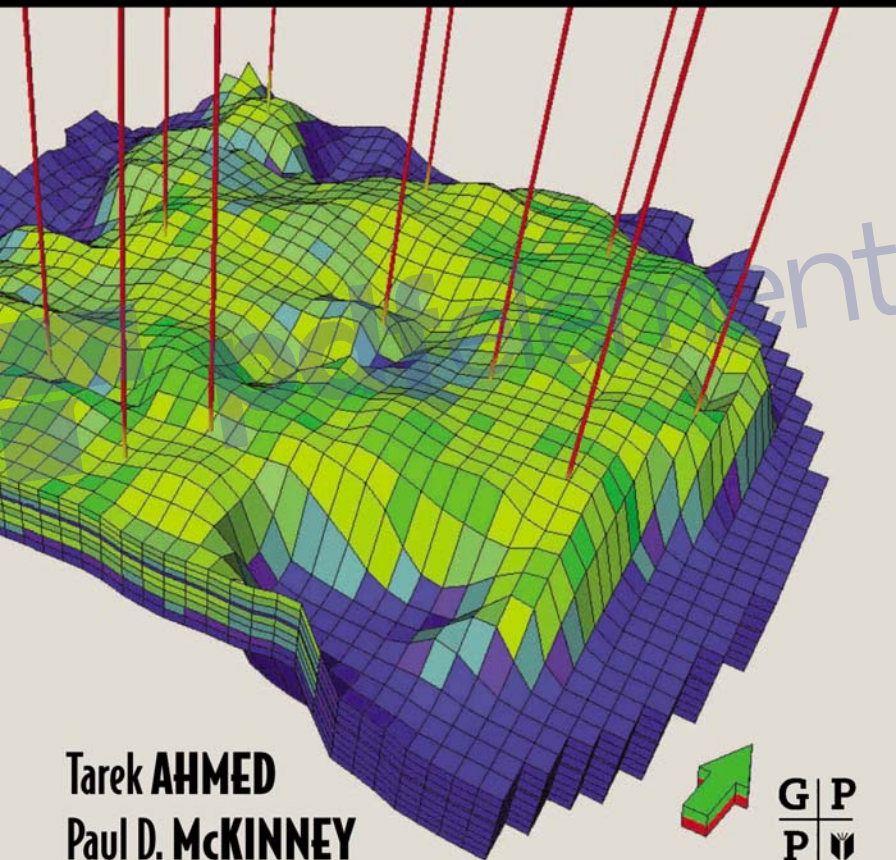# Advanced
Reservoir Engineering

Tarek AHMED
Paul D. McKINNEY

Advanced
Reservoir
Engineering

This page intentionally left blank

Advanced Reservoir Engineering

Tarek Ahmed

Senior Staff Advisor
Anadarko Petroleum Corporation

Paul D. McKinney

V.P. Reservoir Engineering
Anadarko Canada Corporation

Dedication

This book is dedicated to our wonderful and understanding wives, Shanna Ahmed and Teresa McKinney, (without whom this book would have been finished a year ago), and to our beautiful children (NINE of them, wow), Jennifer (the 16 year old nightmare), Justin, Brittany and Carsen Ahmed, and Allison, Sophie, Garretson, Noah and Isabelle McKinney.

This page intentionally left blank

Preface

The primary focus of this book is to present the basic physics of reservoir engineering using the simplest and most straightforward of mathematical techniques. It is only through having a complete understanding of physics of reservoir engineering that the engineer can hope to solve complex reservoir problems in a practical manner. The book is arranged so that it can be used as a textbook for senior and graduate students or as a reference book for practicing engineers.

Chapter 1 describes the theory and practice of well testing and pressure analysis techniques, which is probably one of the most important subjects in reservoir engineering.

Chapter 2 discusses various water-influx models along with detailed descriptions of the computational steps involved in applying these models. Chapter 3 presents the mathematical treatment of unconventional gas reservoirs that include abnormally-pressured reservoirs, coalbed methane, tight gas, gas hydrates, and shallow gas reservoirs. Chapter 4 covers the basic principle oil recovery mechanisms and the various forms of the material balance equation. Chapter 5 focuses on illustrating the practical application of the MBE in predicting the oil reservoir performance under different scenarios of driving mechanisms. Fundamentals of oil field economics are discussed in Chapter 6.

Tarek Ahmed and Paul D. McKinney

This page intentionally left blank

About the Authors

Tarek Ahmed, Ph.D., P.E., is a Senior Staff Advisor with Anadarko Petroleum Corporation. Before joining Anadarko in 2002, Dr. Ahmed served as a Professor and Chairman of the Petroleum Engineering Department at Montana Tech of the University of Montana. After leaving his teaching position, Dr Ahmed has been awarded the rank of Professor of Emeritus of Petroleum Engineering at Montana Tech. He has a Ph.D. from the University of Oklahoma, an M.S. from the University of Missouri-Rolla, and a B.S. from the Faculty of Petroleum (Egypt) – all degrees in Petroleum Engineering. Dr. Ahmed is also the author of 29 technical papers and two textbooks that includes "Hydrocarbon Phase Behavior" (Gulf Publishing Company, 1989) and "Reservoir Engineering Handbook" (Gulf Professional Publishing, 1st edition 2000 and 2nd edition 2002). He taught numerous industry courses and consulted in many countries including, Indonesia, Algeria, Malaysia, Brazil, Argentina, and Kuwait. Dr. Ahmed is an active member of the SPE and serves on the SPE Natural Gas Committee and ABET.

Paul McKinney is Vice President Reservoir Engineering for Anadarko Canada Corporation (a wholly owned subsidiary of Anadarko Petroleum Corporation) overseeing reservoir engineering studies and economic evaluations associated with exploration and development activities, A&D, and planning. Mr. McKinney joined Anadarko in 1983 and has served in staff and managerial positions with the company at increasing levels of responsibility. He holds a Bachelor of Science degree in Petroleum Engineering from Louisiana Tech University and co-authored SPE 75708, "Applied Reservoir Characterization for Maximizing Reserve Growth and Profitability in Tight Gas Sands: A Paradigm Shift in Development Strategies for Low-Permeability Reservoirs."

This page intentionally left blank

Acknowledgements

This page intentionally left blank

Contents

This page intentionally left blank

1

Well Testing Analysis

Contents

1.1 Primary Reservoir Characteristics

Flow in porous media is a very complex phenomenon and cannot be described as explicitly as flow through pipes or conduits. It is rather easy to measure the length and diameter of a pipe and compute its flow capacity as a function of pressure; however, in porous media flow is different in that there are no clear-cut flow paths which lend themselves to measurement.

The analysis of fluid flow in porous media has evolved throughout the years along two fronts: the experimental and the analytical. Physicists, engineers, hydrologists, and the like have examined experimentally the behavior of various fluids as they flow through porous media ranging from sand packs to fused Pyrex glass. On the basis of their analyses, they have attempted to formulate laws and correlations that can then be utilized to make analytical predictions for similar systems.

The main objective of this chapter is to present the mathematical relationships that are designed to describe the flow behavior of the reservoir fluids. The mathematical forms of these relationships will vary depending upon the characteristics of the reservoir. These primary reservoir characteristics that must be considered include:

- types of fluids in the reservoir;
- flow regimes;
- reservoir geometry;
- number of flowing fluids in the reservoir.

1.1.1 Types of fluids

The isothermal compressibility coefficient is essentially the controlling factor in identifying the type of the reservoir fluid. In general, reservoir fluids are classified into three groups:

(1) incompressible fluids;
(2) slightly compressible fluids;
(3) compressible fluids.

The isothermal compressibility coefficient c is described mathematically by the following two equivalent expressions:

In terms of fluid volume:

$$c = \frac{-1}{V}\frac{\partial V}{\partial p} \qquad [1.1.1]$$

In terms of fluid density:

$$c = \frac{1}{\rho}\frac{\partial \rho}{\partial p} \qquad [1.1.2]$$

where

$V =$ fluid volume
$\rho =$ fluid density
$p =$ pressure, psi^{-1}
$c =$ isothermal compressibility coefficient, Ψ^{-1}

Incompressible fluids
An incompressible fluid is defined as the fluid whose volume or density does not change with pressure. That is

$$\frac{\partial V}{\partial p} = 0 \quad \text{and} \quad \frac{\partial \rho}{\partial p} = 0$$

Incompressible fluids do not exist; however, this behavior may be assumed in some cases to simplify the derivation and the final form of many flow equations.

Slightly compressible fluids
These "slightly" compressible fluids exhibit small changes in volume, or density, with changes in pressure. Knowing the volume V_{ref} of a slightly compressible liquid at a reference (initial) pressure p_{ref}, the changes in the volumetric behavior of this fluid as a function of pressure p can be mathematically described by integrating Equation 1.1.1, to give:

$$-c\int_{p_{ref}}^{p}\mathrm{d}p = \int_{V_{ref}}^{V}\frac{\mathrm{d}V}{V}$$

$$\exp\left[c(p_{ref}-p)\right] = \frac{V}{V_{ref}}$$

$$V = V_{ref}\exp\left[c(p_{ref}-p)\right] \qquad [1.1.3]$$

where:

$p =$ pressure, psia
$V =$ volume at pressure p, ft^3
$p_{ref} =$ initial (reference) pressure, psia
$V_{ref} =$ fluid volume at initial (reference) pressure, psia

The exponential e^x may be represented by a series expansion as:

$$e^x = 1 + x + \frac{x^2}{2!} + \frac{x^2}{3!} + \cdots + \frac{x^n}{n!} \qquad [1.1.4]$$

Because the exponent x (which represents the term $c(p_{ref}-p)$) is very small, the e^x term can be approximated by truncating Equation 1.1.4 to:

$$e^x = 1 + x \qquad [1.1.5]$$

Combining Equation 1.1.5 with 1.1.3 gives:

$$V = V_{ref}[1 + c(p_{ref}-p)] \qquad [1.1.6]$$

A similar derivation is applied to Equation 1.1.2, to give:

$$\rho = \rho_{ref}[1 - c(p_{ref}-p)] \qquad [1.1.7]$$

where:

$V =$ volume at pressure p
$\rho =$ density at pressure p
$V_{ref} =$ volume at initial (reference) pressure p_{ref}
$\rho_{ref} =$ density at initial (reference) pressure p_{ref}

It should be pointed out that crude oil and water systems fit into this category.

Compressible fluids
These are fluids that experience large changes in volume as a function of pressure. All gases are considered compressible fluids. The truncation of the series expansion as given by Equation 1.1.5 is not valid in this category and the complete expansion as given by Equation 1.1.4 is used.

The isothermal compressibility of any compressible fluid is described by the following expression:

$$c_g = \frac{1}{p} - \frac{1}{Z}\left(\frac{\partial Z}{\partial p}\right)_T \qquad [1.1.8]$$

Figures 1.1 and 1.2 show schematic illustrations of the volume and density changes as a function of pressure for the three types of fluids.

1.1.2 Flow regimes

There are basically three types of flow regimes that must be recognized in order to describe the fluid flow behavior and reservoir pressure distribution as a function of time. These three flow regimes are:

(1) steady-state flow;
(2) unsteady-state flow;
(3) pseudosteady-state flow.
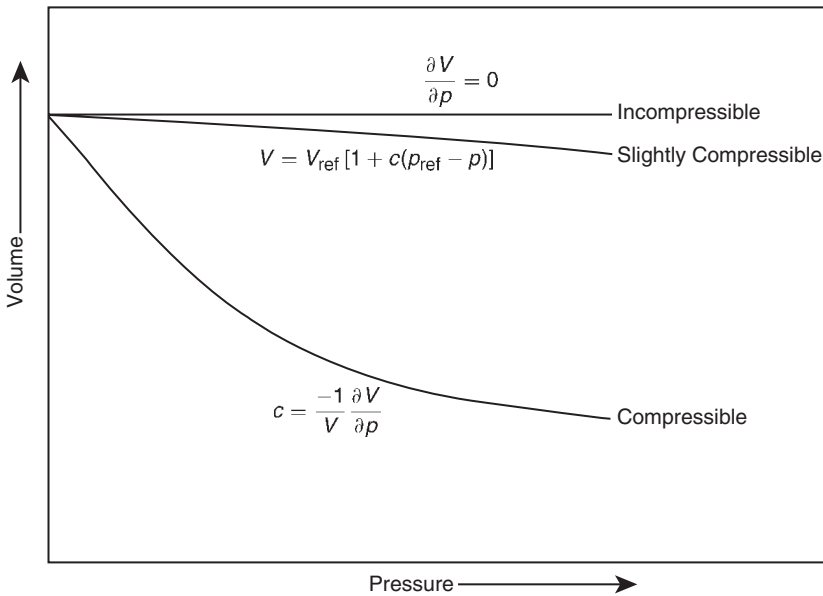
Figure 1.1   *Pressure–volume relationship.*
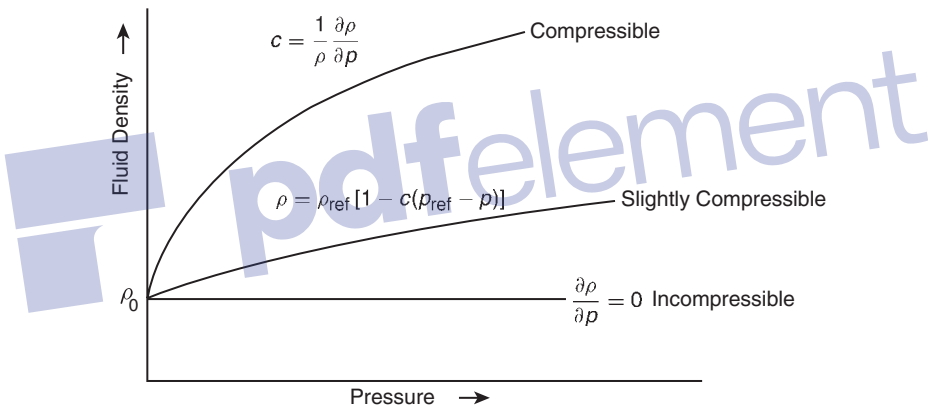
Figure 1.2   *Fluid density versus pressure for different fluid types.*

Steady-state flow

The flow regime is identified as a steady-state flow if the pressure at every location in the reservoir remains constant, i.e., does not change with time. Mathematically, this condition is expressed as:

$$\left(\frac{\partial p}{\partial t}\right)_i = 0 \qquad [1.1.9]$$

This equation states that the rate of change of pressure p with respect to time t at any location i is zero. In reservoirs, the steady-state flow condition can only occur when the reservoir is completely recharged and supported by strong aquifer or pressure maintenance operations.

Unsteady-state flow

Unsteady-state flow (frequently called transient flow) is defined as the fluid flowing condition at which the rate of change of pressure with respect to time at any position in the reservoir is not zero or constant. This definition suggests that the pressure derivative with respect to time is essentially

a function of both position i and time t, thus:

$$\left(\frac{\partial p}{\partial t}\right) = f(i, t) \qquad [1.1.10]$$

Pseudosteady-state flow

When the pressure at different locations in the reservoir is declining linearly as a function of time, i.e., at a constant declining rate, the flowing condition is characterized as pseudosteady-state flow. Mathematically, this definition states that the rate of change of pressure with respect to time at every position is constant, or:

$$\left(\frac{\partial p}{\partial t}\right)_i = \text{constant} \qquad [1.1.11]$$

It should be pointed out that pseudosteady-state flow is commonly referred to as semisteady-state flow and quasisteady-state flow.

Figure 1.3 shows a schematic comparison of the pressure declines as a function of time of the three flow regimes.
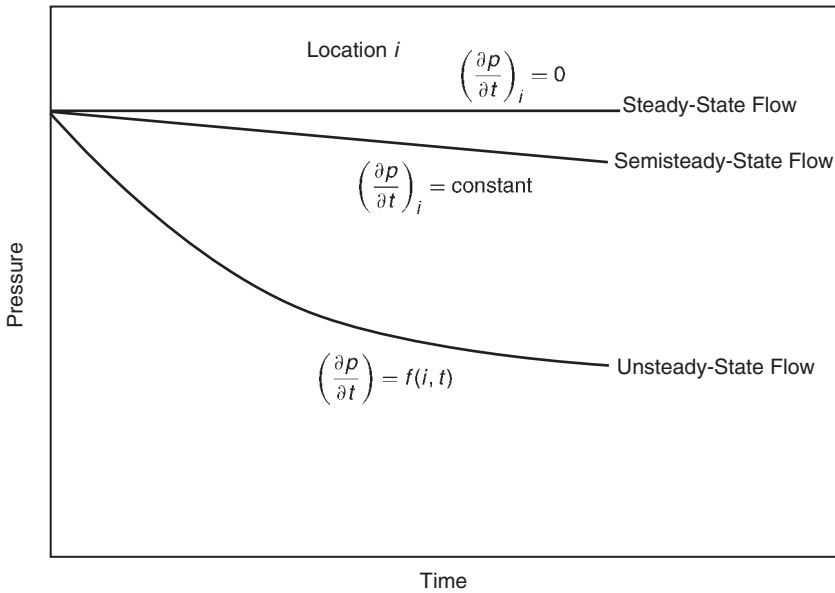
Figure 1.3 *Flow regimes.*
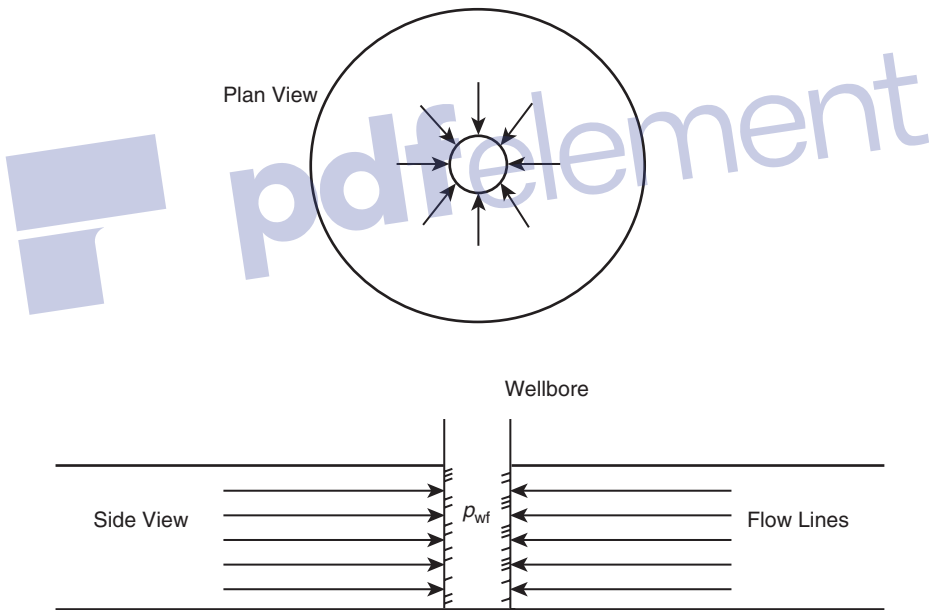
Figure 1.4 *Ideal radial flow into a wellbore.*

1.1.3 Reservoir geometry
The shape of a reservoir has a significant effect on its flow behavior. Most reservoirs have irregular boundaries and a rigorous mathematical description of their geometry is often possible only with the use of numerical simulators. However, for many engineering purposes, the actual flow geometry may be represented by one of the following flow geometries:

- radial flow;
- linear flow;
- spherical and hemispherical flow.

Radial flow
In the absence of severe reservoir heterogeneities, flow into or away from a wellbore will follow radial flow lines a substantial distance from the wellbore. Because fluids move toward the well from all directions and coverage at the wellbore, the term radial flow is used to characterize the flow of fluid into the wellbore. Figure 1.4 shows idealized flow lines and isopotential lines for a radial flow system.

Linear flow
Linear flow occurs when flow paths are parallel and the fluid flows in a single direction. In addition, the cross-sectional
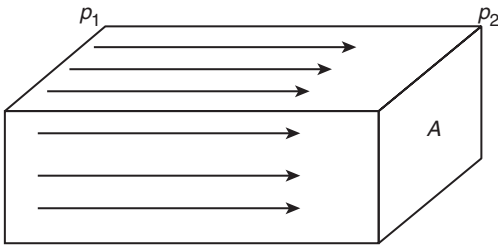
Figure 1.5   *Linear flow.*
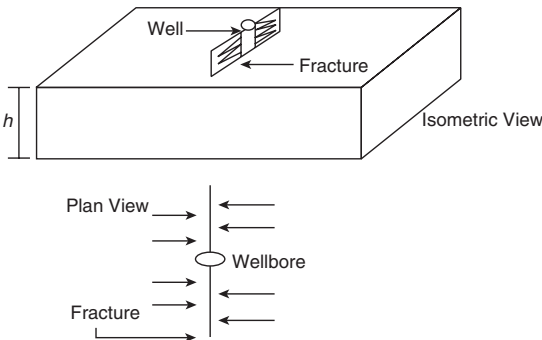
Figure 1.6   *Ideal linear flow into vertical fracture.*
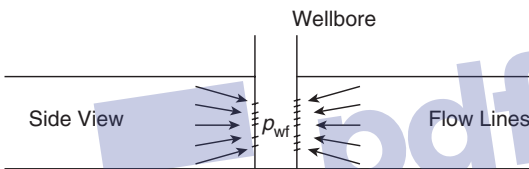
Figure 1.7   *Spherical flow due to limited entry.*
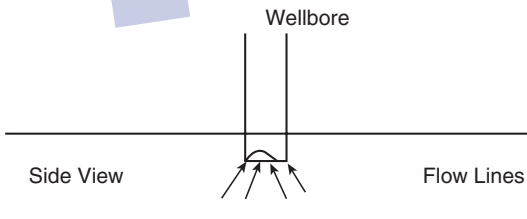
Figure 1.8   *Hemispherical flow in a partially penetrating well.*
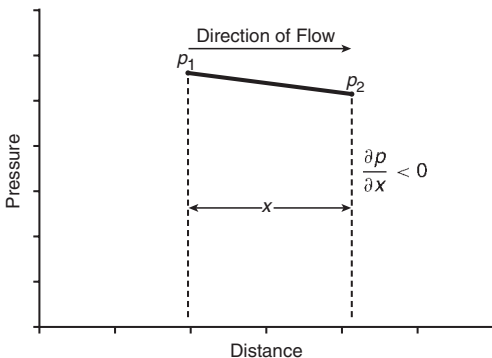
Figure 1.9   *Pressure versus distance in a linear flow.*

area to flow must be constant. Figure 1.5 shows an idealized linear flow system. A common application of linear flow equations is the fluid flow into vertical hydraulic fractures as illustrated in Figure 1.6.

Spherical and hemispherical flow
Depending upon the type of wellbore completion configuration, it is possible to have spherical or hemispherical flow near the wellbore. A well with a limited perforated interval could result in spherical flow in the vicinity of the perforations as illustrated in Figure 1.7. A well which only partially penetrates the pay zone, as shown in Figure 1.8, could result in hemispherical flow. The condition could arise where coning of bottom water is important.

1.1.4 Number of flowing fluids in the reservoir
The mathematical expressions that are used to predict the volumetric performance and pressure behavior of a reservoir vary in form and complexity depending upon the number of mobile fluids in the reservoir. There are generally three cases of flowing system:

(1) single-phase flow (oil, water, or gas);
(2) two-phase flow (oil–water, oil–gas, or gas–water);
(3) three-phase flow (oil, water, and gas).

The description of fluid flow and subsequent analysis of pressure data becomes more difficult as the number of mobile fluids increases.

1.2 Fluid Flow Equations
The fluid flow equations that are used to describe the flow behavior in a reservoir can take many forms depending upon the combination of variables presented previously (i.e., types of flow, types of fluids, etc.). By combining the conservation of mass equation with the transport equation (Darcy's equation) and various equations of state, the necessary flow equations can be developed. Since all flow equations to be considered depend on Darcy's law, it is important to consider this transport relationship first.

1.2.1 Darcy's law
The fundamental law of fluid motion in porous media is Darcy's law. The mathematical expression developed by Darcy in 1956 states that the velocity of a homogeneous fluid in a porous medium is proportional to the pressure gradient, and inversely proportional to the fluid viscosity. For a horizontal linear system, this relationship is:

$$v = \frac{q}{A} = -\frac{k}{\mu}\frac{\mathrm{d}p}{\mathrm{d}x} \qquad [1.2.1a]$$

v is the apparent velocity in centimeters per second and is equal to q/A, where q is the volumetric flow rate in cubic centimeters per second and A is the total cross-sectional area of the rock in square centimeters. In other words, A includes the area of the rock material as well as the area of the pore channels. The fluid viscosity, μ, is expressed in centipoise units, and the pressure gradient, $\mathrm{d}p/\mathrm{d}x$, is in atmospheres per centimeter, taken in the same direction as v and q. The proportionality constant, k, is the permeability of the rock expressed in Darcy units.

The negative sign in Equation 1.2.1a is added because the pressure gradient $\mathrm{d}p/\mathrm{d}x$ is negative in the direction of flow as shown in Figure 1.9.
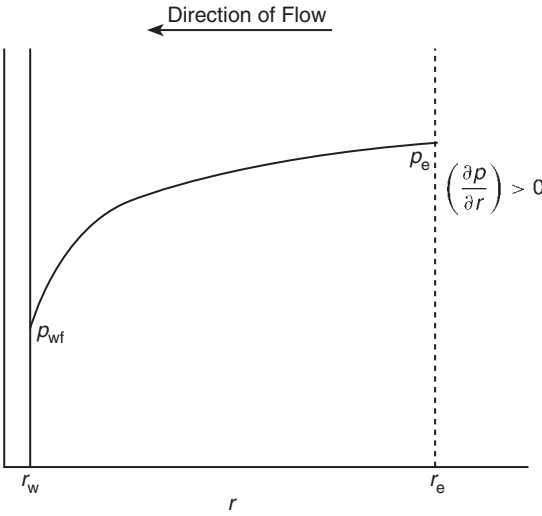
Figure 1.10 *Pressure gradient in radial flow.*

For a horizontal-radial system, the pressure gradient is positive (see Figure 1.10) and Darcy's equation can be expressed in the following generalized radial form:

$$v = \frac{q_r}{A_r} = \frac{k}{\mu}\left(\frac{\partial p}{\partial r}\right)_r \qquad [1.2.1b]$$

where:

q_r = volumetric flow rate at radius r
A_r = cross-sectional area to flow at radius r
$(\partial p/\partial r)_r$ = pressure gradient at radius r
v = apparent velocity at radius r

The cross-sectional area at radius r is essentially the surface area of a cylinder. For a fully penetrated well with a net thickness of h, the cross-sectional area A_r is given by:

$$A_r = 2\pi r h$$

Darcy's law applies only when the following conditions exist:

- laminar (viscous) flow;
- steady-state flow;
- incompressible fluids;
- homogeneous formation.

For turbulent flow, which occurs at higher velocities, the pressure gradient increases at a greater rate than does the flow rate and a special modification of Darcy's equation is needed. When turbulent flow exists, the application of Darcy's equation can result in serious errors. Modifications for turbulent flow will be discussed later in this chapter.

1.2.2 Steady-state flow

As defined previously, steady-state flow represents the condition that exists when the pressure throughout the reservoir does not change with time. The applications of steady-state flow to describe the flow behavior of several types of fluid in different reservoir geometries are presented below. These include:

- linear flow of incompressible fluids;
- linear flow of slightly compressible fluids;
- linear flow of compressible fluids;
- radial flow of incompressible fluids;
- radial flow of slightly compressible fluids;
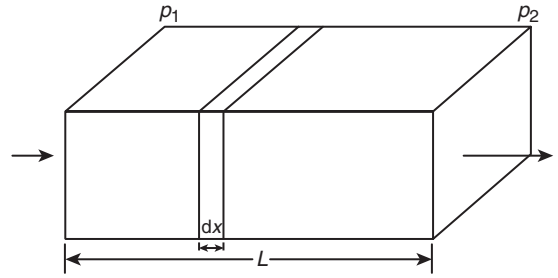
Figure 1.11 *Linear flow model.*

- radial flow of compressible fluids;
- multiphase flow.

Linear flow of incompressible fluids

In a linear system, it is assumed that the flow occurs through a constant cross-sectional area A, where both ends are entirely open to flow. It is also assumed that no flow crosses the sides, top, or bottom as shown in Figure 1.11. If an incompressible fluid is flowing across the element dx, then the fluid velocity v and the flow rate q are constants at all points. The flow behavior in this system can be expressed by the differential form of Darcy's equation, i.e., Equation 1.2.1a. Separating the variables of Equation 1.2.1a and integrating over the length of the linear system:

$$\frac{q}{A}\int_0^L dx = -\frac{k}{u}\int_{p_1}^{p_2} dp$$

which results in:

$$q = \frac{kA(p_1 - p_2)}{\mu L}$$

It is desirable to express the above relationship in customary field units, or:

$$q = \frac{0.001127 kA(p_1 - p_2)}{\mu L} \qquad [1.2.2]$$

where:

q = flow rate, bbl/day
k = absolute permeability, md
p = pressure, psia
μ = viscosity, cp
L = distance, ft
A = cross-sectional area, ft^2

Example 1.1   An incompressible fluid flows in a linear porous media with the following properties:

$L = 2000$ ft,	$h = 20$ ft,	width $= 300$ ft
$k = 100$ md,	$\phi = 15\%$,	$\mu = 2$ cp
$p_1 = 2000$ psi,	$p_2 = 1990$ psi	

Calculate:

(a) flow rate in bbl/day;
(b) apparent fluid velocity in ft/day;
(c) actual fluid velocity in ft/day.

Solution   Calculate the cross-sectional area A:

$$A = (h)(\text{width}) = (20)(100) = 6000 \text{ ft}^2$$

(a) Calculate the flow rate from Equation 1.2.2:

$$q = \frac{0.001127kA(p_1 - p_2)}{\mu L}$$

$$= \frac{(0.001127)(100)(6000)(2000 - 1990)}{(2)(2000)}$$

$$= 1.6905 \text{ bbl/day}$$

(b) Calculate the apparent velocity:

$$v = \frac{q}{A} = \frac{(1.6905)(5.615)}{6000} = 0.0016 \text{ ft/day}$$

(c) Calculate the actual fluid velocity:

$$v = \frac{q}{\phi A} = \frac{(1.6905)(5.615)}{(0.15)(6000)} = 0.0105 \text{ ft/day}$$

The difference in the pressure (p_1-p_2) in Equation 1.2.2 is not the only driving force in a tilted reservoir. The gravitational force is the other important driving force that must be accounted for to determine the direction and rate of flow. The fluid gradient force (gravitational force) is always directed *vertically downward* while the force that results from an applied pressure drop may be in any direction. The force causing flow would then be the *vector sum of these two*. In practice we obtain this result by introducing a new parameter, called "fluid potential," which has the same dimensions as pressure, e.g., psi. Its symbol is Φ. The fluid potential at any point in the reservoir is defined as the pressure at that point less the pressure that would be exerted by a fluid head extending to an arbitrarily assigned datum level. Letting Δz_i be the vertical distance from a point i in the reservoir to this datum level:

$$\Phi_i = p_i - \left(\frac{\rho}{144}\right)\Delta z_i \qquad [1.2.3]$$

where ρ is the density in lb/ft^3.

Expressing the fluid density in g/cm^3 in Equation 1.2.3 gives:

$$\Phi_i = p_i - 0.433\gamma\Delta z \qquad [1.2.4]$$

where:

   $\Phi_i =$ fluid potential at point i, psi
   $p_i =$ pressure at point i, psi
   $\Delta z_i =$ vertical distance from point i to the selected datum level
   $\rho =$ fluid density under reservoir conditions, lb/ft^3
   $\gamma = $ *fluid density* under reservoir conditions, g/cm^3; this is *not* the fluid specific gravity

The datum is usually selected at the gas–oil contact, oil–water contact, or the highest point in formation. In using Equations 1.2.3 or 1.2.4 to calculate the fluid potential Φ_i at location i, the vertical distance z_i is assigned a positive value when the point i is below the datum level and as a negative value when it is above the datum level. That is:

If point i is above the datum level:

$$\Phi_i = p_i + \left(\frac{\rho}{144}\right)\Delta z_i$$

and equivalently:

$$\Phi_i = p_i + 0.433\gamma\Delta z_i$$

If point i is below the datum level:

$$\Phi_i = p_i - \left(\frac{\rho}{144}\right)\Delta z_i$$

and equivalently:

$$\Phi_i = p_i - 0.433\gamma\Delta z_i$$

Applying the above-generalized concept to Darcy's equation (Equation 1.2.2) gives:

$$q = \frac{0.001127kA(\Phi_1 - \Phi_2)}{\mu L} \qquad [1.2.5]$$
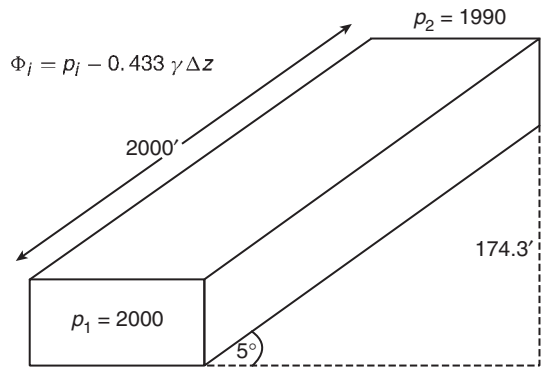
Figure 1.12 *Example of a tilted layer.*

$\Phi_i = p_i - 0.433\,\gamma\,\Delta z$

$p_2 = 1990$

$2000'$

$174.3'$

$p_1 = 2000$

$5°$

It should be pointed out that the fluid potential drop $(\Phi_1-\Phi_2)$ is equal to the pressure drop (p_1-p_2) only when the flow system is horizontal.

Example 1.2 Assume that the porous media with the properties as given in the previous example are tilted with a dip angle of 5° as shown in Figure 1.12. The incompressible fluid has a density of 42 lb/ft^3. Resolve Example 1.1 using this additional information.

Solution

Step 1. For the purpose of illustrating the concept of fluid potential, select the datum level at half the vertical distance between the two points, i.e., at 87.15 ft, as shown in Figure 1.12.

Step 2. Calculate the fluid potential at point 1 and 2.
Since point 1 is below the datum level, then:

$$\Phi_1 = p_1 - \left(\frac{\rho}{144}\right)\Delta z_1 = 2000 - \left(\frac{42}{144}\right)(87.15)$$

$$= 1974.58 \text{ psi}$$

Since point 2 is above the datum level, then:

$$\Phi_2 = p_2 + \left(\frac{\rho}{144}\right)\Delta z_2 = 1990 + \left(\frac{42}{144}\right)(87.15)$$

$$= 2015.42 \text{ psi}$$

Because $\Phi_2 > \Phi_1$, the fluid flows downward from point 2 to point 1. The difference in the fluid potential is:

$$\Delta\Phi = 2015.42 - 1974.58 = 40.84 \text{ psi}$$

Notice that, if we select point 2 for the datum level, then:

$$\Phi_1 = 2000 - \left(\frac{42}{144}\right)(174.3) = 1949.16 \text{ psi}$$

$$\Phi_2 = 1990 + \left(\frac{42}{144}\right)(0) = 1990 \text{ psi}$$

The above calculations indicate that regardless of the position of the datum level, the flow is downward from point 2 to 1 with:

$$\Delta\Phi = 1990 - 1949.16 = 40.84 \text{ psi}$$

Step 3. Calculate the flow rate:

$$q = \frac{0.001127kA(\Phi_1 - \Phi_2)}{\mu L}$$

$$= \frac{(0.001127)(100)(6000)(40.84)}{(2)(2000)} = 6.9 \text{ bbl/day}$$

Step 4. Calculate the velocity:

$$\text{Apparent velocity} = \frac{(6.9)(5.615)}{6000} = 0.0065 \text{ ft/day}$$

$$\text{Actual velocity} = \frac{(6.9)(5.615)}{(0.15)(6000)} = 0.043 \text{ ft/day}$$

Linear flow of slightly compressible fluids

Equation 1.1.6 describes the relationship that exists between pressure and volume for a slightly compressible fluid, or:

$$V = V_{\text{ref}}[1 + c(p_{\text{ref}} - p)]$$

This equation can be modified and written in terms of flow rate as:

$$q = q_{\text{ref}}[1 + c(p_{\text{ref}} - p)] \qquad [1.2.6]$$

where q_{ref} is the flow rate at some reference pressure p_{ref}. Substituting the above relationship in Darcy's equation gives:

$$\frac{q}{A} = \frac{q_{\text{ref}}[1 + c(p_{\text{ref}} - p)]}{A} = -0.001127 \frac{k}{\mu} \frac{dp}{dx}$$

Separating the variables and arranging:

$$\frac{q_{\text{ref}}}{A} \int_0^L dx = -0.001127 \frac{k}{\mu} \int_{p_1}^{p_2} \left[\frac{dp}{1 + c(p_{\text{ref}} - p)} \right]$$

Integrating gives:

$$q_{\text{ref}} = \left[\frac{0.001127 kA}{\mu c L} \right] \ln \left[\frac{1 + c(p_{\text{ref}} - p_2)}{1 + c(p_{\text{ref}} - p_1)} \right] \qquad [1.2.7]$$

where:

q_{ref} = flow rate at a reference pressure p_{ref}, bbl/day
p_1 = upstream pressure, psi
p_2 = downstream pressure, psi
k = permeability, md
μ = viscosity, cp
c = average liquid compressibility, psi^{-1}

Selecting the upstream pressure p_1 as the reference pressure p_{ref} and substituting in Equation 1.2.7 gives the flow rate at point 1 as:

$$q_1 = \left[\frac{0.001127 kA}{\mu c L} \right] \ln \left[1 + c(p_1 - p_2) \right] \qquad [1.2.8]$$

Choosing the downstream pressure p_2 as the reference pressure and substituting in Equation 1.2.7 gives:

$$q_2 = \left[\frac{0.001127 kA}{\mu c L} \right] \ln \left[\frac{1}{1 + c(p_2 - p_1)} \right] \qquad [1.2.9]$$

where q_1 and q_2 are the flow rates at point 1 and 2, respectively.

Example 1.3 Consider the linear system given in Example 1.1 and, assuming a slightly compressible liquid, calculate the flow rate at both ends of the linear system. The liquid has an average compressibility of 21×10^{-5} psi^{-1}.

Solution Choosing the upstream pressure as the reference pressure gives:

$$q_1 = \left[\frac{0.001127 kA}{\mu c L} \right] \ln \left[1 + c(p_1 - p_2) \right]$$

$$= \left[\frac{(0.001127)(100)(6000)}{(2)(21 \times 10^{-5})(2000)} \right]$$

$$\times \ln \left[1 + 21 \times 10^{-5}(2000 - 1990) \right] = 1.689 \text{ bbl/day}$$

Choosing the downstream pressure gives

$$q_2 = \left[\frac{0.001127 kA}{\mu c L} \right] \ln \left[\frac{1}{1 + c(p_2 - p_1)} \right]$$

$$= \left[\frac{(0.001127)(100)(6000)}{(2)(21 \times 10^{-5})(2000)} \right]$$

$$\times \ln \left[\frac{1}{1 + (21 \times 10^{-5})(1990 - 2000)} \right] = 1.692 \text{ bbl/day}$$

The above calculations show that q_1 and q_2 are not largely different, which is due to the fact that the liquid is slightly incompressible and its volume is not a strong function of pressure.

Linear flow of compressible fluids (gases)

For a viscous (laminar) gas flow in a homogeneous linear system, the real-gas equation of state can be applied to calculate the number of gas moles n at the pressure p, temperature T, and volume V:

$$n = \frac{pV}{ZRT}$$

At standard conditions, the volume occupied by the above n moles is given by:

$$V_{\text{sc}} = \frac{nZ_{\text{sc}}RT_{\text{sc}}}{p_{\text{sc}}}$$

Combining the above two expressions and assuming $Z_{\text{sc}} = 1$ gives:

$$\frac{pV}{ZT} = \frac{p_{\text{sc}} V_{\text{sc}}}{T_{\text{sc}}}$$

Equivalently, the above relation can be expressed in terms of the reservoir condition flow rate q, in bbl/day, and surface condition flow rate Q_{sc}, in scf/day, as:

$$\frac{p(5.615q)}{ZT} = \frac{p_{\text{sc}} Q_{\text{sc}}}{T_{\text{sc}}}$$

Rearranging:

$$\left(\frac{p_{\text{sc}}}{T_{\text{sc}}} \right) \left(\frac{ZT}{p} \right) \left(\frac{Q_{\text{sc}}}{5.615} \right) = q \qquad [1.2.10]$$

where:

q = gas flow rate at pressure p in bbl/day
Q_{sc} = gas flow rate at standard conditions, scf/day
Z = gas compressibility factor
$T_{\text{sc}}, p_{\text{sc}}$ = standard temperature and pressure in °R and psia, respectively.

Dividing both sides of the above equation by the cross-sectional area A and equating it with that of Darcy's law, i.e., Equation 1.2.1a, gives:

$$\frac{q}{A} = \left(\frac{p_{\text{sc}}}{T_{\text{sc}}} \right) \left(\frac{ZT}{p} \right) \left(\frac{Q_{\text{sc}}}{5.615} \right) \left(\frac{1}{A} \right) = -0.001127 \frac{k}{\mu} \frac{dp}{dx}$$

The constant 0.001127 is to convert Darcy's units to field units. Separating variables and arranging yields:

$$\left[\frac{Q_{\text{sc}} p_{\text{sc}} T}{0.006328 k T_{\text{sc}} A} \right] \int_0^L dx = -\int_{p_1}^{p_2} \frac{p}{Z \mu_g} dp$$

Assuming that the product of $Z\mu_g$ is constant over the specified pressure range between p_1 and p_2, and integrating, gives:

$$\left[\frac{Q_{\text{sc}} p_{\text{sc}} T}{0.006328 k T_{\text{sc}} A} \right] \int_0^L dx = -\frac{1}{Z \mu_g} \int_{p_1}^{p_2} p \, dp$$

or:

$$Q_{sc} = \frac{0.003164 T_{sc} Ak \left(p_1^2 - p_2^2\right)}{p_{sc} T (Z\mu_g) L}$$

where:

Q_{sc} = gas flow rate at standard conditions, scf/day
k = permeability, md
T = temperature, °R
μ_g = gas viscosity, cp
A = cross-sectional area, ft^2
L = total length of the linear system, ft

Setting $p_{sc} = 14.7$ psi and $T_{sc} = 520$°R in the above expression gives:

$$Q_{sc} = \frac{0.111924 Ak\left(p_1^2 - p_2^2\right)}{TLZ\mu_g} \qquad [1.2.11]$$

It is essential to notice that those gas properties Z and μ_g are very strong functions of pressure, but they have been removed from the integral to simplify the final form of the gas flow equation. The above equation is valid for applications when the pressure is less than 2000 psi. The gas properties must be evaluated at the average pressure $\bar{p}$ as defined below:

$$\bar{p} = \sqrt{\frac{p_1^2 + p_2^2}{2}} \qquad [1.2.12]$$

Example 1.4 A natural gas with a specific gravity of 0.72 is flowing in linear porous media at 140°F. The upstream and downstream pressures are 2100 psi and 1894.73 psi, respectively. The cross-sectional area is constant at 4500 ft^2. The total length is 2500 ft with an absolute permeability of 60 md. Calculate the gas flow rate in scf/day ($p_{sc} = 14.7$ psia, $T_{sc} = 520$°R).

Solution

Step 1. Calculate average pressure by using Equation 1.2.12:

$$\bar{p} = \sqrt{\frac{2100^2 + 1894.73^2}{2}} = 2000 \text{ psi}$$

Step 2. Using the specific gravity of the gas, calculate its pseudo-critical properties by applying the following equations:

$$T_{pc} = 168 + 325\gamma_g - 12.5\gamma_g^2$$

$$= 168 + 325(0.72) - 12.5(0.72)^2 = 395.5°R$$

$$p_{pc} = 677 + 15.0\gamma_g - 37.5\gamma_g^2$$

$$= 677 + 15.0(0.72) - 37.5(0.72)^2 = 668.4 \text{ psia}$$

Step 3. Calculate the pseudo-reduced pressure and temperature:

$$p_{pr} = \frac{2000}{668.4} = 2.99$$

$$T_{pr} = \frac{600}{395.5} = 1.52$$

Step 4. Determine the Z-factor from a Standing–Katz chart to give:

$$Z = 0.78$$

Step 5. Solve for the viscosity of the gas by applying the Lee–Gonzales–Eakin method and using the following sequence of calculations:

$$M_a = 28.96\gamma_g$$

$$= 28.96(0.72) = 20.85$$

$$\rho_g = \frac{pM_a}{ZRT}$$

$$= \frac{(2000)(20.85)}{(0.78)(10.73)(600)} = 8.30 \text{ lb/ft}^3$$

$$K = \frac{(9.4 + 0.02M_a)T^{1.5}}{209 + 19M_a + T}$$

$$= \frac{\left[9.4 + 0.02(20.96)\right](600)^{1.5}}{209 + 19(20.96) + 600} = 119.72$$

$$X = 3.5 + \frac{986}{T} + 0.01M_a$$

$$= 3.5 + \frac{986}{600} + 0.01(20.85) = 5.35$$

$$Y = 2.4 - 0.2X$$

$$= 2.4 - (0.2)(5.35) = 1.33$$

$$\mu_g = 10^{-4}K \exp\left[X\left(\rho_g/62.4\right)^Y\right] = 0.0173 \text{ cp}$$

$$= 10^{-4}\left(119.72 \exp\left[5.35\left(\frac{8.3}{62.4}\right)^{1.33}\right]\right)$$

$$= 0.0173$$

Step 6. Calculate the gas flow rate by applying Equation 1.2.11:

$$Q_{sc} = \frac{0.111924 Ak\left(p_1^2 - p_2^2\right)}{TLZ\mu_g}$$

$$= \frac{(0.111924)(4500)(60)\left(2100^2 - 1894.73^2\right)}{(600)(2500)(0.78)(0.0173)}$$

$$= 1\,224\,242 \text{ scf/day}$$

Radial flow of incompressible fluids

In a radial flow system, all fluids move toward the producing well from all directions. However, before flow can take place, a pressure differential must exist. Thus, if a well is to produce oil, which implies a flow of fluids through the formation to the wellbore, the pressure in the formation at the wellbore must be less than the pressure in the formation at some distance from the well.

The pressure in the formation at the wellbore of a producing well is known as the bottom-hole flowing pressure (flowing BHP, p_{wf}).

Consider Figure 1.13 which schematically illustrates the radial flow of an incompressible fluid toward a vertical well. The formation is considered to have a uniform thickness h and a constant permeability k. Because the fluid is incompressible, the flow rate q must be constant at all radii. Due to the steady-state flowing condition, the pressure profile around the wellbore is maintained constant with time.

Let p_{wf} represent the maintained bottom-hole flowing pressure at the wellbore radius r_w and p_e denotes the external pressure at the external or drainage radius. Darcy's generalized equation as described by Equation 1.2.1b can be used to determine the flow rate at any radius r:

$$v = \frac{q}{A_r} = 0.001127 \frac{k}{\mu} \frac{dp}{dr} \qquad [1.2.13]$$
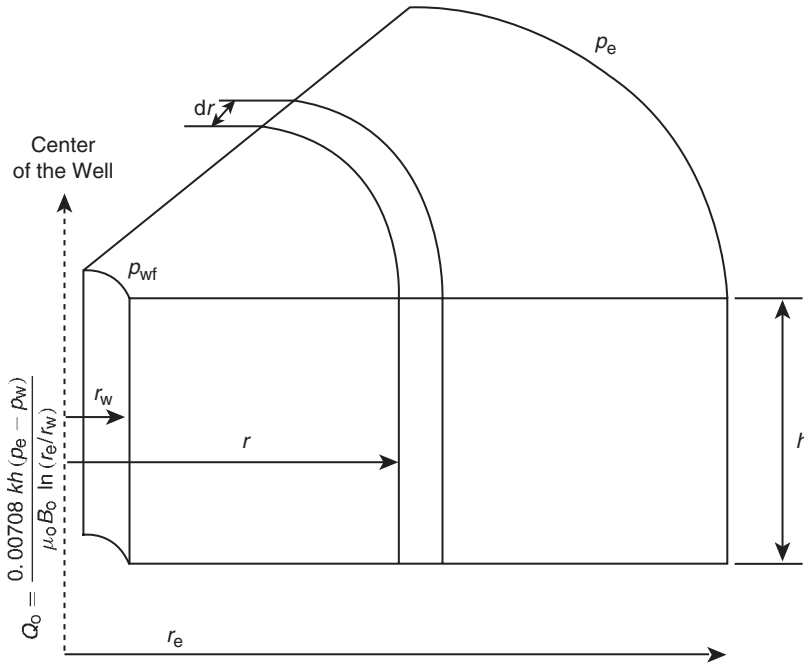
Figure 1.13   *Radial flow model.*

where:

$$v = \text{apparent fluid velocity, bbl/day-ft}^2$$
$$q = \text{flow rate at radius } r, \text{ bbl/day}$$
$$k = \text{permeability, md}$$
$$\mu = \text{viscosity, cp}$$
$$0.001127 = \text{conversion factor to express the equation in field units}$$
$$A_r = \text{cross-sectional area at radius } r$$

The minus sign is no longer required for the radial system shown in Figure 1.13 as the radius increases in the same direction as the pressure. In other words, as the radius increases going away from the wellbore the pressure also increases. At any point in the reservoir the cross-sectional area across which flow occurs will be the surface area of a cylinder, which is $2\pi rh$, or:

$$v = \frac{q}{A_r} = \frac{q}{2\pi rh} = 0.001127 \frac{k}{\mu} \frac{dp}{dr}$$

The flow rate for a crude oil system is customarily expressed in surface units, i.e., stock-tank barrels (STB), rather than reservoir units. Using the symbol Q_o to represent the oil flow as expressed in STB/day, then:

$$q = B_o Q_o$$

where B_o is the oil formation volume factor in bbl/STB. The flow rate in Darcy's equation can be expressed in STB/day, to give:

$$\frac{Q_o B_o}{2\pi rh} = 0.001127 \frac{k}{\mu_o} \frac{dp}{dr}$$

Integrating this equation between two radii, r_1 and r_2, when the pressures are p_1 and p_2, yields:

$$\int_{r_1}^{r_2} \left(\frac{Q_o}{2\pi h} \right) \frac{dr}{r} = 0.001127 \int_{P_1}^{P_2} \left(\frac{k}{\mu_o B_o} \right) dp \qquad [1.2.14]$$

For an incompressible system in a uniform formation, Equation 1.2.14 can be simplified to:

$$\frac{Q_o}{2\pi h} \int_{r_1}^{r_2} \frac{dr}{r} = \frac{0.001127k}{\mu_o B_o} \int_{P_1}^{P_2} dp$$

Performing the integration gives:

$$Q_o = \frac{0.00708kh(p_2 - p_1)}{\mu_o B_o \ln(r_2/r_1)}$$

Frequently the two radii of interest are the wellbore radius r_w and the external or drainage radius r_e. Then:

$$Q_o = \frac{0.00708kh(p_e - p_w)}{\mu_o B_o \ln(r_e/r_w)} \qquad [1.2.15]$$

where:

$$Q_o = \text{oil flow rate, STB/day}$$
$$p_e = \text{external pressure, psi}$$
$$p_{wf} = \text{bottom-hole flowing pressure, psi}$$
$$k = \text{permeability, md}$$
$$\mu_o = \text{oil viscosity, cp}$$
$$B_o = \text{oil formation volume factor, bbl/STB}$$
$$h = \text{thickness, ft}$$
$$r_e = \text{external or drainage radius, ft}$$
$$r_w = \text{wellbore radius, ft}$$

The external (drainage) radius r_e is usually determined from the well spacing by equating the area of the well spacing with that of a circle. That is:

$$\pi r_e^2 = 43\,560A$$

or:

$$r_e = \sqrt{\frac{43\,560A}{\pi}} \qquad [1.2.16]$$

where A is the well spacing in acres.

In practice, neither the external radius nor the wellbore radius is generally known with precision. Fortunately, they enter the equation as a logarithm, so the error in the equation will be less than the errors in the radii.

Equation 1.2.15 can be arranged to solve for the pressure p at any radius r, to give:

$$p = p_{wf} + \left[\frac{Q_o B_o \mu_o}{0.00708 kh} \right] \ln\left(\frac{r}{r_w} \right) \qquad [1.2.17]$$

Example 1.5 An oil well in the Nameless Field is producing at a stabilized rate of 600 STB/day at a stabilized bottom-hole flowing pressure of 1800 psi. Analysis of the pressure buildup test data indicates that the pay zone is characterized by a permeability of 120 md and a uniform thickness of 25 ft. The well drains an area of approximately 40 acres. The following additional data is available:

$$r_w = 0.25 \text{ ft}, \qquad A = 40 \text{ acres}$$

$$B_o = 1.25 \text{ bbl/STB}, \qquad \mu_o = 2.5 \text{ cp}$$

Calculate the pressure profile (distribution) and list the pressure drop across 1 ft intervals from r_w to 1.25 ft, 4 to 5 ft, 19 to 20 ft, 99 to 100 ft, and 744 to 745 ft.

Solution

Step 1. Rearrange Equation 1.2.15 and solve for the pressure p at radius r:

$$p = p_{wf} + \left[\frac{\mu_o B_o Q_o}{0.00708 kh} \right] \ln\left(\frac{r}{r_w} \right)$$

$$= 1800 + \left[\frac{(2.5)(1.25)(600)}{(0.00708)(120)(25)} \right] \ln\left(\frac{r}{0.25} \right)$$

$$= 1800 + 88.28 \ln\left(\frac{r}{0.25} \right)$$

Step 2. Calculate the pressure at the designated radii:

r (ft)	p (psi)	Radius interval	Pressure drop
0.25	1800		
1.25	1942	0.25–1.25	$1942 - 1800 = 142$ psi
4	2045		
5	2064	4–5	$2064 - 2045 = 19$ psi
19	2182		
20	2186	19–20	$2186 - 2182 = 4$ psi
99	2328		
100	2329	99–100	$2329 - 2328 = 1$ psi
744	2506.1		
745	2506.2	744–745	$2506.2 - 2506.1 = 0.1$ psi

Figure 1.14 shows the pressure profile as a function of radius for the calculated data.

Results of the above example reveal that the pressure drop just around the wellbore (i.e., 142 psi) is 7.5 times greater than at the 4 to 5 interval, 36 times greater than at 19–20 ft, and 142 times than that at the 99–100 ft interval. The reason for this large pressure drop around the wellbore is that the fluid flows in from a large drainage area of 40 acres.

The external pressure p_e used in Equation 1.2.15 cannot be measured readily, but p_e does not deviate substantially from the initial reservoir pressure if a strong and active aquifer is present.

Several authors have suggested that the average reservoir pressure p_r, which often is reported in well test results, should be used in performing material balance calculations and flow rate prediction. Craft and Hawkins (1959) showed that the average pressure is located at about 61% of the drainage radius r_e *for a steady-state flow condition.*

Substituting $0.61 r_e$ in Equation 1.2.17 gives:

$$p\,(\text{at } r = 0.61 r_e) = p_r = p_{wf} + \left[\frac{Q_o B_o \mu_o}{0.00708 kh} \right] \ln\left(\frac{0.61 r_e}{r_w} \right)$$

or in terms of flow rate:

$$Q_o = \frac{0.00708 kh(p_r - p_{wf})}{\mu_o B_o \ln(0.61 r_e / r_w)} \qquad [1.2.18]$$

But since $\ln(0.61 r_e / r_w) = \ln(r_e / r_w) - 0.5$, then:

$$Q_o = \frac{0.00708 kh(p_r - p_{wf})}{\mu_o B_o \left[\ln(r_e / r_w) - 0.5 \right]} \qquad [1.2.19]$$

Golan and Whitson (1986) suggested a method for approximating the drainage area of wells producing from a common reservoir. These authors assume that the volume drained by a single well is proportional to its rate of flow. Assuming constant reservoir properties and a uniform thickness, the approximate drainage area of a single well A_w is:

$$A_w = A_T \left(\frac{q_w}{q_T} \right) \qquad [1.2.20]$$

where:

A_w = drainage area of a well
A_T = total area of the field
q_T = total flow rate of the field
q_w = well flow rate

Radial flow of slightly compressible fluids

Terry and co-authors (1991) used Equation 1.2.6 to express the dependency of the flow rate on pressure for slightly compressible fluids. If this equation is substituted into the radial form of Darcy's law, the following is obtained:

$$\frac{q}{A_r} = \frac{q_{ref}\left[1 + c(p_{ref} - p) \right]}{2\pi r h} = 0.001127 \frac{k}{\mu} \frac{dp}{dr}$$

where q_{ref} is the flow rate at some reference pressure p_{ref}.

Separating the variables and assuming a constant compressibility over the entire pressure drop, and integrating over the length of the porous medium:

$$\frac{q_{ref}\mu}{2\pi kh} \int_{r_w}^{r_e} \frac{dr}{r} = 0.001127 \int_{p_{wf}}^{p_e} \frac{dp}{1 + c(p_{ref} - p)}$$

gives:

$$q_{ref} = \left[\frac{0.00708 kh}{\mu c \ln(r_e / r_w)} \right] \ln\left[\frac{1 + c(p_e - p_{ref})}{1 + c(p_{wf} - p_{ref})} \right]$$

where q_{ref} is the oil flow rate at a reference pressure p_{ref}. Choosing the bottom-hole flow pressure p_{wf} as the reference pressure and expressing the flow rate in STB/day gives:

$$Q_o = \left[\frac{0.00708 kh}{\mu_o B_o c_o \ln(r_e / r_w)} \right] \ln\left[1 + c_o(p_e - p_{wf}) \right] \qquad [1.2.21]$$

where:

c_o = isothermal compressibility coefficient, psi^{-1}
Q_o = oil flow rate, STB/day
k = permeability, md

Example 1.6 The following data is available on a well in the Red River Field:

$$p_e = 2506 \text{ psi}, \qquad p_{wf} = 1800 \text{ psi}$$

$$r_e = 745 \text{ ft}, \qquad r_w = 0.25 \text{ ft}$$

$$B_o = 1.25 \text{ bbl/STB}, \quad \mu_o = 2.5 \text{ cp}$$

$$k = 0.12 \text{ darcy}, \qquad h = 25 \text{ ft}$$

$$c_o = 25 \times 10^{-6} \text{ psi}^{-1}$$
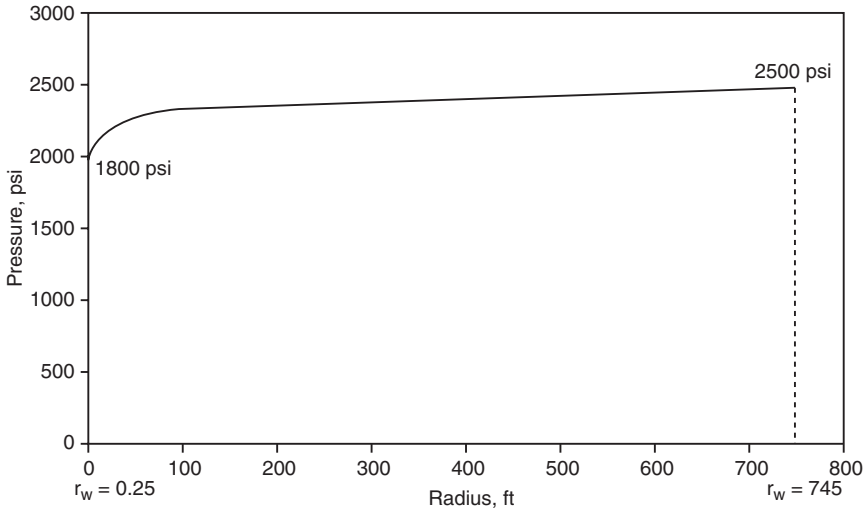
Figure 1.14   *Pressure profile around the wellbore.*

Assuming a slightly compressible fluid, calculate the oil flow rate. Compare the result with that of an incompressible fluid.

Solution   For a slightly compressible fluid, the oil flow rate can be calculated by applying Equation 1.2.21:

$$Q_o = \left[\frac{0.00708kh}{\mu_o B_o c_o \ln(r_e/r_w)} \right] \ln[1 + c_o(p_e - p_{wf})]$$

$$= \left[\frac{(0.00708)(120)(25)}{(2.5)(1.25)(25 \times 10^{-6})\ln(745/0.25)} \right]$$

$$\times \ln\left[1 + (25 \times 10^{-6})(2506 - 1800)\right] = 595 \text{ STB/day}$$

Assuming an incompressible fluid, the flow rate can be estimated by applying Darcy's equation, i.e., Equation 1.2.15:

$$Q_o = \frac{0.00708kh(p_e - p_w)}{\mu_o B_o \ln(r_e/r_w)}$$

$$= \frac{(0.00708)(120)(25)(2506 - 1800)}{(2.5)(1.25)\ln(745/0.25)} = 600 \text{ STB/day}$$

Radial flow of compressible gases
The basic differential form of Darcy's law for a horizontal laminar flow is valid for describing the flow of both gas and liquid systems. For a radial gas flow, Darcy's equation takes the form:

$$q_{gr} = \frac{0.001127(2\pi rh)k}{\mu_g} \frac{dp}{dr} \qquad [1.2.22]$$

where:

$$\begin{aligned} q_{gr} &= \text{gas flow rate at radius } r, \text{ bbl/day} \\ r &= \text{radial distance, ft} \\ h &= \text{zone thickness, ft} \\ \mu_g &= \text{gas viscosity, cp} \\ p &= \text{pressure, psi} \\ 0.001127 &= \text{conversion constant from Darcy units to} \\ &\quad \text{field units} \end{aligned}$$

The gas flow rate is traditionally expressed in scf/day. Referring to the gas flow rate at standard (surface) condition as Q_g, the gas flow rate q_{gr} under wellbore flowing condition can be converted to that of surface condition by applying the definition of the gas formation volume factor B_g to q_{gr} as:

$$Q_g = \frac{q_{gr}}{B_g}$$

where:

$$B_g = \frac{p_{sc}}{5.615T_{sc}} \frac{ZT}{p} \text{ bbl/scf}$$

or:

$$\left(\frac{p_{sc}}{5.615T_{sc}}\right)\left(\frac{ZT}{p}\right)Q_g = q_{gr} \qquad [1.2.23]$$

where:

$$\begin{aligned} p_{sc} &= \text{standard pressure, psia} \\ T_{sc} &= \text{standard temperature, °R} \\ Q_g &= \text{gas flow rate, scf/day} \\ q_{gr} &= \text{gas flow rate at radius } r, \text{ bbl/day} \\ p &= \text{pressure at radius } r, \text{ psia} \\ T &= \text{reservoir temperature, °R} \\ Z &= \text{gas compressibility factor at } p \text{ and } T \\ Z_{sc} &= \text{gas compressibility factor at standard} \\ &\quad \text{condition} \cong 1.0 \end{aligned}$$

Combining Equations 1.2.22 and 1.2.23 yields:

$$\left(\frac{p_{sc}}{5.615T_{sc}}\right)\left(\frac{ZT}{p}\right)Q_g = \frac{0.001127(2\pi rh)k}{\mu_g} \frac{dp}{dr}$$

Assuming that $T_{sc} = 520$°R and $p_{sc} = 14.7$ psia:

$$\left(\frac{TQ_g}{kh}\right)\frac{dr}{r} = 0.703\left(\frac{2p}{\mu_g Z}\right)dp \qquad [1.2.24]$$

Integrating Equation 1.2.24 from the wellbore conditions (r_w and p_{wf}) to any point in the reservoir (r and p) gives:

$$\int_{r_w}^{r}\left(\frac{TQ_g}{kh}\right)\frac{dr}{r} = 0.703\int_{p_{wf}}^{p}\left(\frac{2p}{\mu_g Z}\right)dp \qquad [1.2.25]$$

Imposing Darcy's law conditions on Equation 1.2.25, i.e., steady-state flow, which requires that Q_g is constant at all radii, and homogeneous formation, which implies that k and h are constant, gives:

$$\left(\frac{TQ_g}{kh}\right)\ln\left(\frac{r}{r_w}\right) = 0.703\int_{p_{wf}}^{p}\left(\frac{2p}{\mu_g Z}\right)dp$$

The term:

$$\int_{p_{wf}}^{p}\left(\frac{2p}{\mu_g z}\right)dp$$
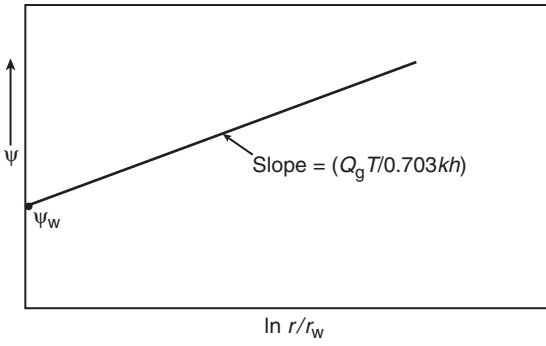
Figure 1.15 *Graph of ψ vs. ln(r/r_w).*

can be expanded to give:

$$\int_{p_{wf}}^{p} \left(\frac{2p}{\mu_g Z} \right) dp = \int_0^p \left(\frac{2p}{\mu_g Z} \right) dp - \int_0^{p_{wf}} \left(\frac{2p}{\mu_g Z} \right) dp$$

Replacing the integral in Equation 1.2.24 with the above expanded form yields:

$$\left(\frac{TQ_g}{kh} \right) \ln \left(\frac{r}{r_w} \right) = 0.703 \left[\int_0^p \left(\frac{2p}{\mu_g Z} \right) dp - \int_0^{p_{wf}} \left(\frac{2p}{\mu_g Z} \right) dp \right]$$

$$[1.2.26]$$

The integral $\int_0^p 2p/(\mu_g Z) dp$ is called the "real-gas pseudo-potential" or "real-gas pseudopressure" and it is usually represented by $m(p)$ or ψ. Thus:

$$m(p) = \psi = \int_0^p \left(\frac{2p}{\mu_g Z} \right) dp \qquad [1.2.27]$$

Equation 1.2.27 can be written in terms of the real-gas pseudopressure as:

$$\left(\frac{TQ_g}{kh} \right) \ln \left(\frac{r}{r_w} \right) = 0.703(\psi - \psi_w)$$

or:

$$\psi = \psi_w + \frac{Q_g T}{0.703kh} \ln \left(\frac{r}{r_w} \right) \qquad [1.2.28]$$

Equation 1.2.28 indicates that a graph of ψ vs. $\ln(r/r_w)$ yields a straight line with a slope of $Q_g T/0.703kh$ and an intercept value of ψ_w as shown in Figure 1.15. The exact flow rate is then given by:

$$Q_g = \frac{0.703kh(\psi - \psi_w)}{T \ln(r/r_w)} \qquad [1.2.29]$$

In the particular case when $r = r_e$, then:

$$Q_g = \frac{0.703kh(\psi_e - \psi_w)}{T \ln(r_e/r_w)} \qquad [1.2.30]$$

where:

ψ_e = real-gas pseudopressure as evaluated from 0 to p_e, psi^2/cp

ψ_w = real-gas pseudopressure as evaluated from 0 to p_{wf}, psi^2/cp

k = permeability, md

h = thickness, ft

r_e = drainage radius, ft

r_w = wellbore radius, ft

Q_g = gas flow rate, scf/day

Because the gas flow rate is commonly expressed in Mscf/day, Equation 1.2.30 can be expressed as:

$$Q_g = \frac{kh(\psi_e - \psi_w)}{1422T \ln(r_e/r_w)} \qquad [1.2.31]$$

where:

Q_g = gas flow rate, Mscf/day

Equation 1.2.31 can be expressed in terms of the average reservoir pressure p_r instead of the initial reservoir pressure p_e as:

$$Q_g = \frac{kh(\psi_r - \psi_w)}{1422T \left[\ln(r_e/r_w) - 0.5 \right]} \qquad [1.2.32]$$

To calculate the integral in Equation 1.2.31, the values of $2p/\mu_g Z$ are calculated for several values of pressure p. Then $2p/\mu_g Z$ vs. p is plotted on a Cartesian scale and the area under the curve is calculated either numerically or graphically, where the area under the curve from $p = 0$ to any pressure p represents the value of ψ corresponding to p. The following example will illustrate the procedure.

Example 1.7 The *PVT* data from a gas well in the Anaconda Gas Field is given below:

p (psi)	μ_g (cp)	Z
0	0.0127	1.000
400	0.01286	0.937
800	0.01390	0.882
1200	0.01530	0.832
1600	0.01680	0.794
2000	0.01840	0.770
2400	0.02010	0.763
2800	0.02170	0.775
3200	0.02340	0.797
3600	0.02500	0.827
4000	0.02660	0.860
4400	0.02831	0.896

The well is producing at a stabilized bottom-hole flowing pressure of 3600 psi. The wellbore radius is 0.3 ft. The following additional data is available:

$k = 65$ md, $\qquad h = 15$ ft, $\qquad T = 600°$R

$p_e = 4400$ psi, $\qquad r_e = 1000$ ft

Calculate the gas flow rate in Mscf/day.

Solution

Step 1. Calculate the term $2p/\mu_g Z$ for each pressure as shown below:

p (psi)	μ_g (cp)	Z	$2p/\mu_g Z$ (psia/cp)
0	0.0127	1.000	0
400	0.01286	0.937	66 391
800	0.01390	0.882	130 508
1200	0.01530	0.832	188 537
1600	0.01680	0.794	239 894
2000	0.01840	0.770	282 326
2400	0.02010	0.763	312 983
2800	0.02170	0.775	332 986
3200	0.02340	0.797	343 167
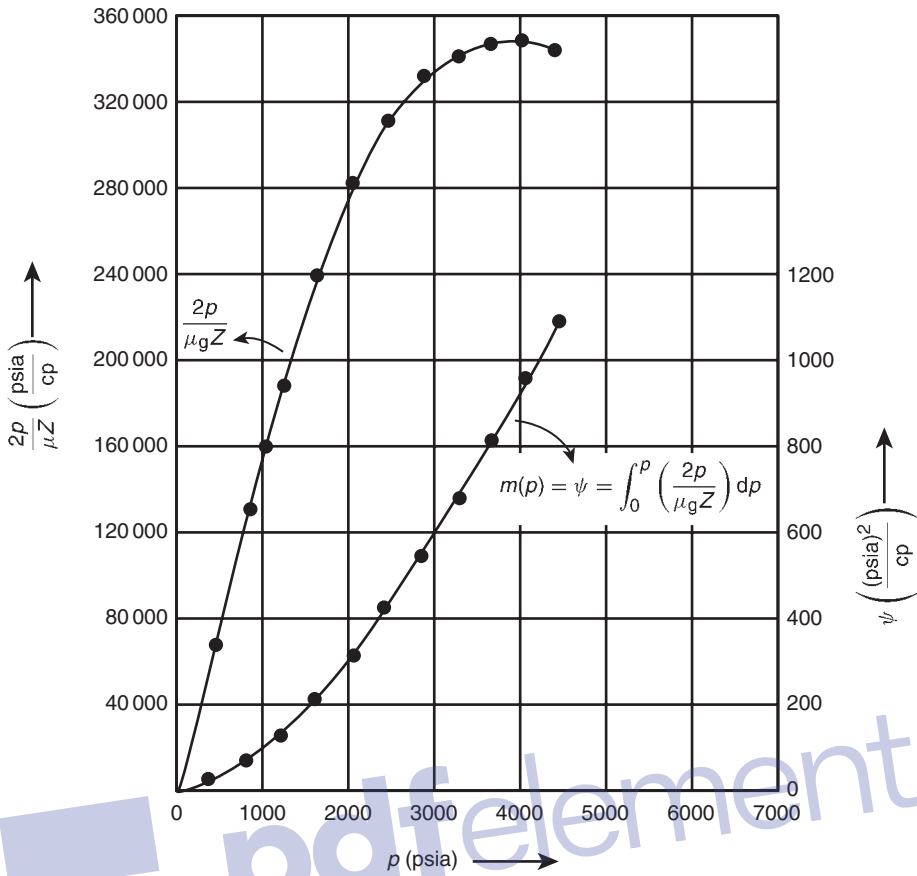
Figure 1.16   *Real-gas pseudopressure data for Example 1.7 (After Donohue and Erekin, 1982).*

p (psi)	μ_g (cp)	Z	$2p/\mu_g Z$ (psia/cp)
3600	0.02500	0.827	348 247
4000	0.02660	0.860	349 711
4400	0.02831	0.896	346 924

Step 2. Plot the term $2p/\mu_g Z$ versus pressure as shown in Figure 1.16.

Step 3. Calculate numerically the area under the curve for each value of p. These areas correspond to the real-gas pseudopressure ψ at each pressure. These ψ values are tabulated below; notice that $2p/\mu_g Z$ vs. p is also plotted in the figure.

p (psi)	ψ (psi^2/cp)
400	13.2×10^6
800	52.0×10^6
1200	113.1×10^6
1600	198.0×10^6
2000	304.0×10^6
2400	422.0×10^6
2800	542.4×10^6
3200	678.0×10^6
3600	816.0×10^6
4000	950.0×10^6
4400	1089.0×10^6

Step 4. Calculate the flow rate by applying Equation 1.2.30:

At $p_w = 3600$ psi: gives $\psi_w = 816.0 \times 10^6$ psi^2/cp

At $p_e = 4400$ psi: gives $\psi_e = 1089 \times 10^6$ psi^2/cp

$$Q_g = \frac{0.703 kh(\psi_e - \psi_w)}{T \ln(r_e/r_w)}$$

$$= \frac{(65)(15)(1089 - 816)10^6}{(1422)(600)\ln(1000/0.25)}$$

$$= 37\,614 \text{ Mscf/day}$$

In the approximation of the gas flow rate, the exact gas flow rate as expressed by the different forms of Darcy's law, i.e., Equations 1.2.25 through 1.2.32, can be approximated by moving the term $2/\mu_g Z$ outside the integral as a constant. It should be pointed out that the product of $Z\mu_g$ is considered constant only under a pressure range of less than 2000 psi. Equation 1.2.31 can be rewritten as:

$$Q_g = \left[\frac{kh}{1422T \ln(r_e/r_w)}\right] \int_{p_{wf}}^{p_e} \left(\frac{2p}{\mu_g Z}\right) dp$$

Removing the term $2/\mu_g Z$ and integrating gives:

$$Q_g = \frac{kh\left(p_e^2 - p_{wf}^2\right)}{1422T \left(\mu_g Z\right)_{avg} \ln\left(r_e/r_w\right)} \qquad [1.2.33]$$

where:

Q_g = gas flow rate, Mscf/day
k = permeability, md

The term $(\mu_g Z)_{avg}$ is evaluated at an average pressure $\bar{p}$ that is defined by the following expression:

$$\bar{p} = \sqrt{\frac{p_{wf}^2 + p_e^2}{2}}$$

The above approximation method is called the pressure-squared method and is limited to flow calculations when the reservoir pressure is less that 2000 psi. Other approximation methods are discussed in Chapter 2.

Example 1.8 Using the data given in Example 1.7, re-solve the gas flow rate by using the pressure-squared method. Compare with the exact method (i.e., real-gas pseudopressure solution).

Solution

Step 1. Calculate the arithmetic average pressure:

$$\bar{p} = \sqrt{\frac{4400^2 + 3600^2}{2}} = 4020 \text{ psi}$$

Step 2. Determine the gas viscosity and gas compressibility factor at 4020 psi:

$$\mu_g = 0.0267$$

$$Z = 0.862$$

Step 3. Apply Equation 1.2.33:

$$Q_g = \frac{kh(p_e^2 - p_{wf}^2)}{1422T(\mu_g Z)_{avg}\ln(r_e/r_w)}$$

$$= \frac{(65)(15)\left[4400^2 - 3600^2\right]}{(1422)(600)(0.0267)(0.862)\ln(1000/0.25)}$$

$$= 38\,314 \text{ Mscf/day}$$

Step 4. Results show that the pressure-squared method approximates the exact solution of 37 614 with an absolute error of 1.86%. This error is due to the limited applicability of the pressure-squared method to a pressure range of less than 2000 psi.

Horizontal multiple-phase flow

When several fluid phases are flowing simultaneously in a horizontal porous system, the concept of the effective permeability of each phase and the associated physical properties must be used in Darcy's equation. For a radial system, the generalized form of Darcy's equation can be applied to each reservoir as follows:

$$q_o = 0.001127\left(\frac{2\pi rh}{\mu_o}\right)k_o\frac{dp}{dr}$$

$$q_w = 0.001127\left(\frac{2\pi rh}{\mu_w}\right)k_w\frac{dp}{dr}$$

$$q_g = 0.001127\left(\frac{2\pi rh}{\mu_g}\right)k_g\frac{dp}{dr}$$

where:

k_o, k_w, k_g = effective permeability to oil, water, and gas, md
μ_o, μ_w, μ_g = viscosity of oil, water, and gas, cp
q_o, q_w, q_g = flow rates for oil, water, and gas, bbl/day
k = absolute permeability, md

The effective permeability can be expressed in terms of the relative and absolute permeability as:

$$k_o = k_{ro}k$$

$$k_w = k_{rw}k$$

$$k_g = k_{rg}k$$

Using the above concept in Darcy's equation and expressing the flow rate in standard conditions yields:

$$Q_o = 0.00708(rhk)\left(\frac{k_{ro}}{\mu_o B_o}\right)\frac{dp}{dr} \quad [1.2.34]$$

$$Q_w = 0.00708(rhk)\left(\frac{k_{rw}}{\mu_w B_w}\right)\frac{dp}{dr} \quad [1.2.35]$$

$$Q_g = 0.00708(rhk)\left(\frac{k_{rg}}{\mu_g B_g}\right)\frac{dp}{dr} \quad [1.2.36]$$

where:

Q_o, Q_w = oil and water flow rates, STB/day
B_o, B_w = oil and water formation volume factor, bbl/STB
Q_g = gas flow rate, scf/day
B_g = gas formation volume factor, bbl/scf
k = absolute permeability, md

The gas formation volume factor B_g is expressed by

$$B_g = 0.005035\frac{ZT}{p} \text{ bbl/scf}$$

Performing the regular integration approach on Equations, 1.2.34 through 1.2.36 yields:

Oil phase:

$$Q_o = \frac{0.00708(kh)(k_{ro})(p_e - p_{wf})}{\mu_o B_o \ln(r_e/r_w)} \quad [1.2.37]$$

Water phase:

$$Q_w = \frac{0.00708(kh)(k_{rw})(p_e - p_{wf})}{\mu_w B_w \ln(r_e/r_w)} \quad [1.2.38]$$

Gas phase:

$$Q_g = \frac{(kh)k_{rg}(\psi_e - \psi_w)}{1422T\ln(r_e/r_w)} \quad \text{in terms of the real-gas potential} \quad [1.2.39]$$

$$Q_g = \frac{(kh)k_{rg}(p_e^2 - p_{wf}^2)}{1422(\mu_g Z)_{avg}T\ln(r_e/r_w)} \quad \text{in terms of the pressure squared} \quad [1.2.40]$$

where:

Q_g = gas flow rate, Mscf/day
k = absolute permeability, md
T = temperature, °R

In numerous petroleum engineering calculations, it is convenient to express the flow rate of any phase as a ratio of other flowing phases. Two important flow ratios are the "instantaneous" water–oil ratio (WOR) and the "instantaneous" gas–oil ratio (GOR). The generalized form of Darcy's equation can be used to determine both flow ratios.

The water–oil ratio is defined as the ratio of the water flow rate to that of the oil. Both rates are expressed in stock-tank barrels per day, or:

$$\text{WOR} = \frac{Q_w}{Q_o}$$

Dividing Equation 1.2.34 by 1.2.36 gives:

$$\text{WOR} = \left(\frac{k_{rw}}{k_{ro}}\right)\left(\frac{\mu_o B_o}{\mu_w B_w}\right) \quad [1.2.41]$$
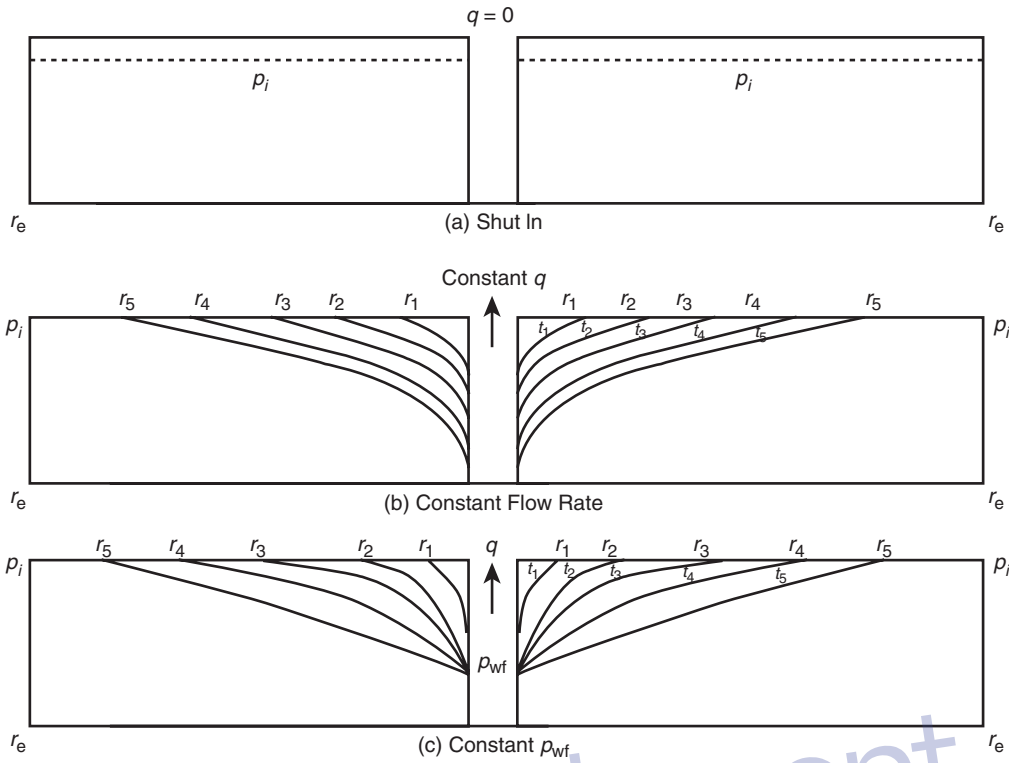
Figure 1.17 *Pressure disturbance as a function of time.*

where:

$$WOR = \text{water–oil ratio, STB/STB}$$

The instantaneous GOR, as expressed in scf/STB, is defined as the *total* gas flow rate, i.e., free gas and solution gas, divided by the oil flow rate, or:

$$GOR = \frac{Q_o R_s + Q_g}{Q_o}$$

or:

$$GOR = R_s + \frac{Q_g}{Q_o} \qquad [1.2.42]$$

where:

GOR = "instantaneous" gas–oil ratio, scf/STB
R_s = gas solubility, scf/STB
Q_g = free gas flow rate, scf/day
Q_o = oil flow rate, STB/day

Substituting Equations 1.2.34 and 1.2.36 into 1.2.42 yields:

$$GOR = R_s + \left(\frac{k_{rg}}{k_{ro}} \right) \left(\frac{\mu_o B_o}{\mu_g B_g} \right) \qquad [1.2.43]$$

where B_g is the gas formation volume factor expressed in bbl/scf.

A complete discussion of the practical applications of the WOR and GOR is given in the subsequent chapters.

1.2.3 Unsteady-state flow

Consider Figure 1.17(a) which shows a shut-in well that is centered in a homogeneous circular reservoir of radius r_e with a uniform pressure p_i throughout the reservoir. This initial reservoir condition represents the zero producing time.

If the well is allowed to flow at a constant flow rate of q, a pressure disturbance will be created at the sand face. The pressure at the wellbore, i.e., p_{wf}, will drop instantaneously as the well is opened. The pressure disturbance will move away from the wellbore at a rate that is determined by:

- permeability;
- porosity;
- fluid viscosity;
- rock and fluid compressibilities.

Figure 1.17(b) shows that at time t_1, the pressure disturbance has moved a distance r_1 into the reservoir. Notice that the pressure disturbance radius is continuously increasing with time. This radius is commonly called the radius of investigation and referred to as r_{inv}. It is also important to point out that as long as the radius of investigation has not reached the reservoir boundary, i.e., r_e, the reservoir will be acting as if it is infinite in size. During this time we say that the reservoir is *infinite acting* because the outer drainage radius r_e, can be mathematically infinite, i.e., $r_e = \infty$. A similar discussion to the above can be used to describe a well that is producing at a constant bottom-hole flowing pressure. Figure 1.17(c) schematically illustrates the propagation of the radius of investigation with respect to time. At time t_4, the pressure disturbance reaches the boundary, i.e., $r_{inv} = r_e$. This causes the pressure behavior to change.

Based on the above discussion, the transient (unsteady-state) flow is defined as that time period during which the boundary has no effect on the pressure behavior in the reservoir and the reservoir will behave as if it is infinite in size. Figure 1.17(b) shows that the transient flow period occurs during the time interval $0 < t < t_t$ for the constant flow rate scenario and during the time period $0 < t < t_4$ for the constant p_{wf} scenario as depicted by Figure 1.17(c).
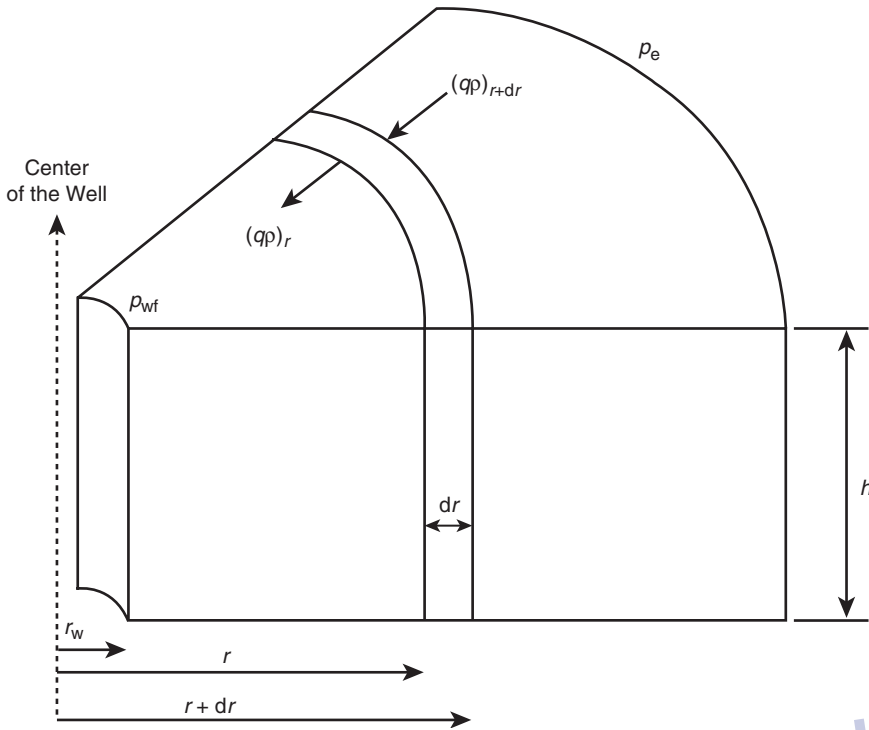
Figure 1.18 *Illustration of radial flow.*

1.2.4 Basic transient flow equation

Under the steady-state flowing condition, the same quantity of fluid enters the flow system as leaves it. In the unsteady-state flow condition, the flow rate into an element of volume of a porous medium may not be the same as the flow rate out of that element and, accordingly, the fluid content of the porous medium changes with time. The other controlling variables in unsteady-state flow *additional* to those already used for steady-state flow, therefore, become:

- time t;
- porosity ϕ;
- total compressibility c_t.

The mathematical formulation of the transient flow equation is based on combining three independent equations and a specifying set of boundary and initial conditions that constitute the unsteady-state equation. These equations and boundary conditions are briefly described below.

Continuity equation: The continuity equation is essentially a material balance equation that accounts for every pound mass of fluid produced, injected, or remaining in the reservoir.

Transport equation: The continuity equation is combined with the equation for fluid motion (transport equation) to describe the fluid flow rate "in" and "out" of the reservoir. Basically, the transport equation is Darcy's equation in its generalized differential form.

Compressibility equation: The fluid compressibility equation (expressed in terms of density or volume) is used in formulating the unsteady-state equation with the objective of describing the changes in the fluid volume as a function of pressure.

Initial and boundary conditions: There are two boundary conditions and one initial condition is required to complete the formulation and the solution of the transient flow equation. The two boundary conditions are:

(1) the formation produces at a constant rate into the wellbore;
(2) there is no flow across the outer boundary and the reservoir behaves as if it were infinite in size, i.e., $r_e = \infty$.

The initial condition simply states that the reservoir is at a uniform pressure when production begins, i.e., time $= 0$.

Consider the flow element shown in Figure 1.18. The element has a width of dr and is located at a distance of r from the center of the well. The porous element has a differential volume of dV. According to the concept of the material balance equation, the rate of mass flow into an element minus the rate of mass flow out of the element during a differential time Δt must be equal to the mass rate of accumulation during that time interval, or:

$$\begin{bmatrix} \text{mass entering} \\ \text{volume element} \\ \text{during interval } \Delta t \end{bmatrix} - \begin{bmatrix} \text{mass leaving} \\ \text{volume element} \\ \text{during interval } \Delta t \end{bmatrix}$$

$$= \begin{bmatrix} \text{rate of mass} \\ \text{accumulation} \\ \text{during interval } \Delta t \end{bmatrix} \qquad [1.2.44]$$

The individual terms of Equation 1.2.44 are described below:
Mass, entering the volume element during time interval Δt
Here:

$$(\text{Mass})_{\text{in}} = \Delta t [A v \rho]_{r+dr} \qquad [1.2.45]$$

where:

$v = $ velocity of flowing fluid, ft/day
$\rho = $ fluid density at $(r + dr)$, lb/ft^3
$A = $ area at $(r + dr)$
$\Delta t = $ time interval, days

The area of the element at the entering side is:

$$A_{r+dr} = 2\pi(r + dr)h \qquad [1.2.46]$$

Combining Equations 1.2.46 with 1.2.35 gives:

$$[\text{Mass}]_{\text{in}} = 2\pi \Delta t(r + dr)h(\nu\rho)_{r+dr} \qquad [1.2.47]$$

Mass leaving the volume element Adopting the same approach as that of the leaving mass gives:

$$[\text{Mass}]_{\text{out}} = 2\pi \Delta t r h(\nu\rho)_r \qquad [1.2.48]$$

Total accumulation of mass The volume of some element with a radius of r is given by:

$$V = \pi r^2 h$$

Differentiating the above equation with respect to r gives:

$$\frac{dV}{dr} = 2\pi r h$$

or:

$$dV = (2\pi r h)\,dr \qquad [1.2.49]$$

Total mass accumulation during $\Delta t = dV[(\phi\rho)_{t+\Delta t} - (\phi\rho)_t]$. Substituting for dV yields:

$$\text{Total mass accumulation} = (2\pi r h)dr[(\phi\rho)_{t+\Delta t} - (\phi\rho)_t] \qquad [1.2.50]$$

Replacing the terms of Equation 1.2.44 with those of the calculated relationships gives:

$$2\pi h(r + dr)\Delta t(\phi\rho)_{r+dr} - 2\pi h r \Delta t(\phi\rho)_r$$
$$= (2\pi r h)dr[(\phi\rho)_{t+\Delta t} - (\phi\rho)_t]$$

Dividing the above equation by $(2\pi r h)dr$ and simplifying gives:

$$\frac{1}{(r)dr}\left[(r + dr)(\nu\rho)_{r+dr} - r(\nu\rho)_r\right] = \frac{1}{\Delta t}\left[(\phi\rho)_{t+\Delta t} - (\phi\rho)_t\right]$$

or:

$$\frac{1}{r}\frac{\partial}{\partial r}[r(\nu\rho)] = \frac{\partial}{\partial t}(\phi\rho) \qquad [1.2.51]$$

where:

ϕ = porosity
ρ = density, lb/ft^3
V = fluid velocity, ft/day

Equation 1.2.51 is called the continuity equation and it provides the principle of conservation of mass in radial coordinates.

The transport equation must be introduced into the continuity equation to relate the fluid velocity to the pressure gradient within the control volume dV. Darcy's law is essentially the basic motion equation, which states that the velocity is proportional to the pressure gradient $\partial p/\partial r$. From Equation 1.2.13:

$$\nu = (5.615)(0.001127)\frac{k}{\mu}\frac{\partial p}{\partial r}$$

$$= (0.006328)\frac{k}{\mu}\frac{\partial p}{\partial r} \qquad [1.2.52]$$

where:

k = permeability, md
v = velocity, ft/day

Combining Equation 1.2.52 with 1.2.51 results in:

$$\frac{0.006328}{r}\frac{\partial}{\partial r}\left(\frac{k}{\mu}(\rho r)\frac{\partial p}{\partial r}\right) = \frac{\partial}{\partial t}(\phi\rho) \qquad [1.2.53]$$

Expanding the right-hand side by taking the indicated derivatives eliminates the porosity from the partial derivative term

on the right-hand side:

$$\frac{\partial}{\partial t}(\phi\rho) = \phi\frac{\partial\rho}{\partial t} + \rho\frac{\partial\phi}{\partial t} \qquad [1.2.54]$$

The porosity is related to the formation compressibility by the following:

$$c_{\text{f}} = \frac{1}{\phi}\frac{\partial\phi}{\partial p} \qquad [1.2.55]$$

Applying the chain rule of differentiation to $\partial\phi/\partial t$:

$$\frac{\partial\phi}{\partial t} = \frac{\partial\phi}{\partial p}\frac{\partial p}{\partial t}$$

Substituting Equation 1.2.55 into this equation:

$$\frac{\partial\phi}{\partial t} = \phi c_{\text{f}}\frac{\partial p}{\partial t}$$

Finally, substituting the above relation into Equation 1.2.54 and the result into Equation 1.2.53 gives:

$$\frac{0.006328}{r}\frac{\partial}{\partial r}\left(\frac{k}{\mu}(\rho r)\frac{\partial p}{\partial r}\right) = \rho\phi c_{\text{f}}\frac{\partial p}{\partial t} + \phi\frac{\partial\rho}{\partial t} \qquad [1.2.56]$$

Equation 1.2.56 is the general partial differential equation used to describe the flow of any fluid flowing in a radial direction in porous media. In addition to the initial assumptions, Darcy's equation has been added, which implies that the flow is laminar. Otherwise, the equation is not restricted to any type of fluid and is equally valid for gases or liquids. However, compressible and slightly compressible fluids must be treated separately in order to develop practical equations that can be used to describe the flow behavior of these two fluids. The treatments of the following systems are discussed below:

- radial flow of slightly compressible fluids;
- radial flow of compressible fluids.

1.2.5 Radial flow of slightly compressibility fluids

To simplify Equation 1.2.56, assume that the permeability and viscosity are constant over pressure, time, and distance ranges. This leads to:

$$\left[\frac{0.006328k}{\mu r}\right]\frac{\partial}{\partial r}\left(r\rho\frac{\partial p}{\partial r}\right) = \rho\phi c_{\text{f}}\frac{\partial p}{\partial t} + \phi\frac{\partial\rho}{\partial t} \qquad [1.2.57]$$

Expanding the above equation gives:

$$0.006328\left(\frac{k}{\mu}\right)\left[\frac{\rho}{r}\frac{\partial p}{\partial r} + \rho\frac{\partial^2 p}{\partial r^2} + \frac{\partial p}{\partial r}\frac{\partial\rho}{\partial r}\right]$$
$$= \rho\phi c_{\text{f}}\left(\frac{\partial p}{\partial t}\right) + \phi\left(\frac{\partial\rho}{\partial t}\right)$$

Using the chain rule in the above relationship yields:

$$0.006328\left(\frac{k}{\mu}\right)\left[\frac{\rho}{r}\frac{\partial p}{\partial r} + \rho\frac{\partial^2 p}{\partial r^2} + \left(\frac{\partial p}{\partial r}\right)^2\frac{\partial\rho}{\partial p}\right]$$
$$= \rho\phi c_{\text{f}}\left(\frac{\partial p}{\partial t}\right) + \phi\left(\frac{\partial p}{\partial t}\right)\left(\frac{\partial\rho}{\partial p}\right)$$

Dividing the above expression by the fluid density ρ gives:

$$0.006328\left(\frac{k}{u}\right)\left[\frac{1}{r}\frac{\partial p}{\partial r} + \frac{\partial^2 p}{\partial r^2} + \left(\frac{\partial p}{\partial r}\right)^2\left(\frac{1}{\rho}\frac{\partial\rho}{\partial p}\right)\right]$$
$$= \phi c_{\text{f}}\left(\frac{\partial p}{\partial t}\right) + \phi\frac{\partial p}{\partial t}\left(\frac{1}{\rho}\frac{\partial\rho}{\partial p}\right)$$

Recalling that the compressibility of any fluid is related to its density by:

$$c = \frac{1}{\rho}\frac{\partial\rho}{\partial p}$$

combining the above two equations gives:

$$0.006328 \left(\frac{k}{\mu}\right)\left[\frac{\partial^2 p}{\partial r^2} + \frac{1}{r}\frac{\partial p}{\partial r} + c\left(\frac{\partial p}{\partial r}\right)^2\right]$$

$$= \phi c_f \left(\frac{\partial p}{\partial t}\right) + \phi c\left(\frac{\partial p}{\partial t}\right)$$

The term $c(\partial p/\partial r)^2$ is considered very small and may be ignored, which leads to:

$$0.006328 \left(\frac{k}{\mu}\right)\left[\frac{\partial^2 p}{\partial r^2} + \frac{1}{r}\frac{\partial p}{\partial r}\right] = \phi\,(c_f + c)\,\frac{\partial p}{\partial t} \qquad [1.2.58]$$

Defining total compressibility, c_t, as:

$$c_t = c + c_f \qquad [1.2.59]$$

and combining Equation 1.2.57 with 1.2.58 and rearranging gives:

$$\frac{\partial^2 p}{\partial r^2} + \frac{1}{r}\frac{\partial p}{\partial r} = \frac{\phi\mu c_t}{0.006328 k}\frac{\partial p}{\partial t} \qquad [1.2.60]$$

where the time t is expressed in days.

Equation 1.2.60 is called the diffusivity equation and is considered one of the most important and widely used mathematical expressions in petroleum engineering. The equation is particularly used in the analysis of well testing data where the time t is commonly reordered in hours. The equation can be rewritten as:

$$\frac{\partial^2 p}{\partial r^2} + \frac{1}{r}\frac{\partial p}{\partial r} = \frac{\phi\mu c_t}{0.0002637 k}\frac{\partial p}{\partial t} \qquad [1.2.61]$$

where:

  $k=$ permeability, md
  $r=$ radial position, ft
  $p=$ pressure, psia
  $c_t=$ total compressibility, psi^{-1}
  $t=$ time, hours
  $\phi=$ porosity, fraction
  $\mu=$ viscosity, cp

When the reservoir contains more than one fluid, total compressibility should be computed as

$$c_t = c_o S_o + c_w S_w + c_g S_g + c_f \qquad [1.2.62]$$

where c_o, c_w, and c_g refer to the compressibility of oil, water, and gas, respectively, and S_o, S_w, and S_g refer to the fractional saturation of these fluids. Note that the introduction of c_t into Equation 1.2.60 does not make this equation applicable to multiphase flow; the use of c_t, as defined by Equation 1.2.61, simply accounts for the compressibility of any immobile fluids which may be in the reservoir with the fluid that is flowing.

The term $0.000264k/\phi\mu c_t$ is called the diffusivity constant and is denoted by the symbol η, or:

$$\eta = \frac{0.0002637 k}{\phi\mu c_t} \qquad [1.2.63]$$

The diffusivity equation can then be written in a more convenient form as:

$$\frac{\partial^2 p}{\partial r^2} + \frac{1}{r}\frac{\partial p}{\partial r} = \frac{1}{\eta}\frac{\partial p}{\partial t} \qquad [1.2.64]$$

The diffusivity equation as represented by relationship 1.2.64 is essentially designed to determine the pressure as a function of time t and position r.

Notice that for a steady-state flow condition, the pressure at any point in the reservoir is constant and does not change with time, i.e., $\partial p/\partial t = 0$, so Equation 1.2.64 reduces to:

$$\frac{\partial^2 p}{\partial r^2} + \frac{1}{r}\frac{\partial p}{\partial r} = 0 \qquad [1.2.65]$$

Equation 1.2.65 is called Laplace's equation for steady-state flow.

Example 1.9   Show that the radial form of Darcy's equation is the solution to Equation 1.2.65.

Solution

Step 1.   Start with Darcy's law as expressed by Equation 1.2.17:

$$p = p_{wf} + \left[\frac{Q_o B_o u_o}{0.00708 kh}\right]\ln\left(\frac{r}{r_w}\right)$$

Step 2.   For a steady-state incompressible flow, the term with the square brackets is constant and labeled as C, or:

$$p = p_{wf} + [C]\ln\left(\frac{r}{r_w}\right)$$

Step 3.   Evaluate the above expression for the first and second derivative, to give:

$$\frac{\partial p}{\partial r} = [C]\left(\frac{1}{r}\right)$$

$$\frac{\partial^2 p}{\partial r^2} = [C]\left(\frac{-1}{r^2}\right)$$

Step 4.   Substitute the above two derivatives in Equation 1.2.65:

$$\frac{-1}{r^2}\,[C] + \left(\frac{1}{r}\right)[C]\left(\frac{1}{r}\right) = 0$$

Step 5.   Results of step 4 indicate that Darcy's equation satisfies Equation 1.2.65 and is indeed the solution to Laplace's equation.

To obtain a solution to the diffusivity equation (Equation 1.2.64), it is necessary to specify an initial condition and impose two boundary conditions. The initial condition simply states that the reservoir is at a uniform pressure p_i when production begins. The two boundary conditions require that the well is producing at a constant production rate and the reservoir behaves as if it were infinite in size, i.e., $r_e = \infty$.

Based on the boundary conditions imposed on Equation 1.2.64, there are two generalized solutions to the diffusivity equation. These are:

(1) the constant-terminal-pressure solution
(2) the constant-terminal-rate solution.

The constant-terminal-pressure solution is designed to provide the cumulative flow at any particular time for a reservoir in which the pressure at one boundary of the reservoir is held constant. This technique is frequently used in water influx calculations in gas and oil reservoirs.

The constant-terminal-rate solution of the radial diffusivity equation solves for the pressure change throughout the radial system providing that the flow rate is held constant at one terminal end of the radial system, i.e., at the producing well. There are two commonly used forms of the constant-terminal-rate solution:

(1) the Ei function solution;
(2) the dimensionless pressure drop p_D solution.

Constant-terminal-pressure solution

In the constant-rate solution to the radial diffusivity equation, the flow rate is considered to be constant at certain radius (usually wellbore radius) and the pressure profile around that radius is determined as a function of time and position. In the constant-terminal-pressure solution, the pressure is known to be constant at some particular radius and the solution is designed to provide the cumulative fluid movement across the specified radius (boundary).

The constant-pressure solution is widely used in water influx calculations. A detailed description of the solution

and its practical reservoir engineering applications is appropriately discussed in the water influx chapter of the book (Chapter 5).

Constant-terminal-rate solution

The constant-terminal-rate solution is an integral part of most transient test analysis techniques, e.g., drawdown and pressure buildup analyses. Most of these tests involve producing the well at a constant flow rate and recording the flowing pressure as a function of time, i.e., $p(r_w, t)$. There are two commonly used forms of the constant-terminal-rate solution:

(1) the Ei function solution;
(2) the dimensionless pressure drop p_D solution.

These two popular forms of solution to the diffusivity equation are discussed below.

The Ei function solution

For an infinite-acting reservoir, Matthews and Russell (1967) proposed the following solution to the diffusivity equation, i.e., Equation 1.2.55:

$$p(r, t) = p_i + \left[\frac{70.6 Q_o \mu B_o}{kh} \right] \text{Ei} \left[\frac{-948 \phi \mu c_t r^2}{kt} \right] \qquad [1.2.66]$$

where:

$p(r,t)$ = pressure at radius r from the well after t hours
t = time, hours
k = permeability, md
Q_o = flow rate, STB/day

The mathematical function, Ei, is called the exponential integral and is defined by:

$$\text{Ei}(-x) = -\int_x^\infty \frac{e^{-u} du}{u}$$
$$= \left[\ln x - \frac{x}{1!} + \frac{x^2}{2\,(2!)} - \frac{x^3}{3\,(3!)} + \cdots \right] \qquad [1.2.67]$$

Craft et al. (1991) presented the values of the Ei function in tabulated and graphical forms as shown in Table 1.1 and Figure 1.19, respectively.

The Ei solution, as expressed by Equation 1.2.66, is commonly referred to as the line source solution. The exponential integral "Ei" can be approximated by the following equation when its argument x is less than 0.01:

$$\text{Ei}(-x) = \ln(1.781x) \qquad [1.2.68]$$

where the argument x in this case is given by:

$$x = \frac{948 \phi \mu c_t r^2}{kt}$$

Equation 1.2.68 approximates the Ei function with less than 0.25% error. Another expression that can be used to approximate the Ei function for the range of $0.01 < x < 3.0$ is given by:

$$\text{Ei}(-x) = a_1 + a_2 \ln(x) + a_3 [\ln(x)]^2 + a_4 [\ln(x)]^3 + a_5 x$$
$$+ a_6 x^2 + a_7 x^3 + a_8/x \qquad [1.2.69]$$

with the coefficients a_1 through a_8 having the following values:

$a_1 = -0.33153973 \qquad a_2 = -0.81512322$

$a_3 = 5.22123384 \times 10^{-2} \qquad a_4 = 5.9849819 \times 10^{-3}$

Table 1.1 Values of $-\text{Ei}(-x)$ as a function of x (After Craft et al. 1991)

x	$-\text{Ei}(-x)$	x	$-\text{Ei}(-x)$	x	$-\text{Ei}(-x)$
0.1	1.82292	3.5	0.00697	6.9	0.00013
0.2	1.22265	3.6	0.00616	7.0	0.00012
0.3	0.90568	3.7	0.00545	7.1	0.00010
0.4	0.70238	3.8	0.00482	7.2	0.00009
0.5	0.55977	3.9	0.00427	7.3	0.00008
0.6	0.45438	4.0	0.00378	7.4	0.00007
0.7	0.37377	4.1	0.00335	7.5	0.00007
0.8	0.31060	4.2	0.00297	7.6	0.00006
0.9	0.26018	4.3	0.00263	7.7	0.00005
1.0	0.21938	4.4	0.00234	7.8	0.00005
1.1	0.18599	4.5	0.00207	7.9	0.00004
1.2	0.15841	4.6	0.00184	8.0	0.00004
1.3	0.13545	4.7	0.00164	8.1	0.00003
1.4	0.11622	4.8	0.00145	8.2	0.00003
1.5	0.10002	4.9	0.00129	8.3	0.00003
1.6	0.08631	5.0	0.00115	8.4	0.00002
1.7	0.07465	5.1	0.00102	8.5	0.00002
1.8	0.06471	5.2	0.00091	8.6	0.00002
1.9	0.05620	5.3	0.00081	8.7	0.00002
2.0	0.04890	5.4	0.00072	8.8	0.00002
2.1	0.04261	5.5	0.00064	8.9	0.00001
2.2	0.03719	5.6	0.00057	9.0	0.00001
2.3	0.03250	5.7	0.00051	9.1	0.00001
2.4	0.02844	5.8	0.00045	9.2	0.00001
2.5	0.02491	5.9	0.00040	9.3	0.00001
2.6	0.02185	6.0	0.00036	9.4	0.00001
2.7	0.01918	6.1	0.00032	9.5	0.00001
2.8	0.01686	6.2	0.00029	9.6	0.00001
2.9	0.01482	6.3	0.00026	9.7	0.00001
3.0	0.01305	6.4	0.00023	9.8	0.00001
3.1	0.01149	6.5	0.00020	9.9	0.00000
3.2	0.01013	6.6	0.00018	10.0	0.00000
3.3	0.00894	6.7	0.00016		
3.4	0.00789	6.8	0.00014		

$a_5 = 0.662318450 \qquad a_6 = -0.12333524$

$a_7 = 1.0832566 \times 10^{-2} \qquad a_8 = 8.6709776 \times 10^{-4}$

The above relationship approximated the Ei values with an average error of 0.5%.

It should be pointed out that for $x > 10.9$, $\text{Ei}(-x)$ can be considered zero for reservoir engineering calculations.

Example 1.10 An oil well is producing at a constant flow rate of 300 STB/day under unsteady-state flow conditions. The reservoir has the following rock and fluid properties:

$B_o = 1.25$ bbl/STB, $\quad \mu_o = 1.5$ cp, $\quad c_t = 12 \times 10^{-6}$ psi^{-1}

$k_o = 60$ md, $\qquad\qquad h = 15$ ft, $\qquad p_i = 4000$ psi

$\phi = 15\%$, $\qquad\qquad r_w = 0.25$ ft

(1) Calculate the pressure at radii of 0.25, 5, 10, 50, 100, 500, 1000, 1500, 2000, and 2500 ft, for 1 hour. Plot the results as:

   (a) pressure versus the logarithm of radius;
   (b) pressure versus radius.
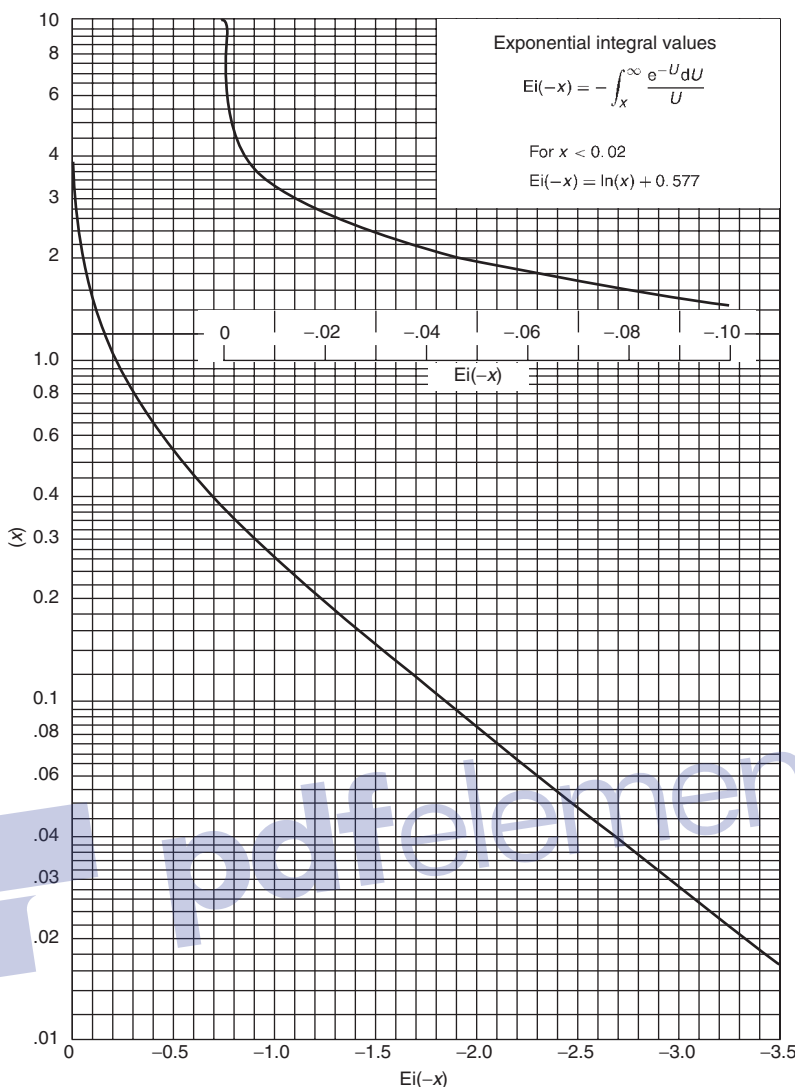
Figure 1.19   *Ei function (After Craft et al., 1991).*

(2) Repeat part 1 for $t = 12$ hours and 24 hours. Plot the results as pressure versus logarithm of radius.

Solution

Step 1. From Equation 1.2.66:

$$p(r,t) = 4000 + \left[\frac{70.6\,(300)\,(1.5)\,(1.25)}{(60)\,(15)} \right]$$

$$\times \text{Ei}\left[\frac{-948\,(1.5)\,(1.5)\,(12 \times 10^{-6})r^2}{(60)\,(t)} \right]$$

$$= 4000 + 44.125\,\text{Ei}\left[(-42.6 \times 10^{-6})\,\frac{r^2}{t} \right]$$

Step 2. Perform the required calculations after 1 hour in the following tabulated form:

r (ft)	$x = (-42.6 \times 10^{-6})r^2/1$	Ei $(-x)$	$p(r,12) = 4000 + 44.125\,\text{Ei}(-x)$
0.25	-2.6625×10^{-6}	-12.26^a	3459
5	-0.001065	-6.27^a	3723
10	-0.00426	-4.88^a	3785
50	-0.1065	-1.76^b	3922
100	-0.4260	-0.75^b	3967
500	-10.65	0	4000
1000	-42.60	0	4000
1500	-95.85	0	4000
2000	-175.40	0	4000
2500	-266.25	0	4000

[a] As calculated from Equation 1.2.17.
[b] From Figure 1.19.
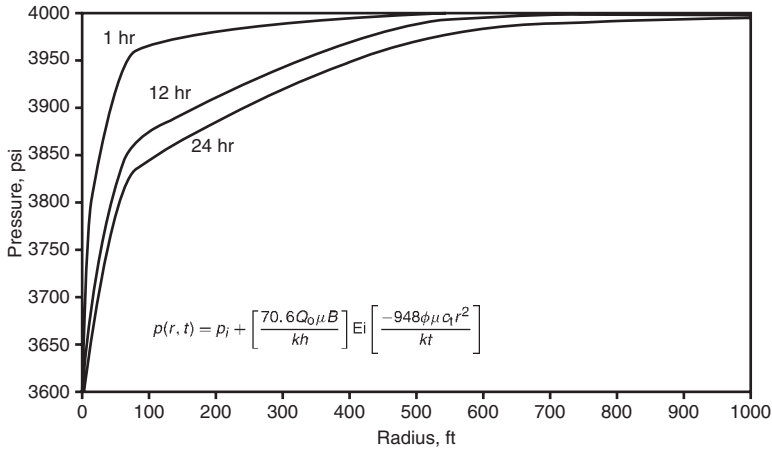
Figure 1.20 *Pressure profiles as a function of time.*

$$p(r, t) = p_i + \left[\frac{70.6 Q_0 \mu B}{kh} \right] \text{Ei} \left[\frac{-948 \phi \mu c_t r^2}{kt} \right]$$
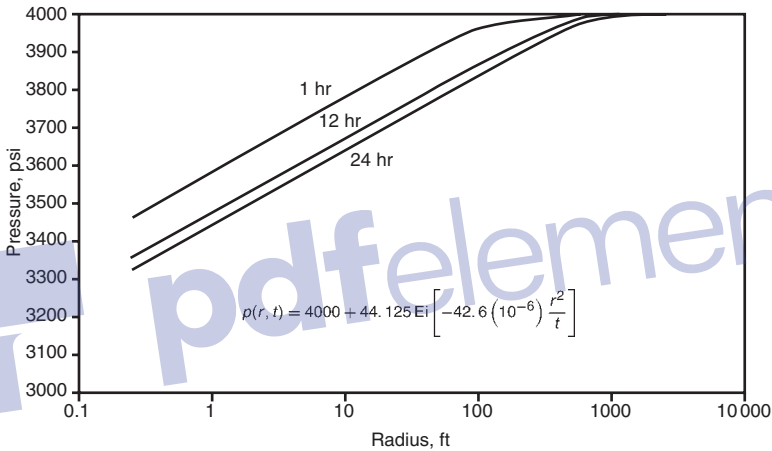
Figure 1.21 *Pressure profiles as a function of time on a semi-log scale.*

$$p(r, t) = 4000 + 44.125 \, \text{Ei} \left[-42.6 \left(10^{-6} \right) \frac{r^2}{t} \right]$$

Step 3. Show the results of the calculation graphically as illustrated in Figures 1.20 and 1.21.

Step 4. Repeat the calculation for $t = 12$ and 24 hours, as in the tables below:

r (ft)	$x = (42.6 \times 10^{-6}) r^2/12$	$\text{Ei}(-x)$	$p(r, 12) = 4000 + 44.125 \, \text{Ei}(-x)$
0.25	0.222×10^{-6}	-14.74^a	3350
5	88.75×10^{-6}	-8.75^a	3614
10	355.0×10^{-6}	-7.37^a	3675
50	0.0089	-4.14^a	3817
100	0.0355	-2.81^b	3876
500	0.888	-0.269	3988
1000	3.55	-0.0069	4000
1500	7.99	-3.77×10^{-5}	4000
2000	14.62	0	4000
2500	208.3	0	4000

[a] As calculated from Equation 1.2.17.
[b] From Figure 1.19.

r (ft)	$x = (-42.6 \times 10^{-6}) r^2/24$	$\text{Ei}(-x)$	$p(r, 24) = 4000 + 44.125 \, \text{Ei}(-x)$
0.25	-0.111×10^{-6}	-15.44^a	3319
5	-44.38×10^{-6}	-9.45^a	3583
10	-177.5×10^{-6}	-8.06^a	3644
50	-0.0045	-4.83^a	3787
100	-0.0178	-8.458^b	3847
500	-0.444	-0.640	3972
1000	-1.775	-0.067	3997
1500	-3.995	-0.0427	3998
2000	-7.310	8.24×10^{-6}	4000
2500	-104.15	0	4000

[a] As calculated from Equation 1.2.17.
[b] From Figure 1.19.

Step 5. Results of step 4 are shown graphically in Figure 1.21.

Figure 1.21 indicates that as the pressure disturbance moves radially away from the wellbore, the reservoir

boundary and its configuration has no effect on the pressure behavior, which leads to the definition of transient flow as: "Transient flow is that time period during which the boundary has no effect on the pressure behavior and the well acts as if it exists in an infinite size reservoir."

Example 1.10 shows that most of the pressure loss occurs close to the wellbore; accordingly, near-wellbore conditions will exert the greatest influence on flow behavior. Figure 1.21 shows that the pressure profile and the drainage radius are continuously changing with time. It is also important to notice that the production rate of the well has no effect on the velocity or the distance of the pressure disturbance since the Ei function is independent of the flow rate.

When the Ei parameter $x < 0.01$, the log approximation of the Ei function as expressed by Equation 1.2.68 can be used in 1.2.66 to give:

$$p(r,t) = p_i - \frac{162.6 Q_o B_o \mu_o}{kh}\left[\log\left(\frac{kt}{\phi \mu c_t r^2}\right) - 3.23\right]$$
[1.2.70]

For most of the transient flow calculations, engineers are primarily concerned with the behavior of the bottom-hole flowing pressure at the wellbore, i.e., $r = r_w$. Equation 1.2.70 can be applied at $r = r_w$ to yield:

$$p_{wf} = p_i - \frac{162.6 Q_o B_o \mu_o}{kh}\left[\log\left(\frac{kt}{\phi \mu c_t r_w^2}\right) - 3.23\right] \quad [1.2.71]$$

where:

k = permeability, md
t = time, hours
c_t = total compressibility, psi^{-1}

It should be noted that Equations 1.2.70 and 1.2.71 cannot be used until the flow time t exceeds the limit imposed by the following constraint:

$$t > 9.48 \times 10^4 \frac{\phi \mu c_t r^2}{k}$$
[1.2.72]

where:

k = permeability, md
t = time, hours

Notice that when a well is producing under unsteady-state (transient) flowing conditions at a constant flow rate, Equation 1.2.71 can be expressed as the equation of a straight line by manipulating the equation to give:

$$p_{wf} = p_i - \frac{162.6 Q_o B_o \mu_o}{kh}\left[\log(t) + \log\left(\frac{k}{\phi \mu c_t r_w^2}\right) - 3.23\right]$$

or:

$$p_{wf} = a + m\log(t)$$

The above equation indicates that a plot of p_{wf} vs. t on a semilogarithmic scale would produce a straight line with an intercept of a and a slope of m as given by:

$$a = p_i - \frac{162.6 Q_o B_o \mu_o}{kh}\left[\log\left(\frac{k}{\phi \mu c_t r_w^2}\right) - 3.23\right]$$

$$m = \frac{162.6 Q_o B_o \mu_o}{kh}$$

Example 1.11 Using the data in Example 1.10, estimate the bottom-hole flowing pressure after 10 hours of production.

Solution

Step 1. Equation 1.2.71 can only be used to calculate p_{wf} at any time that exceeds the time limit imposed by

Equation 1.2.72, or:

$$t > 9.48 \times 10^4 \frac{\phi \mu c_t r^2}{k}$$

$$t = 9.48\left(10^4\right)\frac{(0.15)(1.5)\left(12 \times 10^{-6}\right)(0.25)^2}{60}$$

$$= 0.000267 \text{ hours}$$

$$= 0.153 \text{ seconds}$$

For all practical purposes, Equation 1.2.71 can be used anytime during the transient flow period to estimate the bottom-hole pressure.

Step 2. Since the specified time of 10 hours is greater than 0.000267 hours, the value of p_{wf} can be estimated by applying Equation 1.2.71:

$$p_{wf} = p_i - \frac{162.6 Q_o B_o \mu_o}{kh}\left[\log\left(\frac{kt}{\phi \mu c_t r_w^2}\right) - 3.23\right]$$

$$= 4000 - \frac{162.6(300)(1.25)(1.5)}{(60)(15)}$$

$$\times\left[\log\left(\frac{(60)(10)}{(0.15)(1.5)\left(12 \times 10^{-6}\right)(0.25)^2}\right) - 3.23\right]$$

$$= 3358 \text{ psi}$$

The second form of solution to the diffusivity equation is called the dimensionless pressure drop solution and is discussed below.

The dimensionless pressure drop p_D solution

To introduce the concept of the dimensionless pressure drop solution, consider for example Darcy's equation in a radial form as given previously by Equation 1.2.15

$$Q_o = \frac{0.00708 kh\,(p_e - p_{wf})}{\mu_o B_o \ln(r_e/r_w)} = \frac{kh(p_e - p_{wf})}{141.2\mu_o B_o \ln(r_e/r_w)}$$

Rearranging the above equation gives:

$$\frac{p_e - p_{wf}}{\left(\frac{141.2 Q_o B_o \mu_o}{kh}\right)} = \ln\left(\frac{r_e}{r_w}\right)$$
[1.2.73]

It is obvious that the right-hand side of the above equation has no units (i.e., it is dimensionless) and, accordingly, the left-hand side must be dimensionless. Since the left-hand side is dimensionless, and $p_e - p_{wf}$ has the units of psi, it follows that the term $Q_o B_o \mu_o / 0.00708 kh$ has units of pressure. In fact, any pressure difference divided by $Q_o B_o \mu_o / 0.00708 kh$ is a dimensionless pressure. Therefore, Equation 1.2.73 can be written in a dimensionless form as:

$$p_D = \ln(r_{eD})$$

where:

$$p_D = \frac{p_e - p_{wf}}{\left(\frac{141.2 Q_o B_o \mu_o}{kh}\right)}$$

$$r_{eD} = \frac{r_e}{r_w}$$

The dimensionless pressure drop concept can be extended to describe the changes in the pressure during the unsteady-state flow condition where the pressure is a function of time and radius:

$$p = p(r,t)$$

Therefore, the dimensionless pressure during the unsteady-state flowing condition is defined by:

$$p_D = \frac{p_i - p(r,t)}{\left(\frac{141.2 Q_o B_o \mu_o}{kh}\right)}$$ [1.2.74]

Since the pressure $p(r,t)$, as expressed in a dimensionless form, varies with time and location, it is traditionally presented as a function of dimensionless time t_D and radius r_D as defined below:

$$t_D = \frac{0.0002637 kt}{\phi \mu c_t r_w^2}$$ [1.2.75a]

Another common form of the dimensionless time t_D is based on the total drainage area A as given by:

$$t_{DA} = \frac{0.0002637 kt}{\phi \mu c_t A} = t_A \left(\frac{r_w^2}{A}\right)$$ [1.2.75b]

$$r_D = \frac{r}{r_w}$$ [1.2.76]

and:

$$r_{eD} = \frac{r_e}{r_w}$$ [1.2.77]

where:

p_D = dimensionless pressure drop
r_{eD} = dimensionless external radius
t_D = dimensionless time based on wellbore radius r_w
t_{DA} = dimensionless time based on well drainage area A
A = well drainage area, i.e., πr_e^2, ft^2
r_D = dimensionless radius
t = time, hours
$p(r,t)$ = pressure at radius r and time t
k = permeability, md
μ = viscosity, cp

The above dimensionless groups (i.e., p_D, t_D, and r_D) can be introduced into the diffusivity equation (Equation 1.2.64) to transform the equation into the following dimensionless form:

$$\frac{\partial^2 p_D}{\partial r_D^2} + \frac{1}{r_D}\frac{\partial p_D}{\partial r_D} = \frac{\partial p_D}{\partial t_D}$$ [1.2.78]

Van Everdingen and Hurst (1949) proposed an analytical solution to the above equation by assuming:

- a perfectly radial reservoir system;
- the producing well is in the center and producing at a constant production rate of Q;
- uniform pressure p_i throughout the reservoir before production;
- no flow across the external radius r_e.

Van Everdingen and Hurst presented the solution to Equation 1.2.77 in a form of an infinite series of exponential terms and Bessel functions. The authors evaluated this series for several values of r_{eD} over a wide range of values for t_D and presented the solution in terms of dimensionless pressure drop p_D as a function of dimensionless radius r_{eD} and dimensionless time t_D. Chatas (1953) and Lee (1982) conveniently tabulated these solutions for the following two cases:

(1) infinite-acting reservoir $r_{eD} = \infty$;
(2) finite-radial reservoir.

Infinite-acting reservoir For an infinite-acting reservoir, i.e., $r_{eD} = \infty$, the solution to Equation 1.2.78 in terms of

Table 1.2 p_D *versus* t_D—*infinite radial system, constant rate at the inner boundary (After Lee, J., Well Testing, SPE Textbook Series, permission to publish by the SPE, copyright SPE, 1982)*

t_D	p_D	t_D	p_D	t_D	p_D
0	0	0.15	0.3750	60.0	2.4758
0.0005	0.0250	0.2	0.4241	70.0	2.5501
0.001	0.0352	0.3	0.5024	80.0	2.6147
0.002	0.0495	0.4	0.5645	90.0	2.6718
0.003	0.0603	0.5	0.6167	100.0	2.7233
0.004	0.0694	0.6	0.6622	150.0	2.9212
0.005	0.0774	0.7	0.7024	200.0	3.0636
0.006	0.0845	0.8	0.7387	250.0	3.1726
0.007	0.0911	0.9	0.7716	300.0	3.2630
0.008	0.0971	1.0	0.8019	350.0	3.3394
0.009	0.1028	1.2	0.8672	400.0	3.4057
0.01	0.1081	1.4	0.9160	450.0	3.4641
0.015	0.1312	2.0	1.0195	500.0	3.5164
0.02	0.1503	3.0	1.1665	550.0	3.5643
0.025	0.1669	4.0	1.2750	600.0	3.6076
0.03	0.1818	5.0	1.3625	650.0	3.6476
0.04	0.2077	6.0	1.4362	700.0	3.6842
0.05	0.2301	7.0	1.4997	750.0	3.7184
0.06	0.2500	8.0	1.5557	800.0	3.7505
0.07	0.2680	9.0	1.6057	850.0	3.7805
0.08	0.2845	10.0	1.6509	900.0	3.8088
0.09	0.2999	15.0	1.8294	950.0	3.8355
0.1	0.3144	20.0	1.9601	1000.0	3.8584
		30.0	2.1470		
		40.0	2.2824		
		50.0	2.3884		

Notes: For $t_D < 0.01$: $p_D \cong 2zt_D/x$.
For $100 < t_D < 0.25 r_e^2 D$: $p_D \cong 0.5 (\ln t_D + 0.80907)$.

the dimensionless pressure drop p_D is strictly a function of the dimensionless time t_D, or:

$$p_D = f(t_D)$$

Chatas and Lee tabulated the p_D values for the infinite-acting reservoir as shown in Table 1.2. The following mathematical expressions can be used to approximate these tabulated values of p_D.
For $t_D < 0.01$:

$$p_D = 2\sqrt{\frac{t_D}{\pi}}$$ [1.2.79]

For $t_D > 100$:

$$p_D = 0.5[\ln(t_D) + 0.80907]$$ [1.2.80]

For $0.02 < t_D \leq 1000$:

$$p_D = a_1 + a_2 \ln(t_D) + a_3[\ln(t_D)]^2 + a_4[\ln(t_D)]^3 + a_5 t_D$$
$$+ a_6(t_D)^2 + a_7(t_D)^3 + a_8/t_D$$ [1.2.81]

where the values of the coefficients of the above equations are:

$a_1 = 0.8085064$ $a_2 = 0.29302022$

$a_3 = 3.5264177 \times 10^{-2}$ $a_4 = -1.4036304 \times 10^{-3}$

$a_5 = -4.7722225 \times 10^{-4}$ $a_6 = 5.1240532 \times 10^{-7}$

$a_7 = -2.3033017 \times 10^{-10}$ $a_8 = -2.6723117 \times 10^{-3}$

Finite radial reservoir For a finite radial system, the solution to Equation 1.2.78 is a function of both the dimensionless time t_D and dimensionless time radius r_{eD}, or:

$$p_D = f(t_D, r_{eD})$$

where:

$$r_{eD} = \frac{\text{external radius}}{\text{wellbore radius}} = \frac{r_e}{r_w} \qquad [1.2.82]$$

Table 1.3 presents p_D as a function of t_D for $1.5 < r_{eD} < 10$. It should be pointed out that van Everdingen and Hurst principally applied the p_D function solution to model the performance of water influx into oil reservoirs. Thus, the authors' wellbore radius r_w was in this case the external radius of the reservoir and r_e was essentially the external boundary radius of the aquifer. Therefore, the ranges of the r_{eD} values in Table 1.3 are practical for this application.

Consider the Ei function solution to the diffusivity equations as given by Equation 1.2.66:

$$p(r,t) = p_i + \left[\frac{70.6QB\mu}{kh}\right] \text{Ei}\left[\frac{-948\phi\mu c_t r^2}{kt}\right]$$

This relationship can be expressed in a dimensionless form by manipulating the expression to give:

$$\frac{p_i - p(r,t)}{\left[\frac{141.2Q_oB_o\mu_o}{kh}\right]} = -\frac{1}{2}\text{Ei}\left[\frac{-(r/r_w)^2}{4\left(\frac{0.0002637kt}{\phi\mu c_t r_w^2}\right)}\right]$$

From the definition of the dimensionless variables of Equations 1.2.74 through 1.2.77, i.e., p_D, t_D, and r_D, this relation is expressed in terms of these dimensionless variables as:

$$p_D = -\frac{1}{2}\text{Ei}\left(-\frac{r_D^2}{4t_D}\right) \qquad [1.2.83]$$

Chatas (1953) proposed the following mathematical form for calculated p_D when $25 < t_D$ and $0.25r_{eD}^2 < t_D$:

$$p_D = \frac{0.5 + 2t_D}{r_{eD}^2 - 1} - \frac{r_{eD}^4\left[3 - 4\ln(r_{eD})\right] - 2r_{eD}^2 - 1}{4\left(r_{eD}^2 - 1\right)^2}$$

There are two special cases of the above equation which arise when $r_{eD}^2 \gg 1$ or when $t_D/r_{eD}^2 > 25$:

If $r_{eD}^2 \gg 1$, then:

$$p_D = \frac{2t_D}{r_{eD}^2} + \ln(r_{eD}) - 0.75$$

If $t_D/r_{eD}^2 > 25$, then:

$$p_D = \frac{1}{2}\left[\ln\frac{t_D}{r_D^2} + 0.80907\right] \qquad [1.2.84]$$

The computational procedure of using the p_D function to determine the bottom-hole flowing pressure changing the transient flow period, i.e., during the infinite-acting behavior, is summarized in the following steps:

Step 1. Calculate the dimensionless time t_D by applying Equation 1.2.75:

$$t_D = \frac{0.0002637kt}{\phi\mu c_t r_w^2}$$

Step 2. Determine the dimensionless radius r_{eD}. Note that for an infinite-acting reservoir, the dimensionless radius $r_{eD} = \infty$.

Step 3. Using the calculated value of t_D, determine the corresponding pressure function p_D from the appropriate table or equations, e.g., Equation 1.2.80 or 1.2.84:

For an infinite-acting reservoir $\quad p_D = 0.5[\ln(t_D) + 0.80907]$

For a finite reservoir $p_D = \frac{1}{2}[\ln(t_D/r_D^2) + 0.80907]$

Step 4. Solve for the pressure by applying Equation 1.2.74:

$$p(r_w,t) = p_i - \left(\frac{141.2Q_oB_o\mu_o}{kh}\right)p_D \qquad [1.2.85]$$

Example 1.12 A well is producing at a constant flow rate of 300 STB/day under unsteady-state flow conditions. The reservoir has the following rock and fluid properties (see Example 1.10):

$$B_o = 1.25 \text{ bbl/STB}, \quad \mu_o = 1.5 \text{ cp}, \quad c_t = 12 \times 10^{-6} \text{ psi}^{-1}$$

$$k = 60 \text{ md}, \qquad\qquad h = 15 \text{ ft}, \qquad p_i = 4000 \text{ psi}$$

$$\phi = 15\%, \qquad\qquad r_w = 0.25 \text{ ft}$$

Assuming an infinite-acting reservoir, i.e., $r_{eD} = \infty$, calculate the bottom-hole flowing pressure after 1 hour of production by using the dimensionless pressure approach.

Solution

Step 1. Calculate the dimensionless time t_D from Equation 1.2.75:

$$t_D = \frac{0.0002637kt}{\phi\mu c_t r_w^2}$$

$$= \frac{0.000264\,(60)\,(1)}{(0.15)\,(1.5)\,(12 \times 10^{-6})\,(0.25)^2} = 93\,866.67$$

Step 2. Since $t_D > 100$, use Equation 1.2.80 to calculate the dimensionless pressure drop function:

$$p_D = 0.5[\ln(t_D) + 0.80907]$$

$$= 0.5[\ln(93\,866.67) + 0.80907] = 6.1294$$

Step 3. Calculate the bottom-hole pressure after 1 hour by applying Equation 1.2.85:

$$p(r_w,t) = p_i - \left(\frac{141.2Q_oB_o\mu_o}{kh}\right)p_D$$

$$p(0.25,1) = 4000 - \left[\frac{141.2\,(300)\,(1.25)\,(1.5)}{(60)\,(15)}\right]$$

$$\times\,(6.1294) = 3459 \text{ psi}$$

This example shows that the solution as given by the p_D function technique is identical to that of the Ei function approach. The main difference between the two formulations is that *the p_D function can only be used to calculate the pressure at radius r when the flow rate Q is constant and known*. In that case, the p_D function application is essentially restricted to the wellbore radius because the rate is usually known. On the other hand, the Ei function approach can be used to calculate the pressure at any radius in the reservoir by using the well flow rate Q.

It should be pointed out that, for an infinite-acting reservoir with $t_D > 100$, the p_D function is related to the Ei function by the following relation:

$$p_D = 0.5\left[-\text{Ei}\left(\frac{-1}{4t_D}\right)\right] \qquad [1.2.86]$$

The previous example, i.e., Example 1.12, is not a practical problem, but it is essentially designed to show the physical significance of the p_D solution approach. In transient flow testing, we normally record the bottom-hole flowing pressure as a function of time. Therefore, the dimensionless pressure drop technique can be used to determine one or more of the reservoir properties, e.g. k or kh, as discussed later in this chapter.

1.2.6 Radial flow of compressible fluids

Gas viscosity and density vary significantly with pressure and therefore the assumptions of Equation 1.2.64 are not satisfied for gas systems, i.e., compressible fluids. In order to develop the proper mathematical function for describing

Table 1.3 p_D vs. t_D—finite radial system, constant rate at the inner boundary (After Lee, J., Well Testing, SPE Textbook Series, permission to publish by the SPE, copyright SPE, 1982)

$r_{eD} = 1.5$		$r_{eD} = 2.0$		$r_{eD} = 2.5$		$r_{eD} = 3.0$		$r_{eD} = 3.5$		$r_{eD} = 4.0$	
t_D	p_D	t_D	p_D	t_D	p_D	t_D	p_D	t_D	p_D	t_D	p_D
0.06	0.251	0.22	0.443	0.40	0.565	0.52	0.627	1.0	0.802	1.5	0.927
0.08	0.288	0.24	0.459	0.42	0.576	0.54	0.636	1.1	0.830	1.6	0.948
0.10	0.322	0.26	0.476	0.44	0.587	0.56	0.645	1.2	0.857	1.7	0.968
0.12	0.355	0.28	0.492	0.46	0.598	0.60	0.662	1.3	0.882	1.8	0.988
0.14	0.387	0.30	0.507	0.48	0.608	0.65	0.683	1.4	0.906	1.9	1.007
0.16	0.420	0.32	0.522	0.50	0.618	0.70	0.703	1.5	0.929	2.0	1.025
0.18	0.452	0.34	0.536	0.52	0.628	0.75	0.721	1.6	0.951	2.2	1.059
0.20	0.484	0.36	0.551	0.54	0.638	0.80	0.740	1.7	0.973	2.4	1.092
0.22	0.516	0.38	0.565	0.56	0.647	0.85	0.758	1.8	0.994	2.6	1.123
0.24	0.548	0.40	0.579	0.58	0.657	0.90	0.776	1.9	1.014	2.8	1.154
0.26	0.580	0.42	0.593	0.60	0.666	0.95	0.791	2.0	1.034	3.0	1.184
0.28	0.612	0.44	0.607	0.65	0.688	1.0	0.806	2.25	1.083	3.5	1.255
0.30	0.644	0.46	0.621	0.70	0.710	1.2	0.865	2.50	1.130	4.0	1.324
0.35	0.724	0.48	0.634	0.75	0.731	1.4	0.920	2.75	1.176	4.5	1.392
0.40	0.804	0.50	0.648	0.80	0.752	1.6	0.973	3.0	1.221	5.0	1.460
0.45	0.884	0.60	0.715	0.85	0.772	2.0	1.076	4.0	1.401	5.5	1.527
0.50	0.964	0.70	0.782	0.90	0.792	3.0	1.328	5.0	1.579	6.0	1.594
0.55	1.044	0.80	0.849	0.95	0.812	4.0	1.578	6.0	1.757	6.5	1.660
0.60	1.124	0.90	0.915	1.0	0.832	5.0	1.828			7.0	1.727
0.65	1.204	1.0	0.982	2.0	1.215					8.0	1.861
0.70	1.284	2.0	1.649	3.0	1.506					9.0	1.994
0.75	1.364	3.0	2.316	4.0	1.977					10.0	2.127
0.80	1.444	5.0	3.649	5.0	2.398						

$r_{eD} = 4.5$		$r_{eD} = 5.0$		$r_{eD} = 6.0$		$r_{eD} = 7.0$		$r_{eD} = 8.0$		$r_{eD} = 9.0$		$r_{eD} = 10.0$	
t_D	p_D	t_D	p_D	t_D	p_D	t_D	p_D	t_D	p_D	t_D	p_D	t_D	p_D
2.0	1.023	3.0	1.167	4.0	1.275	6.0	1.436	8.0	1.556	10.0	1.651	12.0	1.732
2.1	1.040	3.1	1.180	4.5	1.322	6.5	1.470	8.5	1.582	10.5	1.673	12.5	1.750
2.2	1.056	3.2	1.192	5.0	1.364	7.0	1.501	9.0	1.607	11.0	1.693	13.0	1.768
2.3	1.702	3.3	1.204	5.5	1.404	7.5	1.531	9.5	1.631	11.5	1.713	13.5	1.784
2.4	1.087	3.4	1.215	6.0	1.441	8.0	1.559	10.0	1.663	12.0	1.732	14.0	1.801
2.5	1.102	3.5	1.227	6.5	1.477	8.5	1.586	10.5	1.675	12.5	1.750	14.5	1.817
2.6	1.116	3.6	1.238	7.0	1.511	9.0	1.613	11.0	1.697	13.0	1.768	15.0	1.832
2.7	1.130	3.7	1.249	7.5	1.544	9.5	1.638	11.5	1.717	13.5	1.786	15.5	1.847
2.8	1.144	3.8	1.259	8.0	1.576	10.0	1.663	12.0	1.737	14.0	1.803	16.0	1.862
2.9	1.158	3.9	1.270	8.5	1.607	11.0	1.711	12.5	1.757	14.5	1.819	17.0	1.890
3.0	1.171	4.0	1.281	9.0	1.638	12.0	1.757	13.0	1.776	15.0	1.835	18.0	1.917
3.2	1.197	4.2	1.301	9.5	1.668	13.0	1.810	13.5	1.795	15.5	1.851	19.0	1.943
3.4	1.222	4.4	1.321	10.0	1.698	14.0	1.845	14.0	1.813	16.0	1.867	20.0	1.968
3.6	1.246	4.6	1.340	11.0	1.757	15.0	1.888	14.5	1.831	17.0	1.897	22.0	2.017
3.8	1.269	4.8	1.360	12.0	1.815	16.0	1.931	15.0	1.849	18.0	1.926	24.0	2.063
4.0	1.292	5.0	1.378	13.0	1.873	17.0	1.974	17.0	1.919	19.0	1.955	26.0	2.108
4.5	1.349	5.5	1.424	14.0	1.931	18.0	2.016	19.0	1.986	20.0	1.983	28.0	2.151
5.0	1.403	6.0	1.469	15.0	1.988	19.0	2.058	21.0	2.051	22.0	2.037	30.0	2.194
5.5	1.457	6.5	1.513	16.0	2.045	20.0	2.100	23.0	2.116	24.0	2.906	32.0	2.236
6.0	1.510	7.0	1.556	17.0	2.103	22.0	2.184	25.0	2.180	26.0	2.142	34.0	2.278
7.0	1.615	7.5	1.598	18.0	2.160	24.0	2.267	30.0	2.340	28.0	2.193	36.0	2.319
8.0	1.719	8.0	1.641	19.0	2.217	26.0	2.351	35.0	2.499	30.0	2.244	38.0	2.360
9.0	1.823	9.0	1.725	20.0	2.274	28.0	2.434	40.0	2.658	34.0	2.345	40.0	2.401
10.0	1.927	10.0	1.808	25.0	2.560	30.0	2.517	45.0	2.817	38.0	2.446	50.0	2.604
11.0	2.031	11.0	1.892	30.0	2.846					40.0	2.496	60.0	2.806
12.0	2.135	12.0	1.975							45.0	2.621	70.0	3.008
13.0	2.239	13.0	2.059							50.0	2.746	80.0	3.210
14.0	2.343	14.0	2.142							60.0	2.996	90.0	3.412
15.0	2.447	15.0	2.225							70.0	3.246	100.0	3.614

Notes: For t_D smaller than values listed in this table for a given r_{eD} reservoir is infinite acting.
Find p_D in Table 1.2.
For $25 < t_D$ and t_D larger than values in table:

$$p_D \cong \frac{(1/2+2t_D)}{r_{eD}^2} - \frac{3r_{eD}^4 - 4r_{eD}^4 \ln r_{eD} - 2r_{eD}^2 - 1}{4\left(r_{eD}^2 - 1\right)^2}$$

For wells in rebounded reservoirs with $r_{eD}^2 \gg 1$:

$$p_D \cong \frac{2t_D}{r_{eD}^2} + \ln r_{eD} - 3/4.$$

the flow of compressible fluids in the reservoir, the following two additional gas equations must be considered:

(1) Gas density equation:

$$\rho = \frac{pM}{ZRT}$$

(2) Gas compressibility equation:

$$c_g = \frac{1}{p} - \frac{1}{Z}\frac{dZ}{dp}$$

Combining the above two basic gas equations with that of Equation 1.2.56 gives:

$$\frac{1}{r}\frac{\partial}{\partial r}\left(r\frac{p}{\mu Z}\frac{\partial p}{\partial r}\right) = \frac{\phi\mu c_t}{0.000264k}\frac{p}{\mu Z}\frac{\partial p}{\partial t} \qquad [1.2.87]$$

where:

$t =$ time, hours
$k =$ permeability, md
$c_t =$ total isothermal compressibility, psi^{-1}
$\phi =$ porosity

Al-Hussainy et al. (1966) linearized the above basic flow equation by introducing the real-gas pseudopressure $m(p)$ into Equation 1.2.87. Recalling the previously defined $m(p)$ equation:

$$m(p) = \int_0^p \frac{2p}{\mu Z}\,dp \qquad [1.2.88]$$

and differentiating this relation with respect to p, gives:

$$\frac{\partial m(p)}{\partial p} = \frac{2p}{\mu Z} \qquad [1.2.89]$$

The following relationships are obtained by applying the chain rule:

$$\frac{\partial m(p)}{\partial r} = \frac{\partial m(p)}{\partial p}\frac{\partial p}{\partial r} \qquad [1.2.90]$$

$$\frac{\partial m(p)}{\partial t} = \frac{\partial m(p)}{\partial p}\frac{\partial p}{\partial t} \qquad [1.2.91]$$

Substituting Equation 1.2.89 into 1.2.90 and 1.2.91, gives:

$$\frac{\partial p}{\partial r} = \frac{\mu Z}{2p}\frac{\partial m(p)}{\partial r} \qquad [1.2.92]$$

and:

$$\frac{\partial p}{\partial t} = \frac{\mu Z}{2p}\frac{\partial m(p)}{\partial t} \qquad [1.2.93]$$

Combining Equations 1.2.92 and 1.2.93 with 1.2.87, yields:

$$\frac{\partial^2 m(p)}{\partial r^2} + \frac{1}{r}\frac{\partial m(p)}{\partial r} = \frac{\phi\mu c_t}{0.000264k}\frac{\partial m(p)}{\partial t} \qquad [1.2.94]$$

Equation 1.2.94 is the radial diffusivity equation for compressible fluids. This differential equation relates the real-gas pseudopressure (real-gas potential) to the time t and the radius r. Al-Hussany et al. (1966) pointed out that in gas well testing analysis, the constant-rate solution has more practical applications than that provided by the constant-pressure solution. The authors provided the exact solution to Equation 1.2.94 that is commonly referred to as the $m(p)$ solution method. There are also two other solutions that approximate the exact solution. These two approximation methods are called the pressure-squared method and the pressure method. In general, there are three forms of mathematical solution to the diffusivity equation:

(1) $m(p)$ solution method (exact solution);
(2) pressure-squared method (p^2 approximation method);
(3) pressure-method (p approximation method).

These three solution methods are presented below.

First solution: m(p) method (exact solution)

Imposing the constant-rate condition as one of the boundary conditions required to solve Equation 1.2.94, Al-Hussany et al. (1966) proposed the following exact solution to the diffusivity equation:

$$m(p_{wf}) = m(p_i) - 57\,895.3\left(\frac{p_{sc}}{T_{sc}}\right)\left(\frac{Q_g T}{kh}\right)$$
$$\times\left[\log\left(\frac{kt}{\phi\mu_i c_{ti}r_w^2}\right) - 3.23\right] \qquad [1.2.95]$$

where:

$p_{wf} =$ bottom-hole flowing pressure, psi
$p_e =$ initial reservoir pressure
$Q_g =$ gas flow rate, Mscf/day
$t =$ time, hours
$k =$ permeability, md
$p_{sc} =$ standard pressure, psi
$T_{sc} =$ standard temperature, °R
$T =$ Reservoir temperature
$r_w =$ wellbore radius, ft
$h =$ thickness, ft
$\mu_i =$ gas viscosity at the initial pressure, cp
$c_{ti} =$ total compressibility coefficient at p_i, psi^{-1}
$\phi =$ porosity

Setting $p_{sc} = 14.7$ psia and $T_{sc} = 520$°R, then Equation 1.2.95 reduces to:

$$m(p_{wf}) = m(p_i) - \left(\frac{1637 Q_g T}{kh}\right)\left[\log\left(\frac{kt}{\phi\mu_i c_{ti}r_w^2}\right) - 3.23\right]$$
$$[1.2.96]$$

The above equation can be simplified by introducing the dimensionless time (as defined previously by Equation 1.2.74) into Equation 1.2.96:

$$t_D = \frac{0.0002637\,kt}{\phi\mu_i c_{ti}r_w^2}$$

Equivalently, Equation 1.2.96 can be written in terms of the dimensionless time t_D as:

$$m(p_{wf}) = m(p_i) - \left(\frac{1637 Q_g T}{kh}\right)\left[\log\left(\frac{4t_D}{\gamma}\right)\right] \qquad [1.2.97]$$

The parameter γ is called Euler's constant and is given by:

$$\gamma = e^{0.5772} = 1.781 \qquad [1.2.98]$$

The solution to the diffusivity equation as given by Equations 1.2.96 and 1.2.97 expresses the bottom-hole real-gas pseudopressure as a function of the transient flow time t. The solution as expressed in terms of $m(p)$ is the recommended mathematical expression for performing gas well pressure analysis due to its applicability in all pressure ranges.

The radial gas diffusivity equation can be expressed in a dimensionless form in terms of the dimensionless real-gas pseudopressure drop ψ_D. The solution to the dimensionless equation is given by:

$$\psi_D = \frac{m(p_i) - m(p_{wf})}{(1422 Q_g T/kh)}$$

or:

$$m(p_{wf}) = m(p_i) - \left(\frac{1422 Q_g T}{kh}\right)\psi_D \qquad [1.2.99]$$

where:

$Q_g =$ gas flow rate, Mscf/day
$k =$ permeability, md

The dimensionless pseudopressure drop ψ_D can be determined as a function of t_D by using the appropriate expression

of Equations 1.2.79 through 1.2.84. When $t_D > 100$, ψ_D can be calculated by applying Equation 1.2.70. That is:

$$\psi_D = 0.5[\ln(t_D) + 0.80907] \qquad [1.2.100]$$

Example 1.13 A gas well with a wellbore radius of 0.3 ft is producing at a constant flow rate of 2000 Mscf/day under transient flow conditions. The initial reservoir pressure (shut-in pressure) is 4400 psi at 140°F. The formation permeability and thickness are 65 md and 15 ft, respectively. The porosity is recorded as 15%. Example 1.7 documents the properties of the gas as well as values of $m(p)$ as a function of pressures. The table is reproduced below for convenience:

P	μ_g (cp)	Z	$m(p)$ (psi^2/cp)
0	0.01270	1.000	0.000
400	0.01286	0.937	13.2×10^6
800	0.01390	0.882	52.0×10^6
1200	0.01530	0.832	113.1×10^6
1600	0.01680	0.794	198.0×10^6
2000	0.01840	0.770	304.0×10^6
2400	0.02010	0.763	422.0×10^6
2800	0.02170	0.775	542.4×10^6
3200	0.02340	0.797	678.0×10^6
3600	0.02500	0.827	816.0×10^6
4000	0.02660	0.860	950.0×10^6
4400	0.02831	0.896	1089.0×10^6

Assuming that the initial total isothermal compressibility is 3×10^{-4} psi^{-1}, calculate the bottom-hole flowing pressure after 1.5 hours.

Solution

Step 1. Calculate the dimensionless time t_D:

$$t_D = \frac{0.0002637kt}{\phi \mu_i c_{ti} r_w^2}$$

$$= \frac{(0.0002637)(65)(1.5)}{(0.15)(0.02831)(3 \times 10^{-4})(0.3^2)} = 224\,498.6$$

Step 2. Solve for $m(p_{wf})$ by using Equation 1.2.97:

$$m(p_{wf}) = m(p_i) - \left(\frac{1637Q_gT}{kh}\right)\left[\log\left(\frac{4t_D}{\gamma}\right)\right]$$

$$= 1089 \times 10^6 - \frac{(1637)(2000)(600)}{(65)(15)}$$

$$\times \left[\log\left(\frac{(4)\,224498.6}{e^{0.5772}}\right)\right] = 1077.5 \times 10^6$$

Step 3. From the given *PVT* data, interpolate using the value of $m(p_{wf})$ to give a corresponding p_{wf} of 4367 psi.

An identical solution can be obtained by applying the ψ_D approach as shown below:

Step 1. Calculate ψ_D from Equation 1.2.100:

$$\psi_D = 0.5[\ln(t_D) + 0.80907]$$

$$= 0.5[\ln(224\,498.6) + 0.8090] = 6.565$$

Step 2. Calculate m(p$_{wf}$) by using Equation 1.2.99:

$$m(p_{wf}) = m(p_i) - \left(\frac{1422Q_gT}{kh}\right)\psi_D$$

$$= 1089 \times 10^6 - \left(\frac{1422\,(2000)\,(600)}{(65)\,(15)}\right)(6.565)$$

$$= 1077.5 \times 10^6$$

By interpolation at $m(p_{wf}) = 1077.5 \times 10^6$, this gives a corresponding value of $p_{wf} = 4367$ psi.

Second solution: pressure-squared method
The first approximation to the exact solution is to move the pressure-dependent term (μZ) outside the integral that defines $m(p_{wf})$ and $m(p_i)$, to give:

$$m(p_i) - m(p_{wf}) = \frac{2}{\overline{\mu Z}} \int_{p_{wf}}^{p_i} p\,dp \qquad [1.2.101]$$

or:

$$m(p_i) - m(p_{wf}) = \frac{p_i^2 - p_{wf}^2}{\overline{\mu Z}} \qquad [1.2.102]$$

The bars over μ and Z represent the values of the gas viscosity and deviation factor as evaluated at the average pressure $\overline{p}$. This average pressure is given by:

$$\overline{p} = \sqrt{\frac{p_i^2 + p_{wf}^2}{2}} \qquad [1.2.103]$$

Combining Equation 1.2.102 with 1.2.96, 1.2.97, or 1.2.99, gives:

$$p_{wf}^2 = p_i^2 - \left(\frac{1637Q_gT\overline{\mu Z}}{kh}\right)\left[\log\left(\frac{kt}{\phi\mu_i c_{ti} r_w^2}\right) - 3.23\right] \qquad [1.2.104]$$

or:

$$p_{wf}^2 = p_i^2 - \left(\frac{1637Q_gT\overline{\mu Z}}{kh}\right)\left[\log\left(\frac{4t_D}{\gamma}\right)\right] \qquad [1.2.105]$$

Equivalently:

$$p_{wf}^2 = p_i^2 - \left(\frac{1422Q_gT\overline{\mu Z}}{kh}\right)\psi_D \qquad [1.2.106]$$

The above approximation solution forms indicate that the product (μZ) is assumed constant at the average pressure $\overline{p}$. This effectively limits the applicability of the p^2 method to reservoir pressures of less than 2000. It should be pointed out that when the p^2 method is used to determine p_{wf} it is perhaps sufficient to set $\overline{\mu Z} = \mu_i Z$.

Example 1.14 A gas well is producing at a constant rate of 7454.2 Mscf/day under transient flow conditions. The following data is available:

$$k = 50 \text{ md}, \quad h = 10 \text{ ft}, \quad \phi = 20\%, \quad p_i = 1600 \text{ psi}$$

$$T = 600°R, \quad r_w = 0.3 \text{ ft}, \quad c_{ti} = 6.25 \times 10^{-4} \text{ psi}^{-1}$$

The gas properties are tabulated below:

P	μ_g (cp)	Z	$m(p)$ (psi^2/cp)
0	0.01270	1.000	0.000
400	0.01286	0.937	13.2×10^6
800	0.01390	0.882	52.0×10^6
1200	0.01530	0.832	113.1×10^6
1600	0.01680	0.794	198.0×10^6

Calculate the bottom-hole flowing pressure after 4 hours by using:

(a) the $m(p)$ method;
(b) the p^2 method.

Solution

(a) The $m(p)$ method:

Step 1. Calculate t_D:

$$t_D = \frac{0.000264\,(50)\,(4)}{(0.2)\,(0.0168)\,(6.25 \times 10^{-4})\,(0.3^2)}$$

$$= 279\,365.1$$

Step 2. Calculate ψ_D:

$$\psi_D = 0.5[\ln(t_D) + 0.80907]$$

$$= 0.5\left[\ln(279\,365.1) + 0.80907\right] = 6.6746$$

Step 3. Solve for $m(p_{wf})$ by applying Equation 1.2.99:

$$m(p_{wf}) = m(p_i) - \left(\frac{1422 Q_g T}{kh}\right)\psi_D$$

$$= (198 \times 10^6) - \left[\frac{1422\,(7454.2)\,(600)}{(50)\,(10)}\right]6.6746$$

$$= 113.1 \times 10^6$$

The corresponding value of $p_{wf} = 1200$ psi.

(b) The p^2 method:

Step 1. Calculate ψ_D by applying Equation 1.2.100:

$$\psi_D = 0.5[\ln(t_D) + 0.80907]$$

$$= 0.5\left[\ln(279\,365.1) + 0.80907\right] = 6.6747$$

Step 2. Calculate p_{wf}^2 by applying Equation 1.2.106:

$$p_{wf}^2 = p_i^2 - \left(\frac{1422 Q_g T \overline{\mu Z}}{kh}\right)\psi_D$$

$$= 1600^2 - \left[\frac{(1422)\,(7454.2)\,(600)\,(0.0168)\,(0.794)}{(50)\,(10)}\right]6.6747$$

$$= 1427491$$

$$p_{wf} = 1195 \text{ psi.}$$

Step 3. The absolute average error is 0.4%.

Third solution: pressure approximation method
The second method of approximation to the exact solution of the radial flow of gases is to treat the gas as a pseudo-liquid. Recal that the gas formation volume factor B_g as expressed in bbl/scf is given by:

$$B_g = \left(\frac{p_{sc}}{5.615 T_{sc}}\right)\left(\frac{ZT}{p}\right)$$

or:

$$B_g = 0.00504\left(\frac{ZT}{p}\right)$$

Solving the above expression for p/Z gives:

$$\frac{p}{Z} = \left(\frac{T p_{sc}}{5.615 T_{sc}}\right)\left(\frac{1}{B_g}\right)$$

The difference in the real-gas pseudopressure is given by:

$$m(p_i) - (p_{wf}) = \int_{p_{wf}}^{p_i} \frac{2p}{\mu Z}\,dp$$

Combining the above two expressions gives:

$$m(p_i) - m(p_{wf}) = \frac{2T p_{sc}}{5.615 T_{sc}} \int_{p_{wf}}^{p_i}\left(\frac{1}{\mu B_g}\right)dp \qquad [1.2.107]$$
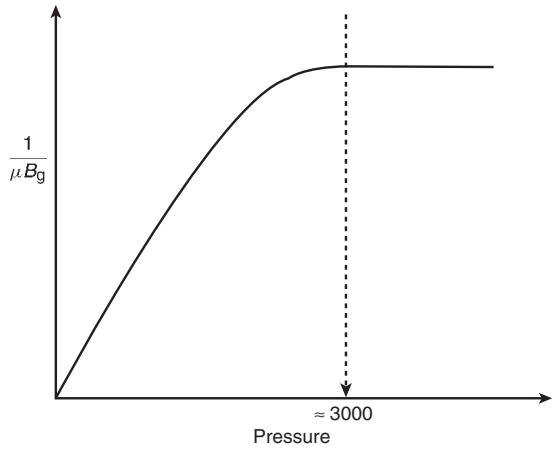
Figure 1.22 Plot of $1/\mu B_g$ vs. pressure.

Fetkovich (1973) suggested that at high pressures above 3000 psi ($p > 3000$), $1/\mu B_g$ is nearly constant as shown schematically in Figure 1.22. Imposing Fetkovich's condition on Equation 1.2.107 and integrating gives:

$$m(p_i) - m(p_{wf}) = \frac{2T p_{sc}}{5.615 T_{sc} \overline{\mu B_g}}(p_i - p_{wf}) \qquad [1.2.108]$$

Combining Equation 1.2.108 with 1.2.96, 1.2.97, or 1.2.99 gives:

$$p_{wf} = p_i - \left(\frac{162.5 \times 10^3 Q_g \overline{\mu B_g}}{kh}\right)\left[\log\left(\frac{kt}{\phi \overline{\mu c_t} r_w^2}\right) - 3.23\right] \qquad [1.2.109]$$

or:

$$p_{wf} = p_i - \left(\frac{(162.5 \times 10^3) Q_g \overline{\mu B_g}}{kh}\right)\left[\log\left(\frac{4 t_D}{\gamma}\right)\right] \qquad [1.2.110]$$

or, equivalently, in terms of dimensionless pressure drop:

$$p_{wf} = p_i - \left(\frac{(141.2 \times 10^3) Q_g \overline{\mu B_g}}{kh}\right)p_D \qquad [1.2.111]$$

where:

Q_g = gas flow rate, Mscf/day
k = permeability, md
B_g = gas formation volume factor, bbl/scf
t = time, hours
p_D = dimensionless pressure drop
t_D = dimensionless

It should be noted that the gas properties, i.e., μ, B_g, and c_t, are evaluated at pressure $\bar{p}$ as defined below:

$$\bar{p} = \frac{p_i + p_{wf}}{2} \qquad [1.2.112]$$

Again, this method is limited only to applications above 3000 psi. When solving for p_{wf}, it might be sufficient to evaluate the gas properties at p_i.

Example 1.15 The data of Example 1.13 is repeated below for convenience.

A gas well with a wellbore radius of 0.3 ft is producing at a constant flow rate of 2000 Mscf/day under transient flow conditions. The initial reservoir pressure (shut-in pressure) is 4400 psi at 140°F. The formation permeability and thickness are 65 md and 15 ft, respectively. The porosity is recorded as 15%. The properties of the gas as well

as values of $m(p)$ as a function of pressures are tabulated below:

P	μ_g (cp)	Z	$m(p)$ (psi^2/cp)
0	0.01270	1.000	0.000
400	0.01286	0.937	13.2×10^6
800	0.01390	0.882	52.0×10^6
1200	0.01530	0.832	113.1×10^6
1600	0.01680	0.794	198.0×10^6
2000	0.01840	0.770	304.0×10^6
2400	0.02010	0.763	422.0×10^6
2800	0.02170	0.775	542.4×10^6
3200	0.02340	0.797	678.0×10^6
3600	0.02500	0.827	816.0×10^6
4000	0.02660	0.860	950.0×10^6
4400	0.02831	0.896	1089.0×10^6

Assuming that the initial total isothermal compressibility is 3×10^{-4}psi^{-1}, calculate, the bottom-hole flowing pressure after 1.5 hours by using the p approximation method and compare it with the exact solution.

Solution

Step 1. Calculate the dimensionless time t_D:

$$t_D = \frac{0.0002637kt}{\phi \mu_i c_{ti} r_w^2}$$

$$= \frac{(0.000264)(65)(1.5)}{(0.15)(0.02831)(3 \times 10^{-4})(0.3^2)} = 224\,498.6$$

Step 2. Calculate B_g at p_i:

$$B_g = 0.00504 \left(\frac{Z_i T}{p_i} \right)$$

$$= 0.00504 \frac{(0.896)(600)}{4400} = 0.0006158 \text{ bbl/scf}$$

Step 3. Calculate the dimensionless pressure p_D by applying Equation 1.2.80:

$$p_D = 0.5[\ln(t_D) + 0.80907]$$

$$= 0.5 \left[\ln(224\,498.6) + 0.80907 \right] = 6.565$$

Step 4. Approximate p_{wf} from Equation 1.2.111:

$$p_{wf} = p_i - \left(\frac{(141.2 10^3) Q_g \overline{\mu} \overline{B_g}}{kh} \right) p_D$$

$$= 4400 - \left[\frac{141.2 \times 10^3 (2000)(0.02831)(0.0006158)}{(65)(15)} \right] 6.565$$

$$= 4367 \text{ psi}$$

The solution is identical to that of the exact solution of Example 1.13.

It should be pointed out that Examples 1.10 through 1.15 are designed to illustrate the use of different solution methods. However, these examples are not practical because, in transient flow analysis, the bottom-hole flowing pressure is usually available as a function of time. All the previous methodologies are essentially used to characterize the reservoir by determining the permeability k or the permeability and thickness product (kh).

1.2.7 Pseudosteady state

In the unsteady-state flow cases discussed previously, it was assumed that a well is located in a very large reservoir and producing at a constant flow rate. This rate creates a pressure disturbance in the reservoir that travels throughout this "infinite-size reservoir." During this transient flow period, reservoir boundaries have no effect on the pressure behavior of the well. Obviously, the time period when this assumption can be imposed is often very short in length. As soon as the pressure disturbance reaches all drainage boundaries, it ends the transient (unsteady-state) flow regime and the beginning of the boundary-dominated flow condition. This different type of flow regime is called pseudosteady (semisteady)-State Flow. It is necessary at this point to impose different boundary conditions on the diffusivity equation and drive an appropriate solution to this flow regime.

Consider Figure 1.23 which shows a well in a radial system that is producing at a constant rate for a long enough period that eventually affects the entire drainage area. During this semisteady-state flow, the change in pressure with time becomes the same throughout the drainage area. Figure 1.23(b) shows that the pressure distributions become paralleled at successive time periods. Mathematically, this important condition can be expressed as:

$$\left(\frac{\partial p}{\partial t} \right)_r = \text{constant} \qquad [1.2.113]$$

The "constant" referred to in the above equation can be obtained from a simple material balance using the definition of the compressibility, assuming no free gas production, thus:

$$c = \frac{-1}{V} \frac{dV}{dp}$$

Rearranging:

$$cV\,dp = -dV$$

Differentiating with respect to time t:

$$cV \frac{dp}{dt} = -\frac{dV}{dt} = q$$

or:

$$\frac{dp}{dt} = -\frac{q}{cV}$$

Expressing the pressure decline rate dp/dt in the above relation in psi/hr gives:

$$\frac{dp}{dt} = -\frac{q}{24cV} = -\frac{Q_o B_o}{24cV} \qquad [1.2.114]$$

where:

$$q = \text{flow rate, bbl/day}$$
$$Q_o = \text{flow rate, STB/day}$$
$$dp/dt = \text{pressure decline rate, psi/hr}$$
$$V = \text{pore volume, bbl}$$

For a radial drainage system, the pore volume is given by:

$$V = \frac{\pi r_e^2 h \phi}{5.615} = \frac{Ah\phi}{5.615} \qquad [1.2.115]$$

where:

$$A = \text{drainage area, ft}^2$$

Combining Equation 1.2.115 with 1.2.114 gives:

$$\frac{dp}{dt} = -\frac{0.23396q}{c_t(\pi r_e^2)h\phi} = \frac{-0.23396q}{c_t Ah\phi} = \frac{-0.23396q}{c_t(\text{pore volume})} \qquad [1.2.116]$$

Examining Equation 1.2.116 reveals the following important characteristics of the behavior of the pressure decline rate
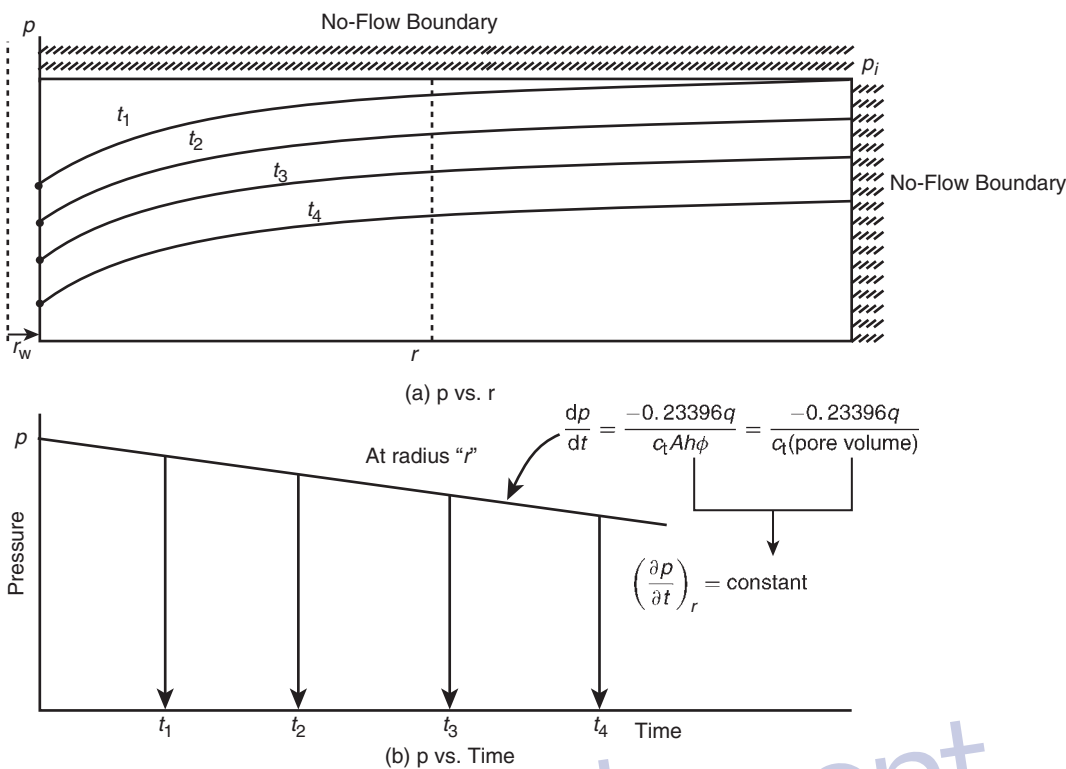
Figure 1.23 *Semisteady-state flow regime.*

dp/dt during the semisteady-state flow:

- the reservoir pressure declines at a higher rate with increasing fluid production rate;
- the reservoir pressure declines at a slower rate for reservoirs with higher total compressibility coefficients;
- the reservoir pressure declines at a lower rate for reservoirs with larger pore volumes.

And in the case of water influx with an influx rate of e_w bbl/day, the equation can be modified as:

$$\frac{dp}{dt} = \frac{-0.23396q + e_w}{c_t(\text{pore volume})}$$

Example 1.16 An oil well is producing at constant oil flow rate of 120 STB/day under a semisteady-state flow regime. Well testing data indicates that the pressure is declining at a constant rate of 0.04655 psi/hr. The following addition data is available:

$$h = 72 \text{ ft}, \qquad \phi = 25\%,$$
$$B_o = 1.3 \text{ bbl/STB}, \quad c_t = 25 \times 10^{-6} \text{ psi}^{-1}$$

Calculate the well drainage area.

Solution Here:
$$q = Q_o B_o = (120)(1.3) = 156 \text{ bbl/day}$$
Apply Equation 1.2.116 to solve for A:
$$\frac{dp}{dt} = -\frac{0.23396q}{c_t(\pi r_e^2)h\phi} = \frac{-0.23396q}{c_t Ah\phi} = \frac{-0.23396q}{c_t(\text{pore volume})}$$
$$-0.04655 = -\frac{0.23396(156)}{(25 \times 10^{-6})(A)(72)(0.25)}$$

$$A = 1\,742\,400 \text{ ft}^2$$

or:

$$A = 1\,742\,400/43\,560 = 40 \text{ acres}$$

Matthews et al. (1954) pointed out that once the reservoir is producing *under the semisteady-state condition*, each well will drain from within its own no-flow boundary independently of the other wells. For this condition to prevail, the pressure decline rate dp/dt must be approximately constant throughout the entire reservoir, otherwise flow would occur across the boundaries causing a readjustment in their positions. Because the pressure at every point in the reservoir is changing at the same rate, it leads to the conclusion that the average reservoir pressure is changing at the same rate. This average reservoir pressure is essentially set equal to the volumetric average reservoir pressure $\bar{p}_r$. It is the pressure that is used to perform flow calculations during the semisteady-state flowing condition. The above discussion indicates that, in principle, Equation 1.2.116 can be used to estimate the average pressure in the well drainage area $\bar{p}$ by replacing the pressure decline rate dp/dt with $(p_i - \bar{p})/t$, or:

$$p_i - \bar{p} = \frac{0.23396qt}{c_t(Ah\phi)}$$

or:

$$\bar{p} = p_i - \left[\frac{0.23396q}{c_t(Ah\phi)}\right]t \qquad [1.2.117]$$

Note that the above expression is essentially an equation of a straight line, with a slope of m\ and intercept of p_i, as

expressed by:

$$\bar{p} = a + m^\setminus t$$

$$m^\setminus = -\left[\frac{0.23396q}{c_t(Ah\phi)}\right] = -\left[\frac{0.23396q}{c_t(\text{pore volume})}\right]$$

$$a = p_i$$

Equation 1.2.117 indicates that the average reservoir pressure, after producing a cumulative oil production of N_p STB, can be roughly approximated by:

$$\bar{p} = p_i - \left[\frac{0.23396 B_o N_p}{c_t(Ah\phi)}\right]$$

It should be noted that when performing material balance calculations, the volumetric average pressure of the entire reservoir is used to calculate the fluid properties. This pressure can be determined from the individual well drainage properties as follows:

$$\bar{p}_r = \frac{\sum_j (\bar{p}V)_j}{\sum_j V_j}$$

in which:

V_j = pore volume of the jth well drainage volume
$(\bar{p})_j$ = volumetric average pressure *within the jth drainage volume*

Figure 1.24 illustrates the concept of the volumetric average pressure. In practice, the V_i are difficult to determine and, therefore, it is common to use individual well flow rates q_i in determining the average reservoir pressure from individual well average drainage pressure:

$$\bar{p}_r = \frac{\sum_j (\bar{p}q)_j}{\sum_j q_j}$$

The flow rates are measured on a routing basis throughout the lifetime of the field, thus facilitating the calculation of the volumetric average reservoir pressure $\bar{p}_r$. Alternatively, the average reservoir pressure can be expressed in terms of the individual well average drainage pressure decline rates and fluid flow rates by:

$$\bar{p}_r = \frac{\sum_j [(\bar{p}q)_j/(\partial \bar{p}/\partial t)_j]}{\sum_j [q_j/(\partial \bar{p}/\partial t)_j]} \qquad [1.2.118]$$

$$\bar{p}_r = \frac{\sum_i (\bar{p}_{ri} q_i)}{\sum_i q_i}$$

$$\bar{p}_r = \frac{\sum_j [(\bar{p}q)_j/(\partial \bar{p}/\partial t)_j]}{\sum_j [q_j/(\partial \bar{p}/\partial t)_j]}$$
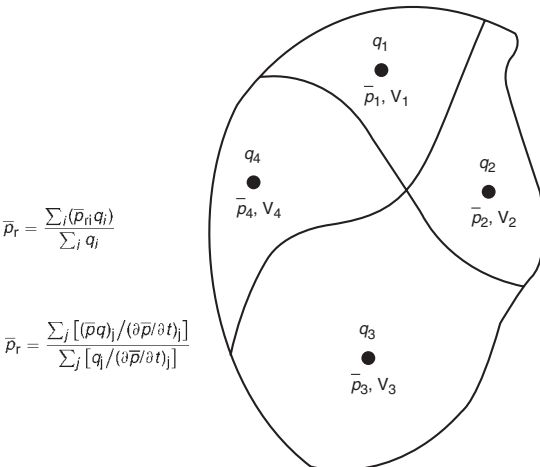
Figure 1.24 *Volumetric average reservoir pressure.*

However, since the material balance equation is usually applied at regular intervals of 3–6 months, i.e., $\Delta t = 3$–6 months, throughout the lifetime of the field, the average field pressure can be expressed in terms of the incremental net change in underground fluid withdrawal $\Delta(F)$ as:

$$\bar{p}_r = \frac{\sum_j \bar{p}_j \Delta(F)_j/\Delta \bar{p}_j}{\sum_j \Delta(F)_j/\Delta \bar{p}_j} \qquad [1.2.119]$$

where the total underground fluid withdrawal at time t and $t + \Delta t$ are given by:

$$F_t = \int_0^t [Q_o B_o + Q_w B_w + (Q_g - Q_o R_s - Q_w R_{sw})B_g]\mathrm{d}t$$

$$F_{t+\Delta t} = \int_0^{t+\Delta t} [Q_o B_o + Q_w B_w + (Q_g - Q_o R_s - Q_w R_{sw})B_g]\mathrm{d}t$$

with:

$$\Delta(F) = F_{t+\Delta t} - F_t$$

and where:

R_s = gas solubility, scf/STB
R_{sw} = gas solubility in the water, scf/STB
B_g = gas formation volume factor, bbl/scf
Q_o = oil flow rate, STB/day
q_o = oil flow rate, bbl/day
Q_w = water flow rate, STB/day
q_w = water flow rate, bbl/day
Q_g = gas flow rate, scf/day

The practical applications of using the pseudosteady-state flow condition to describe the flow behavior of the following two types of fluids are presented below:

(1) radial flow of slightly compressible fluids;
(2) radial flow of compressible fluids.

1.2.8 Radial flow of slightly compressible fluids
The diffusivity equation as expressed by Equation 1.2.61 for the transient flow regime is:

$$\frac{\partial^2 p}{\partial r^2} + \frac{1}{r}\frac{\partial p}{\partial r} = \left(\frac{\phi \mu c_t}{0.000264k}\right)\frac{\partial p}{\partial t}$$

For the semisteady-state flow, the term $\partial p/\partial t$ is constant and is expressed by Equation 1.2.116. Substituting Equation 1.2.116 into the diffusivity equation gives:

$$\frac{\partial^2 p}{\partial r^2} + \frac{1}{r}\frac{\partial p}{\partial r} = \left(\frac{\phi \mu c_t}{0.000264k}\right)\left(\frac{-0.23396q}{c_t Ah\phi}\right)$$

or:

$$\frac{\partial^2 p}{\partial r^2} + \frac{1}{r}\frac{\partial p}{\partial r} = \frac{-887.22q\mu}{Ahk}$$

This expression can be expressed as:

$$\frac{1}{r}\frac{\partial}{\partial r}\left(r\frac{\partial p}{\partial r}\right) = -\frac{887.22q\mu}{(\pi r_e^2)hk}$$

Integrating this equation gives:

$$r\frac{\partial p}{\partial r} = -\frac{887.22q\mu}{(\pi r_e^2)hk}\left(\frac{r^2}{2}\right) + c_1$$

where c_1 is the constant of integration and can be evaluated by imposing the outer no-flow boundary condition (i.e., $(\partial p/\partial r)_{re} = 0$) on the above relation, to give:

$$c_1 = \frac{141.2q\mu}{\pi hk}$$

Combining these two expressions gives:

$$\frac{\partial p}{\partial r} = \frac{141.2q\mu}{hk}\left(\frac{1}{r} - \frac{r}{r_e^2}\right)$$

Integrating again:

$$\int_{p_{wf}}^{p_i} dp = \frac{141.2q\mu}{hk} \int_{rw}^{re} \left(\frac{1}{r} - \frac{r}{r_e^2} \right) dr$$

Performing the above integration and assuming r_w^2/r_e^2 is negligible gives:

$$(p_i - p_{wf}) = \frac{141.2q\mu}{kh} \left[\ln\left(\frac{r_e}{r_w} \right) - \frac{1}{2} \right]$$

A more appropriate form of the above is to solve for the flow rate as expressed in STB/day, to give:

$$Q = \frac{0.00708kh\,(p_i - p_{wf})}{\mu B \left[\ln\left(r_e/r_w \right) - 0.5 \right]} \qquad [1.2.120]$$

where:

Q = flow rate, STB/day
B = formation volume factor, bbl/STB
k = permeability, md

The volumetric average pressure in the well drainage area $\bar{p}$ is commonly used in calculating the liquid flow rate under the semisteady-state flowing condition. Introducing $\bar{p}$ into Equation 1.2.120 gives:

$$Q = \frac{0.00708kh\,(\bar{p} - p_{wf})}{\mu B \left[\ln\left(r_e/r_w \right) - 0.75 \right]} = \frac{(\bar{p} - p_{wf})}{141.2\mu B \left[\ln\left(r_e/r_w \right) - 0.75 \right]}$$

$$[1.2.121]$$

Note that:

$$\ln\left(\frac{r_e}{r_w} \right) - 0.75 = \ln\left(\frac{0.471 r_e}{r_w} \right)$$

The above observation suggests that the volumetric average pressure $\bar{p}$ occur at about 47% of the drainage radius during the semisteady-state condition. That is:

$$Q = \frac{0.00708kh\,(\bar{p} - p_{wf})}{\mu B \left[\ln\left(0.471 r_e/r_w \right) \right]}$$

It should be pointed out that the pseudosteady-state flow occurs regardless of the geometry of the reservoir. Irregular geometries also reach this state when they have been produced long enough for the entire drainage area to be affected.

Rather than developing a separate equation for the geometry of each drainage area, Ramey and Cobb (1971) introduced a correction factor called the shape factor C_A which is designed to account for the deviation of the drainage area from the ideal circular form. The shape factor, as listed in Table 1.4, accounts also for the location of the well within the drainage area. Introducing C_A into Equation 1.2.121 and solving for p_{wf} gives the following two solutions:

(1) In terms of the volumetric average pressure $\bar{p}$:

$$p_{wf} = \bar{p} - \frac{162.6QB\mu}{kh} \log\left(\frac{2.2458A}{C_A r_w^2} \right) \qquad [1.2.122]$$

(2) In terms of the initial reservoir pressure, p_i, recall Equation 1.2.117 which shows the changes of the average reservoir pressure $\bar{p}$ as a function of time and initial reservoir pressure p_i:

$$\bar{p} = p_i - \frac{0.23396qt}{c_t Ah\phi}$$

Combining this equation with Equation 1.2.122 gives:

$$p_{wf} = \left(p_i - \frac{0.23396QBt}{Ah\phi c_t} \right) - \frac{162.6QB\mu}{kh} \log\left(\frac{2.2458A}{C_A r_w^2} \right)$$

$$[1.2.123]$$

where:

k = permeability, md
A = drainage area, ft^2
C_A = shape factor
Q = flow rate, STB/day
t = time, hours
c_t = total compressibility coefficient, psi^{-1}

Equation 1.2.123 can be slightly rearranged as:

$$p_{wf} = \left[p_i - \frac{162.6QB\mu}{kh} \log\left(\frac{2.2458A}{C_A r_w^2} \right) \right] - \left(\frac{0.23396QB}{Ah\phi c_t} \right) t$$

The above expression indicates that under semisteady-state flow and constant flow rate, it can be expressed as an equation of a straight line:

$$p_{wf} = a_{pss} + m_{pss}t$$

with a_{pss} and m_{pss} as defined by:

$$a_{pss} = \left[p_i - \frac{162.6QB\mu}{kh} \log\left(\frac{2.2458A}{C_A r_w^2} \right) \right]$$

$$m_{pss} = -\left(\frac{0.23396QB}{c_t\,(Ah\phi)} \right) = -\left(\frac{0.23396QB}{c_t\,(\text{pore volume})} \right)$$

It is obvious that during the pseudosteady (semisteady)-state flow condition, a plot of the bottom-hole flowing pressure p_{wf} versus time t would produce a straight line with a negative slope of m_{pss} and intercept of a_{pss}.

A more generalized form of Darcy's equation can be developed by rearranging Equation 1.2.122 and solving for Q to give:

$$Q = \frac{kh(\bar{p} - p_{wf})}{162.6B\mu \log\left(2.2458A/C_A r_w^2 \right)} \qquad [1.2.124]$$

It should be noted that if Equation 1.2.124 is applied to a circular reservoir of radius r_e, then:

$$A = \pi r_e^2$$

and the shape factor for a circular drainage area as given in Table 1.4 as:

$$C_A = 31.62$$

Substituting in Equation 1.2.124, it reduces to:

$$Q = \frac{0.00708kh(\bar{p} - p_{wf})}{B\mu[\ln(r_e/r_w) - 0.75]}$$

This equation is identical to that of Equation 1.2.123.

Example 1.17 An oil well is developed on the center of a 40 acre square-drilling pattern. The well is producing at a constant flow rate of 100 STB/day under a semisteady-state condition. The reservoir has the following properties:

$\phi = 15\%$, $\quad\quad h = 30$ ft, $\quad\quad k = 20$ md

$\mu = 1.5$ cp, $\quad\quad B_o = 1.2$ bbl/STB, $\quad c_t = 25 \times 10^{-6}$ psi^{-1}

$p_i = 4500$ psi, $\quad r_w = 0.25$ ft, $\quad\quad A = 40$ acres

(a) Calculate and plot the bottom-hole flowing pressure as a function of time.
(b) Based on the plot, calculate the pressure decline rate. What is the decline in the average reservoir pressure from $t = 10$ to $t = 200$ hours?

Solution

(a) For the p_{wf} calculations:

Step 1. From Table 1.4, determine C_A:

$$C_A = 30.8828$$

Table 1.4 Shape factors for various single-well drainage areas (After Earlougher, R, *Advances in Well Test Analysis*, permission to publish by the SPE, copyright SPE, 1977)

In bounded reservoirs	C_A	$\ln C_A$	$\frac{1}{2}\ln\left(\frac{2.2458}{C_A}\right)$	Exact for $t_{DA}>$	Less than 1% error for $t_{DA}>$	Use infinite system solution with less than 1% error for $t_{DA}>$
(circle, well centered)	31.62	3.4538	−1.3224	0.1	0.06	0.10
(hexagon, well centered)	31.6	3.4532	−1.3220	0.1	0.06	0.10
(triangle)	27.6	3.3178	−1.2544	0.2	0.07	0.09
(60° parallelogram)	27.1	3.2995	−1.2452	0.2	0.07	0.09
(triangle, 1/3)	21.9	3.0865	−1.1387	0.4	0.12	0.08
(triangle, 3:4)	0.098	−2.3227	+1.5659	0.9	0.60	0.015
(square, well centered)	30.8828	3.4302	−1.3106	0.1	0.05	0.09
(square, quartered)	12.9851	2.5638	−0.8774	0.7	0.25	0.03
(square, upper cell)	10132	1.5070	−0.3490	0.6	0.30	0.025
(square, lower rows)	3.3351	1.2045	−0.1977	0.7		0.25 0.01
(2:1 rectangle, centered)	21.8369	3.0836	−1.1373	0.3	0.15	0.025
(2:1 rectangle)	10.8374	2.3830	−0.7870	0.4	0.15	0.025
(2:1 rectangle)	10141	1.5072	−0.3491	1.5	0.50	0.06
(2:1 rectangle)	2.0769	0.7309	−0.0391	1.7	0.50	0.02
(2:1 rectangle)	3.1573	1.1497	−0.1703	0.4	0.15	0.005
(2:1 rectangle)	0.5813	−0.5425	+0.6758	2.0	0.60	0.02
(2:1 rectangle)	0.1109	−2.1991	+1.5041	3.0	0.60	0.005
(4:1 rectangle)	5.3790	1.6825	−0.4367	0.8	0.30	0.01
(4:1 rectangle)	2.6896	0.9894	−0.0902	0.8	0.30	0.01
(4:1 rectangle)	0.2318	−1.4619	+1.1355	4.0	2.00	0.03
(4:1 rectangle)	0.1155	−2.1585	+1.4838	4.0	2.00	0.01
(4:1 rectangle)	2.3606	0.8589	−0.0249	1.0	0.40	0.025

In vertically fractured reservoirs use $(x_e/x_f)^2$ in place of A/r_w^2, for fractured systems

In bounded reservoirs	C_A	$\ln C_A$	$\frac{1}{2}\ln\left(\frac{2.2458}{C_A}\right)$	Exact for $t_{DA}>$	Less than 1% error for $t_{DA}>$	Use infinite system solution with less than 1% error for $t_{DA}>$
$0.1 = x_f/x_e$	2.6541	0.9761	−0.0835	0.175	0.08	cannot use
0.2	2.0348	0.7104	+0.0493	0.175	0.09	cannot use
0.3	1.9986	0.6924	+0.0583	0.175	0.09	cannot use
0.5	1.6620	0.5080	+0.1505	0.175	0.09	cannot use
0.7	1.3127	0.2721	+0.2685	0.175	0.09	cannot use
1.0	0.7887	−0.2374	+0.5232	0.175	0.09	cannot use

In water-drive reservoirs

(circle, well centered)	19.1	2.95	−1.07	–	–	–

In reservoirs of unknown production character

(circle, well centered)	25.0	3.22	−1.20	–	–	–

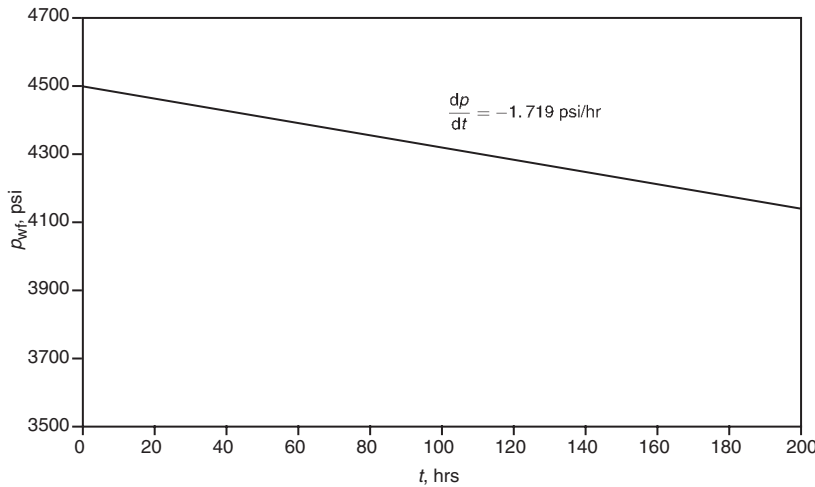$$\frac{\mathrm{d}p}{\mathrm{d}t} = -1.719 \text{ psi/hr}$$

Figure 1.25 *Bottom-hole flowing pressure as a function of time.*

Step 2. Convert the area A from acres to ft^2:

$$A = (40)(43\,560) = 1\,742\,400 \text{ ft}^2$$

Step 3. Apply Equation 1.2.123:

$$p_{\mathrm{wf}} = \left(p_{\mathrm{i}} - \frac{0.23396QBt}{Ah\phi c_{\mathrm{t}}} \right)$$

$$- \frac{162.6QB\mu}{kh} \log\left(\frac{2.2458A}{1 C_A r_{\mathrm{w}}^2} \right)$$

$$= 4500 - 0.143t - 48.78 \log(2\,027\,436)$$

or:

$$p_{\mathrm{wf}} = 4192 - 0.143t$$

Step 4. Calculate p_{wf} at different assumed times, as follows:

t (hr)	$p_{\mathrm{wf}} = 4192 - 0.143t$
10	4191
20	4189
50	4185
100	4178
200	4163

Step 5. Present the results of step 4 in graphical form as shown in Figure 1.25.

(b) It is obvious from Figure 1.25 and the above calculation that the bottom-hole flowing pressure is declining at a rate of 0.143 psi/hr, or:

$$\frac{\mathrm{d}p}{\mathrm{d}t} = -0.143 \text{ psi/hr}$$

The significance of this example is that the rate of pressure decline during the pseudosteady state is the same throughout the drainage area. This means that the *average reservoir pressure*, $\bar{p}_{\mathrm{r}}$, is declining at the same rate of 0.143 psi/hr, therefore the change in $\bar{p}_{\mathrm{r}}$ from 10 to 200 hours is:

$$\Delta\bar{p}_{\mathrm{r}} = (0.143)(200 - 10) = 27.17 \text{ psi}$$

Example 1.18 An oil well is producing under a constant bottom-hole flowing pressure of 1500 psi. The current average reservoir pressure $\bar{p}_{\mathrm{r}}$ is 3200 psi. The well is developed in the center of 40 acre square-drilling pattern. Given the following additional information:

$\phi = 16\%$, $h = 15$ ft, $k = 50$ md,
$\mu = 26$ cp, $B_{\mathrm{o}} = 1.15$ bbl/STB,
$c_{\mathrm{t}} = 10 \times 10^{-6}$ psi^{-1}, $r_{\mathrm{w}} = 0.25$ ft

calculate the flow rate.

Solution
Because the volumetric average pressure is given, solve for the flow rate by applying Equation 1.2.124:

$$Q = \frac{kh\left(\bar{p} - p_{\mathrm{wf}}\right)}{162.6B\mu \log\left[\frac{2.2458A}{C_A r_{\mathrm{w}}^2}\right]}$$

$$= \frac{(50)(15)(3200 - 1500)}{(162.6)(1.15)(2.6) \log\left[\frac{2.2458(40)(43\,560)}{(30.8828)(0.25^2)}\right]}$$

$$= 416 \text{ STB/day}$$

It is interesting to note that Equation 1.2.124 can also be presented in a dimensionless form by rearranging and introducing the dimensionless time t_{D} and dimensionless pressure drop p_{D}, to give:

$$p_{\mathrm{D}} = 2\pi t_{\mathrm{D}A} + \frac{1}{2}\ln\left(\frac{2.3458A}{C_A r_{\mathrm{w}}^2}\right) + s \qquad [1.2.125]$$

with the dimensionless time based on the well drainage given by Equation 1.2.75a as:

$$t_{\mathrm{D}A} = \frac{0.0002637kt}{\phi\mu c_{\mathrm{t}}A} = t_A\left(\frac{r_{\mathrm{w}}^2}{A}\right)$$

where:

   s = skin factor (to be introduced later in the chapter)
  C_A = shape factor
 $t_{\mathrm{D}A}$ = dimensionless time based on the well drainage area πr_{e}^2.

Equation 1.2.125 suggests that during the *boundary-dominated flow*, i.e., pseudosteady state, a plot of p_D vs. t_{DA} on a Cartesian scale would produce a straight line with a slope of 2π. That is:

$$\frac{\partial p_D}{\partial t_{DA}} = 2\pi \qquad [1.2.126]$$

For a well located in a circular drainage area with no skin, i.e., $s = 0$, and taking the logarithm of both sides of Equation 1.2.125 gives:

$$\log(p_D) = \log(2\pi) + \log(t_{DA})$$

which indicates that a plot of p_D vs. t_{DA} on a log–log scale would produce a $45°$ straight line and an intercept of 2π.

1.2.9 Radial flow of compressible fluids (gases)

The radial diffusivity equation as expressed by Equation 1.2.94 was developed to study the performance of a compressible fluid under unsteady-state conditions. The equation has the following form:

$$\frac{\partial^2 m(p)}{\partial r^2} + \frac{1}{r}\frac{\partial m(p)}{\partial r} = \frac{\phi \mu c_t}{0.000264k}\frac{\partial m(p)}{\partial t}$$

For semisteady-state flow, the rate of change of the real-gas pseudopressure with respect to time is constant. That is:

$$\frac{\partial m(p)}{\partial t} = \text{constant}$$

Using the same technique identical to that described previously for liquids gives the following exact solution to the diffusivity equation:

$$Q_g = \frac{kh\left[m(\bar{p}_r) - m(p_{wf})\right]}{1422T\left[\ln\left(\dfrac{r_e}{r_w}\right) - 0.75\right]} \qquad [1.2.127]$$

where:

Q_g = gas flow rate, Mscf/day
T = temperature, °R
k = permeability, md

Two approximations to the above solution are widely used. These are:

(1) the pressure-squared approximation;
(2) the pressure approximation.

Pressure-squared method

As outlined previously, this method provides us with compatible results to that of the exact solution approach when $p < 2000$ psi. The solution has the following familiar form:

$$Q_g = \frac{kh\left(\bar{p}_r^2 - p_{wf}^2\right)}{1422T\bar{\mu}\bar{Z}\left(\ln\left(\dfrac{r_e}{r_w}\right) - 0.75\right)} \qquad [1.2.128]$$

The gas properties $\bar{Z}$ and $\bar{\mu}$ are evaluated at:

$$\bar{p} = \sqrt{\frac{\bar{p}_r^2 + p_{wf}^2}{2}}$$

where:

Q_g = gas flow rate, Mscf/day
T = temperature, °R
k = permeability, md

Pressure approximation method

This approximation method is applicable at $p > 3000$ psi and has the following mathematical form:

$$Q_g = \frac{kh\left(\bar{p}_r - p_{wf}\right)}{1422\bar{\mu}\bar{B}_g\left[\ln\left(r_e/r_w\right) - 0.75\right]} \qquad [1.2.129]$$

with the gas properties evaluated at:

$$\bar{p} = \frac{\bar{p}_r + p_{wf}}{2}$$

where:

Q_g = gas flow rate, Mscf/day
k = permeability, md
$\bar{B}_g$ = gas formation volume factor at a average pressure, bbl/scf

The gas formation volume factor is given by the following expression:

$$B_g = 0.00504\frac{\bar{Z}T}{\bar{p}}$$

In deriving the flow equations, the following two main assumptions were made:

(1) uniform permeability throughout the drainage area;
(2) laminar (viscous) flow.

Before using any of the previous mathematical solutions to the flow equations, the solution must be modified to account for the possible deviation from the above two assumptions. Introducing the following two correction factors into the solution of the flow equation can eliminate these two assumptions:

(1) skin factor;
(2) turbulent flow factor.

1.2.10 Skin factor

It is not unusual during drilling, completion, or workover operations for materials such as mud filtrate, cement slurry, or clay particles to enter the formation and reduce the permeability around the wellbore. This effect is commonly referred to as "wellbore damage" and the region of altered permeability is called the "skin zone." This zone can extend from a few inches to several feet from the wellbore. Many other wells are stimulated by acidizing or fracturing, which in effect increases the permeability near the wellbore. Thus, the permeability near the wellbore is always different from the permeability away from the well where the formation has not been affected by drilling or stimulation. A schematic illustration of the skin zone is shown in Figure 1.26.
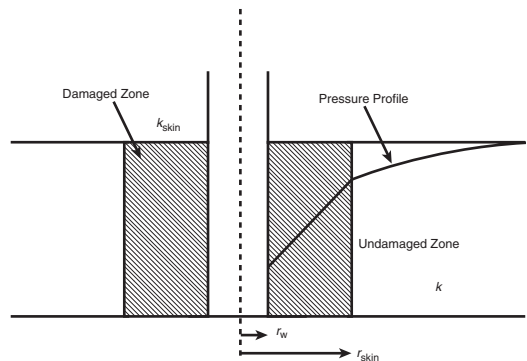

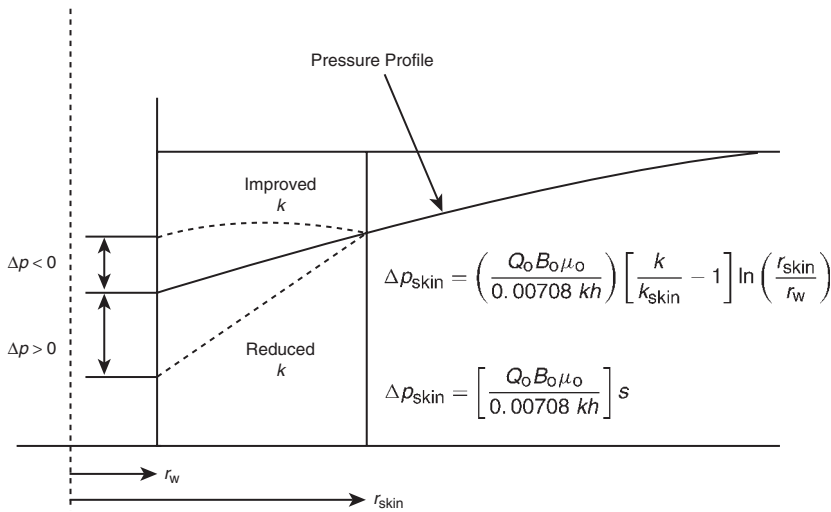**Figure 1.26** *Near-wellbore skin effect.*

Figure 1.27 *Representation of positive and negative skin effects.*

The effect of the skin zone is to alter the pressure distribution around the wellbore. In case of wellbore damage, the skin zone causes an additional pressure loss in the formation. In case of wellbore improvement, the opposite to that of wellbore damage occurs. If we refer to the pressure drop in the skin zone as Δp_{skin}, Figure 1.27 compares the differences in the skin zone pressure drop for three possible outcomes.

- *First outcome*: $\Delta p_{skin} > 0$, which indicates an additional pressure drop due to wellbore damage, i.e., $k_{skin} < k$.
- *Second outcome*: $\Delta p_{skin} < 0$, which indicates less pressure drop due to wellbore improvement, i.e., $k_{skin} > k$.
- *Third outcome*: $\Delta p_{skin} = 0$, which indicates no changes in the wellbore condition, i.e., $k_{skin} = k$.

Hawkins (1956) suggested that the permeability in the skin zone, i.e., k_{skin}, is uniform and the pressure drop across the zone can be approximated by Darcy's equation. Hawkins proposed the following approach:

$$\Delta p_{skin} = \left[\begin{array}{c} \Delta p \text{ in skin zone} \\ \text{due to } k_{skin} \end{array} \right] - \left[\begin{array}{c} \Delta p \text{ in the skin zone} \\ \text{due to } k \end{array} \right]$$

Applying Darcy's equation gives:

$$(\Delta p)_{skin} = \left(\frac{Q_o B_o \mu_o}{0.00708 h k_{skin}} \right) \ln \left(\frac{r_{skin}}{r_w} \right)$$
$$- \left(\frac{Q_o B_o \mu_o}{0.00708 h k} \right) \ln \left(\frac{r_{skin}}{r_w} \right)$$

or:

$$\Delta p_{skin} = \left(\frac{Q_o B_o \mu_o}{0.00708 k h} \right) \left[\frac{k}{k_{skin}} - 1 \right] \ln \left(\frac{r_{skin}}{r_w} \right)$$

where:

k = permeability of the formation, md
k_{skin} = permeability of the skin zone, md

The above expression for determining the additional pressure drop in the skin zone is commonly expressed in the following form:

$$\Delta p_{skin} = \left(\frac{Q_o B_o \mu_o}{0.00708 k h} \right) s = 141.2 \left(\frac{Q_o B_o \mu_o}{k h} \right) s \quad [1.2.130]$$

where s is called the skin factor and defined as:

$$s = \left[\frac{k}{k_{skin}} - 1 \right] \ln \left(\frac{r_{skin}}{r_w} \right) \quad [1.2.131]$$

Depending on the permeability ratio k/k_{skin} and if $\ln(r_{skin}/r_w)$ is always positive, there are only three possible outcomes in evaluating the skin factor s:

(1) *Positive skin factor, $s > 0$*: When the damaged zone near the wellbore exists, k_{skin} is less than k and hence s is a positive number. The magnitude of the skin factor increases as k_{skin} decreases and as the depth of the damage r_{skin} increases.
(2) *Negative skin factor, $s < 0$*: When the permeability around the well k_{skin} is higher than that of the formation k, a negative skin factor exists. This negative factor indicates an improved wellbore condition.
(3) *Zero skin factor, $s = 0$*: Zero skin factor occurs when no alternation in the permeability around the wellbore is observed, i.e., $k_{skin} = k$.

Equation 1.2.131 indicates that a negative skin factor will result in a negative value of Δp_{skin}. This implies that a stimulated well will require less pressure drawdown to produce at rate q than an equivalent well with uniform permeability.

The proposed modification of the previous flow equation is based on the concept that the actual total pressure drawdown will increase or decrease by an amount Δp_{skin}. Assuming that $(\Delta p)_{ideal}$ represents the pressure drawdown for a drainage area with a uniform permeability k, then:

$$(\Delta p)_{actual} = (\Delta p)_{ideal} + (\Delta p)_{skin}$$

or:

$$(p_i - p_{wf})_{actual} = (p_i - p_{wf})_{ideal} + \Delta p_{skin} \quad [1.2.132]$$

The above concept of modifying the flow equation to account for the change in the pressure drop due the wellbore skin effect can be applied to the previous three flow regimes:

(1) steady-state flow;
(2) unsteady-state (transient) flow;
(3) pseudosteady (semisteady)-state flow.

Basically, Equation 1.2.132 can be applied as follows.

Steady state radial flow (accounting for the skin factor)
Substituting Equations 1.2.15 and 1.2.130 into Equation 1.2.132, gives:

$$(\Delta p)_{\text{actual}} = (\Delta p)_{\text{ideal}} + (\Delta p)_{\text{skin}}$$

$$(p_{\text{i}} - p_{\text{wf}})_{\text{actual}} = \left(\frac{Q_{\text{o}}B_{\text{o}}\mu_{\text{o}}}{0.00708kh} \right) \ln \left(\frac{r_{\text{e}}}{r_{\text{w}}} \right) + \left(\frac{Q_{\text{o}}B_{\text{o}}\mu_{\text{o}}}{0.00708kh} \right) s$$

Solving for the flow rate gives:

$$Q_{\text{o}} = \frac{0.00708kh\,(p_{\text{i}} - p_{\text{wf}})}{\mu_{\text{o}}B_{\text{o}} \left[\ln \dfrac{r_{\text{e}}}{r_{\text{w}}} + s \right]} \qquad [1.2.133]$$

where:

Q_{o} = oil flow rate, STB/day
k = permeability, md
h = thickness, ft
s = skin factor
B_{o} = oil formation volume factor, bbl/STB
μ_{o} = oil viscosity, cp
p_{i} = initial reservoir pressure, psi
p_{wf} = bottom-hole flowing pressure, psi

Unsteady-state radial flow (accounting for the skin factor)
For slightly compressible fluids Combining Equations 1.2.71 and 1.2.130 with that of 1.2.132 yields:

$$(\Delta p)_{\text{actual}} = (\Delta p)_{\text{ideal}} + (\Delta p)_{\text{skin}}$$

$$p_{\text{i}} - p_{\text{wf}} = 162.6 \left(\frac{Q_{\text{o}}B_{\text{o}}\mu_{\text{o}}}{kh} \right) \left[\log \frac{kt}{\phi \mu c_{\text{t}} r_{\text{w}}^2} - 3.23 \right]$$

$$+ 141.2 \left(\frac{Q_{\text{o}}B_{\text{o}}\mu_{\text{o}}}{kh} \right) s$$

or:

$$p_{\text{i}} - p_{\text{wf}} = 162.6 \left(\frac{Q_{\text{o}}B_{\text{o}}\mu_{\text{o}}}{kh} \right) \left[\log \frac{kt}{\phi \mu c_{\text{t}} r_{\text{w}}^2} - 3.23 + 0.87s \right]$$
$$[1.2.134]$$

For compressible fluids A similar approach to that of the above gives:

$$m(p_{\text{i}}) - m(p_{\text{wf}}) = \frac{1637 Q_{\text{g}} T}{kh} \left[\log \frac{kt}{\phi \mu c_{\text{t_i}} r_{\text{w}}^2} - 3.23 + 0.87s \right]$$
$$[1.2.135]$$

and in terms of the pressure-squared approach, the difference $[m(p_{\text{i}}) - m(p_{\text{wf}})]$ can be replaced with:

$$m(p_{\text{i}}) - m(p_{\text{wf}}) = \int_{p_{\text{wf}}}^{p_{\text{i}}} \frac{2p}{\mu Z} \, \mathrm{d}p = \frac{p_{\text{i}}^2 - p_{\text{wf}}^2}{\overline{\mu Z}}$$

to give:

$$p_{\text{i}}^2 - p_{\text{wf}}^2 = \frac{1637 Q_{\text{g}} T \overline{Z}\overline{\mu}}{kh} \left[\log \frac{kt}{\phi \mu_{\text{i}} c_{\text{ti}} r_{\text{w}}^2} - 3.23 + 0.87s \right]$$
$$[1.2.136]$$

where:

Q_{g} = gas flow rate, Mscf/day
T = temperature, °R
k = permeability, md
t = time, hours

Pseudosteady-state flow (accounting for the skin factor)
For slightly compressible fluids Introducing the skin factor into Equation 1.2.123 gives:

$$Q_{\text{o}} = \frac{0.00708kh\,(\bar{p}_{\text{r}} - p_{\text{wf}})}{\mu_{\text{o}}B_{\text{o}} \left[\ln \left(\dfrac{r_{\text{e}}}{r_{\text{w}}} \right) - 0.75 + s \right]} \qquad [1.2.137]$$

For compressible fluids

$$Q_{\text{g}} = \frac{kh \left[m(\bar{p}_{\text{r}}) - m(p_{\text{wf}}) \right]}{1422T \left[\ln \left(\dfrac{r_{\text{e}}}{r_{\text{w}}} \right) - 0.75 + s \right]} \qquad [1.2.138]$$

or in terms of the pressure-squared approximation:

$$Q_{\text{g}} = \frac{kh \left(p_{\text{r}}^2 - p_{\text{wf}}^2 \right)}{1422T \overline{\mu}\overline{Z} \left[\ln \left(\dfrac{r_{\text{e}}}{r_{\text{w}}} \right) - 0.75 + s \right]} \qquad [1.2.139]$$

where :

Q_{g} = gas flow rate, Mscf/day
k = permeability, md
T = temperature, °R
$\overline{\mu}_{\text{g}}$ = gas viscosity at average pressure $\bar{p}$, cp
$\overline{Z}_{\text{g}}$ = gas compressibility factor at average pressure $\bar{p}$

Example 1.19 Calculate the skin factor resulting from the invasion of the drilling fluid to a radius of 2 ft. The permeability of the skin zone is estimated at 20 md as compared with the unaffected formation permeability of 60 md. The wellbore radius is 0.25 ft.

Solution
Apply Equation 1.2.131 to calculate the skin factor:

$$s = \left[\frac{60}{20} - 1 \right] \ln \left(\frac{2}{0.25} \right) = 4.16$$

Matthews and Russell (1967) proposed an alternative treatment to the skin effect by introducing the "effective or apparent wellbore radius" r_{wa} that accounts for the pressure drop in the skin. They define r_{wa} by the following equation:

$$r_{\text{wa}} = r_{\text{w}} \mathrm{e}^{-s} \qquad [1.2.140]$$

All of the ideal radial flow equations can be also modified for the skin by simply replacing the wellbore radius r_{w} with that of the apparent wellbore radius r_{wa}. For example, Equation 1.2.134 can be equivalently expressed as:

$$p_{\text{i}} - p_{\text{wf}} = 162.6 \left(\frac{Q_{\text{o}}B_{\text{o}}\mu_{\text{o}}}{kh} \right) \left[\log \left(\frac{kt}{\phi \mu c_{\text{t}} r_{\text{wa}}^2} \right) - 3.23 \right]$$
$$[1.2.141]$$

1.2.11 Turbulent flow factor

All of the mathematical formulations presented so far are based on the assumption that laminar flow conditions are observed during flow. During radial flow, the flow velocity increases as the wellbore is approached. This increase in the velocity might cause the development of turbulent flow around the wellbore. If turbulent flow does exist, it is most likely to occur with gases and causes an additional pressure drop similar to that caused by the skin effect. The term "non-Darcy flow" has been adopted by the industry to describe the additional pressure drop due to the turbulent (non-Darcy) flow.

Referring to the additional real-gas pseudopressure drop due to non-Darcy flow as $\Delta \psi_{\text{non-Darcy}}$, the total (actual) drop is given by:

$$(\Delta \psi)_{\text{actual}} = (\Delta \psi)_{\text{ideal}} + (\Delta \psi)_{\text{skin}} + (\Delta \psi)_{\text{non-Darcy}}$$

Wattenbarger and Ramey (1968) proposed the following expression for calculating $(\Delta \psi)_{\text{non-Darcy}}$:

$$(\Delta \psi)_{\text{non-Darcy}} = 3.161 \times 10^{-12} \left[\frac{\beta T \gamma_{\text{g}}}{\mu_{\text{gw}} h^2 r_{\text{w}}} \right] Q_{\text{g}}^2 \qquad [1.2.142]$$

This equation can be expressed in a more convenient form as;

$$(\Delta \psi)_{\text{non-Darcy}} = F Q_{\text{g}}^2 \qquad [1.2.143]$$

where F is called the "non-Darcy flow coefficient" and given by:

$$F = 3.161 \times 10^{-12} \left[\frac{\beta T \gamma_g}{\mu_{gw} h^2 r_w} \right]$$ [1.2.144]

where:

Q_g = gas flow rate, Mscf/day
μ_{gw} = gas viscosity as evaluated at p_{wf}, cp
γ_g = gas specific gravity
h = thickness, ft
F = non-Darcy flow coefficient, $psi^2/cp/(Mscf/day)^2$
β = turbulence parameter

Jones (1987) proposed a mathematical expression for estimating the turbulence parameter β as:

$$\beta = 1.88(10^{-10})(k)^{-1.47}(\phi)^{-0.53}$$ [1.2.145]

where:

k = permeability, md
ϕ = porosity, fraction

The term FQ_g^2 can be included in all the compressible gas flow equations in the same way as the skin factor. This non-Darcy term is interpreted as a *rate-dependent skin*. The modification of the gas flow equations to account for the turbulent flow condition is given below for the three flow regimes:

(1) unsteady-state (transient) flow;
(2) semisteady-state flow;
(3) steady-state flow.

Unsteady-state radial flow
The gas flow equation for an unsteady-state flow is given by Equation 1.2.135 and can be modified to include the additional drop in the real-gas potential, as:

$$m(p_i) - m(p_{wf}) = \left(\frac{1637 Q_g T}{kh} \right) \left[\log \left(\frac{kt}{\phi \mu_i c_{ti} r_w^2} \right) \right.$$
$$\left. - 3.23 + 0.87s \right] + FQ_g^2$$ [1.2.146]

Equation 1.2.146 is commonly written in a more convenient form as:

$$m(p_i) - m(p_{wf}) = \left(\frac{1637 Q_g T}{kh} \right) \left[\log \left(\frac{kt}{\phi \mu_i c_{ti} r_w^2} \right) \right.$$
$$\left. - 3.23 + 0.87s + 0.87 D Q_g \right]$$ [1.2.147]

where the term DQ_g is interpreted as the rate-dependent skin factor. The coefficient D is called the "inertial or turbulent flow factor" and given by:

$$D = \frac{Fkh}{1422T}$$ [1.2.148]

The true skin factor s which reflects the formation damage or stimulation is usually combined with the non-Darcy rate-dependent skin and labeled as the apparent or total skin factor $s^\backslash$. That is:

$$s^\backslash = s + DQ_g$$ [1.2.149]

or:

$$m(p_i) - m(p_{wf}) = \left(\frac{1637 Q_g T}{kh} \right) \left[\log \left(\frac{kt}{\phi \mu_i c_{ti} r_w^2} \right) \right.$$
$$\left. - 3.23 + 0.87s^\backslash \right]$$ [1.2.150]

Equation 1.2.50 can be expressed in the pressure-squared approximation form as:

$$p_i^2 - p_{wf}^2 = \left(\frac{1637 Q_g T \overline{Z} \overline{\mu}}{kh} \right) \left[\log \frac{kt}{\phi \mu_i c_{ti} r_w^2} - 3.23 + 0.87 s^\backslash \right]$$ [1.2.151]

where:

Q_g = gas flow rate, Mscf/day
t = time, hours
k = permeability, md
μ_i = gas viscosity as evaluated at p_i, cp

Semisteady-state flow
Equation 1.2.138 and 1.2.139 can be modified to account for the non-Darcy flow as follows:

$$Q_g = \frac{kh \left[m(\overline{p}_r) - m(p_{wf}) \right]}{1422T \left[\ln \left(\frac{r_e}{r_w} \right) - 0.75 + s + DQ_g \right]}$$ [1.2.152]

or in terms of the pressure-squared approach:

$$Q_g = \frac{kh \left(\overline{p}_r^2 - p_{wf}^2 \right)}{1422T \overline{\mu} \overline{Z} \left[\ln \left(\frac{r_e}{r_w} \right) - 0.75 + s + DQ_g \right]}$$ [1.2.153]

where the coefficient D is defined as:

$$D = \frac{Fkh}{1422T}$$ [1.2.154]

Steady-state flow
Similar to the above modification procedure, Equations 1.2.32 and 1.2.33 can be expressed as:

$$Q_g = \frac{kh \left[m(p_i) - m(p_{wf}) \right]}{1422T \left[\ln \left(\frac{r_e}{r_w} \right) - 0.5 + s + DQ_g \right]}$$ [1.2.155]

$$Q_g = \frac{kh \left(p_e^2 - p_{wf}^2 \right)}{1422T \overline{\mu} \overline{Z} \left[\ln \left(\frac{r_e}{r_w} \right) - 0.5 + s + DQ_g \right]}$$ [1.2.156]

Example 1.20 A gas well has an estimated wellbore damage radius of 2 feet and an estimated reduced permeability of 30 md. The formation has permeability and porosity of 55 md and 12% respectively. The well is producing at a rate of 20 MMscf/day with a gas gravity of 0.6. The following additional data is available:

$$r_w = 0.25, \ h = 20 \text{ ft}, \ T = 140°F, \ \mu_{gw} = 0.013 \text{ cp}$$

Calculate the apparent skin factor.

Solution

Step 1. Calculate skin factor from Equation 1.2.131:

$$s = \left[\frac{k}{k_{skin}} - 1 \right] \ln \left(\frac{r_{skin}}{r_w} \right)$$
$$= \left[\frac{55}{30} - 1 \right] \ln \left(\frac{2}{0.25} \right) = 1.732$$

Step 2. Calculate the turbulence parameter β by applying Equation 1.2.145:

$$\beta = 1.88(10^{-10})(k)^{-1.47}(\phi)^{-0.53}$$
$$= 1.88 \times 10^{10}(55)^{-1.47}(0.12)^{-0.53}$$
$$= 159.904 \times 10^6$$

Step 3. Calculate the non-Darcy flow coefficient from Equation 1.2.144:

$$F = 3.161 \times 10^{-12} \left[\frac{\beta T \gamma_g}{\mu_{gw} h^2 r_w} \right]$$

$$= 3.1612 \times 10^{-12} \left[\frac{159.904 \times 10^6 (600)(0.6)}{(0.013)(20)^2 (0.25)} \right]$$

$$= 0.14$$

Step 4. Calculate the coefficient D from Equation 1.2.148:

$$D = \frac{Fkh}{1422T}$$

$$= \frac{(0.14)(55)(20)}{(1422)(600)} = 1.805 \times 10^{-4}$$

Step 5. Estimate the apparent skin factor by applying Equation 1.2.149:

$$s^\backslash = s + DQ_g = 1.732 + (1.805 \times 10^{-4})(20\,000)$$

$$= 5.342$$

1.2.12 Principle of superposition

The solutions to the radial diffusivity equation as presented earlier in this chapter appear to be applicable only for describing the pressure distribution in an infinite reservoir that was caused by constant production from a single well. Since real reservoir systems usually have several wells that are operating at varying rates, a more generalized approach is needed to study the fluid flow behavior during the unsteady-state flow period.

The principle of superposition is a powerful concept that can be applied to remove the restrictions that have been imposed on various forms of solution to the transient flow equation. Mathematically the superposition theorem states that any sum of individual solutions to the diffusivity equation is also a solution to that equation. This concept can be applied to account for the following effects on the transient flow solution:

- effects of multiple wells;
- effects of rate change;
- effects of the boundary;
- effects of pressure change.

Slider (1976) presented an excellent review and discussion of the practical applications of the principle of superposition in solving a wide variety of unsteady-state flow problems.

Effects of multiple wells

Frequently, it is desired to account for the effects of more than one well on the pressure at some point in the reservoir. The superposition concept states that the total pressure drop at any point in the reservoir is the sum of the pressure changes at that point caused by the flow in each of the wells in the reservoir. In other words, we simply superimpose one effect upon another.

Consider Figure 1.28 which shows three wells that are producing at different flow rates from an infinite-acting reservoir, i.e., an unsteady-state flow reservoir. The principle of superposition states that the total pressure drop observed at any well, e.g., well 1, is:

$$(\Delta p)_{\text{total drop at well 1}} = (\Delta p)_{\text{drop due to well 1}}$$
$$+ (\Delta p)_{\text{drop due to well 2}}$$
$$+ (\Delta p)_{\text{drop due to well 3}}$$

The pressure drop at well 1 due to its own production is given by the *log approximation* to the Ei function solution
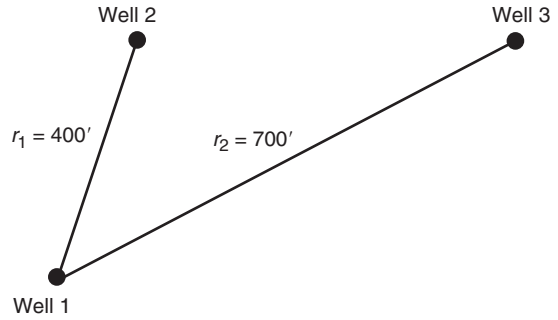
Figure 1.28 *Well layout for Example 1.21.*

presented by Equation 1.2.134, or:

$$(p_i - p_{wf}) = (\Delta p)_{\text{well1}} = \frac{162.6 Q_{o1} B_o \mu_o}{kh} \left[\log \left(\frac{kt}{\phi \mu c_t r_w^2} \right) - 3.23 + 0.87s \right]$$

where:

t = time, hours
s = skin factor
k = permeability, md
Q_{o1} = oil flow rate from well 1

The additional pressure drops at well 1 due to the production from wells 2 and 3 must be written in terms of the Ei function solution, as expressed by Equation 1.2.66, since the log approximation cannot be applied in calculating the pressure at a large distance r from the well where $x > 0.1$. Therefore:

$$p(r,t) = p_i + \left[\frac{70.6 Q_o \mu B_o}{kh} \right] \text{Ei} \left[\frac{-948 \phi \mu_o c_t r^2}{kt} \right]$$

Applying the above expression to calculate the additional pressure drop due to two wells gives:

$$(\Delta p)_{\text{drop due to well 2}} = p_i - p(r_1, t) = - \left[\frac{70.6 Q_{o1} \mu_o B_o}{kh} \right] \times \text{Ei} \left[\frac{-948 \phi \mu_o c_t r_1^2}{kt} \right]$$

$$(\Delta p)_{\text{drop due to well 3}} = p_i - p(r_2, t) = - \left[\frac{70.6 Q_{o2} \mu_o B_o}{kh} \right] \times \text{Ei} \left[\frac{-948 \phi \mu_o c_t r_2^2}{kt} \right]$$

The total pressure drop is then given by:

$$(p_i - p_{wf})_{\text{total at well 1}} = \left(\frac{162.6 Q_{o1} B_o \mu_o}{kh} \right) \left[\log \left(\frac{kt}{\phi \mu c_t r_w^2} \right) - 3.23 + 0.87s \right]$$
$$- \left(\frac{70.6 Q_{o2} B_o \mu_o}{kh} \right) \text{Ei} \left[- \frac{948 \phi \mu c_t r_1^2}{kt} \right]$$
$$- \left(\frac{70.6 Q_{o3} B_o \mu_o}{kh} \right) \text{Ei} \left[- \frac{948 \phi \mu c_t r_2^2}{kt} \right]$$

where Q_{o1}, Q_{o2}, and Q_{o3} refer to the respective producing rates of wells 1, 2, and 3.

The above computational approach can be used to calculate the pressure at wells 2 and 3. Further, it can be extended to include any number of wells flowing under the unsteady-state flow condition. It should also be noted that if the point of interest is an operating well, the skin factor s must be included for that well only.

Example 1.21 Assume that the three wells as shown in Figure 1.28 are producing under a transient flow condition for 15 hours. The following additional data is available:

$$Q_{o1} = 100 \text{ STB/day}, \quad Q_{o2} = 160 \text{ STB/day},$$
$$Q_{o3} = 200 \text{ STB/day}, \quad p_i = 4500 \text{ psi},$$
$$B_o = 1.20 \text{ bbl/STB}, \quad c_t = 20 \times 10^{-6} \text{ psi}^{-1},$$
$$(s)_{\text{well1}} = -0.5, \quad h = 20 \text{ ft},$$
$$\phi = 15\%, \quad k = 40 \text{ md},$$
$$r_w = 0.25 \text{ ft}, \quad \mu_o = 2.0 \text{ cp},$$
$$r_1 = 400 \text{ ft}, \quad r_2 = 700 \text{ ft}.$$

If the three wells are producing at a constant flow rate, calculate the sand face flowing pressure at well 1.

Solution

Step 1. Calculate the pressure drop at well 1 caused by its own production by using Equation 1.2.134:

$$(p_i - p_{\text{wf}}) = (\Delta p)_{\text{well 1}} = \frac{162.6 Q_{o1} B_o \mu_o}{kh}$$
$$\times \left[\log \left(\frac{kt}{\phi \mu c_t r_w^2} \right) - 3.23 + 0.87s \right]$$

$$(\Delta p)_{\text{well 1}} = \frac{(162.6)(100)(1.2)(2.0)}{(40)(20)}$$
$$\times \left[\log \left(\frac{(40)(15)}{(0.15)(2)(20 \times 10^{-6})(0.25)^2} \right) \right.$$
$$\left. - 3.23 + 0.87(0) \right] = 270.2 \text{ psi}$$

Step 2. Calculate the pressure drop at well 1 due to the production from well 2:

$$(\Delta p)_{\text{drop due to well 2}} = p_i - p(r_1, t)$$

$$= - \left[\frac{70.6 Q_{o1} \mu_o B_o}{kh} \right] \text{Ei} \left[\frac{-948 \phi \mu_o c_t r_1^2}{kt} \right]$$

$$(\Delta p)_{\text{due to well 2}} = - \frac{(70.6)(160)(1.2)(2)}{(40)(20)}$$
$$\times \text{Ei} \left[-\frac{(948)(0.15)(2.0)(20 \times 10^{-6})(400)^2}{(40)(15)} \right]$$
$$= 33.888 \left[-\text{Ei}(-1.5168) \right]$$
$$= (33.888)(0.13) = 4.41 \text{ psi}$$

Step 3. Calculate the pressure drop due to production from well 3:

$$(\Delta p)_{\text{drop due to well 3}} = p_i - p(r_2, t)$$

$$= - \left[\frac{70.6 Q_{o2} \mu_o B_o}{kh} \right] \text{Ei} \left[\frac{-948 \phi \mu_o c_t r_2^2}{kt} \right]$$

$$(\Delta p)_{\text{due to well 3}} = - \frac{(70.6)(200)(1.2)(2)}{(40)(20)}$$
$$\text{Ei} \left[- \frac{(948)(0.15)(2.0)(20 \times 10^{-6})(700)^2}{(40)(15)} \right]$$
$$= (42.36) \left[-\text{Ei}(-4.645) \right]$$
$$= (42.36)(1.84 \times 10^{-3}) = 0.08 \text{ psi}$$

Step 4. Calculate the total pressure drop at well 1:

$$(\Delta p)_{\text{total at well 1}} = 270.2 + 4.41 + 0.08 = 274.69 \text{ psi}$$

Step 5. Calculate p_{wf} at well 1:

$$P_{\text{wf}} = 4500 - 274.69 = 4225.31 \text{ psi}$$

Effects of variable flow rates

All of the mathematical expressions presented previously in this chapter require that the wells produce at a constant rate during the transient flow periods. Practically all wells produce at varying rates and, therefore, it is important that we are able to predict the pressure behavior when the rate changes. For this purpose, the concept of superposition states that "Every flow rate change in a well will result in a pressure response which is independent of the pressure responses caused by the other previous rate changes." Accordingly, the total pressure drop that has occurred at any time is the summation of pressure changes caused separately by each net flow rate change.

Consider the case of a shut-in well, i.e., $Q = 0$, that was then allowed to produce at a series of constant rates for the different time periods shown in Figure 1.29. To calculate the total pressure drop at the sand face at time t_4, the composite solution is obtained by adding the individual constant-rate solutions at the specified rate-time sequence, or:

$$(\Delta p)_{\text{total}} = (\Delta p)_{\text{due to}(Q_{o1} - 0)} + (\Delta p)_{\text{due to}(Q_{o2} - Q_{o1})}$$
$$+ (\Delta p)_{\text{due to}(Q_{o3} - Q_{o2})} + (\Delta p)_{\text{due to}(Q_{o4} - Q_{o3})}$$

The above expression indicates that there are four contributions to the total pressure drop resulting from the four individual flow rates:

The first contribution results from increasing the rate from 0 to Q_1 and is in effect over the entire time period t_4, thus:

$$(\Delta p)_{Q_1 - 0} = \left[\frac{162.6(Q_1 - 0)B\mu}{kh} \right]$$
$$\times \left[\log \left(\frac{kt_4}{\phi \mu c_t r_w^2} \right) - 3.23 + 0.87s \right]$$

It is essential to notice the *change* in the rate, i.e., (new rate – old rate), that is used in the above equation. It is the change in the rate that causes the pressure disturbance. Further, it should be noted that the "time" in the equation represents the total elapsed time since the change in the rate has been in effect.

The second contribution results from decreasing the rate from Q_1 to Q_2 at t_1, thus:

$$(\Delta p)_{Q_2 - Q_1} = \left[\frac{162.6(Q_2 - Q_1)B\mu}{kh} \right]$$
$$\times \left[\log \left(\frac{k(t_4 - t_1)}{\phi \mu c_t r_w^2} \right) - 3.23 + 0.87s \right]$$
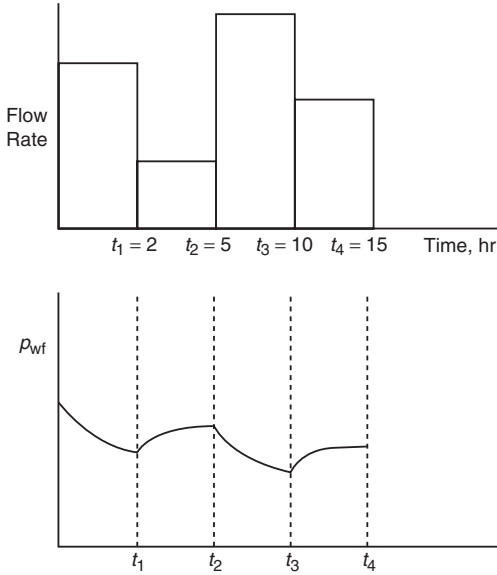
Figure 1.29 *Production and pressure history of a well.*

Using the same concept, the two other contributions from Q_2 to Q_3 and from Q_3 to Q_4 can be computed as:

$$(\Delta p)_{Q_3-Q_2} = \left[\frac{162.6\,(Q_3-Q_2)\,B\mu}{kh}\right]$$

$$\times \left[\log\left(\frac{k\,(t_4-t_2)}{\phi\mu c_t r_w^2}\right) - 3.23 + 0.87s\right]$$

$$(\Delta p)_{Q_4-Q_3} = \left[\frac{162.6\,(Q_4-Q_3)\,B\mu}{kh}\right]$$

$$\times \left[\log\left(\frac{k\,(t_4-t_3)}{\phi\mu c_t r_w^2}\right) - 3.23 + 0.87s\right]$$

The above approach can be extended to model a well with several rate changes. Note, however, that the above approach is valid only if the well is flowing under the unsteady state flow condition for the total time elapsed since the well began to flow at its initial rate.

Example 1.22 Figure 1.29 shows the rate history of a well that is producing under transient flow conditions for 15 hours. Given the following data:

$p_i = 5000$ psi, $h = 20$ ft, $B_o = 1.1$ bbl/STB

$\phi = 15\%$, $\mu_o = 2.5$ cp, $r_w = 0.3$ ft

$c_t = 20 \times 10^{-6}$ psi^{-1}, $s = 0$, $k = 40$ md

calculate the sand face pressure after 15 hours.

Solution

Step 1. Calculate the pressure drop due to the first flow rate for the entire flow period:

$$(\Delta p)_{Q_1-0} = \frac{(162.6)\,(100-0)\,(1.1)\,(2.5)}{(40)\,(20)}$$

$$\times \left[\log\left(\frac{(40)\,(15)}{(0.15)\,(2.5)\,(20\times 10^{-6})\,(0.3)^2}\right) - 3.23 + 0\right]$$

$$= 319.6 \text{ psi}$$

Step 2. Calculate the additional pressure change due to the change of the flow rate from 100 to 70 STB/day:

$$(\Delta p)_{Q_2-Q_1} = \frac{(162.6)\,(70-100)\,(1.1)\,(2.5)}{(40)\,(20)}$$

$$\times \left[\log\left[\frac{(40)\,(15-2)}{(0.15)\,(2.5)\,(20\times 10^{-6})\,(0.3)^2}\right] - 3.23\right]$$

$$= -94.85 \text{ psi}$$

Step 3. Calculate the additional pressure change due to the change of the flow rate from 70 to 150 STB/day:

$$(\Delta p)_{Q_3-Q_2} = \frac{(162.6)\,(150-70)\,(1.1)\,(2.5)}{(40)\,(20)}$$

$$\times \left[\log\left(\frac{(40)\,(15-5)}{(0.15)\,(2.5)\,(20\times 10^{-6})\,(0.3)^2}\right) - 3.23\right]$$

$$= 249.18 \text{ psi}$$

Step 4. Calculate the additional pressure change due to the change of the flow rate from 150 to 85 STB/day:

$$(\Delta p)_{Q_4-Q_3} = \frac{(162.6)\,(85-150)\,(1.1)\,(2.5)}{(40)\,(20)}$$

$$\times \left[\log\left[\frac{(40)\,(15-10)}{(0.15)\,(2.5)\,(20\times 10^{-6})\,(0.3)^2}\right] - 3.23\right]$$

$$= -190.44 \text{ psi}$$

Step 5. Calculate the total pressure drop:

$$(\Delta p)_{\text{total}} = 319.6 + (-94.85) + 249.18 + (-190.44)$$

$$= 283.49 \text{ psi}$$

Step 6. Calculate the wellbore pressure after 15 hours of transient flow:

$$p_{\text{wf}} = 5000 - 283.49 = 4716.51 \text{ psi}$$

Effects of the reservoir boundary

The superposition theorem can also be extended to predict the pressure of a well in a bounded reservoir. Consider Figure 1.30 which shows a well that is located a distance L from the non-flow boundary, e.g., sealing fault. The no-flow boundary can be represented by the following pressure gradient expression:

$$\left(\frac{\partial p}{\partial L}\right)_{\text{Boundary}} = 0$$

Mathematically, the above boundary condition can be met by placing an *image* well, identical to that of the actual well, on the other side of the fault at exactly distance L. Consequently, the effect of the boundary on the pressure behavior of a well would be the same as the effect from an image well located a distance $2L$ from the actual well.

In accounting for the boundary effects, the superposition method is frequently called the *method of images*. Thus, for the problem of the system configuration given in Figure 1.30, the problem reduces to one of determining the effect of the image well on the actual well. The total pressure drop at the actual well will be the pressure drop due to its own production plus the additional pressure drop caused by an identical well at a distance of $2L$, or:

$$(\Delta p)_{\text{total}} = (\Delta p)_{\text{actual well}} + (\Delta p)_{\text{due to image well}}$$
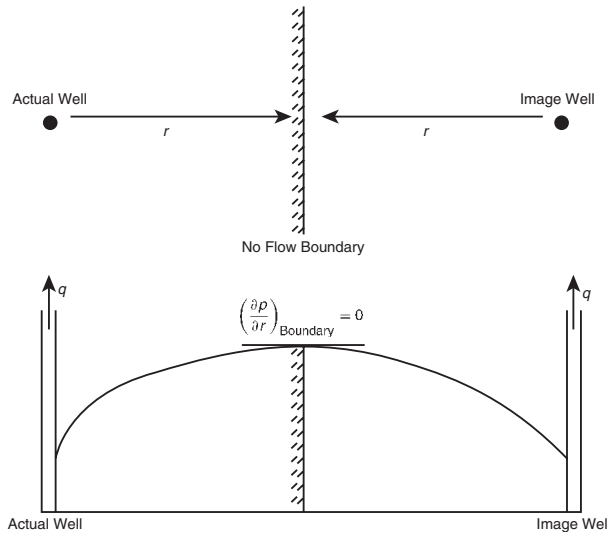
Figure 1.30   *Method of images in solving boundary problems.*

or:

$$(\Delta p)_{\text{total}} = \frac{162.6 Q_o B \mu}{kh} \left[\log \left(\frac{kt}{\phi \mu c_t r_w^2} \right) - 3.23 + 0.87s \right]$$
$$- \left(\frac{70.6 Q_o B \mu}{kh} \right) \text{Ei} \left(- \frac{948 \phi \mu c_t (2L)^2}{kt} \right)$$

[1.2.157]

Notice that this equation assumes the reservoir is infinite except for the indicated boundary. The effect of boundaries is always to cause a greater pressure drop than those calculated for infinite reservoirs.

The concept of image wells can be extended to generate the pressure behavior of a well located within a variety of boundary configurations.

Example 1.23   Figure 1.31 shows a well located between two sealing faults at 400 and 600 feet from the two faults. The well is producing under a transient flow condition at a constant flow rate of 200 STB/day. Given:

$p_i = 500$ psi, $k = 600$ md, $B_o = 1.1$ bbl/STB
$\phi = 17\%$, $\mu_o = 2.0$ cp, $h = 25$ ft
$r_w = 0.3$ ft, $s = 0$, $c_t = 25 \times 10^{-6}$ psi^{-1}

Calculate the sand face pressure after 10 hours.

Solution

Step 1. Calculate the pressure drop due to the actual well flow rate:

$$\left(p_i - p_{wf} \right) = (\Delta p)_{\text{actual}} = \frac{162.6 Q_{o1} B_o \mu_o}{kh}$$
$$\times \left[\log \left(\frac{kt}{\phi \mu c_t r_w^2} \right) - 3.23 + 0.87s \right]$$
$$(\Delta p)_{\text{actual}} = \frac{(162.6)(200)(1.1)(2.0)}{(60)(25)}$$
$$\times \left[\log \left(\frac{(60)(10)}{(0.17)(2)(25 \times 10^{-6})(0.3)^2} \right) - 3.23 + 0 \right]$$
$$= 270.17$$
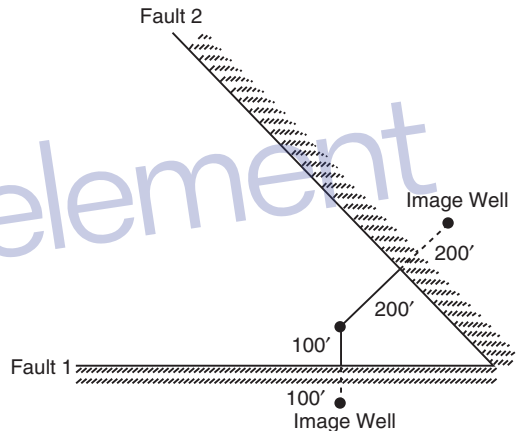
Figure 1.31   *Well layout for Example 1.23.*

Step 2. Determine the additional pressure drop due to the first fault (i.e., image well 1):

$$(\Delta p)_{\text{image well 1}} = p_i - p(2L_1, t)$$
$$= - \left[\frac{70.6 Q_{o2} \mu_o B_o}{kh} \right] \text{Ei} \left[\frac{-948 \phi \mu_o c_t (2L_1)^2}{kt} \right]$$
$$(\Delta p)_{\text{image well 1}} = - \frac{(70.6)(200)(1.1)(2.0)}{(60)(25)}$$
$$\times \text{Ei} \left[- \frac{(948)(0.17)(2)(25 \times 10^{-6})(2 \times 100)^2}{(60)(10)} \right]$$
$$= 20.71 \left[-\text{Ei}(-0.537) \right] = 10.64 \text{ psi}$$

Step 3. Calculate the effect of the second fault (i.e., image well 2):

$$(\Delta p)_{\text{image well 2}} = p_i - p(2L_2, t)$$
$$= - \left[\frac{70.6 Q_{o2} \mu_o B_o}{kh} \right] \text{Ei} \left[\frac{-948 \phi \mu_o c_t (2L_2)^2}{kt} \right]$$

$(\Delta p)_{\text{image well 2}}$

$$= 20.71 \left[-\text{Ei} \left(\frac{-948\,(0.17)\,(2)\,(25 \times 10^{-6})\,(2 \times 200)^2}{(60)\,(10)} \right) \right]$$

$$= 20.71 \left[-\text{Ei}\,(-2.15) \right] = 1.0\ \text{psi}$$

Step 4. The total pressure drop is:

$$(\Delta p)_{\text{total}} = 270.17 + 10.64 + 1.0 = 28.18\ \text{psi}$$

Step 5. $p_{\text{wf}} = 5000 - 281.8 = 4718.2\ \text{psi}.$

Accounting for pressure-change effects

Superposition is also used in applying the constant-pressure case. Pressure changes are accounted for in this solution in much the same way that rate changes are accounted for in the constant-rate case. The description of the superposition method to account for the pressure-change effect is fully described in Chapter 2 in this book.

1.3 Transient Well Testing

Detailed reservoir information is essential to the petroleum engineer in order to analyze the current behavior and future performance of the reservoir. Pressure transient testing is designed to provide the engineer with a quantitative analysis of the reservoir properties. A transient test is essentially conducted by creating a pressure disturbance in the reservoir and recording the pressure response at the wellbore, i.e., bottom-hole flowing pressure p_{wf}, as a function of time. The pressure transient tests most commonly used in the petroleum industry include:

- pressure drawdown;
- pressure buildup;
- multirate;
- interference;
- pulse;
- drill stem (DST);
- falloff;
- injectivity;
- step rate.

It should be pointed out that when the flow rate is changed and the pressure response is recorded in the same well, the test is called a "single-well" test. Drawdown, buildup, injectivity, falloff, and step-rate tests are examples of a single-well test. When the flow rate is changed in one well and the pressure response is measured in another well(s), the test is called a "multiple-well" test.

Several of the above listed tests are briefly described in the following sections.

It has long been recognized that the pressure behavior of a reservoir following a rate change directly reflects the geometry and flow properties of the reservoir. Some of the information that can be obtained from a well test includes:

Drawdown tests	Pressure profile
	Reservoir behavior
	Permeability
	Skin
	Fracture length
	Reservoir limit and shape
Buildup tests	Reservoir behavior
	Permeability
	Fracture length
	Skin
	Reservoir pressure
	Boundaries

DST	Reservoir behavior
	Permeability
	Skin
	Fracture length
	Reservoir limit
	Boundaries
Falloff tests	Mobility in various banks
	Skin
	Reservoir pressure
	Fracture length
	Location of front
	Boundaries
Interference and pulse tests	Communication between wells
	Reservoir-type behavior
	Porosity
	Interwell permeability
	Vertical permeability
Layered reservoir tests	Horizontal permeability
	Vertical permeability
	Skin
	Average layer pressure
	Outer boundaries
Step-rate tests	Formation parting pressure
	Permeability
	Skin

There are several excellent technical and reference books that comprehensively and thoroughly address the subject of well testing and transient flow analysis, in particular:

- C. S. Matthews and D. G. Russell, *Pressure Buildup and Flow Test in Wells* (1967);
- Energy Resources Conservation Board (ERBC), *Theory and Practice of the Testing of Gas Wells* (1975);
- Robert Earlougher, *Advances in Well Test Analysis* (1977);
- John Lee, *Well Testing* (1982);
- M. A. Sabet, *Well Test Analysis* (1991);
- Roland Horn, *Modern Well Test Analysis* (1995).

1.3.1 Drawdown test

A pressure drawdown test is simply a series of bottom-hole pressure measurements made during a period of flow at constant producing rate. Usually the well is shut in prior to the flow test for a period of time sufficient to allow the pressure to equalize throughout the formation, i.e., to reach static pressure. A schematic of the ideal flow rate and pressure history is shown in Figure 1.32.

The fundamental objectives of drawdown testing are to obtain the average permeability, k, of the reservoir rock within the drainage area of the well, and to assess the degree of damage of stimulation induced in the vicinity of the wellbore through drilling and completion practices. Other objectives are to determine the pore volume and to detect reservoir inhomogeneities within the drainage area of the well.

When a well is flowing at a constant rate of Q_{o} under the unsteady-state condition, the pressure behavior of the well will act as if it exists in an infinite-size reservoir. The pressure behavior during this period is described by Equation 1.2.134 as:

$$p_{\text{wf}} = p_{\text{i}} - \frac{162.6 Q_{\text{o}} B_{\text{o}} \mu}{kh} \left[\log \left(\frac{kt}{\phi \mu c_{\text{t}} r_{\text{w}}^2} \right) - 3.23 + 0.87s \right]$$

where:

k = permeability, md
t = time, hours
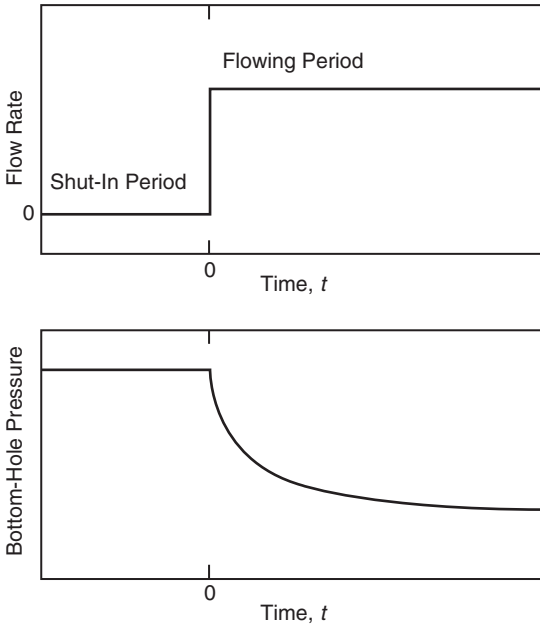r_{w} = wellbore radius, ft
s = skin factor

Figure 1.32 *Idealized drawdown test.*

The above expression can be written as:

$$p_{wf} = p_i - \frac{162.6 Q_o B_o \mu}{kh}$$

$$\times \left[\log(t) + \log\left(\frac{k}{\phi \mu c_t r_w^2}\right) - 3.23 + 0.87 s \right] \quad [1.3.1]$$

This relationship is essentially an equation of a straight line and can be expressed as:

$$p_{wf} = a + m \log(t)$$

where:

$$a = p_i - \frac{162.6 Q_o B_o \mu}{kh} \left[\log\left(\frac{k}{\phi \mu c_t r_w^2}\right) - 3.23 + 0.87 s \right]$$

and the slope m is given by:

$$-m = \frac{-162.6 Q_o B_o \mu_o}{kh} \quad [1.3.2]$$

Equation 1.3.1 suggests that a plot of p_{wf} versus time t on semilog graph paper would yield a straight line with a slope m in psi/cycle. This semilog straight-line portion of the draw-down data, as shown in Figure 1.33, can also be expressed in another convenient form by employing the definition of the slope:

$$m = \frac{p_{wf} - p_{1\,hr}}{\log(t) - \log(1)} = \frac{p_{wf} - p_{1\,hr}}{\log(t) - 0}$$

or:

$$p_{wf} = m \log(t) + p_{1\,hr}$$

Notice that Equation 1.3.2 can also be rearranged to determine the capacity kh of the drainage area of the well. If the thickness is known, then the average permeability is given by:

$$k = \frac{162.6 Q_o B_o \mu_o}{|m| h}$$

where:

k = average permeability, md
$|m|$ = absolute value of slope, psi/cycle

Clearly, kh/μ or k/μ may also be estimated.

The skin effect can be obtained by rearranging Equation 1.3.1 as:

$$s = 1.151 \left[\frac{p_i - p_{wf}}{|m|} - \log t - \log\left(\frac{k}{\phi \mu c_t r_w^2}\right) + 3.23 \right]$$

or, more conveniently, if selecting $p_{wf} = p_{1\,hr}$ which is found on the extension of the straight line at $t = 1$ hr, then:

$$s = 1.151 \left[\frac{p_i - p_{1\,hr}}{|m|} - \log\left(\frac{k}{\phi \mu c_t r_w^2}\right) + 3.23 \right] \quad [1.3.3]$$

where $|m|$ is the absolute value of the slope m.

In Equation 1.2.3, $p_{1\,hr}$ must be obtained from the semilog straight line. If the pressure data measured at 1 hour does not fall on that line, the line must be extrapolated to 1 hour and the extrapolated value of $p_{1\,hr}$ must be used in Equation 1.3.3. This procedure is necessary to avoid calculating an incorrect skin by using a wellbore-storage-influenced pressure. Figure 1.33 illustrates the extrapolation to $p_{1\,hr}$.

Note that the additional pressure drop due to the skin was expressed previously by Equation 1.2.130 as:

$$\Delta p_{skin} = 141.2 \left(\frac{Q_o B_o \mu_o}{kh}\right) s$$

This additional pressure drop can be equivalently written in terms of the semilog straight-line slope m by combining the above expression with that of Equation 1.3.3 to give:

$$\Delta p_{skin} = 0.87 |m| s$$

Another physically meaningful characterization of the skin factor is the flow coefficient E as defined by the ratio of the well actual or observed productivity index J_{actual} and its ideal productivity index J_{ideal}. The ideal productivity index J_{ideal} is the value obtained with no alternation of permeability around the wellbore. Mathematically, the flow coefficient is given by:

$$E = \frac{J_{actual}}{J_{ideal}} = \frac{\bar{p} - p_{wf} - \Delta p_{skin}}{\bar{p} - p_{wf}}$$

where $\bar{p}$ is the average pressure in the well drainage area.

If the drawdown test is long enough, the bottom-hole pressure will deviate from the semilog straight line and make the transition from infinite acting to pseudosteady state. The rate of pressure decline during the pseudosteady-state flow is defined by Equation 1.2.116 as:

$$\frac{dp}{dt} = -\frac{0.23396 q}{c_t(\pi r_e^2) h \phi} = \frac{-0.23396 q}{c_t(A) h \phi} = \frac{-0.23396 q}{c_t (\text{pore volume})}$$

Under this condition, the pressure will decline at a constant rate at any point in the reservoir including the bottom-hole flowing pressure p_{wf}. That is:

$$\frac{dp_{wf}}{dt} = m^\backslash = \frac{-0.23396 q}{c_t A h \phi}$$

This expression suggests that during the semisteady-state flow, a plot of p_{wf} vs. t on a Cartesian scale would produce a straight line with a negative slope of $m^\backslash$ that is defined by:

$$-m^\backslash = \frac{-0.23396 q}{c_t A h \phi}$$

where:

$m^\backslash$ = slope of the *Cartesian straight line* during the pseudosteady state, psi/hr
q = flow rate, bbl/day
A = drainage area, ft^2

Example 1.24[a] Estimate the oil permeability and skin factor from the drawdown data of Figure 1.34.

---

[a]This example problem and the solution procedure are given in Earlougher, R. Advances in Well Test Analysis, Monograph Series, SPE, Dallas (1997).
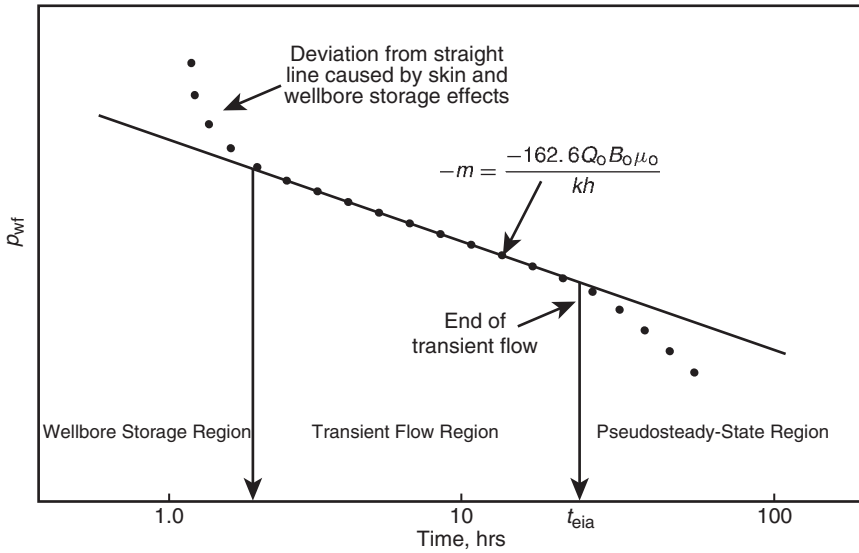
Figure 1.33 *Semilog plot of pressure drawdown data.*
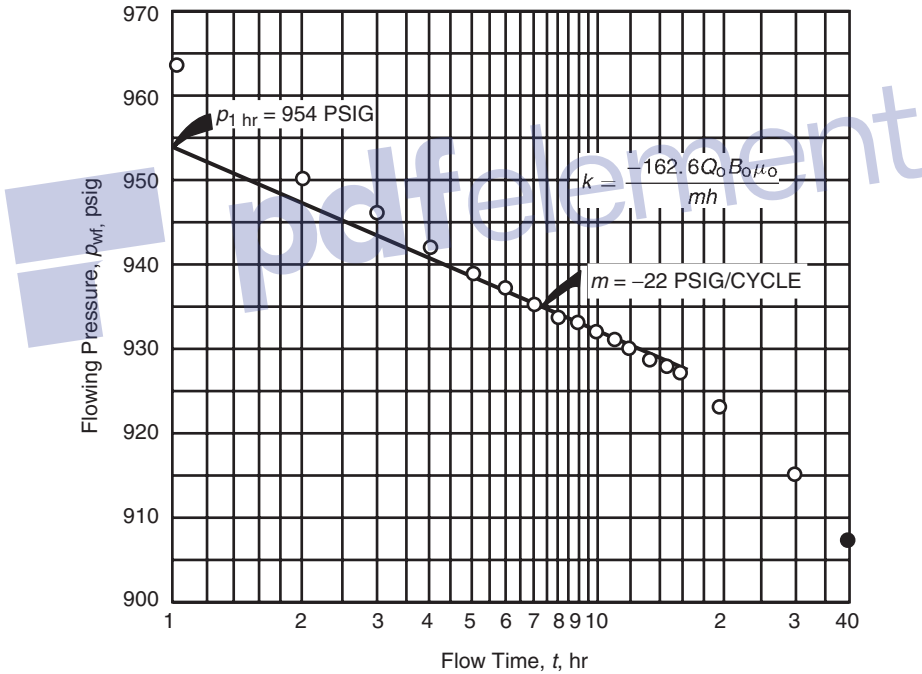
Figure 1.34 *Earlougher's semilog data plot for the drawdown test (Permission to publish by the SPE, copyright SPE, 1977).*

The following reservoir data are available:

$h = 130$ ft, $\phi = 20\%$, $r_w = 0.25$ ft,

$p_i = 1154$ psi, $Q_o = 348$ STB/D, $m = -22$ psi/cycle

$B_o = 1.14$ bbl/STB, $\mu_o = 3.93$ cp, $c_t = 8.74 \times 10^{-6}$ psi^{-1}

Assuming that the wellbore storage effect is not significant, calculate:

- the permeability;
- the skin factor;
- the additional pressure drop due to the skin.

Solution

Step 1. From Figure 1.34, calculate $p_{1\,hr}$:

$$p_{1\,hr} = 954 \text{ psi}$$

Step 2. Determine the slope of the transient flow line:

$$m = -22 \text{ psi/cycle}$$

Step 3. Calculate the permeability by applying Equation 1.3.2:

$$k = \frac{-162.6 Q_o B_o \mu_o}{mh}$$

$$= \frac{-(162.6)(348)(1.14)(3.93)}{(-22)(130)} = 89 \text{ md}$$

Step 4. Solve for the skin factor s by using Equation 1.3.3:

$$s = 1.151 \left[\frac{p_i - p_{1\,hr}}{|m|} - \log\left(\frac{k}{\phi \mu c_t r_w^2} \right) + 3.23 \right]$$

$$= 1.151 \left[\left(\frac{1154 - 954}{22} \right) \right.$$

$$- \log \left(\frac{89}{(0.2)(3.93)(8.74 \times 10^{-6})(0.25)^2} \right)$$

$$\left. + 3.2275 \right] = 4.6$$

Step 5. Calculate the additional pressure drop:

$$\Delta p_{skin} = 0.87 |m| s = 0.87(22)(4.6) = 88 \text{ psi}$$

It should be noted that for a *multiphase flow*, Equations 1.3.1 and 1.3.3 become:

$$p_{wf} = p_i - \frac{162.6 q_t}{\lambda_t h} \left[\log(t) + \log\left(\frac{\lambda_t}{\phi c_t r_w^2} \right) - 3.23 + 0.87 s \right]$$

$$s = 1.151 \left[\frac{p_i - p_{1\,hr}}{|m|} - \log\left(\frac{\lambda_t}{\phi c_t r_w^2} \right) + 3.23 \right]$$

with:

$$\lambda_t = \frac{k_o}{\mu_o} + \frac{k_w}{\mu_w} + \frac{k_g}{\mu_g}$$

$$q_t = Q_o B_o + Q_w B_w + (Q_g - Q_o R_s) B_g$$

or equivalently in terms of GOR as:

$$q_t = Q_o B_o + Q_w B_w + (GOR - R_s) Q_o B_g$$

where:

q_t = total fluid voidage rate, bbl/day
Q_o = oil flow rate, STB/day
Q_w = water flow rate, STB/day
Q_g = total gas flow rate, scf/day
R_s = gas solubility, scf/STB
B_g = gas formation volume factor, bbl/scf
λ_t = total mobility, md/cp
k_o = effective permeability to oil, md
k_w = effective permeability to water, md
k_g = effective permeability to gas, md

The above drawdown relationships indicate that a plot of p_{wf} vs. t on a semilog scale would produce a straight line with a slope m that can be used to determine the total mobility λ_t from:

$$\lambda_t = \frac{162.6 q_t}{mh}$$

Perrine (1956) showed that the effective permeability of each phase, i.e., k_o, k_w, and k_g, can be determined as:

$$k_o = \frac{162.6 Q_o B_o \mu_o}{mh}$$

$$k_w = \frac{162.6 Q_w B_w \mu_w}{mh}$$

$$k_g = \frac{162.6 (Q_g - Q_o R_s) B_g \mu_g}{mh}$$

If the drawdown pressure data is available during both the unsteady-state flow period and the pseudosteady-state flow period, it is possible to estimate the drainage shape and the drainage area of the test well. The transient semilog plot is used to determine its slope m and $p_{1\,hr}$; the Cartesian straight-line plot of the pseudosteady-state data is used to determine its slope $m^\backslash$ and its intercept p_{int}. Earlougher (1977) proposed the following expression to determine the shape factor C_A:

$$C_A = 5.456 \left(\frac{m}{m^\backslash} \right) \exp\left[\frac{2.303(p_{1\,hr} - p_{int})}{m} \right]$$

where:

m = slope of transient semilog straight line, psi/log cycle
$m^\backslash$ = slope of the semisteady-state Cartesian straight line
$p_{1\,hr}$ = pressure at $t = 1$ hour from transient semilog straight line, psi
p_{int} = pressure at $t = 0$ from pseudosteady-state Cartesian straight line, psi

The calculated shape factor from applying the above relationship is compared with those values listed in Table 1.4 to select the geometry of well drainage with a shape factor closest to the calculated value. When extending the drawdown test time with the objective of reaching the drainage boundary of the test well, the test is commonly called the "reservoir limit test."

The reported data of Example 1.24 was extended by Earlougher to include the pseudosteady-state flow period and used to determine the geometry of the test well drainage area as shown in the following example.

Example 1.25 Use the data in Example 1.24 and the Cartesian plot of the pseudosteady-state flow period, as shown in Figure 1.35, to determine the geometry and drainage area of the test well.

Solution

Step 1. From Figure 1.35, determine the slope $m^\backslash$ and intercept p_{int}:

$$m^\backslash = -0.8 \text{ psi/hr}$$

$$p_{int} = 940 \text{ psi}$$

Step 2. From Example 1.24:

$$m = -22 \text{ psi/cycle}$$

$$p_{1\,hr} = 954 \text{ psi}$$

Step 3. Calculate the shape factor C_A from Earlougher's equation:

$$C_A = 5.456 \left(\frac{m}{m^\backslash} \right) \exp\left[\frac{2.303(p_{1\,hr} - p_{int})}{m} \right]$$

$$= 5.456 \left(\frac{-22}{-0.8} \right) \exp\left[\frac{2.303(954 - 940)}{-22} \right]$$

$$= 34.6$$

Step 4. From Table 1.4, $C_A = 34.6$ corresponds to a well in the center of a circle, square, or hexagon:

For a circle: $C_A = 31.62$
For a square: $C_A = 30.88$
For a hexagon: $C_A = 31.60$

Step 5. Calculate the pore volume and drainage area from Equation 1.2.116:

$$\frac{dp}{dt} = m^\backslash = \frac{-0.23396(Q_o B_o)}{c_t (A) h \phi} = \frac{-0.23396(Q_o B_o)}{c_t (\text{pore volume})}$$
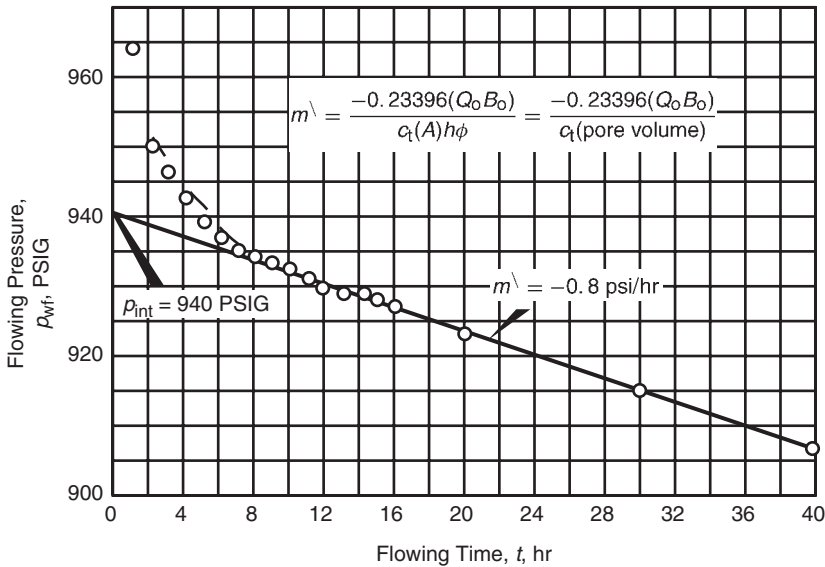
Figure 1.35 *Cartesian plot of the drawdown test data (Permission to publish by the SPE, copyright SPE, 1977).*

Solving for the pore volume gives:

$$\text{Pore volume} = \frac{-0.23396q}{c_t m^\backslash} = \frac{-0.23396(348)(1.4)}{(8.74 \times 10^{-6})(-0.8)}$$

$$= 2.37 \text{ MMbbl}$$

and the drainage area:

$$A = \frac{2.37 \times 10^6 (5.615)}{43460(0.2)(130)} = 11.7 \text{ acres}$$

The above example indicates that the measured bottom-hole flowing pressures are 88 psi more than they would be in the absence of the skin. However, it should be pointed out that when the concept of positive skin factor $+s$ indicates formation damage, whereas a negative skin factor $-s$ suggests formation stimulation, this is essentially a misleading interpretation of the skin factor. The skin factor as determined from any transient well testing analysis represents the composite "total" skin factor that includes the following other skin factors:

- skin due to wellbore damage or stimulation s_d;
- skin due to partial penetration and restricted entry s_r;
- skin due to perforations s_p;
- skin due to turbulence flow s_t;
- skin due to deviated well s_{dw}.

That is:

$$s = s_d + s_r + s_p + s_t + s_{dw}$$

where s is the skin factor as calculated from transient flow analysis. Therefore, to determine if the formation is damaged or stimulated from the skin factor value s obtained from well test analysis, the individual components of the skin factor in the above relationship must be known, to give:

$$s_d = s - s_r - s_p - s_t - s_{dw}$$

There are correlations that can be used to separately estimate these individual skin quantities.

Wellbore storage
Basically, well test analysis deals with the interpretation of the wellbore pressure response to a given change in the flow rate (from zero to a constant value for a drawdown test, or from a constant rate to zero for a buildup test). Unfortunately, the producing rate is controlled at the surface, not at the sand face. Because of the wellbore volume, a constant surface flow rate does not ensure that the entire rate is being produced from the formation. This effect is due to wellbore storage. Consider the case of a drawdown test. When the well is first open to flow after a shut-in period, the pressure in the wellbore drops. This drop in pressure causes the following two types of wellbore storage:

(1) a wellbore storage effect caused by fluid expansion;
(2) a wellbore storage effect caused by changing fluid level in the casing–tubing annulus.

As the bottom-hole pressure drops, the wellbore fluid expands and, thus, the initial surface flow rate is not from the formation, but basically from the fluid that had been stored in the wellbore. This is defined as the *wellbore storage due to fluid expansion*.

The second type of wellbore storage is due to a change in the annulus fluid level (falling level during a drawdown test, rising level during a drawdown test, and rising fluid level during a pressure buildup test). When the well is open to flow during a drawdown test, the reduction in pressure causes the fluid level in the annulus to fall. This annulus fluid production joins that from the formation and contributes to the total flow from the well. The falling fluid level is generally able to contribute more fluid than that by expansion.

The above discussion suggests that part of the flow will be contributed by the wellbore instead of the reservoir. That is:

$$q = q_f + q_{wb}$$

where:

q = surface flow rate, bbl/day
q_f = formation flow rate, bbl/day
q_{wb} = flow rate contributed by the wellbore, bbl/day

During this period when the flow is dominated by the wellbore storage, the measured drawdown pressures will not produce the ideal semilog straight-line behavior that is expected during transient flow. This indicates that the

pressure data collected during the duration of the wellbore storage effect cannot be analyzed by using conventional methods. As production time increases, the wellbore contribution decreases and the formation rate increases until it eventually equals the surface flow rate, i.e., $q = q_f$, which signifies the *end of the wellbore storage effect*.

The effect of fluid expansion and changing fluid level can be quantified in terms of the *wellbore storage factor C* which is defined as:

$$C = \frac{\Delta V_{wb}}{\Delta p}$$

where:

C = wellbore storage coefficient, bbl/psi
ΔV_{wb} = change in the volume of fluid in the wellbore, bbl

The above relationship can be applied to mathematically represent the individual effect of wellbore fluid expansion and falling (or rising) fluid level, to give:

Wellbore storage effect caused by fluid expansion

$$C_{FE} = V_{wb}c_{wb}$$

where:

C_{FE} = wellbore storage coefficient due to fluid expansion, bbl/psi
V_{wb} = total wellbore fluid volume, bbl
c_{wb} = average compressibility of fluid in the wellbore, psi^{-1}

Wellbore storage effect due to changing fluid level

$$C_{FL} = \frac{144 A_a}{5.615 \rho}$$

with:

$$A_a = \frac{\pi[(ID_C)^2 - (OD_T)^2]}{4(144)}$$

where:

C_{FL} = wellbore storage coefficient due to changing fluid level, bbl/psi
A_a = annulus cross-sectional area, ft^2
OD_T = outside diameter of the production tubing, inches
ID_C = inside diameter of the casing, inches
ρ = wellbore fluid density, lb/ft^3

This effect is essentially small if a packer is placed near the producing zone. The total storage effect is the sum of both coefficients. That is:

$$C = C_{FE} + C_{FL}$$

It should be noted during oil well testing that the fluid expansion is generally insignificant due to the small compressibility of liquids. For gas wells, the primary storage effect is due to gas expansion.

To determine the duration of the wellbore storage effect, it is convenient to express the wellbore storage factor in a dimensionless form as:

$$C_D = \frac{5.615C}{2\pi h \phi c_t r_w^2} = \frac{0.8936C}{\phi h c_t r_w^2} \qquad [1.3.4]$$

where:

C_D = dimensionless wellbore storage factor
C = wellbore storage factor, bbl/psi
c_t = total compressibility coefficient, psi^{-1}
r_w = wellbore radius, ft
h = thickness, ft

Horn (1995) and Earlougher (1977), among other authors, have indicated that the wellbore pressure is directly proportional to the time during the wellbore storage-dominated

period of the test and is expressed by:

$$p_D = t_D/C_D \qquad [1.3.5]$$

where:

p_D = dimensionless pressure during wellbore storage domination time
t_D = dimensionless time

Taking the logarithm of both sides of this relationship gives:

$$\log(p_D) = \log(t_D) - \log(C_D)$$

This expression has a characteristic that is diagnostic of wellbore storage effects. It indicates that a plot of p_D vs. t_D on a log–log scale will yield a straight line of a *unit slope, i.e., a straight line with a 45° angle*, during the wellbore storage-dominated period. Since p_D is proportional to pressure drop Δp and t_D is proportional to time t, it is convenient to plot $\log(p_i - p_{wf})$ versus $\log(t)$ and observe where the plot has a slope of one cycle in pressure per cycle in time. This unit slope observation is of major value in well test analysis.

The log–log plot is a valuable aid for recognizing wellbore storage effects in transient tests (e.g., drawdown or buildup tests) when early-time pressure recorded data is available. It is recommended that this plot be made a part of the transient test analysis. As wellbore storage effects become less severe, the formation begins to influence the bottom-hole pressure more and more, and the data points on the log–log plot fall below the unit-slope straight line and signify the end of the wellbore storage effect. At this point, wellbore storage is no longer important and standard semilog data-plotting analysis techniques apply. As a rule of thumb, the time that indicates the end of the wellbore storage effect can be determined from the log–log plot by moving 1 to $1\frac{1}{2}$ cycles in time after the plot starts to deviate from the unit slop and reading the corresponding time on the x axis. This time may be estimated from:

$$t_D > (60 + 3.5s)C_D$$

or:

$$t > \frac{(200\,000 + 12\,000s)C}{(kh/\mu)}$$

where:

t = total time that marks the end of the wellbore storage effect and the beginning of the semilog straight line, hours
k = permeability, md
s = skin factor
μ = viscosity, cp
C = wellbore storage coefficient, bbl/psi

In practice, it is convenient to determine the wellbore storage coefficient C by selecting *a point on the log–log unit-slope straight line* and reading the coordinate of the point in terms of t and Δp, to give:

$$C = \frac{qt}{24\Delta p} = \frac{QBt}{24\Delta p}$$

where:

t = time, hours
Δp = pressure difference $(p_i - p_{wf})$, psi
q = flow rate, bbl/day
Q = flow rate, STB/day
B = formation volume factor, bbl/STB

It is important to note that the volume of fluids stored in the wellbore distorts the early-time pressure response and controls the duration of wellbore storage, especially in deep wells with large wellbore volumes. If the wellbore storage

effects are not minimized or if the test is not continued beyond the end of the wellbore storage-dominated period, the test data will be difficult to analyze with current conventional well testing methods. To minimize wellbore storage distortion and to keep well tests within reasonable lengths of time, it may be necessary to run tubing, packers, and bottom-hole shut-in devices.

Example 1.26   The following data is given for an oil well that is scheduled for a drawdown test:

- volume of fluid in the wellbore $= 180$ bbl
- tubing outside diameter $= 2$ inches
- production oil density in the wellbore $= 7.675$ inches
- average oil density in the wellbore $= 45$ lb/ft^3

$h = 50$ ft,	$\phi = 15\,\%$,
$r_{\mathrm{w}} = 0.25$ ft,	$\mu_{\mathrm{o}} = 2$ cp
$k = 30$ md,	$s = 0$
$c_{\mathrm{t}} = 20 \times 10^{-6}$ psi^{-1},	$c_{\mathrm{o}} = 10 \times 10^{-6}$ psi^{-1}

If this well is placed under a constant production rate, calculate the dimensionless wellbore storage coefficient C_{D}. How long will it take for wellbore storage effects to end?

Solution

Step 1. Calculate the cross-sectional area of the annulus A_{a}:

$$A_{\mathrm{a}} = \frac{\pi[(ID_{\mathrm{C}})^2 - (OD_{\mathrm{T}})^2]}{4(144)}$$

$$= \frac{\pi[(7.675)^2 - (2)^2]}{(4)(144)} = 0.2995 \text{ ft}^2$$

Step 2. Calculate the wellbore storage factor caused by fluid expansion:

$$C_{\mathrm{FE}} = V_{\mathrm{wb}} c_{\mathrm{wb}}$$

$$= (180)(10 \times 10^{-6}) = 0.0018 \text{ bbl/psi}$$

Step 3. Determine the wellbore storage factor caused by the falling fluid level:

$$C_{\mathrm{FL}} = \frac{144 A_{\mathrm{a}}}{5.615 \rho}$$

$$= \frac{144(0.2995)}{(5.615)(45)} = 0.1707 \text{ bbl/psi}$$

Step 4. Calculate the total wellbore storage coefficient:

$$C = C_{\mathrm{FE}} + C_{\mathrm{FL}}$$

$$= 0.0018 + 0.1707 = 0.1725 \text{ bbl/psi}$$

The above calculations show that the effect of fluid expansion C_{FE} can generally be neglected in crude oil systems.

Step 5. Calculate the dimensionless wellbore storage coefficient from Equation 1.3.4:

$$C_{\mathrm{D}} = \frac{0.8936 C}{\phi h c_{\mathrm{t}} r_{\mathrm{w}}^2} = \frac{0.8936(0.1707)}{0.15(50)(20 \times 10^{-6})(0.25)^2}$$

$$= 16\,271$$

Step 6. Approximate the time required for wellbore storage influence to end from:

$$t = \frac{(200\,000 + 12\,000s)C\mu}{kh}$$

$$= \frac{(200\,000 + 0)(0.1725)(2)}{(30)(50)} = 46 \text{ hours}$$

The straight-line relationship as expressed by Equation 1.3.2 is only valid during the infinite-acting behavior of the

well. Obviously, reservoirs are not infinite in extent, so the infinite-acting radial flow period cannot last indefinitely. Eventually the effects of the reservoir boundaries will be felt at the well being tested. The time at which the boundary effect is felt is dependent on the following factors:

- permeability k;
- total compressibility c_{t};
- porosity ϕ;
- viscosity μ;
- distance to the boundary;
- shape of the drainage area.

Earlougher (1977) suggested the following mathematical expression for estimating the duration of the infinite-acting period:

$$t_{\mathrm{eia}} = \left[\frac{\phi \mu c_{\mathrm{t}} A}{0.0002637k} \right] (t_{DA})_{\mathrm{eia}}$$

where:

$t_{\mathrm{eia}} = $ time to the end of infinite-acting period, hours
$A = $ well drainage area, ft^2
$c_{\mathrm{t}} = $ total compressibility, psi^{-1}
$(t_{DA})_{\mathrm{eia}} = $ dimensionless time to the end of the infinite-acting period

This expression is designed to predict the time that marks the end of transient flow in a drainage system of any geometry by obtaining the value of t_{DA} from Table 1.4. The *last three columns* of the table provide with values of t_{DA} that allow the engineer to calculate:

- the maximum elapsed time during which a reservoir is infinite acting;
- the time required for the pseudosteady-state solution to be applied and predict pressure drawdown within 1% accuracy;
- the time required for the pseudosteady-state solution (equations) to be exact and applied.

As an example, for a well centered in a circular reservoir, the maximum time for the reservoir to remain in an infinite-acting system can be determined using the entry in the final column of Table 1.4 to give $(t_{DA})_{\mathrm{eia}} = 0.1$, and accordingly:

$$t_{\mathrm{eia}} = \left[\frac{\phi \mu c_{\mathrm{t}} A}{0.0002637k} \right] (t_{DA})_{\mathrm{eia}} = \left[\frac{\phi \mu c_{\mathrm{t}} A}{0.0002637k} \right] 0.1$$

or:

$$t_{\mathrm{eia}} = \frac{380 \phi \mu c_{\mathrm{t}} A}{k}$$

For example, for a well that is located in the center of a 40 acre circular drainage area with the following properties:

$$k = 60 \text{ md}, \quad c_{\mathrm{t}} = 6 \times 10^{-6} \text{ psi}^{-1}, \quad \mu = 1.5 \text{ cp}, \quad \phi = 0.12$$

the maximum time, in hours, for the well to remain in an infinite-acting system is:

$$t_{\mathrm{eia}} = \frac{380 \phi \mu c_{\mathrm{t}} A}{k} = \frac{380(0.12)(1.4)(6 \times 10^{-6})(40 \times 43560)}{60}$$

$$= 11.1 \text{ hours}$$

Similarly, the pseudosteady-state solution can be applied any time after the semisteady-state flow begins at t_{pss} as estimated from:

$$t_{\mathrm{pss}} = \left[\frac{\phi \mu c_{\mathrm{t}} A}{0.0002637k} \right] (t_{DA})_{\mathrm{pss}}$$

where $(t_{DA})_{\mathrm{pss}}$ can be found from the entry in the fifth column of the table.

Hence, the specific steps involved in a drawdown test analysis are:

(1) Plot $p_{\mathrm{i}} - p_{\mathrm{wf}}$ vs. t on a log–log scale.

(2) Determine the time at which the unit-slope line ends.

(3) Determine the corresponding time at $1\frac{1}{2}$ log cycle, ahead of the observed time in step 2. This is the time that marks the end of the wellbore storage effect and the start of the semilog straight line.

(4) Estimate the wellbore storage coefficient from:

$$C = \frac{qt}{24\,\Delta p} = \frac{QBt}{24\,\Delta p}$$

where t and Δp are values read from a point on the log–log unit-slope straight line and q is the flow rate in bbl/day.

(5) Plot p_{wf} vs. t on a semilog scale.

(6) Determine the start of the straight-line portion as suggested in step 3 and draw the best line through the points.

(7) Calculate the slope of the straight line and determine the permeability k and skin factor s by applying Equations 1.3.2 and 1.3.3, respectively:

$$k = \frac{-162.6Q_o B_o \mu_o}{mh}$$

$$s = 1.151\left[\frac{p_i - p_{1\,hr}}{|m|} - \log\left(\frac{k}{\phi\mu c_t r_w^2}\right) + 3.23\right]$$

(8) Estimate the time to the end of the infinite-acting (transient flow) period, i.e., t_{eia}, which marks the beginning of the pseudosteady-state flow.

(9) Plot all the recorded pressure data after t_{eia} as a function of time on a regular Cartesian scale. This data should form a straight-line relationship.

(10) Determine the slope of the pseudosteady-state line, i.e., dp/dt (commonly referred to as $m^\backslash$) and use Equation 1.2.116 to solve for the drainage area A:

$$A = \frac{-0.23396QB}{c_t h \phi\,(dp/dt)} = \frac{-0.23396QB}{c_t h \phi m^\backslash}$$

where:

$m^\backslash$ = slope of the semisteady-state Cartesian straight line
Q = fluid flow rate, STB/day
B = formation volume factor, bbl/STB

(11) Calculate the shape factor C_A from the expression that was developed by Earlougher (1977):

$$C_A = 5.456\left(\frac{m}{m^\backslash}\right)\exp\left[\frac{2.303(p_{1\,hr} - p_{int})}{m}\right]$$

where:

m = slope of transient semilog straight line, psi/log cycle
$m^\backslash$ = slope of the pseudosteady-state Cartesian straight line
$p_{1\,hr}$ = pressure at $t = 1$ hour from transient semilog straight line, psi
p_{int} = pressure at $t = 0$ from semisteady-state Cartesian straight line, psi

(12) Use Table 1.4 to determine the drainage configuration of the tested well that has a value of the shape factor C_A closest to that of the calculated one, i.e., step 11.

Radius of investigation

The radius of investigation r_{inv} of a given test is the effective distance traveled by the pressure transients, as measured from the tested well. This radius depends on the speed with which the pressure waves propagate through the reservoir rock, which, in turn, is determined by the rock and fluid properties, such as:

- porosity;

- permeability;
- fluid viscosity;
- total compressibility.

As time t increases, more of the reservoir is influenced by the well and the radius of drainage, or investigation, increases as given by:

$$r_{inv} = 0.0325\sqrt{\frac{kt}{\phi\mu c_t}}$$

where:

t = time, hours
k = permeability, md
c_t = total compressibility, psi^{-1}

It should be pointed out that the equations developed for slightly compressible liquids can be extended to describe the behavior of real gases by replacing the pressure with the real-gas pseudopressure $m(p)$, as defined by:

$$m(p) = \int_0^p \frac{2p}{\mu Z}\,dp$$

with the transient pressure drawdown behavior as described by Equation 1.2.151, or:

$$m(p_{wf}) = m(p_i) - \left[\frac{1637Q_g T}{kh}\right]$$

$$\times\left[\log\left(\frac{kt}{\phi\mu_i c_{ti} r_w^2}\right) - 3.23 + 0.87s^\backslash\right]$$

Under constant gas flow rate, the above relation can be expressed in a linear form as:

$$m(p_{wf}) = \left\{m(p_i) - \left[\frac{1637Q_g T}{kh}\right]\right.$$

$$\left.\times\left[\log\left(\frac{k}{\phi\mu_i c_{ti} r_w^2}\right) - 3.23 + 0.87s^\backslash\right]\right\} - \left[\frac{1637Q_g T}{kh}\right]\log(t)$$

or:

$$m(p_{wf}) = a + m\log(t)$$

which indicates that a plot of $m(p_{wf})$ vs. $\log(t)$ would produce a semilog straight line with a negative slope of:

$$m = \frac{1637Q_g T}{kh}$$

Similarly, in terms of the pressure-squared approximation form:

$$p_{wf}^2 = p_i^2 - \left[\frac{1637Q_g T\overline{Z}\overline{\mu}}{kh}\right]$$

$$\times\left[\log\left(\frac{kt}{\phi\mu_i c_{ti} r_w^2}\right) - 3.23 + 0.87s^\backslash\right]$$

or:

$$p_{wf}^2 = \left\{p_i^2 - \left[\frac{1637Q_g T\overline{Z}\overline{\mu}}{kh}\right]\right.$$

$$\times\left[\log\left(\frac{k}{\phi\mu_i c_{ti} r_w^2}\right) - 3.23 + 0.87s^\backslash\right]\right\}$$

$$- \left[\frac{1637Q_g T\overline{Z}\overline{\mu}}{kh}\right]\log(t)$$

This equation is an equation of a straight line that can be simplified to give:

$$p_{wf}^2 = a + m\log(t)$$

which indicates that a plot of p_{wf}^2 vs. $\log(t)$ would produce a semilog straight line with a negative slope of:

$$m = \frac{1637 Q_g T \overline{Z} \overline{\mu}}{kh}$$

The true skin factor s which reflects the formation damage or stimulation is usually combined with the non-Darcy rate-dependent skin and labeled as the apparent or total skin factor:

$$s^\backslash = s + DQ_g$$

with the term DQ_g interpreted as the rate-dependent skin factor. The coefficient D is called the inertial or turbulent flow factor and given by Equation 1.2.148:

$$D = \frac{Fkh}{1422T}$$

where:

Q_g = gas flow rate, Mscf/day
t = time, hours
k = permeability, md
μ_i = gas viscosity as evaluated at p_i, cp

The apparent skin factor $s^\backslash$ is given by:
For pseudopressure approach:

$$s^\backslash = 1.151 \left[\frac{m(p_i) - m(p_{1\,hr})}{|m|} - \log\left(\frac{k}{\phi \mu_{ti} c_{ti} r_w^2}\right) + 3.23 \right]$$

For pressure-squared approach:

$$s^\backslash = 1.151 \left[\frac{p_i^2 - p_{1\,hr}^2}{|m|} - \log\left(\frac{k}{\phi \overline{\mu c_t} r_w^2}\right) + 3.23 \right]$$

If the duration of the drawdown test of the gas well is long enough to reach its boundary, the pressure behavior during the boundary-dominated period (pseudosteady-state condition) is described by an equation similar to that of Equation 1.2.125 as:
For pseudopressure approach:

$$\frac{m(p_i) - m(p_{wf})}{q} = \frac{\Delta m(p)}{q} = \frac{711T}{kh}\left(\ln\frac{4A}{1.781 C_A r_{wa}^2}\right)$$
$$+ \left[\frac{2.356T}{\phi(\mu_g c_g)_i A h}\right] t$$

and as a linear equation by:

$$\frac{\Delta m(p)}{q} = b_{pss} + m^\backslash t$$

This relationship indicates that a plot of $\Delta m(p)/q$ vs. t will form a straight line with:

Intercept: $\quad b_{pss} = \frac{711T}{kh}\left(\ln\frac{4A}{1.781 C_A r_{wa}^2}\right)$

Slope: $\quad m^\backslash = \frac{2.356T}{(\mu_g c_t)_i (\phi hA)} = \frac{2.356T}{(\mu_g c_t)_i (\text{pore volume})}$

For pressure-squared approach:

$$\frac{p_i^2 - p_{wf}^2}{q} = \frac{\Delta(p^2)}{q} = \frac{711 \overline{\mu} \overline{Z} T}{kh}\left(\ln\frac{4A}{1.781 C_A r_{wa}^2}\right)$$
$$+ \left[\frac{2.356 \overline{\mu} \overline{Z} T}{\phi(\mu_g c_g)_i A h}\right] t$$

and in a linear form as:

$$\frac{\Delta(p^2)}{q} = b_{pss} + m^\backslash t$$

This relationship indicates that a plot of $\Delta(p^2)/q$ vs. t on a Cartesian scale will form a straight line with:

Intercept: $\quad b_{pss} = \frac{711 \overline{\mu} \overline{Z} T}{kh}\left(\ln\frac{4A}{1.781 C_A r_{wa}^2}\right)$

Slope: $\quad m^\backslash = \frac{2.356 \overline{\mu} \overline{Z} T}{(\mu_g c_t)_i (\phi hA)} = \frac{2.356 \overline{\mu} \overline{Z} T}{(\mu_g c_t)_i (\text{pore volume})}$

where:

q = flow rate, Mscf/day
A = drainage area, ft^2
T = temperature, °R
t = flow time, hours

Meunier et al. (1987) suggested a methodology for expressing the time t and the corresponding pressure p that allows the use of liquid flow equations without special modifications for gas flow. Meunier and his co-authors introduced the following normalized pseudopressure p_{pn} and normalized pseudotime t_{pn}

$$p_{pn} = p_i + \left[\left(\frac{\mu_i Z_i}{p_i}\right)\int_0^p \frac{p}{\mu Z}\,dp\right]$$

$$t_{pn} = \mu_i c_{ti}\left[\int_0^t \frac{1}{\mu c_t}\,dp\right]$$

The subscript "i" on μ, Z, and c_t refers to the evaluation of these parameters at the initial reservoir pressure p_i. By using the Meunier et al. definition of the normalized pseudopressure and normalized pseudotime there is no need to modify any of the liquid analysis equations. However, care should be exercised when replacing the liquid flow rate with the gas flow rate. It should be noted that in all transient flow equations when applied to the oil phase, the flow rate is expressed as the product of $Q_o B_o$ in bbl/day; that is, in reservoir barrels/day. Therefore, when applying these equations to the gas phase, the product of the gas flow rate and gas formation volume factor $Q_g B_g$ should be given in bbl/day. For example, if the gas flow rate is expressed in scf/day, the gas formation volume factor must be expressed in bbl/scf. The recorded pressure and time are then simply replaced by the normalized pressure and normalized time to be used in all the traditional graphical techniques, including pressure buildup.

1.3.2 Pressure buildup test

The use of pressure buildup data has provided the reservoir engineer with one more useful tool in the determination of reservoir behavior. Pressure buildup analysis describes the buildup in wellbore pressure with time after a well has been shut in. One of the principal objectives of this analysis is to determine the static reservoir pressure without waiting weeks or months for the pressure in the entire reservoir to stabilize. Because the buildup in wellbore pressure will generally follow some definite trend, it has been possible to extend the pressure buildup analysis to determine:

- the effective reservoir permeability;
- the extent of permeability damage around the wellbore;
- the presence of faults and to some degree the distance to the faults;
- any interference between producing wells;
- the limits of the reservoir where there is not a strong water drive or where the aquifer is no larger than the hydrocarbon reservoir.

Certainly all of this information will probably not be available from any given analysis, and the degree of usefulness of any of this information will depend on the experience in the area
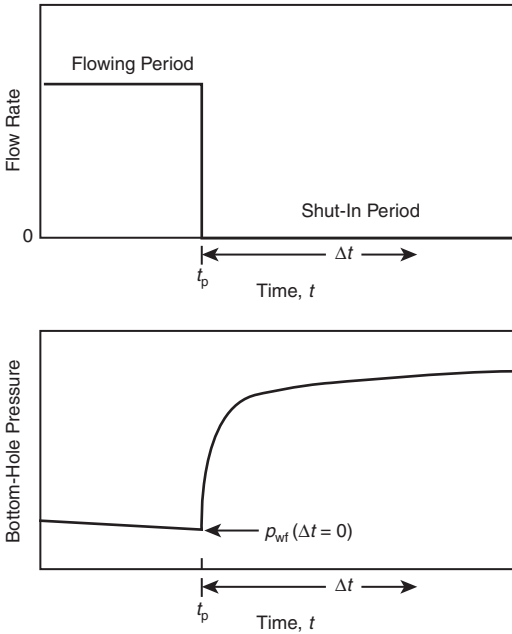
Figure 1.36 *Idealized pressure buildup test.*

and the amount of other information available for correlation purposes.

The general formulas used in analyzing pressure buildup data come from a solution of the diffusivity equation. In pressure buildup and drawdown analyses, the following assumptions, as regards the reservoir, fluid, and flow behavior, are usually made:

- Reservoir: homogeneous; isotropic; horizontal of uniform thickness.
- Fluid: single phase; slightly compressible; constant μ_o and B_o.
- Flow: laminar flow; no gravity effects.

Pressure buildup testing requires shutting in a producing well and recording the resulting increase in the wellbore pressure as a function of shut-in time. The most common and simplest analysis techniques require that the well produce at a constant rate for a flowing time of t_p, either from startup or long enough to establish a stabilized pressure distribution, before shut in. Traditionally, the shut-in time is denoted by the symbol Δt. Figure 1.36 schematically shows the stabilized constant flow rate before shut-in and the ideal behavior of the pressure increase during the buildup period. The pressure is measured immediately before shut-in and is recorded as a function of time during the shut-in period. The resulting pressure buildup curve is then analyzed to determine reservoir properties and the wellbore condition.

Stabilizing the well at a constant rate before testing is an important part of a pressure buildup test. If stabilization is overlooked or is impossible, standard data analysis techniques may provide erroneous information about the formation.

Two widely used methods are discussed below; these are:

(1) the Horner plot;
(2) the Miller–Dyes–Hutchinson method.

1.3.3 Horner plot

A pressure buildup test is described mathematically by using the principle of superposition. Before the shut-in, the well is allowed to flow at a constant flow rate of Q_o STB/day for t_p days. At the end of the flowing period, the well is shut in with a corresponding change in the flow rate from the "old" rate of Q_o to the "new" flow rate of $Q^{new} = 0$, i.e., $Q^{new} - Q^{old} = -Q_o$.

Calculation of the total pressure change which occurs at the sand face during the shut-in time is basically the sum of the pressure changes that are caused by:

- flowing the well at a stabilized flow rate of Q^{old}, i.e., the flow rate before shut-in Q_o, and is in effect over the entire time of $t_p + \Delta t$;
- the net change in the flow rate from Q_o to 0 and is in effect over Δt.

The composite effect is obtained by adding the individual constant-rate solutions at the specified rate–time sequence, as:

$$p_i - p_{ws} = (\Delta p)_{total} = (\Delta p)_{due\ to (Q_o - 0)}$$
$$+ (\Delta p)_{due\ to (0 - Q_o)}$$

where:

$p_i =$ initial reservoir pressure, psi
$p_{ws} =$ wellbore pressure during shut in, psi

The above expression indicates that there are two contributions to the total pressure change at the wellbore resulting from the two individual flow rates.

The first contribution results from increasing the rate from 0 to Q_o and is in effect over the entire time period $t_p + \Delta t$, thus:

$$(\Delta p)_{Q_o - 0} = \left[\frac{162.6(Q_o - 0)B_o\mu_o}{kh} \right]$$
$$\times \left[\log\left(\frac{k(t_p + \Delta t)}{\phi \mu_o c_t r_w^2} \right) - 3.23 + 0.87s \right]$$

The second contribution results from decreasing the rate from Q_o to 0 at t_p, i.e., shut-in time, thus:

$$(\Delta p)_{0 - Q_o} = \left[\frac{162.6(0 - Q_o)B_o\mu_o}{kh} \right]$$
$$\times \left[\log\left(\frac{k\Delta t}{\phi \mu_o c_t r_w^2} \right) - 3.23 + 0.87s \right]$$

The pressure behavior in the well during the shut-in period is then given by:

$$p_i - p_{ws} = \frac{162.6 Q_o \mu_o B_o}{kh} \left[\log \frac{k(t_p + \Delta t)}{\phi \mu_o c_t r_w^2} - 3.23 \right]$$
$$- \frac{162.6(-Q_o)\mu_o B_o}{kh} \left[\log \frac{k\Delta t}{\phi \mu_o c_t r_w^2} - 3.23 \right]$$

Expanding this equation and canceling terms gives:

$$p_{ws} = p_i - \frac{162.6 Q_o \mu_o B_o}{kh} \left[\log\left(\frac{t_p + \Delta t}{\Delta t} \right) \right] \qquad [1.3.6]$$

where:

$p_i =$ initial reservoir pressure, psi
$p_{ws} =$ sand face pressure during pressure buildup, psi
$t_p =$ flowing time before shut-in, hours
$Q_o =$ stabilized well flow rate before shut-in, STB/day
$\Delta t =$ shut-in time, hours

The pressure buildup equation, i.e., Equation 1.3.6 was introduced by Horner (1951) and is commonly referred to as the Horner equation.
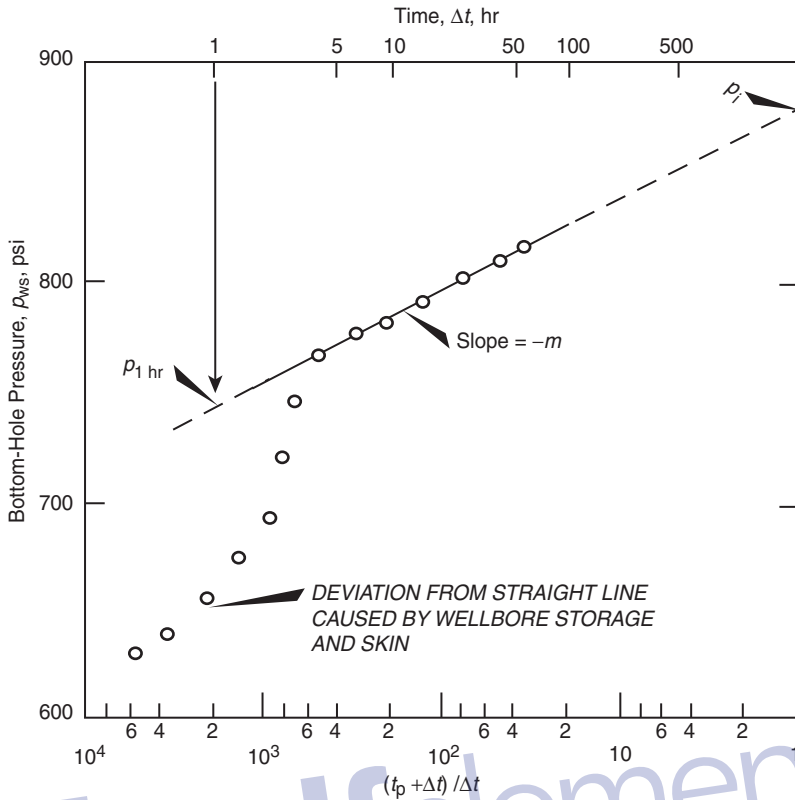
Figure 1.37   Horner plot (After Earlougher, R. Advances in Well Test Analysis) (Permission to publish by the SPE, copyright SPE, 1977).

Equation 1.3.6 is basically an equation of a straight line that can be expressed as:

$$p_{ws} = p_i - m \left[\log \left(\frac{t_p + \Delta t}{\Delta t} \right) \right] \qquad [1.3.7]$$

This expression suggests that a plot of p_{ws} vs. $(t_p + \Delta t)/\Delta t$ on a semilog scale would produce a straight-line relationship with intercept p_i and slope m, where:

$$m = \frac{162.6 Q_o B_o \mu_o}{kh} \qquad [1.3.8]$$

or:

$$k = \frac{162.6 Q_o B_o \mu_o}{mh}$$

and where:

m = slope of straight line, psi/cycle
k = permeability, md

This plot, commonly referred to as the Horner plot, is illustrated in Figure 1.37. Note that on the Horner plot, the scale of time ratio $(t_p + \Delta t)/\Delta t$ increases from right to left. It is observed from Equation 1.3.6 that $p_{ws} = p_i$ when the time ratio is unity. Graphically this means that the initial reservoir pressure, p_i, can be obtained by extrapolating the Horner plot straight line to $(t_p + \Delta t)/\Delta t = 1$.

The time corresponding to the point of shut-in, t_p can be estimated from the following equation:

$$t_p = \frac{24 N_p}{Q_o}$$

where:

N_p = well cumulative oil produced before shut in, STB
Q_o = stabilized well flow rate before shut in, STB/day
t_p = total production time, hours

Earlougher (1977) pointed out that a result of using the superposition principle is that the skin factor, s, does not appear in the general pressure buildup equation, Equation 1.3.6. That means the Horner-plot slope is not affected by the skin factor; however, the skin factor still does affect the shape of the pressure buildup data. In fact, an early-time deviation from the straight line can be caused by the skin factor as well as by wellbore storage, as illustrated in Figure 1.36. The deviation can be significant for the large negative skins that occur in hydraulically fractured wells. The skin factor does affect flowing pressure before shut-in and its value may be estimated from the buildup test data plus the flowing pressure immediately before the buildup test, as given by:

$$s = 1.151 \left[\frac{p_{1\,hr} - p_{wf\,at\Delta t=0}}{|m|} - \log \left(\frac{k}{\phi \mu c_t r_w^2} \right) + 3.23 \right] \qquad [1.3.9]$$

with an additional pressure drop across the altered zone of:

$$\Delta p_{skin} = 0.87 |m| s$$

where:

$p_{wf\,at\Delta t=0}$ = bottom-hole flowing pressure *immediately before shut in*, psi

s = skin factor
$|m|$ = absolute value of the slope in the Horner plot, psi/cycle
r_w = wellbore radius, ft

The value of $p_{1\,hr}$ must be taken from the Horner straight line. Frequently, the pressure data does not fall on the straight line at 1 hour because of wellbore storage effects or large negative skin factors. In that case, the semilog line must be extrapolated to 1 hour and the corresponding pressure is read.

It should be noted that for a *multiphase flow*, Equations 1.3.6 and 1.3.9 become:

$$p_{ws} = p_i - \frac{162.6q_t}{\lambda_t h} \left[\log\left(\frac{t_p + \Delta t}{\Delta t}\right) \right]$$

$$s = 1.151 \left[\frac{p_{1\,hr} - p_{wf\,at\Delta t=0}}{|m|} \right. $$

$$\left. - \log\left(\frac{\lambda_t}{\phi c_t r_w^2}\right) + 3.23 \right]$$

with:

$$\lambda_t = \frac{k_o}{\mu_o} + \frac{k_w}{\mu_w} + \frac{k_g}{\mu_g}$$

$$q_t = Q_o B_o + Q_w B_w + (Q_g - Q_o R_s) B_g$$

or equivalently in terms of GOR as:

$$q_t = Q_o B_o + Q_w B_w + (GOR - R_s) Q_o B_g$$

where:

q_t = total fluid voidage rate, bbl/day
Q_o = oil flow rate, STB/day
Q_w = water flow rate, STB/day
Q_g = gas flow rate, scf/day
R_s = gas solubility, scf/STB
B_g = gas formation volume factor, bbl/scf
λ_t = total mobility, md/cp
k_o = effective permeability to oil, md
k_w = effective permeability to water, md
k_g = effective permeability to gas, md

The regular Horner plot would produce a semilog straight line with a slope m that can be used to determine the total mobility λ_t from:

$$\lambda_t = \frac{162.6q_t}{mh}$$

Perrine (1956) showed that the effective permeability of each phase, i.e., k_o, k_w, and k_g, can be determined as:

$$k_o = \frac{162.6 Q_o B_o \mu_o}{mh}$$

$$k_w = \frac{162.6 Q_w B_w \mu_w}{mh}$$

$$k_g = \frac{162.6 (Q_g - Q_o R_s) B_g \mu_g}{mh}$$

For gas systems, a plot of $m(p_{ws})$ or p_{ws}^2 vs. $(t_p + \Delta t)/\Delta t$ on a semilog scale would produce a straight line relationship with a slope of m and apparent skin factor s as defined by:
For pseudopressure approach:

$$m = \frac{1637 Q_g T}{kh}$$

$$s^\backslash = 1.151 \left[\frac{m(p_{1\,hr}) - m(p_{wf\,at\,\Delta t=0})}{|m|} \right. $$

$$\left. - \log\left(\frac{k}{\phi \mu_i c_{ti} r_w^2}\right) + 3.23 \right]$$

For pressure-squared approach:

$$m = \frac{1637 Q_g \overline{Z} \overline{\mu}_g}{kh}$$

$$s^\backslash = 1.151 \left[\frac{p_{1\,hr}^2 - p_{wf\,at\,\Delta t=0}^2}{|m|} \right. $$

$$\left. - \log\left(\frac{k}{\phi \mu_i c_{ti} r_w^2}\right) + 3.23 \right]$$

where the gas flow rate Q_g is expressed in Mscf/day.

It should be pointed out that when a well is shut in for a pressure buildup test, the well is usually closed at the surface rather than the sand face. Even though the well is shut in, the reservoir fluid continues to flow and accumulates in the wellbore until the well fills sufficiently to transmit the effect of shut-in to the formation. This "afterflow" behavior is caused by the wellbore storage and it has a significant influence on pressure buildup data. During the period of wellbore storage effects, the pressure data points fall below the semilog straight line. The duration of these effects may be estimated by making the log–log data plot described previously of $\log(p_{ws} - p_{wf})$ vs. $\log(\Delta t)$ with p_{wf} as the value recorded immediately before shut-in. When wellbore storage dominates, that plot will have a unit-slope straight line; as the semilog straight line is approached, the log–log plot bends over to a gently curving line with a low slope.

The wellbore storage coefficient C is, by selecting *a point on the log–log unit-slope straight line* and reading the coordinate of the point in terms of Δt and Δp:

$$C = \frac{q\Delta t}{24\Delta p} = \frac{QB\Delta t}{24\Delta p}$$

where

Δt = shut-in time, hours
Δp = pressure difference $(p_{ws} - p_{wf})$, psi
q = flow rate, bbl/day
Q = flow rate, STB/day
B = formation volume factor, bbl/STB

with a dimensionless wellbore storage coefficient as given by Equation 1.3.4 as:

$$C_D = \frac{0.8936C}{\phi h c_t r_w^2}$$

In all the pressure buildup test analyses, the log–log data plot should be made before the straight line is chosen on the semilog data plot. This log–log plot is essential to avoid drawing a semilog straight line through the wellbore storage-dominated data. The beginning of the semilog line can be estimated by observing when the data points on the log–log plot reach the slowly curving low-slope line and adding 1 to $1\frac{1}{2}$ cycles in time after the end of the unit-slope straight line. Alternatively, the time to the beginning of the semilog straight line can be estimated from:

$$\Delta t > \frac{170000\, Ce^{0.14s}}{(kh/\mu)}$$

where:

c = calculated wellbore storage coefficient, bbl/psi
k = permeability, md
s = skin factor
h = thickness, ft

Table 1.5 *Earlougher's pressure buildup data (Permission to publish by the SPE, copyright SPE, 1977.)*

Δt(hr)	$t_p + \Delta t$(hr)	$t_p + \Delta t \Delta t$	p_{ws} (psig)
0.0	–	–	2761
0.10	310.30	3101	3057
0.21	310.21	1477	3153
0.31	310.31	1001	3234
0.52	310.52	597	3249
0.63	310.63	493	3256
0.73	310.73	426	3260
0.84	310.84	370	3263
0.94	310.94	331	3266
1.05	311.05	296	3267
1.15	311.15	271	3268
1.36	311.36	229	3271
1.68	311.68	186	3274
1.99	311.99	157	3276
2.51	312.51	125	3280
3.04	313.04	103	3283
3.46	313.46	90.6	3286
4.08	314.08	77.0	3289
5.03	315.03	62.6	3293
5.97	315.97	52.9	3297
6.07	316.07	52.1	3297
7.01	317.01	45.2	3300
8.06	318.06	39.5	3303
9.00	319.00	35.4	3305
10.05	320.05	31.8	3306
13.09	323.09	24.7	3310
16.02	326.02	20.4	3313
20.00	330.00	16.5	3317
26.07	336.07	12.9	3320
31.03	341.03	11.0	3322
34.98	344.98	9.9	3323
37.54	347.54	9.3	3323

Example 1.27[a] Table 1.5 shows the pressure buildup data from an oil well with an estimated drainage radius of 2640 ft. Before shut-in, the well had produced at a stabilized rate of 4900 STB/day for 310 hours. Known reservoir data is:

depth = 10 476 ft, $r_w = 0.354$ ft, $c_t = 22.6 \times 10^{-6}$ psi^{-1}

$Q_o = 4900$ STB/D, $h = 482$ ft, $p_{wf}(\Delta t = 0) = 2761$ psig

$\mu_o = 0.20$ cp, $B_o = 1.55$ bbl/STB, $\phi = 0.09$

$t_p = 310$ hours, $r_e = 2640$ ft

Calculate:

- the average permeability k;
- the skin factor;
- the additional pressure drop due to skin.

Solution

Step 1. Plot p_{ws} vs. $(t_p + \Delta t)/\Delta t$ on a semilog scale as shown in Figure 1.38).

Step 2. Identify the correct straight-line portion of the curve and determine the slope m:

$$m = 40 \text{ psi/cycle}$$

[a]This example problem and the solution procedure are given in Earlougher, R. *Advance Well Test Analysis*, Monograph Series, SPE, Dallas (1977).

Step 3. Calculate the average permeability by using Equation 1.3.8:

$$k = \frac{162.6 Q_o B_o \mu_o}{mh}$$

$$= \frac{(162.6)(4900)(1.55)(0.22)}{(40)(482)} = 12.8 \text{ md}$$

Step 4. Determine p_{wf} after 1 hour from the straight-line portion of the curve:

$$p_{1\,hr} = 3266 \text{ psi}$$

Step 5. Calculate the skin factor by applying Equation 1.3.9

$$s = 1.151 \left[\frac{p_{1\,hr} - p_{wf \Delta t = 0}}{m} - \log\left(\frac{k}{\phi \mu c_t r_w^2}\right) + 3.23 \right]$$

$$= 1.151 \left[\frac{3266 - 2761}{40} \right.$$

$$\left. - \log\left(\frac{(12.8)}{(0.09)(0.20)(22.6 \times 10^{-6})(0.354)^2}\right) + 3.23 \right]$$

$$= 8.6$$

Step 6. Calculate the additional pressure drop by using:

$$\Delta p_{skin} = 0.87\,|m|\,s$$

$$= 0.87(40)(8.6) = 299.3 \text{ psi}$$

It should be pointed out that Equation 1.3.6 assumes the reservoir to be infinite in size, i.e., $r_e = \infty$, which implies that at some point in the reservoir the pressure would be always equal to the initial reservoir pressure p_i and the Horner straight-line plot will always extrapolate to p_i. However, reservoirs are finite and soon after production begins, fluid removal will cause a pressure decline everywhere in the reservoir system. Under these conditions, the straight line will not extrapolate to the initial reservoir pressure p_i but, instead, the pressure obtained will be a false pressure as denoted by p^*. The false pressure, as illustrated by Matthews and Russell (1967) in Figure 1.39, has no physical meaning but it is usually used to determine the average reservoir pressure $\bar{p}$. It is clear that p^* will *only equal* the initial (original) reservoir pressure p_i when a new well in a newly discovered field is tested. Using the concept of the false pressure p^*, Horner expressions as given by Equations 1.3.6 and 1.3.7 should be expressed in terms of p^* instead of p_i as:

$$p_{ws} = p^* - \frac{162.6 Q_o \mu_o B_o}{kh}\left[\log\left(\frac{t_p + \Delta t}{\Delta t}\right)\right]$$

and:

$$p_{ws} = p^* - m\left[\log\left(\frac{t_p + \Delta t}{\Delta t}\right)\right] \qquad [1.3.10]$$

Bossie-Codreanu (1989) suggested that the well drainage area can be determined from the Horner pressure buildup plot or the MDH plot, discussed next, by selecting the coordinates of any three points located on the semilog straight-line portion of the plot to determine the slope of the pseudosteady-state line m_{pss}. The coordinates of these three points are designated as:

- shut-in time Δt_1 and with a corresponding shut-in pressure p_{ws1};
- shut-in time Δt_2 and with a corresponding shut-in pressure p_{ws2};
- shut-in time Δt_3 and with a corresponding shut-in pressure p_{ws3}.

The selected shut-in times satisfy $\Delta t_1 < \Delta t_2 < \Delta t_3$. The slope of the pseudosteady-state straight-line m_{pss} is then
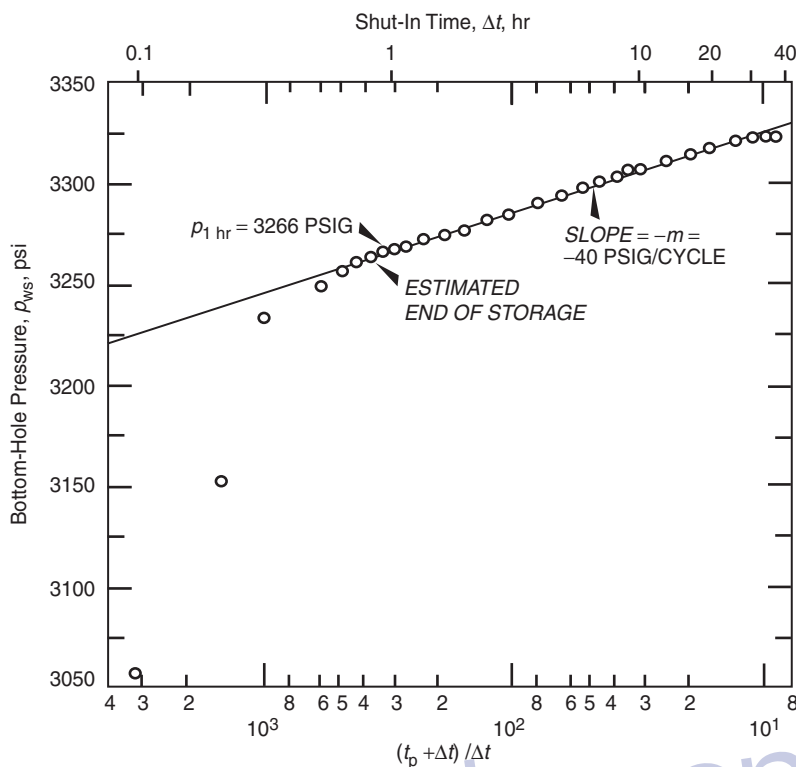
Figure 1.38 *Earlougher's semilog data plot for the buildup test (Permission to publish by the SPE, copyright SPE, 1977).*
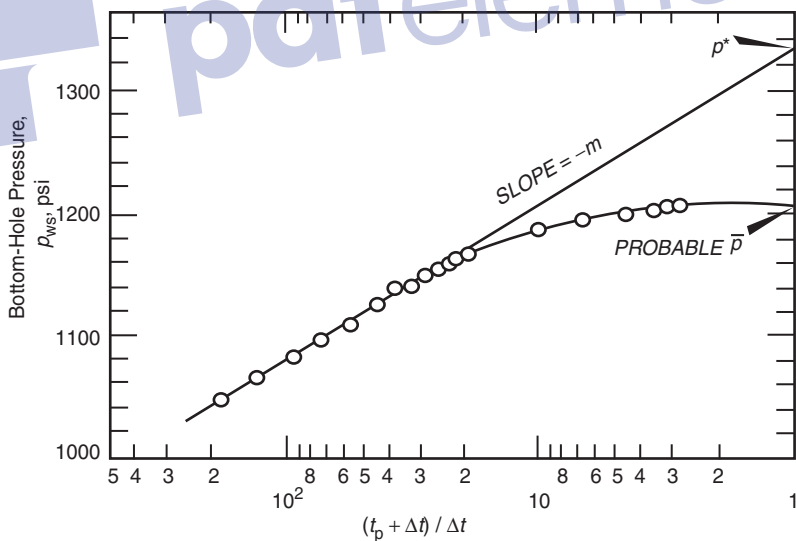
Figure 1.39 *Typical pressure buildup curve for a well in a finite (After Earlougher, R.* Advances in Well Test Analysis*) (Permission to publish by the SPE, copyright SPE, 1977).*

approximated by:

m_{pss}

$$= \frac{(p_{ws2} - p_{ws1})\log(\Delta t_3/\Delta t_1) - (p_{ws3} - p_{ws1})\log[\Delta t_2/\Delta t_1]}{(\Delta t_3 - \Delta t_1)\log(\Delta t_2 \Delta t_1) - (\Delta t_2 - \Delta t_1)\log(\Delta t_3/\Delta t_1)}$$

[1.3.11]

The well drainage area can be calculated from Equation 1.2.116:

$$m^{\backslash} = m_{pss} = \frac{0.23396 Q_o B_o}{c_t A h \phi}$$

Solving for the drainage area gives:

$$A = \frac{0.23396 Q_o B_o}{c_t m_{pss} h \phi}$$

Figure 1.40 *Miller–Dyes–Hutchinson plot for the buildup test (After Earlougher, R.* Advances in Well Test Analysis*)* *(Permission to publish by the SPE, copyright SPE, 1977).*

where:

m_{pss} or $m^\backslash$ = slope of *straight line* during the
pseudosteady-state flow, psi/hr
Q_o = flow rate, bbl/day
A = well drainage area, ft^2

1.3.4 Miller–Dyes–Hutchinson method

The Horner plot may be simplified if the well has been producing long enough to reach a pseudosteady state. Assuming that the production time t_p is much greater than the total shut-in time Δt, i.e., $t_p \gg \Delta t$, the term $t_p + \Delta t \simeq t_p$ and:

$$\log\left(\frac{t_p + \Delta t}{\Delta t}\right) \cong \log\left(\frac{t_p}{\Delta t}\right) = \log(t_p) - \log(\Delta t)$$

Applying the above mathematical assumption to Equation 1.3.10, gives:

$$p_{ws} = p^* - m[\log(t_p) - \log(\Delta t)]$$

or:

$$p_{ws} = [p^* - m\log(t_p)] + m\log(\Delta t)$$

This expression indicates that a plot of p_{ws} vs. $\log(\Delta t)$ would produce a semilog straight line with a positive slope of $+m$ that is identical to that obtained from the Horner plot. The slope is defined mathematically by Equation 1.3.8 as:

$$m = \frac{162.6 Q_o B_o \mu_o}{kh}$$

The semilog straight-line slope m has the same value as of the Horner plot. This plot is commonly called the Miller–Dyes–Hutchinson (MDH) plot. The false pressure p^* may be estimated from the MDH plot by using:

$$p^* = p_{1\,hr} + m\log(t_p + 1) \qquad [1.3.12]$$

where $p_{1\,hr}$ is read from the semilog straight-line plot at $\Delta t = 1$ hour. The MDH plot of the pressure buildup data given in Table 1.5 in terms of p_{ws} vs. $\log(\Delta t)$ is shown in Figure 1.40.

Figure 1.40 shows a positive slope of $m = 40$ psi/cycle that is identical to the value obtained in Example 1.26 with a $p_{1\,hr} = 3266$ psig.

As in the Horner plot, the time that marks the beginning of the MDH semilog straight line may be estimated by making the log–log plot of $(p_{ws} - p_{wf})$ *vs.* Δt and observing when the data points deviate from the 45° angle (unit slope). The exact time is determined by moving 1 to $1\frac{1}{5}$ cycles in time after the end of the unit-slope straight line.

The observed pressure behavior of the test well following the end of the transient flow will depend on:

- shape and geometry of the test well drainage area;
- the position of the well relative to the drainage boundaries;
- length of the producing time t_p before shut-in.

If the well is located in a reservoir with no other wells, the shut-in pressure would eventually become constant (as shown in Figure 1.38) and equal to the *volumetric average reservoir pressure* $\bar{p}_r$. This pressure is required in many reservoir engineering calculations such as:

- material balance studies;
- water influx;
- pressure maintenance projects;
- secondary recovery;
- degree of reservoir connectivity.

Finally, in making future predictions of production as a function of $\bar{p}_r$, pressure measurements throughout the reservoir's life are almost mandatory if one is to compare such a prediction to actual performance and make the necessary adjustments to the predictions. One way to obtain this pressure is to shut in all wells producing from the reservoir for a period of time that is sufficient for pressures to equalize throughout the system to give $\bar{p}_r$. Obviously, such a procedure is not practical.

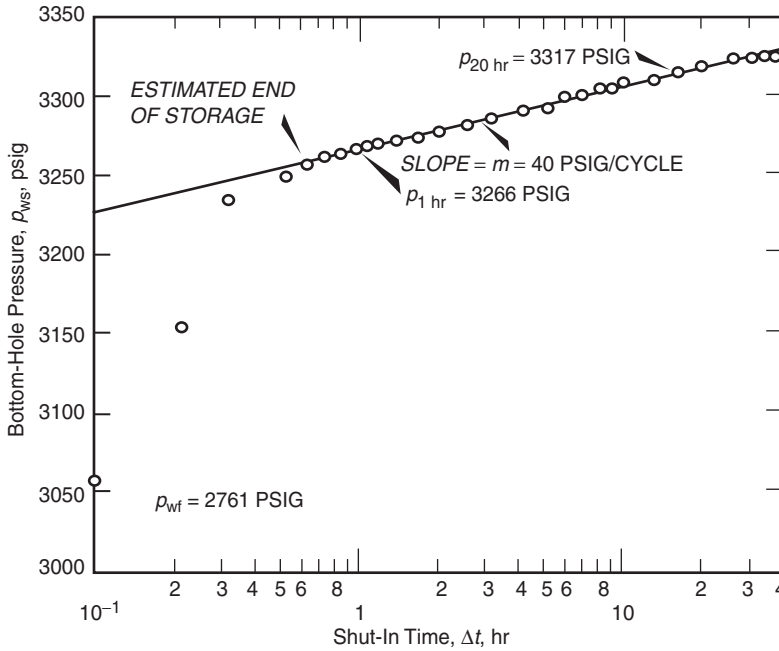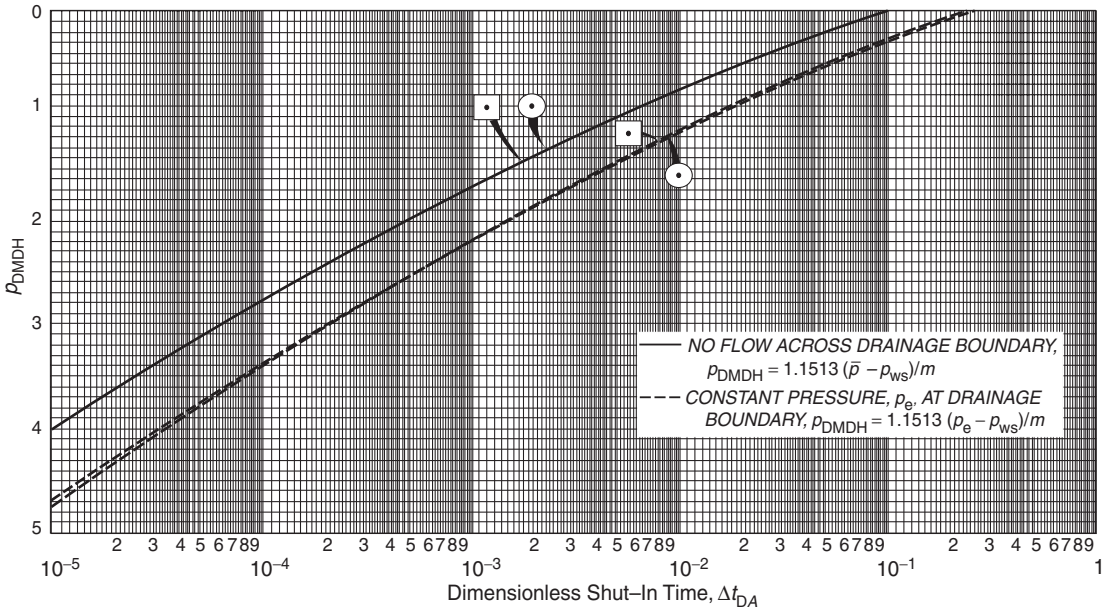**Figure 1.41** *Miller–Dyes–Hutchinson dimensionless pressure for circular and square drainage areas (After Earlougher, R.* Advances in Well Test Analysis*) (Permission to publish by the SPE, copyright SPE, 1977).*

To use the MDH method to estimate average drainage region pressure $\bar{p}_r$ for a circular or square system producing at *pseudosteady state before shut-in*:

(1) Choose any convenient time on the semilog straight line Δt and read the corresponding pressure p_{ws}.
(2) Calculate the dimensionless shut-in time based on the drainage area A from:

$$\Delta t_{DA} = \frac{0.0002637 k \Delta t}{\phi \mu c_t a}$$

(3) Enter Figure 1.41 with the dimensionless time $\Delta t_D A$ and determine an MDH dimensionless pressure p_{DMDH} from the upper curve of Figure 1.41.
(4) Estimate the average reservoir pressure in the closed drainage region from:

$$\bar{p}_r = p_{ws} + \frac{m p_{DMDH}}{1.1513}$$

where m is the semilog straight line of the MDH plot.

There are several other methods for determining $\bar{p}_r$ from a buildup test. Three of these methods are briefly presented below:

(1) the Matthews–Brons–Hazebroek (MBH) method;
(2) the Ramey-Cobb method;
(3) the Dietz method.

1.3.5 MBH method

As noted previously, the buildup test exhibits a semilog straight line which begins to bend down and become flat at the later shut-in times because of the effect of the boundaries. Matthews et al. (1954) proposed a methodology for estimating average pressure from buildup tests in bounded drainage regions. The MBH method is based on theoretical correlations between the extrapolated semilog straight line to the false pressure p^* and current average drainage area pressure $\bar{p}$. The authors point out that the average pressure in the drainage area of each well can be related to p^* if the geometry, shape, and location of the well relative to the drainage boundaries are known. They developed a set of correction charts, as shown in Figures 1.42 through 1.45, for various drainage geometries.

The y axis of these figures represents the MBH dimensionless pressure p_{DMBH} that is defined by:

$$p_{DMBH} = \frac{2.303(p^* - \bar{p})}{|m|}$$

or:

$$\bar{p} = p^* - \left(\frac{|m|}{2.303}\right) p_{DMBH} \qquad [1.3.13]$$

where m is the *absolute* value of the slope obtained from the Horner semilog straight-line plot. The MBH dimensionless pressure is determined at the dimensionless producing time t_{pDA} that corresponds to the flowing time t_p. That is:

$$t_{pDA} = \left[\frac{0.0002637 k}{\phi \mu c_t A}\right] t_p \qquad [1.3.14]$$

where:

t_p = flowing time before shut-in, hours
A = drainage area, ft^2
k = permeability, md
c_t = total compressibility, psi^{-1}

The following steps summarize the procedure for applying the MBH method:

Step 1. Make a Horner plot.
Step 2. Extrapolate the semilog straight line to the value of p^* at $(t_p + \Delta t)/\Delta t = 1.0$.
Step 3. Evaluate the slope of the semilog straight line m.
Step 4. Calculate the MBH dimensionless producing time t_{pDA} from Equation 1.3.14:

$$t_{pDA} = \left[\frac{0.0002637 k}{\phi \mu c_t A}\right] t_p$$

Step 5. Find the closest approximation to the shape of the well drainage area in Figures 1.41 through 1.44 and identify the correction curve.
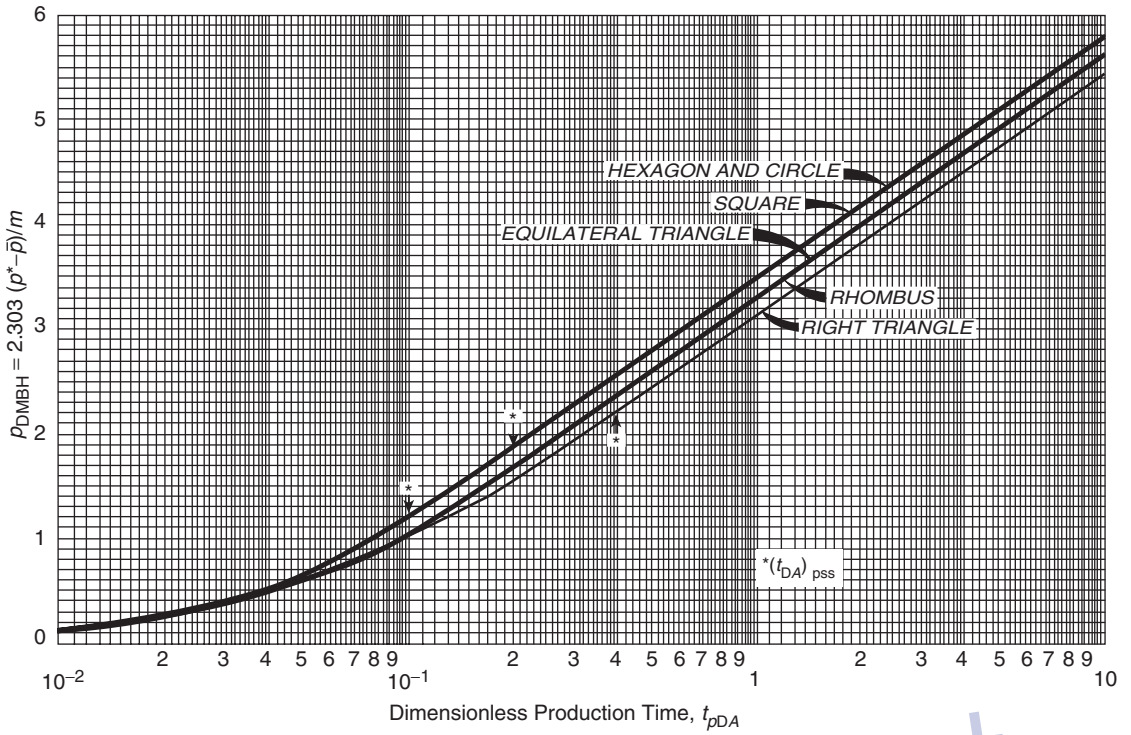
Figure 1.42 *Matthews–Brons–Hazebroek dimensionless pressure for a well in the center of equilateral drainage areas (After Earlougher, R. Advances in Well Test Analysis) (Permission to publish by the SPE, copyright SPE, 1977).*
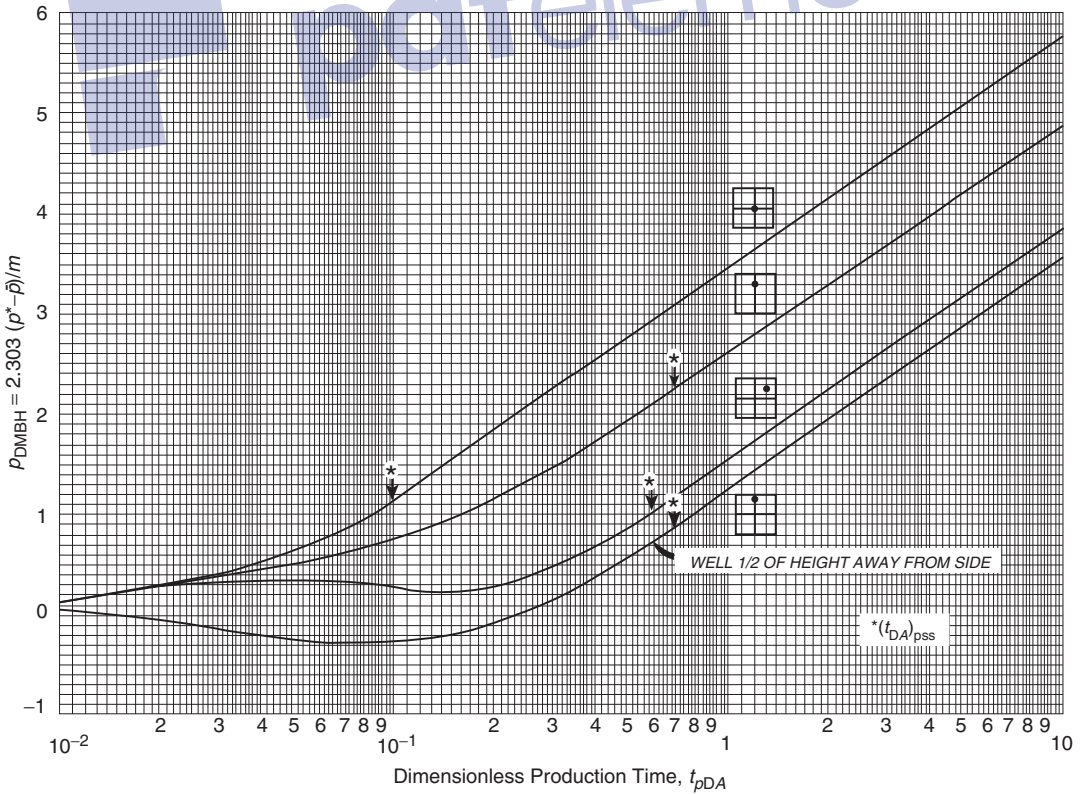
Figure 1.43 *Matthews–Brons–Hazebroek dimensionless pressure for different well locations in a square drainage area. (After Earlougher, R. Advances in Well Test Analysis) (Permission to publish by the SPE, copyright SPE, 1977).*
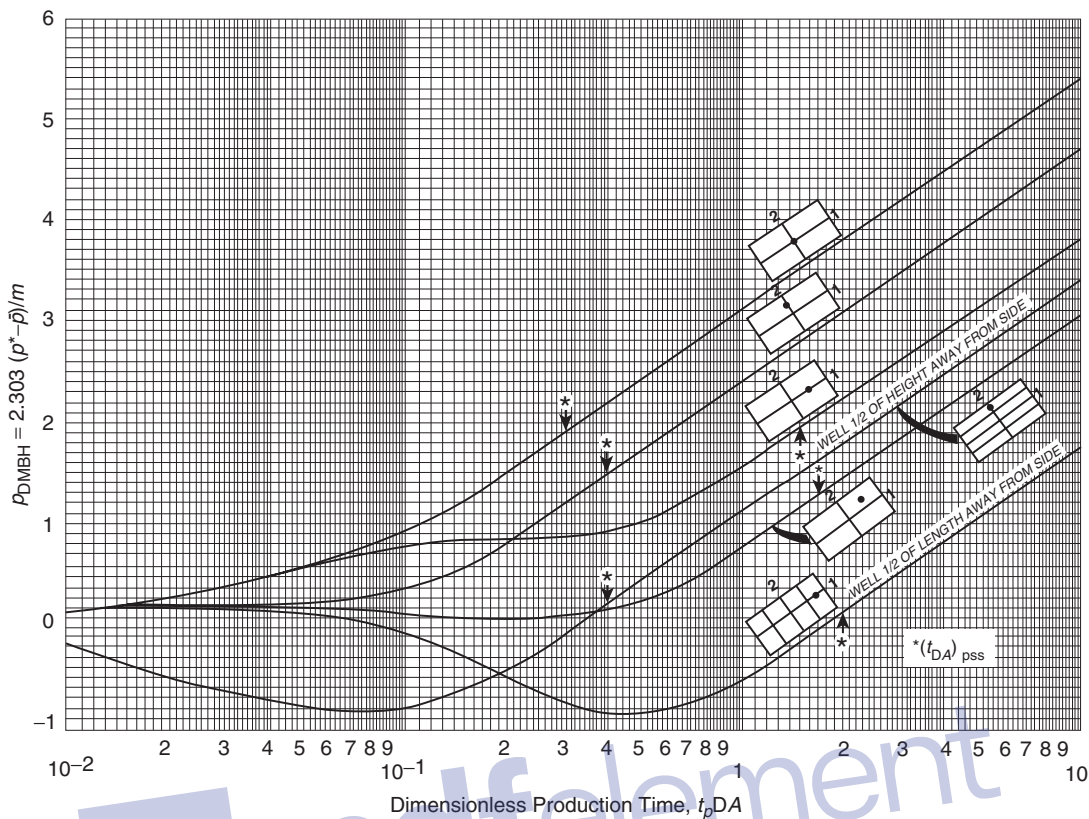
Figure 1.44 *Matthews–Brons–Hazebroek dimensionless pressure for different well locations in a 2:1 rectangular drainage area (After Earlougher, R. Advances in Well Test Analysis) (Permission to publish by the SPE, copyright SPE, 1977).*
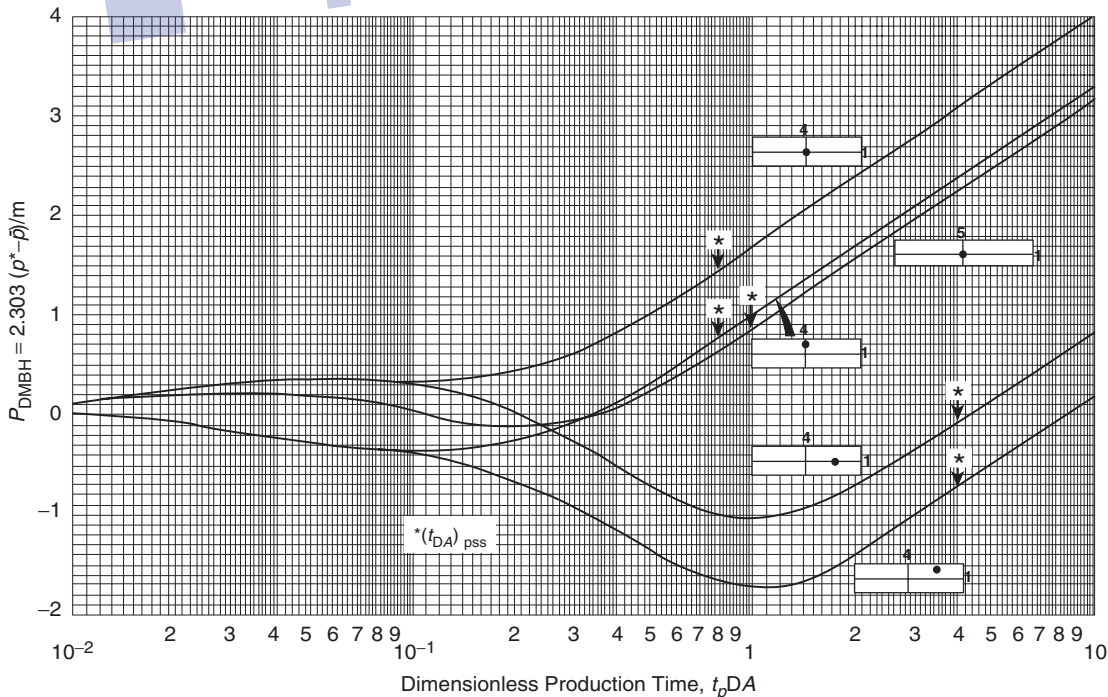
Figure 1.45 *Matthews–Brons–Hazebroek dimensionless pressure for different well locations in 4:1 and 5:1 rectangular drainage areas (After Earlougher, R. Advances in Well Test Analysis) (Permission to publish by the SPE, copyright SPE, 1977).*

Step 6. Read the value of p_{DMBH} from the correction curve at $t_{\text{PD}A}$

Step 7. Calculate the value of $\bar{p}$ from Equation 1.3.13:

$$\bar{p} = p^* - \left(\frac{|m|}{2.303}\right) p_{\text{DMBH}}$$

As in the normal Horner analysis technique, the producing time t_{p} is given by:

$$t_{\text{p}} = \frac{24 N_{\text{p}}}{Q_{\text{o}}}$$

where N_{p} is the cumulative volume produced since the *last pressure buildup test* and Q_{o} is the constant flow rate just before shut-in. Pinson (1972) and Kazemi (1974) indicate that t_{p} should be compared with the time required to reach the pseudosteady state, t_{pss}:

$$t_{\text{pss}} = \left[\frac{\phi \mu c_{\text{t}} A}{0.0002367 k}\right] (t_{\text{D}A})_{\text{pss}} \qquad [1.3.15]$$

For a symmetric closed or circular drainage area, $(t_{\text{D}A})_{\text{pss}} = 0.1$ as given in Table 1.4 and listed in the fifth column.

If $t_{\text{p}} \gg t_{\text{pss}}$, then t_{pss} should ideally replace t_{p} in both the Horner plot and for use with the MBH dimensionless pressure curves.

The above methodology gives the value of $\bar{p}$ in the drainage area of *one well*, e.g., well i. If a number of wells are producing from the reservoir, each well can be analyzed separately to give $\bar{p}$ for its own drainage area. The reservoir average pressure $\bar{p}_{\text{r}}$ can be estimated from these *individual well average drainage pressures* by using one of the relationships given by Equations 1.2.118 and 1.2.119. That is:

$$\bar{p}_{\text{r}} = \frac{\sum_i (\bar{p} q)_i / (\partial \bar{p}/\partial t)_i}{\sum_i q_i / (\partial \bar{p}/\partial t)_i}$$

or:

$$\bar{p}_{\text{r}} = \frac{\sum_i [\bar{p} \Delta(F)/\Delta \bar{p}]_i}{\sum_i [\Delta(F)/\Delta \bar{p}]_i}$$

with:

$$F_{\text{t}} = \int_0^t [Q_{\text{o}} B_{\text{o}} + Q_{\text{w}} B_{\text{w}} + (Q_{\text{g}} - Q_{\text{o}} R_s - Q_{\text{w}} R_{\text{sw}}) B_g] \, \text{d}t$$

$$F_{\text{t}+\Delta t} = \int_0^{t+\Delta t} [Q_{\text{o}} B_{\text{o}} + Q_{\text{w}} B_{\text{w}} + (Q_{\text{g}} - Q_{\text{o}} R_s - Q_{\text{w}} R_{\text{sw}}) B_g] \, \text{d}t$$

and:

$$\Delta(F) = F_{\text{t}+\Delta t} - F_{\text{t}}$$

Similarly, it should be noted that the MBH method and the Figures 1.41 through 1.44 can be applied for compressible gases by defining p_{DMBH} as:

For the pseudopressure approach

$$p_{\text{DMBH}} = \frac{2.303[m(p^*) - m(\bar{p})]}{|m|} \qquad [1.3.16]$$

For the pressure-squared approach

$$p_{\text{DMBH}} = \frac{2.303[(p^*)^2 - (\bar{p})^2]}{|m|} \qquad [1.3.17]$$

Example 1.28 Using the information given in Example 1.27 and pressure buildup data listed in Table 1.5, calculate the average pressure in the well drainage area and the drainage area by applying Equation 1.3.11. The data is listed below for convenience:

$$r_{\text{e}} = 2640 \text{ ft}, \quad r_{\text{w}} = 0.354 \text{ ft}, \quad c_{\text{t}} = 22.6 \times 10^{-6} \text{ psi}^{-1}$$

$$Q_{\text{o}} = 4,900 \text{ STB/D}, \quad h = 482 \text{ ft},$$

$$p_{\text{wf at } \Delta t = 0} = 2761 \text{ psig}$$

$$\mu_{\text{o}} = 0.20 \text{ cp}, \quad B_{\text{o}} = 1.55 \text{ bbl/STB}, \quad \phi = 0.09$$

$$t_{\text{p}} = 310 \text{ hours}, \quad \text{depth} = 10\,476 \text{ ft},$$

reported average pressure $= 3323$ psi

Solution

Step 1. Calculate the drainage area of the well:

$$A = \pi r_{\text{e}}^2 = \pi (2640)^2$$

Step 2. Compare the production time t_{p}, i.e., 310 hours, with the time required to reach the pseudosteady state t_{pss} by applying Equation 1.3.15. Estimate t_{pss} using $(t_{\text{D}A})_{\text{pss}} = 0.1$ to give:

$$t_{\text{pss}} = \left[\frac{\phi \mu c_{\text{t}} A}{0.0002367 k}\right] (t_{\text{D}A})_{\text{pss}}$$

$$= \left[\frac{(0.09)(0.2)(22.6 \times 10^{-6})(\pi)(2640)^2}{(0.0002637)(12.8)}\right] 0.1$$

$$= 264 \text{ hours}$$

Thus, we could replace t_{p} by 264 hours in our analysis because $t_{\text{p}} > t_{\text{pss}}$. However, since t_{p} is only about $1.2 t_{\text{pss}}$, we use the actual production time of 310 hours in the calculation.

Step 3. Figure 1.38 does not show p^* since the semilog straight line is not extended to $(t_{\text{p}} + \Delta t)/\Delta t = 1.0$. However, p^* can be calculated from p_{ws} at $(t_{\text{p}} + \Delta t)/\Delta t = 10.0$ by extrapolating one cycle. That is:

$$p^* = 3325 + (1 \text{ cycle})(40 \text{ psi/cycle}) = 3365 \text{ psig}$$

Step 4. Calculate $t_{\text{pD}A}$ by applying Equation 1.3.14 to give:

$$t_{\text{pD}A} = \left[\frac{0.0002637 k}{\phi \mu c_{\text{t}} A}\right] t_{\text{p}}$$

$$= \left[\frac{0.0002637(12.8)}{(0.09)(0.2)(22.6 \times 10^{-6})(\pi)(2640)^2}\right] 310$$

$$= 0.117$$

Step 5. From the curve of the circle in Figure 1.42, obtain the value of p_{DMBH} at $t_{\text{pD}A} = 0.117$, to give:

$$p_{\text{DMBH}} = 1.34$$

Step 6. Calculate the average pressure from Equation 1.3.13:

$$\bar{p} = p^* - \left(\frac{|m|}{2.303}\right) p_{\text{DMBH}}$$

$$= 3365 - \left(\frac{40}{2.303}\right)(1.34) = 3342 \text{ psig}$$

This is 19 psi higher than the maximum pressure recorded of 3323 psig.

Step 7. Select the coordinates of any three points located on the semilog straight line portion of the Horner plot, to give:

- $(\Delta t_1, p_{\text{ws1}}) = (2.52, 3280)$
- $(\Delta t_2, p_{\text{ws2}}) = (9.00, 3305)$
- $(\Delta t_3, p_{\text{ws3}}) = (20.0, 3317)$

Step 8. Calculate m_{pss} by applying Equation 1.3.11:

$$m_{\text{pss}} = \frac{(p_{\text{ws2}} - p_{\text{ws1}}) \log(\Delta t_3/\Delta t_1) - (p_{\text{ws3}} - p_{\text{ws1}}) \log(\Delta t_2/\Delta t_1)}{(\Delta t_3 - \Delta t_1) \log(\Delta t_2/\Delta t_1) - (\Delta t_2 - \Delta t_1) \log(\Delta t_3/\Delta t_1)}$$

$$= \frac{(3305 - 3280) \log(20/2.51) - (3317 - 3280) \log(9/2.51)}{(20 - 2.51) \log(9/2.51) - (9 - 2.51) \log(20/2.51)}$$

$$= 0.52339 \text{ psi/hr}$$

Step 9. The well drainage area can then be calculated from Equation 1.2.116:

$$A = \frac{0.23396 Q_o B_o}{c_t m_{pss} h \phi}$$

$$= \frac{0.23396(4900)(1.55)}{(22.6 \times 10^{-6})(0.52339)(482)(0.09)}$$

$$= 3\,462\,938 \text{ ft}^2$$

$$= \frac{3\,363\,938}{43\,560} = 80 \text{ acres}$$

The corresponding drainage radius is 1050 ft which differs considerably from the given radius of 2640 ft. Using the calculated drainage radius of 1050 ft and repeating the MBH calculations gives:

$$t_{pss} = \left[\frac{(0.09)(0.2)(22.6 \times 10^{-6})(\pi)(1050)^2}{(0.0002637)(12.8)}\right] 0.1$$

$$= 41.7 \text{ hours}$$

$$t_{pDA} = \left[\frac{0.0002637(12.8)}{(0.09)(0.2)(22.6 \times 10^{-6})(\pi)(1050)^2}\right] 310 = 0.743$$

$$p_{DMBH} = 3.15$$

$$\bar{p} = 3365 - \left(\frac{40}{2.303}\right)(3.15) = 3311 \text{ psig}$$

The value is 12 psi higher than the reported value of average reservoir pressure.

1.3.6 Ramey–Cobb method

Ramey and Cobb (1971) proposed that the average pressure in the well drainage area can be read directly from the Horner semilog straight line if the following data is available:

- shape of the well drainage area;
- location of the well within the drainage area;
- size of the drainage area.

The proposed methodology is based on calculating the dimensionless producing time t_{pDA} as defined by Equation 1.3.14:

$$t_{pDA} = \left[\frac{0.0002637 k}{\phi \mu c_t A}\right] t_p$$

where:

t_p = producing time since the last shut-in, hours
A = drainage area, ft^2

Knowing the shape of the drainage area and well location, determine the dimensionless time to reach pseudosteady state $(t_{DA})_{pss}$, as given in Table 1.4 in the fifth column. Compare t_{pDA} with $(t_{DA})_{pss}$:

- If $t_{pDA} < (t_{DA})_{pss}$, then read the average pressure $\bar{p}$ from the Horner semilog straight line at:

$$\left(\frac{t_p + \Delta t}{\Delta t}\right) = \exp(4\pi t_{pDA}) \qquad [1.3.18]$$

or use the following expression to estimate $\bar{p}$:

$$\bar{p} = p^* - m \log\left[\exp(4\pi t_{pDA})\right] \qquad [1.3.19]$$

- If $t_{pDA} > (t_{DA})_{pss}$, then read the average pressure $\bar{p}$ from the Horner semilog straight-line plot at:

$$\left(\frac{t_p + \Delta t}{\Delta t}\right) = C_A t_{pDA} \qquad [1.3.20]$$

where C_A is the shape factor as determined from Table 1.4.s Equivalently, the average pressure can be estimated from:

$$\bar{p} = p^* - m \log(C_A t_{pDA}) \qquad [1.3.21]$$

where:

m = absolute value of the semilog straight-line slope, psi/cycle
p^* = false pressure, psia
C_A = shape factor, from Table 1.4

Example 1.29 Using the data given in Example 1.27, recalculate the average pressure using the Ramey and Cobb method.

Solution

Step 1. Calculate t_{pDA} by applying Equation (1.3.14):

$$t_{pDA} = \left[\frac{0.0002637 k}{\phi \mu c_t A}\right] t_p$$

$$= \left[\frac{0.0002637(12.8)}{(0.09)(0.2)(22.6 \times 10^{-6})(\pi)(2640)^2}\right](310)$$

$$= 0.1175$$

Step 2. Determine C_A and $(t_{DA})_{pss}$ from Table 1.4 for a well located in the centre of a circle, to give:

$$C_A = 31.62$$
$$(t_{DA})_{pss} = 0.1$$

Step 3. Since $t_{pDA} > (t_{DA})_{pss}$, calculate $\bar{p}$ from Equation 1.3.21:

$$\bar{p} = p^* - m \log(C_A t_{pDA})$$

$$= 3365 - 40 \log[31.62(0.1175)] = 3342 \text{ psi}$$

This value is identical to that obtained from the MBH method.

1.3.7 Dietz method

Dietz (1965) indicated that if the test well has been producing long enough to reach the pseudosteady state before shut-in, the average pressure can be read directly from the MDH semilog straight-line plot, i.e., p_{ws} vs. $\log(\Delta t)$, at the following shut-in time:

$$(\Delta t)_{\bar{p}} = \frac{\phi \mu c_t A}{0.0002637 C_A k} \qquad [1.3.22]$$

where:

Δt = shut-in time, hours
A = drainage area, ft^2
C_A = shape factor
k = permeability, md
c_t = total compressibility, psi^{-1}

Example 1.30 Using the Dietz method and the buildup data given in Example 1.27, calculate the average pressure:

Solution

Step 1. Using the buildup data given in Table 1.5, construct the MDH plot of p_{ws} vs. $\log(\Delta t)$ as shown in Figure 1.40. From the plot, read the following values:

$$m = 40 \text{ psi/cycle}$$
$$p_{1\,hr} = 3266 \text{ psig}$$

Step 2. Calculate false pressure p^* from Equation 1.3.12 to give:

$$p^* = p_{1\,hr} + m\log(t_p + 1)$$

$$= 3266 + 40\log(310 + 1) = 3365.7 \text{ psi}$$

Step 3. Calculate the shut-in time $(\Delta t)_{\bar{p}}$ from Equation 1.3.20:

$$(\Delta t)_{\bar{p}} = \frac{(0.09)(0.2)(22.6 \times 10^{-6})(\pi)(2640)^2}{(0.0002637)(12.8)(31.62)}$$

$$= 83.5 \text{ hours}$$

Step 4. Since the MDH plot does not extend to 83.5 hours, the average pressure can be calculated from the semilog straight-line equation as given by:

$$p = p_{1\,hr} + m\log(\Delta t - 1) \qquad [1.3.23]$$

or:

$$\bar{p} = 3266 + 40\log(83.5 - 1) = 3343 \text{ psi}$$

As indicated earlier, the skin factor s is used to calculate the additional pressure drop in the altered permeability area around the wellbore and to characterize the well through the calculation of the flow coefficient E. That is:

$$\Delta p_{skin} = 0.87\,|m|\,s$$

and:

$$E = \frac{J_{actual}}{J_{ideal}} = \frac{\bar{p} - p_{wf} - \Delta p_{skin}}{\bar{p} - p_{wf}}$$

where $\bar{p}$ is the average pressure in the well drainage area. Lee (1982) suggested that for rapid analysis of the pressure buildup, the flow efficiency can be approximated by using the extrapolated straight-line pressure p^*, to give:

$$E = \frac{J_{actual}}{J_{ideal}} \approx \frac{p^* - p_{wf} - \Delta p_{skin}}{\bar{p} - p_{wf}}$$

Earlougher (1977) pointed out that there are a surprising number of situations where a single pressure point or "spot pressure" is the only pressure information available about a well. The average drainage region pressure $\bar{p}$ can be estimated from the spot pressure reading at shut-in time Δt using:

$$\bar{p} = p_{ws\ at\ \Delta t} + \frac{162.6 Q_o \mu_o B_o}{kh}\left[\log\left(\frac{\phi\mu c_t A}{0.0002637 k C_A \Delta t}\right)\right]$$

For a closed square drainage region $C_A = 30.8828$ and:

$$\bar{p} = p_{ws\ at\ \Delta t} + \frac{162.6 Q_o \mu_o B_o}{kh}\left[\log\left(\frac{122.8\phi\mu c_t A}{k\Delta t}\right)\right]$$

where $p_{ws\ at\ \Delta t}$ is the spot pressure reading at shut-in time Δt and:

Δt = shut-in time, hours
A = drainage area, ft^2
C_A = shape factor
k = permeability, md
c_t = total compressibility, psi^{-1}

It is appropriate at this time to briefly introduce the concept of type curves and discuss their applications in well testing analysis.

1.4 Type Curves

The type curve analysis approach was introduced in the petroleum industry by Agarwal et al. (1970) as a valuable tool when used in conjunction with conventional semilog plots. A type curve is a graphical representation of the theoretical solutions to flow equations. The type curve analysis consists of finding the theoretical type curve that "matches" the actual response from a test well and the reservoir when subjected to changes in production rates or pressures. The match can be found graphically by physically superposing a graph of actual test data with a similar graph of type curve(s) and searching for the type curve that provides the best match. Since type curves are plots of theoretical solutions to transient and pseudosteady-state flow equations, they are usually presented in terms of dimensionless variables (e.g., p_D, t_D, r_D, and C_D) rather than real variables (e.g., Δp, t, r, and C). The reservoir and well parameters, such as permeability and skin, can then be calculated from the dimensionless parameters defining that type curve.

Any variable can be made "dimensionless" by multiplying it by a group of constants with opposite dimensions, but the choice of this group will depend on the type of problem to be solved. For example, to create the dimensionless pressure drop p_D, the actual pressure drop Δp in psi is multiplied by the group A with units of psi^{-1}, or:

$$p_D = A\Delta p$$

Finding the group A that makes a variable dimensionless is derived from equations that describe reservoir fluid flow. To introduce this concept, recall Darcy's equation that describes radial, incompressible, steady-state flow as expressed by:

$$Q = \left[\frac{kh}{141.2B\mu[\ln(r_e/r_{wa}) - 0.5]}\right]\Delta p \qquad [1.4.1]$$

where r_{wa} is the apparent (effective) wellbore radius and defined by Equation 1.2.140 in terms of the skin factor s as:

$$r_{wa} = r_w e^{-s}$$

Group A can be defined by rearranging Darcy's equation as:

$$\ln\left(\frac{r_e}{r_{wa}}\right) - \frac{1}{2} = \left[\frac{kh}{141.2QB\mu}\right]\Delta p$$

Because the left-hand slide of this equation is dimensionless, the right-hand side must be accordingly dimensionless. This suggests that the term $kh/141.2QB\mu$ is essentially group A with units of psi^{-1} that defines the dimensionless variable p_D, or:

$$p_D = \left[\frac{kh}{141.2QB\mu}\right]\Delta p \qquad [1.4.2]$$

Taking the logarithm of both sides of this equation gives:

$$\log(p_D) = \log(\Delta p) + \log\left(\frac{kh}{141.2QB\mu}\right) \qquad [1.4.3]$$

where:

Q = flow rate, STB/day
B = formation, volume factor, bbl/STB
μ = viscosity, cp

For a constant flow rate, Equation 1.4.3 indicates that the logarithm of dimensionless pressure drop, $\log(p_D)$, will differ from the logarithm of the *actual* pressure drop, $\log(\Delta p)$, by a constant amount of:

$$\log\left(\frac{kh}{141.2QB\mu}\right)$$

Similarly, the dimensionless time t_D is given by Equation 1.2.75 as:

$$t_D = \left[\frac{0.0002637k}{\phi\mu c_t r_w^2}\right]t$$

Taking the logarithm of both sides of this equation gives:

$$\log(t_D) = \log(t) + \log\left[\frac{0.0002637k}{\phi\mu c_t r_w^2}\right] \qquad [1.4.4]$$
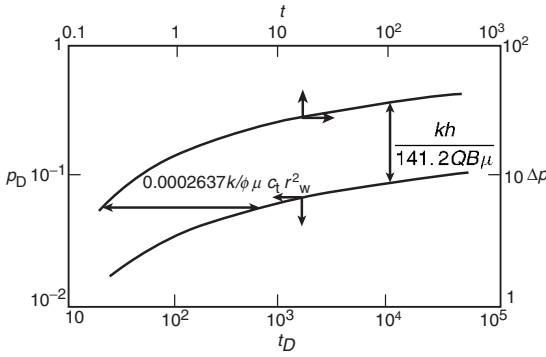
Figure 1.46 *Concept of type curves.*

where:

t = time, hours
c_t = total compressibility coefficient, psi^{-1}
ϕ = porosity

Hence, a graph of $\log(\Delta p)$ vs. $\log(t)$ will have an *identical shape* (i.e., parallel) to a graph of $\log(p_D)$ vs. $\log(t_D)$, although the curve will be shifted by $\log[kh/(141.2QB\mu)]$ vertically in pressure and $\log[0.0002637k/(\phi\mu c_t r_w^2)]$ horizontally in time. This concept is illustrated in Figure 1.46.

Not only do these two curves have the same shape, but if they are *moved relative to each other until they coincide or "match"*, the vertical and horizontal displacements required to achieve the match are related to these constants in Equations 1.4.3 and 1.4.4. Once these constants are determined from the vertical and horizontal displacements, it is possible to estimate reservoir properties such as permeability and porosity. This process of matching two curves through the vertical and horizontal displacements and determining the reservoir or well properties is called type curve matching.

As shown by Equation 1.2.83, the solution to the diffusivity equation can be expressed in terms of the dimensionless pressure drop as:

$$p_D = -\frac{1}{2}\text{Ei}\left(-\frac{r_D^2}{4t_D}\right)$$

Equation 1.2.84 indicates that when $t_D/r_D^2 > 25$, p_D can be approximated by:

$$p_D = \frac{1}{2}\left[\ln\left(t_D/r_D^2\right) + 0.080907\right]$$

Notice that:

$$\frac{t_D}{r_D^2} = \left(\frac{0.0002637k}{\phi\mu c_t r^2}\right)t$$

Taking the logarithm of both sides of this equation, gives:

$$\log\left(\frac{t_D}{r_D^2}\right) = \log\left(\frac{0.0002637k}{\phi\mu c_t r^2}\right) + \log(t) \qquad [1.4.5]$$

Equations 1.4.3 and 1.4.5 indicate that a graph of $\log(\Delta p)$ vs. $\log(t)$ will have an *identical shape* (i.e., parallel) to a graph of $\log(p_D)$ vs. $\log(t_D/r_D^2)$, although the curve will be shifted by $\log(kh141.2/QB\mu)$ vertically in pressure and $\log(0.0002637k/\phi\mu c_t r^2)$ horizontally in time. When these two curves are moved relative to each other until they coincide or "match," the vertical and horizontal movements, in mathematical terms, are given by:

$$\left(\frac{p_D}{\Delta p}\right)_{MP} = \frac{kh}{141.2QB\mu} \qquad [1.4.6]$$

and:

$$\left(\frac{t_D/r_D^2}{t}\right)_{MP} = \frac{0.0002637k}{\phi\mu c_t r^2} \qquad [1.4.7]$$

The subscript "MP" denotes a match point.

A more practical solution then to the diffusivity equation is a plot of the dimensionless p_D vs. t_D/r_D^2 as shown in Figure 1.47 that can be used to determine the pressure at any time and radius from the producing well. Figure 1.47 is basically a type curve that is mostly used in interference tests when analyzing pressure response data in a shut-in observation well at a distance r from an active producer or injector well.

In general, the type curve approach employs the flowing procedure that will be illustrated by the use of Figure 1.47:

Step 1. Select the proper type curve, e.g., Figure 1.47.
Step 2. Place tracing paper over Figure 1.47 and construct a log–log scale having the same dimensions as those of the type curve. This can be achieved by tracing the major and minor grid lines from the type curve to the tracing paper.
Step 3. Plot the well test data in terms of Δp vs. t on the tracing paper.
Step 4. Overlay the tracing paper on the type curve and slide the actual data plot, keeping the x and y axes of both graphs parallel, until the actual data point curve coincides or matches the type curve.
Step 5. Select any arbitrary point match point MP, such as an intersection of major grid lines, and record $(\Delta p)_{MP}$ and $(t)_{MP}$ from the actual data plot and the corresponding values of $(p_D)_{MP}$ and $(t_D/r_D^2)_{MP}$ from the type curve.
Step 6. Using the match point, calculate the properties of the reservoir.

The following example illustrates the convenience of using the type curve approach in an interference test for 48 hours followed by a falloff period of 100 hours.

Example 1.31[a] During an interference test, water was injected at a 170 bbl/day for 48 hours. The pressure response in an observation well 119 ft away from the injector is given below:

t (hrs)	p (psig)	$\Delta p_{ws} = p_i - p$ (psi)
0	$p_i = 0$	0
4.3	22	−22
21.6	82	−82
28.2	95	−95
45.0	119	−119
48.0		injection ends
51.0	109	−109
69.0	55	−55
73.0	47	−47
93.0	32	−32
142.0	16	−16
148.0	15	−15

Other given data includes:

$$p_i = 0 \text{ psi}, \quad B_w = 1.00 \text{ bbl/STB}$$

[a]This example problem and the solution procedure are given in Earlougher, R. *Advanced Well Test Analysis*, Monograph Series, SPE, Dallas (1977).
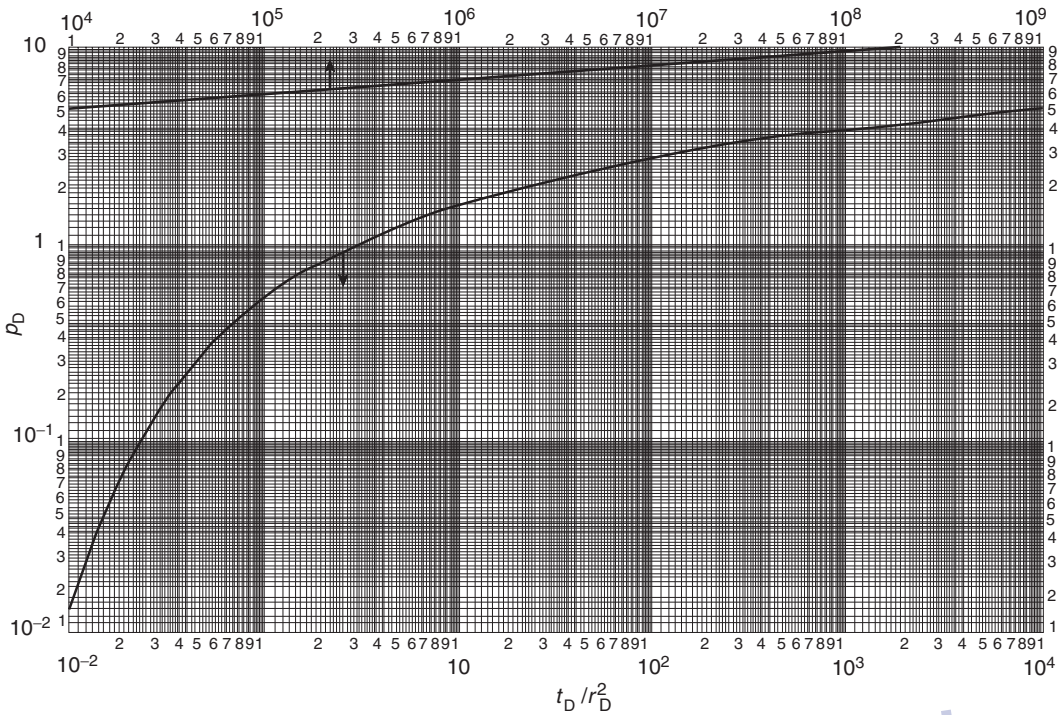
Figure 1.47 *Dimensionless pressure for a single well in an infinite system, no wellbore storage, no skin. Exponential–integral solution (After Earlougher, R.* Advances in Well Test Analysis) *(Permission to publish by the SPE, copyright SPE, 1977).*

$c_t = 9.0 \times 10^{-6} \, \text{psi}^{-1}, \quad h = 45 \, \text{ft}$

$\mu_w = 1.3 \, \text{cp}, \quad q = -170 \, \text{bbl/day}$

Calculate the reservoir permeability and porosity.

Solution

Step 1. Figure 1.48 show a plot of the well test data during the injection period, i.e., 48 hours, in terms of Δp vs. t on tracing paper with the same scale dimensions as in Figure 1.47. Using the overlay technique with the vertical and horizontal movements, find the segment of the type curve that matches the actual data.

Step 2. Select any point on the graph that will be defined as a match point MP, as shown in Figure 1.48. Record $(\Delta p)_{MP}$ and $(t)_{MP}$ from the actual data plot and the corresponding values of $(p_D)_{MP}$ and $(t_D/r_D^2)_{MP}$ from the type curve, to give:

Type curve match values:

$$(p_D)_{MP} = 0.96, \quad (t_D/r_D^2)_{MP} = 0.94$$

Actual data match values:

$$(\Delta p)_{MP} = -100 \, \text{psig}, \quad (t)_{MP} = 10 \, \text{hours}$$

Step 3. Using Equations 1.4.6 and 1.4.7, solve for the permeability and porosity:

$$k = \frac{141.2QB\mu}{h}\left(\frac{p_D}{\Delta p}\right)_{MP}$$

$$= \frac{141.2(-170)(1.0)(1.0)}{45}\left(\frac{0.96}{-100}\right)_{MP} = 5.1 \, \text{md}$$

and:

$$\phi = \frac{0.0002637k}{\mu c_t r^2 [(t_D/r_D^2)/t]_{MP}}$$

$$= \frac{0.0002637(5.1)}{(1.0)(9.0 \times 10^{-6})(119)^2[0.94/10]_{MP}} = 0.11$$

Equation 1.2.83 shows that the dimensionless pressure is related to the dimensionless radius and time by:

$$p_D = -\frac{1}{2}\text{Ei}\left(-\frac{r_D^2}{4t_D}\right)$$

At the wellbore radius where $r = r_w$, i.e., $r_D = 1$, and $p(r,t) = p_{wf}$, the above expression is reduced to:

$$p_D = -\frac{1}{2}\text{Ei}\left(\frac{-1}{4t_D}\right)$$

The log approximation as given by Equation 1.2.80 can be applied to the above solution to give:

$$p_D = \frac{1}{2}[\ln(t_D) + 0.80901]$$

and, to account for the skin s, by:

$$p_D = \frac{1}{2}[\ln(t_D) + 0.80901] + s$$

or:

$$p_D = \frac{1}{2}[\ln(t_D) + 0.80901 + 2s]$$

Notice that the above expressions assume zero wellbore storage, i.e., dimensionless wellbore storage $C_D = 0$. Several authors have conducted detailed studies on the effects and duration of wellbore storage on pressure drawdown and buildup data. Results of these studies were presented in the type curve format in terms of the dimensionless pressure as
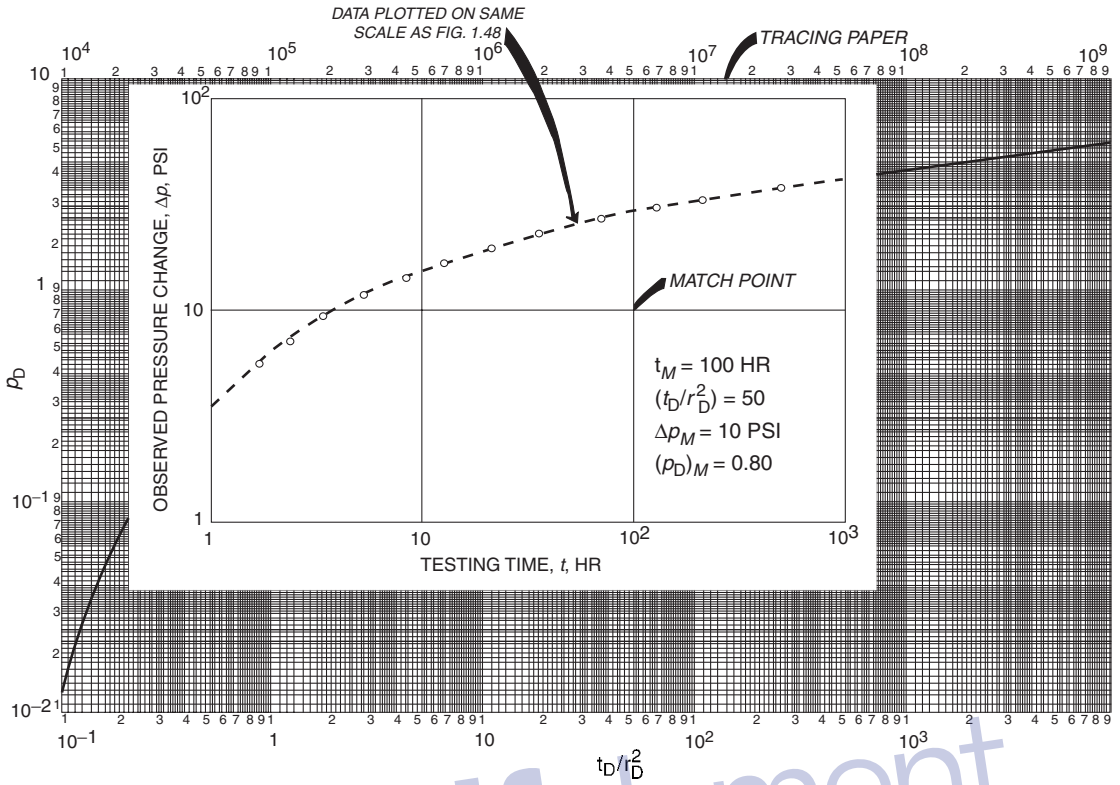
Figure 1.48 *Illustration of type curve matching for an interference test using the type curve (After Earlougher, R. Advances in Well Test Analysis) (Permission to publish by the SPE, copyright SPE, 1977).*

a function of dimensionless time, radius, and wellbore storage, i.e., $p_D = f(t_D, r_D, C_D)$. The following two methods that utilize the concept of the type curve approach are briefly introduced below:

(1) the Gringarten type curve;
(2) the pressure derivative method

1.4.1 Gringarten type curve
During the *early-time period* where the flow is dominated by the wellbore storage, the wellbore pressure is described by Equation 1.3.5 as:

$$p_D = \frac{t_D}{C_D}$$

or:

$$\log(p_D) = \log(t_D) - \log(C_D)$$

This relationship gives the characteristic signature of wellbore storage effects on well testing data which indicates that a plot of p_D vs. t_D on a log–log scale will yield a straight line of a *unit slope*. At the end of the storage effect, which signifies the beginning of the infinite-acting period, the resulting pressure behavior produces the usual straight line on a semilog plot as described by:

$$p_D = \frac{1}{2}[\ln(t_D) + 0.80901 + 2s]$$

It is convenient when using the type curve approach in well testing to include the dimensionless wellbore storage coefficient in the above relationship. Adding and subtracting

$\ln(C_D)$ inside the brackets of the above equation gives:

$$p_D = \frac{1}{2}[\ln(t_D) - \ln(C_D) + 0.80901 + \ln(C_D) + 2s]$$

or, equivalently:

$$p_D = \frac{1}{2}\left[\ln\left(\frac{t_D}{C_D}\right) + 0.80907 + \ln(C_D e^{2s})\right] \qquad [1.4.8]$$

where:

p_D = dimensionless pressure
C_D = dimensionless wellbore storage coefficient
t_D = dimensionless time
s = skin factor

Equation 1.4.8 describes the pressure behavior of a well with a wellbore storage and a skin in a homogeneous reservoir during the transient (infinite-acting) flow period. Gringarten et al. (1979) expressed the above equation in the graphical type curve format shown in Figure 1.49. In this figure, the dimensionless pressure p_D is plotted on a log–log scale versus dimensionless time group t_D/C_D. The resulting curves, characterized by the dimensionless group $C_D e^{2s}$, represent different well conditions ranging from damaged wells to stimulated wells.

Figure 1.49 shows that all the curves merge, in early time, into a unit-slope straight line corresponding to pure wellbore storage flow. At a later time with the end of the wellbore storage-dominated period, curves correspond to infinite-acting radial flow. The end of wellbore storage and the start of infinite-acting radial flow are marked on the type curves of Figure 1.49. There are three dimensionless
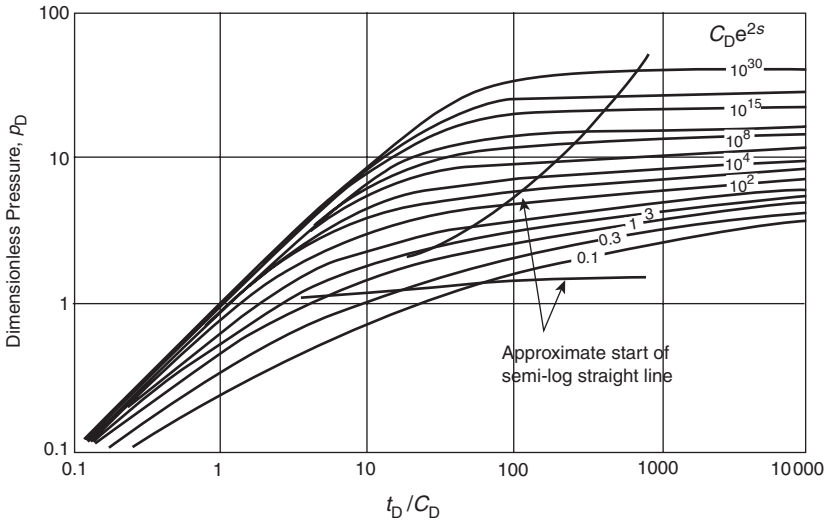
Figure 1.49 *Type curves for a well with wellbore storage and skin in a reservoir with homogeneous behavior (Copyright ©1983 World Oil, Bourdet et al., May 1983).*

groups that Gringarten et al. used when developing the type curve:

(1) dimensionless pressure p_D;
(2) dimensionless ratio t_D/C_D;
(3) dimensionless characterization group $C_D e^{2s}$.

The above three dimensionless parameters are defined mathematically for both the drawdown and buildup tests as follows.

For drawdown
Dimensionless pressure p_D

$$p_D = \frac{kh(p_i - p_{wf})}{141.2QB\mu} = \frac{kh\Delta p}{141.2QB\mu} \quad [1.4.9]$$

where:

k = permeability, md
p_{wf} = bottom-hole flowing pressure, psi
Q = flow rate, bbl/day
B = formation volume factor, bbl/STB

Taking logarithms of both sides of the above equation gives:

$$\log(p_D) = \log(p_i - p_{wf}) + \log\left(\frac{kh}{141.2QB\mu}\right)$$

$$\log(p_D) = \log(\Delta p) + \log\left(\frac{kh}{141.2QB\mu}\right) \quad [1.4.10]$$

Dimensionless ratio t_D/C_D

$$\frac{t_D}{C_D} = \left(\frac{0.0002637kt}{\phi\mu c_t r_w^2}\right)\left(\frac{\phi h c_t r_w^2}{0.8396C}\right)$$

Simplifying gives:

$$\frac{t_D}{C_D} = \left(\frac{0.0002951kh}{\mu C}\right) t \quad [1.4.11]$$

where:

t = flowing time, hours
C = wellbore storage coefficient, bbl/psi

Taking logarithms gives:

$$\log\left(\frac{t_D}{C_D}\right) = \log(t) + \log\left[\frac{0.0002951kh}{\mu C}\right] \quad [1.4.12]$$

Equations 1.4.10 and 1.4.12 indicate that a plot of the actual drawdown data of $\log(\Delta p)$ vs. $\log(t)$ will produce a parallel curve that has an identical shape to a plot of $\log(p_D)$ vs. $\log(t_D/C_D)$. When displacing the actual plot, vertically and horizontally, to find a dimensionless curve that coincides or closely fits the actual data, these displacements are given by the constants of Equations 1.4.9 and 1.4.11 as:

$$\left(\frac{p_D}{\Delta p}\right)_{MP} = \frac{kh}{141.2QB\mu} \quad [1.4.13]$$

and:

$$\left(\frac{t_D/C_D}{t}\right)_{MP} = \frac{0.0002951kh}{\mu C} \quad [1.4.14]$$

where MP denotes a match point.

Equations 1.4.13 and 1.4.14 can be solved for the permeability k (or the flow capacity kh) and the wellbore storage coefficient C respectively:

$$k = \frac{141.2QB\mu}{h}\left(\frac{p_D}{\Delta p}\right)_{MP}$$

and:

$$C = \frac{0.0002951kh}{\mu\left(\frac{t_D/C_D}{t}\right)_{MP}}$$

Dimensionless characterization group $C_D e^{2s}$ The mathematical definition of the dimensionless characterization group $C_D e^{2s}$ as given below is valid for both the drawdown and buildup tests:

$$C_D e^{2s} = \left[\frac{5.615C}{2\pi\phi\mu c_t r_w^2}\right]e^{2s} \quad [1.4.15]$$

where:

ϕ = porosity
c_t = total isothermal compressibility, psi^{-1}
r_w = wellbore radius, ft

When the match is achieved, the dimensionless group $C_D e^{2s}$ describing the matched curve is recorded.

For buildup
It should be noted that *all type curve solutions* are obtained for the drawdown solution. Therefore, these type curves

cannot be used for buildup tests without restriction or modification. The only restriction is that the flow period, i.e., t_p, before shut-in must be somewhat large. However, Agarwal (1980) empirically found that by plotting the buildup data $p_{ws} - p_{wf \text{ at } \Delta t = 0}$ versus "equivalent time" Δt_e instead of the shut-in time Δt, on a log–log scale, the type curve analysis can be made without the requirement of a long drawdown flowing period before shut-in. Agarwal introduced the equivalent time Δt_e as defined by:

$$\Delta t_e = \frac{\Delta t}{1 + \left(\Delta t / t_p\right)} = \left[\Delta t / t_p + \Delta t\right] t_p \qquad [1.4.16]$$

where:

Δt = shut-in time, hours
t_p = total flowing time since the last shut-in, hours
Δt_e = Agarwal equivalent time, hours

Agarwal's equivalent time Δt_e is simply designed to account for the effects of producing time t_p on the pressure buildup test. The concept of Δt_e is that the pressure change $\Delta p = p_{ws} - p_{wf}$ at time Δt during a buildup test is the same as the pressure change $\Delta p = p_i - p_{wf}$ at Δt_e during a drawdown test. Thus, a graph of buildup test in terms of $p_{ws} - p_{wf}$ vs. Δt_e will overlay a graph of pressure change versus flowing time for a drawdown test. Therefore, when applying the type curve approach in analyzing pressure buildup data, the actual shut-in time Δt is replaced by the equivalent time Δt_e.

In addition to the characterization group $C_D e^{2s}$ as defined by Equation 1.4.15, the following two dimensionless parameters are used when applying the Gringarten type curve in analyzing pressure buildup test data.

Dimensionless pressure p_D

$$p_D = \frac{kh(p_{ws} - p_{wf})}{141.2QB\mu} = \frac{kh\Delta p}{141.2QB\mu} \qquad [1.4.17]$$

where:

p_{ws} = shut-in pressure, psi
p_{wf} = flow pressure just before shut-in, i.e., at $\Delta t = 0$, psi

Taking the logarithms of both sides of the above equation gives:

$$\log(p_D) = \log(\Delta p) + \log\left(\frac{kh}{141.2QB\mu}\right) \qquad [1.4.18]$$

Dimensionless ratio t_D / C_D

$$\frac{t_D}{C_D} = \left[\frac{0.0002951kh}{\mu C}\right]\Delta t_e \qquad [1.4.19]$$

Taking the logarithm of each side of Equation 1.4.9 gives:

$$\log\left(\frac{t_D}{C_D}\right) = \log(\Delta t_e) + \log\left(\frac{0.0002951kh}{\mu C}\right) \qquad [1.4.20]$$

Similarly, a plot of actual pressure buildup data of $\log(\Delta p)$ vs. $\log(\Delta t_e)$ would have a shape identical to that of $\log(p_D)$ vs. $\log(t_D / C_D)$. When the actual plot is matched to one of the curves of Figure 1.49, then:

$$\left(\frac{p_D}{\Delta p}\right)_{MP} = \frac{kh}{141.2QB\mu}$$

which can be solved for the flow capacity kh or the permeability k. That is:

$$k = \left[\frac{141.2QB\mu}{h}\right]\left(\frac{p_D}{\Delta p}\right)_{MP} \qquad [1.4.21]$$

and:

$$\left(\frac{t_D / C_D}{\Delta t_e}\right)_{MP} = \frac{0.0002951kh}{\mu C} \qquad [1.4.22]$$

Solving for C gives:

$$C = \left[\frac{0.0002951kh}{\mu}\right]\frac{(\Delta t_e)_{MP}}{(t_D / C_D)_{MP}} \qquad [1.4.23]$$

The recommended procedure for using the Gringarten type curve is given by the following steps:

Step 1. Using the test data, perform *conventional* test analysis and determine:

- wellbore storage coefficient C and C_D;
- permeability k;
- false pressure p^*;
- average pressure $\bar{p}$;
- skin factor s;
- shape factor C_A;
- drainage area A.

Step 2. Plot $p_i - p_{wf}$ versus flowing time t for a drawdown test or $(p_{ws} - p_{wp})$ versus equivalent time Δt_e for a buildup test on log–log paper (tracing paper) with the same size log cycles as the Gringarten type curve.

Step 3. Check the early-time points on the actual data plot for the unit-slope (45° angle) straight line to verify the presence of the wellbore storage effect. If a unit-slope straight line presents, calculate the wellbore storage coefficient C and the dimensionless C_D from any point on the unit-slope straight line with coordinates of $(\Delta p, t)$ or $(\Delta p, \Delta t_e)$, to give:

For drawdown $C = \dfrac{QBt}{24(p_i - p_{wf})} = \dfrac{QB}{24}\left(\dfrac{t}{\Delta p}\right)$

$$[1.4.24]$$

For buildup $C = \dfrac{QB\Delta t_e}{24(p_{ws} - p_{wf})} = \dfrac{QB}{24}\left(\dfrac{\Delta t_e}{\Delta p}\right)$

$$[1.4.25]$$

Estimate the dimensionless wellbore storage coefficient from:

$$C_D = \left[\frac{0.8936}{\phi h c_t r_w^2}\right]C \qquad [1.4.26]$$

Step 4. Overlay the graph of the test data on the type curves and find the type curve that nearly fits most of the actual plotted data. Record the type curve dimensionless group $(C_D e^{2s})_{MP}$.

Step 5. Select a match point MP and record the corresponding values of $(p_D, \Delta p)_{MP}$ from the y axis and $(t_D / C_D, t)_{MP}$ or $(t_D / C_D, \Delta t_e)_{MP}$ from the x axis.

Step 6. From the match, calculate:

$$k = \left[\frac{141.2QB\mu}{h}\right]\left(\frac{p_D}{\Delta p}\right)_{MP}$$

and:

$$C = \left[\frac{0.0002951kh}{\mu}\right]\left(\frac{t}{(t_D / C_D)}\right)_{MP} \quad \text{for drawdown}$$

or:

$$C = \left[\frac{0.0002951kh}{\mu}\right]\left(\frac{\Delta t_e}{(t_D / C_D)}\right)_{MP} \quad \text{for buildup}$$

and:

$$C_D = \left[\frac{0.8936}{\phi h c_t r_w^2}\right]C$$

$$s = \frac{1}{2}\ln\left[\frac{(C_D e^{2s})_{MP}}{C_D}\right] \qquad [1.4.27]$$

Sabet (1991) used the buildup data presented by Bourdet et al. (1983) to illustrate the use of Gringarten type curves. The data is used in the following example:

Example 1.32 Table 1.6 summarizes the pressure buildup data for an oil well that has been producing at a constant flow rate of 174 STB/day before shut-in. Additional pertinent data is given below:

$$\phi = 25\%, \quad c_{t} = 4.2 \times 10^{-6} \text{ psi}^{-1}$$

$$Q = 174 \text{ STB/day}, \quad t_{p} = 15 \text{ hours}$$

$$B = 1.06 \text{ bbl/STB}, \quad r_{w} = 0.29 \text{ ft}$$

$$\mu = 2.5 \text{ cp}, \quad h = 107 \text{ ft}$$

Perform the conventional the pressure buildup analysis by using the Horner plot approach and compare the results with those obtained by using the Gringarten type curve approach.

Table 1.6 Pressure buildup test with afterflow (After Sabet, M. A. "Well Test Analysis" 1991, Gulf Publishing Company)

Δt (hr)	p_{ws} (psi)	Δp (psi)	$\dfrac{t_{p} + \Delta t}{\Delta t}$	Δt_{e}
0.00000	3086.33	0.00	–	0.00000
0.00417	3090.57	4.24	3600.71	0.00417
0.00833	3093.81	7.48	1801.07	0.00833
0.01250	3096.55	10.22	1201.00	0.01249
0.01667	3100.03	13.70	900.82	0.01666
0.02083	3103.27	16.94	721.12	0.02080
0.02500	3106.77	20.44	601.00	0.02496
0.02917	3110.01	23.68	515.23	0.02911
0.03333	3113.25	26.92	451.05	0.03326
0.03750	3116.49	30.16	401.00	0.03741
0.04583	3119.48	33.15	328.30	0.04569
0.05000	3122.48	36.15	301.00	0.04983
0.05830	3128.96	42.63	258.29	0.05807
0.06667	3135.92	49.59	225.99	0.06637
0.07500	3141.17	54.84	201.00	0.07463
0.08333	3147.64	61.31	181.01	0.08287
0.09583	3161.95	75.62	157.53	0.09522
0.10833	3170.68	84.35	139.47	0.10755
0.12083	3178.39	92.06	125.14	0.11986
0.13333	3187.12	100.79	113.50	0.13216
0.14583	3194.24	107.91	103.86	0.14443
0.16250	3205.96	119.63	93.31	0.16076
0.17917	3216.68	130.35	84.72	0.17706
0.19583	3227.89	141.56	77.60	0.19331
0.21250	3238.37	152.04	71.59	0.20953
0.22917	3249.07	162.74	66.45	0.22572
0.25000	3261.79	175.46	61.00	0.24590
0.29167	3287.21	200.88	52.43	0.28611
0.33333	3310.15	223.82	46.00	0.32608
0.37500	3334.34	248.01	41.00	0.36585
0.41667	3356.27	269.94	37.00	0.40541
0.45833	3374.98	288.65	33.73	0.44474
0.50000	3394.44	308.11	31.00	0.48387
0.54167	3413.90	327.57	28.69	0.52279
0.58333	3433.83	347.50	26.71	0.56149
0.62500	3448.05	361.72	25.00	0.60000
0.66667	3466.26	379.93	23.50	0.63830
0.70833	3481.97	395.64	22.18	0.67639
0.75000	3493.69	407.36	21.00	0.71429
0.81250	3518.63	432.30	19.46	0.77075
0.87500	3537.34	451.01	18.14	0.82677
0.93750	3553.55	467.22	17.00	0.88235

Table 1.6 continued

Δt (hr)	p_{ws} (psi)	Δp (psi)	$\dfrac{t_{p} + \Delta t}{\Delta t}$	Δt_{e}
1.00000	3571.75	485.42	16.00	0.93750
1.06250	3586.23	499.90	15.12	0.99222
1.12500	3602.95	516.62	14.33	1.04651
1.18750	3617.41	531.08	13.63	1.10039
1.25000	3631.15	544.82	13.00	1.15385
1.31250	3640.86	554.53	12.43	1.20690
1.37500	3652.85	566.52	11.91	1.25954
1.43750	3664.32	577.99	11.43	1.31179
1.50000	3673.81	587.48	11.00	1.36364
1.62500	3692.27	605.94	10.23	1.46617
1.75000	3705.52	619.19	9.57	1.56716
1.87500	3719.26	632.93	9.00	1.66667
2.00000	3732.23	645.90	8.50	1.76471
2.25000	3749.71	663.38	7.67	1.95652
2.37500	3757.19	670.86	7.32	2.05036
2.50000	3763.44	677.11	7.00	2.14286
2.75000	3774.65	688.32	6.45	2.32394
3.00000	3785.11	698.78	6.00	2.50000
3.25000	3794.06	707.73	5.62	2.67123
3.50000	3799.80	713.47	5.29	2.83784
3.75000	3809.50	723.17	5.00	3.00000
4.00000	3815.97	729.64	4.75	3.15789
4.25000	3820.20	733.87	4.53	3.31169
4.50000	3821.95	735.62	4.33	3.46154
4.75000	3823.70	737.37	4.16	3.60759
5.00000	3826.45	740.12	4.00	3.75000
5.25000	3829.69	743.36	3.86	3.88889
5.50000	3832.64	746.31	3.73	4.02439
5.75000	3834.70	748.37	3.61	4.15663
6.00000	3837.19	750.86	3.50	4.28571
6.25000	3838.94	752.61	3.40	4.41176
6.75000	3838.02	751.69	3.22	4.65517
7.25000	3840.78	754.45	3.07	4.88764
7.75000	3843.01	756.68	2.94	5.10989
8.25000	3844.52	758.19	2.82	5.32258
8.75000	3846.27	759.94	2.71	5.52632
9.25000	3847.51	761.18	2.62	5.72165
9.75000	3848.52	762.19	2.54	5.90909
10.25000	3850.01	763.68	2.46	6.08911
10.75000	3850.75	764.42	2.40	6.26214
11.25000	3851.76	765.43	2.33	6.42857
11.75000	3852.50	766.17	2.28	6.58879
12.25000	3853.51	767.18	2.22	6.74312
12.75000	3854.25	767.92	2.18	6.89189
13.25000	3855.07	768.74	2.13	7.03540
13.75000	3855.50	769.17	2.09	7.17391
14.50000	3856.50	770.17	2.03	7.37288
15.25000	3857.25	770.92	1.98	7.56198
16.00000	3857.99	771.66	1.94	7.74194
16.75000	3858.74	772.41	1.90	7.91339
17.50000	3859.48	773.15	1.86	8.07692
18.25000	3859.99	773.66	1.82	8.23308
19.00000	3860.73	774.40	1.79	8.38235
19.75000	3860.99	774.66	1.76	8.52518
20.50000	3861.49	775.16	1.73	8.66197
21.25000	3862.24	775.91	1.71	8.79310
22.25000	3862.74	776.41	1.67	8.95973
23.25000	3863.22	776.89	1.65	9.11765
24.25000	3863.48	777.15	1.62	9.26752
25.25000	3863.99	777.66	1.59	9.40994
26.25000	3864.49	778.16	1.57	9.54545
27.25000	3864.73	778.40	1.55	9.67456
28.50000	3865.23	778.90	1.53	9.82759
30.00000	3865.74	779.41	1.50	10.00000

Adapted from Bourdet et al. (1983).
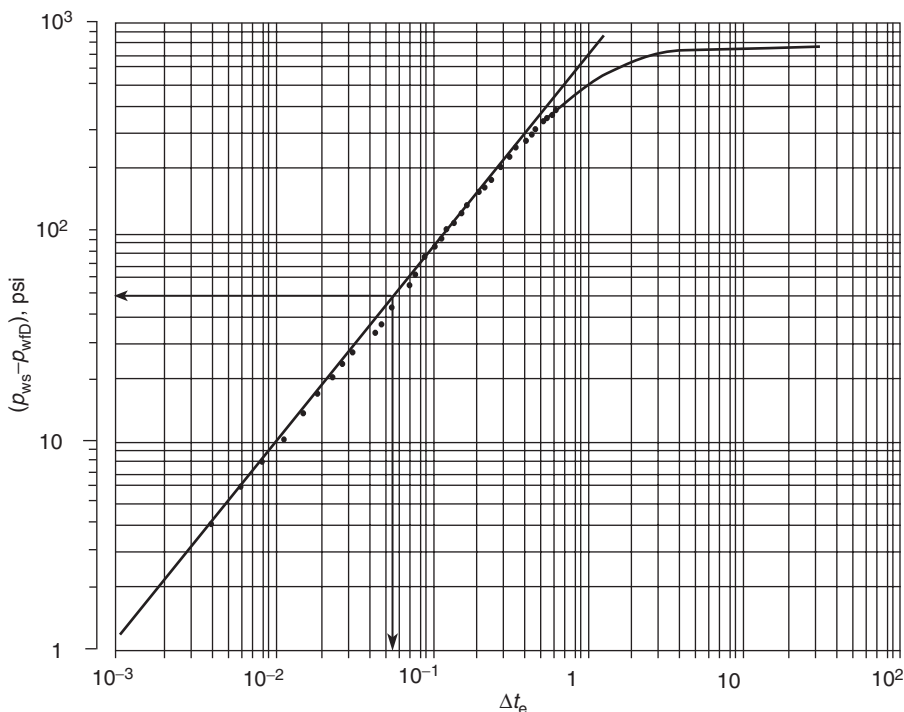
Figure 1.50   *Log–log plot. Data from Table 1.6 (After Sabet, M. A.* Well Test Analysis, *1991, Gulf Publishing Company).*

Solution

Step 1. Plot Δp vs. Δt_e on a log–log scale, as shown in Figure 1.50. The plot shows that the early data form a straight line with a $45°$ angle, which indicates the wellbore storage effect. Determine the coordinates of a point on the straight line, e.g., $\Delta p = 50$ and $\Delta t_e = 0.06$, and calculate C and C_D:

$$C = \frac{QB\Delta t_e}{24\Delta p} = \frac{(174)(1.06)(0.06)}{(24)(50)} = 0.0092 \text{ bbl/psi}$$

$$C_D = \frac{0.8936C}{\phi h c_t r_w^2} = \frac{0.8936(0.0092)}{(0.25)(107)(4.2\times10^{-6})(0.29)^2} = 872$$

Step 2. Make a Horner plot of p_{ws} vs. $(t_p+\Delta t)/\Delta t$ on semilog paper, as shown in Figure 1.51, and perform the conventional well test analysis, to give:

$$m = 65.62 \text{ psi/cycle}$$

$$k = \frac{162.6QB\mu}{mh} \frac{(162.6)(174)(2.5)}{(65.62)(107)} = 10.1 \text{ md}$$

$$p_{1\,hr} = 3797 \text{ psi}$$

$$s = 1.151\left[\frac{p_{1\,hr}-p_{wf}}{(m)} - \log\left(\frac{k}{\phi\mu c_t r_w^2}\right) + 3.23\right]$$

$$= 1.151\left[\frac{3797-3086.33}{65.62}\right.$$

$$\left. -\log\left(\frac{10.1}{(0.25)(2.5)(4.2\times10^{-6})(0.29)^2}\right) + 3.23\right]$$

$$= 7.37$$
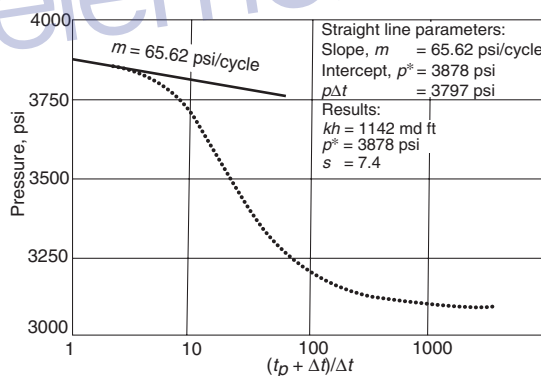
Figure 1.51   *The Horner plot: data from Table 1.6 (Copyright ©1983 World Oil, Bourdet et al., May 1983).*

$$\Delta p_{skin} = (0.87)(65.62)(7.37) = 421 \text{ psi}$$

$$p^* = 3878 \text{ psi}$$

Step 3. Plot Δp vs. Δt_e, on log–log graph paper with the same size log cycles as the Gringarten type curve. Overlay the actual test data plot on the type curve and find the type curve that matches the test data. As shown in Figure 1.52, the data matched the curve with the dimensionless group of $C_D e^{2s} = 10^{10}$ and a match point of:

$$(p_D)_{MP} = 1.79$$
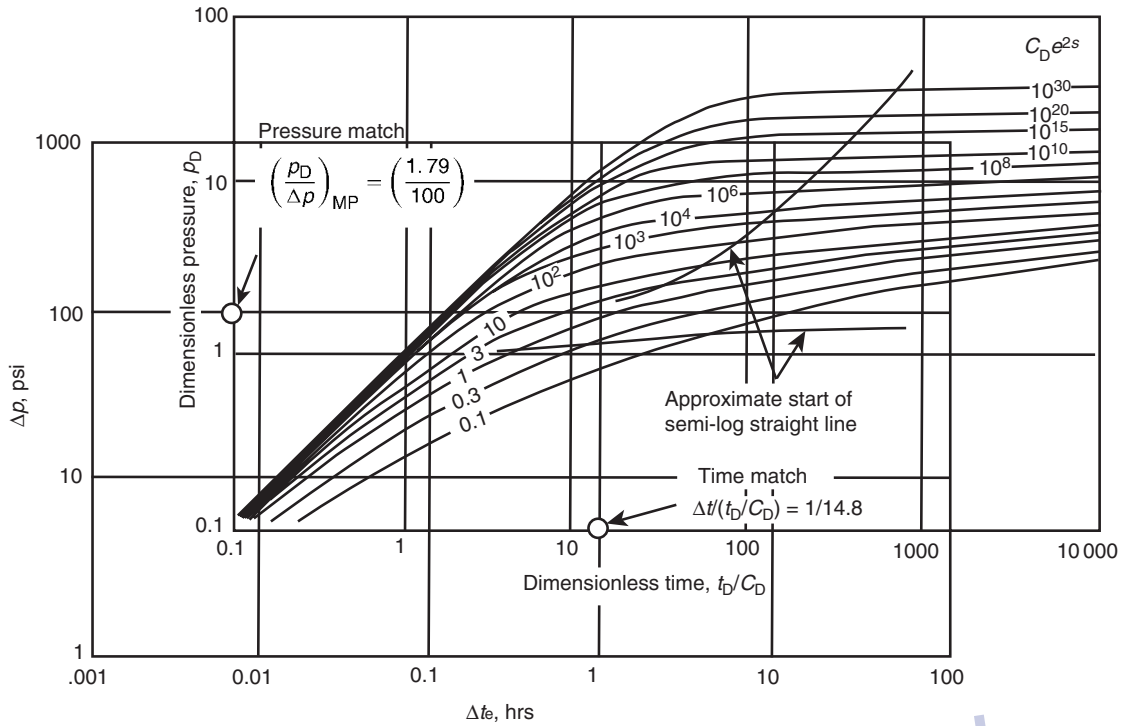
Figure 1.52 *Buildup data plotted on log–log graph paper and matched to type curve by Gringarten et al. (Copyright © 1983 World Oil, Bourdet et al., May 1983).*

$$(\Delta p)_{MP} = 100$$
$$(t_D/C_D) = 14.8$$
$$(\Delta t_e) = 1.0$$

Step 4. From the match, calculate the following properties:

$$k = \left[\frac{141.2QB\mu}{h}\right]\left(\frac{p_D}{\Delta p}\right)_{MP}$$

$$= \frac{141.2(174)(1.06)(2.5)}{(107)}\left(\frac{1.79}{100}\right) = 10.9 \text{ md}$$

$$C = \left[\frac{0.0002951kh}{\mu}\right]\left[\frac{\Delta t_e}{(t_D/C_D)}\right]_{MP}$$

$$= \left[\frac{0.0002951(10.9)(107)}{2.5}\right]\left[\frac{1.0}{14.8}\right] = 0.0093$$

$$C_D = \left[\frac{0.8936}{\phi h c_t r_w^2}\right]C$$

$$= \left[\frac{0.8936}{(0.25)(107)(4.2 \times 10^{-6})(0.29)^2}\right](0.0093)$$

$$= 879$$

$$s = \frac{1}{2}\ln\left[\frac{(C_D e^{2s})_{MP}}{C_D}\right] = \frac{1}{2}\ln\left[\frac{10^{10}}{879}\right] = 8.12$$

Results of the example show a good agreement between the conventional well testing analysis and that of the Gringarten type curve approach.

Similarly, the Gringarten type curve can also be used for gas systems by redefining the dimensionless pressure drop and time as:

For the gas pseudopressure approach $\quad p_D = \dfrac{kh\Delta[m(p)]}{1422Q_g T}$

For the pressure-squared approach $\quad p_D = \dfrac{kh\Delta[p^2]}{1422Q_g\mu_i Z_i T}$

with the dimensionless time as:

$$t_D = \left[\frac{0.0002637k}{\phi\mu c_t r_w^2}\right]t$$

where:

Q_g = gas flow rate, Mscf/day
T = temperature,° R
$\Delta[m(p)] = m(p_{ws}) - m(p_{wf \text{ at } \Delta t=0})$ for the buildup test
$\quad\quad\quad = m(p_i) - m(p_{wf})$ for the drawdown test
$\Delta[p^2] = (p_{ws})^2 - (p_{wf \text{ at } \Delta t=0})^2$ for the buildup test
$\quad\quad\quad = (p_i)^2 - (p_{wf})^2$ for the drawdown test

and for buildup, the shut-in time Δt replaces flowing time t in the above equation.

1.5 Pressure Derivative Method

The type curve approach for the analysis of well testing data was developed to allow for the identification of flow regimes during the wellbore storage-dominated period and the infinite-acting radial flow. As illustrated through Example 1.31, it can be used to estimate the reservoir properties and wellbore condition. However, because of the similarity of curves shapes, it is difficult to obtain a unique solution. As shown in Figure 1.49, all type curves have very similar

Figure 1.53 *Pressure derivative type curve in terms of $P_D^\backslash(t_D/C_D)$ (Copyright ©1983 World Oil, Bourdet et al., May 1983).*

shapes for high values of $C_D e^{2s}$ which lead to the problem of finding a unique match by a simple comparison of shapes and determining the correct values of k, s, and C.

Tiab and Kumar (1980) and Bourdet et al. (1983) addressed the problem of identifying the correct flow regime and selecting the proper interpretation model. Bourdet and his co-authors proposed that flow regimes can have clear characteristic shapes if the "pressure derivative" rather than pressure is plotted versus time on the log–log coordinates. Since the introduction of the pressure derivative type curve, well testing analysis has been greatly enhanced by its use. The use of this pressure derivative type curve offers the following advantages:

- Heterogeneities hardly visible on the conventional plot of well testing data are amplified on the derivative plot.
- Flow regimes have clear characteristic shapes on the derivative plot.
- The derivative plot is able to display in a single graph many separate characteristics that would otherwise require different plots.
- The derivative approach improves the definition of the analysis plots and therefore the quality of the interpretation.

Bourdet et al. (1983) defined the pressure derivative as the derivative of p_D with respect to t_D/C_D as:

$$P_D^\backslash = \frac{d(P_D)}{d(t_D/C_D)} \qquad [1.5.1]$$

It has been shown that during the wellbore storage-dominated period the pressure behavior is described by:

$$P_D = \frac{t_D}{C_D}$$

Taking the derivative of p_D with respect to t_D/C_D gives:

$$\frac{d(P_D)}{d(t_D/C_D)} = P_D^\backslash = 1.0$$

Since $p_D^\backslash = 1$, this implies that multiplying $p_D^\backslash$ by t_D/C_D gives t_D/C_D, or:

$$p_D^\backslash\left(\frac{t_D}{C_D}\right) = \frac{t_D}{C_D} \qquad [1.5.2]$$

Equation 1.5.2 indicates that a plot of $p_D^\backslash(t_D/C_D)$ vs. t_D/C_D in log–log coordinates will produce a unit-slope straight line during the wellbore storage-dominated flow period.

Similarly, during the radial infinite-acting flow period, the pressure behavior is given by Equation 1.5.1 as:

$$p_D = \frac{1}{2}\left[\ln\left(\frac{t_D}{C_D}\right) + 0.80907 + \ln(C_D e^{2s})\right]$$

Differentiating with respect to t_D/C_D, gives:

$$\frac{d(p_D)}{d(t_D/C_D)} = p_D^\backslash = \frac{1}{2}\left[\frac{1}{(t_D/C_D)}\right]$$

Simplifying gives:

$$p_D^\backslash\left(\frac{t_D}{C_D}\right) = \frac{1}{2} \qquad [1.5.3]$$

This indicates that a plot of $p_D^\backslash(t_D/C_D)$ vs. t_D/C_D on a log–log scale will produce a *horizontal line* at $p_D^\backslash(t_D/C_D) = \frac{1}{2}$ during the transient flow (radial infinite-acting) period. As shown by Equations 1.5.2 and 1.5.3 the derivative plot of $p_D^\backslash(t_D/C_D)$ vs. t_D/C_D for the entire well test data will produce *two straight lines* that are characterized by:

- a unit-slope straight line during the wellbore storage-dominated flow;
- a horizontal line at $p_D^\backslash(t_D/C_D) = 0.5$ during the transient flow period.

The fundamental basis for the pressure derivative approach is essentially based on identifying these two straight lines that can be used as reference lines when selecting the proper well test data interpreting model.

Bourdet et al. replotted the Gringarten type curve in terms of $p_D^\backslash(t_D/C_D)$ vs. t_D/C_D on a log–log scale as shown in Figure 1.53. It shows that at the early time during the wellbore storage-dominated flow, the curves follow a unit-slope log–log straight line. When infinite-acting radial flow is reached, the curves become horizontal at a value of $p_D^\backslash(t_D/C_D) = 0.5$ as indicated by Equation 1.5.3. In addition, notice that the transition from pure wellbore storage to infinite-acting behavior gives a "hump" with a height that characterizes the value of the skin factor s.
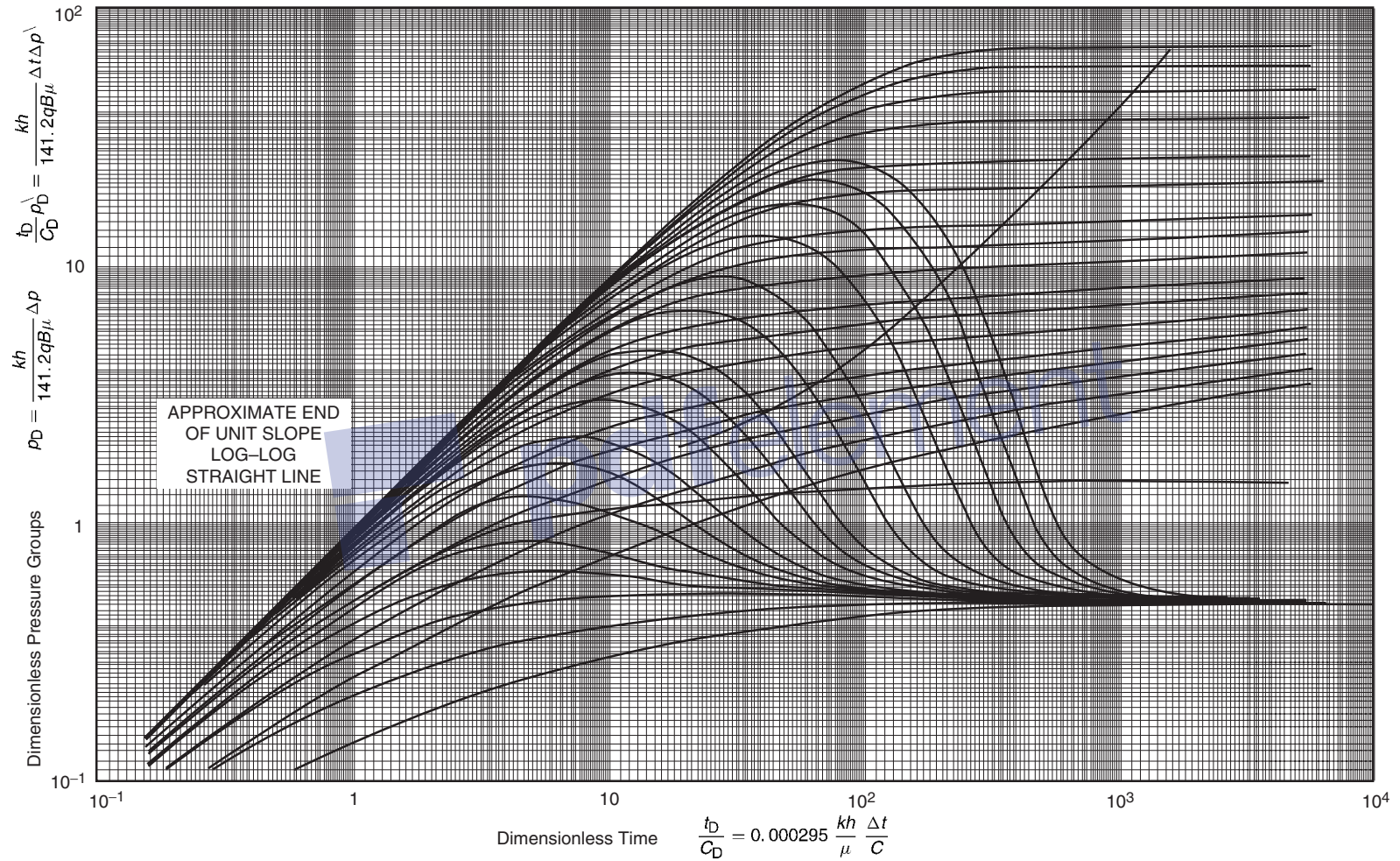
Figure 1.54 *Pressure derivative type curves (Copyright ©1983 World Oil, Bourdet et al., May 1983).*

The axes of the plot are labeled as follows:

Vertical axis (Dimensionless Pressure Groups):
$$p_D = \frac{kh}{141.2qB\mu}\,\Delta p$$
$$\frac{t_D}{C_D}\,p_D{}' = \frac{kh}{141.2qB\mu}\,\Delta t\Delta p'$$

Horizontal axis (Dimensionless Time):
$$\frac{t_D}{C_D} = 0.000295\,\frac{kh}{\mu}\,\frac{\Delta t}{C}$$

APPROXIMATE END OF UNIT SLOPE LOG–LOG STRAIGHT LINE

Figure 1.53 illustrates that the effect of skin is only manifested in the curvature between the straight line due to wellbore storage flow and the *horizontal straight line* due to the infinite-acting radial flow. Bourdet et al. indicated that the data in this curvature portion of the curve is not always well defined. For this reason, the authors found it useful to combine their derivative type curves with that of the Gringarten type curve by superimposing the two type curves, i.e., Figures 1.49 and 1.53, on the same scale. The result of superimposing the two sets of type curves on the same graph is shown in Figure 1.54. The use of the new type curve allows the *simultaneous* matching of pressure-change data and derivative data since both are plotted on the same scale. The derivative pressure data provides, without ambiguity, the pressure match and the time match, while the $C_D e^{2s}$ value is obtained by comparing the label of the match curves for the derivative pressure data and pressure drop data.

The procedure for analyzing well test data using the derivative type curve is summarized by the following steps:

Step 1. Using the actual well test data, calculate the pressure difference Δp and the pressure derivative plotting functions as defined below for drawdown and buildup tests.

For the drawdown tests, for every recorded drawdown pressure point, i.e., flowing time t and a corresponding bottom-hole flowing pressure p_{wf}, calculate:

The pressure difference $\Delta p = p_i - p_{wf}$

The derivative function $t \Delta p^{\backslash} = -t \left(\dfrac{d(\Delta p)}{d(t)} \right)$

[1.5.4]

For the buildup tests, for every recorded buildup pressure point, i.e., shut-in time Δt and corresponding shut-in pressure p_{ws}, calculate:

The pressure difference $\Delta p = p_{ws} - p_{wf \text{ at } \Delta t = 0}$

The derivative function

$$\Delta t_e \Delta p^{\backslash} = \Delta t \left(\frac{t_p + \Delta t}{\Delta t} \right) \left[\frac{d(\Delta p)}{d(\Delta t)} \right]$$

[1.5.5]

The derivatives included in Equations 1.5.4 and 1.5.5, i.e., $[dp_{wf}/dt]$ and $[d(\Delta p_{ws})/d(\Delta t)]$, can be determined numerically at any data point i by using the central difference formula for *evenly spaced time* or the three-point weighted average approximation as shown graphically in Figure 1.55 and mathematically by the following expressions:
Central differences:

$$\left(\frac{dp}{dx} \right)_i = \frac{p_{i+1} - p_{i-1}}{x_{i+1} - x_{i-1}}$$

[1.5.6]

Three-point weighted average:

$$\left(\frac{dp}{dx} \right)_i = \frac{(\Delta p_1 / \Delta x_1) \Delta x_2 + (\Delta p_2 / \Delta x_2) \Delta x_1}{\Delta x_1 + \Delta x_2}$$

[1.5.7]

It should be pointed out that selection of the method of numerical differentiation is a problem that must be considered and examined when applying the pressure derivative method. There are many differentiation methods that use only two points, e.g., backward difference, forward difference, and central difference formulas, and very complex algorithms that utilize several pressure

points. It is important to try several different methods in order to find one which best smoothes the data.

Step 2. On tracing paper with the same size log cycles as the Bourdet–Gringarten type curve graph, i.e., Figure 1.54, plot:

- (Δp) and $(t \Delta p^{\backslash})$ as a function of the flowing time t when analyzing drawdown test data. Notice that there are two sets of data on the same log–log graph as illustrated in Figure 1.56; the first is the analytical solution and the second is the actual drawdown test data.
- The pressure difference Δp versus the equivalent time Δt_e and the derivative function $(\Delta t_e \Delta p^{\backslash})$ versus the *actual shut-in time* Δt. Again, there are two sets of data on the same graph as shown in Figure 1.56.

Step 3. Check the actual early-time pressure points, i.e., pressure difference versus time on a log–log scale, for the unit-slope line. If it exists, draw a line through the points and calculate the wellbore storage coefficient C by selecting a point on the unit-slope line as identified with coordinates of $(t, \Delta p)$ or $(\Delta t_e, \Delta p)$ and applying Equation 1.4.24 or Equation 1.4.25, as follows:

For drawdown $C = \dfrac{QB}{24} \left(\dfrac{t}{\Delta p} \right)$

For buildup $C = \dfrac{QB}{24} \left(\dfrac{\Delta t_e}{\Delta p} \right)$

Step 4. Calculate the dimensionless wellbore storage coefficient C_D by applying Equation 1.4.26 and using the value of C as calculated in Step 3. That is:

$$C_D = \left[\frac{0.8936}{\phi h c_t r_w^2} \right] C$$

Step 5. Check the late-time data points on the *actual pressure derivative* plot to see if they form a horizontal line which indicates the occurrence of transient (unsteady-state) flow. If it exists, draw a horizontal line through these derivative plot points.

Step 6. Place the actual two sets of plots, i.e., the pressure difference plot and derivative function plot, on the Gringarten–Bourdet type curve of Figure 1.54, and force a simultaneous match of the two plots to Gringarten–Bourdet type curves. The unit-slope line should overlay the unit slope on the type curve and the late-time horizontal line should overlay the horizontal line on the type cure which corresponds to a value of 0.5. Note that it is convenient to match both pressure and pressure curves, even though it is redundant. With the double match, a high degree of confidence in the results is obtained.

Step 7. From the match of the best fit, select a match point MP and record the corresponding values of the following:

- From the Gringarten type curve, determine $(p_D, \Delta p)_{MP}$ and the corresponding $(t_D/C_D, t)_{MP}$ or $(t_D/C_D, \Delta t_e)_{MP}$.
- Record the value of the type curve dimensionless group $(C_D e^{2s})_{MP}$ from the Bourdet type curves.

Step 8. Calculate the permeability by applying Equation 1.4.21:

$$k = \left[\frac{141.2 QB\mu}{h} \right] \left[\frac{p_D}{\Delta p} \right]_{MP}$$
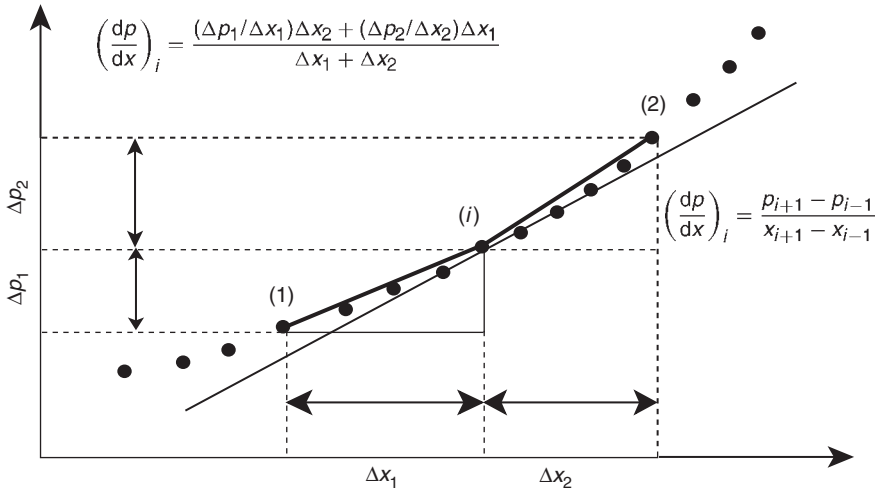
Figure 1.55 *Differentiation algorithm using three points.*
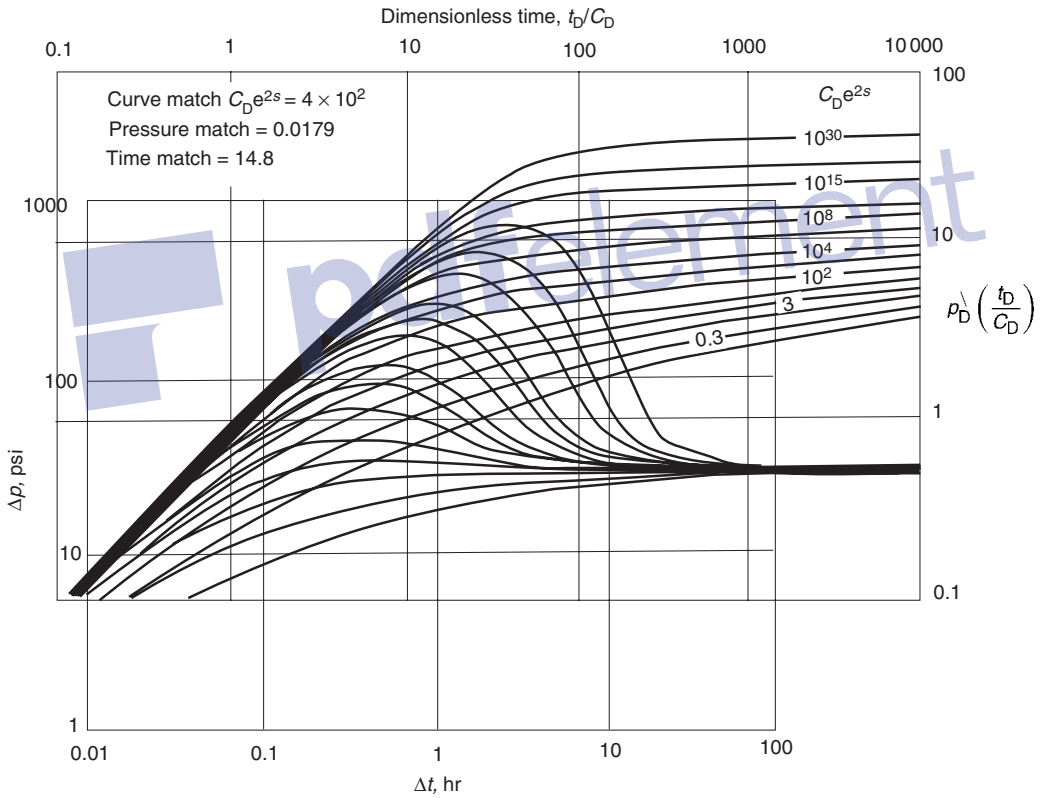
Figure 1.56 *Type curve matching. Data from Table 1.6 (Copyright ©1983 World Oil, Bourdet et al., May 1983).*

Step 9. Recalculate the wellbore storage coefficient C and C_D by applying Equations 1.4.23 and 1.4.26, or:

For drawdown $C = \left[\dfrac{0.0002951kh}{\mu} \right] \dfrac{(t)_{MP}}{(t_D/C_D)_{MP}}$

For buildup $C = \left[\dfrac{0.0002951kh}{\mu} \right] \dfrac{(\Delta t_e)_{MP}}{(t_D/C_D)_{MP}}$

with:

$$C_D = \left[\frac{0.8936}{\phi h c_t r_w^2} \right] C$$

Compare the calculated values of C and C_D with those calculated in steps 3 and 4.

Step 10. Calculate the skin factor s by applying Equation 1.4.27 and using the value of C_D in step 9 and the value of $(C_D e^{2s})_{MP}$ in step 7, to give:

$$s = \frac{1}{2} \ln \left[\frac{(C_D e^{2s})_{MP}}{C_D} \right]$$

Example 1.33 Using the same data of Example 1.31, analyze the given well test data using the pressure derivative approach.

Solution

Step 1. Calculate the derivative function for every recorded data point by applying Equation 1.5.5 or the approximation method of Equation 1.5.6 as tabulated Table 1.7 and shown graphically in Figure 1.57.

Table 1.7 *Pressure derivative method. Data of Table 6.6 After Sabet, M.A. "Well Test Analysis" 1991, Gulf Publishing Company*

Δt (hr)	Δp (psi)	*Slope* (psi/hr)	$\Delta p^{\backslash}$ (psi/hr)	$\Delta t \Delta t^{\backslash}$ $(t_p + \Delta t) t_p$
0.00000	0.00	1017.52	–	–
0.00417	4.24	777.72	897.62	3.74
0.00833	7.48	657.55	717.64	5.98
0.01250	10.22	834.53	746.04	9.33
0.01667	13.70	778.85	806.69	13.46
0.02083	16.94	839.33	809.09	16.88
0.02500	20.44	776.98	808.15	20.24
0.02917	23.68	778.85	777.91	22.74
0.03333	26.92	776.98	777.91	25.99
0.03750	30.16	358.94	567.96	21.35
0.04583	33.15	719.42	539.18	24.79
0.05000	36.15	780.72	750.07	37.63
0.05830	42.63	831.54	806.13	47.18
0.06667	49.59	630.25	730.90	48.95
0.07500	54.84	776.71	703.48	53.02
0.08333	61.31	1144.80	960.76	80.50
0.09583	75.62	698.40	921.60	88.88
0.10833	84.35	616.80	657.60	71.75
0.12083	92.06	698.40	657.60	80.10
0.13333	100.79	569.60	634.00	85.28
0.14583	107.91	703.06	636.33	93.70
0.16250	119.63	643.07	673.07	110.56
0.17917	130.35	672.87	657.97	119.30
0.19583	141.56	628.67	650.77	129.10
0.21250	152.04	641.87	635.27	136.91
0.22917	162.74	610.66	626.26	145.71
0.25000	175.46	610.03	610.34	155.13
0.29167	200.88	550.65	580.34	172.56
0.33333	223.82	580.51	565.58	192.71
0.37500	248.01	526.28	553.40	212.71
0.41667	269.94	449.11	487.69	208.85
0.45833	288.65	467.00	458.08	216.36
0.50000	308.11	467.00	467.00	241.28
0.54167	327.57	478.40	472.70	265.29
0.58333	347.50	341.25	409.82	248.36
0.62500	361.72	437.01	389.13	253.34
0.66667	379.93	377.10	407.05	283.43
0.70833	395.64	281.26	329.18	244.18
0.75000	407.36	399.04	340.15	267.87
0.81250	432.30	299.36	349.20	299.09
0.87500	451.01	259.36	279.36	258.70
0.93750	467.22	291.20	275.28	274.20
1.00000	485.42	231.68	261.44	278.87
1.06250	499.90	267.52	249.60	283.98

Table 1.7 *continued*

Δt (hr)	Δp (psi)	*Slope* (psi/hr)	$\Delta p^{\backslash}$ (psi/hr)	$\Delta t \Delta t^{\backslash}$ $(t_p + \Delta t) t_p$
1.12500	516.62	231.36	249.44	301.67
1.18750	531.08	219.84	225.60	289.11
1.25000	544.82	155.36	187.60	254.04
1.31250	554.53	191.84	173.60	247.79
1.37500	566.52	183.52	187.68	281.72
1.43750	577.99	151.84	167.68	264.14
1.50000	587.48	147.68	149.76	247.10
1.62500	605.94	106.00	126.84	228.44
1.75000	619.19	109.92	107.96	210.97
1.87500	632.93	103.76	106.84	225.37
2.00000	645.90	69.92	86.84	196.84
2.25000	663.38	59.84	64.88	167.88
2.37500	670.66	50.00	54.92	151.09
2.50000	677.11	44.84	47.42	138.31
2.75000	688.32	41.84	43.34	141.04
3.00000	698.78	35.80	38.82	139.75
3.25000	707.73	22.96	29.38	118.17
3.50000	713.47	38.80	30.88	133.30
3.75000	723.17	25.88	32.34	151.59
4.00000	729.64	16.92	21.40	108.43
4.25000	733.87	7.00	11.96	65.23
4.50000	735.62	7.00	7.00	40.95
4.75000	737.37	11.00	9.00	56.29
5.00000	740.12	12.96	11.98	79.87
5.25000	743.36	11.80	12.38	87.74
5.50000	746.31	8.24	10.02	75.32
5.75000	748.37	9.96	9.10	72.38
6.00000	750.86	7.00	8.48	71.23
6.25000	752.51	−1.84	2.58	22.84
6.75000	751.69	5.52	1.84	18.01
7.25000	754.45	4.46	4.99	53.66
7.75000	756.68	3.02	3.74	43.96
8.25000	758.19	3.50	3.26	41.69
8.75000	759.94	2.48	2.99	41.42
9.25000	761.18	2.02	2.25	33.65
9.75000	762.19	2.98	2.50	40.22
10.25000	763.68	1.48	2.23	38.48
10.75000	764.42	2.02	1.75	32.29
11.25000	765.43	1.48	1.75	34.45
11.75000	766.17	2.02	1.75	36.67
12.25000	767.18	1.48	1.75	38.94
12.75000	767.92	1.64	1.56	36.80
13.25000	768.74	0.86	1.25	31.19
13.75000	769.17	1.33	1.10	28.90
14.50000	770.17	1.00	1.17	33.27
15.25000	770.92	0.99	0.99	30.55
16.00000	771.66	1.00	0.99	32.85
16.75000	772.41	0.99	0.99	35.22
17.50000	773.15	0.68	0.83	31.60
18.25000	773.66	0.99	0.83	33.71
19.00000	774.40	0.35	0.67	28.71
19.75000	774.66	0.67	0.51	23.18
20.50000	775.16	1.00	0.83	40.43
21.25000	775.91	0.50	0.75	38.52
22.25000	776.41	0.48	0.49	27.07
23.25000	776.89	0.26	0.37	21.94
24.25000	777.15	0.51	0.38	24.43
25.25000	777.66	0.50	0.50	34.22
26.25000	778.16	0.24	0.37	26.71
27.25000	778.40	0.40^a	0.32^b	24.56^c
28.50000	778.90	0.34	0.37	30.58
30.00000	779.41	25.98	13.16	1184.41

[a] $(778.9 - 778.4)/(28.5 - 27.25) = 0.40.$

[b] $(0.40 + 0.24)/2 = 0.32.$

[c] $27.25 - 0.32 - (15 + 27.25)/15 = 24.56.$
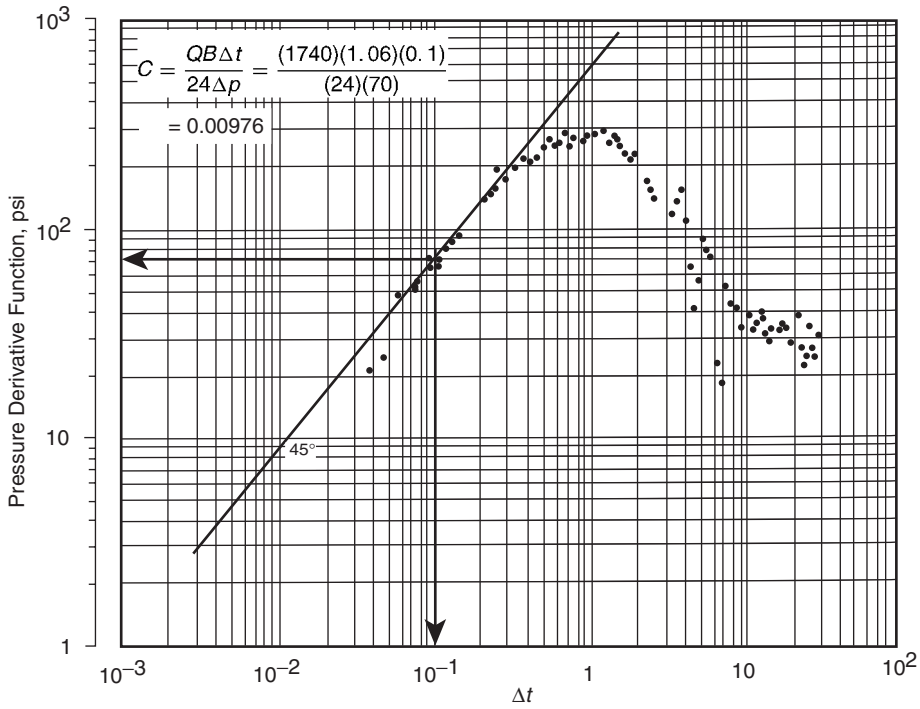
Figure 1.57 Log–log plot. Data from Table 1.7.

Step 2. Draw a straight line with a 45° angle that fits the early-time test points, as shown in Figure 1.57, and select the coordinates of a point on the straight line, to give (0.1, 70). Calculate C and C_D:

$$C = \frac{QB\Delta t}{24\Delta p} = \frac{1740(1.06)(0.1)}{(24)(70)} = 0.00976$$

$$C_D = \left[\frac{0.8936}{\phi h c_t r_w^2}\right] = \frac{0.8936(0.00976)}{(0.25)(107)(4.2 \times 10^{-6})(0.29)^2}$$

$$= 923$$

Step 3. Overlay the pressure difference data and pressure derivative data over the Gringarten–Bourdet type curve to match the type curve, as shown in Figure 1.57, with the following match points:

$$(C_D e^{2s})_{MP} = 4 \times 10^9$$

$$(p_D/\Delta p)_{MP} = 0.0179$$

$$\left[(t_D/C_D)/\Delta t\right]_{MP} = 14.8$$

Step 4. Calculate the permeability k:

$$k = \left[\frac{141.2QB\mu}{h}\right]\left(\frac{p_D}{\Delta p}\right)_{MP}$$

$$= \left[\frac{141.2(174)(1.06)(2.5)}{107}\right](0.0179)$$

$$= 10.9 \text{ md}$$

Step 5. Calculate C and C_D:

$$C = \left[\frac{0.0002951kh}{\mu}\right]\frac{(\Delta t_e)_{MP}}{(t_D/C_D)_{MP}}$$

$$= \left[\frac{0.0002951(10.9)(107)}{2.5}\right]\left(\frac{1}{14.8}\right)$$

$$= 0.0093 \text{ bbl/psi}$$

$$C_D = \frac{0.8936C}{\phi h c_t r_w^2} = \frac{0.8936(0.0093)}{(0.25)(107)(4.2 \times 10^{-6})(0.29)^2}$$

$$= 879$$

Step 6. Calculate the skin factor s:

$$s = \frac{1}{2}\ln\left[\frac{(C_D e^{2s})_{MP}}{C_D}\right] = \frac{1}{2}\ln\left[\frac{4 \times 10^9}{879}\right] = 7.7$$

Notice that the derivative function, as plotted in Figure 1.57, shows an appreciable amount of scatter points and the horizontal line which signifies the radial infinite-acting state is not clear. A practical limitation associated with the use of the pressure derivative approach is the ability to measure pressure transient data with sufficient frequency and accuracy so that it can be differentiated. Generally, the derivative function will show severe oscillations unless the data is smoothed before taking the derivative.

Smoothing of any time series, such as pressure–time data, is not an easy task, and unless it is done with care and know-how, a portion of the data which is representative of the reservoir (signal) could be lost. Signal filtering, smoothing, and interpolation is a very advanced subject of science and engineering, and unless the proper smoothing techniques are applied to the field data, the results could be utterly misleading.
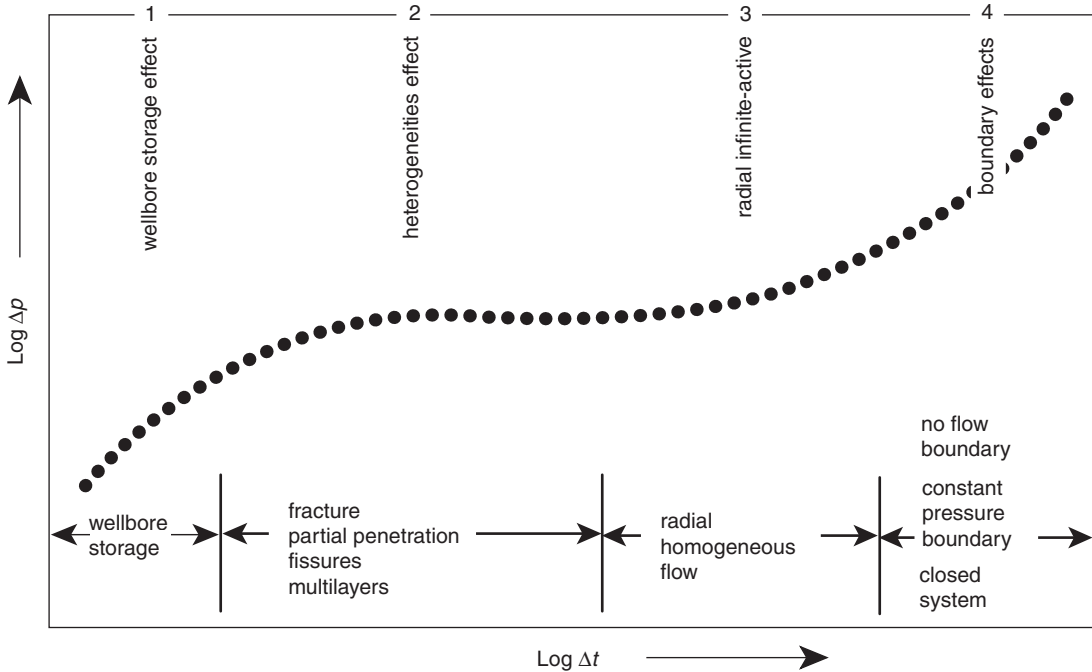
Figure 1.58 Log–log plot of a typical drawdown.

In addition to the reservoir heterogeneity, there are many inner and outer reservoir boundary conditions that will cause the transient state plot to deviate from the expected semilog straight-line behavior during the infinite-acting behavior of the test well, such as:

- faults and other impermeable flow barriers;
- partial penetration;
- phase separation and packer failures;
- interference;
- stratified layers;
- naturally and hydraulically fractured reservoirs;
- boundary;
- lateral increase in mobility.

The theory which describes the unsteady-state flow data is based on the ideal radial flow of fluids in a homogeneous reservoir system of uniform thickness, porosity, and permeability. Any deviation from this ideal concept can cause the predicted pressure to behave differently from the actual measured pressure. In addition, a well test response may have different behavior at different times during the test. In general, the following four different time periods can be identified on a log–log plot of Δp vs. Δt as shown in Figure 1.58:

(1) The *wellbore storage effect* is always the first flow regime to appear.
(2) Evidence of the well and reservoir *heterogeneities effect* will then appear in the pressure behavior response. This behavior may be a result of multilayered formation, skin, hydraulic fractures, or fissured formation.
(3) The pressure response exhibits the *radial infinite-active* behavior and represents an equivalent homogeneous system.
(4) The last period represents the *boundary effects* that may occur at late time.

Thus, many types of flow regimes can appear before and after the actual semilog straight line develops, and they follow a very strict chronology in the pressure response. Only global diagnosis, with identification of all successive regimes present, will indicate exactly when conventional analysis, e.g., the semilog plot technique, is justified. Recognition of the above four different sequences of responses is perhaps the most important element in well test analysis. The difficulty arises from the fact that some of these responses could be missing, overlapping, or undetectable through the traditional graphical semilog straight-line approach. Selection of the correct *reservoir interpretation model* is a prerequisite and an important step before analyzing well test data and interpreting the test results. With proper well test design and sufficient test length for the response to be detected, most pressure transient data can provide an unambiguous indicator of the type and the associated characteristics of the reservoir. However, many well tests cannot or are not run for sufficient test duration to eliminate ambiguity in selecting the proper model to analyze test data. With a sufficient length of well testing time, the reservoir response during well testing is then used to identify a well test interpretation model from which well and reservoir parameters, such as permeability and skin, can be determined. This *model identification* requirement holds for both traditional graphical analyses as well as for computer-aided techniques.

It should be pointed out that both the semilog and log–log plots of pressure versus time data are often insensitive to pressure changes and cannot be solely used as diagnostic plots to find the interpretation model that best represents the dynamic behavior of the well and reservoir during the test. The pressure derivative type curve, however, is the most definitive of the type curves for identifying the proper interpretation model. The pressure derivative approach has been applied with tremendous success as a diagnostic tool for the following reasons:

- It magnifies small pressure changes.
- Flow regimes have *clear characteristic shapes* on the pressure derivative plot.
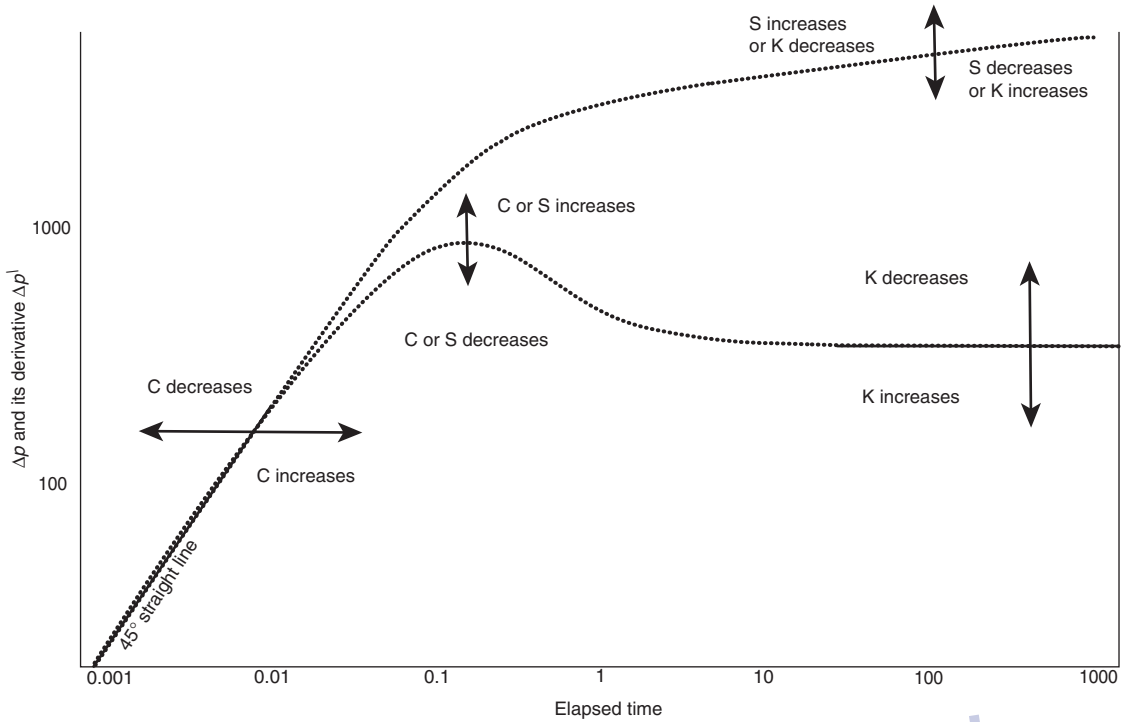
Figure 1.59 Δp and its derivative vs. elapsed time.

- It clearly differentiates between responses of various reservoir models; such as:
  - dual-porosity behavior;
  - naturally and hydraulically fractured reservoirs;
  - closed boundary systems;
  - constant pressure boundaries;
  - faults and impermeable boundaries;
  - infinite acting systems
- It identifies various reservoir behavior and conditions that are not apparent in the traditional well analysis approach.
- It defines a clear recognizable pattern of various flow periods.
- It improves the overall accuracy of test interpretation.
- It provides an accurate estimation of relevant reservoir parameters.

Al-Ghamdi and Issaka (2001) pointed out that there are three major difficulties during the process of identifying the proper interpretation model:

(1) The limited number of available interpretation models that is restricted to prespecified setting and idealized conditions.
(2) The limitation of the majority of existing heterogeneous reservoir models to one type of heterogeneities and its ability to accommodate multiple heterogeneities within the same model.
(3) The non-uniqueness problem where identical responses are generated by completely different reservoir models of totally different geological configuration.

Lee (1982) suggested that the best approach of identifying the correct interpretation model incorporates the following three plotting techniques:

(1) The traditional log–log type curve plot of pressure difference Δp versus time.
(2) The derivative type curve.

(3) The "specialized graph" such as the Horner plot for a homogeneous system among other plots.

Based on knowledge of the shape of different flow regimes, the double plot of pressure and its derivative is used to diagnose the system and choose a well/reservoir model to match the well test data. The specialized plots can then be used to confirm the results of the pressure-derivative type curve match. Therefore, after reviewing and checking the quality of the test raw data, the analysis of well tests can be divided into the following two steps:

(1) The reservoir model identification and various flow regimes encountered during the tests are determined.
(2) The values of various reservoir and well parameters are calculated.

1.5.1 Model identification
The validity of the well test interpretation is totally dependent on two important factors, the accuracy of the measured field data and the applicability of the selected interpretation model. Identifying the correct model for analyzing the well test data can be recognized by plotting the data in several formats to eliminate the ambiguity in model selection. Gringarten (1984) pointed out that the interoperation model consists of three main components that are independent of each other and dominate at different times during the test and they follow the chronology of the pressure response. These are:

(I) *Inner boundaries*. Identification of the inner boundaries is performed on the early-time test data. There are only five possible inner boundaries and flow conditions in and around the wellbore:
  (1) wellbore storage;
  (2) skin;
  (3) phase separation;

(4) partial penetration;
(5) fracture.

(II) *Reservoir behavior*. Identification of the reservoir is performed on the middle-time data during the infinite acting behavior and includes two main types:
(1) homogeneous;
(2) heterogeneous.

(III) *Outer boundaries*. Identification of the outer boundaries is performed on the late-time data. There are two outer boundaries:
(1) no-flow boundary;
(2) constant-pressure boundary.

Each of the above three components exhibits a distinctly different characteristic that can be identified separately, and described by different mathematical forms.

1.5.2 Analysis of early-time test data

Early-time data is meaningful and can be used to obtain unparalleled information on the reservoir around the well-bore. During this early-time period, wellbore storage, fractures, and other inner boundary flow regimes are the dominant flowing conditions and exhibit a distinct different behavior. These inner boundary conditions and their associated flow regimes are briefly discussed below.

Wellbore storage and skin

The most effective procedure for analyzing and under-standing the entire recorded transient well test data is by employing the log–log plot of the pressure difference Δp and its derivative $\Delta p\backslash$ versus elapsed time. Identification of the inner boundaries is performed on early-time test data and starts with the wellbore storage. During this time when the wellbore storage dominates, Δp and its derivative $\Delta p\backslash$ are proportional to the elapsed time and produce a 45° straight line on the log–log plot, as shown in Figure 1.59. On the derivative plot, the transition from the wellbore storage to the infinite-acting radial flow gives a "hump" with a maximum that indicates wellbore damage (positive skin). Conversely, the absence of a maximum indicates a non-damaged or stimulated well.

Phase separation in tubing

Stegemeier and Matthews (1958), in a study of anomalous pressure buildup behavior, graphically illustrated and discussed the effects of several reservoir conditions on the Horner straight-line plot, as shown in Figure 1.60. The problem occurs when gas and oil are segregated in the tubing and annulus during shut-in, which can cause the wellbore pressure to increase. This increase in the pressure could exceed the reservoir pressure and force the liquid to flow back into the formation with a resulting decrease in the well-bore pressure. Stegemeier and Matthews investigated this "humping" effect, as shown in Figure 1.60, which means that bottom-hole pressure builds up to a maximum and then decreases. They attributed this behavior to the rise of bubbles of gas and the redistribution of fluids within the wellbore. Wells which show the humping behavior have the following characteristics:

- They are completed in moderately permeable formations with a considerable skin effect or restriction to flow near the wellbore.
- The annulus is packed off.

The phenomenon does not occur in tighter formations because the production rate is small and thus there is ample space for the segregated gas to move into and expand. Similarly, if there is no restriction to flow near the wellbore, fluid can flow easily back into the formation to equalize the pressure and prevent humping. If the annulus is not packed off,
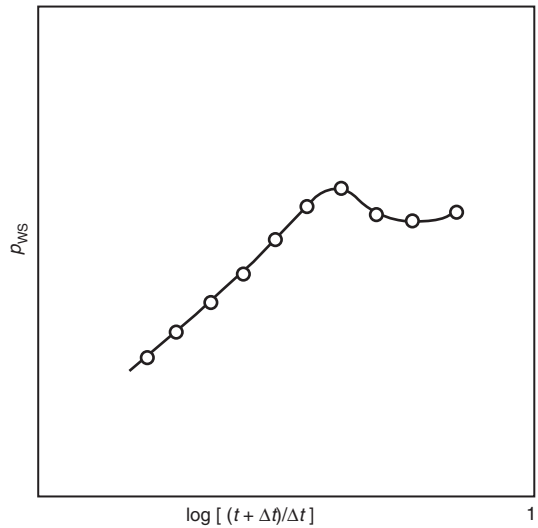
Figure 1.60 *Phase separation in tubing (After Stegemeier and Matthews, 1958).*

bubble rise in the tubing will simply unload liquid into the casing–tubing annulus rather than displace the fluid back into the formation.

Stegemeier and Matthews also showed how *leakage through the wellbore* between dually completed zones at different pressure can cause an anomalous hump in measured pressures. When this leakage this occurs, the pressure differential between zones becomes small, allowing fluid to flow, and causes a hump in the pressure observed in the other zone.

Effect of partial penetration

Depending on the type of wellbore completion configuration, it is possible to have spherical or hemispherical flow near the wellbore. If the well penetrates the reservoir for a short distance below the cap rock, the flow will be hemispherical. When the well is cased through a thick pay zone and only a small part of the casing is perforated, the flow in the immediate vicinity of the wellbore will be spherical. Away from the wellbore, the flow is essentially radial. However, for a short duration of transient test, the flow will remain spherical during the test.

In the case of a pressure buildup test of a partially depleted well, Culham (1974) described the flow by the following expression:

$$p_i - p_{ws} = \frac{2453 QB\mu}{k^{2/3}}\left[\frac{1}{\sqrt{\Delta t}} - \frac{1}{\sqrt{t_p + \Delta t}}\right]$$

This relationship suggests that a plot of $(p_i - p_{ws})$ vs. $[1/\sqrt{\Delta t} - 1/\sqrt{t_p + \Delta t}]$ on a Cartesian scale would be a straight line that passes through the origin with a slope of m as given by:

For spherical flow $\qquad m = \dfrac{2453 QB\mu}{k^{2/3}}$

For hemispherical flow $\qquad m = \dfrac{1226 QB\mu}{k^{2/3}}$

with the *total* skin factor s defined by:

$$s = 34.7 r_{ew}\sqrt{\frac{\phi\mu c_t}{k}}\left[\frac{(p_{ws})_{\Delta t} - p_{wf\ at\ \Delta t=0}}{m} + \frac{1}{\sqrt{\Delta t}}\right] - 1$$

The dimensionless parameter r_{ew} is given by:

For spherical flow $r_{ew} = \dfrac{h_p}{2\ln(h_p/r_w)}$

For hemispherical flow $r_{ew} = \dfrac{h_p}{\ln(2h_p/r_w)}$

where:

$(p_{ws})_{\Delta t}$ = the shut-in pressure at any shut-in time Δt, hours
h_p = perforated length, ft
r_w = wellbore radius, ft

An important factor in determining the partial penetration skin factor is the ratio of the horizontal permeability k_h to the vertical permeability k_v, i.e., k_h/k_v. If the vertical permeability is small, the well will tend to behave as if the formation thickness h is equal to the completion thickness h_P. When the vertical permeability is high, the effect of the partial penetration is to introduce an extra pressure drop near the wellbore. This extra pressure drop will cause a large positive skin factor or smaller apparent wellbore radius when analyzing well test data. Similarly, opening only a few holes in the casing can also cause additional skin damage. Saidikowski (1979) indicated that the total skin factor s as calculated from a pressure transient test is related to the true skin factor caused by formation damage s_d and skin factor due to partial penetration s_P by the following relationship:

$$s = \left(\frac{h}{h_P}\right)s_d + s_P$$

Saidikowski estimated the skin factor due to partial penetration from the following expression:

$$s_P = \left(\frac{h}{h_P} - 1\right)\left[\ln\left(\frac{h}{r_w}\sqrt{\frac{k_h}{k_v}}\right) - 2\right]$$

where:

r_w = wellbore radius, ft
h_p = perforated interval, ft
h = total thickness, ft
k_h = horizontal permeability, md
k_v = vertical permeability, md

1.5.3 Analysis of middle-time test data

Identification of the basic reservoir characteristics is performed during the reservoir infinite-acting period and by using the middle-time test data. Infinite-acting flow occurs after the inner boundary effects have disappeared (e.g., wellbore storage, skin, etc.) and before the outer boundary effects have been felt. Gringarten et al. (1979) suggested that all reservoir behaviors can be classified as homogeneous or heterogeneous systems. The homogeneous system is described by only one porous medium that can be characterized by average rock properties through the conventional well testing approach. Heterogeneous systems are subclassified into the following two categories:

(1) double porosity reservoirs;
(2) multilayered or double-permeability reservoirs.

A brief discussion of the above two categories is given below.

Naturally fractured (double-porosity) reservoirs

Naturally fractured reservoirs are typically characterized by a double-porosity behavior; a primary porosity that represents the matrix ϕ_m and a secondary porosity ϕ_f that represents the fissure system. Basically, "fractures" are created hydraulically for well stimulation while "fissures" are considered natural fractures. The double- or dual-porosity model assumes two porous regions of distinctly different porosities and permeabilities within the formation. Only one, the "fissure system," has a permeability k_f high enough to produce to the well. The matrix system does not produce directly to the well but acts as a source of fluid to the fissure system. A very important characteristic of the double-porosity system is the nature of the fluid exchange between the two distinct porous systems. Gringarten (1984) presented a comprehensive treatment and an excellent review of the behavior of fissured reservoirs and the appropriate methodologies of analyzing well test data.

Warren and Root (1963) presented extensive theoretical work on the behavior of naturally fractured reservoirs. They assumed that the formation fluid flows from the matrix system into the fractures under pseudosteady-state conditions with the fractures acting like conduits to the wellbore. Kazemi (1969) proposed a similar model with the main assumption that the interporosity flow occurs under transient flow. Warren and Root indicated that two characteristic parameters, in addition to permeability and skin, control the behavior of double-porosity systems. These are:

(1) The dimensionless parameter ω that defines the storativity of the fractures as a ratio to that of the total reservoir. Mathematically, it is given by:

$$\omega = \frac{(\phi h c_t)_f}{(\phi h c_t)_{f+m}} = \frac{(\phi h c_t)_f}{(\phi h c_t)_f + (\phi h c_t)_m} \qquad [1.5.8]$$

where:

ω = storativity ratio
h = thickness
c_t = total compressibility, psi^{-1}
ϕ = porosity

The subscripts f and m refer to the fissure and matrix respectively. A typical range of ω is 0.1 to 0.001.

(2) The second parameter λ is the interporosity flow coefficient which describes the ability of the fluid to flow from the matrix into the fissures and is defined by the following relationship:

$$\lambda = \alpha\left(\frac{k_m}{k_f}\right)r_w^2 \qquad [1.5.9]$$

where:

λ = interporosity flow coefficient
k = permeability
r_w = wellbore radius

The factor α is the block-shape parameter that depends on the geometry and the characteristic shape of the matrix–fissures system and has the dimension of a reciprocal of the area defined by the following expression:

$$\alpha = \frac{A}{Vx}$$

where:

A = surface area of the matrix block, ft^2
V = volume of the matrix block
x = characteristic length of the matrix block, ft

Most of the proposed models assume that the matrix–fissures system can be represented by one the following four geometries:

(a) *Cubic* matrix blocks separated by fractures with λ as given by:

$$\lambda = \frac{60}{l_m^2}\left(\frac{k_m}{k_f}\right)r_w^2$$

where l_m is the length of a block side.
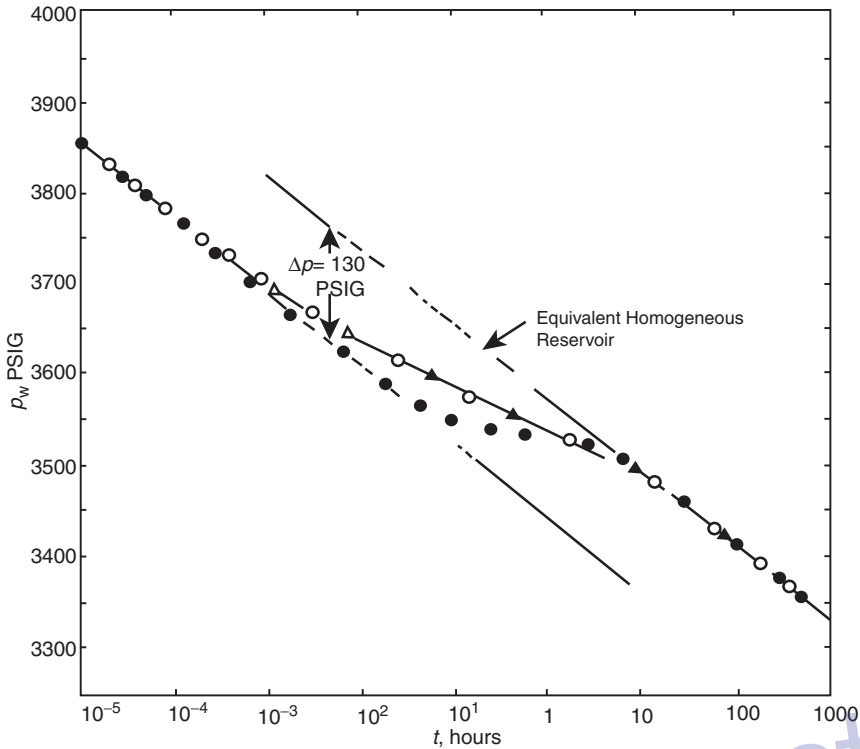
Figure 1.61 *Pressure drawdown according to the model by Warren and Root (Copyright ©1969 SPE, Kazemi, SPEJ, Dec. 1969).*

(b) *Spherical* matrix blocks separated by fractures with λ as given by:

$$\lambda = \frac{15}{r_m^2} \left(\frac{k_m}{k_f} \right) r_w^2$$

where r_m is the radius of the sphere.

(c) *Horizontal strata* (rectangular slab) matrix blocks separated by fractures with λ as given by:

$$\lambda = \frac{12}{h_f^2} \left(\frac{k_m}{k_f} \right) r_w^2$$

where h_f is the thickness of an individual fracture or high-permeability layer.

(d) *Vertical cylinder* matrix blocks separated by fractures with λ as given by:

$$\lambda = \frac{8}{r_m^2} \left(\frac{k_m}{k_f} \right) r_w^2$$

where r_m is the radius of the each cylinder

In general, the value of the interporosity flow parameter ranges between 10^{-3} and 10^{-9}. Cinco and Samaniego (1981) identified the following extreme interporosity flow conditions:

- Restricted interporosity flow which corresponds to a high skin between the least permeable media (matrix) and the highest permeable media (fissures) and is mathematically equivalent to the pseudosteady-state solution, i.e., the Warren and Root model.
- Unrestricted interporosity flow that corresponds to zero skin between the most and highest permeable media and is described be the unsteady-state (transient) solution.

Warren and Root proposed the first identification method of the double-porosity system, as shown by the drawdown semilog plot of Figure 1.61. The curve is characterized by *two parallel straight lines* due to the two separate porosities in the reservoir. Because the secondary porosity (fissures) has the greater transmissivity and is connected to the wellbore, it responds first as described by the first semilog straight line. The primary porosity (matrix), having a much lower transmissivity, responds much later. The combined effect of the two porosities gives rise to the second semilog straight line. The two straight lines are separated by a transition period during which the pressure tends to stabilize.

The first straight line reflects the transient radial flow through the fractures and, thus, *its slope is used to determine the system permeability–thickness product*. However, because the fracture storage is small, the fluid in the fractures is quickly depleted with a combined rapid pressure decline in the fractures. This pressure drop in the fracture allows more fluid to flow from the matrix into the fractures, which causes a slowdown in the pressure decline rate (as shown in Figure 1.61 by the transition period). As the matrix pressure approaches the pressure of the fractures, the pressure is stabilized in the two systems and yields the *second semilog straight line*. It should be pointed out that the first semilog straight line may be shadowed by wellbore storage effects and might not be recognized. Therefore, in practice, only parameters characterizing the homogeneous behavior of the *total* system $k_f h$ can be obtained.

Figure 1.62 shows the pressure buildup data for a naturally fractured reservoir. As for the drawdown, wellbore storage effects may obscure the first semilog straight line. If both semilog straight lines develop, analysis of the total permeability–thickness product is estimated from the slope *m* of either straight line and the use of Equation 1.3.8, or:

$$(k_f h) = \frac{162.6 Q B \mu}{m}$$
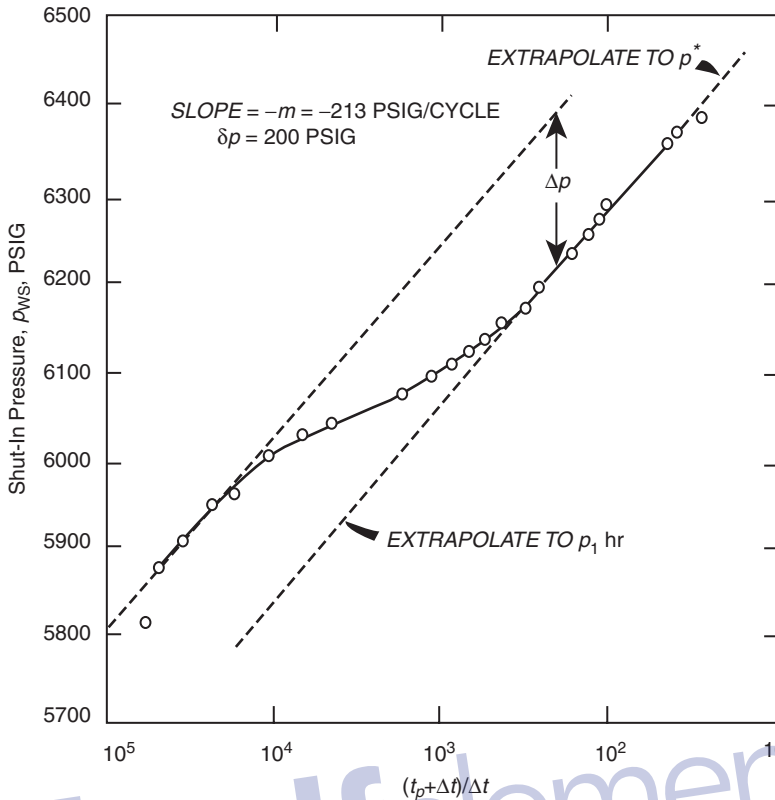
Figure 1.62 *Buildup curve from a fractured reservoir (After Warren and Root, 1963).*

The skin factor s and the false pressure p^* are calculated as described by using the *second straight line*. Warren and Root indicated that the storativity ratio ω can be determined from the vertical displacement between the two straight lines, identified as Δp in Figures 1.61 and 1.62, by the following expression:

$$\omega = 10^{(-\Delta p/m)} \qquad [1.5.10]$$

Bourdet and Gringarten (1980) indicated that by drawing a horizontal line through the *middle* of the transition curve to intersect with both semilog straight lines, as shown in Figures 1.61 and 1.62, the interporosity flow coefficient λ can be determined by reading the corresponding time at the *intersection* of either of the two straight lines, e.g. t_1 or t_2, and applying the following relationships:

In drawdown tests:

$$\lambda = \left[\frac{\omega}{1-\omega}\right]\left[\frac{(\phi h c_t)_m \mu r_w^2}{1.781 k_f t_1}\right] = \left[\frac{1}{1-\omega}\right]\left[\frac{(\phi h c_t)_m \mu r_w^2}{1.781 k_f t_2}\right]$$
$$[1.5.11]$$

In buildup tests:

$$\lambda = \left[\frac{\omega}{1-\omega}\right]\left[\frac{(\phi h c_t)_m \mu r_w^2}{1.781 k_f t_p}\right]\left(\frac{t_p + \Delta t}{\Delta t}\right)_1$$

or:

$$\lambda = \left[\frac{1}{1-\omega}\right]\left[\frac{(\phi h c_t)_m \mu r_w^2}{1.781 k_f t_p}\right]\left(\frac{t_p + \Delta t}{\Delta t}\right)_2 \qquad [1.5.12]$$

where:

k_f = permeability of the fracture, md
t_p = producing time before shut-in, hours
r_w = wellbore radius, ft
μ = viscosity, cp

The subscripts 1 and 2 (e.g., t_1) refer to the first and second line time intersection with the horizontal line drawn through the middle of the transition region pressure response during drawdown or buildup tests.

The above relationships indicate that the value of λ is dependent on the value of ω. Since ω is the ratio of fracture to matrix storage, as defined in terms of the *total* isothermal compressibility coefficients of the matrix and fissures by Equation 1.5.8, thus:

$$\omega = \frac{1}{1 + \left[\dfrac{(\phi h)_m}{(\phi h)_f}\dfrac{(c_t)_m}{(c_t)_f}\right]}$$

it suggests that ω is also dependent on the *PVT* properties of the fluid. It is quite possible for the oil contained in the fracture to be below the bubble point while the oil contained in the matrix is above the bubble point. Thus, ω is pressure dependent and, therefore, λ is greater than 10, so the level of heterogeneity is insufficient for dual porosity effects to be of importance and the reservoir can be treated with a single porosity.

Example 1.34 The pressure buildup data as presented by Najurieta (1980) and Sabet (1991) for a double-porosity system is tabulated below:

Δt (hr)	p_{ws} (psi)	$\frac{t_p + \Delta t}{\Delta t}$
0.003	6617	31 000 000
0.017	6632	516 668
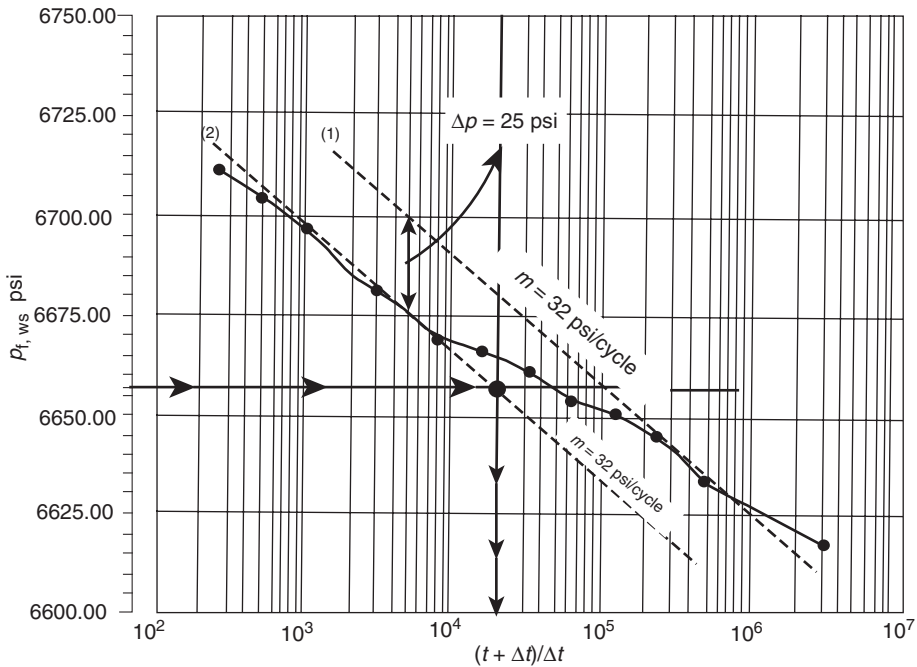
Figure 1.63 *Semilog plot of the buildup test data (After Sabet, M. A.* Well Test Analysis *1991, Gulf Publishing Company).*

Δt (hr)	p_{ws} (psi)	$\frac{t_p + \Delta t}{\Delta t}$
0.033	6644	358 334
0.067	6650	129 168
0.133	6654	64 544
0.267	6661	32 293
0.533	6666	16 147
1.067	6669	8 074
2.133	6678	4 038
4.267	6685	2 019
8.533	6697	1 010
17.067	6704	506
34.133	6712	253

The following additional reservoir and fluid properties are available:

$$p_i = 6789.5 \text{ psi}, \ p_{\text{wf at } \Delta t=0} = 6352 \text{ psi},$$

$$Q_o = 2554 \text{ STB/day}, \ B_o = 2.3 \text{ bbl/STB},$$

$$\mu_o = 1 \text{ cp}, \ t_p = 8611 \text{ hours}$$

$$r_w = 0.375 \text{ ft}, \ c_t = 8.17 \times 10^{-6} \text{ psi}^{-1}, \ \phi_m = 0.21$$

$$k_m = 0.1 \text{ md}, \ h_m = 17 \text{ ft}$$

Estimate ω and λ.

Solution

Step 1. Plot p_{ws} vs. $(t_p + \Delta t)/\Delta t$ on a semilog scale as shown in Figure 1.63.

Step 2. Figure 1.63 shows two parallel semilog straight lines with a slope of $m = 32$ psi/cycle.

Step 3. Calculate $(k_f h)$ from the slope m:

$$(k_f h) = \frac{162.6 Q_o B_o \mu_o}{m} = \frac{162.6(2556)(2.3)(1.0)}{32}$$

$$= 29\,848.3 \text{ md ft}$$

and:

$$k_f = \frac{29848.3}{17} = 1756 \text{ md}$$

Step 4. Determine the vertical distance Δp between the two straight lines:

$$\Delta p = 25 \text{ psi}$$

Step 5. Calculate the storativity ratio ω from Equation 1.5.10:

$$\omega = 10^{-(\Delta p/m)} = 10^{-(25/32)} = 0.165$$

Step 6. Draw a horizontal line through the middle of the transition region to intersect with the two semilog straight lines. Read the corresponding time at the second intersection, to give:

$$\left(\frac{t_p + \Delta t}{\Delta t}\right)_2 = 20000$$

Step 7. Calculate λ from Equation 1.5.12:

$$\lambda = \left[\frac{1}{1-\omega}\right]\left[\frac{(\phi h c_t)_m \mu r_w^2}{1.781 k_f t_p}\right]\left(\frac{t_p + \Delta t}{\Delta t}\right)_2$$

$$= \left[\frac{1}{1-0.165}\right]$$

$$\times \left[\frac{(0.21)(17)(8.17 \times 10^{-6})(1)(0.375)^2}{1.781(1756)(8611)}\right](20000)$$

$$= 3.64 \times 10^{-9}$$

It should be noted that pressure behavior in a naturally fractured reservoir is similar to that obtained in a *layered reservoir with no crossflow*. In fact, in any reservoir system with two predominant rock types, the pressure buildup behavior is similar to that of Figure 1.62.

Gringarten (1987) pointed out that the two straight lines on the semilog plot may or may not be present depending
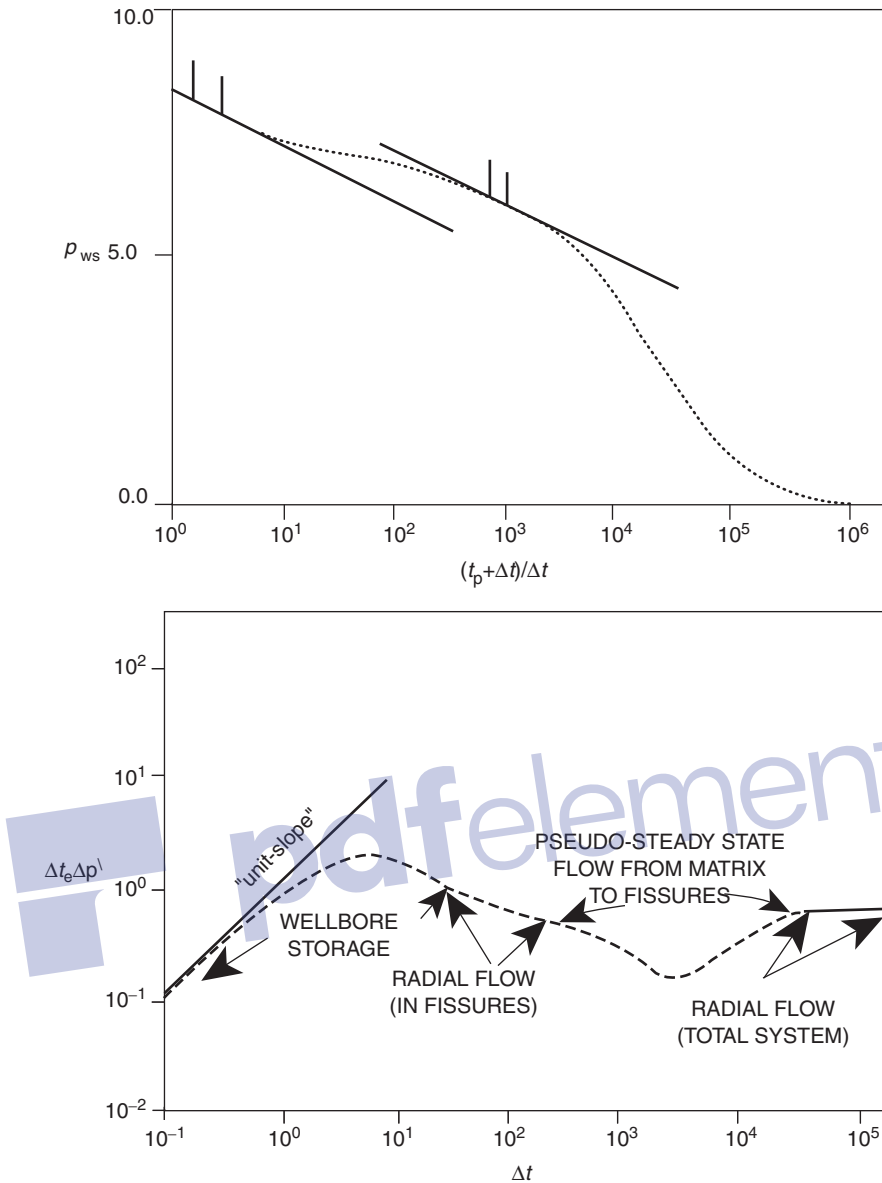
Figure 1.64 *Dual-porosity behavior shows as two parallel semilog straight lines on a semilog plot, as a minimum on a derivative plot.*

on the condition of the well and duration of the test. He concluded that the semilog plot is not an efficient or sufficient tool for identifying double-porosity behavior. In the log–log plot, as shown in Figure 1.62, the double-porosity behavior yields an S-shaped curve. The *initial portion* of the curve represents the homogeneous behavior resulting from depletion in the most permeable medium, e.g., fissures. A *transition period* follows and corresponds to the interporosity flow. Finally, the *last portion* represents the homogeneous behavior of both media when recharge from the least permeable medium (matrix) is fully established and pressure is equalized. The log–log analysis represents a significant improvement over conventional semilog analysis for identifying double-porosity behavior. However, S-shape behavior is difficult to see in highly damaged wells and well behavior can then be erroneously diagnosed as homogeneous.

Furthermore, a similar S-shape behavior may be found in irregularly bounded well drainage systems.

Perhaps the most efficient means for identifying double-porosity systems is the use of the pressure derivative plot. It allows unambiguous identification of the system, provided that the quality of the pressure data is adequate and, more importantly, an accurate methodology is used in calculating pressure derivatives. As discussed previously, the pressure derivative analysis involves a log–log plot of the derivative of the pressure with respect to time versus elapsed time. Figure 1.64 shows the combined log–log plot of pressure and derivative versus time for a dual-porosity system. The derivative plot shows a "minimum" or a "dip" on the pressure derivative curve caused by the interporosity flow during the transition period. The "minimum" is between two horizontal lines; the first represents the radial flow controlled by
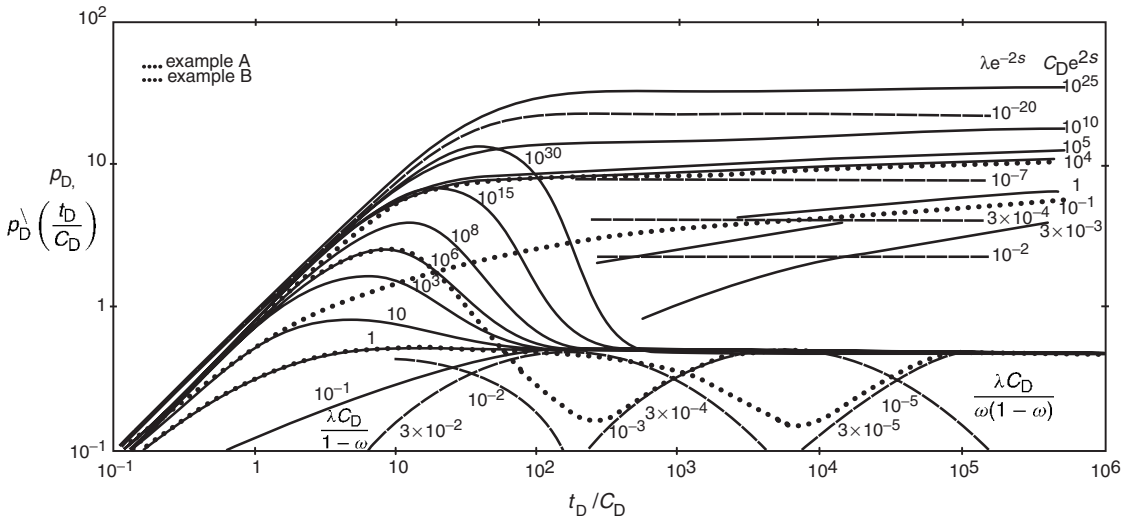
Figure 1.65   *Type curve matching (Copyright ©1984 World Oil, Bourdet et al., April 1984).*

the fissures and the second describes the combined behavior of the double-porosity system. Figure 1.64 shows, at early time, the typical behavior of wellbore storage effects with the deviation from the 45° straight line to a maximum representing a wellbore damage. Gringarten (1987) suggested that the shape of the minimum depends on the double-porosity behavior. For a restricted interporosity flow, the minimum takes a V-shape, whereas unrestricted interporosity yields an open U-shaped minimum.

Based on Warren and Root's double-porosity theory and the work of Mavor and Cinco (1979), Bourdet and Gringarten (1980) developed specialized pressure type curves that can be used for analyzing well test data in dual-porosity systems. They showed that double-porosity behavior is controlled by the following independent variables:

- p_D
- t_D/C_D
- $C_D e^{2s}$
- ω
- λe^{-2s}

with the dimensionless pressure p_D and time t_D as defined below:

$$p_D = \left[\frac{k_f h}{141.2 Q B \mu} \right] \Delta p$$

$$t_D = \frac{0.0002637 k_f t}{[(\phi \mu c_t)_f + (\phi \mu c_t)_m] \mu r_w^2} = \frac{0.0002637 k_f t}{(\phi \mu c_t)_{f+m} \mu r_w^2}$$

where:

k = permeability, md
t = time, hours
μ = viscosity, cp
r_w = wellbore radius, ft

and subscripts:

f = fissure
m = matrix
f + m = total system
D = dimensionless

Bourdet et al. (1984) extended the practical applications of these curves and enhanced their use by introducing the pressure derivative type curves to the solution. They developed two sets of pressure derivative type curves as shown in Figures 1.65 and 1.66. The first set, i.e., Figure 1.65, is based on the assumption that the interporosity flow obeys the pseudosteady-state flowing condition and the other set (Figure 1.66) assumes transient interporosity flow. The use of either set involves plotting the pressure difference Δp and the derivative function, as defined by Equation 1.5.4 for drawdown tests or Equation 1.5.5 for buildup tests, versus time with same size log cycles as the type curve. The controlling variables in each of the two type curve sets are given below.

First type curve set: *pseudo steady-state interporosity flow*   The actual *pressure response*, i.e., pressure difference Δp, is described by the following three component curves:

(1) At early times, the flow comes from the fissures (most permeable medium) and the actual pressure difference plot, i.e., Δp curve, matches one of the homogeneous curves that is labeled $(C_D e^{2s})$ with a corresponding value of $(C_D e^{2s})_f$ that describes the *fissure flow*. This value is designated as $[(C_D e^{2s})_f]_M$.

(2) As the pressure difference response reaches the transition regime, Δp deviates from the $C_D e^{2s}$ curve and follows one of the transition curves that describes this flow regime by λe^{-2s}, designated as $[\lambda e^{-2s}]_M$.

(3) Finally, the pressure difference response leaves the transition curve and matches a new $C_D e^{2s}$ curve below the first one with a corresponding value of $(C_D e^{2s})_{f+m}$ that describes the *total system* behavior, i.e., matrix and fissures. This value is recorded as $[(C_D e^{2s})_{f+m}]_M$.

On the pressure derivative response, the storativity ratio ω defines the shape of the derivative curve during the transition regime that is described by a "depression" or a "minimum." The duration and depth of the depression are linked by the value of ω; a small ω produces a long and therefore deep transition. The interporosity coefficient λ is the second parameter defining the position of the time axis of the transition regime. A decrease of λ value moves the depression to the right side of the plot.
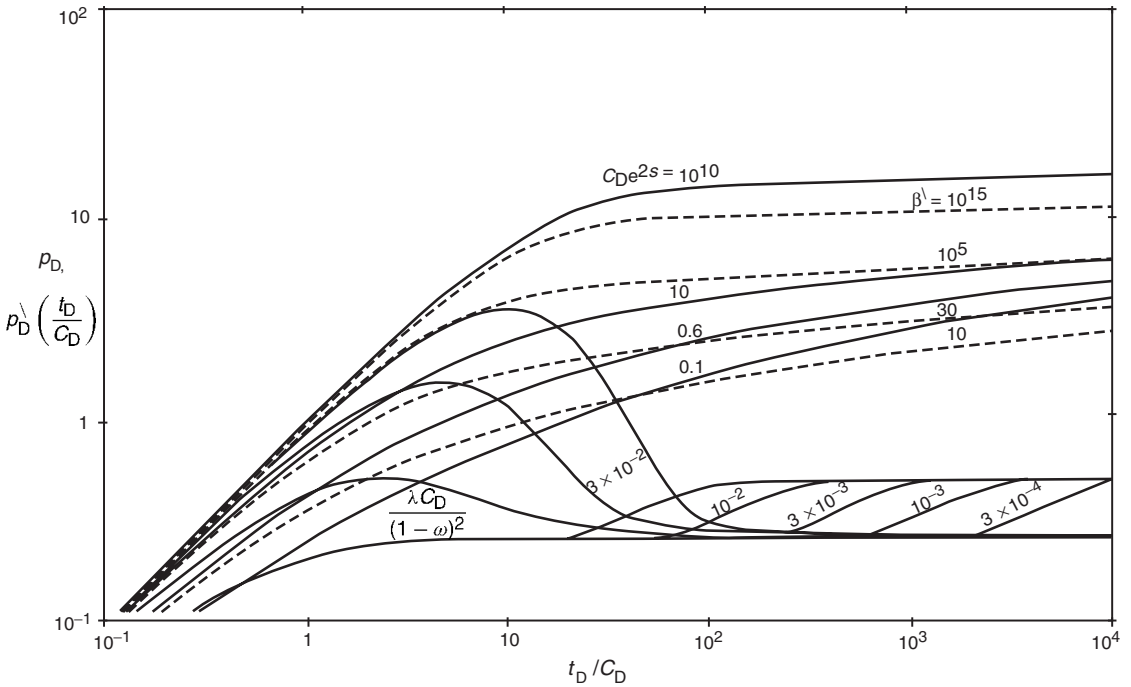
Figure 1.66   *Type curve matching (Copyright ©1984 World Oil, Bourdet et al., April 1984).*

As shown in Figure 1.65, the pressure derivative plots match on four component curves:

(1) The derivative curve follows the fissure flow curve $[(C_D e^{2s})_f]_M$.
(2) The derivative curve reaches an early transition period, expressed by a depression and described by an early transition curve $[\lambda(C_D)_{f+m}/\omega(1-\omega)]_M$.
(3) The derivative pressure curve then matches a late transition curve labeled $[\lambda(C_D)_{f+m}/(1-\omega)]_M$.
(4) The total system behavior is reached on the 0.5 line.

Second type curve set: *transient interporosity flow* As developed by Bourdet and Gringarten (1980) and expanded by Bourdet et al. (1984) to include the pressure derivative approach, this type curve is built in the same way as for the pseudosteady-state interporosity flow. As shown in Figure 1.66, the pressure behavior is defined by three component curves, $(C_D e^{2s})_f$, $\beta^\backslash$, and $(C_D e^{2s})_{f+m}$. The authors defined $\beta^\backslash$ as the interporosity dimensionless group and given by:

$$\beta^\backslash = \delta \left[\frac{(C_D e^{2s})_{f+m}}{\lambda e^{-2s}} \right]$$

where the parameter δ is the shape coefficient with assigned values as given below:

$\delta = 1.0508$ for spherical blocks
$\delta = 1.8914$ for slab matrix blocks

As the first fissure flow is short-lived with transient interporosity flow models, the $(C_D e^{2s})_f$ curves are not seen in practice and therefore have not been included in the derivative curves. The dual-porosity derivative response starts on the derivative of a $\beta^\backslash$ transition curve, then follows a late transition curve labeled $\lambda(C_D)_{f+m}/(1-\omega)^2$ until it reaches the total system regime on the 0.5 line.

Bourdet (1985) points out that the pressure derivative responses during the transition flow regime are very different between the two types of double-porosity model. With the transient interporosity flow solutions, the transition starts from early time and does not drop to a very low level. With pseudosteady-state interporosity flow, the transition starts later and the shape of the depression is much more pronounced. There is *no lower limit* for the depth of the depression when the flow from the matrix to the fissures follows the pseudosteady-state model, whereas for the interporosity transient flow the depth of the *depression does not exceed* 0.25.

In general, the matching procedure and reservoir parameters estimation as applied to the type-curve of Figure 1.66 can be summarized by the following steps:

Step 1. Using the actual well test data, calculate the pressure difference Δp and the pressure derivative plotting functions as defined by Equation 1.5.4 for drawdown or Equation 1.5.5 for buildup tests, i.e.,:
For drawdown tests:

The pressure difference $\Delta p = p_i - p_{wf}$

The derivative function $t \Delta p^\backslash = -t \left(\dfrac{\mathrm{d}(\Delta p)}{\mathrm{d}(t)} \right)$

For buildup tests:

The pressure difference $\Delta p = p_{ws} - p_{wf \text{ at } \Delta t=0}$

The derivative function $\Delta t_e \Delta p^\backslash = \Delta t \left(\dfrac{t_p + \Delta t}{\Delta t} \right) \left[\dfrac{\mathrm{d}(\Delta p)}{\mathrm{d}(\Delta t)} \right]$

Step 2. On tracing paper with the same size log cycles as in Figure 1.66, plot the data of step 1 as a function of flowing time t for drawdown tests or equivalent time Δt_e for buildup tests.

Step 3. Place the actual two sets of plots, i.e., Δp and derivative plots, on Figure 1.65 or Figure 1.66 and force a simultaneous match of the two plots to Gringarten–Bourdet type curves. Read the matched derivative curve $[\lambda(C_D)_{f+m}/(1-\omega)^2]_M$.

Step 4. Choose any point and read its coordinates on both Figures to give:

$$(\Delta p, p_D)_{MP} \quad \text{and} \quad (t \text{ or } \Delta t_e, t_D/C_D)_{MP}$$

Step 5. With the match still maintained, read the values of the curves labeled $(C_D e^{2s})$ which match the initial segment of the curve $[(C_D e^{2s})_f]_M$ and the final segment $[(C_D e^{2s})_{f+m}]_M$ of the data curve.

Step 6. Calculate the well and reservoir parameters from the following relationships:

$$\omega = \frac{[(C_D e^{2s})_{f+m}]_M}{[(C_D e^{2s})_f]_M} \qquad [1.5.13]$$

$$k_f h = 141.2 Q B \mu \left(\frac{p_D}{\Delta p}\right)_{MP} \text{ md ft} \qquad [1.5.14]$$

$$C = \left[\frac{0.000295 k_f h}{\mu}\right] \frac{(\Delta t)_{MP}}{(C_D/C_D)_{MP}} \qquad [1.5.15]$$

$$(C_D)_{f+m} = \frac{0.8926 C}{\phi c_t h r_w^2} \qquad [1.5.16]$$

$$s = 0.5 \ln \left[\frac{[(C_D e^{2s})_{f+m}]_M}{(C_D)_{f+m}}\right] \qquad [1.5.17]$$

$$\lambda = \left[\frac{\lambda(C_D)_{f+m}}{(1-\omega)^2}\right]_M \frac{(1-\omega)^2}{(C_D)_{f+m}} \qquad [1.5.18]$$

The selection of the best solution between the pseudosteady-state and the transient interporosity flow is generally straightforward; with the pseudosteady-state model, the drop of the derivative during transition is a function of the transition duration. Long transition regimes, corresponding to small ω values, produce derivative levels much smaller than the practical 0.25 limit of the transient solution.

The following pressure buildup data as given by Bourdet et al. and reported conveniently by Sabet (1991) is used below as an example to illustrate the use of pressure derivative type curves.

Example 1.35 Table 1.8 shows the pressure buildup and pressure derivative data for a naturally fractured reservoir. The following flow and reservoir data is also given:

$$Q = 960 \text{ STB/day}, \quad B_o = 1.28 \text{ bbl/STB},$$
$$c_t = 1 \times 10^{-5} \text{ psi}^{-1}, \quad \phi = 0.007,$$
$$\mu = 1 \text{ cp}, \quad r_w = 0.29 \text{ ft}, \quad h = 36 \text{ ft}$$

It is reported that the well was opened to flow at a rate of 2952 STB/day for 1.33 hours, shut-in for 0.31 hours, opened again at the same rate for 5.05 hours, closed for 0.39 hours, opened for 31.13 hours at the rate of 960 STB/day, and then shut-in for the pressure buildup test.

Analyze the buildup data and determine the well and reservoir parameters assuming transient interporosity flow.

Solution

Step 1. Calculate the flowing time t_p as follows:

Total oil produced $= N_P$

$$= \frac{2952}{4}[1.33 + 5.05] + \frac{960}{24}31.13 \simeq 2030 \text{ STB}$$

$$t_p = \frac{(24)(2030)}{960} = 50.75 \text{ hours}$$

Table 1.8 *Pressure Buildup Test, Naturally Fractured Reservoir. After Sabet, M. A. "Well Test Analysis" 1991, Gulf Publishing Company*

Δt (hr)	Δp_{ws} (psi)	$\dfrac{t_p + \Delta t}{\Delta t}$	*Slope* (psi/hr)	$\Delta p \backslash \dfrac{t_p + \Delta t}{t_p}$ (psi)
0.00000E+00	0.000		3180.10	
3.48888E−03	11.095	14 547.22	1727.63	8.56
9.04446E−03	20.693	5 612.17	847.26	11.65
1.46000E−02	25.400	3 477.03	486.90	9.74
2.01555E−02	28.105	2 518.92	337.14	8.31
2.57111E−02	29.978	1 974.86	257.22	7.64
3.12666E−02	31.407	1 624.14	196.56	7.10
3.68222E−02	32.499	1 379.24	159.66	6.56
4.23777E−02	33.386	1 198.56	127.80	6.10
4.79333E−02	34.096	1 059.76	107.28	5.64
5.90444E−02	35.288	860.52	83.25	5.63
7.01555E−02	36.213	724.39	69.48	5.36
8.12666E−02	36.985	625.49	65.97	5.51
9.23777E−02	37.718	550.38	55.07	5.60
0.10349	38.330	491.39	48.83	5.39
0.12571	39.415	404.71	43.65	5.83
0.14793	40.385	344.07	37.16	5.99
0.17016	41.211	299.25	34.38	6.11
0.19238	41.975	264.80	29.93	6.21
0.21460	42.640	237.49	28.85	6.33
0.23682	43.281	215.30	30.96	7.12
0.25904	43.969	196.92	25.78	7.39
0.28127	44.542	181.43	24.44	7.10
0.30349	45.085	168.22	25.79	7.67
0.32571	45.658	156.81	20.63	7.61
0.38127	46.804	134.11	18.58	7.53
0.43682	47.836	117.18	17.19	7.88
0.49238	48.791	104.07	16.36	8.34
0.54793	49.700	93.62	15.14	8.72
0.60349	50.541	85.09	12.50	8.44
0.66460	51.305	77.36	12.68	8.48
0.71460	51.939	72.02	11.70	8.83
0.77015	52.589	66.90	11.14	8.93
0.82571	53.208	62.46	10.58	9.11
0.88127	53.796	58.59	10.87	9.62
0.93682	54.400	55.17	8.53	9.26
0.99238	54.874	52.14	10.32	9.54
1.04790	55.447	49.43	7.70	9.64
1.10350	55.875	46.99	8.73	9.26
1.21460	56.845	42.78	7.57	10.14
1.32570	57.686	39.28	5.91	9.17
1.43680	58.343	36.32	6.40	9.10
1.54790	59.054	33.79	6.05	9.93
1.65900	59.726	31.59	5.57	9.95
1.77020	60.345	29.67	5.44	10.08
1.88130	60.949	27.98	4.74	9.93
1.99240	61.476	26.47	4.67	9.75
2.10350	61.995	25.13	4.34	9.87
2.21460	62.477	23.92	3.99	9.62
2.43680	63.363	21.83	3.68	9.79
2.69240	64.303	19.85	3.06[a]	9.55[b]
2.91460	64.983	18.41	3.16	9.59
3.13680	65.686	17.18	2.44	9.34
3.35900	66.229	16.11	19.72	39.68

[a] $(64.983 - 64.303)/(2.9146 - 2.69240) = 3.08$.
[b] $[(3.68 + 3.06)/2] \times 19.85 \times 2.69240^2/50.75 = 9.55$.
Adapted from Bourdet et al. (1984).

Step 2. Confirm the double-porosity behavior by constructing the Horner plot as shown in Figure 1.67. The graph shows the two parallel straight lines confirming the dual-porosity system.
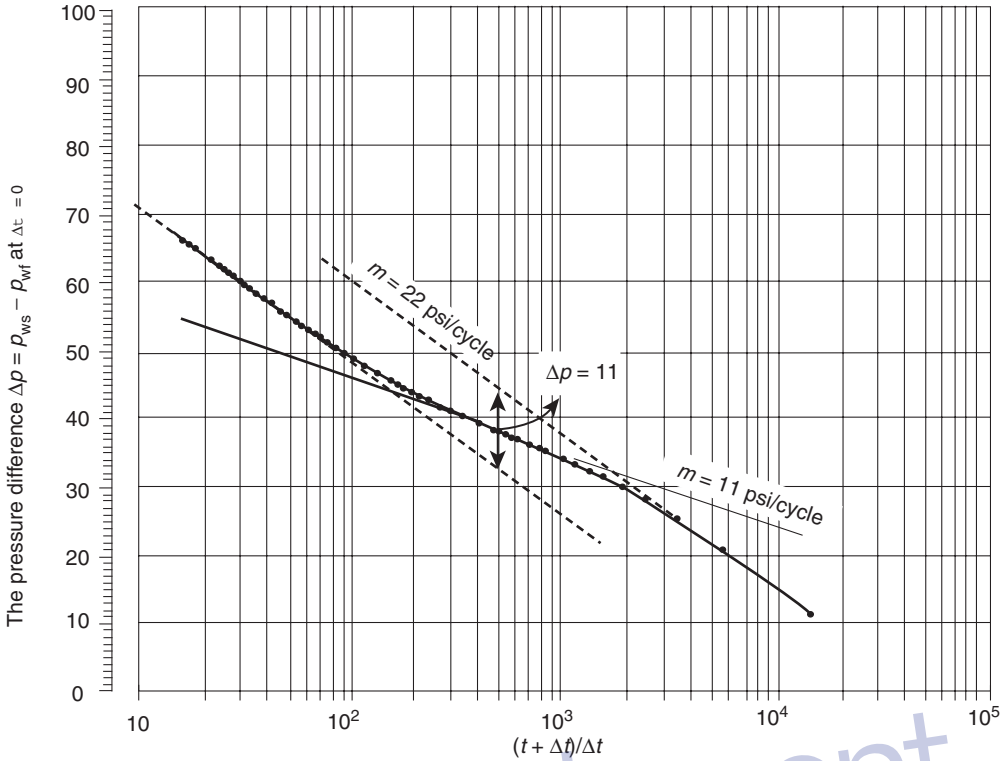
Figure 1.67 *The Horner plot; data from Table 1.8 (After Sabet, M. A.* Well Test Analysis *1991, Gulf Publishing Company).*

Step 3. Using the same grid system of Figure 1.66, plot the *actual pressure derivative* versus shut-in time as shown in Figure 1.68(a) and Δp_{ws} versus time (as shown in Figure 1.68(b)). The 45° line shows that the test was slightly affected by the wellbore storage.

Step 4. Overlay the pressure difference and pressure derivative plots over the transient interporosity type curve, as shown in Figure 1.69, to give the following matching parameters:

$$\left[\frac{p_D}{\Delta p}\right]_{MP} = 0.053$$

$$\left[\frac{t_D/C_D}{\Delta t}\right]_{MP} = 270$$

$$\left[\frac{\lambda(C_D)_{f+m}}{(1-\omega)^2}\right]_M = 0.03$$

$$[(C_D e^{2s})_f]_M = 33.4$$

$$[(C_D e^{2s})_{f+m}]_M = 0.6$$

Step 5. Calculate the well and reservoir parameters by applying Equations 1.5.13 through 1.5.18 to give:

$$\omega = \frac{[(C_D e^{2s})_{f+m}]_M}{[(C_D e^{2s})_f]_M} = \frac{0.6}{33.4} = 0.018$$

Kazemi (1969) pointed out that if the vertical separation between the two parallel slopes Δp is less the 100 psi, the calculation of ω by Equation 1.5.10 will produce a significant error in its values. Figure 1.67

shows that Δp is about 11 psi and Equation 1.5.10 gives an *erroneous value* of:

$$\omega = 10^{-(\Delta p/m)} = 10^{-(11/22)} = 0.316$$

Also:

$$k_f h = 141.2 Q B \mu \left(\frac{p_D}{\Delta p}\right)_{MP}$$

$$= 141.2(960)(1)(1.28)(0.053) = 9196 \text{ md ft}$$

$$C = \left[\frac{0.000295 k_f h}{\mu}\right]\frac{(\Delta t)_{MP}}{(C_D/C_D)_{MP}}$$

$$= \frac{(0.000295)(9196)}{(1.0)(270)} = 0.01 \text{ bbl/psi}$$

$$(C_D)_{f+m} = \frac{0.8926 C}{\phi c_t h r_w^2}$$

$$= \frac{(0.8936)(0.01)}{(0.07)(1 \times 10^{-5})(36)90.29)^2} = 4216$$

$$s = 0.5 \ln\left[\frac{[(C_D e^{2s})_{f+m}]_M}{(C_D)_{f+m}}\right]$$

$$= 0.5 \ln\left[\frac{0.6}{4216}\right] = -4.4$$

$$\lambda = \left[\frac{\lambda(C_D)_{f+m}}{(1-\omega)^2}\right]_M \frac{(1-\omega)^2}{(C_D)_{f+m}}$$

$$= (0.03)\left[\frac{(1-0.018)^2}{4216}\right] = 6.86 \times 10^{-6}$$
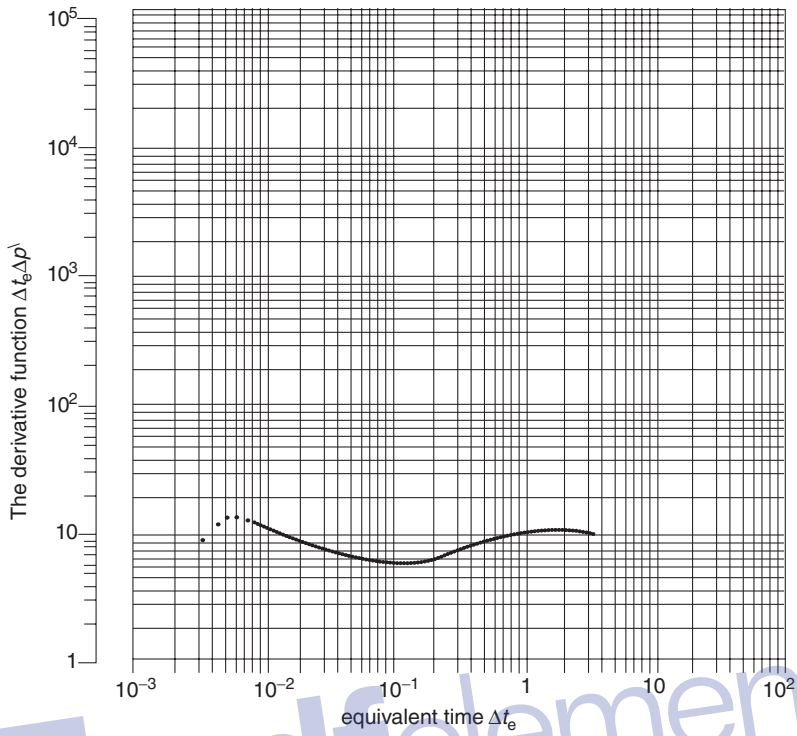
Figure 1.68(a)   *Derivative function.*
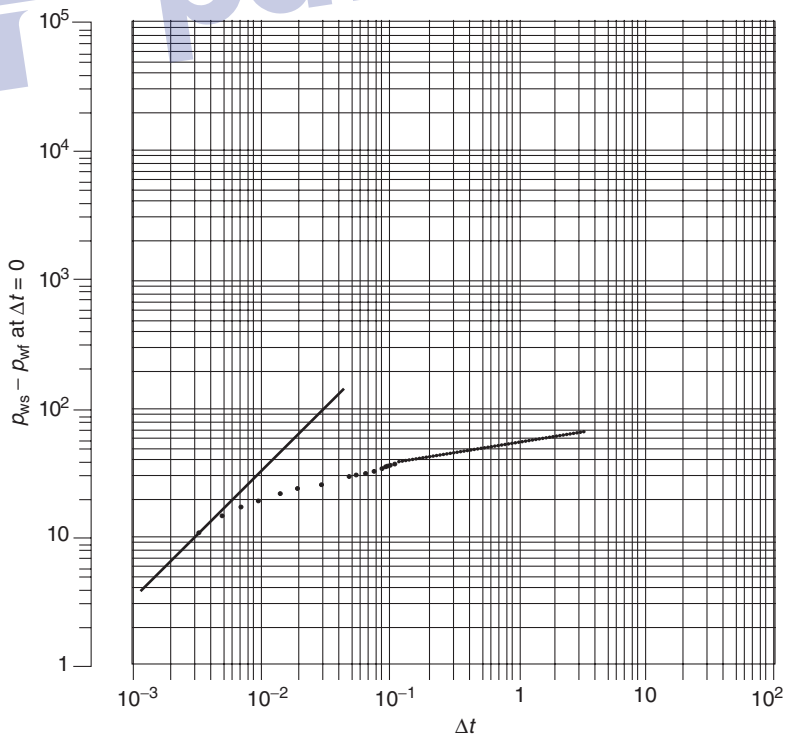
Figure 1.68(b)   *Log–log plot of Δp vs. Δt_e (After Sabet, M. A.* Well Test Analysis *1991, Gulf Publishing Company).*
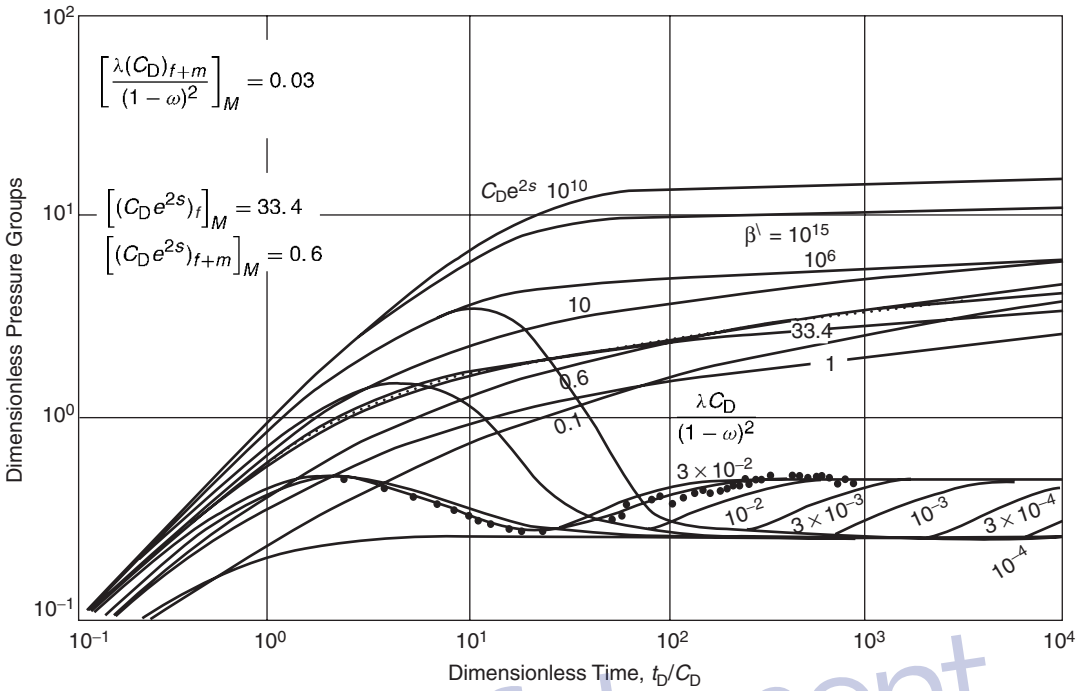
Figure 1.69   *Type curve matching (Copyright ©1984 World Oil, Bourdet et al., April 1984).*

Layered reservoirs

The pressure behavior of a no-crossflow multilayered reservoir with communication only at the wellbore will behave significantly different from a single-layer reservoir. Layered reservoirs can be classified into the following three categories:

(1) *Crossflow layered reservoirs* are those which communicate both in the wellbore and in the reservoir.
(2) *Commingled layered reservoirs* are those which communicate only in the wellbore. A complete permeability barrier exists between the various layers.
(3) *Composite reservoirs* are made up of commingled zones and some of the zones consist of crossflow layers. Each crossflow layer behaves on tests as if it were an homogeneous and isotropic layer; however, the composite reservoir should behave exactly as a commingled reservoir.

Some layered reservoirs behave as double-porosity reservoirs when in fact they are not. When reservoirs are characterized by layers of very low permeabilities interbedded with relatively thin high-permeability layers, they could behave on well tests exactly as if they were naturally fractured systems and could be treated with the interpretation models designed for double-porosity systems. Whether the well produces from a commingled, crossflow, or composite system, the test objectives are to determine skin factor, permeability, and average pressure.

The pressure response of crossflow layered systems during well testing is similar to that of homogeneous systems and can be analyzed with the appropriate conventional semilog and log–log plotting techniques. Results of the well test should be interpreted in terms of the arithmetic total permeability–thickness and porosity–compressibility–thickness products as given by:

$$(kh)_t = \sum_{i=1}^{n \text{ layers}} (kh)_i$$

$$(\phi c_t h)_t = \sum_{i=1}^{n \text{ layers}} (\phi c_t h)_i$$

Kazemi and Seth (1969) proposed that if the total permeability–thickness product $(kh)_t$ is known from a well test, the individual layer permeability k_i may be approximated from the layer flow rate q_i and the total flow rate q_t by applying the following relationship:

$$k_i = \frac{q_i}{q_t} \left[\frac{(kh)_t}{h_i} \right]$$

The pressure buildup behavior of a commingled two-layer system without crossflow is shown schematically in Figure 1.70. The straight line AB that follows the early-time data gives the proper value of the average flow capacity $(kh)_t$ of the reservoir system. The flattening portion BC analogous to a single-layer system attaining statistic pressure indicates that the pressure in the more permeable zone has almost reached its average value. The portion CD represents a repressurization of the more permeable layer by the less depleted, less permeable layer with a final rise DE at the stabilized average pressure. Notice that the buildup is somewhat similar to the buildup in naturally fractured reservoirs.

Sabet (1991) points out that when a commingled system is producing under the pseudosteady-state flow condition, the flow rate from any layer q_i can be approximated from total
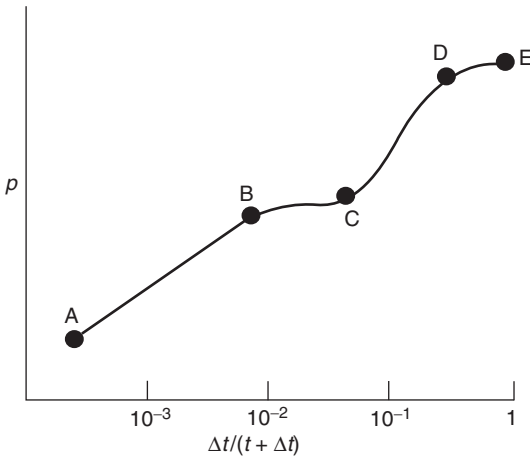
Figure 1.70 *Theoretical pressure buildup curve for two-layer reservoir (Copyright ©1961 SPE, Lefkovits et al., SPEJ, March 1961).*

flow rate and the layer storage capacity $\phi c_t h$ from:

$$q_i = q_t \left[\frac{(\phi c_t h)_i}{\sum_{j=1}^{n} (\phi c_t h_i)_j} \right]$$

1.5.4 Hydraulically fractured reservoirs

A fracture is defined as a single crack initiated from the wellbore by hydraulic fracturing. It should be noted that fractures are different from "fissures," which are the formation of natural fractures. Hydraulically induced fractures are usually vertical, but can be horizontal if the formation is less than approximately 3000 ft deep. Vertical fractures are characterized by the following properties:

- fracture half-length x_f, ft;
- dimensionless radius r_{eD}, where $r_{eD} = r_e/x_f$;
- fracture height h_f, which is often assumed equal to the formation thickness, ft;
- fracture permeability k_f, md;
- fracture width w_f, ft;
- fracture conductivity F_C, where $F_C = k_f w_f$.

The analysis of fractured well tests deals with the identification of well and reservoir variables that would have an impact on future well performance. However, fractured wells are substantially more complicated. The well-penetrating fracture has unknown geometric features, i.e., x_f, w_f, and h_f, and unknown conductivity properties.

Gringarten et al. (1974) and Cinco and Samaniego (1981), among others, propose three transient flow models to consider when analyzing transient pressure data from vertically fractured wells. These are:

(1) infinite conductivity vertical fractures;
(2) finite conductivity vertical fractures;
(3) uniform flux fractures.

Descriptions of the above three types of fractures are given below.

Infinite conductivity vertical fractures

These fractures are created by conventional hydraulic fracturing and characterized by a very high conductivity, which for all practical purposes can be considered as infinite. In this case, the fracture acts similar to a large-diameter pipe with *infinite permeability* and, therefore, there is essentially no pressure drop from the tip of the fracture to the wellbore, i.e., no pressure loss in the fracture. This model assumes that the flow into the wellbore is only through the fracture and exhibits three flow periods:

(1) fracture linear flow period;
(2) formation linear flow period;
(3) infinite-acting pseudoradial flow period.

Several specialized plots are used to identify the start and end of each flow period. For example, an early-time log–log plot of Δp vs. Δt will exhibit a straight line of half-unit slope. These flow periods associated with infinite conductivity fractures and the diagnostic specialized plots will be discussed later in this section.

Finite conductivity fractures

These are very long fractures created by massive hydraulic fracture (MHF). These types of fractures need large quantities of propping agent to keep them open and, as a result, the fracture permeability k_f is reduced as compared to that of the infinite conductivity fractures. These finite conductivity vertical fractures are characterized by measurable pressure drops in the fracture and, therefore, exhibit unique pressure responses when testing hydraulically fractured wells. The transient pressure behavior for this system can include the following four sequence flow periods (to be discussed later):

(1) initially "linear flow within the fracture";
(2) followed by "bilinear flow";
(3) then "linear flow in the formation"; and
(4) eventually "infinite acting pseudoradial flow."

Uniform flux fractures

A uniform flux fracture is one in which the reservoir fluid flow rate from the formation into the fracture is uniform along the entire fracture length. This model is similar to the infinite conductivity vertical fracture in several aspects. The difference between these two systems occurs at the boundary of the fracture. The system is characterized by a variable pressure along the fracture and exhibits essentially two flow periods;

(1) linear flow;
(2) infinite-acting pseudoradial flow.

Except for highly propped and conductive fractures, it is thought that the uniform-influx fracture theory better represents reality than the infinite conductivity fracture; however, the difference between the two is rather small.

The fracture has a much greater permeability than the formation it penetrates; hence it influences the pressure response of a well test significantly. The general solution for the pressure behavior in a reservoir is expressed in terms of dimensionless variables. The following dimensionless groups are used when analyzing pressure transient data in a hydraulically fractured well:

Diffusivity group $\eta_{fD} = \dfrac{k_f \phi c_t}{k \phi_f c_{ft}}$ [1.5.19]

Time group $t_{Dx_f} = \left[\dfrac{0.0002637k}{\phi \mu c_t x_f^2} \right] t = t_D \left(\dfrac{r_w^2}{x_f^2} \right)$

[1.5.20]

Conductivity group $F_{CD} = \dfrac{k_f}{k} \dfrac{w_f}{x_f} = \dfrac{F_C}{k x_f}$ [1.5.21]

Storage group $C_{Df} = \dfrac{0.8937C}{\phi c_t h x_f^2}$ [1.5.22]

(a)

FRACTURE LINEAR FLOW

(b)

BILINEAR FLOW

(c)

FORMATION LINEAR FLOW

(d)

PSEUDO RADIAL FLOW
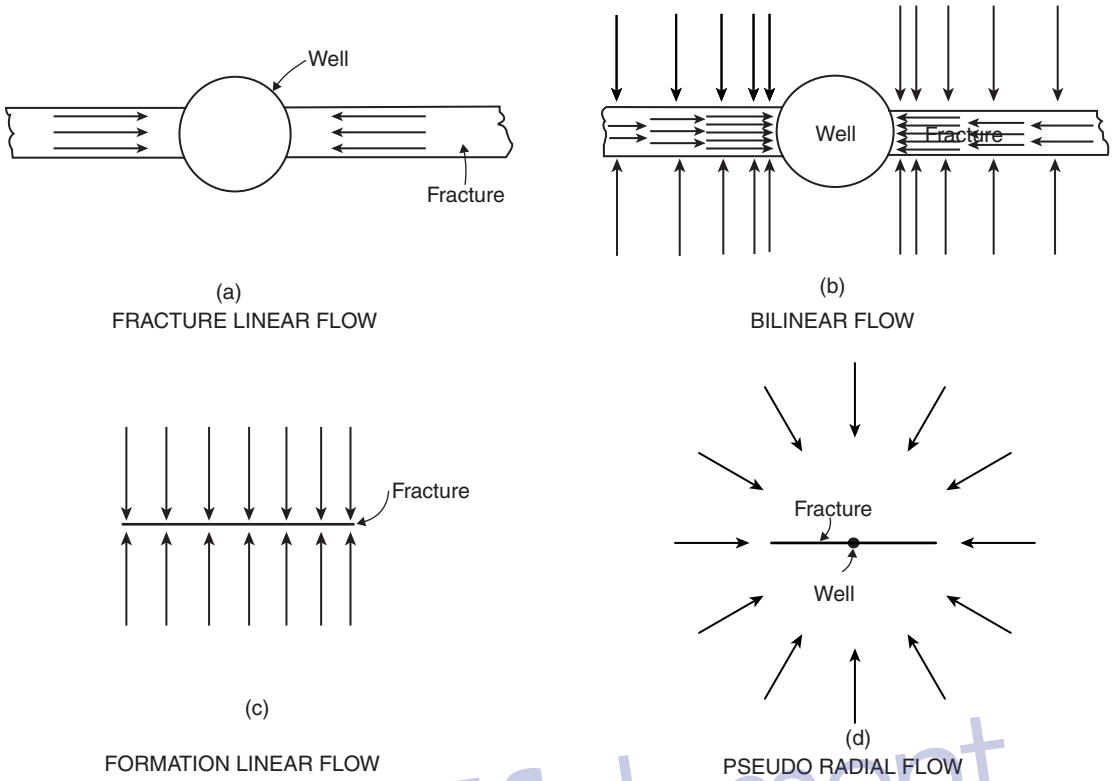
Figure 1.71 *Flow periods for a vertically fractured well (After Cinco and Samaniego, JPT, 1981).*

Pressure group $\quad p_{\mathrm{D}} = \dfrac{kh\Delta p}{141.2QB\mu} \quad$ for oil $\qquad$ [1.5.23]

$$p_{\mathrm{D}} = \frac{kh\Delta m(p)}{1424QT} \quad \text{for gas} \qquad [1.5.24]$$

Fracture group $\quad r_{\mathrm{eD}} = \dfrac{r_{\mathrm{e}}}{x_{\mathrm{f}}}$

where:

$\quad x_{\mathrm{f}}$ = fracture half-length, ft
$\quad w_{\mathrm{f}}$ = fracture width, ft
$\quad k_{\mathrm{f}}$ = fracture permeability, md
$\quad k$ = pre-frac formation permeability, md
$\quad t_{Dx_{\mathrm{f}}}$ = dimensionless time based on the fracture
$\qquad$ half-length x_{f}
$\quad t$ = flowing time in drawdown, Δt or Δt_{e} in buildup,
$\qquad$ hours
$\quad T$ = Temperature, °R
$\quad F_C$ = fracture conductivity, md ft
$\quad F_{\mathrm{CD}}$ = dimensionless fracture conductivity
$\quad \eta$ = hydraulic diffusivity
$\quad c_{\mathrm{ft}}$ = total compressibility of the fracture, psi^{-1}

Notice that the above equations are written in terms of the pressure drawdown tests. These equations should be modified for buildup tests by replacing the pressure and time with the appropriate values as shown below:

Test	Pressure	Time
Drawdown	$\Delta p = p_{\mathrm{i}} - p_{\mathrm{wf}}$	t
Buildup	$\Delta p = p_{\mathrm{ws}} - p_{\mathrm{wf}\ \mathrm{at}\ \Delta t=0}$	Δt or Δt_{e}

In general, a fracture could be classified as an infinite conductivity fracture when the dimensionless fracture conductivity is greater than 300, i.e., $F_{\mathrm{CD}} > 300$.

There are four flow regimes, as shown conceptually in Figure 1.71, associated with the three types of vertical fractures. These are:

(1) fracture linear flow;
(2) bilinear flow;
(3) formation linear flow;
(4) infinite-acting pseudoradial flow.

These flow periods can be identified by expressing the pressure transient data in different type of graphs. Some of these graphs are excellent tools for diagnosis and identification of regimes since test data may correspond to different flow periods.

There are specialized graphs of analysis for each flow period that include:

- a graph of Δp vs. $\sqrt{\text{time}}$ for linear flow;
- a graph of Δp vs. $\sqrt[4]{\text{time}}$ for bilinear flow;
- a graph of Δp vs. log(time) for infinite-acting pseudoradial flow.

These types of flow regimes and the diagnostic plots are discussed below.

Fracture linear flow This is the first flow period which occurs in a fractured system. Most of the fluid enters the wellbore during this period of time as a result of expansion within the fracture, i.e., there is negligible fluid coming from the formation. Flow within the fracture and from the fracture to the wellbore during this time period is linear and can be described by the diffusivity equation as expressed in a linear

form and is applied to both the fracture linear flow and formation linear flow periods. The pressure transient test data during the linear flow period can be analyzed with a graph of Δp vs. $\sqrt{\text{time}}$. Unfortunately, the fracture linear flow occurs at very early time to be of practical use in well test analysis. However, if the fracture linear flow exists (for fractures with $F_{CD} > 300$), the formation linear flow relationships as given by Equations 1.5.19 through 1.5.24 can be used in an exact manner to analyze the pressure data during the formation linear flow period.

If fracture linear flow occurs, the duration of the flow period is short, as it often is in finite conductivity fractures with $F_{CD} < 300$, and care must be taken not to misinterpret the early pressure data. It is common in this situation for skin effects or wellbore storage effects to alter pressures to the extent that the linear flow straight line does not occur or is very difficult to recognize. If the early-time slope is used in determining the fracture length, the slope m_{vf} will be erroneously high, the computed fracture length will be unrealistically small, and no quantitative information will be obtained regarding flow capacity in the fracture.

Cinco et al. (1981) observed that the fracture linear flow ends when:

$$t_{Dx_f} \approx \frac{0.01(F_{CD})^2}{(\eta_{fD})^2}$$

Bilinear flow   This flow period is called bilinear flow because two types of linear flow occur simultaneously. As originally proposed by Cinco (1981), one flow is a linear incompressible flow within the fracture and the other is a linear compressible flow in the formation. Most of the fluid which enters the wellbore during this flow period comes from the formation. Fracture tip effects do not affect well behavior during bilinear flow and, accordingly, it will not be possible to determine the fracture length from the well bilinear flow period data. However, the actual value of the fracture conductivity F_C can be determined during this flow period. The pressure drop through the fracture is significant for the finite conductivity case and the bilinear flow behavior is observed; however, the *infinite conductivity case does not exhibit bilinear flow behavior* because the pressure drop in the fracture is negligible. Thus, identification of the bilinear flow period is very important for two reasons:

(1) It will not be possible to determine a unique fracture length from the well bilinear flow period data. If this data is used to determine the length of the fracture, it will produce a much smaller fracture length than the actual.
(2) The actual fracture conductivity $k_f w_f$ can be determined from the bilinear flow pressure data.

Cinco and Samaniego suggested that during this flow period, the change in the wellbore pressure can be described by the following expressions.

For fractured oil wells   In terms of dimensionless pressure:

$$p_D = \left[\frac{2.451}{\sqrt{F_{CD}}}\right](t_{Dx_f})^{1/4} \qquad [1.5.25]$$

Taking the logarithm of both sides of Equation 1.5.25 gives:

$$\log(p_D) = \log\left[\frac{2.451}{\sqrt{F_{CD}}}\right] + \frac{1}{4}\log(t_{Dx_f}) \qquad [1.5.26]$$

In terms of pressure:

$$\Delta p = \left[\frac{44.1QB\mu}{h\sqrt{F_C}(\phi\mu c_t k)^{1/4}}\right]t^{1/4} \qquad [1.5.27]$$

or equivalently:

$$\Delta p = m_{bf}t^{1/4}$$

Taking the logarithm of both sides of the above expression gives:

$$\log(\Delta p) = \log(m_{bf}) + \frac{1}{4}\log(t) \qquad [1.5.28]$$

with the bilinear slope m_{bf} as given by:

$$m_{bf} = \left[\frac{44.1QB\mu}{h\sqrt{F_C}(\phi\mu c_t k)^{1/4}}\right]$$

where F_C is the fracture conductivity as defined by:

$$F_C = k_f w_f \qquad [1.5.29]$$

For fractured gas wells   In a dimensionless form:

$$m_D = \left[\frac{2.451}{\sqrt{F_{CD}}}\right](t_{Dx_f})^{1/4}$$

or:

$$\log(m_D) = \log\left[\frac{2.451}{\sqrt{F_{CD}}}\right] + \frac{1}{4}\log(t_{Dx_f}) \qquad [1.5.30]$$

In terms of $m(p)$:

$$\Delta m(p) = \left[\frac{444.6QT}{h\sqrt{F_C}(\phi\mu c_t k)^{1/4}}\right]t^{1/4} \qquad [1.5.31]$$

or equivalently:

$$\Delta m(p) = m_{bf}t^{1/4} \qquad [1.5.32]$$

Taking the logarithm of both sides gives:

$$\log[\Delta m(p)] = \log(m_{bf}) + \frac{1}{4}\log(t)$$

Equations 1.5.27 and 1.5.31 indicate that a plot of Δp or $\Delta m(p)$ vs. $(\text{time})^{1/4}$ on a *Cartesian scale* would produce a straight line *passing through the origin* with a slope of "m_{bf} (bilinear flow slope) as given by:
For oil:

$$m_{bf} = \frac{44.1QB\mu}{h\sqrt{F_C}(\phi\mu c_t k)^{1/4}} \qquad [1.5.33]$$

The slope can then be used to solve for fracture conductivity F_C:

$$F_C = \left[\frac{44.1QB\mu}{m_{bf}h(\phi\mu c_t k)^{1/4}}\right]^2$$

For gas:

$$m_{bf} = \frac{444.6QT}{h\sqrt{F_C}(\phi\mu c_t k)^{1/4}} \qquad [1.5.34]$$

with:

$$F_C = \left[\frac{444.6QT}{m_{bf}h(\phi\mu c_t k)^{1/4}}\right]^2$$

It should be noted that *if the straight-line plot does not pass through the origin*, it indicates an additional pressure drop "Δp_s" caused by flow restriction within the fracture in the vicinity of the wellbore (chocked fracture; where the fracture permeability just away from the wellbore is reduced). Examples of restrictions that cause a loss of resulting production include:

- inadequate perforations;
- turbulent flow which can be reduced by increasing the proppant size or concentration;
- overdisplacement of proppant;
- kill fluid was dumped into the fracture.

Similarly, Equations 1.5.28 and 1.5.32 suggest that a plot of Δp or $\Delta m(p)$ versus (time) on a *log–log scale* would produce a straight line with a slope of $m_{bf} = \frac{1}{4}$ and which can be used as a diagnostic tool for bilinear flow detection.

When the bilinear flow ends, the plot will exhibit curvature which could concave upwards or downwards depending upon the value of the dimensionless fracture conductivity F_{CD}, as shown in Figure 1.72. When the values of F_{CD} is < 1.6, the curve will concave downwards, and will concave upwards if $F_{CD} > 1.6$. The upward trend indicates that the
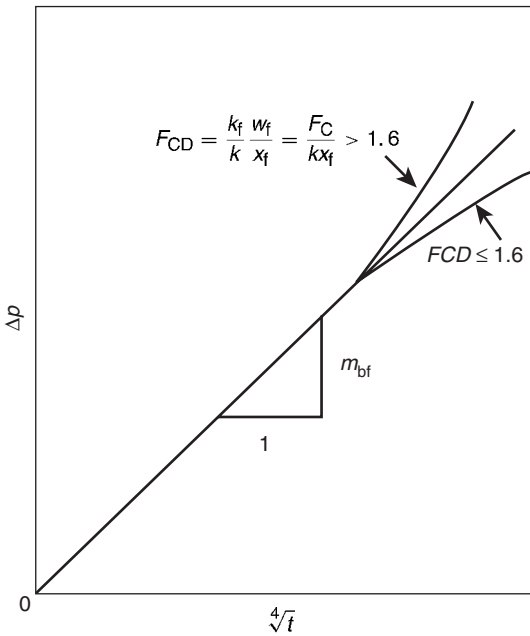
Figure 1.72 *Graph for analysis of pressure data of bilinear flows (After Cinco and Samaniego, 1981).*

fracture tip begins to affect wellbore behavior. If the test is not run sufficiently long for bilinear flow to end when $F_{CD} > 1.6$, it is not possible to determine the length of the fracture. When the dimensionless fracture conductivity $F_{CD} < 1.6$, it indicates that the fluid flow *in the reservoir* has changed from a predominantly one-dimensional linear flow to a two-dimensional flow regime. In this particular case, it is not possible to uniquely determine fracture length even if bilinear flow does end during the test.

Cinco and Samaniego pointed out that the dimensionless fracture conductivity F_{CD} can be estimated from the bilinear flow straight line, i.e., Δp vs. (time)$^{1/4}$, by reading the value of the pressure difference Δp at which the line ends Δp_{ebf} and applying the following approximation:

For oil $\quad F_{CD} = \dfrac{194.9 QB\mu}{kh\Delta p_{ebf}}$ [1.5.35]

For gas $\quad F_{CD} = \dfrac{1965.1 QT}{kh\Delta m(p)_{ebf}}$ [1.5.36]

where:

Q = flow rate, STB/day or Mscf/day
T = temperature, °R

The end of the bilinear flow, "ebf," straight line depends on the fracture conductivity and can be estimated from the following relationships:

For $F_{CD} > 3$ $\qquad t_{Debf} \simeq \dfrac{0.1}{(F_{CD})^2}$

For $1.6 \leq F_{CD} \leq 3$ $\quad t_{Debf} \simeq 0.0205[F_{CD} - 1.5]^{-1.53}$

For $F_{CD} \leq 1.6$ $\qquad t_{Debf} \simeq \left[\dfrac{4.55}{\sqrt{F_{CD}}} - 2.5\right]^{-4}$

The procedure for analyzing the bilinear flow data is summarized by the following steps:

Step 1. Make a plot of Δp versus time on a log–log scale.
Step 2. Determine if any data fall on a straight line with a $\frac{1}{4}$ slope.

Step 3. If data points do fall on the straight line with a $\frac{1}{4}$ slope, replot the data in terms of Δp vs. (time)$^{1/4}$ on a Cartesian scale and identify the data which forms the bilinear straight line.
Step 4. Determine the slope of the bilinear straight line m_{bf} formed in step 3.
Step 5. Calculate the fracture conductivity $F_C = k_f w_f$ from Equation 1.5.33 or Equation 1.5.34:

For oil $\quad F_C = (k_f w_f) = \left[\dfrac{44.1 QB\mu}{m_{bf}h(\phi\mu c_t k)^{1/4}}\right]^2$

For gas $\quad F_C = (k_f w_f) = \left[\dfrac{444.6 QT}{m_{bf}h(\phi\mu c_t k)^{1/4}}\right]^2$

Step 6. Read the value of the pressure difference at which the line ends, Δp_{ebf} or $\Delta m(p)_{ebf}$.
Step 7. Approximate the dimensionless facture conductivity from:

For oil $\quad F_{CD} = \dfrac{194.9 QB\mu}{kh\Delta p_{ebf}}$

For gas $\quad F_{CD} = \dfrac{1965.1 QT}{kh\Delta m(p)_{ebf}}$

Step 8. Estimate the fracture length from the mathematical definition of F_{CD} as expressed by Equation 1.5.21 and the value of F_C of step 5:

$$x_f = \frac{F_C}{F_{CD}k}$$

Example 1.36 A buildup test was conducted on a fractured well producing from a tight gas reservoir. The following reservoir and well parameters are available:

$Q = 7350$ Mscf/day, $\qquad t_p = 2640$ hours
$h = 118$ ft, $\qquad\qquad \phi = 0.10$
$k = 0.025$ md, $\qquad\qquad \mu = 0.0252$
$T = 690°$R, $\qquad\qquad c_t = 0.129 \times 10^{-3}$ psi^{-1}
$p_{wf \text{ at } \Delta t=0} = 1320$ psia, $\quad r_w = 0.28$ ft

The graphical presentation of the buildup data is given in terms of the log–log plot of $\Delta m(p)$ vs. $(\Delta t)^{1/4}$, as shown in Figure 1.73.

Calculate the fracture and reservoir parameters by performing conventional well testing analysis.

Solution

Step 1. From the plot of $\Delta m(p)$ vs. $(\Delta t)^{1/4}$, in Figure 1.73, determine:

$m_{bf} = 1.6 \times 10^8$ psi^2/cphr$^{1/4}$

$t_{sbf} \approx 0.35$ hours (start of bilinear flow)

$t_{ebf} \approx 2.5$ hours (end of bilinear flow)

$\Delta m(p)_{ebf} \approx 2.05 \times 10^8$ psi^2/cp

Step 2. Perform the bilinear flow analysis, as follows:

- Using Equation 1.5.34, calculate fracture conductivity F_C:

$F_C = \left[\dfrac{444.6 QT}{m_{bf}h(\phi\mu c_t k)^{1/4}}\right]^2$

$= \left[\dfrac{444.6(7350)(690)}{(1.62\times 10^8)(118)[(0.1)(0.0252)(0.129\times 10^{-3})(0.025)]^{1/4}}\right]^2$

$= 154$ md ft
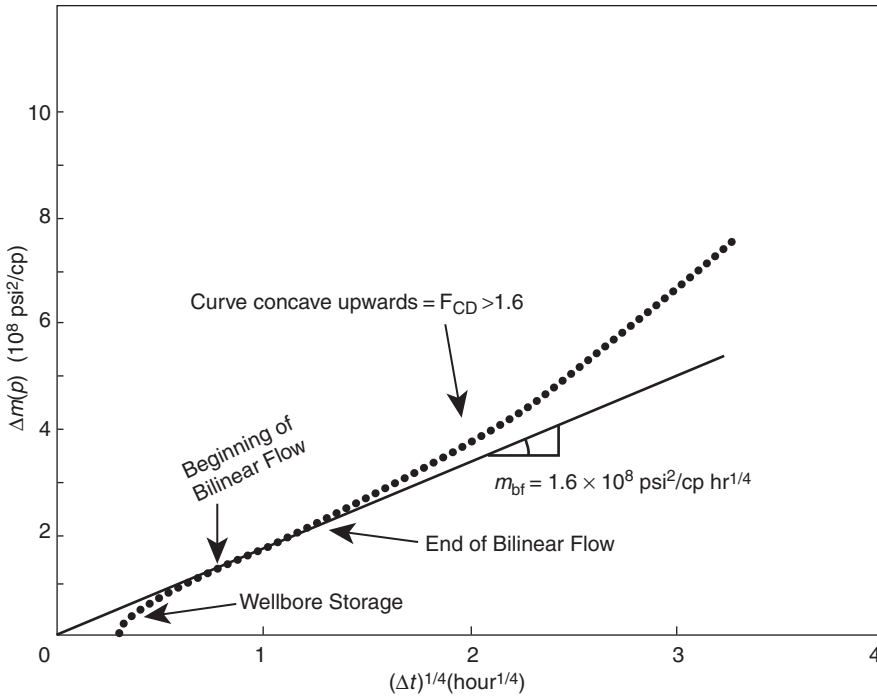
Figure 1.73 *Bilinear flow graph for data of Example 1.36 (After Sabet, M. A.* Well Test Analysis *1991, Gulf Publishing Company).*

- Calculate the dimensionless conductivity F_{CD} by using Equation 1.5.36:

$$F_{CD} = \frac{1965.1QT}{kh\,\Delta m(p)_{ebf}}$$

$$= \frac{1965.1\,(7350)\,(690)}{(0.025)\,(118)\,(2.02 \times 10^8)} = 16.7$$

- Estimate the fracture half-length from Equation 1.5.21:

$$x_f = \frac{F_C}{F_{CD}k}$$

$$= \frac{154}{(16.7)\,(0.025)} = 368 \text{ ft}$$

Formation linear flow At the end of the bilinear flow, there is a transition period after which the fracture tips begin to affect the pressure behavior at the wellbore and a linear flow period might develop. This linear flow period is exhibited by vertical fractures whose dimensionless conductivity is greater that 300, i.e., $F_{CD} > 300$. As in the case of fracture linear flow, the formation linear flow pressure data collected during this period is a function of the fracture length x_f and fracture conductivity F_C. The pressure behavior during this linear flow period can be described by the diffusivity equation as expressed in linear form:

$$\frac{\partial^2 p}{\partial x^2} = \frac{\phi \mu c_t}{0.002637k}\frac{\partial p}{\partial t}$$

The solution to the above linear diffusivity equation can be applied to both fracture linear flow and the formation linear flow, with the solution given in a dimensionless form by:

$$p_D = \left(\pi t_{Dx_f}\right)^{1/2}$$

or in terms of real pressure and time, as:

For oil fractured wells $\Delta p = \left[\dfrac{4.064QB}{hx_f}\sqrt{\dfrac{\mu}{k\phi c_t}}\right]t^{1/2}$

or in simplified form as $\Delta p = m_{vf}\sqrt{t}$

For gas fractured wells $\Delta m(p) = \left[\dfrac{40.925QT}{hx_f}\sqrt{\dfrac{1}{k\phi\mu c_t}}\right]t^{1/2}$

or equivalently as $\Delta m(p) = m_{vf}\sqrt{t}$

The linear flow period may be recognized by pressure data that exhibits a straight line of a $\frac{1}{2}$ slope on a log–log plot of Δp versus time, as illustrated in Figure 1.74. Another diagnostic presentation of pressure data points is the plot of Δp or $\Delta m(p)$ vs. $\sqrt{\text{time}}$ on a Cartesian scale (as shown in Figure 1.75) which would *produce a straight line* with a slope of m_{vf} related to the fracture length by the following equations:

Oil fractured well $x_f = \left[\dfrac{4.064QB}{m_{vf}h}\right]\sqrt{\dfrac{\mu}{k\phi c_t}}$ [1.5.37]

Gas fractured well $x_f = \left[\dfrac{40.925QT}{m_{vf}h}\right]\sqrt{\dfrac{1}{k\phi\mu c_t}}$ [1.5.38]

where:

Q = flow rate, STB/day or Mscf/day
T = temperature, °R
m_{vf} = slope, psi/$\sqrt{\text{hr}}$ or psi^2/cp$\sqrt{\text{hr}}$
k = permeability, md
c_t = total compressibility, psi^{-1}

The straight-line relationships as illustrated by Figures 1.74 and 1.75 provide distinctive and easily recognizable
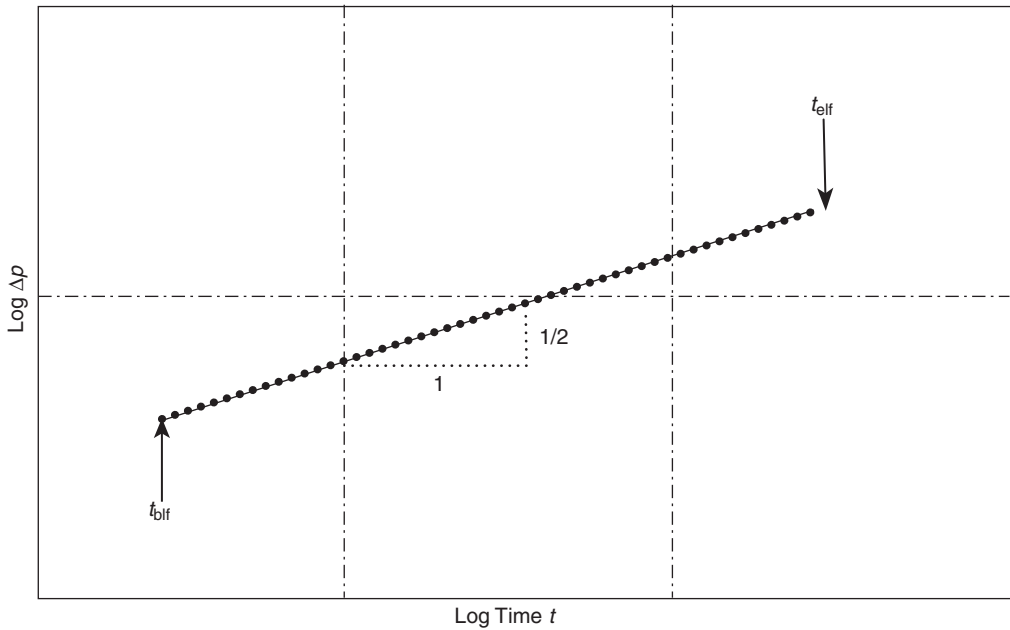
Figure 1.74 *Pressure data for a $\frac{1}{2}$-slope straight line in a log–log graph (After Cinco and Samaniego, 1981).*
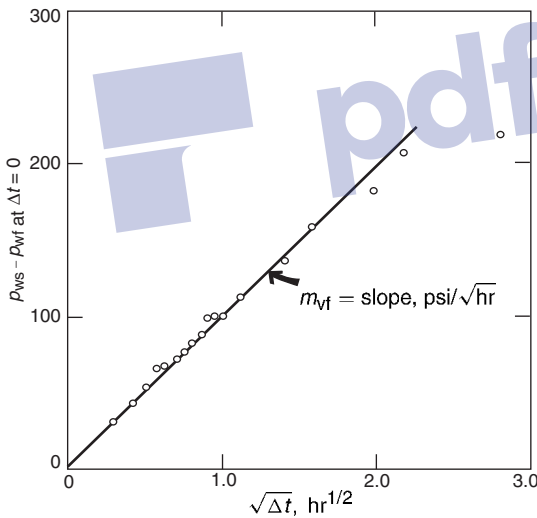
Figure 1.75 *Square-root data plot for buildup test.*

evidence of a fracture. When properly applied, these plots are the best diagnostic tools available for the purpose of detecting a fracture. In practice, the $\frac{1}{2}$ slope is rarely seen except in fractures with high conductivity. Finite conductivity fracture responses generally enter a transition period after the bilinear flow (the $\frac{1}{4}$ slope) and reach the infinite-acting pseudoradial flow regime before ever achieving a $\frac{1}{2}$ slope (linear flow). For a long duration of wellbore storage effect, the bilinear flow pressure behavior may be masked and data analysis becomes difficult with current interpretation methods.

Agarwal et al. (1979) pointed out that the pressure data during the transition period displays a curved portion before straightening to a line of proper slope that represents the fracture linear flow. The duration of the curved portion that represents the transition flow depends on the fracture flow capacity. The lower the fracture flow capacity, the longer the duration of the curved portion. The beginning of formation linear flow, "blf," depends on F_{CD} and can be approximated from the following relationship:

$$t_{Dblf} \approx \frac{100}{(F_{CD})^2}$$

and the end of this linear flow period, "elf," occurs at approximately:

$$t_{Dblf} \approx 0.016$$

Identifying the coordinates of these two points (i.e., beginning and end of the straight line) in terms of time can be used to estimate F_{CD} from:

$$F_{CD} \approx 0.0125 \sqrt{\frac{t_{elf}}{t_{blf}}}$$

where t_{elf} and t_{blf} are given in hours.

Infinite-acting pseudoradial flow During this period, the flow behavior is similar to the radial reservoir flow with a negative skin effect caused by the fracture. The traditional semilog and log–log plots of transient pressure data can be used during this period; for example, the drawdown pressure data can be analyzed by using Equations 1.3.1 through 1.3.3. That is:

$$p_{wf} = p_i - \frac{162.6Q_oB_o\mu}{kh}$$

$$\times \left[\log(t) + \log\left(\frac{k}{\phi\mu c_t r_w^2}\right) - 3.23 + 0.87s \right]$$

or in a linear form as:

$$p_i - p_{wf} = \Delta p = a + m\log(t)$$
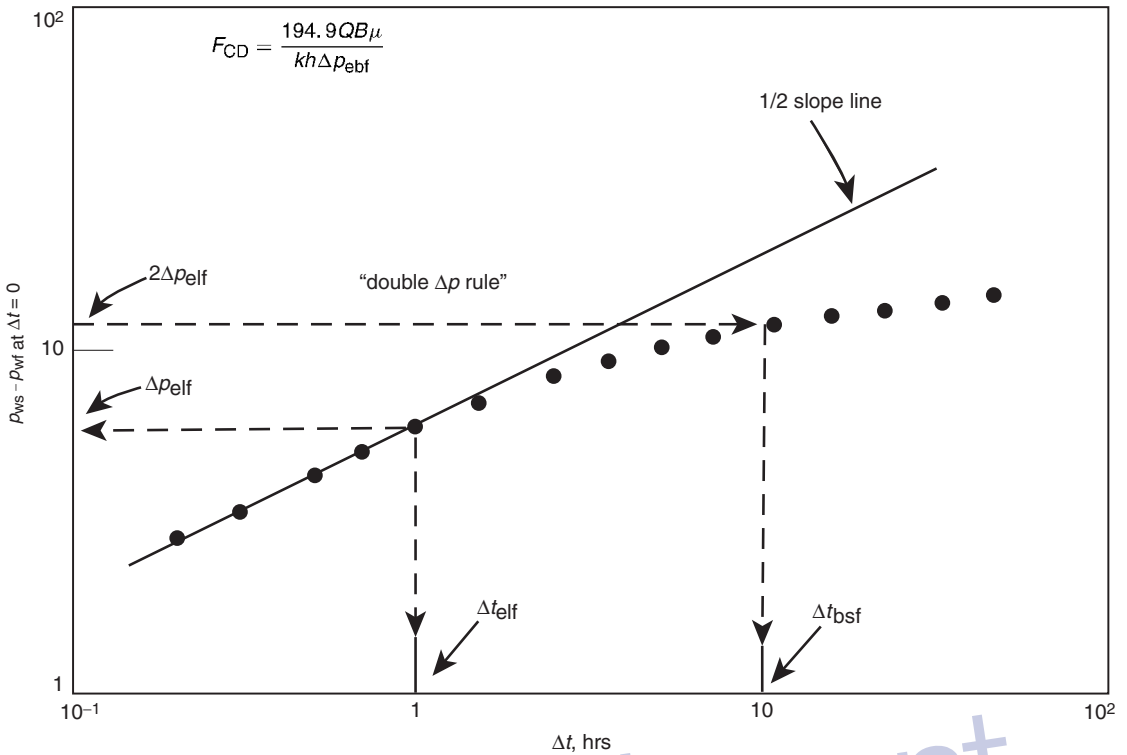
Figure 1.76 *Use of the log–log plot to approximate the beginning of pseudoradial flow.*

with the slope m of:

$$m = \frac{162.6 Q_o B_o \mu_o}{kh}$$

Solving for the formation capacity gives:

$$kh = \frac{162.6 Q_o B_o \mu_o}{|m|}$$

The skin factor s can be calculated by Equation 1.3.3:

$$s = 1.151 \left[\frac{p_i - p_{1\,hr}}{|m|} - \log \left(\frac{k}{\phi \mu c_t r_w^2} \right) + 3.23 \right]$$

If the semilog plot is made in terms of Δp vs. t, notice that the slope m is the same when making the semilog plot in terms of p_{wf} vs. t. Then:

$$s = 1.151 \left[\frac{\Delta p_{1\,hr}}{|m|} - \log \left(\frac{k}{\phi \mu c_t r_w^2} \right) + 3.23 \right]$$

$\Delta p_{1\,hr}$ can then be calculated from the mathematical definition of the slope m, i.e., rise/run, by using two points on the semilog straight line (conveniently, one point could be Δp at $\log(10)$) to give:

$$m = \frac{\Delta p_{at\ \log(10)} - \Delta p_{1\,hr}}{\log(10) - \log(1)}$$

Solving this expression for $\Delta p_{1\,hr}$ gives:

$$\Delta p_{1\,hr} = \Delta p_{at\ \log(10)} - m \qquad [1.5.39]$$

Again, $\Delta p_{at\ \log(10)}$ must be read at the corresponding point on the straight line at $\log(10)$.

Wattenbarger and Ramey (1968) have shown that an approximate relationship exists between the pressure change Δp at the end of the linear flow, i.e., Δp_{elf}, and the

beginning of the infinite acting pseudoradial flow, Δp_{bsf}, as given by:

$$\Delta p_{bsf} \geq 2 \Delta p_{elf} \qquad [1.5.40]$$

The above rule is commonly referred to as the "double-Δp rule" and can be obtained from the log–log plot when the $\frac{1}{2}$ slope ends and by reading the value of Δp, i.e., Δp_{elf}, at this point. For fractured wells, doubling the value of Δp_{elf} will mark the beginning of the infinite-acting pseudoradial flow period. Equivalently, a time rule as referred to as the "$10 \Delta t$ rule" can be applied to mark the beginning of pseudoradial flow by:

$$\text{For drawdown} \quad t_{bsf} \geq 10 t_{elf} \qquad [1.5.41]$$

$$\text{For buildup} \quad \Delta t_{bsf} \geq 10 \Delta t_{elf} \qquad [1.5.42]$$

which indicates that correct infinite-acting pseudoradial flow occurs one log cycle beyond the end of the linear flow. The concept of the above two rules is illustrated graphically in Figure 1.76.

Another approximation that can be used to mark the start of the infinite-acting radial flow period for a finite conductivity fracture is given by:

$$t_{Dbs} \approx 5 \exp[-0.5(F_{CD})^{-0.6}] \quad \text{for} \quad F_{CD} > 0.1$$

Sabet (1991) used the following drawdown test data, as originally given by Gringarten et al. (1975), to illustrate the process of analyzing a hydraulically fractured well test data.

Figure 1.77 *Log–log plot, drawdown test data of Example 1.37 (After Sabet, M. A.* Well Test Analysis *1991, Gulf Publishing Company).*

Example 1.37 The drawdown test data for an infinite conductivity fractured well is tabulated below:

t (hr)	p_{wf} (psi)	Δp (psi)	$\sqrt{t}$ (hr$^{1/2}$)
0.0833	3759.0	11.0	0.289
0.1670	3755.0	15.0	0.409
0.2500	3752.0	18.0	0.500
0.5000	3744.5	25.5	0.707
0.7500	3741.0	29.0	0.866
1.0000	3738.0	32.0	1.000
2.0000	3727.0	43.0	1.414
3.0000	3719.0	51.0	1.732
4.0000	3713.0	57.0	2.000
5.0000	3708.0	62.0	2.236
6.0000	3704.0	66.0	2.449
7.0000	3700.0	70.0	2.646
8.0000	3695.0	75.0	2.828
9.0000	3692.0	78.0	3.000
10.0000	3690.0	80.0	3.162
12.0000	3684.0	86.0	3.464
24.0000	3662.0	108.0	4.899
48.0000	3635.0	135.0	6.928
96.0000	3608.0	162.0	9.798
240.0000	3570.0	200.0	14.142

Additional reservoir parameters are:

$$h = 82 \text{ ft}, \qquad \phi = 0.12$$
$$c_t = 21 \times 10^{-6} \text{ psi}^{-1}, \quad \mu = 0.65 \text{ cp}$$
$$B_o = 1.26 \text{ bbl/STB}, \qquad r_w = 0.28 \text{ ft}$$
$$Q = 419 \text{ STB/day}, \qquad p_i = 3770 \text{ psi}$$

Estimate:

- permeability, k;
- fracture half-length, x_f;
- skin factor, s.

Solution

Step 1. Plot:

- Δp vs. t on a log–log scale, as shown in Figure 1.77;
- Δp vs. $\sqrt{t}$ on a Cartesian scale, as shown in Figure 1.78;
- Δp vs. t on a semilog scale, as shown in Figure 1.79.

Step 2. Draw a straight line through the early points representing $\log(\Delta p)$ vs. $\log(t)$, as shown in Figure 1.77, and determine the slope of the line. Figure 1.77 shows a slope of $\frac{1}{2}$ (not 45° angle) indicating linear flow with no wellbore storage effects. This linear flow lasted for approximately 0.6 hours. That is:

$$t_{elf} = 0.6 \text{ hours}$$

$$\Delta p_{elf} = 30 \text{ psi}$$

and therefore the beginning of the infinite-acting pseudoradial flow can be approximated by the "double Δp rule" or "one log cycle rule," i.e., Equations 1.5.40 and 1.5.41, to give:

$$t_{bsf} \geq 10 t_{elf} \geq 6 \text{ hours}$$

$$\Delta p_{bsf} \geq 2 \Delta p_{elf} \geq 60 \text{ psi}$$

Step 3. From the Cartesian scale plot of Δp vs. $\sqrt{t}$, draw a straight line through the early pressure data points representing the first 0.3 hours of the test (as shown

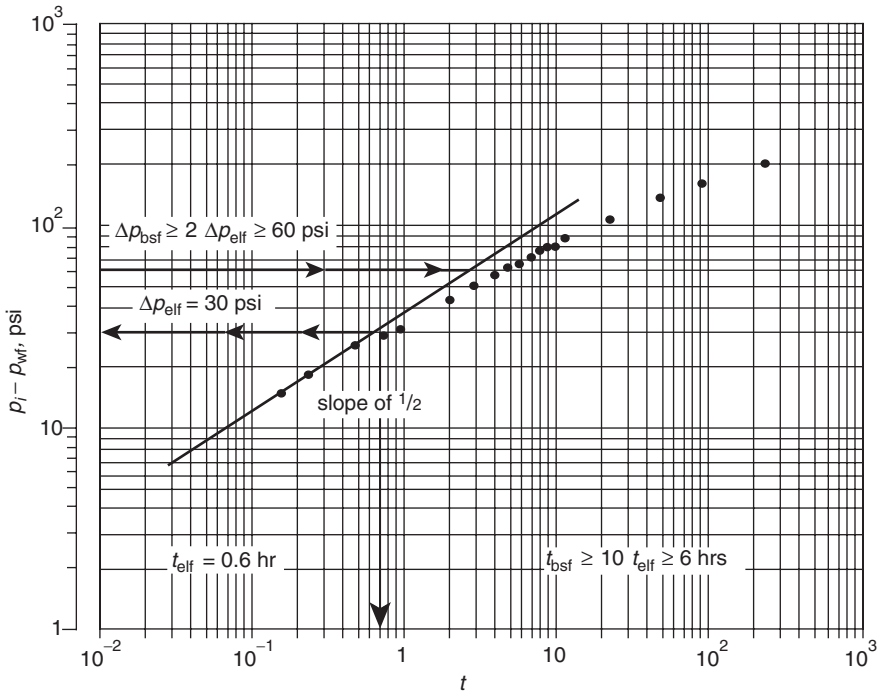**Figure 1.78** *Linear plot, drawdown test data of Example 1.37 (After Sabet, M. A.* Well Test Analysis *1991, Gulf Publishing Company).*

$$k = \frac{162.6 Q_o B_o \mu_o}{mh}$$

$$= \frac{162.6(419)(1.26)(0.65)}{(94.1)(82)} = 7.23 \text{ md}$$

$m = 94.1$ psi/cycle
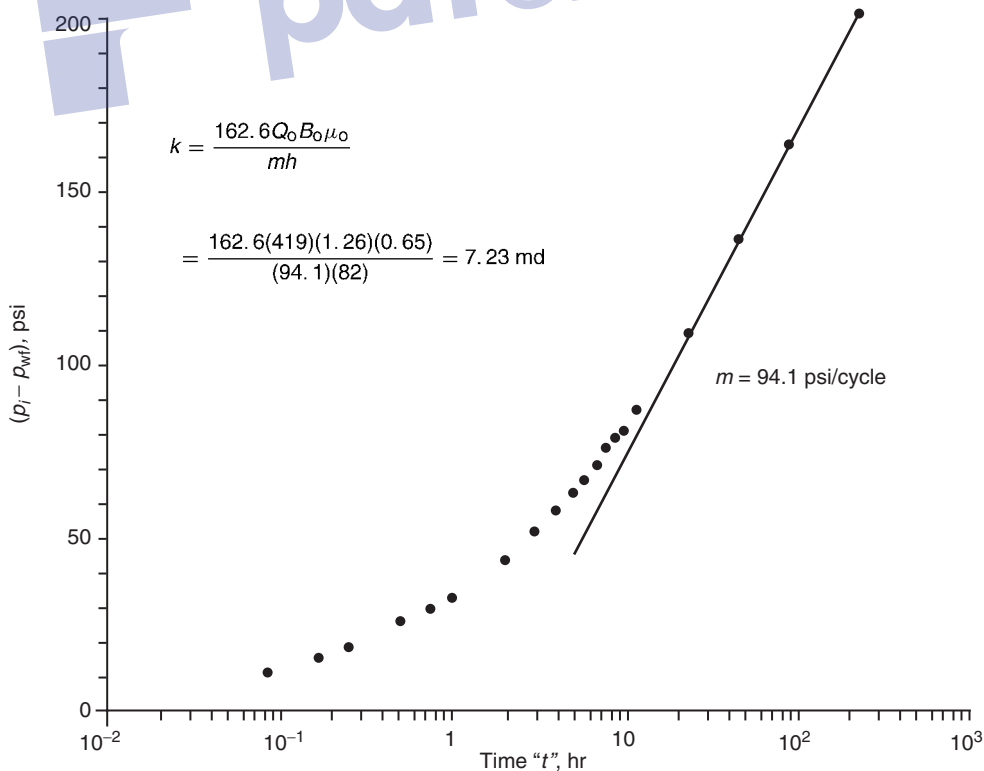
Figure 1.79 *Semilog plot, drawdown test data from Example 1.37.*
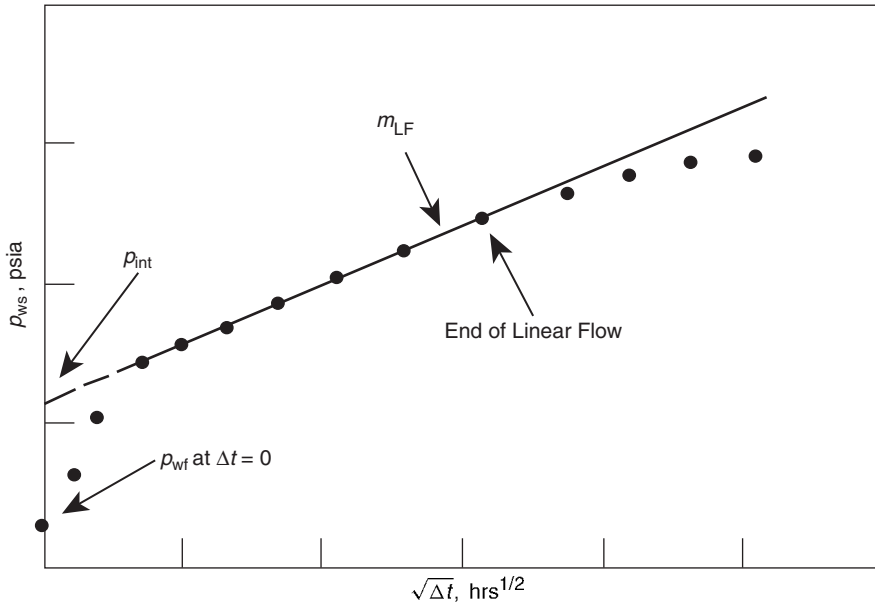
Figure 1.80   *Effect of skin on the square root plot.*

in Figure 1.79) and determine the slope of the line, to give:

$$m_{vf} = 36 \text{ psi/hr}^{1/2}$$

Step 4. Determine the slope of the semilog straight line representing the unsteady-state radial flow in Figure 1.79, to give:

$$m = 94.1 \text{ psi/cycle}$$

Step 5. Calculate the permeability k from the slope:

$$k = \frac{162.6Q_o B_o \mu_o}{mh} = \frac{162.6(419)(1.26)(0.65)}{(94.1)(82)}$$

$$= 7.23 \text{ md}$$

Step 6. Estimate the length of the fracture half-length from Equation 1.5.37, to give:

$$x_f = \left[\frac{4.064QB}{m_{vf}h} \right] \sqrt{\frac{\mu}{k\phi c_t}}$$

$$= \left[\frac{4.064(419)(1.26)}{(36)(82)} \right] \sqrt{\frac{0.65}{(7.23)(0.12)(21 \times 10^{-6})}}$$

$$= 137.3 \text{ ft}$$

Step 7. From the semilog straight line of Figure 1.78, determine Δp at $t = 10$ hours, to give:

$$\Delta p_{\text{at } \Delta t=10} = 71.7 \text{ psi}$$

Step 8. Calculate $\Delta p_{1 \text{ hr}}$ by applying Equation 1.5.39:

$$\Delta p_{1 \text{ hr}} = \Delta p_{\text{at } \Delta t=10} - m = 71.7 - 94.1 = -22.4 \text{ psi}$$

Step 9. Solve for the "total" skin factor s, to give

$$s = 1.151 \left[\frac{\Delta p_{1 \text{ hr}}}{|m|} - \log \left(\frac{k}{\phi \mu c_t r_w^2} \right) + 3.23 \right]$$

$$= 1.151 \left[\frac{-22.4}{94.1} \right.$$

$$\left. - \log \left(\frac{7.23}{0.12(0.65)(21 \times 10^{-6})(0.28)^2} \right) + 3.23 \right]$$

$$= -5.5$$

with an apparent wellbore ratio of:

$$r_w^\backslash = r_w e^{-s} = 0.28 e^{5.5} = 68.5 \text{ ft}$$

Notice that the "total" skin factor is a composite of effects that include:

$$s = s_d + s_f + s_t + s_p + s_{sw} + s_r$$

where:

s_d = skin due to formation and fracture damage
s_f = skin due to the fracture, large negative value $s_f \ll 0$
s_t = skin due to turbulence flow
s_p = skin due to perforations
s_w = skin due to slanted well
s_r = skin due to restricted flow

For fractured oil well systems, several of the skin components are negligible or cannot be applied, mainly s_t, s_p, s_{sw}, and s_r; therefore:

$$s = s_d + s_f$$

or:

$$s_d = s - s_f$$

Smith and Cobb (1979) suggested that the best approach to evaluate damage in a fractured well is to use the square root plot. In an ideal well without damage, the square root straight line will extrapolate to p_{wf} at $\Delta t = 0$, i.e, $p_{wf \text{ at } \Delta t=0}$, however, when a well is damaged the intercept pressure p_{int} will be greater than $p_{wf \text{ at } \Delta t=0}$, as illustrated in Figure 1.80. Note that the well shut-in pressure is described by Equation 1.5.35 as:

$$p_{ws} = p_{wf \text{ at } \Delta t=0} + m_{vf}\sqrt{t}$$

Smith and Cobb pointed out that the total skin factor exclusive of s_f, i.e., $s - s_f$, can be determined from the square root plot by extrapolating the straight line to $\Delta t = 0$ and an intercept pressure p_{int} to give the pressure loss due to skin damage, $(\Delta p_s)_d$, as:

$$(\Delta p_s)_d = p_{int} - p_{wf \text{ at } \Delta t=0} = \left[\frac{141.2QB\mu}{kh} \right] s_d$$

Equation 1.5.35 indicates that if $p_{int} = p_{wf \text{ at } \Delta t=0}$, then the skin due to fracture s_f is equal to the total skin.
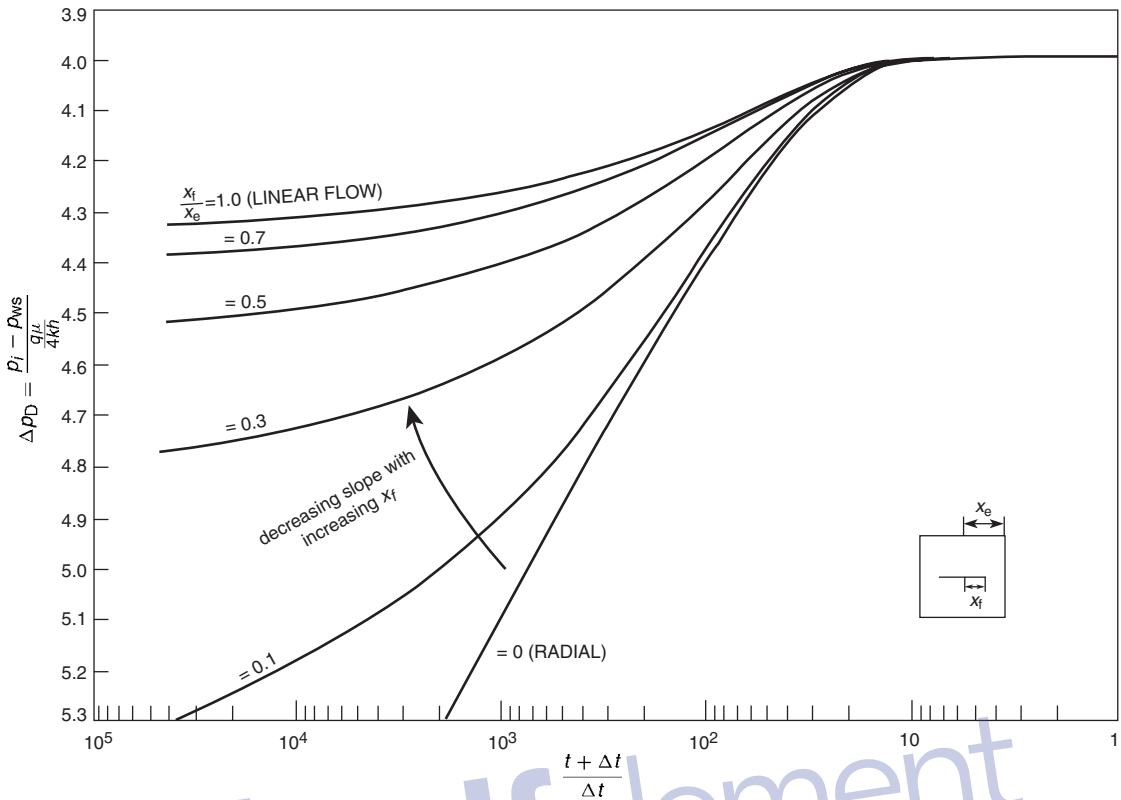
Figure 1.81   *Vertically fractured reservoir, calculated pressure buildup curves (After Russell and Truitt, 1964).*

It should be pointed out that the external boundary can distort the semilog straight line if the fracture half-length is greater than one-third of the drainage radius. The pressure behavior during this infinite-acting period is very dependent on the fracture length. For relatively short fractures, the flow is radial but becomes linear as the fracture length increases as it reaches the drainage radius. As noted by Russell and Truitt (1964), the slope obtained from the traditional well test analysis of a fractured well is erroneously too small and the calculated value of the slope progressively decreases with increasing fracture length. This dependency of the pressure response behavior on the fracture length is illustrated by the theoretical Horner buildup curves given by Russell and Truitt and shown in Figure 1.81. If the fracture penetration ratio x_f/x_e is defined as the ratio of the fracture half-length x_f to the half-length x_e of a closed square-drainage area, then Figure 1.81 shows the effects of fracture penetration on the slope of the buildup curve. For fractures of small penetration, the slope of the buildup curve is only slightly less than that for the unfractured "radial flow" case. However, the slope of the buildup curve becomes progressively smaller with increasing fracture penetrations. This will result in a calculated flow capacity kh which is too large, an erroneous average pressure, and a skin factor which is too small. Obviously a modified method for analyzing and interpreting the data must be employed to account for the effect of length of the fracture on the pressure response during the infinite-acting flow period. Most of the published correction techniques require the use of iterative procedures. The type curve matching approach and other specialized plotting techniques have been accepted by the oil industry as accurate and convenient approaches for analyzing

pressure data from fractured wells, as briefly discussed below.

An alternative and convenient approach to analyzing fractured well transient test data is type curve matching. The type curve matching approach is based on plotting the pressure difference Δp versus time on the same scale as the selected type curve and matching one of the type curves. Gringarten et al. (1974) presented the type curves shown in Figures 1.82 and 1.83 for infinite conductivity vertical fracture and uniform flux vertical fracture, respectively, in a square well drainage area. Both figures present log–log plots of the dimensionless pressure drop p_d (equivalently referred to as dimensionless wellbore pressure p_{wd}) versus dimensionless time t_{Dx_f}. The fracture solutions show an initial period controlled by linear flow where the pressure is a function of the square root of time. In log–log coordinates, as indicated before, this flow period is characterized by a straight line with $\frac{1}{2}$ slope. The infinite-acting pseudoradial flow occurs at a t_{Dx_f} between 1 and 3. Finally, all solutions reach pseudosteady state.

During the matching process a match point is chosen; the dimensionless parameters on the axis of the type curve are used to estimate the formation permeability and fracture length from:

$$k = \frac{141.2QB\mu}{h}\left[\frac{p_D}{\Delta p}\right]_{MP} \qquad [1.5.43]$$

$$x_f = \sqrt{\frac{0.0002637k}{\phi \mu C_t}\left(\frac{\Delta t}{t_{Dx_f}}\right)_{MP}} \qquad [1.5.44]$$
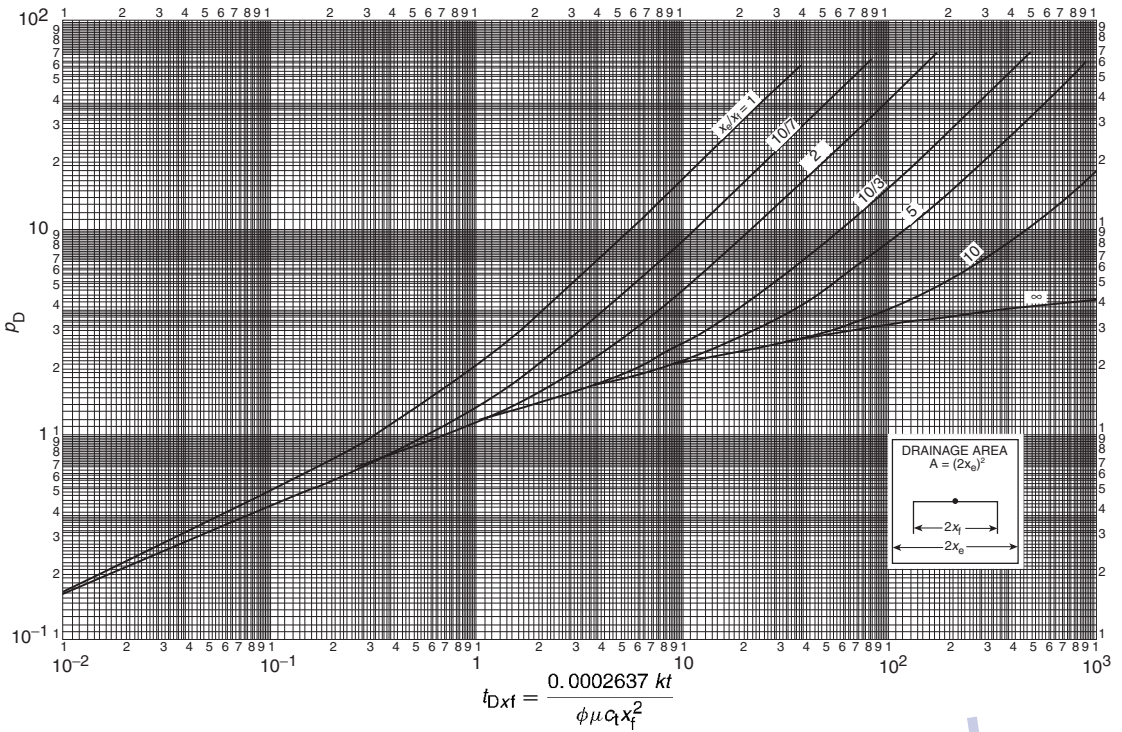
Figure 1.82 *Dimensionless pressure for vertically fractured well in the center of a closed square, no wellbore storage, infinite conductivity fracture (After Gringarten et al., 1974).*

$$t_{Dxf} = \frac{0.0002637\ kt}{\phi \mu c_t x_f^2}$$
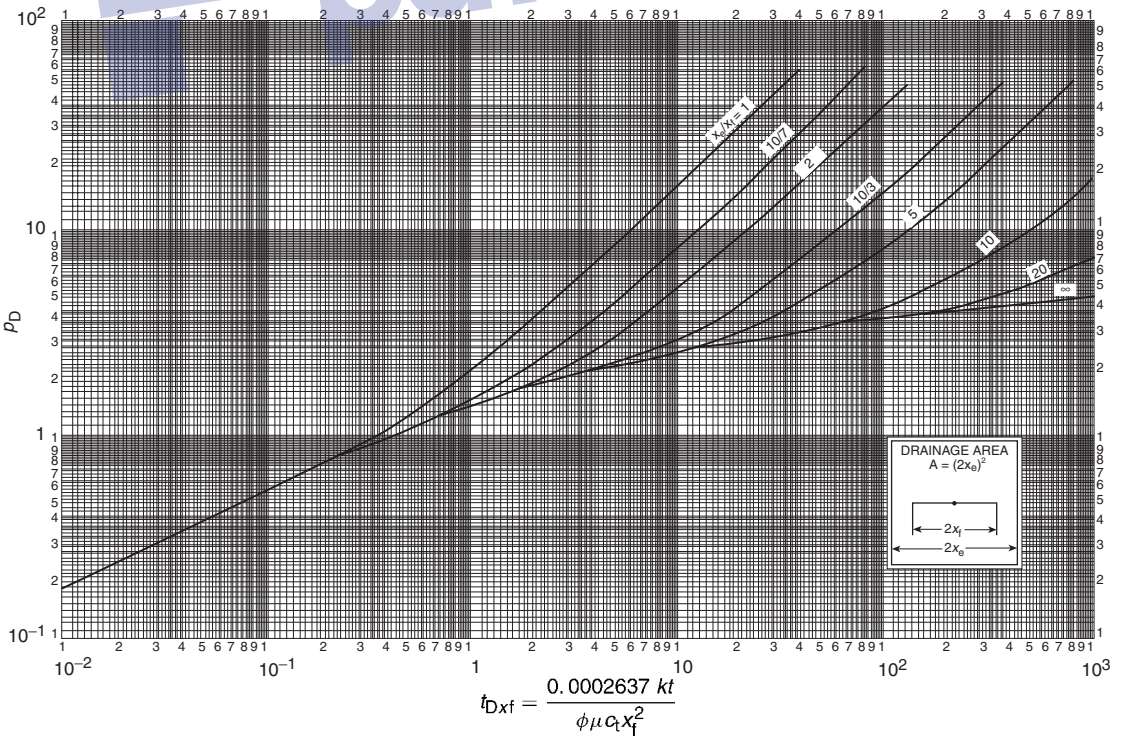
Figure 1.83 *Dimensionless pressure for vertically fractured well in the center of a closed square, no wellbore storage, uniform-flux fracture (After Gringarten et al., 1974).*

$$t_{Dxf} = \frac{0.0002637\ kt}{\phi \mu c_t x_f^2}$$

For large ratios of x_e/x_f, Gringarten and his co-authors suggested that the apparent wellbore radius $r_w^\backslash$ can be approximated from:

$$r_w^\backslash \approx \frac{x_f}{2} = r_w e^{-s}$$

Thus, the skin factor can be approximated from:

$$s = \ln\left(\frac{2r_w}{x_f}\right) \qquad [1.5.45]$$

Earlougher (1977) points out that if all the test data falls on the $\frac{1}{2}$-slope line on the $\log \Delta p$ vs. $\log(\text{time})$ plot, i.e., the test is not long enough to reach the infinite-acting pseudo-radial flow period, then the *formation permeability k cannot be estimated* by either type curve matching or semilog plot. This situation often occurs in tight gas wells. However, the last point on the $\frac{1}{2}$ slope line, i.e., $(\Delta p)_{\text{Last}}$ and $(t)_{\text{Last}}$, may be used to estimate an upper limit of the permeability and a minimum fracture length from:

$$k \leq \frac{30.358 QB\mu}{h(\Delta p)_{\text{last}}} \qquad [1.5.46]$$

$$x_f \geq \sqrt{\frac{0.01648 k(t)_{\text{last}}}{\phi\mu c_t}} \qquad [1.5.47]$$

The above two approximations are only valid for $x_e/x_f \gg 1$ and for infinite conductivity fractures. For uniform-flux fracture, the constants 30.358 and 0.01648 become 107.312 and 0.001648.

To illustrate the use of the Gringarten type curves in analyzing well test data, the authors presented the following example:

Example 1.38 Tabulated below is the pressure buildup data for an infinite conductivity fractured well:

Δt (hr)	p_{ws} (psi)	$p_{ws} - p_{wf \text{ at } \Delta t=0}$ (psi)	$(t_p + \Delta t)\Delta t$
0.000	3420.0	0.0	0.0
0.083	3431.0	11.0	93600.0
0.167	3435.0	15.0	46700.0
0.250	3438.0	18.0	31200.0
0.500	3444.5	24.5	15600.0
0.750	3449.0	29.0	10400.0
1.000	3542.0	32.0	7800.0
2.000	3463.0	43.0	3900.0
3.000	3471.0	51.0	2600.0
4.000	3477.0	57.0	1950.0
5.000	3482.0	62.0	1560.0
6.000	3486.0	66.0	1300.0
7.000	3490.0	70.0	1120.0
8.000	3495.0	75.0	976.0
9.000	3498.0	78.0	868.0
10.000	3500.0	80.0	781.0
12.000	3506.0	86.0	651.0
24.000	3528.0	108.0	326.0
36.000	3544.0	124.0	218.0
48.000	3555.0	135.0	164.0
60.000	3563.0	143.0	131.0
72.000	3570.0	150.0	109.0
96.000	3582.0	162.0	82.3
120.000	3590.0	170.0	66.0
144.000	3600.0	180.0	55.2
192.000	3610.0	190.0	41.6
240.000	3620.0	200.0	33.5

Other available data:

$p_i = 3700$, $r_w = 0.28$ ft,

$\phi = 12\%$, $h = 82$ ft,

$c_t = 21 \times 10^{-6}$ psi^{-1}, $\mu = 0.65$ cp,

$B = 1.26$ bbl/STB, $Q = 419$ STB/day,

$t_p = 7800$ hours

drainage area $= 1600$ acres (not fully developed)

Calculate:

- permeability;
- fracture half-length, x_f;
- skin factor.

Solution

Step 1. Plot Δp vs. Δt on tracing paper with the same scale as the Gringarten type curve of Figure 1.82. Superimpose the tracing paper on the type curve, as shown in Figure 1.84, with the following match points:

$$(\Delta p)_{\text{MP}} = 100 \text{ psi}$$
$$(\Delta t)_{\text{MP}} = 10 \text{ hours}$$
$$(p_D)_{\text{MP}} = 1.22$$
$$(t_D)_{\text{MP}} = 0.68$$

Step 2. Calculate k and x_f by using Equations 1.5.43 and 1.5.44:

$$k = \frac{141.2 QB\mu}{h}\left[\frac{p_D}{\Delta p}\right]_{\text{MP}}$$
$$= \frac{(141.2)(419)(1.26)(0.65)}{(82)}\left[\frac{1.22}{100}\right] = 7.21 \text{ md}$$

$$x_f = \sqrt{\frac{0.0002637 k}{\phi\mu C_t}\left(\frac{\Delta t}{t_{Dxf}}\right)_{\text{MP}}}$$
$$= \sqrt{\frac{0.0002637(7.21)}{(0.12)(0.65)(21\times10^{-6})}\left(\frac{10}{0.68}\right)} = 131 \text{ ft}$$

Step 3. Calculate the skin factor by applying Equation 1.5.45:

$$s = \ln\left(\frac{2r_w}{x_f}\right)$$
$$\approx \ln\left[\frac{(2)(0.28)}{131}\right] = 5.46$$

Step 4. Approximate the time that marks the start of the semilog straight line based on the Gringarten et al. criterion. That is:

$$t_{Dx_f} = \left[\frac{0.0002637 k}{\phi\mu c_t x_f^2}\right] t \geq 3$$

or:

$$t \geq \frac{(3)(0.12)(0.68)(21\times10^{-6})(131)^2}{(0.0002637)(7.21)} \geq 50 \text{ hours}$$

All the data beyond 50 hours can be used in the conventional Horner plot approach to estimate

$$k = \frac{141.2QB\mu}{h}\left[\frac{p_D}{\Delta p}\right]_{MP} \qquad x_f = \sqrt{\frac{0.0002637k}{\phi\mu C_t}\left(\frac{\Delta t}{t_{Dxf}}\right)_{MP}}$$
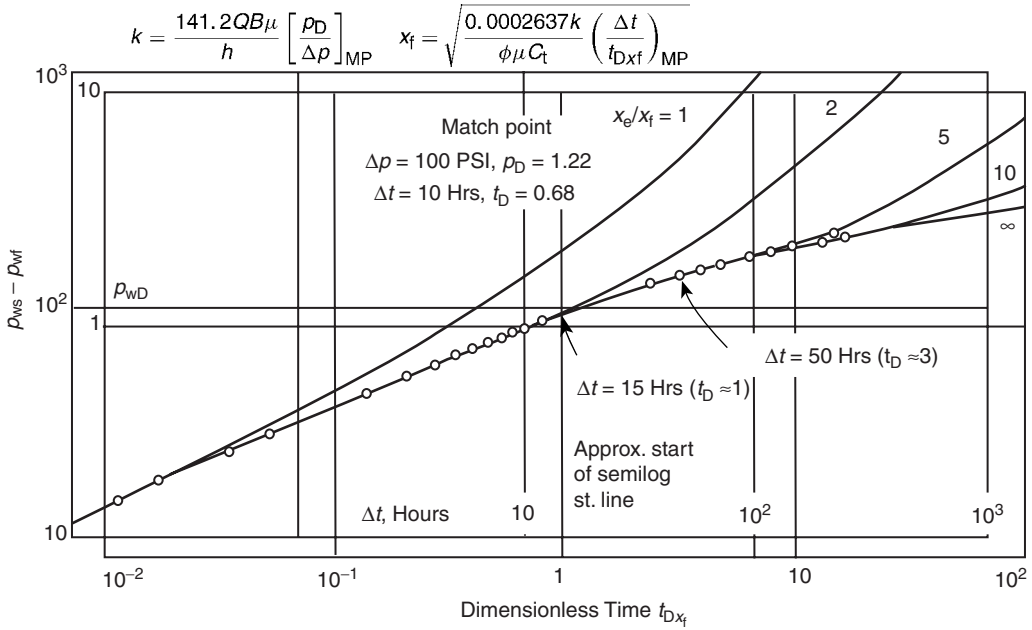
Figure 1.84 *Type curve matching. Data from Example 1.38 (Copyright ©1974 SPE, Gringarten et al., SPEJ, August 1974).*

permeability and skin factor. Figure 1.85 shows a Horner graph with the following results:

$$m = 95 \text{ psi/cycle}$$
$$p^* = 3764 \text{ psi}$$
$$p_{1\,hr} = 3395 \text{ psi}$$
$$k = 7.16 \text{ md}$$
$$s = -5.5$$
$$x_f = 137 \text{ ft}$$

Cinco and Samaniego (1981) developed the type curves shown in Figure 1.86 for finite conductivity vertical fracture. The proposed type curve is based on the bilinear flow theory and presented in terms of $(p_D F_{CD})$ vs. $(t_{Dx_f} F_{CD}^2)$ on a log–log scale for various values of F_{CD} ranging from 0.1π to 1000π. The main feature of this graph is that for all values of F_{CD} the behavior of the bilinear flow ($\frac{1}{4}$ slope) and the formation linear flow ($\frac{1}{2}$ slope) is given by a single curve. Note that there is a transition period between the bilinear and linear flows. The dashed line in this figure indicates the approximate start of the infinite-acting pseudoradial flow.

The pressure data is plotted in terms of $\log(\Delta p)$ vs. $\log(t)$ and the resulting graph is matched to a type curve that is characterized by a dimensionless finite conductivity, $(F_{CD})_M$, with match points of:

- $(\Delta p)_{MP}$, $(p_D F_{CD})_{MP}$;
- $(t)_{MP}$, $(t_{Dx_f} F_{CD}^2)_{MP}$;
- end of bilinear flow $(t_{ebf})_{MP}$;
- beginning of formation linear flow $(t_{blf})_{MP}$;
- beginning of semilog straight line $(t_{bssl})_{MP}$.

From the above match F_{CD} and x_f can be calculated:

For oil $F_{CD} = \left[\dfrac{141.2QB\mu}{hk}\right]\dfrac{(p_D F_{CD})_{MP}}{(\Delta p)_{MP}}$ [1.5.48]

For gas $F_{CD} = \left[\dfrac{1424QT}{hk}\right]\dfrac{(p_D F_{CD})_{MP}}{(\Delta m(p))_{MP}}$ [1.5.49]

The fracture half-length is given by:

$$x_f = \left[\frac{0.0002637k}{\phi\mu c_t}\right]\frac{(t)_{MP}(F_{CD})_M^2}{(t_{Dx_f}F_{CD}^2)_{MP}} \qquad [1.5.50]$$

Defining the dimensionless effective wellbore radius $r_{wD}^\backslash$ as the ratio of the apparent wellbore radius $r_w^\backslash$ to the fracture half-length x_f, i.e., $r_{wD}^\backslash = r_w^\backslash/x_f$, Cinco and Samaniego correlated $r_{wD}^\backslash$ with the dimensionless fracture conductivity F_{CD} and presented the resulting correlation in graphical form, as shown in Figure 1.87.

Figure 1.87 indicates that when the dimensionless fracture conductivity is greater than 100, the dimensionless effective wellbore radius $r_{wD}^\backslash$ is independent of the fracture conductivity with a fixed value of 0.5, i.e., $r_{wD}^\backslash = 0.5$ for $F_{CD} > 100$. The apparent wellbore radius is expressed in terms of the fracture skin factor s_f by:

$$r_w^\backslash = r_w e^{-s_f}$$

Introducing $r_{wD}^\backslash$ into the above expression and solving for s_f gives:

$$s_f = \ln\left[\left(\frac{x_f}{r_w}\right)r_{wD}^\backslash\right]$$

For $F_{CD} > 100$, this gives:

$$s_f = -\ln\left(\frac{x_f}{2r_w}\right)$$

where:

s_f = skin due to fracture
r_w = wellbore radius, ft

It should be kept in mind that specific analysis graphs must be used for different flow regimes to obtain a better estimate of both fracture and reservoir parameters. Cinco and Samaniego used the following pressure buildup data to illustrate the use of their type curve to determine the fracture and reservoir parameters.
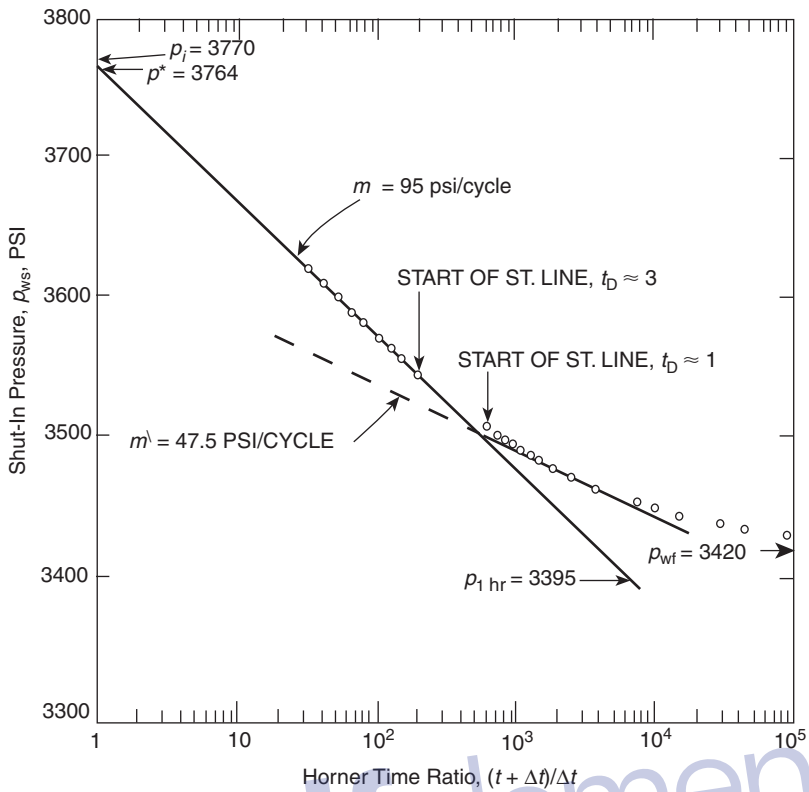
Figure 1.85 *Horner graph for a vertical fracture (infinite conductivity).*
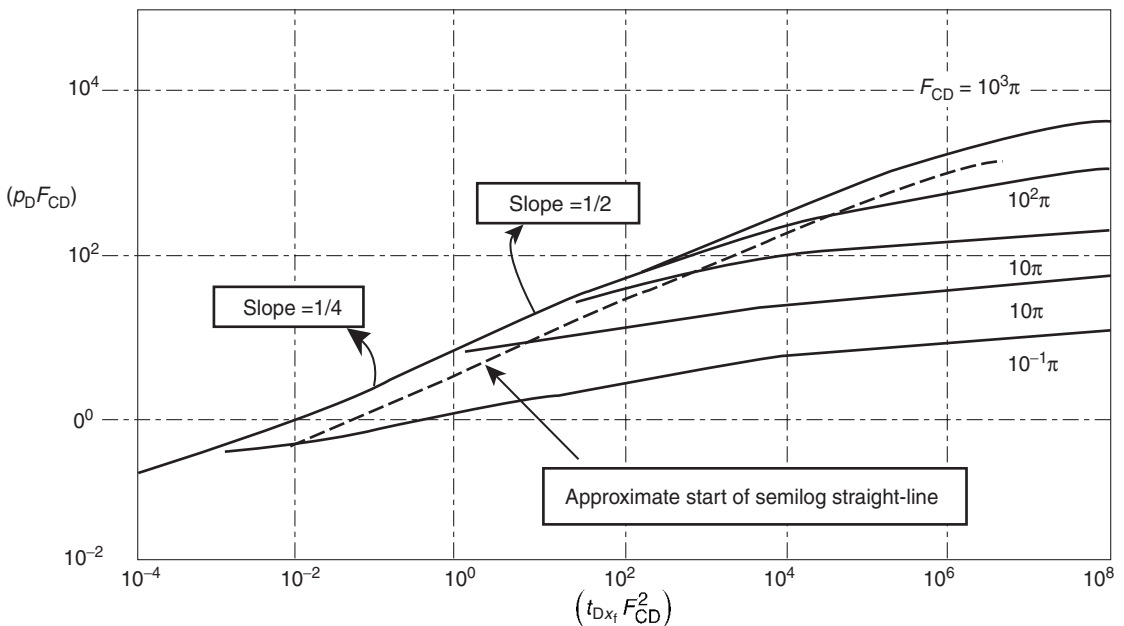
Figure 1.86 *Type curve for vertically fractured gas wells graph (After Cinco and Samaniego, 1981).*
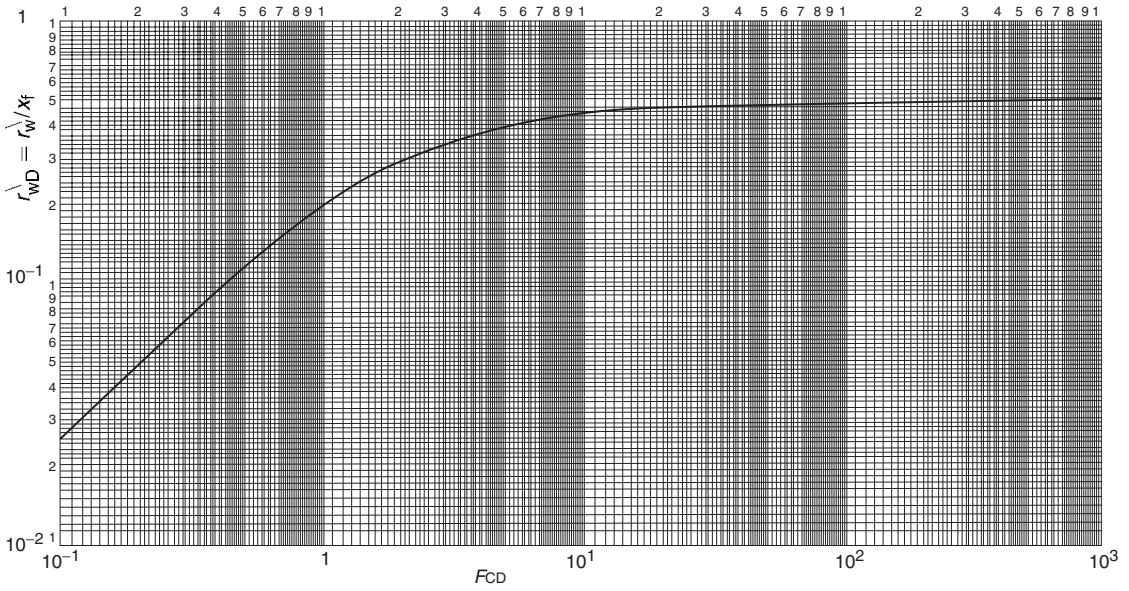
Figure 1.87 *Effective wellbore radius vs. dimensionless fracture conductivity for a vertical fracture graph (After Cinco and Samaniego, 1981).*
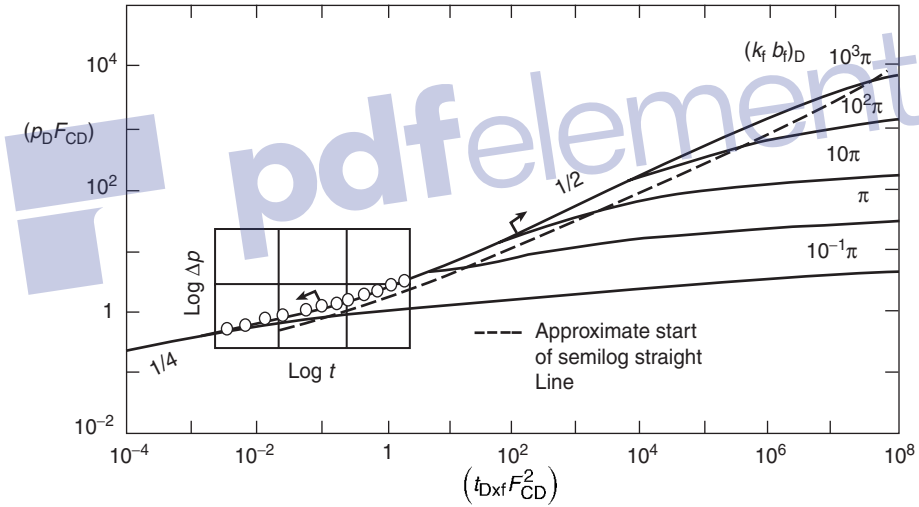
Figure 1.88 *Type curve matching for data in bilinear and transitional flow graph (After Cinco and Samaniego, 1981).*

Example 1.39 The buildup test data as given in Example 1.36 is given below for convenience:

$$Q = 7350 \text{ Mscf/day}, \qquad t_p = 2640 \text{ hours}$$

$$h = 118 \text{ ft}, \qquad \phi = 0.10$$

$$k = 0.025 \text{ md}, \qquad \mu = 0.0252$$

$$T = 690°\text{R}, \qquad c_t = 0.129 \times 10^{-3} \text{ psi}^{-1}$$

$$p_{wf \text{ at } \Delta t=0} = 1320 \text{ psia}, \quad r_w = 0.28 \text{ ft}$$

The graphical presentation of the buildup data is given in the following two forms:

(1) The log–log plot of $\Delta m(p)$ vs. $(\Delta t)^{1/4}$, as shown earlier in Figure 1.73.

(2) The log–log plot of $\Delta m(p)$ vs. (Δt), on the type curve of Figure 1.86 with the resulting match as shown in Figure 1.88.

Calculate the fracture and reservoir parameters by performing conventional and type curve analysis. Compare the results.

Solution

Step 1. From the plot of $\Delta m(p)$ vs. $(\Delta t)^{1/4}$, in Figure 1.73, determine:

$$m_{bf} = 1.6 \times 10^8 \text{ psi}^2/\text{cphr}^{1/4}$$

$$t_{sbf} \approx 0.35 \text{ hrs (start of bilinear flow)}$$

$$t_{ebf} \approx 2.5 \text{ hrs (end of bilinear flow)}$$

$$\Delta m(p)_{ebf} \approx 2.05 \times 10^8 \text{ psi}^2/\text{cp}$$

Step 2. Perform the bilinear flow analysis, as follows:

- Using Equation 1.5.34, calculate fracture conductivity F_C:

$$F_C = \left[\frac{444.6QT}{m_{bf}h(\phi\mu c_t k)^{1/4}} \right]^2$$

$$= \left[\frac{444.6(7350)(690)}{(1.62 \times 10^8)(118)[(0.1)(0.0252)(0.129 \times 10^{-3})(0.025)]^{1/4}} \right]^2$$

$$= 154 \text{ md ft}$$

- Calculate the dimensionless conductivity F_{CD} by using Equation 1.5.36:

$$F_{CD} = \frac{1965.1QT}{kh\Delta m(p)_{ebf}}$$

$$= \frac{1965.1(7350)(690)}{(0.025)(118)(2.02 \times 10^8)} = 16.7$$

- Estimate the fracture half-length from Equation 1.5.21:

$$x_f = \frac{F_C}{F_{CD}k}$$

$$= \frac{154}{(16.7)(0.025)} = 368 \text{ ft}$$

- Estimate the dimensionless ratio $r_w^\backslash/x_f$ from Figure 1.86:

$$\frac{r_w^\backslash}{x_f} \approx 0.46$$

- Calculate the apparent wellbore radius $r_w^\backslash$:

$$r_w^\backslash = (0.46)(368) = 169 \text{ ft}$$

- Calculate the apparent skin factor

$$s = \ln\left(\frac{r_w}{r_w^\backslash}\right) = \ln\left(\frac{0.28}{169}\right) = -6.4$$

Step 3. Perform the type curve analysis as follows:

- Determine the match points from Figure 1.88, to give:

$$\Delta m(p)_{MP} = 10^9 \text{ psi}^2/\text{cp}$$

$$(p_D F_{CD})_{MP} = 6.5$$

$$(\Delta t)_{mp} = 1 \text{ hour}$$

$$[t_{Dx_f}(F_{CD})^2]_{MP} = 3.69 \times 10^{-2}$$

$$t_{sbf} \simeq 0.35 \text{ hour}$$

$$t_{ebf} = 2.5 \text{ hour}$$

- Calculate F_{CD} from Equation

$$F_{CD} = \left[\frac{1424(7350)(690)}{(118)(0.025)} \right] \frac{6.5}{(10^9)} = 15.9$$

- Calculate the fracture half-length from Equation 1.5.49:

$$x_f = \left[\frac{0.0002637(0.025)}{(0.1)(0.0252)(0.129 \times 10^{-3})} \frac{(1)(15.9)^2}{3.69 \times 10^{-2}} \right]^{1/2}$$

$$= 373 \text{ ft}$$

- Calculate F_C from Equation 1.5.21:

$$F_C = F_{CD}x_f k = (15.9)(373)(0.025) = 148 \text{ md ft}$$

- From Figure 1.86 :

$$r_w^\backslash/x_f = 0.46$$

$$r_w^\backslash = (373)(0.46) = 172 \text{ ft}$$

Test results	Type curve analysis	Bilinear flow analysis
F_C	148.0	154.0
x_f	373.0	368.0
F_{CD}	15.9	16.7
$r_w^\backslash$	172.0	169.0

The concept of the pressure derivative can be effectively employed to identify different flow regime periods associated with hydraulically fractured wells. As shown in Figure 1.89, a finite conductivity fracture shows a $\frac{1}{4}$ straight-line slope for both the pressure difference Δp and its derivative; however, the two parallel lines are separated by a factor of 4. Similarly, for an infinite conductivity fracture, two straight parallel lines represent Δp and its derivative with a $\frac{1}{2}$ slope and separation between the lines of a factor of 2 (as shown in Figure 1.90).

In tight reservoirs where the productivity of wells is enhanced by massive hydraulic fracturing (MHF), the resulting fractures are characterized as long vertical fractures with finite conductivities. These wells tend to produce at a constant and low bottom-hole flowing pressure, rather than constant flow rate. The diagnostic plots and the conventional analysis of bilinear flow data can be used when analyzing
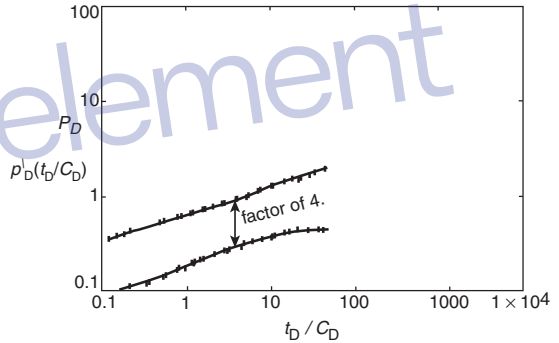
Figure 1.89 Finite conductivity fracture shows as a $\frac{1}{4}$ slope line on a log–log plot, same on a derivative plot. Separation between pressure and derivative is a factor of 4.
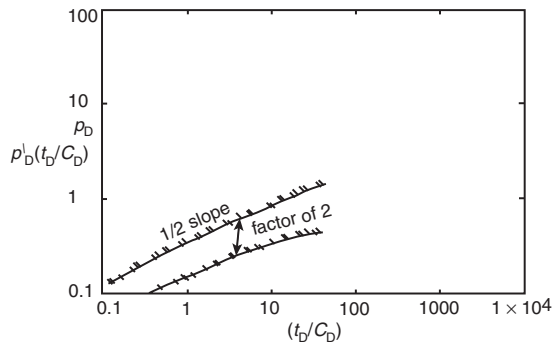
Figure 1.90 Infinite conductivity fracture shows as a $\frac{1}{2}$ slope line on a log–log plot, same on a derivative plot. Separation between pressure and derivative is a factor of 2.

well test data under constant flowing pressure. Equations 1.5.27 through 1.5.31 can be rearranged and expressed in the following forms.

For fractured oil wells

$$\frac{1}{Q} = \left[\frac{44.1B\mu}{h\sqrt{F_C}(\phi\mu c_t k)^{1/4}\Delta p} \right] t^{1/4}$$

or equivalently:

$$\frac{1}{Q} = m_{\text{bf}} t^{1/4}$$

and:

$$\log\left(\frac{1}{Q}\right) = \log(m_{\text{bf}}) + 1/4\log(t)$$

where:

$$m_{\text{bf}} = \frac{44.1B\mu}{h\sqrt{F_C}(\phi\mu c_t k)^{1/4}\Delta p}$$

$$F_C = k_f w_f = \left[\frac{44.1B\mu}{hm_{\text{bf}}(\phi\mu c_t k)^{1/2}\Delta p} \right]^2 \qquad [1.5.51]$$

For fractured gas wells

$$\frac{1}{Q} = m_{\text{bf}} t^{1/4}$$

or:

$$\log\left(\frac{1}{Q}\right) = \log(m)$$

where:

$$m_{\text{bf}} = \frac{444.6T}{h\sqrt{F_C}(\phi\mu c_t k)^{1/4}\Delta m(p)}$$

Solving for F_C:

$$F_C = \left[\frac{444.6T}{hm_{\text{bf}}(\phi\mu c_t k)^{1/4}\Delta m(p)} \right]^2 \qquad [1.5.52]$$

The following procedure can be used to analyze bilinear flow data under constant flow pressure:

Step 1. Plot $1/Q$ vs. t on a log–log scale and determine if any data falls on a straight line of a $\frac{1}{4}$ slope.
Step 2. If any data forms a $\frac{1}{4}$ slope in step 1, plot $1/Q$ vs. $t^{1/4}$ on a Cartesian role and determine the slope m_{bf}.
Step 3. Calculate the fracture conductivity F_C from Equation 1.5.51 or 1.5.52:

$$\text{For oil} \quad F_C = \left[\frac{44.1B\mu}{hm_{\text{bf}}(\phi\mu c_t k)^{1/4}(p_i - p_{\text{wf}})} \right]^2$$

$$\text{For gas} \quad F_C = \left[\frac{444.6T}{hm_{\text{bf}}(\phi\mu c_t k)^{1/4}[m(p_i) - m(p_{\text{wf}})]} \right]^2$$

Step 4. Determine the value of Q when the bilinear straight line ends and designate it as Q_{ebf}.
Step 5. Calculate F_{CD} from Equation 1.5.35 or 1.5.36:

$$\text{For oil} \quad F_{CD} = \frac{194.9Q_{\text{ebf}}B\mu}{kh(p_i - p_{\text{wf}})}$$

$$\text{For gas} \quad F_{CD} = \frac{1965.1Q_{\text{ebf}}T}{kh[m(p_i) - m(p_{\text{wf}})]}$$

Step 6. Estimate the fracture half-length from:

$$x_f = \frac{F_C}{F_{CD}k}$$

Agarwal et al. (1979) presented constant-pressure type curves for finite conductivity fractures, as shown in Figure 1.91. The reciprocal of the dimensionless rate $1/Q_D$ is expressed as a function of dimensionless time t_{Dx_f}, on log–log paper, with the dimensionless fracture conductivity F_{CD} as

a correlating parameter. The reciprocal dimensionless rate $1/Q_D$ is given by:

$$\text{For oil wells} \quad \frac{1}{Q_D} = \frac{kh(p_i - p_{\text{wf}})}{141.2Q\mu B} \qquad [1.5.53]$$

$$\text{For gas wells} \quad \frac{1}{Q_D} = \frac{kh[m(p_i) - m(p_{\text{wf}})]}{1424QT} \qquad [1.5.54]$$

with:

$$t_{Dx_f} = \frac{0.0002637kt}{\phi(\mu c_t)_i x_f^2} \qquad [1.5.55]$$

where:

p_{wf} = wellbore pressure, psi
Q = flow rate, STB/day or Mscf/day
T = temperature, °R
t = time, hours

subscripts:

i = initial
D = dimensionless

The following example, as adopted from Agarwal et al. (1979), illustrates the use of these type curves.

Example 1.40 A pre-frac buildup test was performed on a well producing from a tight gas reservoir, to give a formation permeability of 0.0081 md. Following an MHF treatment, the well produced at a constant pressure with recorded rate-time data as given below:

t (days)	Q (Mscf/day)	$1/Q$ (day/Mscf)
20	625	0.00160
35	476	0.00210
50	408	0.00245
100	308	0.00325
150	250	0.00400
250	208	0.00481
300	192	0.00521

The following additional data is available:

$p_i = 2394$ psi, $\qquad \Delta m(p) = 396 \times 10^6$ psi²/cp

$h = 32$ ft, $\qquad \phi = 0.107$

$T = 720$°R, $\qquad c_{ti} = 2.34 \times 10^{-4}$ psi⁻¹

$\mu_i = 0.0176$ cp, $\quad k = 0.0081$ md

Calculate:

• fracture half-length, x_f;
• fracture conductivity, F_C.

Solution

Step 1. Plot $1/Q$ vs. t on tracing paper, as shown in Figure 1.92, using the log–log scale of the type curves.
Step 2. We must make use of the available values of k, h, and $\Delta m(p)$ by arbitrarily choosing a convenient value of the flow rate and calculating the corresponding $1/Q_D$. Selecting $Q = 1000$ Mscf/day, calculate the corresponding value of $1/Q_D$ by applying Equation 1.5.54:

$$\frac{1}{Q_D} = \frac{kh\Delta m(p)}{1424QT} = \frac{(0.0081)(32)(396 \times 10^6)}{1424(1000)(720)} = 0.1$$

Step 3. Thus, the position of $1/Q = 10^{-3}$ on the y axis of the tracing paper is fixed in relation to $1/Q_D = 0.1$ on the y axis of the type curve graph paper; as shown in Figure 1.93.

$$F_{CD} = \frac{k_f W}{k X_f}$$

$$\frac{1}{q_D} = \frac{kh\Delta(P)^2}{1424 q_g \mu_g zT}$$

$$\frac{1}{q_D} = \frac{kh\Delta\psi(P)}{1424 q_g T}$$

$$t_{Dx_f} = \frac{2.634 \times 10^{-4} kt}{\phi \mu c_t x_f^2}$$
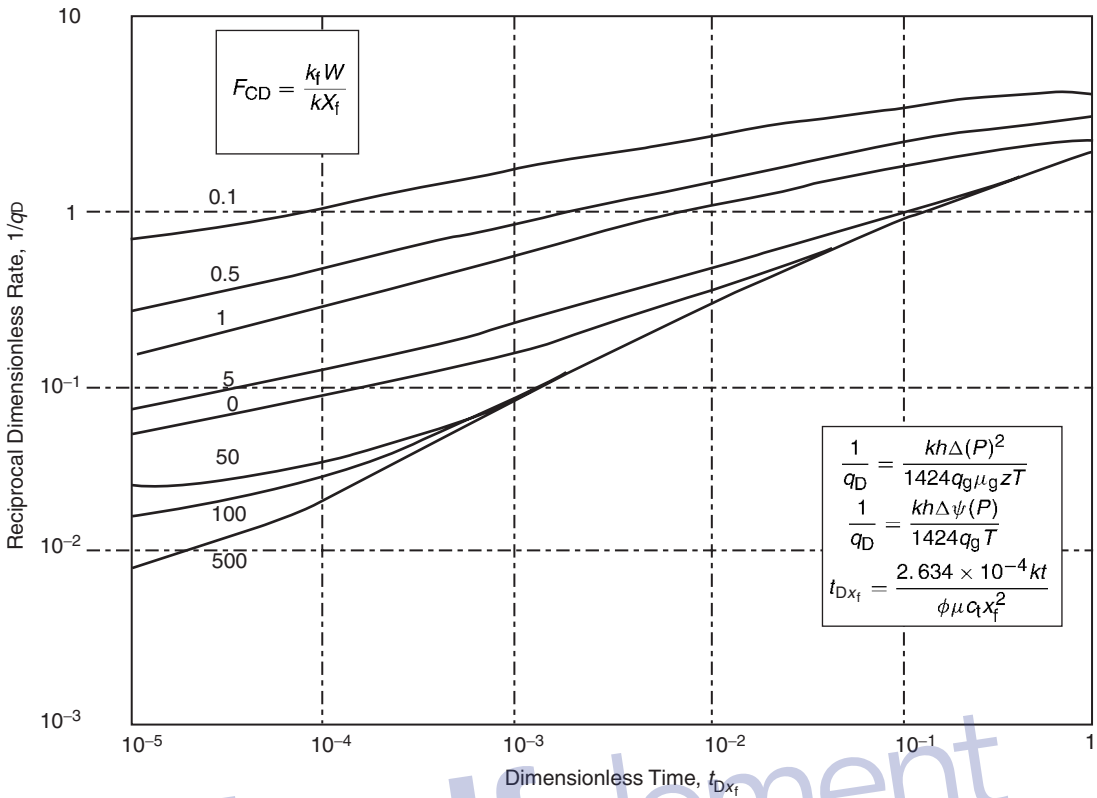
Figure 1.91 *Log–log type curves for finite capacity vertical fractures; constant wellbore pressure (After Agarwal et al., 1979).*
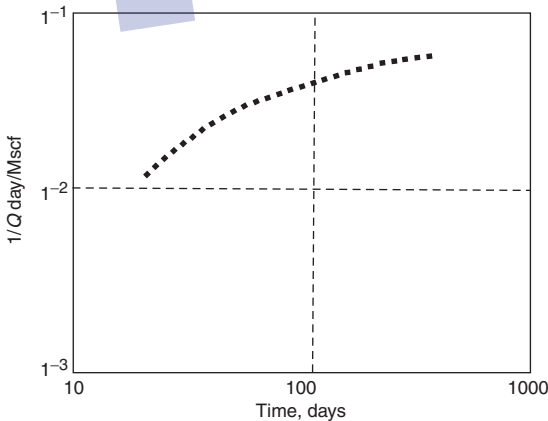
Figure 1.92 *Reciprocal smooth rate vs. time for MHF, Example 1.42.*

Step 4. Move the tracing paper horizontally along the *x* axis until a match is obtained, to give:

$$t = 100 \text{ days} = 2400 \text{ hours}$$
$$t_{Dx_f} = 2.2 \times 10^{-2}$$
$$F_{CD} = 50$$

Step 5. Calculate the fracture half-length from Equation 1.5.55:

$$x_f^2 = \left[\frac{0.0002637k}{\phi(\mu c_t)_i}\right]\left(\frac{t}{t_{Dx_f}}\right)_{MP}$$

$$= \left[\frac{0.0002637(0.0081)}{(0.107)(0.0176)(2.34 \times 10^{-4})}\right]\left(\frac{2400}{2.2 \times 10^{-2}}\right)$$

$$= 528\,174$$

$$x_f \approx 727 \text{ ft}$$

Thus the total fracture length is:

$$2x_f = 1454 \text{ ft}$$

Step 6. Calculate the fracture conductivity F_C from Equation 1.5.2:

$$F_C = F_{CD}kx_f = (50)(0.0081)(727) = 294 \text{ md ft}$$

It should be pointed out that if the pre-fracturing buildup test were not available, matching would require shifting the tracing paper along both the x and y axes to obtain the proper match. This emphasizes the need for determining kh from a pre-fracturing test.

Faults or impermeable barriers

One of the important applications of a pressure buildup test is analyzing the test data to detect or confirm the existence of faults and other flow barriers. When a sealing fault is located near a test well, it significantly affects the recorded well pressure behavior during the buildup test. This pressure

$$x_f^2 = \left[\frac{0.0002637k}{\phi(\mu c_t)_i}\right]\left(\frac{t}{t_{Dx_f}}\right)_{MP}$$

Match points are
t = 100 days
$t_{Dx_f} = 2.15 \times 10^{-2}$
$F_{CD} = 50$

$$F_C = F_{CD}kx_f$$

$$t_{Dx_f} = \left[2.637 \times 10^{-4}kt\right]/\left[\phi\mu_j c_i (x_f)^2\right]$$
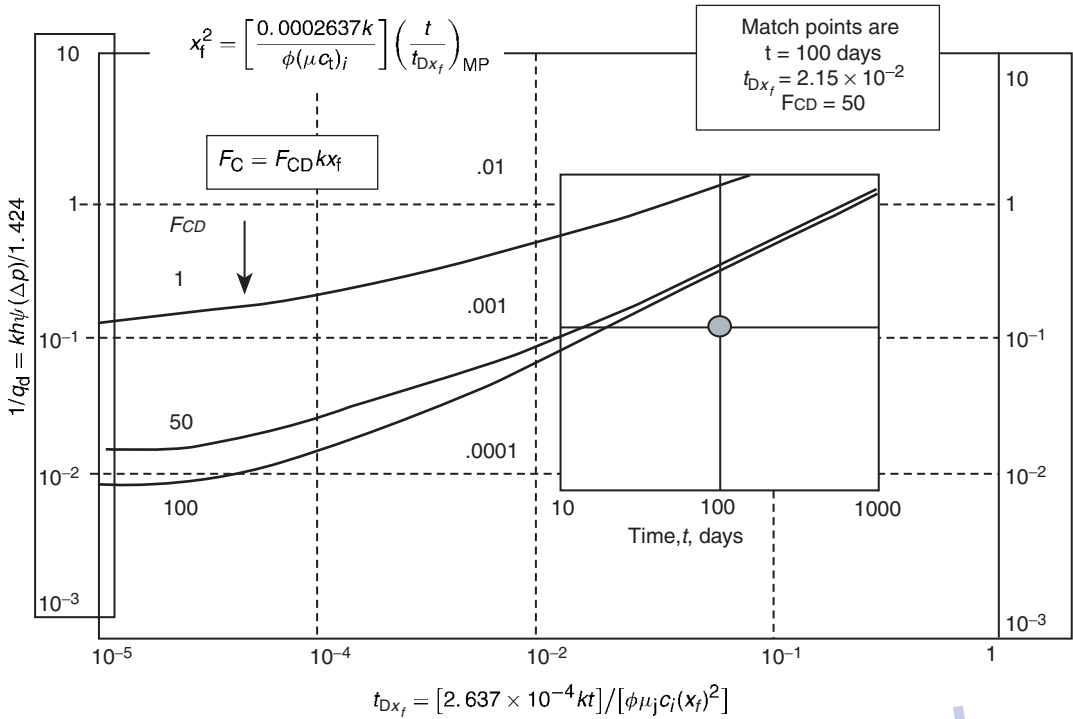
Figure 1.93 *Type curve matching for MHF gas well, Example 1.42.*
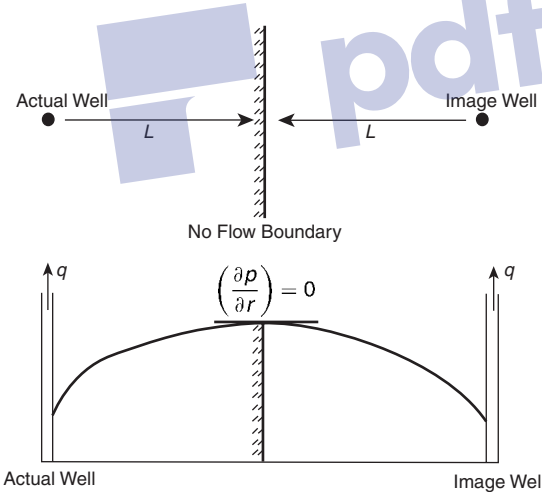
Figure 1.94 *Method of images in solving boundary problems.*

behavior can be described mathematically by applying the principle of superposition as given by the method of images. Figure 1.94 shows a test well that is located at a distance L from a sealing fault. Applying method images, as given Equation 1.2.157, the total pressure drop as a function of time t is:

$$(\Delta p)_{total} = \frac{162.6Q_o B\mu}{kh}\left[\log\left(\frac{kt}{\phi c_t r_w^2}\right) - 3.23 + 0.87s\right]$$

$$- \left(\frac{70.6Q_o B\mu}{kh}\right)\text{Ei}\left(-\frac{948\phi\mu c_t (2L)^2}{kt}\right)$$

When both the test well and image well are shut-in for a buildup test, the principle of superposition can be applied to Equation 1.2.57 to predict the buildup pressure at Δt as:

$$p_{ws} = p_i - \frac{162.6Q_o B_o \mu_o}{kh}\left[\log\left(\frac{t_p + \Delta t}{\Delta t}\right)\right]$$

$$- \left(\frac{70.6Q_o B_o \mu_o}{kh}\right)\text{Ei}\left[\frac{-948\phi\mu c_t (2L)^2}{k(t_p + \Delta t)}\right]$$

$$- \left(\frac{70.6(-Q_o)B_o \mu_o}{kh}\right)\text{Ei}\left[\frac{-948\phi\mu c_t (2L)^2}{k\Delta t}\right] \quad [1.5.56]$$

Recalling that the exponential integral $\text{Ei}(-x)$ can be approximated by Equation 1.2.68 when $x < 0.01$ as:

$$\text{Ei}(-x) = \ln(1.781x)$$

the value of the $\text{Ei}(-x)$ can be set equal to zero when x is greater than 10.9, i.e., $\text{Ei}(-x) = 0$ for $x > 10.9$. Notice that the value of $(2L)^2$ is large and for early buildup times, when Δt is small, the last two terms in can be set equal to zero, or:

$$p_{ws} = p_i - \frac{162.6Q_o B_o \mu_o}{kh}\left[\log\left(\frac{t_p + \Delta t}{\Delta t}\right)\right] \quad [1.5.57]$$

which is essentially the regular Horner equation with a semilog straight-line slope of:

$$m = \frac{162.6Q_o B_o \mu_o}{kh}$$

For a shut-in time sufficiently large that the *logarithmic approximation is accurate for the* Ei *functions*, Equation 1.5.56 becomes:

$$p_{ws} = p_i - \frac{162.6Q_o B_o \mu_o}{kh}\left[\log\left(\frac{t_p + \Delta t}{\Delta t}\right)\right]$$

$$- \frac{162.6Q_o B_o \mu_o}{kh}\left[\log\left(\frac{t_p + \Delta t}{\Delta t}\right)\right]$$

Rearranging this equation by recombining terms gives:

$$p_{ws} = p_i - 2\left(\frac{162.6Q_oB_o\mu_o}{kh}\right)\left[\log\left(\frac{t_p + \Delta t}{\Delta t}\right)\right]$$

Simplifying:

$$p_{ws} = p_i - 2m\left[\log\left(\frac{t_p + \Delta t}{\Delta t}\right)\right] \qquad [1.5.58]$$

Three observations can be made by examining Equations 1.5.57 and 1.5.58:

(1) For early shut-in time buildup data, Equation 1.5.57 indicates that the data from the early shut-in times will form a straight line on the Horner plot with a slope that is identical to a reservoir without sealing fault.

(2) At longer shut-in times, the data will form a *second straight line* on the Horner plot with a slope that is twice that of the first line, i.e., second slope $= 2m$. The presence of the second straight line with a double slope of the first straight line provides a means of recognizing the presence of a fault from pressure buildup data.

(3) The shut-in time required for the slope to double can be approximated from the following expression:

$$\frac{948\phi\mu c_t(2L)^2}{k\Delta t} < 0.01$$

Solving for Δt gives:

$$\Delta t > \frac{380\,000\phi\mu c_t L^2}{k}$$

where:

Δt = minimum shut-in time, hours
k = permeability, md
L = distance between well and the sealing fault, ft

Notice that the value of p^* for use in calculating the average drainage region pressure $\bar{p}$ is obtained by extrapolating the *second straight line* to a unit-time ratio, i.e., to $(t_p + \Delta t)/\Delta t = 1.0$. The permeability and skin factor are calculated in the normal manner described before using the slope of the *first straight line*.

Gray (1965) suggested that for the case in which the slope of the buildup test has the time to double, as shown schematically in Figure 1.95, the distance L from the well to the fault can be calculated by finding the time Δt_x at which the two semilog straight lines intersect. That is:

$$L = \sqrt{\frac{0.000148k\Delta t_x}{\phi\mu c_t}} \qquad [1.5.59]$$

Lee (1982) illustrated Gray's method through the following examples.

Example 1.41 A pressure buildup test was conducted to confirm the existence of a sealing fault near a newly drilled well. Data from the test is given below:

Δt (hr)	p_{ws} (psi)	$(t_p + \Delta t)/\Delta t$
6	3996	47.5
8	4085	35.9
10	4172	28.9
12	4240	24.3
14	4298	20.9
16	4353	18.5
20	4435	15.0
24	4520	12.6
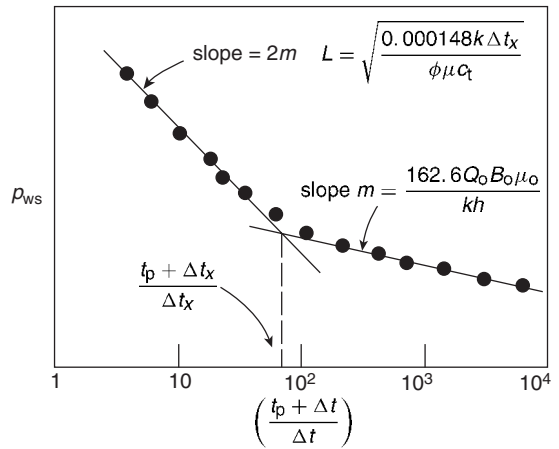
Figure 1.95 *Theoretical Horner plot for a faulted system.*

Δt (hr)	p_{ws} (psi)	$(t_p + \Delta t)/\Delta t$
30	4614	10.3
36	4700	8.76
42	4770	7.65
48	4827	6.82
54	4882	6.17
60	4931	5.65
66	4975	5.23

Other data include the following:

$\phi = 0.15$, $\qquad \mu_o = 0.6$ cp,

$c_t = 17 \times 10^{-6}$ psi^{-1} $\qquad r_w = 0.5$ ft,

$Q_o = 1221$ STB/day, $\qquad h = 8$ ft

$B_o = 1.31$ bbl/STB,

A total of 14 206 STB of oil had been produced before shut-in. Determine whether the sealing fault exists and the distance from the well to the fault.

Solution

Step 1. Calculate total production time t_p:

$$t_p = \frac{24N_p}{Q_o} = \frac{(24)(14206)}{1221} = 279.2 \text{ hours}$$

Step 2. Plot p_{ws} vs. $(t_p + \Delta t)/\Delta t$ as shown in Figure 1.96. The plot clearly shows two straight lines with the first slope of 650 psi/cycle and the second with 1300 psi/cycle. Notice that the second slope is twice that of the first slope indicating the existence of the sealing fault.

Step 3. Using the value of the *first slope*, calculate the permeability k:

$$k = \frac{162.6Q_oB_o\mu_o}{mh} = \frac{162.6(1221)(1.31)(0.6)}{(650)(8)}$$

$$= 30 \text{ md}$$

Step 4. Determine the value of Horner's time ratio at the intersection of the two semilog straight lines shown in Figure 1.96, to give:

$$\frac{t_p + \Delta t_x}{\Delta t_x} = 17$$

or:

$$\frac{279.2 + \Delta t_x}{\Delta t_x} = 17$$
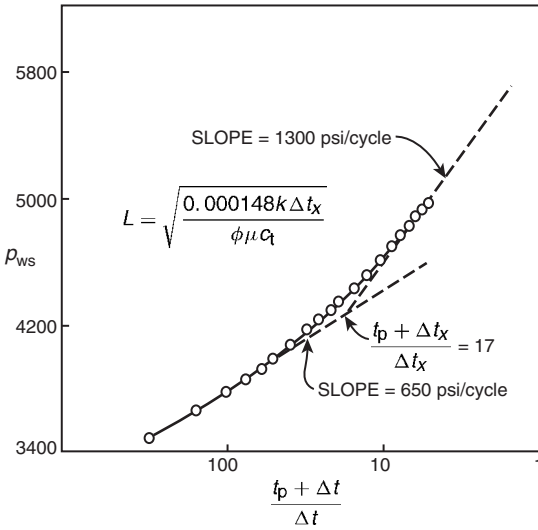
Figure 1.96 *Estimating distance to a no-flow boundary.*

from which:

$$\Delta t_x = 17.45 \text{ hours}$$

Step 5. Calculate the distance L from the well to the fault by applying Equation 1.5.59:

$$L = \sqrt{\frac{0.000148 k \Delta t_x}{\phi \mu c_t}}$$

$$= \sqrt{\frac{0.000148(30)(17.45)}{(0.15)(0.6)(17 \times 10^{-6})}} = 225 \text{ ft}$$

Qualitative interpretation of buildup curves
The Horner plot has been the most widely accepted means for analyzing pressure buildup data since its introduction in 1951. Another widely used aid in pressure transient analysis is the plot of change in pressure Δp versus time on a log–log scale. Economides (1988) pointed out that this log–log plot serves the following two purposes:

(1) the data can be matched to type curves;
(2) the type curves can illustrate the expected trends in pressure transient data for a large variety of well and reservoir systems.

The visual impression afforded by the log–log presentation has been greatly enhanced by the introduction of the pressure derivative which represents the changes of the slope of buildup data with respect to time. When the data produces a straight line on a semilog plot, the pressure derivative plot will, therefore, be constant. That means the pressure derivative plot will be flat for that portion of the data that can be correctly analyzed as a straight line on the Horner plot.

Many engineers rely on the log–log plot of Δp and its derivative versus time to diagnose and select the proper interpretation model for a given set of pressure transient data. Patterns visible in the log–log diagnostic and Horner plots for five frequently encountered reservoir systems are illustrated graphically by Economides as shown in Figure 1.97. The curves on the right represent buildup responses for five different patterns, a through e, with the curves on the left representing the corresponding responses when the data is plotted in the log–log format of Δp and $(\Delta t \Delta p^\setminus)$ versus time.

The five different buildup examples shown in Figure 1.97 were presented by Economides (1988) and are briefly discussed below:

Example a illustrates the most common response—that of a homogeneous reservoir with wellbore storage and skin. Wellbore storage derivative transients are recognized as a "hump" in early time. The flat derivative portion in late time is easily analyzed as the Horner semilog straight line.

Example b shows the behavior of an infinite conductivity, which is characteristic of a well that penetrates a natural fracture. The $\frac{1}{2}$ slopes in both the pressure change and its derivative result in two parallel lines during the flow regime, representing linear flow to the fracture.

Example c shows the homogeneous reservoir with a single vertical planar barrier to flow or a fault. The level of the second-derivative plateau is twice the value of the level of the first-derivative plateau, and the Horner plot shows the familiar slope-doubling effect.

Example d illustrates the effect of a closed drainage volume. Unlike the drawdown pressure transient, this has a unit-slope line in late time that is indicative of pseudosteady-state flow; the buildup pressure derivative drops to zero. The permeability and skin cannot be determined from the Horner plot because no portion of the data exhibits a flat derivative for this example. When transient data resembles example d, the only way to determine the reservoir parameters is with a type curve match.

Example e exhibits a valley in the pressure derivative that is indicative of reservoir heterogeneity. In this case, the feature results from dual-porosity behavior, for the case of pseudosteady flow from matrix to fractures.

Figure 1.97 clearly shows the value of the pressure/pressure derivative presentation. An important advantage of the log–log presentation is that the transient patterns have a standard appearance as long as the data is plotted with square log cycles. The visual patterns in semilog plots are amplified by adjusting the range of the vertical axis. Without adjustment, many or all of the data may appear to lie on one line and subtle changes can be overlooked.

Some of the pressure derivative patterns shown are similar to those characteristics of other models. For example, the pressure derivative doubling associated with a fault (example c) can also indicate transient interporosity flow in a dual-porosity system. The sudden drop in the pressure derivative in buildup data can indicate either a closed outer boundary or constant-pressure outer boundary resulting from a gas cap, an aquifer, or pattern injection wells. The valley in the pressure derivative (example e) could indicate a layered system instead of dual porosity. For these cases and others, the analyst should consult geological, seismic, or core analysis data to decide which model to use in an interpretation. With additional data, a more conclusive interpretation for a given transient data set may be found.

An important place to use the pressure/pressure derivative diagnosis is on the well site. If the objective of the test is to determine permeability and skin, the test can be terminated once the derivative plateau is identified. If heterogeneities or boundary effects are detected in the transient, the test can be run longer to record the entire pressure/pressure derivative response pattern needed for the analysis.

1.6 Interference and Pulse Tests

When the flow rate is changed and the pressure response is recorded in the same well, the test is called a "single-well" test. Examples of single-well tests are drawdown, buildup, injectivity, falloff and step-rate tests. When the flow rate is changed in one well and the pressure response is recorded in another well, the test is called a "multiple-well" test.
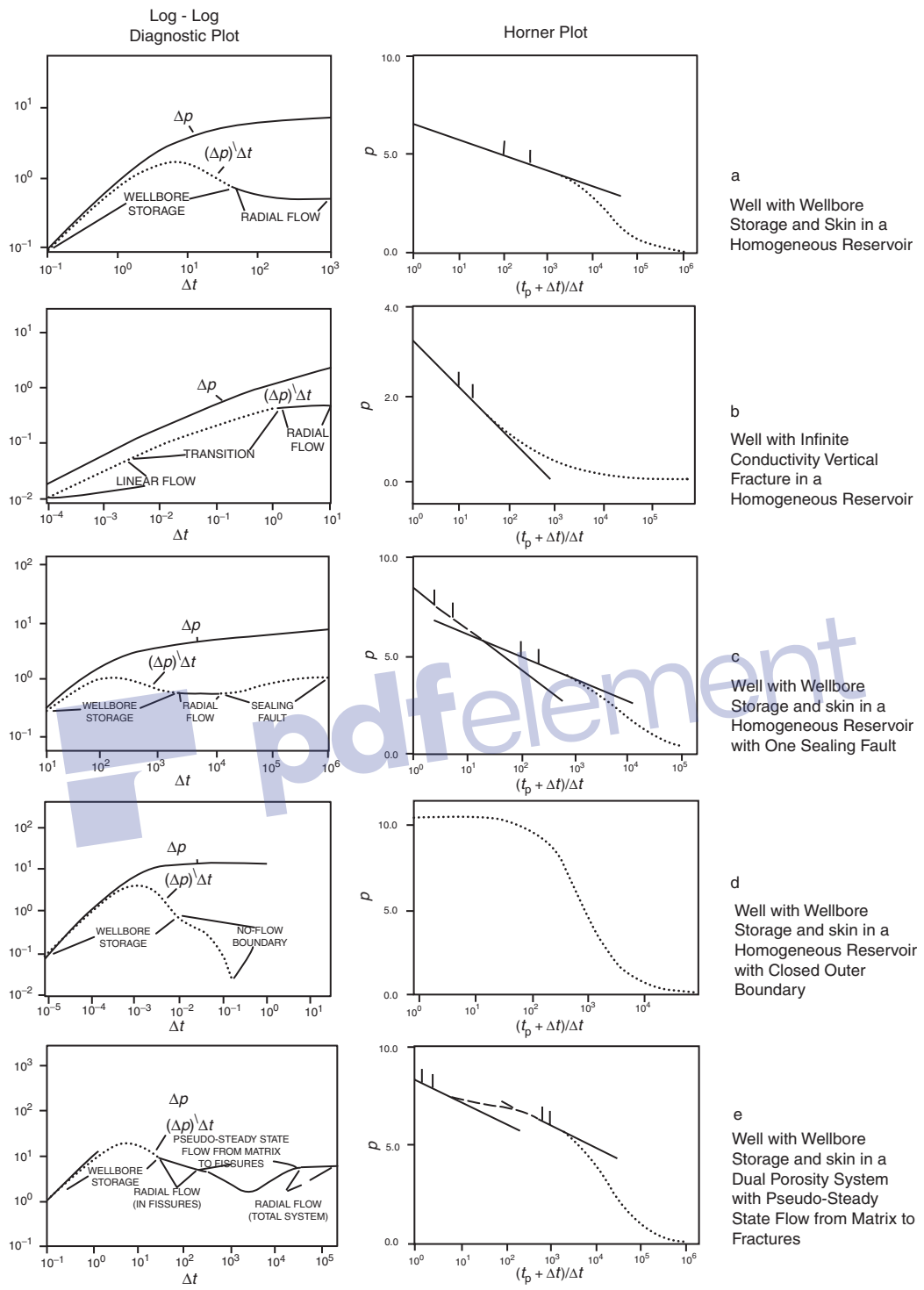
Figure 1.97 *Qualitative interpretation of buildup curves (After Economides, 1988).*
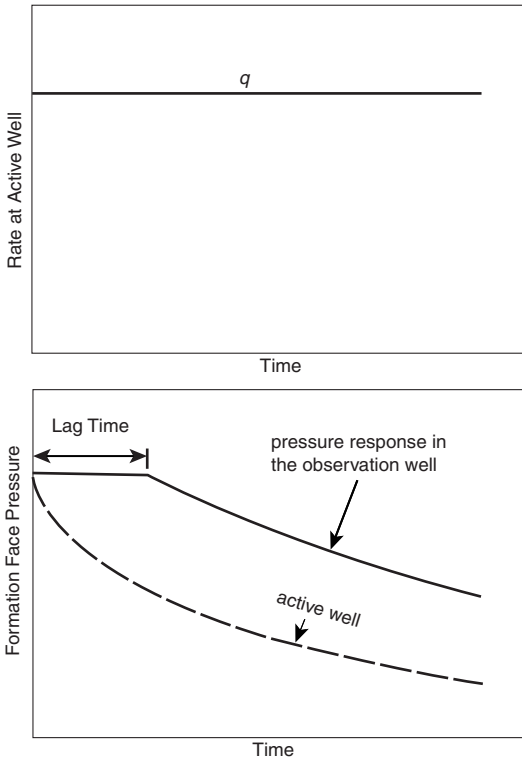
Figure 1.98   *Rate history and pressure response of a two-well interference test conducted by placing the active well on production at constant rate.*
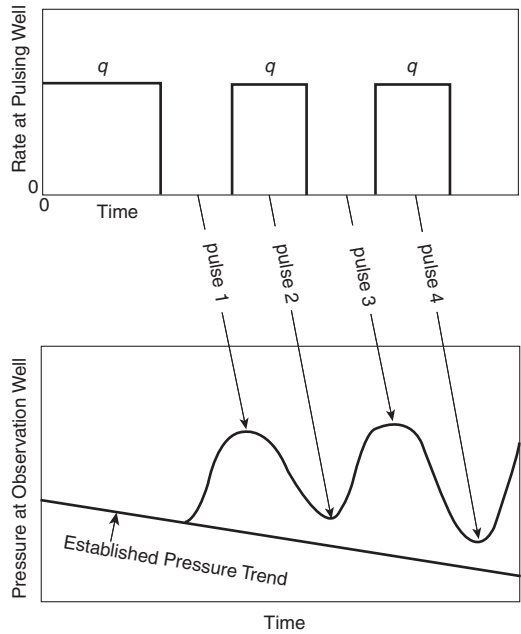
Figure 1.99   *Illustration of rate history and pressure response for a pulse test (After Earlougher, R. Advances in Well Test Analysis) (Permission to publish by the SPE, copyright SPE, 1977).*

Examples of multiple-well tests are interference and pulse tests.

Single-well tests provide valuable reservoir and well characteristics that include flow capacity kh, wellbore conditions, and fracture length as examples of these important properties. However, these tests do not provide the directional nature of reservoir properties (such as permeability in the x, y, and z direction) and have inabilities to indicate the degree of communication between the test wells and adjacent wells. Multiple-well tests are run to determine:

- the presence or lack of communication between the test well and surrounding wells;
- the mobility–thickness product kh/μ;
- the porosity–compressibility–thickness product $\phi c_t h$;
- the fracture orientation if intersecting one of the test wells;
- the permeability in the direction of the major and minor axes.

The multiple-well test requires at least one active (producing or injecting) well and at least one pressure observation well, as shown schematically in Figure 1.98. In an interference test, all the test wells are shut-in until their wellbore pressures stabilize. The active well is then allowed to produce or inject at constant rate and the pressure response in the observation well(s) is observed. Figure 1.98 indicates this concept with one active well and one observation well. As the figure indicates, when the active well starts to produce, the pressure in the shut-in observation well begins to respond after some "time lag" that depends on the reservoir rock and fluid properties.

Pulse testing is a form of interference testing. The producer or injector is referred to as "the pulser or the active well" and the observation well is called "the responder." The tests are conducted by sending a series of short-rate pulses from the active well (producer or injector) to a shut-in observation well(s). Pulses generally are alternating periods of production (or injection) and shut-in, with the same rate during each production (injection) period, as illustrated in Figure 1.99 for a two-well system.

Kamal (1983) provided an excellent review of interference and pulse testing and summarized various methods that are used to analyze test data. These methods for analyzing interference and pulse tests are presented below.

1.6.1 Interference testing in homogeneous isotropic reservoirs

A reservoir is classified as "homogeneous" when the porosity and thickness do not change significantly with location. An "isotropic" reservoir indicates that the permeability is the same throughout the system. In these types of reservoirs, the type curve matching approach is perhaps the most convenient to use when analyzing interference test data in a homogeneous reservoir system. As given previously by Equation 1.2.66, the pressure drop at any distance r from an active well (i.e., distance between an active well and a shut-in observation well) is expressed as:

$$p_i - p(r,t) = \Delta p = \left[\frac{-70.6QB\mu}{kh} \right] \mathrm{Ei} \left[\frac{-948\phi c_t r^2}{kt} \right]$$

Earlougher (1977) expressed the above expression in a dimensionless form as:

$$\frac{p_i - p(r,t)}{\frac{141.2QB\mu}{kh}} = -\frac{1}{2}\mathrm{Ei}\left[\left(\frac{-1}{4} \right) \left(\frac{\phi\mu c_t r_w^2}{0.0002637 kt} \right) \left(\frac{r}{r_w} \right)^2 \right]$$

From the definitions of the dimensionless parameters p_D, t_D, and r_D, the above equations can be expressed in a
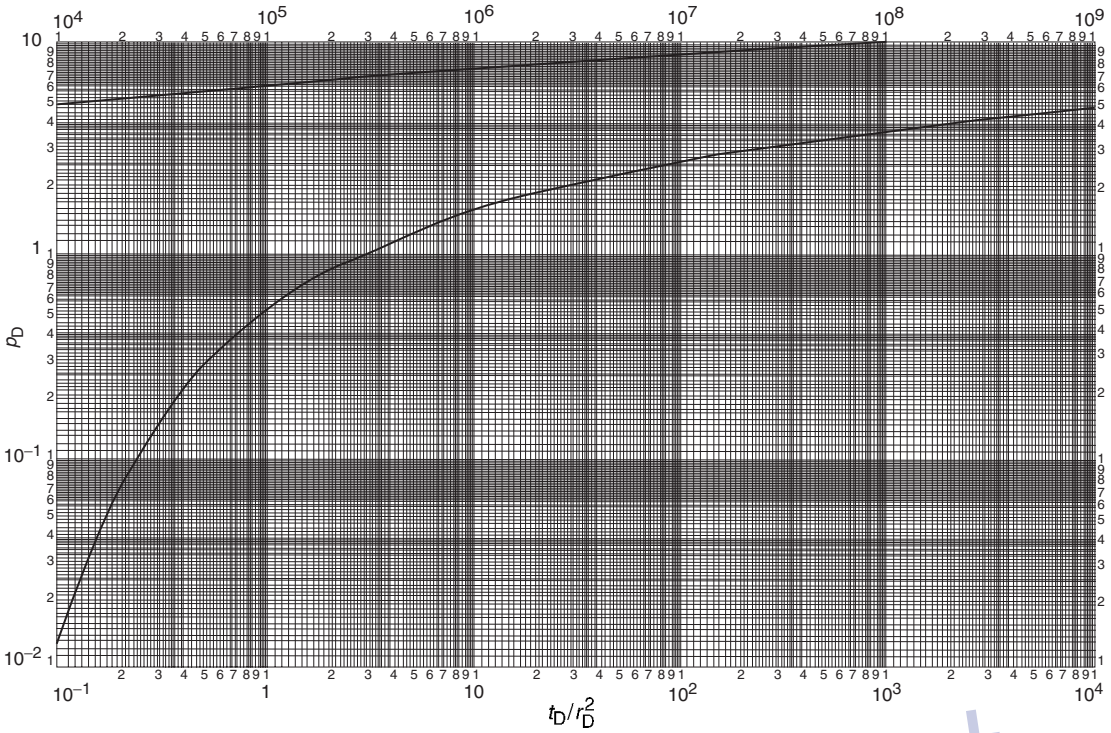
Figure 1.100 *Dimensionless pressure for a single well in an infinite system, no wellbore storage, no skin. Exponential–integral solution (After Earlougher, R. Advances in Well Test Analysis) (Permission to publish by the SPE, copyright SPE, 1977).*

dimensionless form as:

$$p_D = -\frac{1}{2}\text{Ei}\left[\frac{-r_D^2}{4t_D}\right] \qquad [1.6.1]$$

with the dimensionless parameters as defined by:

$$p_D = \frac{[p_i - p(r,t)]kh}{141.2QB\mu}$$

$$r_D = \frac{r}{r_w}$$

$$t_D = \frac{0.0002637kt}{\phi\mu c_t r_w^2}$$

where:

$p(r,t)$ = pressure at distance r and time t, psi
r = distance between the active well and a shut-in observation well
t = time, hours
p_i = reservoir pressure
k = permeability, md

Earlougher expressed in Equation 1.6.1 a type curve form as shown previously in Figure 1.47 and reproduced for convenience as Figure 1.100.

To analyze an interference test by type curve matching, plot the observation well(s) pressure change Δp versus time on tracing paper laid over Figure 1.100 using the matching procedure described previously. When the data is matched to the curve, any convenient match point is selected and match point values from the tracing paper and the underlying type curve grid are read. The following expressions can then be

applied to estimate the average reservoir properties:

$$k = \left[\frac{141.2QB\mu}{h}\right]\left[\frac{p_D}{\Delta p}\right]_{MP} \qquad [1.6.2]$$

$$\phi = \frac{0.0002637}{c_t r^2}\left[\frac{k}{\mu}\right]\left[\frac{t}{t_D/r_D^2}\right]_{MP} \qquad [1.6.3]$$

where:

r = distance between the active and observation wells, ft
k = permeability, md

Sabet (1991) presented an excellent discussion on the use of the type curve approach in analyzing interference test data by making use of test data given by Strobel et al. (1976). The data, as given by Sabet, is used in the following example to illustrate the type curve matching procedure:

Example 1.42 An interference test was conducted in a dry gas reservoir using two observation wells, designated as Well 1 and Well 3, and an active well, designated as Well 2. The interference test data is listed below:

- Well 2 is the producer, $Q_g = 12.4$ MMscf/day;
- Well 1 is located 8 miles east of Well 2, i.e., $r_{12} = 8$ miles;
- Well 3 is located 2 miles west of Well 2, i.e., $r_{23} = 2$ miles.

Flow rate	Time	Observed pressure (psia)			
Q	t	Well 1		Well 3	
(MMscf/day)	(hr)	p_1	Δp_1	p_3	Δp_3
0.0	24	2912.045	0.000	2908.51	0.00
12.4	0	2912.045	0.000	2908.51	0.00
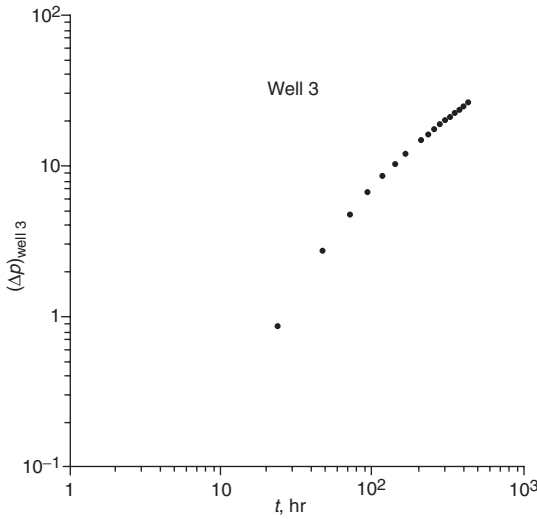
Figure 1.101 *Interference data of Well 3. (After Sabet, M. A. Well Test Analysis 1991, Gulf Publishing Company).*
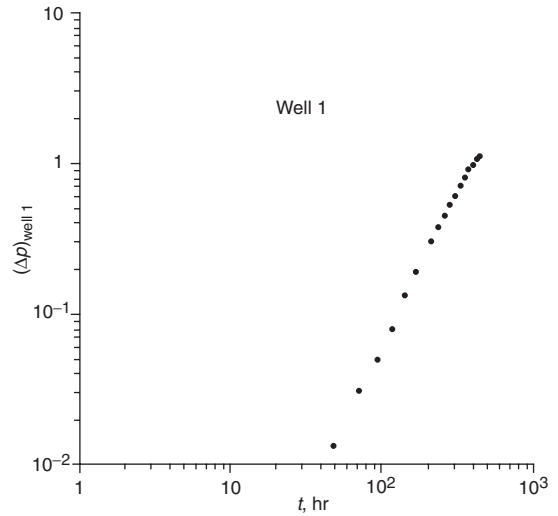
Figure 1.102 *Interference data of Well 1. (After Sabet, M. A. Well Test Analysis 1991, Gulf Publishing Company).*

Flow rate	Time	Observed pressure (psia)			
Q	t	Well 1		Well 3	
(MMscf/day)	(hr)	p_1	Δp_1	p_3	Δp_3
12.4	24	2912.035	0.010	2907.66	0.85
12.4	48	2912.032	0.013	2905.80	2.71
12.4	72	2912.015	0.030	2903.79	4.72
12.4	96	2911.997	0.048	2901.85	6.66
12.4	120	2911.969	0.076	2899.98	8.53
12.4	144	2911.918	0.127	2898.25	10.26
12.4	169	2911.864	0.181	2896.58	11.93
12.4	216	2911.755	0.290	2893.71	14.80
12.4	240	2911.685	0.360	2892.36	16.15
12.4	264	2911.612	0.433	2891.06	17.45
12.4	288	2911.533	0.512	2889.79	18.72
12.4	312	2911.456	0.589	2888.54	19.97
12.4	336	2911.362	0.683	2887.33	21.18
12.4	360	2911.282	0.763	2886.16	22.35
12.4	384	2911.176	0.869	2885.01	23.50
12.4	408	2911.108	0.937	2883.85	24.66
12.4	432	2911.030	1.015	2882.69	25.82
12.4	444	2910.999	1.046	2882.11	26.40
0.0	450	Well 2 shut-in			
0.0	480	2910.833	1.212	2881.45	27.06
0.0	504	2910.714	1.331	2882.39	26.12
0.0	528	2910.616	1.429	2883.52	24.99
0.0	552	2910.520	1.525	2884.64	23.87
0.0	576	2910.418	1.627	2885.67	22.84
0.0	600	2910.316	1.729	2886.61	21.90
0.0	624	2910.229	1.816	2887.46	21.05
0.0	648	2910.146	1.899	2888.24	20.27
0.0	672	2910.076	1.969	2888.96	19.55
0.0	696	2910.012	2.033	2889.60	18.91

The following additional reservoir data is available:

$T = 671.6°R$, $h = 75$ ft, $c_{ti} = 2.74 \times 10^{-4}$ psi^{-1}

$B_{gi} = 920.9$ bbl/MMscf, $r_w = 0.25$ ft, $Z_i = 0.868$,

$S_w = 0.21$, $\gamma_g = 0.62$, $\mu_{gi} = 0.0186$ cp

Using the type curve approach, characterize the reservoir in terms of permeability and porosity.

Solution

Step 1. Plot Δp vs. t on a log–log tracing paper with the same dimensions as those of Figure 1.100, as shown in Figures 1.101 and 1.102 for Wells 1 and 3, respectively.

Step 2. Figure 1.103 shows the match of interference data for Well 3, with the following matching points:

$$(p_D)_{MP} = 0.1 \quad \text{and} \quad (\Delta p)_{MP} = 2 \text{ psi}$$

$$(t_D/r_D^2)_{MP} = 1 \quad \text{and} \quad (t)_{MP} = 159 \text{ hours}$$

Step 3. Solve for k and ϕ between Well 2 and Well 3 by applying Equations 1.6.2 and 1.6.3

$$k = \left[\frac{141.2QB\mu}{h}\right]\left[\frac{p_D}{\Delta p}\right]_{MP}$$

$$= \left[\frac{141.2(12.4)(920.9)(0.0186)}{75}\right]\left(\frac{0.1}{2}\right) = 19.7 \text{ md}$$

$$\phi = \frac{0.0002637}{c_t r^2}\left[\frac{k}{\mu}\right]\left[\frac{t}{t_D/r_D^2}\right]_{MP}$$

$$= \frac{0.0002637}{(2.74 \times 10^{-4})(2 \times 5280)^2}\left(\frac{19.7}{0.0186}\right)\left(\frac{159}{1}\right)$$

$$= 0.00144$$

Step 4. Figure 1.104 shows the match of the test data for Well 1 with the following matching points:

$$(p_D)_{MP} = 1 \quad \text{and} \quad (\Delta p)_{MP} = 5.6 \text{ psi}$$

$$(t_D/r_D^2)_{MP} = 0.1 \quad \text{and} \quad (t)_{MP} = 125 \text{ hours}$$
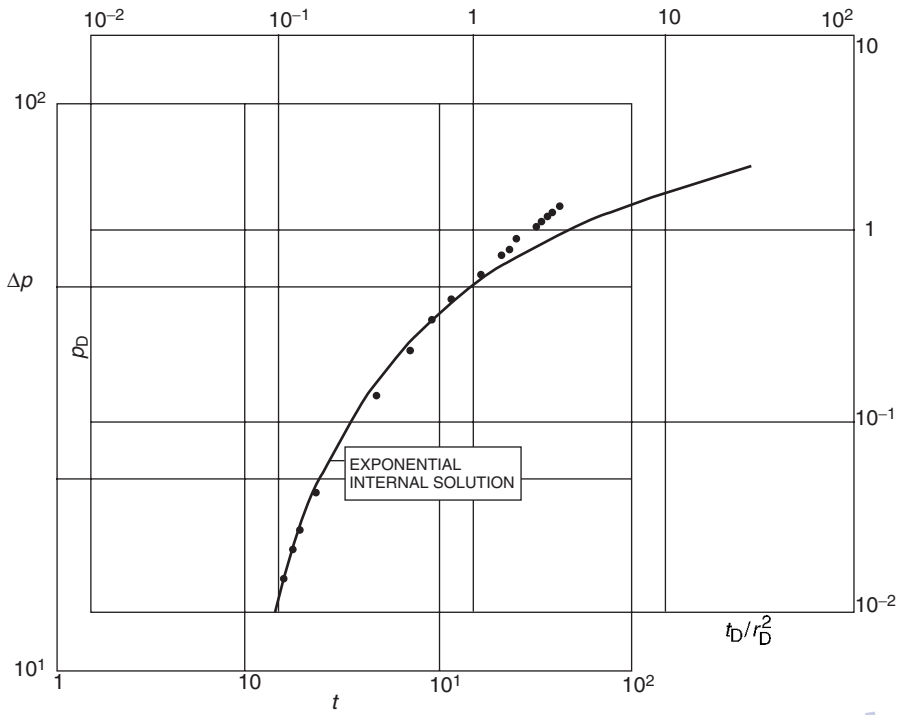
Figure 1.103 *Match of interference data of Well 3. (After Sabet, M. A. Well Test Analysis 1991, Gulf Publishing Company).*
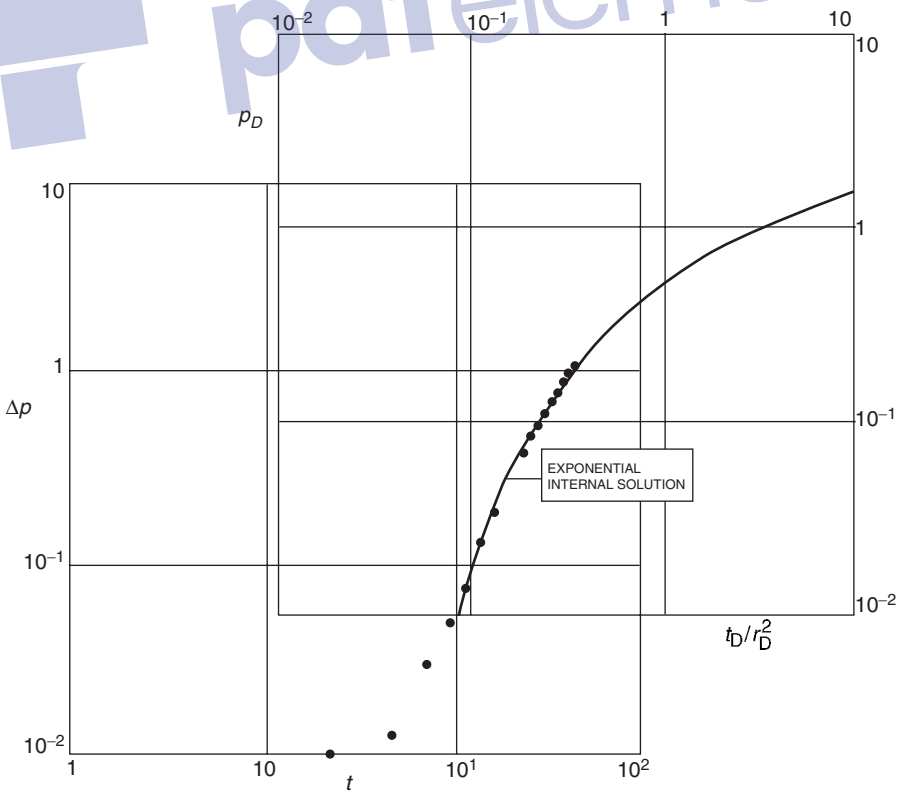
Figure 1.104 *Match of interference data of Well 1.*

Step 5. Calculate k and ϕ:

$$k = \left[\frac{141.2(12.4)(920.9)(0.0186)}{75} \right] \left(\frac{1}{5.6} \right)$$

$$= 71.8 \text{ md}$$

$$\phi = \frac{0.0002637}{(2.74 \times 10^{-4})(8 \times 5280)^2} \left(\frac{71.8}{0.0180} \right) \left(\frac{125}{0.1} \right)$$

$$= 0.0026$$

In a homogeneous and isotropic reservoir, i.e., permeability is the same throughout the reservoir, the minimum area of the reservoir investigated during an interference test between two wells located a distance r apart is obtained by drawing two circles of radius r centered at each well.

1.6.2 Interference testing in homogeneous anisotropic reservoirs

A homogeneous anisotropic reservoir is one in which the porosity ϕ and thickness h are the same throughout the system, but the permeability varies with direction. Using multiple observation wells when conducting an interference test in a homogeneous anisotropic reservoir, it is possible to determine the maximum and minimum permeabilities, i.e., k_{max} and k_{min}, and their directions relative to well locations. Based on the work of Papadopulos (1965), Ramey (1975) adopted the Papadopulos solution for estimating anisotropic reservoir properties from an interference test that requires at least three observation wells for analysis. Figure 1.105 defines the necessary nomenclature used in the analysis of interference data in a homogeneous anisotropic reservoir.

Figure 1.105 shows an active well, with its coordinates at the *origin*, and several observation wells are each located at coordinates defined by (x, y). Assuming that all the wells in the testing area have been shut in for a sufficient time to equalize the pressure to p_i, placing the active well on production (or injection) will cause a change in pressure of Δp, i.e., $\Delta p = p_i - p(x, y, t)$, at all observation wells. This change in

the pressure will occur after a lag period with a length that depends, among other parameters, on:

- the distance between the active well and observation well;
- permeability;
- wellbore storage in the active well;
- the skin factor following a lag period.

Ramey (1975) showed that the change in pressure at an observation well with coordinates of (x, y) at any time t is given by the Ei function as:

$$p_D = -\frac{1}{2} \text{Ei} \left[\frac{-r_D^2}{4t_D} \right]$$

The dimensionless variables are defined by:

$$p_D = \frac{\bar{k}h[p_i - p(x, y, t)]}{141.2QB\mu} \tag{1.6.4}$$

$$\frac{t_D}{r_D^2} = \left[\frac{(\bar{k})^2}{y^2 k_x + x^2 k_y - 2xyk_{xy}} \right] \left(\frac{0.0002637t}{\phi \mu c_t} \right) \tag{1.6.5}$$

with:

$$\bar{k} = \sqrt{k_{max}k_{min}} = \sqrt{k_x k_y - k_{xy}^2} \tag{1.6.6}$$

Ramey also developed the following relationships:

$$k_{max} = \frac{1}{2} \left[(k_x + k_y) + \sqrt{(k_x k_y)^2 + 4k_{xy}^2} \right] \tag{1.6.7}$$

$$k_{min} = \frac{1}{2} \left[(k_x + k_y)^2 - \sqrt{(k_x k_y)^2 + 4k_{xy}^2} \right] \tag{1.6.8}$$

$$\theta_{max} = \arctan \left(\frac{k_{max} - k_x}{k_{xy}} \right) \tag{1.6.9}$$

$$\theta_{min} = \arctan \left(\frac{k_{min} - k_y}{k_{xy}} \right) \tag{1.6.10}$$

where:

k_x = permeability in x direction, md
k_y = permeability in y direction, md
k_{xy} = permeability in xy direction, md
k_{min} = minimum permeability, md
k_{max} = maximum permeability, md
$\bar{k}$ = average system permeability, md
θ_{max} = direction (angle) of k_{max} as measured from the $+x$ axis
θ_{min} = direction (angle) of k_{min} as measured from the $+y$ axis
x, y = coordinates, ft
t = time, hours

Ramey pointed out that if $\phi \mu c_t$ is not known, solution of the above equations will require that a minimum of three observation wells is used in the test, otherwise the required information can be obtained with only two observation wells. Type curve matching is the first step of the analysis technique. Observed pressure changes at each observation well, i.e., $\Delta p = p_i - p(x, y, t)$, are plotted on log–log paper and matched with the exponential–integral type curve shown in Figure 1.100. The associated specific steps of the methodology of using the type curve in determining the properties of a homogeneous anisotropic reservoir are summarized below:

Step 1. From at least three observation wells, plot the observed pressure change Δp versus time t for each well on the same size scale as the type curve given in Figure 1.100.

Step 2. Match each of the observation well data set to the type curve of Figure 1.100. Select a convenient match point for each data set so that the pressure match point $(\Delta p, p_D)_{MP}$ is the same for all observation well
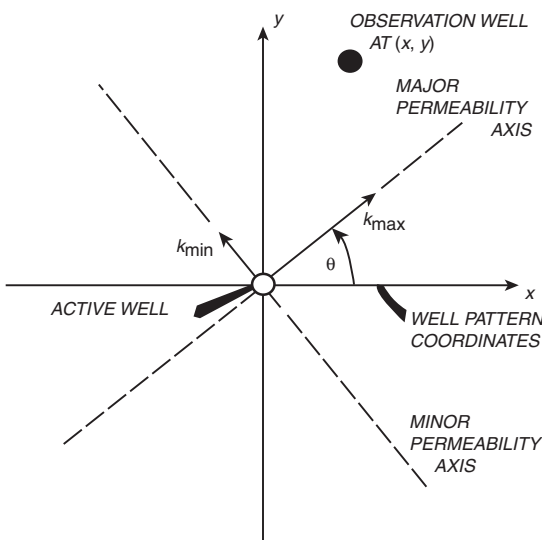
Figure 1.105 *Nomenclature for anisotropic permeability system (After Ramey, 1975).*

responses, while the time match points $(t, t_D/r_D^2)_{MP}$ vary.

Step 3. From the pressure match point $(\Delta p, p_D)_{MP}$, calculate the average system permeability from:

$$\bar{k} = \sqrt{k_{min}k_{max}} = \left[\frac{141.2QB\mu}{h}\right]\left(\frac{p_D}{\Delta p}\right)_{MP} \quad [1.6.11]$$

Notice from Equation 1.6.6 that:

$$(\bar{k})^2 = k_{min}k_{max} = k_x k_y - k_{xy}^2 \quad [1.6.12]$$

Step 4. Assuming *three observation wells*, use the time match $[(t, (t_D/r_D^2)]_{MP}$ for each observation well to write:

Well 1:

$$\left[\frac{(t_D/r_D^2)}{t}\right]_{MP} = \left(\frac{0.0002637}{\phi\mu c_t}\right)$$

$$\times \left(\frac{(\bar{k})^2}{y_1^2 k_x + x_1^2 k_y - 2x_1y_1k_{xy}}\right)$$

Rearranging gives:

$$y_1^2 k_x + x_1^2 k_y - 2x_1y_1k_{xy} = \left(\frac{0.0002637}{\phi\mu c_t}\right)$$

$$\times \left(\frac{(\bar{k})^2}{\left[\frac{(t_D/r_D^2)}{t}\right]_{MP}}\right)$$

$$[1.6.13]$$

Well 2:

$$\left[\frac{(t_D/r_D^2)}{t}\right]_{MP} = \left(\frac{0.0002637}{\phi\mu c_t}\right)$$

$$\times \left(\frac{(\bar{k})^2}{y_2^2 k_x + x_2^2 k_y - 2x_2y_2k_{xy}}\right)$$

$$y_2^2 k_x + x_2^2 k_y - 2x_2y_2k_{xy} = \left(\frac{0.0002637}{\phi\mu c_t}\right)$$

$$\times \left(\frac{(\bar{k})^2}{\left[\frac{(t_D/r_D^2)}{t}\right]_{MP}}\right)$$

$$[1.6.14]$$

Well 3:

$$\left[\frac{(t_D/r_D^2)}{t}\right]_{MP} = \left(\frac{0.0002637}{\phi\mu c_t}\right)$$

$$\times \left(\frac{(\bar{k})^2}{y_3^2 k_x + x_3^2 k_y - 2x_3y_3k_{xy}}\right)$$

$$y_3^2 k_x + x_3^2 k_y - 2x_3y_3k_{xy} = \left(\frac{0.0002637}{\phi\mu c_t}\right)$$

$$\times \left(\frac{(\bar{k})^2}{\left[\frac{(t_D/r_D^2)}{t}\right]_{MP}}\right)$$

$$[1.6.15]$$

Equations 1.6.12 through 1.6.15 contain the following four unknowns:

k_x = permeability in x direction

k_y = permeability in y direction
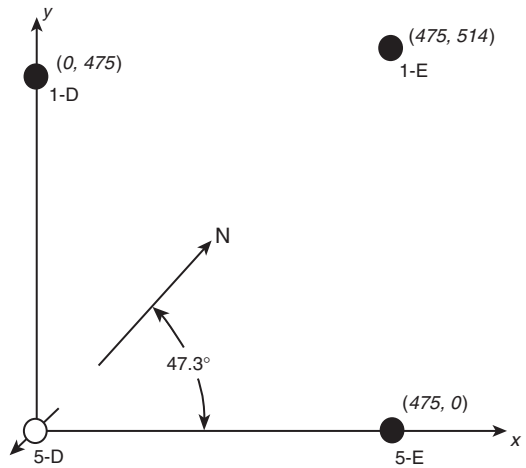
Figure 1.106 Well locations for Example 1.43 (After Earlougher, R. Advances in Well Test Analysis) (Permission to publish by the SPE, copyright SPE, 1977).

k_{xy} = permeability in xy direction

$\phi\mu c_t$ = porosity group

These four equations can be solved simultaneously for the above four unknowns. The following example as given by Ramey (1975) and later by Earlougher (1977) is used to clarify the use of the proposed methodology for determining the properties of an anisotropic reservoir.

Example 1.43   The following data is for an interference test in a nine-spot pattern with one active well and eight observation wells. Before testing, all wells were shut in. The test was conducted by injecting at -115 STB/day and observing the fluid levels in the remaining eight shut-in wells. Figure 1.106 shows the well locations. For simplicity, only the recorded pressure data for three observation wells, as tabulated below, is used to illustrate the methodology. These selected wells are labeled Well 5-E, Well 1-D, and Well 1-E.

Well 1-D		Well 5-E		Well 1-E	
t (hr)	Δp (psi)	t (hr)	Δp (psi)	t (hr)	Δp (psi)
23.5	−6.7	21.0	−4.0	27.5	−3.0
28.5	−7.2	47.0	−11.0	47.0	−5.0
51.0	−15.0	72.0	−16.3	72.0	−11.0
77.0	−20.0	94.0	−21.2	95.0	−13.0
95.0	−25.0	115.0	−22.0	115.0	−16.0
			−25.0		

The well coordinates (x, y) are as follows:

	Well	x (ft)	y (ft)
1	1-D	0	475
2	5-E	475	0
3	1-E	475	514

$i_w = -115$ STB/day, $B_w = 1.0$ bbl/STB, $\mu_w = 1.0$ cp,

$\phi = 20\%$, $T = 75°$ F, $h = 25$ ft,

$c_o = 7.5 \times 10^{-6}$ psi^{-1}, $c_w = 3.3 \times 10^{-6}$ psi^{-1},

$c_f = 3.7 \times 10^{-6}$ psi^{-1}, $r_w = 0.563$ ft, $p_i = 240$ psi

Calculate k_{max}, k_{min}, and their directions relative to the x axis.
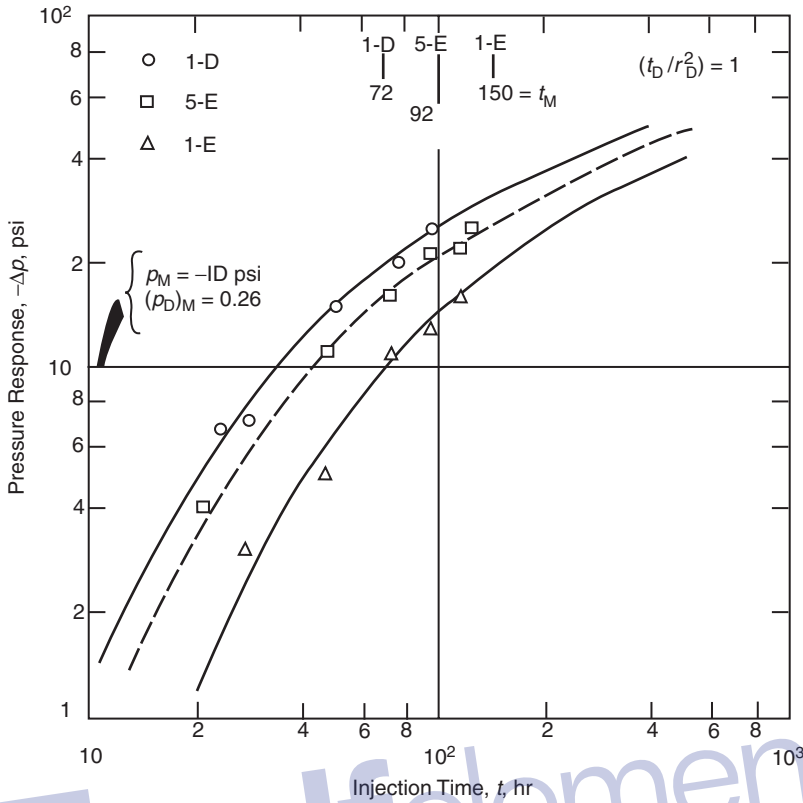
Figure 1.107   *Interference data of Example 1.6 matched to Figure 1.100. Pressure match is the same of all curves. (After Earlougher, R. Advances in Well Test Analysis). (Permission to publish by the SPE, copyright SPE, 1977).*

Solution

Step 1. Plot Δp versus time t for each of the three observation wells on a log–log plot of the same scale as that of Figure 1.100. The resulting plots with the associated match on the type curve are shown in Figure 1.107.

Step 2. Select the same pressure match point on the pressure scale for all the observation wells; however, the match point on the time scale is different for all wells:

Match point	Well 1-D	Well 5-E	Well 1-E
$(p_D)_{MP}$	0.26	0.26	0.26
$(t_D/r_D^2)_{MP}$	1.00	1.00	1.00
$(\Delta p)_{MP}$	−10.00	−10.00	−10.00
$(t)_{MP}$	72.00	92.00	150.00

Step 3. From the pressure match point, use Equation 1.6.11 to solve for $\bar{k}$:

$$\bar{k} = \sqrt{k_{\min}k_{\max}} = \left[\frac{141.2QB\mu}{h}\right]\left(\frac{p_D}{\Delta p}\right)_{MP}$$

$$= \sqrt{k_{\min}k_{\max}} = \left[\frac{141.2(-115)(1.0)(1.0)}{25}\right]\left(\frac{0.26}{-10}\right)$$

$$= 16.89 \text{ md}$$

or:

$$k_{\min}k_{\max} = (16.89)^2 = 285.3$$

Step 4. Using the time match point $(t, t_D/r_D^2)_{MP}$ for each observation well, apply Equations 1.6.13 through 1.6.15 to give:
For Well 1-D with $(x_1, y_1) = (0, 475)$:

$$y_1^2 k_x + x_1^2 k_y - 2x_1 y_1 k_{xy} = \left(\frac{0.0002637}{\phi \mu c_t}\right)$$

$$\times \left(\frac{(\bar{k})^2}{\left[\dfrac{(t_D/r_D^2)}{t}\right]_{MP}}\right)$$

$$(475)^2 k_x + (0)^2 k_y - 2(0)(475)$$

$$= \frac{0.0002637(285.3)}{\phi \mu c_t}\left(\frac{72}{1.0}\right)$$

Simplifying gives:

$$k_x = \frac{2.401 \times 10^{-5}}{\phi \mu c_t} \qquad \text{(A)}$$

For Well 5-E with $(x_2, y_2) = (475, 0)$:

$$(0)^2 k_x + (475)^2 k_y - 2(475)(0)k_{xy}$$

$$= \frac{0.0002637(285.3)}{\phi \mu C_t}\left(\frac{92}{1.0}\right)$$

or:

$$k_y = \frac{3.068 \times 10^{-5}}{\phi \mu c_t} \qquad (B)$$

For Well 1-E with $(x_3, y_3) = (475, 514)$:

$$(514)^2 k_x + (475)^2 k_y - 2(475)(514)k_{xy}$$

$$= \frac{0.0002637(285.3)}{\phi \mu c_t} \left(\frac{150}{1.0}\right)$$

or:

$$0.5411 k_x + 0.4621 k_y - k_{xy} = \frac{2.311 \times 10^{-5}}{\phi \mu c_t} \qquad (C)$$

Step 5. Combine Equations A through C to give:

$$k_{xy} = \frac{4.059 \times 10^{-6}}{\phi \mu c_t} \qquad (D)$$

Step 6. Using Equations A, B, and D in Equation 1.6.12 gives:

$$[k_x k_y] - k_{xy}^2 = (\bar{k})^2$$

$$\left[\frac{(2.401 \times 10^{-5})}{(\phi \mu c_t)} \frac{(3.068 \times 10^{-5})}{(\phi \mu c_t)}\right]$$

$$- \frac{(4.059 \times 10^{-6})^2}{(\phi \mu c_t)} = (16.89)^2 = 285.3$$

or:

$$\phi \mu c_t = \sqrt{\frac{(2.401 \times 10^{-5})(3.068 \times 10^{-5}) - (4.059 \times 10^{-6})^2}{285.3}}$$

$$= 1.589 \times 10^{-6} \text{ cp/psi}$$

Step 7. Solve for c_t:

$$c_t = \frac{1.589 \times 10^{-6}}{(0.20)(1.0)} = 7.95 \times 10^{-6} \text{ psi}^{-1}$$

Step 8. Using the calculated value of $\phi \mu c_t$ from step 6, i.e., $\phi \mu c_t = 1.589 \times 10^{-6}$, in Equations A, B, and D, solve for k_x, k_y, and k_{xy}:

$$k_x = \frac{2.401 \times 10^{-5}}{1.589 \times 10^{-6}} = 15.11 \text{ md}$$

$$k_y = \frac{3.068 \times 10^{-5}}{1.589 \times 10^{-6}} = 19.31 \text{ md}$$

$$k_{xy} = \frac{4.059 \times 10^{-6}}{1.589 \times 10^{-6}} = 2.55 \text{ md}$$

Step 9. Estimate the maximum permeability value by applying Equation 1.6.7, to give:

$$k_{max} = \frac{1}{2}\left[(k_x + k_y) + \sqrt{(k_x k_y)^2 + 4k_{xy}^2}\right]$$

$$= \frac{1}{2}\left[(15.11 + 19.31)\right.$$

$$\left. + \sqrt{(15.11 - 19.31)^2 + 4(2.55)^2}\right] = 20.5 \text{ md}$$

Step 10. Estimate the minimum permeability value by applying Equation 1.6.8:

$$k_{min} = \frac{1}{2}\left[(k_x + k_y)^2 - \sqrt{(k_x k_y)^2 + 4k_{xy}^2}\right]$$

$$= \frac{1}{2}\left[(15.11 + 19.31)\right.$$

$$\left. - \sqrt{(15.11 - 19.31)^2 + 4(2.55)^2}\right] = 13.9 \text{ md}$$

Step 11. Estimate the direction of k_{max} from Equation 1.6.9:

$$\theta_{max} = \arctan\left(\frac{k_{max} - k_x}{k_{xy}}\right)$$

$$= \arctan\left(\frac{20.5 - 15.11}{2.55}\right)$$

$$= 64.7° \text{ as measured from the } +x \text{ axis}$$

1.6.3 Pulse testing in homogeneous isotropic reservoirs

Pulse tests have the same objectives as conventional interference tests, which include:

- estimation of permeability k;
- estimation of porosity–compressibility product ϕc_t;
- whether pressure communication exists between wells.

The tests are conducted by sending a sequence of flow disturbances "pulses" into the reservoir from an active well and monitoring the pressure responses to these signals at shut-in observation wells. The pulse sequence is created by producing from (or injecting into) the active well, then shutting it in, and repeating that sequence in a regular pattern, as depicted by Figure 1.108. The figure is for an active producing well that is pulsed by shutting in, continuing production, and repeating the cycle.

The production (or injection) rate should be the same during each period. The lengths of all production periods and all shut-in periods should be equal; however, production periods do not have to equal shut-in periods. These pulses create a very distinctive pressure response at the observation well which can be easily distinguished from any pre-existing trend in reservoir pressure, or random pressure perturbations "noise," which could otherwise be misinterpreted.

It should be noted that pulse testing offers several advantages over conventional interference tests:

- Because the pulse length used in a pulse test is short, ranging from a few hours to a few days, boundaries seldom affect the test data.
- Because of the distinctive pressure response, there are fewer interpretation problems caused by random "noise" and by trends in reservoir pressure at the observation well.
- Because of shorter test times, pulse tests cause less disruption of normal field operations than interference test.

For each pulse, the pressure response at the observation well is recorded (as illustrated in Figure 1.109) with a very sensitive pressure gauge. In pulse tests, pulse 1 and pulse 2 have characteristics that differ from those of all subsequent pulses. Following these pulses, all odd pulses have similar characteristics and all even pulses also have similar characteristics. Any one of the pulses can be analyzed for k and ϕc_t. Usually, several pulses are analyzed and compared.

Figure 1.109, which depicts the rate history of the active well and the pressure response at an observation well, illustrates the following five parameters which are required for the analysis of a pulse test:

(1) The "pulse period" Δt_p represents the length of the shut-in time.
(2) The "cycle period" Δt_C represents the total time length of a cycle, i.e., the shut-in period plus the flow or injection period.
(3) The "flowing or injection period" Δt_f represents the length of the flow or injection time.
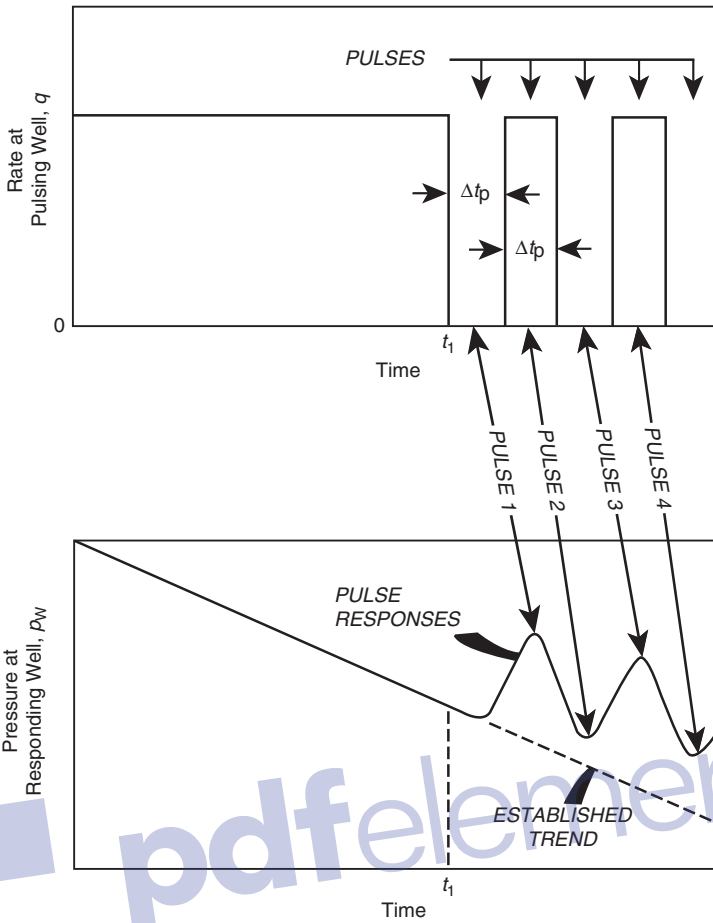
**Figure 1.108** *Schematic illustration of rate (pulse) history and pressure response for a pulse test (After Earlougher, R. Advances in Well Test Analysis) (Permission to publish by the SPE, copyright SPE, 1977).*
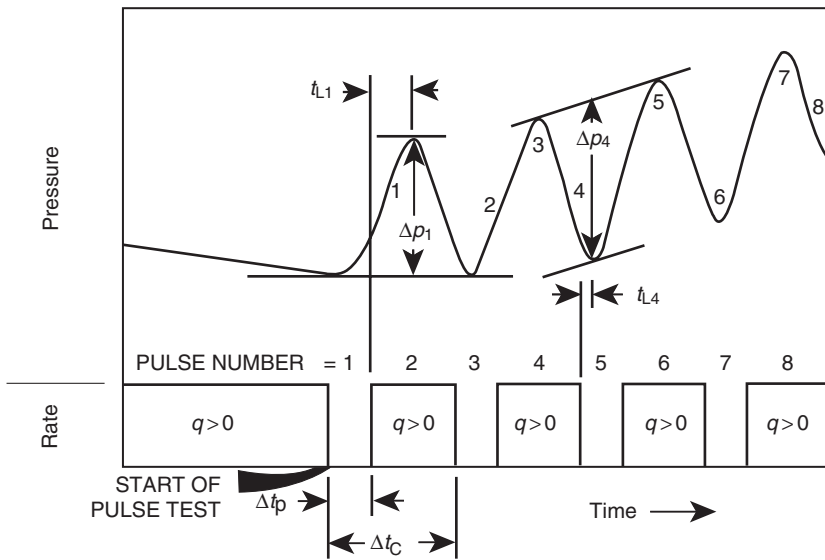
Figure 1.109 *Schematic pulse test rate and pressure history showing definition of time lag (t_L) and pulse response amplitude (Δp) curves. (After Earlougher, R. Advances in Well Test Analysis) (Permission to publish by the SPE, copyright SPE, 1977).*
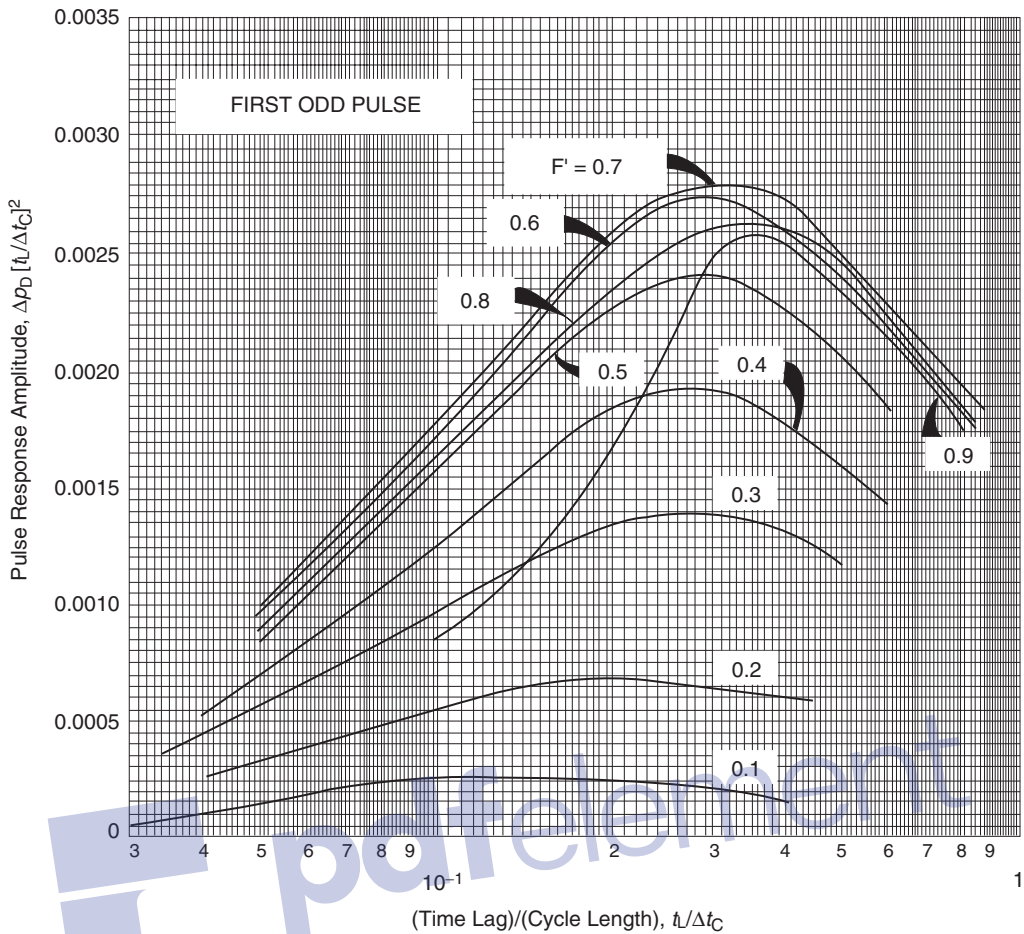
Figure 1.110 *Pulse testing: relation between time lag and response amplitude for first odd pulse. (After Kamal and Brigham, 1976).*

(4) The "time lag" t_L represents the elapsed time between the end of a pulse and the pressure peak caused by the pulse. This time lag t_L is associated with each pulse and essentially describes the time required for a pulse created when the rate is changed to move from the active well to the observation well. It should be pointed out that a flowing (or injecting) period is a "pulse" and a shut-in period is another pulse; the combined two pulses constitute a "cycle."

(5) The "pressure response amplitude" Δp is the vertical distance between two adjacent peaks (or valleys) and a line parallel to this through the valley (or peak), as illustrated in Figure 1.109. Analysis of simulated pulse tests show that pulse 1, i.e., the "first odd pulse," and pulse 2, i.e., the "first even pulse," have characteristics that differ from all subsequent pulses. Beyond these *initial pulses*, all odd pulses have similar characteristics, and all even pulses exhibit similar behavior.

Kamal and Brigham (1975) proposed a pulse test analysis technique that uses the following four dimensionless groups:

(1) Pulse ratio $F^\backslash$, as defined by:

$$F^\backslash = \frac{\text{pulse period}}{\text{cycle period}} = \frac{\Delta t_p}{\Delta t_p + \Delta t_f} = \frac{\Delta t_p}{\Delta t_C} \qquad [1.6.16]$$

where the time is expressed in hours.

(2) Dimensionless time lag $(t_L)_D$, as given by:

$$(t_L)_D = \frac{t_L}{\Delta t_C} \qquad [1.6.17]$$

where:

$\bar{k}$ = average permeability, md

(3) Dimensionless distance (r_D) between the active and observation wells:

$$r_D = \frac{r}{r_w} \qquad [1.6.18]$$

where:

r = distance between the active well and the observation well, ft

(4) Dimensionless pressure response amplitude Δp_D:

$$\Delta p_D = \left[\frac{\bar{k} h}{141.2 B \mu} \frac{\Delta p}{Q} \right] \qquad [1.6.19]$$

where Q is the rate at the active well while it is active, with the sign convention that $\Delta p/Q$ is always positive, i.e., the absolute value of $\left| \Delta p/Q \right|$.

Kamal and Brigham developed a family of curves, as shown in Figures 1.110 through 1.117, that correlates the
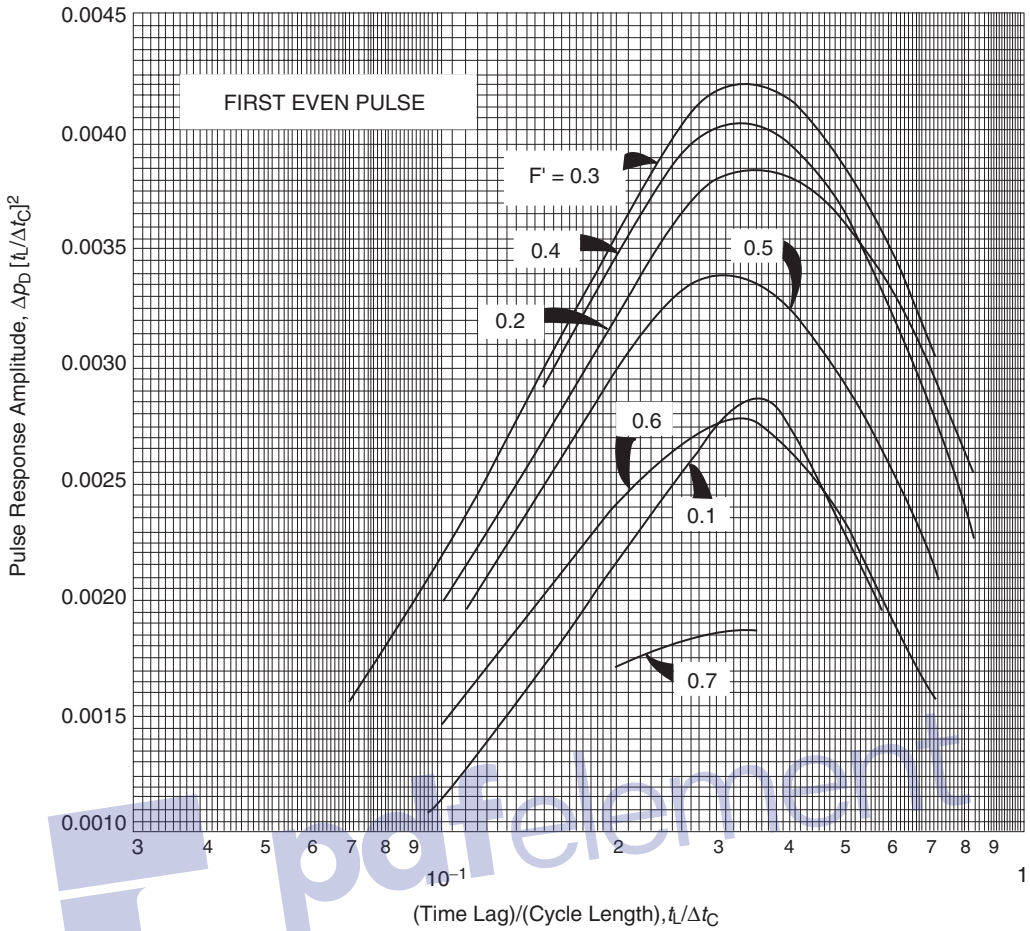
Figure 1.111 *Pulse testing: relation between time lag and response amplitude for first even pulse. (After Kamal and Brigham, 1976).*

pulse ratio $F^{\backslash}$ and the dimensionless time lag $(t_L)_D$ to the dimensionless pressure Δp_D. These curves are specifically designated to analyze the pulse test data for the following conditions:

- *First* odd pulse: Figures 1.110 and 1.114.
- *First* even pulse: Figures 1.111 and 1.115.
- All the *remaining odd pulses* except the first: Figures 1.112 and 1.116.
- All the *remaining even pulses* except the first: Figures 1.113 and 1.117.

The time lag t_L and pressure response amplitude Δp from one or more pulse responses are used to estimate the average reservoir permeability from:

$$\bar{k} = \left[\frac{141.2 QB\mu}{h\Delta p[(t_L)_D]^2}\right]\left[\Delta p_D (t_L/\Delta t_C)^2\right]_{\text{Fig}} \qquad [1.6.20]$$

The term $\left[\Delta p_D (t_L/\Delta t_C)^2\right]_{\text{Fig}}$ is determined from Figures 1.110, 1.111, 1.112, or 1.113 for the appropriate values of $t_L/\Delta t_C$ and $F^{\backslash}$. The other parameters of Equation 1.6.20 are defined below:

Δp = amplitude of the pressure response from the obs-ervation well for the *pulse being analyzed*, psi

Δt_C = cycle length, hours
Q = production (injection) rate during active period, STB/day
$\bar{k}$ = average permeability, md

Once the permeability is estimated from Equation 1.6.20, the porosity–compressibility product can be estimated from:

$$\phi c_t = \left[\frac{0.0002637\bar{k}(t_L)}{\mu r^2}\right]\frac{1}{[(t_L)_D/r_D^2]_{\text{Fig}}} \qquad [1.6.21]$$

where:

t_L = time lag, hours
r = distance between the active well and observation well, ft

The term $\left[(t_L)_D/r_D^2\right]_{\text{Fig}}$ is determined from Figures 1.114, 1.115, 1.116, or 1.117. Again, the appropriate figure to be used in analyzing the pressure response data depends on whether the first-odd or fist-even pulse or one of the remaining pulses is being analyzed.

Example 1.44[a] In a pulse test following rate stabilization, the active well was shut in for 2 hours, then produced for 2 hours, and the sequence was repeated several times.

[a]After John Lee, *Well Testing* (1982).
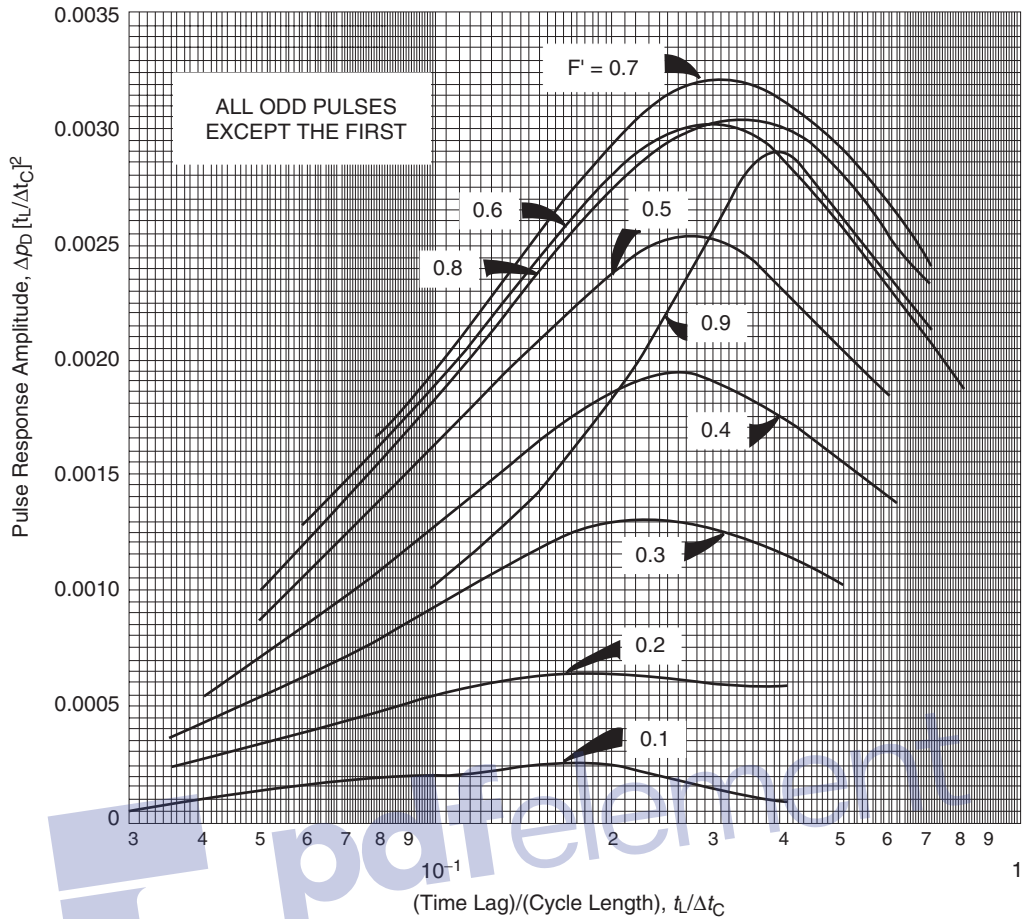
Figure 1.112 *Pulse testing: relation between time lag and response amplitude for all odd pulses after the first. (After Kamal and Brigham, 1976).*

An observation well at 933 ft from the active well recorded an amplitude pressure response of 0.639 psi during the *fourth* pulse and a time lag of 0.4 hours. The following additional data is also available:

$$Q = 425 \text{ STB/day}, \quad B = 1.26 \text{ bbl/STB},$$
$$r = 933 \text{ ft}, \quad h = 26 \text{ ft},$$
$$\mu = 0.8 \text{ cp}, \quad \phi = 0.08$$

Estimate $\bar{k}$ and ϕc_t.

Solution

Step 1. Calculate the pulse ratio $F^\backslash$ from Equation 1.6.16, to give:

$$F^\backslash = \frac{\Delta t_p}{\Delta t_C} = \frac{\Delta t_p}{\Delta t_p + \Delta t_f} = \frac{2}{2+2} = 0.5$$

Step 2. Calculate the dimensionless time lag $(t_L)_D$ by applying Equation 1.6.17:

$$(t_L)_D = \frac{t_L}{\Delta t_C} = \frac{0.4}{4} = 0.1$$

Step 3. Using the values of $(t_L)_D = 0.1$ and $F^\backslash = 0.5$, use Figure 1.113 to get:

$$\left[\Delta p_D (t_L/\Delta t_C)^2\right]_{\text{Fig}} = 0.00221$$

Step 4. Estimate the average permeability from Equation 1.6.20, to give:

$$\bar{k} = \left[\frac{141.2QB\mu}{h\Delta p[(t_L)_D]^2}\right]\left[\Delta p_D(t_L/\Delta t_C)^2\right]_{\text{Fig}}$$

$$= \left[\frac{(141.2)(425)(1.26)(0.8)}{(26)(0.269)[0.1]^2}\right](0.00221) = 817 \text{ md}$$

Step 5. Using $(t_L)_D = 0.1$ and $F^\backslash = 0.5$, use Figure 1.117 to get:

$$\left[(t_L)_D/r_D^2\right]_{\text{Fig}} = 0.091$$

Step 6. Estimate the product ϕc_t by applying Equation 1.6.21

$$\phi c_t = \left[\frac{0.0002637\bar{k}(t_L)}{\mu r^2}\right]\frac{1}{[(t_L)_D/r_D^2]_{\text{Fig}}}$$

$$= \left[\frac{0.0002637(817)(0.4)}{(0.8)(933)^2}\right]\frac{1}{(0.091)}$$

$$= 1.36 \times 10^{-6}$$

Step 7. Estimate c_t as:

$$c_t = \frac{1.36 \times 10^{-6}}{0.08} = 17 \times 10^{-6} \text{ psi}^{-1}$$
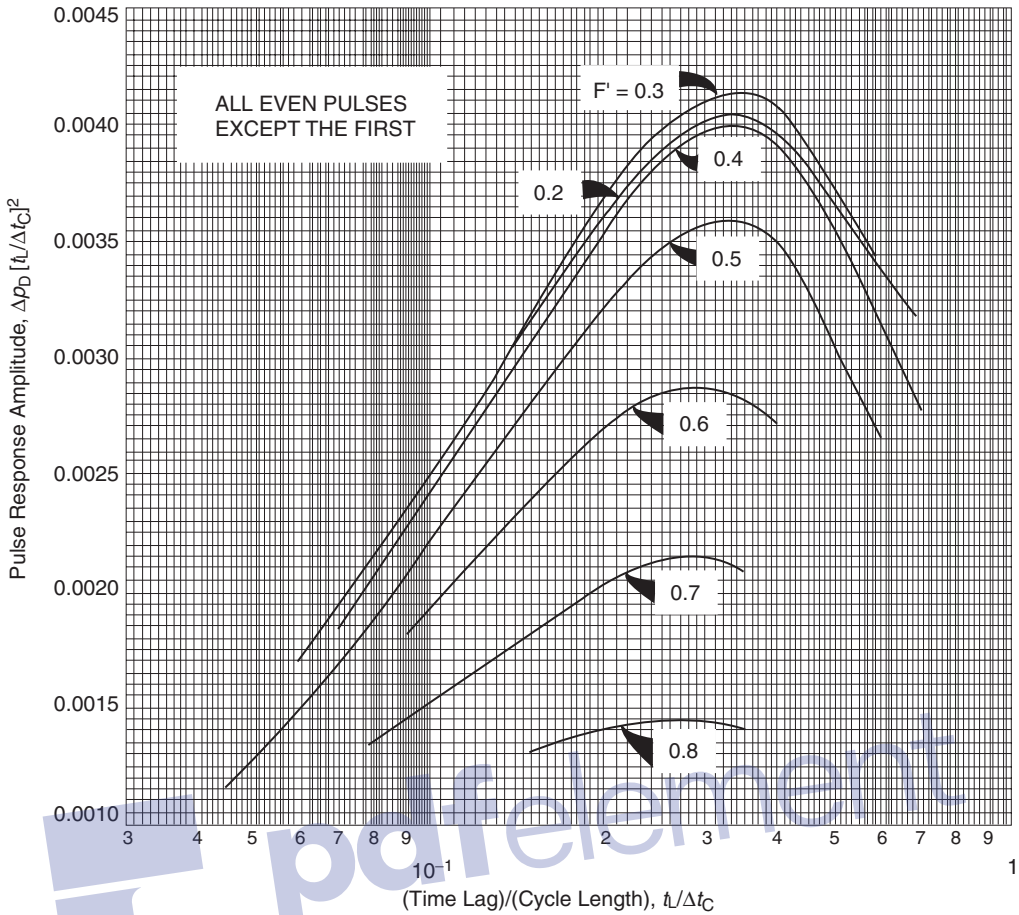
Figure 1.113 *Pulse testing: relation between time lag and response amplitude for all even pulses after the first. (After Kamal and Brigham, 1976).*

Example 1.45[a] A pulse test was conducted using an injection well as the pulsing well in a five-spot pattern with the four offsetting production wells as the responding wells. The reservoir was at its static pressure conditions when the first injection pulse was initiated at 9:40 a.m., with an injection rate of 700 bbl/day. The injection rate was maintained for 3 hours followed by a shut-in period for 3 hours. The injection shut-in periods were repeated several times and the results of pressure observation are given in Table 1.9. The following additional data is available:

$$\mu = 0.87 \text{ cp}, \quad c_t = 9.6 \times 10^{-6} \text{ psi}^{-1},$$

$$\phi = 16\%, \qquad r = 330 \text{ ft}$$

Calculate the permeability and average thickness.

Solution

Step 1. Plot the pressure response from one of the observations well as a function of time, as shown in Figure 1.118.
Analyzing first odd-pulse pressure data

Step 1. From Figure 1.118 determine the amplitude pressure response and time lag during the first pulse,

to give:

$$\Delta p = 6.8 \text{ psi}$$

$$t_L = 0.9 \text{ hour}$$

Step 2. Calculate the pulse ratio F' from Equation 1.6.16, to give:

$$F' = \frac{\Delta t_p}{\Delta t_C} = \frac{3}{3+3} = 0.5$$

Step 3. Calculate the dimensionless time lag $(t_L)_D$ by applying Equation 1.6.17:

$$(t_L)_D = \frac{t_L}{\Delta t_C} = \frac{0.9}{6} = 0.15$$

Step 4. Using the values of $(t_L)_D = 0.15$ and $F' = 0.5$, use Figure 1.110 to get:

$$\left[\Delta p_D (t_L/\Delta t_C)^2\right]_{\text{Fig}} = 0.0025$$

Step 5. Estimate average hk from Equation 1.6.20, to give:

$$h\bar{k} = \left[\frac{141.2QB\mu}{\Delta p[(t_L)_D]^2}\right]\left[\Delta p_D (t_L/\Delta t_C)^2\right]_{\text{Fig}}$$

$$= \left[\frac{(141.2)(700)(1.0)(0.86)}{(6.8)[0.15]^2}\right](0.0025)$$

$$= 1387.9 \text{ md ft}$$

[a]Data reported by H. C. Slider, *Worldwide Practical Petroleum Reservoir Engineering Methods*, Penn Well Books, 1983.
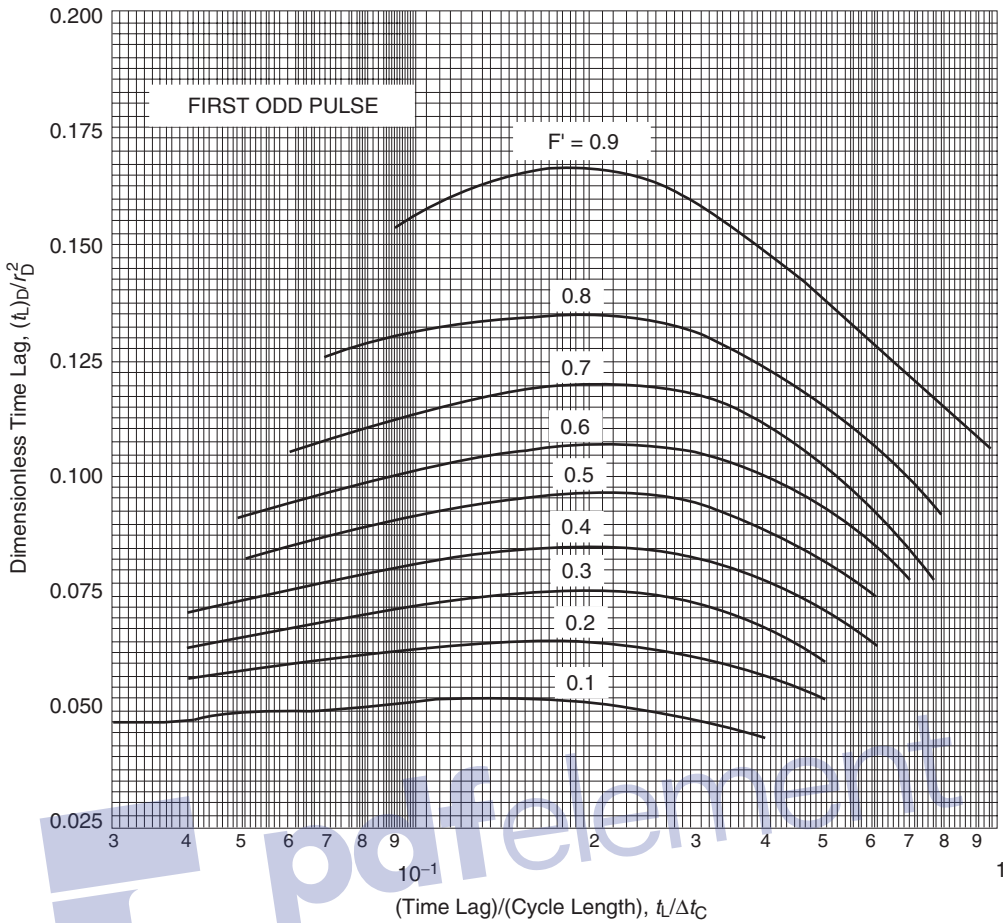
Figure 1.114 *Pulse testing: relation between time lag and cycle length for first odd pulse. (After Kamal and Brigham, 1976).*

Step 6. Using $(t_L)_D = 0.15$ and $F^\backslash = 0.5$, use Figure 1.114 to get:

$$\left[(t_L)_D / r_D^2\right]_{\text{Fig}} = 0.095$$

Step 7. Estimate the average permeability by rearranging Equation 1.6.21 as:

$$\bar{k} = \left[\frac{\phi c_t \mu r^2}{0.0002637(t_L)}\right]\left[(t_L)_D / r_D^2\right]_{\text{Fig}}$$

$$= \left[\frac{(0.16)(9.6 \times 10^{-6})(0.86)(330)^2}{0.0002637(0.9)}\right](0.095)$$

$$= 57.6 \text{ md}$$

Estimate the thickness *h* from the value of the product *hk* as calculated in step 5 and the above average permeability. That is:

$$\bar{k} = \left[\frac{h\bar{k}}{\bar{k}}\right] = \left[\frac{1387.9}{57.6}\right] = 24.1 \text{ ft}$$

Analyzing the fifth pulse pressure data

Step 1. From Figure 1.110 determine the amplitude pressure response and time lag during the fifth pulse, to give:

$$\Delta p = 9.2 \text{ psi}$$

$$t_L = 0.7 \text{ hour}$$

Step 2. Calculate the pulse ratio $F^\backslash$ from Equation 1.6.16 to give:

$$F^\backslash = \frac{\Delta t_p}{\Delta t_C} = \frac{\Delta t_p}{\Delta t_p + \Delta t_f} = \frac{3}{3+3} = 0.5$$

Step 3. Calculate the dimensionless time lag $(t_L)_D$ by applying Equation 1.6.17:

$$(t_L)_D = \frac{t_L}{\Delta t_C} = \frac{0.7}{6} = 0.117$$

Step 4. Using the values of $(t_L)_D = 0.117$ and $F^\backslash = 0.5$, use Figure 1.111 to get:

$$\left[\Delta p_D (t_L / \Delta t_C)^2\right]_{\text{Fig}} = 0.0018$$

Step 5. Estimate average *hk* from equation 1.6.20, to give:

$$h\bar{k} = \left[\frac{141.2 QB\mu}{\Delta p[(t_L)_D]^2}\right]\left[\Delta p_D (t_L / \Delta t_C)^2\right]_{\text{Fig}}$$

$$= \left[\frac{(141.2)(700)(1.0)(0.86)}{(9.2)[0.117]^2}\right](0.0018)$$

$$= 1213 \text{ md ft}$$

Step 6. Using $(t_L)_D = 0.117$ and $F^\backslash = 0.5$, use Figure 1.115 to get:

$$\left[(t_L)_D / r_D^2\right]_{\text{Fig}} = 0.093$$
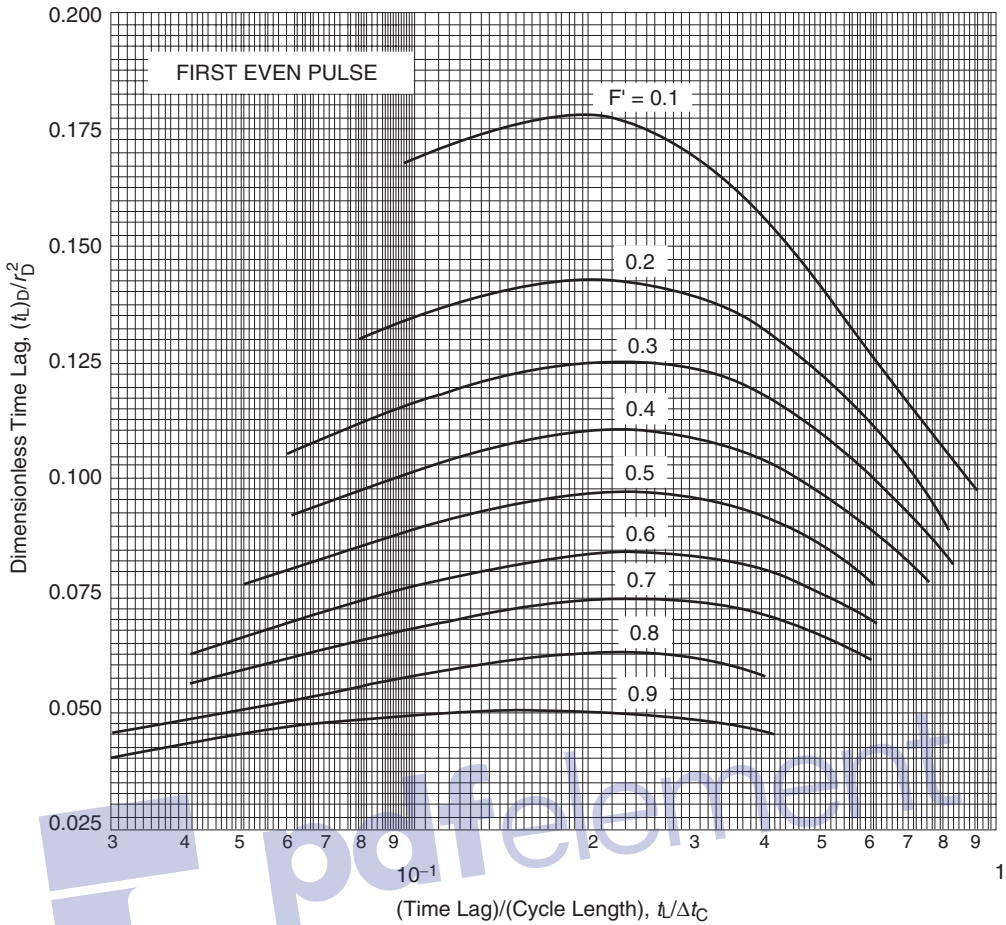
Figure 1.115 *Pulse testing: relation between time lag and cycle length for first even pulse. (After Kamal and Brigham, 1976).*

Step 7. Estimate the average permeability by rearranging Equation 1.6.21 as:

$$\overline{k} = \left[\frac{\phi c_t \mu r^2}{0.0002637(t_L)} \right] [(t_L)_D / r_D^2]_{Fig}$$

$$= \left[\frac{(0.16)(9.6 \times 10^{-6})(0.86)(330)^2}{0.0002637(0.7)} \right] (0.095)$$

$$= 72.5 \text{ md}$$

Estimate the thickness h from the value of the product hk as calculated in step 5 and the above average permeability. That is:

$$\overline{k} = \left[\frac{h\overline{k}}{\overline{k}} \right] = \left[\frac{1213}{72.5} \right] = 16.7 \text{ ft}$$

The above calculations should be repeated for all other pulses and the results should be compared with core and conventional well testing analysis to determine the best values that describe these properties.

1.6.4 Pulse testing in homogeneous anisotropic reservoirs

The analysis for the pulse test case is the same as that for the homogeneous isotropic case, except the average permeability $\overline{k}$ as defined by Equation 1.6.6 is introduced into 1.6.20 and 1.6.21, to give:

$$\overline{k} = \sqrt{k_x k_y - k_{xy}^2} = \left[\frac{141.2QB\mu}{h\Delta p[(t_L)_D]^2} \right] \left[\Delta p_D (t_L/\Delta t_C)^2 \right]_{Fig}$$
[1.6.22]

and:

$$\phi c_t = \left[\frac{0.0002637(t_L)}{\mu r^2} \right] \left[\frac{(\overline{k})^2}{y^2 k_x + x^2 k_y - 2xyk_{xy}} \right]$$

$$\times \frac{1}{\left[(t_L)_D / r_D^2 \right]_{Fig}}$$
[1.6.23]

The solution methodology outlined in analyzing interference test data in homogeneous anisotropic reservoirs can be employed when estimating various permeability parameters from pulse testing.

1.6.5 Pulse test design procedure

Prior knowledge of the expected pressure response is important so that the range and sensitivity of the pressure gauge
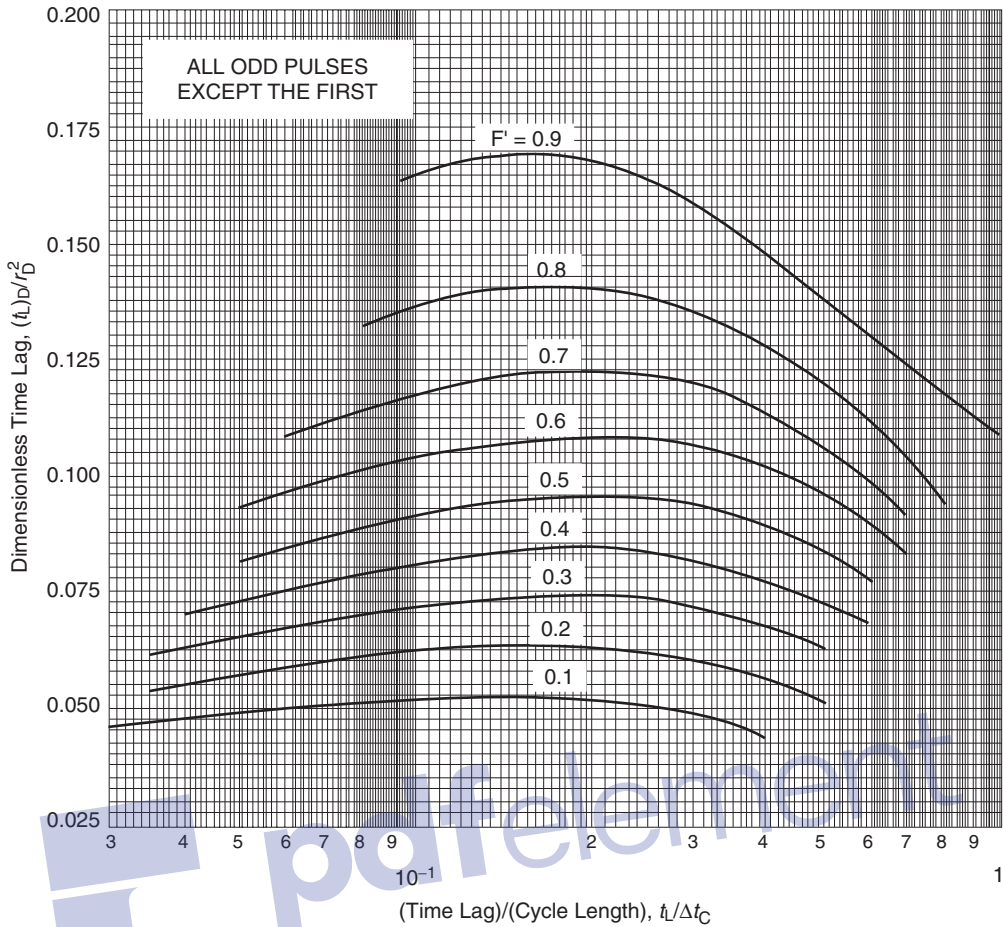
Figure 1.116 Pulse testing: relation between time lag and cycle length for all odd pulses after the first. (After Kamal and Brigham, 1976).

and length of time needed for the test can be predetermined. To design a pulse test, Kamal and Brigham (1975) recommend the following procedure:

Step 1. The first step in designing a pulse test is to select the appropriate pulse ratio $F^\backslash$ as defined by Equation 1.6.16, i.e., pulse ratio = pulse period/cycle period. A pulse ratio near 0.7 is recommended if analyzing the odd pulses; and near 0.3 if analyzing the even pulses. It should be noted the $F^\backslash$ should not exceed 0.8 or drop below 0.2.

Step 2. Calculate the dimensionless time lag from one of the following approximations:

For odd pulses $\quad (t_L)_D = 0.09 + 0.3 F^\backslash \qquad$ [1.6.24]

For even pulses $\quad (t_L)_D = 0.027 - 0.027 F^\backslash$

[1.6.25]

Step 3. Using the values of $F^\backslash$ and $(t_L)_D$ from step 1 and step 2 respectively, determine the dimensionless parameter $\left[(t_L)_D / r_D^2\right]$ from Figure 1.114 or Figure 1.115.

Step 4. Using the values of $F^\backslash$ and $(t_L)_D$, determine the dimensionless response amplitude $\left[\Delta p_D (t_L/\Delta t_C)^2\right]_{\text{Fig}}$ from the appropriate curve in Figure 1.110 or Figure 1.111.

Step 5. Using the following parameters:

- estimates of k, h, ϕ, μ, and c_t,
- values of $\left\lfloor (t_L)_D / r_D^2 \right\rfloor_{\text{Fig}}$ and $\left[\Delta p_D (t_L/\Delta t_C)^2\right]_{\text{Fig}}$ from step 3 and 4, and
- Equations 1.6.1 and 1.6.2

calculate the cycle period (Δt_C) and the response amplitude Δp from:

$$t_L = \left[\frac{\phi \mu c_t r^2}{0.0002637 \bar{k}}\right] \left[(t_L)_D / r_D^2\right]_{\text{Fig}} \qquad [1.6.26]$$

$$\Delta t_C = \frac{t_L}{(t_L)_D} \qquad [1.6.27]$$

$$\Delta p = \left[\frac{141.2 Q B \mu}{h \bar{k} \left[(t_L)_D\right]^2}\right] \left[\Delta p_D (t_L/\Delta t_C)^2\right]_{\text{Fig}} \qquad [1.6.28]$$

Step 6. Using the pulse ratio $F^\backslash$ and cycle period Δt_C, calculate the pulsing (shut-in) period and flow period from:

Pulse (shut-in) period $\quad \Delta t_p = F^\backslash \Delta t_C$

Flow period $\quad \Delta t_f = \Delta t_C - \Delta t_p$
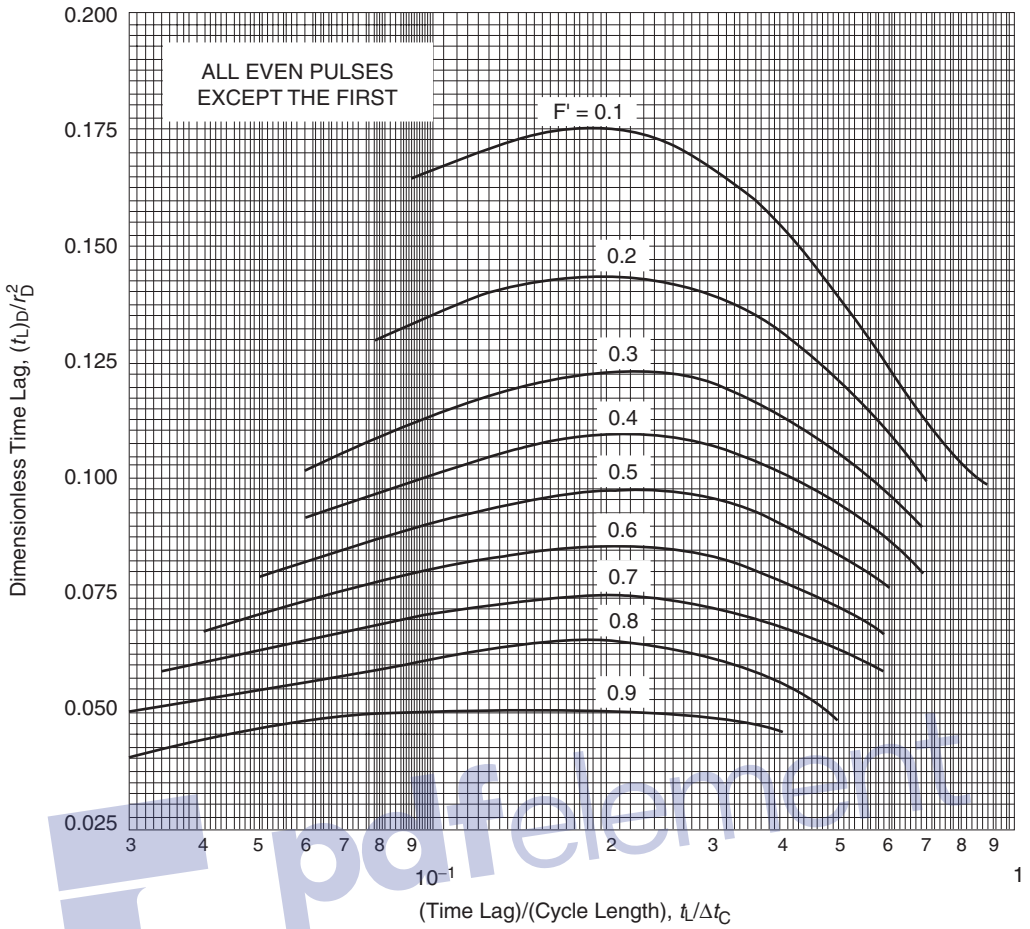
Figure 1.117 *Pulse testing: relation between time lag and cycle length for all even pulses after the first. (After Kamal and Brigham, 1976).*

Table 1.9 *Pressure behaviour of producing Well. After Slider, H. C., Worldwide Practical Petroleum Reservoir Engineering Methods, copyright ©1983, Penn Well Publishing*

Time	Pressure (psig)	Time	Pressure (psig)	Time	Pressure (psig)
9:40 a.m	390.1	2:23 p.m.	411.6	11:22 p.m.	425.1
10:10 a.m.	390.6	2:30 p.m.	411.6	12:13 a.m.	429.3
10:30 a.m.	392.0	2:45 p.m.	411.4	12:40 a.m.	431.3
10:40 a.m.	393.0	3:02 p.m.	411.3	1:21 a.m.	433.9
10:48 a.m.	393.8	3:30 p.m.	411.0	1:53 a.m.	433.6
11:05 a.m.	395.8	4:05 p.m	410.8	2:35 a.m.	432.0
11:15 a.m.	396.8	4:30 p.m.	412.0	3:15 a.m.	430.2
11:30 a.m.	398.6	5:00 p.m.	413.2	3:55 a.m.	428.5
11:45 a.m.	400.7	5:35 p.m.	416.4	4:32 a.m.	428.8
12:15 p.m.	403.8	6:00 p.m.	418.9	5:08 a.m.	430.6
12:30 p.m.	405.8	6:35 p.m.	422.3	5:53 a.m.	434.5
12:47 p.m.	407.8	7:05 p.m.	424.6	6:30 a.m.	437.4
1:00 p.m.	409.1	7:33 p.m.	425.3	6:58 a.m.	440.3
1:20 p.m.	410.7	7:59 p.m.	425.1	7:30 a.m.	440.9
1:32 p,m.	411.3	8:31 p.m.	423.9	7:58 a.m.	440.7
1:45 p.m.	411.7	9:01 p,m,	423.1	8:28 a.m.	439.6
2:00 p.m.	411.9	9:38 p.m.	421.8	8:57 a.m.	438.6
2:15 p.m.	411.9	10:26 p.m.	421.4	9:45 a.m.	437.0
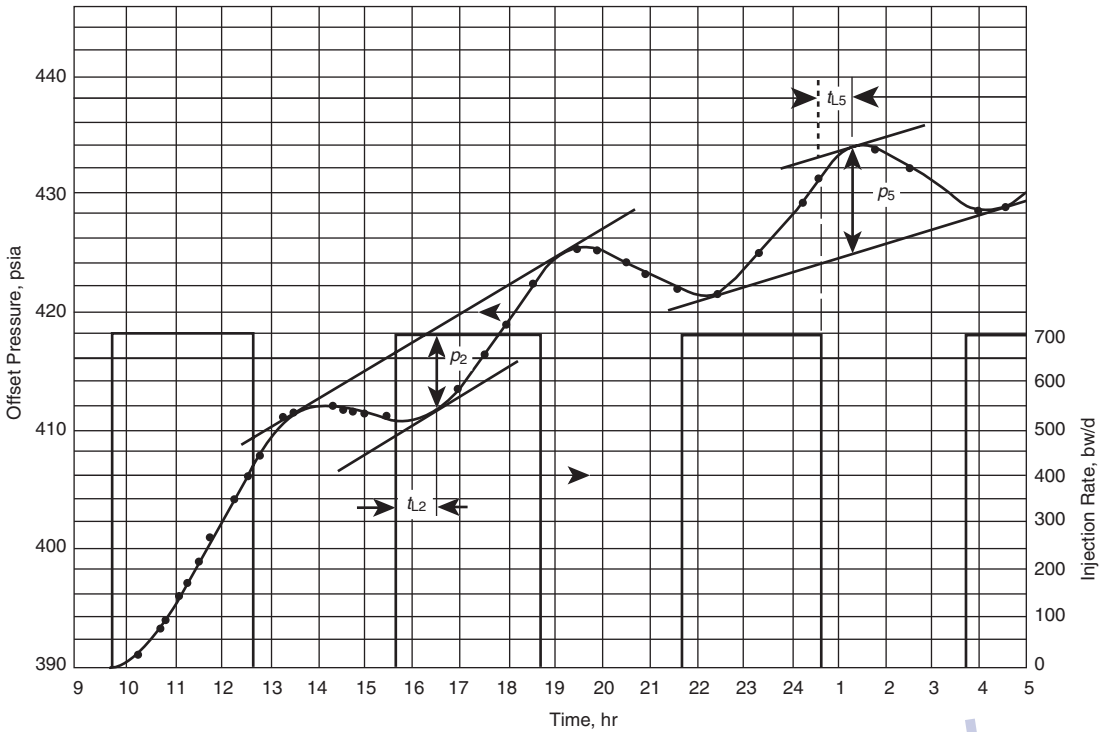
Figure 1.118   *Pulse pressure response for Example 1.45.*

Example 1.46   Design a pulse test using the following approximate properties:

$$\mu = 3 \text{ cp}, \quad \phi = 0.18, \quad k = 200 \text{ md}$$

$$h = 25 \text{ ft}, \quad r = 600 \text{ ft}, \quad c_t = 10 \times 10^{-6} \text{ psi}^{-1}$$

$$B = 1 \text{ bbl/STB}, \quad Q = 100 \text{ bbl/day}, \quad F^\backslash = 0.6$$

Solution

Step 1. Calculate $(t_L)_D$ from Equation 1.6.24 or 1.6.25. Since $F^\backslash$ is 0.6, the odd pulses should be used and therefore from Equation 1.6.24:

$$(t_L)_D = 0.09 + 0.3(0.6) = 0.27$$

Step 2. Selecting the first odd pulse, determine the dimensionless cycle period from Figure 1.114 to get:

$$\left[(t_L)_D / r_D^2\right]_{\text{Fig}} = 0.106$$

Step 3. Determine the dimensionless response amplitude from Figure 1.110 to get:

$$\left[\Delta p_D (t_L/\Delta t_C)^2\right]_{\text{Fig}} = 0.00275$$

Step 4. Solve for t_L, Δt_C, and Δp by applying Equations 1.6.26 through 1.6.28, to give:
   Time lag:

$$t_L = \left[\frac{\phi \mu C_t r^2}{0.0002637 \bar{k}}\right] \left[(t_L)_D / r_D^2\right]_{\text{Fig}}$$

$$= \left[\frac{(0.18)(3)(10 \times 10^{-6})(660)^2}{(0.0002637)(200)}\right](0.106)$$

$$= 4.7 \text{ hours}$$

Cycle time:

$$\Delta t_C = \frac{t_L}{(t_L)_D} = \frac{4.7}{0.27} = 17.5 \text{ hours}$$

Pulse length (shut-in):

$$\Delta t_P = \Delta t_C F^\backslash = (17.5)(0.27) \approx 5 \text{ hours}$$

Flow period:

$$\Delta t_f = \Delta t_C - \Delta t_P = 17.5 - 4.7 \approx 13 \text{ hours}$$

Step 5. Estimate the pressure response from Equation 1.6.28:

$$\Delta p = \left[\frac{141.2 Q B \mu}{h \bar{k} \left[(t_L)_D\right]^2}\right] \left[\Delta p_D (t_L/\Delta t_C)^2\right]_{\text{Fig}}$$

$$= \left[\frac{(141.2)(100)(1)(3)}{(25)(200)(0.27)^2}\right](0.00275) = 0.32 \text{ psi}$$

This is the expected response amplitude for *odd-pulse* analysis. We shut in the well for 5 hours and produced for 13 hours and repeated each cycle with a period of 18 hours.

The above calculations can be repeated if we desire to analyze the first even-pulse response.

1.7 Injection Well Testing

Injectivity testing is a pressure transient test during injection into a well. Injection well testing and the associated analysis are essentially simple, as long as the mobility ratio between the injected fluid and the reservoir fluid is unity. Earlougher (1977) pointed out that the unit-mobility ratio is a reasonable approximation for many reservoirs under water floods. The objectives of injection tests are similar to those

of production tests, namely the determination of:

- permeability;
- skin;
- average pressure;
- reservoir heterogeneity;
- front tracking.

Injection well testing involves the application of one or more of the following approaches:

- injectivity test;
- pressure falloff test;
- step-rate injectivity test.

The above three analyses of injection well testing are briefly presented below.

1.7.1 Injectivity test analysis

In an injectivity test, the well is shut in until the pressure is stabilized at initial reservoir pressure p_i. At this time, the injection begins at a constant rate q_{inj}, as schematically illustrated in Figure 1.119, while recording the bottom-hole pressure p_{wf}. For a unit-mobility ratio system, the injectivity test would be identical to a pressure drawdown test except that the constant rate is negative with a value of q_{inj}. However, in all the preceding relationships, the injection rate will be treated as a positive value, i.e., $q_{inj} > 0$.

For a constant injection rate, the bottom-hole pressure is given by the linear form of Equation 1.3.1 as:

$$p_{wf} = p_{1\,hr} + m \log(t) \qquad [1.7.1]$$

The above relationship indicates that a plot of bottom-hole injection pressure versus the logarithm of injection time would produce a straight-line section as shown in Figure 1.119, with an intercept of $p_{1\,hr}$ and a slope m as defined by:

$$m = \frac{162.6 q_{inj} B \mu}{kh}$$

where:

q_{inj} = absolute value of injection rate, STB/day
m = slope, psi/cycle
k = permeability, md
h = thickness, ft
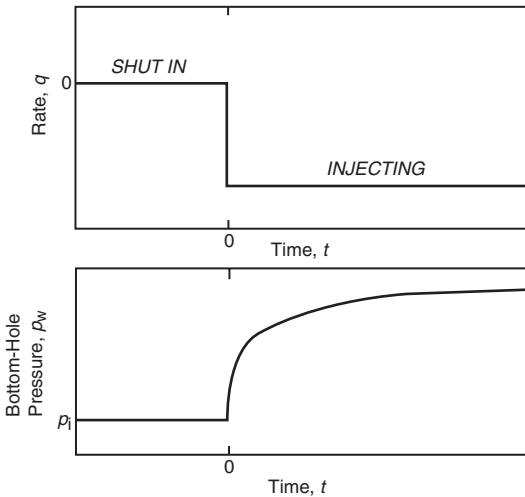
Figure 1.119 *Idealized rate schedule and pressure response for injectivity testing.*

Sabet (1991) pointed out that, depending on whether the density of the injected fluid is higher or lower than the reservoir fluid, the injected fluid will tend to override or underride the reservoir fluid and, therefore the net pay h which should be used in interpreting injectivity tests would not be the same as the net pay which is used in interpreting drawdown tests.

Earlougher (1977) pointed out that, as in drawdown testing, the wellbore storage has great effects on the recorded injectivity test data due to the expected large value of the wellbore storage coefficient. Earlougher recommended that all injectivity test analyses must include the log–log plot of $(p_{wf} - p_i)$ versus injection time with the objective of determining the duration of the wellbore storage effects. As defined previously, the beginning of the semilog straight line, i.e., the end of the wellbore storage effects, can be estimated from the following expression:

$$t > \frac{(200\,000 + 12\,000s)C}{kh/\mu} \qquad [1.7.2]$$

where:

t = time that marks the end of wellbore storage effects, hours
k = permeability, md
s = skin factor
C = wellbore storage coefficient, bbl/psi
μ = viscosity, cp

Once the semilog straight line is identified, the permeability and skin can be determined as outlined previously by:

$$k = \frac{162.6 q_{inj} B \mu}{mh} \qquad [1.7.3]$$

$$s = 1.1513 \left[\frac{p_{1\,hr} - p_i}{m} - \log\left(\frac{k}{\phi \mu c_t r_w^2} \right) + 3.2275 \right] \qquad [1.7.4]$$

The above relationships are valid as long as the mobility ratio is approximately equal to 1. If the reservoir is under water flood and a water injection well is used for the injectivity test, the following steps summarize the procedure of analyzing the test data assuming a unit-mobility ratio:

Step 1. Plot $(p_{wf} - p_i)$ versus injection time on a log–log scale.
Step 2. Determine the time at which the unit-slope line, i.e., 45° line, ends.
Step 3. Move $1\frac{1}{2}$ log cycles ahead of the observed time in step 2 and read the corresponding time which marks the start of the semilog straight line.
Step 4. Estimate the wellbore storage coefficient C by selecting any point on the unit-slope line and reading its coordinates, i.e., Δp and t, and applying the following expression:

$$C = \frac{q_{inj} B t}{24 \Delta p} \qquad [1.7.5]$$

Step 5. Plot p_{wf} vs. t on a semilog scale and determine the slope m of the straight line that represents the transient flow condition.
Step 6. Calculate the permeability k and skin factor from Equations 1.7.3 and 1.7.4 respectively.
Step 7. Calculate the radius of investigation r_{inv} at the end of injection time. That is:

$$r_{inv} = 0.0359 \sqrt{\frac{kt}{\phi \mu c_t}} \qquad [1.7.6]$$

Step 8. Estimate the radius to the leading edge of the water bank r_{wb} before the initiation of the injectivity
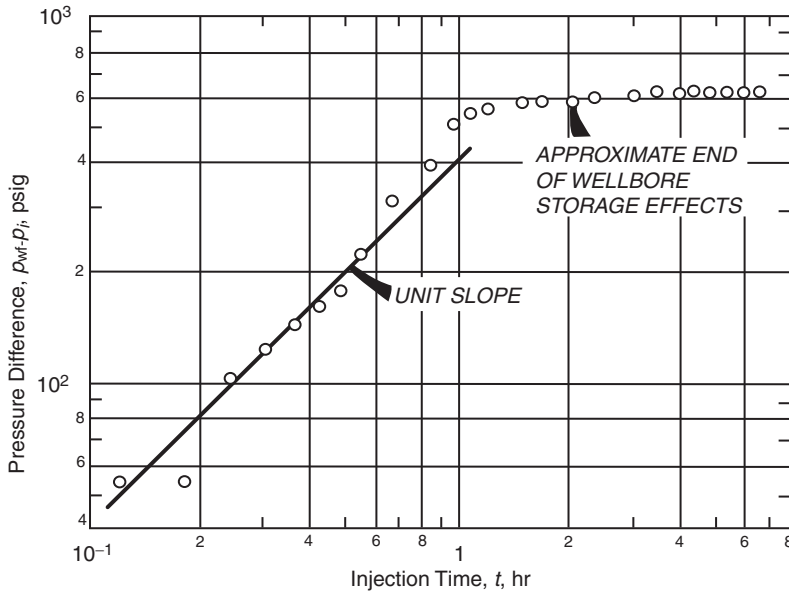
Figure 1.120 *Log–log data plot for the injectivity test of Example 1.47. Water injection into a reservoir at static conditions (After Earlougher, R. Advances in Well Test Analysis) (Permission to publish by the SPE, copyright SPE, 1977).*

test from:

$$r_{wb} = \sqrt{\frac{5.615W_{inj}}{\pi h \phi (\overline{S}_w - S_{wi})}} = \sqrt{\frac{5.615W_{inj}}{\pi h \phi (\Delta S_w)}} \quad [1.7.7]$$

where:

r_{wb} = radius to the water bank, ft
W_{inj} = cumulative water injected at the start of the test, bbl
$\overline{S}_w$ = average water saturation at the start of the test
s_{wi} = initial water saturation

Step 9. Compare r_{wb} with r_{inv}: if $r_{inv} < r_{wb}$, the unit-mobility ratio assumption is justified.

Example 1.47[a] Figures 1.120 and 1.121 show pressure response data for a 7 hour injectivity test in a water-flooded reservoir in terms of $\log(p_{wf} - p_i)$ vs. $\log(t)$ and $\log(p_{wf})$ vs. $\log(t)$ respectively. Before the test, the reservoir had been under water flood for 2 years with a constant injection rate of 100 STB/day. The injectivity test was initiated after shutting in all wells for several weeks to stabilize the pressure at p_i. The following data is available:

$c_t = 6.67 \times 10^{-6}$ psi^{-1}

$B = 1.0$ bbl/STB, $\mu = 1.0$ cp

$S_w = 62.4$ lb/ft^3, $\phi = 0.15$, $q_{inj} = 100$ STB/day

$h = 16$ ft, $r_w = 0.25$ ft, $p_i = 194$ psig

$\Delta S_w = 0.4$,   depth $= 1002$ ft,   total test time $= 7$ hours

The well is completed with 2 inch tubing set on a packer. Estimate the reservoir permeability and skin factor.

[a]After Robert Earlougher, *Advances in Well Test Analysis*, 1977.

Solution

Step 1. The log–log data plot of Figure 1.120 indicates that the data begins to deviate from the unit-slope line at about 0.55 hours. Using the rule of thumb of moving 1 to $1\frac{1}{2}$ cycles in time after the data starts deviating from the unit-slope line, suggests that the start of the semilog straight line begins after 5 to 10 hours of testing. However, Figures 1.120 and 1.121 clearly show that the wellbore storage effects have ended after 2 to 3 hours.

Step 2. From the unit-slope portion of Figure 1.120, select the coordinates of a point (i.e., Δp and t) end calculate the wellbore storage coefficient C by applying Equation 1.7.5:

$$\Delta p = 408 \text{ psig}$$

$$t = 1 \text{ hour}$$

$$C = \frac{q_{inj}Bt}{24\Delta p}$$

$$= \frac{(100)(1.0)(1)}{(24)(408)} = 0.0102 \text{ bbl/psi}$$

Step 3. From the semilog plot in Figure 1.121, determine the slope of the straight line m to give:

$$m = 770 \text{ psig/cycle}$$

Step 4. Calculate the permeability and skin factor by using Equations 1.7.3 and 1.7.4:

$$k = \frac{162.6q_{inj}B\mu}{mh}$$

$$= \frac{(162.6)(100)(1.0)(1.0)}{(80)(16)} - 12.7 \text{ md}$$

Figure 1.121 *Semilog plot for the injectivity test of Example 1.47. Water injection into a reservoir at static conditions (After Earlougher, R. Advances in Well Test Analysis) (Permission to publish by the SPE, copyright SPE, 1977).*

$$s = 1.1513 \left[\frac{p_{1\,hr} - p_i}{m} - \log\left(\frac{k}{\phi \mu c_t r_w^2} \right) + 3.2275 \right]$$

$$= 1.1513 \left[\frac{770 - 194}{80} \right.$$

$$- \log \left(\frac{12.7}{(0.15)(1.0)(6.67 \times 10^{-6})(0.25)^2} \right)$$

$$\left. + 3.2275 \right] = 2.4$$

Step 5. Calculate the radius of investigation after 7 hours by applying Equation 1.7.6:

$$r_{inv} = 0.0359 \sqrt{\frac{kt}{\phi \mu c_t}}$$

$$= 0.0359 \sqrt{\frac{(12.7)(7)}{(0.15)(1.0)(6.67 \times 10^{-6})}} \simeq 338\ \text{ft}$$

Step 6. Estimate the distance of the leading edge of the water bank before the start of the test from Equation 1.7.7:

$$W_{inj} \cong (2)(365)(100)(1.0) = 73\,000\ \text{bbl}$$

$$r_{wb} = \sqrt{\frac{5.615 W_{inj}}{\pi h \phi (\Delta S_w)}}$$

$$= \sqrt{\frac{(5.615)(73\,000)}{\pi (16)(0.15)(0.4)}} \cong 369\ \text{ft}$$

Since $r_{inv} < r_{wb}$, the use of the unit-mobility ratio analysis is justified.

1.7.2 Pressure falloff test

A pressure falloff test is usually preceded by an injectivity test of a long duration. As illustrated schematically in Figure 1.122, falloff testing is analogous to pressure buildup testing in a production well. After the injectivity test that lasted for a total injection time of t_p at a constant injection
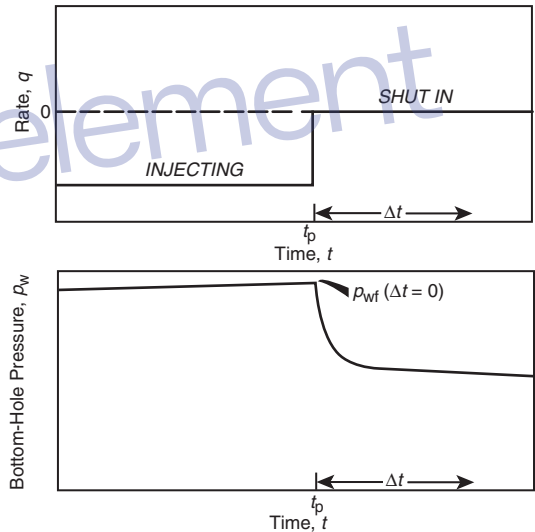
Figure 1.122 *Idealized rate schedule and pressure response for falloff testing.*

rate of q_{inj}, the well is then shut in. The pressure data taken immediately before and during the shut in period is analyzed by the Horner plot method.

The recorded pressure falloff data can be represented by Equation 1.3.11, as:

$$p_{ws} = p^* + m \left[\log\left(\frac{t_p + \Delta t}{\Delta t} \right) \right]$$

with:

$$m = \left| \frac{162.6 q_{inj} B \mu}{kh} \right|$$

where p^* is the false pressure that is only equal to the initial (original) reservoir pressure in a newly discovered field. As
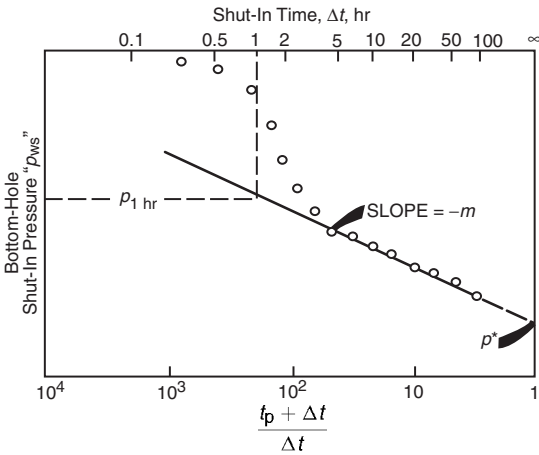
Figure 1.123 Horner plot of a typical falloff test.

shown in Figure 1.123, a plot of p_{ws} vs. $\log\left[(t_p + \Delta t)/\Delta t\right]$ would form a straight-line portion with an intercept of p^* at $(t_p + \Delta t)/\Delta t = 1$ and a negative slope of m.

It should be pointed out that the log–log data plot should be constructed to identify the end of the wellbore storage effects and beginning of the proper semilog straight line. The permeability and skin factor can be estimated as outlined previously by the expressions:

$$k = \frac{162.6 q_{inj} B \mu}{|m| h}$$

$$s = 1.513 \left[\frac{p_{wf\ at\ \Delta t=0} - p_{1\ hr}}{|m|} - \log\left(\frac{k}{\phi \mu c_t r_w^2}\right) + 3.2275 \right]$$

Earlougher (1977) indicated that if the injection rate varies before the falloff test, the equivalent injection time may be approximated by:

$$t_p = \frac{24 W_{inj}}{q_{inj}}$$

where W_{inj} is the cumulative volume injected since the last pressure equalization, i.e., last shut-in, and q_{inj} is the injection rate just before shut-in.

It is not uncommon for a falloff test to experience a change in wellbore storage after the test begins at the end of the injectivity test. This will occur in any well which goes on vacuum during the test. An injection well will go on vacuum when the bottom-hole pressure decreases to a value which is insufficient to support a column of water to the surface. Prior to going on vacuum, an injection well will experience storage due to water expansion; after going on vacuum, the storage will be due to a falling fluid level. This change in storage will generally exhibit itself as a decrease in the rate of pressure decline.

The falloff data can also be expressed in graphical form by plotting p_{ws} vs. $\log(\Delta t)$ as proposed by MDH (Miller–Dyes–Hutchinson). The mathematical expression for estimating the false pressure p^* from the MDH analysis is given by Equation 1.3.12 as:

$$p* = p_{1\ hr} - |m| \log(t_p + 1) \qquad [1.7.8]$$

Earlougher pointed out that the MDH plot is more practical to use unless t_p is less than about twice the shut-in time.

The following example, as adopted from the work of McLeod and Coulter (1969) and Earlougher (1977), is used to illustrate the methodology of analyzing the falloff pressure data.

Example 1.48[a]   During a stimulation treatment, brine was injected into a well and the falloff data, as reported by McLeod and Coulter (1969), is shown graphically in Figures 1.124 through 1.126. Other available data includes:

total injection time $t_p = 6.82$ hours,
total falloff time $= 0.67$ hours
$q_{inj} = 807$ STB/day, $B_w = 1.0$ bbl/STB,
$c_w = 3.0 \times 10^{-6}$ psi^{-1}
$\phi = 0.25$, $h = 28$ ft, $\mu_w = 1.0$ cp
$c_t = 1.0 \times 10^{-5}$ psi^{-1}, $r_w = 0.4$ ft, $S_w = 67.46$ lb/ft^3
depth $= 4819$ ft,
hydrostatic fluid gradient $= 0.4685$ psi/ft

The recorded shut-in pressures are expressed in terms of *wellhead pressures* p_{ts} with $p_{tf\ at\ \Delta t=0} = 1310$ psig. Calculate:

• the wellbore storage coefficient;
• the permeability;
• the skin factor;
• the average pressure.

Solution

Step 1. From the log–log plot of Figure 1.124, the semilog straight line begins around 0.1 to 0.2 hours after shut-in. Using $\Delta p = 238$ psi at $\Delta t = 0.01$ hours as the selected coordinates of a point on the unit-slope straight line, calculate the wellbore storage coefficient from Equation 1.7.5, to give:

$$C = \frac{q_{inj} B t}{24 \Delta p}$$
$$= \frac{(807)(1.0)(0.01)}{(24)(238)} = 0.0014 \text{ bbl/psi}$$

Step 2. Figures 1.125 and 1.126 show the Horner plot, i.e., "wellhead pressures vs. $\log\left[(t_p + \Delta t)/\Delta t\right]$," and the MDH plot, i.e., "wellhead pressures vs. $\log(\Delta t)$," respectively, with both plots giving:

$$m = 270 \text{ psig/cycle}$$
$$p_{1\ hr} = 85 \text{ psig}$$

Using these two values, calculate k and s:

$$k = \frac{162.6 q_{inj} B \mu}{|m| h}$$
$$= \frac{(162.6)(807)(1.0)(1.0)}{(270)(28)} = 17.4 \text{ md}$$

$$s = 1.513 \left[\frac{p_{wf\ at\ \Delta t=0} - p_{1\ hr}}{|m|} - \log\left(\frac{k}{\phi \mu c_t r_w^2}\right) + 3.2275 \right]$$

$$= 1.513 \left[\frac{1310 - 85}{270} - \log\left(\frac{17.4}{(0.25)(1.0)(1.0 \times 10^{-5})(0.4)^2}\right) \right]$$

$$+ 3.2275 = 0.15$$

Step 3. Determine p^* from the extrapolation of the Horner plot of Figure 1.125 to $(t_p + \Delta t)/\Delta t = 1$, to give:

$$p_{ts}^* = -151 \text{ psig}$$

Equation 1.7.8 can be used to approximate p^*:

$$p^* = p_{1\ hr} - |m| \log(t_p + 1)$$
$$p_{ts}^* = 85 - (270) \log(6.82 + 1) = -156 \text{ psig}$$

[a]Robert Earlougher, *Advances in Well Test Analysis*, 1977.
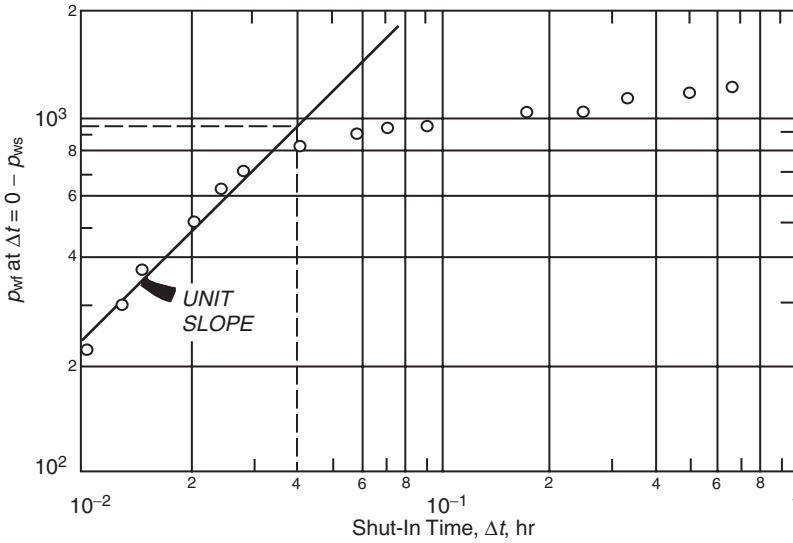
Figure 1.124 *Log–log data plot for a falloff test after brine injection, Example 1.48 (After Earlougher, R. Advances in Well Test Analysis) (Permission to publish by the SPE, copyright SPE, 1977).*
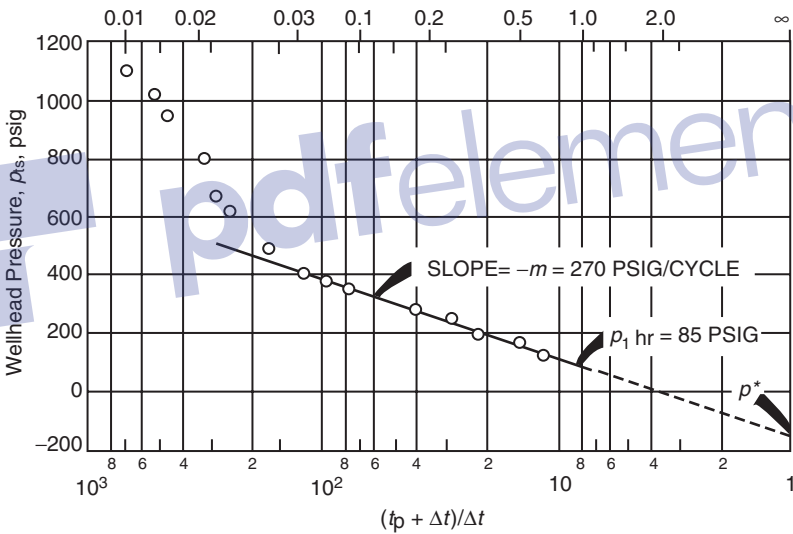
Figure 1.125 *Horner plot of pressure falloff after brine injection, Example 1.48.*

This is the false pressure at the wellhead, i.e., the surface. Using the hydrostatic gradient of 0.4685 psi/ft and the depth of 4819 ft, the reservoir false pressure is:

$$p^* = (4819)(0.4685) - 151 = 2107 \text{ psig}$$

and since injection time t_p is short compared with the shut-in time, we can assume that:

$$\bar{p} = p^* = 2107 \text{ psig}$$

Pressure falloff analysis in non-unit-mobility ratio systems
Figure 1.127 shows a plan view of the saturation distribution in the vicinity of an injection well. This figure shows two distinct zones.

Zone 1. represents the water bank with its leading edge at a distance of r_{f1} from the injection well. The mobility λ of the injected fluid in this zone, i.e., zone 1, is defined as the ratio of effective permeability of the injected fluid at its average saturation to its viscosity, or:

$$\lambda_1 = (k/\mu)_1$$

Zone 2. represents the oil bank with the leading edge at a distance of r_{f2} from the injection well. The mobility λ of the oil bank in this zone, i.e., zone 2, is defined as the ratio of oil effective permeability as evaluated at initial or connate water saturation to its viscosity, or:

$$\lambda_2 = (k/\mu)_2$$
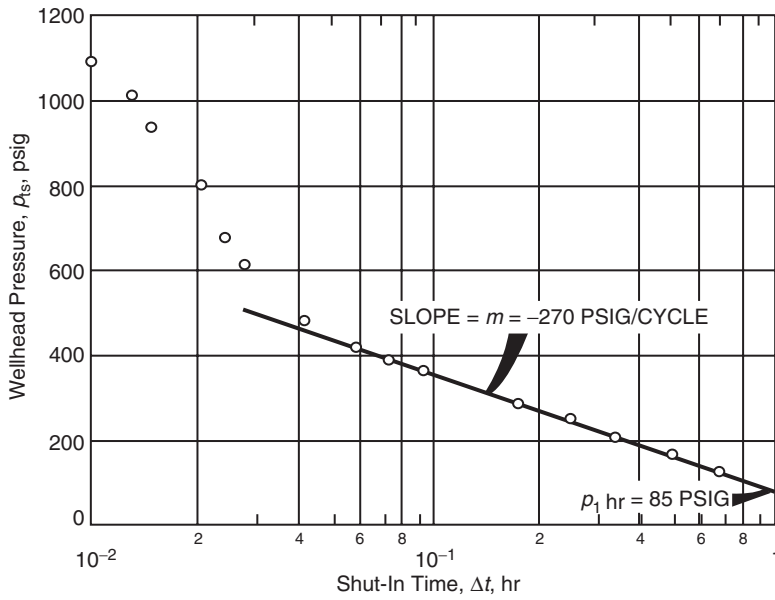
Figure 1.126 *Miller–Dyes–Hutchinson plot of pressure falloff after brine injection, Example 1.48.*
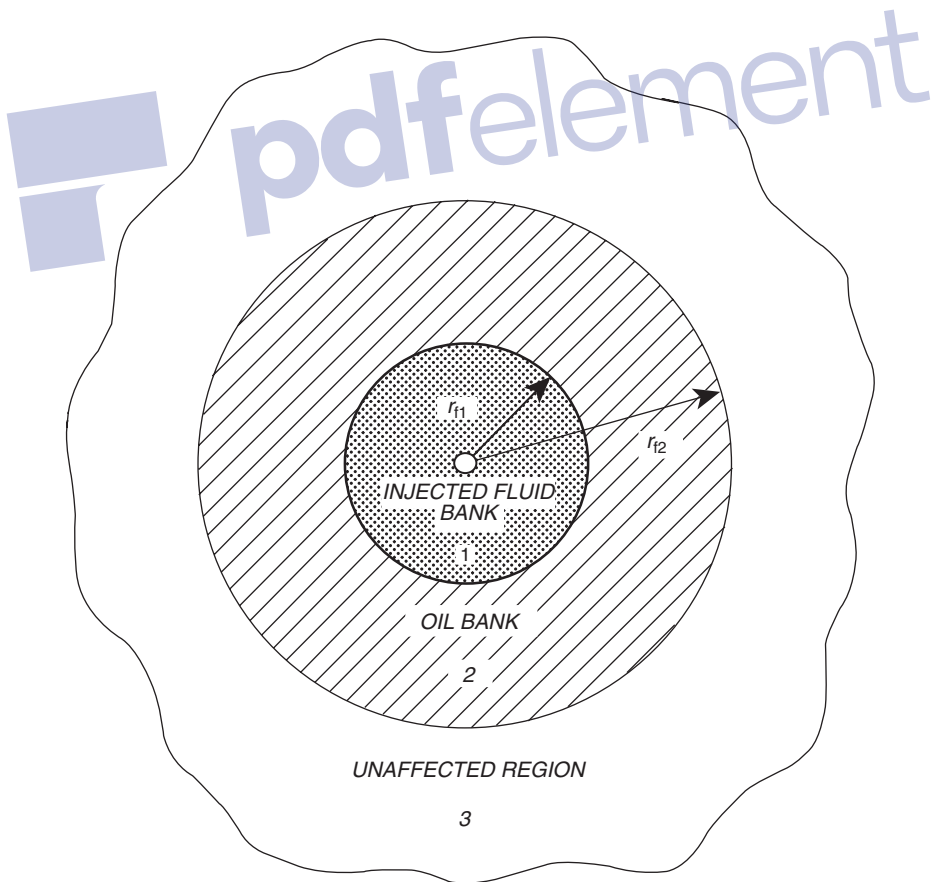
Figure 1.127 *Schematic diagram of fluid distribution around an injection well (composite reservoir).*
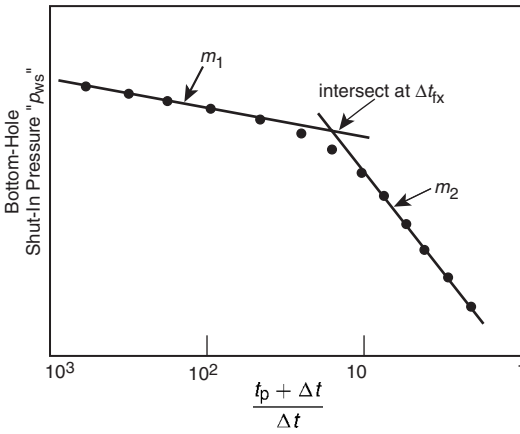
Figure 1.128 Pressure falloff behavior in a two-bank system.

Figure 1.129 Relationship between mobility ratio, slope ratio, and storage ratio. (After Merrill, et al. 1974).

The assumption of a two-bank system is applicable if the reservoir is filled with liquid or if the maximum shut-in time of the falloff test is such that the radius of investigation of the test does not exceed the outer radius of the oil bank. The ideal behavior of the falloff test in a two-bank system as expressed in terms of the Horner plot is illustrated in Figure 1.128.

Figure 1.128 shows two distinct straight lines with slopes of m_1 and m_2, that intersect at Δt_{fx}. The slope m_1 of the first line is used to estimate the effective permeability to water k_w in the flooded zone and the skin factor s. It is commonly believed that the slope of the second line m_2 will yield the mobility of the oil bank λ_o. However, Merrill et al. (1974) pointed out that the slope m_2 can be used only to determine the oil zone mobility if $r_{f2} > 10 r_{f1}$ and $(\phi c_t)_1 = (\phi c_t)_2$, and developed a technique that can be used to determine the distance r_{f1} and mobility of each bank. The technique requires knowing the values of (ϕc_t) in the first and second zone, i.e., $(\phi c_t)_1$ and $(\phi c_t)_2$. The authors proposed the following expression:

$$\lambda = \frac{k}{\mu} = \frac{162.6 QB}{m_2 h}$$

The authors also proposed two graphical correlations, as shown in Figures 1.129 and 1.130, that can be used with the Horner plot to analyze the pressure falloff data.

The proposed technique is summarized by the following:

Step 1. Plot Δp vs. Δt on a log–log scale and determine the end of the wellbore storage effect.
Step 2. Construct the Horner plot or the MDH plot and determine m_1, m_2, and Δt_{fx}.
Step 3. Estimate the effective permeability in the first zone, i.e., injected fluid invaded zone, "zone 1," and the skin factor from:

$$k_1 = \frac{162.6 q_{\text{inj}} B \mu}{|m_1| h} \qquad [1.7.9]$$

$$s = 1.513 \left[\frac{p_{\text{wf at } \Delta t=0} - p_{1\,\text{hr}}}{|m_1|} \right. $$
$$\left. - \log \left(\frac{k_1}{\phi \mu_1 (c_t)_1 r_w^2} \right) + 3.2275 \right]$$

where the subscript "1" denotes zone 1, the injected fluid zone.

Step 4. Calculate the following dimensionless ratios:

$$\frac{m_2}{m_1} \quad \text{and} \quad \frac{(\phi c_t)_1}{(\phi c_t)_2}$$

with the subscripts "1" and "2" denoting zone 1 and zone 2 respectively.
Step 5. Use Figure 1.129 with the two dimensionless ratios of step 4 and read the mobility ratio λ_1/λ_2.
Step 6. Estimate the effective permeability in the second zone from the following expression:

$$k_2 = \left(\frac{\mu_2}{\mu_1} \right) \frac{k_1}{\lambda_1/\lambda_2} \qquad [1.7.10]$$

Step 7. Obtain the dimensionless time Δt_{Dfx} from Figure 1.130.
Step 8. Calculate the distance to the leading edge of the injected fluid bank r_{f1} from:

$$r_{f1} = \sqrt{ \left[\frac{0.0002637 (k/\mu)_1}{(\phi c_t)_1} \right] \left(\frac{\Delta t_{\text{fx}}}{\Delta t_{\text{Dfx}}} \right) } \qquad [1.7.11]$$

To illustrate the technique, Merrill et al. (1974) presented the following example.

Example 1.49 Figure 1.131 shows the MDH semilog plot of simulated falloff data for a two-zone water flood with no apparent wellbore storage effects. Data used in the simulation is given below:

$$r_w = 0.25 \text{ ft}, \quad h = 20 \text{ ft}, \quad r_{f1} = 30 \text{ ft}$$
$$r_{f2} = r_e = 3600 \text{ ft}, \quad (k/\mu)_1 = \eta_1 = 100 \text{ md/cp}$$
$$(k/\mu)_2 = \eta_2 = 50 \text{ md/cp}, \quad (\phi c_t)_1 = 8.95 \times 10^{-7} \text{ psi}^{-1}$$
$$(\phi c_t)_2 = 1.54 \times 10^{-6} \text{ psi}^{-1}, \quad q_{\text{inj}} = 400 \text{ STB/day}$$
$$B_w = 1.0 \text{ bbl/STB}$$

Calculate λ_1, λ_2, and r_{f1} and compare with the simulation data.
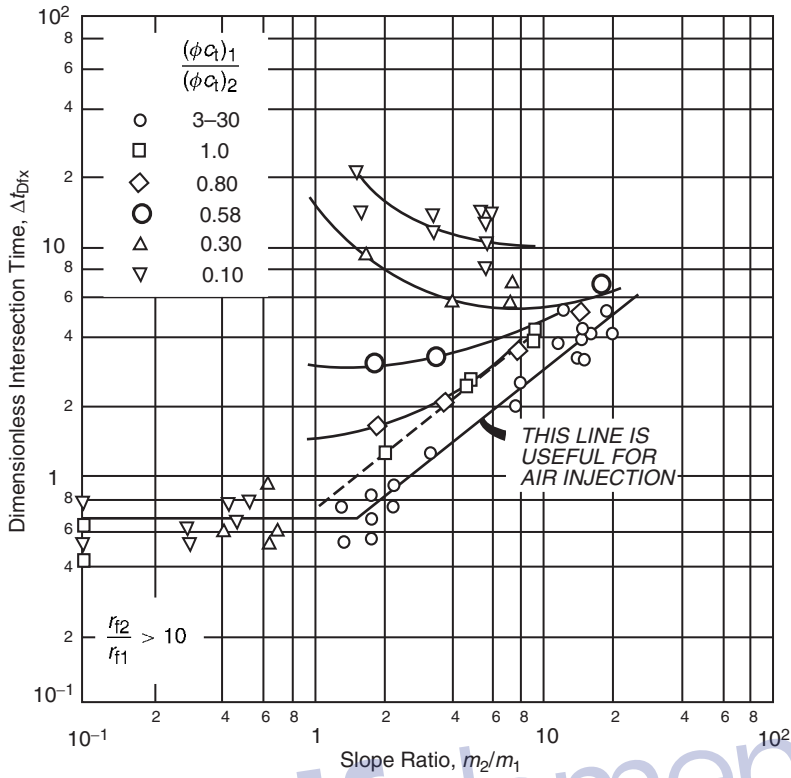
Figure 1.130 Correlation of dimensionless intersection time, Δt_{Dfx}, for falloff data from a two-zone reservoir. (After Merrill et al.1974).
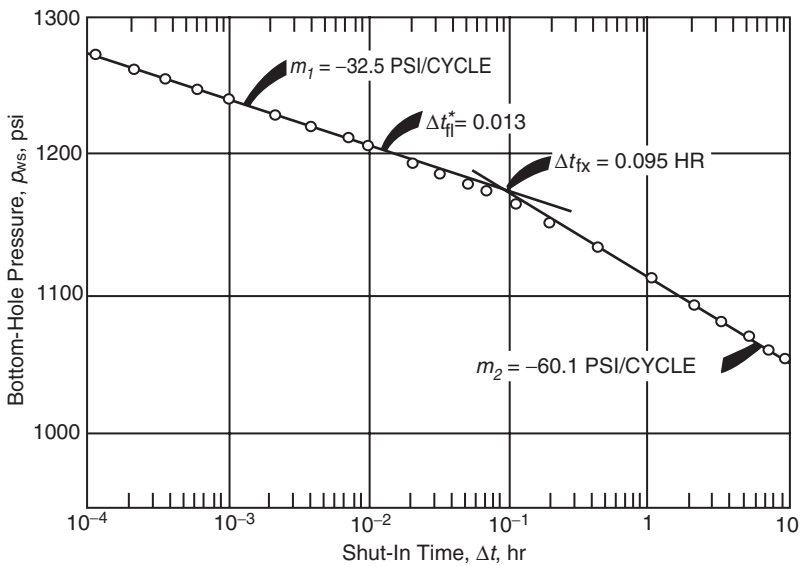
Figure 1.131 Falloff test data for Example 1.49. (After Merrill et al. 1974).
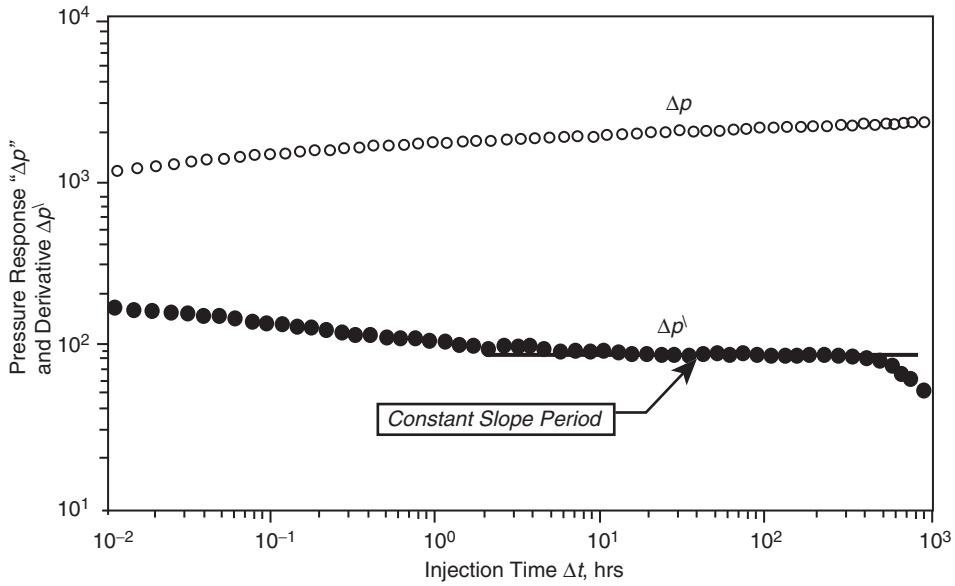
Figure 1.132 *Injection pressure response and derivative (base case).*

Solution

Step 1. From Figure 1.131, determine m_1, m_2, and Δt_{fx} to give:

$$m_1 = 32.5 \text{ psi/cycle}$$

$$m_2 = 60.1 \text{ psi/cycle}$$

$$\Delta t_{fx} = 0.095 \text{ hour}$$

Step 2. Estimate $(k/\mu)_1$, i.e., mobility of water bank, from Equation 1.7.9:

$$\left(\frac{k}{\mu}\right)_1 = \frac{162.6 q_{inj} B}{|m_1| h} = \frac{162.6(400)(1.0)}{(32.5)(20)}$$

$$= 100 \text{ md/cp}$$

The value matches the value used in the simulation.

Step 3. Calculate the following dimensionless ratios:

$$\frac{m_2}{m_1} = \frac{-60.1}{-32.5} = 1.85$$

$$\frac{(\phi c_t)_1}{(\phi c_t)_2} = \frac{8.95 \times 10^{-7}}{1.54 \times 10^{-6}} = 0.581$$

Step 4. Using the two dimensionless ratios as calculated in step 4, determine the ratio λ_1/λ_2 from Figure 1.129:

$$\frac{\lambda_1}{\lambda_2} = 2.0$$

Step 5. Calculate the mobility in the second zone, i.e., oil bank mobility $\lambda_2 = (k/\mu)_2$, from Equation 1.7.10:

$$\left(\frac{k}{\mu}\right)_2 = \frac{(k/\mu)_1}{(\lambda_1/\lambda_2)} = \frac{100}{2.0} = 50 \text{ md/cp}$$

with the exact match of the input data.

Step 6. Determine Δt_{Dfx} from Figure 1.130:

$$\Delta t_{Dfx} = 3.05$$

Step 7. Calculate r_{fl} from Equation 1.7.11:

$$r_{fl} = \sqrt{\frac{(0.0002637)(100)(0.095)}{(8.95 \times 10^{-7})(3.05)}} = 30 \text{ ft}$$

Yeh and Agarwal (1989) presented a different approach of analyzing the recorded data from the injectivity and falloff tests. Their methodology uses the pressure derivate Δp and Agarwal equivalent time Δt_e (see Equation 1.4.16) in performing the analysis. The authors defined the following nomenclature:

During the injectivity test period:

$$\Delta p_{wf} = p_{wf} - p_i$$

$$\Delta p_{wf}^{\backslash} = \frac{d(\Delta p_{wf})}{d(\ln t)}$$

where:

p_{wf} = bottom-hole pressure at time t during injection, psi
t = injection time, hours
$\ln t$ = natural logarithm of t

During the falloff test period:

$$\Delta p_{ws} = p_{wf \text{ at } \Delta t=0} - p_{ws}$$

$$\Delta p_{ws}^{\backslash} = \frac{d(\Delta p_{ws})}{d(\ln \Delta te)}$$

with:

$$\Delta t_e = \frac{t_p \Delta t}{t_p + \Delta t}$$

where:

Δt = shut-in time, hours
t_p = injection time, hours

Through the use of a numerical simulator, Yeh and Agarwal simulated a large number of injectivity and falloff tests and made the following observations for both tests:

Pressure behavior during injectivity tests

(1) A log–log plot of the injection pressure difference Δp_{wf} and its derivative $\Delta p_{wf}^{\backslash}$ versus injection time will exhibit a constant-slope period, as shown in Figure 1.132, and designated as $(\Delta p_{wf}^{\backslash})_{const}$. The water mobility λ_1 in
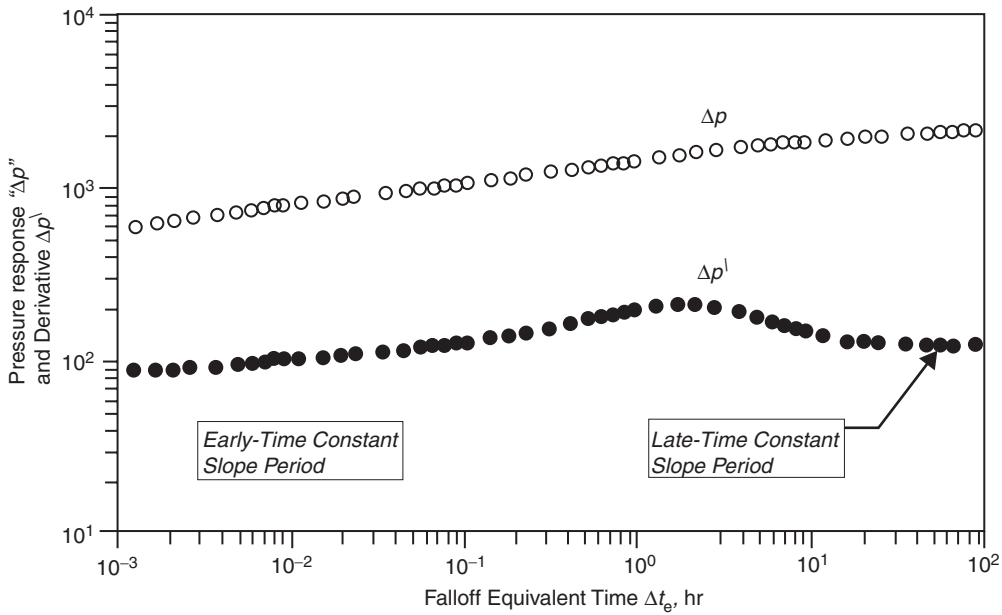
Figure 1.133 *Falloff pressure response and derivative (base case).*

the floodout zone, i.e., water bank, can be estimated from:

$$\lambda_1 = \left(\frac{k}{\mu}\right)_1 = \frac{70.62 q_{inj} B}{h(\Delta p_{wf}^{\backslash})_{const}}$$

Notice that the constant 70.62 is used instead of 162.6 because the pressure derivative is calculated with respect to the natural logarithm of time.

(2) The skin factor as calculated from the semilog analysis method is usually in excess of its true value because of the contrast between injected and reservoir fluid properties.

Pressure behavior during falloff tests

(1) The log–log plot of the pressure falloff response in terms of Δp and its derivative as a function of the falloff equivalent time Δt_e is shown in Figure 1.133. The resulting derivative curve shows two constant-slope periods, $(\Delta p_{ws}^{\backslash})_1$ and $(\Delta p_{ws}^{\backslash})_2$, which reflect the radial flow in the floodout zone, i.e., water bank, and, the radial flow in the unflooded zone, i.e., oil bank.

These two derivative constants can be used to estimate the mobility of the water bank λ_1 and the oil bank λ_2 from:

$$\lambda_1 = \frac{70.62 q_{inj} B}{h(\Delta p_{ws}^{\backslash})_1}$$

$$\lambda_2 = \frac{70.62 q_{inj} B}{h(\Delta p_{ws}^{\backslash})_2}$$

(2) The skin factor can be estimated from the first semilog straight line and closely represents the actual mechanical skin on the wellbore.

1.7.3 Step-rate test

Step-rate injectivity tests are specifically designed to determine the pressure at which fracturing could be induced in the reservoir rock. In this test, water is injected at a constant rate for about 30 minutes before the rate is increased and maintained for successive periods, each of which also
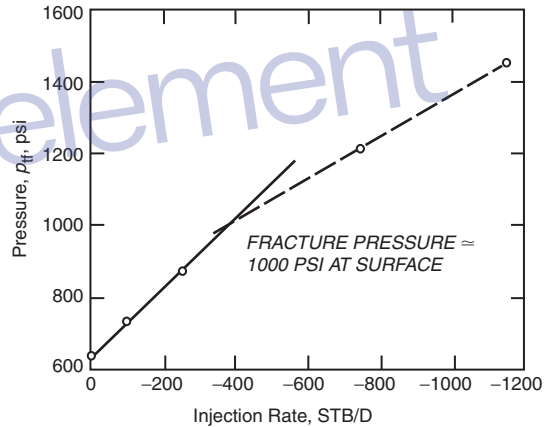
Figure 1.134 *Step-rate injectivity data plot.*

lasts for 30 minutes. The pressure observed at the end of each injection rate is plotted versus the rate. This plot usually shows two straight lines which intersect at the fracture pressure of the formation, as shown schematically in Figure 1.134. The suggested procedure is summarized below:

Step 1. Shut in the well and allow the bottom-hole pressure to stabilize (if shutting in the well is not possible, or not practical, stabilize the well at a low flow rate). Measure the stabilized pressure.

Step 2. Open the well at a low injection rate and maintain this rate for a preset time. Record the pressure at the end of the flow period.

Step 3. Increase the rate, and at the end of an interval of time equal to that used in step 2, again record the pressure.

Step 4. Repeat step 3 for a number of increasing rates until the parting pressure is noted on the step-rate plot depicted by Figure 1.134.

As pointed out by Horn (1995), data presented in graphical form is much easier to understand than a single table of numbers. Horn proposed the following "toolbox" of graphing functions that is considered an essential part of computer-aided well test interpretation system:

Flow period	Characteristic	Plot used
Infinite-acting radial flow drawdown)	Semilog straight line	p vs. $\log \Delta t$ (semilog plot, sometimes called MDH plot)
Infinite-acting radial flow (buildup)	Horner straight line	p vs. $\log(t_p + \Delta t)/\Delta t$ (Horner plot)
Wellbore storage	Straight line p vs. t, or unit-slope $\log \Delta p$ vs. $\log \Delta t$	$\log \Delta p$ vs. $\log \Delta t$ (log–log plot, type curve)
Finite conductivity fracture	Straight-line slope $\frac{1}{4}$, $\log \Delta p$ vs. $\log \Delta t$ plot	$\log \Delta p$ vs. $\log \Delta t$, or Δp vs. $\Delta t^{1/4}$
Infinite conductivity fracture	Straight-line slope $\frac{1}{2}$, $\log \Delta p$ vs. $\log \Delta t$ plot	$\log \Delta p$ vs. $\log \Delta t$, or Δp vs. $\Delta t^{1/2}$
Dual-porosity behavior	S-shaped transition between parallel semilog straight lines	p vs. $\log \Delta t$ (semilog plot)
Closed boundary	Pseudosteady state, pressure linear with time	p vs. Δt (Cartesian plot)
Impermeable fault	Doubling of slope on semilog straight line	p vs. $\log \Delta t$ (semilog plot)
Constant-pressure boundary	Constant pressure, flat line on all p, t plots	Any

Chaudhry (2003) presented another useful "toolbox" that summarizes the pressure derivative trends for common flow regimes that have been presented in this chapter, as shown in Table 1-10.

Kamal et al. (1995) conveniently summarized; in tabulated form, various plots and flow regimes most commonly used in transient tests and the information obtained from each test as shown in Tables 1-11 and 1-12.

Table 1.10   *Pressure Derivative Trends for Common Flow Regimes.*

Wellbore storage dual-porosity matrix to fissure flow	Semilog straight lines with slope 1.151
	Parallel straight-line responses are characteristics of naturally fractured reservoirs
Dual porosity with pseudosteady-state interporosity flow	Pressure change slope → increasing, leveling off, increasing
	Pressure derivative slope = 0, valley = 0
	Additional distinguishing characteristic is middle-time valley trend during more than 1 log cycle
Dual porosity with transient inter-porosity flow	Pressure change slope → steepening
	Pressure derivative slope = 0, upward trend = 0
	Additional distinguishing characteristic → middle-time slope doubles
Pseudosteady state	Pressure change slope → for drawdown and zero for buildup
	Pressure derivative slope → for drawdown and steeply descending for buildup
	Additional distinguishing characteristic → late time drawdown pressure change and derivative are overlain; slope of 1 occurs much earlier in the derivative
Constant-pressure boundary (steady state)	Pressure change slope → 0
	Pressure derivative slope → steeply descending
	Additional distinguishing characteristic → cannot be distinguished from psuedosteady state in pressure buildup test
Single sealing fault (pseudoradial flow)	Pressure change slope → steeping
	Pressure derivative slope → 0, upward trend → 0
	Additional distinguishing characteristic → late-time slope doubles
Elongated reservoir linear flow	Pressure change slope → 0.5
	Pressure derivative slope → 0.5
	Additional distinguishing characteristic → late-time pressure change and derivative are offset by factor of 2; slope of 0.5 occurs much earlier in the derivative
Wellbore storage infinite-acting radial flow	Pressure change slope = 1, pressure derivative slope = 1
	Additional distinguishing characteristics are: early time pressure change, and derivative are overlain
Wellbore storage, partial penetration, infinite-acting radial flow	Pressure change increases and pressure derivative slope = 0
	Additional distinguishing characteristic is: middile-time flat derivative
Linear flow in an infinite conductivity vertical fracture	$K(x_f)^2 \rightarrow$ calculate from specialized plot
	Pressure slope = 0.5 and pressure derivative slope = 0.5
	Additional distinguishing characteristics are: early-time pressure change and the derivative are offset by a factor of 2
Bilinear flow to an infinite conductivity vertical fracture	$K_f w \rightarrow$ calculate from specialized plot
	Pressure slope = 0.25 and pressure derivative slope = 0.25
	Additional distinguishing characteristic are: early-time pressure change and derivative are offset by factor of 4

(continued)

Table 1.10 *Pressure Derivative Trends for Common Flow Regimes (continued)*

Wellbore storage infinite acting radial flow	Sealing fault
Wellbore storage	No flow boundary
Wellbore storage linear flow	$Kb^2 \rightarrow$ calculate from specialized plot

Table 1.11 *Reservoir properties obtainable from various transient tests (After Kamal et al. 1995).*

Drill item tests	Reservoir behavior Permeability Skin	Step-rate tests	Formation parting pressure Permeability Skin
	Fracture length Reservoir pressure Reservoir limit Boundaries	Falloff tests	Mobility in various banks Skin Reservoir pressure Fracture length
Repeat/multiple-formation tests	Pressure profile		Location of front Boundaries
Drawdown tests	Reservoir behavior Permeability Skin Fracture length Reservoir limit Boundaries	Interference and pulse tests	Communication between wells Reservoir type behavior Porosity Interwell permeability Vertical permeability
Buildup tests	Reservoir behavior Permeability Skin Fracture length Reservoir pressure Boundaries	Layered reservoir tests	Properties of individual layers Horizontal permeability Vertical permeability Skin Average layer pressure Outer Boundaries

Table 1.12 *Plots and flow regimes of transient tests (After Kamal et al. 1995)*

	Plot				
Flow regime	Cartesian	$\sqrt{\Delta t}$	$\sqrt[4]{\Delta t}$	Log–log	Semilog
Wellbore storage	Straight line Slope $\rightarrow C$ Intercept $\rightarrow \Delta t_c$ Δp_c			Unit slope on Δp and $p^\backslash$ Δp and $p^\backslash$ coincide	Positive s Negative s
Linear flow		Straight line Slope $= m_f \rightarrow l_f$ Intercept = fracture damage		Slope $= \frac{1}{2}$ on $p^\backslash$ and on Δp if $s = 0$ Slope $< \frac{1}{2}$ on Δp if $s \neq 0$ $p^\backslash$ at half the level of Δp	
Bilinear flow			Straight line Slope $= m_{bf} \rightarrow C_{fd}$	Slope $= \frac{1}{4}$ $p^\backslash$ at $\frac{1}{4}$ level of Δp	
First IARF [a] (high-k layer, fractures)	Decreasing slope			$p^\backslash$ horizontal at $p_D^\backslash = 0.5$	Straight line Slope $= m \rightarrow kh$ $\Delta p_{1\,hr} \rightarrow s$
Transition	More decreasing slope			$\Delta p = \lambda e^{-2s}$ or $B^\backslash$ $p_D^\backslash = 0.25$ (transition) $= < 0.25$ (pseudo-steady state)	Straight line Slope $= m/2$ (transition) $= 0$ (pseudo-steady state)
Second IARF (total system)	Similar slope to first IARF			$p^\backslash$ horizontal at $p_D^\backslash = 0.5$	Straight line Slope $= m \rightarrow kh, p^*$ $\Delta p_{1\,hr} \rightarrow s$
Single no-flow boundary				$p^\backslash$ horizontal at $p_D^\backslash = 1.0$	Straight line Slope $= 2m$ Intersection with IARF$\rightarrow$distance to boundary
Outer no-flow boundaries (drawdown test only)	Straight line Slope $= m^* \rightarrow \phi Ah$ $p_{int} \rightarrow C_A$			Unit slope for Δp and $p^\backslash$ Δp and $p^\backslash$ coincide	Increasing slope

[a] IARF = Infinite-Acting Radial Flow.

Problems

1. An incompressible fluid flows in a linear porous media with the following properties.

   $L = 2500$ ft, $h = 30$ ft,   width $= 500$ ft, $k = 50$ md,
   $\phi = 17\%$, $\mu = 2$ cp, inlet pressure $= 2100$ psi,
   $Q = 4$ bbl/day, $\rho = 45$ lb/ft^3

   Calculate and plot the pressure profile throughout the linear system.

2. Assume the reservoir linear system as described in problem 1 is tilted with a dip angle of $7°$. Calculate the fluid potential through the linear system.

3. A gas of 0.7 specific gravity is flowing in a linear reservoir system at $150°$F. The upstream and downstream pressures are 2000 and 1800 psi, respectively. The system has the following properties:

   $L = 2000$ ft, $W = 300$ ft, $h = 15$ ft
   $k = 40$ md, $\phi = 15\%$

   Calculate the gas flow rate.

4. An oil well is producing a crude oil system at 1000 STB/day and 2000 psi of bottom-hole flowing pressure. The pay zone and the producing well have the following characteristics.

   $h = 35$ ft, $r_w = 0.25$ ft,   drainage area $= 40$ acres
   API $= 45°$, $\gamma_g = 0.72$, $R_s = 700$ scf/STB
   $k = 80$ md

   Assuming steady-state flowing conditions, calculate and plot the pressure profile around the wellbore.

5. Assuming steady-state flow and an incompressible fluid, calculate the oil flow rate under the following conditions:

   $p_e = 2500$ psi, $p_{wf} = 2000$ psi, $r_e = 745$ ft
   $r_w = 0.3$ ft, $\mu_o = 2$ cp, $B_o = 1.4$ bbl/STB
   $h = 30$ ft, $k = 60$ md

6. A gas well is flowing under a bottom-hole flowing pressure of 900 psi. The current reservoir pressure is 1300 psi. The following additional data is available:

   $T = 140°$F, $\gamma_g = 0.65$, $r_w = 0.3$ ft
   $k = 60$ md, $h = 40$ ft, $r_e = 1000$ ft

   Calculate the gas flow rate by using

   (a) the real-gas pseudopressure approach;
   (b) the pressure-squared method.

7. After a period of shut-in of an oil well, the reservoir pressure has stabilized at 3200 psi. The well is allowed to flow at a constant flow rate of 500 STB/day under a transient flow condition. Given:

   $B_o = 1.1$ bbl/STB, $\mu_o = 2$ cp, $c_t = 15 \times 10^{-6}$ psi^{-1}
   $k = 50$ md, $h = 20$ ft, $\phi = 20\%$
   $r_w = 0.3$ ft, $p_i = 3200$ psi

   calculate and plot the pressure profile after 1, 5, 10, 15, and 20 hours.

8. An oil well is producing at a constant flow rate of 800 STB/day under a transient flow condition. The following data is available:

   $B_o = 1.2$ bbl/STB, $\mu_o = 3$ cp, $c_t = 15 \times 10^{-6}$ psi^{-1}
   $k = 100$ md, $h = 25$ ft, $\phi = 15\%$
   $r_w = 0.5$, $p_i = 4000$ psi,

Using the Ei function approach and the p_D method, calculate the bottom-hole flowing pressure after 1, 2, 3, 5, and 10 hours. Plot the results on a semilog scale and Cartesian scale.

9. A well is flowing under a drawdown pressure of 350 psi and produces at a constant flow rate of 300 STB/day. The net thickness is 25 ft. Given:

   $r_e = 660$ ft, $r_w = 0.25$ ft
   $\mu_o = 1.2$ cp, $B_o = 1.25$ bbl/STB

   calculate:

   (a) the average permeability;
   (b) the capacity of the formation.

10. An oil well is producing from the center of a 40 acre square drilling pattern. Given:

    $\phi = 20\%$, $h = 15$ft, $k = 60$ md
    $\mu_o = 1.5$ cp, $B_o = 1.4$ bbl/STB, $r_w = 0.25$ ft
    $p_i = 2000$ psi, $p_{wf} = 1500$ psi

    calculate the oil flow rate.

11. A shut-in well is located at a distance of 700 ft from one well and 1100 ft from a second well. The first well flows for 5 days at 180 STB/day, at which time the second well begins to flow at 280 STB/day. Calculate the pressure drop in the shut-in well when the second well has been flowing for 7 days. The following additional data is given:

    $p_i = 3000$ psi, $B_o = 1.3$ bbl/STB, $\mu_o = 1.2$ cp,
    $h = 60$ ft, $c_t = 15 \times 10^{-6}$ psi^{-1}, $\phi = 15\%$, $k = 45$ md

12. A well is opened to flow at 150 STB/day for 24 hours. The flow rate is then increased to 360 STB/day and lasts for another 24 hours. The well flow rate is then reduced to 310 STB/day for 16 hours. Calculate the pressure drop in a shut-in well 700 ft away from the well, given:

    $\phi = 15\%$, $h = 20$ ft, $k = 100$ md
    $\mu_o = 2$ cp, $B_o = 1.2$ bbl/STB, $r_w = 0.25$ ft
    $p_i = 3000$ psi, $c_t = 12 \times 10^{-6}$ psi^{-1}

13. A well is flowing under unsteady-state flowing conditions for 5 days at 300 STB/day. The well is located at 350 ft and 420 ft distance from two sealing faults. Given:

    $\phi = 17\%$, $c_t = 16 \times 10^{-6}$ psi^{-1}, $k = 80$ md
    $p_i = 3000$ psi, $B_o = 1.3$ bbl/STB, $\mu_o = 1.1$ cp
    $r_w = 0.25$ ft, $h = 25$ ft

    calculate the pressure in the well after 5 days.

14. A drawdown test was conducted on a new well with results as given below:

t (hr)	p_{wf} (psi)
1.50	2978
3.75	2949
7.50	2927
15.00	2904
37.50	2876
56.25	2863
75.00	2848
112.50	2810
150.00	2790
225.00	2763

Given:

$p_i = 3400$ psi, $h = 25$ ft, $Q = 300$ STB/day
$c_t = 18 \times 10^{-6}$ psi^{-1}, $\mu_o = 1.8$ cp,
$B_o = 1.1$ bbl/STB, $r_w = 0.25$ ft, $\phi = 12\%$,

and assuming no wellbore storage, calculate:

(a) the average permeability;
(b) the skin factor.

15. A drawdown test was conducted on a discovery well. The well was allowed to flow at a constant flow rate of 175 STB/day. The fluid and reservoir data is given below:

$S_{wi} = 25\%$, $\phi = 15\%$, $h = 30$ ft, $c_t = 18 \times 10^{-6}$ psi^{-1}
$r_w = 0.25$ ft, $p_i = 4680$ psi, $\mu_o = 1.5$ cp,
$B_o = 1.25$ bbl/STB

The drawdown test data is given below:

t (hr)	p_{wf} (psi)
0.6	4388
1.2	4367
1.8	4355
2.4	4344
3.6	4334
6.0	4318
8.4	4309
12.0	4300
24.0	4278
36.0	4261
48.0	4258
60.0	4253
72.0	4249
84.0	4244
96.0	4240
108.0	4235
120.0	4230
144.0	4222
180.0	4206

Calculate:

(a) the drainage area;
(b) the skin factor;
(C) the oil flow rate at a bottom-hole flowing pressure of 4300 psi, assuming a semisteady-state flowing conditions.

16. A pressure buildup test was conducted on a well that had been producing at 146 STB/day for 53 hours.

The reservoir and fluid data is given below.

$B_o = 1.29$ bbl/STB, $\mu_o = 0.85$ cp,
$c_t = 12 \times 10^{-6}$ psi^{-1}, $\phi = 10\%$, $p_{wf} = 1426.9$ psig,
$A = 20$ acres

The buildup data is as follows:

Time	p_{ws} (psig)
0.167	1451.5
0.333	1476.0
0.500	1498.6
0.667	1520.1
0.833	1541.5
1.000	1561.3
1.167	1581.9
1.333	1599.7
1.500	1617.9
1.667	1635.3
2.000	1665.7
2.333	1691.8
2.667	1715.3
3.000	1736.3
3.333	1754.7
3.667	1770.1
4.000	1783.5
4.500	1800.7
5.000	1812.8
5.500	1822.4
6.000	1830.7
6.500	1837.2
7.000	1841.1
7.500	1844.5
8.000	1846.7
8.500	1849.6
9.000	1850.4
10.000	1852.7
11.000	1853.5
12.000	1854.0
12.667	1854.0
14.620	1855.0

Calculate:

(a) the average reservoir pressure;
(b) the skin factor;
(c) the formation capacity;
(d) an estimate of the drainage area and compare with the given value.

This page intentionally left blank

2   Water Influx

Contents

Water-bearing rocks called aquifers surround nearly all hydrocarbon reservoirs. These aquifers may be substantially larger than the oil or gas reservoirs they adjoin as to appear infinite in size, and they may be so small in size as to be negligible in their effect on reservoir performance.

As reservoir fluids are produced and reservoir pressure declines, a pressure differential develops from the surrounding aquifer into the reservoir. Following the basic law of fluid flow in porous media, the aquifer reacts by encroaching across the original hydrocarbon–water contact. In some cases, water encroachment occurs due to hydrodynamic conditions and recharge of the formation by surface waters at an outcrop. In many cases, the pore volume of the aquifer is not significantly larger than the pore volume of the reservoir itself. Thus, the expansion of the water in the aquifer is negligible relative to the overall energy system, and the reservoir behaves volumetrically. In this case, the effects of water influx can be ignored. In other cases, the aquifer permeability may be sufficiently low such that a very large pressure differential is required before an appreciable amount of water can encroach into the reservoir. In this instance, the effects of water influx can be ignored as well.

The objective of this chapter, however, concern those reservoir–aquifer systems in which the size of the aquifer is large enough and the permeability of the rock is high enough that water influx occurs as the reservoir is depleted. This chapter is designed to provide the various water influx calculation models and a detailed description of the computational steps involved in applying these models.

2.1 Classification of Aquifers

Many gas and oil reservoirs are produced by a mechanism termed "water drive." Often this is called natural water drive to distinguish it from artificial water drive that involves the injection of water into the formation. Hydrocarbon production from the reservoir and the subsequent pressure drop prompt a response from the aquifer to offset the pressure decline. This response comes in the form of a water influx, commonly called water encroachment, which is attributed to:

- expansion of the water in the aquifer;
- compressibility of the aquifer rock;
- artesian flow where the water-bearing formation outcrop is located structurally higher than the pay zone.

Reservoir–aquifer systems are commonly classified on the basis described in the following subsections.

2.1.1 Degree of pressure maintenance
Based on the degree of reservoir pressure maintenance provided by the aquifer, the natural water drive is often qualitatively described as:

- the active water drive;
- the partial water drive;
- the limited water drive.

The term "active" water drive refers to the water encroachment mechanism in which the rate of water influx equals the reservoir *total* production rate. Active water drive reservoirs are typically characterized by a gradual and slow reservoir pressure decline. If during any long period the production rate and reservoir pressure remain reasonably constant, the reservoir voidage rate must be equal to the water influx rate:

$$\begin{bmatrix} \text{water influx} \\ \text{rate} \end{bmatrix} = \begin{bmatrix} \text{oil flow} \\ \text{rate} \end{bmatrix} + \begin{bmatrix} \text{free gas} \\ \text{flow rate} \end{bmatrix} + \begin{bmatrix} \text{water} \\ \text{production} \\ \text{rate} \end{bmatrix}$$

or:

$$e_{\text{w}} = Q_{\text{o}}B_{\text{o}} + Q_{g}B_{g} + Q_{\text{w}}B_{\text{w}} \qquad [2.1.1]$$

where:

e_{w} = water influx rate, bbl/day
Q_{o} = oil flow rate, STB/day
B_{o} = oil formation volume factor, bbl/STB
Q_{g} = free gas flow rate, scf/day
B_{g} = gas formation volume factor, bbl/scf
Q_{w} = water flow rate, STB/day
B_{w} = water formation volume factor, bbl/STB

Equation 2.1.1 can be equivalently expressed in terms of cumulative production by introducing the following derivative terms:

$$e_{\text{w}} = \frac{dW_{\text{e}}}{dt} = B_{\text{o}}\frac{dN_{\text{p}}}{dt} + (\text{GOR} - R_{\text{s}})\frac{dN_{\text{p}}}{dt}B_{g} + \frac{dW_{\text{p}}}{dt}B_{\text{w}}$$
$$[2.1.2]$$

where:

W_{e} = cumulative water influx, bbl
t = time, days
N_{p} = cumulative oil production, STB
GOR = current gas–oil ratio, scf/STB
R_{s} = current gas solubility, scf/STB
B_{g} = gas formation volume factor, bbl/scf
W_{p} = cumulative water production, STB
dN_{p}/dt = daily oil flow rate Q_{o}, STB/day
dW_{p}/dt = daily water flow rate Q_{w}, STB/day
dW_{e}/dt = daily water influx rate e_{w}, bbl/day
$(\text{GOR} - R_{\text{s}})dN_{\text{p}}/dt$ = daily free gas rate, scf/day

Example 2.1 Calculate the water influx rate e_{w} in a reservoir whose pressure is stabilized at 3000 psi. Given:

initial reservoir pressure = 3500 psi,

$dN_{\text{p}}/dt = 32\,000$ STB/day

$B_{\text{o}} = 1.4$ bbl/STB, $\text{GOR} = 900$ scf/STB, $R_{\text{s}} = 700$ scf/STB

$B_{g} = 0.00082$ bbl/scf, $dW_{\text{p}}/dt = 0$, $B_{\text{w}} = 1.0$ bbl/STB

Solution Applying Equation 2.1.1 or 2.1.2 gives:

$$e_{\text{w}} = \frac{dW_{\text{e}}}{dt} = B_{\text{o}}\frac{dN_{\text{p}}}{dt} + (\text{GOR} - R_{\text{s}})\frac{dN_{\text{p}}}{dt}B_{g} + \frac{dW_{\text{p}}}{dt}B_{\text{w}}$$

$$= (1.4)(32\,000) + (900 - 700)(32\,000)(0.00082) + 0$$

$$= 50\,048 \text{ bbl/day}$$

2.1.2 Outer boundary conditions
The aquifer can be classified as infinite or finite (bounded). Geologically all formations are finite but may act as infinite if the changes in the pressure at the oil–water contact are not "felt" at the aquifer boundary. Some aquifers outcrop and are infinite acting because of surface replenishment. In general, the outer boundary governs the behavior of the aquifer and can be classified as follows:

- Infinite system indicates that the effect of the pressure changes at the oil/aquifer boundary can never be felt at the outer boundary. This boundary is for all intents and purposes at a constant pressure equal to initial reservoir pressure.
- Finite system indicates that the aquifer outer limit is affected by the influx into the oil zone and that the pressure at this outer limit changes with time.

2.1.3 Flow regimes
There are basically three flow regimes that influence the rate of water influx into the reservoir. As previously described in Chapter 1, these flow regimes are:
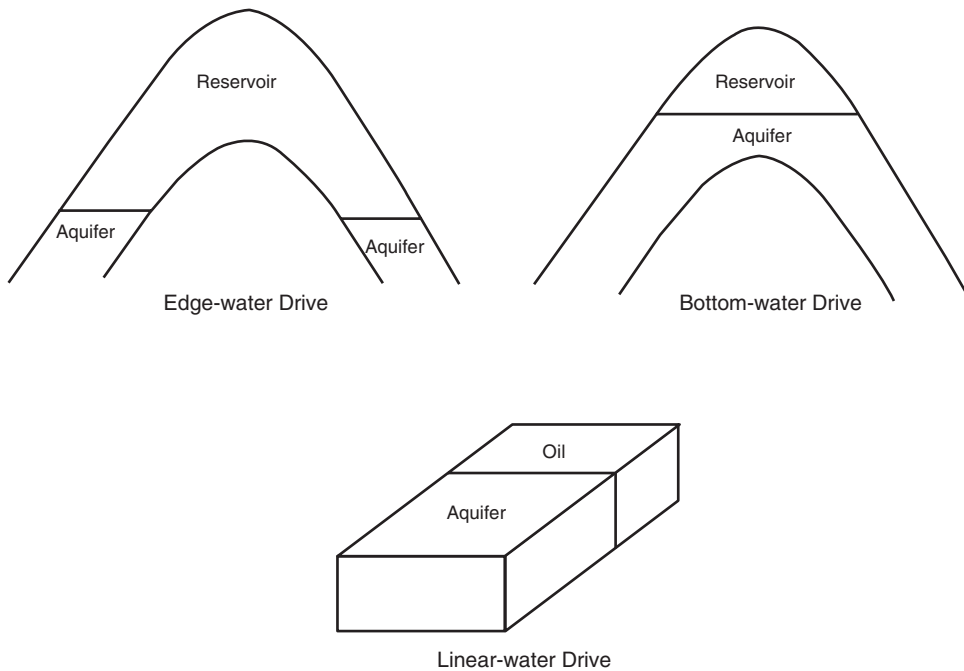
(1) steady state;

Figure 2.1 *Flow geometries.*

(2) semi(pseudo)steady state;
(3) unsteady state.

2.1.4 Flow geometries

Reservoir–aquifer systems can be classified on the basis of flow geometry as:

- edge-water drive;
- bottom-water drive;
- linear-water drive.

In edge-water drive, as shown in Figure 2.1, water moves into the flanks of the reservoir as a result of hydrocarbon production and pressure drop at the reservoir–aquifer boundary. The flow is essentially radial with negligible flow in the vertical direction.

Bottom-water drive occurs in reservoirs with large areal extent and a gentle dip where the reservoir–water contact completely underlies the reservoir. The flow is essentially radial and, in contrast to the edge-water drive, the bottom-water drive has significant vertical flow.

In linear–water drive, the influx is from one flank of the reservoir. The flow is strictly linear with a constant cross-sectional area.

2.2 Recognition of Natural Water Influx

Normally very little information is obtained during the exploration and development period of a reservoir concerning the presence or characteristics of an aquifer that could provide a source of water influx during the depletion period. Natural water drive may be assumed by analogy with nearby producing reservoirs, but early reservoir performance trends can provide clues. A comparatively low, and decreasing, rate of reservoir pressure decline with increasing cumulative withdrawals is indicative of fluid influx. Successive calculations of barrels withdrawn per psi change in reservoir pressure can

supplement performance graphs. However, if the reservoir limits have not been delineated by the developmental dry holes the influx could be from an undeveloped area of the reservoir not accounted for in averaging reservoir pressure. If the reservoir pressure is below the oil saturation pressure, a low rate of increase in produced GOR is also indicative of fluid influx.

Early water production from edge wells is indicative of water encroachment. Such observations must be tempered by the possibility that the early water production is due to formation fractures, thin high-permeability streaks, or to coning in connection with a limited aquifer. The water production may be due to casing leaks.

Calculation of increasing original oil-in-place from successive reservoir pressure surveys by using the material balance and assuming no water influx is also indicative of fluid influx.

2.3 Water Influx Models

It should be appreciated that there are more uncertainties attached to this part of reservoir engineering than to any other. This is simply because one seldom drills wells into an aquifer to gain the necessary information about the porosity, permeability, thickness, and fluid properties. Instead, these properties have frequently to be inferred from what has been observed in the reservoir. Even more uncertain, however, is the geometry and areal continuity of the aquifer itself.

Several models have been developed for estimating water influx that is based on assumptions that describe the characteristics of the aquifer. Due to the inherent uncertainties in the aquifer characteristics, all of the proposed models require historical reservoir performance data to evaluate constants representing aquifer property parameters since these are rarely known from exploration and development drilling with sufficient accuracy for direct application. The material balance equation can be used to determine

historical water influx provided original oil-in-place is known from pore volume estimates. This permits evaluation of the constants in the influx equations so that future water influx rate can be forecast.

The mathematical water influx models that are commonly used in the petroleum industry include:

- pot aquifer;
- Schilthuis steady state;
- Hurst modified steady state;
- van Everdingen and Hurst unsteady state:
  - edge-water drive;
  - bottom-water drive;
- Carter–Tracy unsteady state;
- Fetkovich method:
  - radial aquifer;
  - linear aquifer.

The following sections describe the above models and their practical applications in water influx calculations.

2.3.1 The pot aquifer model

The simplest model that can be used to estimate the water influx into a gas or oil reservoir is based on the basic definition of compressibility. A drop in the reservoir pressure, due to the production of fluids, causes the aquifer water to expand and flow into the reservoir. The compressibility is defined mathematically as:

$$c = \frac{1}{V}\frac{\partial V}{\partial p} = \frac{1}{V}\frac{\Delta V}{\Delta p}$$

or:

$$\Delta V = cV\,\Delta p$$

Applying the above basic compressibility definition to the aquifer gives:

Water influx = (aquifer compressibility)

$$\times \text{(initial volume of water)}\,\text{(pressure drop)}$$

or:

$$W_e = c_t W_i (p_i - p) \quad c_t = c_w + c_f \qquad [2.3.1]$$

where:

W_e = cumulative water influx, bbl
c_t = aquifer total compressibility, psi^{-1}
c_w = aquifer water compressibility, psi^{-1}
c_f = aquifer rock compressibility, psi^{-1}
W_i = initial volume of water in the aquifer, bbl
p_i = initial reservoir pressure, psi
p = current reservoir pressure (pressure at oil–water contact), psi

Calculating the initial volume of water in the aquifer requires knowledge of aquifer dimensions and properties. These, however, are seldom measured since wells are not deliberately drilled into the aquifer to obtain such information. For instance, if the aquifer shape is radial, then:

$$W_i = \left[\frac{\pi\,(r_a^2 - r_e^2)\,h\phi}{5.615}\right] \qquad [2.3.2]$$

where:

r_a = radius of the aquifer, ft
r_e = radius of the reservoir, ft
h = thickness of the aquifer, ft
ϕ = porosity of the aquifer

Figure 2.2 *Radial aquifer geometries.*

Equation 2.3.2 suggests that water is encroaching in a radial form from all directions. Quite often, water does not encroach on all sides of the reservoir, or the reservoir is not circular in nature. To account for these cases, a modification to Equation 2.3.2 must be made in order to properly describe the flow mechanism. One of the simplest modifications is to include the fractional encroachment angle f in the equation, as illustrated in Figure 2.2, to give:

$$W_e = (c_w + c_f)\,W_i\,f\,(p_i - p) \qquad [2.3.3]$$

where the fractional encroachment angle f is defined by:

$$f = \frac{(\text{encroachment angle})^{\circ}}{360^{\circ}} = \frac{\theta}{360^{\circ}} \qquad [2.3.4]$$

The above model is only applicable to a small aquifer, i.e., pot aquifer, whose dimensions are of the same order of magnitude as the reservoir itself. Dake (1978) pointed out that because the aquifer is considered relatively small, a pressure drop in the reservoir is instantaneously transmitted throughout the entire reservoir–aquifer system. Dake suggested that for large aquifers, a mathematical model is required which includes time dependence to account for the fact that it takes a finite time for the aquifer to respond to a pressure change in the reservoir.

Example 2.2 Calculate the cumulative water influx that result from a pressure drop of 200 psi at the oil–water contact with an encroachment angle of 80°. The reservoir–aquifer system is characterized by the following properties:

	Reservoir	*Aquifer*
radius, ft	2600	10 000
porosity	0.18	0.12
c_f, psi^{-1}	4×10^{-6}	3×10^{-6}
c_w, psi^{-1}	5×10^{-6}	4×10^{-6}
h, ft	20	25

Solution

Step 1. Calculate the initial volume of water in the aquifer from Equation 2.3.2:

$$W_i = \left[\frac{\pi \left(r_a^2 - r_e^2 \right) h\phi}{5.615} \right]$$

$$= \left[\frac{\pi \left(10\,000^2 - 2600^2 \right) (25)(0.12)}{5.615} \right] = 156.5 \text{ MMbbl}$$

Step 2. Determine the cumulative water influx by applying Equation 2.3.3:

$$W_e = (c_w + c_f) W_i f (p_i - p)$$

$$= (4.0 + 3.0)10^{-6}(156.5 \times 10^6)\left(\frac{80}{360}\right)(200) = 48689 \text{ bbl}$$

2.3.2 The Schilthuis steady-state model

Schilthuis (1936) proposed that for an aquifer that is flowing under the steady-state flow regime, the flow behavior could be described by Darcy's equation. The rate of water influx e_w can then be determined by applying Darcy's equation:

$$\frac{dW_e}{dt} = e_w = \left[\frac{0.00708 kh}{\mu_w \ln(r_a/r_e)} \right] (p_i - p) \qquad [2.3.5]$$

This relationship can be more conveniently expressed as:

$$\frac{dW_e}{dt} = e_w = C(p_i - p) \qquad [2.3.6]$$

where:

e_w = rate of water influx, bbl/day
k = permeability of the aquifer, md
h = thickness of the aquifer, ft
r_a = radius of the aquifer, ft
r_e = radius of the reservoir, ft
t = time, days

The parameter C is called the "water influx constant" and expressed in bbl/day/psi. This water influx constant C may be calculated from the reservoir historical production data over a number of selected time intervals, provided the rate of water influx e_w has been determined independently from a different expression. For instance, the parameter C may be estimated by combining Equations 2.1.1 with 2.3.6. Although the influx constant can only be obtained in this manner when the reservoir pressure stabilizes, once it has been found it may be applied to both stabilized and changing reservoir pressures.

Example 2.3 The data given in Example 2.1 is used in this example:

$p_i = 3500$ psi, $\quad p = 3000$ psi, $\quad Q_o = 32\,000$ STB/day

$B_o = 1.4$ bbl/STB GOR = 900 scf/STB $R_s = 700$ scf/STB

$B_g = 0.00082$ bbl/scf $\quad Q_w = 0$ $\quad B_w = 1.0$ bbl/STB

Calculate the Schilthuis water influx constant.

Solution

Step 1. Solve for the rate of water influx e_w by using Equation 2.1.1:

$$e_w = Q_o B_o + Q_g B_g + Q_w B_w$$

$$= (1.4)(32\,000) + (900 - 700)(32\,000)(0.00082) + 0$$

$$= 50\,048 \text{ bbl/day}$$

Step 2. Solve for the water influx constant from Equation 2.3.6:

$$\frac{dW_e}{dt} = e_w = C(p_i - p)$$

or:

$$C = \frac{e_w}{p_i - p} = \frac{50\,048}{3500 - 3000} = 100 \text{ bbl/day/psi}$$

If the steady-state approximation is considered to adequately describe the aquifer flow regime, the values of the calculated water influx constant C will be constant over the historical period.

Note that the pressure drops contributing to the influx are the cumulative pressure drops from the initial pressure.

In terms of the cumulative water influx W_e, Equation 2.3.6 is integrated to give the common Schilthuis expression for water influx as:

$$\int_0^{W_e} dW_e = \int_0^t C(p_i - p)\, dt$$

or:

$$W_e = C \int_0^t (p_i - p)\, dt \qquad [2.3.7]$$

where:

W_e = cumulative water influx, bbl
C = water influx constant, bbl/day/psi
t = time, days
p_i = initial reservoir pressure, psi
p = pressure at the oil–water contact at time t, psi

When the pressure drop $(p_i - p)$ is plotted versus the time t, as shown in Figure 2.3, the area under the curve represents
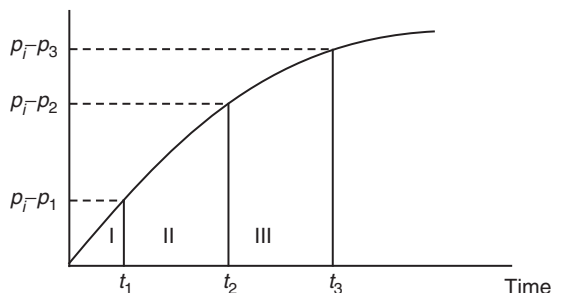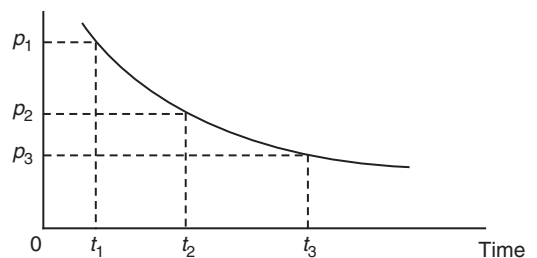
Figure 2.3 *Calculating the area under the curve.*

the integral $\int_0^t (p_i - p)dt$. This area at time t can be determined numerically by using the trapezoidal rule (or any other numerical integration method) as:

$$\int_o^t (p_i - p)\mathrm{d}t = \mathrm{area_I} + \mathrm{area_{II}} + \mathrm{area_{III}} + \cdots$$

$$= \left(\frac{p_i - p_1}{2}\right)(t_1 - 0)$$

$$+ \frac{(p_i - p_1) + (p_i - p_2)}{2}(t_2 - t_1)$$

$$+ \frac{(p_i - p_2) + (p_i - p_3)}{2}(t_3 - t_2) + \cdots$$

Equation 2.3.7 can then be written as:

$$W_e = C \sum_0^t (\Delta p)\Delta t \qquad [2.3.8]$$

Example 2.4   The pressure history of a water drive oil reservoir is given below:

t (days)	p (psi)
0	
100	3450
200	3410
300	3380
400	3340

The aquifer is under a steady-state flowing condition with an estimated water influx constant of 130 bbl/day/psi. Given the initial reservoir pressure is 3500 psi, calculate the cumulative water influx after 100, 200, 300, and 400 days using the steady-state model.

Solution

Step 1.   Calculate the total pressure drop at each time t:

t (days)	p	$p_i - p$
0	3500	0
100	3450	50
200	3410	90
300	3380	120
400	3340	160

Step 2.   Calculate the cumulative water influx after 100 days:

$$W_e = C\left[\left(\frac{p_i - p_1}{2}\right)(t_1 - 0)\right] = 130\left(\frac{50}{2}\right)(100 - 0)$$

$$= 325\,000\ \mathrm{bbl}$$

Step 3.   Determine W_e after 200 days:

$$W_e = C\left\{\left(\frac{p_i - p_1}{2}\right)(t_1 - 0)\right.$$

$$\left. + \left[\frac{(p_i - p_1) + (p_i - p_2)}{2}\right](t_2 - t_1)\right\}$$

$$= 130\left[\left(\frac{50}{2}\right)(100 - 0) + \left(\frac{50 + 90}{2}\right)(200 - 100)\right]$$

$$= 1\,235\,000\ \mathrm{bbl}$$

Step 4. W_e after 300 days:

$$W_e = C\left\{\left(\frac{p_i - p_1}{2}\right)(t_1 - 0)\right.$$

$$+ \left[\frac{(p_i - p_1) + (p_i - p_2)}{2}\right](t_2 - t_1)$$

$$\left. + \frac{(p_i - p_2) + (p_i - p_3)}{2}(t_3 - t_2)\right\}$$

$$= 130\left[\left(\frac{50}{2}\right)(100) + \left(\frac{50 + 90}{2}\right)(200 - 100)\right.$$

$$\left. + \left(\frac{120 + 90}{2}\right)(300 - 200)\right] = 2\,600\,000\ \mathrm{bbl}$$

Step 5.   Similarly, calculate W_e after 400 days:

$$W_e = 130\left[2500 + 7000 + 10\,500\right.$$

$$\left. + \left(\frac{160 + 120}{2}\right)(400 - 300)\right]$$

$$= 4\,420\,000\ \mathrm{bbl}$$

2.3.3 The Hurst modified steady-state equation

One of the problems associated with the Schilthuis steady-state model is that as the water is drained from the aquifer, the aquifer drainage radius r_a will increase as the time increases. Hurst (1943) proposed that the "apparent" aquifer radius r_a would increase with time and, therefore, the dimensionless radius r_a/r_e may be replaced with a *time-dependent function* as given below:

$$r_a/r_e = at \qquad [2.3.9]$$

Substituting Equation 2.3.9 into Equation 2.3.5 gives:

$$e_w = \frac{\mathrm{d}W_e}{\mathrm{d}t} = \frac{0.00708\,kh(p_i - p)}{\mu_w \ln(at)} \qquad [2.3.10]$$

The Hurst modified steady-state equation can be written in a more simplified form as:

$$e_w = \frac{\mathrm{d}W_e}{\mathrm{d}t} = \frac{C(p_i - p)}{\ln(at)} \qquad [2.3.11]$$

and in terms of the cumulative water influx:

$$W_e = C\int_0^t \left[\frac{p_i - p}{\ln(at)}\right]\mathrm{d}t \qquad [2.3.12]$$

Approximating the integral with a summation gives:

$$W_e = C\sum_0^t \left[\frac{\Delta p}{\ln(at)}\right]\Delta t \qquad [2.3.13]$$

The Hurst modified steady-state equation contains two unknown constants, i.e., a and C, that must be determined from the reservoir–aquifer pressure and water influx historical data. The procedure for determining the constants a and C is based on expressing Equation 2.3.11 as a linear relationship:

$$\left(\frac{p_i - p}{e_w}\right) = \frac{1}{C}\ln(at)$$

or:

$$\frac{p_i - p}{e_w} = \left(\frac{1}{C}\right)\ln(a) + \left(\frac{1}{C}\right)\ln(t) \qquad [2.3.14]$$

Equation 2.3.14 indicates that a plot of the term $(p_i - p)/e_w$ vs. $\ln(t)$ would produce a straight line with a slope of $1/C$ and intercept of $(1/C)\ln(a)$, as shown schematically in Figure 2.4.
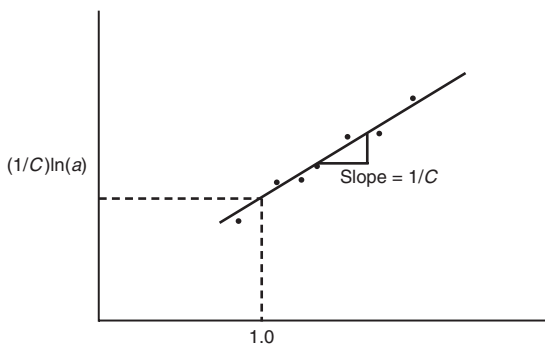
Figure 2.4 *Graphical determination of C and a.*

Example 2.5 The following data, as presented by Craft and Hawkins (1959), documents the reservoir pressure as a function of time for a water drive reservoir. Using the reservoir historical data, Craft and Hawkins calculated the water influx by applying the material balance equation (see Chapter 4). The rate of water influx was also calculated numerically at each time period:

Time (days)	Pressure (psi)	W_e (M bbl)	e_w (bbl/day)	$p_i - p$ (psi)
0	3793	0	0	0
182.5	3774	24.8	389	19
365.0	3709	172.0	1279	84
547.5	3643	480.0	2158	150
730.0	3547	978.0	3187	246
912.5	3485	1616.0	3844	308
1095.0	3416	2388.0	4458	377

It is predicted that the boundary pressure would drop to 3379 psi after 1186.25 days of production. Calculate the cumulative water influx at that time.

Solution

Step 1. Construct the following table.

t (days)	$\ln(t)$	$p_i - p$	e_w (bbl/day)	$(p_i - p)/e_w$
0	–	0	0	–
182.5	5.207	19	389	0.049
365.0	5.900	84	1279	0.066
547.5	6.305	150	2158	0.070
730.0	6.593	246	3187	0.077
912.5	6.816	308	3844	0.081
1095.0	6.999	377	4458	0.085

Step 2. Plot the term $(p_i - p)/e_w$ vs. $\ln(t)$ and draw the best straight line through the points as shown in Figure 2.5, and determine the slope of the line:

$$\text{Slope} = 1/C = 0.020$$

Step 3. Determine the coefficient C of the Hurst equation from the slope:

$$C = 1/\text{slope} = 1/0.02 = 50$$

Step 4. Use any point on the straight line and solve for the parameter a by applying Equation 2.3.11:

$$a = 0.064$$

Step 5. The Hurst equation is represented by:

$$W_e = 50 \int_0^t \left[\frac{p_i - p}{\ln(0.064t)} \right] dt$$

Step 6. Calculate the cumulative water influx after 1186.25 days from:

$$W_e = 2388 \times 10^3 + \int_{1095}^{1186.25} 50 \left[\frac{p_i - p}{\ln(0.064t)} \right] dt$$

$$= 2388 \times 10^3 + 50 \big[((3793 - 3379)/\ln(0.064 \times 1186.25)$$

$$+ (3793 - 3416)/\ln(0.064 \times 1095)) \big/ 2 \big] (1186.25 - 1095)$$

$$= 2388 \times 10^3 + 420.508 \times 10^3 = 2809 \text{ Mbbl}$$
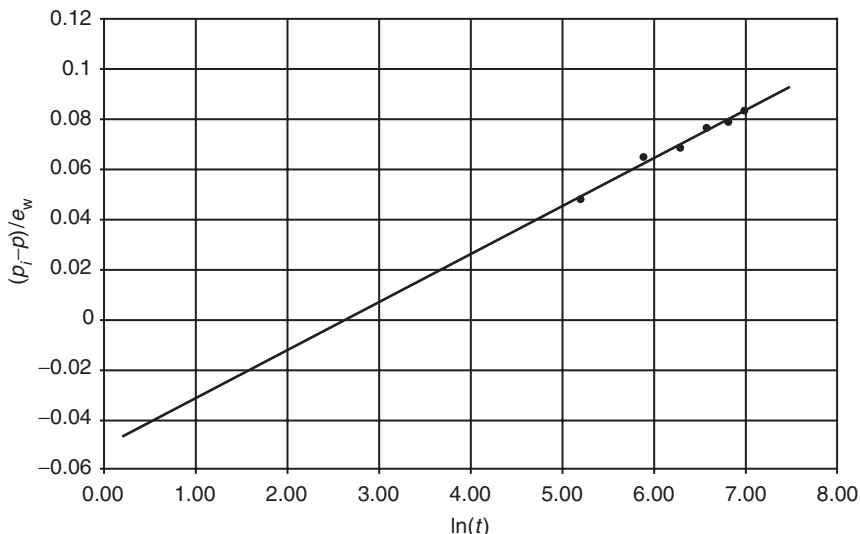
Figure 2.5 *Determination of C and n for Example 2-5.*

2.3.4 The van Everdingen and Hurst unsteady-state model

The mathematical formulations that describe the flow of a crude oil system into a wellbore are identical in form to those equations that describe the flow of water from an aquifer into a cylindrical reservoir, as shown schematically in Figure 2.6. When an oil well is brought on production at a constant flow rate after a shut-in period, the pressure behavior is essentially controlled by the transient (unsteady-state) flowing condition. This flowing condition is defined as the time period during which the boundary has no effect on the pressure behavior.

The dimensionless form of the diffusivity equation, as presented in Chapter 1 by Equation 1.2.78, is basically the general mathematical equation that is designed to model the transient flow behavior in reservoirs or aquifers. In a dimensionless form, the diffusivity equation is:

$$\frac{\partial^2 P_D}{\partial r_D^2} + \frac{1}{r_D}\frac{\partial P_D}{\partial r_D} = \frac{\partial P_D}{\partial t_D}$$
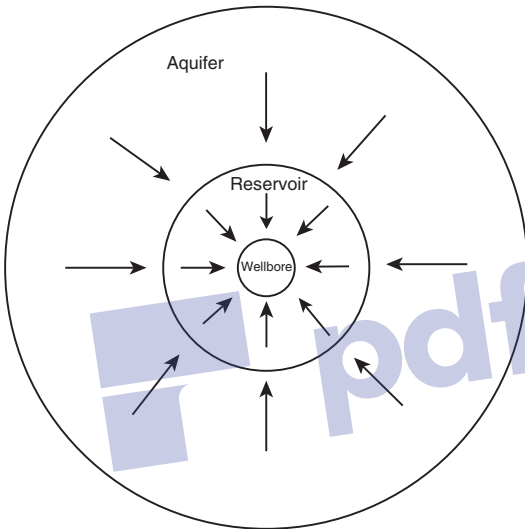
Figure 2.6 *Water influx into a cylindrical reservoir.*

Van Everdingen and Hurst (1949) proposed solutions to the dimensionless diffusivity equation for the following two reservoir–aquifer boundary conditions:

(1) constant terminal rate;
(2) constant terminal pressure.

For the constant-terminal-rate boundary condition, the rate of water influx is assumed constant for a given period, and the pressure drop at the reservoir–aquifer boundary is calculated.

For the constant-terminal-pressure boundary condition, a boundary pressure drop is assumed constant over some finite time period, and the water influx rate is determined.

In the description of water influx from an aquifer into a reservoir, there is greater interest in calculating the influx rate rather than the pressure. This leads to the determination of the water influx as a function of a given pressure drop at the inner boundary of the reservoir–aquifer system.

Van Everdingen and Hurst (1949) solved the diffusivity equation for the aquifer–reservoir system by applying the Laplace transformation to the equation. The authors' solution can be used to determine the water influx in the following systems:

- edge-water drive system (radial system);
- bottom-water drive system;
- linear-water drive system.

Edge-water drive
Figure 2.7 shows an idealized radial flow system that represents an edge-water drive reservoir. The inner boundary is defined as the interface between the reservoir and the aquifer. The flow across this inner boundary is considered horizontal and encroachment occurs across a cylindrical plane encircling the reservoir. With the interface as the inner boundary, it is possible to impose a constant terminal pressure at the inner boundary and determine the rate of water influx across the interface.

Van Everdingen and Hurst proposed a solution to the dimensionless diffusivity equation that utilizes the constant-terminal-pressure condition in addition to the following initial and outer boundary conditions:
Initial conditions:

$p = p_i$ for all values of radius r
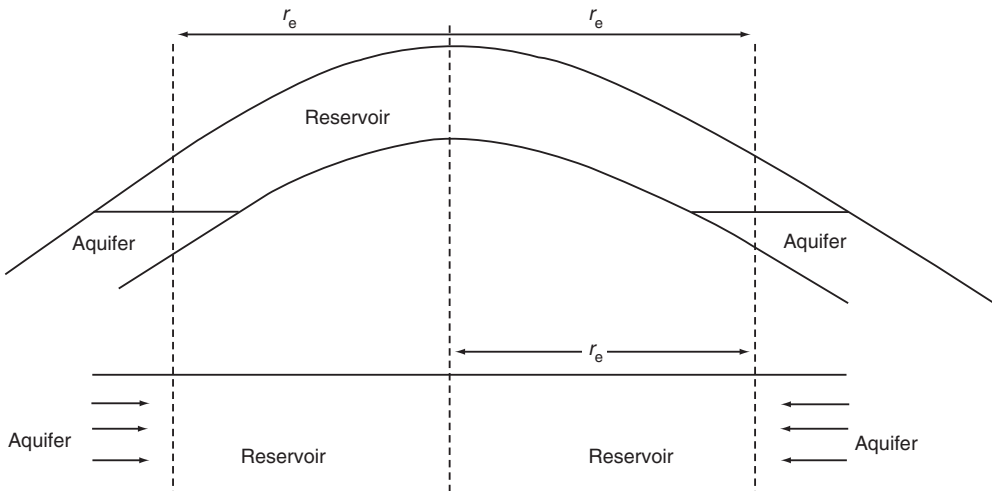
Figure 2.7 *Idealized radial flow model.*

Outer boundary conditions:

- For an infinite aquifer:

$$p = p_i \quad \text{at } r = \infty$$

- For a bounded aquifer:

$$\frac{\partial p}{\partial r} = 0 \quad \text{at } r = r_a$$

Van Everdingen and Hurst assumed that the aquifer is characterized by:

- uniform thickness;
- constant permeability;
- uniform porosity;
- constant rock compressibility;
- constant water compressibility.

The authors expressed their mathematical relationship for calculating the water influx in the form of a dimensionless parameter called dimensionless water influx W_{eD}. They also expressed the dimensionless water influx as a function of the dimensionless time t_D and dimensionless radius r_D; thus they made the solution to the diffusivity equation generalized and it can be applied to any aquifer where the flow of water into the reservoir is essentially radial. The solutions were derived for the cases of bounded aquifers and aquifers of infinite extent. The authors presented their solution in tabulated and graphical forms as reproduced here in Figures 2.8 through 2.11 and Tables 2.1 and 2.2. The two dimensionless parameters t_D and r_D are given by:

$$t_D = 6.328 \times 10^{-3} \frac{kt}{\phi \mu_w c_t r_e^2} \qquad [2.3.15]$$

$$r_D = \frac{r_a}{r_e} \qquad [2.3.16]$$

$$c_t = c_w + c_f \qquad [2.3.17]$$

where:

$$
\begin{aligned}
t &= \text{time, days} \\
k &= \text{permeability of the aquifer, md} \\
\phi &= \text{porosity of the aquifer} \\
\mu_w &= \text{viscosity of water in the aquifer, cp} \\
r_a &= \text{radius of the aquifer, ft} \\
r_e &= \text{radius of the reservoir, ft} \\
c_w &= \text{compressibility of the water, psi}^{-1} \\
c_f &= \text{compressibility of the aquifer formation, psi}^{-1} \\
c_t &= \text{total compressibility coefficient, psi}^{-1}
\end{aligned}
$$

The water influx is then given by:

$$W_e = B \Delta p W_{eD} \qquad [2.3.18]$$

with:

$$B = 1.119 \phi c_t r_e^2 h \qquad [2.3.19]$$

where:

$$
\begin{aligned}
W_e &= \text{cumulative water influx, bbl} \\
B &= \text{water influx constant, bbl/psi} \\
\Delta p &= \text{pressure drop at the boundary, psi} \\
W_{eD} &= \text{dimensionless water influx}
\end{aligned}
$$

Equation 2.3.19 assumes that the water is encroaching in a radial form. Quit often water does not encroach on all sides of the reservoir, or the reservoir is not circular in nature. In these cases, some modifications must be made in Equation 2.3.19 to properly describe the flow mechanism. One of the simplest modifications is to introduce the encroachment angle, as a dimensionally parameter f, to the water influx constant B, as follows:

$$f = \frac{\theta}{360} \qquad [2.3.20]$$

$$B = 1.119 \phi c_t r_e^2 h f \qquad [2.3.21]$$
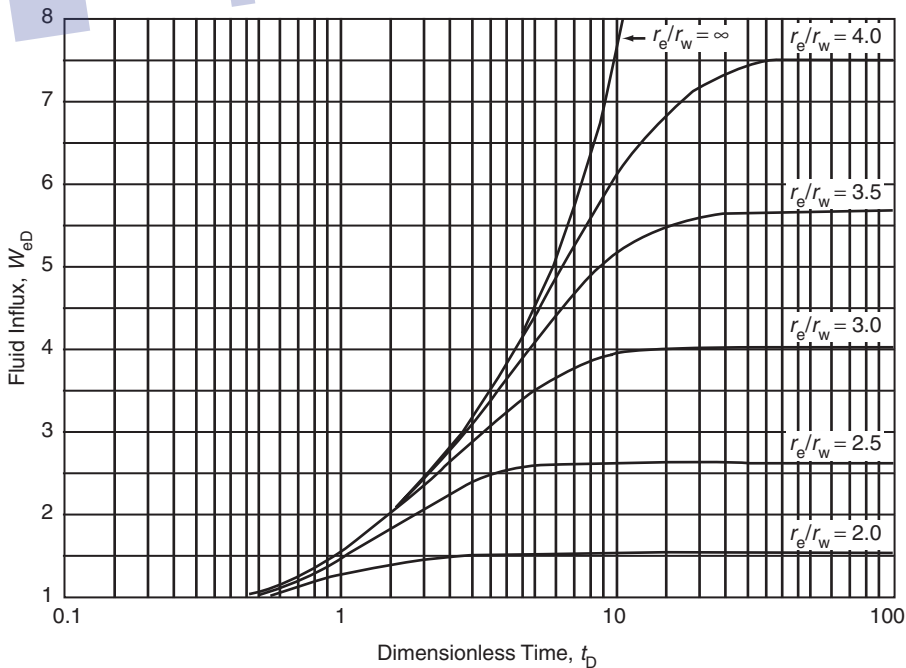
Figure 2.8 *Dimensionless water influx* W_{eD} *for several values of* r_e/r_R, *i.e.,* r_a/r_e *(Van Everdingen and Hurst* W_{eD}. *Permission to publish by the SPE).*

Figure 2.9 *Dimensionless water influx W_{eD} for several values of r_e/r_R, i.e., r_a/r_e (van Everdingen and Hurst W_{eD} values. Permission to publish by the SPE).*

Figure 2.10 *Dimensionless water influx W_{eD} for infinite aquifer (van Everdingen and Hurst W_{eD} values. Permission to publish by the SPE).*

Figure 2.11 *Dimensionless water influx* W_{eD} *for infinite aquifer (van Everdingen and Hurst* W_{eD} *values. Permission to publish by the SPE).*

Table 2.1 *Dimensionless Water Influx* W_{eD} *for Infinite Aquifer (van Everdingen and Hurst* W_{eD}. *Permission to publish by the SPE).*

Dimensionless time t_D	Fluid influx W_{eD}	Dimensionless time t_D	Fluid influx W_{eD}	Dimensionless time t_D	Fluid influx W_{eD}	Dimensionless time t_D	Fluid influx W_{eD}	Dimensionless time t_D	Fluid influx W_{eD}	Dimensionless time t_D	Fluid influx W_{eD}
0.00	0.000	79	35.697	455	150.249	1190	340.843	3250	816.090	35.000	6780.247
0.01	0.112	80	36.058	460	151.640	1200	343.308	3300	827.088	40.000	7650.096
0.05	0.278	81	36.418	465	153.029	1210	345.770	3350	838.067	50.000	9363.099
0.10	0.404	82	36.777	470	154.416	1220	348.230	3400	849.028	60.000	11047.299
0.15	0.520	83	37.136	475	155.801	1225	349.460	3450	859.974	70.000	12708.358
0.20	0.606	84	37.494	480	157.184	1230	350.688	3500	870.903	75.000	13531.457
0.25	0.689	85	37.851	485	158.565	1240	353.144	3550	881.816	80.000	14350.121
0.30	0.758	86	38.207	490	159.945	1250	355.597	3600	892.712	90.000	15975.389
0.40	0.898	87	38.563	495	161.322	1260	358.048	3650	903.594	100.000	17586.284
0.50	1.020	88	38.919	500	162.698	1270	360.496	3700	914.459	125.000	21560.732
0.60	1.140	89	39.272	510	165.444	1275	361.720	3750	925.309	$1.5(10)^5$	$2.538(10)^4$
0.70	1.251	90	39.626	520	168.183	1280	362.942	3800	936.144	2.0"	3.308"
0.80	1.359	91	39.979	525	169.549	1290	365.386	3850	946.966	2.5"	4.066"
0.90	1.469	92	40.331	530	170.914	1300	367.828	3900	957.773	3.0"	4.817"
1	1.569	93	40.684	540	173.639	1310	370.267	3950	968.566	4.0"	6.267"
2	2.447	94	41.034	550	176.357	1320	372.704	4000	979.344	5.0"	7.699"
3	3.202	95	41.385	560	179.069	1325	373.922	4050	990.108	6.0"	9.113"
4	3.893	96	41.735	570	181.774	1330	375.139	4100	1000.858	7.0"	$1.051(10)^5$
5	4.539	97	42.084	575	183.124	1340	377.572	4150	1011.595	8.0"	1.189"
6	5.153	98	42.433	580	184.473	1350	380.003	4200	1022.318	9.0"	1.326"
7	5.743	99	42.781	590	187.166	1360	382.432	4250	1033.028	$1.0(10)6'$	1.462"
8	6.314	100	43.129	600	189.852	1370	384.859	4300	1043.724	1.5"	2.126"
9	6.869	105	44.858	610	192.533	1375	386.070	4350	1054.409	2.0"	2.781"
10	7.411	110	46.574	620	195.208	1380	387.283	4400	1065.082	2.5"	3.427"
11	7.940	115	48.277	625	196.544	1390	389.705	4450	1075.743	3.0"	4.064"
12	8.457	120	49.968	630	197.878	1400	392.125	4500	1086.390	4.0"	5.313"
13	8.964	125	51.648	640	200.542	1410	394.543	4550	1097.024	5.0"	6.544"
14	9.461	130	53.317	650	203.201	1420	396.959	4600	1107.646	6.0"	7.761"
15	9.949	135	54.976	660	205.854	1425	398.167	4650	1118.257	7.0"	8.965"
16	10.434	140	56.625	670	208.502	1430	399.373	4700	1128.854	8.0"	$1.016(10)^6$

(continued)

Table 2.1 *Dimensionless Water Influx* W_{eD} *for Infinite Aquifer (van Everdingen and Hurst* W_{eD}. *Permission to publish by the SPE).*

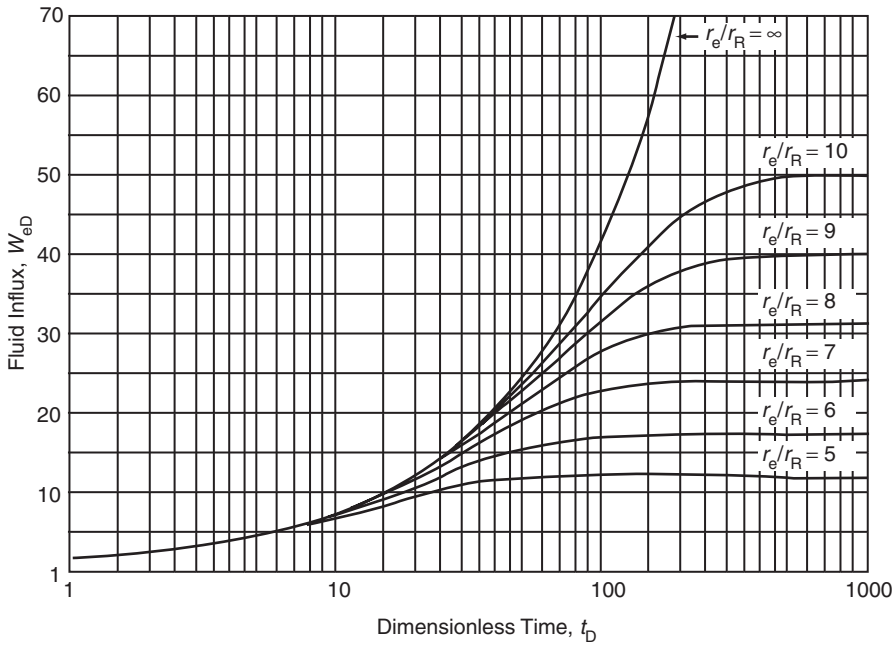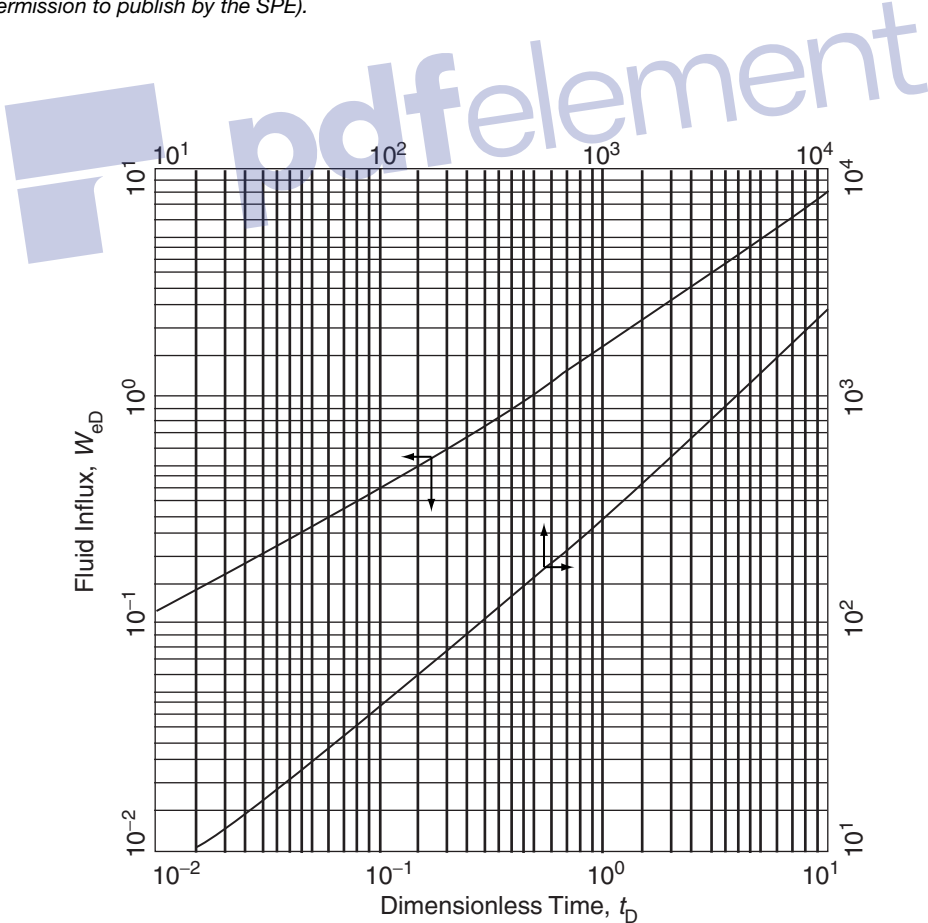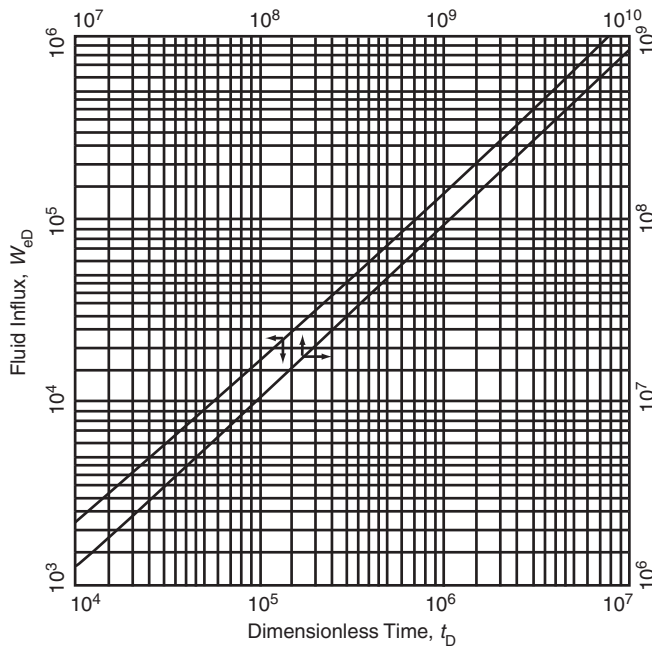| Dimensionless time t_D	Fluid influx W_{eD}	Dimensionless time t_D	Fluid influx W_{eD}	Dimensionless time t_D	Fluid influx W_{eD}	Dimensionless time t_D	Fluid influx W_{eD}	Dimensionless time t_D	Fluid influx W_{eD}	Dimensionless time t_D	Fluid influx W_{eD}
17	10.913	145	58.265	675	209.825	1440	401.786	4750	1139.439	9.0"	1.134"
18	11.386	150	59.895	680	211.145	1450	404.197	4800	1150.012	$1.0(10)^7$	1.252"
19	11.855	155	61.517	690	213.784	1460	406.606	4850	1160.574	1.5"	1.828"
20	12.319	160	63.131	700	216.417	1470	409.013	4900	1171.125	2.0"	2.398"
21	12.778	165	64.737	710	219.046	1475	410.214	4950	1181.666	2.5"	2.961"
22	13.233	170	66.336	720	221.670	1480	411.418	5000	1192.198	3.0"	3.517"
23	13.684	175	67.928	725	222.980	1490	413.820	5100	1213.222	4.0"	4.610"
24	14.131	180	69.512	730	224.289	1500	416.220	5200	1234.203	5.0"	5.689"
25	14.573	185	71.090	740	226.904	1525	422.214	5300	1255.141	6.0"	6.758"
26	15.013	190	72.661	750	229.514	1550	428.196	5400	1276.037	7.0"	7.816"
27	15.450	195	74.226	760	232.120	1575	434.168	5500	1296.893	8.0"	8.866"
28	15.883	200	75.785	770	234.721	1600	440.128	5600	1317.709	9.0"	9.911"
29	16.313	205	77.338	775	236.020	1625	446.077	5700	1338.486	$1.0(10)^8$	$1.095(10)^7$
30	16.742	210	78.886	780	237.318	1650	452.016	5800	1359.225	1.5"	1.604"
31	17.167	215	80.428	790	239.912	1675	457.945	5900	1379.927	2.0"	2.108"
32	17.590	220	81.965	800	242.501	1700	463.863	6000	1400.593	2.5"	2.607"
33	18.011	225	83.497	810	245.086	1725	469.771	6100	1421.224	3.0"	3.100"
34	18.429	230	85.023	820	247.668	1750	475.669	6200	1441.820	4.0"	4.071"
35	18.845	235	86.545	825	248.957	1775	481.558	6300	1462.383	5.0"	5.032"
36	19.259	240	88.062	830	250.245	1800	487.437	6400	1482.912	6.0"	5.984"
37	19.671	245	89.575	840	252.819	1825	493.307	6500	1503.408	7.0"	6.928"
38	20.080	250	91.084	850	255.388	1850	499.167	6600	1523.872	8.0"	7.865"
39	20.488	255	92.589	860	257.953	1875	505.019	6700	1544.305	9.0"	8.797"
40	20.894	260	94.090	870	260.515	1900	510.861	6800	1564.706	$1.0(10)^9$	9.725"
41	21.298	265	95.588	875	261.795	1925	516.695	6900	1585.077	1.5"	$1.429(10)^8$
42	21.701	270	97.081	880	263.073	1950	522.520	7000	1605.418	2.0"	1.880"
43	22.101	275	98.571	890	265.629	1975	528.337	7100	1625.729	2.5"	2.328"
44	22.500	280	100.057	900	268.181	2000	534.145	7200	1646.011	3.0"	2.771"
45	22.897	285	101.540	910	270.729	2025	539.945	7300	1666.265	4.0"	3.645"
46	23.291	290	103.019	920	273.274	2050	545.737	7400	1686.490	5.0"	4.510"
47	23.684	295	104.495	925	274.545	2075	551.522	7500	1706.688	6.0"	5.368"
48	24.076	300	105.968	930	275.815	2100	557.299	7600	1726.859	7.0"	6.220"
49	24.466	305	107.437	940	278.353	2125	563.068	7700	1747.002	8.0"	7.066"
50	24.855	310	108.904	950	280.888	2150	568.830	7800	1767.120	9.0"	7.909"
51	25.244	315	110.367	960	283.420	2175	574.585	7900	1787.212	$1.0(10)^{10}$	8.747"
52	25.633	320	111.827	970	285.948	2200	580.332	8000	1807.278	1.5"	$1.288"(10)^9$
53	26.020	325	113.284	975	287.211	2225	586.072	8100	1827.319	2.0"	1.697"
54	26.406	330	114.738	980	288.473	2250	591.806	8200	1847.336	2.5"	2.103"
55	26.791	335	116.189	990	290.995	2275	597.532	8300	1867.329	3.0"	2.505"
56	27.174	340	117.638	1000	293.514	2300	603.252	8400	1887.298	4.0"	3.299"
57	27.555	345	119.083	1010	296.030	2325	608.965	8500	1907.243	5.0"	4.087"
58	27.935	350	120.526	1020	298.543	2350	614.672	8600	1927.166	6.0"	4.868"
59	28.314	355	121.966	1025	299.799	2375	620.372	8700	1947.065	7.0"	5.643"
60	28.691	360	123.403	1030	301.053	2400	626.066	8800	1966.942	8.0"	6.414"
61	29.068	365	124.838	1040	303.560	2425	631.755	8900	1986.796	9.0"	7.183"
62	29.443	370	126.720	1050	306.065	2450	637.437	9000	2006.628	$1.0(10)^{11}$	7.948"
63	29.818	375	127.699	1060	308.567	2475	643.113	9100	2026.438	1.5"	$1.17(10)^{10}$
64	30.192	380	129.126	1070	311.066	2500	648.781	9200	2046.227	2.0"	1.55"
65	30.565	385	130.550	1075	312.314	2550	660.093	9300	2065.996	2.5"	1.92"
66	30.937	390	131.972	1080	313.562	2600	671.379	9400	2085.744	3.0"	2.29"
67	31.308	395	133.391	1090	316.055	2650	682.640	9500	2105.473	4.0"	3.02"
68	31.679	400	134.808	1100	318.545	2700	693.877	9600	2125.184	5.0"	3.75"
69	32.048	405	136.223	1110	321.032	2750	705.090	9700	2144.878	6.0"	4.47"
70	32.417	410	137.635	1120	323.517	2800	716.280	9800	2164.555	7.0"	5.19"
71	32.785	415	139.045	1125	324.760	2850	727.449	9900	2184.216	8.0"	5.89"
72	33.151	420	140.453	1130	326.000	2900	738.598	10 000	2203.861	9. 0"	6.58"
73	33.517	425	141.859	1140	328.480	2950	749.725	12 500	2688.967	$1.0(10)^{12}$	7.28"
74	33.883	430	143.262	1150	330.958	3000	760.833	15 000	3164.780	1.5"	$1.08(10)^{11}$
75	34.247	435	144.664	1160	333.433	3050	771.922	17 500	3633.368	2.0"	1.42"
76	34.611	440	146.064	1170	335.906	3100	782.992	20 000	4095.800		
77	34.974	445	147.461	1175	337.142	3150	794.042	25 000	5005.726		
78	35.336	450	148.856	1180	338.376	3200	805.075	30 000	5899.508		

Table 2.2 *Dimensionless Water Influx W_{eD} for Several Values of r_e/r_R, i.e., r_a/r_e (Van Everdingen and Hurst W_{eD}. Permission to publish by the SPE).*

| $r_e/r_R = 1.5$ | | $r_e/r_R = 2.0$ | | $r_e/r_R = 2.5$ | | $r_e/r_R = 3.0$ | | $r_e/r_R = 3.5$ | | $r_e/r_R = 4.0$ | | $r_e/r_R = 4.5$ | |
Dimensionless time t_D	Fluid influx W_{eD}	Dimensionless time t_D	Fluid influx W_{eD}	Dimensionless time t_D	Fluid influx W_{eD}	Dimensionless time t_D	Fluid influx W_{eD}	Dimensionless time t_D	Fluid influx W_{eD}	Dimensionless time t_D	Fluid influx W_{eD}	Dimensionless time t_D	Fluid influx W_{eD}
$5.0(10)^{-2}$	0.276	$5.0(10)^{-2}$	0.278	$1.0(10)^{-1}$	0.408	$3.0(10)^{-1}$	0.755	1.00	1.571	2.00	2.442	2.5	2.835
6.0"	0.304	7.5"	0.345	1.5"	0.509	4.0"	0.895	1.20	1.761	2.20	2.598	3.0	3.196
7.0"	0.330	$1.0(10)^{-1}$	0.404	2.0"	0.599	5.0"	1.023	1.40	1.940	2.40	2.748	3.5	3.537
8.0"	0.354	1.25"	0.458	2.5"	0.681	6.0"	1.143	1.60	2.111	2.60	2.893	4.0	3.859
9.0"	0.375	1.50"	0.507	3.0"	0.758	7.0"	1.256	1.80	2.273	2.80	3.034	4.5	4.165
$1.0(10)^{-1}$	0.395	1.75"	0.553	3.5"	0.829	8.0"	1.363	2.00	2.427	3.00	3.170	5.0	4.454
1.1"	0.414	2.00"	0.597	4.0"	0.897	9.0"	1.465	2.20	2.574	3.25	3.334	5.5	4.727
1.2"	0.431	2.25"	0.638	4.5"	0.962	1.00	1.563	2.40	2.715	3.50	3.493	6.0	4.986
1.3"	0.446	2.50"	0.678	5.0"	1.024	1.25	1.791	2.60	2.849	3.75	3.645	6.5	5.231
1.4"	0.461	2.75"	0.715	5.5"	1.083	1.50	1.997	2.80	2.976	4.00	3.792	7.0	5.464
1.5"	0.474	3.00"	0.751	6.0"	1.140	1.75	2.184	3.00	3.098	4.25	3.932	7.5	5.684
1.6"	0.486	3.25"	0.785	6.5"	1.195	2.00	2.353	3.25	3.242	4.50	4.068	8.0	5.892
1.7"	0.497	3.50"	0.817	7.0"	1.248	2.25	2.507	3.50	3.379	4.75	4.198	8.5	6.089
1.8"	0.507	3.75"	0.848	7.5"	1.299	2.50	2.646	3.75	3.507	5.00	4.323	9.0	6.276
1.9"	0.517	4.00"	0.877	8.0"	1.348	2.75	2.772	4.00	3.628	5.50	4.560	9.5	6.453
2.0"	0.525	4.25"	0.905	8.5"	1.395	3.00	2.886	4.25	3.742	6.00	4.779	10	6.621
2.1"	0.533	4.50"	0.932	9.0"	2.440	3.25	2.990	4.50	3.850	6.50	4.982	11	6.930
2.2"	0.541	4.75"	0.958	9.5"	1.484	3.50	3.084	4.75	3.951	7.00	5.169	12	7.208
2.3"	0.548	5.00"	0.993	1.0	1.526	3.75	3.170	5.00	4.047	7.50	5.343	13	7.457
2.4"	0.554	5.50"	1.028	1.1	1.605	4.00	3.247	5.50	4.222	8.00	5.504	14	7.680
2.5"	0.559	6.00"	1.070	1.2	1.679	4.25	3.317	6.00	4.378	8.50	5.653	15	7.880
2.6"	0.565	6.50"	1.108	1.3	1.747	4.50	3.381	6.50	4.516	9.00	5.790	16	8.060
2.8"	0.574	7.00"	1.143	1.4	1.811	4.75	3.439	7.00	4.639	9.50	5.917	18	8.365
3.0"	0.582	7.50"	1.174	1.5	1.870	5.00	3.491	7.50	4.749	10	6.035	20	8.611
3.2"	0.588	8.00"	1.203	1.6	1.924	5.50	3.581	8.00	4.846	11	6.246	22	8.809
3.4"	0.594	9.00"	1.253	1.7	1.975	6.00	3.656	8.50	4.932	12	6.425	24	8.968
3.6"	0.599	1.00"	1.295	1.8	2.022	6.50	3.717	9.00	5.009	13	6.580	26	9.097
3.8"	0.603	1.1	1.330	2.0	2.106	7.00	3.767	9.50	5.078	14	6.712	28	9.200
4.0"	0.606	1.2	1.358	2.2	2.178	7.50	3.809	10.00	5.138	15	6.825	30	9.283
4.5"	0.613	1.3	1.382	2.4	2.241	8.00	3.843	11	5.241	16	6.922	34	9.404
5.0"	0.617	1.4	1.402	2.6	2.294	9.00	3.894	12	5.321	17	7.004	38	9.481
6.0"	0.621	1.6	1.432	2.8	2.340	10.00	3.928	13	5.385	18	7.076	42	9.532
7.0"	0.623	1.7	1.444	3.0	2.380	11.00	3.951	14	5.435	20	7.189	46	9.565
8.0"	0.624	1.8	1.453	3.4	2.444	12.00	3.967	15	5.476	22	7.272	50	9.586
		2.0	1.468	3.8	2.491	14.00	3.985	16	5.506	24	7.332	60	9.612
		2.5	1.487	4.2	2.525	16.00	3.993	17	5.531	26	7.377	70	9.621
		3.0	1.495	4.6	2.551	18.00	3.997	18	5.551	30	7.434	80	9.623
		4.0	1.499	5.0	2.570	20.00	3.999	20	5.579	34	7.464	90	9.624
		5.0	1.500	6.0	2.599	22.00	3.999	25	5.611	38	7.481	100	9.625
				7.0	2.613	24.00	4.000	30	5.621	42	7.490		
				8.0	2.619			35	5.624	46	7.494		
				9.0	2.622			40	5.625	50	7.499		
				10.0	2.624								

| $r_e/r_R = 5.0$ | | $r_e/r_R = 6.0$ | | $r_e/r_R = 7.0$ | | $r_e/r_R = 8.0$ | | $r_e/r_R = 9.0$ | | $r_e/r_R = 10.0$ | |
Dimensionless time t_D	Fluid influx W_{eD}	Dimensionless time t_D	Fluid influx W_{eD}	Dimensionless time t_D	Fluid influx W_{eD}	Dimensionless time t_D	Fluid influx W_{eD}	Dimensionless time t_D	Fluid influx W_{eD}	Dimensionless time t_D	Fluid influx W_{eD}
3.0	3.195	6.0	5.148	9.0	6.861	9	6.861	10	7.417	15	9.96
3.5	3.542	6.5	5.440	9.50	7.127	10	7.398	15	9.945	20	12.32
4.0	3.875	7.0	5.724	10	7.389	11	7.920	20	12.26	22	13.22
4.5	4.193	7.5	6.002	11	7.902	12	8.431	22	13.13	24	14.95
5.0	4.499	8.0	6.273	12	8.397	13	8.930	24	13.98	26	14.95
5.5	4.792	8.5	6.537	13	8.876	14	9.418	26	14.79	28	15.78
6.0	5.074	9.0	6.795	14	9.341	15	9.895	26	15.59	30	16.59
6.5	5.345	9.5	7.047	15	9.791	16	10.361	30	16.35	32	17.38
7.0	5.605	10.0	7.293	16	10.23	17	10.82	32	17.10	34	18.16
7.5	5.854	10.5	7.533	17	10.65	18	11.26	34	17.82	36	18.91

Table 2.2 *Dimensionless Water Influx W_{eD} for Several Values of r_e/r_R, i.e., r_a/r_e (Van Everdingen and Hurst W_{eD}. Permission to publish by the SPE) (continued)*

$r_e/r_R = 5.0$		$r_e/r_R = 6.0$		$r_e/r_R = 7.0$		$r_e/r_R = 8.0$		$r_e/r_R = 9.0$		$r_e/r_R = 10.0$	
Dimensionless time t_D	Fluid influx W_{eD}	Dimensionless time t_D	Fluid influx W_{eD}	Dimensionless time t_D	Fluid influx W_{eD}	Dimensionless time t_D	Fluid influx W_{eD}	Dimensionless time t_D	Fluid influx W_{eD}	Dimensionless time t_D	Fluid influx W_{eD}
8.0	6.094	11	7.767	18	11.06	19	11.70	36	18.52	38	19.65
8.5	6.325	12	8.220	19	11.46	20	12.13	38	19.19	40	20.37
9.0	6.547	13	8.651	20	11.85	22	12.95	40	19.85	42	21.07
9.5	6.760	14	9.063	22	12.58	24	13.74	42	20.48	44	21.76
10	6.965	15	9.456	24	13.27	26	14.50	44	21.09	46	22.42
11	7.350	16	9.829	26	13.92	28	15.23	46	21.69	48	23.07
12	7.706	17	10.19	28	14.53	30	15.92	48	22.26	50	23.71
13	8.035	18	10.53	30	15.11	34	17.22	50	22.82	52	24.33
14	8.339	19	10.85	35	16.39	38	18.41	52	23.36	54	24.94
15	8.620	20	11.16	40	17.49	40	18.97	54	23.89	56	25.53
16	8.879	22	11.74	45	18.43	45	20.26	56	24.39	58	26.11
18	9.338	24	12.26	50	19.24	50	21.42	58	24.88	60	26.67
20	9.731	25	12.50	60	20.51	55	22.46	60	25.36	65	28.02
22	10.07	31	13.74	70	21.45	60	23.40	65	26.48	70	29.29
24	10.35	35	14.40	80	22.13	70	24.98	70	27.52	75	30.49
26	10.59	39	14.93	90	22.63	80	26.26	75	28.48	80	31.61
28	10.80	51	16.05	100	23.00	90	27.28	80	29.36	85	32.67
30	10.98	60	16.56	120	23.47	100	28.11	85	30.18	90	33.66
34	11.26	70	16.91	140	23.71	120	29.31	90	30.93	95	34.60
38	11.46	80	17.14	160	23.85	140	30.08	95	31.63	100	35.48
42	11.61	90	17.27	180	23.92	160	30.58	100	32.27	120	38.51
46	11.71	100	17.36	200	23.96	180	30.91	120	34.39	140	40.89
50	11.79	110	17.41	500	24.00	200	31.12	140	35.92	160	42.75
60	11.91	120	17.45			240	31.34	160	37.04	180	44.21
70	11.96	130	17.46			280	31.43	180	37.85	200	45.36
80	11.98	140	17.48			320	31.47	200	38.44	240	46.95
90	11.99	150	17.49			360	31.49	240	39.17	280	47.94
100	12.00	160	17.49			400	31.50	280	39.56	320	48.54
120	12.00	180	17.50			500	31.50	320	39.77	360	48.91
		200	17.50					360	39.88	400	49.14
		220	17.50					400	39.94	440	49.28
								440	39.97	480	49.36
								480	39.98		

θ is the angle subtended by the reservoir circumference, i.e., for a full circle $\theta = 360°$ and for a semicircular reservoir against a fault $\theta = 180°$, as shown in Figure 2.12.

Example 2.6[a]   Calculate the water influx at the end of 1, 2, and 5 years into a circular reservoir with an aquifer of infinite extent, i.e., $r_{eD} = \infty$. The initial and current reservoir pressures are 2500 and 2490 psi, respectively. The reservoir-aquifer system has the following properties.

	Reservoir	Aquifer
radius, ft	2000	∞
h, ft	20	22.7
k, md	50	100
ϕ, %	15	20
μ_w, cp	0.5	0.8
c_w, psi^{-1}	1×10^{-6}	0.7×10^{-6}
c_f, psi^{-1}	2×10^{-6}	0.3×10^{-6}

[a]Data for this example was reported by Cole, Frank *Reservoir Engineering Manual*, Gulf Publishing Company, 1969.
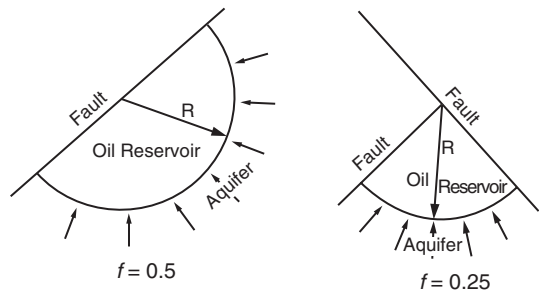
Figure 2.12 *Gas cap drive reservoir (After Cole, F., Reservoir Engineering Manual, Gulf Publishing Company, 1969).*

Solution

Step 1. Calculate the aquifer total compressibility coefficient c_t from Equation 2.3.17:

$$c_t = c_w + c_f$$

$$= 0.7(10^{-6}) + 0.3(10^{-6}) = 1 \times 10^{-6} \text{ psi}^{-1}$$

Step 2. Determine the water influx constant from Equation 2.3.21:

$$B = 1.119 \phi c_t r_e^2 h f$$

$$= 1.119(0.2)(1 \times 10^{-6})(2000)^2(22.7)(360/360)$$

$$= 20.4$$

Step 3. Calculate the corresponding dimensionless time after 1, 2, and 5 years:

$$t_D = 6.328 \times 10^{-3} \frac{kt}{\phi \mu_w c_t r_e^2}$$

$$= 6.328 \times 10^{-3} \frac{100t}{(0.8)(0.2)(1 \times 10^{-6})(2000)^2}$$

$$= 0.9888t$$

Thus in tabular form:

t (days)	$t_D = 0.9888t$
365	361
730	722
1825	1805

Step 4. Using Table 2.1, determine the dimensionless water influx W_{eD}:

t (days)	t_D	W_{eD}
365	361	123.5
730	722	221.8
1825	1805	484.6

Step 5. Calculate the cumulative water influx by applying Equation 2.3.18:

$$W_e = B \Delta p W_{eD}$$

t (days)	W_{eD}	$W_e = (20.4)(2500 \times 2490)W_{eD}$
365	123.5	25 194 bbl
730	221.8	45 247 bbl
1825	484.6	98 858 bbl

Example 2.6 shows that, for a given pressure drop, doubling the time interval will not double the water influx. This example also illustrates how to calculate water influx as a result of a single pressure drop. As there will usually be many of these pressure drops occurring throughout the prediction period, it is necessary to analyze the procedure to be used where these multiple pressure drops are present.

Consider Figure 2.13 which illustrates the decline in the boundary pressure as a function of time for a radial reservoir–aquifer system. If the boundary pressure in the reservoir shown in Figure 2.13 is suddenly reduced at time t, from p_i to p_1, a pressure drop of $(p_i - p_1)$ will be imposed across the aquifer. Water will continue to expand and the new reduced pressure will continue to move outward into the aquifer. Given a sufficient length of time the pressure at the outer edge of the aquifer will finally be reduced to p_1.

If some time after the boundary pressure has been reduced to p_1, a second pressure p_2 is suddenly imposed at the boundary, a new pressure wave will begin moving outward into the aquifer. This new pressure wave will also cause water expansion and therefore encroachment into the reservoir. However, *this new pressure drop will not* be $p_i - p_2$, but will be $p_1 - p_2$. This second pressure wave will be moving behind the first pressure wave. Just ahead of the second pressure wave will be the pressure at the end of the first pressure drop, p_1.

Since these pressure waves are assumed to occur at different times, they are entirely independent of each other. Thus, water expansion will continue to take place as a result of the first pressure drop, even though additional water influx is also taking place as a result of one or more later pressure drops. This is essentially an application of the principle of superposition. In order to determine the total water influx into a reservoir at any given time, it is necessary to determine the water influx as a result of each successive pressure drop that has been imposed on the reservoir and aquifer.
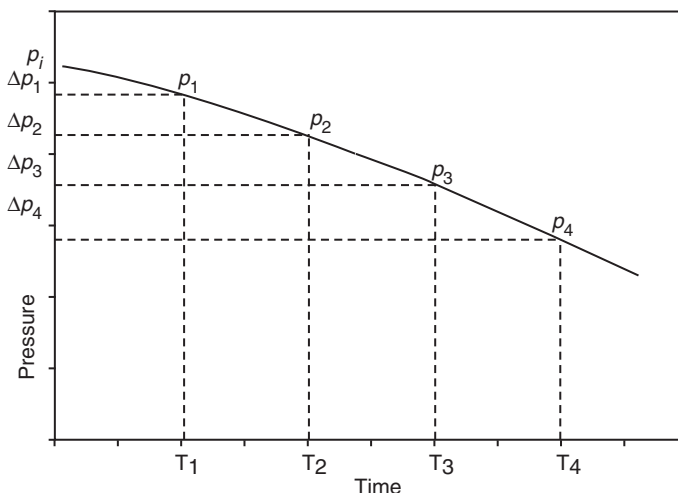
Figure 2.13   Boundary pressure versus time.
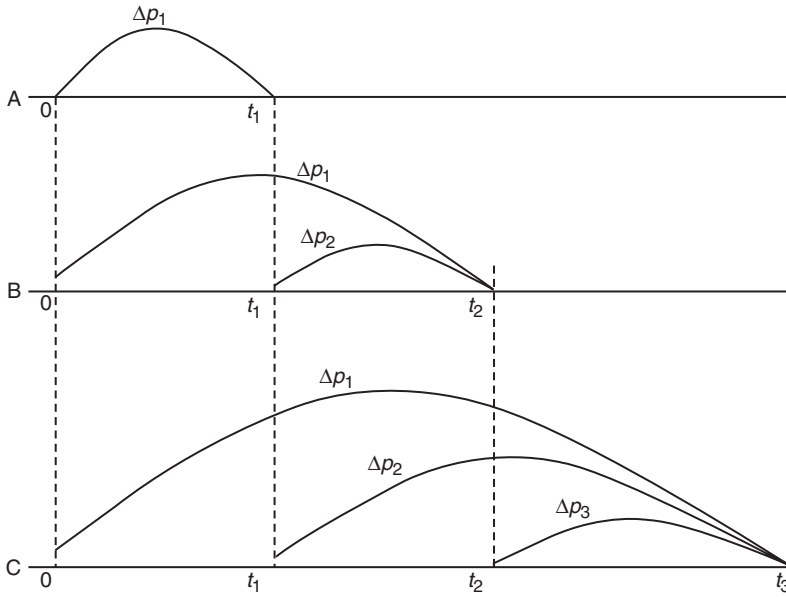
Figure 2.14 *Illustration of the superposition concept.*

In calculating the cumulative water influx into a reservoir at successive intervals, it is necessary to calculate the total water influx from the beginning. This is required because of the different times during which the various pressure drops have been effective.

The van Everdingen and Hurst computational procedure for determining the water influx as a function of time and pressure is summarized by the following steps and described conceptually in Figure 2.14:

Step 1. Assume that the boundary pressure has declined from its initial value of p_i to p_1 after t_1 days. To determine the cumulative water influx in response to this first pressure drop $\Delta p_1 = p_i - p_1$ can be simply calculated from Equation 2.3.18, or:

$$W_e = B \Delta p_1 (W_{eD})_{t_1}$$

where W_e is the cumulative water influx due to the first pressure drop Δp_1. The dimensionless water influx $(W_{eD})_{t_1}$ is evaluated by calculating the dimensionless time at t_1 days. This simple calculation step is shown by A in Figure 2.14.

Step 2. Let the boundary pressure decline again to p_2 after t_2 days with a pressure drop of $\Delta p_2 = p_1 - p_2$. The total cumulative water influx after t_2 days will result from the first pressure drop Δp_1 and the second pressure drop Δp_2, or:

$$W_e = \text{water influx due to } \Delta p_1$$
$$+ \text{ water influx due to } \Delta p_2$$

$$W_e = (W_e)_{\Delta p_1} + (W_e)_{\Delta p_2}$$

where:

$$(W_e)_{\Delta p_1} = B \Delta p_1 (W_{eD})_{t_2}$$
$$(W_e)_{\Delta p_2} = B \Delta p_2 (W_{eD})_{t_2 - t_1}$$

The above relationships indicate that the effect of the first pressure drop Δp_1 will continue for the entire time t_2, while the effect of the second pressure drop

will continue only for $(t_2 - t_1)$ days as shown by B in Figure 2.14.

Step 3. A third pressure drop of $\Delta p_3 = p_2 - p_3$ would cause an additional water influx as illustrated by C in Figure 2.14. The total cumulative water influx can then be calculated from:

$$W_e = (W_e)_{\Delta p_1} + (W_e)_{\Delta p_2} + (W_e)_{\Delta p_3}$$

where:

$$(W_e)_{\Delta p_1} = B \Delta p_1 (W_{eD})_{t_3}$$
$$(W_e)_{\Delta p_2} = B \Delta p_2 (W_{eD})_{t_3 - t_1}$$
$$(W_e)_{\Delta p_3} = B \Delta p_3 (W_{eD})_{t_3 - t_2}$$

The van Everdingen and Hurst water influx relationship can then be expressed in a more generalized form as:

$$W_e = B \sum \Delta p W_{eD} \qquad [2.3.22]$$

The authors also suggested that instead of using the entire pressure drop for the first period, a better approximation is to consider that one-half of the pressure drop, $\frac{1}{2}(p_i - p_1)$, is effective during the entire first period. For the second period the effective pressure drop then is one-half of the pressure drop during the first period, $\frac{1}{2}(p_i - p_2)$, which simplifies to:

$$\frac{1}{2}(p_i - p_1) + \frac{1}{2}(p_1 - p_2) = \frac{1}{2}(p_i - p_2)$$

Similarly, the effective pressure drop for use in the calculations for the third period would be one-half of the pressure drop during the second period, $\frac{1}{2}(p_1 - p_2)$, plus one-half of the pressure drop during the third period, $\frac{1}{2}(p_2 - p_3)$, which simplifies to $\frac{1}{2}(p_1 - p_3)$. The time intervals must all be equal in order to preserve the accuracy of these modifications.

Example 2.7 Using the data given in Example 2.6, calculate the cumulative water influx at the end of 6, 12, 18, and

24 months. The predicted boundary pressure at the end of each specified time period is given below:

Time (days)	Time (months)	Boundary pressure (psi)
0	0	2500
182.5	6	2490
365.0	12	2472
547.5	18	2444
730.0	24	2408

Data from Example 2.6 is listed below:

$$B = 20.4$$

$$t_D = 0.9888\,t$$

Solution   *Water influx after 6 months:*

Step 1. Determine water influx constant B. Example 2.6 gives a value of:

$$B = 20.4 \text{ bbl/psi}$$

Step 2. Calculate the dimensionless time t_D at $t = 182.5$ days:

$$t_D = 0.9888t = 0.9888(182.5) = 180.5$$

Step 3. Calculate the first pressure drop Δp_1. This pressure is taken as one-half of the actual pressured drop, or:

$$\Delta p_1 = \frac{p_i - p_1}{2} = \frac{2500 - 2490}{2} = 5 \text{ psi}$$

Step 4. Determine the dimensionless water influx W_{eD} from Table 2.1 at $t_D = 180.5$, to give:

$$(W_{eD})_{t_1} = 69.46$$

Step 5. Calculate the cumulative water influx at the end of 182.5 days *due to the first pressure drop* of 5 psi, i.e., $(W_e)_{\Delta p_1 = 5}$, by using the van Everdingen and Hurst equation, or:

$$(W_e)_{\Delta p_1 = 5 \text{ psi}} = B\Delta p_1 (W_{eD})_{t_1}$$

$$= (20.4)(5)(69.46) = 7085 \text{ bbl}$$

Cumulative water influx after 12 months:

Step 1. After an additional 6 months, the pressure has declined from 2490 psi to 2472 psi. This second pressure Δp_2 is taken as one-half the actual pressure drop during the first period, plus one-half the actual pressure drop during the second period, or:

$$\Delta p_2 = \frac{p_i - p_2}{2} = \frac{2500 - 2472}{2} = 14 \text{ psi}$$

Step 2. The total cumulative water influx at the end of 12 months would result from the first pressure drop Δp_1 and the second pressure drop Δp_2.
The first pressure drop Δp_1 has been effective for a year, but the second pressure drop, Δp_2, has been effective for only 6 months, as shown in Figure 2.15. Separate calculations must be made for the two pressure drops because of this time difference, and the results added in order to determine the total water influx. That is:

$$W_e = (W_e)_{\Delta p_1} + (W_e)_{\Delta p_2}$$

Figure 2.15   *Duration of the pressure drop in Example 2.7.*

Step 3. Calculate the dimensionless time at 365 days, as:

$$t_D = 0.9888t = 0.9888(365) = 361$$

Step 4. Determine the dimensionless water influx at $t_D = 361$ from Table 2.1, to give:

$$W_{eD} = 123.5$$

Step 5. Calculate the water influx due to the first and second pressure drop, i.e., $(W_e)_{\Delta p_1}$ and $(W_e)_{\Delta p_2}$, or:

$$(W_e)_{\Delta p_1 = 5} = (20.4)(5)(123.5) = 12\,597 \text{ bbl}$$

$$(W_e)_{\Delta p_2 = 14} = (20.4)(14)(69.46) = 19\,838 \text{ bbl}$$

Step 6. Calculate the total cumulative water influx after 12 months:

$$W_e = (W_e)_{\Delta p_1} + (W_e)_{\Delta p_2}$$

$$= 12\,597 + 19\,938 = 32\,435 \text{ bbl}$$

Water influx after 18 months:

Step 1. Calculate the third pressure drop Δp_3 which is taken as one-half of the actual pressure drop during the second period plus one-half of the *actual* pressure drop during the third period, or:

$$\Delta p_3 = \frac{p_1 - p_3}{2} = \frac{2490 - 2444}{2} = 23 \text{ psi}$$

Step 2. Calculate the dimensionless time after 6 months:

$$t_D = 0.9888t = 0.9888(547.5) = 541.5$$

Step 3. Determine the dimensionless water influx from Table 2.1 at $t_D = 541.5$:

$$W_{eD} = 173.7$$

Step 4. The first pressure drop will have been effective for the entire 18 months, the second pressure drop will have been effective for 12 months, and the last pressure drop will have been effective for only 6 months, as shown in Figure 2.16. Therefore, the cumulative water influx is as calculated below:

Time (days)	t_D	Δp	W_{eD}	$B\Delta p W_{eD}$
547.5	541.5	5	173.7	17\,714
365	361	14	123.5	35\,272
182.5	180.5	23	69.40	32\,291
$W_e = 85\,277$ bbl				

Water influx after 24 months:
The first pressure drop has now been effective for the entire 24 months, the second pressure drop has been effective for 18 months, the third pressure drop has been effective for
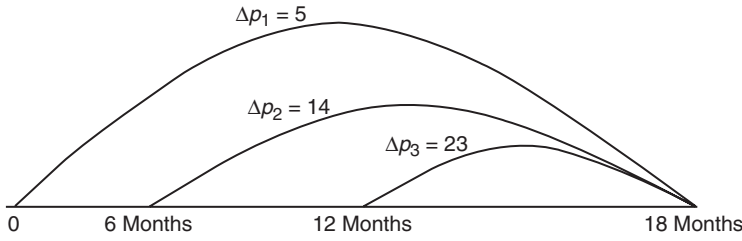
Figure 2.16 *Pressure drop data for Example 2.7.*

12 months, and the fourth pressure drop has been effective only 6 months. A summary of the calculations is given below:

Time (days)	t_D	Δp	W_{eD}	$B\Delta p W_{eD}$
730	722	5	221.8	22 624
547.5	541.5	14	173.7	49 609
365	361	23	123.5	57 946
182.5	180.5	32	69.40	45 343
$W_e = 175\,522$ bbl				

Edwardson et al. (1962) developed three sets of simple polynomial expressions for calculating the dimensionless water influx W_{eD} for infinite-acting aquifers. The proposed three expressions essentially approximate the W_{eD} data in three dimensionless time regions.

(1) For $t_D < 0.01$:

$$W_{eD} = \sqrt{\frac{t_D}{\pi}} \qquad [2.3.23]$$

(2) For $0.01 < t_D < 200$:

$$W_{eD} = \left(1.2838\sqrt{t_D} + 1.19328\,t_D + 0.269872\,(t_D)^{3/2}\right.$$
$$\left. + 0.00855294\,(t_D)^2\right)/\left(1 + 0.616599\sqrt{t_D}\right.$$
$$\left. + 0.0413008\,t_D\right) \qquad [2.3.24]$$

(3) For $t_D > 200$:

$$W_{eD} = \frac{-4.29881 + 2.02566\,t_D}{\ln(t_D)} \qquad [2.3.25]$$

Bottom-water drive

The van Everdingen and Hurst solution to the *radial* diffusivity equation is considered the most rigorous aquifer influx model to date. However, the proposed solution technique is not adequate to describe the vertical water encroachment in bottom-water drive systems. Coats (1962) presented a mathematical model that takes into account the vertical flow effects from bottom-water aquifers. He correctly noted that in many cases reservoirs are situated on top of an aquifer with a continuous horizontal interface between the reservoir fluid and the aquifer water and with a significant aquifer thickness. He stated that in such situations significant bottom-water drive would occur. He modified the diffusivity equation to account for the vertical flow by including an additional term in the equation, to give:

$$\frac{\partial^2 p}{\partial r^2} + \frac{1}{r}\frac{\partial p}{\partial r} + F_k\frac{\partial^2 p}{\partial z^2} = \frac{\mu\phi c}{k}\frac{\partial p}{\partial t} \qquad [2.3.26]$$

where F_k is the ratio of vertical to horizontal permeability, or:

$$F_k = k_v/k_h \qquad [2.3.27]$$

where:

k_v = vertical permeability
k_h = horizontal permeability

Allard and Chen (1988) pointed out that there are an infinite number of solutions to Equation 2.3.26, representing all possible reservoir–aquifer configurations. They suggested that it is possible to derive a general solution that is applicable to a variety of systems by the solution to Equation 2.3.26 in terms of the dimensionless time t_D, dimensionless radius r_D, and a newly introduced dimensionless variable, z_D.

$$z_D = \frac{h}{r_e\sqrt{F_k}} \qquad [2.3.28]$$

where:

z_D = dimensionless vertical distance
h = aquifer thickness, ft

Allen and Chen used a numerical model to solve Equation 2.3.26. The authors developed a solution to the bottom-water influx that is comparable in form with that of van Everdingen and Hurst:

$$W_e = B\sum\Delta p\,W_{eD} \qquad [2.3.29]$$

They defined the water influx constant B as identical to that of Equation 2.3.19, or

$$B = 1.119\phi c_t r_e^2 h \qquad [2.3.30]$$

Note that the water influx constant B in bottom-water drive reservoirs *does not include* the encroachment angle θ.

The actual values of W_{eD} are different from those of the van Everdingen and Hurst model because W_{eD} for the bottom-water drive is also a function of the vertical permeability. Allard and Chen tabulated the values of W_{eD} as a function of r_D, t_D, and z_D. These values are presented in Tables 2.3 through 2.7.

The solution procedure of a bottom-water influx problem is identical to the edge-water influx problem outlined in Example 2.7. Allard and Chen illustrated results of their method in the following example.

Example 2.8 An infinite-acting bottom-water aquifer is characterized by the following properties:

$r_a = \infty$, $k_h = 50$ md, $F_k = 0.04$, $\phi = 0.1$,
$\mu_w = 0.395$ cp, $c_t = 8 \times 10^{-6}$ psi^{-1}, $h = 200$ ft,
$r_e = 2000$ ft, $\theta = 360°$

Table 2.3 *Dimensionless Water Influx, W$_{eD}$, for Infinite Aquifer (Permission to publish by the SPE)*

				Z'_D			
t_D	*0.05*	*0.1*	*0.3*	*0.5*	*0.7*	*0.9*	*1.0*
0.1	0.700	0.677	0.508	0.349	0.251	0.195	0.176
0.2	0.793	0.786	0.696	0.547	0.416	0.328	0.295
0.3	0.936	0.926	0.834	0.692	0.548	0.440	0.396
0.4	1.051	1.041	0.952	0.812	0.662	0.540	0.486
0.5	1.158	1.155	1.059	0.918	0.764	0.631	0.569
0.6	1.270	1.268	1.167	1.021	0.862	0.721	0.651
0.7	1.384	1.380	1.270	1.116	0.953	0.806	0.729
0.8	1.503	1.499	1.373	1.205	1.039	0.886	0.803
0.9	1.621	1.612	1.477	1.286	1.117	0.959	0.872
1	1.743	1.726	1.581	1.347	1.181	1.020	0.932
2	2.402	2.393	2.288	2.034	1.827	1.622	1.509
3	3.031	3.018	2.895	2.650	2.408	2.164	2.026
4	3.629	3.615	3.477	3.223	2.949	2.669	2.510
5	4.217	4.201	4.048	3.766	3.462	3.150	2.971
6	4.784	4.766	4.601	4.288	3.956	3.614	3.416
7	5.323	5.303	5.128	4.792	4.434	4.063	3.847
8	5.829	5.808	5.625	5.283	4.900	4.501	4.268
9	6.306	6.283	6.094	5.762	5.355	4.929	4.680
10	6.837	6.816	6.583	6.214	5.792	5.344	5.080
11	7.263	7.242	7.040	6.664	6.217	5.745	5.468
12	7.742	7.718	7.495	7.104	6.638	6.143	5.852
13	8.196	8.172	7.943	7.539	7.052	6.536	6.231
14	8.648	8.623	8.385	7.967	7.461	6.923	6.604
15	9.094	9.068	8.821	8.389	7.864	7.305	6.973
16	9.534	9.507	9.253	8.806	8.262	7.682	7.338
17	9.969	9.942	9.679	9.218	8.656	8.056	7.699
18	10.399	10.371	10.100	9.626	9.046	8.426	8.057
19	10.823	10.794	10.516	10.029	9.432	8.793	8.411
20	11.241	11.211	10.929	10.430	9.815	9.156	8.763
21	11.664	11.633	11.339	10.826	10.194	9.516	9.111
22	12.075	12.045	11.744	11.219	10.571	9.874	9.457
23	12.486	12.454	12.147	11.609	10.944	10.229	9.801
24	12.893	12.861	12.546	11.996	11.315	10.581	10.142
25	13.297	13.264	12.942	12.380	11.683	10.931	10.481
26	13.698	13.665	13.336	12.761	12.048	11.279	10.817
27	14.097	14.062	13.726	13.140	12.411	11.625	11.152
28	14.493	14.458	14.115	13.517	12.772	11.968	11.485
29	14.886	14.850	14.501	13.891	13.131	12.310	11.816
30	15.277	15.241	14.884	14.263	13.488	12.650	12.145
31	15.666	15.628	15.266	14.634	13.843	12.990	12.473
32	16.053	16.015	15.645	15.002	14.196	13.324	12.799
33	16.437	16.398	16.023	15.368	14.548	13.659	13.123
34	16.819	16.780	16.398	15.732	14.897	13.992	13.446
35	17.200	17.160	16.772	16.095	15.245	14.324	13.767
36	17.579	17.538	17.143	16.456	15.592	14.654	14.088
37	17.956	17.915	17.513	16.815	15.937	14.983	14.406
38	18.331	18.289	17.882	17.173	16.280	15.311	14.724
39	18.704	18.662	18.249	17.529	16.622	15.637	15.040
40	19.088	19.045	18.620	17.886	16.964	15.963	15.356
41	19.450	19.407	18.982	18.240	17.305	16.288	15.671
42	19.821	19.777	19.344	18.592	17.644	16.611	15.985
43	20.188	20.144	19.706	18.943	17.981	16.933	16.297
44	20.555	20.510	20.065	19.293	18.317	17.253	16.608
45	20.920	20.874	20.424	19.641	18.651	17.573	16.918
46	21.283	21.237	20.781	19.988	18.985	17.891	17.227
47	21.645	21.598	21.137	20.333	19.317	18.208	17.535
48	22.006	21.958	21.491	20.678	19.648	18.524	17.841
49	22.365	22.317	21.844	21.021	19.978	18.840	18.147

(continued)

Table 2.3   *Dimensionless Water Influx, W$_{eD}$, for Infinite Aquifer (Permission to publish by the SPE) (continued)*

				Z'_D			
t_D	*0.05*	*0.1*	*0.3*	*0.5*	*0.7*	*0.9*	*1.0*
50	22.722	22.674	22.196	21.363	20.307	19.154	18.452
51	23.081	23.032	22.547	21.704	20.635	19.467	18.757
52	23.436	23.387	22.897	22.044	20.962	19.779	19.060
53	23.791	23.741	23.245	22.383	21.288	20.091	19.362
54	24.145	24.094	23.593	22.721	21.613	20.401	19.664
55	24.498	24.446	23.939	23.058	21.937	20.711	19.965
56	24.849	24.797	24.285	23.393	22.260	21.020	20.265
57	25.200	25.147	24.629	23.728	22.583	21.328	20.564
58	25.549	25.496	24.973	24.062	22.904	21.636	20.862
59	25.898	25.844	25.315	24.395	23.225	21.942	21.160
60	26.246	26.191	25.657	24.728	23.545	22.248	21.457
61	26.592	26.537	25.998	25.059	23.864	22.553	21.754
62	26.938	26.883	26.337	25.390	24.182	22.857	22.049
63	27.283	27.227	26.676	25.719	24.499	23.161	22.344
64	27.627	27.570	27.015	26.048	24.616	23.464	22.639
65	27.970	27.913	27.352	26.376	25.132	23.766	22.932
66	28.312	28.255	27.688	26.704	25.447	24.088	23.225
67	28.653	28.596	28.024	27.030	25.762	24.369	23.518
68	28.994	28.936	28.359	27.356	26.075	24.669	23.810
69	29.334	29.275	28.693	27.681	26.389	24.969	24.101
70	29.673	29.614	29.026	28.008	26.701	25.268	24.391
71	30.011	29.951	29.359	28.329	27.013	25.566	24.881
72	30.349	30.288	29.691	28.652	27.324	25.864	24.971
73	30.686	30.625	30.022	28.974	27.634	26.161	25.260
74	31.022	30.960	30.353	29.296	27.944	26.458	25.548
75	31.357	31.295	30.682	29.617	28.254	26.754	25.836
76	31.692	31.629	31.012	29.937	28.562	27.049	26.124
77	32.026	31.963	31.340	30.257	28.870	27.344	26.410
78	32.359	32.296	31.668	30.576	29.178	27.639	26.697
79	32.692	32.628	31.995	30.895	29.485	27.933	25.983
80	33.024	32.959	32.322	31.212	29.791	28.226	27.268
81	33.355	33.290	32.647	31.530	30.097	28.519	27.553
82	33.686	33.621	32.973	31.846	30.402	28.812	27.837
83	34.016	33.950	33.297	32.163	30.707	29.104	28.121
84	34.345	34.279	33.622	32.478	31.011	29.395	28.404
85	34.674	34.608	33.945	32.793	31.315	29.686	28.687
86	35.003	34.935	34.268	33.107	31.618	29.976	28.970
87	35.330	35.263	34.590	33.421	31.921	30.266	29.252
88	35.657	35.589	34.912	33.735	32.223	30.556	29.534
89	35.984	35.915	35.233	34.048	32.525	30.845	29.815
90	36.310	36.241	35.554	34.360	32.826	31.134	30.096
91	36.636	36.566	35.874	34.672	33.127	31.422	30.376
92	36.960	36.890	36.194	34.983	33.427	31.710	30.656
93	37.285	37.214	36.513	35.294	33.727	31.997	30.935
94	37.609	37.538	36.832	35.604	34.026	32.284	31.215
95	37.932	37.861	37.150	35.914	34.325	32.570	31.493
96	38.255	38.183	37.467	36.223	34.623	32.857	31.772
97	38.577	38.505	37.785	36.532	34.921	33.142	32.050
98	38.899	38.826	38.101	36.841	35.219	33.427	32.327
99	39.220	39.147	38.417	37.149	35.516	33.712	32.605
100	39.541	39.467	38.733	37.456	35.813	33.997	32.881
105	41.138	41.062	40.305	38.987	37.290	35.414	34.260
110	42.724	42.645	41.865	40.508	38.758	36.821	35.630
115	44.299	44.218	43.415	42.018	40.216	38.221	36.993
120	45.864	45.781	44.956	43.520	41.666	39.612	38.347
125	47.420	47.334	46.487	45.012	43.107	40.995	39.694
130	48.966	48.879	48.009	46.497	44.541	42.372	41.035
135	50.504	50.414	49.523	47.973	45.967	43.741	42.368

(continued)

Table 2.3 *Dimensionless Water Influx,* W$_{eD}$, *for Infinite Aquifer (Permission to publish by the SPE) (continued)*

t_D	Z'_D 0.05	0.1	0.3	0.5	0.7	0.9	1.0
140	52.033	51.942	51.029	49.441	47.386	45.104	43.696
145	53.555	53.462	52.528	50.903	48.798	46.460	45.017
150	55.070	54.974	54.019	52.357	50.204	47.810	46.333
155	56.577	56.479	55.503	53.805	51.603	49.155	47.643
160	58.077	57.977	56.981	55.246	52.996	50.494	48.947
165	59.570	59.469	58.452	56.681	54.384	51.827	50.247
170	61.058	60.954	59.916	58.110	55.766	53.156	51.542
175	62.539	62.433	61.375	59.534	57.143	54.479	52.832
180	64.014	63.906	62.829	60.952	58.514	55.798	54.118
185	65.484	65.374	64.276	62.365	59.881	57.112	55.399
190	66.948	66.836	65.718	63.773	61.243	58.422	56.676
195	68.406	68.293	67.156	65.175	62.600	59.727	57.949
200	69.860	69.744	68.588	66.573	63.952	61.028	59.217
205	71.309	71.191	70.015	67.967	65.301	62.326	60.482
210	72.752	72.633	71.437	69.355	66.645	63.619	61.744
215	74.191	74.070	72.855	70.740	67.985	64.908	63.001
220	75.626	75.503	74.269	72.120	69.321	66.194	64.255
225	77.056	76.931	75.678	73.496	70.653	67.476	65.506
230	78.482	78.355	77.083	74.868	71.981	68.755	66.753
235	79.903	79.774	78.484	76.236	73.306	70.030	67.997
240	81.321	81.190	79.881	77.601	74.627	71.302	69.238
245	82.734	82.602	81.275	78.962	75.945	72.570	70.476
250	84.144	84.010	82.664	80.319	77.259	73.736	71.711
255	85.550	85.414	84.050	81.672	78.570	75.098	72.943
260	86.952	86.814	85.432	83.023	79.878	76.358	74.172
265	88.351	88.211	86.811	84.369	81.182	77.614	75.398
270	89.746	89.604	88.186	85.713	82.484	78.868	76.621
275	91.138	90.994	89.558	87.053	83.782	80.119	77.842
280	92.526	92.381	90.926	88.391	85.078	81.367	79.060
285	93.911	93.764	92.292	89.725	86.371	82.612	80.276
290	95.293	95.144	93.654	91.056	87.660	83.855	81.489
295	96.672	96.521	95.014	92.385	88.948	85.095	82.700
300	98.048	97.895	96.370	93.710	90.232	86.333	83.908
305	99.420	99.266	97.724	95.033	91.514	87.568	85.114
310	100.79	100.64	99.07	96.35	92.79	88.80	86.32
315	102.16	102.00	100.42	97.67	94.07	90.03	87.52
320	103.52	103.36	101.77	98.99	95.34	91.26	88.72
325	104.88	104.72	103.11	100.30	96.62	92.49	89.92
330	106.24	106.08	104.45	101.61	97.89	93.71	91.11
335	107.60	107.43	105.79	102.91	99.15	94.93	92.30
340	108.95	108.79	107.12	104.22	100.42	96.15	93.49
345	110.30	110.13	108.45	105.52	101.68	97.37	94.68
350	111.65	111.48	109.78	106.82	102.94	98.58	95.87
355	113.00	112.82	111.11	108.12	104.20	99.80	97.06
360	114.34	114.17	112.43	109.41	105.45	101.01	98.24
365	115.68	115.51	113.76	110.71	106.71	102.22	99.42
370	117.02	116.84	115.08	112.00	107.96	103.42	100.60
375	118.36	118.18	116.40	113.29	109.21	104.63	101.78
380	119.69	119.51	117.71	114.57	110.46	105.83	102.95
385	121.02	120.84	119.02	115.86	111.70	107.04	104.13
390	122.35	122.17	120.34	117.14	112.95	108.24	105.30
395	123.68	123.49	121.65	118.42	114.19	109.43	106.47
400	125.00	124.82	122.94	119.70	115.43	110.63	107.64
405	126.33	126.14	124.26	120.97	116.67	111.82	108.80
410	127.65	127.46	125.56	122.25	117.90	113.02	109.97
415	128.97	128.78	126.86	123.52	119.14	114.21	111.13
420	130.28	130.09	128.16	124.79	120.37	115.40	112.30
425	131.60	131.40	129.46	126.06	121.60	116.59	113.46
430	132.91	132.72	130.75	127.33	122.83	117.77	114.62

(continued)

Table 2.3   *Dimensionless Water Influx, W*$_{eD}$*, for Infinite Aquifer (Permission to publish by the SPE) (continued)*

t_D	Z'_D						
	0.05	*0.1*	*0.3*	*0.5*	*0.7*	*0.9*	*1.0*
435	134.22	134.03	132.05	128.59	124.06	118.96	115.77
440	135.53	135.33	133.34	129.86	125.29	120.14	116.93
445	136.84	136.64	134.63	131.12	126.51	121.32	118.08
450	138.15	137.94	135.92	132.38	127.73	122.50	119.24
455	139.45	139.25	137.20	133.64	128.96	123.68	120.39
460	140.75	140.55	138.49	134.90	130.18	124.86	121.54
465	142.05	141.85	139.77	136.15	131.39	126.04	122.69
470	143.35	143.14	141.05	137.40	132.61	127.21	123.84
475	144.65	144.44	142.33	138.66	133.82	128.38	124.98
480	145.94	145.73	143.61	139.91	135.04	129.55	126.13
485	147.24	147.02	144.89	141.15	136.25	130.72	127.27
490	148.53	148.31	146.16	142.40	137.46	131.89	128.41
495	149.82	149.60	147.43	143.65	138.67	133.06	129.56
500	151.11	150.89	148.71	144.89	139.88	134.23	130.70
510	153.68	153.46	151.24	147.38	142.29	136.56	132.97
520	156.25	156.02	153.78	149.85	144.70	138.88	135.24
530	158.81	158.58	156.30	152.33	147.10	141.20	137.51
540	161.36	161.13	158.82	154.79	149.49	143.51	139.77
550	163.91	163.68	161.34	157.25	151.88	145.82	142.03
560	166.45	166.22	163.85	159.71	154.27	148.12	144.28
570	168.99	168.75	166.35	162.16	156.65	150.42	146.53
580	171.52	171.28	168.85	164.61	159.02	152.72	148.77
590	174.05	173.80	171.34	167.05	161.39	155.01	151.01
600	176.57	176.32	173.83	169.48	163.76	157.29	153.25
610	179.09	178.83	176.32	171.92	166.12	159.58	155.48
620	181.60	181.34	178.80	174.34	168.48	161.85	157.71
630	184.10	183.85	181.27	176.76	170.83	164.13	159.93
640	186.60	186.35	183.74	179.18	173.18	166.40	162.15
650	189.10	188.84	186.20	181.60	175.52	168.66	164.37
660	191.59	191.33	188.66	184.00	177.86	170.92	166.58
670	194.08	193.81	191.12	186.41	180.20	173.18	168.79
680	196.57	196.29	193.57	188.81	182.53	175.44	170.99
690	199.04	198.77	196.02	191.21	184.86	177.69	173.20
700	201.52	201.24	198.46	193.60	187.19	179.94	175.39
710	203.99	203.71	200.90	195.99	189.51	182.18	177.59
720	206.46	206.17	203.34	198.37	191.83	184.42	179.78
730	208.92	208.63	205.77	200.75	194.14	186.66	181.97
740	211.38	211.09	208.19	203.13	196.45	188.89	184.15
750	213.83	213.54	210.62	205.50	198.76	191.12	186.34
760	216.28	215.99	213.04	207.87	201.06	193.35	188.52
770	218.73	218.43	215.45	210.24	203.36	195.57	190.69
780	221.17	220.87	217.86	212.60	205.66	197.80	192.87
790	223.61	223.31	220.27	214.96	207.95	200.01	195.04
800	226.05	225.74	222.68	217.32	210.24	202.23	197.20
810	228.48	228.17	225.08	219.67	212.53	204.44	199.37
820	230.91	230.60	227.48	222.02	214.81	206.65	201.53
830	233.33	233.02	229.87	224.36	217.09	208.86	203.69
840	235.76	235.44	232.26	226.71	219.37	211.06	205.85
850	238.18	237.86	234.65	229.05	221.64	213.26	208.00
860	240.59	240.27	237.04	231.38	223.92	215.46	210.15
870	243.00	242.68	239.42	233.72	226.19	217.65	212.30
880	245.41	245.08	241.80	236.05	228.45	219.85	214.44
890	247.82	247.49	244.17	238.37	230.72	222.04	216.59
900	250.22	249.89	246.55	240.70	232.98	224.22	218.73
910	252.62	252.28	248.92	243.02	235.23	226.41	220.87
920	255.01	254.68	251.28	245.34	237.49	228.59	223.00
930	257.41	257.07	253.65	247.66	239.74	230.77	225.14
940	259.80	259.46	256.01	249.97	241.99	232.95	227.27

(continued)

Table 2.3 Dimensionless Water Influx, W_{eD}, for Infinite Aquifer (Permission to publish by the SPE) (continued)

| t_D | Z_D' | | | | | | |
	0.05	0.1	0.3	0.5	0.7	0.9	1.0
950	262.19	261.84	258.36	252.28	244.24	235.12	229.39
960	264.57	264.22	260.72	254.59	246.48	237.29	231.52
970	266.95	266.60	263.07	256.89	248.72	239.46	233.65
980	269.33	268.98	265.42	259.19	250.96	241.63	235.77
990	271.71	271.35	267.77	261.49	253.20	243.80	237.89
1000	274.08	273.72	270.11	263.79	255.44	245.96	240.00
1010	276.35	275.99	272.35	265.99	257.58	248.04	242.04
1020	278.72	278.35	274.69	268.29	259.81	250.19	244.15
1030	281.08	280.72	277.03	270.57	262.04	252.35	246.26
1040	283.44	283.08	279.36	272.86	264.26	254.50	248.37
1050	285.81	285.43	281.69	275.15	266.49	256.66	250.48
1060	288.16	287.79	284.02	277.43	268.71	258.81	252.58
1070	290.52	290.14	286.35	279.71	270.92	260.95	254.69
1080	292.87	292.49	288.67	281.99	273.14	263.10	256.79
1090	295.22	294.84	290.99	284.26	275.35	265.24	258.89
1100	297.57	297.18	293.31	286.54	277.57	267.38	260.98
1110	299.91	299.53	295.63	288.81	279.78	269.52	263.08
1120	302.28	301.87	297.94	291.07	281.98	271.66	265.17
1130	304.60	304.20	300.25	293.34	284.19	273.80	267.26
1140	306.93	308.54	302.56	295.61	286.39	275.93	269.35
1150	309.27	308.87	304.87	297.87	288.59	278.06	271.44
1160	311.60	311.20	307.18	300.13	290.79	280.19	273.52
1170	313.94	313.53	309.48	302.38	292.99	282.32	275.61
1180	316.26	315.86	311.78	304.64	295.19	284.44	277.69
1190	318.59	318.18	314.08	306.89	297.38	286.57	279.77
1200	320.92	320.51	316.38	309.15	299.57	288.69	281.85
1210	323.24	322.83	318.67	311.39	301.76	290.81	283.92
1220	325.56	325.14	320.96	313.64	303.95	292.93	286.00
1230	327.88	327.46	323.25	315.89	306.13	295.05	288.07
1240	330.19	329.77	325.54	318.13	308.32	297.16	290.14
1250	332.51	332.08	327.83	320.37	310.50	299.27	292.21
1260	334.82	334.39	330.11	322.61	312.68	301.38	294.28
1270	337.13	336.70	332.39	324.85	314.85	303.49	296.35
1280	339.44	339.01	334.67	327.08	317.03	305.60	298.41
1290	341.74	341.31	336.95	329.32	319.21	307.71	300.47
1300	344.05	343.61	339.23	331.55	321.38	309.81	302.54
1310	346.35	345.91	341.50	333.78	323.55	311.92	304.60
1320	348.65	348.21	343.77	336.01	325.72	314.02	306.65
1330	350.95	350.50	346.04	338.23	327.89	316.12	308.71
1340	353.24	352.80	348.31	340.46	330.05	318.22	310.77
1350	355.54	355.09	350.58	342.68	332.21	320.31	312.82
1360	357.83	357.38	352.84	344.90	334.38	322.41	314.87
1370	360.12	359.67	355.11	347.12	336.54	324.50	316.92
1380	362.41	361.95	357.37	349.34	338.70	326.59	318.97
1390	364.69	364.24	359.63	351.56	340.85	328.68	321.02
1400	366.98	366.52	361.88	353.77	343.01	330.77	323.06
1410	369.26	368.80	364.14	355.98	345.16	332.86	325.11
1420	371.54	371.08	366.40	358.19	347.32	334.94	327.15
1430	373.82	373.35	368.65	360.40	349.47	337.03	329.19
1440	376.10	375.63	370.90	362.61	351.62	339.11	331.23
1450	378.38	377.90	373.15	364.81	353.76	341.19	333.27
1460	380.65	380.17	375.39	367.02	355.91	343.27	335.31
1470	382.92	382.44	377.64	369.22	358.06	345.35	337.35
1480	385.19	384.71	379.88	371.42	360.20	347.43	339.38
1490	387.46	386.98	382.13	373.62	362.34	349.50	341.42
1500	389.73	389.25	384.37	375.82	364.48	351.58	343.45
1525	395.39	394.90	389.96	381.31	369.82	356.76	348.52

(continued)

Table 2.3 *Dimensionless Water Influx, W$_{eD}$, for Infinite Aquifer (Permission to publish by the SPE) (continued)*

t_D	Z'_D 0.05	0.1	0.3	0.5	0.7	0.9	1.0
1550	401.04	400.55	395.55	386.78	375.16	361.93	353.59
1575	406.68	406.18	401.12	392.25	380.49	367.09	358.65
1600	412.32	411.81	406.69	397.71	385.80	372.24	363.70
1625	417.94	417.42	412.24	403.16	391.11	377.39	368.74
1650	423.55	423.03	417.79	408.60	396.41	382.53	373.77
1675	429.15	428.63	423.33	414.04	401.70	387.66	378.80
1700	434.75	434.22	428.85	419.46	406.99	392.78	383.82
1725	440.33	439.79	434.37	424.87	412.26	397.89	388.83
1750	445.91	445.37	439.89	430.28	417.53	403.00	393.84
1775	451.48	450.93	445.39	435.68	422.79	408.10	398.84
1880	457.04	456.48	450.88	441.07	428.04	413.20	403.83
1825	462.59	462.03	456.37	446.46	433.29	418.28	408.82
1850	468.13	467.56	461.85	451.83	438.53	423.36	413.80
1875	473.67	473.09	467.32	457.20	443.76	428.43	418.77
1900	479.19	478.61	472.78	462.56	448.98	433.50	423.73
1925	484.71	484.13	478.24	467.92	454.20	438.56	428.69
1950	490.22	489.63	483.69	473.26	459.41	443.61	433.64
1975	495.73	495.13	489.13	478.60	464.61	448.66	438.59
2000	501.22	500.62	494.56	483.93	469.81	453.70	443.53
2025	506.71	506.11	499.99	489.26	475.00	458.73	448.47
2050	512.20	511.58	505.41	494.58	480.18	463.76	453.40
2075	517.67	517.05	510.82	499.89	485.36	468.78	458.32
2100	523.14	522.52	516.22	505.19	490.53	473.80	463.24
2125	528.60	527.97	521.62	510.49	495.69	478.81	468.15
2150	534.05	533.42	527.02	515.78	500.85	483.81	473.06
2175	539.50	538.86	532.40	521.07	506.01	488.81	477.96
2200	544.94	544.30	537.78	526.35	511.15	493.81	482.85
2225	550.38	549.73	543.15	531.62	516.29	498.79	487.74
2250	555.81	555.15	548.52	536.89	521.43	503.78	492.63
2275	561.23	560.56	553.88	542.15	526.56	508.75	497.51
2300	566.64	565.97	559.23	547.41	531.68	513.72	502.38
2325	572.05	571.38	564.58	552.66	536.80	518.69	507.25
2350	577.46	576.78	569.92	557.90	541.91	523.65	512.12
2375	582.85	582.17	575.26	563.14	547.02	528.61	516.98
2400	588.24	587.55	580.59	568.37	552.12	533.56	521.83
2425	593.63	592.93	585.91	573.60	557.22	538.50	526.68
2450	599.01	598.31	591.23	578.82	562.31	543.45	531.53
2475	604.38	603.68	596.55	584.04	567.39	548.38	536.37
2500	609.75	609.04	601.85	589.25	572.47	553.31	541.20
2550	620.47	619.75	612.45	599.65	582.62	563.16	550.86
2600	631.17	630.43	623.03	610.04	592.75	572.99	560.50
2650	641.84	641.10	633.59	620.40	602.86	582.80	570.13
2700	652.50	651.74	644.12	630.75	612.95	592.60	579.73
2750	663.13	662.37	654.64	641.07	623.02	602.37	589.32
2800	673.75	672.97	665.14	651.38	633.07	612.13	598.90
2850	684.34	683.56	675.61	661.67	643.11	621.88	608.45
2900	694.92	694.12	686.07	671.94	653.12	631.60	617.99
2950	705.48	704.67	696.51	682.19	663.13	641.32	627.52
3000	716.02	715.20	706.94	692.43	673.11	651.01	637.03
3050	726.54	725.71	717.34	702.65	683.08	660.69	646.53
3100	737.04	736.20	727.73	712.85	693.03	670.36	656.01
3150	747.53	746.68	738.10	723.04	702.97	680.01	665.48
3200	758.00	757.14	748.45	733.21	712.89	689.64	674.93
3250	768.45	767.58	758.79	743.36	722.80	699.27	684.37
3300	778.89	778.01	769.11	753.50	732.69	708.87	693.80
3350	789.31	788.42	779.42	763.62	742.57	718.47	703.21
3400	799.71	798.81	789.71	773.73	752.43	728.05	712.62
3450	810.10	809.19	799.99	783.82	762.28	737.62	722.00

(continued)

Table 2.3   *Dimensionless Water Influx, W_{eD}, for Infinite Aquifer (Permission to publish by the SPE) (continued)*

t_D	Z'_D 0.05	0.1	0.3	0.5	0.7	0.9	1.0
3500	820.48	819.55	810.25	793.90	772.12	747.17	731.38
3550	830.83	829.90	820.49	803.97	781.94	756.72	740.74
3600	841.18	840.24	830.73	814.02	791.75	766.24	750.09
3650	851.51	850.56	840.94	824.06	801.55	775.76	759.43
3700	861.83	860.86	851.15	834.08	811.33	785.27	768.76
3750	872.13	871.15	861.34	844.09	821.10	794.76	778.08
3800	882.41	881.43	871.51	854.09	830.86	804.24	787.38
3850	892.69	891.70	881.68	864.08	840.61	813.71	796.68
3900	902.95	901.95	891.83	874.05	850.34	823.17	805.96
3950	913.20	912.19	901.96	884.01	860.06	832.62	815.23
4000	923.43	922.41	912.09	893.96	869.77	842.06	824.49
4050	933.65	932.62	922.20	903.89	879.47	851.48	833.74
4100	943.86	942.82	932.30	913.82	889.16	860.90	842.99
4150	954.06	953.01	942.39	923.73	898.84	870.30	852.22
4200	964.25	963.19	952.47	933.63	908.50	879.69	861.44
4250	974.42	973.35	962.53	943.52	918.16	889.08	870.65
4300	984.58	983.50	972.58	953.40	927.60	898.45	879.85
4350	994.73	993.64	982.62	963.27	937.43	907.81	889.04
4400	1004.9	1003.8	992.7	973.1	947.1	917.2	898.2
4450	1015.0	1013.9	1002.7	983.0	956.7	926.5	907.4
4500	1025.1	1024.0	1012.7	992.8	966.3	935.9	916.6
4550	1035.2	1034.1	1022.7	1002.6	975.9	945.2	925.7
4600	1045.3	1044.2	1032.7	1012.4	985.5	954.5	934.9
4650	1055.4	1054.2	1042.6	1022.2	995.0	963.8	944.0
4700	1065.5	1064.3	1052.6	1032.0	1004.6	973.1	953.1
4750	1075.5	1074.4	1062.6	1041.8	1014.1	982.4	962.2
4800	1085.6	1084.4	1072.5	1051.6	1023.7	991.7	971.4
4850	1095.6	1094.4	1082.4	1061.4	1033.2	1000.9	980.5
4900	1105.6	1104.5	1092.4	1071.1	1042.8	1010.2	989.5
4950	1115.7	1114.5	1102.3	1080.9	1052.3	1019.4	998.6
5000	1125.7	1124.5	1112.2	1090.6	1061.8	1028.7	1007.7
5100	1145.7	1144.4	1132.0	1110.0	1080.8	1047.2	1025.8
5200	1165.6	1164.4	1151.7	1129.4	1099.7	1065.6	1043.9
5300	1185.5	1184.3	1171.4	1148.8	1118.6	1084.0	1062.0
5400	1205.4	1204.1	1191.1	1168.2	1137.5	1102.4	1080.0
5500	1225.3	1224.0	1210.7	1187.5	1156.4	1120.7	1098.0
5600	1245.1	1243.7	1230.3	1206.7	1175.2	1139.0	1116.0
5700	1264.9	1263.5	1249.9	1226.0	1194.0	1157.3	1134.0
5800	1284.6	1283.2	1269.4	1245.2	1212.8	1175.5	1151.9
5900	1304.3	1302.9	1288.9	1264.4	1231.5	1193.8	1169.8
6000	1324.0	1322.6	1308.4	1283.5	1250.2	1211.9	1187.7
6100	1343.6	1342.2	1327.9	1302.6	1268.9	1230.1	1205.5
6200	1363.2	1361.8	1347.3	1321.7	1287.5	1248.3	1223.3
6300	1382.8	1381.4	1366.7	1340.8	1306.2	1266.4	1241.1
6400	1402.4	1400.9	1386.0	1359.8	1324.7	1284.5	1258.9
6500	1421.9	1420.4	1405.3	1378.8	1343.3	1302.5	1276.6
6600	1441.4	1439.9	1424.6	1397.8	1361.9	1320.6	1294.3
6700	1460.9	1459.4	1443.9	1416.7	1380.4	1338.6	1312.0
6800	1480.3	1478.8	1463.1	1435.6	1398.9	1356.6	1329.7
6900	1499.7	1498.2	1482.4	1454.5	1417.3	1374.5	1347.4
7000	1519.1	1517.5	1501.5	1473.4	1435.8	1392.5	1365.0
7100	1538.5	1536.9	1520.7	1492.3	1454.2	1410.4	1382.6
7200	1557.8	1556.2	1539.8	1511.1	1472.6	1428.3	1400.2
7300	1577.1	1575.5	1559.0	1529.9	1491.0	1446.2	1417.8
7400	1596.4	1594.8	1578.1	1548.6	1509.3	1464.1	1435.3
7500	1615.7	1614.0	1597.1	1567.4	1527.6	1481.9	1452.8
7600	1634.9	1633.2	1616.2	1586.1	1545.9	1499.7	1470.3
7700	1654.1	1652.4	1635.2	1604.8	1564.2	1517.5	1487.8

(continued)

Table 2.3 *Dimensionless Water Influx, W_{eD}, for Infinite Aquifer (Permission to publish by the SPE) (continued)*

				Z'_D			
t_D	*0.05*	*0.1*	*0.3*	*0.5*	*0.7*	*0.9*	*1.0*
7800	1673.3	1671.6	1654.2	1623.5	1582.5	1535.3	1505.3
7900	1692.5	1690.7	1673.1	1642.2	1600.7	1553.0	1522.7
8000	1711.6	1709.9	1692.1	1660.8	1619.0	1570.8	1540.1
8100	1730.8	1729.0	1711.0	1679.4	1637.2	1588.5	1557.6
8200	1749.9	1748.1	1729.9	1698.0	1655.3	1606.2	1574.9
8300	1768.9	1767.1	1748.8	1716.6	1673.5	1623.9	1592.3
8400	1788.0	1786.2	1767.7	1735.2	1691.6	1641.5	1609.7
8500	1807.0	1805.2	1786.5	1753.7	1709.8	1659.2	1627.0
8600	1826.0	1824.2	1805.4	1772.2	1727.9	1676.8	1644.3
8700	1845.0	1843.2	1824.2	1790.7	1746.0	1694.4	1661.6
8800	1864.0	1862.1	1842.9	1809.2	1764.0	1712.0	1678.9
8900	1883.0	1881.1	1861.7	1827.7	1782.1	1729.6	1696.2
9000	1901.9	1900.0	1880.5	1846.1	1800.1	1747.1	1713.4
9100	1920.8	1918.9	1899.2	1864.5	1818.1	1764.7	1730.7
9200	1939.7	1937.4	1917.9	1882.9	1836.1	1782.2	1747.9
9300	1958.6	1956.6	1936.6	1901.3	1854.1	1799.7	1765.1
9400	1977.4	1975.4	1955.2	1919.7	1872.0	1817.2	1782.3
9500	1996.3	1994.3	1973.9	1938.0	1890.0	1834.7	1799.4
9600	2015.1	2013.1	1992.5	1956.4	1907.9	1852.1	1816.6
9700	2033.9	2031.9	2011.1	1974.7	1925.8	1869.6	1833.7
9800	2052.7	2050.6	2029.7	1993.0	1943.7	1887.0	1850.9
9900	2071.5	2069.4	2048.3	2011.3	1961.6	1904.4	1868.0
1.00×10^4	2.090×10^3	2.088×10^3	2.067×10^3	2.029×10^3	1.979×10^3	1.922×10^3	1.885×10^3
1.25×10^4	2.553×10^3	2.551×10^3	2.526×10^3	2.481×10^3	2.421×10^3	2.352×10^3	2.308×10^3
1.50×10^4	3.009×10^3	3.006×10^3	2.977×10^3	2.925×10^3	2.855×10^3	2.775×10^3	2.724×10^3
1.75×10^4	3.457×10^3	3.454×10^3	3.421×10^3	3.362×10^3	3.284×10^3	3.193×10^3	3.135×10^3
2.00×10^4	3.900×10^3	3.897×10^3	3.860×10^3	3.794×10^3	3.707×10^3	3.605×10^3	3.541×10^3
2.50×10^4	4.773×10^3	4.768×10^3	4.724×10^3	4.646×10^3	4.541×10^3	4.419×10^3	4.341×10^3
3.00×10^4	5.630×10^3	5.625×10^3	5.574×10^3	5.483×10^3	5.361×10^3	5.219×10^3	5.129×10^3
3.50×10^4	6.476×10^3	6.470×10^3	6.412×10^3	6.309×10^3	6.170×10^3	6.009×10^3	5.906×10^3
4.00×10^4	7.312×10^3	7.305×10^3	7.240×10^3	7.125×10^3	6.970×10^3	6.790×10^3	6.675×10^3
4.50×10^4	8.139×10^3	8.132×10^3	8.060×10^3	7.933×10^3	7.762×10^3	7.564×10^9	7.437×10^3
5.00×10^4	8.959×10^3	8.951×10^3	8.872×10^3	8.734×10^3	8.548×10^3	8.331×10^3	8.193×10^3
6.00×10^4	1.057×10^4	1.057×10^4	1.047×10^4	1.031×10^4	1.010×10^4	9.846×10^3	9.684×10^3
7.00×10^4	1.217×10^4	1.217×10^4	1.206×10^4	1.188×10^4	1.163×10^4	1.134×10^4	1.116×10^4
8.00×10^4	1.375×10^4	1.375×10^4	1.363×10^4	1.342×10^4	1.315×10^4	1.283×10^4	1.262×10^4
9.00×10^4	1.532×10^4	1.531×10^4	1.518×10^4	1.496×10^4	1.465×10^4	1.430×10^4	1.407×10^4
1.00×10^5	1.687×10^4	1.686×10^4	1.672×10^4	1.647×10^4	1.614×10^4	1.576×10^4	1.551×10^4
1.25×10^5	2.071×10^4	2.069×10^4	2.052×10^4	2.023×10^4	1.982×10^4	1.936×10^4	1.906×10^4
1.50×10^5	2.448×10^4	2.446×10^4	2.427×10^4	2.392×10^4	2.345×10^4	2.291×10^4	2.256×10^4
2.00×10^5	3.190×10^4	3.188×10^4	3.163×10^4	3.119×10^4	3.059×10^4	2.989×10^4	2.945×10^4
2.50×10^5	3.918×10^4	3.916×10^4	3.885×10^4	3.832×10^4	3.760×10^4	3.676×10^4	3.622×10^4
3.00×10^5	4.636×10^4	4.633×10^4	4.598×10^4	4.536×10^4	4.452×10^4	4.353×10^4	4.290×10^4
4.00×10^5	6.048×10^4	6.044×10^4	5.999×10^4	5.920×10^4	5.812×10^4	5.687×10^4	5.606×10^4
5.00×10^5	7.438×10^4	7.431×10^4	7.376×10^4	7.280×10^4	7.150×10^4	6.998×10^4	6.900×10^4
6.00×10^5	8.805×10^4	8.798×10^4	8.735×10^4	8.623×10^4	8.471×10^4	8.293×10^4	8.178×10^4
7.00×10^5	1.016×10^5	1.015×10^5	1.008×10^5	9.951×10^4	9.777×10^4	9.573×10^4	9.442×10^4
8.00×10^5	1.150×10^5	1.149×10^5	1.141×10^5	1.127×10^5	1.107×10^5	1.084×10^5	1.070×10^5
9.00×10^5	1.283×10^5	1.282×10^5	1.273×10^5	1.257×10^5	1.235×10^5	1.210×10^5	1.194×10^5
1.00×10^6	1.415×10^5	1.412×10^5	1.404×10^5	1.387×10^5	1.363×10^5	1.335×10^5	1.317×10^5
1.50×10^6	2.059×10^5	2.060×10^5	2.041×10^5	2.016×10^5	1.982×10^5	1.943×10^5	1.918×10^5
2.00×10^6	2.695×10^5	2.695×10^5	2.676×10^5	2.644×10^5	2.601×10^5	2.551×10^5	2.518×10^5
2.50×10^6	3.320×10^5	3.319×10^5	3.296×10^5	3.254×10^5	3.202×10^5	3.141×10^5	3.101×10^5
3.00×10^6	3.937×10^5	3.936×10^5	3.909×10^5	3.864×10^5	3.803×10^5	3.731×10^5	3.684×10^5
4.00×10^6	5.154×10^5	5.152×10^5	5.118×10^5	5.060×10^5	4.981×10^5	4.888×10^5	4.828×10^5
5.00×10^6	6.352×10^5	6.349×10^5	6.308×10^5	6.238×10^5	6.142×10^5	6.029×10^5	5.956×10^5

(continued)

Table 2.3 *Dimensionless Water Influx, W_{eD}, for Infinite Aquifer (Permission to publish by the SPE) (continued)*

t_D	0.05	0.1	0.3	0.5	0.7	0.9	1.0
6.00×10^6	7.536×10^5	7.533×10^5	7.485×10^5	7.402×10^5	7.290×10^5	7.157×10^5	7.072×10^5
7.00×10^6	8.709×10^5	8.705×10^5	8.650×10^5	8.556×10^5	8.427×10^5	8.275×10^5	8.177×10^5
8.00×10^6	9.972×10^5	9.867×10^5	9.806×10^5	9.699×10^5	9.555×10^5	9.384×10^5	9.273×10^5
9.00×10^6	1.103×10^6	1.102×10^6	1.095×10^6	1.084×10^6	1.067×10^6	1.049×10^6	1.036×10^6
1.00×10^7	1.217×10^6	1.217×10^6	1.209×10^6	1.196×10^6	1.179×10^6	1.158×10^6	1.144×10^6
1.50×10^7	1.782×10^6	1.781×10^6	1.771×10^6	1.752×10^6	1.727×10^6	1.697×10^6	1.678×10^6
2.00×10^7	2.337×10^6	2.336×10^6	2.322×10^6	2.298×10^6	2.266×10^6	2.227×10^6	2.202×10^6
2.50×10^7	2.884×10^6	2.882×10^6	2.866×10^6	2.837×10^6	2.797×10^6	2.750×10^6	2.720×10^6
3.00×10^7	3.425×10^6	3.423×10^6	3.404×10^6	3.369×10^6	3.323×10^6	3.268×10^6	3.232×10^6
4.00×10^7	4.493×10^6	4.491×10^6	4.466×10^6	4.422×10^6	4.361×10^6	4.290×10^6	4.244×10^6
5.00×10^7	5.547×10^6	5.544×10^6	5.514×10^6	5.460×10^6	5.386×10^6	5.299×10^6	5.243×10^6
6.00×10^7	6.590×10^6	6.587×10^6	6.551×10^6	6.488×10^6	6.401×10^6	6.299×10^6	6.232×10^6
7.00×10^7	7.624×10^6	7.620×10^6	7.579×10^6	7.507×10^6	7.407×10^6	7.290×10^6	7.213×10^6
8.00×10^7	8.651×10^6	8.647×10^6	8.600×10^6	8.519×10^6	8.407×10^6	8.274×10^6	8.188×10^6
9.00×10^7	9.671×10^6	9.666×10^6	9.615×10^6	9.524×10^6	9.400×10^6	9.252×10^6	9.156×10^6
1.00×10^8	1.069×10^7	1.067×10^7	1.062×10^7	1.052×10^7	1.039×10^7	1.023×10^7	1.012×10^7
1.50×10^8	1.567×10^7	1.567×10^7	1.555×10^7	1.541×10^7	1.522×10^7	1.499×10^7	1.483×10^7
2.00×10^8	2.059×10^7	2.059×10^7	2.048×10^7	2.029×10^7	2.004×10^7	1.974×10^7	1.954×10^7
2.50×10^8	2.546×10^7	2.545×10^7	2.531×10^7	2.507×10^7	2.476×10^7	2.439×10^7	2.415×10^7
3.00×10^8	3.027×10^7	3.026×10^7	3.010×10^7	2.984×10^7	2.947×10^7	2.904×10^7	2.875×10^7
4.00×10^8	3.979×10^7	3.978×10^7	3.958×10^7	3.923×10^7	3.875×10^7	3.819×10^7	3.782×10^7
5.00×10^8	4.920×10^7	4.918×10^7	4.894×10^7	4.851×10^7	4.793×10^7	4.724×10^7	4.679×10^7
6.00×10^8	5.852×10^7	5.850×10^7	5.821×10^7	5.771×10^7	5.702×10^7	5.621×10^7	5.568×10^7
7.00×10^8	6.777×10^7	6.774×10^7	6.741×10^7	6.684×10^7	6.605×10^7	6.511×10^7	6.450×10^7
8.00×10^8	7.700×10^7	7.693×10^7	7.655×10^7	7.590×10^7	7.501×10^7	7.396×10^7	7.327×10^7
9.00×10^8	8.609×10^7	8.606×10^7	8.564×10^7	8.492×10^7	8.393×10^7	8.275×10^7	8.199×10^7
1.00×10^9	9.518×10^7	9.515×10^7	9.469×10^7	9.390×10^7	9.281×10^7	9.151×10^7	9.066×10^7
1.50×10^9	1.401×10^8	1.400×10^8	1.394×10^8	1.382×10^8	1.367×10^8	1.348×10^8	1.336×10^8
2.00×10^9	1.843×10^8	1.843×10^8	1.834×10^8	1.819×10^8	1.799×10^8	1.774×10^8	1.758×10^8
2.50×10^9	2.281×10^8	2.280×10^8	2.269×10^8	2.251×10^8	2.226×10^8	2.196×10^8	2.177×10^8
3.00×10^9	2.714×10^8	2.713×10^8	2.701×10^8	2.680×10^8	2.650×10^8	2.615×10^8	2.592×10^8
4.00×10^9	3.573×10^8	3.572×10^8	3.558×10^8	3.528×10^8	3.489×10^8	3.443×10^8	3.413×10^8
5.00×10^9	4.422×10^8	4.421×10^8	4.401×10^8	4.367×10^8	4.320×10^8	4.263×10^8	4.227×10^8
6.00×10^9	5.265×10^8	5.262×10^8	5.240×10^8	5.199×10^8	5.143×10^8	5.077×10^8	5.033×10^8
7.00×10^9	6.101×10^8	6.098×10^8	6.072×10^8	6.025×10^8	5.961×10^8	5.885×10^8	5.835×10^8
8.00×10^9	6.932×10^8	6.930×10^8	6.900×10^8	6.847×10^8	6.775×10^8	6.688×10^8	6.632×10^8
9.00×10^9	7.760×10^8	7.756×10^8	7.723×10^8	7.664×10^8	7.584×10^8	7.487×10^8	7.424×10^8
1.00×10^{10}	8.583×10^8	8.574×10^8	8.543×10^8	8.478×10^8	8.389×10^8	8.283×10^8	8.214×10^8
1.50×10^{10}	1.263×10^9	1.264×10^9	1.257×10^9	1.247×10^9	1.235×10^9	1.219×10^9	1.209×10^9
2.00×10^{10}	1.666×10^9	1.666×10^9	1.659×10^9	1.646×10^9	1.630×10^9	1.610×10^9	1.596×10^9
2.50×10^{10}	2.065×10^9	2.063×10^9	2.055×10^9	2.038×10^9	2.018×10^9	1.993×10^9	1.977×10^9
3.00×10^{10}	2.458×10^9	2.458×10^9	2.447×10^9	2.430×10^9	2.405×10^9	2.376×10^9	2.357×10^9
4.00×10^{10}	3.240×10^9	3.239×10^9	3.226×10^9	3.203×10^9	3.171×10^9	3.133×10^9	3.108×10^9
5.00×10^{10}	4.014×10^9	4.013×10^9	3.997×10^9	3.968×10^9	3.929×10^9	3.883×10^9	3.852×10^9
6.00×10^{10}	4.782×10^9	4.781×10^9	4.762×10^9	4.728×10^9	4.682×10^9	4.627×10^9	4.591×10^9
7.00×10^{10}	5.546×10^9	5.544×10^9	5.522×10^9	5.483×10^9	5.430×10^9	5.366×10^9	5.325×10^9
8.00×10^{10}	6.305×10^9	6.303×10^9	6.278×10^9	6.234×10^9	6.174×10^9	6.102×10^9	6.055×10^9
9.00×10^{10}	7.060×10^9	7.058×10^9	7.030×10^9	6.982×10^9	6.914×10^9	6.834×10^9	6.782×10^9
1.00×10^{11}	7.813×10^9	7.810×10^9	7.780×10^9	7.726×10^9	7.652×10^9	7.564×10^9	7.506×10^9
1.50×10^{11}	1.154×10^{10}	1.153×10^{10}	1.149×10^{10}	1.141×10^{10}	1.130×10^{10}	1.118×10^{10}	1.109×10^{10}
2.00×10^{11}	1.522×10^{10}	1.521×10^{10}	1.515×10^{10}	1.505×10^{10}	1.491×10^{10}	1.474×10^{10}	1.463×10^{10}
2.50×10^{11}	1.886×10^{10}	1.885×10^{10}	1.878×10^{10}	1.866×10^{10}	1.849×10^{10}	1.828×10^{10}	1.814×10^{10}
3.00×10^{11}	2.248×10^{10}	2.247×10^{10}	2.239×10^{10}	2.224×10^{10}	2.204×10^{10}	2.179×10^{10}	2.163×10^{10}
4.00×10^{11}	2.965×10^{10}	2.964×10^{10}	2.953×10^{10}	2.934×10^{10}	2.907×10^{10}	2.876×10^{10}	2.855×10^{10}
5.00×10^{11}	3.677×10^{10}	3.675×10^{10}	3.662×10^{10}	3.638×10^{10}	3.605×10^{10}	3.566×10^{10}	3.540×10^{10}

(continued)

Table 2.3 *Dimensionless Water Influx, W_{eD}, for Infinite Aquifer (Permission to publish by the SPE) (continued)*

t_D	Z'_D						
	0.05	0.1	0.3	0.5	0.7	0.9	1.0
6.00×10^{11}	4.383×10^{10}	4.381×10^{10}	4.365×10^{10}	4.337×10^{10}	4.298×10^{10}	4.252×10^{10}	4.221×10^{10}
7.00×10^{11}	5.085×10^{10}	5.082×10^{10}	5.064×10^{10}	5.032×10^{10}	4.987×10^{10}	4.933×10^{10}	4.898×10^{10}
8.00×10^{11}	5.783×10^{10}	5.781×10^{10}	5.706×10^{10}	5.723×10^{10}	5.673×10^{10}	5.612×10^{10}	5.572×10^{10}
9.00×10^{11}	6.478×10^{10}	6.746×10^{10}	6.453×10^{10}	6.412×10^{10}	6.355×10^{10}	6.288×10^{10}	6.243×10^{10}
1.00×10^{12}	7.171×10^{10}	7.168×10^{10}	7.143×10^{10}	7.098×10^{10}	7.035×10^{10}	6.961×10^{10}	6.912×10^{10}
1.50×10^{12}	1.060×10^{11}	1.060×10^{11}	1.056×10^{11}	1.050×10^{11}	1.041×10^{11}	1.030×10^{11}	1.022×10^{11}
2.00×10^{12}	1.400×10^{11}	1.399×10^{11}	1.394×10^{11}	1.386×10^{11}	1.374×10^{11}	1.359×10^{11}	1.350×10^{11}

Table 2.4 *Dimensionless Water Influx, W_{eD}, for $r'_D = 4$ (Permission to publish by the SPE)*

t_D	Z'_D						
	0.05	0.1	0.3	0.5	0.7	0.9	1.0
2	2.398	2.389	2.284	2.031	1.824	1.620	1.507
3	3.006	2.993	2.874	2.629	2.390	2.149	2.012
4	3.552	3.528	3.404	3.158	2.893	2.620	2.466
5	4.053	4.017	3.893	3.627	3.341	3.045	2.876
6	4.490	4.452	4.332	4.047	3.744	3.430	3.249
7	4.867	4.829	4.715	4.420	4.107	3.778	3.587
8	5.191	5.157	5.043	4.757	4.437	4.096	3.898
9	5.464	5.434	5.322	5.060	4.735	4.385	4.184
10	5.767	5.739	5.598	5.319	5.000	4.647	4.443
11	5.964	5.935	5.829	5.561	5.240	4.884	4.681
12	6.188	6.158	6.044	5.780	5.463	5.107	4.903
13	6.380	6.350	6.240	5.983	5.670	5.316	5.113
14	6.559	6.529	6.421	6.171	5.863	5.511	5.309
15	6.725	6.694	6.589	6.345	6.044	5.695	5.495
16	6.876	6.844	6.743	6.506	6.213	5.867	5.671
17	7.014	6.983	6.885	6.656	6.371	6.030	5.838
18	7.140	7.113	7.019	6.792	6.523	6.187	5.999
19	7.261	7.240	7.140	6.913	6.663	6.334	6.153
20	7.376	7.344	7.261	7.028	6.785	6.479	6.302
22	7.518	7.507	7.451	7.227	6.982	6.691	6.524
24	7.618	7.607	7.518	7.361	7.149	6.870	6.714
26	7.697	7.685	7.607	7.473	7.283	7.026	6.881
28	7.752	7.752	7.674	7.563	7.395	7.160	7.026
30	7.808	7.797	7.741	7.641	7.484	7.283	7.160
34	7.864	7.864	7.819	7.741	7.618	7.451	7.350
38	7.909	7.909	7.875	7.808	7.719	7.585	7.496
42	7.931	7.931	7.909	7.864	7.797	7.685	7.618
46	7.942	7.942	7.920	7.898	7.842	7.752	7.697
50	7.954	7.954	7.942	7.920	7.875	7.808	7.764
60	7.968	7.968	7.965	7.954	7.931	7.898	7.864
70	7.976	7.976	7.976	7.968	7.965	7.942	7.920
80	7.982	7.982	7.987	7.976	7.976	7.965	7.954
90	7.987	7.987	7.987	7.984	7.983	7.976	7.965
100	7.987	7.987	7.987	7.987	7.987	7.983	7.976
120	7.987	7.987	7.987	7.987	7.987	7.987	7.987

Table 2.5 *Dimensionless Water Influx, W_{eD}, for $r'_D = 6$ (Permission to publish by the SPE)*

t_D	Z'_D						
	0.05	0.1	0.3	0.5	0.7	0.9	1.0
6	4.780	4.762	4.597	4.285	3.953	3.611	3.414
7	5.309	5.289	5.114	4.779	4.422	4.053	3.837
8	5.799	5.778	5.595	5.256	4.875	4.478	4.247
9	6.252	6.229	6.041	5.712	5.310	4.888	4.642
10	6.750	6.729	6.498	6.135	5.719	5.278	5.019

(continued)

Table 2.5 *Dimensionless Water Influx, W_{eD}, for $r_D^\backslash = 6$ (Permission to publish by the SPE) (continued)*

	Z_D'						
t_D	0.05	0.1	0.3	0.5	0.7	0.9	1.0
11	7.137	7.116	6.916	6.548	6.110	5.648	5.378
12	7.569	7.545	7.325	6.945	6.491	6.009	5.728
13	7.967	7.916	7.719	7.329	6.858	6.359	6.067
14	8.357	8.334	8.099	7.699	7.214	6.697	6.395
15	8.734	8.709	8.467	8.057	7.557	7.024	6.713
16	9.093	9.067	8.819	8.398	7.884	7.336	7.017
17	9.442	9.416	9.160	8.730	8.204	7.641	7.315
18	9.775	9.749	9.485	9.047	8.510	7.934	7.601
19	10.09	10.06	9.794	9.443	8.802	8.214	7.874
20	10.40	10.37	10.10	9.646	9.087	8.487	8.142
22	10.99	10.96	10.67	10.21	9.631	9.009	8.653
24	11.53	11.50	11.20	10.73	10.13	9.493	9.130
26	12.06	12.03	11.72	11.23	10.62	9.964	9.594
28	12.52	12.49	12.17	11.68	11.06	10.39	10.01
30	12.95	12.92	12.59	12.09	11.46	10.78	10.40
35	13.96	13.93	13.57	13.06	12.41	11.70	11.32
40	14.69	14.66	14.33	13.84	13.23	12.53	12.15
45	15.27	15.24	14.94	14.48	13.90	13.23	12.87
50	15.74	15.71	15.44	15.01	14.47	13.84	13.49
60	16.40	16.38	16.15	15.81	15.34	14.78	14.47
70	16.87	16.85	16.67	16.38	15.99	15.50	15.24
80	17.20	17.18	17.04	16.80	16.48	16.06	15.83
90	17.43	17.42	17.30	17.10	16.85	16.50	16.29
100	17.58	17.58	17.49	17.34	17.12	16.83	16.66
110	17.71	17.69	17.63	17.50	17.34	17.09	16.93
120	17.78	17.78	17.73	17.63	17.49	17.29	17.17
130	17.84	17.84	17.79	17.73	17.62	17.45	17.34
140	17.88	17.88	17.85	17.79	17.71	17.57	17.48
150	17.92	17.91	17.88	17.84	17.77	17.66	17.58
175	17.95	17.95	17.94	17.92	17.87	17.81	17.76
200	17.97	17.97	17.96	17.95	17.93	17.88	17.86
225	17.97	17.97	17.97	17.96	17.95	17.93	17.91
250	17.98	17.98	17.98	17.97	17.96	17.95	17.95
300	17.98	17.98	17.98	17.98	17.98	17.97	17.97
350	17.98	17.98	17.98	17.98	17.98	17.98	17.98
400	17.98	17.98	17.98	17.98	17.98	17.98	17.98
450	17.98	17.98	17.98	17.98	17.98	17.98	17.98
500	17.98	17.98	17.98	17.98	17.98	17.98	17.98

Table 2.6 *Dimensionless Water Influx, W_{eD}, for $r_D^\backslash = 8$ (Permission to publish by the SPE)*

	Z_D'						
t_D	0.05	0.1	0.3	0.5	0.7	0.9	1.0
9	6.301	6.278	6.088	5.756	5.350	4.924	4.675
10	6.828	6.807	6.574	6.205	5.783	5.336	5.072
11	7.250	7.229	7.026	6.650	6.204	5.732	5.456
12	7.725	7.700	7.477	7.086	6.621	6.126	5.836
13	8.173	8.149	7.919	7.515	7.029	6.514	6.210
14	8.619	8.594	8.355	7.937	7.432	6.895	6.578
15	9.058	9.032	8.783	8.351	7.828	7.270	6.940
16	9.485	9.458	9.202	8.755	8.213	7.634	7.293
17	9.907	9.879	9.613	9.153	8.594	7.997	7.642
18	10.32	10.29	10.01	9.537	8.961	8.343	7.979
19	10.72	10.69	10.41	9.920	9.328	8.691	8.315
20	11.12	11.08	10.80	10.30	9.687	9.031	8.645
22	11.89	11.86	11.55	11.02	10.38	9.686	9.280
24	12.63	12.60	12.27	11.72	11.05	10.32	9.896
26	13.36	13.32	12.97	12.40	11.70	10.94	10.49

(continued)

Table 2.6 *Dimensionless Water Influx,* W_{eD}, *for* $r_D^\rangle = 8$ *(Permission to publish by the SPE) (continued)*

t_D	Z_D'						
	0.05	*0.1*	*0.3*	*0.5*	*0.7*	*0.9*	*1.0*
28	14.06	14.02	13.65	13.06	12.33	11.53	11.07
30	14.73	14.69	14.30	13.68	12.93	12.10	11.62
34	16.01	15.97	15.54	14.88	14.07	13.18	12.67
38	17.21	17.17	16.70	15.99	15.13	14.18	13.65
40	17.80	17.75	17.26	16.52	15.64	14.66	14.12
45	19.15	19.10	18.56	17.76	16.83	15.77	15.21
50	20.42	20.36	19.76	18.91	17.93	16.80	16.24
55	21.46	21.39	20.80	19.96	18.97	17.83	17.24
60	22.40	22.34	21.75	20.91	19.93	18.78	18.19
70	23.97	23.92	23.36	22.55	21.58	20.44	19.86
80	25.29	25.23	24.71	23.94	23.01	21.91	21.32
90	26.39	26.33	25.85	25.12	24.24	23.18	22.61
100	27.30	27.25	26.81	26.13	25.29	24.29	23.74
120	28.61	28.57	28.19	27.63	26.90	26.01	25.51
140	29.55	29.51	29.21	28.74	28.12	27.33	26.90
160	30.23	30.21	29.96	29.57	29.04	28.37	27.99
180	30.73	30.71	30.51	30.18	29.75	29.18	28.84
200	31.07	31.04	30.90	30.63	30.26	29.79	29.51
240	31.50	31.49	31.39	31.22	30.98	30.65	30.45
280	31.72	31.71	31.66	31.56	31.39	31.17	31.03
320	31.85	31.84	31.80	31.74	31.64	31.49	31.39
360	31.90	31.90	31.88	31.85	31.78	31.68	31.61
400	31.94	31.94	31.93	31.90	31.86	31.79	31.75
450	31.96	31.96	31.95	31.94	31.91	31.88	31.85
500	31.97	31.97	31.96	31.96	31.95	31.93	31.90
550	31.97	31.97	31.97	31.96	31.96	31.95	31.94
600	31.97	31.97	31.97	31.97	31.97	31.96	31.95
700	31.97	31.97	31.97	31.97	31.97	31.97	31.97
800	31.97	31.97	31.97	31.97	31.97	31.97	31.97

Table 2.7 *Dimensionless Water Influx,* W_{eD}, *for* $r_D^\rangle = 10$ *(Permission to publish by the SPE)*

t_D	Z_D'						
	0.05	*0.1*	*0.3*	*0.5*	*0.7*	*0.9*	*1.0*
22	12.07	12.04	11.74	11.21	10.56	9.865	9.449
24	12.86	12.83	12.52	11.97	11.29	10.55	10.12
26	13.65	13.62	13.29	12.72	12.01	11.24	10.78
28	14.42	14.39	14.04	13.44	12.70	11.90	11.42
30	15.17	15.13	14.77	14.15	13.38	12.55	12.05
32	15.91	15.87	15.49	14.85	14.05	13.18	12.67
34	16.63	16.59	16.20	15.54	14.71	13.81	13.28
36	17.33	17.29	16.89	16.21	15.35	14.42	13.87
38	18.03	17.99	17.57	16.86	15.98	15.02	14.45
40	18.72	18.68	18.24	17.51	16.60	15.61	15.02
42	19.38	19.33	18.89	18.14	17.21	16.19	15.58
44	20.03	19.99	19.53	18.76	17.80	16.75	16.14
46	20.67	20.62	20.15	19.36	18.38	17.30	16.67
48	21.30	21.25	20.76	19.95	18.95	17.84	17.20
50	21.92	21.87	21.36	20.53	19.51	18.38	17.72
52	22.52	22.47	21.95	21.10	20.05	18.89	18.22
54	23.11	23.06	22.53	21.66	20.59	19.40	18.72
56	23.70	23.64	23.09	22.20	21.11	19.89	19.21
58	24.26	24.21	23.65	22.74	21.63	20.39	19.68
60	24.82	24.77	24.19	23.26	22.13	20.87	20.15

(continued)

Table 2.7 Dimensionless Water Influx, W_{eD}, for $r_D^\backslash = 10$ (Permission to publish by the SPE) (continued)

	Z_D'						
t_D	0.05	0.1	0.3	0.5	0.7	0.9	1.0
65	26.18	26.12	25.50	24.53	23.34	22.02	21.28
70	27.47	27.41	26.75	25.73	24.50	23.12	22.36
75	28.71	28.55	27.94	26.88	25.60	24.17	23.39
80	29.89	29.82	29.08	27.97	26.65	25.16	24.36
85	31.02	30.95	30.17	29.01	27.65	26.10	25.31
90	32.10	32.03	31.20	30.00	28.60	27.03	26.25
95	33.04	32.96	32.14	30.95	29.54	27.93	27.10
100	33.94	33.85	33.03	31.85	30.44	28.82	27.98
110	35.55	35.46	34.65	33.49	32.08	30.47	29.62
120	36.97	36.90	36.11	34.98	33.58	31.98	31.14
130	38.28	38.19	37.44	36.33	34.96	33.38	32.55
140	39.44	39.37	38.64	37.56	36.23	34.67	33.85
150	40.49	40.42	39.71	38.67	37.38	35.86	35.04
170	42.21	42.15	41.51	40.54	39.33	37.89	37.11
190	43.62	43.55	42.98	42.10	40.97	39.62	38.90
210	44.77	44.72	44.19	43.40	42.36	41.11	40.42
230	45.71	45.67	45.20	44.48	43.54	42.38	41.74
250	46.48	46.44	46.01	45.38	44.53	43.47	42.87
270	47.11	47.06	46.70	46.13	45.36	44.40	43.84
290	47.61	47.58	47.25	46.75	46.07	45.19	44.68
310	48.03	48.00	47.72	47.26	46.66	45.87	45.41
330	48.38	48.35	48.10	47.71	47.16	46.45	46.03
350	48.66	48.64	48.42	48.08	47.59	46.95	46.57
400	49.15	49.14	48.99	48.74	48.38	47.89	47.60
450	49.46	49.45	49.35	49.17	48.91	48.55	48.31
500	49.65	49.64	49.58	49.45	49.26	48.98	48.82
600	49.84	49.84	49.81	49.74	49.65	49.50	49.41
700	49.91	49.91	49.90	49.87	49.82	49.74	49.69
800	49.94	49.94	49.93	49.92	49.90	49.85	49.83
900	49.96	49.96	49.94	49.94	49.93	49.91	49.90
1000	49.96	49.96	49.96	49.96	49.94	49.93	49.93
1200	49.96	49.96	49.96	49.96	49.96	49.96	49.96

The boundary pressure history is given below:

Time (days)	p (psi)
0	3000
30	2956
60	2917
90	2877
120	2844
150	2811
180	2791
210	2773
240	2755

Calculate the cumulative water influx as a function of time by using the bottom-water drive solution and compare with the edge-water drive approach.

Solution Step 1. Calculate the dimensionless radius for an infinite-acting aquifer:

$$r_D = \infty$$

Step 2. Calculate z_D from Equation 2.3.28:

$$z_D = \frac{h}{r_e \sqrt{F_k}}$$

$$= \frac{200}{2000 \sqrt{0.04}} = 0.5$$

Step 3. Calculate the water influx constant B:

$$B = 1.119 \phi c_t r_e^2 h$$

$$= 1.119(0.1)(8 \times 10^{-6})(2000)^2(200)$$

$$= 716 \text{ bbl/psi}$$

Step 4. Calculate the dimensionless time t_D:

$$t_D = 6.328 \times 10^{-3} \frac{kt}{\phi \mu_w c_t r_e^2}$$

$$= 6.328 \times 10^{-3} \left[\frac{50}{(0.1)(0.395)(8 \times 10^{-6})(2000)^2} \right] t$$

$$= 0.2503t$$

Step 5. Calculate the water influx by using the bottom-water model and edge-water model. Note that the

difference between the two models lies in the approach used in calculating the dimensionless water influx W_{eD}:

$$W_e = B \sum \Delta p \, W_{eD}$$

t	t_D	Δp	Bottom-water model		Edge-water model	
(days)		(psi)	W_{eD}	W_e (Mbbl)	W_{eD}	W_e (Mbbl)
0	0	0	–	–	–	–
30	7.5	22	5.038	79	6.029	95
60	15.0	41.5	8.389	282	9.949	336
90	22.5	39.5	11.414	572	13.459	678
120	30.0	36.5	14.994	933	16.472	1103
150	37.5	33.0	16.994	1353	19.876	1594
180	45.0	26.5	19.641	1810	22.897	2126
210	52.5	19.0	22.214	2284	25.827	2676
240	60.0	18.0	24.728	2782	28.691	3250

Linear water drive

As shown by van Everdingen and Hurst, the water influx from a linear aquifer is proportional to the square root of time. The van Everdingen and Hurst dimensionless water influx is replaced by the square root of time, as given by:

$$W_e = B_L \sum \left[\Delta p_n \sqrt{t - t_n} \right]$$

where:

B_L = linear-aquifer water influx constant, bbl/psi/$\sqrt{\text{time}}$
t = time (any convenient time units, e.g., months, years)
Δp = pressure drop as defined previously for the radial edge-water drive

The linear-aquifer water influx constant B_L is determined for the material balance equation as described in Chapter 4.

2.3.5 The Carter and Tracy water influx model

The van Everdingen and Hurst methodology provides the exact solution to the radial diffusivity equation and therefore is considered the correct technique for calculating water influx. However, because superposition of solutions is required, their method involves tedious calculations. To reduce the complexity of water influx calculations, Carter and Tracy (1960) proposed a calculation technique that does not require superposition and allows direct calculation of water influx.

The primary difference between the Carter–Tracy technique and the van Everdingen and Hurst technique is that Carter–Tracy assumes constant water influx rates over each finite time interval. Using the Carter–Tracy technique, the cumulative water influx at any time, t_n, can be calculated directly from the previous value obtained at t_{n-1}, or:

$$(W_e)_n = (W_e)_{n-1} + \left[(t_D)_n - (t_D)_{n-1} \right]$$

$$\times \left[\frac{B \Delta p_n - (W_e)_{n-1} (p_D^{\backslash})_n}{(p_D)_n - (t_D)_{n-1} (p_D^{\backslash})_n} \right] \qquad [2.3.31]$$

where:

B = the van Everdingen and Hurst water influx constant as defined by Equation 2.3.21
t_D = the dimensionless time as defined by Equation 2.3.15

n = the *current* time step
$n - 1$ = the *previous* time step
Δp_n = total pressure drop, $p_i - p_n$, psi
p_D = dimensionless pressure
$p_D^{\backslash}$ = dimensionless pressure derivative

Values of the dimensionless pressure p_D as a function of t_D and r_D are tabulated in Chapter 1, Table 1.2. In addition to the curve-fit equations given in Chapter 1 (Equations 1.2.79 through 1.2.84, Edwardson et al. (1962) developed the following approximation of p_D for an infinite-acting aquifer:

$$p_D = \frac{370.529\sqrt{t_D} + 137.582 t_D + 5.69549\,(t_D)^{1.5}}{328.834 + 265.488\sqrt{t_D} + 45.2157 t_D + (t_D)^{1.5}}$$

$$[2.3.32]$$

The dimensionless pressure derivative can then be approximated by:

$$p_D^{\backslash} = \frac{E}{F} \qquad [2.3.33]$$

where:

$E = 716.441 + 46.7984\,(t_D)^{0.5} + 270.038 t_D + 71.0098\,(t_D)^{1.5}$
$F = 1296.86\,(t_D)^{0.5} + 1204.73 t_D + 618.618\,(t_D)^{1.5}$
$\quad + 538.072\,(t_D)^2 + 142.41\,(t_D)^{2.5}$

When the dimensionless time $t_D > 100$, the following approximation can be used for p_D:

$$p_D = \frac{1}{2}[\ln(t_D) + 0.80907]$$

with the derivative given by:

$$p_D^{\backslash} = \frac{1}{2 t_D}$$

Fanchi (1985) matched the van Everdingen and Hurst tabulated values of the dimensionless pressure p_D as a function of t_D and r_D in Table 1.2 by using a regression model and proposed the following expression:

$$p_D = a_0 + a_1 t_D + a_2 \ln(t_D) + a_2 [\ln(t_D)]^2$$

in which the regression coefficients are given below:

r_{eD}	a_0	a_1	a_2	a_3
1.5	0.10371	1.6665700	−0.04579	−0.01023
2.0	0.30210	0.6817800	−0.01599	−0.01356
3.0	0.51243	0.2931700	0.015340	−0.06732
4.0	0.63656	0.1610100	0.158120	−0.09104
5.0	0.65106	0.1041400	0.309530	−0.11258
6.0	0.63367	0.0694000	0.41750	−0.11137
8.0	0.40132	0.0410400	0.695920	−0.14350
10.0	0.14386	0.0264900	0.896460	−0.15502
∞	0.82092	−0.000368	0.289080	0.028820

It should be noted that the Carter and Tracy method is not an exact solution to the diffusivity equation and should be considered as an approximation.

Example 2.9 Rework Example 2.7 by using the Carter and Tracy method.

Solution Example 2.7 shows the following preliminary results:

• water influx constant $B = 20.4$ bbl/psi;
• $t_D = 0.9888t$.

Step 1. For each time step n, calculate the total pressure drop $\Delta p_n = p_i - p_n$ and the corresponding t_D:

n	t_1 (days)	p_n	Δp_n	t_D
0	0	2500	0	0
1	182.5	2490	10	180.5
2	365.0	2472	28	361.0
3	547.5	2444	56	541.5
4	730.0	2408	92	722.0

Step 2. Since the values of t_D are greater than 100, use Equation 1.2.80 to calculate p_D and its derivative $p_D^{\backslash}$. That is:

$$p_D = \frac{1}{2}[\ln(t_D) + 0.80907]$$

$$p_D^{\backslash} = \frac{1}{2t_D}$$

n	t	t_D	p_D	$p_D^{\backslash}$
0	0	0	–	–
1	182.5	180.5	3.002	2.770×10^{-3}
2	365.0	361.0	3.349	1.385×10^{-3}
3	547.5	541.5	3.552	0.923×10^{-3}
4	730.0	722.0	3.696	0.693×10^{-3}

Step 3. Calculate cumulative water influx by applying Equation 2.3.31

W_e after 182.5 days:

$$(W_e)_n = (W_e)_{n-1} + [(t_D)_n - (t_D)_{n-1}]$$

$$\times \left[\frac{B\Delta p_n - (W_e)_{n-1}\left(p_D^{\backslash}\right)_n}{(p_D)_n - (t_D)_{n-1}\left(p_D^{\backslash}\right)_n} \right]$$

$$= 0 + [180.5 - 0]$$

$$\times \left[\frac{(20.4)(10) - (0)(2.77 \times 10^{-3})}{3.002 - (0)(2.77 \times 10^{-3})} \right]$$

$$= 12\,266 \text{ bbl}$$

W_e after 365 days:

$$W_e = 12\,266 + [361 - 180.5]$$

$$\times \left[\frac{(20.4)(28) - (12\,266)(1.385 \times 10^{-3})}{3.349 - (180.5)(1.385 \times 10^{-3})} \right]$$

$$= 42\,545 \text{ bbl}$$

W_e after 547.5 days:

$$W_e = 42\,546 + [541.5 - 361]$$

$$\times \left[\frac{(20.4)(56) - (42\,546)(0.923 \times 10^{-3})}{3.552 - (361)(0.923 \times 10^{-3})} \right]$$

$$= 104\,406 \text{ bbl}$$

W_e after 720 days:

$$W_e = 104\,406 + [722 - 541.5]$$

$$\times \left[\frac{(20.4)(92) - (104\,406)(0.693 \times 10^{-3})}{3.696 - (541.5)(0.693 \times 10^{-3})} \right]$$

$$= 202\,477 \text{ bbl}$$

The following table compares the results of the Carter and Tracy water influx calculations with those of the van Everdingen and Hurst method.

Time (months)	Carter and Tracy, W_e (bbl)	van Everdingen and Hurst, W_e, bbl
0	0	0
6	12\,266	7085
12	42\,546	32\,435
18	104\,400	85\,277
24	202\,477	175\,522

The above comparison indicates that the Carter and Tracy method considerably overestimates the water influx. However, this is due to the fact that a large time step of 6 months was used in the Carter and Tracy method to determine the water influx. The accuracy of this method can be increased substantially by restricting the time step to one month. Recalculating the water influx on a monthly basis produces an excellent match with the van Everdingen and Hurst method as shown below.

Time (months)	Time (days)	p (psi)	Δp (psi)	t_D	p_D	$p_D^{\backslash}$	Carter–Tracy W_e (bbl)	van Everdingen and Hurst W_e (bbl)
0	0	2500.0	0.00	0	0.00	0	0.0	0
1	30	2498.9	1.06	30.0892	2.11	0.01661	308.8	
2	61	2497.7	2.31	60.1784	2.45	0.00831	918.3	
3	91	2496.2	3.81	90.2676	2.66	0.00554	1860.3	
4	122	2494.4	5.56	120.357	2.80	0.00415	3171.7	
5	152	2492.4	7.55	150.446	2.91	0.00332	4891.2	
6	183	2490.2	9.79	180.535	3.00	0.00277	7057.3	7088.9
7	213	2487.7	12.27	210.624	3.08	0.00237	9709.0	
8	243	2485.0	15.00	240.713	3.15	0.00208	12\,884.7	
9	274	2482.0	17.98	270.802	3.21	0.00185	16\,622.8	
10	304	2478.8	21.20	300.891	3.26	0.00166	20\,961.5	
11	335	2475.3	24.67	330.981	3.31	0.00151	25\,938.5	
12	365	2471.6	28.38	361.070	3.35	0.00139	31\,591.5	32\,435.0
13	396	2467.7	32.34	391.159	3.39	0.00128	37\,957.8	
14	426	2463.5	36.55	421.248	3.43	0.00119	45\,074.5	
15	456	2459.0	41.00	451.337	3.46	0.00111	52\,978.6	
16	487	2454.3	45.70	481.426	3.49	0.00104	61\,706.7	

Time (months)	Time (days)	p (psi)	Δp (psi)	t_D	p_D	$p_D^{\backslash}$	Carter–Tracy W_e (bbl)	van Everdingen and Hurst W_e (bbl)
17	517	2449.4	50.64	511.516	3.52	0.00098	71 295.3	
18	547	2444.3	55.74	541.071	3.55	0.00092	81 578.8	85 277.0
19	578	2438.8	61.16	571.130	3.58	0.00088	92 968.2	
20	608	2433.2	66.84	601.190	3.60	0.00083	105 323.	
21	638	2427.2	72.75	631.249	3.63	0.00079	118 681.	
22	669	2421.1	78.92	661.309	3.65	0.00076	133 076.	
23	699	2414.7	85.32	691.369	3.67	0.00072	148 544.	
24	730	2408.0	91.98	721.428	3.70	0.00069	165 119.	175 522.0

2.3.6 The Fetkovich method

Fetkovich (1971) developed a method of describing the approximate water influx behavior of a finite aquifer for radial and linear geometries. In many cases, the results of this model closely match those determined using the van Everdingen and Hurst approach. The Fetkovich theory is much simpler, and, like the Carter–Tracy technique, this method does not require the use of superposition. Hence, the application is much easier, and this method is also often utilized in numerical simulation models.

The Fetkovich model is based on the premise that the productivity index concept will adequately describe water influx from a finite aquifer into a hydrocarbon reservoir. That is, the water influx rate is directly proportional to the pressure drop between the average aquifer pressure and the pressure at the reservoir–aquifer boundary. The method neglects the effects of any transient period. Thus, in cases where pressures are changing rapidly at the aquifer–reservoir interface, predicted results may differ somewhat from the more rigorous van Everdingen and Hurst or Carter–Tracy approaches. However, in many cases pressure changes at the waterfront are gradual and this method offers an excellent approximation to the two methods discussed above.

This approach begins with two simple equations. The first is the productivity index (PI) equation for the aquifer, which is analogous to the PI equation used to describe an oil or gas well:

$$e_w = \frac{dW_e}{dt} = J\left(\bar{p}_a - p_r\right) \qquad [2.3.34]$$

where:

e_w = water influx rate from aquifer, bbl/day
J = productivity index for the aquifer, bbl/day/psi
$\bar{p}_a$ = average aquifer pressure, psi
p_r = inner aquifer boundary pressure, psi

The second equation is an aquifer material balance equation for a constant compressibility, which states that the amount of pressure depletion in the aquifer is directly proportional to the amount of water influx from the aquifer, or:

$$W_e = c_t W_i \left(p_i - \bar{p}_a\right) f \qquad [2.3.35]$$

where:

W_i = initial volume of water in the aquifer, bbl
c_t = total aquifer compressibility, $c_w + c_f$, psi^{-1}
p_i = initial pressure of the aquifer, psi
f = $\theta/360$

Equation 2.3.25 suggests that the *maximum* possible water influx occurs if $\bar{p}_a = 0$, or:

$$W_{ei} = c_t W_i p_i f \qquad [2.3.36]$$

where:

W_{ei} = maximum water influx, bbl

Combining Equation 2.3.36 with 2.3.35 gives:

$$\bar{p}_a = p_i \left(1 - \frac{W_e}{c_t W_i p_i}\right) = p_i \left(1 - \frac{W_e}{W_{ei}}\right) \qquad [2.3.37]$$

Equation 2.3.35 provides a simple expression to determine the average aquifer pressure $\bar{p}_a$ after removing W_e bbl of water from the aquifer to the reservoir, i.e., cumulative water influx.

Differentiating Equation 2.3.37 with respect to time gives:

$$\frac{dW_e}{dt} = -\frac{W_{ei}}{p_i} \frac{d\bar{p}_a}{dt} \qquad [2.3.38]$$

Fetkovich combined Equation 2.3.38 with 2.3.34 and integrated to give the following form:

$$W_e = \frac{W_{ei}}{p_i} \left(p_i - p_r\right) \exp\left(\frac{-Jp_i t}{W_{ei}}\right) \qquad [2.3.39]$$

where:

W_e = cumulative water influx, bbl
p_r = reservoir pressure, i.e., pressure at the oil or gas–water contact
t = time, days

Equation 2.3.39 has no practical applications since it was derived for a constant inner boundary pressure. To use this solution in the case in which the boundary pressure is varying continuously as a function of time, the superposition technique must be applied. Rather than using superposition, Fetkovich suggested that, if the reservoir–aquifer boundary pressure history is divided into a finite number of time intervals, the incremental water influx during the nth interval is:

$$\left(\Delta W_e\right)_n = \frac{W_{ei}}{p_i} \left[\left(\bar{p}_a\right)_{n-1} - \left(\bar{p}_r\right)_n\right] \left[1 - \exp\left(-\frac{Jp_i \Delta t_n}{W_{ei}}\right)\right] \qquad [2.3.40]$$

where $\left(\bar{p}_a\right)_{n-1}$ is the average aquifer pressure at the end of the previous time step. This average pressure is calculated from Equation 2.3.37 as:

$$\left(\bar{p}_a\right)_{n-1} = p_i \left(1 - \frac{\left(W_e\right)_{n-1}}{W_{ei}}\right) \qquad [2.3.41]$$

The average reservoir boundary pressure $\left(\bar{p}_r\right)_n$ is estimated from:

$$\left(\bar{p}_r\right)_n = \frac{\left(p_r\right)_n + \left(p_r\right)_{n-1}}{2} \qquad [2.3.42]$$

The productivity index J used in the calculation is a function of the geometry of the aquifer. Fetkovich calculated the productivity index from Darcy's equation for bounded aquifers. Lee and Wattenbarger (1996) pointed out that the Fetkovich method can be extended to infinite-acting aquifers by requiring that the ratio of water influx rate to pressure drop is approximately constant throughout the productive life of the reservoir. The productivity index J of the aquifer is given by the following expressions:

Type of outer aquifer boundary	J for radial flow (bbl/day/psi)	J for linear flow (bbl/day/psi)	Equation
Finite, no flow	$J = \dfrac{0.00708khf}{\mu_w\left[\ln(r_D) - 0.75\right]}$	$J = \dfrac{0.003381kwh}{\mu_w L}$	[2.3.43]
Finite, constant pressure	$J = \dfrac{0.00708khf}{\mu_w\left[\ln(r_D)\right]}$	$J = \dfrac{0.001127kwh}{\mu_w L}$	[2.3.44]
Infinite	$J = \dfrac{0.00708khf}{\mu_w \ln(a/r_e)}$ $a = \sqrt{0.0142kt/(\phi\mu_w c_t)}$	$J = \dfrac{0.001kwh}{\mu_w\sqrt{0.0633kt/(\phi\mu_w c_t)}}$	[2.3.45]

where:

w = width of the linear aquifer, ft
L = length of the linear aquifer, ft
r_D = dimensionless radius, r_a/r_e
k = permeability of the aquifer, md
t = time, days
θ = encroachment angle
h = thickness of the aquifer
$f = \theta/360$

The following steps describe the methodology of using the Fetkovich model in predicting the cumulative water influx:

Step 1. Calculate the initial volume of water in the aquifer from:

$$W_i = \frac{\pi}{5.615}\left(r_a^2 - r_e^2\right)h\phi$$

Step 2. Calculate the maximum possible water influx W_{ei} by applying Equation 2.3.36, or:

$$W_{ei} = c_t W_i p_i f$$

Step 3. Calculate the productivity index J based on the boundary conditions and aquifer geometry.

Step 4. Calculate the incremental water influx $(\Delta W_e)_n$ from the aquifer during the nth time interval by using Equation 2.3.40. For example, during the first time step Δt_1:

$$\left(\Delta W_e\right)_1 = \frac{W_{ei}}{p_i}\left[p_i - (\bar{p}_r)_1\right]\left[1 - \exp\left(\frac{-Jp_i\Delta t_1}{W_{ei}}\right)\right]$$

with:

$$(\bar{p}_r)_1 = \frac{p_i + (p_r)_1}{2}$$

For the second time interval Δt_2:

$$\left(\Delta W_e\right)_2 = \frac{W_{ei}}{p_i}\left[(\bar{p}_a)_1 - (\bar{p}_r)_2\right]\left[1 - \exp\left(\frac{-Jp_i\Delta t_2}{W_{ei}}\right)\right]$$

where $(\bar{p}_a)_1$ is the average aquifer pressure at the end of the first period and removing $(\Delta W_e)_1$ barrels of water from the aquifer to the reservoir. From Equation 2.3.41:

$$(\bar{p}_a)_1 = p_i\left(1 - \frac{(\Delta W_e)_1}{W_{ei}}\right)$$

Step 5. Calculate the cumulative (total) water influx at the end of any time period from:

$$W_e = \sum_{i=1}^{n}\left(\Delta W_e\right)_i$$

Example 2.10[b] Using the Fetkovich method, calculate the water influx as a function of time for the following reservoir–aquifer and boundary pressure data:
$p_i = 2740$ psi, $h = 100$ ft, $c_t = 7 \times 10^{-6}$ psi^{-1}
$\mu_w = 0.55$ cp, $k = 200$ md, $\theta = 140°$
reservoir area = 40 363 acres,
aquifer area = 1 000 000 acres

Time (days)	p_r (psi)
0	2740
365	2500
730	2290
1095	2109
1460	1949

Figure 2.17[c] shows the wedge reservoir–aquifer system with an encroachment angle of 140°.

Solution   Step 1. Calculate the reservoir radius r_e

$$r_e = \left(\frac{\theta}{360}\right)\sqrt{\frac{43\,560A}{\pi}} = 9200 \text{ ft}$$

$$= \left(\frac{140}{360}\right)\sqrt{\frac{(43\,560)(2374)}{\pi}} = 9200 \text{ ft}$$

Step 2. Calculate the equivalent aquifer radius r_a:

$$r_a = \left(\frac{140}{360}\right)\sqrt{\frac{(43\,560)(1\,000\,000)}{\pi}} = 46\,000 \text{ ft}$$

Step 3. Calculate the dimensionless radius r_D:

$$r_D = r_a/r_e = 46\,000/9200 = 5$$

Step 4. Calculate initial water-in-place W_i:

$$W_i = \pi\left(r_a^2 - r_e^2\right)h\theta/5.615$$

$$= \frac{\pi(46\,000^2 - 9200^2)(100)(0.25)}{5.615}$$

$$= 28.41 \text{ MMMbbl}$$

Step 5. Calculate W_{ei} from Equation 2.3.36:

$$W_{ei} = c_t W_i p_i f$$

$$= 7 \times 10^{-6}(28.41 \times 10^9)(2740)\left(\frac{140}{360}\right)$$

$$= 211.9 \text{ MMMbbl}$$

[b]Data for this example is given by L.P. Dake *Fundamentals of Reservoir Engineering* 1978, Elsevier Publishing Company.
[c]Data for this example is given by L.P. Dake *Fundamentals of Reservoir Engineering* 1978, Elsevier Publishing Company.
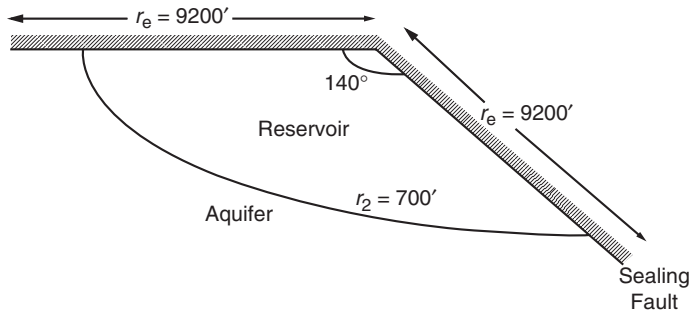
Figure 2.17 *Aquifer-reservoir geometry for Example 2.10.*

Step 6. Calculate the productivity index J of the radial aquifer from Equation 2.3.43

$$J = \frac{0.00708\,(200)\,(100)\left(\frac{140}{360}\right)}{0.55\ln(5)}$$

$$= 116.5\text{ bbl/day/psi}$$

and therefore:

$$\frac{Jp_i}{W_{ei}} = \frac{(116.5)(2740)}{211.9 \times 10^6} = 1.506 \times 10^{-3}$$

Since the time step Δt is fixed at 365 days, then:

$$1 - \exp^{(-Jp_i\Delta t/W_{ei})} = 1 - \exp^{(-1.506\times10^{-3}\times365)}$$

$$= 0.4229$$

Substituting in Equation 2.3.41 gives:

$$(\Delta W_e)_n = \frac{W_{ei}}{p_i}\left[(\bar{p}_a)_{n-1} - (\bar{p}_r)_n\right]$$

$$\times \left[1 - \exp\left(-\frac{Jp_i\Delta t_n}{W_{ei}}\right)\right]$$

$$= \frac{211.9 \times 10^6}{2740}\left[(\bar{p}_a)_{n-1} - (\bar{p}_r)_n\right](0.4229)$$

$$= 32705\left[(\bar{p}_a)_{n-1} - (\bar{p}_r)_n\right]$$

Step 7. Calculate the cumulative water influx as shown in the following table.

n	t (days)	p_r	$(\bar{p}_r)_n$	$(\bar{p}_a)_{n-1}$	$(\bar{p}_a)_{n-1}$ $-(\bar{p}_r)_n$	$(\Delta W_e)_n$ (MMbbl)	W_e (MMbbl)
0	0	2740	2740	–	–	–	–
1	365	2500	2620	2740	120	3.925	3.925
2	730	2290	2395	2689	294	9.615	13.540
3	1095	2109	2199	2565	366	11.970	25.510
4	1460	1949	2029	2409	381	12.461	37.971

Problems

1. Calculate the cumulative water influx that result from a pressure drop of 200 psi at the oil–water contact with an encroachment angle of 50°. The reservoir–aquifer system is characterized by the following properties:

	Reservoir	*Aquifer*
radius, ft	6000	20 000
porosity	0.18	0.15
c_f, psi^{-1}	4×10^{-6}	3×10^{-6}
c_w, psi^{-1}	5×10^{-6}	4×10^{-6}
h, ft	25	20

2. An active water drive oil reservoir is producing under steady-state flowing conditions. The following data is available:

$p_i = 4000$ psi, $p = 3000$ psi,
$Q_o = 40\,000$ STB/day $B_o = 1.3$ bbl/STB,
GOR $= 700$ scf/STB, $R_s = 500$ scf/STB
$Z = 0.82$, $T = 140°$F,
$Q_w = 0$, $B_w = 1.0$ bbl/STB

Calculate the Schilthuis water influx constant.

3. The pressure history of a water drive oil reservoir is given below:

t (days)	p (psi)
0	4000
120	3950
220	3910
320	3880
420	3840

The aquifer is under a steady-state flowing condition with an estimated water influx constant of 80 bbl/day/psi. Using the steady-state model, calculate and plot the cumulative water influx as a function of time.

4. A water drive reservoir has the following boundary pressure history:

Time (months)	*Boundary pressure* (psi)
0	2610
6	2600
12	2580
18	2552
24	2515

The aquifer–reservoir system is characterized by the following data:

	Reservoir	*Aquifer*
radius, ft	2000	∞
h, ft	25	30
k, md	60	80
ϕ, %	17	18
μ_w, cp	0.55	0.85
c_w, psi^{-1}	0.7×10^{-6}	0.8×10^{-6}
c_f, psi^{-1}	0.2×10^{-6}	0.3×10^{-6}

If the encroachment angle is 360°, calculate the water influx as a function of time by using:

(a) the van Everdingen and Hurst method;
(b) the Carter and Tracy Method.

5. The following table summarizes the original data available on the West Texas water drive reservoir:

	Oil zone	*Aquifer*
Geometry	Circular	Semicircular
Area, acres	640	Infinite
Initial reservoir pressure, psia	4000	4000
Initial oil saturation	0.80	0
Porosity, %	22	–
B_{oi}, bbl/STB	1.36	–
B_{wi}, bbl/STB	1.00	1.05
c_o, psi	6×10^{-6}	–
c_w, psi^{-1}	3×10^{-6}	7×10^{-6}

The geological data of the aquifer estimates the water influx constant at 551 bbl/psi. After 1120 days of production, the reservoir average pressure has dropped to 3800 psi and the field has produced 860 000 STB of oil.

The field condition after 1120 days of production is given below:

$p = 3800$ psi, $N_p = 860\,000$ STB,
$B_o = 1.34$ bbl/STB, $B_w = 1.05$ bbl/STB,
$W_e = 991\,000$ bbl,
$t_D = 32.99$ (dimensionless time after 1120 days),
$W_p = 0$ bbl

It is expected that the average reservoir pressure will drop to 3400 psi after 1520 days (i.e., from the start of production). Calculate the cumulative water influx after 1520 days.

6. A wedge reservoir–aquifer system with an encroachment angle of 60° has the following boundary pressure history:

Time (days)	*Boundary pressure* (psi)
0	2850
365	2610
730	2400
1095	2220
1460	2060

Given the following aquifer data:

$h = 120$ ft, $c_f = 5 \times 10^{-6}$ psi^{-1},
$c_w = 4 \times 10^{-6}$ psi^{-1}, $\mu_w = 0.7$ cp,
$k = 60$ md, $\phi = 12\%$,
reservoir area = 40 000 acres
aquifer area = 980 000 acres, $T = 140°$F

calculate the cumulative influx as a function of time by using:

(a) the van Everdingen and Hurst method;
(b) the Carter and Tracy method;
(c) the Fetkovich method.

This page intentionally left blank

3

Unconventional Gas Reservoirs

Contents

Efficient development and operation of a natural gas reservoir depend on understanding the reservoir characteristics and the well performance. Predicting the future recovery of the reservoir and the producing wells is the most important part in the economic analysis of the field for further development and expenditures. To forecast the performance of a gas field and its existing production wells, sources of energy for producing the hydrocarbon system must be identified and their contributions to reservoir behavior evaluated.

The objective of this chapter is to document the methods that can be used to evaluate and predict:

- vertical and horizontal gas well performance;
- conventional and non-conventional gas field performance.

3.1 Vertical Gas Well Performance

Determination of the flow capacity of a gas well requires a relationship between the inflow gas rate and the sand face pressure or flowing bottom-hole pressure. This inflow performance relationship may be established by the proper solution of Darcy's equation. Solution of Darcy's law depends on the conditions of the flow existing in the reservoir or the flow regime.

When a gas well is first produced after being shut in for a period of time, the gas flow in the reservoir follows an unsteady-state behavior until the pressure drops at the drainage boundary of the well. Then the flow behavior passes through a short transition period, after which it attains a steady-state or semisteady (pseudosteady)-state condition. The objective of this chapter is to describe the empirical as well as analytical expressions that can be used to establish the inflow performance relationships under the pseudosteady-state flow condition.

3.1.1 Gas flow under laminar (viscous) flowing conditions
The exact solution to the differential form of Darcy's equation for compressible fluids under the pseudosteady-state flow condition was given previously by Equation 1.2.138, as:

$$Q_g = \frac{kh\left[\overline{\psi}_r - \psi_{wf}\right]}{1422T\left[\ln\left(r_e/r_w\right) - 0.75 + s\right]} \qquad [3.1.1]$$

with:

$$\overline{\psi}_r = m(\overline{p}_r) = 2\int_0^{\overline{p}_r}\frac{p}{\mu Z}\,dp$$

$$\psi_{wf} = m(p_{wf}) = 2\int_0^{p_{wf}}\frac{p}{\mu Z}\,dp$$

where:

Q_g = gas flow rate, Mscf/day
k = permeability, md
$m(\overline{p}_r) = \overline{\psi}_r$ = average reservoir real-gas pseudo-pressure, psi^2/cp
T = temperature, °R
s = skin factor
h = thickness
r_e = drainage radius
r_w = wellbore radius

Note that the shape factor C_A, which is designed to account for the deviation of the drainage area from the ideal circular form as introduced in Chapter 1 and given in Table 1.4, can be included in Darcy's equation to give:

$$Q_g = \frac{kh\left[\overline{\psi}_r - \psi_{wf}\right]}{1422T\left[\frac{1}{2}\ln\left(4A/1.781C_A r_w^2\right) + s\right]}$$
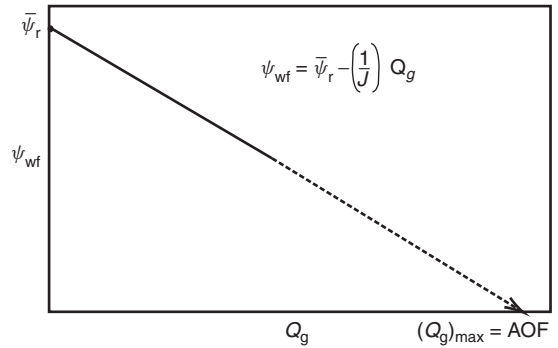
Figure 3.1   Steady-state gas well flow.

with:

$$A = \pi r_e^2$$

where:

A = drainage area, ft^2
C_A = shape factor with values as given in Table 1.4

For example, a circular drainage area has a shape factor of 31.62, i.e., $C_A = 31.62$, as shown in Table 1.4, and reduces the above equation into Equation 3.1.1.

The productivity index J for a gas well can be written analogously to that for oil wells with the definition as the production rate per unit pressure drop. That is:

$$J = \frac{Q_g}{\left[\overline{\psi}_r - \psi_{wf}\right]} = \frac{kh}{1422T\left[\frac{1}{2}\ln\left(4A/1.781C_A r_w^2\right) + s\right]}$$

For the most commonly used flow geometry, i.e., a circular drainage area, the above equation is reduced to:

$$J = \frac{Q_g}{\overline{\psi}_r - \psi_{wf}} = \frac{kh}{1422T\left[\ln\left(r_e/r_w\right) - 0.75 + s\right]} \qquad [3.1.2]$$

or:

$$Q_g = J\left(\overline{\psi}_r - \psi_{wf}\right) \qquad [3.1.3]$$

With the absolute open flow potential (AOF), i.e., maximum gas flow rate $(Q_g)_{max}$, as calculated by setting $\psi_{wf} = 0$, then:

$$\text{AOF} = (Q_g)_{max} = J(\overline{\psi}_r - 0)$$

or:

$$\text{AOF} = (Q_g)_{max} = J\overline{\psi}_r \qquad [3.1.4]$$

where:

J = productivity index, Mscf/day/psi^2/cp
$(Q_g)_{max}$ = Maximum gas flow rate, Mscf/day
AOF = Absolute open flow potential, Mscf/day

Equation 3.1.3 can be expressed in a linear relationship as:

$$\psi_{wf} = \overline{\psi}_r - \left(\frac{1}{J}\right)Q_g \qquad [3.1.5]$$

Equation 3.1.5 indicates that a plot of ψ_{wf} vs. Q_g would produce a straight line with a slope of $1/J$ and intercept of $\overline{\psi}_r$, as shown in Figure 3.1. If two different stabilized flow rates are available, the line can be extrapolated and the slope is determined to estimate AOF, J, and $\overline{\psi}_r$.

Equation 3.1.1 can be written alternatively in the following integral form:

$$Q_g = \frac{kh}{1422T\left[\ln\left(r_e/r_w\right) - 0.75 + s\right]}\int_{p_{wf}}^{\overline{p}_r}\left(\frac{2p}{\mu_g Z}\right)dp \quad [3.1.6]$$

Note that $(p/\mu_g Z)$ is directly proportional to $(1/\mu_g B_g)$ where B_g is the gas formation volume factor and defined as:

$$B_g = 0.00504 \frac{ZT}{p} \qquad [3.1.7]$$

where:

B_g = gas formation volume factor, bbl/scf
Z = gas compressibility factor
T = temperature, °R

Equation 3.1.6 can then be written in terms of B_g of Equation 3.1.7, as follows. Arrange Equation 3.1.6 to give:

$$\frac{p}{ZT} = \frac{0.00504}{B_g}$$

Arrange Equation 3.1.7 in the following form:

$$Q_g = \frac{kh}{1422\left[\ln\left(r_e/r_w\right) - 0.75 + s\right]} \int_{p_{wf}}^{\bar{p}_r} \left(\frac{2}{\mu_g} \frac{p}{TZ}\right) dp$$

Combining the above two expressions:

$$Q_g = \left[\frac{7.08\left(10^{-6}\right)kh}{\ln\left(r_e/r_w\right) - 0.75 + s}\right] \int_{p_{wf}}^{\bar{p}_r} \left(\frac{1}{\mu_g B_g}\right) dp \qquad [3.1.8]$$

where:

Q_g = gas flow rate, Mscf/day
μ_g = gas viscosity, cp
k = permeability, md

Figure 3.2 shows a typical plot of the gas pressure functions $(2p/\mu Z)$ and $(1/\mu_g B_g)$ versus pressure. The integral in Equations 3.1.6 and 3.1.8 represents the area under the curve between $\bar{p}_r$ and p_{wf}. As illustrated in Figure 3.2, the pressure function exhibits the following three distinct pressure application regions.

High-pressure region
When the bottom-hole flowing pressure p_{wf} and average reservoir pressure $\bar{p}_r$ are both higher than 3000 psi, the pressure functions $(2p/\mu_g Z)$ and $(1/\mu_g B_g)$ are nearly constant, as shown by Region III in Figure 3.2. This observation suggests that the pressure term $(1/\mu_g B_g)$ in Equation 3.1.8 can be treated as a constant and can be removed outside the integral, to give:

$$Q_g = \left[\frac{7.08\left(10^{-6}\right)kh}{\ln\left(r_e/r_w\right) - 0.75 + s}\right]\left(\frac{1}{\mu_g B_g}\right) \int_{p_{wf}}^{\bar{p}_r} dp$$

or:

$$Q_g = \frac{7.08\left(10^{-6}\right)kh\left(\bar{p}_r - p_{wf}\right)}{\left(\mu_g B_g\right)_{avg}\left[\ln\left(r_e/r_w\right) - 0.75 + s\right]} \qquad [3.1.9]$$
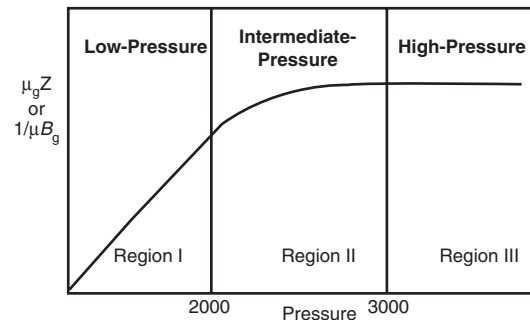
Figure 3.2 Gas PVT data.

where:

Q_g = gas flow rate, Mscf/day
B_g = gas formation volume factor, bbl/scf
k = permeability, md

The gas viscosity μ_g and formation volume factor B_g should be evaluated at the average pressure p_{avg} as given by:

$$p_{avg} = \frac{\bar{p}_r + p_{wf}}{2} \qquad [3.1.10]$$

The method of determining the gas flow rate by using Equation 3.1.9 is commonly called the "pressure approximation method."

It should be pointed out the concept of the productivity index J cannot be introduced into Equation 3.1.9 since this equation is only valid for applications when both p_{wf} and $\bar{p}_r$ are above 3000 psi.

Note that deviation from the circular drainage area can be treated as an additional skin by including the shape factor C_A in Equation 3.1.9, to give:

$$Q_g = \frac{7.08\left(10^{-6}\right)kh\left(\bar{p}_r - p_{wf}\right)}{\left(\mu_g B_g\right)_{avg}\left[\frac{1}{2}\ln\left(4A/1.781 C_A r_w^2\right) + s\right]}$$

Intermediate-pressure region
Between 2000 and 3000 psi, the pressure function shows distinct curvature. When the bottom-hole flowing pressure and average reservoir pressure are both between 2000 and 3000 psi, the pseudopressure gas pressure approach (i.e., Equation 3.1.1) should be used to calculate the gas flow rate:

$$Q_g = \frac{kh\left[\bar{\psi}_r - \psi_{wf}\right]}{1422T\left[\ln\left(r_e/r_w\right) - 0.75 + s\right]}$$

and for a non-circular drainage area, the above flow should be modified to include the shape factor C_A and the drainage area, to give:

$$Q_g = \frac{kh\left[\bar{\psi}_r - \psi_{wf}\right]}{1422T\left[\frac{1}{2}\ln\left(4A/1.781 C_A r_w^2\right) + s\right]}$$

Low-pressure region
At low pressures, usually less than 2000 psi, the pressure functions $(2p/\mu Z)$ and $(1/\mu_g B_g)$ exhibit a linear relationship with pressure as shown in Figure 3.2 and is identified as Region I. Golan and Whitson (1986) indicated that the product $(\mu_g Z)$ is essentially constant when evaluating any pressure below 2000 psi. Implementing this observation in Equation 3.1.6 and integrating gives:

$$Q_g = \frac{kh}{1422T\left[\ln\left(r_e/r_w\right) - 0.75 + s\right]}\left(\frac{2}{\mu_g Z}\right) \int_{p_{wf}}^{\bar{p}_r} p \, dp$$

or:

$$Q_g = \frac{kh\left(\bar{p}_r^2 - p_{wf}^2\right)}{1422T\left(\mu_g Z\right)_{avg}\left[\ln\left(r_e/r_w\right) - 0.75 + s\right]} \qquad [3.1.11]$$

and for a non-circular drainage area:

$$Q_g = \frac{kh\left(\bar{p}_r^2 - p_{wf}^2\right)}{1422T\left(\mu_g Z\right)_{avg}\left[\frac{1}{2}\ln\left(4A/1.781 C_A r_w^2\right) + s\right]}$$

where:

Q_g = gas flow rate, Mscf/day
k = permeability, md
T = temperature, °R
Z = gas compressibility factor
μ_g = gas viscosity, cp

It is recommended that the Z factor and gas viscosity be evaluated at the average pressure p_{avg} as defined by:

$$p_{\text{avg}} = \sqrt{\frac{\bar{p}_{\text{r}}^2 + p_{\text{wf}}^2}{2}}$$

It should be pointed out that, for the remainder of this chapter, it will be assumed that the well is draining a circular area with a shape factor of 31.16.

The method of calculating the gas flow rate by Equation 3.1.11 is called the "pressure-squared approximation method."

If both $\bar{p}_{\text{r}}$ and p_{wf} are lower than 2000 psi, Equation 3.1.11 can be expressed in terms of the productivity index J as:

$$Q_{\text{g}} = J\left(\bar{p}_{\text{r}}^2 - p_{\text{wf}}^2\right) \qquad [3.1.12]$$

with:

$$\left(Q_{\text{g}}\right)_{\text{max}} = \text{AOF} = J\bar{p}_{\text{r}}^2 \qquad [3.1.13]$$

where:

$$J = \frac{kh}{1422T\left(\mu_g Z\right)_{\text{avg}}\left[\ln\left(r_{\text{e}}/r_{\text{w}}\right) - 0.75 + s\right]} \qquad [3.1.14]$$

Example 3.1 The *PVT* properties of a gas sample taken from a dry gas reservoir are given below:

p (psi)	μ_g (cp)	Z	ψ (psi^2/cp)	B_g (bbl/scf)
0	0.01270	1.000	0	–
400	0.01286	0.937	13.2×10^6	0.007080
1200	0.01530	0.832	113.1×10^6	0.002100
1600	0.01680	0.794	198.0×10^6	0.001500
2000	0.01840	0.770	304.0×10^6	0.001160
3200	0.02340	0.797	678.0×10^6	0.000750
3600	0.02500	0.827	816.0×10^6	0.000695
4000	0.02660	0.860	950.0×10^6	0.000650

The reservoir is producing under the pseudosteady-state condition. The following additional data is available:

$k = 65$ md, $\quad h = 15$ ft, $\qquad T = 600°$R

$r_{\text{e}} = 1000$ ft, $\quad r_{\text{w}} = 0.25$ ft, $\quad s = -0.4$

Calculate the gas flow rate under the following conditions:

(a) $\bar{p}_{\text{r}} = 4000$ psi, $p_{\text{wf}} = 3200$ psi;
(b) $\bar{p}_{\text{r}} = 2000$ psi, $p_{\text{wf}} = 1200$ psi.

Use the appropriate approximation methods and compare results with the exact solution.

Solution

(a) Calculation of Q_{g} at $\bar{p}_{\text{r}} = 4000$ and $p_{\text{wf}} = 3200$ psi:

Step 1. Select the approximation method. Because $\bar{p}_{\text{r}}$ and p_{wf} are both greater than 3000, the pressure approximation method is used, i.e., Equation 3.1.9.

Step 2. Calculate average pressure and determine the corresponding gas properties.

$$\bar{p} = \frac{4000 + 3200}{2} = 3600 \text{ psi}$$

$$\mu_g = 0.025 \quad B_g = 0.000695$$

Step 3. Calculate the gas flow rate by applying Equation 3.1.9:

$$Q_{\text{g}} = \frac{7.08\left(10^{-6}\right)kh\left(\bar{p}_{\text{r}} - p_{\text{wf}}\right)}{\left(\mu_g B_g\right)_{\text{avg}}\left[\ln\left(r_{\text{e}}/r_{\text{w}}\right) - 0.75 + s\right]}$$

$$= \frac{7.08\left(10^{-6}\right)(65)(15)(4000 - 3200)}{(0.025)(0.000695)\left[\ln\left(1000/0.25\right) - 0.75 - 0.4\right]}$$

$$= 44\,490 \text{ Mscf/day}$$

Step 4. Recalculate Q_{g} by using the pseudopressure equation, i.e., Equation 3.1, to give:

$$Q_{\text{g}} = \frac{kh\left[\bar{\psi}_{\text{r}} - \psi_{\text{wf}}\right]}{1422T\left[\ln\left(r_{\text{e}}/r_{\text{w}}\right) - 0.75 + s\right]}$$

$$= \frac{(65)(15)(950.0 - 678.0)10^6}{(1422)(600)\left[\ln\left(1000/0.25\right) - 0.75 - 0.4\right]}$$

$$= 43\,509 \text{ Mscf/day}$$

Comparing results of the pressure approximation method with the pseudopressure approach indicates that the gas flow rate can be approximated using the "pressure method" with an absolute percentage error of 2.25%.

(b) Calculation of Q_{g} at $\bar{p}_{\text{r}} = 2000$ and $p_{\text{wf}} = 1200$:

Step 1. Select the appropriate approximation method. Because $\bar{p}_{\text{r}}$ and $p_{\text{wf}} \leq 2000$, use the pressure-squared approximation.

Step 2. Calculate average pressure and the corresponding μ_g and Z:

$$\bar{p} = \sqrt{\frac{2000^2 + 1200^2}{2}} = 1649 \text{ psi}$$

$$\mu_g = 0.017, \quad Z = 0.791$$

Step 3. Calculate Q_{g} by using the pressure-squared equation, i.e., Equation 3.1.11:

$$Q_{\text{g}} = \frac{kh\left(\bar{p}_{\text{r}}^2 - p_{\text{wf}}^2\right)}{1422T\left(\mu_g Z\right)_{\text{avg}}\left[\ln\left(r_{\text{e}}/r_{\text{w}}\right) - 0.75 + s\right]}$$

$$= \frac{(65)(15)\left(2000^2 - 1200^2\right)}{1422(600)(0.017)(0.791)\left[\ln\left(1000/0.25\right) - 0.75 - 0.4\right]}$$

$$= 30\,453 \text{ Mscf/day}$$

Step 4. Using the tabulated values of real-gas pseudopressure, calculate the exact Q_{g} by applying Equation 3.1.1:

$$Q_{\text{g}} = \frac{kh\left[\bar{\psi}_{\text{r}} - \psi_{\text{wf}}\right]}{1422T\left[\ln\left(r_{\text{e}}/r_{\text{w}}\right) - 0.75 + s\right]}$$

$$= \frac{(65)(15)(304.0 - 113.1)10^6}{(1422)(600)\left[\ln\left(1000/0.25\right) - 0.75 - 0.4\right]}$$

$$= 30\,536 \text{ Mscf/day}$$

Comparing results of the two methods, the pressure-squared approximation predicted the gas flow rate with an average absolute error of 0.27%.

3.1.2 Gas flow under turbulent flow conditions

All of the mathematical formulations presented thus far in this chapter are based on the assumption that laminar (viscous) flow conditions are observed during the gas flow. During radial flow, the flow velocity increases as the wellbore

is approached. This increase of the gas velocity might cause the development of a turbulent flow around the wellbore. If turbulent flow does exist, it causes an additional pressure drop similar to that caused by the mechanical skin effect.

As presented in Chapter 1 by Equations 1.2.152 through 1.2.154, the semisteady-state flow equation for compressible fluids can be modified to account for the additional pressure drop due to the turbulent flow by *including the rate-dependent skin factor DQ_g*, where the term D is called the turbulent flow factor. The resulting pseudosteady-state equations are given in the following three forms:

(1) Pressure-squared approximation form:

$$Q_g = \frac{kh\left(\bar{p}_r^2 - p_{wf}^2\right)}{1422T\left(\mu_g Z\right)_{avg}\left[\ln\left(r_e/r_w\right) - 0.75 + s + DQ_g\right]}$$

[3.1.15]

where D is the inertial or turbulent flow factor and is given by Equation 1.2.148 as:

$$D = \frac{Fkh}{1422T}$$ [3.1.16]

and where the non-Darcy flow coefficient F is defined by Equation 1.2.144 as:

$$F = 3.161\left(10^{-12}\right)\left[\frac{\beta T \gamma_g}{\mu_g h^2 r_w}\right]$$ [3.1.17]

where:

F = non-Darcy flow coefficient
k = permeability, md
T = temperature, °R
γ_g = gas gravity
r_w = wellbore radius, ft
h = thickness, ft
β = turbulence parameter as given by Equation 1.2.145:
$\beta = 1.88(10^{-10})k^{-1.47}\phi^{-0.53}$

and ϕ is the porosity.

(2) Pressure approximation form:

$$Q_g = \frac{7.08\left(10^{-6}\right)kh\left(\bar{p}_r - p_{wf}\right)}{\left(\mu_g B_g\right)_{avg}T\left[\ln\left(r_e/r_w\right) - 0.75 + s + DQ_g\right]}$$

[3.1.18]

(3) Real-gas pseudopressure form:

$$Q_g = \frac{kh\left(\bar{\psi}_r - \psi_{wf}\right)}{1422T\left[\ln\left(r_e/r_w\right) - 0.75 + s + DQ_g\right]}$$ [3.1.19]

Equations 3.1.15, 3.1.18, and 3.1.19 are essentially quadratic relationships in Q_g and, thus, they do not represent explicit expressions for calculating the gas flow rate. There are two separate empirical treatments that can be used to represent the turbulent flow problem in gas wells. Both treatments, with varying degrees of approximation, are directly derived and formulated from the three forms of the pseudosteady-state equations, i.e., Equations 3.1.15 through 3.1.17. These two treatments are called:

(1) the simplified treatment approach;
(2) the laminar–inertial–turbulent (LIT) treatment.

These two empirical treatments of the gas flow equation are presented below.

Simplified treatment approach
Based on the analysis for flow data obtained from a large number of gas wells, Rawlins and Schellardt (1936) postulated that the relationship between the gas flow rate and pressure can be expressed in the pressure-squared form,

i.e., Equation 3.1.11, by including an exponent n to account for the additional pressure drop due to the turbulent flow as:

$$Q_g = \frac{kh}{1422T\left(\mu_g Z\right)_{avg}\left[\ln\left(r_e/r_w\right) - 0.75 + s\right]}[\bar{p}_r^2 - p_{wf}^2]^n$$

Introducing the performance coefficient C into the above equation, as defined by:

$$C = \frac{kh}{1422T\left(\mu_g Z\right)_{avg}\left[\ln\left(r_e/r_w\right) - 0.75 + s\right]}$$

gives:

$$Q_g = C[\bar{p}_r^2 - p_{wf}^2]^n$$ [3.1.20]

where:

Q_g = gas flow rate, Mscf/day
$\bar{p}_r$ = average reservoir pressure, psi
n = exponent
C = performance coefficient, Mscf/day/psi^2

The exponent n is intended to account for the additional pressure drop caused by the high-velocity gas flow, i.e., turbulence. Depending on the flowing conditions, the exponent n may vary from 1.0 for completely laminar flow to 0.5 for fully turbulent flow, i.e., $0.5 \leq n \leq 1.0$.

The performance coefficient C in Equation 3.1.20 is included to account for:

- reservoir rock properties;
- fluid properties;
- reservoir flow geometry.

It should be pointed out that Equation 3.1.20 is based on the assumption that the gas flow obeys the pseudosteady-state or the steady-state flowing condition as required by Darcy's equation. This condition implies that the well has established a constant drainage radius r_e, and, therefore, the performance coefficient C should remain constant. On the other hand, during the unsteady-state (transient) flow condition, the well drainage radius is continuously changing.

Equation 3.1.20 is commonly called the deliverability or back-pressure equation. If the coefficients of the equation (i.e., n and C) can be determined, the gas flow rate Q_g at any bottom-hole flow pressure p_{wf} can be calculated and the inflow performance relationship (IPR) curve constructed.

taking the logarithm of both sides of Equation 3.1.20 gives:

$$\log(Q_g) = \log(C) + n\log\left(\bar{p}_r^2 - p_{wf}^2\right)$$ [3.1.21]

Equation 3.1.21 suggests that a plot of Q_g vs. $\left(\bar{p}_r^2 - p_{wf}^2\right)$ on a log–log scale should yield a straight line having a slope of n. In the natural gas industry, the plot is traditionally reversed by plotting $\left(\bar{p}_r^2 - p_{wf}^2\right)$ vs. Q_g on a logarithmic scale to produce a straight line with a slope of $1/n$. This plot as shown schematically in Figure 3.3 is commonly referred to as the deliverability graph or the back-pressure plot.

The deliverability exponent n can be determined from any two points on the *straight line*, i.e., $(Q_{g1}, \Delta p_1^2)$ and $(Q_{g2}, \Delta p_2^2)$, according to the flowing expression:

$$n = \frac{\log\left(Q_{g1}\right) - \log\left(Q_{g2}\right)}{\log\left(\Delta p_1^2\right) - \log\left(\Delta p_2^2\right)}$$ [3.1.22]

Given n, any point on the straight line can be used to compute the performance coefficient C from:

$$C = \frac{Q_g}{\left(\bar{p}_r^2 - p_{wf}^2\right)^n}$$ [3.1.23]

The coefficients of the back-pressure equation or any of the other empirical equations are traditionally determined from analyzing gas well testing data. Deliverability testing has
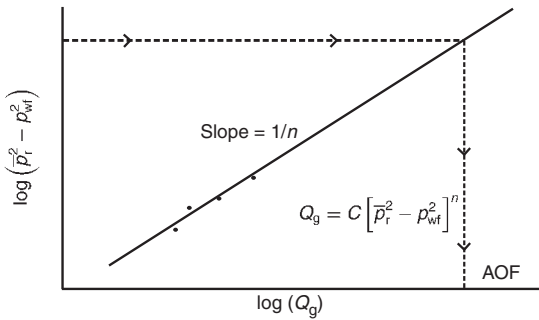
Figure 3.3   Well deliverability graph.
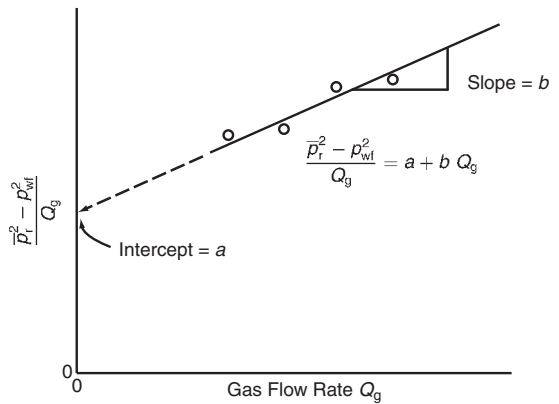
Figure 3.4   Graph of the pressure-squared data.

been used for more than 60 years by the petroleum industry to characterize and determine the flow potential of gas wells. There are essentially three types of deliverability tests:

(1) conventional deliverability (back-pressure) test;
(2) isochronal test;
(3) modified isochronal test.

These tests basically consist of flowing wells at multiple rates and measuring the bottom-hole flowing pressure as a function of time. When the recorded data is properly analyzed, it is possible to determine the flow potential and establish the inflow performance relationships of the gas well. The deliverability test is discussed later in this chapter for the purpose of introducing basic techniques used in analyzing the test data.

Laminar–inertial–turbulent (LIT) approach
Essentially, this approach is based on expressing the total pressure drop in terms of the pressure drop due to Darcy's (laminar) flow and the additional pressure drop due to the turbulent flow. That is:

$$(\Delta p)_{\text{Total}} = (\Delta p)_{\text{Laminar Flow}} + (\Delta p)_{\text{Turbulent Flow}}$$

The three forms of the semisteady-state equation as presented by Equations 3.1.15, 3.1.18, and 3.1.19, i.e., the pseudopressure, pressure-squared, and pressure approach, can be rearranged in quadratic forms for the purpose of separating the "laminar" and "inertial–turbulent" terms and composing these equations as follows

Pressure-squared quadratic form   Equation 3.1.15 can be written in a more simplified form as:

$$Q_g = \frac{kh\left(\bar{p}_r^2 - p_{\text{wf}}^2\right)}{1422T\left(\mu_g Z\right)_{\text{avg}}\left[\ln\left(r_e/r_w\right) - 0.75 + s + DQ_g\right]}$$

Rearranging this equation gives:

$$\bar{p}_r^2 - p_{\text{wf}}^2 = aQ_g + bQ_g^2 \qquad [3.1.24]$$

with:

$$a = \left(\frac{1422T\mu_g Z}{kh}\right)\left[\ln\left(\frac{r_e}{r_w}\right) - 0.75 + s\right] \qquad [3.1.25]$$

$$b = \left(\frac{1422T\mu_g Z}{kh}\right)D \qquad [3.1.26]$$

where:

a = laminar flow coefficient
b = inertial–turbulent flow coefficient
Q_g = gas flow rate, Mscf/day
Z = gas deviation factor
k = permeability, md
μ_g = gas viscosity, cp

Equation 3.1.24 indicates that the first term on the right-hand side of the equation (i.e., aQ_g) represents the pressure drop due to laminar (Darcy) flow while the second term represents aQ_g^2, the pressure drop due to the turbulent flow.

The term aQ_g in Equation 3.1.26 represents the pressure-squared drop due to laminar flow while the term bQ_g^2 accounts for the pressure-squared drop due to inertial–turbulent flow effects.

Equation 3.1.24 can be liberalized by dividing both sides of the equation by Q_g, to yield:

$$\frac{\bar{p}_r^2 - p_{\text{wf}}^2}{Q_g} = a + bQ_g \qquad [3.1.27]$$

The coefficients a and b can be determined by plotting $\left(\bar{p}_r^2 - p_{\text{wf}}^2/2\right)$ vs. Q_g on a Cartesian scale and should yield a straight line with a slope of b and intercept of a. As presented later in this chapter, data from deliverability tests can be used to construct the linear relationship as shown schematically in Figure 3.4.

Given the values of a and b, the quadratic flow equation, i.e., Equation 3.1.24, can be solved for Q_g at any p_{wf} from:

$$Q_g = \frac{-a + \sqrt{a^2 + 4b\left(\bar{p}_r^2 - p_{\text{wf}}^2\right)}}{2b} \qquad [3.1.28]$$

Furthermore, by assuming various values of p_{wf} and calculating the corresponding Q_g from Equation 3.1.28, the current IPR of the gas well at the current reservoir pressure $\bar{p}_r$ can be generated.

It should be pointed out that the following assumptions were made in developing Equation 3.1.24:

(1) single-phase flow;
(2) a homogeneous and isotropic reservoir;
(3) the permeability is independent of pressure;
(4) the product of the gas viscosity and compressibility factor, i.e., $(\mu_g Z)$, is constant.

This method is recommended for applications at pressures below 2000 psi.

Pressure quadratic form   The pressure approximation equation, i.e., Equation 3.1.18, can be rearranged and expressed in the following quadratic form:

$$Q_g = \frac{7.08\left(10^{-6}\right)kh\left(\bar{p}_r - p_{\text{wf}}\right)}{\left(\mu_g B_g\right)_{\text{avg}}T\left[\ln\left(r_e/r_w\right) - 0.75 + s + DQ_g\right]}$$
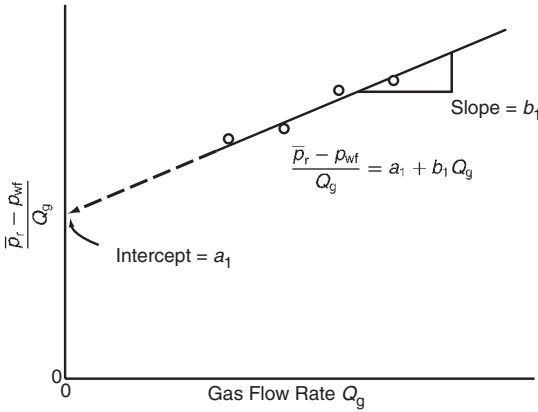
Figure 3.5 *Graph of the pressure method data.*

Figure 3.6 *Graph of real-gas pseudopressure data.*

Rearranging gives:

$$\bar{p}_r - p_{wf} = a_1 Q_g + b_1 Q_g^2 \qquad [3.1.29]$$

where:

$$a_1 = \frac{141.2\,(10^{-3})\,(\mu_g B_g)}{kh}\left[\ln\left(\frac{r_e}{r_w}\right) - 0.75 + s\right] \qquad [3.1.30]$$

$$b_1 = \left[\frac{141.2\,(10^{-3})\,(\mu_g B_g)}{kh}\right] D \qquad [3.1.31]$$

The term $a_1 Q_g$ represents the pressure drop due to laminar flow, while the term $b_1 Q_g^2$ accounts for the additional pressure drop due to the turbulent flow condition. In a linear form, Equation 3.17 can be expressed as:

$$\frac{\bar{p}_r - p_{wf}}{Q_g} = a_1 + b_1 Q_g \qquad [3.1.32]$$

The laminar flow coefficient a_1 and inertial–turbulent flow coefficient b_1 can be determined from the linear plot of the above equation as shown in Figure 3.5.

Once the coefficients a_1 and b_1 are determined the gas flow rate can be determined at any pressure from:

$$Q_g = \frac{-a_1 + \sqrt{a_1^2 + 4b_1\,(\bar{p}_r - p_{wf})}}{2b_1} \qquad [3.1.33]$$

The application of Equation 3.1.29 is also restricted by the assumptions listed for the pressure-squared approach. However, the pressure method is applicable at pressures higher than 3000 psi.

Pseudopressure quadratic approach   The pseudopressure equation has the form:

$$Q_g = \frac{kh\,(\bar{\psi}_r - \psi_{wf})}{1422T\,[\ln(r_e/r_w) - 0.75 + s + DQ_g]}$$

This expression can be written in a more simplified form as:

$$\bar{\psi}_r - \psi_{wf} = a_2 Q_g + b_2 Q_g^2 \qquad [3.1.34]$$

where:

$$a_2 = \left(\frac{1422}{kh}\right)\left[\ln\left(\frac{r_e}{r_w}\right) - 0.75 + s\right] \qquad [3.1.35]$$

$$b_2 = \left(\frac{1422}{kh}\right) D \qquad [3.1.36]$$

The term $a_2 Q_g$ in Equation 3.1.34 represents the pseudopressure drop due to laminar flow while the term $b_2 Q_g^2$ accounts for the pseudopressure drop due to inertial–turbulent flow effects.

Equation 3.1.34 can be liberalized by dividing both sides of the equation by Q_g, to yield:

$$\frac{\bar{\psi}_r - \psi_{wf}}{Q_g} = a_2 + b_2 Q_g \qquad [3.1.37]$$

The above expression suggests that a plot of $(\bar{\psi}_r - \psi_{wf}/Q_g)$ vs. Q_g on a Cartesian scale should yield a straight line with a slope of b_2 and intercept of a_2 as shown in Figure 3.6.

Given the values of a_2 and b_2, the gas flow rate at any p_{wf} is calculated from:

$$Q_g = \frac{-a_2 + \sqrt{a_2^2 + 4b_2\,(\bar{\psi}_r - \psi_{wf})}}{2b_2} \qquad [3.1.38]$$

It should be pointed out that the pseudopressure approach is more rigorous than either the pressure-squared or pressure method and is applicable to all ranges of pressure.

In the next subsection, the back-pressure test is introduced. However, the material is intended only to be an introduction. There are several excellent books by the following authors that address transient flow and well testing in great detail:

- Earlougher (1977);
- Matthews and Russell (1967);
- Lee (1982);
- Canadian Energy Resources Conservation Board (ERCB) (1975).

3.1.3 Back-pressure test

Rawlins and Schellhardt (1936) proposed a method for testing gas wells by gauging the ability of the well to flow against particular pipeline back-pressures greater than atmospheric pressure. This type of flow test is commonly referred to as the "conventional deliverability test." The required procedure for conducting this back-pressure test consists of the following steps:

Step 1. Shut in the gas well sufficiently long for the formation pressure to equalize at the volumetric average pressure $\bar{p}_r$.

Step 2. Place the well on production at a constant flow rate Q_{g1} for a sufficient time to allow the bottom-hole flowing pressure to stabilize at p_{wf1}, i.e., to reach the pseudosteady state.

Step 3. Repeat step 2 for several rates and record the stabilized bottom-hole flow pressure at each corresponding flow rate. If three or four rates are used, the test may be referred to as a three-point or four-point flow test.
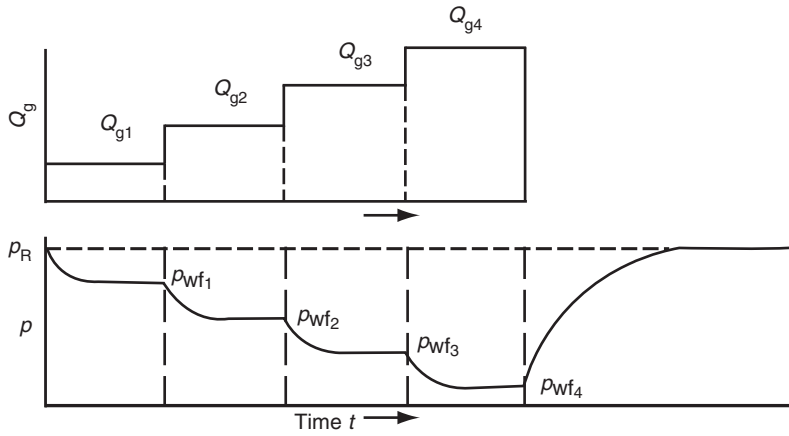
Figure 3.7 *Conventional back-pressure test.*

The rate and pressure history of a typical four-point test is shown in Figure 3.7. The figure illustrates a normal sequence of rate changes where the rate is increased during the test. Tests may also be run, however, using a reverse sequence. Experience indicates that a normal rate sequence gives better data in most wells. The most important factor to be considered in performing the conventional deliverability test is the length of the flow periods. It is required that each rate be maintained sufficiently long for the well to stabilize, i.e., to reach the pseudosteady state. The pseudosteady-state time is defined as the time when the rate of change of pressure with respect to time, i.e., dp/dt, is constant through the reservoir at a constant flow rate. This stabilization time for a well in the center of a circular or square drainage area may be estimated from:

$$t_{pss} = \frac{15.8\phi\mu_{gi}c_{ti}A}{k} \qquad [3.1.39]$$

with:

$$c_{ti} = S_w c_{wi} + (1 - S_w)c_{gi} + c_f$$

where:

t_{pss} = stabilization (pseudosteady-state) time, days
c_{ti} = total compressibility coefficient at initial pressure, psi^{-1}
c_{wi} = water compressibility coefficient at initial pressure, psi^{-1}
c_f = formation compressibility coefficient, psi^{-1}
c_{gi} = gas compressibility coefficient at initial pressure, psi^{-1}
ϕ = porosity, fraction
μ_g = gas viscosity, cp
k = effective gas permeability, md
A = drainage area, ft^2

In order to properly apply Equation 3.1.39, the fluid properties and system compressibility must be determined at the average reservoir pressure. However, evaluating these parameters at initial reservoir pressure has been found to provide a good first-order approximation of the time required to reach the pseudosteady-state condition and establish a constant drainage area. The recorded bottom-hole flowing pressure p_{wf} versus flow rate Q_g can be analyzed in several graphical forms to determine the coefficients of the selected flow gas flow equation. That is:

Back-pressure equation $\log(Q_g) = \log(C) + n\log(\bar{p}_r^2 - p_{wf}^2)$

Pressure-squared equation $\bar{p}_r^2 - p_{wf}^2 = aQ_g + bQ_g^2$

Pressure equation $\dfrac{\bar{p}_r - p_{wf}}{Q_g} = a_1 + b_1 Q_g$

Pseudopressure equation $\overline{\psi}_r - \psi_{wf} = a_2 Q_g + b_2 Q_g^2$

The application of the back-pressure test data to determine the coefficients of any of the empirical flow equations is illustrated in the following example.

Example 3.2 A gas well was tested using a three-point conventional deliverability test with an initial average reservoir pressure of 1952 psi. The recorded data during the test is given below:

p_{wf} (psia)	$m(p_{wf}) = \psi_{wf}$ (psi^2/cp)	Q_g (Mscf/day)
1952	316×10^6	0
1700	245×10^6	2624.6
1500	191×10^6	4154.7
1300	141×10^6	5425.1

Figure 3.8 shows the gas pseudopressure ψ as a function of pressure. Generate the current IPR by using the following methods.

(a) simplified back-pressure equation;
(b) laminar–inertial–turbulent (LIT) methods:
  (i)   pressure-squared approach, Equation 3.1.29
  (ii) pressure approach, Equation 3.1.33
  (iii) pseudopressure approach, Equation 3.1.26;
(c) compare results of the calculation.

Solution

(a) Back-pressure equation:

Step 1. Prepare the following table:

p_{wf}	p_{wf}^2 ($psi^2 \times 10^3$)	$(\bar{p}_r^2 - p_{wf}^2)$ ($psi^2 \times 10^3$)	Q_g (Mscf/day)
$\overline{p}_r = 1952$	3810	0	0
1700	2890	920	2624.6
1500	2250	1560	4154.7
1300	1690	2120	5425.1
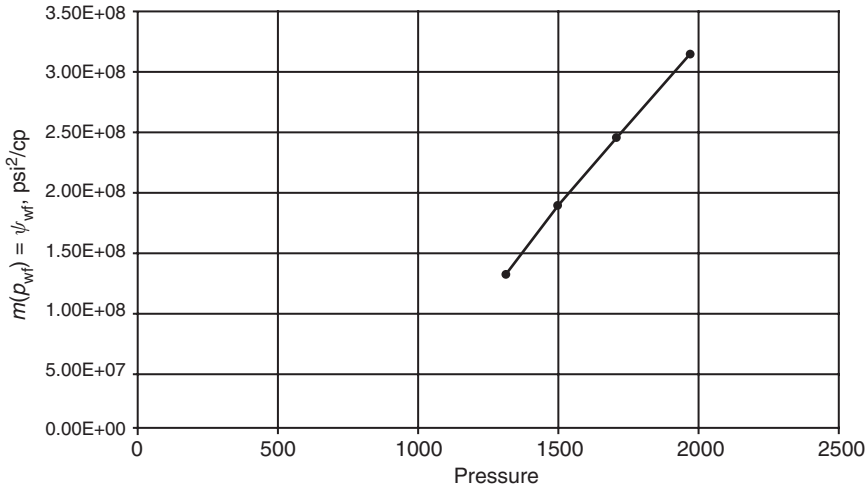
Figure 3.8 *Real-gas potential versus pressure.*
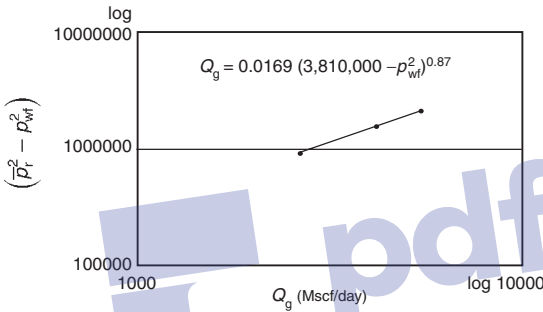
Figure 3.9 *Back-pressure curve.*

Step 2. Plot $(\bar{p}_r^2 - p_{wf}^2)$ vs. Q_g on a log–log scale as shown in Figure 3.9. Draw the best straight line through the points.

Step 3. Using any two points on the straight line, calculate the exponent n from Equation 3.1.22, as:

$$n = \frac{\log(Q_{g1}) - \log(Q_{g2})}{\log(\Delta p_1^2) - \log(\Delta p_2^2)}$$

$$= \frac{\log(4000) - \log(1800)}{\log(1500) - \log(600)} = 0.87$$

Step 4. Determine the performance coefficient C from Equation 3.1.23 by using the coordinate of any point on the straight line, or:

$$C = \frac{Q_g}{\left(\bar{p}_r^2 - p_{wf}^2\right)^n}$$

$$= \frac{1800}{(600\,000)^{0.87}} = 0.0169 \text{ Mscf/psi}^2$$

Step 5. The back-pressure equation is then expressed as:

$$Q_g = 0.0169(3\,810\,000 - p_{wf}^2)^{0.87}$$

Step 6. Generate the IPR data by assuming various values of p_{wf} and calculate the corresponding Q_g:

p_{wf}	Q_g (Mscf/day)
1952	0
1800	1720
1600	3406
1000	6891
500	8465
0	8980

where the absolute open flow potential AOF $= (Q_g)_{max} = 8980$ Mscf/day.

(b) LIT method:

(i) Pressure-squared method:

Step 1. Construct the following table:

p_{wf}	$(\bar{p}_r^2 - p_{wf}^2)$ (psi$^2 \times 10^3$)	Q_g (Mscf/day)	$(\bar{p}_r^2 - p_{wf}^2)/Q_g$
$\bar{p}_r = 1952$	0	0	–
1700	920	2624.6	351
1500	1560	4154.7	375
1300	2120	5425.1	391

Step 2. Plot $(\bar{p}_r^2 - p_{wf}^2)/Q_g$ vs. Q_g on a Cartesian scale and draw the best straight line as shown in Figure 3.10.

Step 3. Determine the intercept and the slope of the straight line, to give:

$$\text{intercept } a = 318$$

$$\text{slope } b = 0.01333$$

Step 4. The quadratic form of the pressure-squared approach is given by Equation 3.1.24 as:

$$\bar{p}_r^2 - p_{wf}^2 = aQ_g + bQ_g^2$$

$$(3\,810\,000 - p_{wf}^2) = 318Q_g + 0.01333Q_g^2$$
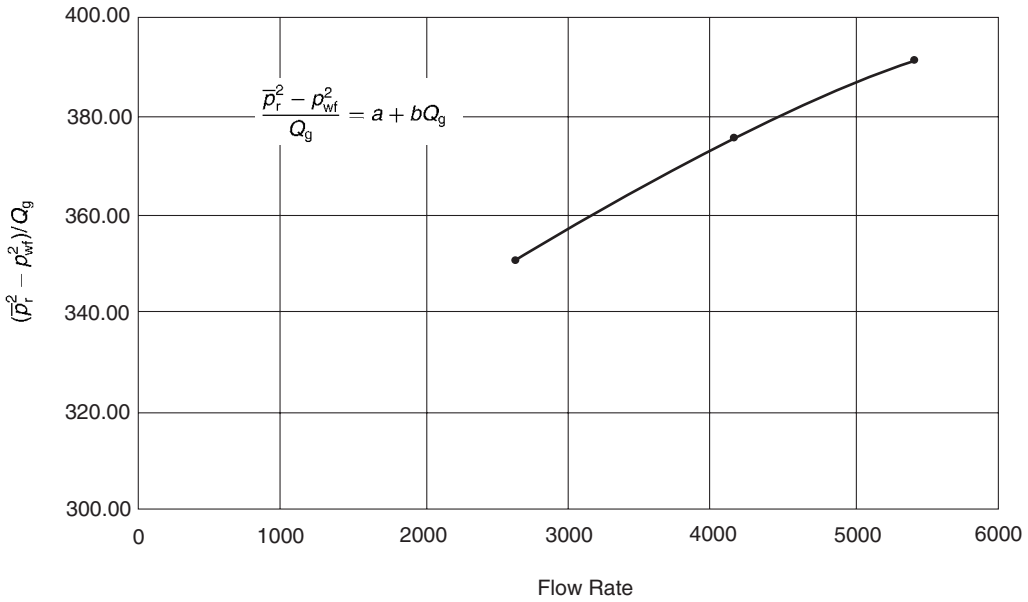
Figure 3.10 *Pressure-squared method.*

Step 5. Construct the IPR data by assuming various values of p_{wf} and solving for Q_g by using Equation 3.1.28:

p_{wf}	$(\bar{p}_r^2 - p_{wf}^2)$ psi$^2 \times 10^3$	Q_g (Mscf/day)
1952	0	0
1800	570	1675
1600	1250	3436
1000	2810	6862
500	3560	8304
0	3810	8763 = AOF = $(Q_g)_{max}$

(ii) Pressure method:

Step 1. Construct the following table:

p_{wf}	$(\bar{p}_r - p_{wf})$	Q_g (Mscf/day)	$(\bar{p}_r - p_{wf})/Q_g$
$\bar{p}_r = 1952$	0	0	–
1700	252	262.6	0.090
1500	452	4154.7	0.109
1300	652	5425.1	0.120

Step 2. Plot $(\bar{p}_r - p_{wf})/Q_g$ vs. Q_g on a cartesan scale as shown in Figure 3.11. Draw the best straight line and determine the intercept and slope as:

$$\text{intercept } a_1 = 0.06$$

$$\text{slope } b_1 = 1.111 \times 10^{-5}$$

Step 3. The quadratic form of the pressure method is then given by:

$$\bar{p}_r - p_{wf} = a_1 Q_g + b_1 Q_g^2$$

or:

$$(1952 - p_{wf}) = 0.06 Q_g + (1.111 \times 10^{-5}) Q_g^2$$

Step 4. Generate the IPR data by applying Equation 3.1.33:

p_{wf}	$(\bar{p}_r - p_{wf})$	Q_g (Mscf/day)
1952	0	0
1800	152	1879
1600	352	3543
1000	952	6942
500	1452	9046
0	1952	10 827

(iii) Pseudopressure approach:

Step 1. Construct the following table:

p_{wf}	ψ (psi^2/cp)	$(\bar{\psi}_r - \psi_{wf})$	Q_g (Mscf/day)	$(\bar{\psi}_r - \psi_{wf})/Q_g$
$\bar{p}_r = 1952$	316×10^6	0	0	–
1700	245×10^6	71×10^6	262.6	27.05×10^3
1500	191×10^6	125×10^6	4154.7	30.09×10^3
1300	141×10^6	175×10^6	5425.1	32.26×10^3

Step 2. Plot $(\bar{\psi}_r - \psi_{wf})/Q_g$ on a Cartesian scale as shown in Figure 3.12 and determine the intercept a_2 and slope b_2 as:

$$a_2 = 22.28 \times 10^3$$

$$b_2 = 1.727$$

Step 3. The quadratic form of the gas pseudopressure method is given by Equation 3.1.34:

$$\bar{\psi}_r - \psi_{wf} = a_2 Q_g + b_2 Q_g^2$$

$$(316 \times 10^6 - \psi_{wf}) = 22.28 \times 10^3 Q_g + 1.727 Q_g^2$$
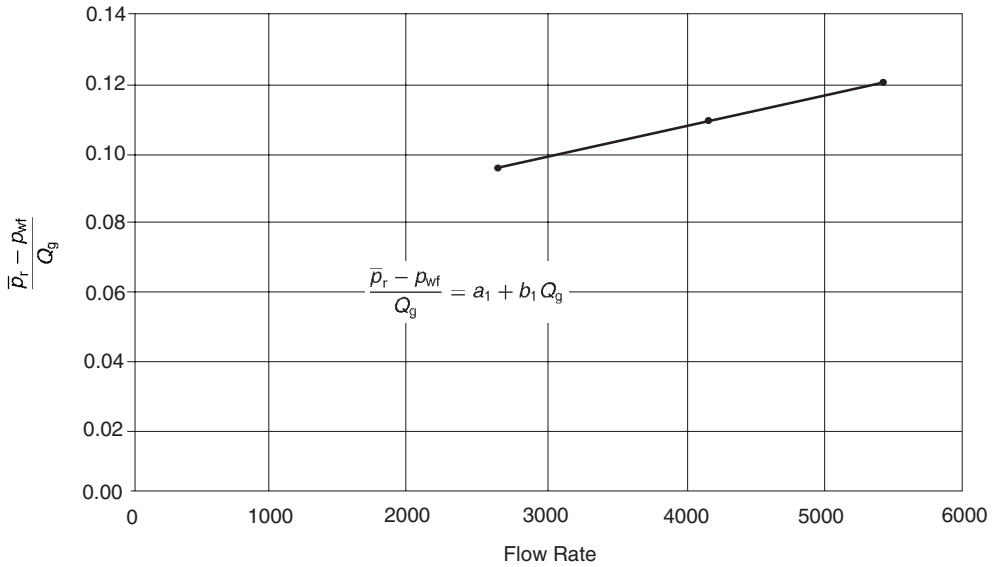
Figure 3.11 *Pressure approximation method.*

$$\frac{\overline{p}_r - p_{wf}}{Q_g} = a_1 + b_1 Q_g$$
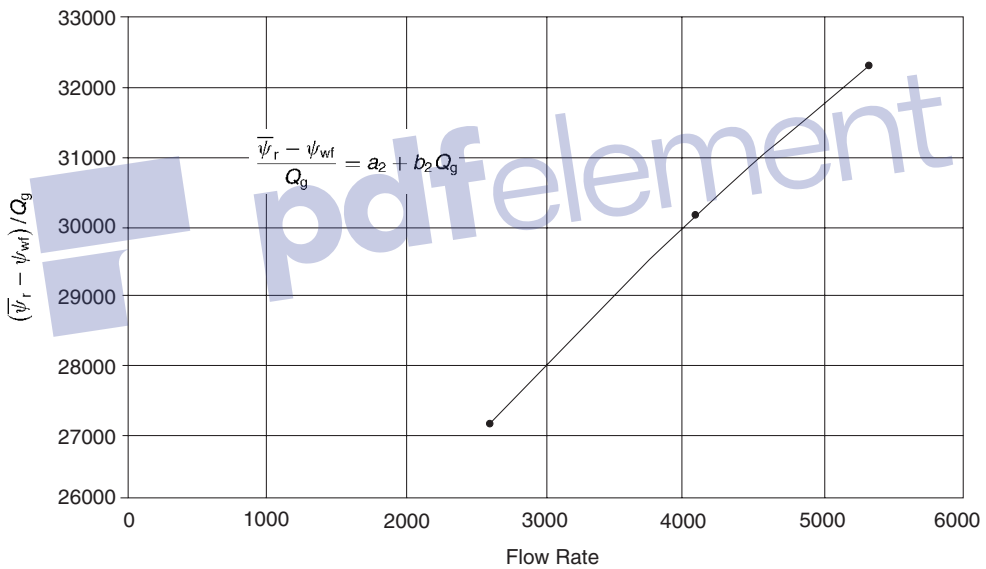
Figure 3.12 *Pseudopressure method.*

$$\frac{\overline{\psi}_r - \psi_{wf}}{Q_g} = a_2 + b_2 Q_g$$

Step 4. Generate the IPR data by assuming various values of p_{wf}, i.e., ψ_{wf}, and calculating the corresponding Q_g from Equation 3.1.38:

p_{wf}	$m(p)$ or ψ	$\overline{\psi}_r - \psi_{wf}$	Q_g (Mscf/day)
1952	316×10^6	0	0
1800	270×10^6	46×10^6	1794
1600	215×10^6	101×10^6	3503
1000	100×10^6	216×10^6	6331
500	40×10^6	276×10^6	7574
0	0	316×10^6	$8342 = \text{AOF} (Q_g)_{\max}$

(c) Compare the gas flow rates as calculated by the four different methods. Results of the IPR calculation are documented below:

	Gas flow rate (Mscf/day)			
Pressure	*Back-pressure*	p^2 *approach*	p *approach*	ψ *approach*
1952	0	0	0	0
1800	1720	1675	1879	1811
1600	3406	3436	3543	3554
1000	6891	6862	6942	6460
500	8465	8304	9046	7742
0	8980	8763	10 827	8536
	6.0%	5.4%	11%	–
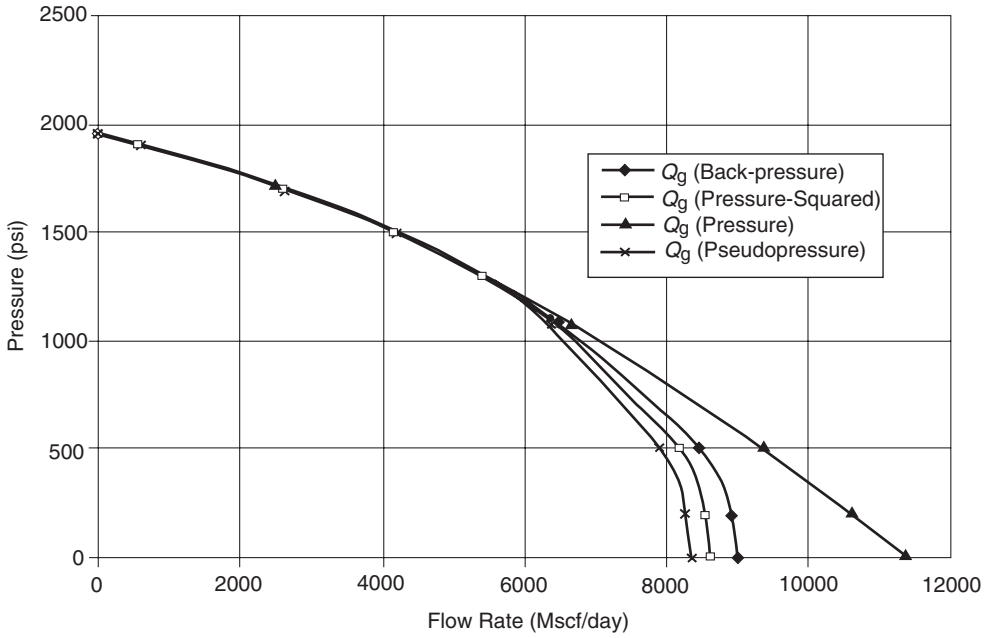
Figure 3.13 *IPR for all methods.*

Since the pseudopressure analysis is considered more accurate and rigorous than the other three methods, the accuracy of each of the methods in predicting the IPR data is compared with that of the ψ approach. Figure 3.13 compares graphically the performance of each method with that of the ψ approach. Results indicate that the pressure-squared equation generated the IPR data with an absolute average error of 5.4% as compared with 6% and 11% for the back-pressure equation and the pressure approximation method, respectively.

It should be noted that the pressure approximation method is limited to applications for pressures greater than 3000 psi.

3.1.4 Future inflow performance relationships

Once a well has been tested and the appropriate deliverability or inflow performance equation established it is essential to predict the IPR data as a function of average reservoir pressure. The gas viscosity μ_g and gas compressibility factor Z are considered the parameters that are subject to the greatest change as reservoir pressure $\bar{p}_r$ changes.

Assume that the current average reservoir pressure is $\bar{p}_{r1}$, with gas viscosity of μ_{g1} and compressibility factor of Z_1. At a selected future average reservoir pressure $\bar{p}_{r2}$, μ_{g2} and Z_2 represent the corresponding gas properties. To approximate the effect of reservoir pressure changes, i.e., from $\bar{p}_{r1}$ to $\bar{p}_{r2}$, on the coefficients of the deliverability equation, the following methodology is recommended.

Back-pressure equation
Recall the back-pressure equation:

$$Q_g = C[\bar{p}_r^2 - p_{wf}^2]^n$$

where the coefficient C describes the gas and reservoir properties by:

$$C = \frac{kh}{1422T \left(\mu_g Z\right)_{avg} \left[\ln\left(r_e/r_w\right) - 0.75 + s\right]}$$

The performance coefficient C is considered a pressure-dependent parameter and should be adjusted with each change of the reservoir pressure. Assuming that the reservoir pressure has declined from p_{r1} to p_{r2}, the performance coefficient at p_1 can be adjusted to reflect the pressure drop by applying the following simple approximation:

$$C_2 = C_1 \left[\frac{\mu_{g1} Z_1}{\mu_{g2} Z_2}\right] \tag{3.1.40}$$

The value of n is considered essentially constant. Subscripts 1 and 2 refer to the properties at p_{r1} and p_{r2}.

LIT methods
The laminar flow coefficients a and the inertial–turbulent flow coefficient b of any of the previous LIT methods, i.e., Equations 3.1.24, 3.1.29, and 3.1.34, are modified according to the following simple relationships:

Pressure-squared method   The pressure-squared equation is written as:

$$\bar{p}_r^2 - p_{wf}^2 = aQ_g + bQ_g^2$$

The coefficients of the above expression are given by:

$$a = \left(\frac{1422T\mu_g Z}{kh}\right)\left[\ln\left(\frac{r_e}{r_w}\right) - 0.75 + s\right]$$

$$b = \left(\frac{1422T\mu_g Z}{kh}\right) D$$

Obviously the coefficients a and b are pressure dependent and should be modified to account for the change of the reservoir pressure from $\bar{p}_{r1}$ to $\bar{p}_{r2}$. The proposed relationships for adjusting the coefficients are as follows:

$$a_2 = a_1 \left[\frac{\mu_{g2} Z_2}{\mu_{g1} Z_1}\right] \tag{3.1.41}$$

$$b_2 = b_1 \left[\frac{\mu_{g2} Z_2}{\mu_{g1} Z_1}\right] \tag{3.1.42}$$

where the subscripts 1 and 2 represent conditions at reservoir pressures $\bar{p}_{r1}$ to $\bar{p}_{r2}$, respectively.

Pressure approximation method   The pressure approximation equation for calculating the gas rate is given by:

$$\bar{p}_r - p_{wf} = a_1 Q_g + b_1 Q_g^2$$

with:

$$a_1 = \frac{141.2\left(10^{-3}\right)\left(\mu_g B_g\right)}{kh}\left[\ln\left(\frac{r_e}{r_w}\right) - 0.75 + s\right]$$

$$b_1 = \left[\frac{141.2\left(10^{-3}\right)\left(\mu_g B_g\right)}{kh}\right]D$$

The recommended methodology for adjusting the coefficients a and b is based on applying the following simple two expressions:

$$a_2 = a_1\left[\frac{\mu_{g2}B_{g2}}{\mu_{g1}B_{g1}}\right] \qquad [3.1.43]$$

$$b_2 = b_1\left[\frac{\mu_{g2}B_{g2}}{\mu_{g1}B_{g1}}\right] \qquad [3.1.44]$$

where B_g is the gas formation volume factor in bbl/scf.

Pseudopressure approach   Recall the pseudopressure equation:

$$\bar{\psi}_r - \psi_{wf} = a_2 Q_g + b_2 Q_g^2$$

The coefficients are described by:

$$a_2 = \left(\frac{1422}{kh}\right)\left[\ln\left(\frac{r_e}{r_w}\right) - 0.75 + s\right]$$

$$b_2 = \left(\frac{1422}{kh}\right)D$$

Note that the coefficients a and b of the pseudopressure approach are essentially independent of the reservoir pressure and can be treated as constants.

Example 3.3   In addition to the data given in Example 3.2, the following information is available.

- $(\mu_g Z) = 0.01206$ at 1952 psi;
- $(\mu_g Z) = 0.01180$ at 1700 psi.

Using the following methods:

(a) backpressure equation,
(b) pressure-squared equation, and
(c) pseudopressure equation

generate the IPR data for the well when the reservoir pressure drops from 1952 to 1700 psi.

Solution

Step 1. Adjust the coefficients a and b of each equation.

- For the back-pressure equation: Adjust C by using Equation 3.1.40:

$$C_2 = C_1\left[\frac{\mu_{g1}Z_1}{\mu_{g2}Z_2}\right]$$

$$C = 0.0169\left(\frac{0.01206}{0.01180}\right) = 0.01727$$

and therefore the future gas flow rate is expressed by:

$$Q_g = 0.01727\left(1700^2 - p_{wf}^2\right)^{0.87}$$

- Pressure-squared method: Adjust a and b by applying Equations 3.1.41 and 3.1.42:

$$a_2 = a_1\left[\frac{\mu_{g2}B_{g2}}{\mu_{g1}B_{g1}}\right]$$

$$a = 318\left(\frac{0.01180}{0.01206}\right) = 311.14$$

$$b_2 = b_1\left[\frac{\mu_{g2}B_{g2}}{\mu_{g1}B_{g1}}\right]$$

$$b = 0.01333\left(\frac{0.01180}{0.01206}\right) = 0.01304$$

$$\left(1700^2 - p_{wf}^2\right) = 311.14Q_g + 0.01304Q_g^2$$

- Pseudopressure method: No adjustments are needed because the coefficients are independent of the pressure:

$$\left(245 \times 10^6 - \psi_{wf}\right) = 22.28 \times 10^3 Q_g + 1.727 Q_g^2$$

Step 2. Generate the IPR data:

Gas flow rate Q_g (Mscf/day)

p_{wf}	Back-pressure	p^2 method	ψ method
$\bar{p}_r = 1700$	0	0	0
1600	1092	1017	1229
1000	4987	5019	4755
500	6669	6638	6211
0	7216	7147	7095

Figure 3.14 compares graphically the IPR data as predicted by the above three methods.

It should be pointed out that all the various well tests and inflow performance relationships previously discussed are intended to evaluate the formation capacity to deliver gas to the wellbore for a specified average reservoir pressure $\bar{p}_r$ and a bottom-hole flowing pressure p_{wf}. The volume of gas which can actually be delivered to the surface will also depend on the surface tubing head pressure p_t and the pressure drop from the wellbore to the surface due to the weight of the gas column and friction loss through the tubing. Cullender and Smith (1956) described the pressure loss by the following expression:

$$p_{wf}^2 = e^S p_t^2 + \frac{L}{H}\left(F_r Q_g \overline{T}\,\overline{Z}\right)^2\left(e^S - 1\right)$$

with:

$$S = \frac{0.0375\gamma_g H}{\overline{T}\,\overline{Z}}$$

$$F_r = \frac{0.004362}{d^{0.224}} \qquad \text{when } d \leq 4.277 \text{ inches}$$

$$F_r = \frac{0.004007}{d^{0.164}} \qquad \text{when } d > 4.277 \text{ inches}$$

where:

p_{wf} = bottom-hole flowing pressure, psi
p_t = tubing head (wellhead) pressure, psi
Q_g = gas flow rate, Mscf/day
L = actual tubing flow length, ft
H = vertical depth of the well to midpoint of perforation, ft
$\overline{T}$ = arithmetic average temperature, i.e., $(T_t + T_b)/2$, °R
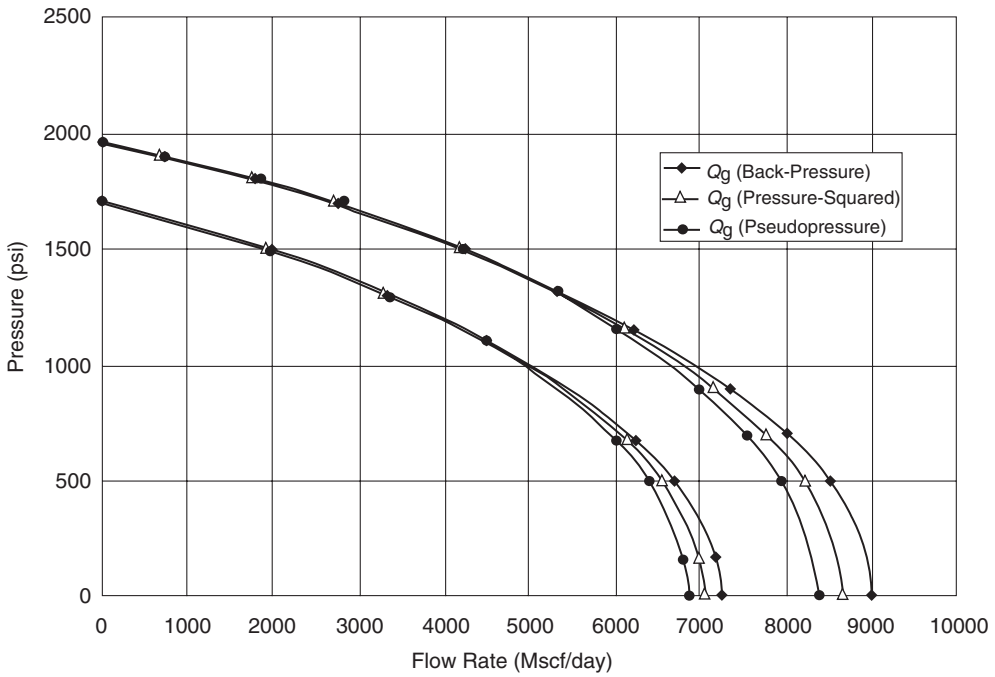
Figure 3.14   IPR comparison.

T_t = tubing head temperature, °R
T_b = wellbore temperature, °R
$\overline{Z}$ = gas deviation factor at arithmetic average pressure, i.e., $(p_t + p_{wf})/2$
F_r = friction factor for tubing ID
d = inside tubing diameter, inches
γ_g = specific gravity of the gas

The Cullender and Smith equation can be combined with the back-pressure equation by the gas flow rate Q_g to give:

$$\frac{p_{wf}^2 - e^S p_t^2}{\frac{L}{H}(F_r \overline{T}\,\overline{Z})^2 (e^S - 1)} = C(p_r^2 - p_{wf}^2)^{2n}$$

This equation must be satisfied iteratively be solving for the p_{wf} which satisfy the equality. The correct value of p_{wf} can then be used to establish the gas deliverability of the well.

3.2 Horizontal Gas Well Performance

Many low-permeability gas reservoirs are historically considered to be non-commercial due to low production rates. Most vertical wells drilled in tight gas reservoirs are stimulated using hydraulic fracturing and/or acidizing treatments to attain economical flow rates. In addition, to deplete a tight gas reservoir, vertical wells must be drilled at close spacing to efficiently drain the reservoir. This would require a large number of vertical wells. In such reservoirs, horizontal wells provide an attractive alternative to effectively deplete tight gas reservoirs and attain high flow rates. Joshi (1991) pointed out that horizontal wells are applicable in both low-permeability reservoirs as well as in high-permeability reservoirs. The excellent reference textbook by Joshi (1991) gives a comprehensive treatment of horizontal well performance in oil and gas reservoirs.

In calculating the gas flow rate from a horizontal well, Joshi (1991) introduced the concept of the effective wellbore radius $r_w^\backslash$ into the gas flow equation. The effective wellbore radius is given by:

$$r_w^\backslash = \frac{r_{eh}(L/2)}{a\left[1 + \sqrt{1 - (L/2a)^2}\,\right]\left[h/(2r_w)\right]^{h/L}} \quad [3.2.1]$$

with:

$$a = \left(\frac{L}{2}\right)\left[0.5 + \sqrt{0.25 + (2r_{eh}/L)^4}\,\right]^{0.5} \quad [3.2.2]$$

and:

$$r_{eh} = \sqrt{\frac{43\,560A}{\pi}} \quad [3.2.3]$$

where:

L = length of the horizontal well, ft
h = thickness, ft
r_w = wellbore radius, ft
r_{eh} = horizontal well drainage radius, ft
a = half the major axis of the drainage ellipse, ft
A = drainage area of the horizontal well, acres

For a pseudosteady-state flow, Joshi (1991) expressed Darcy's equation of a laminar flow in the following two familiar forms:

(1) Pressure-squared form:

$$Q_g = \frac{kh\left(\bar{p}_r^2 - p_{wf}^2\right)}{1422T\left(\mu_g Z\right)_{avg}\left[\ln\left(r_{eh}/r_w^\backslash\right) - 0.75 + s\right]} \quad [3.2.4]$$

where:

Q_g = gas flow rate, Mscf/day
s = skin factor
k = permeability, md
T = temperature, °R

(2) Pseudo-pressure form:

$$Q_g = \frac{kh \left(\overline{\psi}_r - \psi_{wf} \right)}{1422T \left[\ln \left(r_{eh}/r_w^\backslash \right) - 0.75 + s \right]} \qquad [3.2.5]$$

Example 3.4 A horizontal gas well 2000 foot long is draining an area of approximately 120 acres. The following data is available.

$$\overline{p}_r = 2000 \text{ psi}, \quad \overline{\psi}_r = 340 \times 10^6 \text{ psi}^2/\text{cp}$$

$$p_{wf} = 1200 \text{ psi}, \quad \psi_{wf} = 128 \times 10^6 \text{ psi}^2/\text{cp}$$

$$(\mu_g Z)_{avg} = 0.011826, \quad r_w = 0.3 \text{ ft}, \quad s = 0.5$$

$$h = 20 \text{ ft}, \quad T = 180°\text{F}, \quad k = 1.5 \text{ md}$$

Assuming a pseudosteady-state flow, calculate the gas flow rate by using the pressure-squared and pseudopressure methods.

Solution

Step 1. Calculate the drainage radius of the horizontal well:

$$r_{eh} = \sqrt{\frac{(43\,560)(120)}{\pi}} = 1290 \text{ ft}$$

Step 2. Calculate half the major axis of the drainage ellipse by using Equation 3.2.2:

$$a = \left[\frac{2000}{2} \right] \left[0.5 + \sqrt{0.25 + \left[\frac{(2)(1290)}{2000} \right]^4} \right]^{0.5} = 1495.8$$

Step 3. Calculate the effective wellbore radius $r_w^\backslash$ from Equation 3.2.1:

$$(h/2r_w)^{h/L} = \left[\frac{20}{(2)(0.3)} \right]^{20/2000} = 1.0357$$

$$1 + \sqrt{1 - \left(\frac{L}{2a} \right)^2} = 1 + \sqrt{1 - \left(\frac{2000}{2(1495.8)} \right)^2} = 1.7437$$

Applying Equation 3.2.1 gives:

$$r_w^\backslash = \frac{1290 \, (2000/2)}{1495.8 \, (1.7437) \, (1.0357)} = 477.54 \text{ ft}$$

Step 4. Calculate the flow rate by using the pressure-squared approximation approach by using Equation 3.2.4:

$$Q_g = \frac{(1.5)(20)(2000^2 - 1200^2)}{(1422)(640)(0.011826) \left[\ln \left(\frac{1290}{477.54} \right) - 0.75 + 0.5 \right]}$$

$$= 9594 \text{ Mscf/day}$$

Step 5. Calculate the flow rate by using the ψ approach as described by Equation 3.2.5:

$$Q_g = \frac{(1.5)(20)(340 - 128)(10^6)}{(1422)(640) \left[\ln \left(\frac{1290}{477.54} \right) - 0.75 + 0.5 \right]}$$

$$= 9396 \text{ Mscf/day}$$

For turbulent flow, Darcy's equation must be modified to account for the additional pressure caused by the non-Darcy flow by including the rate-dependent skin factor DQ_g. In practice, the back-pressure equation and the LIT approach are used to calculate the flow rate and construct the IPR curve for

the horizontal well. Multirate tests, i.e., deliverability tests, must be performed on the horizontal well to determine the coefficients of the selected flow equation.

3.3 Material Balance Equation for Conventional and Unconventional Gas Reservoirs

Reservoirs that initially contain free gas as the only hydrocarbon system are termed gas reservoirs. Such a reservoir contains a mixture of hydrocarbon components that exists wholly in the gaseous state. The mixture may be a "dry," "wet," or "condensate" gas, depending on the composition of the gas and the pressure and temperature at which the accumulation exists.

Gas reservoirs may have water influx from a contiguous water-bearing portion of the formation or may be volumetric (i.e., have no water influx).

Most gas engineering calculations involve the use of gas formation volume factor B_g and gas expansion factor E_g. The equations for both these factors are summarized below for convenience.

- Gas formation volume factor B_g is defined as the volume occupied by n moles of gas at certain pressure p and temperature T to that occupied at standard conditions. Applying the real-gas equation of state to both conditions gives:

$$B_g = \frac{p_{sc}}{T_{sc}} \frac{ZT}{p} = 0.02827 \frac{ZT}{p} \text{ ft}^3/\text{scf} \qquad [3.3.1]$$

Expressing B_g in bb/scf gives:

$$B_g = \frac{p_{sc}}{5.616 T_{sc}} \frac{ZT}{p} = 0.00504 \frac{ZT}{p} \text{ bbl/scf}$$

- The gas expansion factor is simply the reciprocal of B_g, or:

$$E_g = \frac{1}{B_g} = \frac{T_{sc}}{p_{sc}} \frac{p}{ZT} = 35.37 \frac{p}{ZT} \text{ scf/ft}^3 \qquad [3.3.2]$$

Expressing E_g in scf/bbl gives

$$E_g = \frac{5.615 T_{sc}}{p_{sc}} \frac{p}{ZT} = 198.6 \frac{p}{ZT} \text{ scf/bbl}$$

One of the primary concerns when conducting a reservoir study on a gas field is the determination of the initial gas-in-place G. There are commonly two approaches that are extensively used in natural gas engineering:

(1) the volumetric method;
(2) the material balance approach.

3.3.1 The volumetric method

Data used to estimate the gas-bearing reservoir pore volume (PV) include, but are not limited to, well logs, core analyses, bottom-hole pressure (BHP) and fluid sample information, and well tests. This data typically is used to develop various subsurface maps. Of these, structural and stratigraphic cross-sectional maps help to establish the reservoir's areal extent and to identify reservoir discontinuities such as pinch-outs, faults, or gas–water contacts. Subsurface contour maps, usually drawn relative to a known or marker formation, are constructed with lines connecting points of equal elevation and therefore portray the geologic structure. Subsurface isopachous maps are constructed with lines of equal net gas-bearing formation thickness. With these maps, the reservoir PV can then be estimated by planimetering the areas between the isopachous lines and using an approximate volume calculation technique, such as pyramidal or trapezoidal methods.

The volumetric equation is useful in reserve work for estimating gas-in-place at any stage of depletion. During the

development period before reservoir limits have been accurately defined, it is convenient to calculate gas-in-place per acre-foot of bulk reservoir rock. Multiplication of this unit figure by the best available estimate of bulk reservoir volume then gives gas-in-place for the lease, tract, or reservoir under consideration. Later in the life of the reservoir, when the reservoir volume is defined and performance data is available, volumetric calculations provide valuable checks on gas-in-place estimates obtained from material balance methods.

The equation for calculating gas-in-place is:

$$G = \frac{43\,560 Ah\phi\,(1 - S_{wi})}{B_{gi}} \qquad [3.3.3]$$

with:

$$B_{gi} = 0.02827 \frac{Z_i T}{p_i} \text{ ft}^3/\text{scf}$$

where:

G = gas-in-place, scf
A = area of reservoir, acres
h = average reservoir thickness, ft
ϕ = porosity
S_{wi} = water saturation
B_{gi} = gas formation volume factor at initial pressure p_i, ft^3/scf.

This equation can be applied at the initial pressure p_i and at a depletion pressure p in order to calculate the cumulative gas production G_p:

Gas produced = initial gas in place − remaining gas

$$G_p = \frac{43\,560 Ah\phi\,(1 - S_{wi})}{B_{gi}} - \frac{43\,560 Ah\phi\,(1 - S_{wi})}{B_g}$$

or

$$G_p = 43\,560 Ah\phi\,(1 - S_{wi}) \left(\frac{1}{B_{gi}} - \frac{1}{B_g} \right)$$

Rearranging gives:

$$\frac{1}{B_g} = \frac{1}{B_{gi}} - \left[\frac{1}{43\,560 Ah\phi\,(1 - S_{wi})} \right] G_p$$

From the definition of the gas expansion factor E_g, i.e., $E_g = 1/B_g$, the above form of the material balance equation can be expressed as:

$$E_g = E_{gi} - \left[\frac{1}{43\,560 Ah\phi\,(1 - S_{wi})} \right] G_p$$

or:

$$E_g = E_{gi} - \left[\frac{1}{(pv)\,(1 - S_{wi})} \right] G_p$$

This relationship indicates that a plot of E_g vs. G_p will produce a straight line with an intercept on the x axis with a value of E_{gi} and on the y axis with a value that represents the initial gas-in-place. Note that when $p = 0$, the gas expansion factor is also zero, $E_g = 0$, and that will reduce the above equation to:

$$G_p = \text{(pore volume)}\,(1 - S_{wi})E_{gi} = G$$

The same approach can be applied at both initial and *abandonment conditions* in order to calculate the recoverable gas.

Applying Equation 3.3.3 to the above expression gives:

$$G_p = \frac{43\,560 Ah\phi\,(1 - S_{wi})}{B_{gi}} - \frac{43\,560 Ah\phi\,(1 - S_{wi})}{B_{ga}}$$

or:

$$G_p = 43\,560 Ah\phi\,(1 - S_{wi}) \left(\frac{1}{B_{gi}} - \frac{1}{B_{ga}} \right) \qquad [3.3.4]$$

where B_{ga} is evaluated at abandonment pressure. Application of the volumetric method assumes that the pore volume occupied by gas is constant. If water influx is occurring, A, h, and S_w will change.

Example 3.5 A gas reservoir has the following characteristics:

$A = 3000$ acres, $h = 30$ ft, $\phi = 0.15$, $S_{wi} = 20\%$

$T = 150°\text{F}$, $p_i = 2600$ psi, $Z_i = 0.82$

p	Z
2600	0.82
1000	0.88
400	0.92

Calculate the cumulative gas production and recovery factor at 1000 and 400 psi.

Solution

Step 1. Calculate the reservoir PV:

$$\text{PV} = 43\,560 Ah\phi$$

$$= 43\,560 (3000)(30)(0.15) = 588.06 \text{ MMft}^3$$

Step 2. Calculate B_g at every given pressure by using Equation 3.3.1:

$$B_g = 0.02827 \frac{ZT}{p} \text{ ft}^3/\text{scf}$$

p	Z	B_g (ft^3/scf)
2600	0.82	0.0054
1000	0.88	0.0152
400	0.92	0.0397

Step 3. Calculate initial gas-in-place at 2600 psi:

$$G = \frac{43\,560 Ah\phi\,(1 - S_{wi})}{B_{gi}} = \frac{(\text{PV})\,(1 - S_{wi})}{B_{gi}}$$

$$= 588.06(10^6)(1 - 0.2)/0.0054 = 87.12 \text{ MMMscf}$$

Step 4. Since the reservoir is assumed volumetric, calculate the remaining gas at 1000 and 400 psi.
Remaining gas at 1000 psi:

$$G_{1000\,\text{psi}} = \frac{(\text{PV})\,(1 - S_{wi})}{(B_g)_{1000\,\text{psi}}}$$

$$= 588.06(10^6)^n(1 - 0.2)/0.0152$$

$$= 30.95 \text{ MMMscf}$$

Remaining gas at 400 psi:

$$G_{400\,\text{psi}} = \frac{(\text{PV})\,(1 - S_{wi})}{(B_g)_{400\,\text{psi}}}$$

$$= 588.06(10^6)(1 - 0.2)/0.0397$$

$$= 11.95 \text{ MMMscf}$$

Step 5. Calculate cumulative gas production G_p and the recovery factor RF at 1000 and 400 psi.

At 1000 psi:

$$G_p = (G - G_{1000\,psi}) = (87.12 - 30.95) \times 10^9$$

$$= 56.17 \text{ MMMscf}$$

$$RF = \frac{56.17 \times 10^9}{87.12 \times 10^9} = 64.5\%$$

At 400 psi:

$$G_p = (G - G_{400\,psi}) = (87.12 - 11.95) \times 10^9$$

$$= 75.17 \text{ MMMscf}$$

$$RF = \frac{75.17 \times 10^9}{87.12 \times 10^9} = 86.3\%$$
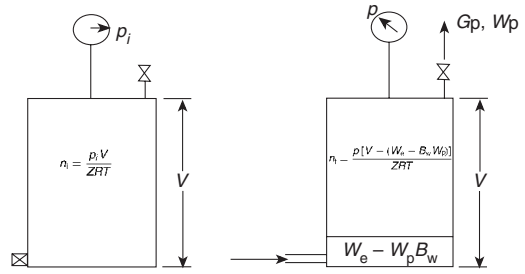
The recovery factors for volumetric gas reservoirs will range from 80% to 90%. If a strong water drive is present, trapping of residual gas at higher pressures can reduce the recovery factor substantially, to the range of 50% to 80%.

3.3.2 The material balance method

Material balance is one of the fundamental tools of reservoir engineering. Pletcher (2000) presented excellent documentation of the material balance equation in its various forms and discussed some procedures of improving their performances in predicting gas reserves. If enough production–pressure history is available for a gas reservoir in terms of:

- cumulative gas production G_p as a function of pressure,
- gas properties as a function of pressure at reservoir temperature, and
- the initial reservoir pressure, p_i,

then the gas reserves can be calculated without knowing the areal extend of the reservoir or the drainage area of the well A, thickness h, porosity ϕ, or water saturation S_w. This can be accomplished by forming a mass or mole balance on the gas, as:

$$n_p = n_i - n_f \qquad [3.3.5]$$

where:

n_p = moles of gas produced
n_i = moles of gas initially in the reservoir
n_f = moles of gas remaining in the reservoir

Representing the gas reservoir by an idealized gas container, as shown schematically in Figure 3.15, the gas moles in Equation 3.3.5 can be replaced by their equivalents using the real-gas law, to give:

$$n_p = \frac{p_{sc} G_p}{Z_{sc} R T_{sc}}$$

$$n_i = \frac{p_i V}{ZRT}$$

$$n_f = \frac{p\left[V - (W_e - B_w W_p)\right]}{ZRT}$$

Substituting the above three relationships into Equation 3.3.5 and knowing $Z_{sc} = 1$ gives:

$$\frac{p_{sc} G_p}{R T_{sc}} = \frac{p_i V}{ZRT} - \frac{p\left[V - (W_e - B_w W_p)\right]}{ZRT} \qquad [3.3.6]$$

where:

p_i = initial reservoir pressure
G_p = cumulative gas production, scf
p = current reservoir pressure
V = original gas volume, ft³
Z_i = gas deviation factor at p_i

Figure 3.15 Idealized water-drive gas reservoir.

Z = gas deviation factor at p
T = temperature, °R
W_e = cumulative water influx, ft³
W_p = cumulative water production, stock-tank ft³

Equation 3.3.6 is essentially the general material balance equation (MBE). It can be expressed in numerous forms depending on the type of the application and the driving mechanism. In general, dry gas reservoirs can be classified into two categories:

(1) volumetric gas reservoirs;
(2) water drive gas reservoirs.

These two types of gas reservoirs are presented next.

3.3.3 Volumetric gas reservoirs

For a volumetric reservoir and assuming no water production, Equation 3.3.6 is reduced to:

$$\frac{p_{sc} G_p}{T_{sc}} = \left(\frac{p_i}{Z_i T}\right) V - \left(\frac{p}{ZT}\right) V \qquad [3.3.7]$$

Equation 3.3.7 is commonly expressed in the following two forms:

(1) in terms of p/Z;
(2) in terms of B_g.

The above two forms of the MBE for volumetric gas reservoirs are discussed below.

Form 1: MBE as expressed in terms of p/Z
Rearranging Equation 3.1.7 and solving for p/Z gives:

$$\frac{p}{Z} = \frac{p_i}{Z_i} - \left(\frac{p_{sc} T}{T_{sc} V}\right) G_p \qquad [3.3.8]$$

or equivalently:

$$\frac{p}{Z} = \frac{p_i}{Z_i} - (m)\, G_p$$

Equation 3.3.8 is the equation of a straight line with a negative slope m, when p/Z is plotted versus the cumulative gas production G_p as shown in Figure 3.16. This straight-line relationship is perhaps one of the most widely used relationships in gas-reserve determination. Equation 3.3.8 reveals the straight-line relationship provides the engineer with the following four characteristics of plot:

(1) Slope of the straight line is equal to:

$$-m = -\frac{p_{sc} T}{T_{sc} V}$$

or:

$$V = \frac{p_{sc} T}{T_{sc}\, m} \qquad [3.3.9]$$
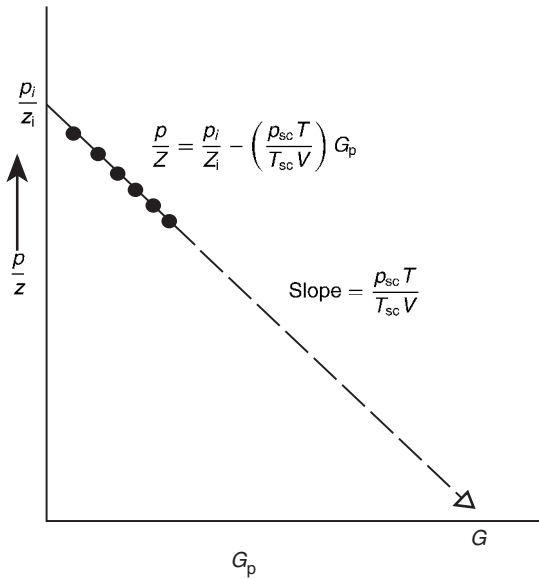
Figure 3.16   *Gas material balance equation.*

Time, t (years)	Reservoir pressure, p (psia)	Z	Cumulative production, G_p (MMMscf)
0.0	1798	0.869	0.00
0.5	1680	0.870	0.96
1.0	1540	0.880	2.12
1.5	1428	0.890	3.21
2.0	1335	0.900	3.92

The following data is also available:

$$\phi = 13\%, \quad S_{wi} = 0.52, \quad A = 1060 \text{ acres}, \quad h = 54 \text{ ft},$$

$$T = 164°F$$

Calculate the gas initially in place volumetrically and from the MBE.

Solution

Step 1. Calculate B_{gi} from Equation 3.3.1:

$$B_{gi} = 0.02827 \frac{(0.869)(164 + 460)}{1798} = 0.00853 \text{ ft}^3/\text{scf}$$

Step 2. Calculate the gas initially in place volumetrically by applying Equation 3.3.3:

$$G = \frac{43560 Ah\phi(1 - S_{wi})}{B_{gi}}$$

$$= 43560(1060)(54)(0.13)(1 - 0.52)/0.00853$$

$$= 18.2 \text{ MMMscf}$$

Step 3. Plot p/Z versus G_p as shown in Figure 3.17 and determine G as:

$$G = 14.2 \text{ MMMscf}$$

The value of the gas initially in place as calculated form the MBE compares reasonably with the volumetric value.

The calculated reservoir gas volume V can be used to determine the areal extend of the reservoir from:

$$V = 43560 Ah\phi(1 - S_{wi})$$

That is:

$$A = V/[43560 h\phi(1 - S_{wi})]$$

If reserve calculations are performed on a well-by-well basis, the drainage radius of the well can then estimated from:

$$r_e = \sqrt{\frac{43560A}{\pi}}$$

where A is the area of the reservoir in acres.

(2) Intercept at $G_p = 0$ gives p_i/Z_i.

(3) Intercept at $p/Z = 0$ gives the gas initially in place G in scf. Notice that when $p/Z = 0$, Equation 3.3.8 is reduced to:

$$0 = \frac{p_i}{Z_i} - \left(\frac{p_{sc}T}{T_{sc}V}\right)G_p$$

Rearranging:

$$\frac{T_{sc}}{p_{sc}} \frac{p_i}{TZ_i} V = G_p$$

This equation is essentially $E_{gi}V$ and therefore:

$$E_{gi}V = G$$

(4) Cumulative gas production or gas recovery at any pressure.

Example 3.6[a]   A volumetric gas reservoir has the following production history.

[a]After Ikoku, C. *Natural Gas Reservoir Engineering*, John Wiley & Sons (1984).

Figure 3.17   *Relationship of p/z vs. G_p for Example 3.6.*

The reservoir gas volume V can be expressed in terms of the volume of gas at standard conditions by:

$$V = B_{gi}G = \left(\frac{p_{sc}}{T_{sc}}\frac{Z_i T}{p_i}\right)G$$

Combining the above relationship with that of Equation 3.3.8:

$$\frac{p}{Z} = \frac{p_i}{Z_i} - \left(\frac{p_{sc}T}{T_{sc}V}\right)G_p$$

gives:

$$\frac{p}{Z} = \frac{p_i}{Z_i} - \left[\left(\frac{p_i}{Z_i}\right)\frac{1}{G}\right]G_p \qquad [3.3.10]$$

or:

$$\frac{p}{Z} = \frac{p_i}{Z_i} - [m]G_p$$

The above equation indicates that a plot of p/Z vs. G_p would produce a straight line with a slope of m and intercept of p_i/Z_i, with the slope m defined by:

$$m = \left(\frac{p_i}{Z_i}\right)\frac{1}{G}$$

Equation 3.3.10 can be rearranged to give:

$$\frac{p}{Z} = \frac{p_i}{Z_i}\left[1 - \frac{G_p}{G}\right] \qquad [3.3.11]$$

Again, Equation 3.3.10 shows that for a volumetric reservoir, the relationship between p/Z and G_p is essentially linear. This popular equation indicates that extrapolation of the straight line to the abscissa, i.e., at $p/Z = 0$, will give the value of the gas initially in place as $G = G_p$. Note that when $p/Z = 0$, Equations 3.3.10 and 3.3.11 give:

$$G = G_p$$

The graphical representation of Equation 3.3.10 can be used to detect the presence of water influx, as shown in Figure 3.18. When the plot of p/Z vs. G_p deviates from the linear relationship, it indicates the presence of water encroachment.

Field average p/Z   From the individual well performance in terms of p/Z vs. G_p, the recovery performance of the entire field can be estimated form the following relationship:

$$\left(\frac{p}{Z}\right)_{\text{Field}} = \frac{p_i}{Z_i} - \frac{\sum_{j=1}^{n}(G_p)_j}{\sum_{j=1}^{n}\left[G_p\bigg/\frac{p_i}{Z_i} - \frac{p}{Z}\right]_j}$$
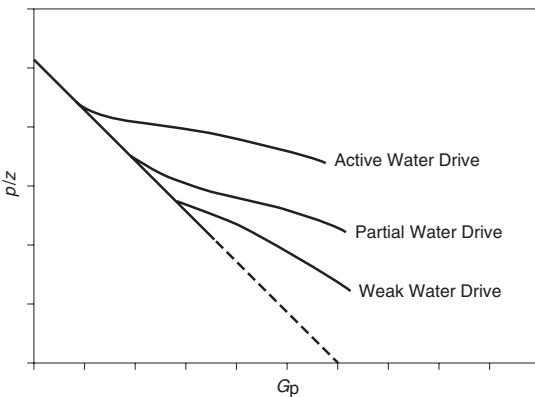
Figure 3.18   *Effect of water drive on p/z vs. G_p relationship.*

The summation $\sum$ is taken over the total number of the field gas wells n, i.e. $j = 1, 2, ..., n$. The total field performance in terms of $(p/Z)_{\text{Field}}$ vs. $(G_p)_{\text{Field}}$ can then be constructed from the estimated values of the field p/Z and actual total field production, i.e., $(p/Z)_{\text{Field}}$ vs. $\sum G_p$. The above equation is applicable as long as all wells are producing with defined static boundaries, i.e. under pseudosteady-state conditions.

When using the MBE for reserve analysis for the entire reservoir that is characterized by a distinct lack of pressure equilibrium throughout the reservoir, the following average pressure decline $(p/Z)_{\text{Field}}$ can be used:

$$\left(\frac{p}{Z}\right)_{\text{Field}} = \frac{\sum_{j=1}^{n}\left(\frac{p\Delta G_p}{\Delta p}\right)_j}{\sum_{j=1}^{n}\left(\frac{\Delta G_p}{\Delta p/Z}\right)_j}$$

where Δp and ΔG_p are the incremental pressure difference and cumulative production, respectively.

Form 2: MBE as expressed in terms of B_g
From the definition of the initial gas formation volume factor, it can be expressed as:

$$B_{gi} = \frac{V}{G}$$

Replacing B_{gi} in the relation with Equation 3.3.1 gives:

$$\frac{p_{sc}}{T_{sc}}\frac{Z_i T}{p_i} = \frac{V}{G} \qquad [3.3.12]$$

where:

V = volume of gas originally in place, ft³
G = volume of gas originally in place, scf
p_i = original reservoir pressure
Z_i = gas compressibility factor at p_i

Recalling Equation 3.3.8:

$$\frac{p}{Z} = \frac{p_i}{Z_i} - \left(\frac{p_{sc}T}{T_{sc}V}\right)G_p$$

Equation 3.3.12 can be combined with Equation 3.3.8 to give:

$$G = \frac{G_p B_g}{B_g - B_{gi}} \qquad [3.3.13]$$

Equation 3.3.13 suggests that to calculate the initial gas volume, the information required is production data, pressure data, gas specific gravity for obtaining Z factors, and reservoir temperature. However, early in the producing life of a reservoir, *the denominator of the right-hand side of the MBE is very small*, while the numerator is relatively large. A small change in the denominator will result in a large discrepancy in the calculated value of initial gas-in-place. Therefore, the MBE should not be relied on early in the producing life of the reservoir.

Material balances on volumetric gas reservoirs are simple. Initial gas-in-place may be computed from Equation 3.3.13 by substituting cumulative gas produced and appropriate gas formation volume factors at corresponding reservoir pressures during the history period. If successive calculations at various times during the history give consistent and constant values for initial gas-in-place, the reservoir is operating *under volumetric control and the computed G is reliable*, as shown in Figure 3.19). Once G has been determined and the absence of water influx established in this fashion, the same equation can be used to make future predictions of cumulative gas production as a function of reservoir pressure.

$$G = \frac{G_p B_g}{B_g - B_{gi}}$$
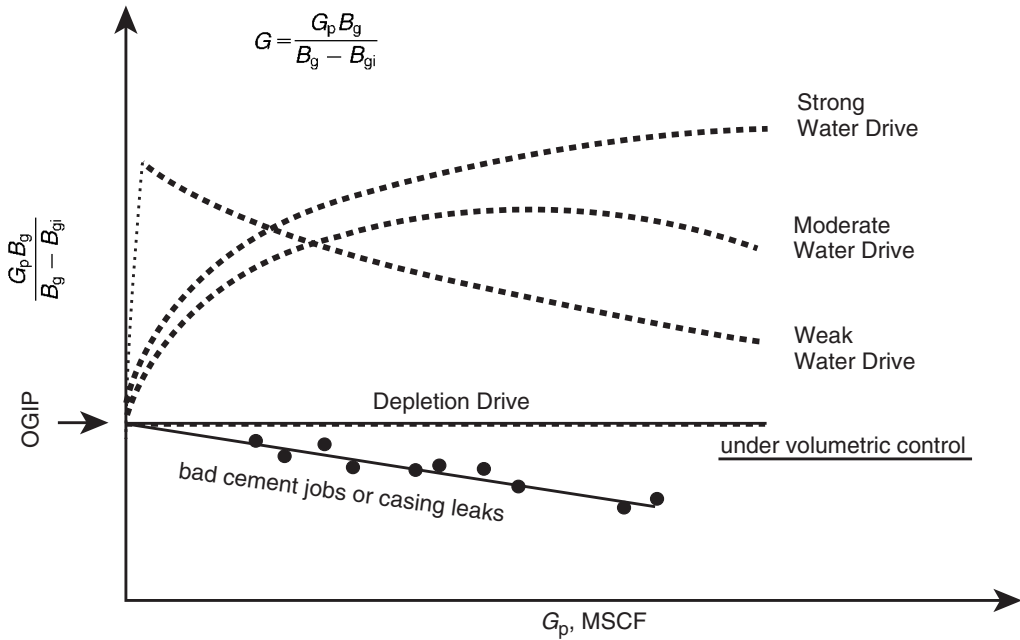
Figure 3.19   *Gas-in-place in a depletion driver reservoir.*

It should be pointed out that the successive application of Equation 3.3.13 can yield increasing or decreasing values of the gas initially in place G. Two different situations therefore exist:

(1) When the calculated value of the gas initially in place G appears to increase with time, the reservoir might be under drive. The invasion of water reduces the pressure drop for a given amount of production, making the reservoir appear larger as time progresses. The reservoir should in this case be classified as a water drive gas reservoir. Another possibility, if no known aquifer exists in the region, is that gas from a different reservoir or zone might migrate through fractures or leaky faults.

(2) If the calculated value of G decreases with time, the pressure drops more rapidly than would be the case in a volumetric reservoir. This implies loss of gas to other zones, leaky cementing job or casing leaks, among other possibilities.

Example 3.7   After producing 360 MMscf of gas from a volumetric gas reservoir, the pressure has declined from 3200 psi to 3000 psi. Calculate.

(a) The gas initially in place, given:

$$B_{gi} = 0.005278 \text{ ft}^3/\text{scf}, \text{ at } p_i = 3200 \text{ psi}$$

$$B_g = 0.005390 \text{ ft}^3/\text{scf}, \text{ at } p = 3000 \text{ psi}$$

(b) Recalculate the gas initially in place assuming that the pressure measurements were incorrect and the true average pressure is 2900 psi, instead of 2900 psi. The gas formation volume factor at this pressure is 0.00558 ft^3/scf.

Solution

(a) Using Equation 3.1.14, calculate G:

$$G = \frac{G_p B_g}{B_g - B_{gi}}$$

$$= \frac{360 \times 10^6 (0.00539)}{0.00539 - 0.005278} = 17.325 \text{ MMMscf}$$

(b) Recalculate G by using the correct value of B_g:

$$G = \frac{360 \times 10^6 (0.00558)}{0.00558 - 0.005278} = 6.652 \text{ MMMscf}$$

Thus, an error of 100 psia, which is only 3.5% of the total reservoir pressure, resulted in an increase in calculated gas-in-place of approximately 160%. Note that a similar error in reservoir pressure later in the producing life of the reservoir will not result in an error as large as that calculated early in the producing life of the reservoir.

Gas recovery factor

The gas recovery factor (RF) at any depletion pressure is defined as the cumulative gas produced G_p at this pressure divided by the gas initially in place G:

$$RF = \frac{G_p}{G}$$

Introducing the gas RF into Equation 3.3.11 gives:

$$\frac{p}{Z} = \frac{p_i}{Z_i} \left[1 - \frac{G_p}{G} \right]$$

or:

$$\frac{p}{Z} = \frac{p_i}{Z_i} [1 - RF]$$

Solving for the RF at any depletion pressure gives:

$$RF = 1 - \left[\frac{p}{Z} \frac{Z_i}{p_i} \right]$$

$$G + \frac{W_e}{B_g - B_{gi}} = \frac{G_p B_g + W_p B_w}{B_g - B_{gi}}$$

$$C = \frac{W_e}{B_g - B_{gi}}$$

True Value of G
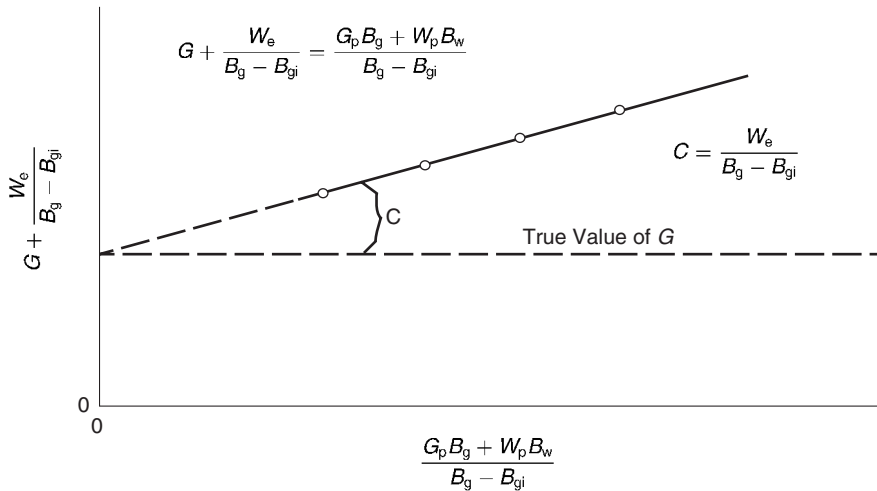
Figure 3.20 *Effect of water influx on calculating the gas initially in place.*

3.3.4 Water drive gas reservoirs

The plot of p/Z versus cumulative gas production G_p is a widely accepted method for solving gas material balance under depletion drive conditions. The extrapolation of the plot to atmospheric pressure provides a reliable estimate of the original gas-in-place. If a water drive is present the plot often appears to be linear, but the extrapolation will give an erroneously high value for gas-in-place. If the gas reservoir has a water drive, then there will be two unknowns in the MBE, even though production data, pressure, temperature, and gas gravity are known. These two unknowns are initial gas-in-place and cumulative water influx. In order to use the MBE to calculate initial gas-in-place, some independent method of estimating W_e, the cumulative water influx, must be developed.

Equation 3.1.13 can be modified to include the cumulative water influx and water production, to give:

$$G = \frac{G_p B_g - (W_e - W_p B_w)}{B_g - B_{gi}} \qquad [3.3.14]$$

The above equation can be arranged and expressed as:

$$G + \frac{W_e}{B_g - B_{gi}} = \frac{G_p B_g + W_p B_w}{B_g - B_{gi}} \qquad [3.3.15]$$

where:

B_g = gas formation volume factor, bbl/scf
W_e = cumulative water influx, bbl

Equation 3.3.15 reveals that for a volumetric reservoir, i.e., $W_e = 0$, the right-hand side of the equation will be constant and equal to the initial gas-in-place "G" regardless of the amount of gas G_p which has been produced. That is:

$$G + 0 = \frac{G_p B_g + W_p B_w}{B_g - B_{gi}}$$

For a water drive reservoir, the values of the right-hand side of Equation 3.3.15 will continue to increase because of the $W_e/(B_g - B_{gi})$ term. A plot of several of these values at successive time intervals is illustrated in Figure 3.20. Extrapolation of the line formed by these points back to the point where $G_p = 0$ shows the true value of G, because when $G_p = 0$, then $W_e/(B_g - B_{gi})$ is also zero.

This graphical technique can be used to estimate the value of W_e, because at any time the difference between the horizontal line (i.e., true value of G) and the straight line $G + [W_e/(B_g - B_{gi})]$ will give the value of $W_e/(B_g - B_{gi})$.

Because gas often is bypassed and trapped by the encroaching water, recovery factors for gas reservoirs with water drive can be significantly lower than for volumetric reservoirs produced by simple gas expansion. In addition, the presence of reservoir heterogeneities, such as low-permeability stringers or layering, may reduce gas recovery further. As noted previously, ultimate recoveries of 80% to 90% are common in volumetric gas reservoirs, while typical recovery factors in water drive gas reservoirs can range from 50% to 70%. The amount of gas that is trapped in the region that has been flooded by water encroachment can be estimated by defining the following characteristic reservoir parameters and the steps as outlined below:

(PV) = reservoir pore volume, ft^3
(PV)$_{water}$ = pore volume of the water-invaded zone, ft^3
S_{grw} = residual gas saturation to water displacement
S_{wi} = initial water saturation
G = gas initially in place, scf
G_p = cumulative gas production at depletion pressure "p", scf
B_{gi} = initial gas formation volume factor, ft^3/scf
B_g = gas formation volume factor at depletion pressure "p", ft^3/scf
Z = gas deviation factor at depletion pressure "p"

Step 1. Express the reservoir pore volume (PV) in terms of the initial gas-in-place G as follows:

$$GB_{gi} = (PV)(1 - S_{wi})$$

Solving for the reservoir pore volume gives:

$$(PV) = \frac{GB_{gi}}{1 - S_{wi}}$$

Step 2. Calculate the pore volume in the water-invaded zone, as:

$$W_e - W_p B_w = (PV)_{water}(1 - S_{wi} - S_{grw})$$
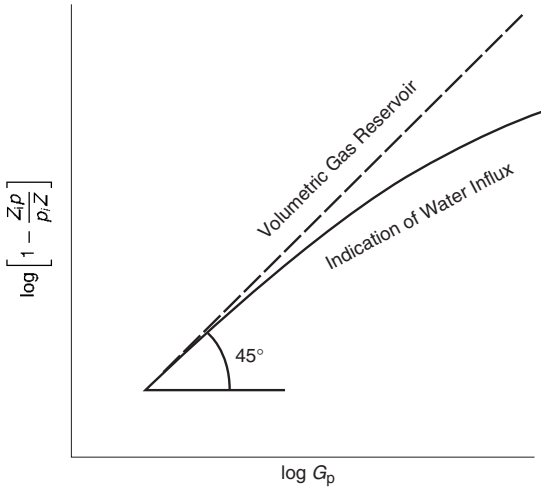
Figure 3.21 *Energy plot.*

Solving for the pore volume of the water-invaded zone, $(PV)_{water}$, gives:

$$(PV)_{water} = \frac{W_e - W_p B_w}{1 - S_{wi} - S_{grw}}$$

Step 3. Calculate trapped gas volume in the water-invaded zone, or:

Trapped gas volume $= (PV)_{water} S_{grw}$

Trapped gas volume $= \left(\dfrac{W_e - W_p B_w}{1 - S_{wi} - S_{grw}} \right) S_{grw}$

Step 4. Calculate the number of moles of gas n trapped in the water-invaded zone by using the equation of state, or:

$$p(\text{trapped gas volume}) = ZnRT$$

Solving for n, gives:

$$n = \frac{p \left(\dfrac{W_e - W_p B_w}{1 - S_{wi} - S_{grw}} \right) S_{grw}}{ZRT}$$

This indicates that the higher the pressure, the greater the quantity of tapped gas. Dake (1994) pointed out that if the pressure is reduced by rapid gas withdrawal the volume of gas trapped in each individual pore space, i.e., S_{grw}, will remain unaltered but its quantity n is reduced

Step 5. The gas saturation at any pressure can be adjusted to account for the trapped gas as follows:

S_g

$= \dfrac{\text{remaining gas volume} - \text{trapped gas volume}}{\text{reservoir pore volume} - \text{pore volume of water invaded zone}}$

$$S_g = \frac{(G - G_p)B_g - \left(\dfrac{W_e - W_p B_w}{1 - S_{wi} - S_{grw}} \right) S_{grw}}{\left(\dfrac{GB_{gi}}{1 - S_{wi}} \right) - \left(\dfrac{W_e - W_p B_w}{1 - S_{wi} - S_{grw}} \right)}$$

There are several methods of expressing the MBE in a convenient graphical form that can be used to describe the recovery performance of a volumetric or water drive gas reservoir including:

- Energy plot;
- MBE as a straight line;
- Cole plot;
- modified Cole plot;
- Roach plot;
- modified Roach plot;
- Fetkovich et al. plot;
- Paston et al. plot;
- Hammerlindl method.

These methods are presented below.

The energy plot
Many graphical methods have been proposed for solving the gas MBE that are useful in detecting the presence of water influx. One such graphical technique is called the energy plot, which is based on arranging Equation 3.3.11:

$$\frac{p}{Z} = \frac{p_i}{Z_i} \left[1 - \frac{G_p}{G} \right]$$

to give:

$$1 - \left[\frac{p}{Z} \frac{Z_i}{p_i} \right] = \frac{G_p}{G}$$

Taking the logarithm of both sides of this equation:

$$\log \left[1 - \frac{Z_i p}{p_i Z} \right] = \log G_p - \log G \qquad [3.3.16]$$

Figure 3.21 shows a schematic illustration of the plot.

From Equation 3.3.16, it is obvious that a plot of $[1 - (Z_i p)/(p_i Z)]$ vs. G_p on log–log coordinates will yield a straight line with a slope of 1 (45° angle). An extrapolation to 1 on the vertical axis ($p = 0$) yields a value for initial gas-in-place, G. The graphs obtained from this type of analysis have been referred to as energy plots. They have been found to be useful in detecting water influx early in the life of a reservoir. If W_e is not zero, the slope of the plot will be less than one, and will also decrease with time, since W_e increases with time. *An increasing slope can only occur as a result of either gas leaking from the reservoir or bad data*, since the increasing slope would imply that the gas occupied PV was increasing with time.

Generalized MBE as a straight line
Havlena and Odeh (1963, 1964) expressed the material balance in terms of gas production, fluid expansion, and water influx as:

$$\begin{bmatrix} \text{underground} \\ \text{withdrawal} \end{bmatrix} = \begin{bmatrix} \text{gas} \\ \text{expansion} \end{bmatrix} + \begin{bmatrix} \text{water expansion and} \\ \text{pore compaction} \end{bmatrix}$$
$$+ \begin{bmatrix} \text{water} \\ \text{influx} \end{bmatrix} + \begin{bmatrix} \text{fluid} \\ \text{injection} \end{bmatrix}$$

and mathematically as:

$$G_p B_g + W_p B_w = G \left(B_g - B_{gi} \right) + G B_{gi} \frac{(c_w S_{wi} + c_f)}{1 - S_{wi}} \Delta p$$
$$+ W_e + (W_{inj} B_w + G_{inj} B_{ginj})$$

Assuming no water or gas injection, i.e., W_{inj} and $G_{inj} = 0$, the above generalized MBE reduces to:

$$G_p B_g + W_p B_w = G(B_g - B_{gi}) + G B_{gi} \frac{(c_w S_{wi} + c_f)}{1 - S_{wi}} \Delta p + W_e$$
$$[3.3.17]$$

where:

$\Delta p = p_i - p$
$B_g = $ gas formation volume factor, bbl/scf

Using the nomenclature of Havlena and Odeh, Equation 3.3.17 can be written in the following form:

$$F = G(E_G + E_{f,w}) + W_e \qquad [3.3.18]$$

with the terms F, E_G, and $E_{f,w}$ as defined by:

Underground fluid withdrawal F:

$$F = G_p B_g + W_p B_w \qquad [3.3.19]$$

Gas expansion term E_G:

$$E_G = B_g - B_{gi} \qquad [3.3.20]$$

Water and rock expansion $E_{f,w}$:

$$E_{f,w} = B_{gi} \frac{(c_w S_{wi} + c_f)}{1 - S_{wi}} \Delta p \qquad [3.3.21]$$

Equation 3.3.18 can be further simplified by introducing the total system expansion term E_t that combined both compressibilities E_G and $E_{f,w}$ as defined by:

$$E_t = E_G + E_{f,w}$$

to give:

$$F = G E_t + W_e$$

Note that for a volumetric gas reservoir with no water influx or production, Equation 3.3.17 is expressed in an expanded form as:

$$G_p B_g = G(B_g - B_{gi}) + G B_{gi} \frac{(c_w S_{wi} + c_f)}{1 - S_{wi}} \Delta p$$

Dividing both sides of the above equation by G and rearranging gives:

$$\frac{G_p}{G} = 1 - \left[1 - \frac{(c_w S_{wi} + c_f)\,\Delta p}{1 - S_{wi}}\right] \frac{B_{gi}}{B_g}$$

Inserting the typical values of $c_w = 3 \times 10^{-6}$ psi^{-1}, $c_f = 10 \times 10^{-6}$ psi^{-1}, and $S_{wi} = 0.25$ in above relationship and considering a large pressure drop of $\Delta p = 1000$ psi, the term in the square brackets becomes:

$$\left[1 - \frac{(c_w S_{wi} + c_f)\,\Delta p}{1 - S_{wi}}\right] = 1 - \frac{[3 \times 0.25 + 10]10^{-6}(1000)}{1 - 0.25}$$

$$= 1 - 0.014$$

The above value of 0.014 suggests that the inclusion of the term accounting for the reduction in the hydrocarbon PV due to connate water expansion and shrinkage of the PV only alters the material balance by 1.4%, and therefore the term is frequently neglected. The main reason for the omission is because the water and formation compressibilities are usually, although not always, insignificant in comparison with the gas compressibility.

Assuming that the rock and water expansion term $E_{f,w}$ is negligible in comparison with the gas expansion term E_G, Equation 3.3.8 is reduced to:

$$F = G E_G + W_e \qquad [3.3.22]$$

Finding the proper model that can be used to determine the cumulative water influx W_e is perhaps the biggest unknown when applying the MBE. The water influx is usually replaced with the analytical aquifer model that must be known or determined from the MBE. The MBE can be expressed as the equation of a straight line by dividing both sides of the above equation by the gas expansion E_G to give:

$$\frac{F}{E_G} = G + \frac{W_e}{E_G} \qquad [3.3.23]$$

The graphical presentation of Equation 3.3.23 is given in Figure 3.22). Assuming that the water influx can be adequately described by the van Everdingen and Hurst
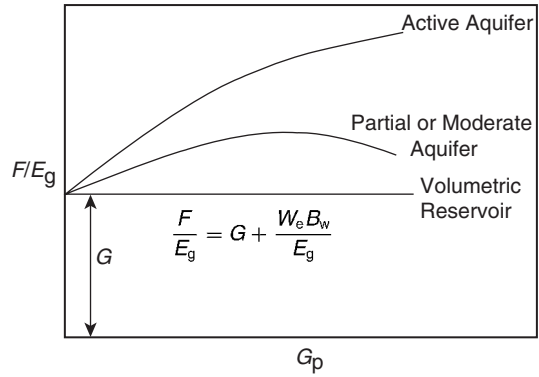
Figure 3.22 *Defining the reservoir driving mechanism.*

(1949) unsteady-state model, the selected water influx model can be integrated into Equation 3.3.23; to give:

$$\frac{F}{E_G} = G + B \frac{\sum [\Delta p W_{eD}]}{E_G}$$

This expression suggests that a graph of F/E_G vs. $\sum \Delta p W_{eD}/E_G$ will yield a straight line, provided the unsteady-state influx summation, $\sum \Delta p W_{eD}$, is accurately assumed. The resulting straight line intersects the y axis at the initial gas-in-place G and has a slope equal to the water influx constant B; as illustrated in Figure 3.23.

Non-linear plots will result if the aquifer is improperly characterized. A systematic upward or downward curvature suggests that the summation term is too small or too large, respectively, while an S-shaped curve indicates that a linear (instead of a radial) aquifer should be assumed. The points should plot sequentially from left to right. A reversal of this plotting sequence indicates that an unaccounted aquifer boundary has been reached and that a smaller aquifer should be assumed in computing the water influx term.

A linear infinite system rather than a radial system might better represent some reservoirs, such as reservoirs formed as fault blocks in salt domes. The van Everdingen and Hurst dimensionless water influx W_{eD} is replaced by the square root of time, as:

$$W_e = C \sum \Delta p_n \sqrt{t - t_n} \qquad [3.3.24]$$

where:

C = water influx constant, ft^3/psi
t = time (any convenient units, i.e., days, years, etc.)

The water influx constant C must be determined by using the past production and pressure of the field in conjunction with the Havlena and Odeh methodology. For the linear system, the underground withdrawal F is plotted versus $\left[\sum \Delta p_n \sqrt{t - t_n} / (B_g - B_{gi})\right]$ on a Cartesian graph. The plot should result in a straight line with G being the intercept and the water influx constant C being the slope of the straight line.

To illustrate the use of the linear aquifer model in the gas MBE as expressed as the equation of a straight line, i.e., Equation Havlena and Odeh proposed the following problem.

Example 3.8 The volumetric estimate of the gas initially in place for a dry gas reservoir ranges from 1.3 to
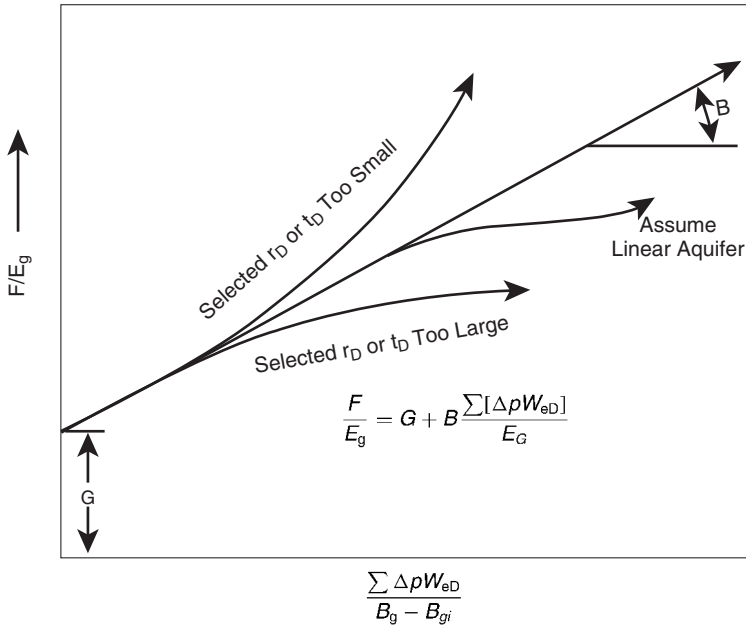
Figure 3.23 *Havlena–Odeh MBE plot for a gas reservoir.*

Table 3.1 *Havlena–Odeh Dry-Gas Reservoir Data for Example 8-8*

Time (months)	Average reservoir pressure (psi)	$E_g = (B_g - B_{gi}) \times 10^{-6}$ (ft³/scf)	$E_g = (G_p - B_g) \times 10^6$ (ft³)	$\dfrac{\sum \Delta p_n Zt - t_n}{B_g - B_{gi}}$ (10⁶)	$F/E_g = \dfrac{G_p B_g}{B_g - B_{gi}}$ (10¹²)
0	2883	0.0	–	–	–
2	2881	4.0	5.5340	0.3536	1.3835
4	2874	18.0	24.5967	0.4647	1.3665
6	2866	34.0	51.1776	0.6487	1.5052
8	2857	52.0	76.9246	0.7860	1.4793
10	2849	68.0	103.3184	0.9306	1.5194
12	2841	85.0	131.5371	1.0358	1.5475
14	2826	116.5	180.0178	1.0315	1.5452
16	2808	154.5	240.7764	1.0594	1.5584
18	2794	185.5	291.3014	1.1485	1.5703
20	2782	212.0	336.6281	1.2426	1.5879
22	2767	246.0	392.8592	1.2905	1.5970
24	2755	273.5	441.3134	1.3702	1.6136
26	2741	305.5	497.2907	1.4219	1.6278
28	2726	340.0	556.1110	1.4672	1.6356
30	2712	373.5	613.6513	1.5714	1.6430
32	2699	405.0	672.5969	1.5714	1.6607
34	2688	432.5	723.0868	1.6332	1.6719
36	2667	455.5	771.4902	1.7016	1.6937

1.65×10^{12} scf. Production, pressures, and the pertinent gas expansion term, i.e., $E_g = B_g - B_{gi}$, are presented in Table 3.1. Calculate the original gas-in-place G.

Solution

Step 1. Assume a volumetric gas reservoir.

Step 2. Plot p/Z vs. G_p or $G_p B_g/(B_g - B_{gi})$ vs. G_p.

Step 3. A plot of $G_p B_g/(B_g - B_{gi})$ vs. $G_p B_g$ shows upward curvature, as shown in Figure 3.24 indicating water influx.

Step 4. Assuming a linear water influx, plot $G_p B_g/(B_g - B_{gi})$ vs. $(\sum \Delta p_n \sqrt{t - t_n})/(B_g - B_{gi})$ as shown in Figure 3.25.
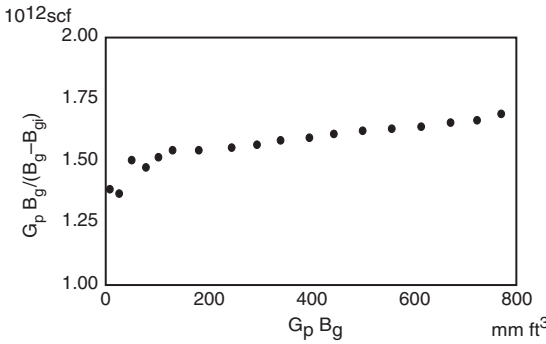
Figure 3.24   *Indication of the water influx.*
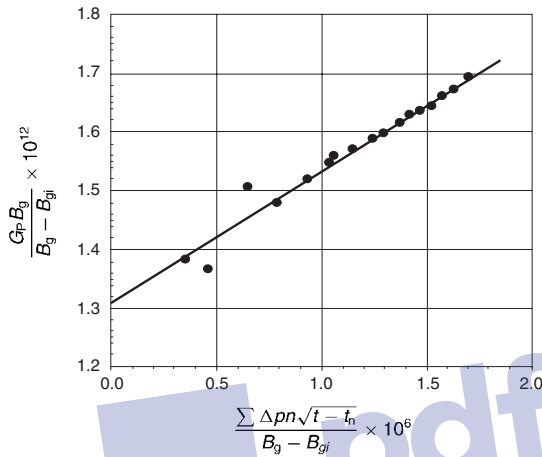
Figure 3.25   *Havlena–Odeh MBE plot for Example 3.8.*

Step 5. As evident from Figure 3.25, the necessary straight-line relationship is regarded as satisfactory evidence for the presence of the linear aquifer.

Step 6. From Figure 3.25, determine the original gas-in-place G and the linear water influx constant C, to give:

$$G = 1.325 \times 10^{12} \text{ scf}$$

$$C = 212.7 \times 10^3 \text{ ft}^3/\text{psi}$$

Drive indices for gas reservoirs   Drive indices have been defined for oil reservoirs (see Chapter 4) to indicate the relative magnitude of the various energy forces contributing to the driving mechanism of the reservoir. Similarly, drive indices can be defined for gas reservoirs by dividing Equation 3.3.17 by $G_p B_g + W_p B_w$, to give:

$$\frac{G}{G_p}\left(1 - \frac{B_{gi}}{B_g}\right) + \frac{G}{G_p}\frac{E_{f,w}}{B_g} + \frac{W_e - W_p B_w}{G_p B_g} = 1$$

Define the following three drive indices:

(1) Gas drive index (GDI) as:

$$\text{GDI} = \frac{G}{G_p}\left(1 - \frac{B_{gi}}{B_g}\right)$$

(2) Compressibility drive index (CDI) as:

$$\text{CDI} = \frac{G}{G_p}\frac{E_{f,w}}{B_g}$$

(3) Water drive index (WDI) as:

$$\text{WDI} = \frac{W_e - W_p B_w}{G_p B_g}$$

Substituting the above three indices into the MBE gives:

$$\text{GDI} + \text{CDI} + \text{WDI} = 1$$

Pletcher (2000) pointed out that if the drive indices do not sum to 1.0, this indicates that the solution to the MBE has not been obtained or is simply incorrect. In practice, however, drive indices calculated from actual field data rarely sum exactly to 1.0 unless accurate recording of production data is achieved. The summed drive indices typically fluctuate above or below one depending on the quality of the collected production data with time.

The Cole plot
The Cole plot is a useful tool for distinguishing between water drive and depletion drive reservoirs. The plot is derived from the generalized MBE as given in an expanded form by Equation 3.3.15 as:

$$\frac{G_p B_g + W_p B_w}{B_g - B_{gi}} = G + \frac{W_e}{B_g - B_{gi}}$$

or in a compact form by Equation 3.3.23 as:

$$\frac{F}{E_G} = G + \frac{W_e}{E_G}$$

Cole (1969) proposed ignoring the water influx term W_e/E_G and simply plotting the left-hand side of the above expression as a function of the cumulative gas production, G_p. This is simply for display purposes to inspect its variation during depletion. Plotting F/E_G versus production time or pressure decline, Δp, can be equally illustrative.

Dake (1994) presented an excellent discussion of the strengths and weaknesses of the MBE as a straight line. He pointed out that the plot will have one of the three shapes depicted previously in Figure 3.19. If the reservoir is of the volumetric depletion type, $W_e = 0$, then the values of F/E_G evaluated, say, at six monthly intervals, should plot as a straight line parallel to the abscissa, whose ordinate value is the gas initially in place. Alternatively, if the reservoir is affected by natural water influx then the plot of F/E_G will usually produce a concave-downward-shaped arc whose exact form is dependent upon the aquifer size and strength and the gas off-take rate. Backward extrapolation of the F/E_G trend to the ordinate should nevertheless provide an estimate of the gas initially in place ($W_e \sim 0$); however, the plot can be highly non-linear in this region yielding a rather uncertain result. The main advantage in the F/E_G vs. G_p plot, however, is that it is much more sensitive than other methods in establishing whether the reservoir is being influenced by natural water influx or not.

However, in the presence of a weak water drive, the far right-hand term in the above expression, i.e., $[W_e/(B_g - B_{gi})$, would decrease with time because the denominator would increase faster than the numerator. Therefore, the plotted points will exhibit a negative slope as shown in Figure 3.19. As reservoir depletion progresses in a weak water drive reservoir, the points migrate vertically down and to the right toward the time value of G. Therefore, under a weak water drive, the apparent initial gas-in-place decreases with time, contrary to that for a strong or moderate water drive. Pletcher (2000) pointed out that the weak water drive curve begins with a positive slope in the very early stages of reservoir depletion (as shown in Figure 3.19) prior to developing the signature negative slope. The very early points are difficult to use for determining G because they frequently exhibit a wide scatter behavior that is introduced by even small errors in pressure measurements early in the reservoir life.

Therefore, the curve is a "hump-shaped" curve similar to the moderate water drive with the exception that the positive-slope portion of the hump is very short and in practice will not appear if early data is *not* obtained.

Modified Cole plot

Pore compressibility can be very large in shallow unconsolidated reservoirs with values in excess of 100×10^{-6} psi^{-1}. Such large values have been measured, for instance, in the Bolivar Coast Fields in Venezuela and therefore it would be inadmissible to omit c_f from the gas MBE. In such cases, the term $E_{f,w}$ should be included when constructing the Cole plot and the equation should be written as:

$$\frac{F}{E_t} = G + \frac{W_e}{E_t}$$

As pointed out by Pletcher, the left-hand term F/E_t now incorporates energy contributions from the formation (and water) compressibility as well as the gas expansion. The modified Cole plot consists of plotting F/E_t on the y axis versus G_p on the x axis. Vertically; the points will lie closer to the true value of G than the original Cole plot. In reservoirs where formation compressibility is a significant contributor to reservoir energy, such as abnormally pressured reservoirs, the original Cole plot will exhibit a negative slope even if no water drive is present. The modified plot, however, will be a horizontal line assuming the correct value of c_f is used in calculating the term F/E_t. Thus, constructing *both* the original and modified Cole plots will distinguish between the following two possibilities:

(1) Reservoirs that are subject to *weak aquifer and significant c_f*. In this case, both plots, i.e., the original and modified Cole plots, will have a negative slope.
(2) Reservoirs where c_f *is significant but there is no aquifer attached*. In this particular case, the original Cole plot will have a negative slope while the modified plot will be horizontal.

It should be pointed out that negative slopes in the original and modified Cole plots could result from any unaccounted-for source of energy that is decreasing with time relative to gas expansion. This could include, for example, communication with other depleting reservoirs.

An "abnormally pressured" gas reservoir (sometimes called an "overpressured" or "geo-pressured" gas reservoir) is defined as a reservoir with pressures greater than a normal pressure gradient, i.e., over 0.5 psi/ft. A typical p/Z vs. G_p plot for an abnormally pressured gas reservoir will exhibit two straight lines as shown in Figure 3.26.

(1) The first straight line corresponds to the "apparent" gas reservoir behavior with an extrapolation that gives the "apparent gas-in-place G_{app}."
(2) The second straight line corresponds to the "normal pressure behavior" with an extrapolation that gives the "actual initial gas-in-place G."

Hammerlindl (1971) pointed out that in abnormally high-pressure volumetric gas reservoirs, two distinct slopes are evident when the plot of p/Z vs. G_p is used to predict reserves because of the formation and fluid compressibility effects as shown in Figure 3.26. The final slope of the p/Z plot is steeper than the initial slope; consequently, reserve estimates based on the early life portion of the curve are erroneously high. The initial slop is due to gas expansion and significant pressure maintenance brought about by formation compaction, crystal expansion, and water expansion. At approximately normal pressure gradient, the formation compaction is essentially complete and the reservoir assumes the characteristics of a normal gas expansion reservoir. This accounts for the second slope. Most early
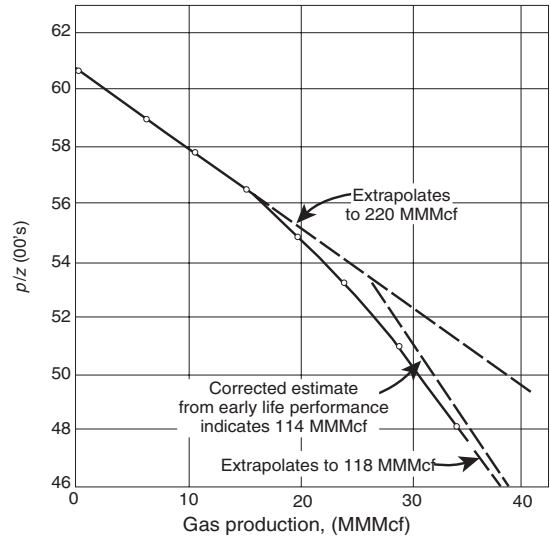
Figure 3.26 *p/Z versus cumulative production—North Ossum Field, Lafayette Parish, Louisiana NS2B reservoir (After Hammerlindl, 1971).*

decisions are made based on the early life extrapolation of the p/Z plot; therefore, the effects of hydrocarbon PV change on reserve estimates, productivity, and abandonment pressure must be understood.

All gas reservoir performance is related to effective compressibility, not gas compressibility. When the pressure is abnormal and high, the effective compressibility may equal two or more times the gas compressibility. If the effective compressibility is equal to twice the gas compressibility, then the first cubic foot of gas produced is due to 50% gas expansion and 50% formation compressibility and water expansion. As the pressure is lowered in the reservoir, the contribution due to gas expansion becomes greater because the gas compressibility is approaching the effective compressibility. Using formation compressibility, gas production, and shut-in bottom-hole pressures, two methods are presented for correcting the reserve estimates from the early life data (assuming no water influx).

Gunawan Gan and Blasingame (2001) provided a comprehensive literature review of the methods and theories that have been proposed to explain the non-linear behavior of p/Z vs. G_p. There are essentially two theories for such behavior:

(1) rock collapse theory;
(2) shale water influx theory.

These theories are briefly addressed below.

Rock collapse theory Harville and Hawkins (1969) suggested that the non-linear behavior that is characterized with two straight-line plots can be attributed to "pore collapse" and formation compaction. They concluded from a study on the North Ossum Field (Louisiana) that the initial slope is a result of the continuous increase in the *net* overburden pressure as the pore pressure declines with production. This increase in the net overburden pressure causes rock failure, i.e., rock collapse, which subsequently causes a continuous decrease in the rock compressibility c_f. This process continues until c_f eventually reaches a "normal value" which marks the beginning of the second slope. At this point, the reservoir

performance becomes similar to that for a constant-volume, normally pressured, gas reservoir system.

Shale water influx theory Several investigators have attributed the non-linear behavior of p/Z vs. G_p to shale water influx or peripheral water influx from a limited aquifer and the treatment of PV compressibility as a constant. Bourgoyne (1990) demonstrated that reasonable values of shale permeability and compressibility, treated as a function of pressure, can be used to match abnormal gas reservoir performance behavior to yield the first straight line. The second straight line is a result of a decrease in pressure support from the surrounding shales as the gas reservoir is depleted.

Fetkovich et al. (1998) differentiated between two different PV compressibilities, the "total" and the "instantaneous." The total PV compressibility is defined mathematically by the following expression:

$$\overline{c}_f = \frac{1}{(PV)_i} \left[\frac{(PV)_i - (PV)_p}{p_i - p} \right]$$

The term in the square brackets is the slope of the chord from initial condition $(P_i, (PV)_i)$ to any lower pressure $(P, (PV)_p)$, where:

$\overline{c}_f$ = cumulative pore volume (formation or rock) compressibility, psi^{-1}
p_i = initial pressure, psi
p = pressure, psi
$(PV)_i$ = pore volume at initial reservoir pressure
$(PV)_p$ = pore volume at pressure p

The instantaneous pore volume (rock or formation) compressibility is defined as:

$$c_f = \frac{1}{(PV)_P} \frac{\partial(PV)}{\partial p}$$

The instantaneous compressibility c_f should be used in reservoir simulation, while the cumulative compressibility $\overline{c}_f$ must be used with forms of the material balance that apply cumulative pressure drop $(p_i - p)$.

Both types of compressibilities are pressure dependent and best determined by special core analysis. An example of this analysis is shown below for a Gulf Coast sandstone as given by Fetkovich et al.:

p (psia)	$p_i - p$ (psi)	$(PV)_i - (PV)_p$ (cm^3)	$\overline{c}_f$ (10^{-6} psi^{-1})	c_f (10^{-6} psi^{-1})
$p_i = 9800$	0	0.000	16.50	16.50
9000	800	0.041	14.99	13.70
8000	1800	0.083	13.48	11.40
7000	2800	0.117	12.22	9.10
6000	3800	0.144	11.08	6.90
5000	4800	0.163	9.93	5.00
4000	5800	0.177	8.92	3.80
3000	6800	0.190	8.17	4.10
2000	7800	0.207	7.76	7.30
1000	8800	0.243	8.07	16.80
500	9300	0.276	8.68	25.80

Figure 3.27 shows how c_f and $\overline{c}_f$ vary as a function of pressure for this overpressured Gulf Coast sandstone reservoir. Figure 3.27 gives the proper definition of the "pore collapse" which is the condition when the instantaneous PV compressibility begins to increase at decreasing reservoir pressure.

Roach plot for abnormally pressured gas reservoirs
Roach (1981) proposed a graphical technique for analyzing abnormally pressured gas reservoirs. The MBE as

expressed by Equation 3.3.17 may be written in the following form for a volumetric gas reservoir:

$$\left(\frac{p}{Z}\right) c_t = \left(\frac{p_i}{Z_i}\right) \left[1 - \frac{G_p}{G} \right] \tag{3.3.25}$$

where:

$$c_t = 1 - \frac{(c_f + c_w S_{wi})(p_i - p)}{1 - S_{wi}} \tag{3.3.26}$$

Defining the rock expansion term E_R as:

$$E_R = \frac{c_f + c_w S_{wi}}{1 - S_{wi}} \tag{3.3.27}$$

Equation 3.3.26 can be expressed as:

$$c_t = 1 - E_R(p_i - p) \tag{3.3.28}$$

Equation 3.3.25 indicates that plotting the term $(p/Z) c_t$ versus cumulative gas production G_p on Cartesian coordinates results in a straight line with an x intercept at the original gas-in-place and a y intercept at the original $(p/Z)_i$. Since c_t is unknown and must be found by choosing the compressibility values resulting in the best straight-line fit, this method is a trial-and-error procedure.

Roach used the data published by Duggan (1972) for the Mobil–David Anderson Gas Field to illustrate the application of Equations 3.3.25 and 3.3.28 to determine graphically the gas initially in place. Duggan reported that the reservoir had an initial pressure of 9507 psig at 11300 ft. Volumetric estimates of original gas-in-place indicated that the reservoir contains 69.5 MMMscf. The historical p/Z vs. G_p plot produced an initial gas-in-place of 87 MMMscf, as shown in Figure 3.28.

Using the trial-and-error approach, Roach showed that a value of the rock expansion term E_r of 1805×10^{-6} would result in a straight line with an initial gas-in-place of 75 MMMscf, as shown in Figure 3.28.

To avoid the trial-and-error procedure, Roach proposed that Equations 3.3.25 and 3.3.28 can be combined and expressed in a linear form by:

$$\frac{(p/Z)_i/(p/Z) - 1}{p_i - p} = \frac{1}{G} \left[\frac{(p/Z)_i/(p/Z)}{p_i - p} \right] G_p - \frac{S_{wi} c_w + c_f}{1 - S_{wi}} \tag{3.3.29}$$

or equivalently as:

$$\alpha = \left(\frac{1}{G}\right) \beta - E_R \tag{3.3.30}$$

with:

$$\alpha = \frac{\left[(p_i/Z_i)/(p/Z) \right] - 1}{(p_i - p)} \tag{3.3.31}$$

$$\beta = \left[\frac{(p_i/Z_i)/(p/Z)}{(p_i - p)} \right] G_p \tag{3.3.32}$$

$$E_R = \frac{S_{wi} c_w + c_f}{1 - S_{wi}}$$

where:

G = initial gas-in-place, scf
E_R = rock and water expansion term, psi^{-1}
S_{wi} = initial water saturation

Equation 3.3.30 shows that a plot of α vs. β will yield a straight line with:

$$\text{slope} = 1/G$$

$$y \text{ intercept} = -E_R$$

To illustrate the proposed methodology, Roach applied Equation 3.3.30 to the Mobil–David Gas Field with the results as shown graphically in Figure 3.29. The slope of the straight

Cumulative PV compressibility as a chord slope.
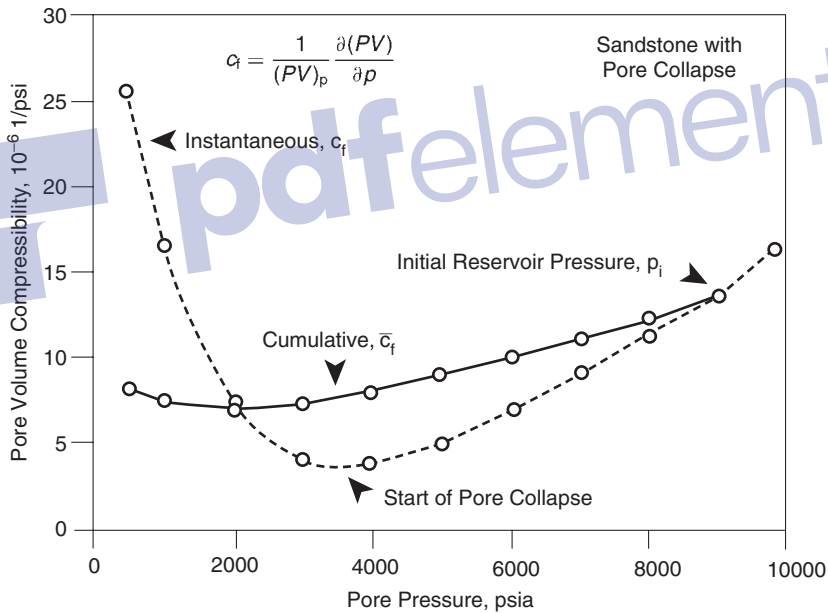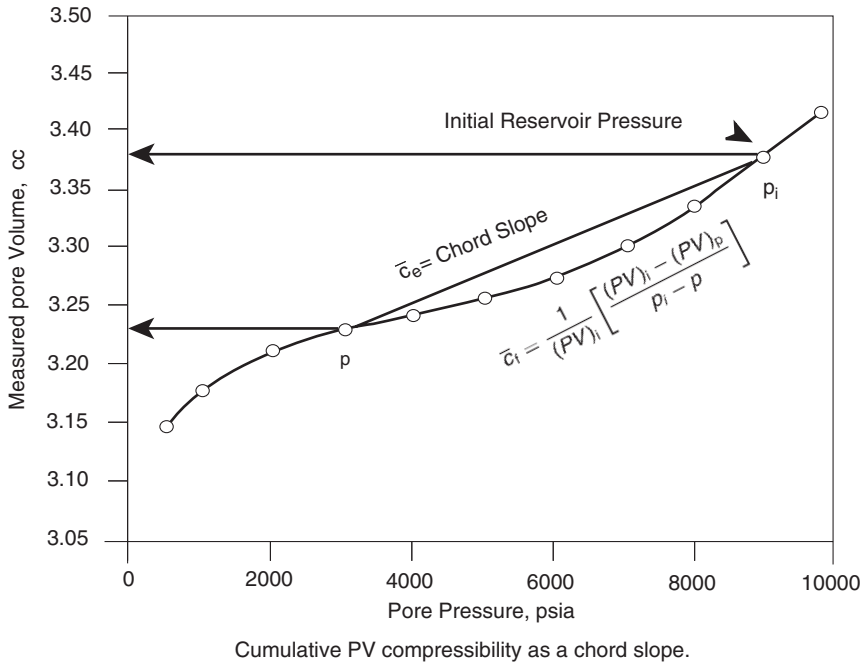
Figure 3.27 *Cumulative and instantaneous c_f.*

line gives $G = 75.2$ MMMscf and the intercept gives $E_R = 1805 \times 10^{-6}$.

Begland and Whitehead (1989) proposed a method to predict the percentage recovery of volumetric, high-pressured gas reservoirs from the initial pressure to the abandonment pressure when only initial reservoir data is available. The proposed technique allows the PV and water compressibilities to be pressure dependent. The authors derived the following form of the MBE for a volumetric gas reservoir:

$$r = \frac{G_p}{G} = \frac{B_g - B_{gi}}{B_g} + \frac{\frac{B_{gi} S_{wi}}{1 - S_{wi}} \left[\frac{B_{tw}}{B_{twi}} - 1 + \frac{c_f (p_i - p)}{S_{wi}} \right]}{B_g} \quad [3.3.33]$$

where:

r = recovery factor
B_g = gas formation volume factor, bbl/scf
c_f = formation compressibility, psi^{-1}
B_{tw} = two-phase water formation volume factor, bbl/STB
B_{twi} = initial two-phase water formation volume factor, bbl/STB

The water two-phase formation volume factor (FVF) is determined from:

$$B_{tw} = B_w + B_g (R_{swi} - R_{sw})$$
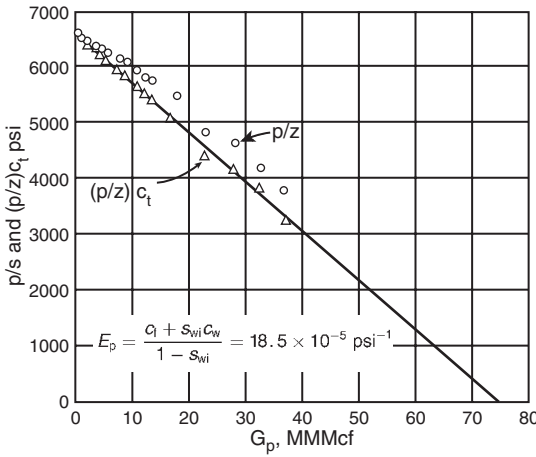
Figure 3.28 *Mobil–David Anderson "L" p/Z versus cumulative production (After Roach, 1981).*
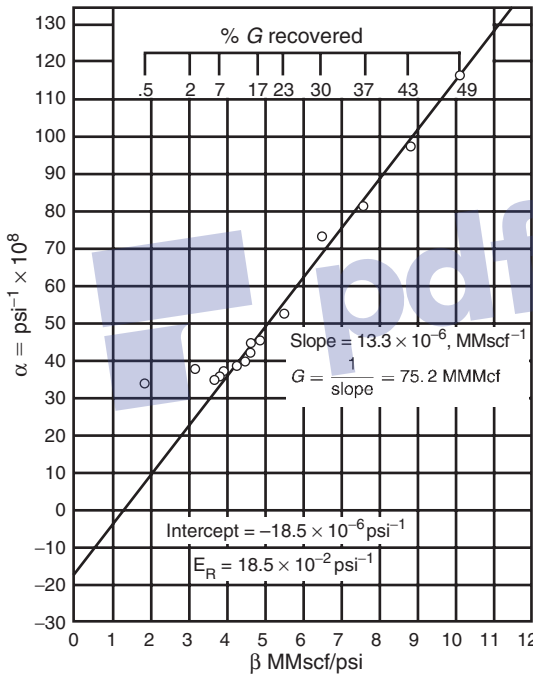
Figure 3.29 *Mobil–David Anderson "L" p/Z gas material balance (After Roach, 1981).*

where:

R_{sw} = gas solubility in the water phase, scf/STB
B_w = water FVF, bbl/STB
B_g = gas FVF, bbl/scf

The following three assumptions are inherent in Equation 3.3.33:

(1) a volumetric, single-phase gas reservoir;
(2) no water production;
(3) the formation compressibility c_f remains constant over the pressure drop $(p_i - p)$.

The authors point out that the change in water compressibility c_w is implicit in the change of B_{tw} with pressure as determined above.

Begland and Whitehead suggested that because c_f is pressure dependent, Equation 3.3.33 is not correct as reservoir pressure declines from the initial pressure to some value several hundred psi lower. The pressure dependence of c_f can be accounted for in Equation 3.3.33 and is solved in an incremental manner.

Modified Roach plot for pot aquifer gas reservoirs
Assuming that the aquifer can be described adequately by a pot aquifer model with a total water volume of W_{aq}, the MBE can be arranged to give:

$$\frac{(p/Z)_i/(p/Z) - 1}{p_i - p}$$

$$= \frac{1}{G}\left[\frac{(p/Z)_i/(p/Z)\,G_p + \dfrac{W_p B_w}{B_{gi}}}{p_i - p}\right]$$

$$- \left[\frac{S_{wi}c_w + c_f}{1 - S_{wi}} + \frac{(c_w + c_f)W_{aq}}{GB_{gi}}\right]$$

or equivalently as the equation of a straight line:

$$\alpha = \left(\frac{1}{G}\right)\beta - E_R$$

with:

$$\alpha = \frac{\left[(p_i/Z_i)/(p/Z)\right] - 1}{(p_i - p)}$$

$$\beta = \left[\frac{(p_i/Z_i)/(p/Z)\,G_p + \dfrac{W_p B_w}{B_{gi}}}{(p_i - p)}\right]$$

$$E_R = \frac{S_{wi}c_w + c_f}{1 - S_{wi}} + \frac{(c_w + c_f)W_{aq}}{GB_{gi}}$$

Plotting α vs. β will produce a straight line with a correct slope of $1/G$ and constant intercept of E_R.

Fetkovich et al. plot for abnormal pressure gas reservoirs
Fetkovich et al. (1998) adopted the *shale water influx theory* and developed a general gas MBE that accounts for the total *cumulative* effects of the various reservoir compressibilities as well as the total water associated with the reservoir. The "associated" water includes:

• connate water;
• water within interbedded shales and non-pay reservoir rock;
• volume of water in the attached aquifer.

The authors expressed the associated water as a ratio of the total volume of the associated water to that of the reservoir pore volume, or:

$$M = \frac{\text{total associated water volume}}{\text{reservoir pore volume}}$$

where M is a dimensionless volume ratio.

In the development of the general MBE, the authors also introduced the cumulative effective compressibility term $\bar{c}_e$ as defined by:

$$\bar{c}_e = \frac{S_{wi}\bar{c}_w + M(\bar{c}_f + \bar{c}_w) + \bar{c}_f}{1 - S_{wi}} \qquad [3.3.34]$$

where:

$\bar{c}_e$ = cumulative effective compressibility, psi^{-1}
$\bar{c}_f$ = total PV (formation) compressibility, psi^{-1}
$\bar{c}_w$ = cumulative total water compressibility, psi^{-1}
S_{wi} = initial water saturation

The gas MBE can then be expressed as:

$$\frac{p}{Z}\left[1 - \bar{c}_e(p_i - p)\right] = \frac{p_i}{Z_i} - \left[\frac{(p_i/Z_i)}{G}\right]G_p \qquad [3.3.35]$$

The $\bar{c}_e$ function represents the cumulative change in hydrocarbon PV caused by compressibility effects and water influx from interbedded shales and non-pay reservoir rock, and water influx from a small limited aquifer. The effect of the compressibility function $\bar{c}_e$ on the MBE depends strongly on the magnitude of $\bar{c}_w$, $\bar{c}_f$, and the dimensionless parameter M. The non-linear behavior of the p/Z vs. G_p plot is basically attributed to changes in the magnitude of $\bar{c}_e$ with declining reservoir pressure, as follows:

- The first straight line in the "early-time" trend is developed in the abnormal pressure period where the effect of $\bar{c}_w$ and $\bar{c}_f$ (as described by the $\bar{c}_e$ function) is significant.
- The second straight line in the "late-time" trend is a result of increasing the magnitude of the gas compressibility significantly to dominate the reservoir driving mechanism.

The procedure for estimating the initial gas-in-place G from Equation 3.3.35 is summarized in the following steps:

Step 1. Using the available rock and water compressibilities ($\bar{c}_f$ and $\bar{c}_w$ as a function of pressure) in Equation 3.3.34, generate a family of $\bar{c}_e$ curves for several assumed values of the dimensionless volume rates M:

$$\bar{c}_e = \frac{S_{wi}\bar{c}_w + M(\bar{c}_f + \bar{c}_w) + \bar{c}_f}{1 - S_{wi}}$$

Step 2. Assume a range of values for G with the largest value based on extrapolation of the early depletion data, and the lowest value being somewhat larger than the current G_p. For an *assumed value* of G, calculate $\bar{c}_e$ from Equation 3.3.35 for each measured p/Z and G_p data point, or:

$$\bar{c}_e = \left[1 - \frac{(p/Z)_i}{(p/Z)}\left(1 - \frac{G_p}{G}\right)\right]\frac{1}{p_i - p}$$

Step 3. For a given assumed value of G, plot the calculated values of $\bar{c}_e$ from step 2 as a function of pressure and repeat for all other values of G. This family of $\bar{c}_e$ curves is essentially generated independently from the MBE to *match* the $\bar{c}_e$ values as calculated in step 1.

Step 4. The match gives G, the M value, and the $\bar{c}_e$ function that can be used to predict the p/Z vs. G_p plot by rearranging Equation 3.3.35 and assuming several values of p/Z and calculating the corresponding G_p, to give:

$$G_p = G\left\{1 - \left(\frac{Z_i}{p_i}\frac{p}{Z}\right)\left[1 - \bar{c}_e(p_i - p)\right]\right\}$$

Paston et al. plot for abnormal pressure gas reservoirs
Harville and Hawkins (1969) attributed the concave-downward shape of the p/Z vs. G_p curve for overpressured gas reservoirs to pore collapse and formation compaction. Hammerlindl (1971) calculated the changes in the PV and indicated that the system isothermal compressibility changed from 28×10^{-6} psi^{-1} at initial conditions to 6×10^{-6} psi^{-1} at final condition. Poston and Berg (1997) suggested

that the gas MBE can be arranged to solve for the original gas-in-place, formation compressibility, and water influx values simultaneously. The MBE as presented by Equation 3.3.17 can be rearranged to give:

$$\frac{1}{\Delta p}\left[\left(\frac{p_i Z}{pZ_i}\right) - 1\right] = \left(\frac{1}{G}\right)\left[\left(\frac{Zp_i}{Z_i p}\right)\left(\frac{G_p}{\Delta p}\right)\right] - (c_e + W_{en})$$

where the energy term for the net water influx W_{en} and effective compressibility c_e are given by:

$$W_{en} = \frac{(W_e - W_p)B_w}{\Delta p G B_{gi}}$$

$$c_e = \frac{c_w S_{wi} + c_f}{1 - S_{wi}}$$

where:

G = gas initially in place, scf
B_{gi} = initial gas FVF, bbl/scf
c_w = water compressibility coefficient, psi^{-1}
$\Delta p = p_i - p$

The above form of the MBE indicates that for a volumetric gas reservoir (i.e., $W_e = 0$) with a constant effective compressibility, a plot of the left-hand side of the equation versus $(Zp_i/Z_i p)(G_p/\Delta p)$ would produce a straight line with a slope of $1/G$ and a negative intercept of $-c_e$ that can be used to solve the above equation for the formation compressibility c_f, to give:

$$c_f = -c_e(1 - S_{wi}) - c_w S_{wi}$$

Experience has shown that c_f values should range over $6 \times 10^{-6} < c_f < 25 \times 10^{-6}$ psi^{-1}, a value over 25×10^{-6} as calculated from the above expression; that is, c_e, might indicate water influx.

Hammerlindl method for abnormal pressure gas reservoirs
Hammerlindl (1971) proposed two methods to correct apparent gas-in-place G_{app} obtained by extrapolation of the early straight-line of the p/Z vs. G_p graph. Both methods use the initial reservoir pressure p_i and another average reservoir pressure p_1 at some time while the reservoir is still behaving as an abnormally pressured reservoir. The proposed mathematical expressions for both methods are given below.

Method I Hammerlindl suggested that the actual gas-in-place G can be estimated by correcting the apparent gas-in-place G_{app} by incorporating the ratio R of the effective total system compressibility to the gas compressibility, to give:

$$G = \frac{G_{app}}{R}$$

with:

$$R = \frac{1}{2}\left(\frac{c_{eff,i}}{c_{gi}} + \frac{c_{eff,1}}{c_{g1}}\right)$$

where the effective total system compressibility $c_{eff,i}$ at the initial reservoir pressure and the effective system compressibility $c_{eff,1}$ at reservoir pressure p_1 are given by:

$$c_{eff,i} = \frac{S_{gi}c_{gi} + S_{wi}c_{wi} + c_f}{S_{gi}}$$

$$c_{eff,1} = \frac{S_{gi}c_{g1} + S_{wi}c_{w1} + c_f}{S_{gi}}$$

where:

p_i = initial reservoir pressure, psi
p_1 = average reservoir pressure during the abnormally pressured behavior, psi
c_{gi} = gas compressibility at p_i, psi^{-1}
c_{g1} = gas compressibility at p_1, psi^{-1}
c_{wi} = water compressibility at p_i, psi^{-1}
c_{w1} = water compressibility at p_1, psi^{-1}
S_{wi} = initial water saturation

Method II Hammerlindl's second method also uses two pressures p_i and p_1 to compute actual gas-in-place from the following relationship:

$$G = \text{Corr } G_{app}$$

where the correction factor "Corr" is given by:

$$\text{Corr} = \frac{(B_{g1} - B_{gi})S_{gi}}{(B_{g1} - B_{gi})S_{gi} + B_{gi}(p_i - p_1)(c_f + c_w S_{wi})}$$

and B_g is the gas formation volume factor at p_i and p_1 as expressed in ft^3/scf by:

$$B_g = 0.02827 \frac{ZT}{p}$$

Effect of gas production rate on ultimate recovery
Volumetric gas reservoirs are essentially depleted by expansion and, therefore, the ultimate gas recovery is independent of the field production rate. The gas saturation in this type of reservoirs is never reduced, only the number of pounds of gas occupying the pore spaces is reduced. Therefore, it is important to reduce the abandonment pressure to the lowest possible level. In closed gas reservoirs, it is not uncommon to recover as much as 90% of the initial gas-in-place.

Cole (1969) pointed out that for water drive gas reservoirs, recovery may be rate dependent. There are two possible influences which producing rate may have on ultimate recovery. First, in an active water drive reservoir, the abandonment pressure may be quite high, sometimes only a few psi below initial pressure. In such a case, the gas remaining in the pore spaces at abandonment will be relatively great. However, the encroaching water reduces the initial gas saturation. Therefore, the high abandonment pressure is somewhat offset by the reduction in initial gas saturation. If the reservoir can be produced at a rate greater than the rate of water influx rate, without water coning, then a high producing rate could result in maximum recovery by taking advantage of a combination of reduced abandonment pressure and reduction in initial gas saturation. Second, the water-coning problems may be very severe in gas reservoirs, in which case it will be necessary to restrict withdrawal rates to reduce the magnitude of this problem.

Cole suggested that recovery from water drive gas reservoirs is substantially less than recovery from closed gas reservoirs. As a rule of thumb, recovery from a water drive reservoir will be approximately 50% to 0% of the initial gas-in-place. The structural location of producing wells and the degree of water coning are important considerations in determining ultimate recovery. A set of circumstances could exist—such as the location of wells very high on the structure with very little coning tendencies—where water drive recovery would be greater than depletion drive recovery. Abandonment pressure is a major factor in determining recovery efficiency, and permeability is usually the most important factor in determining the magnitude of the abandonment pressure. Reservoirs with low permeability will have higher abandonment pressures than reservoirs with high permeability. A certain minimum flow rate must be sustained, and a higher permeability will permit this minimum flow rate at a lower pressure.

3.4 Coalbed Methane (CBM)

The term "coal" refers to sedimentary rocks that contain more than 50% by weight and more than 70% by volume of organic materials consisting mainly of carbon, hydrogen, and oxygen in addition to inherent moisture. Coals generate an extensive suite of hydrocarbons and non-hydrocarbon components. Although the term "methane" is used frequently in the industry, in reality the produced gas is typically a mixture of C_1, C_2, traces of C_3, and heavier N_2 and CO_2. Methane, as one such hydrocarbon constituent of coal, is of special interest for two reasons:

(1) Methane is usually present in high concentration, in coal, depending on composition, temperature, pressure, and other factors.
(2) Of the many molecular species trapped within coal, methane can be easily liberated by simply reducing the pressure in the bed. Other hydrocarbon components are tightly held and generally can be liberated only through different extraction methods.

Levine (1991) suggested that the materials comprising a coalbed fall broadly into the following two categories:

(1) "Volatile" low-molecular-weight materials (components) that can be liberated from the coal by pressure reduction, mild heating, or solvent extraction.
(2) Materials that will remain in the solid state after the separation of volatile components.

Most of the key data needed for estimating gas-in-place and performing other performance calculations is obtained mainly from the following core tests:

- *Canister desorption tests*: These tests are conducted on coal samples to determine:
    - the total adsorbed gas content G_c of the coal sample as measured in scf/ton of coal;
    - desorption time t that is defined by the time required to disrobe 63% of the total adsorbed gas.
- *Proximate tests:* These tests are designed to determine coal composition in terms of:
    - percentage of ash;
    - fixed carbon;
    - moisture content;
    - volatile matter.

Remner et al. (1986) presented a comprehensive study on the effects of coal seam properties on the coalbed methane drainage process. The authors pointed out that reservoir characteristics of coalbeds are complex because they are naturally fractured reservoirs that are characterized by two distinct porosity systems, i.e. dual-porosity systems. These are:

(1) *Primary porosity system:* The matrix primary porosity system in these reservoirs is composed of very fine pores, "micropores," with extremely low permeability. These micropores contain a large internal surface area on which substantial quantities of gas may be adsorbed. With such low permeability, the primary porosity is both impermeable to gas and inaccessible to water. However, the desorbed gas can flow (transport) through the primary porosity system by the diffusion process, as discussed later in this section. The micropores are essentially responsible for most of the porosity in coal.
(2) *Secondary porosity system:* The secondary porosity system (macropores) of coal seams consists of the natural fracture network of cracks and fissures inherent in all coals. The macropores, known as cleats, act as a sink to the primary porosity system and provide the permeability for fluid flow. They act as conduits to the production
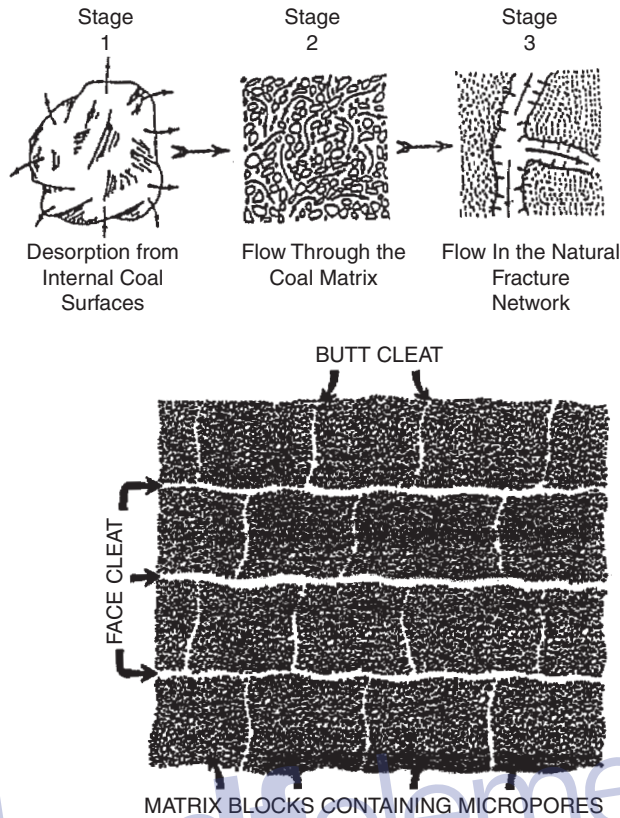
Figure 3.30 *Schematic of methane flow dynamics in a coal seam system (After King et al., 1986).*

wells as shown in Figure 3.30. The cleats are mainly composed of the following two major components:

(a) *The face cleat*: The face cleat, as shown conceptually in Figure 3.30 by Remner et al., is continuous throughout the reservoir and is capable of draining large areas.
(b) *The butt cleat*: Butt cleats contact a much smaller area of the reservoir and thus are limited in their drainage capacities.

In addition to the cleat system, a fracture system caused by tectonic activity may also be present in coals. Water and gas flow to coalbed methane wells occurs in the cleat and fracture systems. These cleats and fractures combine to make up the bulk permeability measured from well tests conducted on coalbed methane wells.

The bulk of the methane, i.e., gas-in-place, is stored in an adsorbed state on internal coal surfaces and is considered a near liquid-like state as opposed to a free gas phase. The coal cleats are considered initially saturated with water and must be removed (produced) from the natural fractures, i.e., cleats, to lower the reservoir pressure. When the pressure is reduced, the gas is released (desorbed) from the coal matrix into the fractures. The gas production is then controlled by a four-step process that includes:

Step 1. Removal of water from the coal cleats and lowering the reservoir pressure to that of the gas desorption pressure. This process is called dewatering the reservoir.
Step 2. Desorption of gas from the coal internal surface area.

Step 3. Diffusion of the desorbed gas to the coal cleat system.
Step 4. Flow of the gas through fractures to the wellbore.

The economical development of coalbed methane (CBM) reservoirs depends on the following four coal seam characteristics:

(1) gas content G_c;
(2) density of the coal ρ_B
(3) deliverability and drainage efficiency;
(4) permeability and porosity.

Hughes and Logan (1990) pointed out that an economic reservoir must first contain a sufficient amount of adsorbed gas (gas content), must have adequate permeability to produce that gas, have enough pressure for adequate gas storage capacity, and, finally, the desorption time must be such that it is economical to produce that gas. These four characteristic coal seam parameters that are required to economically develop the reservoir are discussed below.

3.4.1 Gas content
The gas present in the coal is molecularly adsorbed on the coal's extensive surface area. Gas content estimation methods involve placing freshly cut reservoir coal samples in airtight gas desorption canisters and measuring the volume of gas that desorbs as a function of time at ambient temperature and pressure conditions. A disadvantage of this analysis procedure is that the measured desorbed gas volume is not equal to the total gas content since a large amount of gas is commonly lost by desorption during sample recovery.
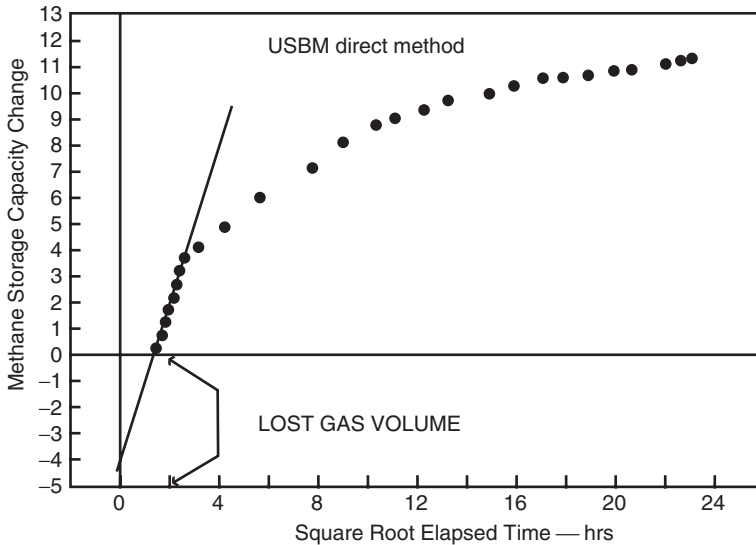
Figure 3.31 *Plot of test data used to determine lost gas volume.*

The volume of gas lost during this core recovery time is referred to as "lost gas." The volume of the lost gas can be estimated by using the USBM direct method, as illustrated in Figure 3.31. The method simply involves plotting the desorbed gas volume versus the square root of time, $\sqrt{t}$, on a Cartesian scale and extrapolating the early-time desorption data back to time zero. Experience has shown that this technique works adequately in shallow, low-pressure, low-temperature coals with a lost gas volume in the range of 5–10% of the total adsorbed gas content of the coal. However, in higher-pressure coal seams, the lost gas volume may exceed 50% of the total adsorbed gas content.

It should be pointed out that some of the gas may not desorb from coal by the end of desorption measurements and remains absorbed in the core sample. The term "residual gas" is commonly referred to the gas that remains at the end of the desorption test. McLennan and Schafer (1995) and Nelson (1999) pointed out that the rate of gas desorption from coals is so very slow that impractically long time intervals would be required for complete gas desorption to occur. This residual gas content remaining at the end of desorption measurements is determined by crushing the sample and measuring the released gas volume. The chief limitation of this direct method analysis procedure is that it yields different gas content values depending upon the coal sample type, gas desorption testing conditions, and lost gas estimation method. Nelson (1999) pointed out that the failure to quantify and account for any residual gas volume that may remain in the coal sample at the end of gas desorption measurements would result in significant underestimation error in coalbed gas-in-place evaluations. This residual gas volume can be a significant fraction, ranging between 5% and 50%, of the total adsorbed gas content.

Another important laboratory measurement is known as the "sorption isotherm" and is required to relate the gas storage capacity of a coal sample to pressure. This information is required to predict the volume of gas that will be released from the coal as the reservoir pressure declines. *Note that the gas content G_c is a measurement of the actual (total) gas contained in a given coal reservoir, while the sorption isotherm defines the relationship of pressure to the capacity of a given coal to hold gas at a constant temperature.*

Accurate determinations of both gas content and the sorption isotherm are required to estimate recoverable reserve and production profiles. An example of a typical sorption isotherm relationship is shown in Figure 3.32 as given by Mavor et al. (1990). This sorption isotherm was measured on a sample collected from a well in the Fruitland Formation Coal Seam of the San Juan Basin, New Mexico. The authors pointed out that the total gas content G_c of the coal was determined to be 355 scf/ton by desorption canister tests performed on whole core samples at the well location. The gas content is less than the sorption isotherm gas storage capacity of 440 scf/ton at the initial reservoir pressure of 1620 psia. This implies that the pressure must be reduced to 648 psia which corresponds to 355 scf/ton on the sorption isotherm curve. This pressure is known as the critical or desorption pressure p_d. This value will determine whether a coal seam is saturated or undersaturated. A saturated coal seam holds as much adsorbed gas as it possibly can for the given reservoir pressure and temperature. An analogy would be an oil reservoir having a bubble point equal to the initial reservoir pressure. If the initial reservoir pressure is greater than the critical desorption pressure, the coalbed is considered an undersaturated one as in the case of Fruitland Formation Coal. An undersaturated coal seam is undesirable since more water will have to be produced (dewatering process) before gas begins to flow.

For an undersaturated reservoir, i.e., $p_i > p_d$, the total volume of water that must be removed to drop from the initial reservoir pressure p_i to the desorption pressure p_d can be estimated from the total isothermal compressibility coefficient:

$$c_t = \frac{1}{W_i} \frac{W_p}{p_i - p_d} \qquad [3.4.1]$$

where:

W_p = total volume of water removed, bbl
W_i = total volume of water in the reservoir (area), bbl
p_i = initial reservoir pressure, psi
p_d = desorption pressure, psi
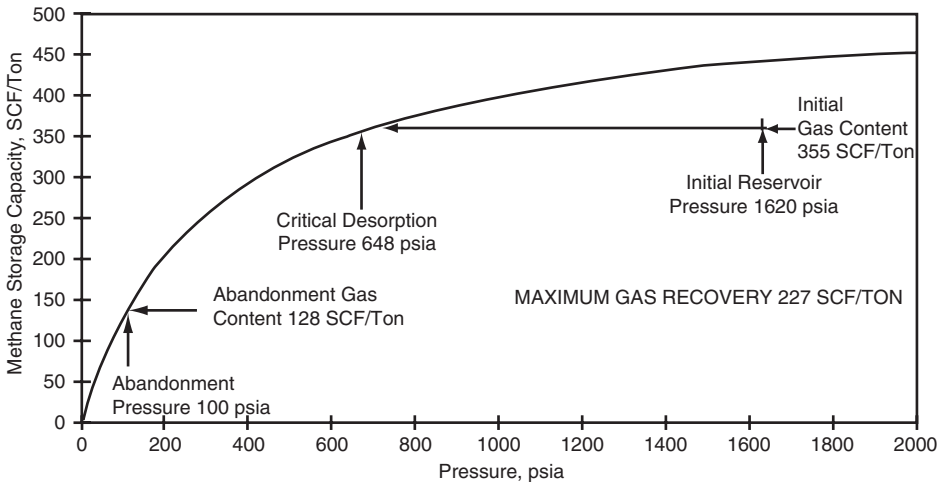
Figure 3.32 *Sorption isotherm curve (After Mavor et al. 1990).*

c_t = total system compressibility coefficient in psi^{-1} as given by:

$$c_t = c_w + c_f$$

with:

c_w = water compressibility
c_f = formation compressibility

Solving Equation 3.4.1 for water removed gives:

$$W_p = c_t W_i (p_i - p_d) \qquad [3.4.2]$$

Example 3.9 An undersaturated coal system has the following reservoir parameters:

Drainage area = 160 acres,   thickness = 15 ft,   porosity = 3%

Initial pressure = 650 psia,   desorption pressure = 450 psia,

total compressibility = 16×10^{-5} psi^{-1}

Estimate the total volume of water that must be produced for the reservoir pressure to decline from initial pressure to desorption pressure.

Solution

Step 1. Calculate the total volume of water initially in the drainage area:

$$W_i = 7758 A h \phi S_{wi}$$

$$W_i = 7758(160)(15)(0.03)(1.0) = 558\,576 \text{ bbl}$$

Step 2. Estimate the total water volume to be produced to reach the desorption pressure from Equation 3.4.2:

$$W_p = 16(10^{-5})(558\,576)(650 - 450) = 17\,874 \text{ bbl}$$

Step 3. Assuming the area is being drained with only one well that is discharging at 300 bbl/day, the total time to reach the desorption pressure is:

$$t = 17\,874/300 = 60 \text{ days}$$

For most coal seams, the quantity of gas held in the coal is primarily a function of coal rank, ash content, and the initial reservoir pressure. The adsorbed capacity of the coal seam varies non-linearly with pressure. A common method of utilizing sorption isotherm data is to assume that the relationship between gas storage capacity and pressure can be described by a relationship that was originally proposed

by Langmuir (1918). The sorption isotherm data that fits this relationship is known as a "Langmuir isotherm" and is given by:

$$V = V_L \frac{p}{p + p_L} \qquad [3.4.3]$$

where:

V = volume of gas currently adsorbed at p, scf/ft^3 of coal
V_L = Langmuir's volume, scf/ft^3
p_L = Langmuir's pressure, psi
p = reservoir pressure, psi

Because the amount of gas adsorbed depends on mass of coal, not volume, a more useful form of the Langmuir equation which expresses the adsorbed volume in scf/ton is:

$$V = V_m \frac{bp}{1 + bp} \qquad [3.4.4]$$

where:

V = volume of gas currently adsorbed at p, scf/ton
V_m = Langmuir's isotherm constant, scf/ton
b = Langmuir's pressure constant, psi^{-1}
p = pressure, psi

The two sets of Langmuir's constants are related by:

$$V_L = 0.031214 V_m \rho_B$$

and:

$$p_L = \frac{1}{b}$$

where ρ_B is the bulk density of the coal deposit in gm/cm^3.

The Langmuir pressure b and volume V_m can be estimated by fitting the sorption isotherm data to Equation 3.4.4. The equation can be linearized as follows:

$$V = V_m - \left(\frac{1}{b}\right) \frac{V}{p} \qquad [3.4.5]$$

The above relationship suggests that a plot of the desorbed gas volume V versus the ratio V/p on a Cartesian scale would produce a straight line with a slope of $-1/b$ and intercept of V_m.

Similarly, when expressing the adsorbed gas volume in scf/ft^3, Equation 3.4.3 can be expressed as the equation of a
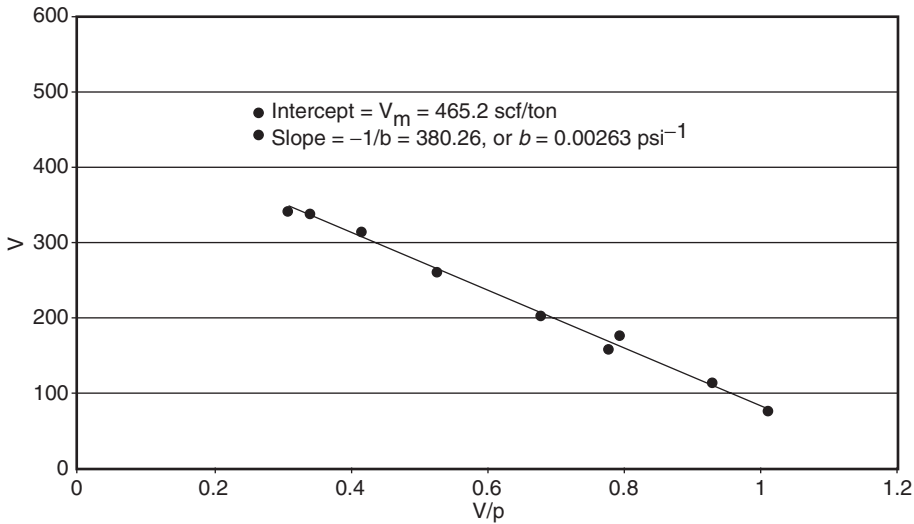
Figure 3.33   *Volume V versus the ratio V/p of Example 3.10.*

straight line to give:

$$V = V_L - p_L \left(\frac{V}{p} \right)$$

A plot of V in scf/ft^3 as a function V/P would produce a straight line with an intercept of V_L and a negative slope of $-p_L$.

Example 3.10   The following sorption isotherm data is given by Mavor et al. (1990) for a coal sample from the San Juan Basin:

p (psi)	76.0	122.0	205.0	221.0	305.0	504.0	507.0	756.0	1001.0	1008.0
V (scf/ton)	77.0	113.2	159.8	175.0	206.4	265.3	267.2	311.9	339.5	340.5

Calculate the Langmuir isotherm constant V_m and the Langmuir pressure constant b for the San Juan Basin coal sample.

Solution

Step 1.   Calculate V/p for each of the measured data points and construct the following table:

p	V	V/p
76.0	77.0	1.013158
122.0	113.2	0.927869
205.0	159.8	0.779512
221.0	175.0	0.791855
305.0	206.4	0.676721
504.0	265.3	0.526389
507.0	267.2	0.527022
756.0	311.9	0.412566
1001.0	339.5	0.339161
1108.0	340.5	0.307310

Step 2.   Plot V vs. V/p on a Cartesian scale, as shown in Figure 3.33, and draw the best straight line through the points.

Step 3.   Determine the coefficient of the straight line, i.e., slope and intercept, to give:

Intercept $= V_m = 465.2$ scf/ton

Slope $= -1/b = -380.26$, or $b = 0.00263$ psi^{-1}

Step 4.   The Langmuir equation, i.e., Equation 3.4.4, can be written as:

$$V = 465.2 \frac{0.00263p}{1 + 0.00263p}$$

Seidle and Arrl (1990) proposed that the desorbed gas will begin to flow through the cleats at the time that is required for a well to reach the semisteady-state. For a gas well centered in a circular or square drainage area, the semisteady-state flow begins when the dimension time t_{DA} is 0.1, or:

$$t_{DA} = 0.1 = \frac{2.637(10^{-4})k_g t}{\phi(\mu_g c_t)_i A}$$

Solving for the time t gives:

$$t = \frac{379.2\phi(\mu_g c_t)_i A}{K_g}$$

where:

t = time, hours
A = drainage area, ft^2
k_g = gas effective compressibility, md
ϕ = cleat porosity, fraction
μ_g = gas viscosity, cp
c_t = total system compressibility, psi^{-1}

Both gas viscosity and system compressibility are calculated at the desorption pressure. The total system compressibility is given by:

$$c_t = c_p + S_w c_w + S_g c_g + c_s$$

where:

c_p = cleat volume compressibility, psi^{-1}
S_w = water saturation

S_g = gas saturation
c_w = water compressibility, psi^{-1}
c_g = gas compressibility, psi^{-1}
c_s = apparent sorption compressibility, psi^{-1}

The authors pointed out that the adsorption of the gas on the coal surface increases the total system compressibility by c_s, i.e., apparent sorption compressibility, that is given by:

$$c_s = \frac{0.17525 B_g V_m \rho_B b}{\phi(1 + b p)^2} \qquad [3.4.6]$$

where:

B_g = gas formation volume factor, bbl/scf
ρ_B = bulk density of the coal deposit, gm/cm^3
V_m, b = Langmuir's constants

Example 3.11 In addition to the data given in Example 3.10 for the San Juan coal, the following properties are also available:

$\rho_B = 1.3$ g/cm^3, $\quad \phi = 2\%$, $\quad T = 575°R$

$p_d = 600$ psi, $\quad S_w = 0.9$, $\quad S_g = 0.1$

$c_f = 15 \times 10^{-6}$ psi^{-1}, $\quad c_w = 10 \times 10^{-6}$ psi^{-1},

$c_g = 2.3 \times 10^{-3}$ psi^{-1}

$A = 40$ acres, $\quad k_g = 5$ md, $\quad \mu_g = 0.012$ cp

$Z =$ factor at 600 psi $= 0.86$

Calculate the time required to achieve the semisteady state.

Solution

Step 1. From Example 3.10:

$$V_m = 465.2 \text{ scf/ton}$$

$$b = 0.00263 \text{ psi}^{-1}$$

Step 2. Calculate B_g in bbl/scf from Equation 3.2.6 or:

$$B_g = 0.00504 \frac{ZT}{P}$$

$$= 0.00504 \frac{(0.86)(575)}{600} = 0.00415 \text{ bbl/scf}$$

Step 3. Apply Equation 3.4.6 to calculate c_s to give:

$$c_s = \frac{0.17525(0.00415)(465.2)(1.3)(0.00263)}{0.02[1 + (0.00263)(600)]^2}$$

$$= 8.71 \times 10^{-3} \text{ psi}^{-1}$$

Step 4. Calculate c_t:

$$c_t = 15(10^{-6}) + 0.9(10)(10^{-6}) + 0.1(2.3)(10^{-3})$$

$$+ 8.71(10^{-3}) = 0.011 \text{ psi}^{-1}$$

Step 5. Calculate the time to reach semisteady state:

$$t = \frac{(379.2)(0.03)(0.012)(0.011)(40)(43560)}{5}$$

$$= 523 \text{ hours}$$

Seidle and Arrl (1990) proposed the use of conventional black-oil simulators to model the production behavior of coalbed methane. The authors pointed out that the amount of gas held by coal at a given pressure is analogous to the amount of gas dissolved in a crude oil system at a given pressure. The Langmuir isotherm of coalbeds is comparable to the solution gas–oil ratio R_s of conventional oil reservoirs. A conventional reservoir simulator can be used to describe

coalbed methane by treating the gas adsorbed to the surface of the coal as a dissolved gas in immobile oil.

Seidle and Arrl suggested that the introduction of the oil phase requires increasing the porosity and altering the initial saturations. The gas–water relative permeability curves must be modified and fluid properties of the immobile oil must be also adjusted. The required adjustments for use in a conventional black-oil simulator are summarized below:

Step 1. Select any arbitrary initial oil saturation S_{om} for the model, with the subscript m denoting a model value. The initial value may be set as the residual oil saturation and must remain constant throughout the simulation.

Step 2. Adjust the actual coalbed cleat porosity ϕ_m by the following expression:

$$\phi_m = \frac{\phi}{1 - S_{om}} \qquad [3.4.7]$$

Step 3. Adjust the actual water and gas saturations, i.e., S_w and S_g, to equivalent model saturations S_{wm} and S_{gm} from:

$$S_{wm} = (1 - S_{om})S_w \qquad [3.4.8]$$

$$S_{gm} = (1 - S_{om})S_g \qquad [3.4.9]$$

These two equations are used to adjust gas–water relative permeability data for input into the simulator. The relative permeability corresponding to the actual S_g or S_w is assigned to the equivalent model saturation S_{gm} or S_{wm}.

Step 4. To ensure that the oil phase will remain immobile, assign a zero oil relative permeability $K_{ro} = 0$ for all saturations and/or specifying a very large oil viscosity, i.e., $\mu_o = 10^6$ cp.

Step 5. To link the gas dissolved in the immobile oil, i.e., R_s in immobile oil, convert the sorption isotherm data to gas solubility data using the following expression:

$$R_s = \left(\frac{0.17525 \rho_B}{\phi_m S_{om}}\right) V \qquad [3.4.10]$$

where:

R_s = equivalent gas solubility, scf/STB
V = gas content, scf/STB
ρ_B = bulk coal seam density, g/cm^3

Equation 3.4.10 can be expressed equally in terms of Langmuir's constants by replacing the gas content V with Equation 3.4.4 to give:

$$R_s = \left(\frac{0.17525 \rho_B}{\phi_m S_{om}}\right)(V_m)\left(\frac{b p}{1 + b p}\right) \qquad [3.4.11]$$

Step 6. To conserve mass over the course of simulation, the oil formation volume factor must be constant with a value of 1.0 bbl/STB.

Using the relative permeability and coal seam properties as given by Ancell et al. (1980) and Seidle and Arrl (1990), the following example illustrates the use of the above methodology.

Example 3.12 The following coal seam properties and relative permeability are available:

$S_{gi} = 0.0$, $\quad V_m = 660$ scf/ton, $\quad b = 0.00200$ psi^{-1}

$\rho_B = 1.3$ g/cm^3, $\quad \phi = 3\%$

S_g	$S_w = 1 - S_g$	K_{rg}	K_{rw}
0.000	1.000	0.000	1.000
0.100	0.900	0.000	0.570
0.200	0.800	0.000	0.300
0.225	0.775	0.024	0.256
0.250	0.750	0.080	0.210
0.300	0.700	0.230	0.140
0.350	0.650	0.470	0.090
0.400	0.600	0.750	0.050
0.450	0.550	0.940	0.020
0.475	0.525	0.980	0.014
0.500	0.500	1.000	0.010
0.600	0.400	1.000	0.000
1.000	0.000	1.000	0.000

Adjust the above relative permeability data and convert the sorption isotherm data into gas solubility for use in a black-oil model.

Solution

Step 1. Select any arbitrary initial oil saturation, to get:

$$S_{om} = 0.1$$

Step 2. Adjust the actual cleat porosity by using Equation 3.4.7:

$$\phi_m = \frac{0.03}{1 - 0.1} = 0.0333$$

Step 3. Retabulate the relative permeability data by only readjusting the saturation values using Equations 3.4.8 and 3.4.9, to give:

S_g	S_w	$S_{gm} = 0.9S_g$	$S_{wm} = 0.9S_w$	k_{rg}	k_{rw}
0.0000	1.0000	0.0000	0.9000	0.0000	1.0000
0.1000	0.9000	0.9000	0.8100	0.0000	0.5700
0.2000	0.8000	0.1800	0.7200	0.0000	0.3000
0.2250	0.7750	0.2025	0.6975	0.0240	0.2560
0.2500	0.7500	0.2250	0.6750	0.0800	0.2100
0.3000	0.7000	0.2700	0.6300	0.2300	0.1400
0.3500	0.6500	0.3150	0.5850	0.4700	0.0900
0.4000	0.6000	0.3600	0.5400	0.7500	0.0500
0.4500	0.5500	0.4045	0.4950	0.9400	0.0200
0.4750	0.5250	0.4275	0.4275	0.9800	0.0140
0.5000	0.5000	0.4500	0.4500	1.0000	0.0100
0.6000	0.4000	0.5400	0.3600	1.0000	0.0000
1.0000	0.0000	0.9000	0.0000	1.0000	0.0000

Step 4. Calculate R_s from either Equation 3.4.8 or 3.4.9 at different assumed pressures:

$$R_s = \left[\frac{(0.17525)(1.30)}{(0.0333)(0.1)} \right] V = 68354V$$

with:

$$V = (660) \frac{0.0002p}{1 + 0.002p}$$

to give:

p (psia)	V (scf/ton)	R_s (scf/STB)
0.0	0.0	0.0
50.0	60.0	4101.0
100.0	110.0	7518.0
150.0	152.3	10520.0
200.0	188.6	12890.0
250.0	220.0	15040.0
300.0	247.5	16920.0

p (psia)	V (scf/ton)	R_s (scf/STB)
350.0	271.8	18570.0
400.0	293.3	20050.0
450.0	312.6	21370.0
500.0	330.0	22550.0

For pressures below the critical desorption pressure, the fractional gas recovery could be roughly estimated from the following relationship:

$$RF = 1 - \left[\left(\frac{V_m}{G_c} \right) \left(\frac{bp}{1 + bp} \right) \right]^a \qquad [3.4.12]$$

where:

RF = gas recovery factor
V_m, b = Langmuir's constants
V = gas content at pressure p, scf/ton
G_c = gas content at critical desorption pressure, scf/ton
p = reservoir pressure, psi
a = recovery exponent

The recovery exponent a is included to account for the deliverability, heterogeneity, and well spacing, among other factors that affect the gas recovery. The recovery exponent usually ranges between 0.5 and 0.85 and can be estimated from the recorded field recovery factor at pressure p. A detailed discussion of the MBE calculations and predicting the recovery performance of coal seems are presented later in this chapter.

Example 3.13 In addition to the data given in Example 3.10, the following information is also available:

$$G_c = 330 \text{ scf/ton at } 500 \text{ psia}, \quad a = 0.82$$

Estimate the gas recovery factor as a function of pressure to an abandonment pressure of 100 psia.

Solution

Step 1. Substitute Langmuir's constants, i.e., V_m and b, and the recovery exponent into Equation 3.4.12, to give:

$$RF = 1 - \left[\left(\frac{660}{330} \right) \left(\frac{0.002p}{1 + 0.002p} \right) \right]^{0.82}$$

$$= 1 - \left[\frac{0.0004p}{1 + 0.002p} \right]^{0.82}$$

Step 2. Assume several reservoir pressures and calculate the recovery factor in the following tabulated form:

p (psi)	RF (%)
450	4.3
400	9.2
350	14.7
300	21.0
250	28.3
200	36.8
150	47.0
100	59.4

Many factors influence the measured gas content G_c and sorption isotherm and, consequently, affect the determination of the initial gas-in-place. Among these factors are:

- moisture content of the coal;
- temperature;
- rank of the coal.
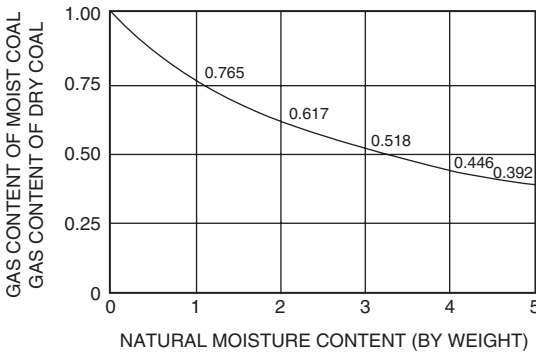
Figure 3.34 *Effect of moisture content on gas storage capacity.*
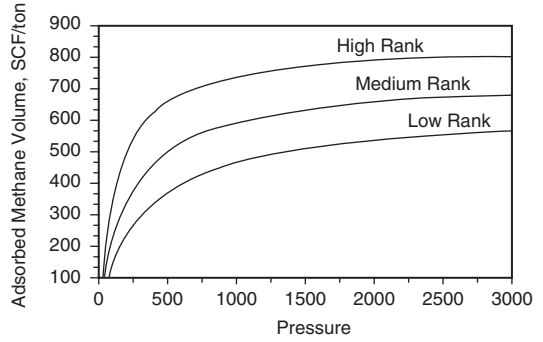
Figure 3.36 *Relationship between rank and sorptive capacity.*

These parameters are briefly discussed below.

- *Moisture content:* One of the major difficulties in measuring the gas content and sorption isotherm is the reproduction of the coal content at reservoir conditions. The moisture content of coal is the weight of the water in the coal matrix, not the water contained as free water in the fracture system. The gas storage capacity of coal is significantly affected by moisture content as shown in Figures 3.34 and 3.35. Figure 3.34 illustrates Langmuir isotherms as the moisture increases from 0.37% to 7.41% with apparent reduction of the methane storage capacity. Figure 3.35 shows that the quantity of methane adsorbed in coal is inversely proportional to the inherent moisture content. As evidenced by these two figures, an increase in the moisture content decreases the ability of coal to store gas.

- *Temperature:* This affects both the volume of gas retained by the coal and the rate at which it is desorbed. Numerous laboratory studies confirmed the following two observations:
  (a) the rate of gas desorption from the coal is exponentially dependent upon temperature (i.e., the higher the temperature, the faster the desorption);
  (b) the gas sorption capacity of the coal is inversely proportional to temperature (i.e., the storage capacity of the coal decreases with increasing temperature as shown in Figure 3.34).

- *Rank of the coal:* According to the American Society for Testing and Materials (ASTM), coal rank is the assignment of a distinct maturation level to a coal derived through the measurement of chemical and physical properties of the coal. The properties most commonly used for rank classification include the fixed carbon content, volatile matter content, and calorific value, among older properties. Coal rank determination is important as the capability of the coal to have generated gas is related to the rank of the coal. Figure 3.36 shows that the gas content and the storage capacity of the coal increase with higher coal ranks. Coals with higher ranks have more capacities to both store and generate gas.

3.4.2 Density of the coal

Gas-in-place volume G is the total amount of gas stored within a specific reservoir rock volume. The basic equation used to calculate G is:

$$G = 1359.7 Ah\rho_B G_c \qquad [3.4.13]$$
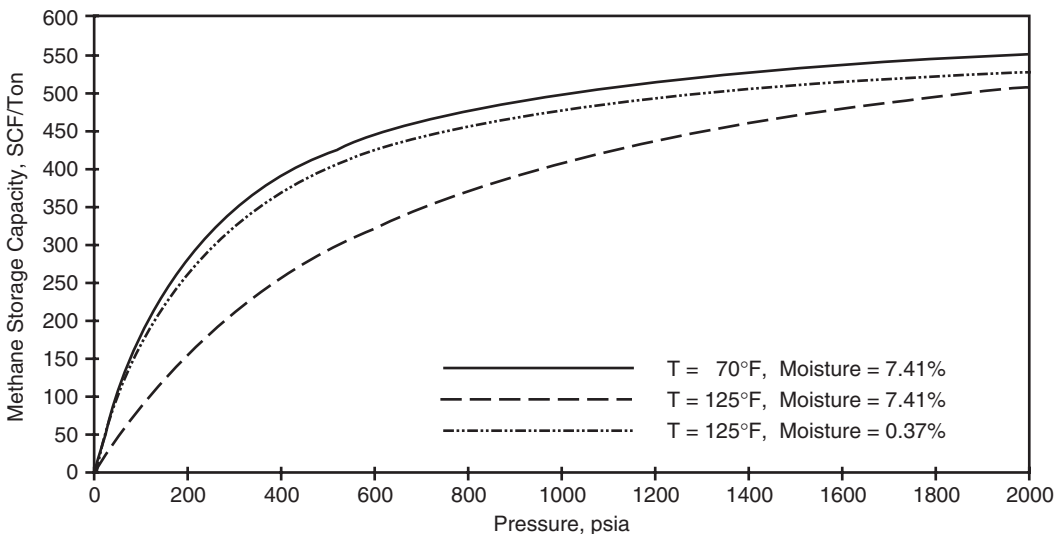
Figure 3.35 *Sorption isotherm temperature and moisture content sensitivity.*

where:

G = initial gas-in-place, scf
A = drainage area, acres
h = thickness, ft
ρ_B = average coal bulk density, g/cm^3
G_c = average gas content, scf/ton

Mavor and Nelson (1997) pointed out that the use of Equation 3.4.13 requires accurate determination of the four parameters in the equation, i.e., A, h, G_c, and ρ_B. The accuracy of G estimates is limited by uncertainties or errors in the parameters. Nelson (1999) pointed out the density of the coal is a strong function of its composition. Since the mineral matter component of coal has a significantly higher density than the bulk organic matter, coal density will be directly correlated to the mineral matter content. Coal density and compositional properties are not uniform throughout the coal seam but vary vertically and laterally as a function of coal rank, moisture content, and mineral matter content, among other depositional environment geological variables. To illustrate the significant vertical and lateral changes in coal density, Mavor and Nelson (1997) used the basal Fruitland Formation coalbed reservoirs at three well locations in the San Juan Basin as examples for this density variation. As shown below, these examples list the variations in ash content, gas content, and average density.

Well	Interval	Avg. ash content (%)	Avg. density (g/cm^3)	Avg. gas content (scf/ton)
1	Intermediate	27.2	1.49	370
	Basal	20.4	1.44	402
2	Intermediate	36.4	1.56	425
	Basal	31.7	1.52	460
3	Intermediate	61.3	1.83	343
	Basal	43.3	1.63	512

It is commonly assumed that interbedded rocks, having densities greater than 1.75 g/cm^3 have negligible gas storage capacity.

Due to its organic richness, coal has a much lower bulk density than, for example, shale or sandstone, and, as a result, the gross thickness of coal-bearing intervals can be readily quantified using geophysical log data. Nelson (1999) pointed out that the commonly used analysis practice for coalbed reservoir thickness is to use 1.75 g/cm^3 as the maximum log density value for the gas-bearing seams. The author stated that the density of ash in San Juan Basin coal is typically 2.4 to 2.5 g/cm^3. The amount of gas stored in coalbed reservoir rocks between the density values of 1.75 and 2.5 g/cm^3 can be significant. This suggests that if the reservoir thickness analysis is based upon a maximum log density value of 1.75 g/cm^3, the calculated gas-in-place volume as expressed by Equation 3.4.13 can greatly underestimate the gas-in-place. It should be pointed out that the moisture content, which varies inversely as a function of coal rank, substantially affects the coal density. As shown by Equation 3.4.13, the gas initially in place G is a function of coal density ρ_c. Neavel et al. (1999), Unsworth et al. (1989), Pratt et al. (1999), and Nelson (1989) observed that high-rank coals (bituminous coals) have a low moisture content of less than 10%, whereas low-rank coals (sub-bituminous coals) have a very high moisture content ($>$25%). The authors pointed out that at 5% ash content, Powder River Basin sub-bituminous coal has a dry-basis density of 1.4 g/cm^3; however, with a moisture content of 27% and ash content of 5%, the density is only 1.33 g/cm^3. This density value difference indicates

how crucial the accurate moisture content is for a reliable estimate of gas-in-place.

3.4.3 Deliverability and drainage efficiency

Interest has grown recently in utilizing the vast resources of coalbed methane reservoirs. As indicated earlier, methane is held in an adsorbed state on the surface of the coal pores by reservoir pressure; this pressure must be reduced to allow desorption of methane from coal surfaces and subsequent methane production. The reservoir pressure is caused by an existing static pressure due to groundwater. Hence, unlike a conventional gas reservoir, gas production is obtained from coal seams by first dewatering and depressurizing the coal seam. Typically, coal seams are naturally fractured and contain laterally extensive, closed, spaced vertical fractures (i.e., cleats). Because the intrinsic permeability of the coal matrix is usually very small, these cleats must be well developed with the minimum required permeability (usually $>$ 1 md) to economically develop the reservoir. Holditch et al. (1988) proposed that to produce gas at economic rates from a coal seam, the following three criteria must be met:

(1) an extensive cleat system must exist to provide the needed permeability;
(2) the gas content must be large enough to provide a source that is worth developing;
(3) the cleat system must be connected to the wellbore.

Therefore, large-scale coalbed methane field development requires significant initial investment before any gas production can occur. Most coalbed methane reservoirs require:

- hydraulic fracture stimulation to supplement the coal cleats and to interconnect the cleat system to the wellbore;
- artificial lift of the reservoir water;
- water disposal facilities;
- complete well pattern development.

In general, proper well spacing and stimulation govern the economic attractiveness of the gas production from coalbeds.

Construction of a complete theory of coal well deliverability is difficult as it is necessary to consider the two-phase flow of gas and water in the coalbed. However, coal wells produce substantial amounts of water before the reservoir pressure declines to the desorption pressure. Once the drainage area of a coal well has been dewatered and the gas rate peaks, water production often declines to negligible rates. This peak in gas rate is essentially a function of:

- the ability of the primary porosity, i.e., porosity of the coal matrix, to supply gas to the secondary porosity system (cleat system);
- the conductivity of the cleat system to water.

Unlike conventional gas and oil reservoirs where minimal well interference is desired, the design of efficient dewatering and depressurizing systems requires maximum well interference for *maximum drawdown*. Well performance in coalbed reservoirs is strongly dependent on this amount of pressure interference between wells which allows the reservoir pressure to be lowered rapidly and consequently allows gas to be released from the coal matrix. This objective can be accomplished by optimizing the following two decision variables:

(1) optimal well spacing;
(2) optimal drilling pattern shape.

Wick et al. (1986) used a numerical simulator to examine the effect of well spacing on single-well production. The investigation examined the recovery factors from a 160 acre

coalbed that contains 1676 MMscf of gas as a function of well spacing for a total of simulation time of 15 years. Results of the study for 20, 40, 80, and 160 acre well spacing are given below:

Well spacing (acres)	Wells on 160 acres	Gas-in-place per well (MMscf)	Cum. gas prod. per well (MMscf)		Recovery factor (%)	Total gas prod. from 160 acres (MMscf)
			5 years	15 years		
160	1	1676	190	417	25	417
80	2	838	208	388	46	776
40	4	419	197	292	70	1170
20	8	209.5	150	178	85	1429

These results suggest that gas recovery over 15 years from an *individual well increases* with larger well spacing, while gas recoveries from the first five years are very similar for the 40, 80, and 160 acre cases. This is largely a result of the need to dewater the drainage area for a particular well before gas production becomes efficient. Percentage gas recovery ranges from 25% on 160 acre spacing to 85% on 20 acre spacing. Drilling on 20 acre spacing produces the most gas from a 160 acre area in 15 years. At this time, 85% of the gas-in-place has been produced but only 25% gas recovery with one well on the 160 acre spacing. In determining optimal well spacing, an *economic evaluation that includes current and predicted future gas price* must be made by the operator to maximize both gas recovery and profit.

Selecting the optimum pattern depends heavily on the following variables:

- the coal characteristics, i.e., isotropic or anisotropic permeability behavior;
- reservoir configuration;
- locations of existing wells and total number of wells;
- initial water pressure and desorption pressure;
- volume of water to be removed and the required drawdown.

3.4.4 Permeability and porosity

Permeability in coals is essentially controlled by the magnitude of the net stress in the reservoir. The variations in the net stress throughout the coal seam can cause local variations in permeability. It has been also shown by several investigators that the coal permeability can increase as gas is desorbed from the coal matrix. Numerous laboratory measurements have shown the dependence of permeability and porosity on the stress conditions in coal seams with relationships that are unique for each coal seam. With the production, cleat properties experience changes due to the following two distinct and opposing mechanisms:

(1) cleat porosity and permeability *decline* due to compaction and the reduction of net stress $\Delta\sigma$;
(2) cleat porosity and permeability *increase* due to coal matrix shrinkage as a result of gas desorption.

Walsh (1981) suggested that the change in the net stress $\Delta\sigma$ can be expressed in terms of reservoir pressure by:

$$\sigma = \sigma - \sigma_o = s(p_o - p) = s\Delta p \qquad [3.4.14]$$

where:

Δp = pressure drop from p_o to p, psi
p_o = original pressure, psia
p = current pressure, psia
σ_o = original effective stress, psia
σ = effective stress, psia
s = constant relating change in psia pressure to change in effective stress

The effective stress is defined as the total stress minus the seam fluid pressure. The effective stress tends to close the cleats and to reduce permeability within the coal. If the effective stress σ is not known, it can be approximated at any given depth D by:

$$\sigma = 0.572D$$

Equation 3.4.14 can be simplified by setting the constant s equal to 0.572, to give:

$$\Delta\sigma = 0.572\Delta p$$

Defining the average pore compressibility by the following expression:

$$\bar{c}_p = \frac{1}{p_o - p} \int_p^{p_o} c_p \, dp$$

where:

$\bar{c}_p$ = average pore compressibility, psi^{-1}
c_p = pore volume compressibility, psi^{-1}

the desired relationships for expressing the changes in porosity and permeability as a function of the reservoir pressure are given by:

$$\phi = \frac{A}{1 + A} \qquad [3.4.15]$$

with:

$$A = \frac{\phi_o}{1 + \phi_o} \exp^{-s\bar{c}_p(\Delta p)} \qquad [3.4.16]$$

and:

$$k = k_o \left(\frac{\phi}{\phi_o}\right)^3$$

where ϕ is the porosity and the subscript o represents the value at initial conditions.

Somerton et al. (1975) proposed a correlation that allows the formation permeability to vary with the changes in the net stress $\Delta\sigma$ as follows:

$$k = k_o \left[\exp\left(\frac{-0.003\Delta\sigma}{(k_o)^{0.1}}\right) + 0.0002\,(\Delta\sigma)^{1/3}\,(k_o)^{1/3}\right]$$

where:

k_o = original permeability at zero net stress, md
k = permeability at net stress $\Delta\sigma$, md
$\Delta\sigma$ = net stress, psia

3.4.5 Material balance equation for coalbed methane

The MBE is a fundamental tool for estimating the original gas-in-place G and predicting the recovery performance of conventional gas reservoirs. The MBE as expressed by Equation 3.3.8 is:

$$\frac{p}{Z} = \frac{p_i}{Z_i} - \left(\frac{p_{sc}T}{T_{sc}V}\right)G_p$$

The great utility of the p/Z plots and the ease of their constructions for conventional gas reservoirs have led to many efforts, in particular the work of King (1993) and Seidle (1999), to extend this approach to unconventional gas resources such as coalbed methane (CBM).

The MBE for CBM can be expressed in the following generalized form:

Gas produced G_P = gas originally adsorbed G + original

free gas G_F − gas currently adsorbed

at this pressure G_A − remaining free G_R

or:

$$G_p = G + G_F - G_A - G_R \qquad [3.4.17]$$

For a saturated reservoir (i.e., initial reservoir pressure p_i = desorption pressure p_d) with no water influx, the four main

components of the right-hand-side of the above equality can be determined individually as follows.

Gas originally adsorbed G   As defined previously by Equation 3.4.13, the gas-in-place G is given by:

$$G = 1359.7Ah\rho_B G_c$$

where:

G = gas initially in place, scf
ρ_B = bulk density of coal, g/cm^3
G_c = gas content, scf/ton
A = drainage area, acres
h = Average thickness, ft

Original free gas G_F   For this:

$$G_F = 7758Ah\phi(1 - S_{wi})E_{gi} \qquad [3.4.18]$$

where:

G_F = original free gas-in-place, scf
S_{wi} = initial water saturation
ϕ = porosity
E_{gi} = gas expansion factor at p_i in scf/bbl and given by:

$$E_{gi} = \frac{5.615 Z_{sc}T_{sc}}{p_{sc_i}}\frac{p_i}{TZ_i} = 198.6\frac{p_i}{TZ_i}$$

Gas currently adsorbed at p, G_A   The gas stored by adsorption at any pressure p is typically expressed with the adsorption isotherm or mathematically by Langmuir's equation, i.e., Equation 3.4.4, as:

$$V = V_m\frac{bp}{1 + bp}$$

where:

V = volume of gas currently adsorbed at p, scf/ton
V_m = Langmuir's isotherm constant, scf/ton
b = Langmuir's pressure constant, psi^{-1}

The volume of the adsorbed gas V as expressed in scf/ton at reservoir pressure p can be converted into scf by the following relationship:

$$G_A = 1359.7Ah\rho_B V \qquad [3.4.19]$$

where:

G_A = adsorbed gas at p, scf
ρ_B = average bulk density of the coal, g/cm^3
V = adsorbed gas at p, scf/ton

Remaining free gas G_R   During the dewatering phase of the reservoir, formation compaction (matrix shrinkage) and water expansion will significantly effect water production. Some of the desorbed gas remains in the coal–cleat system and occupies a PV that will be available with water production. King (1993) derived the following expression for calculating the average water saturation remaining in the coal cleats during the dewatering phase:

$$S_w = \frac{S_{wi}[1 + c_w(p_i - p)] - \dfrac{B_w W_p}{7758Ah\phi}}{1 - (p_i - p)c_f} \qquad [3.4.20]$$

where:

p_i = initial pressure, psi
p = current reservoir pressure, psi
W_p = cumulative water produced, bbl
B_w = water formation volume factor, bbl/STB
A = drainage area, acres
c_w = isothermal compressibility of the water, psi^{-1}
c_f = isothermal compressibility of the formation, psi^{-1}
S_{wi} = initial water saturation

Using the above estimated average water saturation, the following relationship for the remaining gas in cleats is developed:

$$G_R = 7758Ah\phi$$

$$\times \left[\frac{\dfrac{B_w W_p}{7758Ah\phi} + (1 - S_{wi}) - (p_i - p)(c_f + c_w S_{wi})}{1 - (p_i - p)c_f}\right]E_g$$

$$[3.4.21]$$

where:

G_R = remaining gas at pressure p, scf
W_p = cumulative water produced, bbl
A = drainage area, acres

and with the gas expansion factor given by:

$$E_g = 198.6\frac{p}{TZ} \text{ scf/bbl}$$

Substituting the above derived four terms into Equation 3.4.17 and rearranging gives:

$$G_p = G + G_F - G_A - G_R$$

or:

$$G_p + \frac{B_w W_p E_g}{1 - (c_f \Delta P)} = Ah\left[1359.7\rho_B\left(G_c - \frac{V_m bp}{1 + bp}\right)\right.$$

$$+ \frac{7758\phi[\Delta P(c_f + S_{wi}c_{wi}) - (1 - S_{wi})]E_g}{1 - (c_f \Delta P)}\right]$$

$$+ 7758Ah\phi(1 - S_{wi})E_{g_i} \qquad [3.4.22]$$

In terms of the volume of gas adsorbed V, this equation can be expressed as:

$$G_p + \frac{B_w W_p E_g}{1 - (c_f \Delta P)} = Ah\left[1359.7\rho_B(G_c - V)\right.$$

$$+ \frac{7758\phi[\Delta P(c_f + S_{wi}c_{wi}) - (1 - S_{wi})]E_g}{1 - (c_f \Delta P)}\right]$$

$$+ 7758Ah\phi((1 - S_{wi})E_{g_i} \qquad [3.4.23]$$

Each of the above two forms of the generalized MBE is the equation of a straight line and can be written as:

$$y = mx + a$$

with:

$$y = G_p + \frac{B_w W_p E_g}{1 - (c_f \Delta P)}$$

$$x = 1359.7\rho_B\left(G_c - \frac{V_m bp}{1 + bp}\right)$$

$$+ \frac{7758\phi[\Delta P(c_f + S_{wi}c_{wi}) - (1 - S_{wi})]E_g}{1 - (c_f \Delta P)}$$

or equivalently:

$$x = 1359.7\rho_B(G_c - V)$$

$$+ \frac{7758\phi[\Delta P(c_f + S_{wi}c_{wi}) - (1 - S_{wi})]E_g}{1 - (c_f \Delta P)}$$

with a slope of :

$$m = Ah$$

and intercept as:

$$a = 7758Ah\phi(1 - S_{wi})E_{g_i}$$

A plot of y as defined above and using the production and pressure drop data versus the term x would produce a straight line with a slope m of Ah and intercept of a.

The drainage area A as calculated from the slope m and the intercept a must be the same. That is:

$$A = \frac{m}{h} = \frac{a}{7758h\phi(1 - S_{wi})E_{gi}}$$

For scattered points, the correct straight line must satisfy the above equality.

Neglecting the rock and fluid compressibility, Equation 3.4.23 is reduced to:

$$G_p + B_w W_p E_g$$

$$= Ah\left[1359.7\rho_B\left(G_c - V_m\frac{bp}{1 + bp}\right) - 7758\phi(1 - S_{wi})E_g\right]$$

$$+ 7758Ah\phi(1 - S_{wi})E_{gi} \qquad [3.4.24]$$

This expression is again the equation of a straight line, i.e., $y = mx + a$, where:

$$y = G_p + B_w W_p E_g$$

$$x = 1359.7\rho_B(G_c - V_m\frac{bp}{1 + bp}) - 7758\phi(1 - S_{wi})E_g$$

slope: $m = Ah$
intercept: $a = 7758Ah\phi(1 - S_{wi})E_{gi}$

In terms of the adsorbed gas volume V, Equation 3.4.24 is expressed as:

$$G_p + B_w W_p E_g = Ah\left[1359.7\rho_B(G_c - V) - 7758\phi(1 - S_{wi})E_g\right]$$

$$+ 7758Ah\phi(1 - S_{wi})E_{gi} \qquad [3.4.25]$$

With the calculation of the bulk volume Ah, the original gas-in-place G can then be calculated from:

$$G = 1359.7(Ah)\rho_B G_c$$

Example 3.14 A coal well is draining a homogeneous 320 acre coal deposit.

The actual well production and pertinent coal data is given below:

Time (days)	G_p (MMscf)	W_p (METB)	p (psia)	p/Z (psia)
0	0	0	1500	1704.5
730	265.086	157 490	1315	1498.7
1460	968.41	290 238	1021	1135.1
2190	1704.033	368 292	814.4	887.8
2920	2423.4	425 473	664.9	714.1
3650	2992.901	464 361	571.1	607.5

Langmuir's pressure constant $b = 0.00276$ psi^{-1}
Langmuir's volume constant $V_m = 428.5$ scf/ton
Average bulk density $\rho_B = 1.70$ g/cm^3
Average thickness $h = 50$ ft
Initial water saturation $S_{wi} = 0.95$
Drainage area $A = 320$ acres
Initial pressure $p_i = 1500$ psia
Critical (desorption) pressure $p_d = 1500$ psia
Temperature $T = 105^o$F
Initial gas content $G_c = 345.1$ scf/ton
Formation volume factor $B_w = 1.00$ bbl/STB
Porosity $\phi = 0.01$
Water compressibility $c_w = 3 \times 10^{-6}$ psi^{-1}
Formation compressibility $c_f = 6 \times 10^{-6}$ psi^{-1}

(a) Neglecting formation and water compressibility coefficients, calculate the well drainage area and original gas-in-place.
(b) Repeat the above calculations by including water and formation compressibilities.

Solution

Step 1. Calculate E_g and V as a function of pressure by applying the following expressions:

$$E_g = 198.6\frac{p}{Tz} = 0.3515\frac{p}{z} \text{ scf/bbl}$$

$$V = V_m\frac{bp}{1 + bp} = 1.18266\frac{p}{1 + 0.00276p} \text{ scf/ton}$$

p (psi)	p/Z (psi)	E_g (scf/bbl)	V (scf/ton)
1500	1704.5	599.21728	345.0968
1315	1498.7	526.86825	335.903
1021	1135.1	399.04461	316.233
814.4	887.8	312.10625	296.5301
664.9	714.1	251.04198	277.3301
571.1	607.5	213.56673	262.1436

Step 2. Neglecting c_w and c_f, the MBE is given by Equation 3.4.25 or:

$$G_p + B_w W_p E_g = Ah[1359.7\rho_B(G_c - V)$$

$$- 7758\phi(1 - S_{wi})E_g] + 7758Ah\phi(1 - S_{wi})E_{gi}$$

or:

$$G_p + B_w W_p E_g = Ah[2322.66(345.1 - V)$$

$$- 3.879E_g] + 2324.64(Ah)$$

Use the given data in the MBE to construct the following table:

p (psi)	V (scf/ton)	G_p (MMscf)	W_p (MMETB)	E_g (scf/bbl)	$y = G_p + W_pE_g$ (MMscf)	$x = 2322.66$ $(345.1 - V)$ $-3.879E_g$ (scf/acre-ft)
1500	345.097	0	0	599.21	0	0
1315	335.90	265.086	0.15749	526.87	348.06	19310
1021	316.23	968.41	0.290238	399.04	1084.23	65494
814.4	296.53	1704.033	0.368292	312.11	1818.98	111593
664.9	277.33	2423.4	0.425473	251.04	2530.15	156425
571.1	262.14	2992.901	0.464361	213.57	3092.07	191844

Step 3. Plot $G_p + B_w W_p E_g$ vs. $2322.66(345.1 - V) - 3.879E_g$ on a Cartesian scale, as shown in Figure 3.37.
Step 4. Draw the best straight line through the points and determine the slope, to give:

$$\text{Slope} = Ah = 15\,900 \text{ acre ft}$$

or:

$$\text{Area } A = \frac{15\,900}{50} = 318 \text{ acres}$$

Step 5. Calculate the initial gas-in-place:

$$G = 1359.7Ah\rho_B G_c$$

$$= 1359.7(318)(50)(1.7)(345.1)$$

$$= 12.68 \text{ Bscf}$$

$$G_F = 77.58Ah\phi(1 - S_{wi})E_{gi}$$

$$= 7758(318)(50)(0.01)(0.05)(599.2)$$

$$= 0.0369 \text{ Bscf}$$

Total gas-in-place $= G + G_F = 12.68 + 0.0369$
$= 12.72$ Bscf
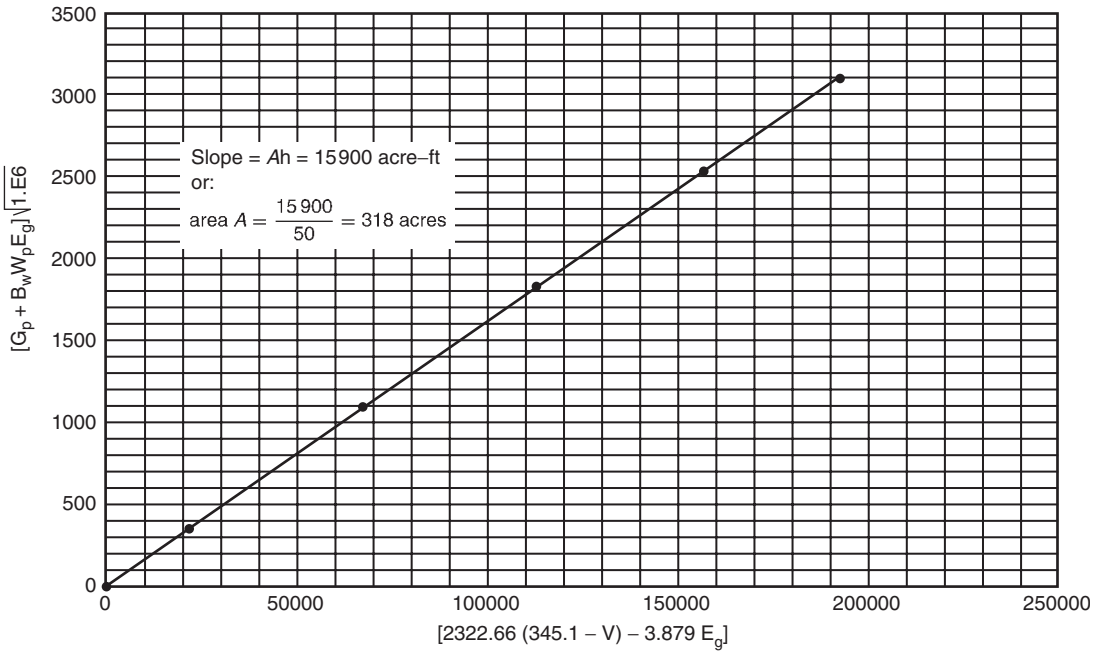
Figure 3.37 *Graphical determination of drainage area.*

Step 1. Using the given values of c_w and c_f in Equation 3.4.23, calculate the Y and X terms and tabulate the results as a function of pressure as follows:

$$y = G_p + \frac{W_p E_g}{1 - [6(10^{-6})(1500 - p)]}$$

$$x = 1359.7(1.7)(345.1 - V)$$

$$+ \frac{7758(0.01)[(1500 - p)(6(10^{-6}) + 0.95c_{wi}) - (1 - 0.95)]E_g}{1 - [6.(10^{-6})(1500 - p)]}$$

p (psi)	V (scf/ton)	X	Y
1315	335.903	1.90E+04	3.48E+08
1021	316.233	6.48E+04	1.08E+09
814.4	296.5301	1.11E+05	1.82E+09
664.9	277.3301	1.50E+05	2.53E+09
571.1	262.1436	1.91E+05	3.09E+09

Step 2. Plot the x and y values on a Cartesian scale, as shown in Figure 3.38, and draw the best straight line through the points.

Step 3. Calculate the slope and intercept of the line, to give:

$$\text{Slope} = Ah = 15\,957 \text{ acre ft}$$

or:

$$A = \frac{15\,957}{50} = 319 \text{ acres}$$

To confirm the above calculated drainage area of the well, it can be also determined from the intercept of the straight line; to give:

$$\text{Intercept} = 3.77(10^7) = 7758Ah\phi(1 - S_{wi})E_{gi}$$

or:

$$A = \frac{3.708(10^7)}{7758(50)(0.01)(0.05)(599.2)} = 324 \text{ acres}$$

Step 4. Calculate the initial gas-in-place to give:

$$\text{Total} = G + G_F$$

$$= 12.72 + 0.037 = 12.76 \text{ Bscf}$$

Under the conditions imposed on Equation 3.4.24 and assuming 100% initial water saturation, the usefulness of the equation can be extended to estimate the average reservoir pressure p from the historical production data, i.e., G_p and W_p. Equation 3.4.24 is given as:

$$G_p + W_p E_g = (1359.7\rho_B Ah)\left[\left(G_c - V_m \frac{bp}{1 + bp}\right)\right]$$

Or in terms of G:

$$G_p + W_p E_g = G - (1359.7\rho_B Ah)V_m \frac{bp}{1 + bp} \qquad [3.4.26]$$

At the initial reservoir pressure p_i, initial gas-in-place G is given by:

$$G = [1359.7\rho_B Ah]G_c$$

$$= [1359.7\rho_B Ah]\left(V_m \frac{bp_i}{1 + bp_i}\right) \qquad [3.4.27]$$

Combining Equation 3.4.27 with 3.4.26 and rearranging gives:

$$\left[\left(\frac{p}{p_i}\right)\left(\frac{1 + bp_i}{1 + bp}\right)\right] = 1 - \left[\frac{1}{G}(G_p + B_w W_p E_g)\right]$$

or:

$$\left[\left(\frac{p}{p_i}\right)\left(\frac{1 + bp_i}{1 + bp}\right)\right] = 1 - \frac{1}{G}\left(G_p + 198.6\frac{p}{ZT}B_w W_p\right)$$

$$[3.4.28]$$
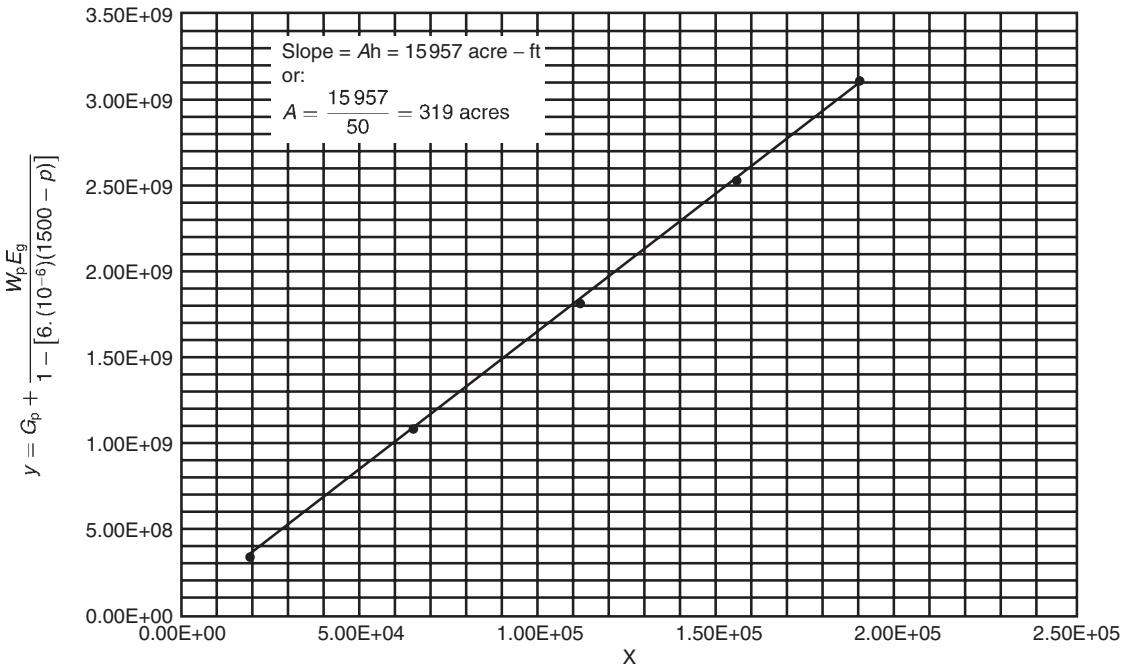
Figure 3.38 *Straight-line relationship of y as a function of x.*

where:

G = initial gas-in-place; scf
G_p = cumulative gas produced, scf
W_p = cumulative water produced, STB
E_g = gas formation volume factor, scf/bbl
p_i = initial pressure
T = temperature, °R
Z = z-factor at pressure p

Equation 3.4.28 is the equation of a straight line with a slope of $-1/G$ and intercept of 1.0. In a more convenient form, Equation 3.4.28 is written as:

$$y = 1 + mx$$

where:

$$y = \left[\left(\frac{p}{p_i} \right) \left(\frac{1 + bp_i}{1 + bp} \right) \right] \qquad [3.4.29]$$

$$x = G_p + 198.6 \frac{p}{ZT} B_w W_p \qquad [3.4.30]$$

$$m = \frac{1}{G}$$

Figure 3.39 shows the graphical linear relationship of Equation 3.4.28. Solving this linear relationship for the average reservoir pressure p requires an iterative procedure as summarized in the following steps:

Step 1. On a Cartesian scale, draw a straight line that originates from 1 on the y axis and with a negative slope of $1/G$, as shown in Figure 3.39.
Step 2. At a given G_p and W_p, guess the reservoir pressure p and calculate the y and x terms as given by Equations 3.4.29 and 3.4.30 respectively.
Step 3. Plot the coordinate of the calculated point, i.e., (x, y), on Figure 3.39. If the coordinate of the point falls
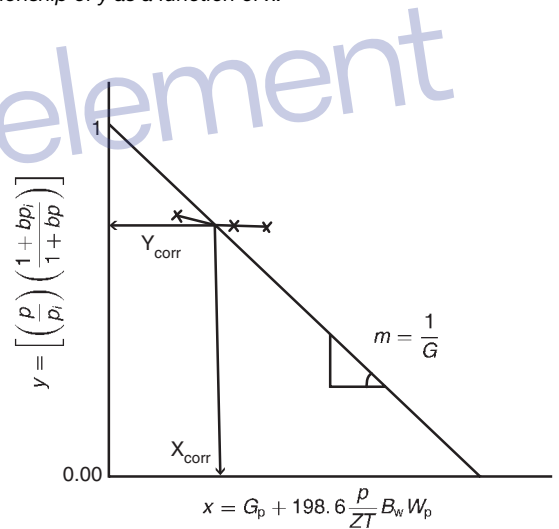
Figure 3.39 *Graphical determination of reservoir pressure.*

on the straight line, it indicates that the assumed reservoir pressure is correct, otherwise the process is repeated at a different pressure. The process can be rapidly converged by assuming three different pressure values and connecting the coordinate plotted points with a smooth curve that intersects with the straight line at (x_{corr}, y_{corr}). The reservoir pressure at the given W_p and G_p is calculated from:

$$p = \frac{p_i y_{corr}}{1 + bP_i (1 - y_{corr})}$$

3.4.6 Prediction of CBM reservoir performance

The MBE as given by its various mathematical forms, i.e., Equations 3.4.22 through 3.4.25 can be used to predict future performance of CBM reservoirs as a function of reservoir pressure. Assuming, for simplicity, that the water and formation compressibility coefficients are negligible, Equation 3.4.22 can be expressed as:

$$G_p + B_w W_p E_g = G - (1359.7 A h \rho_B V_m b) \frac{p}{1+bp}$$
$$- 7758 \phi A h (1 - S_{wi}) E_g + 7758 A h \phi ((1 - S_{wi}) E_{gi}$$

where:

G = initial gas-in-place, scf
A = drainage area, acres
h = average thickness, ft
S_{wi} = initial water saturation
E_g = gas formation volume factor, scf/bbl
b = Langmuir's pressure constant, psi^{-1}
V_m = Langmuir's volume constant, scf/ton

In a more convenient form, the above expression is written as:

$$G_p + B_w W_p E_g = G - \frac{a_1 P}{1+bp} + a_2 (E_{gi} - E_g) \qquad [3.4.31]$$

where the coefficients a_1 and a_2 are given by:

$$a_1 = 1359.7 A h b V_m$$

$$a_2 = 7758 A h \phi (1 - S_{wi})$$

Differentiating with respect to pressure gives:

$$\frac{\partial (G_p + B_w W_p E_g)}{\partial p} = -\frac{a_1}{(1+bp)^2} - a_2 \frac{\partial E_g}{\partial p}$$

Expressing the above derivative in finite difference form gives:

$$G_p^{n+1} + B_w^{n+1} W_p^{n+1} E_g^{n+1} = G_p^n + B_w^n W_p^n E_g^n + \frac{a_1 (p^n - p^{n+1})}{(1+bp^{n+1})}$$
$$+ a_2 (E_g^n - E_g^{n+1}) \qquad [3.4.32]$$

where the superscripts n and $n+1$ indicate the current and future time levels respectively, and:

p^n, p^{n+1} = current and future reservoir pressures, psia
G_p^n, G_p^{n+1} = current and future cumulative gas production, scf
W_p^n, W_p^{n+1} = current and future cumulative water production, STB
E_g^n, E_g^{n+1} = current and future gas expansion factor, scf/bbl

Equation 3.4.32 contains two unknowns, G_p^{n+1} and W_p^{n+1}, and requires two additional relations:

(1) the producing gas–water ratio (GWR) equation;
(2) the gas saturation equation.

The gas–water ratio relationship is given by:

$$\frac{Q_g}{Q_w} = GWR = \frac{k_{rg}}{k_{rw}} \frac{\mu_w B_w}{\mu_g B_g} \qquad [3.4.33]$$

where:

GWR = gas–water ratio, scf/STB
k_{rg} = relative permeability to gas
k_{rw} = relative permeability to water
μ_w = water viscosity, cp
μ_g = gas viscosity, cp
B_w = water formation volume factor, bbl/STB
B_g = gas formation volume factor, bbl/STB
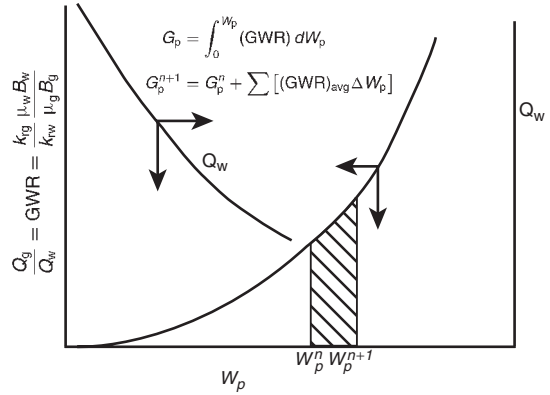
Figure 3.40 *Relationships between GWR, Q_w, and W_p.*

The cumulative gas produced G_p is related to the EWR by the following expression:

$$G_p = \int_0^{W_p} (GWR) dW_p \qquad [3.4.34]$$

This expression suggests that the cumulative gas production at any time is essentially the area under the curve of the GWR versus the W_p relationship, as shown in Figure 3.40.

Also, the incremental cumulative gas produced ΔG_p between W_p^n and W_p^{n+1} is given by:

$$G_p^{n+1} - G_p^n = \Delta G_p = \int_{W_p^n}^{W_p^{n+1}} (GWR) dW_p \qquad [3.4.35]$$

This expression can be approximated by using the trapezoidal rule, to give:

$$G_p^{n+1} - G_p^n = \Delta G_p = \left[\frac{(GWR)^{n+1} + (GWR)^n}{2} \right] (W_p^{n+1} - W_p^n)$$
$$[3.4.36]$$

or:

$$G_p^{n+1} = G_p^n + \sum [(GWR)_{avg} \Delta W_p] \qquad [3.4.37]$$

The other auxiliary mathematical expression needed to predict the recovery performance of a coalbed gas reservoir is the gas saturation equation. Neglecting the water and formation compressibilities, the gas saturation is given by:

$$S_g^{n+1} = \frac{(1 - S_{wi}) - (p_i - p^{n+1})(c_f + c_w S_{wi}) + \dfrac{B_w^{n+1} W_p^{n+1}}{7758 A h \phi}}{1 - [(p_i - p^{n+1}) c_f]}$$
$$[3.4.38]$$

The required computations are performed in a series of pressure drops that proceed from a known reservoir condition at pressure p^n to the new lower pressure p^{n+1}. It is accordingly assumed that the cumulative gas and water production has increased from G_p^n and W_p^n to G_p^{n+1} and W_p^{n+1}, while flow rates have changed from Q_g^n and Q_w^n to Q_g^{n+1} and Q_w^{n+1}. The proposed methodology for predicting the reservoir performance consists of the following steps:

Step 1. Using the gas–water relative permeability data, prepare a plot of the relative permeability ratio k_{rg}/k_{rw} versus gas saturation S_g on a semilog scale.
Step 2. Knowing the reservoir temperature T and specific gravity of the gas γ_g, calculate and prepare a plot

of E_g, B_g, and gas viscosity μ_g as a function of pressure, where:

$$E_g = 198.6 \frac{p}{ZT}, \text{ scf/bbl}$$

$$B_g = \frac{1}{E_g} = 0.00504 \frac{ZT}{p}, \text{ bbl/scf}$$

Step 3. Select a future reservoir pressure p^{n+1} below the current reservoir pressure p^n. If the current reservoir pressure p^n is the initial reservoir pressure, set W_p^n and G_p^n equal to zero.

Step 4. Calculate B_w^{n+1}, E_g^{n+1}, and B_g^{n+1} at the selected pressure p^{n+1}.

Step 5. Estimate or guess the cumulative water production W_p^{n+1} and solve Equation 3.4.32 for G_p^{n+1}, to give:

$$G_p^{n+1} = G_p^n + (B_w^n W_p^n E_g^n - B_w^{n+1} W_p^{n+1} E_g^{n+1})$$
$$+ \frac{a_1(p^n - p^{n+1})}{(1 + bp^{n+1})} + a_2(E_g^n - E_g^{n+1})$$

Step 6. Calculate the gas saturation at p^{n+1} and W_p^{n+1} by applying Equation 3.4.38:

$$S_g^{n+1} = \frac{(1 - S_{wi}) - (p_i - p^{n+1})(c_f + c_w S_{wi}) + \frac{B_w^{n+1} W_p^{n+1}}{7758Ah\phi}}{1 - [(p_i - p^{n+1})c_f]}$$

Step 7. Determine the relative permeability ratio k_{rg}/k_{rw} at S_g^{n+1} and estimate the GWR from Equation 3.4.33, or:

$$(GWR)^{n+1} = \frac{k_{rg}}{k_{rw}} \left(\frac{\mu_w B_w}{\mu_g B_g} \right)^{n+1}$$

Step 8. Recalculate the cumulative gas production G_p^{n+1} by applying Equation 3.4.36:

$$G_p^{n+1} = G_p^n + \frac{(GWR)^{n+1} + (GWR)^n}{2} (W_p^{n+1} - W_p^n)$$

Step 9. The total gas produced G_p^{n+1} as calculated from the MBE in step 5 and that of the GWR in step 8 provide two independent methods for determining the cumulative gas production. If the two values agree, the assumed value of W_p^{n+1} and the calculated G_p^{n+1} are correct. Otherwise, assume a new value for W_p^{n+1} and repeat Steps 5 through 9. In order to simplify this iterative process, three values of W_p^{n+1} can be assumed which yield three different solutions of G_p^{n+1} for each of the equations (i.e., MBE and GWR equations). When the computed values of G_p^{n+1} are plotted versus the assumed values of W_p^{n+1}, the resulting two curves (one representing results of step 5 and the one from step 8), will intersect. The coordinates of the intersection give the correct G_p^{n+1} and W_p^{n+1}.

Step 10. Calculate the incremental cumulative gas production ΔG_p from:

$$\Delta G_p = G_p^{n+1} - G_p^n$$

Step 11. Calculate the gas and water flow rates from Equations 3.1.11 and 3.4.33, to give:

$$Q_g^{n+1} = \frac{0.703hk(k_{rg})^{n+1}(p^{n+1} - p_{wf})}{T(\mu_g Z)_{avg}[\ln(r_e/r_w) - 0.75 + s]}$$

$$Q_w^{n+1} = \left(\frac{k_{rw}}{k_{rg}} \right)^{n+1} \left(\frac{\mu_g B_g}{\mu_w B_w} \right)^{n+1} Q_g^{n+1}$$

where:

Q_g = gas flow rate, scf/day
Q_w = water flow rate, STB/day
k = absolute permeability, md
T = temperature, °R
r_e = drainage radius, ft
r_w = wellbore radius, ft
s = skin factor

Step 12. Calculate the average gas flow rate as the reservoir pressure declines from p^n to p^{n+1}, as:

$$(Q_g)_{avg} = \frac{Q_g^n + Q_g^{n+1}}{2}$$

Step 13. Calculate the incremental time Δt required for the incremental gas production ΔG_p during the pressure drop from p^n to p^{n+1}, as:

$$\Delta t = \frac{\Delta G_P}{(Q_g)_{avg}} = \frac{G_p^{n+1} - G_p^n}{(Q_g)_{avg}}$$

where:

Δt = incremental time, days

Step 14. Calculate the total time t:

$$t = \sum \Delta t$$

Step 15. Get:

$$W_p^n = W_p^{n+1}$$
$$G_p^n = G_p^{n+1}$$
$$Q_g^n = Q_g^{n+1}$$
$$Q_w^n = Q_w^{n+1}$$

and repeat steps 3 through 15.

3.4.7 Flow of desorbed gas in cleats and fractures

Flow in conventional gas reservoirs obeys, depending on the flow regime, Darcy's equation in response to a pressure gradient. In coal seams, the gas is physically adsorbed on the internal surfaces of the coal matrix. As discussed in previous sections, coal seam reservoirs are characterized by a dual-porosity system: primary (matrix) porosity and secondary (cleats) porosity. The secondary porosity system ϕ_2 of coal seams consists of the natural-fracture (cleats) system inherent in these reservoirs. These cleats act as a sink to the primary porosity (porosity of the coal matrix) and as a conduit to production wells. The porosity ϕ_2 in this system ranges between 2% and 4%. Therefore, methane production from coal seams occurs by a three-stage process in which the methane:

(1) diffuses through the coal matrix to the cleat and obeys Fick's law;
(2) desorbs at the matrix-cleat interface; then
(3) flows through the cleat system to the wellbore as described by Darcy's equation.

The primary porosity system in these seams is composed of very fine pores that contain a large internal surface area on which large quantities of gas are stored. The permeability of the coal matrix system is extremely low, and, in effect, the primary porosity system (coal matrix) is both impermeable to gas and inaccessible to water. In the absence of gas flow in the matrix, the gas is transported according to gradients in concentration, i.e., diffusion process. Diffusion is a process where flow occurs via random motion of molecules from a

high concentration area to an area with lower concentration, in which the flow obeys Fick's law as given by:

$$Q_g = -379.4 DA \frac{dC_m}{ds} \qquad [3.4.39]$$

where:

Q_g = matrix-fracture gas flow rate, scf/day
s = fracture spacing, ft
D = diffusion coefficient, ft^2/day
C_m = molar concentration, lb$_m$-mole/ft^3
A = surface area of the coal matrix, ft^2

The volume of the adsorbed gas can be converted into molar concentration C_m from the following expression:

$$C_m = 0.5547(10^{-6}) \gamma_g \rho_B V \qquad [3.4.40]$$

where:

C_m = molar concentration lb$_m$-mole/ft^3
ρ_B = coal bulk density, g/cm^3
V = adsorbed gas volume, scf/ton
γ_g = specific gravity of the gas

Zuber et al. (1987) pointed out that the diffusion coefficient D can be determined indirectly from the canister desorption test. The authors correlated the diffusion coefficient with the coal cleat spacing s and desorption time t. The average cleat spacing can be determined by visual observation of coal cores. The proposed expression is given by:

$$D = \frac{s^2}{8\pi t} \qquad [3.4.41]$$

where:

D = diffusion coefficient, ft^2/day
t = desorption time from the canister test, days
s = coal cleat spacing, ft

The desorption time t is determined from canister tests on a core sample as defined by the time required to disrobe 63% of the total adsorbed gas.

3.5 Tight Gas Reservoirs

Gas reservoirs with permeability less than 0.1 md are considered "tight gas" reservoirs. They present unique problems to reservoir engineers when applying the MBE to predict the gas-in-place and recovery performance.

The use of the conventional material balance in terms of p/Z plot is commonly utilized as a powerful tool for evaluating the performance of gas reservoirs. For a volumetric gas reservoir, the MBE is expressed in different forms that will produce a linear relationship between p/Z and the cumulative gas production G_p. Two such forms are given by Equations 3.3.10 and 3.3.11 as:

$$\frac{p}{Z} = \frac{p_i}{Z_i} - \left[\left(\frac{p_i}{Z_i} \right) \frac{1}{G} \right] G_p$$

$$\frac{p}{Z} = \frac{p_i}{Z_i} \left[1 - \frac{G_p}{G} \right]$$

The MBE as expressed by any of the above equations is very simple to apply because it is not dependent on flow rates, reservoir configuration, rock properties, or well details. However, there are fundamental assumptions that must be satisfied when applying the equation, including:

- uniform saturation throughout the reservoir at any time;
- there is small or no pressure variation within the reservoir;
- the reservoir can be represented by a single weighted average pressure at any time;

- the reservoir is represented by a tank, i.e., constant drainage area, of homogeneous properties.

Payne (1996) pointed out that the assumption of uniform pressure distributions is required to ensure that pressure measurements taken at different well locations represent true average reservoir pressures. This assumption implies that the average reservoir pressure to be used in the MBE can be described with one pressure value. In high-permeability reservoirs, small pressure gradients exist away from the wellbore and the average reservoir pressure estimates can be readily made with short-term shut-in buildups or static pressure surveys.

Unfortunately, the concept of the straight-line p/Z plot as described by the conventional MBE fails to produce this linear behavior when applied to tight gas reservoirs that had not established a constant drainage area. Payne (1996) suggested that the essence of the errors associated with the use of p/Z plots in tight gas reservoirs is that substantial pressure gradients exist within the formation, resulting in a violation of the basic tank assumption. These gradients manifest themselves in terms of scattered, generally curved, and rate-dependent p/Z plot behavior. This non-linear behavior of p/Z plots, as shown in Figure 3.41, may significantly underestimate gas initially in place (GIIP) when interpreting by the conventional straight-line method. Figure 3.41(a) reveals that the reservoir pressure declines very rapidly as the area surrounding the well cannot be recharged as fast as it is depleted by the well. This early, rapid pressure decline is seen often in tight gas reservoirs and is an indication that the use of p/Z plot analysis may be inappropriate. It is clearly apparent that the use of early points would dramatically underestimate GIIP, as shown in Figure 3.41(a) for the Waterton Gas Field with an apparent GIIP of 7.5 Bm^3. However, late-time production and pressure data shows a nearly double GIIP of 16.5 Bm^3, as shown in Figure 3.41(b).

The main problem with tight gas reservoirs is the difficulty of accurately estimating the average reservoir pressure required for p/Z plots as a function of G_p or time. If the
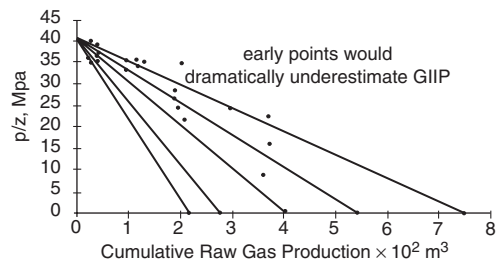
Figure 3.41(a) *Real-life example of p/Z plot from Sheet IVc in the Waterton Gas Field.*
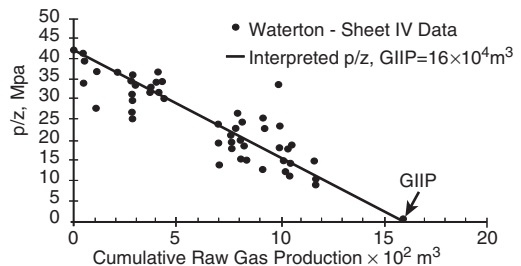
Figure 3.41(b) *Real-life example of p/Z plot from Sheet IV in the Waterton Gas Field.*

pressures obtained during shut-in do not reflect the average reservoir pressure, the resulting analysis will be inaccurate. In tight gas reservoirs, excessive shut-in times of months or years may be required to obtain accurate estimates of average reservoir pressure. The minimum shut-in time that is required to obtain a reservoir pressure that represents the average reservoir pressure must be at least equal to time to reach the pseudosteady state t_{pss}. This time is given by Equation 3.1.39 for a well in the centre of a circular or square drainage area, as:

$$t_{pss} = \frac{15.8\phi\mu_{gi}c_{ti}A}{k}$$

with:

$$c_{ti} = S_{wi}c_{wi} + S_g c_{gi} + c_f$$

where:

t_{pss} = stabilization (pseudosteady-state) time, days
c_{ti} = total compressibility coefficient at initial pressure, psi^{-1}
c_{wi} = water compressibility coefficient at initial pressure, psi^{-1}
c_f = formation compressibility coefficient, psi^{-1}
c_{gi} = gas compressibility coefficient at initial pressure, psi^{-1}
ϕ = porosity, fraction

With most tight gas reservoirs being hydraulically fractured, Earlougher (1977) proposed the following expression for estimating the minimum shut-in time to reach the semisteady state:

$$t_{pss} = \frac{474\phi\mu_g c_t x_f^2}{k} \qquad [3.5.1]$$

where:

x_f = fracture half-length, ft
k = permeability, md

Example 3.15 Estimate the time required for a shut-in gas well reach its 40 acre drainage area. The well is located in the centre of a square-drainage boundary with the following properties:

$\phi = 14\%, \quad \mu_{gi} = 0.016$ cp, $\quad c_{ti} = 0.0008$ psi
$A = 40$ acres, $\quad k = 0.1$ md

Solution Calculate the stabilization time by applying Equation 3.1.39 to give:

$$t_{pss} = \frac{15.8(0.14)(0.016)(0.0008)(40)(43560)}{0.1} = 493 \text{ days}$$

The above example indicates that an excessive shut-in time of approximately 16 months is required to obtain a reliable average reservoir pressure.

Unlike curvature in the p/Z plot which can be caused by:

- an aquifer,
- an oil leg,
- formation compressibility, or
- liquid condensation,

scatter in the p/Z plot is diagnostic of substantial reservoir pressure gradients. Hence, if substantial scatter is seen in a p/Z plot, the tank assumption is being violated and the plot should not be used to determine GIIP. One obvious solution to the material balance problem in tight gas reservoirs is the use of a numerical simulator. Two other relatively new approaches for solving the material balance problem that can be used if reservoir simulation software is not available are:

(1) the compartmental reservoir approach;
(2) the combined decline curve and type curve approach.

These two methodologies are discussed below.

3.5.1 Compartmental reservoir approach
A compartmental reservoir is defined as a reservoir that consists of two or more distinct regions that are allowed to communicate. Each compartment or "tank" is described by its own material balance, which is coupled to the material balance of the neighboring compartments through influx or efflux gas across the common boundaries. Payne (1996) and Hagoort and Hoogstra (1999) proposed two different robust and rigorous schemes for the numerical solution of the MBEs, of compartmented gas reservoirs. The main difference between the two approaches is that Payne solves for the pressure in each compartment explicitly and Hagoort and Hoogstra implicitly. However, *both schemes* employ the following basic approach:

- Divide the reservoir into a number of compartments with each compartment containing one or more production wells that are proximate and that measure consistent reservoir pressures. The initial division should be made with as few tanks as possible with each compartment having different dimensions in terms of length L, width W, and height h.
- Each compartment must be characterized by a historical production and pressure decline data as a function of time.
- If the initial division is not capable of matching the observed pressure decline, additional compartments can be added either by subdividing the previously defined tanks or by adding tanks that do not contain drainage points, i.e., production wells.

The practical application of the compartmental reservoir approach is illustrated by the following two methods:

(1) the Payne method
(2) the Hagoort and Hoogstra method

Payne method
Rather than using the conventional single-tank MBE in describing the performance of tight gas reservoirs, Payne (1996) suggested a different approach that is based on subdividing the reservoir into a number of tanks, i.e., compartments, which are allowed to communicate. Such compartments can be depleted either directly by wells or indirectly through other tanks. The flow rate between tanks is set proportionally to either the difference in the square of tank pressure or the difference in pseudopressures, i.e., $m(p)$. To illustrate the concept, consider a reservoir that consists of two compartments, 1 and 2, as shown schematically in Figure 3.42.

Initially, i.e., before the start of production, both compartments are in equilibrium with the same initial reservoir pressure. Gas production can be produced from either one or both compartments. With gas production, the pressures in the reservoir compartments will decline at a different rate depending on the production rate from each compartment and the crossflow rate between the two compartments. Adopting the convention that influx is positive if gas flows from compartment 1 into compartment 2, the linear gas flow rate between the two compartments in terms of gas pseudopressure is given by Equation 1.2.11 of Chapter 1 as:

$$Q_{12} = \left(\frac{0.111924kA}{TL}\right)[m(p_1) - m(p_2)]$$
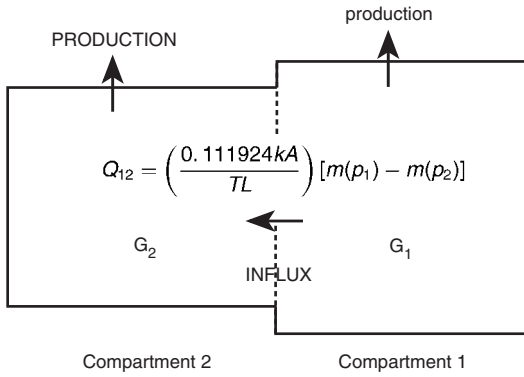
Figure 3.42 *Schematic representation of compartmented reservoir consisting of two reservoir compartments separated by a permeable boundary.*

where:

Q_{12} = flow rate between the two compartments, scf/day

$m(p_1)$ = gas pseudopressure in compartment (tank) 1, psi²/cp

$m(p_2)$ = gas pseudopressure in compartment (tank) 2, psi²/cp

k = permeability, md

L = distance between the center of the two compartments, ft

A = cross-sectional area, i.e., width height, ft²

T = temperature, °R

The above equation can be expressed in a more compact form by including a "communication factor" C_{12} between the two compartments, as:

$$Q_{12} = C_{12}[m(p_1) - m(p_2)] \qquad [3.5.2]$$

The communication factor C_{12} between the two compartments is computed by calculating the individual communication factor for each compartment and employing an average technique. The communication factor for each of the two compartments is given by:

For compartment 1 $C_1 = \dfrac{0.111924k_1A_1}{TL_1}$

For compartment 2 $C_2 = \dfrac{0.111924k_2A_2}{TL_2}$

And the communication factor between two compartments, C_{12}, is given by the following average technique:

$$C_{12} = \frac{2C_1C_2}{(C_1 + C_2)}$$

where:

C_{12} = communication factor between two compartments, scf/day/psi²/cp

C_1 = communication factor for compartment 1, scf/day/psi²/cp

C_2 = communication factor for compartment 2, scf/day/psi²/cp

L_1 = length of compartment 1, ft

L_2 = length of compartment 2, ft

A_1 = cross-sectional area of compartment 1, ft²

A_2 = cross-sectional area of compartment 2, ft²

The cumulative gas in flux G_{p12} from compartment 1 to compartment 2 is given by the integration of flow rate over

time t as:

$$G_{p12} = \int_0^t Q_{12}\,dt = \sum_0^t (\Delta Q_{12})\Delta t \qquad [3.5.3]$$

Payne proposed that *individual* compartment pressures are determined by assuming a straight-line relationship of p/Z vs. G_{pt} with the total gas production G_{pt} from an individual compartment as defined by the following expression:

$$G_{pt} = G_p + G_{p12}$$

where G_p is the cumulative gas produced from wells in the compartment and G_{p12} is the cumulative gas efflux/influx between the connected compartments. Solving Equation 3.3.10 for the pressure in each compartment and assuming a positive flow from compartment 1 to 2 gives:

$$p_1 = \left(\frac{p_i}{Z_i}\right) Z_1 \left(1 - \frac{G_{p1} + G_{p12}}{G_1}\right) \qquad [3.5.4]$$

$$p_2 = \left(\frac{p_i}{Z_i}\right) Z_2 \left(1 - \frac{G_{p2} - G_{p12}}{G_2}\right) \qquad [3.5.5]$$

with:

$$G_1 = 43560A_1h_1\phi_1(1S_{wi})/B_{gi} \qquad [3.5.6]$$

$$G_2 = 43560A_2h_2\phi_2(1S_{wi})/B_{gi} \qquad [3.5.7]$$

where:

G_1 = initial gas-in-place in compartment 1, scf

G_2 = initial gas-in-place in compartment 2, scf

G_{p1} = actual cumulative gas production from compartment 1, scf.

G_{p2} = actual cumulative gas production from compartment 2, scf.

A_1 = areal extent of compartment 1, acres

A_2 = areal extent of compartment 2, acres

h_1 = average thickness of compartment 1, ft

h_2 = average thickness of compartment 2, ft

B_{gi} = initial gas formation volume factor, ft³/scf

ϕ_1 = average porosity in compartment 1

ϕ_2 = average porosity in compartment 2

The subscripts 1 and 2 denote the two compartments 1 and 2, while the subscript i refers to initial condition. The required input data for the Payne method consists of:

- amount of gas contained in each tank, i.e., tank dimensions, porosity, and saturation;
- intercompartment communication factors C_{12};
- initial pressure in each compartment;
- production data profiles from the individual tanks.

Payne's technique is performed fully explicit in time. At each time step, the pressures in various tanks are calculated, yielding a pressure profile that can be matched to the actual pressure decline. The specific steps of this iterative method are summarized below:

Step 1. Prepare the available gas properties data in tabulated and graphical forms that include:

Z vs. p

μ_g vs. p

$2p/(\mu_g Z)$ vs. p

$m(p)$ vs. p

Step 2. Divide the reservoir into compartments and determine the dimensions of each compartments in terms of:

length L

height h

width W

cross-sectional area A

Step 3. For each compartment, determine the initial gas-in-place G. Assuming two compartments for example, then calculate G_1 and G_2 from Equations 3.5.6 and 3.5.7:

$$G_1 = 43560 A_1 h_1 \phi_1 (1 S_{wi})/B_{gi}$$

$$G_2 = 43560 A_2 h_2 \phi_2 (1 S_{wi})/B_{gi}$$

Step 4. For each compartment, make a plot of p/Z vs. G_P that can be constructed by simply drawing a drawing a straight line between p_i/Z_i with initial gas-in-place in both compartments, i.e., G_1 and G_2.

Step 5. Calculate the communication factors for each compartment and between compartments. For two compartments:

$$C_1 = \frac{0.111924 k_1 A_1}{T L_1}$$

$$C_2 = \frac{0.111924 k_2 A_2}{T L_2}$$

$$C_{12} = \frac{2 C_1 C_2}{(C_1 + C_2)}$$

Step 6. Select a small time step Δt and determine the corresponding *actual* cumulative gas production G_p from each compartment. Assign $G_p = 0$ if the compartment does not include a well.

Step 7. Assume (guess) the pressure distributions throughout the selected compartmental system and determine the gas deviation factor Z at each pressure. For a two-compartment system, let the initial values be denoted by p_1^k and p_2^k.

Step 8. Using the assumed values of the pressure p_1^k and p_2^k, determine the corresponding $m(p_1)$ and $m(p_2)$ from the data of step 1.

Step 9. Calculate the gas influx rate Q_{12} and cumulative gas influx G_{p12} by applying Equations 3.5.2 and 3.5.3, respectively.

$$Q_{12} = C_{12}[m(p_1) - m(p_2)]$$

$$G_{p12} = \int_0^t Q_{12} dt = \sum_0^t (\Delta Q_{12}) \Delta t$$

Step 10. Substitute the values of G_{p12}, the Z factor, and actual values of G_{p1} and G_{p2} in Equations 3.5.4 and 3.5.5 to calculate the pressure in each compartment as denoted by p_1^{k+1} and p_2^{k+1}:

$$p_1^{k+1} = \left(\frac{p_i}{Z_i}\right) Z_1 \left(1 - \frac{G_{p1} + G_{p12}}{G_1}\right)$$

$$p_2^{k+1} = \left(\frac{p_i}{Z_i}\right) Z_2 \left(1 - \frac{G_{p2} - G_{p12}}{G_2}\right)$$

Step 11. Compare the assumed and calculated values, i.e., $\left|p_1^k - p_1^{k+1}\right|$ and $\left|p_2^k - p_2^{k+1}\right|$. If a satisfactory match is achieved within a tolerance of 5–10 psi for all the pressure values, then steps 3 through 7 are repeated at the new time level with the corresponding historical gas production data. If the match is not satisfactory, repeat the iterative cycle of steps 4 through 7 and set $p_1^k = p_1^{k+1}$ and $p_2^k = p_2^{k+1}$.

Step 12. Repeat steps 6 through 11 to produce a pressure decline profile for each compartment that can be compared with the actual pressure profile for each compartment or that from step 4.

Performing a material balance history match consists of varying the number of compartments required, the dimension of the compartments, and the communication factors until an acceptable match of the pressure decline is obtained. The improved accuracy in estimating the original gas-in-place, resulting from determining the optimum number and size of compartments, stems from the ability of the proposed method to incorporate reservoir pressure gradients, which are completely neglected in the single-tank conventional p/Z plot method.

Hagoort and Hoogstra method

Based on the Payne method, Hagoort and Hoogstra (1999) developed a numerical method to solve the MBE of compartmental gas reservoirs that employs an implicit, iterative procedure, and that recognizes the pressure dependency of the gas properties. The iterative technique relies on adjusting the size of compartments and the transmissibility values to match the historical pressure data for each compartment as a function of time. Referring to Figure 3.42, the authors assume a thin permeable layer with a transmissibility of Γ_{12} separating the two compartments. Hagoort and Hoogstra expressed the instantaneous gas influx through the thin permeable layer by Darcy's equation as given by (in Darcy's units):

$$Q_{12} = \frac{\Gamma_{12}(p_1^2 - p_2^2)}{2 p_1 (\mu_g B_g)_{avg}}$$

where:

$\Gamma_{12} = $ the transmissibility between compartments

Here, we suggest a slightly different approach for estimating the gas influx between compartments by modifying Equation 1.2.11 in Chapter 1 to give:

$$Q_{12} = \frac{0.111924 \Gamma_{12}(p_1^2 - p_2^2)}{TL} \qquad [3.5.8]$$

with:

$$\Gamma_{12} = \frac{\Gamma_1 \Gamma_2 (L_1 + L_2)}{L_1 \Gamma_2 + L_2 \Gamma_1} \qquad [3.5.9]$$

$$\Gamma_1 = \left[\frac{kA}{Z\mu_g}\right]_1 \qquad [3.5.10]$$

$$\Gamma_2 = \left[\frac{kA}{Z\mu_g}\right]_2 \qquad [3.5.11]$$

where:

$Q_{12} = $ influx gas rate, scf/day
$L = $ distance between the centers of compartments 1 and 2, ft
$A = $ cross-sectional area, ft^2
$\mu_g = $ gas viscosity, cp
$Z = $ gas deviation factor
$k = $ permeability, md
$p = $ pressure, psia
$T = $ temperature, °R
$L_1 = $ length of compartment 1, ft
$L_2 = $ length of compartment 2, ft

The subscripts 1 and 2 refer to compartments 1 and 2, respectively.

Using Equation 3.3.10, the material balance for the two reservoir compartments can be modified to include the gas influx from compartment 1 to compartment 2 as:

$$\frac{p_1}{Z_1} = \frac{p_1}{Z_1}\left(1 - \frac{G_{p1} + G_{p12}}{G_1}\right) \qquad [3.5.12]$$

$$\frac{p_2}{Z_2} = \frac{p_1}{Z_1}\left(1 - \frac{G_{p2} - G_{p12}}{G_2}\right) \qquad [3.5.13]$$

where:

p_1 = initial reservoir pressure, psi
Z_1 = initial gas deviation factor
G_p = actual (historical) cumulative gas production, scf
G_1, G_2 = initial gas-in-place in compartment 1 and 2, scf
G_{p12} = cumulative gas influx from compartment 1 to 2 in scf, as given in Equation 3.5.13

Again, subscripts 1 and 2 represent compartments 1 and 2, respectively.

To solve the MBEs as represented by the relationships 3.5.7 and 3.5.10 for the two unknowns p_1 and p_2, the two expressions can be arranged and equated to zero, to give:

$$F_1(p_1, p_2) = p_1 - \left(\frac{p_i}{Z_i}\right) Z_1 \left(1 - \frac{G_{p1} + G_{p12}}{G_1}\right) = 0 \quad [3.5.14]$$

$$F_2(p_1, p_2) = p_2 - \left(\frac{p_i}{Z_i}\right) Z_2 \left(1 - \frac{G_{p2} - G_{p12}}{G_2}\right) = 0 \quad [3.5.15]$$

The general methodology of applying the method is very similar to that of Payne's and involves the following specific steps:

Step 1. Prepare the available gas properties data in tabulated and graphical forms that include, Z vs. p and μ_g vs. p.

Step 2. Divide the reservoir into compartments and determine the dimensions of each compartments in terms of:

length L
height h
width W
cross-sectional area A

Step 3. For each compartment, determine the initial gas-in-place G. For reasons of clarity, assume two gas compartments and calculate G_1 and G_2 from Equations 3.5.6 and 3.5.7:

$$G_1 = 43560 A_1 h_1 \phi_1 (1 S_{wi})/B_{gi}$$

$$G_2 = 43560 A_2 h_2 \phi_2 (1 S_{wi})/B_{gi}$$

Step 4. For each compartment, make a plot of p/Z vs. G_p that can be constructed by simply drawing a drawing a straight line between p_i/Z_i with initial gas-in-place in both compartments, i.e., G_1 and G_2.

Step 5. Calculate the transmissibility by applying Equation 3.5.9:

Step 6. Select a time step Δt and determine the corresponding actual cumulative gas production G_{p1} and G_{p2}.

Step 7. Calculate the gas influx rate Q_{12} and cumulative gas influx G_{p12} by applying Equations 3.5.8 and 3.5.3, respectively:

$$Q_{12} = \frac{0.111924 \Gamma_{12} (p_1^2 - p_2^2)}{TL}$$

$$G_{p12} = \int_0^t Q_{12} dt = \sum_0^t (\Delta Q_{12}) \Delta t$$

Step 8. Start the iterative solution by assuming initial estimates of the pressure for compartments 1 and 2 (i.e., p_1^k and p_2^k). Using the Newton–Raphson iterative scheme, calculate new improved values of the pressure p_1^{k+1} and p_2^{k+1} by solving the following

linear equations as expressed in a matrix form:

$$\begin{bmatrix} p_1^{k+1} \\ p_2^{k+1} \end{bmatrix} = \begin{bmatrix} p_1^k \\ p_2^k \end{bmatrix} - \begin{bmatrix} \dfrac{\partial F_1(p_1^k, p_2^k)}{\partial p_1} & \dfrac{\partial F_1(p_1^k, p_2^k)}{\partial p_2} \\ \dfrac{\partial F_2(p_1^k, p_2^k)}{\partial p_1} & \dfrac{\partial F_2(p_1^k, p_2^k)}{\partial p_2} \end{bmatrix}^{-1}$$

$$\times \begin{bmatrix} -F_1(p_1^k, p_2^k) \\ -F_2(p_1^k, p_2^k) \end{bmatrix}$$

where the superscript 1 denotes the inverse of the matrix. The partial derivatives in the above system of equations can be expressed in analytical form by differentiating Equations 3.5.14 and 3.5.15 with respect to p_1 and p_2. During an iterative cycle, the derivatives are evaluated at the updated new pressures, i.e., p_1^{k+1} and p_2^{k+1}. The iteration is stopped when $\left|p_1^{k+1} - p_1^k\right|$ and $\left|p_2^{k+1} - p_2^k\right|$ are less than a certain pressure tolerance, i.e., 5–10 psi.

Step 9. Generate the pressure profile as a function of time for each compartment by repeating steps 2 and 3.

Step 10. Repeat steps 6 through 11 to produce a pressure decline profile for each compartment that can be compared with the actual pressure profile for each compartment or that from step 4.

Compare the calculated pressure profiles with those of the observed pressures. If a match has not been achieved, adjust the size and number of compartments (i.e., initial gas-in-place) and repeat steps 2 through 10.

3.5.2 Combined decline curve and type curve analysis approach

Production decline analysis is the analysis of past trends of declining production performance, i.e., rate versus time and rate versus cumulative production plots, for wells and reservoirs. During the past 30 years, various methods have been developed for estimating reserves in tight gas reservoirs. These methods range from the basic MBE to decline and type curve analysis techniques. There are two kinds of decline curve analysis techniques, namely:

(1) the classical curve fit of historical production data;
(2) the type curve matching technique.

Some graphical solutions use a combination of decline curves and type curves with varying limitations. General principles of both types and methods of combining both approaches to determine gas reserves are briefly presented below.

Decline curve analysis
Decline curves are one of the most extensively used forms of data analysis employed in evaluating gas reserves and predicting future production. The decline curve analysis technique is based on the assumption that the past production trend with its controlling factors will continue in the future and, therefore, can be extrapolated and described by a mathematical expression.

The method of extrapolating a "trend" for the purpose of estimating future performance must satisfy the condition that the factors which caused changes in the past performance, i.e., decline in the flow rate, will operate in the same way in the future. These decline curves are characterized by three factors:

(1) initial production rate, or the rate at some particular time;
(2) curvature of the decline;
(3) rate of decline.
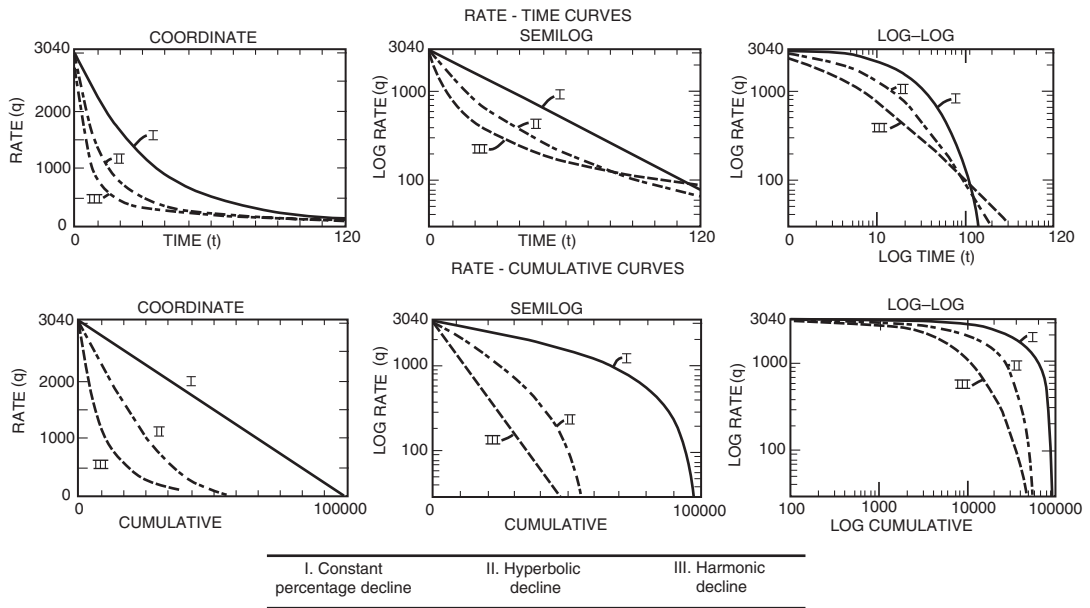
Figure 3.43 *Classification of production decline curves. (After Arps, J.J. "Estimation of Primary Oil Reserves," Courtesy of Trans. AIME, vol. 207, 1956).*

These factors are a complex function of numerous parameters within the reservoir, wellbore, and surface-handling facilities.

Ikoku (1984) presented a comprehensive and rigorous treatment of production decline curve analysis. He pointed out that the following three conditions must be considered when performing production decline curve analysis:

(1) Certain conditions must prevail before we can analyze a production decline curve with any degree of reliability. The production must have been stable over the period being analyzed; that is, a flowing well must have been produced with constant choke size or constant wellhead pressure and a pumping well must have been pumped off or produced with constant fluid level. These indicate that the well must have been produced at capacity under a given set of conditions. The production decline observed should truly reflect reservoir productivity and not be the result of external causes, such as a change in production conditions, well damage, production controls, and equipment failure.

(2) Stable reservoir conditions must also prevail in order to extrapolate decline curves with any degree of reliability. This condition will normally be met as long as the producing mechanism is not altered. However, when action is taken to improve the recovery of gas, such as infill drilling, fluid injection, fracturing, and acidizing, decline curve analysis can be used to estimate the performance of the well or reservoir in the absence of the change and compare it to the actual performance with the change. This comparison will enable us to determine the technical and economic success of our efforts.

(3) Production decline curve analysis is used in the evaluation of new investments and the audit of previous expenditures. Associated with this is the sizing of equipment and facilities such as pipelines, plants, and treating facilities. Also associated with the economic analysis is

the determination of reserves for a well, lease, or field. This is an independent method of reserve estimation, the result of which can be compared with volumetric or material balance estimates.

Arps (1945) proposed that the "curvature" in the production rate versus time curve can be expressed mathematically by one of the hyperbolic family of equations. Arps recognized the following three types of rate decline behavior:

(1) exponential decline;
(2) harmonic decline;
(3) hyperbolic decline.

Each type of decline curve has a different curvature as shown in Figure 3.43. This figure depicts the characteristic shape of each type of decline when the flow rate is plotted versus time or versus cumulative production on Cartesian, semilog, and log–log scales. The main characteristics of these decline curves are discussed below and can be used to select the flow rate decline model that is appropriate for describing the rate–time relationship of the hydrocarbon system:

• For exponential decline: A straight-line relationship will result when flow rate is plotted versus time on a *semilog scale* and also when the flow rate versus cumulative production is plotted on a *Cartesian scale*.
• For harmonic decline: Rate versus cumulative production is a straight line on a *semilog scale* with all other types of decline curves having some curvature. There are several shifting techniques that are designed to straighten out the resulting curve of plotting flow rate versus time when plotted on a log–log scale.
• For hyperbolic decline: None of the above plotting scales, i.e., Cartesian, semilog, or log–log, will produce a straight-line relationship for a hyperbolic decline. However, if the flow rate is plotted versus time on log–log paper, the

$$q_t = \frac{q_i}{(1 + bD_i t)^{1/b}}$$

Exponential	$b = 0$	$q_t = q_i \exp(-D_i t)$
Hyperbolic	$0 < b < 1$	$q_t = \dfrac{q_i}{(1 + bD_i t)^{1/b}}$
Harmonic	$b = 1$	$q_t = \dfrac{q_i}{(1 + D_i t)}$
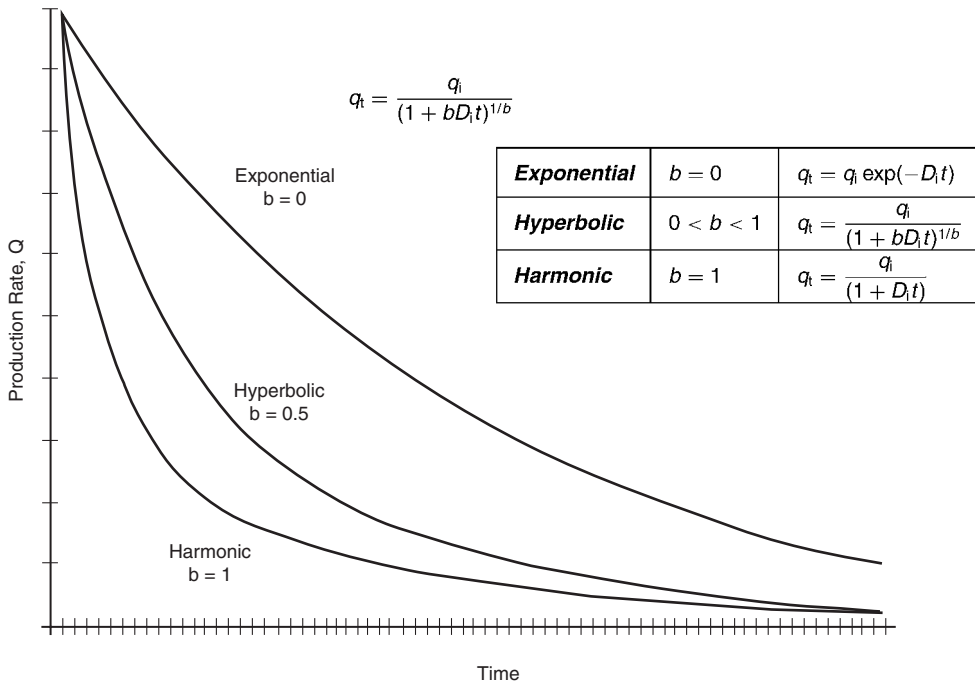
Figure 3.44 *Decline curve—rate/time (exponential, harmonic, hyperbolic).*

resulting curve can be straightened out by using shifting techniques.

Nearly all conventional decline curve analysis is based on empirical relationships of production rate versus time given by Arps (1945) as:

$$q_t = \frac{q_i}{(1 + bD_i t)^{1/b}} \qquad [3.5.16]$$

where:

q_t = gas flow rate at time t, MMscf/day
q_i = initial gas flow rate, MMscf/day
t = time, days
D_i = initial decline rate, day^1
b = Arps's decline curve exponent

The mathematical description of these production decline curves is greatly simplified with the use of the instantaneous (nominal) decline rate D. This decline rate is defined as the rate of change of the natural logarithm of the production rate, i.e., $\ln(q)$, with respect to time t, or:

$$D = -\frac{d(\ln q)}{dt} = -\frac{1}{q}\frac{dq}{dt} \qquad [3.5.17]$$

The minus sign has been added since dq and dt have opposite signs and it is convenient to have D always positive. Not that the decline rate equation, i.e., Equation 3.5.17, describes the instantaneous changes in the slope of the curvature dq/dt with changing of the flow rate q with time.

The parameters determined from the classical fit of the historical data, namely the decline rate D and the exponent b, can be used to predict future production. This type of decline curve analysis can be applied to individual wells or the entire reservoir. The accuracy of the entire reservoir application is sometimes better than for individual wells due to smoothing of the rate data. Based on the type of rate decline behavior of the hydrocarbon system, the value of b ranges from 0

to 1 and, accordingly, Arps's equation can be conveniently expressed in the following three forms:

Case	b	Rate–time relationship	
Exponential	$b = 0$	$q_t = q_i \exp(-D_i t)$	[3.5.18]
Hyperbolic	$0 < b < 1$	$q_t = \dfrac{q_i}{(1 + bD_i t)^{1/b}}$	[3.5.19]
Harmonic	$b = 1$	$q_t = \dfrac{q_i}{(1 + D_i t)}$	[3.5.20]

Figure 3.44 illustrates the general shape of the three curves at different possible values of b.

It should be pointed out that the above forms of decline curve equations are strictly applicable *only* when the well/reservoir is under pseudosteady (semisteady)-state flow conditions, i.e., boundary-dominated flow conditions. Arps's equation has been often misused and applied to model the performance of oil and gas wells whose flow regimes are in a transient flow. As presented in Chapter 1, when a well is first open to flow, it is under a transient (unsteady-state) condition. It remains under this condition until the production from the well affects the total reservoir system by reaching its drainage boundary, then the well is said to be flowing under pseudosteady-state or boundary-dominated flow conditions. The following is a list of inherent assumptions that must be satisfied before performing rate–time decline curve analysis:

- The well is draining a constant drainage area, i.e., the well is under boundary-dominated flow conditions.
- The well is produced at or near capacity.
- The well is produced at a *constant bottom-hole pressure*.

Again, the above conditions must be satisfied before applying any of the decline curve analysis methods to describe the production performance of a reservoir. In most cases, tight gas wells are producing at capacity and approach a constant

bottom-hole pressure, if produced at a constant line pressure. However, it can be extremely difficult to determine when a tight gas well has defined its drainage area and the start of the pseudosteady-state flowing condition.

The area under the decline curve of q versus time between times t_1 and t_2 is a measure of the cumulative gas production G_p during this period as expressed mathematically by:

$$G_p = \int_{t_1}^{t_2} q_t \mathrm{d}t \qquad [3.5.21]$$

Replacing the flow rate q_t in the above equation with the three individual expressions that describe types of decline curves, i.e., Equations 3.5.18 through 3.5.20, and integrating gives:

Exponential $b = 0$	$G_{p(t)} = \dfrac{1}{D_i}(q_i - q_t)$ [3.5.22]
Hyperbolic $0 < b < 1$	$G_{p(t)} = \left[\dfrac{(q_i)}{D_i(1-b)}\right]\left[1 - \left(\dfrac{q_t}{q_i}\right)^{1-b}\right]$ [3.5.23]
Harmonic $b = 1$	$G_{p(t)} = \left(\dfrac{q_i}{D_i}\right)\ln\left(\dfrac{q_i}{q_t}\right)$ [3.5.24]

where:

$G_{p(t)}$ = cumulative gas production at time t, MMscf
q_i = initial gas flow rate at time $t = 0$, MMscf/unit time
t = time, unit time
q_t = gas flow rate at time t, MMscf/unit time
D_i = nominal (initial) decline rate, 1/unit time

All the above expressions as given by Equations 3.5.18 through 3.5.24 require consistent units. Any convenient unit time can be used but, again, care should be taken to make certain that the time base of rates, i.e., q_i and q_t, matches the time unit of the decline rate D_i, e.g., for flow rate q in scf/month with D_i in month^{-1}.

Note that the *traditional* Arps decline curve analysis, as given by Equations 3.5.22 through 3.5.24, gives a reasonable estimation of reserves but it has its failings, the most important one being that it *completely ignores the flowing pressure data*. As a result, it can underestimate or over estimate the reserves. The practical applications of these three commonly used decline curves are documented below.

Exponential decline, b=0 The graphical presentation of this type of decline curve indicates that a plot of q_t vs. t on a semilog scale or a plot of q_t vs. $G_{p(t)}$ on a Cartesian scale will produce linear relationships that can be described mathematically by:

$$q_t = q_i \exp(-D_i t)$$

or linearly as:

$$\ln(q_t) = \ln(q_i) - D_i t$$

And similarly:

$$G_{p(t)} = \frac{q_i - q_t}{D_i}$$

or linearly as:

$$q_t = q_i - D_i G_{p(t)}$$

This type of decline curve is perhaps the simplest to use and perhaps the most conservative. It is widely used in the industry for the following reasons:

- Many wells follow a constant decline rate over a great portion of their productive life and will deviate significantly from this trend toward the end of this period.
- The mathematics involved, as described by the above line expressions, is easier to apply than the other line types.

Assuming that the historical production from a well or field is recognized by its exponential production decline behavior, the following steps summarize the procedure to predict the behavior of the well or the field as a function of time.

Step 1. Plot q_t vs. G_p on a Cartesian scale and q_t vs. t on semilog paper.

Step 2. For both plots, draw the best straight line through the points.

Step 3. Extrapolate the straight line on q_t vs. G_p to $G_p = 0$ which intercepts the y axis with a flow rate value that is identified as q_i.

Step 4. Calculate the initial decline rate D_i by selecting a point on the Cartesian straight line with coordinates of (q_t, G_{pt}) or on a semilog line with coordinates of (q_t, t) and solve for D_i by applying Equation 3.5.20 or 3.5.22:

$$D_i = \frac{\ln(q_i/q_t)}{t} \qquad [3.5.25]$$

or equivalently as:

$$D_i = \frac{q_i - q_t}{G_{p(t)}} \qquad [3.5.26]$$

If the method of least squares is used to determine the decline rate by analyzing the entire production data, then

$$D_i = \frac{\sum_t \left[t \ln(q_i/q_t)\right]}{\sum_t t^2} \qquad [3.5.27]$$

or equivalently as:

$$D_i = \frac{q_i \sum_t G_{p(t)} - \sum_t q_t G_{p(t)}}{\sum_t [G_{p(t)}]^2} \qquad [3.5.28]$$

Step 5. Calculate the time to reach the economic flow rate q_a (or any rate) and the corresponding cumulative gas production from Equations 3.5.18 and 3.5.22:

$$t_a = \frac{\ln(q_i/q_a)}{D_i}$$

$$G_{pa} = \frac{q_i - q_a}{t_a}$$

where:

G_{pa} = cumulative gas production when reaching the economic flow rate or at abandonment, mmscf
q_i = initial gas flow rate at time $t = 0$, MMscf/unit time
t = abandonment time, unit time
q_a = economic (abandonment) gas flow rate, MMscf/unit time
D_i = nominal (initial) decline rate, 1/time unit

Example 3.16 The following production data is available from a dry gas field:

q_t (MMscf/day)	G_p (MMscf)	q_t (MMscf/day)	G_p (MMscf)
320	16000	208	304000
336	32000	197	352000
304	48000	184	368000
309	96000	176	384000
272	160000	184	400000
248	240000		

Estimate:

(a) the future cumulative gas production when gas flow rate reaches 80 MMscf/day;
(b) the *extra* time to reach 80 MMscf/day.

Solution

(a) Use the following steps:

Step 1. A plot of G_p vs. q_t on a Cartesian scale as shown in Figure 3.45 produces a straight line indicating an exponential decline.
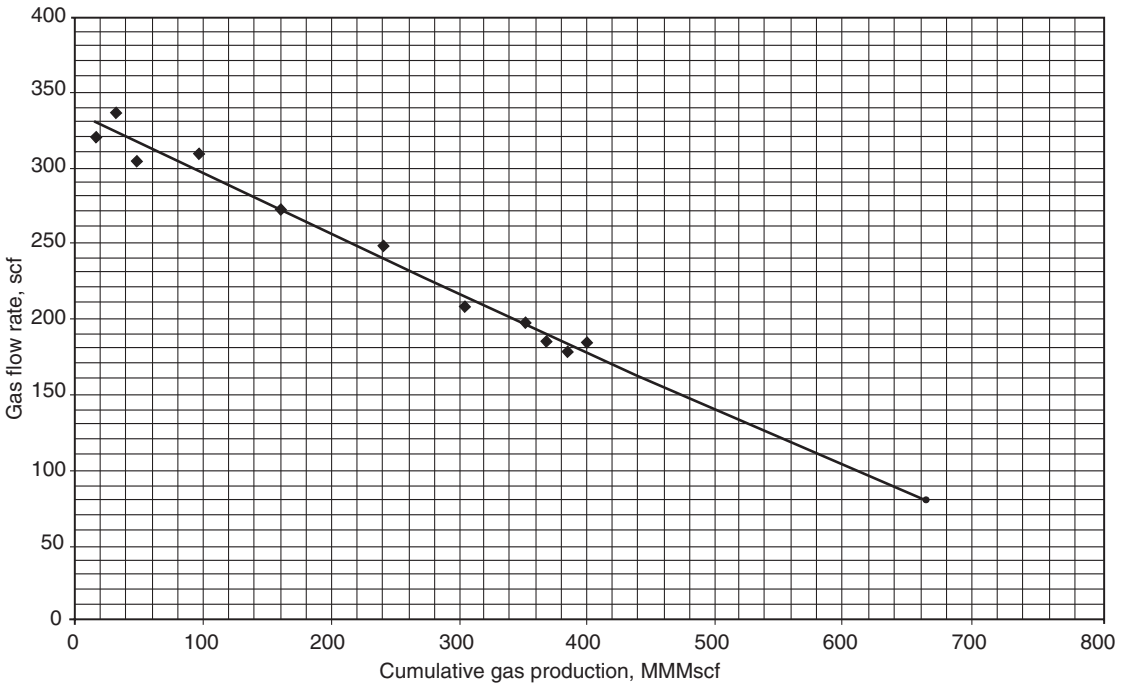
Figure 3.45 *Decline curve data for Example 3.16.*

Step 2. From the graph, cumulative gas production is 633 600 MMscf at $q_t = 80$ MMscf/day indicating an extra production of $633.6 - 400.0 = 233.6$ MMMscf.

Step 3. The intercept of the straight line with the y axis gives a value of $q_i = 344$ MMscf/day.

Step 4. Calculate the initial (nominal) decline rate D_i by selecting a point *on* the straight line and solving for D_i by applying Equation 3.5.25. At $G_{p(t)}$ of 352 MMscf, q_t is 197 MMscf/day or:

$$D_i = \frac{q_i - q_t}{G_{p(t)}} = \frac{344 - 197}{352000} = 0.000418 \text{ day}^{-1}$$

It should be pointed out that the monthly and yearly nominal decline can be determined as:

$$D_{im} = (0.000418)(30.4) = 0.0126 \text{ month}^{-1}$$

$$D_{iy} = (0.0126)(12) = 0.152 \text{ year}^{-1}$$

Using the least-squares approach, i.e., Equation 3.5.28, gives:

$$D_i = \frac{0.3255(10^9) - 0.19709(10^9)}{0.295(10^{12})}$$

$$= 0.000425 \text{ day}^{-1}$$

(b) To calculate the *extra* time to reach 80 MMscf/day, use the following steps:

Step 1. Calculate the time to reach the last recorded flow rate of 184 MMscf from Equation 3.5.25.

$$t = \frac{\ln(344/184)}{0.000425} = 1472 \text{ days} = 4.03 \text{ years}$$

Step 2. Calculate total time to reach a gas flow rate of 80 MMscf/day:

$$t = \frac{\ln(344/80)}{0.000425} = 3432 \text{ days} = 9.4 \text{ years}$$

Step 3. Extra time $= 9.4 - 4.03 = 5.37$ years.

Example 3.17 A gas well has the following production history:

Date	Time (months)	q_t (MMscf/month)
1-1-02	0	1240
2-1-02	1	1193
3-1-02	2	1148
4-1-02	3	1104
5-1-02	4	1066
6-1-02	5	1023
7-1-02	6	986
8-1-02	7	949
9-1-02	8	911
10-1-02	9	880
11-1-02	10	843
12-1-02	11	813
1-1-03	12	782

(a) Use the first six months of the production history data to determine the coefficient of the decline curve equation.
(b) Predict flow rates and cumulative gas production from August 1, 2002 through January 1, 2003.
(c) Assuming that the economic limit is 30 MMscf/month, estimate the time to reach the economic limit and the corresponding cumulative gas production.

Solution

(a) Use the following steps:

Step 1. A plot of q_t vs. t on a semilog scale as shown in Figure 3.46 indicates an exponential decline.

Step 2. Determine the initial decline rate D_i by selecting a point on the straight line and substituting the coordinates of the point in Equation 3.5.25
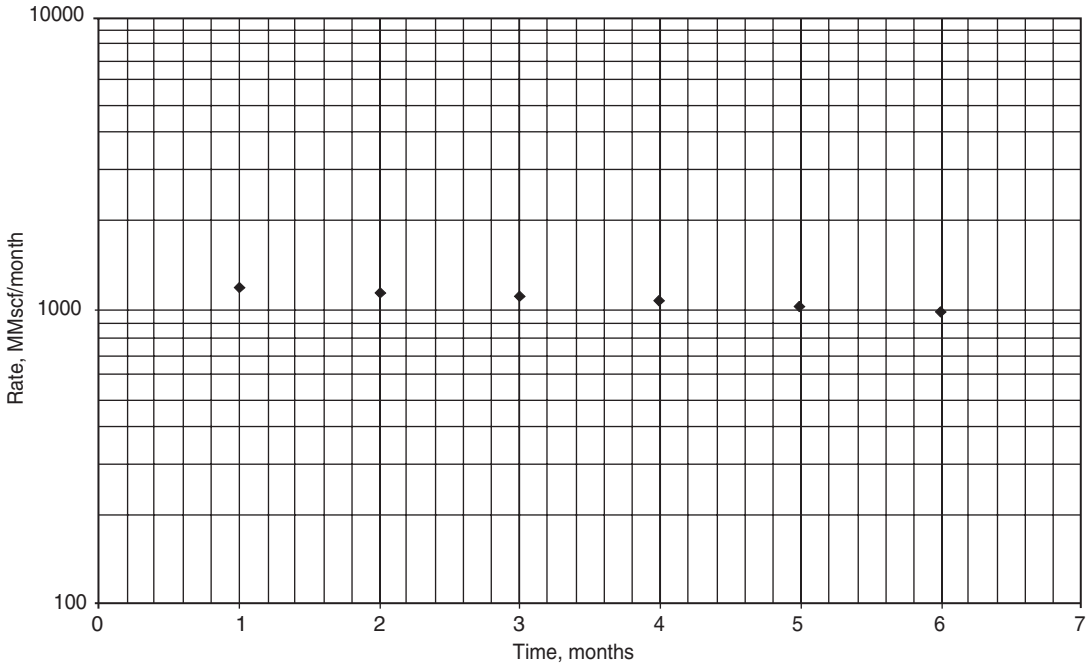
Figure 3.46 *Decline curve data for Example 3.17.*

or using the least-squares method, to give, from Equation 3.5.25:

$$D_i = \frac{\ln(q_i/q_t)}{t}$$

$$= \frac{\ln(1240/986)}{6} = 0.0382 \text{ month}^{-1}$$

Similarly; from Equation 3.5.27:

$$D_i = \frac{\sum_t \left[t \ln(q_i/q_t) \right]}{\sum_t t^2}$$

$$= \frac{3.48325}{91} = 0.0383 \text{ month}^{-1}$$

(b) Use Equations 3.5.18 and 3.5.22 to calculate q_t and $G_{p(t)}$ in the following tabulated form:

$$q_t = 1240 \exp(-0.0383t)$$
$$G_{pt} = (q_i - q_t)/0.0383$$

Date	Time (months)	Actual q_t (MMscf/ month)	Calculated q_t (MMscf/ month)	$G_{p(t)}$ (MMscf/ month)
2-1-02	1	1193	1193	1217
3-1-02	2	1148	1149	2387
4-1-02	3	1104	1105	3514
5-1-02	4	1066	1064	4599
6-1-02	5	1023	1026	4643
7-1-02	6	986	986	6647
8-1-02	7	949	949	7614
9-1-02	8	911	913	8545

Date	Time (months)	Actual q_t (MMscf/ month)	Calculated q_t (MMscf/ month)	$G_{p(t)}$ (MMscf/ month)
10-1-02	9	880	879	9441
11-1-02	10	843	846	10303
12-1-02	11	813	814	11132
1-1-03	12	782	783	11931

(c) Use Equations 3.5.25 and 3.5.26 to calculate the time to reach an economic flow rate of 30 MMscf/month and the corresponding reserves:

$$t = \frac{\ln(1240/30)}{0.0383} = 97 \text{ months} = 8 \text{ years}$$

$$G_{pt} = \frac{(1240 - 30)10^6}{0.0383} = 31.6 \text{ MMMscf}$$

Harmonic decline, b=1 The production recovery performance of a hydrocarbon system that follows a harmonic decline, i.e., $b = 1$ in Equation 3.5.16, is described by Equations 3.5.20 and 3.5.24:

$$q_t = \frac{q_i}{1 + D_i t}$$

$$G_{p(t)} = \left(\frac{q_i}{D_i} \right) \ln \left(\frac{q_i}{q_t} \right)$$

The above two expressions can be rearranged and expressed respectively as:

$$\frac{1}{q_t} = \frac{1}{q_i} + \left(\frac{D_i}{q_i} \right) t \qquad [3.5.29]$$

$$\ln(q_t) = \ln(q_i) - \left(\frac{D_i}{q_i} \right) G_{p(t)} \qquad [3.5.30]$$

The basic two plots for harmonic decline curve analysis are based on the above two relationships. Equation 3.5.29 indicates that a plot of $1/q_t$ vs. t on a Cartesian scale will yield a straight line with a slope of (D_i/q_i) and intercept of $1/q_i$. Equation 3.5.30 suggests that a plot of q_t vs. $G_{p(t)}$ on a semilog scale will yield a straight line with a negative slope of (D_i/q_i) and an intercept of q_i. The method of least squares can also be sued to calculate the decline rate D_i, to give:

$$D_i = \frac{\sum_t (tq_i/q_t) - \sum_t t}{\sum_t t^2}$$

Other relationships that can be derived from Equations 3.5.29 and 3.5.30 include the time to reach the economic flow rate q_a (or any flow rate) and the corresponding cumulative gas production $G_{p(a)}$:

$$t_a = \frac{q_i - q_a}{q_a D_i} \qquad [3.5.31]$$

$$G_{p(a)} = \left(\frac{q_i}{D_i}\right) \ln\left(\frac{q_a}{q_t}\right)$$

Hyperbolic decline, 0 < b < 1 The two governing relationships for a reservoir or a well when its production follows the hyperbolic decline behavior are given by Equations 3.5.19 and 3.5.23, or:

$$q_t = \frac{q_i}{(1 + bD_it)^{1/b}}$$

$$G_{p(t)} = \left[\frac{q_i}{D_i(1-b)}\right]\left[1 - \left(\frac{q_t}{q_i}\right)^{1-b}\right]$$

The following simplified iterative method is designed to determine D_i and b from the historical production data:

Step 1. Plot q_t vs. t on a semilog scale and draw a *smooth curve* through the points.
Step 2. Extend the curve to intercept the y axis at $t = 0$ and read q_i.
Step 3. Select the other end point of the smooth curve and record the coordinates of the point and refer to it as (t_2, q_2).
Step 4. Determine the coordinates of the middle point on the smooth curve that corresponds to (t_1, q_1) with the value of q_1 as obtained from the following expression:

$$q_1 = \sqrt{q_i q_2} \qquad [3.5.32]$$

The corresponding value of t_1 is read from the smooth curve at q_1.

Step 5. Solve the following equation iteratively for b:

$$f(b) = t_2\left(\frac{q_i}{q_1}\right)^b - t_1\left(\frac{q_i}{q_2}\right)^b - (t_2 - t_1) = 0$$
$$[3.5.33]$$

The Newton–Raphson iterative method can be employed to solve the above non-linear function by using the following recursion technique:

$$b^{k+1} = b^k - \frac{f(b^k)}{f'(b^k)} \qquad [3.5.34]$$

where the derivative $f^{\backslash}(b^k)$ is given by:

$$f^{\backslash}(b^k) = t_2\left(\frac{q_i}{q_1}\right)^{b^k}\ln\left(\frac{q_i}{q_1}\right) - t_1\left(\frac{q_i}{q_2}\right)^{b^k}\ln\left(\frac{q_i}{q_2}\right)$$
$$[3.5.35]$$

Starting with an initial value of $b = 0.5$, i.e., $b^k = 0.5$, the method will usually converge after 4–5 iterations when setting the convergence criterion at $b^{k+1} - b^k \leq 10^{-6}$.

Step 6. Solve for D_i by solving Equation 3.5.19 for D_i and using the calculated value of b from step 5 and the
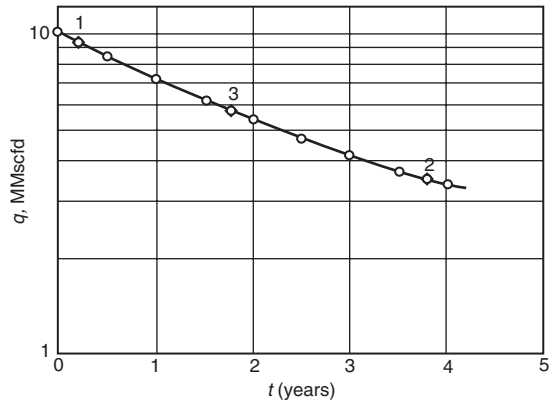
Figure 3.47 *Rate–time plot for Example 3.18.*

coordinates of a point on the smooth graph, i.e., (t_2, q_2), to give:

$$D_i = \frac{(q_i/q_2)^b - 1}{bt_2} \qquad [3.5.36]$$

The following example illustrates the proposed methodology for determining b and D_i.

Example 3.18[a] The following production data is reported by Ikoku for a gas well:

Date	Time (years)	q_t (MMscf/day)	$G_{p(t)}$ (MMscf)
Jan. 1, 1979	0.0	10.00	0.00
July 1, 1979	0.5	8.40	1.67
Jan. 1, 1980	1.0	7.12	3.08
July 1, 1980	1.5	6.16	4.30
Jan. 1, 1981	2.0	5.36	5.35
July 1, 1981	2.5	4.72	6.27
Jan. 1, 1982	3.0	4.18	7.08
July 1, 1982	3.5	3.72	7.78
Jan. 1, 1983	4.0	3.36	8.44

Estimate the future production performance for the next 16 years.

Solution

Step 1. Determine the type of decline that adequately represents the historical data. This can be done by constructing the following two plots:

   (1) Plot q_t vs. t on a semilog scale as shown in Figure 3.47. The plot does not yield a straight line and, thus, the decline is *not exponential*.
   (2) Plot q_t vs. $G_{p(t)}$ on semilog paper as shown in Figure 3.48. The plot again does not produce a straight line and, therefore, the decline is *not a harmonic*.

The generated two plots indicate that the decline must be hyperbolic

Step 2. From Figure 3.47, determine the initial flow rate q_i by extending the smooth curve to intercept with the y axis, i.e., at $t = 0$, to give:

$$q_i = 10 \text{ MMscf/day}$$

[a]Ikoku, C. *Natural Gas Reservoir Engineering*, John Wiley & Sons (1984).
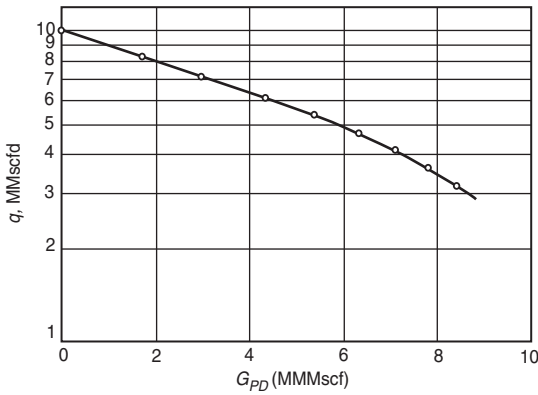
Figure 3.48   *Rate—cumulative plot for Example 3.18.*

Step 3. Select the coordinates of the other end point on the smooth curve as (t_2, q_2), to give:

$$t_2 = 4 \text{ years}$$

$$q_2 = 3.36 \text{ MMscf/day}$$

Step 4. Calculate q_1 from Equation 3.5.32 and determine the corresponding time:

$$q_1 = \sqrt{q_i q_2} = \sqrt{(10)(3.36)} = 5.8 \text{ MMscf/day}$$

The corresponding time $t_1 = 1.719$ years.

Step 5. Assume $b = 0.5$, and solve Equation 3.5.33 iteratively for b:

$$f(b) = t_2 \left(\frac{q_i}{q_1}\right)^b - t_1 \left(\frac{q_i}{q_2}\right)^b - (t_2 - t_1)$$

$$f(b) = 4(1.725)^b - 1.719(2.976)^b - 2.26$$

and:

$$f'(b^k) = t_2 \left(\frac{q_i}{q_1}\right)^{b^k} \ln\left(\frac{q_i}{q_1}\right) - t_1 \left(\frac{q_i}{q_2}\right)^{b^k} \ln\left(\frac{q_i}{q_2}\right)$$

$$f'(b) = 2.18(1.725)^b - 1.875(2.976)^b$$

with:

$$b^{k+1} = b^k - \frac{f(b^k)}{f'(b^k)}$$

The iterative method can be conveniently performed by constructing the following table:

k	b^k	$f(b)$	$f'(b)$	b^{k+1}
0	0.500000	7.57×10^{-3}	-0.36850	0.520540
1	0.520540	-4.19×10^{-4}	-0.40950	0.519517
2	0.519517	-1.05×10^{-6}	-0.40746	0.519514
3	0.519514	-6.87×10^{-9}	-0.40745	0.519514

The method converges after three iterations with a value of $b = 0.5195$.

Step 6. Solve for D_i by using Equation 3.5.36:

$$D_i = \frac{(q_i/q_2)^b - 1}{b t_2}$$

$$= \frac{(10/3.36)^{0.5195} - 1}{(0.5195)(4)} = 0.3668 \text{ year}^{-1}$$

or on a monthly basis $D_i = 0.3668/12 = 0.0306 \text{ month}^{-1}$
or on a daily basis $D_i = 0.3668/365 = 0.001 \text{ day}^{-1}$

Step 7. Use Equations 3.5.19 and 3.5.23 to predict the future production performance of the gas well. Note in Equation 3.5.19 that the denominator contains $D_i t$ and, therefore, the product must be dimensionless, or:

$$q_t = \frac{10(10^6)}{[1 + 0.5195 D_i t]^{(1/0.5195)}}$$

$$= \frac{(10)(10^6)}{[1 + 0.5195(0.3668)(t)]^{(1/0.5195)}}$$

where:

q_t = flow rate, MMscf/day
t = time, years
D_i = decline rate, year^{-1}

In Equation 3.5.23, the time basis in q_i is expressed in days and, therefore, D_i must be expressed in day^{-1}, or:

$$G_{p(t)} = \left[\frac{q_i}{D_i(1-b)}\right]\left[1 - \left(\frac{q_t}{q_i}\right)^{1-b}\right]$$

$$= \left[\frac{(10)(10^6)}{(0.001)(1 - 0.5195)}\right]$$

$$\times \left[1 - \left(\frac{q_t}{(10)(10^6)}\right)^{1-0.5195}\right]$$

Results of step 7 are tabulated below and shown graphically in Figure 3.49:

Time (years)	Actual q (MMscf/day)	Calculated q (MMscf/day)	Actual cum. gas (MMMscf)	Calc. cum. gas (MMMscf)
0	10	10	0	0
0.5	8.4	8.392971	1.67	1.671857
1	7.12	7.147962	3.08	3.08535
1.5	6.16	6.163401	4.3	4.296641
2	5.36	5.37108	5.35	5.346644
2.5	4.72	4.723797	6.27	6.265881
3	4.18	4.188031	7.08	7.077596
3.5	3.72	3.739441	7.78	7.799804
4	3.36	3.36	8.44	8.44669
5		2.757413		9.557617
6		2.304959		10.477755
7		1.956406		11.252814
8		1.68208		11.914924
9		1.462215		12.487334
10		1.283229		12.987298
11		1.135536		13.427888
12		1.012209		13.819197
13		0.908144		14.169139
14		0.819508		14.484015
15		0.743381		14.768899
16		0.677503		15.027928
17		0.620105		15.264506
18		0.569783		15.481464
19		0.525414		15.681171
20		0.486091		15.86563

Gentry (1972) developed a graphical method for the coefficients b and D_i as shown in Figures 3.50 and 3.51. Arps's decline curve exponent b is expressed in Figure 3.50 in terms of the ratios q_i/q and $G_p/(tq_i)$ with an upper limit for q_i/q at 100. To determine the exponent b, enter the graph with the abscissa with a value of $G_p/(tq_i)$ that corresponds to the last
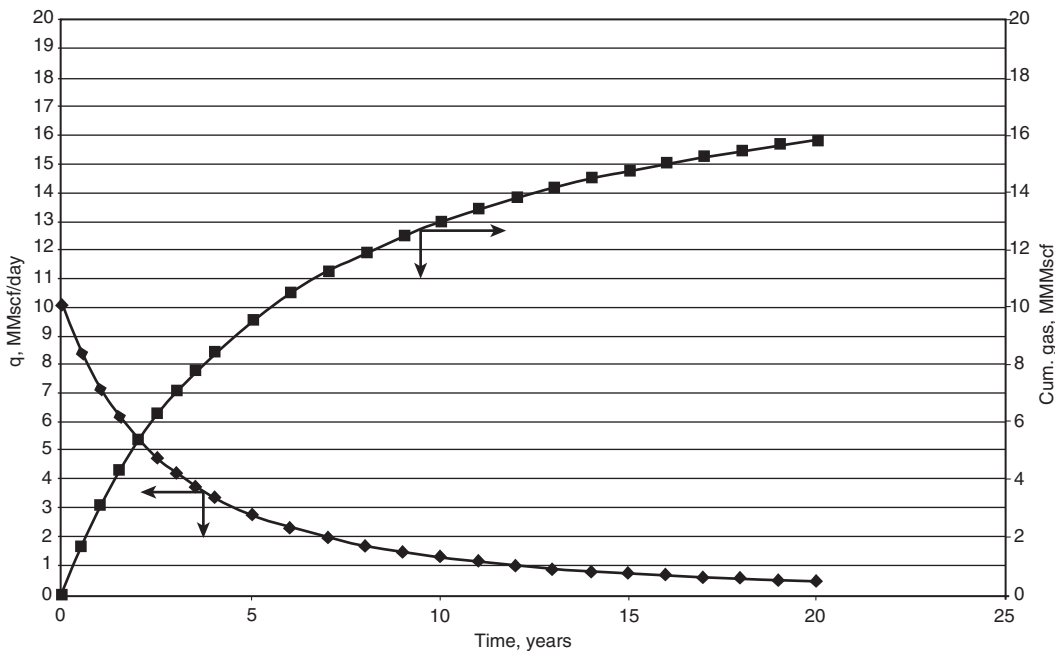
Figure 3.49   *Decline curve data for Example 3.18.*
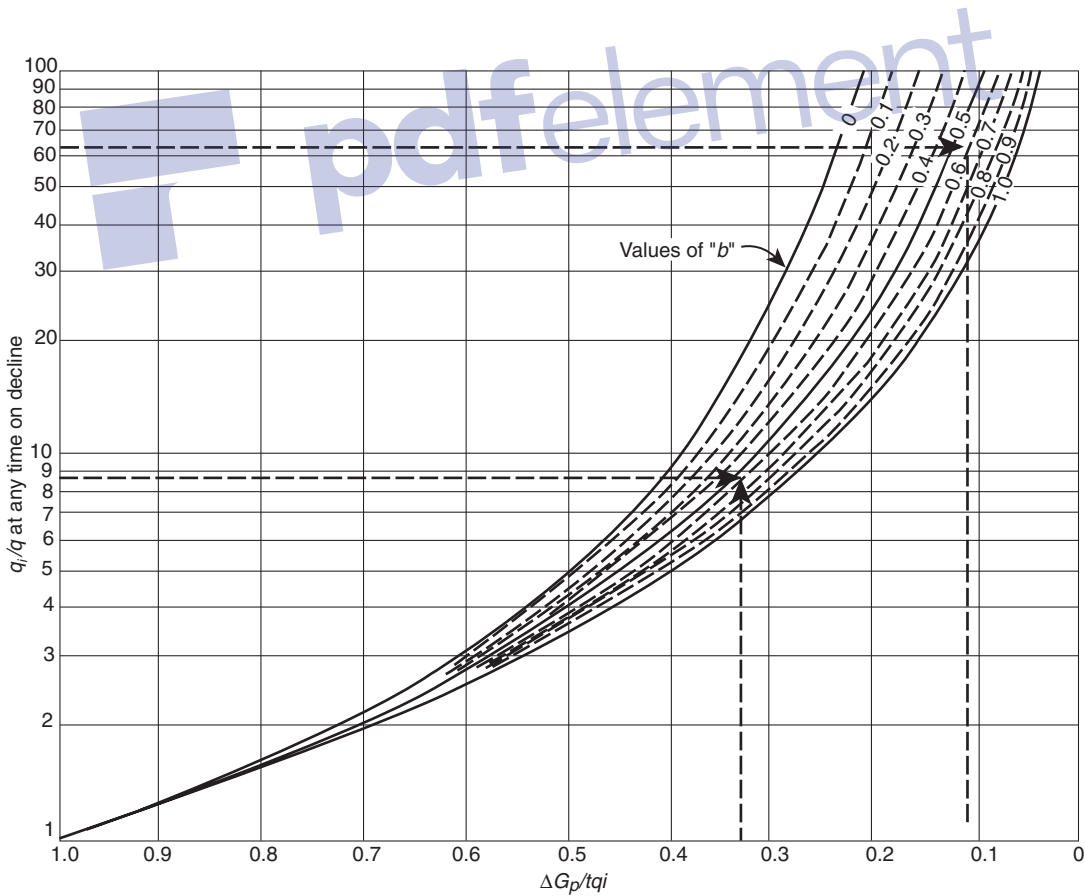
Figure 3.50   *Relationship between production rate and cumulative production (After Gentry, 1972).*
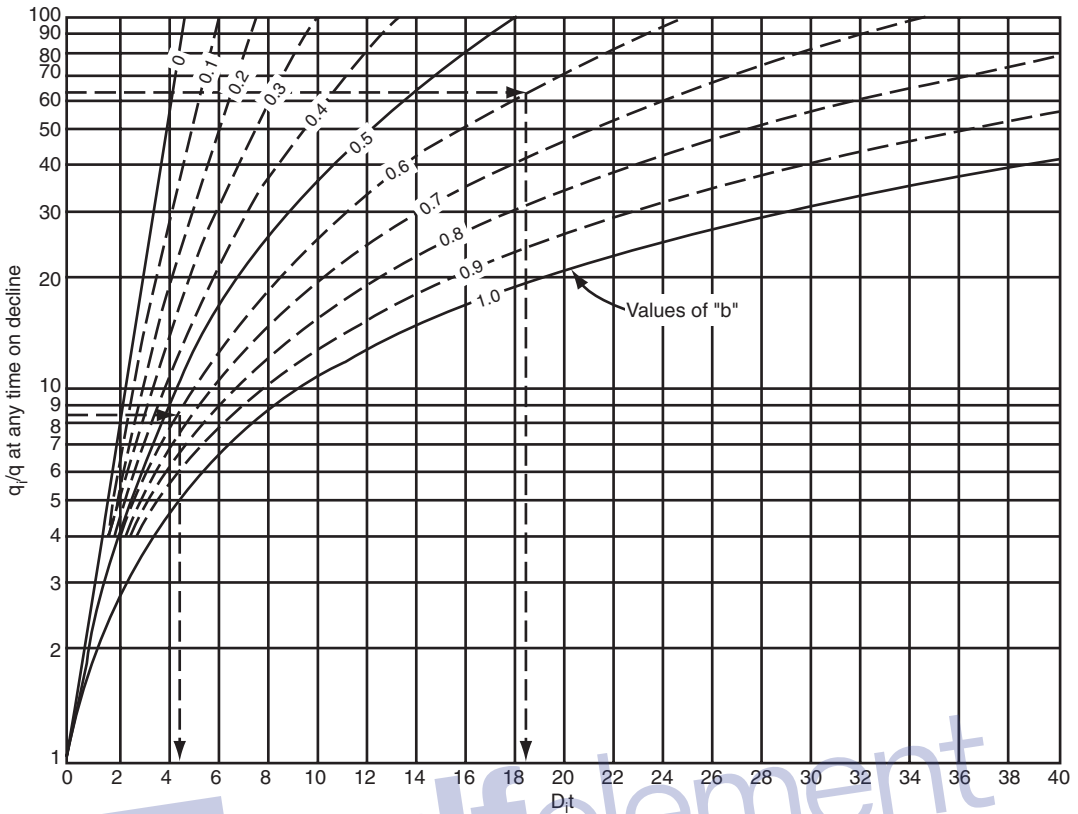
Figure 3.51   *Relationship betweeen production rate and time (After Gentry, 1972).*

data point on the decline curve and enter the coordinates with the value of the ratio of initial production rate to that of the last rate on the decline curve q_i/q. The exponent b is read by the intersection of these two values. The initial decline rate D_i can be determined from Figure 3.51 by entering the ordinate with the value of q_i/q and moving to the right to the curve that corresponds to the value of b. The initial decline rate D_i can be found by reading the value on the abscissa divided by the time t from q_i to q.

Example 3.19   Using the data given in Example 3.18, recalculate the coefficients b and D_i by using Gentry's graphs.

Solution

Step 1. Calculate the ratios q_i/q and $G_p/(tq_i)$ as:
$$q_i/q = 10/3.36 = 2.98$$
$$G_p/(tq_i) = 8440/[(4 \times 365)(10)] = 0.58$$

Step 2. From Figure 3.50, draw a horizontal line from the y axis at 2.98 and a vertical line from the x axis at 0.58 and read the value of b at the intersection of the two lines, to give:
$$b = 0.5$$

Step 3. Figure 3.51 with the values of 2.98 and 0.5 to give:
$$D_i t = 1.5 \quad \text{or} \quad D_i = 1.5/4 = 0.38 \text{ year}^{-1}$$

In many cases gas wells are not produced at their full capacity during their early life for various reasons, such as

limited capacity of flow lines, transportation, low demand, or other types of restrictions. Figure 3.52 illustrates a model for estimating the time pattern of production where the rate is restricted.

Figure 3.52 shows that the well produces at a restricted flow rate of q_r for a total time of t_r with a cumulative production of G_{pr}. The proposed methodology for estimating the restricted time t_r is to set the total cumulative production $G_{p(tr)}$ that would have occurred under normal decline from the initial well capacity q_i down to q_r equal to G_{pr}. Eventually, the well will reach the time t_r where it begins to decline with a behavior that is similar to other wells in the area. The proposed method for predicting the decline rate behavior for a
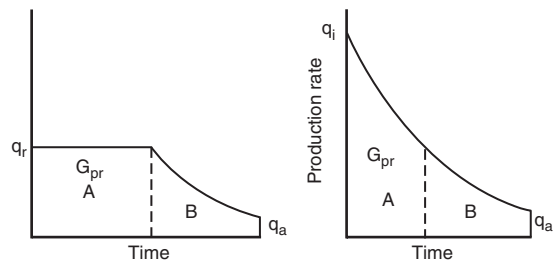
Figure 3.52   *Estimation of the effect of restricting maximum production rate.*

well under restricted flow is based on the assumption that the following data is available and applicable to the well:

- coefficients of Arps's equation, i.e., D_i and b by analogy with other wells;
- abandonment (economic) gas flow rate q_a;
- ultimate recoverable reserves G_{pa};
- allowable (restricted) flow rate q_r.

The methodology is summarized in the following steps:

Step 1. Calculate the initial well flow capacity q_i that would have occurred with no restrictions, as follows:

For exponential $q_i = G_{pa}D_i + q_a$ [3.5.37]

For harmonic $q_i = q_r \left[1 + \dfrac{D_i G_{pa}}{q_r} - \ln\left(\dfrac{q_r}{q_a}\right) \right]$ [3.5.38]

For hyperbolic $q_i = \left\{ (q_r)^b + \dfrac{D_i b G_{pa}}{(q_r)^{1-b}} - \dfrac{b(q_r)^b}{1-b} \right.$

$\left. \times \left[1 - \left(\dfrac{q_a}{q_r}\right)^{1-b} \right] \right\}^{1/b}$ [3.5.39]

Step 2. Calculate the cumulative gas production during the restricted flow rate period:

For exponential $G_{pr} = \dfrac{q_i - q_r}{D_i}$ [3.5.40]

For harmonic $G_{pr} = \left(\dfrac{q_i}{D_i}\right) \ln\left(\dfrac{q_i}{q_r}\right)$ [3.5.41]

For hyperbolic $G_{pr} = \left[\dfrac{q_i}{D_i(1-b)} \right] \left[1 - \left(\dfrac{q_r}{q_i}\right)^{1-b} \right]$ [3.5.42]

Step 3. Regardless of the type of decline, calculate the total time of the restricted flow rate from:

$t_r = \dfrac{G_{pr}}{q_r}$ [3.5.43]

Step 4. Generate the well production performance as a function of time by applying the appropriate decline relationships as given by Equations 3.5.18 through 3.5.29.

Example 3.20 The volumetric calculations on a gas well show that the ultimate recoverable reserves G_{pa} are 25 MMMscf of gas. By analogy with other wells in the area, the following data is assigned to the well:

exponential decline
allowable (restricted) production rate $= 425$ MMscf/month
economic limit $= 30$ MMscf/month
nominal decline rate $= 0.044$ month^{-1}

Calculate the yearly production performance of the well.

Solution

Step 1. Estimate the initial flow rate q_i from Equation 3.5.37:

$q_i = G_{pa}D_i + q_a$

$= (0.044)(25\,000) + 30 = 1130$ MMscf/month

Step 2. Calculate the cumulative gas production during the restricted flow period by using Equation 3.5.40:

$G_{pr} = \dfrac{q_i - q_r}{D_i}$

$= \dfrac{1130 - 425}{0.044} = 16.023$ MMscf

Step 3. Calculate the total time of the restricted flow from Equation 3.5.43:

$t_r = \dfrac{G_{pr}}{q_r}$

$= \dfrac{16\,023}{425} = 37.7$ months $= 3.14$ years

Step 4. The yearly production during the first three years is:

$q = (425)(12) = 5100$ MMscf/year

The fourth year is divided into 1.68 months, i.e., 0.14 years, of constant production plus 10.32 months of declining production, or:

For the first 1.68 months $(1.68)(425) = 714$ MMscf

At the end of the fourth year:

$q = 425 \exp\left[-0.044(10.32)\right] = 270$ MMscf/month

Cumulative gas production for the last 10.32 months is:

$\dfrac{425 - 270}{0.044} = 3523$ MMscf

Total production for the fourth year is:

$714 + 3523 = 4237$ MMscf

Year	Production (MMscf/year)
1	5100
2	5100
3	5100
4	4237

The flow rate at the end of the fourth year, i.e., 270 MMscf/month, is set equal to the *initial flow rate at the beginning of the fifth year*. The flow rate at the end of the fifth year, q_{end}, is calculated from Equation 3.5.40 as:

$q_{end} = q_i \exp[-D_i(12)]$

$= 270 \exp[-0.044(12)] = 159$ MMscf/month

with a cumulative gas production of:

$G_p = \dfrac{q_i - q_{end}}{D_i} = \dfrac{270 - 159}{0.044} = 2523$ MMscf

And for the sixth year:

$q_{end} = 159 \exp[-0.044(12)] = 94$ MMscf/month

as:

$G_p = \dfrac{159 - 94}{0.044} = 1482$ MMscf

Results of the above repeated procedure are tabulated below:

t (years)	q_i (MMscf/ month)	q_{end} (MMSCF/ month)	*Yearly production* (MMscf/year)	*Cumulative production* (MMMscf)
1	425	425	5100	5.100
2	425	425	5100	10.200
3	425	425	5100	15.300
4	425	270	4237	19.537
5	270	159	2523	22.060
6	159	94	1482	23.542
7	94	55	886	24.428
8	55	33	500	24.928

Reinitialization of Data Fetkovich (1980) pointed out that there are several obvious situations where rate–time data must be reinitialized for reasons that include among others:

- the drive or production mechanism has changed;
- an abrupt change in the number of wells on a lease or a field due to infill drilling;
- changing the size of tubing would change q_i and also the decline exponent b.

Providing a well is not tubing or equipment limited, the effects of stimulation will result in a change in deliverability q_i and possibly the remaining recoverable gas. However, the decline exponent b normally can be assumed constant. Fetkovich et al. (1996) suggested a "rule-of-thumb" equation to approximate an increase in rate due to stimulation as:

$$(q_i)_{new} = \left[\frac{7 + s_{old}}{7 + s_{new}} \right] (q_t)_{old}$$

where:

$(q_t)_{old}$ = producing rate just prior to stimulation
s = skin factor

Arps's equation, i.e., Equation 3.5.16, can be expressed as:

$$q_t = \frac{(q_i)_{new}}{(1 + bt(D_i)_{new})^{1/b}}$$

with:

$$(D_i)_{new} = \frac{(q_i)_{new}}{(1 - b) G}$$

where:

G = gas-in-place, scf

Type curve analysis
As presented in Chapter 1, type curve analysis of production data is a technique where actual production rate and time are history matched to a theoretical model. The production data and theoretical model are generally expressed graphically in dimensionless forms. Any variable can be made "dimensionless" by multiplying it by a group of constants with opposite dimensions, but the choice of this group will depend on the type of problem to be solved. For example, to create the dimensionless pressure drop p_D, the actual pressure drop in psi is multiplied by the group A with units of psi^{-1}, or:

$$p_D = A\Delta p$$

Finding group A that makes a variable dimensionless is derived from equations that describe reservoir fluid flow. To introduce this concept, recall Darcy's equation that describes the radial, incompressible, steady-state flow as expressed by:

$$Q = \left[\frac{0.00708\, kh}{B\mu[\ln(r_e/r_{wa}) - 0.5]} \right] \Delta p$$

where r_{wa} is the apparent (effective) wellbore radius and defined by Equation 1.2.140 in terms of the skin factor s as:

$$r_{wa} = r_w e^{-s}$$

Group A can be defined by rearranging Darcy's equation as:

$$\ln \left(\frac{r_e}{r_{wa}} \right) - \frac{1}{2} = \left[\frac{0.00708\, kh}{QB\mu} \right] \Delta p$$

Because the left-hand slide of the above equation is dimensionless, the right-hand side must be accordingly dimensionless. This suggests that the term $0.00708kh/QB\mu$ is essentially group A with units of psi^{-1} that defines the dimensionless variable p_D, or:

$$p_D = \left[\frac{0.00708\, kh}{QB\mu} \right] \Delta p$$

Or the ratio of p_D to Δp as:

$$\frac{p_D}{\Delta p} = \left[\frac{kh}{141.2QB\mu} \right]$$

Taking the logarithm of both sides of this equation gives:

$$\log(p_D) = \log(\Delta p) + \log \left(\frac{0.00708\, kh}{QB\mu} \right) \qquad [3.5.44]$$

where:

Q = flow rate, STB/day
B = formation volume factor, bbl/STB
μ = viscosity, cp

For a constant flow rate, Equation 3.5.44 indicates that the logarithm of the dimensionless pressure drop, $\log(p_D)$, will differ from the logarithm of the *actual* pressure drop, $log(\Delta p)$, by a constant amount of:

$$\log \left(\frac{0.00708\, kh}{QB\mu} \right)$$

Similarly, the dimensionless time t_D is given in Chapter 1 by Equation 1.2.75, with time t given in days, as:

$$t_D = \left[\frac{0.006328\, k}{\phi\mu c_t r_w^2} \right] t$$

Taking the logarithm of both sides of this equation gives:

$$\log(t_D) = \log(t) + \log \left[\frac{0.006328\, k}{\phi\mu c_t r_w^2} \right] \qquad [3.5.45]$$

where:

t = time, days
c_t = total compressibility coefficient, psi^{-1}
ϕ = porosity

Hence, a graph of $\log(\Delta p)$ vs. $\log(t)$ will have an *identical shape* (i.e., parallel) to a graph of $\log(p_D)$ vs. $\log(t_D)$, although the curve will be shifted by $\log(0.00708kh/QB\mu)$ vertically in pressure and $\log(0.000264k/\phi\mu c_t r_w^2)$ horizontally in time. This concept is illustrated in Chapter 1 by Figure 1.46 and reproduced in this chapter for convenience.
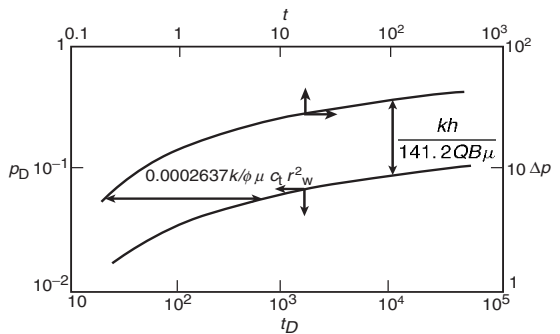
Figure 1.46 *Concept of type curves.*

Not only do these two curves have the same shape, but if they are *moved relative to each other until they coincide or "match,"* the vertical and horizontal displacements required to achieve the match are related to these constants in Equations 3.5.44 and 3.5.45. Once these constants are determined from the vertical and horizontal displacements, it is possible to estimate reservoir properties such as permeability and porosity. This process of matching two curves through the vertical and horizontal displacements and determining the reservoir or well properties is called *type curve matching*.

To fully understand the power and convenience of using the dimensionless concept approach in solving engineering problems, this concept is illustrated through the following example.

Example 3.21 A well is producing under transient (unsteady-state) flow conditions. The following properties are given:

$p_i = 3500$ psi, $B = 1.44$ bbl/STB

$c_t = 17.6 \times 10^{-6}$ psi^{-1}, $\phi = 15\%$

$\mu = 1.3$ cp, $h = 20$ ft

$Q = 360$ STB/day, $k = 22.9$ md

$s = 0$

(a) Calculate the pressure at radii 10 ft and 100 ft for the flowing time 0.1, 0.5, 1.0, 2.0, 5.0, 10, 20, 50, and 100 hours. Plot $p_i - p(r, t)$ vs. t on a log–log scale.

(b) Present the data from part (a) in terms of $p_i - p(r, t)$ vs. (t/r^2) on a log–log scale.

Solution

(a) During transient flow, Equation 1.2.66 is designed to describe the pressure at any radius r and any time t as given by:

$$p(r, t) = p_i + \left[\frac{70.6 QB\mu}{kh} \right] \text{Ei} \left[\frac{-948\phi\mu c_t r^2}{kt} \right]$$

or:

$$p_i - p(r, t) = \left[\frac{-70.6(360)(1.444)(1.3)}{(22.9)(20)} \right]$$

$$\times \text{Ei} \left[\frac{-948(0.15)(1.3)(17.6 \times 10^{-6} r^2)}{(22.9)t} \right]$$

$$p_i - p(r, t) = -104 \text{Ei} \left[-0.0001418 \frac{r^2}{t} \right]$$

Values of $p_i - p(r, t)$ are presented as a function of time and radius (i.e., at $r = 10$ feet and 100 feet) in the following table and graphically in Figure 3.53:

Assumed		$r = 10$ feet	
t (hours)	t/r^2	Ei$[-0.0001418 r^2/t]$	$p_i - p(r, t)$
0.1	0.001	-1.51	157
0.5	0.005	-3.02	314
1.0	0.010	-3.69	384
2.0	0.020	-4.38	455
5.0	0.050	-5.29	550
10.0	0.100	-5.98	622
20.0	0.200	-6.67	694
50.0	0.500	-7.60	790
100.0	1.000	-8.29	862

Assumed		$r = 100$ feet	
t (hours)	t/r^2	Ei$[-0.0001418 r^2/t]$	$p_i - p(r, t)$
0.1	0.00001	0.00	0
0.5	0.00005	-0.19	2
1.0	0.00010	-0.12	12
2.0	0.00020	-0.37	38
5.0	0.00050	-0.95	99
10.0	0.00100	-1.51	157
20.0	0.00200	-2.14	223
50.0	0.00500	-3.02	314
100.0	0.00100	-3.69	386

(b) Figure 3.53 shows two different curves for the 10 and 100 feet radii. Obviously, the same calculations can be repeated for any number of radii and, consequently, the same number of curves will be generated. However, the solution can be greatly simplified by examining Figure 3.54. This plot shows that when the pressure difference $p_i - p(r, t)$ is plotted versus t/r^2, the data for both radii forms a common curve. In fact, the pressure difference for any reservoir radius will plot on this exact same curve.
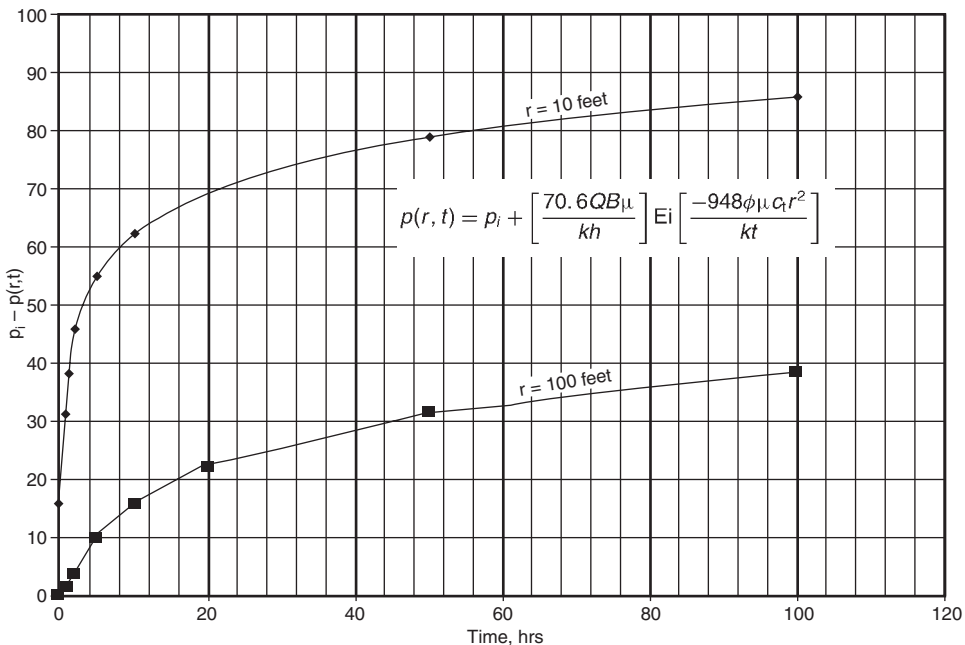
Figure 3.53 *Pressure profile at 10 feet and 100 feet as a function of time.*
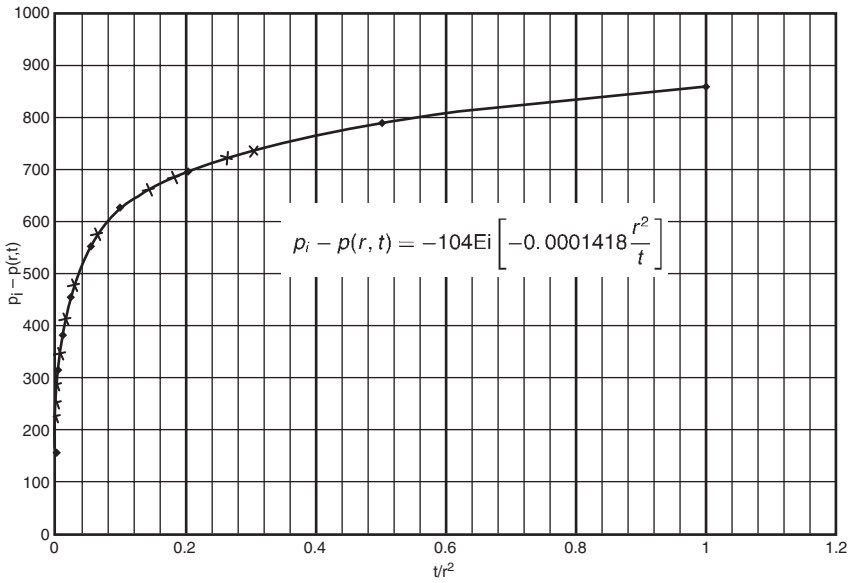
Figure 3.54 *Pressure profile at 10 feet and 100 feet as a function of t/r^2.*

For example, in the same reservoir to calculate the pressure p at 150 feet after 200 hours of transient flow, then:

$$t/r^2 = 200/150^2 = 0.0089$$

From Figure 3.54:

$$p_i - p(r, t) = 370 \text{ psi}$$

Thus:

$$p(r, t) = p_i - 370 = 5000 - 370 = 4630 \text{ psi}$$

Several investigators have employed the dimensionless variables approach to determine reserves and to describe the recovery performance of hydrocarbon systems with time, notably:

- Fetkovich;
- Carter;
- Palacio and Blasingame;
- Flowing material balance;
- Anash et al.;
- Decline curve analysis for fractured wells.

All the methods are based on defining a set of "Decline curve dimensionless variables" that includes:

- decline curve dimensionless rate q_{Dd};
- decline curve dimensionless cumulative production Q_{Dd};
- decline curve dimensionless time t_{Dd}.

These methods were developed with the objective of providing the engineer with an additional convenient tool for estimating reserves and determining other reservoir properties for oil and gas wells using the available performance data. A review of these methods and their practical applications are documented below.

Fetkovich type curve Type curve matching is an advanced form of decline analysis proposed by Fetkovich (1980). The author proposed that the concept of the dimensionless variables approach can be extended for use in decline curve analysis to simplify the calculations. He introduced the decline curve dimensionless flow rate variable q_{dD} and decline curve dimensionless time t_{dD} that are used in all decline curve and type curve analysis techniques. Arps's

relationships can be expressed in the following dimensionless forms:

$$\text{Hyperbolic} \quad \frac{q_t}{q_i} = \frac{1}{[1 + bD_i t]^{1/b}}$$

In a dimensionless form:

$$q_{Dd} = \frac{1}{[1 + bt_{Dd}]^{1/b}} \qquad [3.5.46]$$

where the decline curve dimensionless variables q_{Dd} and t_{Dd} are defined by:

$$q_{Dd} = \frac{q_t}{q_i} \qquad [3.5.47]$$

$$t_{Dd} = D_i t \qquad [3.5.48]$$

$$\text{Exponential} \quad \frac{q_t}{q_i} = \frac{1}{\exp[D_i t]}$$

Similarly:

$$q_{Dd} = \frac{1}{\exp[t_{Dd}]} \qquad [3.5.49]$$

$$\text{Harmonic} \quad \frac{q_t}{q_i} = \frac{1}{1 + D_i t}$$

or:

$$q_{Dd} = \frac{1}{1 + t_{Dd}} \qquad [3.5.50]$$

where q_{Dd} and t_{Dd} are the decline curve dimensionless variables as defined by Equations 3.5.47 and 3.5.48, respectively. During the boundary-dominated flow period, i.e., steady-state or semisteady-state flow conditions, Darcy's equation can be used to describe the initial flow rate q_i as:

$$q_i = \frac{0.00708kh\Delta p}{B\mu \left[\ln(r_e/r_{wa}) - \frac{1}{2}\right]} = \frac{kh(p_i - p_{wf})}{142.2B\mu \left[\ln(r_e/r_{wa}) - \frac{1}{2}\right]}$$
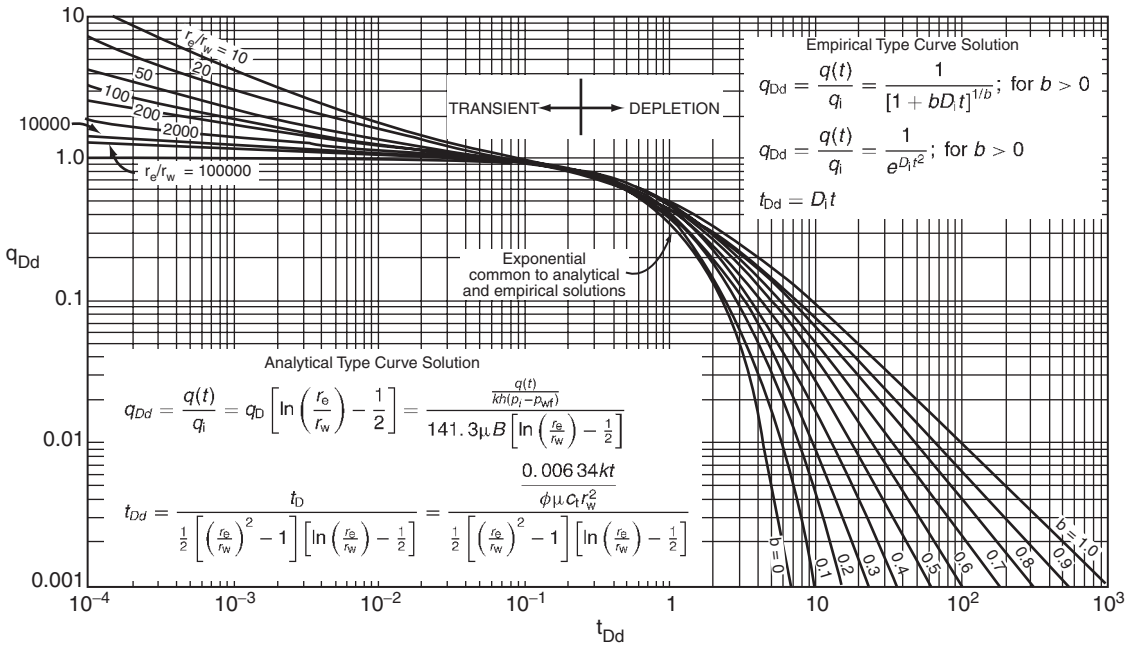
Figure 3.55 *Fetkovich type curves (After Fetkovich, 1980, JPT June 1980, copyright SPE 1980).*

where:

q = flow rate, STB/day
B = formation, volume factor, bbl/STB
μ = viscosity, cp
k = permeability, md
h = thickness, ft
r_e = drainage radius, ft
r_{wa} = apparent (effective) wellbore radius, ft

The ratio r_e/r_{wa} is commonly referred to as the dimensionless drainage radius r_D. That is:

$$r_D = r_e/r_{wa} \qquad [3.5.51]$$

with:

$$r_{wa} = r_w e^{-s}$$

The ratio r_e/r_{wa} in of Darcy's equation can be replaced with r_D, to give:

$$q_i = \frac{kh(p_i - p_{wf})}{141.2B\mu\left[\ln(r_D) - \frac{1}{2}\right]}$$

Rearranging Darcy's equation gives:

$$\left[\frac{141.2B\mu}{kh\Delta p}\right]q_i = \frac{1}{\ln(r_D) - \frac{1}{2}}$$

It is obvious that the right-hand side of this equation is dimensionless, which indicates that the left-hand side of the equation is also dimensionless. The above relationship then defines the dimensionless rate q_D as:

$$q_D = \left[\frac{141.2B\mu}{kh\Delta p}q_i\right] = \frac{1}{\ln(r_D) - \frac{1}{2}} \qquad [3.5.52]$$

Recalling the dimensionless form of the diffusivity equation, i.e., Equation 1.2.78, as:

$$\frac{\partial^2 p_D}{\partial r_D^2} + \frac{1}{r_D}\frac{\partial p_D}{\partial r_D} = \frac{\partial p_D}{\partial r_D}$$

Fetkovich demonstrated that the analytical solutions to the above transient flow diffusivity equation and the

pseudosteady-state decline curve equations could be combined and presented in a family of "log–log" dimensionless curves. To develop this link between the two flow regimes, Fetkovich expressed the decline curve dimensionless variables q_{Dd} and t_{Dd} in terms of the transient dimensionless rate q_D and time t_D. Combining Equation 3.5.47 with Equation 3.5.52, gives:

$$q_{Dd} = \frac{q_t}{q_i} = \frac{\frac{q_t}{kh(p_i - p)}}{141.2B\mu\left[\ln(r_D) - \frac{1}{2}\right]}$$

or:

$$q_{Dd} = q_D\left[\ln(r_D) - \frac{1}{2}\right] \qquad [3.5.53]$$

Fetkovich expressed the decline curve dimensionless time t_{Dd} in terms of the transient dimensionless time t_D by:

$$t_{Dd} = \frac{t_D}{\frac{1}{2}\left[r_D^2 - 1\right]\left[\ln(r_D) - \frac{1}{2}\right]} \qquad [3.5.54]$$

Replacing the dimensionless time t_D by Equation 1.2.75 gives:

$$t_{Dd} = \frac{1}{\frac{1}{2}\left[r_D^2 - 1\right]\left[\ln(r_D) - \frac{1}{2}\right]}\left[\frac{0.006328t}{\phi(\mu c_t)r_{wa}^2}\right] \qquad [3.5.55]$$

Although Arps's exponential and hyperbolic equations were developed empirically on the basis of production data, Fetkovich was able to place a physical basis to Arps's coefficients. Equations 3.5.48 and 3.5.55 indicate that the initial decline rate D_i can be defined mathematically by the following expression:

$$D_i = \frac{1}{\frac{1}{2}\left[r_D^2 - 1\right]\left[\ln(r_D) - \frac{1}{2}\right]}\left[\frac{0.006328}{\phi(\mu c_t)r_{wa}^2}\right] \qquad [3.5.56]$$

Fetkovich arrived at his unified type curve; as shown in Figure 3.55, by solving the dimensionless form of the diffusivity equation using the constant-terminal solution approach for several assumed values of r_D and t_{Dd} and the solution to Equation 3.5.46 as a function of t_{Dd} for several values of b ranging from 0 to 1.

Notice in Figure 3.55 that all curves coincide and become indistinguishable at $t_{Dt} \approx 0.3$. Any data existing before a t_{Dt} of 0.3 will appear to be exponentially declining regardless of the true value of b and, thus, will plot as a straight line on semilog paper.

With regard to the initial rate q_i, it is not simply a producing rate at early time; it is very specifically a pseudosteady-state rate at the surface. It can be substantially less that the actual early-time transient flow rates as would be produced from low-permeability wells with large negative skins.

The basic steps used in Fetkovich type curve matching of declining rate–time data are given below:

Step 1. Plot the historical flow rate q_t versus time t in any convenient units on log–log paper or tracing paper with the same logarithmic cycles as the Fetkovich type curve.

Step 2. Place the tracing paper data plot over the type curve and slide the tracing paper with the plotted data, keeping the coordinate axes parallel, until the actual data points match one of the type curves with a specific value of b.

Because decline type curve analysis is based on *boundary-dominated flow conditions*, there is no basis for choosing the proper b values for future boundary-dominated production if only transient data is available. In addition, because of the similarity of curve shapes, unique type curve matches are difficult to obtain with transient data only. If it is apparent that boundary-dominated (i.e., pseudosteady-state) data is present and can be matched on a curve for a particular value of b the actual curve can simply be extrapolated following the trend of the type curve into the future.

Step 3. From the match of that particular type curve of step 2, record values of the reservoir dimensionless radius r_e/r_{wa} and the parameter b.

Step 4. Select any convenient match point "MP" on the actual data plot (q_t and t)$_{MP}$ and the corresponding values lying beneath that point on the type curve grid (q_{Dd}, t_{Dd})$_{MP}$.

Step 5. Calculate the initial surface gas flow rate q_i at $t = 0$ from the rate match point:

$$q_i = \left[\frac{q_t}{q_{D_i}} \right]_{MP} \qquad [3.5.57]$$

Step 6. Calculate the initial decline rate D_i from the time match point:

$$D_i = \left[\frac{t_{Dd}}{t} \right]_{MP} \qquad [3.5.58]$$

Step 7. Using the value of r_e/r_{wa} from step 3 and the calculated value of q_i, calculate the formation permeability k by applying Darcy's equation in one of the following three forms:

• Pseudopressure form:

$$k = \frac{1422[\ln(r_e/r_{wa}) - 0.5]q_i}{h[m(p_i) - m(p_{wf})]} \qquad [3.5.59]$$

• Pressure-squared form:

$$k = \frac{1422T(\mu_g Z)_{avg}[\ln(r_e/r_{wa}) - 0.5]q_i}{h(p_i^2 - p_{wf}^2)} \qquad [3.5.60]$$

• Pressure approximation form:

$$k = \frac{141.2(10^3)T(\mu_g B_g)[\ln(r_e/r_{wa}) - 0.5]q_i}{h(p_i - p_{wf})} \qquad [3.5.61]$$

where:

k = permeability, md
p_i = initial pressure, psia
p_{wf} = bottom-hole flowing pressure, psia
$m(P)$ = pseudopressure, psi^2/cp
q_i = initial gas flow rate, Mscf/day
T = temperature, °R
h = thickness, ft
μ_g = gas viscosity, cp
Z = gas deviation factor
B_g = gas formation volume factor, bbl/scf

Step 8. Determine the reservoir pore volume (PV) of the well drainage area at the beginning of the boundary-dominated flow from the following expression:

$$PV = \frac{56.54T}{(\mu_g c_t)_i[m(p_i) - m(p_{wf})]} \left(\frac{q_i}{D_i} \right) \qquad [3.5.62]$$

or in terms of pressure squared:

$$PV = \frac{28.27T(\mu_g Z)_{avg}}{(\mu_g c_t)_i[p_i^2 - p_{wf}^2]} \left(\frac{q_i}{D_i} \right) \qquad [3.5.63]$$

with:

$$r_e = \sqrt{\frac{PV}{\pi h \phi}} \qquad [3.5.64]$$

$$A = \frac{\pi r e^2}{43\,560} \qquad [3.5.65]$$

where:

PV = pore volume, ft^3
ϕ = porosity, fraction
μ_g = gas viscosity, cp
c_t = total compressibility coefficient, psi^{-1}
q_i = initial gas rate, Mscf/day
D_i = decline rate, day^{-1}
r_e = drainage radius of the well, ft
A = drainage area, acres

subscripts:

i = initial
avg = average

Step 9. Calculate the skin factor s from the r_e/r_{wa} matching parameter and the calculated values of A and r_e from step 8:

$$s = \ln \left[\left(\frac{r_e}{r_{wa}} \right)_{MP} \left(\frac{r_w}{r_e} \right) \right] \qquad [3.5.66]$$

Step 10. Calculate the initial gas-in-place G from:

$$G = \frac{(PV)[1 - S_w]}{5.615 B_{gi}} \qquad [3.5.67]$$

The initial gas-in-place can also estimated from the following relationship:

$$G = \frac{q_i}{D_i(1 - b)} \qquad [3.5.68]$$

where:

G = initial gas-in-place, scf
S_w = initial water saturation
B_{gi} = gas formation volume factor at p_i, bbl/scf
PV = pore volume, ft^3

An inherent problem when applying decline curve analysis is having sufficient rate–time data to determine a unique value for b as shown in the Fetkovich type curve. It illustrates that for a shorter the producing time, the b value curves

$$PV = \frac{56.54T}{(\mu_g c_t)_i [m(p_i) - m(p_{wf})]} \left(\frac{q_i}{D_i}\right)$$
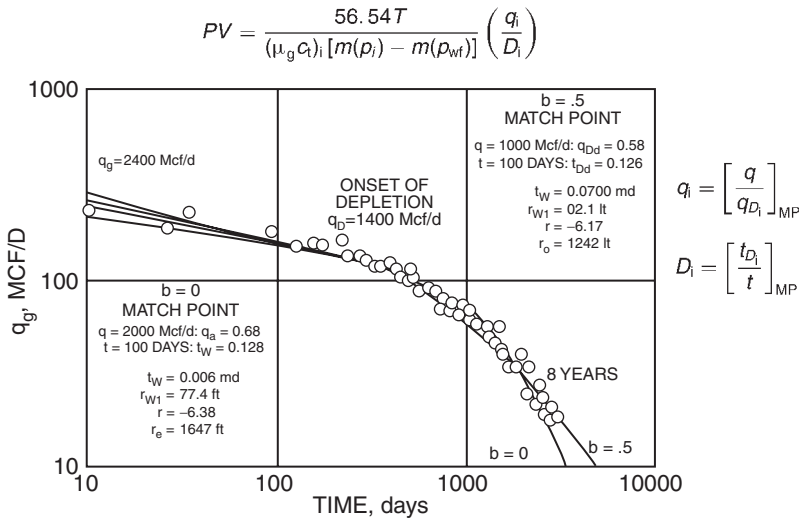
Figure 3.56 *West Virginia gas well A type curve fit (Copyright SPE 1987).*

approach one another, which leads to difficulty in obtaining a unique match. Arguably, applying the type curve approach with only three years of production history may be too short for some pools. Unfortunately, since time is plotted on a log scale, the production history becomes compressed so that even when incremental history is added, it may still be difficult to differentiate and clearly identify the appropriate decline exponent b.

The following example illustrates the use of the type curve approach to determine reserves and other reservoir properties.

Example 3.22 Well A is a low-permeability gas well located in West Virginia. It produces from the Onondaga chert that has been hydraulically fractured with 50 000 gal of 3% gelled acid and 30 000 lb of sand. A conventional Horner analysis of pressure buildup data on the well indicated the following:

$p_i = 3268$ psia, $m(p_i) = 794.8 \times 10^6$ psi^2/cp

$k = 0.082$ md, $s = -5.4$

The Fetkovich et al. (1987) provided the following additional data on the gas well:

$p_{wf} = 500$ psia, $m(p_{wf}) = 20.8 \times 10^6$ psi^2/cp

$\mu_{gi} = 0.0172$ cp, $c_{ti} = 177 \times (10^{-6})$ psi^{-1}

$T = 620°$R, $h = 70$ ft

$\phi = 0.06$, $B_{gi} = 0.000853$ bbl/scf

$S_w = 0.35$, $r_w = 0.35$ ft

The historical rate time data for eight years was plotted and matched to r_e/r_{wa} stem of 20 and $b = 0.5$, as shown in Figure 3.56, with the following match point:

$q_t = 1000$ Mscf/day, $t = 100$ days

$q_{Dd} = 0.58$, $t_{Dd} = 0.126$

Using the above data, calculate:

- permeability k;
- drainage area A;
- skin factor s;
- gas-in-place G.

Solution

Step 1. Using the match point, calculate q_i and D_i by applying Equations 3.5.57 and 3.5.58, respectively:

$$q_i = \left[\frac{q_t}{q_{Dt}}\right]_{MP}$$

$$= \frac{1000}{0.58} = 1724 \text{ Mscf/day}$$

and:

$$D_i = \left[\frac{t_{Dd}}{t}\right]_{MP}$$

$$= \frac{0.126}{100} = 0.00126 \text{ day}^{-1}$$

Step 2. Calculate the permeability k from Equation 3.5.59

$$k = \frac{1442T[\ln(r_e/r_{wa}) - 0.5]q_i}{h[m(p_i) - m(p_{wf})]}$$

$$= \frac{1422(620)[\ln(20) - 0.5](1724.1)}{(70)[794.8 - 20.8](10^6)} = 0.07 \text{ md}$$

Step 3. Calculate the reservoir PV of the well drainage area by using Equation 3.5.62:

$$PV = \frac{56.54T}{(\mu_g c_t)_i[m(p_i) - m(p_{wf})]} \left(\frac{q_i}{D_i}\right)$$

$$= \frac{56.54(620)}{(0.0172)(177)(10^{-6})[794.8 - 20.8](10^6)}$$

$$\times \frac{1724.1}{0.00126} = 20.36 \times 10^6 \text{ ft}^3$$

Step 4. Calculate the drainage radius and area by applying Equations 3.5.64 and 3.5.65:

$$r_e = \sqrt{\frac{PV}{\pi h \phi}}$$

$$= \sqrt{\frac{(20.36)10^6}{\pi (70)(0.06)}} = 1242 \text{ ft}$$

and:

$$A = \frac{\pi \, re^2}{43\,560}$$

$$= \frac{\pi \, (1242)^2}{43\,560} = 111 \text{ acres}$$

Step 5. Determine the skin factor from Equation 3.5.66:

$$s = \ln\left[\left(\frac{r_e}{r_{wa}}\right)_{MP}\left(\frac{r_w}{r_e}\right)\right]$$

$$= \ln\left[(20)\left(\frac{0.35}{1242}\right)\right] = -5.18$$

Step 6. Calculate the initial gas-in-place by using Equation 3.5.67:

$$G = \frac{(PV)[1 - S_w]}{5.615 B_{gi}}$$

$$= \frac{(20.36)(10^6)[1 - 0.35]}{(5.615)(0.000853)} = 2.763 \text{ Bscf}$$

The initial gas G can also be estimated from Equation 3.5.68, to give:

$$G = \frac{q_i}{D_i(1 - b)}$$

$$= \frac{1.7241(10^6)}{0.00126(1 - 0.5)} = 2.737 \text{ Bscf}$$

Limits of exponent b and decline analysis of stratified no-crossflow reservoirs Most reservoirs consist of several layers with varying reservoir properties. Due to the fact that no-crossflow reservoirs are perhaps the most prevalent and important, reservoir heterogeneity is of considerable significance in long-term prediction and reserve estimates. In layered reservoirs with crossflow, adjacent layers can simply be combined into a single equivalent layer that can be described as a homogeneous layer with averaging reservoir properties of the cross-flowing layers. As shown later in this section, the decline curve exponent b for a single homogeneous layer ranges between 0 and a maximum value of 0.5. For layered no-crossflow systems, values of the decline curve exponent b range between 0.5 and 1 and therefore can be used to identify the stratification. These separated layers might have the greatest potential for increasing current production and recoverable reserves.

Recalling the back-pressure equation, i.e., Equation 3.1.20:

$$q_g = C(p_r^2 - p_{wf}^2)^n$$

where:

n = back-pressure curve exponent
c = performance coefficient
p_r = reservoir pressure

Fetkovich et al. (1996) suggested that the Arps decline exponent b and the decline rate can be expressed in terms of the exponent n by:

$$b = \frac{1}{2n}\left[(2n - 1) - \left(\frac{p_{wf}}{p_i}\right)^2\right] \qquad [3.5.69]$$

$$D_i = 2n\left(\frac{q_i}{G}\right) \qquad [3.5.70]$$

where G is the initial gas-in-place. Equation 3.5.69 indicates that as the reservoir pressure p_i approaches p_{wf} with depletion, all the non-exponential decline ($b \neq 0$) will shift toward exponential decline ($b = 0$) as depletion proceeds. Equation 3.5.69 also suggests that if the well is producing at a very low

bottom-hole flowing pressure ($p_{wf} = 0$) or $p_{wf} \ll p_i$, it can be reduced to the following expression:

$$b = 1 - \frac{1}{2n} \qquad [3.5.71]$$

The exponent n from a gas well back-pressure performance curve can therefore be used to calculate or estimate b and D_i. Equation 3.5.70 provides the physical limits of b, which is between 0 and 0.5, over the accepted theoretical range of n which is between 0.5 and 1.0 for a single-layer homogeneous system, as follows:

n	b
(high k) 0.50	0.0
0.56	0.1
0.62	0.2
0.71	0.3
0.83	0.4
(low k) 1.00	0.5

However, the harmonic decline exponent, $b = 1$, cannot be obtained from the back-pressure exponent. The b value of 0.4 should be considered as a good limiting value for gas wells when not clearly defined by actual production data.

The following is a tabulation of the values of b that should be expected for single-layer homogeneous or layered crossflow systems.

b	System characterization and identification
0.0	Gas wells undergoing liquid loading
	Wells with high back-pressure
	High-pressure gas
	Low-pressure gas with back-pressure curve exponent of $n \approx 0.5$
	Poor water-flood performance (oil wells)
	Gravity drainage with no solution gas (oil wells)
	Solution gas drive with unfavorable k_g/k_o (oil wells)
0.3	Typical for solution gas drive reservoirs
0.4–0.5	Typical for gas wells, $b = 0$, for $p_{wf} \approx 0$; $b = 0$, for $p_{wf} \approx 0.1p_i$
0.5	Gravity drainage for solution gas and for water-drive oil reservoirs
Undeterminable	Constant-rate or increasing-rate production period
	Flow rates are all in transient or infinite-acting period
$0.5 < b < 0.9$	Layered or composite reservoir

The significance of the decline curve exponent b value is that for a single-layer reservoir, the value of b will lie between 0 and 0.5. With layered no-crossflow performance, however, the b value can be between 0.5 and 1.0. As pointed out by Fetkovich et al. (1996), the further the b value is driven towards a value of 1.0, the more the unrecovered reserves remain in the tight low-permeability layer and the greater the potential to increase production and recoverable reserves through stimulation of the low-permeability layer. This suggests that decline curve analysis can be used to recognize and identify layered no-crossflow performance using only readily available historical production data. Recognition of the layers that are not being adequately drained compared to other layers, i.e., differential depletion, is where the opportunity lies. Stimulation of the less productive layers can allow both increased production and reserves. Figure 3.57 presents the standard Arps depletion decline curves, as presented by Fetkovich et al. (1996). Eleven curves are shown
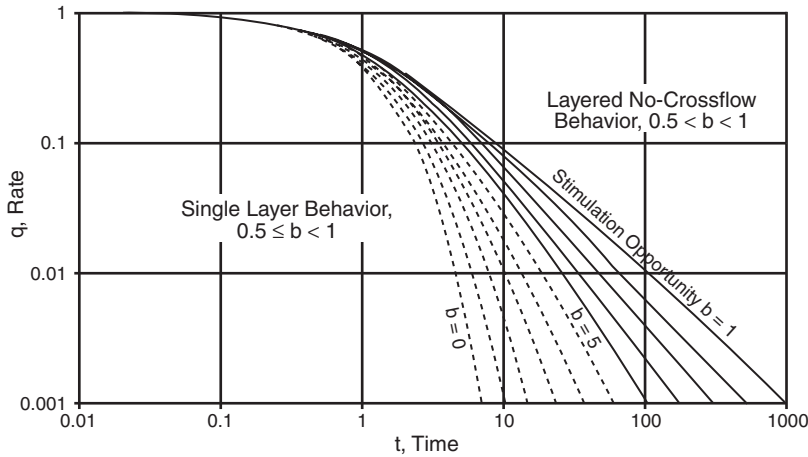
Figure 3.57 *Depletion decline curves (After Fetkovich, 1997, copyright SPE 1997).*

with each being described by a *b* value which ranges between 0 and 1 in increments of 0.1. All of the values have meaning and should be understood in order to apply decline curve analysis properly. *When decline curve analysis yields a b value greater than 0.5 (layered no-crossflow production) it is inaccurate to simply to make a prediction from the match point values.* This is because the match point represents a best fit of the surface production data that includes production from all layers. Multiple combinations of layer production values can give the same composite curve and, therefore, unrealistic forecasts in late time may be generated.

To demonstrate the effect of the layered no-crossflow reservoir system on the exponent *b*, Fetkovich et al. (1996) evaluated the production depletion performance of a two-layered gas reservoir producing from two non-communicated layers. The field produces from 10 wells and contains an estimated 1.5 Bscf of gas-in-place at an initial reservoir pressure of 428 psia. The reservoir has a gross thickness of 350 ft with a shale barrier averaging 50 ft thick that is clearly identified across the field and separates the two layers. Core data indicates a bimodal distribution with a permeability ratio between 10:1 and 20:1.

A type curve analysis and regression fit of the total field composite $\log(q_i)$ vs. $\log(t)$ yielded $b = 0.89$ that is identical to all values obtained from individual well analysis. To provide a quantitative analysis and an early recognition of a non-crossflow layered reservoir, Fetkovich (1980) expressed the rate–time equation for a gas well in terms of the back-pressure exponent *n* with a constant p_{wf} of zero. The derivation is based on combining Arps's hyperbolic equation with the MBE (i.e., p/Z vs. G_p) and back-pressure equation to give:

For $0.5 < n < 1, 0 < b < 0.5$:

$$q_t = \frac{q_i}{\left[1 + (2n-1)\left(\frac{q_i}{G}\right)t\right]^{\frac{2n}{2n-1}}} \quad [3.5.72]$$

$$G_{p(t)} = G\left\{1 - \left[1 + (2n-1)\left(\frac{q_i}{G}\right)t\right]^{\frac{1}{2n-1}}\right\} \quad [3.5.73]$$

For $n = 0.5, b = 0$:

$$q_t = q_i \exp\left[-\left(\frac{q_i}{G}\right)t\right] \quad [3.5.74]$$

$$G_{p(t)} = G\left\{1 - \exp\left[-\left(\frac{q_i}{G}\right)t\right]\right\} \quad [3.5.75]$$

For $n = 1, b = 0.5$:

$$q_t = \frac{q_i}{\left[1 + \left(\frac{q_i}{G}\right)t\right]^2} \quad [3.5.76]$$

$$G_{p(t)} = G - \frac{G}{1 + \left(\frac{q_i t}{G}\right)} \quad [3.5.77]$$

The above relationships are based on $p_{wf} = 0$, which implies that $q_i = q_{max}$ as given by:

$$q_i = q_{i\,max} = \frac{kh p_i^2}{1422T(\mu_g Z)_{avg}[\ln(r_e/r_w) - 0.75 + s]} \quad [3.5.78]$$

where:

$q_{i\,max}$ = stabilized absolute open-flow potential, i.e., at $P_{wf} = 0$, Mscf/day
G = initial gas-in-place, Mscf
q_t = gas flow rate at time t, Mscf/day
t = time
$G_{p(t)}$ = cumulative gas production at time t, Mscf

For a commingled well producing from two layers at a constant p_{wf}, the total flow rate $(q_t)_{total}$ is essentially the sum of the flow rate from each layer, or:

$$(q_t)_{total} = (q_t)_1 + (q_t)_2$$

where the subscripts 1 and 2 represent the more permeable layer and less permeable layer, respectively. For a hyperbolic exponent of $b = 0.5$, Equation 3.5.76 can be substituted into the above expression to give:

$$\frac{(q_{max})_{total}}{\left[1 + t\left(\frac{q_{max}}{G}\right)_{total}\right]^2} = \frac{(q_{max})_1}{\left[1 + t\left(\frac{q_{max}}{G}\right)_1\right]^2} + \frac{(q_{max})_2}{\left[1 + t\left(\frac{q_{max}}{G}\right)_2\right]^2} \quad [3.5.79]$$

Equation 3.5.79 indicates that only if $(q_{max}/G)_1 = (q_{max}/G)_2$ will the value of $b = 0.5$ for each layer yield a composite rate–time value of $b = 0.5$.

Mattar and Anderson (2003) presented an excellent review of methods that are available for analyzing production data using traditional and modern type curves. Basically, modern type curve analysis methods incorporate the flowing pressure data along with production rates and they use the analytical solutions to calculate hydrocarbon-in-place.

Two important features of modern decline analysis that improve upon the traditional techniques are:

(1) *Normalizing of rates using flowing pressure drop:* Plotting a normalized rate $(q/\Delta p)$ enables the effects of back-pressure changes to be accommodated in the reservoir analysis.
(2) *Handling the changing in gas compressibility with pressure:* Using pseudotime as the time function, instead of real time, enables the gas material balance to be handled rigorously as the reservoir pressure declines with time.

Carter type curve Fetkovich originally developed his type curves for gas and oil wells that are producing at constant pressures. Carter (1985) presented a new set of type curves developed exclusively for the analysis of gas rate data. Carter noted that the changes in fluid properties with pressure significantly affect reservoir performance predictions. Of utmost importance is the variation in the gas viscosity–compressibility product $\mu_g c_g$, which was ignored by Fetkovich. Carter developed another set of decline curves for boundary-dominated flow that uses a new correlating parameter λ to represent the changes in $\mu_g c_g$ during depletion. The λ parameter, called the "dimensionless drawdown correlating parameter," is designated to reflect the magnitude of pressure drawdown on $\mu_g c_g$ and defined by:

$$\lambda = \frac{(\mu_g c_g)_i}{(\mu_g c_g)_{avg}} \qquad [3.5.80]$$

or equivalently:

$$\lambda = \frac{(\mu_g c_g)_i}{2} \left[\frac{m(p_i) - m(p_{wf})}{\dfrac{p_i}{Z_i} - \dfrac{p_{wf}}{Z_{wf}}} \right] \qquad [3.5.81]$$

where:

c_g = gas compressibility coefficient, psi^{-1}
$m(p)$ = real-gas pseudopressure, psi^2/cp
p_{wf} = bottom-hole flowing pressure, psi
p_i = initial pressure, psi
μ_g = gas viscosity, cp
Z = gas deviation factor

For $\lambda = 1$, this indicates a negligible drawdown effect and corresponds to $b = 0$ on the Fetkovich exponential decline curve. Values of λ range between 0.55 and 1.0. The type curves presented by Carter are based on specially defined for dimensionless parameters:

(1) dimensionless time t_D;
(2) dimensionless rate q_D;
(3) dimensionless geometry parameter (η) that characterizes the dimensionless radius r_{eD} and flow geometry;
(4) dimensionless drawdown correlating parameter λ.

Carter used a finite difference radial gas model to generate the data for constructing the type curves shown in Figure 3.58.

The following steps summarize the type curve matching procedure:

Step 1. Using Equation 3.5.80 or 3.5.81, calculates the parameter λ:

$$\lambda = \frac{(\mu_g c_g)_i}{(\mu_g c_g)_{avg}}$$

or:

$$\lambda = \frac{(\mu_g c_g)_i}{2} \left[\frac{m(p_i) - m(p_{wf})}{\dfrac{p_i}{Z_i} - \dfrac{p_{wf}}{Z_{wf}}} \right]$$

Step 2. Plot gas rate q in Mscf/day or MMscf/day as a function of time (t) in days using the same log–log scale as the type curves. If the actual rate values are erratic or fluctuate, it may be best to obtain averaged values of rate by determining the slope of straight lines drawn through adjacent points spaced at regular intervals on the plot of cumulative production G_p versus time, i.e., slope = $dG_p/dt = q_g$. The resulting plot of q_g vs. t should be made on tracing paper or on a transparency so that it can be laid over the type curves for matching.

Step 3. Match the rate data to a type curve corresponding to the computed value of λ in step 1. If the computed value of λ is not as one of the values for which a type curve is shown, the needed curve can be obtained by interpolation and graphical construction.

Step 4. From the match, values of $(q_D)_{MP}$ and $(t_D)_{MP}$ corresponding to specific values for $(q)_{MP}$ and $(t)_{MP}$ are recorded. Also, a value for the dimensionless geometry parameter η is also obtained from the match. It is strongly emphasized that late-time data points (boundary-dominated pseudosteady-state flow condition) are to be matched in preference to early-time data points (unsteady-state flow condition) because matching some early rate data often will be impossible.

Step 5. Estimate the gas that would be recoverable by reducing the average reservoir pressure from its initial value to p_{wf} from the following expression:

$$\Delta G = G_i - G_{pwf} = \frac{(qt)_{MP}}{(q_D t_D)_{MP}} \frac{\eta}{\lambda} \qquad [3.5.82]$$

Step 6. Calculate the initial gas-in-place G_i from:

$$G_i = \left[\frac{\dfrac{p_i}{Z_i}}{\dfrac{p_i}{Z_i} - \dfrac{p_{wf}}{Z_{wf}}} \right] \Delta G \qquad [3.5.83]$$

Step 7. Estimate the drainage area of the gas well from:

$$A = \frac{B_{gi} G_i}{43\,560 \phi h (1 - S_{wi})} \qquad [3.5.84]$$

where:

B_{gi} = gas formation volume factor at p_i, ft^3/scf
A = drainage area, acres
h = thickness, ft
ϕ = porosity
S_{wi} = initial water saturation

Example 3.23 The following production and reservoir data was used by Carter to illustrate the proposed calculation procedure.

p (psia)	μ_g (cp)	Z
1	0.0143	1.0000
601	0.0149	0.9641
1201	0.0157	0.9378
1801	0.0170	0.9231
2401	0.0188	0.9207
3001	0.0208	0.9298
3601	0.0230	0.9486
4201	0.0252	0.9747
4801	0.0275	1.0063
5401	0.0298	1.0418
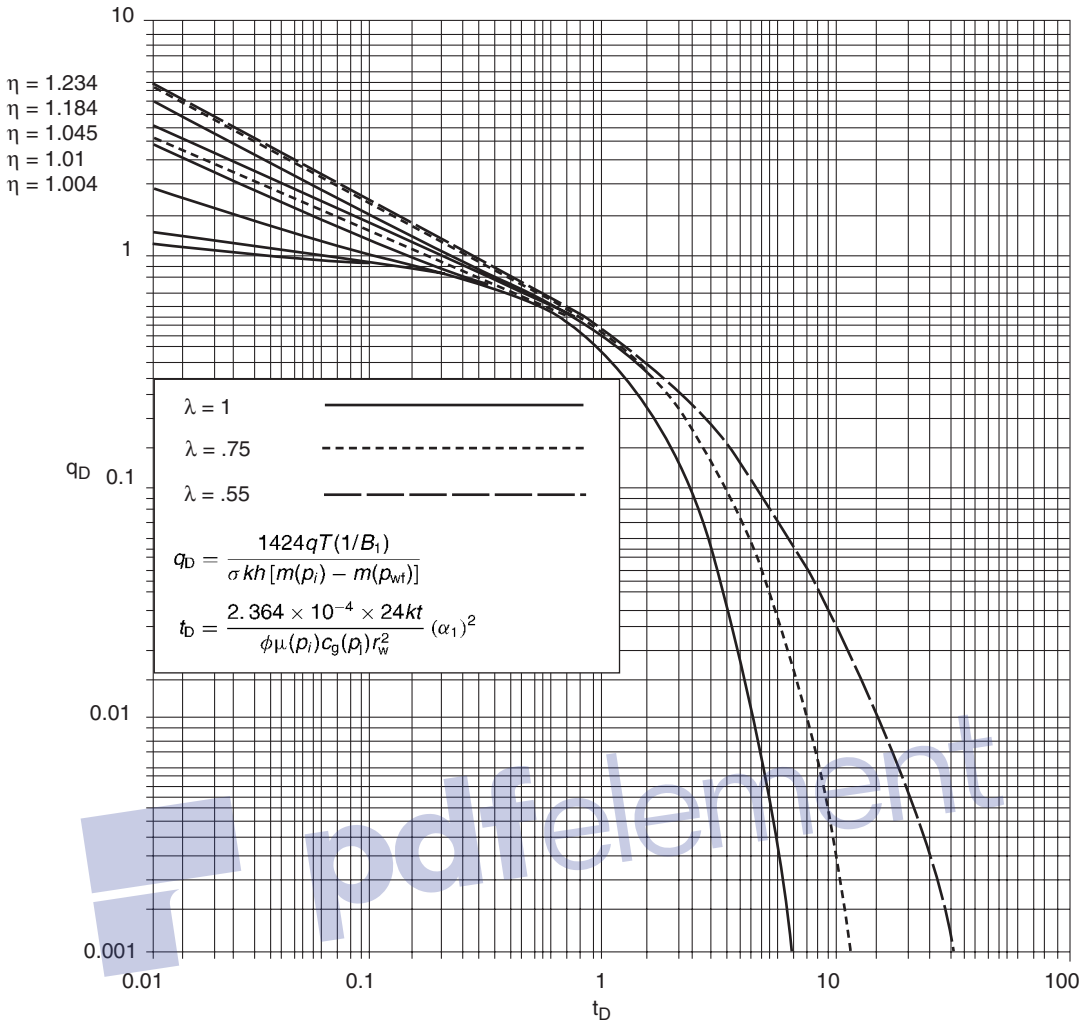
Figure 3.58 *Radial–linear gas reservoir type curves (After Carter, SPEJ 1985, copyright SPE 1985).*

$p_i = 5400$ psia, $p_{wf} = 500$ psi,

$T = 726°$R, $h = 50$ ft

$\phi = 0.070$, $S_{wi} = 0.50$,

$\lambda = 0.55$

Time (days)	q_t (MMscf/day)
1.27	8.300
10.20	3.400
20.50	2.630
40.90	2.090
81.90	1.700
163.80	1.410
400.00	1.070
800.00	0.791
1600.00	0.493
2000.00	0.402
3000.00	0.258
5000.00	0.127
10 000.00	0.036

Calculate the initial gas-in-place and the drainage area.

Solution

Step 1. The calculated value of λ is given as 0.55 and, therefore, the type curve for a λ value of 0.55 can be used directly from Figure 3.58.

Step 2. Plot the production data, as shown in Figure 3.59, on the same log–log scale as Figure 3.55 and determine the match points of:

$$(q)_{MP} = 1.0 \text{ MMscf/day}$$

$$(t)_{MP} = 1,000 \text{ days}$$

$$(q_D)_{MP} = 0.605$$

$$(t_D)_{MP} = 1.1$$

$$\eta = 1.045$$

Step 3. Calculate ΔG from Equation 3.5.82:

$$\Delta G = G_i - G_{pwf} = \frac{(qt)_{MP}}{(q_D t_D)_{MP}} \frac{\eta}{\lambda}$$

$$= \frac{(1)(1000)}{(0.605)(1.1)} \frac{1.045}{0.55} = 2860 \text{ MMscf}$$
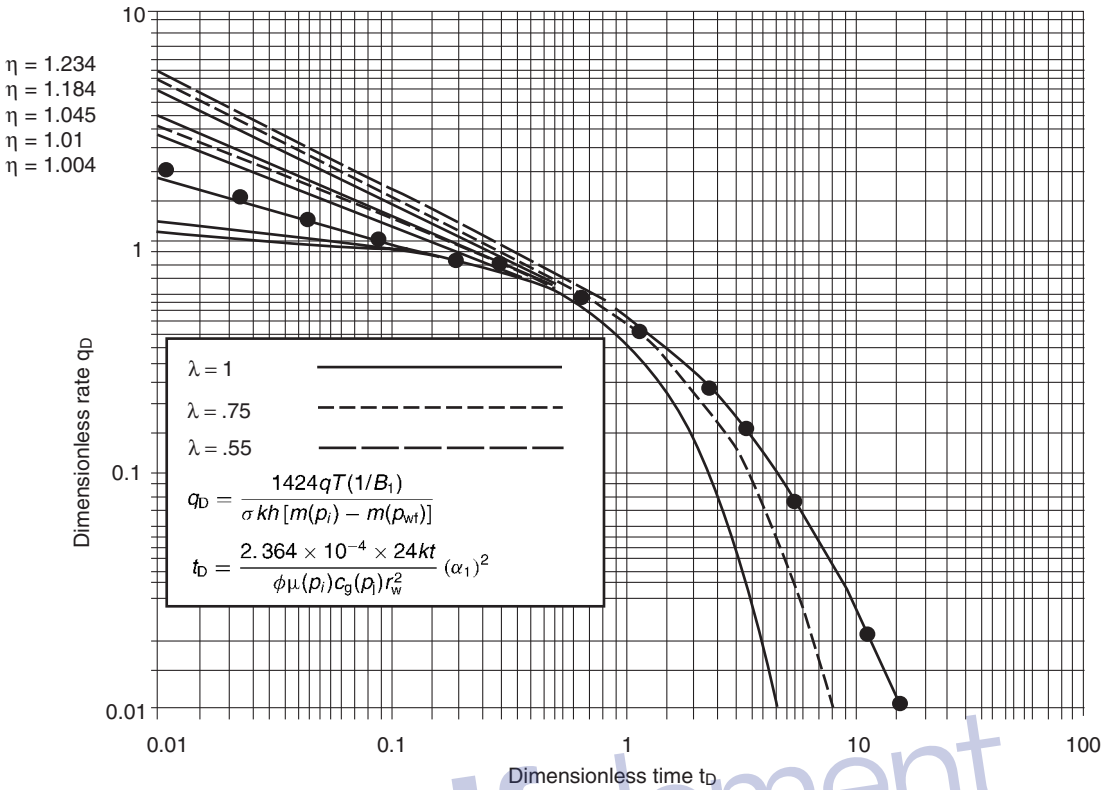
Figure 3.59   *Carter type curves for Example 3.23.*

Step 4. Estimate the initial gas-in-place by applying Equation 3.5.83.

$$G_i = \left[\frac{\frac{p_i}{Z_i}}{\frac{p_i}{Z_i} - \frac{p_{wf}}{Z_{wf}}} \right] \Delta G$$

$$= \left[\frac{\frac{5400}{1.0418}}{\frac{5400}{1.0418} - \frac{500}{0.970}} \right] 2860 = 3176 \text{ MMscf}$$

Step 5. Calculate the gas formation volume factor B_{gi} at p_i.

$$B_{gi} = 0.0287 \frac{Z_i T}{p_i} = 0.02827 \frac{(1.0418)(726)}{5400}$$

$$= 0.00396 \text{ ft}^3/\text{scf}$$

Step 6. Determine the drainage area from Equation 3.5.84:

$$A = \frac{B_{gi} G_i}{43\,560 \phi h (1 - S_{wi})}$$

$$= \frac{0.00396(3176)(10^6)}{43\,560(0.070)(50)(1 - 0.50)} = 105 \text{ acres}$$

Palacio–Blasingame type curves

Palacio and Blasingame (1993) presented an innovative technique for converting gas well production data with variable rates and bottom-hole flowing pressures into "equivalent constant-rate liquid data" that allows the liquid solutions to be used to model gas flow. The reasoning for this approach is that the constant-rate type curve solutions for liquid flow

problems are well established from the traditional well test analysis approach. The new solution for the gas problem is based on a material-balance-like time function and an algorithm that allows:

• the use of decline curves that are specifically developed for liquids;
• modeling of actual variable rate–variable pressure drop production conditions;
• explicit computation of gas-in-place.

Under pseudosteady-state flow conditions, Equation 1.2.123 in Chapter 1 describes the radial flow of slightly compressible liquids as:

$$p_{wf} = \left[p_i - \frac{0.23396 QBt}{Ah\phi c_t} \right] - \frac{162.6 QB\mu}{kh} \log \left[\frac{4A}{1.781 C_A r_w^2} \right]$$

where:

k = permeability, md
A = drainage area, ft^2
C_A = shape factor
Q = flow rate, STB/day
t = time, hours
c_t = total compressibility coefficient, psi^{-1}

Expressing the time t in days and converting from "log" to natural logarithm "ln," the above relation can be written as:

$$\frac{p_i - p_{wf}}{q} = \frac{\Delta p}{q} = 70.6 \frac{B\mu}{kh} \ln \left[\frac{4A}{1.781 C_A r_{wa}^2} \right] + \left[\frac{5.615 B}{Ah\phi C_t} \right] t$$

[3.5.85]

or more conveniently as:

$$\frac{\Delta p}{q} = b_{pss} + mt \qquad [3.5.86]$$

This expressions suggests that, under a pseudosteady-state flowing condition, a plot of $\Delta p/q$ vs. t on a Cartesian scale would yield a straight line with an intercept of b_{pss} and slope of m, with:

Intercept $\quad b_{pss} = 70.6 \dfrac{B\mu}{kh} \ln\left[\dfrac{4A}{1.781 C_A r_{wa}^2}\right] \qquad [3.5.87]$

Slope $\quad m = \dfrac{5.615B}{Ah\phi c_t} \qquad [3.5.88]$

where:

b_{pss} = constant in the pseudosteady-state "pss" equation
t = time, days
k = permeability, md
A = drainage area, ft^2
q = flow rate, STB/day
B = formation volume factor, bbl/STB
C_A = shape factor
c_t = total compressibility, psi^{-1}
r_{wa} = apparent (effective) wellbore radius, ft

For a gas system flowing under pseudosteady-state conditions, a similar equation to that of Equation 3.5.85 can be expressed as:

$$\frac{m(p_i) - m(p_{wf})}{q} = \frac{\Delta m(p)}{q} = \frac{711T}{kh}\left(\ln\frac{4A}{1.781 C_A r_{wa}^2}\right)$$
$$+ \left[\frac{56.54T}{\phi(\mu_g c_g)_i Ah}\right]t \qquad [3.5.89]$$

And in a linear form as:

$$\frac{\Delta m(p)}{q} = b_{pss} + mt \qquad [3.5.90]$$

Similar to the liquid system, Equation 3.5.90 indicates that a plot of $\Delta m(p)/q$ vs. t will form a straight line with:

Intercept $\quad b_{pss} = \dfrac{711T}{kh}\left(\ln\dfrac{4A}{1.781 C_A r_{wa}^2}\right)$

Slope $\quad m = \dfrac{56.54T}{(\mu_g c_t)_i(\phi hA)} = \dfrac{56.54T}{(\mu_g c_t)_i(PV)}$

where:

q = flow rate, Mscf/day
A = drainage area, ft^2
T = temperature, °R
t = flow time, days

The linkage that allows for the transformation of converting gas production data into equivalent constant-rate liquid data is based on the use of a new time function called "pseudo-equivalent time or normalized material balance pseudo-time," as defined by:

$$t_a = \frac{(\mu_g c_g)_i}{q_t}\int_o^t\left[\frac{q_t}{\overline{\mu_g c_g}}\right]dt = \frac{(\mu_g c_g)_i}{q_t}\frac{Z_i G}{2p_i}[m(\overline{p}_i) - \overline{m}(p)]$$
$$[3.5.91]$$

where:

t_a = pseudo-equivalent (normalized material balance) time, days
t = time, days

G = original gas-in-place, Mscf
q_t = gas flow rate at time t, Mscf/day
$\overline{p}$ = average pressure, psi
$\overline{\mu}_g$ = gas viscosity at $\overline{p}$, cp
$\overline{c}_g$ = gas compressibility at $\overline{p}$, psi^{-1}
$\overline{m}(p)$ = normalized gas pseudo pressure, psi^2/cp

In order to perform decline curve analysis under variable rates and pressures, the authors derived a theoretical expression for decline curve analysis that combines:

- the material balance relation;
- the pseudosteady-state equation;
- the normalized material balance time function t_a.

to give the following relationship:

$$\left[\frac{q_g}{\overline{m}(p_i) - \overline{m}(p_{wf})}\right]b_{pss} = \frac{1}{1 + \left(\frac{m}{b_{pss}}\right)t_a} \qquad [3.5.92]$$

where $\overline{m}(p)$ is the normalized pseudopressure as defined by:

$$\overline{m}(p_i) = \frac{\mu_{gi}Z_i}{p_i}\int_0^{p_i}\left[\frac{p}{\mu_g Z}\right]dp \qquad [3.5.93]$$

$$\overline{m}(p) = \frac{\mu_{gi}Z_i}{p_i}\int_0^{p}\left[\frac{p}{\mu_g Z}\right]dp \qquad [3.5.94]$$

and:

$$m = \frac{1}{Gc_{ti}} \qquad [3.5.95]$$

$$b_{pss} = \frac{70.6\mu_{gi}B_{gi}}{k_g h}\left[\ln\left(\frac{4A}{1.781 C_A r_{wa}^2}\right)\right] \qquad [3.5.96]$$

where:

G = original gas-in-place, Mscf
c_{gi} = gas compressibility at p_i, psi^{-1}
c_{ti} = total system compressibility at p_i, psi^{-1}
q_g = gas flow rate, Mscf/day
k_g = effective permeability to gas, md
$\overline{m}(p)$ = normalized pseudo-pressure, psia
p_i = initial pressure
r_{wa} = effective (apparent) wellbore radius, ft
B_{gi} = gas formation volume factor at p_i, bbl/Mscf

Notice that Equation 3.5.92 is essentially expressed in the same dimensionless form as the Fetkovich equation, i.e., Equation 3.5.148, or

$$q_{Dd} = \frac{1}{1 + (t_a)_{Dd}} \qquad [3.5.97]$$

with:

$$q_{Dd} = \left[\frac{q_g}{\overline{m}(p_i) - \overline{m}(p_{wf})}\right]b_{pss} \qquad [3.5.98]$$

$$(t_a)_{Dd} = \left(\frac{m}{b_{pss}}\right)t_a \qquad [3.5.99]$$

It must be noted that the q_{Dd} definition is now in terms of normalized pseudopressures and the modified dimensionless decline time function $(t_a)_{Dt}$ is not in terms of real time but in terms of the material balance pseudotime. *Also note that Equation 3.5.98 traces the path of a harmonic decline on the Fetkovich type curve with a hyperbolic exponent of $b = 1$.*

However, there is a computational problem when applying Equation 3.5.91 because it requires the value of G or the average pressure $\overline{p}$ which is itself a function of G. The method is iterative in nature and requires rearranging of Equation 3.5.92 in the following familiar form of linear relationship:

$$\frac{\overline{m}(p_i) - \overline{m}(p)}{q_g} = b_{pss} + mt_a \qquad [3.5.100]$$

The iterative procedure for determining G and $\overline{p}$ is described in the following steps:

Step 1. Using the available gas properties, set up a table of Z, μ, p/Z, $(p/Z\mu)$ vs. p for the gas system:

Time	p	Z	μ	p/Z	$p/(Z\mu)$
0	p_i	Z_i	μ_i	p_i/Z_i	$p_i/(Z\mu)_i$
.	.	.	.	.	.
.	.	.	.	.	.
.	.	.	.	.	.

Step 2. Plot $(p/Z\mu)$ vs. p on a Cartesian scale and numerically determine the area under the curve for several values of p. Multiply each area by $(Z_i\mu_i/p_i)$ to give the normalized pseudopressure as:

$$\overline{m}(p) = \frac{\mu_{gi}Z_i}{p_i} \int_0^p \left[\frac{p}{\mu_g Z} \right] dp$$

The required calculations of this step can be performed in the following tabulated form:

p	Area $= \int_0^p \left[\frac{p}{\mu_g Z} \right] dp$	$\overline{m}(p) = $ (area)$\frac{\mu_{gi}Z_i}{p_i}$
0	0	0
.	.	.
p_i	.	.

Step 3. Draw plots of $\overline{m}(p)$ and p/Z vs. p on a Cartesian scale.

Step 4. Assume a value for the initial gas-in-place G.

Step 5. For *each* production data point of G_p and t, calculate $\overline{p}/\overline{Z}$ from the gas MBE, i.e., Equation 3.3.11:

$$\frac{\overline{p}}{\overline{Z}} = \frac{p_i}{Z_i}\left(1 - \frac{G_p}{G}\right)$$

Step 6. From the plot generated in step 3, use the graph of p vs. p/Z for *each* value of the ratio $\overline{p}/\overline{Z}$ and determine the value of the corresponding average reservoir pressure $\overline{p}$. For each value of the average reservoir pressure $\overline{p}$, determine the values $\overline{m}(\overline{p})$ for each $\overline{p}$.

Step 7. For *each* production data point, calculate t_a by applying Equation 3.5.91:

$$t_a = \frac{(\mu_g c_g)_i}{q_t}\frac{Z_i G}{2p_i}[\overline{m}(p_i) - \overline{m}(\overline{p})]$$

The calculation of t_a can be conveniently performed in the following tabulated form:

t	q_t	G_p	$\overline{p}$	$\overline{m}(\overline{p})$	$t_a = \frac{(\mu_g c_g)_i}{q_i}\frac{Z_i G}{2p_i}[\overline{m}p_i - \overline{m}(\overline{p})]$
.	.	.	.	.	.
.	.	.	.	.	.
.	.	.	.	.	.

Step 8. Based on the linear relationship given by Equation 3.5.100, plot $\left[\overline{m}(p_i) - \overline{m}(\overline{p})\right]/q_g$ vs. t_a on a Cartesian scale and determine the slope m.

Step 9. Recalculate the initial gas-in-place G by using the value m from step 8 and applying Equation 3.5.95 to give:

$$G = \frac{1}{c_{ti}m}$$

Step 10. The new value of G from step 8 is used for the next iteration, i.e., step 4, and this process could continue until some convergence tolerance for G is met.

Palacio and Blasingame developed a modified Fetkovich–Carter type curve, as shown in Figure 3.60, to give the performance of constant-rate and constant-pressure gas flow solutions, the traditional Arps curve stems. To obtain a more accurate match to decline type curves than using flow rate data alone, the authors introduced the following two complementary plotting functions:

Integral function $(q_{Dd})_i$:

$$(q_{Dd})_i = \frac{1}{t_a} \int_0^{t_a} \left(\frac{q_g}{\overline{m}(p_i) - \overline{m}(p_{wf})} \right) dt_a \qquad [3.5.101]$$

Derivative of the integral function $(q_{Dd})_{id}$:

$$(q_{Dd})_{id} = \left(\frac{-1}{t_a} \right) \frac{d}{dt_a}\left[\frac{1}{t_a} \int_0^{t_a} \left(\frac{q_g}{\overline{m}(p_i) - \overline{m}(p_{wf})} \right) dt_a \right] \qquad [3.5.102]$$

Both functions can easily be generated by using simple numerical integration and differentiation methods.

To analyze gas production data, the proposed method involves the following basic steps:

Step 1. Calculate the initial gas-in-place G as outlined previously.

Step 2. Construct the following table:

t	q_g	t_a	p_{wf}	$\overline{m}(p_{wf})$	$\frac{q_g}{[\overline{m}(p_i) - \overline{m}(p_{wf})]}$
.	.	.	.	.	.
.	.	.	.	.	.
.	.	.	.	.	.

Plot $q_g/\left[\overline{m}(p_i) - \overline{m}(\overline{p})\right]$ vs. t_a on a Cartesian scale.

Step 3. Using the well production data as tabulated and plotted in step 2, compute the two complementary plotting functions as given by Equations 3.5.101 and 3.5.102 as a function of t_a:

$$(q_{Dd})_i = \frac{1}{t_a} \int_0^{t_a} \left(\frac{q_g}{\overline{m}(p_i) - \overline{m}(p_{wf})} \right) dt_a$$

$$(q_{Dd})_{id} = \left(\frac{-1}{t_a} \right) \frac{d}{dt_a}\left[\frac{1}{t_a} \int_0^{t_a} \left(\frac{q_g}{\overline{m}(p_i) - \overline{m}(p_{wf})} \right) dt_a \right]$$

Step 4. Plot both functions, i.e., $(q_{Dd})_i$ and $(q_{Dd})_{id}$, versus t_a on tracing paper so it can be laid over the type curve of Figure 3.60 for matching.

Step 5. Establish a match point MP and the corresponding dimensionless radius r_{eD} value to confirm the final value of G and to determine other properties:

$$G = \frac{1}{c_{ti}}\left[\frac{t_a}{t_{Dd}} \right]_{MP}\left[\frac{(q_{Dd})_i}{q_{Dd}} \right]_{MP} \qquad [3.5.103]$$

$$A = \frac{5.615 G B_{gi}}{h\phi(1 - S_{wi})}$$

$$r_e = \sqrt{\frac{A}{\pi}}$$

$$r_{wa} = \frac{r_e}{r_{eD}}$$

$$s = -\ln\left(\frac{r_{wa}}{r_w} \right)$$

$$k = \frac{141.2 B_{gi}\mu_{gi}}{h}\left[\ln\left(\frac{r_e}{r_w} \right) - \frac{1}{2} \right]\left[\frac{(q_{Dd})_i}{q_{Dd}} \right]_{MP} \qquad [3.5.104]$$

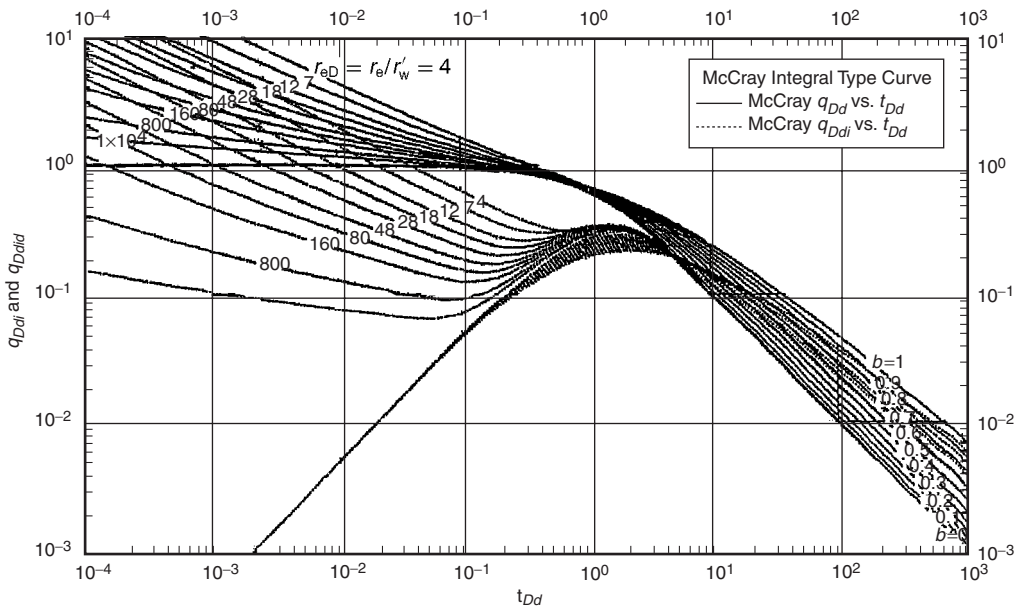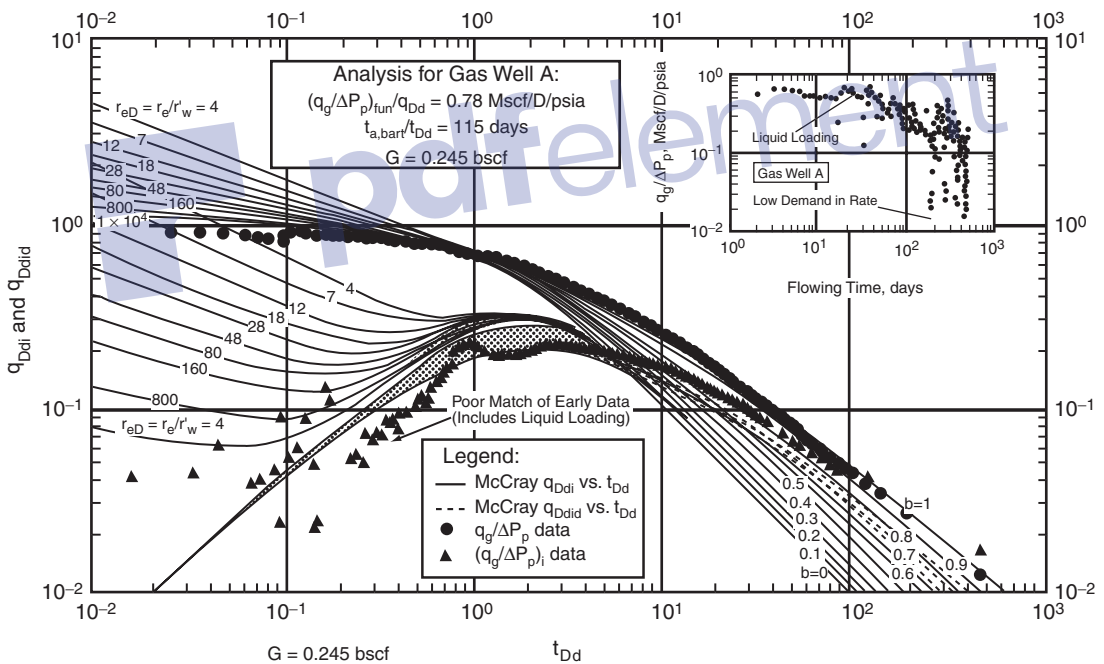**Figure 3.60** *Palacio-Blasingame type curve.*

Figure 3.61 *Palacio-Blasingame West Virginia gas well example.*

where:

  G = gas-in-place, Mscf
  B_{gi} = gas formation volume factor at p_i, bbl/Mscf
  A = drainage area, ft^2
  s = skin factor
  r_{eD} = dimensionless drainage radius
  S_{wi} = connate water saturation

The authors used the West Virginia gas well "A," as given by Fetkovich in Example 3.22, to demonstrate the use of

the proposed type curve. The resulting fit of the data given in Example 3.22 to Placio and Blasingame is shown in Figure 3.61.

Flowing material balance The flowing material balance method is a new technique that can be used to estimate the original gas-in-place (OGIP). The method as introduced by Mattar and Anderson (2003) uses the concept of the normalized rate and material balance pseudotime to create a simple linear plot, which extrapolates to fluids-in-place.

The method uses the available production data in a manner similar to that of Palacio and Blasingame's approach. The authors showed that for a depletion drive gas reservoir flowing under pseudosteady-state conditions, the flow system can be described by:

$$\frac{q}{m(p_i) - m(p_{wf})} = \frac{q}{\Delta m(p)} = \left(\frac{-1}{Gb'_{pss}}\right) Q_N + \frac{1}{b'_{pss}}$$

where Q_N is the normalized cumulative production as given by:

$$Q_N = \frac{2q_t p_i t_a}{(c_t \mu_i Z_i) \Delta m(p)}$$

and t_a is the Palacio and Blasingame normalized material balance pseudotime as given by:

$$t_a = \frac{(\mu_g c_g)_i}{q_t} \frac{Z_i G}{2p_i} [\overline{m}(p_i) - \overline{m}(\overline{p})]$$

The authors defined b'_{pss} as the inverse productivity index, in psi^2/cp-MMscf, as:

$$b'_{pss} = \frac{1.417 \times 10^6 T}{kh} \left[\ln(r_e/r_{wa}) - \frac{3}{4}\right]$$

where:

p_i = initial pressure, psi
G = Original gas in place
r_e = drainage radius, ft
r_{wa} = apparent well bore radius, ft

Thus, the above expression suggests that a plot of $q/\Delta m(p)$ versus $2qp_i t_a/(c_t \mu_i Z_i \Delta m(p))$ on a Cartesian scale would produce a straight line with following characteristics:

- x axis intercept gives gas-in-place G;
- y axis intercept gives b'_{pss};
- slope gives $(-1/Gb'_{pss})$.

Specific steps in estimating G are summarized below:

Step 1. Using the available gas properties, set up a table of Z, μ, p/Z, $(p/Z\mu)$ vs. p for the gas system.
Step 2. Plot $(p/Z\mu)$ vs. p on a Cartesian scale and numerically determine the area under the curve for several values of p to give $m(p)$ at each pressure.
Step 3. Assume a value for the initial gas-in-place G.
Step 4. Using the assumed value of G and for *each* production data point of G_p at time t, calculate $\overline{p}/\overline{Z}$ from the gas MBE, i.e., Equation 3.3.11:

$$\frac{\overline{p}}{\overline{Z}} = \frac{p_i}{Z_i}\left(1 - \frac{G_p}{G}\right)$$

Step 5. For each production data point of q_t and t, calculate t_a and the normalized cumulative production Q_N:

$$t_a = \frac{(\mu_g c_g)_i}{q_t} \frac{Z_i G}{2p_i}[\overline{m}(p_i) - \overline{m}(\overline{p})]$$

$$Q_N = \frac{2q_t p_i t_a}{(c_t \mu_i Z_i) \Delta m(p)}$$

Step 6. Plot $q/\Delta p$ vs. Q_N on a Cartesian scale and obtain the best line through the date points. Extrapolate the line to the x axis and read the original-gas-in-place G.
Step 7. The new value of G from step 5 is used for the next iteration, i.e., step 3, and this process could continue until some convergence tolerance for G is met.

Anash et al. type curves The changes in gas properties can significantly affect reservoir performance during depletion; of utmost importance is the variation in the gas viscosity–compressibility product $\mu_g c_g$ which was ignored by Fetkovich in developing his type curves. Anash et al. (2000) proposed three functional forms to describe the

product $\mu_g c_t$ as a function of pressure. They conveniently expressed the pressure in a dimensionless form as generated from the gas MBE, to give:

$$\frac{p}{Z} = \frac{p_i}{Z_i}\left(1 - \frac{G_p}{G}\right)$$

In a dimensionless form, the above MBE is expressed as:

$$p_D = (1 - G_{pD})$$

where:

$$p_D = \frac{p/Z}{p_i/Z_i} \quad G_{pD} = \frac{G_p}{G} \qquad [3.5.105]$$

Anash and his co-authors indicated that the product $(\mu_g c_t)$ can be expressed in a "dimensionless ratio" of $(\mu_g c_t)_i/\mu_g c_t)$ as a function of the dimensionless pressure p_D by one of the following three forms:

(1) *First-order polynomial*: The first form is a first-degree polynomial that is adequate in describing the product $\mu_g c_t$ as a function of pressure at low gas reservoir pressure below 5000 psi, i.e., $p_i < 5000$. The polynomial is expressed in a dimensionless form as:

$$\frac{\mu_i c_{ti}}{\mu c_t} = p_D \qquad [3.5.106]$$

where:

c_{ti} = total system compressibility at p_i, psi^{-1}
μ_i = gas viscosity at p_i, cp

(2) *Exponential model*: The second form is adequate in describing the product $\mu_g c_t$ for high-pressure gas reservoirs, i.e., $p_i > 8000$ psi:

$$\frac{\mu_i c_{ti}}{\mu c_t} = \beta_o \exp(\beta_1 p_D) \qquad [3.5.107]$$

(3) *General polynomial model*: A third-or fourth-degree polynomial is considered by the authors as a general model that is applicable to all gas reservoir systems with any range of pressures, as given by

$$\frac{\mu_i c_{ti}}{\mu c_t} = a_0 + a_1 p_D + a_2 p_D^2 + a_3 p_D^3 + a_4 p_D^4 \qquad [3.5.108]$$

The coefficients in Equations 3.5.107 and 3.5.108, i.e., β_0, β_1, a_0, a_1, etc., can be determined by plotting the dimensionless ratio $\mu_i c_{ti}/\mu_t c_t$ vs. p_D on a Cartesian scale, as shown in Figure 3.62, and using the least-squares type regression model to determine the coefficients.

The authors also developed the following fundamental form of the stabilized gas flow equation as:

$$\frac{dG_p}{dt} = q_g = \frac{J_g}{c_{ti}}\int_{p_{wD}}^{p_D}\left[\frac{\mu_i c_{ti}}{\mu c_t}\right]dp_D$$

with the dimensionless bottom-hole flowing pressure as defined by:

$$p_{wD} = \frac{p_{wf}/Z_{wf}}{p_i/Z_i}$$

where:

q_g = gas flow rate, scf/day
p_{wf} = flowing pressure, psia
Z_{wf} = gas deviation factor at p_{wf}
J_g = productivity index, scf/day, psia

Anash et al. presented their solutions in a "type curve" format in terms of a set of the familiar dimensionless variables q_{Dd}, t_{Dd}, r_{eD}, and a newly introduced correlating parameter β that is a function of the dimensionless pressure. They presented three type curve sets, as shown in Figures 3.63 through 3.65, one for each of the functional forms selected to describe the product μc_t (i.e., first-order polynomial, exponential model, or general polynomial).
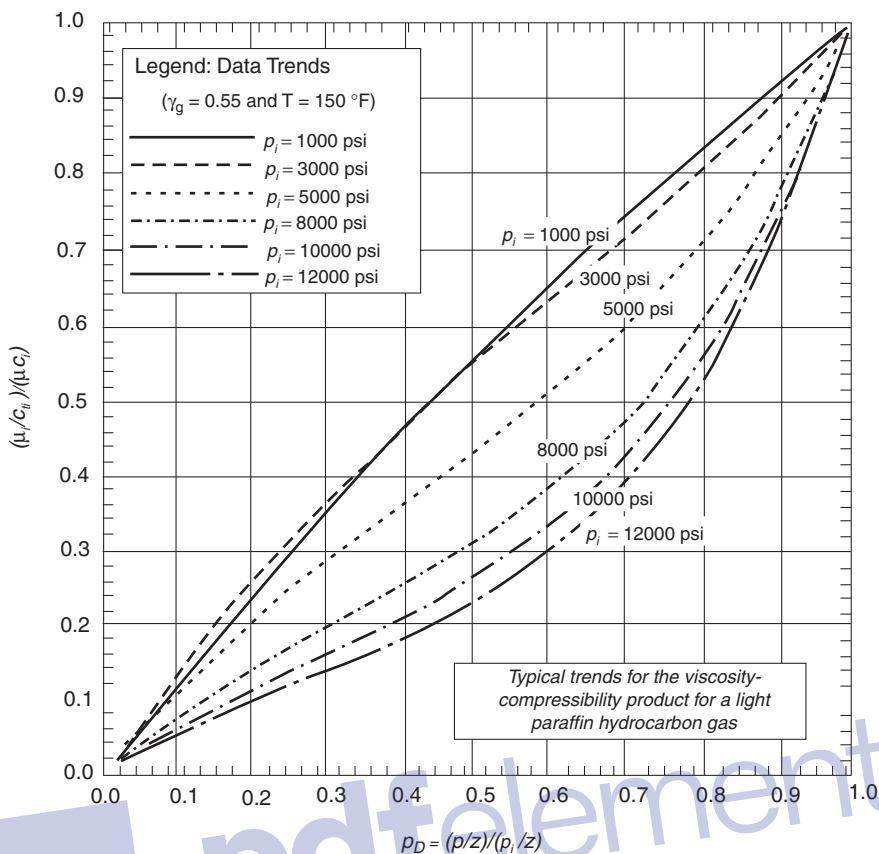
Figure 3.62 *Typical distribution of the viscosity–compressibility function (After Anash et al., 2000).*
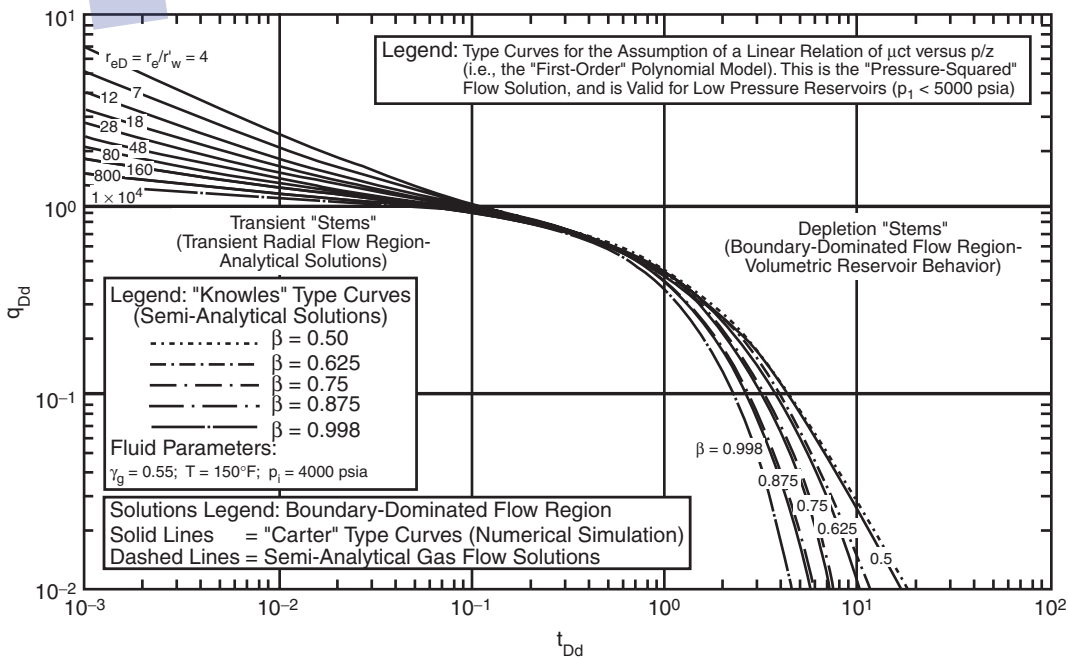

Figure 3.63 *"First-order" polynomial solution for real-gas flow under boundary-dominated flow conditions. Solution assumes a $\mu\,c_t$ profile that is linear with p_D (Permission to copy by the SPE, 2000).*
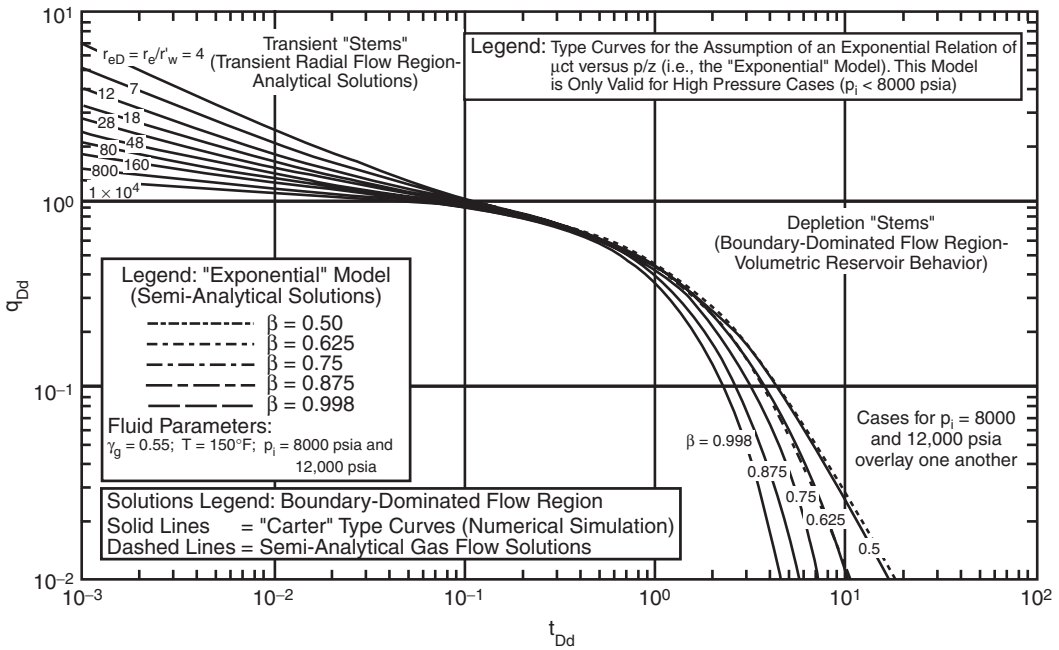
Figure 3.64   "Exponential" solutions for real-gas flow under boundary-dominated flow conditions (Permission to copy by the SPE, 2000).
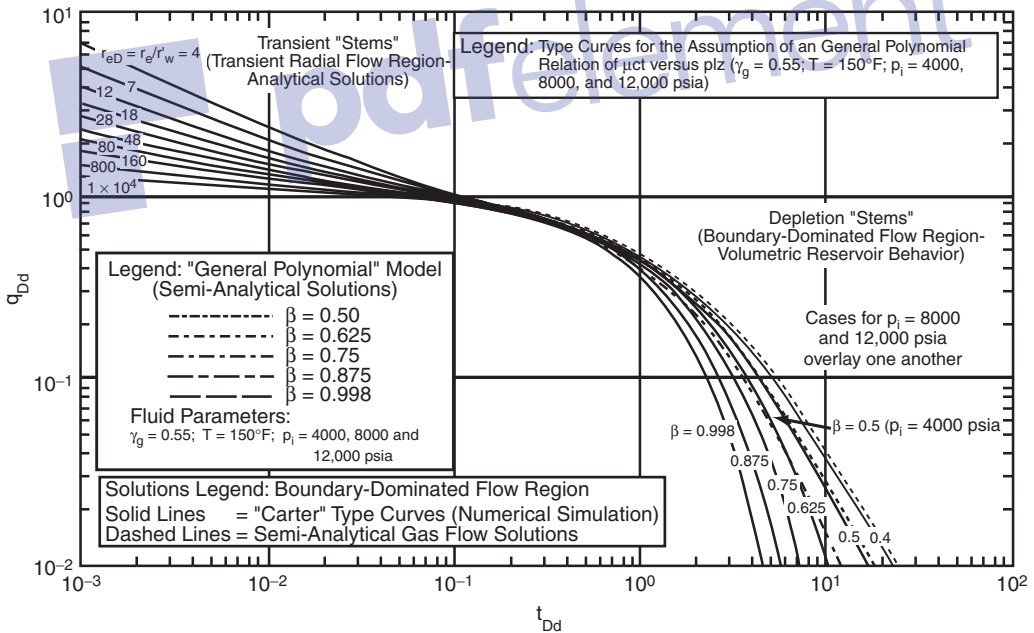

Figure 3.65   "General polynomial" solution for real-gas flow under boundary-dominated flow conditions (Permission to copy by the SPE, 2000).

The methodology of employing the Anash et al. type curve is summarized by the following steps:

Step 1. Using the available gas properties, prepare a plot of $(\mu_i c_{ti}/\mu c_t)$ vs. p_D, where:

$$p_D = \frac{p/Z}{p_i/Z_i}$$

Step 2. From the generated plot, select the appropriate functional form that describes the resulting curve. That is:
First-order polynomial:

$$\frac{\mu_i c_{ti}}{\mu c_t} = p_D$$

Exponential model:

$$\frac{\mu_i c_{ti}}{\mu c_t} = \beta_0 \exp(\beta_1 p_D)$$

General polynomial model:

$$\frac{\mu_i c_{ti}}{\mu c_t} = a_o + a_1 p_D + a_2 p_D^2 + a_3 p_D^3 + a_4 p_D^4$$

Use a regression model, i.e., leastsquares, determine the coefficient of the selected functional form that adequately describes $(\mu_i c_{ti}/\mu c_t)$ vs. p_D.

Step 3. Plot the historical flow rate q_g versus time t on log–log scale with the same logarithmic cycles as the one given by the selected type curves (i.e., Figures 3.63 through 3.65).

Step 4. Using the type curve matching technique described previously, select a match point and record:

$$(q_g)_{MP} \quad \text{and} \quad (q_{Dd})_{MP}$$

$$(t)_{MP} \quad \text{and} \quad (t_{Dd})_{MP}$$

$$(r_{eD})_{MP}$$

Step 5. Calculate the dimensionless pressure p_{wD} using the bottom-hole flowing pressure:

$$p_{wD} = \frac{p_{wf}/Z_{wf}}{p_i/Z_i}$$

Step 6. Depending on the selected functional form in step 2, calculate the constant α for the selected functional model:

For the first-order polynomial:

$$\alpha = \frac{1}{2}(1 - p_{wD}^2) \qquad [3.5.109]$$

For the exponential model:

$$\alpha = \frac{\beta_0}{\beta_1}\left[\exp(\beta_1) - \exp(\beta_1 p_{wD})\right] \qquad [3.5.110]$$

where β_0 and β_1 are the coefficients of the exponential model.

For the polynomial function (assuming a fourth degree polynomial)

$$\alpha = A_0 + A_1 + A_2 + A_3 + A_4 \qquad [3.5.111]$$

where:

$$A_0 = -(A_1 p_{wD} + A_2 p_{wD}^2 + A_3 p_{wD}^3 + A_4 p_{wD}^4) \qquad [3.5.112]$$

where:

$$A_1 = a_0 \quad A_2 = \frac{a_1}{2} \quad A_3 = \frac{a_2}{3} \quad A_4 = \frac{a_3}{4}$$

Step 7. Calculate the well productivity index J_g, in scf/day-psia, by using the flow rate match point and the constant α of step 6 in the following relation:

$$J_g = \frac{C_{ti}}{\alpha}\left(\frac{q_g}{q_{Dd}}\right)_{MP} \qquad [3.5.113]$$

Step 8. Estimate the original gas-in-place G, in scf, from the time match point:

$$G = \frac{J_g}{C_{ti}}\left(\frac{t}{t_{Dd}}\right)_{MP} \qquad [3.5.114]$$

Step 9. Calculate the reservoir drainage area A, in ft^2, from the following expression:

$$A = \frac{5.615 B_{gi} G}{\phi h(1 - S_{wi})} \qquad [3.5.115]$$

where:

A = drainage area, ft^2
B_{gi} = gas formation volume factor at p_i, bbl/scf
S_{wi} = connate water saturation

Step 10. Calculate the permeability k, in md, from the match curve of the dimensionless drainage radius r_{eD}:

$$k = \frac{141.2 \mu_i B_{gi} J_g}{h}\left(\ln[r_{eD}]_{MP} - \frac{1}{2}\right) \qquad [3.5.116]$$

Step 11. Calculate the skin factor from the following relationships:

Drainage radius $r_e = \sqrt{\dfrac{A}{\pi}} \qquad [3.5.117]$

Apparent wellbore radius $r_{wa} = \dfrac{r_e}{(r_{eD})_{MP}} \qquad [3.5.118]$

Skin factor $s = -\ln\left(\dfrac{r_{wa}}{r_w}\right) \qquad [3.5.119]$

Example 3.24 The West Virginia gas well "A" is a vertical gas well which has been hydraulically fractured and is undergoing depletion. The production data was presented by Fetkovich and used in Example 3.22. A summary of the reservoir and fluid properties is given below:

$r_w = 0.354$ ft, $\qquad\qquad h = 70$ ft
$\phi = 0.06$, $\qquad\qquad T = 160°$F
$s = 5.17$, $\qquad\qquad k = 0.07$ md
$\gamma_g = 0.57$, $\qquad\qquad B_{gi} = 0.00071$ bbl/scf
$\mu_{gi} = 0.0225$ cp, $\qquad\qquad c_{ti} = 0.000184$ psi^{-1}
$p_i = 4,175$ psia, $\qquad\qquad p_{wf} = 710$ psia
$\alpha = 0.4855$ (first-order polynomial)
$S_{wi} = 0.35$

Solution

Step 1. Figure 3.66 shows the type curve match of the production data with that of Figure 3.63 to give:

$$(q_{Dd})_{MP} = 1.0$$

$$(q_g)_{MP} = 1.98 \times 10^6 \text{ scf/day}$$

$$(t_{Dd})_{MP} = 1.0$$

$$(t)_{MP} = 695 \text{ days}$$

$$(r_{eD})_{MP} = 28$$

Step 2. Calculate the productivity index from Equation 3.5.113:

$$J_g = \frac{C_{ti}}{\alpha}\left(\frac{q_g}{q_{Dd}}\right)_{MP}$$

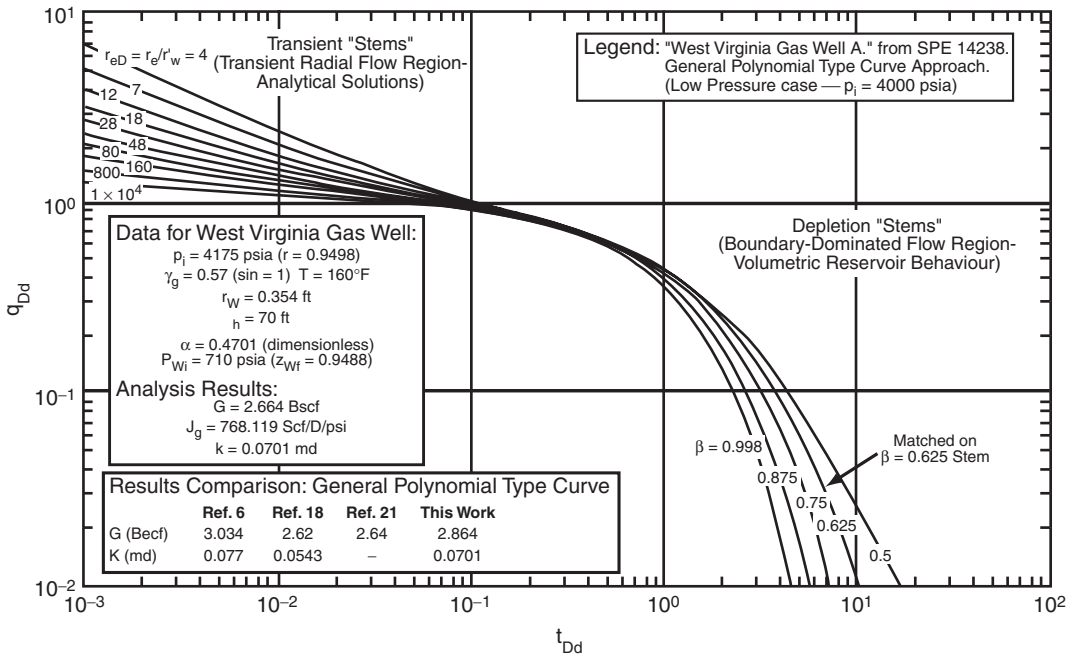$$= \frac{0.000184}{0.4855}\left(\frac{1.98 \times 10^6}{1.0}\right) = 743.758 \text{ scf/day-psi}$$

Step 3. Solve for G by applying Equation 3.5.114:

$$G = \frac{J_g}{C_{ti}}\left(\frac{t}{t_{Dd}}\right)_{MP}$$

$$= \frac{743.758}{0.0001824}\left(\frac{695}{1.0}\right) = 2.834 \text{ Bscf}$$

Step 4. Calculate the drainage area from Equation 3.5.115:

$$A = \frac{5.615 B_{gi} G}{\phi h(1 - S_{wi})}$$

$$= \frac{5.615(0.00071)(2.834 \times 10^9)}{(0.06)(70)(1 - 0.35)}$$

$$= 4.1398 \times 10^6 \text{ ft}^2 = 95 \text{ acres}$$

Figure 3.66 *Type curve analysis of West Virginia gas well "A" (SPE 14238). "General polynomial" type curve analysis approach (Permission to copy by the SPE, 2000)*

Step 5. Compute the permeability from the match on the $r_{eD} = 28$ transient stem by using Equation 3.5.116:

$$k = \frac{(141.2)(0.0225)(0.00071)(743.76)}{70}\left(\ln(28) - \frac{1}{2}\right)$$

$$= 0.0679 \text{ md}$$

Step 6. Calculate the skin factor by applying Equations 3.5.117 and 3.5.118:

$$r_e = \sqrt{\frac{A}{\pi}} = \sqrt{\frac{4.1398 \times 10^6}{\pi}} = 1147.9 \text{ ft}$$

$$r_{wa} = \frac{r_e}{(r_{eD})_{MP}} = \frac{1147.9}{28} = 40.997 \text{ ft}$$

$$s = -\ln\left(\frac{r_{wa}}{r_w}\right) = -\ln\left(\frac{40.997}{0.354}\right) = -4.752$$

Decline curve analysis for fractured wells Pratikno et al. (2003) developed a new set of type curves specifically for finite conductivity, vertically fractured wells centered in bounded circular reservoirs. The authors used analytical solutions to develop these type curves and to establish a relation for the decline variables.

Recall that the general dimensionless pressure equation for a bounded reservoir during pseudosteady-state flow is given by Equation 1.2.125:

$$p_D = 2\pi t_{DA} + \frac{1}{2}[\ln(A/r_w^2)] + \frac{1}{2}[\ln(2.2458/C_A)] + s$$

with the dimensionless time based on the wellbore radius t_D or drainage area t_{DA} as given by Equations 1.2.75a and 1.2.75b as:

$$t_D = \frac{0.0002637kt}{\phi\mu c_t r_w^2}$$

$$t_{DA} = \frac{0.0002637kt}{\phi\mu c_t A} = t_A\left(\frac{r_w^2}{A}\right)$$

The authors adopted the above form and suggested that for a well producing under pseudosteady-state (pss) at a constant rate with a finite conductivity fracture in a circular reservoir, the dimensionless pressure drop can be expressed as:

$$p_D = 2\pi t_{DA} + b_{Dpss}$$

or:

$$b_{Dpss} = p_D - 2\pi t_{DA}$$

Where the term b_{Dpss} is the dimensionless pseudosteady-state constant that is independent of time; however, b_{Dpss} is a function of:

• the dimensionless radius r_{eD} and
• the dimensionless fracture conductivity F_{CD}.

The above two dimensionless parameters were defined in Chapter 1 by:

$$F_{CD} = \frac{k_f}{k}\frac{w_f}{x_f} = \frac{F_C}{kx_f}$$

$$r_{eD} = \frac{r_e}{x_f}$$

The authors noted that during pseudosteady flow, the equation describing the flow during this period yields a constant value for a given values of r_{eD} and F_{CD} that is closely given by the following relationship:

$$b_{Dpss} = \ln(r_{eD}) - 0.049298 + \frac{0.43464}{r_{eD}^2}$$

$$+ \frac{a_1 + a_2 u + a_3 u^2 + a_4 u^3 + a_5 u^4}{1 + b_1 u + b_2 u^2 + b_3 u^3 + b_4 u^4}$$

with:

$$u = \ln(F_{CD})$$

Fetkovich-McCray Type Curve for a Vertical Well with a
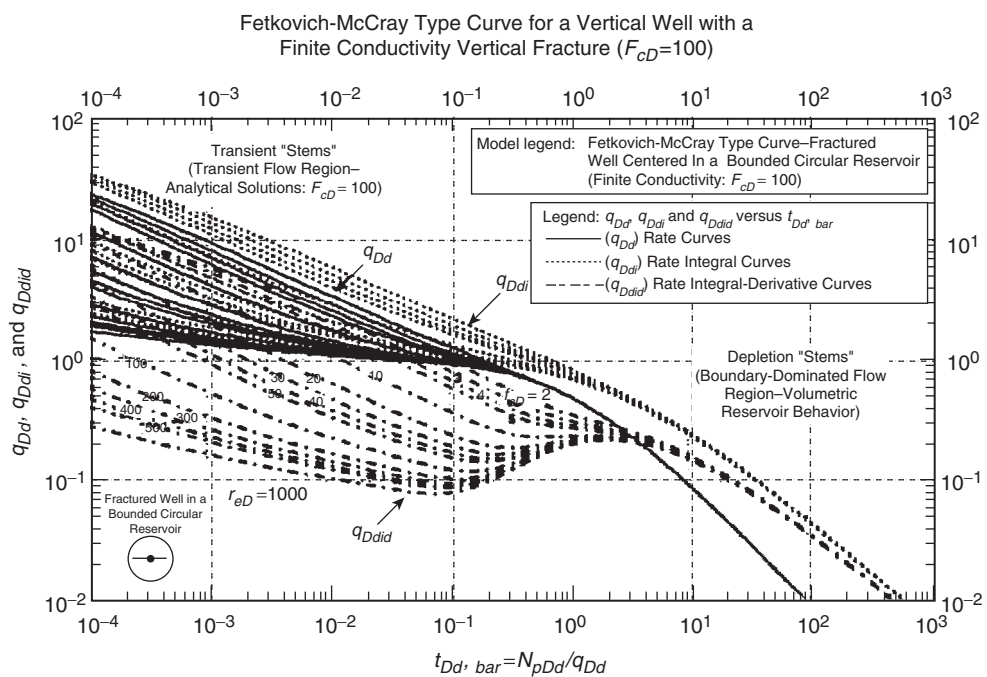Finite Conductivity Vertical Fracture ($F_{cD}= 0.1$)
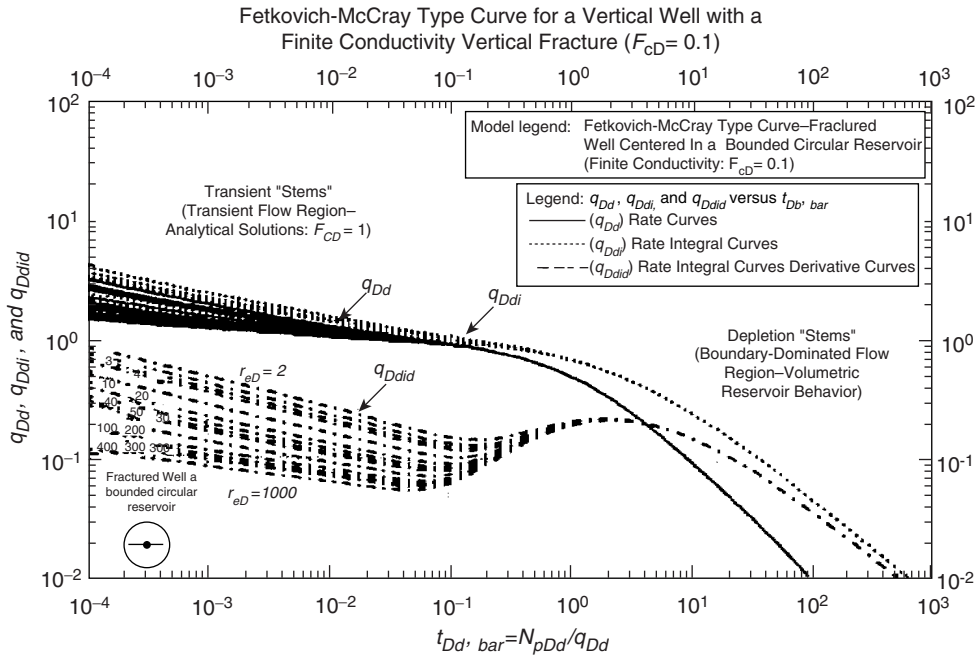
Figure 3.67 *Fetkovich–McCray decline type curve—rate versus material balance time format for a well with a finite conductivity vertical fracture ($F_{cD} = 0.1$) (Permission to copy by the SPE, 2003).*

where:

$a_1 = 0.93626800$ $b_1 = -0.38553900$
$a_2 = -1.0048900$ $b_2 = -0.06988650$
$a_3 = 0.31973300$ $b_3 = -0.04846530$
$a_4 = -0.0423532$ $b_4 = -0.00813558$
$a_5 = 0.00221799$

Based on the above equations, Pratikno et al. used Palacio and Blasingame's previously defined functions (i.e., t_a, $(q_{Dd})_i$, and $(q_{Dd})_{id}$) and the parameters r_{eD} and F_{CD} to generate a set of decline curves for a sequence of 13 values for F_{CD} with a sampling of $r_{eD} = 2, 3, 4, 5, 10, 20, 30, 40, 50, 100, 200, 300, 400, 500,$ and 1000. Type curves for F_{CD} of 0.1, 1, 10, 100, 1000 are shown in Figures 3.67 through 3.71.

The authors recommended the following type curve matching procedure that is similar to the methodology used in applying Palacio and Blasingame's type curve:

Solution

Step 1. Analyze the available well testing data using the Gringarten or Cinco–Samaniego method, as presented in Chapter 1, to calculate the dimensionless fracture conductivity F_{CD} and the fracture half-length x_f.

Step 2. Assemble the available well data in terms of bottom-hole pressure and the flow rate q_t (in STB/day for oil or Mscf/day for gas) as a function of time. Calculate the material balance pseudotime t_a for *each given data point* by using:

For oil $t_a = \dfrac{N_p}{q_t}$

For gas $t_a = \dfrac{(\mu_g c_g)_i}{q_t}\dfrac{Z_i G}{2p_i}[\overline{m}(p_i) - \overline{m}(\bar{p})]$

where $\overline{m}(p_i)$ and $\overline{m}(p)$ are the normalized pseudopressures as defined by Equations 3.5.93

and 3.5.94:

$$\overline{m}(p_i) = \frac{\mu_{gi}Z_i}{p_i}\int_0^{p_i}\left[\frac{p}{\mu_g Z}\right]dp$$

$$\overline{m}(p) = \frac{\mu_{gi}Z_i}{p_i}\int_0^{p}\left[\frac{p}{\mu_g Z}\right]dp$$

Note that the initial gas-in-place G must be calculated iteratively, as illustrated previously by Palacio and Blasingame.

Step 3. Using the well production data as tabulated and plotted in step 2, compute the following three complementary plotting functions:

(1) pressure drop normalized rate q_{Dd};
(2) pressure drop normalized rate integral function $(q_{Dd})_i$;
(3) pressure drop normalized rate integral–derivative function $(q_{Dd})_{id}$.

For gas:

$$q_{Dd} = \frac{q_g}{\overline{m}(p_i) - \overline{m}(p_{wf})}$$

$$(q_{Dd})_i = \frac{1}{t_a}\int_0^{t_a}\left(\frac{q_g}{\overline{m}(p_i) - \overline{m}(p_{wf})}\right)dt_a$$

$$(q_{Dd})_{id} = \left(\frac{-1}{t_a}\right)\frac{d}{dt_a}\left[\frac{1}{t_a}\int_0^{t_a}\left(\frac{q_g}{\overline{m}(p_i) - \overline{m}(p_{wf})}\right)dt_a\right]$$

For oil:

$$q_{Dd} = \frac{q_o}{p_i - p_{wf}}$$

$$(q_{Dd})_i = \frac{1}{t_a}\int_0^{t_a}\left(\frac{q_o}{p_i - p_{wf}}\right)dt_a$$

$$(q_{Dd})_{id} = \left(\frac{-1}{t_a}\right)\frac{d}{dt_a}\left[\frac{1}{t_a}\int_0^{ta}\left(\frac{q_o}{p_i - p_{wf}}\right)dt_a\right]$$
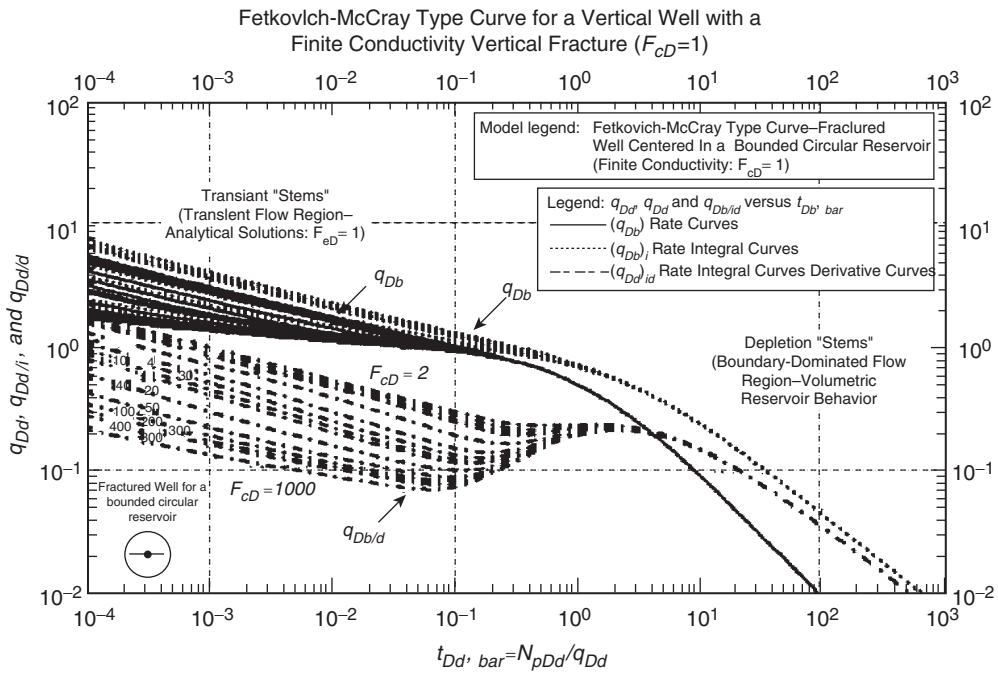
Figure 3.68 *Fetkovich–McCray decline type curve—rate versus material balance time format for a well with a finite conductivity vertical fracture (F_{cD} = 1) (Permission to copy by the SPE, 2003).*
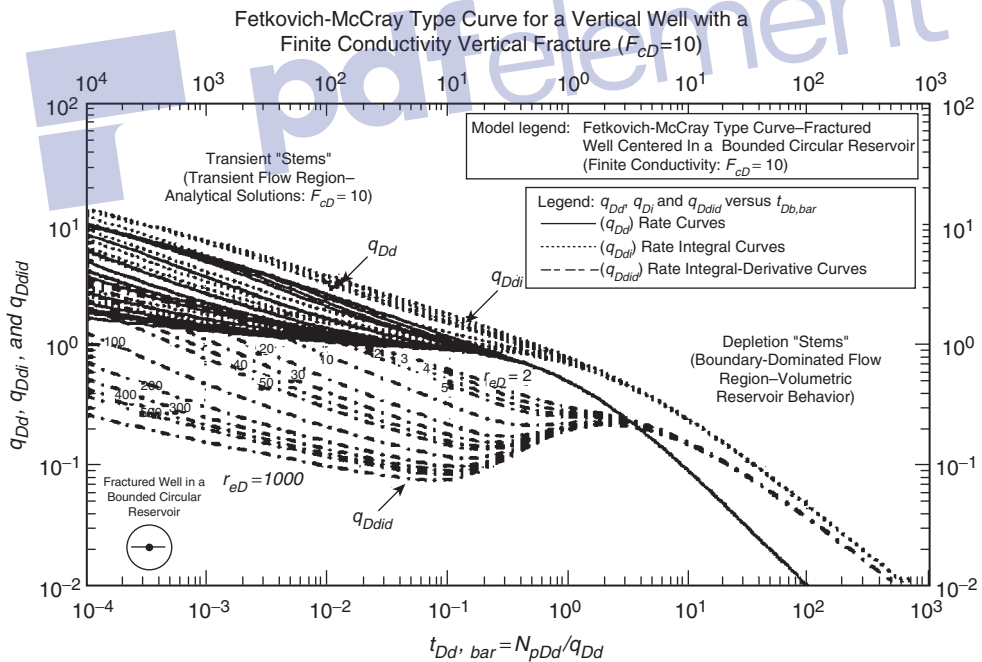
Figure 3.69 *Fetkovich–McCray decline type curve—rate versus material balance time format for a well with a finite conductivity vertical fracture (F_{cD} = 10) (Permission to copy by the SPE, 2003).*

Step 4. Plot the three gas or oil functions, i.e., q_{Dd}, $(q_{Dd})_i$, and $(q_{Dd})_{id}$, versus t_a on tracing paper so it can be laid over the type curve with the appropriate value F_{CD}.

Step 5. Establish a match point "MP" for each of the three functions (q_{Dd}, $(q_{Dd})_i$ and $(q_{Dd})_{id}$). Once a "match" is

obtained, record the "time" and "rate" match points as well as the dimensionless radius r_{eD} value:

(1) Rate-axis "match point": Any $(q/\Delta p)_{MP}$ – $(q_{Dd})_{MP}$ pair.

Fetkovich-McCray Type Curve for a Vertical Well with a
Finite Conductivity Vertical Fracture (F_{cD}=100)

Figure 3.70 *Fetkovich–McCray decline type curve—rate versus material balance time format for a well with a finite conductivity vertical fracture (F_{cD} = 100) (Permission to copy by the SPE, 2003).*

Fetkovich-McCray Type Curve for a Vertical Well with a
Finite Conductivity Vertical Fracture (F_{cD}=1000)
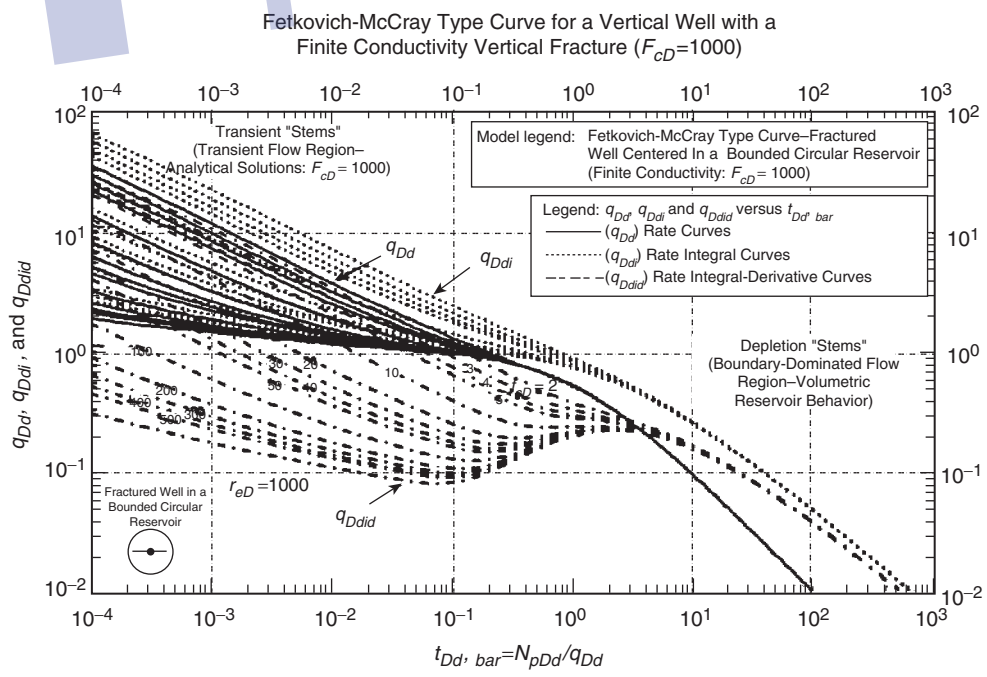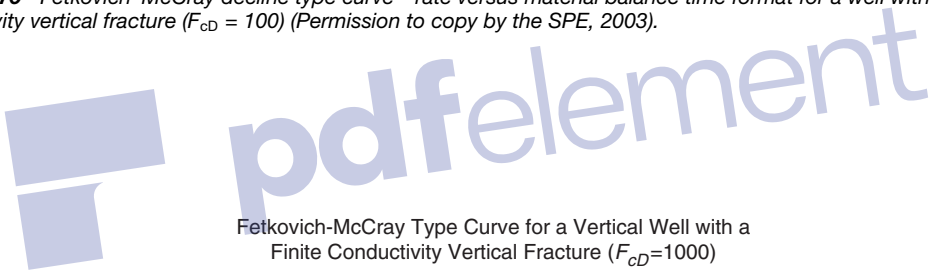
Figure 3.71 *Fetkovich–McCray decline type curve—rate versus material balance time format for a well with a finite conductivity vertical fracture (F_{cD} = 1000) (Permission to copy by the SPE, 2003).*

Felkovich-McCray Type Curve for a Vertical Well with a Finite Conductivity Vertical Fracture (F_{cD}= 5)
[Example 1–Low Permeability/High Pressure Gas Reservoir (Texas)]
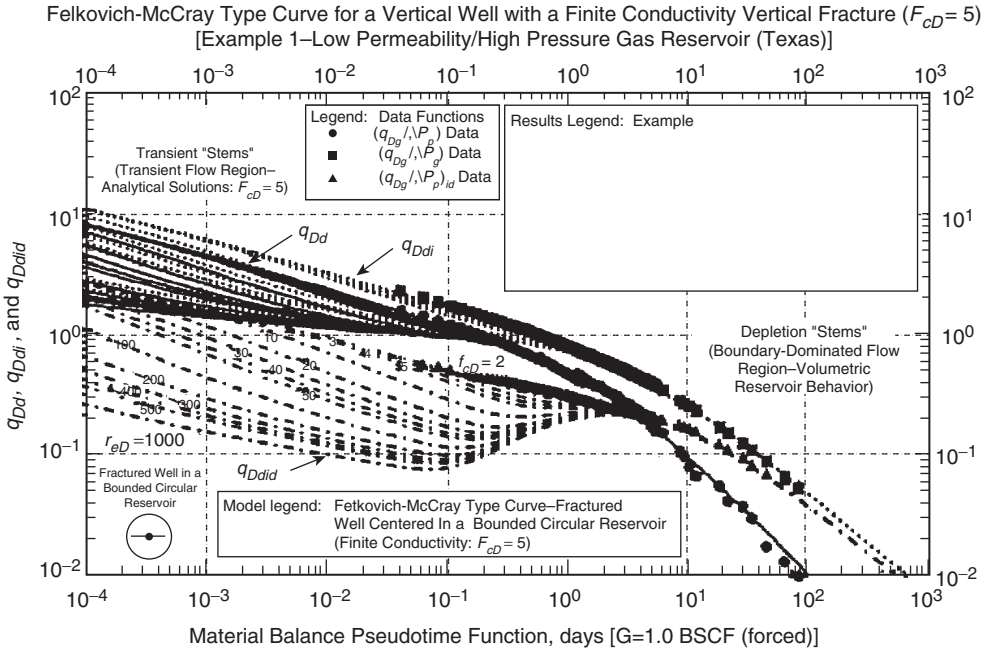
Figure 3.72   *Match of production data for Example 1 on the Fetkovich–McCray decline type curve (pseudopressure drop normalized rate versus material balance time format) for a well with a finite conductivity vertical fracture (F_{cD} = 5) (Permission to copy by the SPE, 2003).*

(2) Time-axis "match point": Any $(\bar{t})_{MP} - (t_{Dd})_{MP}$ pair.
(3) Transient flow stem: Select $(q/\Delta p)$, $(q/\Delta p)_i$, and $(q/\Delta p)_{id}$ functions that best match the transient data stem and record r_{eD}.

Step 6. Solve for b_{Dpss} by using the values of F_{CD} and r_{eD}:
$$u = \ln(F_{CD})$$

$$b_{Dpss} = \ln(r_{eD}) - 0.049298 + \frac{0.43464}{r_{eD}^2}$$

$$+ \frac{a_1 + a_2 u + a_3 u^2 + a_4 u^3 + a_5 u^4}{1 + b_1 u + b_2 u^2 + b_3 u^3 + b_4 u^4}$$

Step 7. Using the results of the match point, estimate the following reservoir properties:
For gas:
$$G = \frac{1}{c_{ti}} \left[\frac{t_a}{t_{Dd}} \right]_{MP} \left[\frac{(q_g/\Delta m(\bar{p}))}{q_{Dd}} \right]_{MP}$$

$$k_g = \frac{141.2 B_{gi} \mu_{gi}}{h} \left[\frac{(q_g/\Delta m(\bar{p})_{MP})}{(q_{Dd})_{MP}} \right] b_{Dpss}$$

$$A = \frac{5.615 G B_{gi}}{h\phi(1 - S_{wi})}$$

$$r_e = \sqrt{\frac{A}{\pi}}$$

For oil:
$$N = \frac{1}{c_t} \left[\frac{t_a}{t_{Dd}} \right]_{MP} \left[\frac{(q_o/\Delta p)_i}{q_{Dd}} \right]_{MP}$$

$$k_o = \frac{141.2 B_{oi} \mu_{goi}}{h} \left[\frac{(q_o/\Delta p)_{MP}}{(q_{Dd})_{MP}} \right] b_{Dpss}$$

$$A = \frac{5.615 N B_{oi}}{h\phi(1 - S_{wi})}$$

$$r_e = \sqrt{\frac{A}{\pi}}$$

where:

G = gas-in-place, Mscf
N = oil-in-place, STB
B_{gi} = gas formation volume factor at p_i, bbl/Mscf
A = drainage area, ft^2
r_e = drainage radius, ft
S_{wi} = connate water saturation

Step 8. Calculate the fracture half-length x_f and compare with step 1:
$$x_f = \frac{r_e}{r_{eD}}$$

Example 3.25   The Texas Field vertical gas well has been hydraulically fractured and is undergoing depletion. A summary of the reservoir and fluid properties is given below:

$r_w = 0.333$ ft, $h = 170$ ft
$\phi = 0.088$, $T = 300°F$
$\gamma_g = 0.70$, $B_{gi} = 0.5498$ bblM/scf
$\mu_{gi} = 0.0361$ cp, $c_{ti} = 5.1032 \times 10^{-5}$ psi^{-1}
$p_i = 9330$ psia, $p_{wf} = 710$ psia
$S_{wi} = 0.131$, $F_{CD} = 5.0$

Figure 3.72 shows the type curve match for $F_{CD} = 5$, with the matching points as given below:
$$(q_{Dd})_{MP} = 1.0$$

$$[(q_g/\Delta m(\bar{p}))]_{MP} = 0.89 \text{ Mscf/psi}$$

$$(t_{Dd})_{MP} = 1.0$$

$$(t_a)_{MP} = 58 \text{ days}$$

$$(r_{eD})_{MP} = 2.0$$

Perform type curve analysis on this gas well.

Solution

Step 1. Solve for b_{Dpss} by using the values of F_{CD} and r_{eD}:

$$u = \ln(F_{CD}) = \ln(5) = 1.60944$$

$$b_{Dpss} = \ln(r_{eD}) - 0.049298 + \frac{0.43464}{r_{eD}^2}$$

$$+ \frac{a_1 + a_2 u + a_3 u^2 + a_4 u^3 + a_5 u^4}{1 + b_1 u + b_2 u^2 + b_3 u^3 + b_4 u^4}$$

$$= \ln(2) - 0.049298 + \frac{0.43464}{2^2}$$

$$+ \frac{a_1 + a_2 u + a_3 u^2 + a_4 u^3 + a_5 u^4}{1 + b_1 u + b_2 u^2 + b_3 u^3 + b_4 u^4} = 1.00222$$

Step 2. Using the results of the match point, estimate the following reservoir properties:

$$G = \frac{1}{c_{ti}} \left[\frac{t_a}{t_{Dd}} \right]_{MP} \left[\frac{(q_g/\Delta m(\bar{p}))}{q_{Dd}} \right]_{MP}$$

$$= \frac{1}{5.1032 \times 10^{-5}} \left[\frac{58}{1.0} \right]_{MP} \left[\frac{0.89}{1.0} \right]$$

$$= 1.012 \times 10^6 \text{ MMscf}$$

$$k_g = \frac{141.2 B_{gi}\mu_{gi}}{h} \left[\frac{(q_g/\Delta m(\bar{p})_{MP})}{(q_{Dd})_{MP}} \right] b_{Dpss}$$

$$= \frac{141.2(0.5498)(0.0361)}{170} \left[\frac{0.89}{1.0} \right] 1.00222$$

$$= 0.015 \text{ md}$$

$$A = \frac{5.615 G B_{gi}}{h\phi(1 - S_{wi})}$$

$$= \frac{5.615(1.012 \times 10^6)(0.5498)}{(170)(0.088)(1 - 0.131)} = 240\,195 \text{ ft}^2$$

$$= 5.51 \text{ acres}$$

$$r_e = \sqrt{\frac{A}{\pi}} = \sqrt{\frac{240\,195}{\pi}} = 277 \text{ ft}$$

Step 3. Calculate the fracture half-length x_f and compare with step 1:

$$x_f = \frac{r_e}{r_{eD}} = \frac{277}{2} = 138 \text{ ft}$$

3.6 Gas Hydrates

Gas hydrates are solid crystalline compounds formed by the physical combination of gas and water under pressure and temperatures considerably above the freezing point of water. In the presence of free water, hydrate will form when the temperature is below a certain degree; this temperature is called "hydrate temperature T_h." Gas hydrate crystals resemble ice or wet snow in appearance but do not have the solid structure of ice. The main framework of the hydrate crystal is formed with water molecules. The gas molecules occupy void spaces (cages) in the water crystal lattice; however, enough cages must be filled with hydrocarbon molecules to stabilize the crystal lattice. When the hydrate "snow" is tossed on the ground, it causes a distinct cracking sound resulting from the escaping of gas molecules as they rupture the crystal lattice of the hydrate molecules.

Two types of hydrate crystal lattices are known, with each containing void spaces of two different sizes:

(1) Structure I of the lattice has voids of the size to accept small molecules such as methane and ethane. These "guest" gas molecules are called "hydrate formers." In general, light components such as C_1, C_2, and CO_2 form structure I hydrates.
(2) Structure II of the lattice has larger voids (i.e., "cages or cavities") that allow the entrapment of the heavier alkanes with medium-sized molecules, such as C_3, $i - C_4$, and $n - C_4$, in addition to methane and ethane, to form structure II hydrates. Several studies have shown that a stable hydrate structure is hydrate structure II. However, the gases are very lean; structure I is expected to be the hydrate stable structure.

All components heavier than C_4, i.e., C_{5+}, do not contribute to the formation of hydrates and therefore are identified as "non-hydrate components."

Gas hydrates generate considerable operational and safety concerns in subsea pipelines and process equipment. The current practice in the petroleum industry for avoiding gas hydrate is to operate outside the hydrate stability zone. During the flow of natural gas, it becomes necessary to define, and thereby avoid, conditions that promote the formation of hydrates. This is essential since hydrates can cause numerous problems such as:
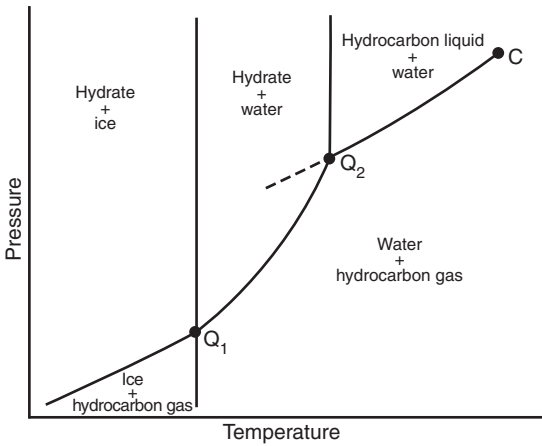
- choking the flow string, surface lines, and other equipment;
- completely blocking flow lines and surface equipment;
- hydrate formation in the flow string resulting in a lower value of measured wellhead pressures.

Sloan (2000) listed several conditions that tend to promote the formation of gas hydrates. These are:

- the presence of free water and gas molecules that range in size from methane to butane;
- the presence of H_2S or CO_2 as a substantial factor contributing to the formation of hydrate since these acid gases are more soluble in water than hydrocarbons;
- temperatures below the "hydrate formation temperature" for the pressure and gas composition considered;
- high operating pressures that increase the "hydrate formation temperature";
- high velocity or agitation through piping or equipment;
- the presence of small "seed" crystal of hydrate;
- natural gas at or below its water dewpoint with liquid water present.

The above conditions necessary for hydrate formation lead to the following four classic, thermodynamic prevention methods:

(1) Water removal provides the best protection.
(2) Maintaining a high temperature throughout the flow system, i.e., insulation, pipe bundling, or electrical heating.
(3) Hydrate prevention is achieved most frequently by injecting an inhibitor, such as methanol or monoethylene glycol, which acts as antifreezes.
(4) Kinetic inhibitors are low-molecular-weight polymers dissolved in a carrier solvent and injected into the water phase in the pipeline. These inhibitors bond to the hydrate surface and prevent significant crystal growth for a period longer than the free water residence time in a pipeline.

Figure 3.73 *Phase diagram for a typical mixture of water and light hydrocarbon.*

Figure 3.74 *Pressure–temperature curves for predicting hydrate (Courtesy Gas Processors Suppliers Association).*

3.6.1 Phase diagrams for hydrates

The temperature and pressure conditions for hydrate formation in surface gas processing facilities are generally much lower than those considered in production and reservoir engineering. The conditions of initial hydrate formation are often given by simple p–T phase diagrams for water–hydrocarbon systems. A schematic illustration of the phase diagram for a typical mixture of water and light hydrocarbon is shown in Figure 3.73. This graphical illustration of the diagram shows a lower quadruple point "Q_1" and upper quadruple point "Q_2." The quadruple point defines the condition at which four phases are in equilibrium.

Each quadruple point is at the intersection of four three-phase lines. The lower quadruple point Q_1 represents the point at which ice, hydrate, water, and hydrocarbon gas exist in equilibrium. At temperatures below the temperature that corresponds to point Q_1, hydrates form from vapor and ice. The upper quadruple point Q_2 represents the point at which water, liquid hydrocarbon, hydrocarbon gas, and hydrate exist in equilibrium, and marks the upper temperature limit for hydrate formation for that particular gas–water system. Some of the lighter natural-gas components, such as methane and nitrogen, do not have an upper quadruple point, so no upper temperature limit exists for hydrate formation. This is the reason that hydrates can still form at high temperatures (up to 120°F) in the surface facilities of high-pressure wells.

The line Q_1–Q_2 separates the area in which water and gas combine to form hydrates. The vertical line extending from point Q_2 separates the area of water and hydrocarbon liquid from the area of hydrate and water.

It is convenient to divide hydrate formation into the following two categories:

Category I: Hydrate formation due to a decrease in temperature with no sudden pressure drop, such as in the flow string or surface line.

Category II: Hydrate formation where sudden expansion occurs, such as in orifices, back-pressure regulators, or chokes.

Figure 3.74 presents a graphical method for approximating hydrate formation conditions and for estimating the permissible expansion condition of natural gases without the formation of hydrates. This figure shows the hydrate-forming conditions as described by a family of "hydrate formation lines" representing natural gases with various specific gravities. Hydrates will form whenever the coordinates of the point representing the pressure and temperature are located to the *left of the hydrate formation line for the gas in question*. This graphical correlation can be used to approximate the hydrate-forming temperature as the temperature deceases along flow string and flow lines, i.e., category I.
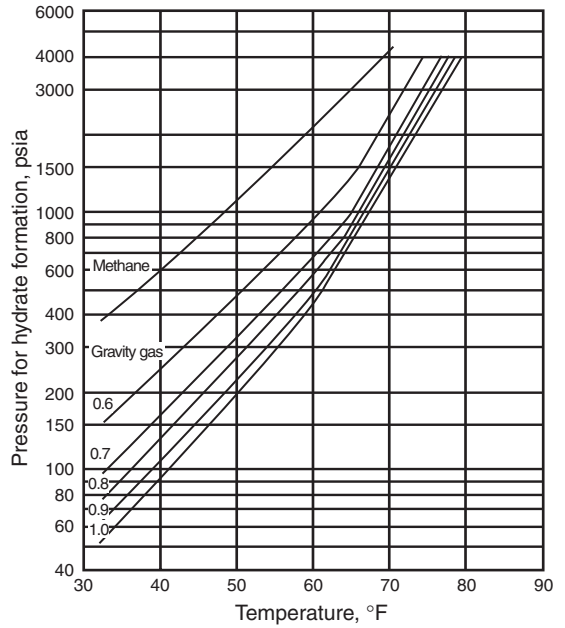
Example 3.26 A gas of 0.8 specific gravity is at 1000 psia. To what extent can the temperature be lowered without hydrate formation in the presence of free water?

Solution   From Figure 3.74, at a specific gravity of 0.8 and a pressure of 1000 psia, hydrate temperature is 66°F. Thus, hydrates may form at or below 66°F.

Example 3.27 A gas has a specific gravity of 0.7 and exists at 60°F. What would be the pressure above which hydrates could be expected to form?

*Solution*   From Figure 3.74, hydrate will form above 680 psia.

It should be pointed out that the graphical correlation presented in Figure 3.74 was developed for pure water–gas systems; however, the presence of dissolved solids in the water will reduce the temperatures at which natural gases will form hydrates.

When a water–wet gas expands rapidly through a valve, orifice, or other restrictions, hydrates may form because of rapid gas cooling caused by Joule–Thomson expansion. That is:

$$\frac{\partial T}{\partial p} = \frac{RT^2}{pC_P}\left(\frac{\partial Z}{\partial T}\right)_P$$

where:

T = temperature
p = pressure
Z = gas compressibility factor
C_P = specific heat at constant pressure
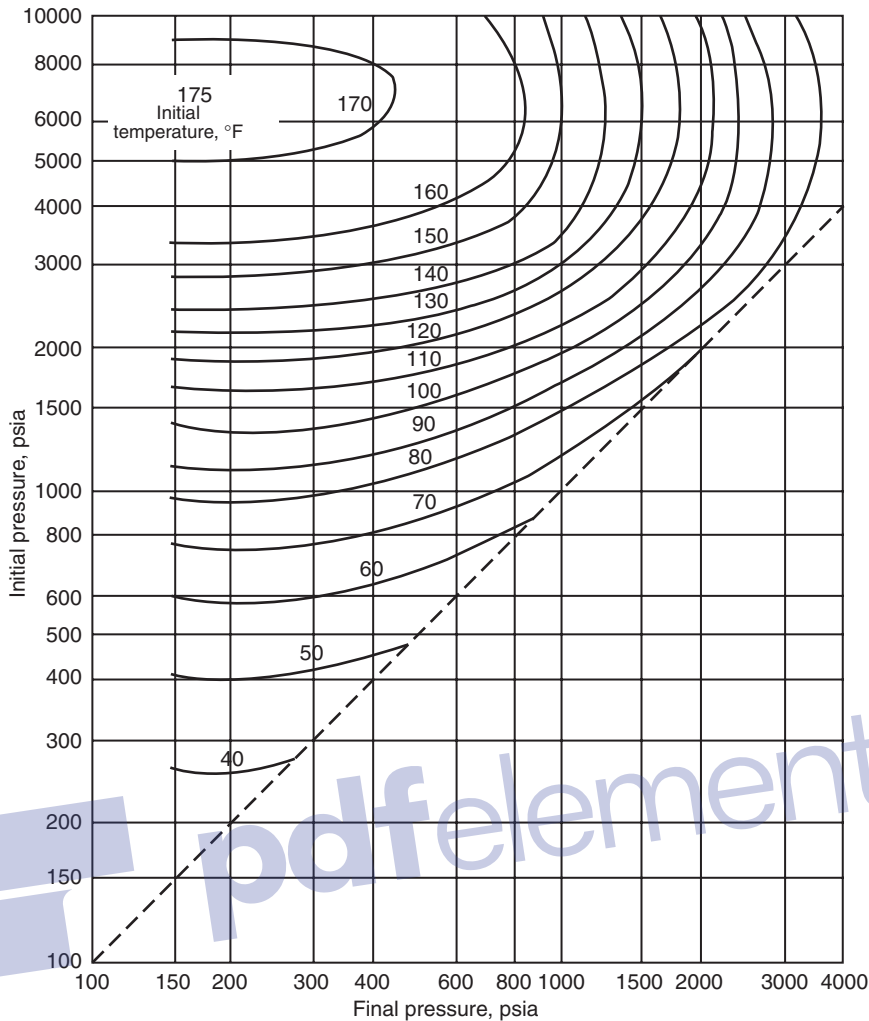
Figure 3.75 *Permissible expansion of a 0.6 gravity natural gas without hydrate formation (Courtesy Gas Processors Suppliers Association).*

This reduction in temperature due to the sudden reduction in pressure, i.e., $\partial T / \partial p$, could cause the condensation of water vapor from the gas and bring the mixture to the conditions necessary for hydrate formation. Figures 3.75 through 3.79 can be used to estimate the maximum reduction in pressure without causing the formation of hydrates.

The chart is entered at the intersection of the initial pressure and initial temperature isotherm; and the lowest pressure to which the gas can be expanded without forming hydrate is read directly from the x axis below the intersection.

Example 3.28 How far can a gas of 0.7 specific gravity at 1500 psia and 120°F be expanded without hydrate formation?

Solution From Figure 3.76, select the graph on the y axis with the initial pressure of 1500 psia and move horizontally to the right to intersect with the 120°F temperature isotherm. Read the "final" pressure on the x axis, to give 300 psia. Hence, this gas may be expanded to a final pressure of 300 psia without the possibility of hydrate formation.

Ostergaard et al. (2000) proposed a new correlation to predict the hydrate-free zone of reservoir fluids that range in composition from black oil to lean natural-gas systems. The authors separated the components of the hydrocarbon system into the following two groups:

(1) hydrate-forming hydrocarbons "h" that include methane, ethane, propane, and butanes;
(2) non-hydrate-forming hydrocarbons "nh" that include pentanes and heavier components.

Define the following correlating parameters:

$$f_h = y_{C1} + y_{C2} + y_{C3} + y_{i-C4} + y_{n-C4} \qquad [3.6.1]$$

$$f_{nh} = y_{C5+} \qquad [3.6.2]$$

$$F_m = \frac{f_{nh}}{f_h} \qquad [3.6.3]$$

$$\gamma_h = \frac{m_h}{28.96} = \frac{\sum_{i=C_1}^{n-C_4} y_i m_i}{28.96} \qquad [3.6.4]$$
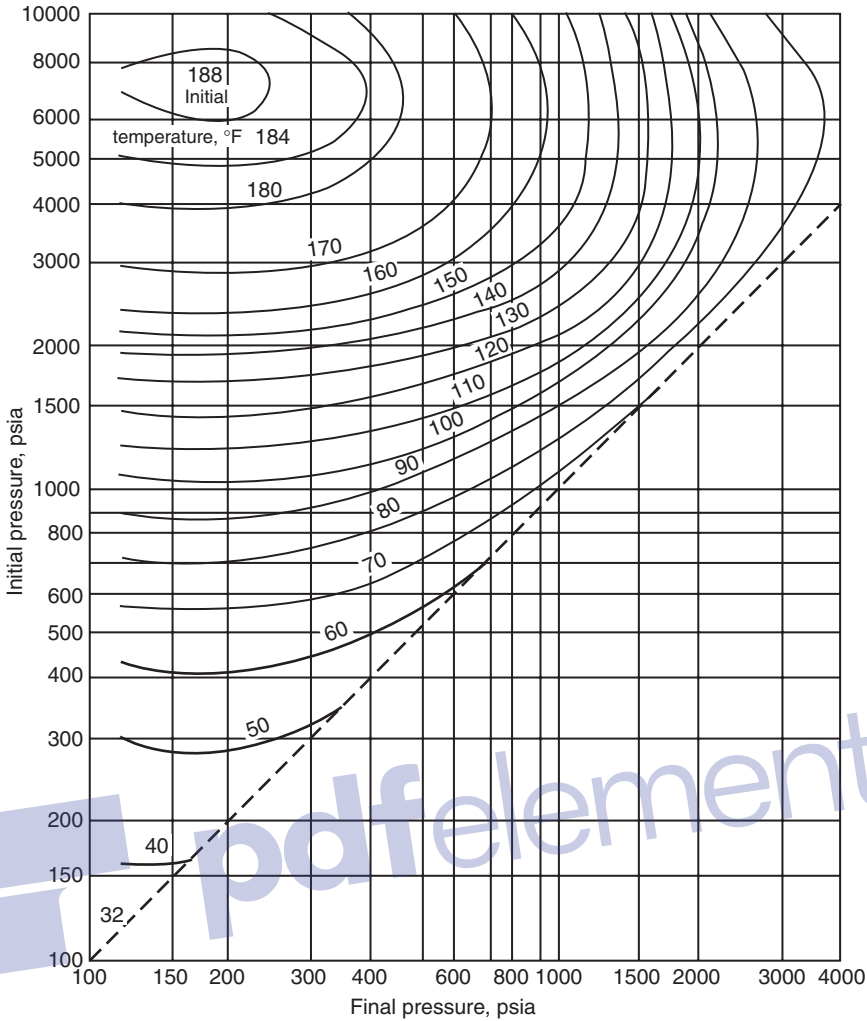
Figure 3.76 *Permissible expansion of a 0.7 gravity natural gas without hydrate formation (Courtesy Gas Processors Suppliers Association).*

where:

$\quad$ h $=$ hydrate-forming components C_1 through C_4
$\quad$ nh $=$ non-hydrate-forming components, C_5 and heavier
$\quad F_m =$ molar ratio between the non-hydrate-forming and hydrate-forming components
$\quad \gamma_h =$ specific gravity of hydrate-forming components

The authors correlated the hydrate dissociation pressure p_h of fluids containing only hydrocarbons as a function of the above defined parameters by the following expression:

$$p_h = 0.1450377 \exp \left\{ \left[\frac{a_1}{(\gamma_h + a_2)^3} + a_3 F_m + a_4 F_m^2 + a_5 \right] T \right.$$

$$\left. + \frac{a_6}{(\gamma_h + a_7)^3} + a_8 F_m + a_9 F_m^2 + a_{10} \right\} \qquad [3.6.5]$$

where:

$\quad p_h =$ hydrate dissociation pressure, psi
$\quad T =$ temperature, °R
$\quad a_i =$ constants as given below

a_i	*Value*
a_1	2.5074400×10^{-3}
a_2	0.4685200
a_3	1.2146440×10^{-2}
a_4	$-4.6761110 \times 10^{-4}$
a_5	0.0720122
a_6	3.6625000×10^{-4}
a_7	-0.4850540
a_8	-5.4437600
a_9	3.8900000×10^{-3}
a_{10}	-29.9351000

Equation 3.6.5 was developed using data on black oil, volatile oil, gas condensate, and natural gas systems in the range of 32°F to 68°F, which covers the practical range of hydrate formation for reservoir fluids transportation.
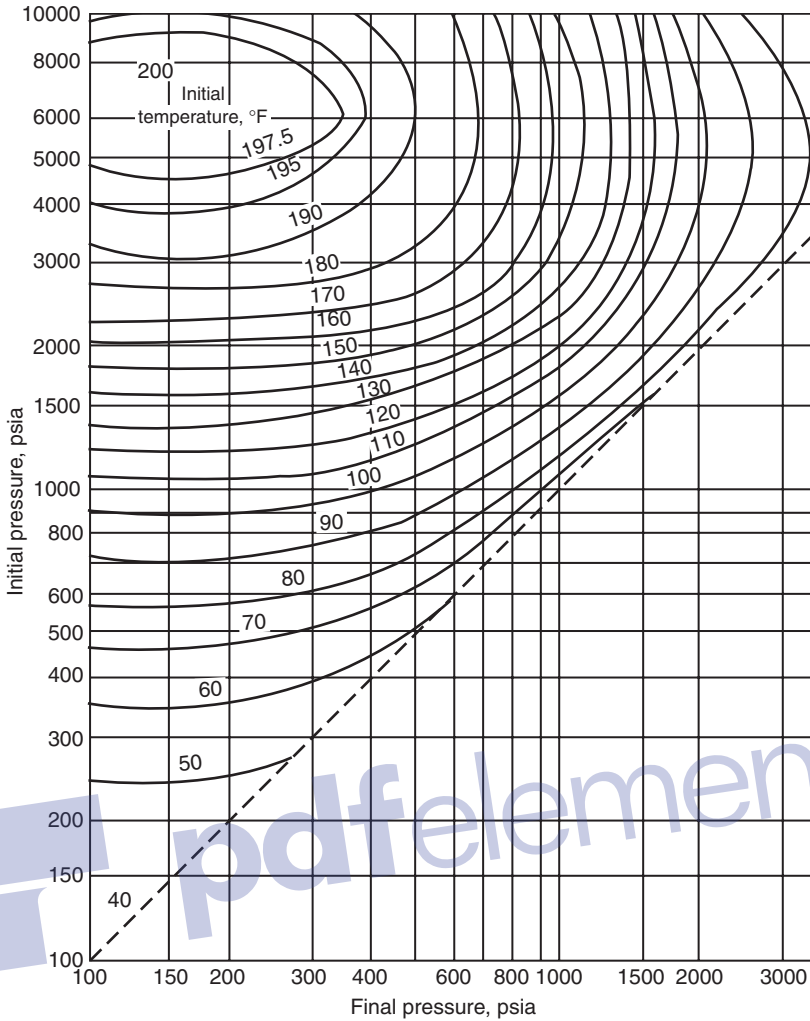
Figure 3.77 *Permissible expansion of a 0.8 gravity natural gas without hydrate formation (Courtesy Gas Processors Suppliers Association).*

Equation 3.6.5 can also be arranged and solved for the temperature, to give:

$$T = \frac{\ln(6.89476 p_h) - \frac{a_6}{(\gamma_h + a_7)^3} + a_8 F_m + a_9 F_m^2 + a_{10}}{\left[\frac{a_1}{(\gamma_h + a_2)^3} + a_3 F_m + a_4 F_m^2 + a_5\right]}$$

The authors pointed out that N_2 and CO_2 do not obey the general trend given for hydrocarbons in Equation 3.6.5. Therefore, to account for the pressure of N_2 and CO_2 in the hydrocarbon system, they treated each of these two non-hydrocarbon fractions separately and developed the following correction factors:

$$E_{CO_2} = 1.0 + \left[(b_1 F_m + b_2)\frac{y_{CO_2}}{1 - y_{N_2}}\right] \qquad [3.6.6]$$

$$E_{N_2} = 1.0 + \left[(b_3 F_m + b_4)\frac{y_{N_2}}{1 - \gamma_{CO_2}}\right] \qquad [3.6.7]$$

with:

$$b_1 = -2.0943 \times 10^{-4}\left(\frac{T}{1.8} - 273.15\right)^3 + 3.809 \times 10^{-3}$$
$$\times \left(\frac{T}{1.8} - 273.15\right)^2 - 2.42 \times 10^{-2}\left(\frac{T}{1.8} - 273.15\right)$$
$$+ 0.423 \qquad [3.6.8]$$

$$b_2 = 2.3498 \times 10^{-4}\left(\frac{T}{1.8} - 273.15\right)^2$$
$$- 2.086 \times 10^{-3}\left(\frac{T}{1.8} - 273.15\right)^2$$
$$+ 1.63 \times 10^{-2}\left(\frac{T}{1.8} - 273.15\right) + 0.650 \qquad [3.6.9]$$
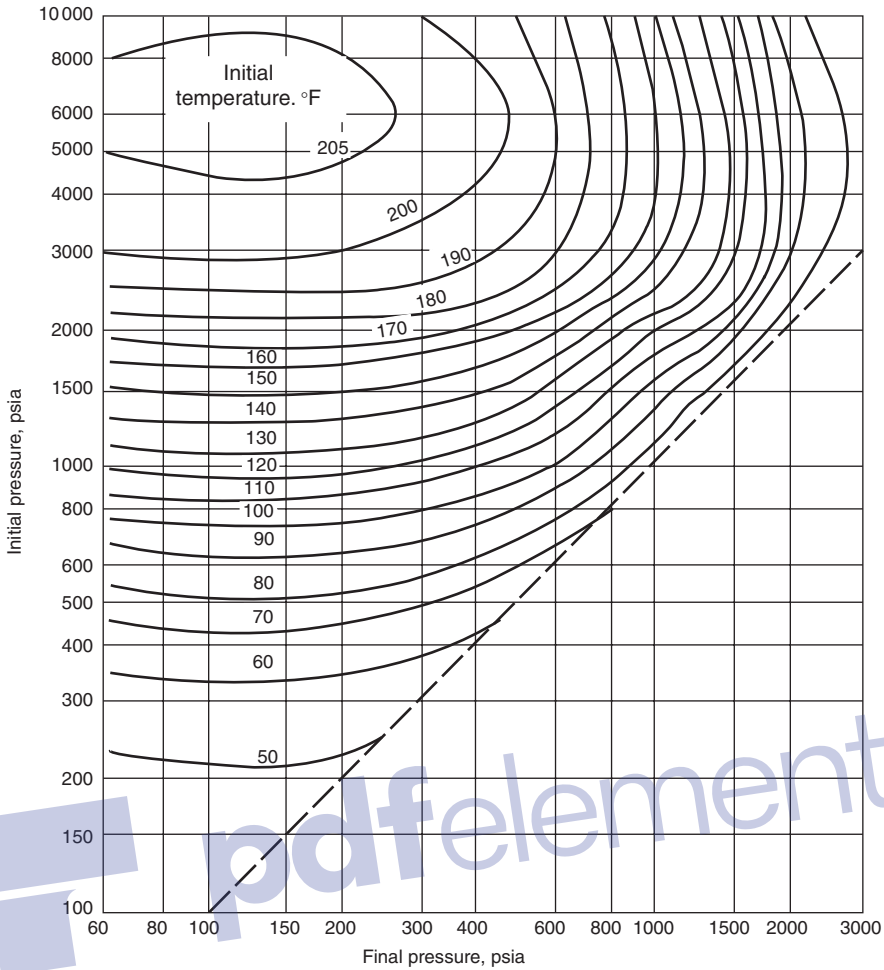
Figure 3.78 *Permissible expansion of a 0.9 gravity natural gas without hydrate formation (Courtesy Gas Processors Suppliers Association).*

$$b_3 = 1.1374 \times 10^{-4} \left(\frac{T}{1.8} - 273.15 \right)^3$$

$$+ 2.61 \times 10^{-4} \left(\frac{T}{1.8} - 273.15 \right)^2$$

$$+ 1.26 \times 10^{-2} \left(\frac{T}{1.8} - 273.15 \right) + 1.123 \qquad [3.6.10]$$

$$b_4 = 4.335 \times 10^{-5} \left(\frac{T}{1.8} - 273.15 \right)^3$$

$$- 7.7 \times 10^{-5} \left(\frac{T}{1.8} - 273.15 \right)^2$$

$$+ 4.0 \times 10^{-3} \left(\frac{T}{1.8} - 273.15 \right) + 1.048 \qquad [3.6.11]$$

where:

y_{N_2} = mole fraction of N_2
y_{CO_2} = mole fraction of CO_2
T = temperature, °R
F_m = molar ratio as defined by Equation 3.6.3

The total, i.e., corrected, hydrate dissociation pressure p_{corr} is given by:

$$p_{corr} = p_h E_{N_2} E_{CO_2} \qquad [3.6.12]$$

To demonstrate these correlations, Ostergaard and coworkers presented the following example:

Example 3.29 A gas condensate system has the following composition:

Component	y_{i_1} (%)	M_i
CO_2	2.38	44.01
N_2	0.58	28.01
C_1	73.95	16.04
C_2	7.51	30.07
C_3	4.08	44.10
i-C_4	0.61	58.12
n-C_4	1.58	58.12
i-C_5	0.50	72.15
n-C_5	0.74	72.15
C_6	0.89	84.00
C_{7+}	7.18	–

Calculate the hydrate dissociation pressure at 45°F, i.e., 505°R.
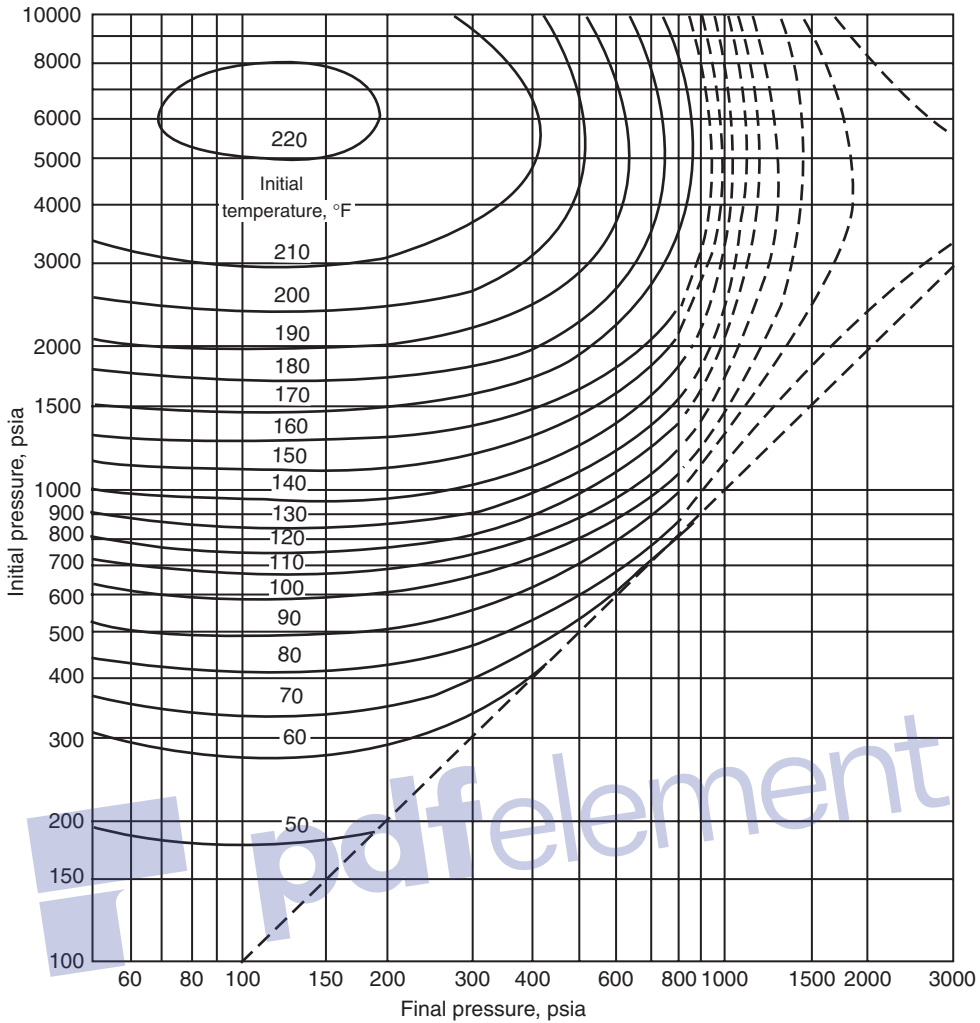
Figure 3.79 *Permissible expansion of a 1.0 gravity natural gas without hydrate formation (Courtesy Gas Processors Suppliers Association).*

Solution

Step 1. Calculate f_h and f_{nh} from Equations 3.6.1 and 3.6.2:

$$f_h = y_{C1} + y_{C2} + y_{C3} + y_{i-C4} + y_{n-C4}$$

$$= 73.95 + 7.51 + 4.08 + 0.61 + 1.58 = 87.73\%$$

$$f_{nh} = y_{C5+} = y_{i-C5} + y_{n-C5} + y_{C6} + y_{C7+}$$

$$= 0.5 + 0.74 + 0.89 + 7.18 = 9.31\%$$

Step 2. Calculate F_m by applying Equation 3.6.3:

$$F_m = \frac{f_{nh}}{f_h} = \frac{9.31}{87.73} = 0.1061$$

Step 3. Determine the specific gravity of the hydrate-forming components by normalizing their mole fractions as shown below:

Component	y_i	Normalized y_i^*	M_i	$M_i y_i^*$
C_1	0.7395	0.8429	16.04	13.520
C_2	0.0751	0.0856	30.07	2.574
C_3	0.0408	0.0465	44.10	2.051

Component	y_i	Normalized y_i^*	M_i	$M_i y_i^*$
i-C_4	0.0061	0.0070	58.12	0.407
n-C_4	0.0158	0.0180	58.12	1.046
	$\sum = 0.8773$	$\sum = 1.0000$		$\sum = 19.5980$

$$\gamma_h = \frac{19.598}{28.96} = 0.6766$$

Step 4. Using the temperature T and the calculated values of F_m and γ_h in Equation 3.6.5 gives:

$$p_h = 236.4 \text{ psia}$$

Step 5. Calculate the constants b_1 and b_2 for CO_2 by applying Equations 3.6.8 and 3.6.9 to give:

$$b_1 = -2.0943 \times 10^{-4} \left(\frac{505}{1.8} - 273.15 \right)^3$$

$$+ 3.809 \times 10^{-3} \left(\frac{505}{1.8} - 273.15 \right)^2 - 2.42 \times 10^{-2}$$

$$\times \left(\frac{505}{1.8} - 273.15 \right) + 0.423 = 0.368$$

$$b_2 = 2.3498 \times 10^{-4} \left(\frac{505}{1.8} - 273.15 \right)^2$$

$$- 2.086 \times 10^{-3} \left(\frac{505}{1.8} - 273.15 \right)^2 + 1.63 \times 10^{-2}$$

$$\times \left(\frac{505}{1.8} - 273.15 \right) + 0.650 = 0.752$$

Step 6. Calculate the CO_2 correction factor E_{CO_2} by using Equation 3.6.6:

$$E_{CO_2} = 1.0 + \left[(b_1 F_m + b_2) \frac{y_{CO_2}}{1 - y_{N_2}} \right]$$

$$= 1.0 + \left[(0.368 \times 0.1061 + 0.752) \frac{0.0238}{1 - 0.0058} \right]$$

$$= 1.019$$

Step 7. Correct for the presence of N_2, to give:

$$b_3 = 1.1374 \times 10^{-4} \left(\frac{505}{1.8} - 273.15 \right)^3$$

$$+ 2.61 \times 10^{-4} \left(\frac{505}{1.8} - 273.15 \right)^2 + 1.26 \times 10^{-2}$$

$$\times \left(\frac{505}{1.8} - 273.15 \right) + 1.123 = 1.277$$

$$b_4 = 4.335 \times 10^{-5} \left(\frac{505}{1.8} - 273.15 \right)^3$$

$$- 7.7 \times 10^{-5} \left(\frac{505}{1.8} - 273.15 \right)^2 + 4.0 \times 10^{-3}$$

$$\times \left(\frac{505}{1.8} - 273.15 \right) + 1.048 = 1.091$$

$$E_{N_2} = 1.0 + \left[(b_3 F_m + b_4) \frac{y_{N_2}}{1 - \gamma_{CO_2}} \right]$$

$$= 1.0 + \left[(1.277 \times 0.1061 + 1.091) \frac{0.0058}{1 - 0.00238} \right]$$

$$= 1.007$$

Step 8. Estimate the total (corrected) hydrate dissociation pressure by using Equation 3.6.12, to give:

$$p_{corr} = p_h E_{N_2} E_{CO_2}$$

$$= (236.4)(1.019)(1.007) = 243 \text{ psia}$$

Makogon (1981) developed an analytical relationship between hydrate and conditions in terms of pressure and temperature as a function of specific gravity of the gas. The expression is given by:

$$\log(p) = b + 0.0497(T + kT^2) \qquad [3.6.13]$$

where:

T = temperature, °C
p = pressure, atm

The coefficients b and k are expressed graphically as a function of the specific gravity of the gas, as shown in Figure 3.80.

Example 3.30   Find the pressure at which hydrate forms at $T = 40°F$ for a natural gas with a specific gravity of 0.631, using Equation 3.6.13.

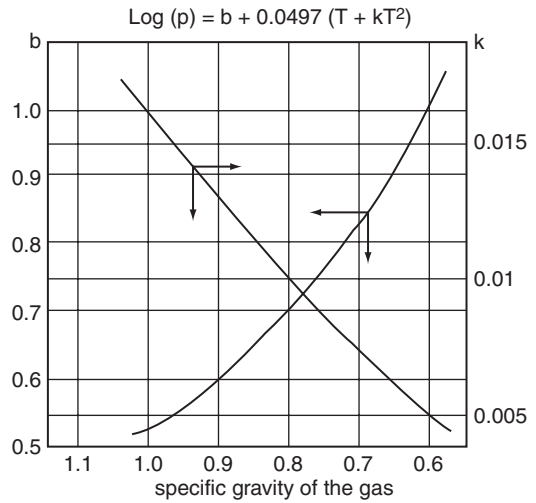**Figure 3.80**   Coefficients b and k of Equation 3.6.14.

Solution

Step 1. Convert the given temperature from °F to °C:
$$T = (40 - 32)/1.8 = 4.4°C$$

Step 2. Determine values of the coefficients b and k from Figure 3.80, to give:
$$b = 0.91$$
$$k = 0.006$$

Step 3. Solve for p by applying Equation 3.6.13
$$\log(p) = b + 0.0497(T + kT^2)$$

$$= 0.91 + 0.0497[4.4 + 0.006(4.4)^2]$$

$$= 1.1368$$

$$p = 10^{1.1368} = 13.70 \text{ atm} = 201 \text{ psia}$$

Figure 3.76 gives a value of 224 psia as compared with the above value of 201.

Carson and Katz (1942) adopted the concept of the equilibrium ratios, i.e., K values, for estimating hydrate-forming conditions. They proposed that hydrates are the equivalent of solid solutions and not mixed crystals, and therefore postulated that hydrate-forming conditions could be estimated from empirically determined vapor–solid equilibrium ratios as defined by:

$$K_{i(v-s)} = \frac{y_i}{x_{i(s)}} \qquad [3.6.14]$$

where:

$K_{i(v-s)}$ = equilibrium ratio of component i between vapor and solid
y_i = mole fraction of component i in the vapor (gas) phase
$x_{i(s)}$ = mole fraction of component i in the solid phase on a water-free basis

The calculation of the hydrate-forming conditions in terms of pressure or temperature is analogous to the dewpoint calculation of gas mixtures. In general, a gas in the presence of free water phase will form a hydrate when:

$$\sum_{i=1}^{n} \frac{y_i}{K_{i(v-s)}} = 1 \qquad [3.6.15]$$
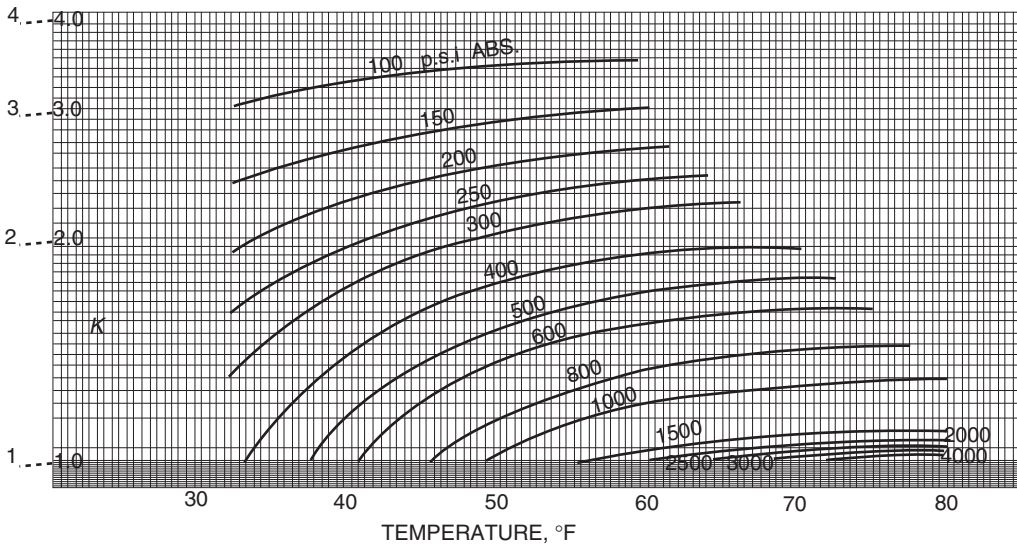
Figure 3.81   *Vapor–solid equilibrium constant for methane (Carson & Katz, 1942, courtesy SPE-AIME).*

Whitson and Brule (2000) pointed out that the vapor–solid equilibrium ratio cannot be used to perform flash calculations and determine hydrate-phase splits or equilibrium-phase compositions, since $K_{i(s)}$ is based on the mole fraction of a "guest" component in the solid-phase hydrate mixture on a water-free basis.

Carson and Katz developed K value charts for the hydrate-forming molecules that include methane through butanes, CO_2, and H_2S, as shown in Figures 3.81 through 3.87. It should be noted that $K_{i(s)}$ for non-hydrate formers are assumed to be infinity, i.e., $K_{i(s)} = \infty$.

The solution of Equation 3.6.15 for the hydrate-forming pressure or temperature is an iterative process. The process involves assuming several values of p or T and calculating the equilibrium ratios at each assumed value until the constraint represented by Equation 3.6.15 is met, i.e., summation is equal to 1.

Example 3.31   Using the equilibrium ratio approach, calculate the hydrate formation pressure p_h at 50°F for the following gas mixture:

Component	y_i
CO_2	0.002
N_2	0.094
C_1	0.784
C_2	0.060
C_3	0.036
i-C_4	0.005
n-C_4	0.019

The experimentally observed hydrate formation pressure is 325 psia at 50°F.

Solution

Step 1. For simplicity, assume two different pressures, 300 psia and 350 psia, and calculate the equilibrium ratios

at these pressures, to give:

Component	y_i	At 300 psia		At 350 psia	
		$K_{i(v-s)}$	$y_i/K_{i(v-s)}$	$K_{i(v-s)}$	$y_i/K_{i(v-s)}$
CO_2	0.002	3.0	0.0007	2.300	0.0008
N_2	0.094	∞	0	∞	0
C_1	0.784	2.04	0.3841	1.900	0.4126
C_2	0.060	0.79	0.0759	0.630	0.0952
C_3	0.036	0.113	0.3185	0.086	0.4186
i-C_4	0.005	0.0725	0.0689	0.058	0.0862
n-C_4	0.019	0.21	0.0900	0.210	0.0900
$\sum$	1.000		0.9381		1.1034

Step 2. Interpolating linearly at $\sum y_i/K_{i(v-s)} = 1$ gives:

$$\frac{350 - 300}{1.1035 - 0.9381} = \frac{p_h - 300}{1.0 - 0.9381}$$

Hydrate-forming pressure $p_h = 319$ psia, which compares favorably with the observed value of 325 psia.

Example 3.32   Calculate the temperature for hydrate formation at 435 psi for a gas with a 0.728 specific gravity with the following composition:

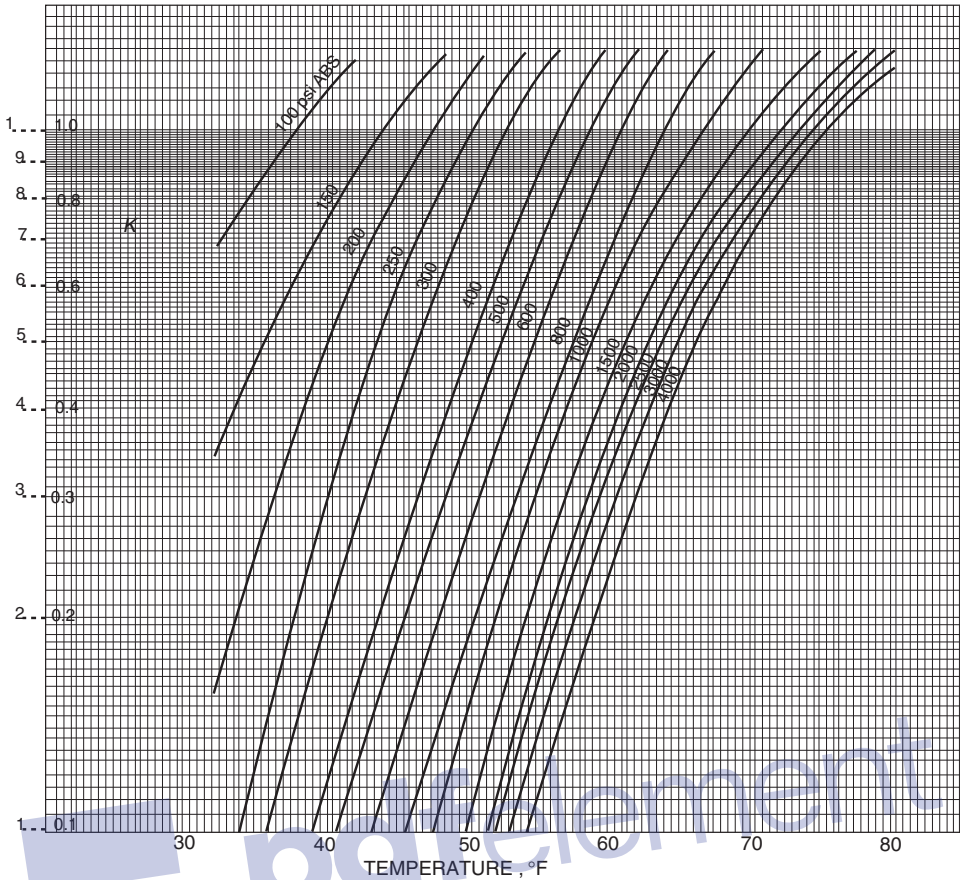| Component	y_i
CO_2	0.04
N_2	0.06
C_1	0.78
C_2	0.06
C_3	0.03
i-C_4	0.01
C_{5+}	0.02

Figure 3.82   *Vapor–solid equilibrium constant for ethane (Carson & Katz, 1942, courtesy SPE-AIME).*

Solution   The iterative procedure for estimating the hydrate-forming temperature is given in the following tabulated form:

Component	y_i	$T = 59°F$		$T = 50°F$		$T = 54°F$	
		$K_{i(v-s)}$	$y_i/K_{i(v-s)}$	$K_{i(v-s)}$	$y_i/K_{i(v-s)}$	$K_{i(v-s)}$	$y_i/K_{i(v-s)}$
CO_2	0.04	5.00	0.0008	1.700	0.0200	3.000	0.011
N_2	0.06	∞	0	∞	0	∞	0
C_1	0.78	1.80	0.4330	1.650	0.4730	1.740	0.448
C_2	0.06	1.30	0.0460	0.475	0.1260	0.740	0.081
C_3	0.03	0.27	0.1100	0.066	0.4540	0.120	0.250
i-C_4	0.01	0.08	0.1250	0.026	0.3840	0.047	0.213
C_{5+}	0.02	∞	0	∞	0	∞	0
Total	1.00				1.457		1.003

The temperature at which hydrate will form is approximately 54°F.

Sloan (1984) curve–fitted the Katz-Carson charts by the following expression:

$$\ln\left(K_{i(v-s)}\right) = A_0 + A_1 T + A_2 p + \frac{A_3}{T} + \frac{A_4}{p} + A_5 p T$$
$$+ A_6 T^2 + A_7 p^2 + A_8\left(\frac{p}{T}\right) + A_9 \ln\left(\frac{p}{T}\right)$$
$$+ \frac{A_{10}}{p^2} + A_{11}\left(\frac{T}{p}\right) + A_{12}\left(\frac{T^2}{p}\right) + A_{13}\left(\frac{p}{T^2}\right)$$
$$+ A_{14}\left(\frac{T}{p^3}\right) + A_{15} T^3 + A_{16}\left(\frac{p^3}{T^2}\right) + A_{17} T^4$$

where:

T = temperature, °F
p = pressure, psia

The coefficients A_0 through A_{17} are given in Table 3.2.

Example 3.33   Resolve Example 3.32 by using Equation 3.6.13.

Solution

Step 1. Convert the given pressure from psia to atm:
$$p = 435/14.7 = 29.6$$

Step 2. Determine the coefficients b and k from Figure 3.82 at the specific gravity of the gas, i.e., 0.728, to give:
$$b = 0.8$$
$$k = 0.0077$$

Step 3. Apply Equation 3.6.13, to give:
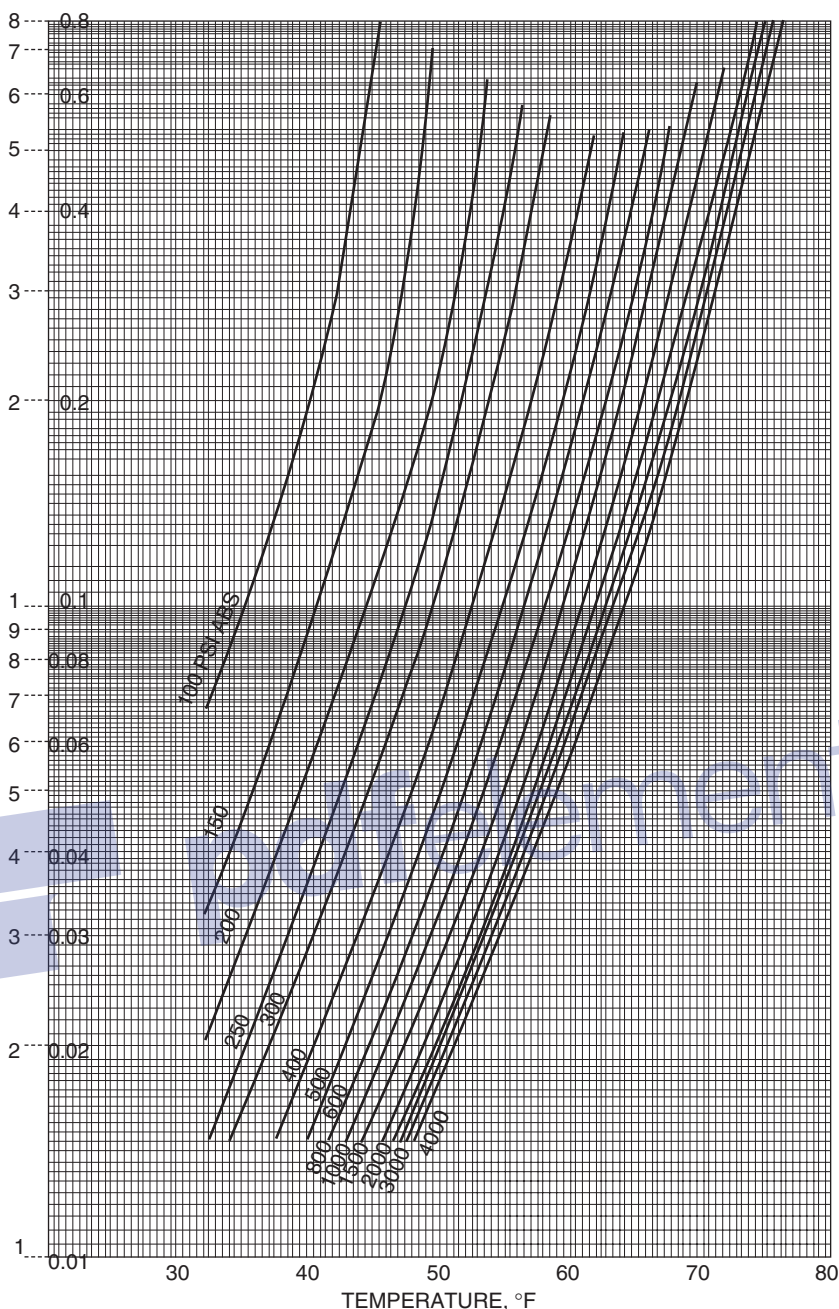$$\log(p) = b + 0.0497(T + kT^2)$$
$$\log(29.6) = 0.8 + 0.0497(T + 0.0077T^2)$$
$$0.000383T^2 + 0.0497T - 0.6713 = 0$$

Using the quadratic formula, gives:
$$T = \frac{-0.497 + \sqrt{(0.0497)^2 - (4)(0.000383)(-0.6713)}}{(2)(0.000383)}$$
$$= 12.33°C$$

Figure 3.83 *Vapor–solid equilibrium constant for propane (Carson & Katz, 1942, courtesy SPE-AIME).*

or:

$$T = (1.8)(12.33) + 32 = 54.2°F$$

3.6.2 Hydrates in subsurface

One explanation for hydrate formation is that the entrance of the gaseous molecules into vacant lattice cavities in the liquid water structure causes the water to solidify at temperatures above the freezing point of water. In general, ethane, propane, and butane raise the hydrate formation temperature for methane. For example, 1% of propane raises the hydrate-forming temperature from 41° to 49°F at 600 psia. Hydrogen sulfide and carbon dioxide are also relatively significant contributors in causing hydrates, whereas N_2 and C_{5+} have no noticeable effect. These solid ice-like mixtures of natural gas and water have been found in formations under deep water along the continental margins of America and beneath the permafrost (i.e., permanently frozen ground) in Arctic basins. The permafrost occurs where the mean atmospheric temperature is just under 32°F.

Muller (1947) suggested that lowering of the earth's temperature took place in early Pleistocene times, "perhaps a
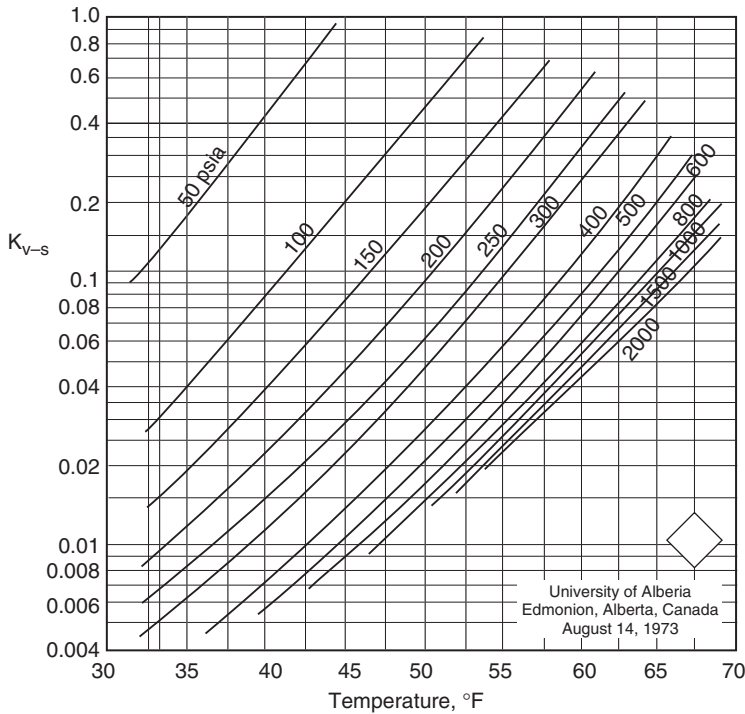
Figure 3.84   *Vapor–solid equilibrium constant for i-butane (Carson & Katz, 1942, courtesy SPE-AIME).*

million years ago." If formation natural gases were cooled under pressure in the presence of free water, hydrates would form in the cooling process before ice temperatures were reached. If further lowering of temperature brought the layer into a permafrost condition, then the hydrates would remain as such. In colder climates (such as Alaska, northern Canada, and Siberia) and beneath the oceans, conditions are appropriate for gas hydrate formation.

The essential condition for gas hydrate stability at a given depth is that the actual earth temperature at that depth is lower than the hydrate-forming temperature corresponding to the pressure and gas composition conditions. The thickness of a potential hydrate zone can be an important variable in drilling operations where drilling through hydrates requires special precautions. It can also be of significance in determining regions where hydrate occurrences might be sufficiently thick to justify gas recovery. The existence of a gas hydrate stability condition, however, *does not ensure that hydrates exist in that region*, but only that they can exist. In addition, if gas and water coexist within the hydrate stability zone, then they must exist in gas hydrate form.

Consider the earth temperature curve for the Cape Simpson area of Alaska, as shown in Figure 3.88. Pressure data from a drill stem test (DST) and a repeated formation test (RFT) indicates a pressure gradient of 0.435 psi/ft. Assuming a 0.6 gas gravity with its hydrate-forming pressure and temperature as given in Figure 3.74, this hydrate p–T curve can be converted into a depth versus temperature plot by dividing the pressures by 0.435, as shown by Katz (1971) in Figure 3.88. These two curves intersect at 2100 ft in depth. Katz pointed out that at Cape Simpson, we would expect to find water in the form of ice down to 900 ft and hydrates between 900 and 2100 ft of 0.6 gas gravity.

Using the temperature profile as a function of depth for the Prudhoe Bay Field as shown in Figure 3.89, Katz (1971)

estimated that the hydrate zone thickness at Prudhoe Bay for a 0.6 gravity gas might occur between 2000 and 4000 ft. Godbole et al. (1988) pointed out that the first confirmed evidence of the presence of gas hydrates in Alaska was obtained on March 15, 1972, when Arco and Exxon recovered gas hydrate core samples in pressurized core barrels at several depths between 1893 and 2546 ft from the Northwest Eileen well 2 in the Prudhoe Bay Field.

Studies by Holder et al. (1987) and Godbole et al. (1988) on the occurrence of in-situ natural-gas hydrates in the Arctic North Slope of Alaska and beneath the ocean floor suggest that the factors controlling the depth and thickness of natural-gas–hydrate zones in these regions and affecting their stabilities include:

- geothermal gradient;
- pressure gradient;
- gas composition;
- permafrost thickness;
- ocean-bottom temperature;
- mean average annual surface temperature;
- water salinity.

Various methods have been proposed for harvesting the gas in hydrate form that essentially require heat to melt the hydrate or lowering the pressure on the hydrate to release the gas. Specifically:

- steam injection;
- hot brine injection;
- fire-flood;
- chemicals injection;
- depressurizing.

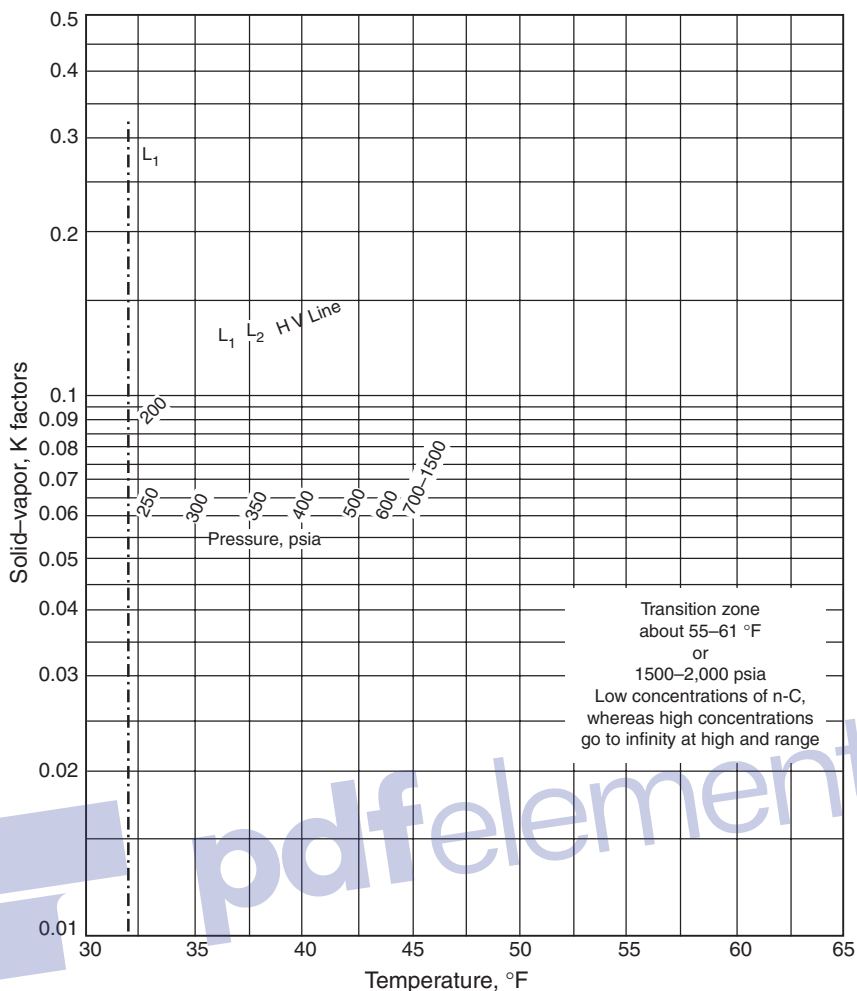Holder and Anger (1982) suggested that in the depressurizing scheme, pressure reduction causes destabilization

Figure 3.85   *Vapor–solid equilibrium constant for n-butane (Carson & Katz, 1942, courtesy SPE-AIME).*
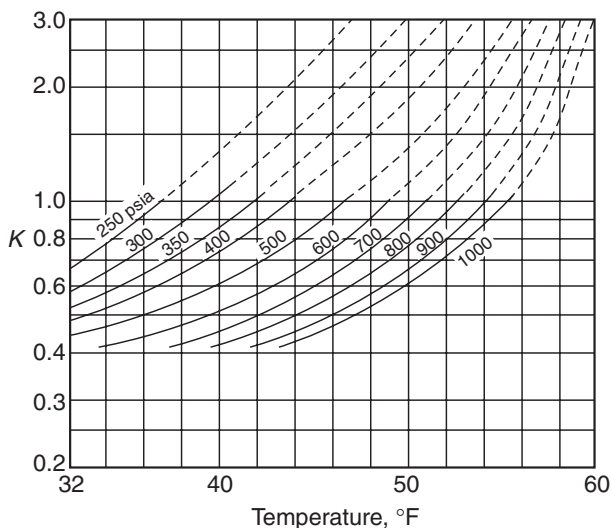

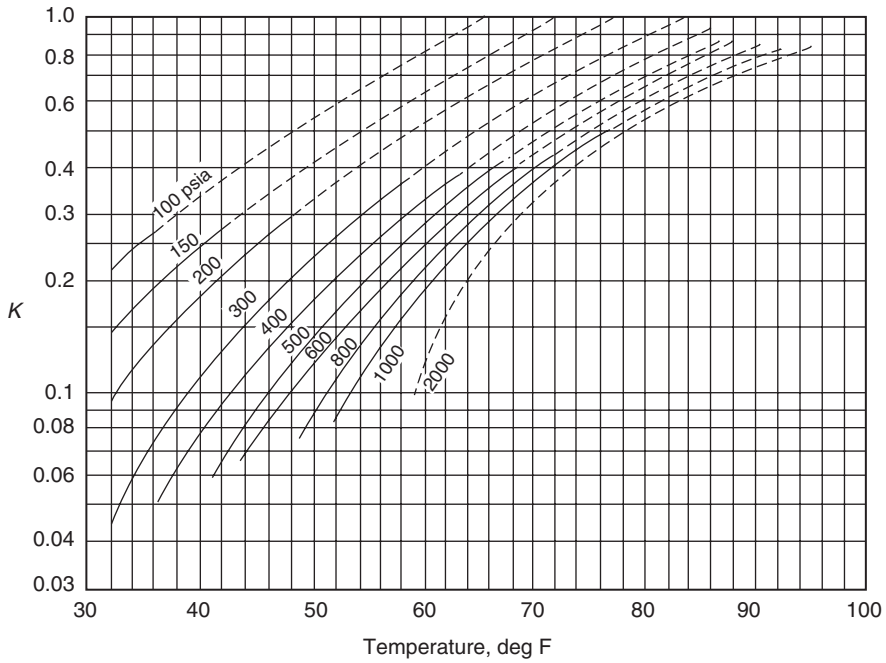**Figure 3.86**   *Vapor–solid equilibrium constant for CO_2 (Carson & Katz, 1942, courtesy SPE-AIME).*

Figure 3.87   Vapor–solid equilibrium constant for H_2S (Carson & Katz, 1942, courtesy SPE-AIME).

Table 3.2   Values of coefficients A_0 through A_{17} in Slolan's equation

Component	A_0	A_1	A_2	A_3	A_4	A_5
CH_4	1.63636	0.0	0.0	31.6621	−49.3534	5.31×10^{-6}
C_2H_6	6.41934	0.0	0.0	−290.283	2629.10	0.0
C_3H_8	−7.8499	0.0	0.0	47.056	0.0	-1.17×10^{-6}
$i\text{-}C_4H_{10}$	−2.17137	0.0	0.0	0.0	0.0	0.0
$n\text{-}C_4H_{10}$	−37.211	0.86564	0.0	732.20	0.0	0.0
N_2	1.78857	0.0	−0.001356	−6.187	0.0	0.0
CO_2	9.0242	0.0	0.0	−207.033	0.0	4.66×10^{-5}
H_2S	−4.7071	0.06192	0.0	82.627	0.0	-7.39×10^{-6}

	A_6	A_7	A_8	A_9	A_{10}	A_{11}
CH_4	0.0	0.0	0.128525	−0.78338	0.0	0.0
C_2H_6	0.0	9.0×10^{-8}	0.129759	−1.19703	-8.46×10^{4}	−71.0352
C_3H_8	7.145×10^{-4}	0.0	0.0	0.12348	1.669×10^{4}	0.0
$i\text{-}C_4H_{10}$	1.251×10^{-3}	1.0×10^{-8}	0.166097	−2.75945	0.0	0.0
$n\text{-}C_4H_{10}$	0.0	9.37×10^{-6}	−1.07657	0.0	0.0	−66.221
N_2	0.0	2.5×10^{-7}	0.0	0.0	0.0	0.0
CO_2	-6.992×10^{-3}	2.89×10^{-6}	-6.223×10^{-3}	0.0	0.0	0.0
H_2S	0.0	0.0	0.240869	−0.64405	0.0	0.0

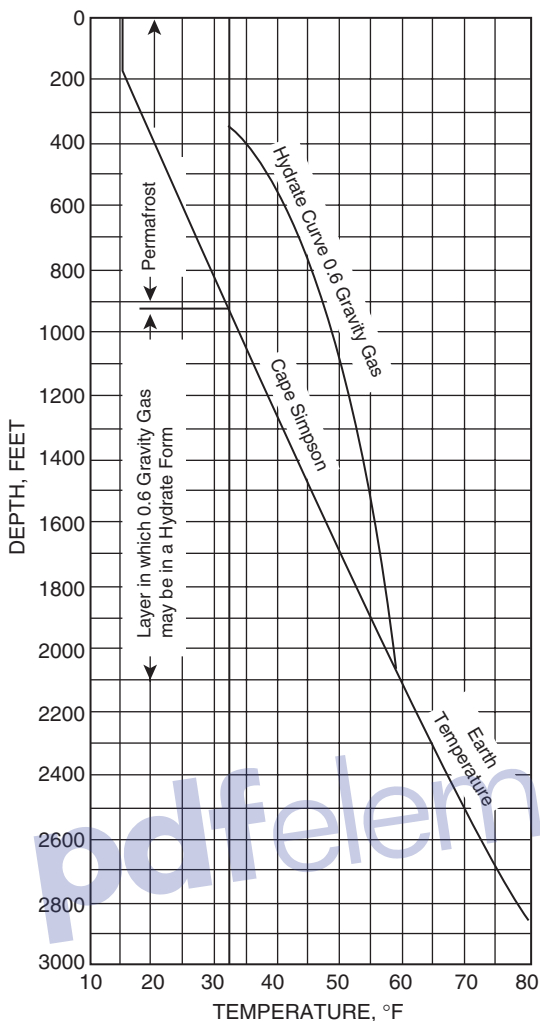|	A_{12}	A_{13}	A_{14}	A_{15}	A_{16}	A_{17}
CH_4	0.0	−5.3569	0.0	-2.3×10^{-7}	-2.0×10^{-8}	0.0
C_2H_6	0.596404	−4.7437	7.82×10^{4}	0.0	0.0	0.0
C_3H_8	0.23319	0.0	-4.48×10^{4}	5.5×10^{-6}	0.0	0.0
$i\text{-}C_4H_{10}$	0.0	0.0	-8.84×10^{2}	0.0	-5.7×10^{-7}	-1.0×10^{-8}
$n\text{-}C_4H_{10}$	0.0	0.0	9.17×10^{5}	0.0	4.98×10^{-6}	-1.26×10^{-6}
N_2	0.0	0.0	5.87×10^{5}	0.0	1.0×10^{-8}	1.1×10^{-7}
CO_2	0.27098	0.0	0.0	8.82×10^{-5}	2.55×10^{-6}	0.0
H_2S	0.0	−12.704	0.0	-1.3×10^{-6}	0.0	0.0

Figure 3.88 *Method for locating the thickness of hydrate layer (Permission to copy SPE, copyright SPE 1971).*
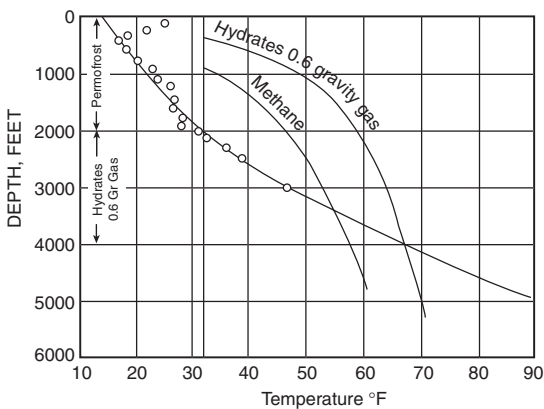

Figure 3.89 *Hydrate zone thickness for temperature gradient at Prudhoe Bay (Permission to copy SPE, copyright SPE 1971).*

of hydrates. As hydrates dissociate, they absorb heat from the surrounding formation. The hydrates continue to dissociate until they generate enough gas to raise the reservoir pressure to the equilibrium pressure of hydrates at a new temperature, which is lower than the original value. A temperature gradient is thus generated between the hydrates (sink) and surrounding media (source), and heat flows to the hydrates. The rate of dissociation of hydrates, however, is controlled by the rate of heat influx from the surrounding media or by the thermal conductivity of the surrounding rock matrix.

Many question need to be answered if gas is to be produced from hydrates. For example:

• The form in which hydrates exist in a reservoir should be known. Hydrates may exist in different types (all hydrates, excess water, and excess ice, in conjunction with free gas or oil) and in different forms (massive, laminated, dispersed, or nodular). Each case will have a different effect on the method of production and on the economics.

• The saturation of hydrates in the reservoir.
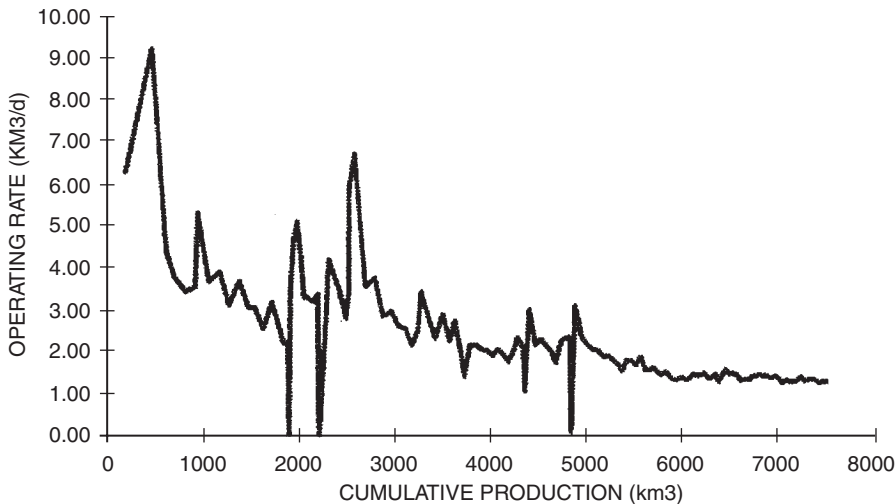
Figure 3.90   *Production history for a typical Medicine Hat property (Permission to copy SPE, copyright SPE 1995).*

- There could be several problems associated with gas production, such as pore blockage by ice and blockage of the wellbore resulting from re-formation of hydrates during flow of gas through the production well.
- Economics of the project is perhaps the most important impacting factor for the success of gas recovery from subsurface hydrate accumulations.

Despite the above concerns, subsurface hydrates exhibit several characteristics, especially compared with other unconventional gas resources, that increase their importance as potential energy resources and make their future recovery likely. These include a higher concentration of gas in hydrated form, enormously large deposits of hydrates, and their wide occurrence in the world.

3.7 Shallow Gas Reservoirs

Tight, shallow gas reservoirs present a number of unique challenges in determining reserves accurately. Traditional methods such as decline analysis and material balance are inaccurate due to the formation's low permeability and the usually poor-quality pressure data. The low permeabilities cause long transient periods that are not separated early from production decline with conventional decline analysis, resulting in lower confidence in selecting the appropriate decline characteristics which effect recovery factors and remaining reserves significantly. In an excellent paper, West and Cochrane (1994) used the Medicine Hat Field in western Canada as an example of these types of reservoirs and developed a methodology, called the extended material balance technique, to evaluate gas reserves and potential infill drilling.

The Medicine Hat Field is a tight, shallow gas reservoir producing from multiple highly interbedded, silty sand formations with poor permeabilities of less than 0.1 md. This poor permeability is the main characteristic of these reservoirs that affects conventional decline analysis. Due to these low permeabilities, and in part to commingled multilayer production effects, wells experience long transient periods before they begin experiencing pseudosteady-state flow that represents the decline portion of their lives. One of the principal assumptions often neglected when conducting decline analysis is that the pseudosteady state must have been achieved. The initial transient production trend of a

well or group of wells is not indicative of the long-term decline of the well. Distinguishing the transient production of a well from its pseudosteady-state production is often difficult, and this can lead to errors in determining the decline characteristic (exponential, hyperbolic, or harmonic) of the well. Figure 3.90 shows the production history from a tight, shallow gas well and illustrates the difficulty in selecting the correct decline. Another characteristic of tight, shallow gas reservoirs that affects conventional decline analysis is that constant reservoir conditions, an assumption required for conventional decline analysis, do not exist because of increasing drawdown, changing operating strategies, erratic development, and deregulation.

Material balance is affected by tight, shallow gas reservoirs because the pressure data is limited, of poor quality, and non-representative of a majority of the wells. Because the risk of drilling dry holes is low and drill stem tests (DSTs) are not cost-effective in the development of shallow gas, DST data is very limited. Reservoir pressures are recorded only for government-designated "control" wells, which account for only 5% of all wells. Shallow gas produces from multiple formations, and production from these formations is typically commingled, exhibiting some degree of pressure equalization. Unfortunately, the control wells are segregated by tubing/packers, and consequently the control-well pressure data is not representative of most commingled wells. In addition, pressure monitoring has been very inconsistent. Varied measurement points (downhole or wellhead), inconsistent shut-in times, and different analysis types (e.g., buildup and static gradient) make quantitative pressure tracking difficult. As Figure 3.91 shows, both these problems result in a scatter of data, which makes material balance extremely difficult.

Wells in the Medicine Hat shallow gas area are generally cased, perforated, and fractured in one, two, or all three formations as ownerships vary not only areally but between formations. The Milk River and Medicine Hat formations are usually produced commingled. Historically, the Second White Specks formation has been segregated from the other two; recently, however, commingled production from all three formations has been approved. Spacing for shallow gas is usually two to four wells per section.

As a result of the poor reservoir quality and low pressure, well productivity is very low. Initial rates rarely
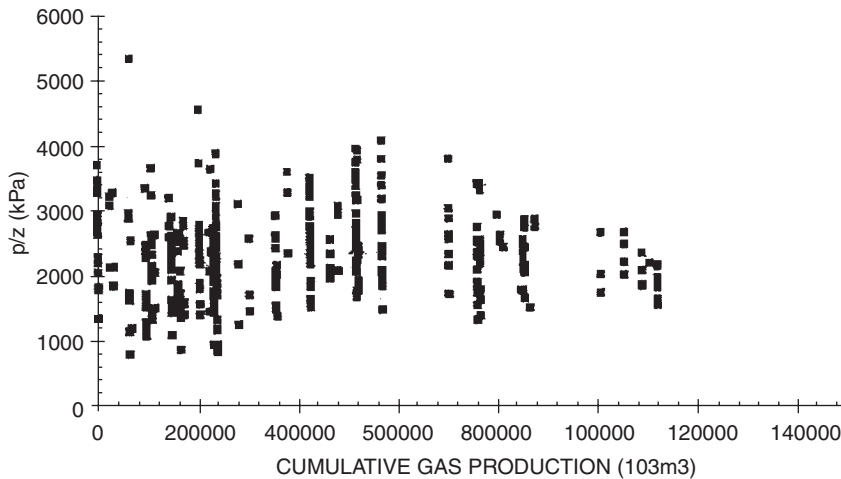
Figure 3.91 *Scatter pressure data for a typical Medicine Hat property (Permission to copy SPE, copyright SPE 1995).*

exceed 700 Mscf/day. Current average production per well is approximately 50 Mscf/day for a three-formation completion. There are approximately 24 000 wells producing from the Milk River formation in southern Alberta and Saskatchewan with total estimated gas reserves of 5.3 Tscf. West and Cochrane (1994) developed an iterative methodology, called extended material balance "EMB", to determine gas reserves in 2300 wells in the Medicine Hat Field.

The EMB technique is essentially an iterative process for obtaining a suitable p/Z vs. G_p line for a reservoir where pressure data is inadequate. It combines the principles of volumetric gas depletion with the gas deliverability equation. The deliverability equation for radial flow of gas describes the relationship between the pressure differential in the wellbore and the gas flow rate from the well:

$$Q_g = C[p_r^2 - p_{wf}^2]^n \qquad [3.7.1]$$

Due to the very low production rates from the wells in Medicine Hat shallow gas, a laminar flow regime exists which can be described with an exponent $n = 1$. The terms making up the coefficient C in Equation 3.7.1 are either fixed reservoir parameters (kh, r_e, r_w, and T) that do not vary with time or terms that fluctuate with pressure, temperature, and gas composition, i.e., μ_g and Z. The performance coefficient C is given by:

$$C = \frac{kh}{1422T\mu_g Z[\ln(r_e/r_w) - 0.5]} \qquad [3.7.2]$$

Because the original reservoir pressure in these shallow formations is low, the differences between initial and abandonment pressures are not significant and the variation in the pressure-dependent terms over time can be assumed negligible. C may be considered constant for a given Medicine Hat shallow gas reservoir over its life. With these simplifications for shallow gas, the deliverability equation becomes:

$$Q_g = C[p_r^2 - p_{wf}^2] \qquad [3.7.3]$$

The sum of the instantaneous production rates with time will yield the relationship between G_p and reservoir pressure, similar to the MBE. By use of this common relationship, with the unknowns being reservoir pressure p and the performance coefficient C, the EMB method involves iterating to find the correct p/Z vs. G_p relationship to give a constant C with time. The proposed iterative method is applied as outlined in the following steps:

Step 1. To avoid calculating individual reserves for each of the 2300 wells, West and Cochrane (1995) grouped

wells by formation and by date on production. The authors verified this simplification on a test group by ensuring that the reserves from the group of wells yielded the same results as the sum of the individual well reserves. These groupings were used for each of the 10 properties, and the results of the groupings combined to give a property production forecast. Also, to estimate the reservoir decline characteristics more accurately, the rates were normalized to reflect changes in the bottom-hole flowing pressure (BHFP).

Step 2. Using the gas specific gravity and reservoir temperature, calculate the gas deviation factor Z as a function of pressure and plot p/Z vs. p on a Cartesian scale.

Step 3. An initial estimate for the p/Z variation with G_p is made by guessing an initial pressure p_i, and a linear slope m of Equation 3.3.10:

$$\frac{p}{Z} = \frac{p_i}{Z_i} - [m]\,G_p$$

with the slope m as defined by:

$$m = \left(\frac{p_i}{Z_i}\right)\frac{1}{G}$$

Step 4. Starting at the initial production date for the property, the p/Z versus time relationship is established by simply substituting the actual cumulative production G_p into the MBE with estimated slope m and p_i because actual cumulative production G_p versus time is known. The *reservoir pressure p* can then be constructed as a function of time from the plot of p/Z as a function of p, i.e., step 2.

Step 5. Knowing the actual production rates, Q_g, and BHFPs p_{wf} for each monthly time interval, and having estimated reservoir pressures p from step 3, C is calculated for each time interval with Equation 3.7.3:

$$C = \frac{Q_g}{p^2 - p_{wf}^2}$$

Step 6. C is plotted versus time. If C is not constant (i.e., the plot is not a horizontal line), a new p/Z versus G_p is guessed and the process repeated from step 3 through step 5.

Step 7. Once a constant C solution is obtained, the representative p/Z relationship has been defined for reserves determination.
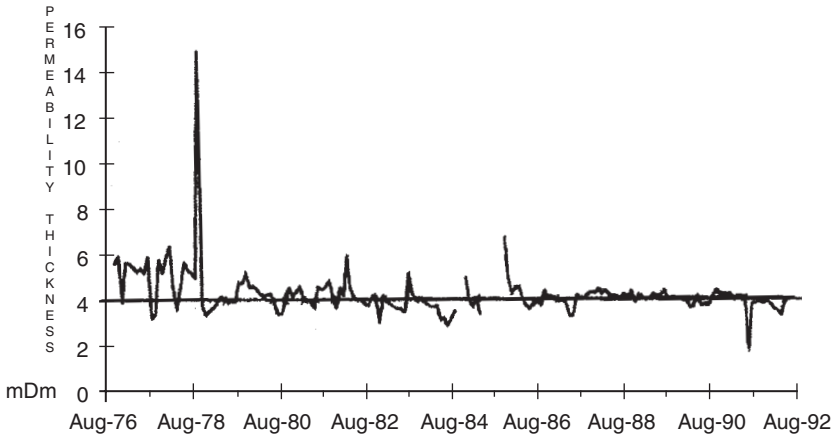
Figure 3.92 *Example of a successful EMB solution–flat kh profile (Permission to copy SPE, copyright SPE1995).*

Use of the EMB method in the Medicine Hat shallow gas makes the fundamental assumptions (1) that the gas pool depletes volumetrically (i.e., no water influx) and (2) that all wells behave like an average well with the same deliverability constant, turbulence constant, and BHFP, which is a reasonable assumption given the number of wells in the area, the homogeneity of the rocks, and the observed well production trends.

In the EMB evaluation, West and Cochrane pointed out that wells for each property were grouped according to producing interval so that the actual production from the wells could be related to a particular reservoir pressure trend. When calculating the coefficient C as outlined above, a total C based on grouped production was calculated and then divided by the number of wells producing in a given time interval to give an average C value. This average C value was used to calculate an average permeability/thickness, kh, for comparison with actual kh data obtained through buildup analysis for the reservoir from:

$$kh = 1422T\mu_g Z[\ln(r_e/r_w) - 0.5]C$$

For that reason kh versus time was plotted instead of C versus time in the method. Figure 3.92 shows a flat kh versus time profile indicating a valid p/Z vs. G_p relationship.

Problems

1. The following information is available on a volumetric gas reservoir:

    Initial reservoir temperature, $T_i = 155°F$

    Initial reservoir pressure, $p_i = 3500$ psia

    Specific gravity of gas, $\gamma_g = 0.65(\text{air} = 1)$

    Thickness of reservoir, $h = 20$ ft

    Porosity of the reservoir, $\phi = 10\%$

    Initial water saturation, $S_{wi} = 25\%$

    After producing 300 MMscf, the reservoir pressure declined to 2500 psia. Estimate the areal extent of this reservoir.

2. The following pressures and cumulative production data[a] is available for a natural-gas reservoir:

p (psia)	Z	G_p (MMMscf)
2080	0.759	0
1885	0.767	6.873
1620	0.787	14.002
1205	0.828	23.687
888	0.866	31.009
645	0.900	36.207

   (a) Estimate the initial gas-in-place.
   (b) Estimate the recoverable reserves at an abandonment pressure of 500 psia. Assume $z_a = 1.00$.
   (c) What is the recovery factor at the abandonment pressure of 500 psia?

3. A gas field with an active water drive showed a pressure decline from 3000 to 2000 psia over a 10 month period. From the following production data, match the past history and calculate the original hydrocarbon gas in the reservoir. Assume $z = 0.8$ in the range of reservoir pressures and $T = 140°F$.

Data[a]				
t, months	0	2.5	5.0	7.5	10.0
p, psia	3000	2750	2500	2250	2000
G_p, MMscf	0	97.6	218.9	355.4	500.0

4. A volumetric gas reservoir produced 600 MMscf of gas of 0.62 specific gravity when the reservoir pressure declined from 3600 to 2600 psi. The reservoir temperature is reported at 140°F. Calculate:

   (a) gas initially in place;
   (b) remaining reserves to an abandonment pressure of 500 psi;
   (c) ultimate gas recovery at abandonment.

[a]Chi Ikoku, *Natural Gas Reservoir Engineering*, John Wiley & Sons, 1984.

5. The following information on a water drive gas reservoir is given:

$$\text{Bulk volume} = 100\,000 \text{ acre-ft}$$
$$\text{Gas gravity} = 0.6$$
$$\text{Porosity} = 15\%$$
$$S_{wi} = 25\%$$
$$T = 140°F$$
$$p_i = 3500 \text{ psi}$$

Reservoir pressure has declined to 3000 psi while producing 30 MMMscf of gas and no water production. Calculate the cumulative water influx.

6. The pertinent data for the Mobil–David Field is given below:

$$G = 70 \text{ MMMscf}$$
$$p_i = 9507 \text{ psi}$$
$$f = 24\% \quad f S_{wi} = 35\%$$
$$c_w = 401 \times 10^{-6} \text{ psi}^{-1},$$
$$c_f = 3.4 \times 10^{-6} \text{ psi}^{-1},$$
$$\gamma_g = 0.74$$
$$T = 266°F$$

For this volumetric abnormally pressured reservoir, calculate and plot cumulative gas production as a function of pressure.

7. A gas well is producing under a constant bottom-hole flowing pressure of 1000 psi. The specific gravity of the produced gas is 0.65. Given:

$$p_i = 1500 \text{ psi}$$
$$r_w = 0.33 \text{ ft}$$
$$r_e = 1000 \text{ ft}$$
$$k = 20 \text{ md}$$
$$h = 20 \text{ ft}$$
$$T = 140°F$$
$$s = 0.40$$

calculate the gas flow rate by using:

(a) the real-gas pseudopressure approach;
(b) the pressure-squared approximation.

8. The following data[a] was obtained from a back-pressure test on a gas well:

Q_g (Mscf/day)	p_{wf} (psi)
0	481
4928	456
6479	444
8062	430
9640	415

(a) Calculate values of C and n.
(b) Determine the AOF.
(c) Generate the IPR curves at reservoir pressures of 481 and 300 psi.

[a]Chi Ikoku, *Natural Gas Reservoir Engineering*, John Wiley & Sons, 1984.

9. The following back-pressure test data is available:

Q_g (Mscf/day)	p_{wf} (psi)
0	5240
1000	4500
1350	4191
2000	3530
2500	2821

Given:

$$\text{gas gravity} = 0.78$$
$$\text{porosity} = 12\%$$
$$s_{wi} = 15\%$$
$$T = 281°F$$

(a) generate the current IPR curve by using:
  (i) the simplified back-pressure equation;
  (ii) the laminar–Inertial–turbulent (LIT) methods:

  - pressure-squared approach
  - pressure-approach
  - pseudo-pressure approach;

(b) repeat part (a) for a future reservoir pressure of 4000 psi.

10. A 3000 foot horizontal gas well is draining an area of approximately 180 acres, given:

$$p_i = 2500 \text{ psi}, \quad p_{wf} = 1500 \text{ psi}, \quad k = 25 \text{ md}$$
$$T = 120°F, \quad r_w = 0.25, \quad h = 20 \text{ ft}$$
$$\gamma_g = 0.65$$

Calculate the gas flow rate.

11. Given the sorption isotherm data below for a coal sample from the CBM field, calculate Langmuir's isotherm constant V_m and Langmuir's pressure constant b:

p (psi)	V, (scf/ton)
87.4	92.4
140.3	135.84
235.75	191.76
254.15	210
350.75	247.68
579.6	318.36
583.05	320.64
869.4	374.28
1151.15	407.4
1159.2	408.6

12. The following production data is available from a dry gas field:

q_t (MMscf/day)	G_p (MMscf)	q_t (MMscf/day)	G_p (MMscf)
384	19 200	249.6	364 800
403.2	38 400	236.4	422 400
364.8	57 600	220.8	441 600
370.8	115 200	211.2	460 800
326.4	192 000	220.8	480 000
297.6	288 000		

Estimate:

(a) the future cumulative gas production when gas flow rate reaches 100 MMscf/day;
(b) extra time to reach 100 MMscf/day.

13. A gas well has the following production history:

Date	Time (months)	q_t (MMscf/month)
1/1/2000	0	1017
2/1/2000	1	978
3/1/2000	2	941
4/1/2000	3	905
5/1/2000	4	874
6/1/2000	5	839
7/1/2000	6	809
8/1/2000	7	778
9/1/2000	8	747
10/1/2000	9	722
11/1/2000	10	691
12/1/2000	11	667
1/1/2001	12	641

    (a) Use the first six months of the production history data to determine the coefficient of the decline curve equation.

    (b) Predict flow rates and cumulative gas production from August 1, 2000 through January 1, 2001.

    (c) Assuming that the economic limit is 20 MMscf/month, estimate the time to reach the economic limit and the corresponding cumulative gas production.

14. The volumetric calculations on a gas well show that the ultimate recoverable reserves G_{pa} are 18 MMMscf of gas. By analogy with other wells in the area, the following data is assigned to the well:

Exponential decline

Allowable (restricted) production rate = 425 MMscf/month

Economic limit = 20 MMscf/month

Nominal decline rate = 0.034 month^{-1}

Calculate the yearly production performance of the well.

15. The following data is available on a gas well production:

$p_i = 4100$ psia, $p_{wf} = 400$ psi, $T = 600°R$

$h = 40$ ft, $\phi = 0.10$, $S_{wi} = 0.30$

$\gamma_g = 0.65$,

Time (days)	q_t (MMscf/day)
0.7874	5.146
6.324	2.108
12.71	1.6306
25.358	1.2958
50.778	1.054
101.556	0.8742
248	0.6634
496	0.49042
992	0.30566
1240	0.24924
1860	0.15996
3100	0.07874
6200	0.02232

Calculate the initial gas-in-place and the drainage area.

16. A gas of 0.7 specific gravity is at 800 psia. To what extent can the temperature be lowered without hydrate formation in the presence of free water?

17. A gas has a specific gravity of 0.75 and exists at 70°F. What would be the pressure above which hydrates could be expected to form?

18. How far can a 0.76 gravity gas at 1400 psia and 110°F be expanded without hydrate formation?

4

Performance of Oil Reservoirs

Contents

Each reservoir is composed of a unique combination of geometric form, geological rock properties, fluid characteristics, and primary drive mechanism. Although no two reservoirs are identical in all aspects, they can be grouped according to the primary recovery mechanism by which they produce. It has been observed that each drive mechanism has certain typical performance characteristics in terms of:

- ultimate recovery factor;
- pressure decline rate;
- gas–oil ratio;
- water production.

The recovery of oil by any of the natural drive mechanisms is called "primary recovery." The term refers to the production of hydrocarbons from a reservoir without the use of any process (such as fluid injection) to supplement the natural energy of the reservoir.

The two main objectives of this chapter are:

(1) To introduce and give a detailed discussion of the various primary recovery mechanisms and their effects on the overall performance of oil reservoirs.
(2) To provide the basic principles of the material balance equation and other governing relationships that can be used to predict the volumetric performance of oil reservoirs.

4.1 Primary Recovery Mechanisms

For a proper understanding of reservoir behavior and predicting future performance, it is necessary to have knowledge of the driving mechanisms that control the behavior of fluids within reservoirs.

The overall performance of oil reservoirs is largely determined by the nature of the energy, i.e., driving mechanism, available for moving the oil to the wellbore. There are basically six driving mechanisms that provide the natural energy necessary for oil recovery:

(1) rock and liquid expansion drive;
(2) depletion drive;
(3) gas cap drive;
(4) water drive;
(5) gravity drainage drive;
(6) combination drive.

These six driving mechanisms are presented below.

4.1.1 Rock and liquid expansion

When an oil reservoir initially exists at a pressure higher than its bubble point pressure, the reservoir is called an "undersaturated oil reservoir." At pressures above the bubble point pressure, crude oil, connate water, and rock are the only materials present. As the reservoir pressure declines, the rock and fluids expand due to their individual compressibilities. The reservoir rock compressibility is the result of two factors:

(1) expansion of the individual rock grains, and
(2) formation compaction.

Both of these factors are the results of a decrease of fluid pressure within the pore spaces, and both tend to reduce the pore volume through the reduction of the porosity.

As the expansion of the fluids and reduction in the pore volume occur with decreasing reservoir pressure, the crude oil and water will be forced out of the pore space to the wellbore. Because liquids and rocks are only slightly compressible, the reservoir will experience a rapid pressure decline. The oil reservoir under this driving mechanism is characterized by a constant gas–oil ratio that is equal to the gas solubility at the bubble point pressure.

This driving mechanism is considered the least efficient driving force and usually results in the recovery of only a small percentage of the total oil-in-place.

4.1.2 Depletion drive mechanism

This driving form may also be referred to by the following various terms:

- solution gas drive;
- dissolved gas drive;
- internal gas drive.

In this type of reservoir, the principal source of energy is a result of gas liberation from the crude oil and the subsequent expansion of the solution gas as the reservoir pressure is reduced. As pressure falls below the bubble point pressure, gas bubbles are liberated within the microscopic pore spaces. These bubbles expand and force the crude oil out of the pore space as shown conceptually in Figure 4.1.

Cole (1969) suggests that a depletion drive reservoir can be identified by the following characteristics:

Pressure behavior: The reservoir pressure declines rapidly and continuously. This reservoir pressure behavior is attributed to the fact that no extraneous fluids or gas caps are available to provide a replacement of the gas and oil withdrawals.

Water production: The absence of a water drive means there will be little or no water production with the oil during the entire producing life of the reservoir.

A depletion drive reservoir is characterized by a rapidly increasing gas–oil ratio from all wells, regardless of their structural position. After the reservoir pressure has been reduced below the bubble point pressure, gas evolves from solution throughout the reservoir. Once the gas saturation exceeds the critical gas saturation, free gas begins to flow toward the wellbore and the gas–oil ratio increases. The gas will also begin a vertical movement
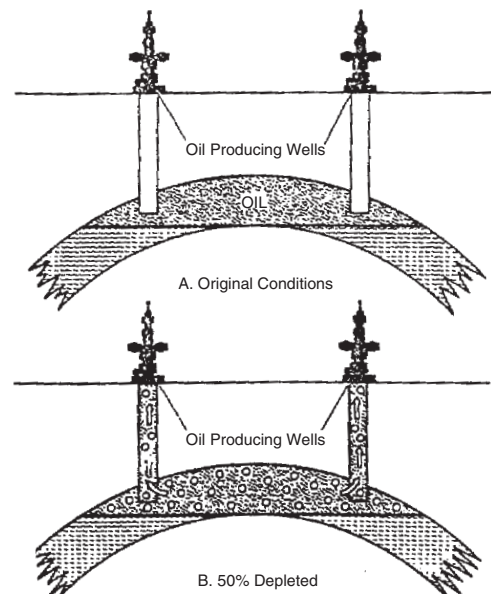
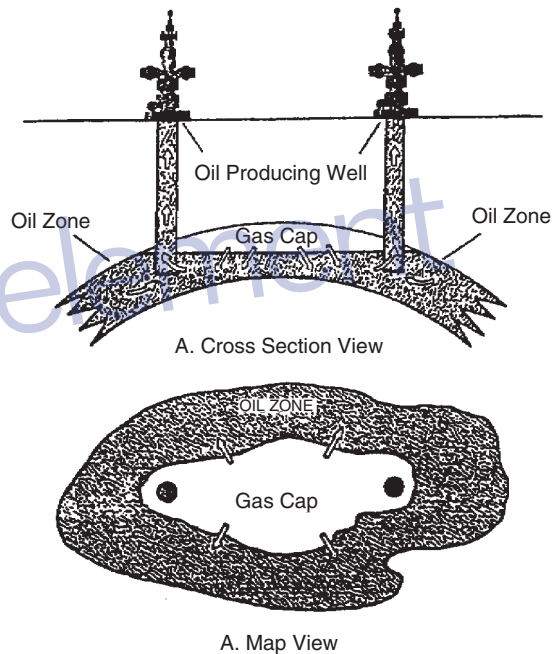**Figure 4.1** *Solution gas drive reservoir. (After Clark, N.J., Elements of Petroleum Reservoirs, SPE, 1969).*
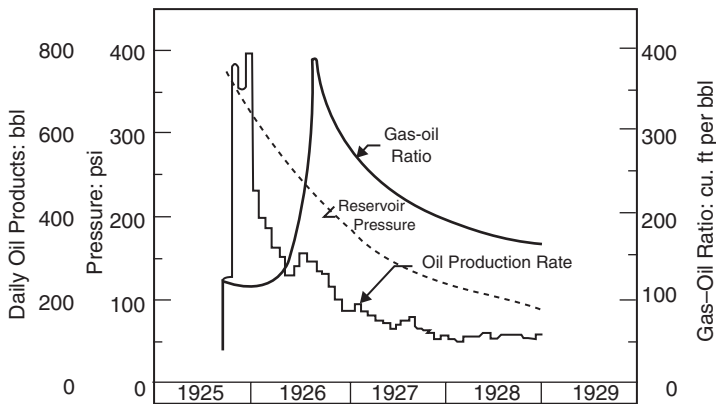
Figure 4.2 *Production data for a solution gas drive reservoir. (After Clark, N.J., Elements of Petroleum Reservoirs, SPE, 1969).*

due to gravitational forces, which may result in the formation of a secondary gas cap. Vertical permeability is an important factor in the formation of a secondary gas cap. *Unique oil recovery:* Oil production by depletion drive is usually the least efficient recovery method. This is a direct result of the formation of gas saturation throughout the reservoir. Ultimate oil recovery from depletion drive reservoirs may vary from less than 5% to about 30%. The low recovery from this type of reservoir suggests that large quantities of oil remain in the reservoir and, therefore, depletion drive reservoirs are considered the best candidates for secondary recovery applications.

The above characteristic trends occurring during the production life of depletion drive reservoirs are shown in Figure 4.2 and summarized below:

Characteristics	Trend
Reservoir pressure	Declines rapidly and continuously
Gas–oil ratio	Increases to maximum and then declines
Water production	None
Well behavior	Requires pumping at early stage
Oil recovery	5% to 30%

4.1.3 Gas cap drive

Gas cap drive reservoirs can be identified by the presence of a gas cap with little or no water drive as shown in Figure 4.3. Due to the ability of the gas cap to expand, these reservoirs are characterized by a slow decline in the reservoir pressure. The natural energy available to produce the crude oil comes from the following two sources:

(1) expansion of the gas cap gas, and
(2) expansion of the solution gas as it is liberated.

Cole (1969) and Clark (1969) presented a comprehensive review of the characteristic trends associated with gas cap drive reservoirs. These characteristic trends are summarized below:

Reservoir pressure: The reservoir pressure falls slowly and continuously. Pressure tends to be maintained at a higher level than in a depletion drive reservoir. The degree of pressure maintenance depends upon the volume of gas in the gas cap compared to the oil volume.

Figure 4.3 *Gas cap drive reservoir (After Clark, N.J., Elements of Petroleum Reservoirs, SPE, 1969).*

Water production: Absent or negligible water production.
Gas–oil ratio: The gas–oil ratio rises continuously in upstructure wells. As the expanding gas cap reaches the producing intervals of upstructure wells, the gas–oil ratio from the affected wells will increase to high values.
Ultimate oil recovery: Oil recovery by gas cap expansion is actually a frontal drive displacing mechanism which, therefore, yields considerably larger recovery efficiency than that of depletion drive reservoirs. This larger recovery efficiency is also attributed to the fact that no gas saturation is being formed throughout the reservoir at the same time. Figure 4.4 shows the relative positions of the gas–oil contact at different times in the producing life of the reservoir. The expected oil recovery ranges from 20% to 40%.
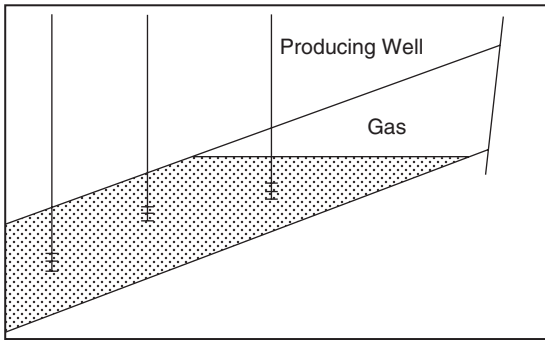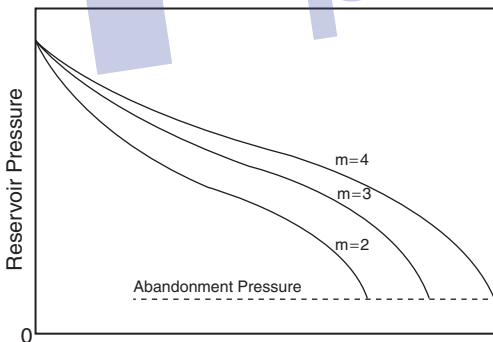
A. Initial fluid distribution
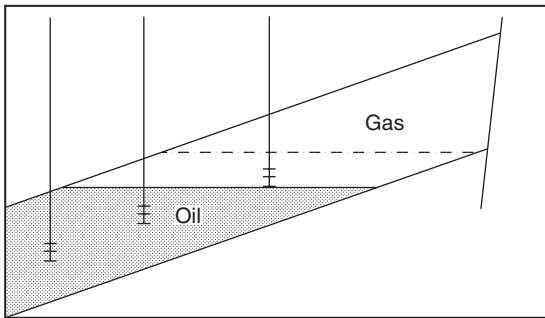
B. Gas cap expansion due to oil production

Figure 4.4 *Gas cap drive reservoir (After Cole, F., Reservoir Engineering Manual, Gulf Publishing Company, 1969).*

Figure 4.5 *Effect of gas cap size on ultimate oil recovery (After Cole, F., Reservoir Engineering Manual, Gulf Publishing Company, 1969).*

The ultimate oil recovery from a gas cap drive reservoir will vary depending largely on the following six important parameters:

(1) Size of the original gas cap: As shown graphically in Figure 4.5, the ultimate oil recovery increases with increasing size of the gas cap.
(2) Vertical permeability: Good vertical permeability will permit the oil to move downward with less bypassing of gas.
(3) Oil viscosity: As the oil viscosity increases, the amount of gas bypassing will also increase, which leads to a lower oil recovery.

(4) Degree of conservation of the gas: In order to conserve gas, and thereby increase ultimate oil recovery, it is necessary to shut in the wells that produce excessive gas.
(5) Oil production rate: As the reservoir pressure declines with production, solution gas evolves from the crude oil and the gas saturation increases continuously. If the gas saturation exceeds the critical gas saturation, the evolved gas begins to flow in the oil zone. As a result of creating a mobile gas phase in the oil zone, the following two events will occur: (1) the effective permeability to oil will be decreased as a result of the increased gas saturation; and (2) the effective permeability to gas will be increased, thereby increasing the flow of gas.

The formation of the free gas saturation in the oil zone cannot be prevented without resorting to pressure maintenance operations. Therefore, in order to achieve maximum benefit from a gas cap drive-producing mechanism, gas saturation in the oil zone must be kept to an absolute minimum. This can be accomplished by taking advantage of gravitational segregation of the fluids. In fact, an efficiently operated gas cap drive reservoir must also have an efficient gravity segregation drive. As the gas saturation is formed in the oil zone it must be allowed to migrate upstructure to the gas cap. Thus, a gas cap drive reservoir is in reality a combination-driving reservoir, although it is not usually considered as such.

Lower producing rates will permit the maximum amount of free gas in the oil zone to migrate to the gas cap. Therefore gas cap drive reservoirs are rate sensitive, as lower producing rates will usually result in increased recovery.

(6) Dip angle: The size of the gas cap determines the overall field oil recovery. When the gas cap is considered the main driving mechanism, its size is a measure of the reservoir energy available to produce the crude oil system. Such recovery normally will be 20% to 40% of the original oil-in-place, but if some other features are present to assist, such as steep angle of dip which allows good oil drainage to the bottom of the structure, considerably higher recoveries (up to 60% or greater) may be obtained. Conversely, extremely thin oil columns (where early breakthrough of the advancing gas cap occurs in producing wells) may limit oil recovery to lower figures regardless of the size of the gas cap. Figure 4.6 shows typical production and pressure data for a gas cap drive reservoir.

Well behavior: Because of the effects of gas cap expansion on maintaining reservoir pressure and the effect of decreased liquid column weight as it is produced out the well, gas cap drive reservoirs tend to flow longer than depletion drive reservoirs.

4.1.4 Water drive mechanism

Many reservoirs are bounded on a portion or all of their peripheries by water-bearing rocks called aquifers. The aquifers may be so large compared to the reservoir they adjoin as to appear infinite for all practical purposes, and they may range down to those so small as to be negligible in their effects on the reservoir performance.

The aquifer itself may be entirely bounded by impermeable rock so that the reservoir and aquifer together form a closed (volumetric) unit. On the other hand, the reservoir may outcrop at one or more places where it may be replenished by surface water as shown schematically in Figure 4.7.
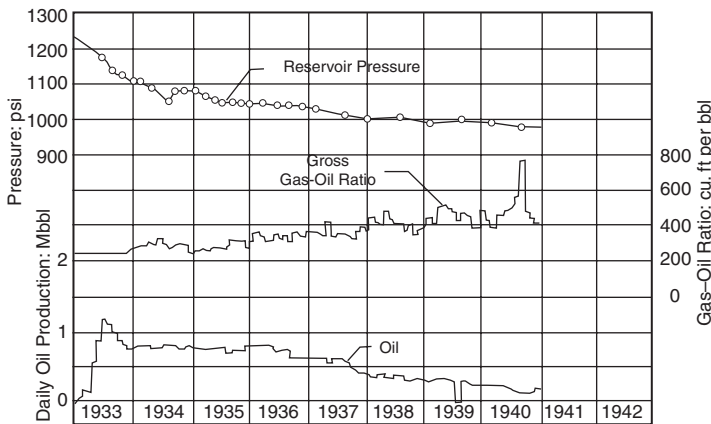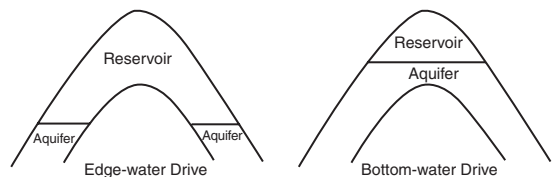
Figure 4.6 *Production data for a gas cap drive reservoir (After Clark, N.J., Elements of Petroleum Reservoirs, SPE, 1969. Courtesy of API).*
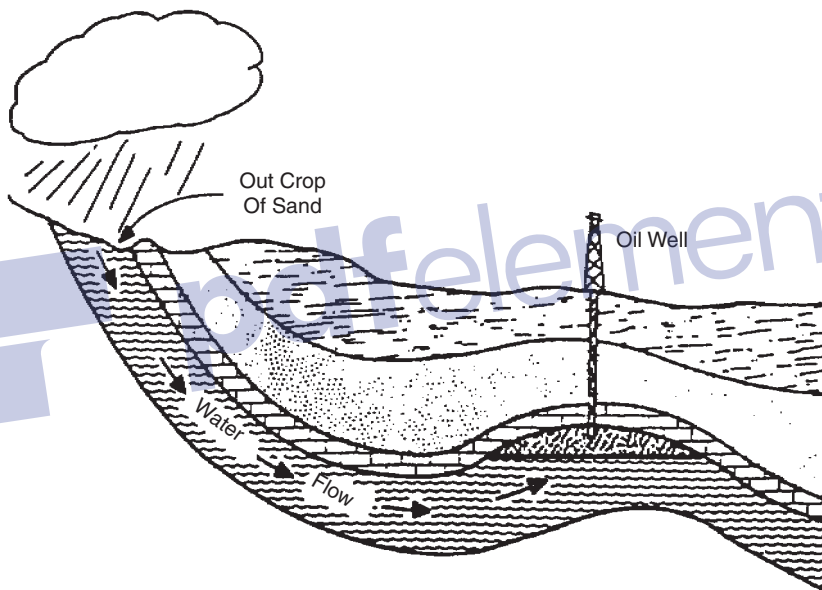
Figure 4.7 *Reservoir having artesian water drive (After Clark, N.J., Elements of Petroleum Reservoirs, SPE, 1969).*

It is common to speak of edge water or bottom water in discussing water influx into a reservoir. Bottom water occurs directly beneath the oil and edge water occurs off the flanks of the structure at the edge of the oil as illustrated in Figure 4.8. Regardless of the source of water, the water drive is the result of water moving into the pore spaces originally occupied by oil, replacing the oil and displacing it to the producing wells.

Cole (1969) presented the following discussion on the characteristics that can be used for identification of the water-driving mechanism.

Reservoir pressure
The decline in the reservoir pressure is usually very gradual. Figure 4.9 shows the pressure–production history of a typical water drive reservoir. It is not uncommon for many thousands of barrels of oil to be produced for each pound per

Figure 4.8 *Aquifer geometries.*

square inch drop in reservoir pressure. The reason for the small decline in reservoir pressure is that oil and gas withdrawals from the reservoir are replaced almost volume for volume by water encroaching into the oil zone. Several large oil reservoirs in the Gulf Coast areas of the United States
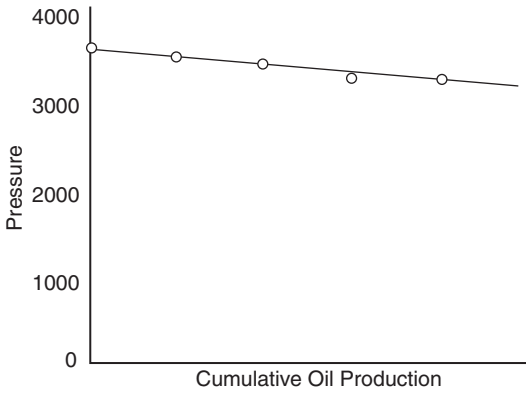
Figure 4.9 *Pressure–production history for a water drive reservoir.*

have such active water drives that the reservoir pressure has declined by only about 1 psi per million barrels of oil produced. Although pressure history is normally plotted versus cumulative oil production, it should be understood that total reservoir fluid withdrawals are the really important criteria in the maintenance of reservoir pressure. In a water drive reservoir, only a certain number of barrels of water can move into the reservoir as a result of a unit pressure drop within the reservoir. Since the principal income production is from oil, if the withdrawals of water and gas can be minimized, then the withdrawal of oil from the reservoir can be maximized with minimum pressure decline. Therefore, it is extremely important to reduce water and gas production to an absolute minimum. This can usually be accomplished by shutting in wells that are producing large quantities of these fluids, and where possible transferring their allowable oil production to other wells producing with lower water–oil or gas–oil ratios.

Water production
Early excess water production occurs in structurally low wells. This is characteristic of a water drive reservoir, and provided the water is encroaching in a uniform manner, nothing can or should be done to restrict this encroachment, as the water will probably provide the most efficient displacing mechanism possible. If the reservoir has one or more lenses of very high permeability, then the water may be moving through this more permeable zone. In this case, it may be economically feasible to perform remedial operations to shut off this permeable zone producing water. It should be realized that in most cases the oil which is being recovered from a structurally low well will be recovered from wells located higher on the structure and any expenses involved in remedial work to reduce the water–oil ratio of structurally low wells may be needless expenditure.

Gas–oil ratio
There is normally little change in the producing gas–oil ratio during the life of the reservoir. This is especially true if the reservoir does not have an initial free gas cap. Pressure will be maintained as a result of water encroachment and therefore there will be relatively little gas released from solution.

Ultimate oil recovery
Ultimate recovery from water drive reservoirs is usually much larger than recovery under any other producing mechanism. Recovery is dependent upon the efficiency of

the flushing action of the water as it displaces the oil. In general, as the reservoir heterogeneity increases, the recovery will decrease, due to the uneven advance of the displacing water. The rate of water advance is normally faster in zones of high permeability. This results in earlier high water–oil ratios and consequent earlier economic limits. Where the reservoir is more or less homogeneous, the advancing waterfront will be more uniform, and when the economic limit, due primarily to high water–oil ratios, has been reached, a greater portion of the reservoir will have been contacted by the advancing water.

Ultimate oil recovery is also affected by the degree of activity of the water drive. In a very active water drive where the degree of pressure maintenance is good, the role of solution gas in the recovery process is reduced to almost zero, with maximum advantage being taken of the water as a displacing force. This should result in maximum oil recovery from the reservoir. The ultimate oil recovery normally ranges from 35% to 75% of the original oil-in-place. The characteristic trends of a water drive reservoir are shown graphically in Figure 4.10 and summarized below:

Characteristics	Trend
Reservoir pressure	Remains high
Surface gas–oil ratio	Remains low
Water production	Starts early and increases to appreciable amounts
Well behavior	Flow until water production gets excessive
Expected oil recovery	35% to 75%

4.1.5 Gravity drainage drive
The mechanism of gravity drainage occurs in petroleum reservoirs as a result of differences in densities of the reservoir fluids. The effects of gravitational forces can be simply illustrated by placing a quantity of crude oil and a quantity of water in a jar and agitating the contents. After agitation, the jar is placed at rest, and the more dense fluid (normally water) will settle to the bottom of the jar, while the less dense fluid (normally oil) will rest on top of the denser fluid. The fluids have separated as a result of the gravitational forces acting on them.

The fluids in petroleum reservoirs have all been subjected to the forces of gravity, as evidenced by the relative positions of the fluids, i.e., gas on top, oil underlying the gas, and water underlying oil. The relative positions of the reservoir fluids are shown in Figure 4.11. Due to the long periods of time involved in the petroleum accumulation and migration process, it is generally assumed that the reservoir fluids are in equilibrium. If the reservoir fluids are in equilibrium then the gas–oil and oil–water contacts should be essentially horizontal. Although it is difficult to determine precisely the reservoir fluid contacts, the best available data indicates that, in most reservoirs, the fluid contacts actually are essentially horizontal.

Gravity segregation of fluids is probably present to some degree in all petroleum reservoirs, but it may contribute substantially to oil production in some reservoirs.

Cole (1969) stated that reservoirs operating largely under a gravity drainage producing mechanism are characterized by the following.

Reservoir pressure
Variable rates of pressure decline depend principally upon the amount of gas conservation. Strictly speaking, where the gas is conserved, and reservoir pressure is maintained, the reservoir would be operating under combined gas cap drive
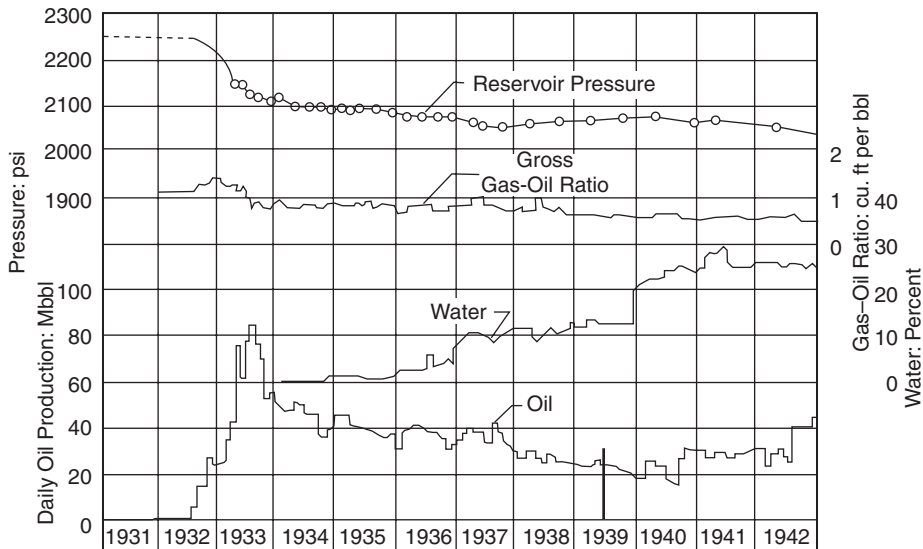
Figure 4.10 *Production data for a water drive reservoir (After Clark, N.J., Elements of Petroleum Reservoirs, SPE, 1969. Courtesy of API).*
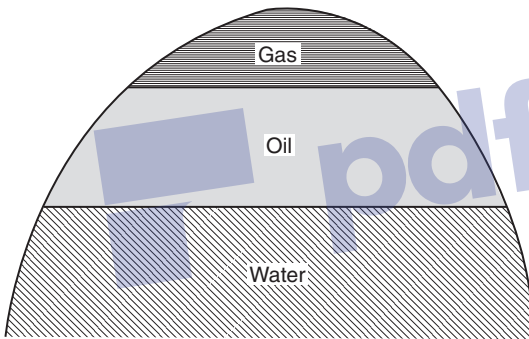
Figure 4.11 *Initial fluids distribution in an oil reservoir.*

and gravity drainage mechanisms. Therefore, for the reservoir to be operating solely as a result of gravity drainage, the reservoir would show a rapid pressure decline. This would require the upstructure migration of the evolved gas where it later was produced from structurally high wells, resulting in rapid loss of pressure.

Gas–oil ratio
These types of reservoirs typically show low gas–oil ratios from structurally located low wells. This is caused by migration of the evolved gas upstructure due to gravitational segregation of the fluids. On the other hand, the structurally high wells will experience an increasing gas–oil ratio as a result of the upstructure migration of the gas released from the crude oil.

Secondary gas cap
A secondary gas cap can be found in reservoirs that initially were undersaturated. Obviously the gravity drainage mechanism does not become operative until the reservoir pressure has declined below the saturation pressure, since above the saturation pressure there will be no free gas in the reservoir.

Water production
Gravity drainage reservoirs have little or no water production. Water production is essentially indicative of a water drive reservoir.

Ultimate oil recovery
Ultimate recovery from gravity drainage reservoirs will vary widely, due primarily to the extent of depletion by gravity drainage alone. Where gravity drainage is good, or where producing rates are restricted to take maximum advantage of the gravitational forces, recovery will be high. There are reported cases where recovery from gravity drainage reservoirs has exceeded 80% of the initial oil-in-place. In other reservoirs where depletion drive also plays an important role in the oil recovery process, the ultimate recovery will be less.

In operating gravity drainage reservoirs, it is essential that the oil saturation in the vicinity of the wellbore must be maintained as high as possible. There are two obvious reasons for this requirement:

(1) high oil saturation means a higher oil flow rate;
(2) high oil saturation means a lower gas flow rate.

If the liberated solution gas is allowed to flow upstructure instead of toward the wellbore, then high oil saturation in the vicinity of the wellbore can be maintained.

In order to take maximum advantage of the gravity drainage producing mechanism, wells should be located as low as structurally possible. This will result in maximum conservation of the reservoir gas. A typical gravity drainage reservoir is shown in Figure 4.12.

As discussed by Cole (1969), there are five factors that affect ultimate recovery from gravity drainage reservoirs:

(1) Permeability in the direction of dip: Good permeability, particularly in the vertical direction and in the direction of migration of the oil, is a prerequisite for efficient gravity drainage. For example, a reservoir with little structural relief which also contained many more or less continuous shale "breaks" could probably not be operated under gravity drainage because the oil could not flow to the base of the structure.
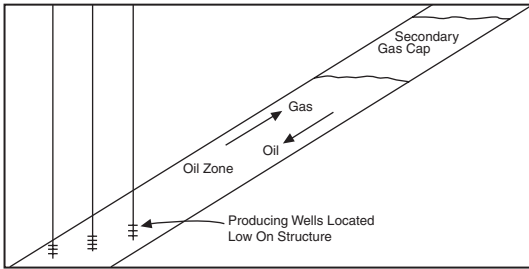
Figure 4.12 *Gravity drainage reservoir (After Cole, F., Reservoir Engineering Manual, Gulf Publishing Company, 1969).*

(2) Dip of the reservoir: In most reservoirs, the permeability in the direction of dip is considerably larger than the permeability transverse to the direction of dip. Therefore, as the dip of the reservoir increases, the oil and gas can flow along the direction of dip (which is also the direction of greatest permeability) and still achieve their desired structural position.

(3) Reservoir producing rates: Since the gravity drainage rate is limited, the reservoir producing rates should be limited to the gravity drainage rate, and then maximum recovery will result. If the reservoir producing rate exceeds the gravity drainage rate the depletion drive producing mechanism will become more significant with a consequent reduction in ultimate oil recovery.

(4) Oil viscosity: Oil viscosity is important because the gravity drainage rate is dependent upon the viscosity of the oil. In the fluid flow equations, as the viscosity decreases the flow rate increases. Therefore, the gravity drainage rate will increase as the reservoir oil viscosity decreases.

(5) Relative permeability characteristics: For an efficient gravity drive mechanism to be operative, the gas must flow upstructure while the oil flows downstructure. Although this situation involves counterflow of the oil and gas, both fluids are flowing and therefore relative permeability characteristics of the formation are very important.

4.1.6 Combination drive mechanism

The driving mechanism most commonly encountered is one in which both water and free gas are available in some degree to displace the oil toward the producing wells. The most common type of drive encountered, therefore, is a combination drive mechanism as illustrated in Figure 4.13.

Two combinations of driving forces are usually present in combination drive reservoirs:

(1) depletion drive and a weak water drive, or
(2) depletion drive with a small gas cap and a weak water drive.

In addition, gravity segregation can also play an important role in any of these two drives. In general, combination drive reservoirs can be recognized by the occurrence of a combination of some of the following factors.

Reservoir pressure

These types of reservoirs usually experience a relatively rapid pressure decline. Water encroachment and/or external gas cap expansion are insufficient to maintain reservoir pressures.
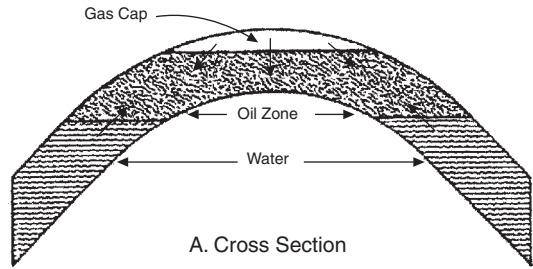
A. Cross Section
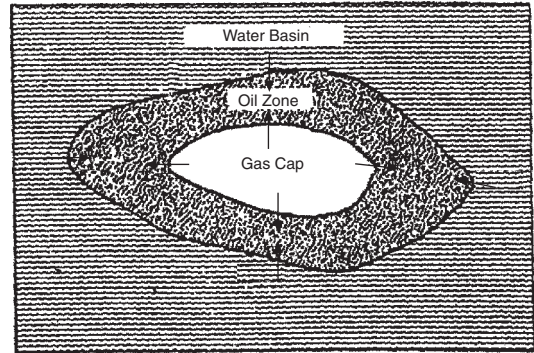
B. Map View

Figure 4.13 *Combination-drive reservoir (After Clark, N.J., Elements of Petroleum Reservoirs, SPE, 1969).*

Water production

The producing wells that are structurally located near the initial oil–water contact will slowly exhibit increasing water producing rates due to the increase in the water encroachment from the associated aquifer.

Gas–oil ratio

If a small gas cap is present the structurally high wells will exhibit continually increasing gas–oil ratios, provided the gas cap is expanding. It is possible that the gas cap will shrink due to production of excess free gas, in which case the structurally high wells will exhibit a decreasing gas–oil ratio. This condition should be avoided whenever possible, as large volumes of oil can be lost as a result of a shrinking gas cap.

Ultimate oil recovery

As a substantial percentage of the total oil recovery may be due to the depletion drive mechanism, the gas–oil ratio of structurally low wells will also continue to increase, due to evolution of solution gas from the crude oil throughout the reservoir as pressure is reduced. Ultimate recovery from combination drive reservoirs is usually greater than recovery from depletion drive reservoirs but less than recovery from water drive or gas cap drive reservoirs. Actual recovery will depend upon the degree to which it is possible to reduce the magnitude of recovery by depletion drive. In most combination drive reservoirs it will be economically feasible to institute some type of pressure maintenance operation, either gas injection or water injection, or both gas and water injection, depending upon the availability of the fluids.

4.2 The Material Balance Equation

The material balance equation (MBE) has long been recognized as one of the basic tools of reservoir engineers

for interpreting and predicting reservoir performance. The MBE, when properly applied, can be used to:

- estimate initial hydrocarbon volumes in place;
- predict reservoir pressure;
- calculate water influx;
- predict future reservoir performance;
- predict ultimate hydrocarbon recovery under various types of primary drive mechanisms.

Although in some cases it is possible to solve the MBE simultaneously for the initial hydrocarbon volumes, i.e., oil and gas volumes, and the water influx, generally one or the other must be known from other data or methods that do not depend on the material balance calculations. The accuracy of the calculated values depends on the reliability of the available data and if the reservoir characteristics meet the assumptions that are associated with the development of the MBE. The equation is structured to simply keep inventory of all materials entering, leaving, and accumulating in the reservoir.

The concept the MBE was presented by Schilthuis in 1936 and is simply based on the principle of the volumetric balance. It states that the cumulative withdrawal of reservoir fluids is equal to the combined effects of fluid expansion, pore volume compaction, and water influx. In its simplest form, the equation can be written on a volumetric basis as:

Initial volume = volume remaining + volume removed

Since oil, gas, and water are present in petroleum reservoirs, the MBE can be expressed for the total fluids or for any one of the fluids present. Three different forms of the MBE are presented below in details. These are:

(1) generalized MBE;
(2) MBE as an equation of a straight line;
(3) Tracy's form of the MBE.

4.3 Generalized MBE

The MBE is designed to treat the reservoir as a *single tank* or region that is characterized by homogeneous rock properties and described by an average pressure, i.e., no pressure variation throughout the reservoir, at any particular time or stage of production. Therefore, the MBE is commonly referred to as a tank model or zero-dimensional (0-D) model. These assumptions are of course unrealistic since reservoirs are generally considered heterogeneous with considerable variation in pressures throughout the reservoir. However, it is shown that the tank-type model accurately predict the behavior of the reservoir in most cases if accurate average pressures and production data are available.

4.3.1 Basic assumptions in the MBE

The MBE keeps an inventory on all material entering, leaving, or accumulating within a region over discrete periods of time during the production history. The calculation is most vulnerable to many of its underlying assumptions early in the depletion sequence when fluid movements are limited and pressure changes are small. Uneven depletion and partial reservoir development compound the accuracy problem.

The basic assumptions in the MBE are as follows:

Constant temperature

Pressure–volume changes in the reservoir are assumed to occur without any temperature changes. If any temperature changes occur, they are usually sufficiently small to be ignored without significant error.

Reservoir characteristics

The reservoir has uniform porosity, permeability, and thickness characteristics. In addition, the shifting in the gas–oil contact or oil–water contact is uniform throughout the reservoir.

Fluid recovery

The fluid recovery is considered independent of the rate, number of wells, or location of the wells. The *time* element is not explicitly expressed in the material balance when applied to predict future reservoir performance.

Pressure equilibrium

All parts of the reservoir have the same pressure and fluid properties are therefore constant throughout. Minor variations in the vicinity of the wellbores may usually be ignored. Substantial pressure variation across the reservoir may cause excessive calculation error.

It is assumed that the *PVT* samples or data sets represent the actual fluid compositions and that reliable and representative laboratory procedures have been used. Notably, the vast majority of material balances assume that differential depletion data represents reservoir flow and that separator flash data may be used to correct for the wellbore transition to surface conditions. Such "black-oil" *PVT* treatments relate volume changes to temperature and pressure only. They lose validity in cases of volatile oil or gas condensate reservoirs where compositions are also important. Special laboratory procedures may be used to improve *PVT* data for volatile fluid situations.

Constant reservoir volume

Reservoir volume is assumed to be constant except for those conditions of rock and water expansion or water influx that are specifically considered in the equation. The formation is considered to be sufficiently competent that no significant volume change will occur through movement or reworking of the formation due to overburden pressure as the internal reservoir pressure is reduced. The constant-volume assumption also relates to an area of interest to which the equation is applied.

Reliable production data

All production data should be recorded with respect to the same time period. If possible, gas cap and solution gas production records should be maintained separately.

Gas and oil gravity measurements should be recorded in conjunction with the fluid volume data. Some reservoirs require a more detailed analysis and the material balance to be solved for volumetric segments. The produced fluid gravities will aid in the selection of the volumetric segments and also in the averaging of fluid properties. There are essentially three types of production data that must be recorded in order to use the MBE in performing reliable reservoir calculations. These are:

(1) Oil production data, even for properties not of interest, can usually be obtained from various sources and is usually fairly reliable.
(2) Gas production data is becoming more available and reliable as the market value of this commodity increases; unfortunately, this data will often be more questionable where gas is flared.
(3) The water production term need represent only the net withdrawals of water; therefore, where subsurface disposal of produced brine is to the same source formation, most of the error due to poor data will be eliminated.

Developing the MBE

Before deriving the material balance, it is convenient to denote certain terms by symbols for brevity. The symbols used conform where possible to the standard nomenclature adopted by the Society of Petroleum Engineers.

p_i	Initial reservoir pressure, psi
p	Volumetric average reservoir pressure
Δp	Change in reservoir pressure $= p_i - p$, psi
p_b	Bubble point pressure, psi
N	Initial (original) oil-in-place, STB
N_p	Cumulative oil produced, STB
G_p	Cumulative gas produced, scf
W_p	Cumulative water produced
R_p	Cumulative gas–oil ratio, scf/STB
GOR	Instantaneous gas–oil ratio, scf/STB
R_{si}	Initial gas solubility, scf/STB
R_s	Gas solubility, scf/STB
B_{oi}	Initial oil formation volume factor, bbl/STB
B_o	Oil formation volume factor, bbl/STB
B_{gi}	Initial gas formation volume factor, bbl/scf
B_g	Gas formation volume factor, bbl/scf
W_{ing}	Cumulative water injected, STB
G_{inj}	Cumulative gas injected, scf
W_e	Cumulative water influx, bbl
m	Ratio of initial gas cap gas reservoir volume to initial reservoir oil volume, bbl/bbl
G	Initial gas cap gas, scf
PV	Pore volume, bbl
c_w	Water compressibility, psi^{-1}
c_f	Formation (rock) compressibility, psi^{-1}

Several of the material balance calculations require the total pore volume (PV) as expressed in terms of the initial oil volume N and the volume of the gas cap. The expression for the total PV can be derived by conveniently introducing the parameter m into the relationship as follows.

Define the ratio m as:

$$m = \frac{\text{initial volume of gas cap in bbl}}{\text{volume of oil initially in place in bbl}} = \frac{GB_{gi}}{NB_{oi}}$$

Solving for the volume of the gas cap gives:

Initial volume of the gas cap, $GB_{gi} = mNB_{oi}$, bbl

The total initial volume of the hydrocarbon system is then given by:

Initial oil volume + initial gas cap volume $= (PV)(1 - S_{wi})$

$$NB_{oi} + mNB_{oi} = (PV)(1 - S_{wi})$$

Solving for PV gives:

$$PV = \frac{NB_{oi}(1 + m)}{1 - S_{wi}} \qquad [4.3.1]$$

where:

S_{wi} = initial water saturation
N = initial oil-in-place, STB
PV = total pore volume, bbl
m = ratio of initial gas cap gas reservoir volume to initial reservoir oil volume, bbl/bbl

Treating the reservoir PV as an idealized container as illustrated in Figure 4.14, volumetric balance expressions can be derived to account for all volumetric changes which occur during the natural productive life of the reservoir. The MBE can be written in a generalized form as follows:

PV occupied by the oil initially in place at p_i

  $+$ PV occupied by the gas in the gas cap at p_i

  $=$ PV occupied by the remaining oil at p

    $+$ PV occupied by the gas in the gas cap at p

    $+$ PV occupied by the evolved solution gas at p

    $+$ PV occupied by the net water influx at p

    $+$ change in PV due to connate water expansion and

    $+$ pore volume reduction due to rock expansion

    $+$ PV occupied by the injected gas at p

    $+$ PV occupied by the injected water at p [4.3.2]

The above nine terms composing the MBE can be determined separately from the hydrocarbon *PVT* and rock properties, as follows.
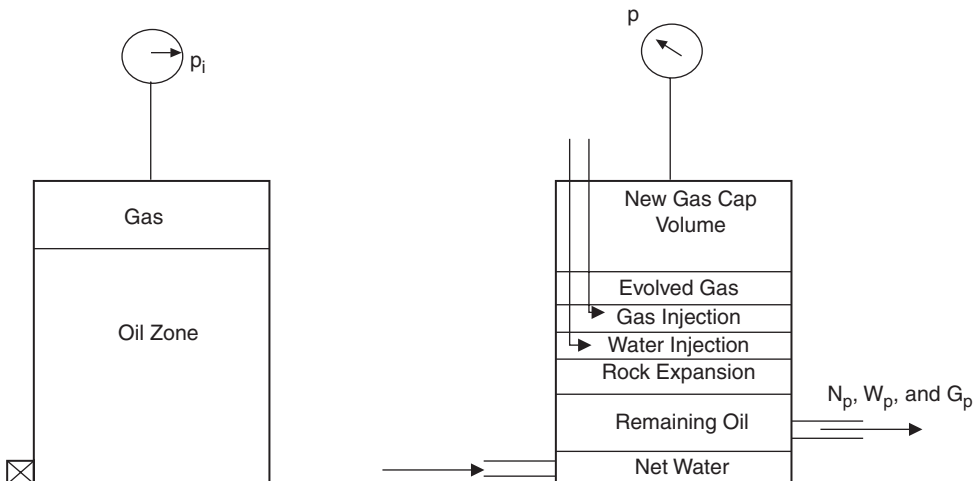
Figure 4.14   *Tank-model concept.*

Hydrocarbon PV occupied by the oil initially in place

Volume occupied by initial oil in place $= NB_{oi}$, bbl   [4.3.3]

where:

$N =$ oil initially in place, STB
$B_{oi} =$ oil formation volume factor at initial reservoir pressure p_i, bbl/STB

Hydrocarbon PV occupied by the gas in the gas cap

Volume of gas cap $= mNB_{oi}$, bbl   [4.3.4]

where m is a dimensionless parameter and defined as the ratio of gas cap volume to the oil zone volume.

Hydrocarbon PV occupied by the remaining oil

Volume of the remaining oil $= (N - N_p)B_o$, bbl   [4.3.5]

where:

$N_p =$ cumulative oil production, STB
$B_o =$ oil formation volume factor at reservoir pressure p, bbl/STB

Hydrocarbon PV occupied by the gas cap
at reservoir pressure p

As the reservoir pressure drops to a new level p, the gas in the gas cap expands and occupies a larger volume. Assuming no gas is produced from the gas cap during the pressure declines, the new volume of the gas cap can be determined as:

Volume of the gas cap at $p = \left[\dfrac{mNB_{oi}}{B_{gi}}\right]B_g$, bbl   [4.3.6]

where:

$B_{gi} =$ gas formation volume factor at initial reservoir pressure, bbl/scf
$B_g =$ current gas formation volume factor, bbl/scf

Hydrocarbon PV occupied by the evolved solution gas
Some of the solution gas that has been evolved from the oil will remain in the pore space and occupies a certain volume that can be determined by applying the following material balance on the solution gas:

$$\begin{bmatrix}\text{volume of the evolved gas}\\ \text{that remains in the PV}\end{bmatrix} = \begin{bmatrix}\text{volume of gas initially}\\ \text{in solution}\end{bmatrix}$$

$$-\begin{bmatrix}\text{volume of gas}\\ \text{produced}\end{bmatrix}$$

$$-\begin{bmatrix}\text{volume of gas}\\ \text{remaining in solution}\end{bmatrix}$$

or:

$$\begin{bmatrix}\text{volume of the evolved}\\ \text{gas that remains}\\ \text{in the PV}\end{bmatrix} = \left[NR_{si} - N_pR_p - (N - N_p)R_s\right]B_g$$

[4.3.7]

where:

$N_p =$ cumulative oil produced, STB
$R_p =$ net cumulative produced gas–oil ratio, scf/STB
$R_s =$ current gas solubility factor, scf/STB
$B_g =$ current gas formation volume factor, bbl/scf
$R_{si} =$ gas solubility at initial reservoir pressure, scf/STB

PV occupied by the net water influx

Net water influx $= W_e - W_pB_w$ [4.3.8]

where:

$W_e =$ cumulative water influx, bbl
$W_p =$ cumulative water produced, STB
$B_w =$ water formation volume factor, bbl/STB

Change in PV due to initial water and rock expansion
The component describing the reduction in the hydrocarbon PV due to the expansion of initial (connate) water and the reservoir rock cannot be neglected for an undersaturated oil reservoir. The water compressibility c_w and rock compressibility c_f are generally of the same order of magnitude as the compressibility of the oil. However, the effect of these two components can generally be neglected for gas cap drive reservoirs or when the reservoir pressure drops below the bubble point pressure.

The compressibility coefficient c which describes the changes in the volume (expansion) of the fluid or material with changing pressure is given by:

$$c = \frac{-1}{V}\frac{\partial V}{\partial p}$$

or:

$$\Delta V = Vc\Delta p$$

where ΔV represents the net changes or expansion of the material as a result of changes in the pressure. Therefore, the reduction in the PV due to the expansion of the connate water in the oil zone and the gas cap is given by:

Connate water expansion $= \left[(PV)S_{wi}\right]c_w\Delta p$

Substituting for PV with Equation 4.3.1, gives:

Expansion of connate water $= \left[\dfrac{NB_{oi}(1 + m)}{1 - S_{wi}}S_{wi}\right]c_w\Delta p$

[4.3.9]

where:

$\Delta p =$ change in reservoir pressure, $p_i - p$
$c_w =$ water compressibility coefficient, psi^{-1}
$m =$ ratio of the volume of the gas cap gas to the reservoir oil volume, bbl/bbl

Similarly, as fluids are produced and pressure declines, the entire reservoir PV is reduced (compaction) and this negative change in PV expels an equal volume of fluid as production. The reduction in the PV due to the expansion of the reservoir rock is given by:

Change in PV $= \dfrac{NB_{oi}(1 + m)}{1 - S_{wi}}c_f\Delta p$ [4.3.10]

Combining the expansions of the connate water and formation as represented by Equations 4.3.9 and 4.3.10 gives:

Total changes in the PV $= NB_{oi}(1 + m)\left(\dfrac{S_{wi}c_w + c_f}{1 - S_{wi}}\right)\Delta p$

[4.3.11]

The connate water and formation compressibilities are generally small in comparison to the compressibility of oil and gas. However, values of c_w and c_f are significant for undersaturated oil reservoirs and they account for an appreciable

fraction of the production above the bubble point. Ranges of compressibilities are given below:

Undersaturated oil	$5–50 \times 10^{-6}$ psi^{-1}
Water	$2–4 \times 10^{-6}$ psi^{-1}
Formation	$3–10 \times 10^{-6}$ psi^{-1}
Gas at 1000 psi	$500–1000 \times 10^{-6}$ psi^{-1}
Gas at 5000 psi	$50–200 \times 10^{-6}$ psi^{-1}

PV occupied by the injection gas and water
Assuming that G_{inj} volumes of gas and W_{ing} volumes of water have been injected for pressure maintenance, the total PV occupied by the two injected fluids is given by:

$$\text{Total volume} = G_{inj}B_{ginj} + W_{inj}B_w \qquad [4.3.12]$$

where:

G_{inj} = cumulative gas injected, scf
B_{ginj} = injected gas formation volume factor, bbl/scf
W_{ing} = cumulative water injected, STB
B_w = water formation volume factor, bbl/STB

Combining Equations 4.3.3 through 4.3.12 with Equation 4.3.2 and rearranging gives:

$$N = \Big(N_p B_o + (G_p - N_p R_s)B_g - (W_e - W_p B_w) - G_{inj}B_{ginj}$$
$$- W_{inj}B_w\Big) \Big/ \Big((B_o - B_{oi}) + (R_{si} - R_s)B_g + mB_{oi}\big[(B_g/B_{gi})$$
$$-1\big] + B_{oi}(1+m)\big[(S_{wi}c_w + c_f)/(1 - S_{wi})\big]\Delta p\Big) \qquad [4.3.13]$$

where:

N = initial oil-in-place, STB
G_p = cumulative gas produced, scf
N_p = cumulative oil produced, STB
R_{si} = gas solubility at initial pressure, scf/STB
m = ratio of gas cap gas volume to oil volume, bbl/bbl
B_{gi} = gas formation volume factor at p_i, bbl/scf
B_{ginj} = gas formation volume factor of the injected gas, bbl/scf

Recognizing that the cumulative gas produced G_p can be expressed in terms of the cumulative gas–oil ratio R_p and cumulative oil produced, then:

$$G_p = R_p N_p \qquad [4.3.14]$$

Combining Equation 4.3.14 with 4.3.13 gives:

$$N = \Big(N_p[B_o + (R_p - R_s)B_g] - (W_e - W_p B_w)$$
$$- G_{inj}B_{ginj} - W_{inj}B_{wi}\Big) \Big/ \Big((B_o - B_{oi}) + (R_{si} - R_s)B_g$$
$$+ mB_{oi}\big[(B_g/B_{gi}) - 1\big] + B_{oi}(1+m)$$
$$\times \big[(S_{wi}c_w + c_f)/(1 - S_{wi})\big]\Delta p\Big) \qquad [4.3.15]$$

This relationship is referred to as the generalized MBE. A more convenient form of the MBE can be arrived at, by introducing the concept of the total (two-phase) formation volume factor B_t into the equation. This oil *PVT* property is defined as:

$$B_t = B_o + (R_{si} - R_s)B_g \qquad [4.3.16]$$

Introducing B_t into Equation 4.3.15 and assuming, for the sake of simplicity, that there is no water or gas injection, gives:

$$N = \Big(N_p[B_t + (R_p - R_{si})B_g] - (W_e - W_p B_w)\Big) \Big/$$
$$\Big((B_t - B_{ti}) + mB_{ti}\big[B_g/B_{gi}/ - 1\big]$$
$$+ B_{ti}(1+m)\big[(S_{wi}c_w + c_f)/(1 - S_{wi})\big]\Delta p\Big) \qquad [4.3.17]$$

(note that $B_{ti} = B_{oi}$) where:

S_{wi} = initial water saturation
R_p = cumulative produced gas–oil ratio, scf/STB
Δp = change in the volumetric average reservoir pressure, psi
B_g = gas formation volume factor, bbl/scf

Example 4.1 The Anadarko Field is a combination drive reservoir. The current reservoir pressure is estimated at 2500 psi. The reservoir production data and *PVT* information are given below:

	Initial reservoir condition	*Current reservoir condition*
p, psi	3000	2500
B_o, bbl/STB	1.35	1.33
R_s, scf/STB	600	500
N_p, MMSTB	0	5
G_p, MMMscf	0	5.5
B_w, bbl/STB	1.00	1.00
W_e, MMbbl	0	3
W_p, MMbbl	0	0.2
B_g, bbl/scf	0.0011	0.0015
c_f, c_w	0	0

The following additional information is available:

Volume of bulk oil zone = 100 000 acres-ft

Volume of bulk gas zone = 20 000 acres-ft

Calculate the initial oil-in-place.

Solution

Step 1. Assuming the same porosity and connate water for the oil and gas zones, calculate m:

$$m = \frac{7758\phi(1 - S_{wi})(Ah)_{\text{gas cap}}}{7758\phi(1 - S_{wi})(Ah)_{\text{oil zone}}}$$
$$= \frac{7758\phi(1 - S_{wi})20\,000}{7758\phi(1 - S_{wi})100\,000}$$
$$= \frac{20\,000}{100\,000} = 0.2$$

Step 2. Calculate the cumulative gas–oil ratio R_p:

$$R_p = \frac{G_p}{N_p}$$
$$= \frac{5.5 \times 10^9}{5 \times 10^6} = 1100 \text{ scf/STB}$$

Step 3. Solve for the initial oil-in-place by applying Equation 4.3.15:

$$N = \left(N_p[B_o + (R_p - R_s)B_g] - (W_e - W_pB_w) \right) \Big/$$

$$\left((B_o - B_{oi}) + (R_{si} - R_s)B_g + mB_{oi}[(B_g/B_{gi}) - 1] \right.$$

$$\left. + B_{oi}(1 + m)[(S_{wi}c_w + c_f)(1 - S_{wi})]\Delta p \right)$$

$$= \left(5 \times 10^6[1.33 + (1100 - 500)0.0015] \right.$$

$$\left. - (3 \times 10^6 - 0.2 \times 10^6) \right) \Big/ \left((1.35 - 1.33) \right.$$

$$+ (600 - 500)0.0015 + (0.2)(1.35)$$

$$\left. \times [(0.0015/0.0011) - 1] \right) = 31.14 \text{ MMSTB}$$

4.3.2 Increasing primary recovery

It should be obvious that many steps can be taken to increase the ultimate primary recovery from a reservoir. Some of these steps can be surmised from the previous discussions, and others have been specifically noted when various subjects have been discussed. At this point we get involved with the problem of semantics when we attempt to define primary recovery. Strictly speaking, we can define secondary recovery as any production obtained using artificial energy in the reservoir. This automatically places pressure maintenance through gas or water injection in the secondary recovery category. Traditionally, most engineers in the oil patch prefer to think of pressure maintenance as an aid to primary recovery. It appears that we can logically classify the measures available for improving oil recovery during primary production as:

- well control procedures, and
- reservoir control procedures, e.g., pressure maintenance.

Well control
It should be stated that any steps taken to increase the oil or gas producing rate from an oil or gas reservoir generally increase the ultimate recovery from that reservoir by placing the economic limit further along the cumulative production scale. It is recognized that there is a particular rate of production at which the producing costs equal the operating expenses. Producing from an oil or gas well below this particular rate results in a net loss. If the productive capacity of a well can be increased it is clear that additional oil will be produced before the economic rate is reached. Consequently, acidizing, paraffin control, sand control, clean-out, and other means actually increase ultimate production from that well.

It is clear that production of gas and water decreases the natural reservoir energy. If the production of gas and water from an oil reservoir can be minimized, a larger ultimate production may be obtained. The same concept can be similarly applied for minimizing the production of water from a gas reservoir.

Proper control of the individual well rate is a big factor in the control of gas and water coning or fingering. This general problem is not restricted to water drive and gas cap drive reservoirs. In a solution gas drive reservoir it may be possible to produce a well at too high a rate from an ultimate recovery standpoint because excessive drawdown of the producing well pressure results in an excessive gas–oil ratio and corresponding waste of the solution gas. The engineer should be aware of this possibility and test wells in a solution gas drive reservoir to see if the gas–oil ratio is sensitive.

It should be observed that excessive drawdown in a solution gas drive reservoir through excessive producing rates often causes excessive deposition of paraffin in the tubing and occasionally in the reservoir itself. Keeping gas in solution in the oil by keeping the well pressure as high as possible minimizes the paraffin deposition. Of course, deposition of paraffin in the tubing is not serious when compared to the deposition of paraffin in the reservoir. Given enough time and money, the paraffin can be cleaned from the tubing and flow lines. However, it is problematic whether paraffin deposited in the pores of the formation around the wellbore can be cleaned from these pores. Consequently, the operator should be very careful to avoid such deposition in the formation.

Another adverse effect that may be caused by an excess producing rate is the production of sand. Many unconsolidated formations tend to flow sand through perforations and into the producing system when flow rates are excessive. It may be possible to improve this situation with screens, gravel packing, or consolidating materials.

The proper positioning of wells in a reservoir also plays a big part in the control of gas and water production. It is obvious that wells should be positioned as far as possible from the original gas–oil, water–oil, and gas–water contacts in order to minimize the production of unwanted gas and water. The positioning of the producing wells must, or course, be consistent with the needs for reservoir drainage, the total reservoir producing capacity, and the cost of development.

In determining the proper well spacing to use in a particular reservoir, the engineer should make certain that full recognition is given to the pressure distribution that will prevail in the drainage area of a well when the economic limit is reached. In a continuous reservoir there is no limit on the amount of reservoir that can be affected by one well. However, the engineer should be concerned with the additional oil that can be recovered prior to reaching the economic limit rate by increasing the drainage volume, or radius, of a well. In very tight reservoirs we may be able to accomplish only a small reduction in the reservoir pressure in the additional reservoir volume. This effect may be nearly offset by the reduction of the well rate caused by the increase in the drainage radius. Thus, care should be exercised to ensure that the greatest well spacing possible is also the most economical.

Total reservoir control
The effect of water and gas production on the recovery in an oil reservoir can be shown by solving Equation 4.3.15 for the produced oil:

$$N_p = \frac{N[B_o - B_{oi} + (R_{si} - R_s)B_g + (c_f + c_wS_{wc})\Delta p B_{oi}/(1 - S_{wc})]}{B_o - R_sB_g}$$

$$- \frac{B_gG_p - mNB_{oi}\left(\dfrac{B_g}{B_{gi}} - 1\right) - W_e + W_pB_w}{B_o - R_sB_g}$$

It should be noted that the oil production obtainable at a particular reservoir pressure is almost directly reduced by the reservoir volume of gas (G_pB_g) and water produced (W_pB_w). Furthermore, the derivation of the MBE shows that the cumulative gas production, G_p, is the net produced gas defined as the produced gas less the injected gas. Similarly, if the water encroachment, W_e, is defined as the natural water encroachment, the produced water, W_p, must represent the net water produced, defined as the water produced less the water injected. Therefore, if produced water or produced

gas can be injected without adversely affecting the amount of water or gas produced, the amount of oil produced at a particular reservoir pressure can be increased.

It is well known that the most efficient natural reservoir drive is water encroachment. The next most efficient is gas cap expansion, and the least efficient is solution gas drive. Consequently, it is important for the reservoir engineer to control production from a reservoir so that as little oil as possible is produced by solution gas drive and as much oil as possible is produced by water drive. However, when two or more drives operate in a reservoir, it is not always clear how much production results from each drive. One convenient method of estimating the amount of production resulting from each drive is to use material balance drive indices.

4.3.3 Reservoir driving indices

In a combination drive reservoir where all the driving mechanisms are simultaneously present, it is of a practical interest to determine the relative magnitude of each of the driving mechanisms and its contribution to the production. This objective can be achieved by rearranging Equation 4.3.15 in the following generalized form:

$$\frac{N(B_t - B_{ti})}{A} + \frac{NmB_{ti}(B_g - B_{gi})/B_{gi}}{A} + \frac{W_e - W_pB_w}{A}$$

$$+ \frac{NB_{oi}(1 + m)\left[\dfrac{c_wS_{wi} + c_f}{1 - S_{wi}}\right](p_i - p)}{A}$$

$$+ \frac{W_{inj}B_{winj}}{A} + \frac{G_{inj}B_{ginj}}{A} = 1 \qquad [4.3.18]$$

with the parameter A as defined by:

$$A = N_p\left[B_t + (R_p - R_{si})B_g\right] \qquad [4.3.19]$$

Equation 4.3.18 can be abbreviated and expressed as:

$$\text{DDI} + \text{SDI} + \text{WDI} + \text{EDI} + \text{WII} + \text{GII} = 1.0 \qquad [4.3.20]$$

where:

- DDI = depletion drive index
- SDI = segregation (gas cap) drive index
- WDI = water drive index
- EDI = expansion (rock and liquid) depletion index
- WII = injected water index
- GII = injected gas index

The numerators of the six terms in Equation 4.3.18 represent the total net change in the volume due to gas cap and fluid expansions, net water influx, and fluid injection, while the denominator represents the cumulate reservoir voidage of produced oil and gas. Since the total volume increase must be equal to the total voidage, the sum of the four indices must therefore be necessarily equal to 1. Furthermore, the value of each index must be less than or equal to unity, but cannot be negative. The four terms on the left-hand side of Equation 4.3.20 represent the four major primary driving mechanisms by which oil may be recovered from oil reservoirs. As presented earlier in this chapter, these driving forces are as follows.

Depletion drive Depletion drive is the oil recovery mechanism wherein the production of the oil from its reservoir rock is achieved by the expansion of the original oil volume with all its original dissolved gas. This driving mechanism is represented mathematically by the first term of Equation 4.3.18 or:

$$\text{DDI} = N\left(B_t - B_{ti}\right)/A \qquad [4.3.21]$$

where DDI is termed the depletion drive index.

Segregation drive Segregation drive (gas cap drive) is the mechanism wherein the displacement of oil from the formation is accomplished by the expansion of the original free gas cap. This driving force is described by the second term of Equation 4.3.18, or:

$$\text{SDI} = \left[NmB_{ti}\left(B_g - B_{gi}\right)/B_{gi}\right]/A \qquad [4.3.22]$$

where SDI is termed the segregation drive index. It should be pointed out that it is usually impossible to eliminate the production of the gas cap gas and, thus, cause gas cap shrinkage. This distinct possibility of the shrinkage of the gas cap, and, therefore, reducing SDI, could be a result of the random location of producing wells. It will be necessary to eliminate gas cap shrinkage by either shutting in wells that produce gas from the gas cap or returning fluid to the gas cap to replace the gas which has been produced. It is common practice to return some of the produced gas to the reservoir in order to maintain the size of the gas cap. In some cases, it has been more economical to return water instead of gas to the gas cap. This may be feasible when there are no facilities readily available for compressing the gas. Cole (1969) pointed out that this particular technique has been successfully applied in several cases, although the possibility of gravity segregation has to be considered.

Water drive Water drive is the mechanism wherein the displacement of the oil is accomplished by the net encroachment of water into the oil zone. This mechanism is represented by the third term of Equation 4.3.18, or:

$$\text{WDI} = (W_e - W_pB_w)/A \qquad [4.3.23]$$

where WDI is referred to as the water drive index.

Expansion drive index For undersaturated oil reservoirs with no water influx, the principal source of energy is a result of the rock and fluid expansion as represented by the fourth term in Equation 4.3.18 as:

$$\text{EDI} = \frac{NB_{oi}(1 + m)\left[\dfrac{c_wS_{wi} + c_f}{1 - S_{wi}}\right](p_i - p)}{A}$$

When all the other three driving mechanisms are contributing to the production of oil and gas from the reservoir, the contribution of the rock and fluid expansion to the oil recovery is usually too small and essentially negligible and can be ignored.

Injected water drive index The relative efficiency of the water injection pressure maintenance operations is expressed by:

$$\text{WII} = \frac{W_{inj}B_{winj}}{A}$$

The magnitude of WII indicates the importance of the injected water as an improved recovery agent.

Injected gas drive index Similar to the injected water drive index, the magnitude of its value indicates the relative importance this drive mechanism as compared to the other indices, as given by:

$$\text{GII} = \frac{G_{inj}B_{ginj}}{A}$$

Note that for a depletion drive reservoir under pressure maintenance operations by gas injection, Equation 4.3.20 is reduced to:

$$\text{DDI} + \text{EDI} + \text{GII} = 1.0$$

Since the recovery by depletion drive and expansion of the fluid and rock are usually poor, it is essential to maintain a high injected gas drive index. If the reservoir pressure can be maintained constant or declining at a slow rate, the values of DDI and EDI will be minimized because the changes in the numerators of both terms will essentially approach zeros. Theoretically, the highest recovery would occur at

constant reservoir pressure; however, economic factors and feasibility of operation may dictate some pressure reduction.

In the absence of gas or water injection, Cole (1969) pointed out that since the sum of the remaining four driving indexes is equal to 1, it follows that if the magnitude of one of the index terms is reduced, then one or both of the remaining terms must be correspondingly increased. An effective water drive will usually result in maximum recovery from the reservoir. Therefore, if possible, the reservoir should be operated to yield a maximum water drive index and minimum values for the depletion drive index and the gas cap drive index. Maximum advantage should be taken of the most efficient drive available, and where the water drive is too weak to provide an effective displacing force, it may be possible to utilize the displacing energy of the gas cap. In any event, the depletion drive index should be maintained as low as possible at all times, as this is normally the most inefficient driving force available.

Equation 4.3.20 can be solved at any time to determine the magnitude of the various driving indexes. The forces displacing the oil and gas from the reservoir are subject to change from time to time and for this reason Equation 4.3.20 should be solved periodically to determine whether there has been any change in the driving indexes. Changes in fluid withdrawal rates are primarily responsible for changes in the driving indexes. For example, reducing the oil producing rate could result in an increased water drive index and a correspondingly reduced depletion drive index in a reservoir containing a weak water drive. Also, by shutting in wells producing large quantities of water, the water drive index could be increased, as the net water influx (gross water influx minus water production) is the important factor.

When the reservoir has a very weak water drive, but has a fairly large gas cap, the most efficient reservoir producing mechanism may be the gas cap, in which case a large gas cap drive index is desirable. Theoretically, recovery by gas cap drive is independent of producing rate, as the gas is readily expansible. Low vertical permeability could limit the rate of expansion of the gas cap, in which case the gas cap drive index would be rate sensitive. Also, gas coning into producing wells will reduce the effectiveness of the gas cap expansion due to the production of free gas. Gas coning is usually a rate-sensitive phenomenon: the higher the producing rates, the greater the amount of coning.

An important factor in determining the effectiveness of a gas cap drive is the degree of conservation of the gas cap gas. As a practical mater, it will often be impossible, because of royalty owners or lease agreements, to completely eliminate gas cap gas production. Where free gas is being produced, the gas cap drive index can often be markedly increased by shutting in high gas–oil-ratio wells, and, if possible, transferring their allowables to other low gas–oil-ratio wells.

Figure 4.15 shows a set of plots that represents various driving indexes for a combination drive reservoir. At point A some of the structurally low wells are reworked to reduce water production. This results in an effective increase in the water drive index. At point B workover operations are complete, water, gas, and oil producing rates are relatively stable, and the driving indexes show no change. At point C some of the wells which have been producing relatively large, but constant, volumes of water are shut in, which results in an increase in the water drive index. At the same time some of the upstructure, high gas–oil-ratio wells have been shut in and their allowables transferred to wells lower on the structure producing with normal gas–oil ratios. At point D gas is being returned to the reservoir, and the gas cap drive index is exhibiting a decided increase. The water drive index is relatively constant, although it is decreasing somewhat, and the depletion drive index is showing a marked decline. This is indicative of a more efficient reservoir operation, and if the depletion drive index can be reduced to zero, relatively good recovery can be expected from the reservoir. Of course, to achieve a zero depletion drive index would require the complete maintenance of reservoir pressure, which is often difficult to accomplish. It can be noted from Figure 4.15 that the sum of the various drive indexes is always equal to 1.

Example 4.2 A combination drive reservoir contains 10 MMSTB of oil initially in place. The ratio of the original gas cap volume to the original oil volume, i.e., m, is estimated as 0.25. The initial reservoir pressure is 3000 psia at 150°F. The reservoir produced 1 MMSTB of oil, 1100 MMscf of gas of 0.8 specific gravity, and 50 000 STB of water by the time the reservoir pressure dropped to 2800 psi. The following *PVT* data is available:

	3000 psi	2800 psi
B_o, bbl/STB	1.58	1.48
R_s, scf/STB	1040	850
B_g, bbl/scf	0.00080	0.00092
B_t, bbl/STB	1.58	1.655
B_w, bbl/STB	1.000	1.000
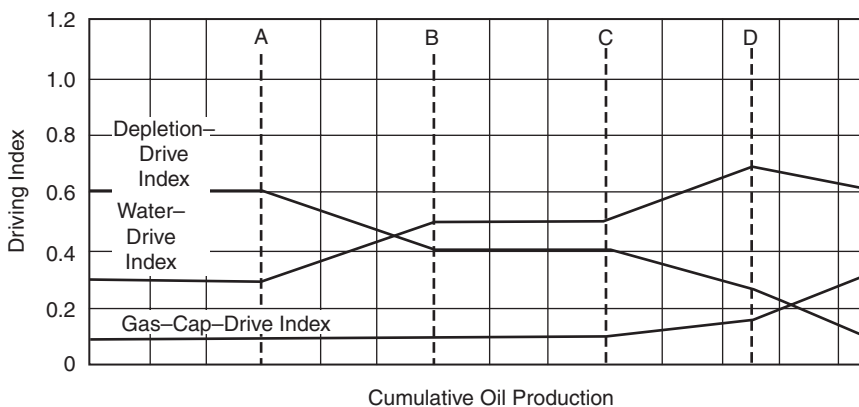
Figure 4.15 Driving indexes in a combination drive reservoir (After Clark N.J., Elements of Petroleum Reservoirs, SPE, 1969).

The following data is also available:

$S_{wi} = 0.20$, $c_w = 1.5 \times 10^{-6} \text{ psi}^{-1}$, $c_f = 1 \times 10^{-6} \text{ psi}^{-1}$

Calculate:

(a) the cumulative water influx;
(b) the net water influx;
(c) the primary driving indices at 2800 psi.

Solution Because the reservoir contains a gas cap, the rock and fluid expansion can be neglected, i.e., set c_f and $c_w = 0$. However, for illustration purposes, the rock and fluid expansion term will be included in the calculations.

(a) The cumulative water influx:

Step 1. Calculate the cumulative gas–oil ratio R_p:

$$R_p = \frac{G_p}{N_p} = \frac{1100 \times 10^6}{1 \times 10^6} = 1100 \text{ scf/STB}$$

Step 2. Arrange Equation 4.3.17 to solve for W_e:

$$W_e = N_p\left[B_t + (R_p - R_{si})B_g\right]$$

$$- N\left[(B_t - B_{ti}) + mB_{ti}\left(\frac{B_g}{B_{gi}} - 1\right)\right.$$

$$\left. + B_{ti}(1+m)\left(\frac{S_{wi}c_w + c_f}{1 - S_{wi}}\right)\Delta p\right] + W_p B_{wp}$$

$$= 10^6\left[1.655 + (1100 - 1040)0.00092\right] - 10^7$$

$$\times \left[(1.655 - 1.58) + 0.25(1.58)\left(\frac{0.00092}{0.00080} - 1\right)\right.$$

$$+ 1.58(1 + 0.25)\left(\frac{0.2(1.5 \times 10^{-6})}{1 - 0.2}\right)$$

$$\left. \times (3000 - 2800)\right] + 50000 = 411281 \text{ bbl}$$

Neglecting the rock and fluid expansion term, the cumulative water influx is 417 700 bbl.

(b) The net water influx:

Net water influx $= W_e - W_p B_w = 411\,281 - 50\,000$

$$= 361\,281 \text{ bbl}$$

(c) The primary recovery indices:

Step 1. Calculate the parameter A by using Equation 4.3.19:

$$A = N_p\left[B_t + (R_p - R_{si})B_g\right]$$

$$= (1.0 \times 10^6)[1.655 + (1100 - 1040)0.00092]$$

$$= 1\,710\,000$$

Step 2. Calculate DDI, SDI, and WDI by applying Equations 4.3.21 through 4.3.23, respectively:

$$DDI = N(B_t - B_{ti})/A$$

$$= \frac{10 \times 10^6 (1.655 - 1.58)}{1\,710\,000} = 0.4385$$

$$SDI = \left[NmB_{ti}(B_g - B_{gi})/B_{gi}\right]/A$$

$$= \frac{10 \times 10^6 (0.25)(1.58)(0.00092 - 0.0008)/0.0008}{1710000}$$

$$= 0.3465$$

$$WDI = (W_e - W_p B_w)/A$$

$$= \frac{411\,281 - 50\,000}{1\,710\,000} = 0.2112$$

Since:

$$DDI + SDI + WDI + EDI = 1.0$$

then:

$$EDI = 1 - 0.4385 - 0.3465 - 0.2112 = 0.0038$$

The above calculations show that 43.85% of the recovery was obtained by depletion drive, 34.65% by gas cap drive, 21.12% by water drive, and only 0.38% by connate water and rock expansion. The results suggest that the expansion drive index term can be neglected in the presence of a gas cap or when the reservoir pressure drops below the bubble point pressure. However, in high-PV compressibility reservoirs such as chalks and unconsolidated sands, the energy contribution of the rock and water expansion cannot be ignored even at high gas saturations.

A source of error is often introduced in the MBE calculations when determining the average reservoir pressure and the associated problem of correctly weighting or averaging the individual well pressures. An example of such a problem is when the producing formations are comprised of two or more zones of different permeabilities. In this case, the pressures are generally higher in the zone of low permeability and because the measured pressures are nearer to those in high-permeability zones, the measured static pressures tend to be lower and the reservoir behaves as if it contained less oil. Schilthuis explained this phenomenon by referring to the oil in the more permeable zones as active oil and by observing that the *calculated active oil usually increases with time* because the oil and gas in low-permeability zones slowly expand to offset the pressure decline. This is also true for fields that are not fully developed, because the average pressure can be that of the developed portion only, whereas the pressure is higher in the undeveloped portions. Craft et al. (1991) pointed out that the effect of pressure errors on the calculated values of initial oil and water influx depends on the size of the errors in relation to the reservoir pressure decline. Notice that the pressure enters the MBE mainly when determining the *PVT* differences in terms of:

$$(B_o - B_{oi})$$
$$(B_g - B_{gi})$$
$$(R_{si} - R_s)$$

Because water influx and gas cap expansion tend to offset pressure decline, the pressure errors are more serious than for the undersaturated reservoirs. In the case of very active water drives or gas caps that are large compared to the oil zone, the MBE usually produces considerable errors when determining the initial oil-in-place because of the very small pressure decline.

Dake (1994) pointed out that there are two "necessary" conditions that must be satisfied for a meaningful application of the MBE to a reservoir:

(1) There should be adequate data collection in terms of production pressure, and *PVT*, in both frequency and quality for proper use of the MBE.
(2) It must be possible to define an average reservoir pressure trend as a function of time or production for the field.

Establishing an average pressure decline trend can be possible even if there are large pressure differentials across the field under normal conditions. Averaging *individual well pressure* declines can possibly be used to determine a uniform trend in the entire reservoir. The concept of average well pressure and its use in determining the reservoir volumetric average pressure was introduced in Chapter 1 as illustrated by Figure 1.24. This figure shows that if $(\bar{p})_j$ and V_j represents the pressure and volume drained by the jth

well, the volumetric average pressure of the entire reservoir can be estimated from:

$$\bar{p}_r = \frac{\sum_j (\bar{p}V)_j}{\sum_j V_j}$$

in which:

V_j = the PV of the jth well drainage volume

$(\bar{p})_j$ = volumetric average pressure *within the jth drainage volume*

In practice, the V_j are difficult to determine and, therefore, it is common to use individual well flow rates q_i in determining the average reservoir pressure from individual well average drainage pressure. From the definition of the isothermal compressibility coefficient:

$$c = \frac{1}{V}\frac{\partial V}{\partial P}$$

differentiating with time gives:

$$\frac{\partial p}{\partial t} = \frac{1}{cV}\frac{\partial V}{\partial t}$$

or:

$$\frac{\partial p}{\partial t} = \frac{1}{cV}(q)$$

This expression suggests that for a reasonably constant c at the time of measurement:

$$V \propto \frac{q}{\partial p/\partial t}$$

Since the flow rates are measured on a routine basis throughout the lifetime of the field, the average reservoir pressure can be alternatively expressed in terms of the individual well average drainage pressure decline rates and fluid flow rates by:

$$\bar{p}_r = \frac{\sum_j \left[(\bar{p}q)_j/(\partial\bar{p}/\partial t)_j\right]}{\sum_j \left[q_j/(\partial\bar{p}/\partial t)_j\right]}$$

However, since the MBE is usually applied at regular intervals of 3–6 months, i.e., Δt = 3–6 months, throughout the lifetime of the field, the average field pressure can be expressed in terms of the incremental net change in underground fluid withdrawal, $\Delta(F)$, as:

$$\bar{p}_r = \frac{\sum_j \bar{p}_j \Delta(F)_j/\Delta\bar{p}_j}{\sum_j \Delta(F)_j/\Delta\bar{p}_j}$$

where the total underground fluid withdrawal at time t and $t + \Delta t$ are given by:

$$F_t = \int_0^t \left[Q_oB_o + Q_wB_w + (Q_g - Q_oR_s - Q_wR_{sw})B_g\right]dt$$

$$F_{t+\Delta t} = \int_0^{t+\Delta t} \left[Q_oB_o + Q_wB_w + (Q_g - Q_oR_s - Q_wR_{sw})B_g\right]dt$$

with:

$$\Delta(F) = F_{t+\Delta t} - F_t$$

where:

R_s = gas solubility, scf/STB
R_{sw} = gas solubility in the water, scf/STB
B_g = gas formation volume factor, bbl/scf
Q_o = oil flow rate, STB/day
Q_w = water flow rate, STB/day
Q_g = gas flow rate, scf/day

For a volumetric reservoir with total fluid production and initial reservoir pressure as the only available data, the average

pressure can be *roughly approximated* by using the following expression:

$$\bar{p}_r = p_i - \left[\frac{5.371 \times 10^{-6}F_t}{c_t(Ah\phi)}\right]$$

with the total fluid production F_t as defined above by:

$$F_t = \int_0^t \left[Q_oB_o + Q_wB_w + (Q_g - Q_oR_s - Q_wR_{sw})B_g\right]dt$$

where:

A = well or reservoir drainage area, acres
h = thickness, ft
c_t = total compressibility coefficient, psi^{-1}
ϕ = porosity
p_i = initial reservoir pressure, psi

The above expression can be employed in a incremental manner, i.e., from time t to $t + \Delta t$, by:

$$(\bar{p}_r)_{t+\Delta t} = (\bar{p}_r)_t - \left[\frac{5.371 \times 10^{-6}\Delta F}{c_t(Ah\phi)}\right]$$

with:

$$\Delta(F) = F_{t+\Delta t} - F_t$$

4.4 The Material Balance as an Equation of a Straight Line

An insight into the general MBE, i.e., Equation 4.3.15, may be gained by considering the physical significance of the following groups of terms from which it is comprised;

- $N_p[B_o + (R_p - R_s)B_g]$ represents the reservoir volume of cumulative oil and gas produced;
- $[W_e - W_pB_w]$ refers to the net water influx that is retained in the reservoir;
- $[G_{inj}B_{ginj} + W_{inj}B_w]$, the pressure maintenance term, represents cumulative fluid injection in the reservoir;
- $[mB_{oi}(B_g/B_{gi} - 1)]$ represents the net expansion of the gas cap that occurs with the production of N_p stock-tank barrels of oil (as expressed in bbl/STB of original oil-in-place).

There are essentially three unknowns in Equation (4.3.15):

(1) the original oil-in-place N,
(2) the cumulative water influx W_e, and
(3) the original size of the gas cap as compared to the oil zone size m.

In developing a methodology for determining the above three unknowns, Havlena and Odeh (1963, 1964) expressed Equation 4.3.15 in the following form:

$$N_p[B_o + (R_p - R_s)B_g] + W_pB_w = N[(B_o - B_{oi})$$

$$+ (R_{si} - R_s)B_g] + mNB_{oi}\left(\frac{B_g}{B_{gi}} - 1\right) + N(1+m)B_{oi}$$

$$\times \left(\frac{c_wS_{wi} + c_f}{1 - S_{wi}}\right)\Delta p + W_e + W_{inj}B_w + G_{inj}B_{ginj} \quad [4.4.1]$$

Havlena and Odeh further expressed Equation 4.4.1 in a more condensed form as:

$$F = N\left[E_o + mE_g + E_{f,w}\right] + \left(W_e + W_{inj}B_w + G_{inj}B_{ginj}\right)$$

Assuming, for the purpose of simplicity, that no pressure maintenance by gas or water injection is being considered, the above relationship can be further simplified and written as:

$$F = N\left[E_o + mE_g + E_{f,w}\right] + W_e \quad [4.4.2]$$

in which the terms F, E_o, E_g, and $E_{f,w}$ are defined by the following relationships:

- F represents the underground withdrawal and is given by:

$$F = N_p \left[B_o + (R_p - R_s)B_g \right] + W_p B_w \qquad [4.4.3]$$

In terms of the two-phase formation volume factor B_t, the underground withdrawal "F" can be written as:

$$F = N_p \left[B_t + (R_p - R_{si})B_g \right] + W_p B_w \qquad [4.4.4]$$

- E_o describes the expansion of oil and its originally dissolved gas and is expressed in terms of the oil formation volume factor as:

$$E_o = (B_o - B_{oi}) + (R_{si} - R_s)B_g \qquad [4.4.5]$$

Or, equivalently, in terms of B_t;

$$E_o = B_t - B_{ti} \qquad [4.4.6]$$

- E_g is the term describing the expansion of the gas cap gas and is defined by the following expression:

$$E_g = B_{oi}[(B_g/B_{gi}) - 1] \qquad [4.4.7]$$

In terms of the two-phase formation volume factor B_t, essentially $B_{ti} = B_{oi}$ or:

$$E_g = B_{ti}[(B_g/B_{gi}) - 1]$$

- $E_{f,w}$ represents the expansion of the initial water and the reduction in the PV and is given by:

$$E_{f,w} = (1 + m)B_{oi} \left[\frac{c_w S_{wi} + c_f}{1 - S_{wi}} \right] \Delta p \qquad [4.4.8]$$

Havlena and Odeh examined several cases of varying reservoir types with Equation 4.4.2 and pointed out that the relationship can be rearranged in the form of a straight line. For example, in the case of a reservoir which has no initial gas cap (i.e., $m = 0$) or water influx (i.e., $W_e = 0$), and negligible formation and water compressibilities (i.e., c_f and $c_w = 0$), Equation 4.4.2 reduces to:

$$F = NE_o$$

This expression suggests that a plot of the parameter F as a function of the oil expansion parameter E_o would yield a straight line with slope N and intercept equal to 0.

The straight-line method requires the plotting of a variable group versus another variable group, with the variable group selection depending on the mechanism of production under which the reservoir is producing. The most important aspect of this method of solution is that it attaches significance to the sequence of the plotted points, the direction in which they plot, and to the shape of the resulting plot.

The significance of the straight-line approach is that the sequence of plotting is important and if the plotted data deviates from this straight line there is some reason for it. This significant observation will provide the engineer with valuable information that can be used in determining the following unknowns:

- initial oil-in-place N;
- size of the gas cap m;
- water influx W_e;
- driving mechanism;
- average reservoir pressure.

The applications of the straight-line form of the MBE in solving reservoir engineering problems are presented next to illustrate the usefulness of this particular form. Six cases of applications are presented and include:

Case 1: Determination of N in volumetric undersaturated reservoirs
Case 2: Determination of N in volumetric saturated reservoirs

Case 3: Determination of N and m in gas cap drive reservoirs
Case 4: Determination of N and W_e in water drive reservoirs
Case 5: Determination of N, m, and W_e in combination drive reservoirs
Case 6: Determination of average reservoir pressure $\bar{p}$

4.4.1 Case 1: Volumetric Undersaturated Oil Reservoirs

The linear form of the MBE as expressed by Equation 4.4.2 can be written as:

$$F = N \left[E_o + mE_g + E_{f,w} \right] + W_e \qquad [4.4.9]$$

Assuming no water or gas injection, several terms in the above relationship may disappear when imposing the conditions associated with the assumed reservoir driving mechanism. For a volumetric and undersaturated reservoir, the conditions associated with driving mechanism are:

$$W_e = 0 \text{ since the reservoir is volumetric}$$
$$m = 0 \text{ since the reservoir is undersaturated}$$
$$R_s = R_{si} = R_p \text{ since all produced gas is dissolved in the oil}$$

Applying the above conditions on Equation 4.1.9 gives:

$$F = N(E_o + E_{f,w}) \qquad [4.4.10]$$

or:

$$N = \frac{F}{E_o + E_{f,w}} \qquad [4.4.11]$$

with:

$$F = N_p B_o + W_p B_w \qquad [4.4.12]$$

$$E_o = B_o - B_{oi} \qquad [4.4.13]$$

$$E_{f,w} = B_{oi} \left[\frac{c_w S_w + c_f}{1 - S_{wi}} \right] \Delta p \qquad [4.4.14]$$

$$\Delta p = p_i - \bar{p}_r$$

where:

N = initial oil-in-place, STB
p_i = initial reservoir pressure
$\bar{p}_r$ = volumetric average reservoir pressure

When a new field is discovered, one of the first tasks of the reservoir engineer is to determine if the reservoir can be classified as a volumetric reservoir, i.e., $W_e = 0$. The classical approach of addressing this problem is to assemble all the necessary data (i.e., production, pressure, and PVT) that is required to evaluate the right-hand side of Equation 4.4.11. The term $F/(E_o + E_{f,w})$ for each pressure and time observation is plotted versus cumulative production N_p or time, as shown in Figure 4.16. Dake (1994) suggested that such a plot can assume two various shapes:

(1) If all the calculated points of $F/(E_o + E_{f,w})$ lie on a horizontal straight line (see line A in Figure 4.16, it implies that the reservoir can be classified as a volumetric reservoir. This defines a purely depletion drive reservoir whose energy derives solely from the expansion of the rock, connate water, and the oil. Furthermore, the ordinate value of the plateau determines the initial oil-in-place N.

(2) Alternately, if the calculated values of the term $F/(E_o + E_{f,w})$ rise, as illustrated by the curves B and C, it indicates that the reservoir has been energized by water influx, abnormal pore compaction, or a combination of these two. Curve B in Figure 4.16 might be for a strong water drive field in which the aquifer is displaying an infinite-acting behavior, whereas curve C represents an aquifer whose outer boundary had been felt and the
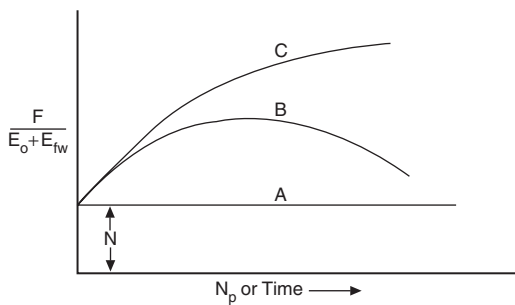
Figure 4.16 *Classification of the reservoir.*

aquifer is depleting in unison with the reservoir itself. The downward trend in points on curve C as time progresses denotes the diminishing degree of energizing by the aquifer. Dake (1994) pointed out that in water drive reservoirs, the shape of the curve, i.e., $F/(E_o + E_{f,w})$ versus time, is highly rate dependent. For instance, if the reservoir is producing at a higher rate than the water influx rate, the calculated values of $F/(E_o + E_{f,w})$ will dip downward, revealing a lack of energizing by the aquifer, whereas if the rate is decreased the reverse happens and the points are elevated.

Similarly Equation 4.4.10 could be used to verify the characteristic of the reservoir driving mechanism and to determine the initial oil-in-place. A plot of the underground withdrawal F versus the expansion term $(E_o + E_{f,w})$ should result in a straight line going through the origin with N being the slope. It should be noted that the origin is a "must" point; thus, one has a fixed point to guide the straight-line plot (as shown in Figure 4.17).

This interpretation technique is useful in that, if the linear relationship is expected for the reservoir and yet the actual plot turns out to be non-linear, then this deviation can itself be diagnostic in determining the actual drive mechanisms in the reservoir.

A linear plot of the underground withdrawal F vs. $(E_o + E_{f,w})$ indicates that the field is producing under volumetric performance, i.e., no water influx, and strictly by pressure depletion and fluid expansion. On the other hand, a non-linear plot indicates that the reservoir should be characterized as a water drive reservoir.

Example 4.3 The Virginia Hills Beaverhill Lake Field is a volumetric undersaturated reservoir. Volumetric calculations indicate the reservoir contains 270.6 MMSTB of oil
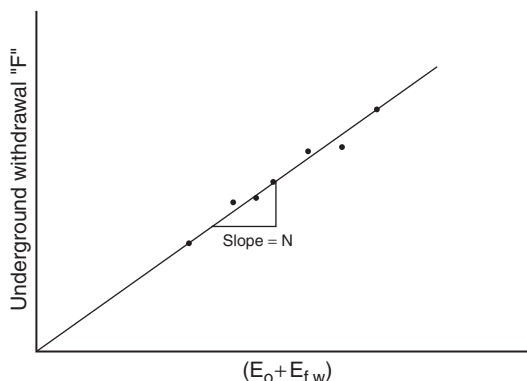

Figure 4.17 *Underground withdrawal versus $E_o + E_{f,w}$.*

initially in place. The initial reservoir pressure is 3685 psi. The following additional data is available:

$S_{wi} = 24\%$, $B_w = 1.0$ bbl/STB,
$c_w = 3.62 \times 10^{-6}$ psi^{-1}, $p_b = 1500$ psi,
$c_f = 4.95 \times 10^{-6}$ psi^{-1}

The field production and *PVT* data is summarized below:

Volumetric average pressure	No. of producing wells	B_o (bbl/STB)	N_p (MSTB)	W_p (MSTB)
3685	1	1.3102	0	0
3680	2	1.3104	20.481	0
3676	2	1.3104	34.750	0
3667	3	1.3105	78.557	0
3664	4	1.3105	101.846	0
3640	19	1.3109	215.681	0
3605	25	1.3116	364.613	0
3567	36	1.3122	542.985	0.159
3515	48	1.3128	841.591	0.805
3448	59	1.3130	1273.53	2.579
3360	59	1.3150	1691.887	5.008
3275	61	1.3160	2127.077	6.500
3188	61	1.3170	2575.330	8.000

Calculate the initial oil-in-place by using the MBE and compare with the volumetric estimate of N.

Solution

Step 1. Calculate the initial water and rock expansion term $E_{f,w}$ from Equation 4.4.14:

$$E_{f,w} = B_{oi}\left[\frac{c_w S_w + c_f}{1 - S_{wi}}\right]\Delta p$$

$$= 1.3102\left[\frac{3.62 \times 10^{-6}(0.24) + 4.95 \times 10^{-6}}{1 - 0.24}\right]\Delta p$$

$$= 10.0 \times 10^{-6}(3685 - \bar{p}_r)$$

Step 2. Construct the following table using Equations 4.4.12 and 4.4.13:

$$F = N_p B_o + W_p B_w$$

$$E_o = B_o - B_{oi}$$

$$E_{f,w} = 10.0 \times 10^{-6}(3685 - \bar{p}_r)$$

| $\bar{p}_r$ (psi)	F (Mbbl)	E_o (bbl/STB)	Δp	$E_{f,w}$	$E_o + E_{f,w}$
3685	–	–	0	0	–
3680	26.84	0.0002	5	50×10^{-6}	0.00025
3676	45.54	0.0002	9	90×10^{-6}	0.00029
3667	102.95	0.0003	18	180×10^{-6}	0.00048
3664	133.47	0.0003	21	210×10^{-6}	0.00051
3640	282.74	0.0007	45	450×10^{-6}	0.00115
3605	478.23	0.0014	80	800×10^{-6}	0.0022
3567	712.66	0.0020	118	1180×10^{-6}	0.00318
3515	1105.65	0.0026	170	1700×10^{-6}	0.0043
3448	1674.72	0.0028	237	2370×10^{-6}	0.00507
3360	2229.84	0.0048	325	3250×10^{-6}	0.00805
3275	2805.73	0.0058	410	4100×10^{-6}	0.0099
3188	3399.71	0.0068	497	4970×10^{-6}	0.0117
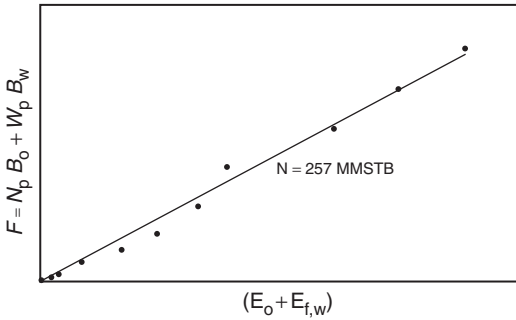
Figure 4.18 F vs. $E_o + E_{f,w}$ for Example 4.3.

Step 3. Plot the underground withdrawal term F against the expansion term $(E_o + E_{f,w})$ on a Cartesian scale, as shown in Figure 4.18.

Step 4. Draw the best straight through the points and determine the slope of the line and the volume of the active initial oil-in-place as:

$$N = 257 \text{ MMSTB}$$

It should be noted that the value of the initial oil-in-place as determined from the MBE is referred to as the "effective" or "active" initial oil-in-place. This value is usually smaller than that of the volumetric estimate due to oil being trapped in undrained fault compartments or low-permeability regions of the reservoir.

4.4.2 Case 2: Volumetric saturated oil reservoirs

An oil reservoir that originally exists at *its bubble point pressure* is referred to as a "saturated oil reservoir." The main driving mechanism in this type of reservoir results from the liberation and expansion of the solution gas as the pressure drops below the bubble point pressure. The only unknown in a volumetric saturated oil reservoir is the initial oil-in-place N. Normally, the water and rock expansion term $E_{f,w}$ is negligible in comparison to the expansion of solution gas; however, it is recommended to include the term in the calculations. Equation 4.4.9 can be simplified to give an identical form to that of Equation 4.4.10. That is:

$$F = N(E_o + E_{f,w}) \qquad \text{[4.4.15]}$$

However, the parameters F and E_o that constitute the above expression are given in an expanded form to reflect the reservoir condition as the pressure drops below the bubble point. The underground withdrawal F and the expansion term $(E_o + E_{f,w})$ are defined by:

F in terms of B_o $F = N_p[B_o + (R_p - R_s)B_g] + W_p B_w$

or equivalently in terms of B_t $F = N_p[B_t + (R_p - R_{si})B_g] + W_p B_w$

E_o in terms of B_o $E_o = (B_o - B_{oi}) + (R_{si} - R_s)B_g$

or equivalently in terms of B_t $E_o = B_t - B_{ti}$

and:

$$E_{f,w} = B_{oi}\left[\frac{c_w S_w + c_f}{1 - S_{wi}}\right]\Delta p$$

Equation 4.4.15 indicates that a plot of the underground withdrawal F, evaluated by using the actual reservoir production data, as a function of the fluid expansion term $(E_o + E_{f,w})$ should result in a straight line going through the origin with a slope of N.

The above interpretation technique is useful in that, if a simple linear relationship such as Equation 4.4.15 is expected for a reservoir and yet the actual plot turns out to be non-linear, then this deviation can itself be diagnostic in determining the actual drive mechanisms in the reservoir. For instance, Equation 4.4.15 may turn out to be non-linear because there is an unsuspected water influx into the reservoir, helping to maintain the pressure.

Example 4.4[a] A volumetric undersaturated oil reservoir has a bubble point pressure of 4500. The initial reservoir pressure is 7150 psia and the volumetric calculations indicate the reservoir contains 650 MMSTB of oil initially in place. The field is a tight, naturally fractured, chalk reservoir and was developed without pressure support by water injection. The initial reservoir pressure is 3685 psi. The following additional data is available:

$S_{wi} = 43\%$,

$c_f = 3.3 \times 10^{-6} \text{psi}^{-1}$,

$B_w = 1.0 \text{ bbl/STB}$,

$c_w = 3.00 \times 10^{-6} \text{ psi}^{-1}$,

$p_b = 1500 \text{ psi}$

The field production and *PVT* data summarized below:

p (psia)	Q_o (STB/day)	Q_g (MMscf/day)	B_o (bbl/STB)	R_s (scf/STB)	B_g (bbl/scf)	N_p (MMSTB)	R_p (scf/STB)
7150	–	–	1.743	1450	–	0	1450
6600	44 230	64.110	1.760	1450	–	8.072	1450
5800	79 326	115.616	1.796	1450	–	22.549	1455
4950	75 726	110.192	1.830	1450	–	36.369	1455
4500	–	–	1.850	1450	–	43.473	1447
4350	70 208	134.685	1.775	1323	0.000797	49.182	1576
4060	50 416	147.414	1.670	1143	0.000840	58.383	1788
3840	35 227	135.282	1.611	1037	0.000881	64.812	1992
3600	26 027	115.277	1.566	958	0.000916	69.562	2158
3480	27 452	151.167	1.523	882	0.000959	74.572	2383
3260	20 975	141.326	1.474	791	0.001015	78.400	2596
3100	15 753	125.107	1.440	734	0.001065	81.275	2785
2940	14 268	116.970	1.409	682	0.001121	83.879	2953
2800	13 819	111.792	1.382	637	0.001170	86.401	3103

[a]L.P. Dake, *The Practice of Reservoir Engineering*, 1994, Elsevier.

Calculate the initial oil-in-place by using the MBE and compare with the volumetric estimate of N.

Solution

Step 1. For the undersaturated performance, the initial oil-in-place is described by Equation 4.41 as:

$$N = \frac{F}{E_o + E_{f,w}}$$

where:

$$F = N_p B_o$$

$$E_o = B_o - B_{oi}$$

$$E_{f,w} = B_{oi} \left[\frac{c_w S_w + c_f}{1 - S_{wi}} \right] \Delta p$$

$$= 1.743 \left[\frac{3.00 \times 10^{-6} (0.43) + 3.30 \times 10^{-6}}{1 - 0.43} \right] \Delta p$$

$$= 8.05 \times 10^{-6} (7150 - \bar{p}_r)$$

Step 2. Calculate N using the undersaturated reservoir data:

$$F = N_p B_o$$

$$E_o = B_o - B_{oi} = B_o - 1.743$$

$$E_{f,w} = 8.05 \times 10^{-6} (7150 - \bar{p}_r)$$

$\bar{p}_r$ (psi)	F (MMbbl)	E_o (bbl/STB)	Δp (psi)	$E_{f,w}$ bbl/STB	$N = F/$ $(E_o + E_{f,w})$ (MMSTB)
7150	–	–	0	0	–
6600	14.20672	0.0170	550	0.00772	574.7102
5800	40.49800	0.0530	1350	0.018949	562.8741
4950	66.55527	0.0870	2200	0.030879	564.6057
4500	80.42505	0.1070	2650	0.037195	557.752

The above calculations suggest that the initial oil-in-place as calculated from the undersaturated reservoir performance data is around 558 MMSTB, which is lower by about 14% of the volumetric estimation of 650 MMSTB.

Step 3. Calculate N using the entire reservoir data:

$$F = N_p [B_o + (R_p - R_s) B_g]$$

$$E_o = (B_o - B_{oi}) + (R_{si} - R_s) B_g$$

$\bar{p}_r$ (psi)	F (MMbbl)	E_o (bbl/STB)	Δp (psi)	$E_{f,w}$ (bbl/STB)	$N = F/$ $(E_o + E_{f,w})$ (MMSTB)
7150	–	–	0	0	–
6600	14.20672	0.0170	550	0.00772	574.7102
5800	40.49800	0.0530	1350	0.018949	562.8741
4950	66.55527	0.0870	2200	0.030879	564.6057
4500	80.42505	0.1070	2650	0.037195	557.752
4350	97.21516	0.133219	2800	0.09301	563.5015
4060	129.1315	0.184880	3090	0.043371	565.7429
3840	158.9420	0.231853	3310	0.046459	571.0827
3600	185.3966	0.273672	3550	0.048986	574.5924
3480	220.9165	0.324712	3670	0.051512	587.1939
3260	259.1963	0.399885	3890	0.054600	570.3076
3100	294.5662	0.459540	4050	0.056846	570.4382
2940	331.7239	0.526928	4210	0.059092	566.0629
2800	368.6921	0.590210	4350	0.061057	566.1154
Average					570.0000

It should be pointed out that as the reservoir pressures continues to decline below the bubble point and with increasing volume of the liberated gas, it reaches the time when the saturation of the liberated gas exceeds the critical gas saturation and, as a result, the gas will start to be produced in disproportionate quantities compared to the oil. At this stage of depletion, there is little that can be done to avert this situation during the primary production phase. As indicated earlier, the primary recovery from these types of reservoirs seldom exceeds 30%. However, under very favorable conditions, the oil and gas might separate with the gas moving structurally updip in the reservoir that might lead to preservation of the natural energy of the reservoir with a consequent improvement in overall oil recovery. Water injection is traditionally used by the oil industry to maintain the pressure above the bubble point pressure or alternatively to pressurize the reservoir to the bubble point pressure. In such type of reservoirs, as the reservoir pressure drops below the bubble point pressure, some volume of the liberated gas will remain in the reservoir as a free gas. This volume, as expressed in scf, is given by Equation 4.4.7 as:

$$[\text{volume of the free gas in scf}] = NR_{si} - (N - N_p)R_s - N_p R_p$$

However, the total volume of the liberated gas at any depletion pressure is given by:

$$\begin{bmatrix} \text{total volume of the} \\ \text{liberated gas, in scf} \end{bmatrix} = NR_{si} - (N - N_p) R_s$$

Therefore, the fraction of the total solution gas that has been retained in the reservoir as a free gas, α_g, at any depletion stage is then given by:

$$\alpha_g = \frac{NR_{si} - (N - N_p)R_s - N_p R_p}{NR_{si} - (N - N_p)R_s}$$

$$= 1 - \left[\frac{N_p R_p}{NR_{si} - (N - N_p)R_s} \right]$$

Alternatively, this can be expressed as a fraction of the total initial gas-in-solution, by:

$$\alpha_{gi} = \frac{NR_{si} - (N - N_p)R_s - N_p R_p}{NR_{si}}$$

$$= 1 - \left[\frac{(N - N_p)R_s + N_p R_p}{NR_{si}} \right]$$

The calculation of the changes in the fluid saturations with declining reservoir pressure is an integral part of using the MBE. The remaining volume of each phase can be determined by calculating different phase saturation, recalling:

$$\text{Oil saturation } S_o = \frac{\text{oil volume}}{\text{pore volume}}$$

$$\text{Water saturation } S_w = \frac{\text{water volume}}{\text{pore volume}}$$

$$\text{Gas saturation } S_g = \frac{\text{gas volume}}{\text{pore volume}}$$

and:

$$S_o + S_w + S_g = 1.0$$

If we consider a volumetric saturated oil reservoir that contains N stock-tank barrels of oil at the initial reservoir

pressure p_i, i.e., p_b, the initial oil saturation at the bubble point pressure is given by:

$$S_{oi} = 1 - S_{wi}$$

From the definition of oil saturation:

$$\frac{\text{oil volume}}{\text{pore volume}} = \frac{NB_{oi}}{\text{pore volume}} = 1 - S_{wi}$$

or:

$$\text{pore volume} = \frac{NB_{oi}}{1 - S_{wi}}$$

If the reservoir has produced N_p stock-tank barrels of oil, the remaining oil volume is given by:

$$\text{Remaining oil volume} = (N - N_p)B_o$$

This indicates that for a volumetric-type oil reservoir, the oil saturation at any depletion state below the bubble point pressure can be represented by:

$$S_o = \frac{\text{oil volume}}{\text{pore volume}} = \frac{(N - N_p)B_o}{\left(\dfrac{NB_{oi}}{1 - S_{wi}}\right)}$$

Rearranging:

$$S_o = (1 - S_{wi})\left(1 - \frac{N_p}{N}\right)\frac{B_o}{B_{oi}}$$

As the solution gas evolves from the oil with declining reservoir pressure, the gas saturation (assuming constant water saturation S_{wi}) is simply given by:

$$S_g = 1 - S_{wi} - S_o$$

or:

$$S_g = 1 - S_{wi} - \left[(1 - S_{wi})\left(1 - \frac{N_p}{N}\right)\frac{B_o}{B_{oi}}\right]$$

Simplifying:

$$S_g = (1 - S_{wi})\left[1 - \left(1 - \frac{N_p}{N}\right)\frac{B_o}{B_{oi}}\right]$$

Another important function of the MBE is history matching the production–pressure data of individual wells. Once the reservoir pressure declines below the bubble point pressure, it is essential to perform the following tasks:

- Generate, the pseudo-relative permeability ratio k_{rg}/k_{ro} for the entire reservoir or for individual wells drainage area.
- Assess the solution gas driving efficiency.
- Examine the field gas–oil ratio as compared to the laboratory solution gas solubility R_s to define the bubble point pressure and critical gas saturation.

The instantaneous gas–oil ratio (GOR), as discussed in detail in Chapter 5, is given by:

$$\text{GOR} = \frac{Q_g}{Q_o} = R_s + \left(\frac{k_{rg}}{k_{ro}}\right)\left(\frac{\mu_o B_o}{\mu_g B_g}\right)$$

This can be arranged to solve for the relative permeability ratio k_{rg}/k_{ro} to give:

$$\left(\frac{k_{rg}}{k_{ro}}\right) = (\text{GOR} - R_s)\left(\frac{\mu_g B_g}{\mu_o B_o}\right)$$

One of the most practical applications of the MBE is its ability to generate the field relative permeability ratio as a function of gas saturation that can be used to adjust the laboratory core relative permeability data. *The main advantage of the field-or well-generated relative permeability ratio is that it incorporates some of the complexities of reservoir heterogeneity and degree of segregation of the oil and the evolved gas.*

It should be noted that the laboratory relative permeability data applies to an *unsegregated* reservoir, i.e., no change in fluid saturation with height. The laboratory relative permeability is most suitable for applications with the zero-dimensional tank model. For reservoirs with complete gravity segregation, it is possible to generate a pseudo-relative permeability ratio k_{rg}/k_{ro}. A complete segregation means that the upper part of the reservoir contains gas and immobile oil, i.e., residual oil S_{or}, while the lower part contains oil and immobile gas that exists at it critical saturation S_{gc}. Vertical communication implies that as the gas evolves in the lower region, any gas with saturation above S_{gc} moves rapidly upward and leaves that region, while in the upper region any oil above S_{or} drains downward and moves into the lower region. On the basis of these assumption, Poston (1987) proposed the following two relationships:

$$\frac{k_{rg}}{k_{ro}} = \frac{(S_g - S_{gc})(k_{rg})_{or}}{(S_o - S_{or})(k_{ro})_{gc}}$$

$$k_{ro} = \left[\frac{S_o - S_{or}(k_{rg})_{or}}{1 - S_w - S_{gc} - S_{or}}\right](k_{ro})_{gc}$$

where:

$(k_{ro})_{gc}$ = relative permeability to oil at critical gas saturation

$(k_{go})_{or}$ = relative permeability to gas at residual oil saturation

If the reservoir is initially undersaturated, i.e., $p_i > p_b$, the reservoir pressure will continue to decline with production until it eventually reaches the bubble point pressure. It is recommended that the material calculations should be performed in two stages: first from p_i to p_b and second from p_b to different depletion pressures p. As the pressure declines from p_i to p_b, the following changes will occur as a result:

- Based on the water compressibility c_w, the connate water will expand with a resulting increase in the connate water saturation (providing that there is no water production).
- Based on the formation compressibility c_f, a reduction (compaction) in the entire reservoir pore volume.

Therefore, there are several volumetric calculations that must be performed to reflect the reservoir condition at the bubble point pressure. These calculations are based on defining the following parameters:

- Initial oil-in-place at p_i, N_i, with *initial* oil and water saturations of $S_{oi}^{\backslash}$ and $S_{woi}^{\backslash}$.
- Cumulative oil produced at the bubble point pressure N_{pb}.
- Oil remaining at the bubble point pressure, i.e., *initial* oil at the bubble point:

$$N_b = N_i - N_{pb}$$

- Total pore volume at the bubble point pressure, $(PV)_b$:

$$(PV)_b = \text{remaining oil volume} + \text{connate water volume}$$

$$+ \text{connate water expansion}$$

$$- \text{reduction in PV due to compaction}$$

$$(PV)_b = (N_i - N_{pb})B_{ob} + \left[\frac{N_i B_{oi}}{1 - S_{wi}^{\backslash}}\right]S_{wi}^{\backslash}$$

$$+ \left[\frac{N_i B_{oi}}{1 - S_{wi}}\right](p_i - p_b)(-c_f + c_w S_{wi}^{\backslash})$$

Simplifying:

$$(PV)_b = (N_i - N_{pb})B_{ob} + \left[\frac{N_i B_{oi}}{1 - S_{wi}^{\backslash}} \right]$$

$$\times \left[S_{wi}^{\backslash} + (p_i - p_b)(-c_f + c_w S_{wi}^{\backslash}) \right]$$

- Initial oil and water saturations *at the bubble point pressure*, i.e., S_{oi} and S_{wi} are:

$$S_{oi} = \frac{(N_i - N_{pb})B_{ob}}{(PV)_b}$$

$$= \frac{(N_i - N_{pb})B_{ob}}{(N_i - N_{pb})B_{ob} + \left[\dfrac{N_i B_{oi}}{1 - S_{wi}^{\backslash}} \right] [S_{wi}^{\backslash} + (p_i - p_b)(-c_f + c_w S_{wi}^{\backslash})]}$$

$$S_{wi} =$$

$$\frac{\left[\dfrac{N_i B_{oi}}{1 - S_{wi}^{\backslash}} \right] [S_{wi}^{\backslash} + (p_i - p_b)(-c_f + c_w S_{wi}^{\backslash})]}{(N_i - N_{pb})B_{ob} + \left[\dfrac{N_i B_{oi}}{1 - S_{wi}^{\backslash}} \right] [S_{wi}^{\backslash} + (p_i - p_b)(-c_f + c_w S_{wi}^{\backslash})]}$$

$$= 1 - S_{oi}$$

- Oil saturation S_o at any pressure below p_b is given by: ·

$$S_o = \frac{(N_i - N_p)B_o}{(PV)_b}$$

$$= \frac{(N_i - N_p)B_o}{(N_i - N_{pb})B_{ob} + \left[\dfrac{N_i B_{oi}}{1 - S_{wi}^{\backslash}} \right] [S_{wi}^{\backslash} + (p_i - p_b)(-c_f + c_w S_{wi}^{\backslash})]}$$

Gas saturation S_g at any pressure below p_b, assuming no water production, is given by:

$$S_g = 1 - S_o - S_{wi}$$

where:

N_i = initial oil-in-place at p_i, i.e., $p_i > p_b$, STB
N_b = initial oil-in-place at the bubble point pressure, STB
N_{pb} = cumulative oil produced at the bubble point pressure, STB

$S_{oi}^{\backslash}$ = oil saturation at p_i, $p_i > p_b$
S_{oi} = initial oil saturation at p_b
$S_{wi}^{\backslash}$ = water saturation at p_i, $p_i > p_b$
S_{wi} = initial water saturation at p_b

It is very convenient also to qualitatively represent the fluid production graphically by employing the concept of the bubble map. The bubble map essentially illustrates the growing size of the drainage area of a production well. The drainage area of each well is represented by a circle with an oil bubble radius r_{ob} of:

$$r_{ob} = \sqrt{\frac{5.615 N_p}{\pi \phi h \left(\frac{1 - S_{wi}}{B_{oi}} - \frac{S_o}{B_o} \right)}}$$

This expression is based on the assumption that the saturation is evenly distributed throughout a homogeneous drainage area, where:

r_{ob} = oil bubble radius, ft
N_p = well current cumulative oil production, bbl
S_o = current oil saturation

Similarly, the growing bubble of the reservoir free gas can be described graphically by calculating gas bubble radius r_{gb} as:

$$r_{gb} = \sqrt{\frac{5.615 \left[NR_{si} - (N - N_p) R_s - N_p R_p \right] B_g}{\pi \phi h (1 - S_o - S_{wi})}}$$

where:

r_{gb} = gas bubble radius, ft
N_p = well current cumulative oil production, bbl
B_g = current gas formation volume factor, bbl/scf
S_o = current oil saturation

Example 4.5 In addition to the data given in Example 4.4 for the chalk reservoir, the oil–gas viscosity ratios a function of pressure are included with the *PVT* data as shown below:

p (psia)	Q_o (STB/day)	Q_g (MMscf/day)	B_o (bbl/STB)	R_s (scf/STB)	B_g (bbl/scf)	μ_o/μ_g	N_p (MMSTB)	R_p (scf/STB)
7150	–	–	1.743	1450	–	–	0	1450
6600	44 230	64.110	1.760	1450	–	–	8.072	1450
5800	79 326	115.616	1.796	1450	–	–	22.549	1455
4950	75 726	110.192	1.830	1450	–	–	36.369	1455
4500	–	–	1.850	1450	–	5.60	43.473	1447
4350	70 208	134.685	1.775	1323	0.000797	6.02	49.182	1576
4060	50 416	147.414	1.670	1143	0.000840	7.24	58.383	1788
3840	35 227	135.282	1.611	1037	0.000881	8.17	64.812	1992
3600	26 027	115.277	1.566	958	0.000916	9.35	69.562	2158
3480	27 452	151.167	1.523	882	0.000959	9.95	74.572	2383
3260	20 975	141.326	1.474	791	0.001015	11.1	78.400	2596
3100	15 753	125.107	1.440	734	0.001065	11.9	81.275	2785
2940	14 268	116.970	1.409	682	0.001121	12.8	83.879	2953
2800	13 819	111.792	1.382	637	0.001170	13.5	86.401	3103

Using the given pressure–production history of the field, estimate the following:

- Percentage of the liberated solution gas retained in the reservoir as the pressure declines below the bubble point pressure. Express the retained gas volume as a percentage of the total gas liberated α_g and also of total initial gas-in-solution α_{gi}.
- Oil and gas saturations.
- Relative permeability ratio k_{rg}/k_{ro}.

Solution

Step 1. Tabulate the values of α_g and α_{gi} as calculated from:

$$\alpha_g = 1 - \left[\frac{N_p R_p}{N R_{si} - (N - N_p) R_s} \right]$$

$$= 1 - \left[\frac{N_p R_p}{570(1450) - (570 - N_p) R_s} \right]$$

$$\alpha_{gi} = 1 - \left[\frac{(N - N_p) R_s + N_p R_p}{N R_{si}} \right]$$

$$= 1 - \left[\frac{(570 - N_p) R_s + N_p R_p}{570(1450)} \right]$$

That is:

p (psia)	R_s (scf/STB)	N_p (MMSTB)	R_p (scf/STB)	α_g (%)	α_{gi} (%)
7150	1450	0	1450	0.00	0.00
6600	1450	8.072	1450	0.00	0.00
5800	1450	22.549	1455	0.00	0.00
4950	1450	36.369	1455	0.00	0.00
4500	1450	43.473	1447	0.00	0.00
4350	1323	49.182	1576	43.6	7.25
4060	1143	58.383	1788	56.8	16.6
3840	1037	64.812	1992	57.3	21.0
3600	958	69.562	2158	56.7	23.8
3480	882	74.572	2383	54.4	25.6
3260	791	78.400	2596	53.5	28.3
3100	734	81.275	2785	51.6	29.2
2940	682	83.879	2953	50.0	29.9
2800	637	86.401	3103	48.3	30.3

Step 2. Calculate the PV at the bubble point pressure from:

$$(\text{PV})_b = (N_i - N_{pb}) B_{ob} + \left[\frac{N_i B_{oi}}{1 - S'_{wi}} \right]$$

$$\times [S'_{wi} + (p_i - p_b)(-c_f + c_w S'_{wi})]$$

$$= (570 - 43.473)1.85 + \left[\frac{570(1.743)}{1 - 0.43} \right]$$

$$\times [0.43 + (7150 - 4500)(-3.3 \times 10^{-6}$$

$$+ 3.0 \times 10^{-6}(0.43))]$$

$$= 1.71 \times 10^9 \text{ bbl}$$

Step 3. Calculate the initial oil and water saturations at the bubble point pressure:

$$S_{oi} = \frac{(N_i - N_{pb}) B_{ob}}{(\text{PV})_b}$$

$$= \frac{(570 - 43.473)10^6(1.85)}{1.71 \times 10^9} = 0.568$$

$$S_{wi} = 1 - S_{oi} = 0.432$$

Step 4. Calculate the oil and gas saturations as a function of pressure below p_b:

$$S_o = \frac{(N_i - N_p) B_o}{(\text{PV})_b}$$

$$= \frac{(570 - N_p)10^6 B_o}{1.71 \times 10^9}$$

Gas saturation S_g at any pressure below p_b is given by:

$$S_g = 1 - S_o - 0.432$$

p (psia)	N_p (MMSTB)	S_o (%)	S_g (%)
4500	43.473	56.8	0.00
4350	49.182	53.9	2.89
4060	58.383	49.8	6.98
3840	64.812	47.5	9.35
3600	69.562	45.7	11.1
3480	74.572	44.0	12.8
3260	78.400	42.3	14.6
3100	81.275	41.1	15.8
2940	83.879	40.0	16.9
2800	86.401	39.0	17.8

Step 5. Calculate the gas–oil ratio as function of pressure $p < p_b$:

$$\text{GOR} = \frac{Q_g}{Q_o}$$

p (psia)	Q_o (STB/day)	Q_g (MMscf/day)	$\text{GOR} = Q_g/Q_o$ (scf/STB)
4500	–	–	1450
4350	70 208	134.685	1918
4060	50 416	147.414	2923
3840	35 227	135.282	3840
3600	26 027	115.277	4429
3480	27 452	151.167	5506
3260	20 975	141.326	6737
3100	15 753	125.107	7942
2940	14 268	116.970	8198
2800	13 819	111.792	8090

Step 6. Calculate the relative permeability ratio k_{rg}/k_{ro}:

$$\left(\frac{k_{rg}}{k_{ro}} \right) = (\text{GOR} - R_s) \left(\frac{\mu_g B_g}{\mu_o B_o} \right)$$

p (psi)	N_p (MMSTB)	S_o (%)	S_g (%)	R_s (scf/STB)	μ_o/μ_g	B_o (bbl/STB)	B_g (bbl/scf)	GOR = Q_g/Q_o (scf/STB)	k_{rg}/k_{ro}
4500	43.473	56.8	0.00	1450	5.60	1.850	–	1450	–
4350	49.182	53.9	2.89	1323	6.02	1.775	0.000797	1918	0.0444
4060	58.383	49.8	6.98	1143	7.24	1.670	0.000840	2923	0.1237
3840	64.812	47.5	9.35	1037	8.17	1.611	0.000881	3840	0.1877
3600	69.562	45.7	11.1	958	9.35	1.566	0.000916	4429	0.21715
3480	74.572	44.0	12.8	882	9.95	1.523	0.000959	5506	0.29266
3260	78.400	42.3	14.6	791	11.1	1.474	0.001015	6737	0.36982
3100	81.275	41.1	15.8	734	11.9	1.440	0.001065	7942	0.44744
2940	83.879	40.0	16.9	682	12.8	1.409	0.001121	8198	0.46807
2800	86.401	39.0	17.8	637	13.5	1.382	0.001170	8090	0.46585

If the laboratory relative permeability data is available, the following procedure is recommended for generating the field relative permeability data:

(1) Use as much past reservoir production and pressure history as possible to calculate relative permeability ratio k_{rg}/k_{ro} vs. S_o, as shown in Example 4.5.
(2) Plot the permeability ratio k_{rg}/k_{ro} versus liquid saturation S_L, i.e., $S_L = S_o + S_{wc}$, on semilog paper.
(3) Plot the lab relative permeability data on the same graph prepared in step 2. Extend the field-calculated permeability data parallel to the lab data.
(4) Extrapolated field data from step 3 is considered the relative permeability characteristics of the reservoir and should be used in predicting the future reservoir performance.

It should be pointed out that it is a characteristic of most solution gas drive reservoirs that only a fraction of the oil-in-place is recoverable by primary depletion methods. However, the liberated solution gas can move much more freely than the oil through the reservoir. The displacement of the oil by the expanding liberated gas is essentially the main driving mechanism in these types of reservoirs. In general, it is possible to estimate the amount of gas that will be recovered during the primary depletion method, which can provide us with an estimate of an *end point*, i.e., maximum, on the oil recovery performance curve. A log–log plot of the cumulative gas (on the *y* axis) versus cumulative oil (on the *x* axis) *provides the recovery trend of the hydrocarbon recovery*. The generated curve can be extrapolated to the total gas available, e.g., (NR_{si}), and to read the upper limit on oil recovery at abandonment.

Example 4.6 Using the data given in Example 4.5, estimate the oil recovery factor and cumulative oil production after producing 50% of the solution gas.

Solution

Step 1. Using in-place values from Example 4.5 and from the definition of the recovery factor, construct the following table:

Oil-in place	$N = 570$ MMSTB
Gas-in-solution	$G = NR_{si} = 570 \times 1450$
	$= 826.5$ MMMscf
Cum. gas produced	$G_p = N_p R_p$
Oil recovery factor	$RF = N_p/N$
Gas recovery factor	$RF = G_p/G$

Months	p (psia)	N_p (MMSTB)	R_p (scf/STB)	$G_p = N_p R_p$ (MMMscf)	Oil RF (%)	Gas RF (%)
0	7150	0	1450	0	0	0
6	6600	8.072	1450	11.70	1.416	1.411
12	5800	22.549	1455	32.80	4.956	3.956
18	4950	36.369	1455	52.92	6.385	6.380
21	4500	43.473	1447	62.91	7.627	7.585
24	4350	49.182	1576	77.51	8.528	9.346
30	4060	58.383	1788	104.39	10.242	12.587
36	3840	64.812	1992	129.11	11.371	15.567
42	3600	69.562	2158	150.11	12.204	18.100
48	3480	74.572	2383	177.71	13.083	21.427
54	3260	78.400	2596	203.53	13.754	24.540
60	3100	81.275	2785	226.35	14.259	27.292
66	2940	83.879	2953	247.69	14.716	29.866
72	2800	86.401	3103	268.10	15.158	32.327

Step 2. From the log–log plot of N_p vs. G_p and the Cartesian plot of oil recovery factor versus gas recover factor, as shown in Figures 4.19 and 4.20:

Oil recovery factor $= 17\%$

Cumulative oil $N_p = 0.17 \times 570 = 96.9$ MMSTB

Cumulative gas $G_p = 0.50 \times 826.5$
$= 413.25$ MMMscf

4.4.3 Case 3: Gas cap drive reservoirs
For a reservoir in which the expansion of the gas cap gas is the predominant driving mechanism, the effect of water and pore compressibilities as a contributing driving mechanism can be considered negligible as compared to that of the high compressibility of the gas. However, Havlena and Odeh (1963, 1964) acknowledged that whenever a gas cap is present or its size is to be determined, an exceptional degree of accuracy of pressure data is required. The specific problem with reservoir pressure is that the underlying oil zone in a gas cap drive reservoir exists initially near its bubble point pressure. Therefore, the flowing pressures are obviously below the bubble point pressure, which exacerbates the difficulty in conventional pressure buildup interpretation to determine average reservoir pressure.

Assuming that there is no natural water influx or it is negligible (i.e., $W_e = 0$), the Havlena and Odeh material balance can be expressed as:

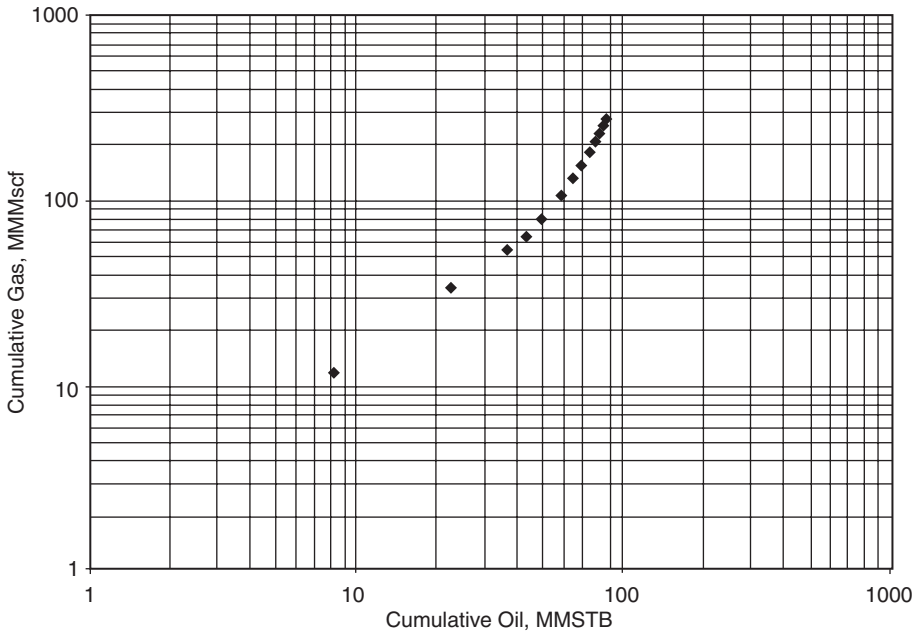$$F = N[E_o + mE_g] \qquad [4.4.16]$$
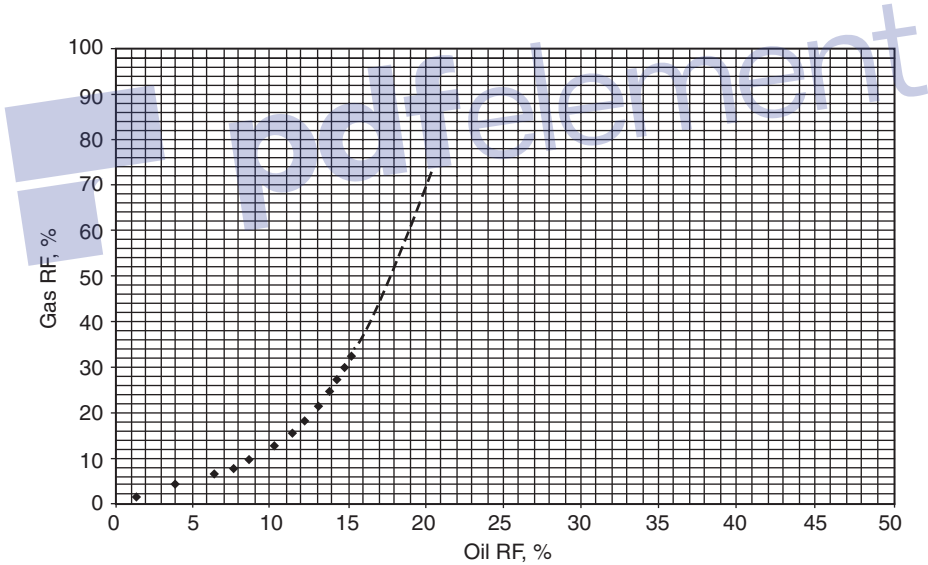
Figure 4.19 G_p vs. N_p, Example 4.6.

Figure 4.20 Gas recovery factor versus oil recovery factor.

in which the variables F, E_o, and E_g are given by:

$$F = N_p[B_o + (R_p - R_s)B_g] + W_pB_w$$

$$= N_p[B_t + (R_p - R_{si})B_g] + W_pB_w$$

$$E_o = (B_o - B_{oi}) + (R_{si} - R_s)B_g$$

$$= B_t - B_{ti}$$

$$E_g = B_{oi}[(B_g/B_{gi}) - 1]$$

The methodology in which Equation 4.4.16 can be used depends on the number of unknowns in the equation. There are three possible unknowns in Equation 4.4.16. These are:

(1) N is unknown, m is known;
(2) m is unknown, N is known;
(3) N and m are unknown.

The practical use of Equation 4.4.16 in determining the three possible unknowns is presented below.

Unknown N, known m   Equation 4.4.16 indicates that a plot of F versus $(E_o + mE_g)$ on a Cartesian scale would produce a
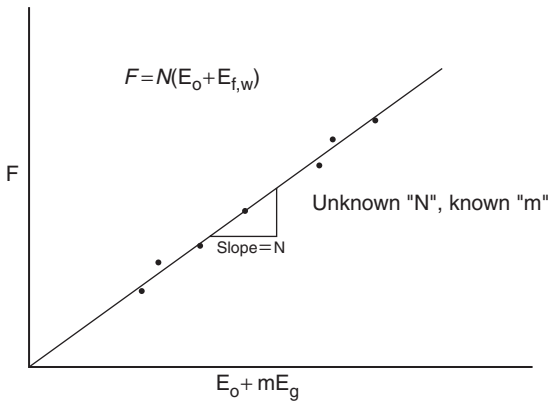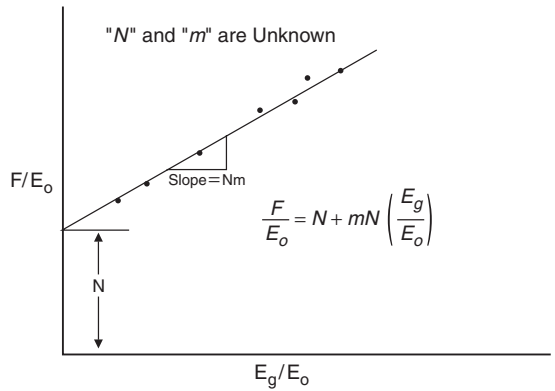
Figure 4.21 F vs. $E_o + mE_g$.

Figure 4.23 F/E_o vs. E_g/E_o.

straight line through the origin with a slope of N, as shown in Figure 4.21. In making the plot, the underground withdrawal F can be calculated at various times as a function of the production terms N_p and R_p.

Conclusion $N = $ slope

Unknown m, known N   Equation 4.4.16 can be rearranged as an equation of straight line, to give:

$$\left(\frac{F}{N} - E_o \right) = mE_g \qquad [4.4.17]$$

This relationship shows that a plot of the term $(F/N - E_o)$ vs. E_g would produce a straight line with a slope of m. One advantage of this particular arrangement is that the straight line must pass through the origin which, therefore, acts as a control point. Figure 4.22 shows an illustration of such a plot.

Conclusion $m = $ slope

Also Equation 4.4.16 can be rearranged to solve for m, to give:

$$m = \frac{F - NE_o}{NE_g}$$

This relationship shows that a plot of the term $(F/N - E_o)$ vs. E_g would produce a straight line with a slope of m. One advantage of this particular arrangement is that the straight line must pass through the origin
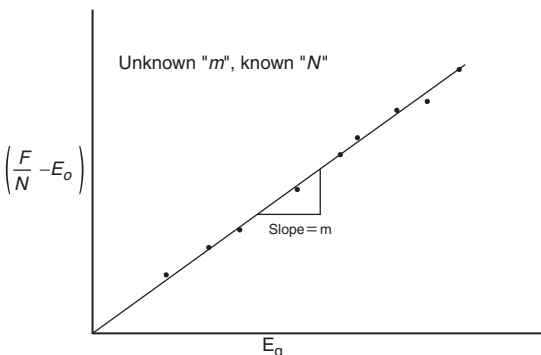

Figure 4.22 $(F/N - E_o)$ vs. E_g.

N and m are unknown   If there is uncertainty in both the values of N and m, Equation 4.4.16 can be re-expressed as:

$$\frac{F}{E_o} = N + mN \left(\frac{E_g}{E_o} \right) \qquad [4.4.18]$$

A plot of F/E_o versus E_g/E_o should then be linear with intercept N and slope mN. This plot is illustrated in Figure 4.23.

Conclusions $N = $ intercept
$mN = $ slope
$m = $ slope/intercept $= $ slope/N

Example 4.7   Reliable volumetric calculations on a well-developed gas cap drive reserve show the flowing results:

$N = 736$ MMSTB,	$G = 320$ Bscf
$p_i = 2808$ psia,	$B_{oi} = 1.39$ bbl/STB
$B_{gi} = 0.000919$ bbl/STB,	$R_{si} = 755$ scf/STB

The production history in terms of parameter F and the *PVT* data are given below:

$\bar{p}$ (psi)	F (MMbbl)	B_t (bbl/STB)	B_g (bbl/scf)
2803	7.8928	1.3904	0.0009209
2802	7.8911	1.3905	0.0009213
2801	7.8894	1.3906	0.0009217
2800	7.8877	1.3907	0.0009220
2799	7.8860	1.3907	0.0009224
2798	7.8843	1.3908	0.0009228

Estimate the gas–oil volume ratio m and compare with the calculated value

Solution

Step 1. Calculate the actual m from the results of the volumetric calculation:

$$m = \frac{GB_{gi}}{NB_{oi}} = \frac{(3200 \times 10^9)(0.000919)}{(736 \times 10^6)(1.390)} \approx 2.9$$

Step 2. Using the production data, calculate E_o, E_g, and m

$$E_o = B_t - B_{ti}$$

$$E_g = B_{ti}[(B_g/B_{gi}) - 1]$$

$$m = \frac{F - NE_o}{NE_g}$$

$\bar{p}$ (psi)	F (MMbbl)	E_o (bbl/STB)	E_g (bbl/scf)	$m = (F - NE_o)/NE_g$
2803	7.8928	0.000442	0.002874	3.58
2802	7.8911	0.000511	0.003479	2.93
2801	7.8894	0.000581	0.004084	2.48
2800	7.8877	0.000650	0.004538	2.22
2799	7.8860	0.000721	0.005143	1.94
2798	7.8843	0.000791	0.005748	1.73

The above tabulated results appear to confirm the volumetric m value of 2.9; however, the results also show the sensitivity of the m value to the reported average reservoir pressure.

Example 4.8 The production history and the *PVT* data of a gas cap drive reservoir are given below:

Date	$\bar{p}$ (psi)	N_p (MSTB)	G_p (Mscf)	B_t (bbl/STB)	B_g (bbl/scf)
5/1/89	4415	–	–	1.6291	0.00077
1/1/91	3875	492.5	751.3	1.6839	0.00079
1/1/92	3315	1015.7	2409.6	1.7835	0.00087
1/1/93	2845	1322.5	3901.6	1.9110	0.00099

The initial gas solubility R_{si} is 975 scf/STB. Estimate the initial oil-and gas-in-place.

Solution

Step 1. Calculate the cumulative produced gas–oil ratio R_p

$\bar{p}$	G_p (Mscf)	N_p (MSTB)	$R_p = G_p/N_p$ (scf/STB)
4415	–	–	–
3875	751.3	492.5	1525
3315	2409.6	1015.7	2372
2845	3901.6	1322.5	2950

Step 2. Calculate F, E_o, and E_g from:

$$F = N_p[B_t + (R_p - R_{si})B_g] + W_p B_w$$

$$E_o = B_t - B_{ti}$$

$$E_g = B_{ti}[(B_g/B_{gi}) - 1]$$

$\bar{p}$	F	E_o	E_g
3875	2.04×10^6	0.0548	0.0529
3315	8.77×10^6	0.1540	0.2220
2845	17.05×10^6	0.2820	0.4720

Step 3. Calculate F/E_o and E_g/E_o:

$\bar{p}$	F/E_o	E_g/E_o
3875	3.72×10^7	0.96
3315	5.69×10^7	0.44
2845	6.00×10^7	0.67

Step 4. Plot F/E_o vs. E_g/E_o as shown in Figure 4.24, to give:

$$\text{Intercept} = N = 9 \text{ MMSTB}$$

$$\text{Slope} = Nm = 3.1 \times 10^7$$
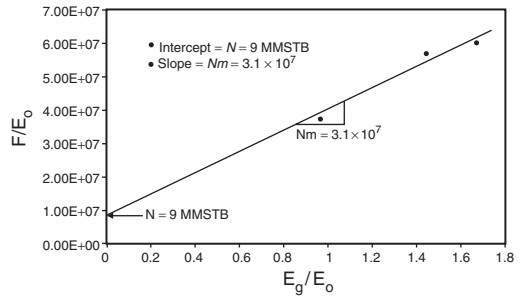
Figure 4.24 Calculation of m and N for Example 4.8.

Step 5. Calculate m:

$$m = 3.1 \times 10^7/(9 \times 10^6) = 3.44$$

Step 6. Calculate the initial gas cap gas volume G from the definition of m:

$$m = \frac{GB_{gi}}{NB_{oi}}$$

or:

$$G = \frac{mNB_{oi}}{B_{gi}} = \frac{(3.44)(9 \times 10^6)(1.6291)}{0.00077}$$

$$= 66 \text{ MMMscf}$$

4.4.4 Case 4: Water drive reservoirs

In a water drive reservoir, identifying the type of the aquifer and characterizing its properties are perhaps the most challenging tasks involved in conducting a reservoir engineering study. Yet, without an accurate description of the aquifer, future reservoir performance and management cannot be properly evaluated.

The full MBE can be expressed again as:

$$F = N(E_o + mE_g + E_{f,w}) + W_e$$

Dake (1978) pointed out that the term $E_{f,w}$ can frequently be neglected in water drive reservoirs. This is not only for the usual reason that the water and pore compressibilities are small, but also because a water influx helps to maintain the reservoir pressure and, therefore, the Δp appearing in the $E_{f,w}$ term is reduced, or:

$$F = N(E_o + mE_g) + W_e \qquad [4.4.19]$$

If, in addition, the reservoir has an initial gas cap, then Equation 4.4.18 can be further reduced to:

$$F = NE_o + W_e \qquad [4.4.20]$$

In attempting to use the above two equations to match the production and pressure history of a reservoir, the greatest uncertainty is always the determination of the water influx W_e. In fact, in order to calculate the water influx the engineer is confronted with what is inherently the greatest uncertainty in the whole subject of reservoir engineering. The reason is that the calculation of W_e requires a mathematical model which itself relies on knowledge of aquifer properties. These, however, are seldom measured since wells are not deliberately drilled into the aquifer to obtain such information.

For a water drive reservoir with no gas cap, Equation 4.4.20 can be rearranged and expressed as:

$$\frac{F}{E_o} = N + \frac{W_e}{E_o} \qquad [4.4.21]$$

Several water influx models have been described in Chapter 2, including:

- the pot aquifer model;
- the Schilthuis steady-state method;
- the van Everdingen and Hurst model.

The use of these models in connection with Equation 4.4.21 to simultaneously determine N and W_e is described below.

Pot aquifer model in the MBE
Assume that the water influx could be properly described by using the simple pot aquifer model as described by Equation 2.3.3, as:

$$W_e = (c_w + c_f) W_i f (p_i - p) \qquad [4.4.22]$$

$$f = \frac{(\text{encroachment angle})^{\circ}}{360^{\circ}} = \frac{\theta}{360^{\circ}}$$

$$W_i = \left[\frac{\pi \left(r_a^2 - r_e^2 \right) h\phi}{5.615} \right]$$

where:

r_a = radius of the aquifer, ft
r_e = radius of the reservoir, ft
h = thickness of the aquifer, ft
ϕ = porosity of the aquifer
θ = encroachment angle
c_w = aquifer water compressibility, psi^{-1}
c_f = aquifer rock compressibility, psi^{-1}
W_i = initial volume of water in the aquifer, bbl

Since the ability to use Equation 4.4.22 relies on knowledge of the aquifer properties, i.e., c_w, c_f, h, r_a, and θ, these properties could be combined and treated as one unknown K in Equation 4.4.22, or:

$$W_e = K \Delta p \qquad [4.4.23]$$

where the water influx constant K represents the combined pot aquifer properties as:

$$K = (c_w + c_f) W_i f$$

Combining Equation 4.4.23 with 4.4.21 gives:

$$\frac{F}{E_o} = N + K \left(\frac{\Delta p}{E_o} \right) \qquad [4.4.24]$$

Equation 4.4.24 indicates that a plot of the term F/E_o as a function of $\Delta p/E_o$ would yield a straight line with an intercept of N and slope of K, as illustrated in Figure 4.25.
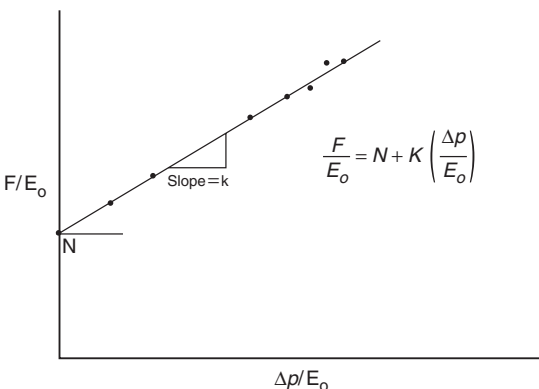
If a gas gap with a known value of m exists, Equation 4.4.19 can be expressed in the following linear form:

$$\frac{F}{E_o + mE_g} = N + K \left(\frac{\Delta p}{E_o + mE_g} \right)$$

This form indicates that a plot of the term $F/(E_o + mE_g)$ as a function of $\Delta p/(E_o + mE_g)$ would yield a straight line with an intercept of N and slope of K.

The Steady-State Model in the MBE
The steady-state aquifer model as proposed by Schilthuis (1936) is given by:

$$W_e = C \int_0^t (p_i - p) \, dt \qquad [4.4.25]$$

where:

W_e = cumulative water influx, bbl
C = water influx constant, bbl/day/psi
t = time, days
p_i = initial reservoir pressure, psi
p = pressure at the oil–water contact at time t, psi

Combining Equation 4.4.25 with 4.4.21 gives:

$$\frac{F}{E_o} = N + C \left(\frac{\int_0^t (p_i - p) \, dt}{E_o} \right) \qquad [4.4.26]$$

Plotting F/E_o vs. $\int_0^t (p_i - p) \, dt/E_o$ results in a straight line with an intercept that represents the initial oil-in-place N and a slope that describes the water influx constant C as shown in Figure 4.26.

And for a known gas gap; Equation 4.4.26 can be expressed in the following linear form:

$$\frac{F}{E_o + mE_g} = N + C \left(\frac{\int_0^t (p_i - p) \, dt}{E_o + mE_g} \right)$$

Plotting $F/(E_o + mE_g)$ vs. $\int_0^t (p_i - p) dt/(E_o + mE_g)$ results in a straight line with an intercept that represents the initial oil-in-place N and a slope that describes the water influx constant C.

The unsteady-state model in the MBE
The van Everdingen and Hurst unsteady-state model is given by:

$$W_e = B \Sigma \Delta p W_{eD} \qquad [4.4.27]$$

with:

$$B = 1.119 \phi c_t r_e^2 hf$$
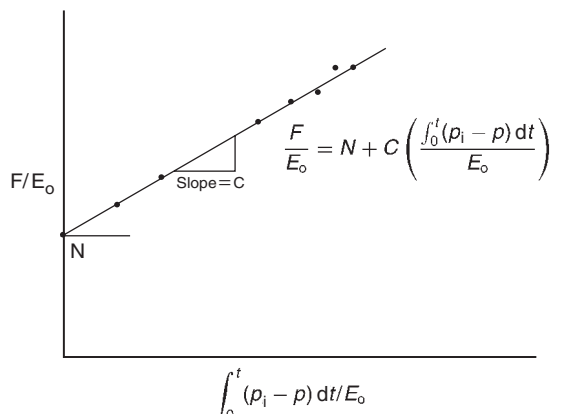

Figure 4.25 F/E_o vs. $\Delta p/E_o$.

Figure 4.26 Graphical determination of N and c.

Van Everdingen and Hurst presented the dimensionless water influx W_{eD} as a function of the dimensionless time t_D and dimensionless radius r_D that are given by:

$$t_D = 6.328 \times 10^{-3} \frac{kt}{\phi \mu_w c_t r_e^2}$$

$$r_D = \frac{r_a}{r_e}$$

$$c_t = c_w + c_f$$

where:

t = time, days
k = permeability of the *aquifer*, md
ϕ = porosity of the *aquifer*
μ_w = viscosity of water in the *aquifer*, cp
r_a = radius of the *aquifer*, ft
r_e = radius of the reservoir, ft
c_w = compressibility of the water, psi^{-1}

Combining Equation 4.4.27 with 4.4.21 gives:

$$\frac{F}{E_o} = N + B \left(\frac{\sum \Delta p W_{eD}}{E_o} \right) \qquad [4.4.28]$$

The proper methodology of solving the above linear relationship is summarized in the following steps.

Step 1. From the field past production and pressure history, calculate the underground withdrawal F and oil expansion E_o.
Step 2. Assume an aquifer configuration, i.e., linear or radial.
Step 3. Assume the aquifer radius r_a and calculate the dimensionless radius r_D.
Step 4. Plot F/E_o vs. $(\sum \Delta p W_{eD})/E_o$ on a Cartesian scale. If the assumed aquifer parameters are correct, the plot will be a straight line with N being the intercept and the water influx constant B being the slope. It should be noted that four other different plots might result. These are:

  (1) Complete random scatter of the individual points, which indicates that the calculation and/or the basic data are in error.
  (2) A systematically upward-curved line, which suggests that the assumed aquifer radius (or dimensionless radius) is too small.
  (3) A systematically downward-curved the indicating that the selected aquifer radius (or dimensionless radius) is too large.
  (4) An S-shaped curve indicates that a better fit could be obtained if a linear water influx is assumed.

Figure 4.27 shows a schematic illustration of the Havlena and Odeh methodology in determining the aquifer fitting parameters.

It should be noted that in many large fields, an infinite linear water drive satisfactorily describes the production–pressure behavior. For a Unit pressure drop, the cumulative water influx in an infinite linear case is simply proportional to $\sqrt{t}$ and does not require the estimation of the dimensionless time t_D. Thus, the Van Everdingen and Hurst dimensionless water influx W_{eD} in Equation 4.4.27 is replaced by the square root of time, to give:

$$W_w = B \sum \left[\Delta p_n \sqrt{(t - t_n)} \right]$$

Therefor, the linear form of the MBE can be expressed as:

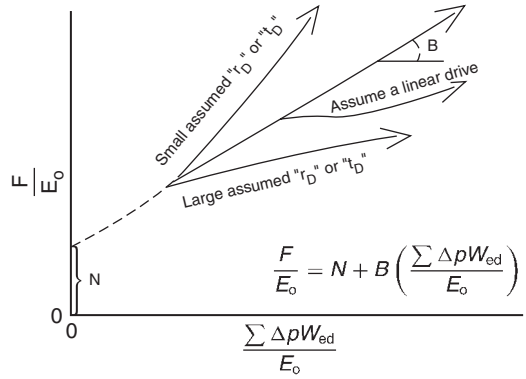$$\frac{F}{E_o} = N + B \left(\frac{\sum \Delta p_n \sqrt{t - t_n}}{E_o} \right)$$

Figure 4.27 Havlena and Odeh straight-line plot (After: Havlena and ODeh, 1963).

Example 4.9 The material balance parameters, the underground withdrawal F, and the oil expansion E_o of a saturated oil reservoir (i.e., $m = 0$) are given below:

$\bar{p}$	F	E_o
3500	–	–
3488	2.04×10^6	0.0548
3162	8.77×10^6	0.1540
2782	17.05×10^6	0.2820

Assuming that the rock and water compressibilities are negligible, calculate the initial oil-in-place.

Solution

Step 1. The most important step in applying the MBE is to verify that no water influx exists. Assuming that the reservoir is volumetric, calculate the initial oil-in-place N by using every individual production data point in Equation 4.4.15, or:

$$N = F/E_o$$

F	E_o	$N = F/E_o$
2.04×10^6	0.0548	37 MMSTB
8.77×10^6	0.1540	57 MMSTB
17.05×10^6	0.2820	60 MMSTB

Step 2. The above calculations show that the calculated values of the initial oil-in-place are increasing, as shown graphically in Figure 4.28, which indicates a water encroachment, i.e., water drive reservoir.
Step 3. For simplicity, select the pot aquifer model to represent the water encroachment calculations in the MBE as given by Equation 4.4.24, or:

$$\frac{F}{E_o} = N + K \left(\frac{\Delta p}{E_o} \right)$$

Step 4. Calculate the terms F/E_o and $\Delta p/E_o$ of Equation 4.4.24:

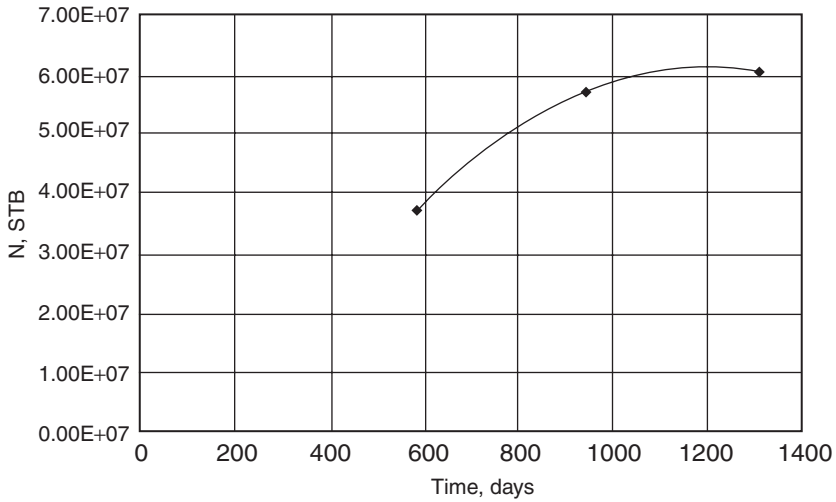| $\bar{p}$	Δp	F	E_o	F/E_o	$\Delta p/E_o$
3500	0	–	–	–	–
3488	12	2.04×10^6	0.0548	37.23×10^6	219.0
3162	338	8.77×10^6	0.1540	56.95×10^6	2194.8
2782	718	17.05×10^6	0.2820	60.46×10^6	2546

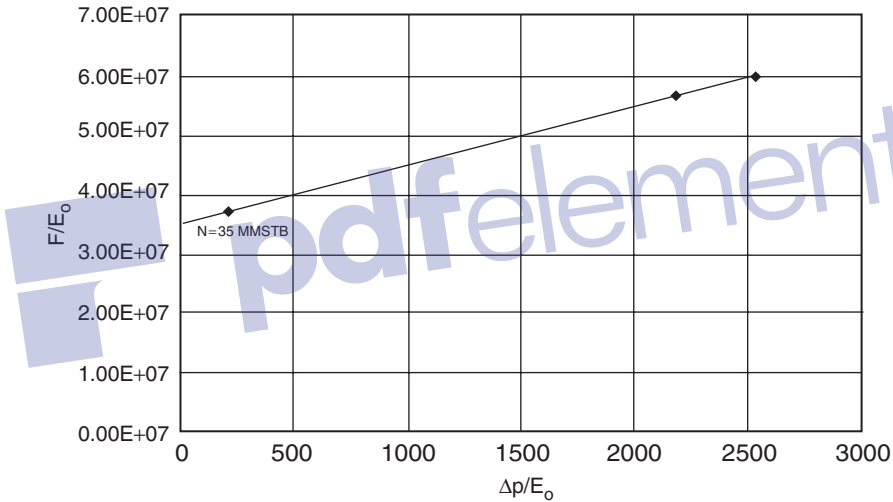**Figure 4.28** *Indication of water influx.*

Figure 4.29 *F/E_o vs. $\Delta p/E_o$.*

Step 5. Plot F/E_o vs. $\Delta p/E_o$, as shown in Figure 4.29 and determine the intercept and the slope:

$$\text{Intercept} = N = 35 \text{ MMSTB}$$

$$\text{Slope} = K = 9983$$

4.4.5 Case 5: Combination drive reservoirs

This relatively complicated case involves the determination of the following three unknowns:

(1) initial oil-in-place N;
(2) size of the gas cap m;
(3) Water influx W_e.

The general MBE that includes the above three unknown is given by Equation 4.4.9 as:

$$F = N(E_o + mE_g) + W_e$$

where the variables constituting the above expression are defined by:

$$F = N_p[B_o + (R_p - R_s)B_g] + W_p B_w$$
$$= N_p[B_t + (R_p - R_{si})B_g] + W_p B_w$$
$$E_o = (B_o - B_{oi}) + (R_{si} - R_s)B_g$$
$$= B_t - B_{ti}$$
$$E_g = B_{oi}[(B_g/B_{gi}) - 1]$$

Havlena and Odeh differentiated Equation 4.4.9 with respect to pressure and rearranged the resulting equation to eliminate m, to give:

$$\frac{FE_g^\backslash - F^\backslash E_g}{E_o E_g^\backslash - E_o^\backslash E_g} = N + \frac{W_e E_g^\backslash - W_e^\backslash E_g}{E_o E_g^\backslash - E_o^\backslash E_g} \qquad [4.4.29]$$

in which the reversed primes denote derivatives with respect to pressure. That is:

$$E_g^\backslash = \frac{\partial E_g}{\partial p} = \left(\frac{B_{oi}}{B_{gi}}\right)\frac{\partial B_g}{\partial p} \approx \left(\frac{B_{oi}}{B_{gi}}\right)\frac{\Delta B_g}{\Delta p}$$

$$E_o^\backslash = \frac{\partial E_o}{\partial p} = \frac{\partial B_t}{\partial p} \approx \frac{\Delta B_t}{\Delta p}$$

$$F^\backslash = \frac{\partial F}{\partial p} \approx \frac{\Delta F}{\Delta p}$$

$$W_e^\backslash = \frac{\partial W_e}{\partial p} \approx \frac{\Delta W_e}{\Delta p}$$

A plot of the left-hand side of Equation 4.4.29 versus the second term on the right for a selected aquifer model should, if the choice is correct, provide a straight line with unit slope whose intercept on the ordinate gives the initial oil-in-place N. After having correctly determined N and W_e, Equation 4.4.9 can be solved directly for m, to give:

$$m = \frac{F - NE_o - W_e}{NE_g}$$

Note that all the above derivatives can be evaluated numerically using one of the finite difference techniques; e.g., forward, backward, or central difference formula.

4.4.6 Case 6: Average reservoir pressure

To gain any understanding of the behavior of a reservoir with free gas, e.g., solution gas drive or gas cap drive, it is essential that every effort be made to determine reservoir pressures with accuracy. In the absence of reliable pressure data, the MBE can be used to estimate average reservoir pressure if accurate values of m and N are available from volumetric calculations. The general MBE is given by Equation 4.4.16 as:

$$F = N\left[E_o + mE_g\right]$$

Solving Equation 4.4.16 for the average pressure using the production history of the field involves the following graphical procedure:

Step 1. Select the time at which the average reservoir pressure is to be determined and obtain the corresponding production data, i.e., N_p, G_p, and R_p.

Step 2. Assume several average reservoir pressure values and determine the left-hand side F of Equation 4.4.16 at each assumed pressure. That is:

$$F = N_p[B_o + (R_p - R_s)B_g] + W_pB_w$$

Step 3. Using the same assumed average reservoir pressure values of step 2, calculate the right-hand side (RHS) of Equation 4.4.16:

$$\text{RHS} = N[E_o + mE_g]$$

where:

$$E_o = (B_o - B_{oi}) + (R_{si} - R_s)B_g$$
$$E_g = B_{oi}[(B_g/B_{gi}) - 1]$$

Step 4. Plot the left- and right-hand sides of the MBE, as calculated in steps 2 and 3, on Cartesian paper as a function of assumed average pressure. The point of intersection gives the average reservoir pressure that corresponds to the selected time of step 1. An illustration of the graph is shown in Figure 4.30.

Step 5. Repeat steps 1 through 4 to estimate reservoir pressure at each selected depletion time.

4.5 Tracy's Form of the MBE

Neglecting the formation and water compressibilities, the general MBE as expressed by Equation 4.3.13 can be reduced to the following:

$$N = \frac{N_pB_o + (G_p - N_pR_s)B_g - (W_e - W_pB_w)}{(B_o - B_{oi}) + (R_{si} - R_s)B_g + mB_{oi}\left[\dfrac{B_g}{B_{gi}} - 1\right]} \quad [4.5.1]$$

Tracy (1955) suggested that the above relationship can be rearranged into a more usable form as:

$$N = N_p\Phi_o + G_p\Phi_g + (W_pB_w - W_e)\Phi_w \quad [4.5.2]$$

Where Φ_o, Φ_g, and Φ_w are considered *PVT*-related properties that are functions of pressure and defined by:

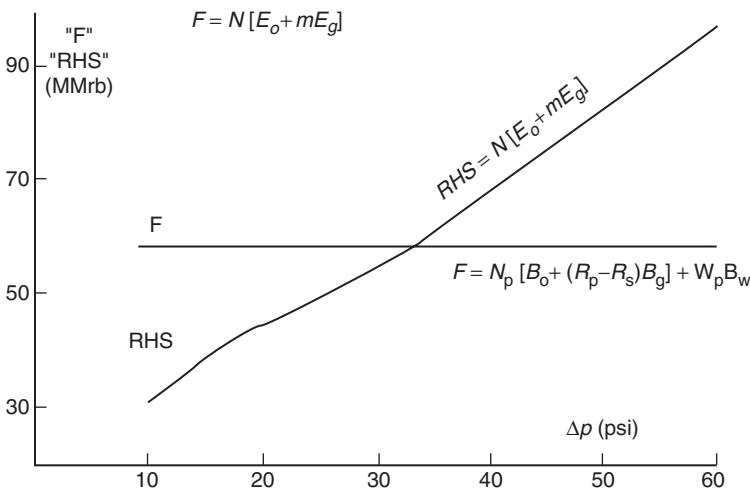$$\Phi_o = \frac{B_o - R_sB_g}{\text{Den}} \quad [4.5.3]$$

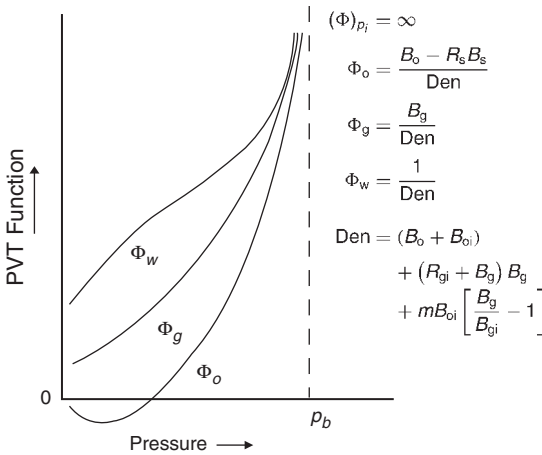**Figure 4.30** *Solution of the material balance for the pressure.*

Figure 4.31   *Tracy's PVT functions.*

$$\Phi_g = \frac{B_g}{\text{Den}} \qquad [4.5.4]$$

$$\Phi_w = \frac{1}{\text{Den}} \qquad [4.5.5]$$

with:

$$\text{Den} = (B_o - B_{oi}) + (R_{si} - R_s) B_g + m B_{oi} \left[\frac{B_g}{B_{gi}} - 1 \right] \qquad [4.5.6]$$

where:

Φ_o = oil *PVT* function
Φ_g = gas *PVT* function
Φ_w = water *PVT* function

Figure 4.31 shows a graphical presentation of the behavior of Tracy's *PVT* functions with changing pressure.

Note that Φ_o is negative at low pressures and all Φ functions are approaching infinity at bubble point pressure because the value of the denominator "Den" in Equations 4.5.3 through 4.5.5 approaches zero. Tracy's form is valid only for initial pressures equal to the bubble point pressure, and cannot be used at pressures above the bubble point. Furthermore, shapes of the Φ function curves illustrate that small errors in pressure and/or production can cause large errors in calculated oil-in-place at pressures near the bubble point. However, Steffensen (1987) pointed out that Tracy's equation uses the oil formation volume factor at the bubble point pressure B_{ob} for the initial B_{oi} which causes all the *PVT* functions Φ to become infinity at the bubble point pressure. Steffensen suggested that Tracy's equation could be extended for applications above the bubble point pressure, i.e., for undersaturated oil reservoirs, by simply using the value of B_o at the initial reservoir pressure. He concluded that Tracy's methodology could predict reservoir performance for the entire pressure range from any initial pressure down to abandonment.

It should be pointed out that because the rock and water compressibility are relatively unimportant below the bubblepoint pressure; they were not included in Tracy's material balance formulation. They can be included indirectly, however, by the use of pseudovalues of the oil formation volume factor at pressures below the initial pressure.

These pseudovalues, B_o^*, given by:

$$B_o^* = B_o + B_{oi} \left(\frac{S_w c_w + c_f}{1 - S_w} \right) (p_i - p)$$

These pesudovalues include the additional pressure support of water and rock compressibilities in the material balance computations.

$$g_{\text{gas}} < \frac{\text{d}p}{\text{d}z} < g_{\text{oil}}$$

with:

$$g_{\text{gas}} = \frac{\rho_g}{144}$$

$$g_{\text{oil}} = \frac{\rho_o}{144}$$

where:

g_{oil} = oil gradient, psi/ft
ρ_o = oil density; lb/ft^3
g_{gas} = gas gradient, psi/ft
ρ_g = gas density; lb/ft^3
$\text{d}p/\text{d}z$ = reservoir pressure gradient, psi/ft

The following example is given by Tracy (1955) to illustrate his proposed approach.

Example 4.10   The production history of a saturated oil reservoir is as follows:

$\bar{p}$ (psia)	N_p (MSTB)	G_p (MMscf)
1690	0	0
1600	398	38.6
1500	1570	155.8
1100	4470	803

The calculated values of the *PVT* functions are given below:

p	Φ_o	Φ_g
1600	36.60	0.4000
1500	14.30	0.1790
1100	2.10	0.0508

Calculate the oil-in-place N.

Solution   The calculations can be conveniently performed in following tabulated form using:

$$N = N_p \Phi_o + G_p \Phi_g + 0$$

$\bar{p}$ (psia)	N_p (MSTB)	G_p (MMscf)	$(N_p \Phi_o)$	$(G_p \Phi_g)$	N (STB)
1600	398	38.6	14.52×10^6	15.42×10^6	29.74×10^6
1500	155.8	155.8	22.45×10^6	27.85×10^6	50.30×10^6
1100	803.0	803.0	9.39×10^6	40.79×10^6	50.18×10^6

The above results show that the original oil in place in this reservoir is approximately 50 MMSTB of oil. The calculation at 1600 psia is a good example of the sensitivity of such a calculation near the bubble point pressure. Since the last two values of the original oil-in-place agree so well, the first calculation is probably wrong.

Problems

1. You have the following data on an oil reservoir:

	Oil	Aquifer
Geometry	circular	semicircular
Encroachment angle	–	180°
Radius, ft	4000	80 000
Flow regime	semisteady state	unsteady state
Porosity	–	0.20
Thickness, ft	–	30
Permeability, md	200	50
Viscosity, cp	1.2	0.36
Original pressure	3800	3800
Current pressure	3600	–
Original volume factor	1.300	1.04
Current volume factor	1.303	1.04
Bubble point pressure	3000	–

The field has been on production for 1120 days, and has produced 800 000 STB of oil and 60 000 STB of water. Water and formation compressibilities are estimated to be 3×10^{-6} and 3×10^{-6} psi^{-1}, respectively.
Calculate the original oil-in-place.

2. The following rock and fluid properties data is available on the Nameless Field:

Reservoir area = 1000 acres, porosity = 10%
thickness = 20 ft, $T = 140°F$
$s_{wi} = 20\%$, $p_i = 4000$ psi
$p_b = 4000$ psi

The gas compressibility factor and relative permeability ratio are given by the following expressions:

$$Z = 0.8 - 0.00002(p - 4000)$$

$$\frac{k_{rg}}{k_{ro}} = 0.00127 \exp(17.269 S_g)$$

The production history of the field is given below:

	4000 psi	3500 psi	3000 psi
μ_o, cp	1.3	1.25	1.2
μ_g, cp	–	0.0125	0.0120
B_o, bbl/STB	1.4	1.35	1.30
R_s, scf/STB	–	–	450
GOR, scf/STB	600	–	1573

Subsurface information indicates that there is no aquifer and there has been no water production.
Calculate:

(a) the remaining oil-in-place at 3000 psi;
(b) the cumulative gas produced at 3000 psi.

3. The following *PVT* and production history data is available on an oil reservoir in West Texas.

Original oil-in-place = 10 MMSTB

Initial water saturation = 22%

Initial reservoir pressure = 2496 psia

Bubble point pressure = 2496 psi

Pressure (psi)	B_o (bbl/STB)	R_s (scf/STB)	B_g (bbl/scf)	μ_o (cp)	μ_g (cp)	GOR (scf/STB)
2496	1.325	650	0.000796	0.906	0.016	650
1498	1.250	486	0.001335	1.373	0.015	1360
1302	1.233	450	0.001616	1.437	0.014	2080

The cumulative gas–oil ratio at 1302 psi is recorded at 953 scf/STB. Calculate:

(a) the oil saturation at 1302 psia;
(b) the volume of the free gas in the reservoir at 1302 psia;
(c) the relative permeability ratio (k_g/k_o) at 1302 psia.

4. The Nameless field is an undersaturated oil reservoir. The crude oil system and rock type indicate-that the reservoir is *highly compressible*. The available reservoir and production data is given below:

$S_{wi} = 0.25$, $\phi = 20\%$,
area = 1000 acres, $h = 70$ ft,
$T = 150°F$, Bubble point pressure = 3500 psia

	Original conditions	Current conditions
Pressure, psi	5000	4500
B_o, bbl/STB	1.905	1.920
R_s, scf/STB	700	700
N_p, MSTB	0	610.9

Calculate the cumulative oil production at 3900 psi. The *PVT* data shows that the oil formation volume factor is equal to 1.938 bbl/STB at 3900 psia.

5. The following data[b] is available on a gas cap drive reservoir:

Pressure (psi)	N_p (MMSTB)	R_p (scf/STB)	B_o (RB/STB)	R_s (scf/STB)	B_g (RB/scf)
3330			1.2511	510	0.00087
3150	3.295	1050	1.2353	477	0.00092
3000	5.903	1060	1.2222	450	0.00096
2850	8.852	1160	1.2122	425	0.00101
2700	11.503	1235	1.2022	401	0.00107
2550	14.513	1265	1.1922	375	0.00113
2400	17.730	1300	1.1822	352	0.00120

Calculate the initial oil and free gas volumes.

6. If 1 million STB of oil have been produced from the Calgary Reservoir at a cumulative produced GOR of 2700 scf/STB, causing the reservoir pressure to drop from the initial reservoir pressure of 400 psia to 2400 psia, what is the initial stock-tank oil-in-place?

7. The following data is taken from an oil field that had no original gas cap and no water drive:

Oil pore volume of reservoir = 75 MM ft^3
Solubility of gas in crude = 0.42 scf/STB/psi
Initial bottom-hole pressure = 3500 psia
Bottom-hole temperature = 140°F
Bubble point pressure of the reservoir = 3000 psia
Formation volume factor at 3500 psia = 1.333 bbl/STB

[b] *Fundamental of Reservoir Engineering, Elsevier Publishing Co.*, Amsterdam, 1978.

Compressibility factor of the gas at 1000 psia and 140°F = 0.95

Oil produced when pressure is 2000 psia = 1.0 MMSTB

Net cumulative produced GOR = 2800 scf/STB

(a) Calculate the initial STB of oil in the reservoir.
(b) Calculate the initial scf of gas in the reservoir.
(c) Calculate the initial dissolved GOR of the reservoir.
(d) Calculate the scf of gas remaining in the reservoir at 2000 psia.
(e) Calculate the scf of free gas in the reservoir at 2000 psia.
(f) Calculate the gas volume factor of the escaped gas at 2000 psia at standard conditions of 14.7 psia and 60°F.
(g) Calculate the reservoir volume of the free gas at 2000 psia.
(h) Calculate the total reservoir GOR at 2000 psia.
(i) Calculate the dissolved GOR at 2000 psia.
(j) Calculate the liquid volume factor of the oil at 2000 psia.
(k) Calculate the total, or two-phase, oil volume factor of the oil and its initial complement of dissolved gas at 2000 psia.

8. Production data, along with reservoir and fluid data, for an undersaturated reservoir follows. There was no measureable water produced, and it can be assumed that there was no free gas flow in the reservoir. Determine the following:

(a) The saturations of oil, gas, and water at a reservoir pressure of 2258.
(b) Has water encroachment occurred and, if so, what is the volume?

Gas gravity = 0.78
Reservoir temperature = 160°F
Initial water saturation = 25%
Original oil-in-place = 180 MMSTB
Bubble point pressure = 2819 psia

The following expressions for B_o and R_{so} as functions of pressure were determined from laboratory data:

$$B_o = 1.00 + 0.00015p, \text{ bbl/STB}$$

$$R_{so} = 50 + 0.42p, \text{ scf/STB}$$

Pressure (psia)	Cumulative oil produced (MMSTB)	Cumulative gas produced (MMscf)	Instantaneous GOR (scf/STB)
2819	0	0	1000
2742	4.38	4.380	1280
2639	10.16	10.360	1480
2506	20.09	21.295	2000
2403	27.02	30.260	2500
2258	34.29	41.150	3300

9. The Wildcat Reservoir was discovered in 1970. The reservoir had an initial pressure of 3000 psia and laboratory data indicated a bubble point pressure of 2500 psia. The connate water saturation was 22%. Calculate the fractional recovery, N_p/N, from initial conditions down to a pressure of 2300 psia. State any assumptions which you make relative to the calculations.

Porosity = 0.165

Formation compressibility = 2.5×10^{-6} psia^{-1}

Reservoir temperature = 150°F

Pressure (psia)	B_o (bbl/STB)	R_{so} (scf/STB)	Z	B_g (bbl/scf)	Viscosity ratio μ_o/μ_g
3000	1.315	650	0.745	0.000726	53.91
2500	1.325	650	0.680	0.000796	56.60
2300	1.311	618	0.663	0.000843	61.46

This page intentionally left blank

5 Predicting Oil Reservoir Performance

Contents

Most reservoir engineering calculations involve the use of the material balance equation (MBE). Some of the most useful applications of the MBE require the concurrent use of fluid flow equations, e.g., Darcy's equation. Combining the two concepts would enable the engineer to predict the reservoir future production performance as a function of time. Without the fluid flow concepts, the MBE simply provides performance as a function of the average reservoir pressure. Prediction of the reservoir future performance is ordinarily performed in the following three phases:

Phase 1: The first phase involves the use of the MBE in a predictive mode to estimate cumulative hydrocarbon production and fractional oil recovery as a function of declining reservoir pressure and increasing gas–oil ratio (GOR). These results are incomplete, however, because they give no indication of the time that it will take to recover oil at any depletion stage. In addition, this stage of calculations is performed without considering:

- the actual number of wells;
- the location of wells;
- the production rate of individual wells;
- the time required to deplete the reservoir.

Phase 2: To determine recovery profile as a function of time, it is necessary to generate individual well performance profile with declining reservoir pressure. This phase documents different techniques that are designed to model the production performance of vertical and horizontal wells.

Phase 3: The third stage of prediction is the time–production phase. In these calculations, the reservoir and well performance data is correlated with time. It is necessary in this phase to account for the number of wells and the productivity of individual well.

5.1 Phase 1. Reservoir Performance Prediction Methods

The MBE in its various mathematical forms as presented in Chapter 4 is designed to provide estimates of the initial oil-in-place N, size of the gas cap m, and water influx W_e. To use the MBE to predict the reservoir future performance, two additional relations are required:

(1) the equation of producing (instantaneous) GOR;
(2) the equation for relating saturations to cumulative oil production.

These auxiliary mathematical expressions are presented below.

5.1.1 Instantaneous GOR
The produced GOR at any particular time is the ratio of the standard cubic feet of total gas being produced at any time to the stock-tank barrels of oil being produced at that same instant—hence, the name instantaneous GOR. Equation (1.2.42) in Chapter 1 describes the GOR mathematically by the following expression:
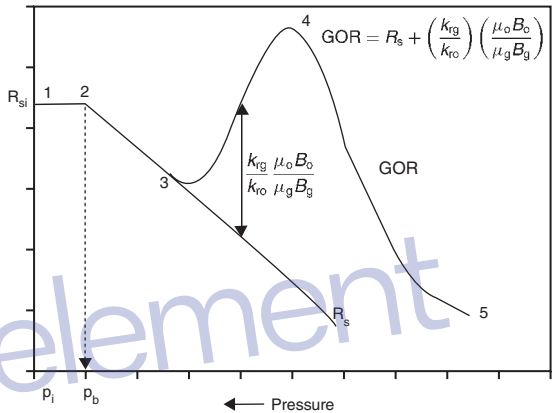
$$GOR = R_s + \left(\frac{k_{rg}}{k_{ro}}\right)\left(\frac{\mu_o B_o}{\mu_g B_g}\right) \qquad [5.1.1]$$

where:

GOR = instantaneous gas–oil ratio, scf/STB
R_s = gas solubility, scf/STB
k_{rg} = relative permeability to gas
k_{ro} = relative permeability to oil
B_o = oil formation volume factor, bbl/STB
B_g = gas formation volume factor, bbl/scf
μ_o = oil viscosity, cp
μ_g = gas viscosity, cp
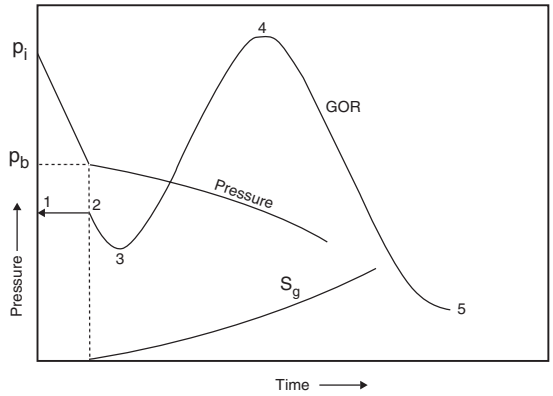
Figure 5.1 *Characteristics of solution gas drive reservoirs.*

Figure 5.2 *History of GOR and R_s for a solution gas drive reservoir.*

The instantaneous GOR equation is of fundamental importance in reservoir analysis. The importance of Equation 5.1.1 can appropriately be discussed in conjunction with Figures 5.1 and 5.2. Those illustrations show the history of the GOR of a hypothetical depletion drive reservoir that is typically characterized by the following points:

Point 1. When the reservoir pressure p is above the bubble point pressure p_b, there is no free gas in the formation, i.e., $k_{rg} = 0$, and therefore:

$$GOR = R_{si} = R_{sb} \qquad [5.1.2]$$

The GOR remains constant at R_{si} until the pressure reaches the bubble point pressure at point 2.

Point 2. As the reservoir pressure declines below p_b, the gas begins to evolve from solution and its saturation increases. However, this free gas cannot flow until the gas saturation S_g reaches the critical gas saturation S_{gc} at point 3. From point 2 to point 3, the instantaneous GOR is described by a decreasing gas solubility, as:

$$GOR = R_s \qquad [5.1.3]$$

Point 3. At this point, the free gas begins to flow with the oil and the values of GOR progressively increase with the declining reservoir pressure to point 4. During this pressure decline period, the GOR is described by Equation 5.1.1, or:

$$GOR = R_s + \left(\frac{k_{rg}}{k_{ro}}\right)\left(\frac{\mu_o B_o}{\mu_g B_g}\right)$$

Point 4. At this point, the maximum GOR is reached due to the fact that the supply of gas has reached a maximum and marks the beginning of the blow-down period to point 5.
Point 5. This point indicates that all the producible free gas has been produced and the GOR is essentially equal to the gas solubility and continues to decline following the R_s curve.

There are three types of GORs, all expressed in scf/STB, which must be clearly distinguished from each other. These are:

- instantaneous GOR (defined by Equation 5.5.1);
- solution GOR, i.e., gas solubility R_s;
- cumulative GOR R_p.

The solution GOR is a *PVT* property of the crude oil system. It is commonly referred to as "gas solubility" and denoted by R_s. It measures the tendency of the gas to dissolve in or evolve from the oil with changing pressures. It should be pointed out that as long as the evolved gas remains immobile, i.e., gas saturation S_g is less than the critical gas saturation, the instantaneous GOR is equal to the gas solubility. That is:

$$\text{GOR} = R_s$$

The cumulative GOR R_p, as defined previously in the MBE, should be clearly distinguished from the producing (instantaneous) GOR. The cumulative GOR is defined as:

$$R_p = \frac{\text{cumulative (total) gas produced}}{\text{cumulative oil produced}}$$

or:

$$R_p = \frac{G_p}{N_p} \qquad [5.1.4]$$

where:

R_p = cumulative GOR, scf/STB
G_p = cumulative gas produced, scf
N_p = cumulative oil produced, STB

The cumulative gas produced G_p is related to the instantaneous GOR and cumulative oil production by the expression:

$$G_p = \int_0^{N_p} (\text{GOR}) dN_p \qquad [5.1.5]$$

Equation 5.1.5 simply indicates that the cumulative gas production at any time is essentially the area under the curve of the GOR vs. N_p relationship, as shown in Figure 5.3.
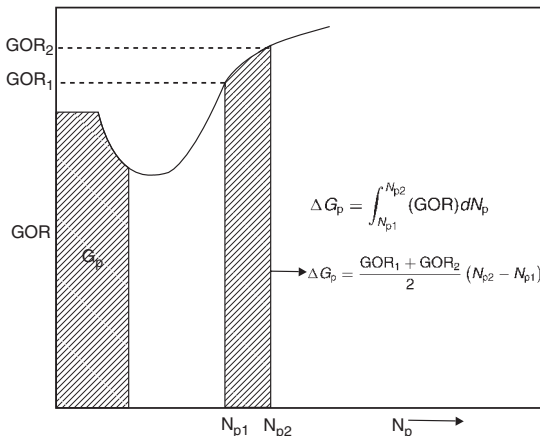

Figure 5.3 *Relationship between GOR and G_p.*

The incremental cumulative gas produced, ΔG_p, between N_{p1} and N_{p2} is then given by:

$$\Delta G_p = \int_{N_{p1}}^{N_{p2}} (\text{GOR}) dN_p \qquad [5.1.6]$$

This integral can be approximated by using the trapezoidal rule, to give:

$$\Delta G_p = \left[\frac{(\text{GOR})_1 + (\text{GOR})_2}{2} \right] (N_{p2} - N_{p1})$$

or:

$$\Delta G_p = (\text{GOR})_{\text{avg}} \Delta N_p$$

Equation 5.1.5 can then be approximated as:

$$G_p = \sum_0 (\text{GOR})_{\text{avg}} \Delta N_p \qquad [5.1.7]$$

Example 5.1 The following production data is available on a depletion drive reservoir:

p (psi)	GOR (scf/STB)	N_p (MMSTB)
	1340	0
2600	1340	1.380
2400	1340	2.260
	1340	3.445
1800	1936	7.240
1500	3584	12.029
1200	6230	15.321

The initial reservoir pressure is 2925 psia with a bubble point pressure of 2100 psia. Calculate cumulative gas produced G_p and cumulative GOR at each pressure.

Solution

Step 1. Construct the following table by applying Equations 5.1.4 and 5.1.7:

$$R_p = \frac{G_p}{N_p}$$

$$\Delta G_p = \left[\frac{(\text{GOR})_1 + (\text{GOR})_2}{2} \right] (N_{p2} - N_{p1}) = (\text{GOR})_{\text{avg}} \Delta N_p$$

$$G_p = \sum_0 (\text{GOR})_{\text{avg}} \Delta N_p$$

p (psi)	GOR (scf/STB)	$(\text{GOR})_{\text{avg}}$ (scf/STB)	N_p (MMSTB)	ΔN_p (MMSTB)	ΔG_p (MMscf)	G_p (MMscf)	R_p (scf/STB)
2925	1340	1340	0	0	0	0	–
2600	1340	1340	1.380	1.380	1849	1849	1340
2400	1340	1340	2.260	0.880	1179	3028	1340
2100	1340	1340	3.445	1.185	1588	4616	1340
1800	1936	1638	7.240	3.795	6216	10 832	1496
1500	3584	2760	12.029	4.789	13 618	24 450	2033
1200	6230	4907	15.321	3.292	16 154	40 604	2650

It should be pointed out that the crude oil PVT properties used in the MBE are appropriate for moderate-low volatility "***black oil***" systems which, when produced at the surface, is separated into oil and solution gas. These properties; as defined mathematically below are designed to relate surface volumes to reservoir volumes and vice versa.

$$R_s = \frac{\begin{array}{c}\text{volume of solution gas dissolved}\\ \text{in the oil at reservoir condition}\end{array}}{\text{volume of the oil at stock} - \text{tank conditions}}$$

$$B_o = \frac{\text{volume of oil at reservoir condition}}{\text{volume of the oil at stock} - \text{tank conditions}}$$

$$B_g = \frac{\text{volume of the free gas at reservoir condition}}{\text{volume of free gas at stock} - \text{tank conditions}}$$

Whitson and Brule (2000) point out that the above three properties constitute the classical (**black oil**) PVT data required for various type of applications of the MBE. However; in formulating the material balance equation; the following assumptions were made when using the black oil PVT data:

(1) Reservoir gas does not yield liquid when brought to the surface
(2) Reservoir oil consists of two surface "components"; stock-tank oil and total surface separator gas
(3) Properties of stock-tank oil in terms of its *API* gravity and surface gas do not change with depletion pressure.
(4) Surface gas released from the reservoir oil has the same properties as the reservoir gas

This situation is more complex when dealing with volatile oils. This type of crude oil systems are characterized by significant hydrocarbon liquid recovery from their produced reservoir gases. As the reservoir pressure drops below the bubblepoint pressure; the evolved solution gas liberated in the reservoir contains enough heavy components to yield appreciable condensate dropout at the separators that is combined with the stock-tank oil. This is in contrast to black oils for which little error is introduced by the assumption that there is negligible hydrocarbon liquid recovery from produced gas. Also, volatile oils evolve gas and develop free-gas saturation in the reservoir more rapidly than normal black oils as pressure declined below the bubblepoint. This causes relatively high GOR's at the wellhead. Thus, performance predictions differ from those discussed for black oils mainly because of the need to account for liquid recovery from the produced gas. Conventional material balances with standard laboratory PVT (black-oil) data *underestimate* oil recovery. The error increases for increasing oil volatility.

Consequently, depletion performance of volatile oil reservoirs below bubblepoint is strongly influenced by the rapid shrinkage of oil and by the large amounts of gas evolved. This results in relatively high gas saturation, high producing GOR's, and low to moderate production of reservoir oil. The produced gas can yield a substantial volume of hydrocarbon liquids in the processing equipment. This liquid recovery at the surface can equal or exceed the volume of stock-tank oil produced from the reservoir liquid phase. Depletion-drive recoveries are often between 15 and 30% of the original oil in place.

For volatile oil reservoir primary-performance prediction methods, the key requirements are correct handling of the oil shrinkage, gas evolution, gas and oil flow in the reservoir, and liquids recovery at the surface. If

Q_o = Black oil flow rate, STB/day
$Q_o^\backslash$ = Total flow rate including condensate, STB/day
R_s = Gas solubility, scf/STB
GOR = Total measured gas-oil ratio, scf/STB
r_s = Condensate yield, STB/scf

Then:

$$Q_o = Q_o^\backslash - (Q_o^\backslash \text{GOR} - Q_o R_s) r_s$$

Solving for Q_o, gives:

$$Q_o = Q_o^\backslash \left[\frac{1 - (r_s \text{GOR})}{1 - (r_s R_s)} \right]$$

The above expression can be used to adjust the cumulative "black oil" production, N_p, to account for the condensate

production. The black oil cumulative production is then calculated from:

$$N_p = \int_0^t Q_o \, dt \approx \sum_0^t (\Delta Q_o \Delta t)$$

The cumulative total gas production "G_p" and the *adjusted* cumulative black oil production "N_p" is used in Equation 5.1.4 to calculate the cumulative gas-oil ratio; i.e.,:

$$R_p = \frac{G_p}{N_p}$$

Whitson, C, and Brule, M: *Phase Behavior*, SPE Monograph Volume 20, Society of Petroleum Engineers, Richardson, Texas, 2000.

5.1.2 The Reservoir Saturation Equations and Their Adjustments

The saturation of a fluid (gas, oil, or water) in the reservoir is defined as the volume of the fluid divided by the pore volume, or:

$$S_o = \frac{\text{oil volume}}{\text{pore volume}} \qquad [5.1.8]$$

$$S_w = \frac{\text{water volume}}{\text{pore volume}} \qquad [5.1.9]$$

$$S_g = \frac{\text{gas volume}}{\text{pore volume}} \qquad [5.1.10]$$

$$S_o + S_w + S_g = 1.0 \qquad [5.1.11]$$

Consider a volumetric oil reservoir with no gas cap that contains N stock-tank barrels of oil at the initial reservoir pressure p_i. Assuming no water influx gives:

$$S_{oi} = 1 - S_{wi}$$

where the subscript i indicates the initial reservoir condition. From the definition of oil saturation:

$$1 - S_{wi} = \frac{NB_{oi}}{\text{pore volume}}$$

or:

$$\text{Pore volume} = \frac{NB_{oi}}{1 - S_{wi}} \qquad [5.1.12]$$

If the reservoir has produced N_p stock-tank barrels of oil, the remaining oil volume is given by:

$$\text{Remaining oil volume} = (N - N_p)B_o \qquad [5.1.13]$$

Substituting Equations 5.1.13 and 5.1.12 into 5.1.8 gives:

$$S_o = \frac{\text{remaining oil volume}}{\text{pore volume}} = \frac{(N - N_p)B_o}{\left(\frac{NB_{oi}}{1 - S_{wi}} \right)} \qquad [5.1.14]$$

or:

$$S_o = \left(1 - S_{wi} \right) \left(1 - \frac{N_p}{N} \right) \frac{B_o}{B_{oi}} \qquad [5.1.15]$$

and therefore:

$$S_g = 1 - S_o - S_{wi} \qquad [5.1.16]$$

Example 5.2 A volumetric solution gas drive reservoir has an initial water saturation of 20%. The initial oil formation volume factor is reported at 1.5 bbl/STB. When 10% of the initial oil was produced, the value of B_o decreased to 1.38. Calculate the oil saturation and gas saturation.

Solution   From Equations 5.1.15 and 5.1.16:

$$S_o = (1 - S_{wi})\left(1 - \frac{N_p}{N}\right)\frac{B_o}{B_{oi}}$$

$$= (1 - 0.2)(1 - 0.1)\left(\frac{1.38}{1.50}\right) = 0.662$$

$$S_g = 1 - S_o - S_{wi}$$

$$= 1 - 0.662 - 0.20 = 0.138$$

It should be pointed out that the values of the relative permeability ratio k_{rg}/k_{ro} as a function of oil saturation can be generated by using the actual field production as expressed in terms of N_p, GOR, and *PVT* data. The recommended methodology involves the following steps:

Step 1. Given the actual field cumulative oil production N_p and the *PVT* data as a function of pressure, calculate the oil and gas saturations from Equations 5.1.15 and 5.1.16:

$$S_o = (1 - S_{wi})\left(1 - \frac{N_p}{N}\right)\frac{B_o}{B_{oi}}$$

$$S_g = 1 - S_o - S_{wi}$$

Step 2. Using the actual field instantaneous GORs, solve Equation 5.1.1 for the relative permeability ratio, as:

$$\frac{k_{rg}}{k_{ro}} = (\text{GOR} - R_s)\left(\frac{\mu_g B_g}{\mu_o B_o}\right)$$

Step 3. The relative permeability ratio is traditionally expressed graphically by plotting k_{rg}/k_{ro} vs. S_o on semilog paper. This is obviously not the case in a gravity drainage reservoir and will result in the calculation of abnormally low oil saturation.

Notice that Equation 5.1.14 suggests that all the remaining oil saturation at any depletion stage is distributed uniformly throughout the reservoir. In dealing with gravity drainage reservoirs, water drive reservoirs, or gas cap drive reservoirs, adjustments must be made to the oil saturation as calculated by Equation 5.1.14 to account for:

• migration of the evolved gas upstructure;
• trapped oil in the water-invaded region;
• trapped oil in the gas cap expansion zone;
• loss of oil saturation in the gas cap shrinkage zone.

Oil saturation adjustment in gravity drainage reservoirs
In these types of reservoirs, the gravity effects result in much lower producing GORs than would be expected from reservoirs producing without the benefit of gravity drainage. This is due to the upstructure migration of the gas and consequent *higher oil saturation* in the vicinity of the completion intervals of the production wells which should be used when calculating the oil relative permeability k_{ro}. The following steps summarize the recommended procedure for adjusting Equation 5.1.14 to reflect the migration of gas to the top of the structure:

Step 1. Calculate the volume of the evolved gas that will migrate to the top of the formation to form the *secondary gas cap* from the following relationship:

$$(\text{gas})_{\text{migrated}} = [NR_{si} - (N - N_p)R_s - N_p R_p]B_g$$

$$- \left[\frac{NB_{oi}}{1 - S_{wi}} - (\text{PV})_{\text{SGC}}\right]S_{gc}$$

where:

$(\text{PV})_{\text{SGC}}$ = pore volume of the secondary gas cap, bbl

S_{gc} = critical gas saturation
B_g = current gas formation volume factor, bbl/scf

Step 2. Recalculate the volume of the evolved gas that will form the secondary gas cap from following relationship:

$$(\text{gas})_{\text{migrated}} = [1 - S_{wi} - S_{org}](\text{PV})_{\text{SGC}}$$

where:

$(\text{PV})_{\text{SGC}}$ = pore volume of the secondary gas cap, bbl
S_{org} = residual oil saturation to gas displacement
S_{wi} = connate or initial water saturation

Step 3. Equating the two derived relationships and solving for secondary gas cap pore volume gives:

$$(\text{PV})_{\text{SGC}} = \frac{[NR_{si} - (N - N_p)R_s - N_p R_p]B_g - \left[\dfrac{NB_{oi}}{1 - S_{wi}}\right]S_{gc}}{(1 - S_{wi} - S_{org} - S_{gc})}$$

Step 4. Adjust Equation 5.1.14 to account for the migration of the evolved gas to the secondary gas cap, to give:

$$S_o = \frac{(N - N_p)B_o - (\text{PV})_{\text{SGC}}S_{org}}{\left(\dfrac{NB_{oi}}{1 - S_{wi}}\right) - (\text{PV})_{\text{SGC}}} \qquad [5.1.17]$$

It should be noted that the oil recovery by gravity drainage involves two fundamental mechanisms:

(1) the formation of the secondary gas cap as presented by Equation 5.1.17
(2) the gravity drainage rate

For an efficient gravity drive mechanism, the gas must flow upstructure while the oil flows downstructure, i.e., both phases are moving in opposite directions; this is called the "counterflow" of oil and gas. Since both fluids are flowing, gas–oil relative permeability characteristics of the formation are very important. Since the gas saturation is not uniform throughout the oil column, the field calculated, k_{rg}/k_{ro}, that is based on the material balance calculations, must be used. For the counterflow to occur, the actual reservoir pressure gradient must be between the static gradient of the oil and gas. That is:

$$\rho_{\text{gas}} < \left(\frac{dp}{dz}\right) < \rho_{\text{oil}}$$

where:

ρ_{oil} = oil gradient, psi/ft
ρ_{gas} = gas gradient, psi/ft
dp/dz = reservoir pressure gradient, psi/ft

Terwilliger et al. (1951) pointed out that oil recovery by gravity segregation is rate sensitive and that a rather sharp decrease in recovery would occur at production rates above the maximum rate of gravity drainage and, hence, production should not exceed this particular maximum rate. The maximum rate of gravity drainage is defined as the "rate at which complete counterflow exists" and mathematically by the following expression:

$$q_o = \frac{7.83 \times 10^{-6}k k_{ro}A(\rho_o - \rho_g)\sin(\alpha)}{\mu_o}$$

where:

q_o = oil production rate, bbl/day
ρ_o = oil density, lb/ft^3
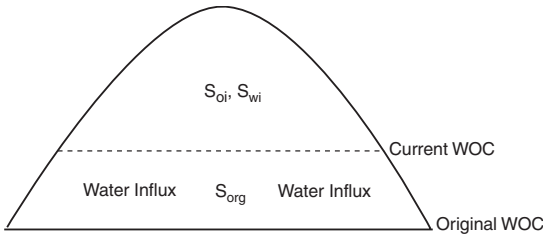
Figure 5.4 *Oil saturation adjustment for water influx.*

ρ_g = gas density, lb/ft^3
A = cross-sectional area open to flow, ft^2
k = absolute permeability, md
α = dip angle

This calculated value of q_o represents the maximum oil rate that should not be exceeded without causing the gas to flow downward.

Oil saturation adjustment due to water influx
The proposed oil saturation adjustment methodology is illustrated in Figure 5.4 and described by the following steps:

Step 1. Calculate the PV in the water-invaded region, as:

$$W_e - W_p B_w = (PV)_{water}(1 - S_{wi} - S_{orw})$$

Solving for the PV of the water-invaded zone, $(PV)_{water}$, gives:

$$(PV)_{water} = \frac{W_e - W_p B_w}{1 - S_{wi} - S_{orw}} \qquad [5.1.18]$$

where:

$(PV)_{water}$ = pore volume in water-invaded zone, bbl
S_{orw} = residual oil saturated in the imbibition water–oil system

Step 2. Calculate the oil volume in the water-invaded zone, or:

$$\text{Volume of oil} = (PV)_{water} S_{orw} \qquad [5.1.19]$$

Step 3. Adjust Equation 5.1.14 to account for the trapped oil by using Equations 5.1.18 and 5.1.19:

$$S_o = \frac{(N - N_p)B_o - \left[\dfrac{W_e - W_p B_w}{1 - S_{wi} - S_{orw}}\right]S_{orw}}{\left(\dfrac{NB_{oi}}{1 - S_{wi}}\right) - \left[\dfrac{W_e - W_p B_w}{1 - S_{wi} - S_{orw}}\right]} \qquad [5.1.20]$$

Oil saturation adjustment due to gas cap expansion
The oil saturation adjustment procedure is illustrated in Figure 5.5 and summarized below:

Step 1. Assuming no gas is produced from the gas cap, calculate the net expansion of the gas cap, from:
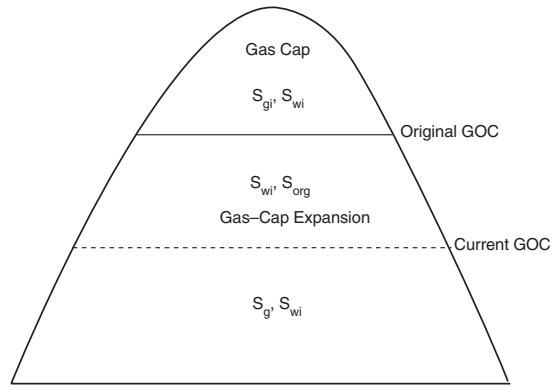
$$\text{Expansion of the gas cap} = mNB_{oi}\left(\frac{B_g}{B_{gi}} - 1\right) \qquad [5.1.21]$$

Step 2. Calculate the PV of the gas-invaded zone, $(PV)_{gas}$, by solving the following simple material balance:

$$mNB_{oi}\left(\frac{B_g}{B_{gi}} - 1\right) = (PV)_{gas}(1 - S_{wi} - S_{org})$$

or:

$$(PV)_{gas} = \frac{mNB_{oi}\left(\dfrac{B_g}{B_{gi}} - 1\right)}{1 - S_{wi} - S_{org}} \qquad [5.1.22]$$

Figure 5.5 *Oil saturation adjustment for gas cap expansion.*

where:

$(PV)_{gas}$ = pore volume of the gas-invaded zone
S_{org} = residual oil saturation in gas–oil system

Step 3. Calculate the volume of oil in the gas-invaded zone.

$$\text{Oil volume} = (PV)_{gas} S_{org} \qquad [5.1.23]$$

Step 4. Adjust Equation 5.1.14 to account for the trapped oil in the gas expansion zone by using Equations 5.1.22 and 5.1.23, to give:

$$S_o = \frac{(N - N_p)B_o - \left[\dfrac{mNB_{oi}\left(\dfrac{B_g}{B_{gi}} - 1\right)}{1 - S_{wi} - S_{org}}\right]S_{org}}{\left(\dfrac{NB_{oi}}{1 - S_{wi}}\right) - \left[\dfrac{mNB_{oi}}{1 - S_{wi} - S_{org}}\right]\left(\dfrac{B_g}{B_{gi}} - 1\right)} \qquad [5.1.24]$$

Oil saturation adjustment for combination drive
For a combination drive reservoir, i.e., water influx and gas cap, the oil saturation equation as given by Equation 5.1.14 can be adjusted to account for both driving mechanisms, as:

$$S_o = \frac{(N - N_p)B_o - \left[\dfrac{mNB_{oi}\left(\dfrac{B_g}{B_{gi}} - 1\right)S_{org}}{1 - S_{wi} - S_{org}} + \dfrac{(W_e - B_w W_p)S_{orw}}{1 - S_{wi} - S_{orw}}\right]}{\dfrac{NB_{oi}}{1 - S_{wi}} - \left[\dfrac{mNB_{oi}\left(\dfrac{B_g}{B_{gi}} - 1\right)}{1 - S_{wi} - S_{org}} + \dfrac{W_e - W_p B_w}{1 - S_{wi} - S_{orw}}\right]} \qquad [5.1.25]$$

Oil saturation adjustment for shrinking gas cap
The control of the gas cap size is very often a reliable guide to the efficiency of reservoir operations. A shrinking gas cap will cause the loss of a substantial amount of oil, which might otherwise be recovered. Normally, there is little or no oil saturation in the gas cap, and if the oil migrates into the original gas zone there will necessarily be some residual oil saturation remaining in this portion of the gas cap at abandonment. As pointed out by Cole (1961), the magnitude of this loss may be quite large and depends on:

- the area of the gas–oil contact;
- the rate of gas cap shrinkage;
- the relative permeability characteristics;
- the vertical permeability.

A shrinking gas cap can be controlled by either shutting in wells which are producing large quantities of gas cap gas

or returning some of the produced gas back to the gas cap portion of the reservoir. In many cases, the shrinkage cannot be completely eliminated by shutting in wells, as there is a practical limit to the number of wells that can be shut in. The amount of oil lost by the shrinking gas cap can be very well the engineer's most important economic justification for the installation of gas return facilities.

The difference between the original volume of the gas cap and the volume occupied by the gas cap at any subsequent time is a measure of the volume of oil that has migrated into the gas cap. If the size of the original gas cap is mNB_{oi}, then the expansion of the original free gas resulting from reducing the pressure from p_i to p is:

Expansion of the original gas cap $= mNB_{oi}[(B_g/B_{gi}) - 1)]$

where:

mNB_{oi} = original gas cap volume, bbl
B_g = gas formation volume factor, bbl/scf

If the gas cap is shrinking, then the volume of the produced gas must be larger than the gas cap expansion. All of the oil that moves into the gas cap will not be lost, as this oil will also be subject to the various driving mechanisms. Assuming no original oil saturation in the gas zone, the oil that will be lost is essentially the residual oil saturation remaining at abandonment. If the cumulative gas production from the gas cap is G_{pc} scf, the volume of the gas cap shrinkage as expressed in barrels is equal to:

Gas cap shrinkage $= G_{pc}B_g - mNB_{oi}[(B_g/B_{gi}) - 1)$

From the volumetric equation:

$G_{pc}B_g - mNB_{oi}\left[(B_g/B_{gi}) - 1\right] = 7758Ah\phi(1 - S_{wi} - S_{gr})$

where:

A = average cross-sectional area of the gas–oil contact, acres
h = average change in depth of the gas–oil contact, ft
S_{gr} = residual gas saturation in the shrinking zone

The volume of oil lost as a result of oil migration to the gas cap can also be calculated from the volumetric equation as follows:

Oil lost $= 7758Ah\phi S_{org}/B_{oa}$

where:

S_{org} = residual oil saturation in the gas cap shrinking zone
B_{oa} = oil formation volume factor at abandonment

Combining the above relationships and eliminating the term $7758Ah\phi$, gives the following expression for estimating the volume of oil in barrels lost in the gas cap:

Oil lost $= \dfrac{[G_{pc}B_g - mNB_{oi}\left(\dfrac{B_g}{B_{gi}} - 1\right)]S_{org}}{(1 - S_{wi} - S_{gr})B_{oa}}$

where:

G_{pc} = cumulative gas production for the gas cap, scf
B_g = gas formation volume factor, bbl/scf

All the methodologies that have been developed to predict the future reservoir performance are essentially based on employing and combining the above relationships that include:

• the MBE;

• the saturation equations;
• the instantaneous GOR;
• the equation relating the cumulative GOR to the instantaneous GOR.

Using the above information, it is possible to predict the field primary recovery performance with declining reservoir pressure. There are three methodologies that are widely used in the petroleum industry to perform a reservoir study. These are:

(1) the Tracy method;
(2) the Muskat method;
(3) the Tarner method.

All three methods yield essentially the same results when small intervals of pressure or time are used. The methods can be used to predict the performance of a reservoir under any driving mechanism, including:

• solution gas drive;
• gas cap drive;
• water drive;
• combination drive.

The practical use of all the techniques is illustrated in predicting the primary recovery performance of a volumetric solution gas drive reservoir. Using the appropriate saturation equation, e.g., Equation 5.1.20 for a water drive reservoir, any of the available reservoir prediction techniques could be applied to other reservoirs operating under different driving mechanisms.

The following two cases of the solution gas drive reservoir are considered.

(1) undersaturated oil reservoirs;
(2) saturated oil reservoirs.

5.1.3 Undersaturated oil reservoirs

When the reservoir pressure is above the bubble point pressure of the crude oil system, the reservoir is considered as undersaturated. The general material balance is expressed in Chapter 4 by Equation 4.3.15:

$$N = \frac{N_p[B_o + (R_p - R_s)B_g] - (W_e - W_pB_w) - G_{inj}B_{ginj} - W_{inj}B_{wi}}{(B_o - B_{oi}) + (R_{si} - R_s)B_g + mB_{oi}\left[\dfrac{B_g}{B_{gi}} - 1\right] + B_{oi}(1 + m)\left[\dfrac{S_{wi}c_w + c_f}{1 - S_{wi}}\right]\Delta p}$$

where:

S_{org} = residual oil saturation in the gas cap shrinking zone
B_{oa} = oil formation volume factor at abandonment

For a volumetric undersaturated reservoir with no fluid injection, the following conditions are observed:

• $m = 0$;
• $W_e = 0$;
• $R_s = R_{si} = R_p$.

Imposing the above conditions on the MBE reduces the equation to the following simplified form:

$$N = \frac{N_pB_o}{(B_o - B_{oi}) + B_{oi}\left[\dfrac{S_{wi}c_w + c_f}{1 - S_{wi}}\right]\Delta p} \qquad [5.1.26]$$
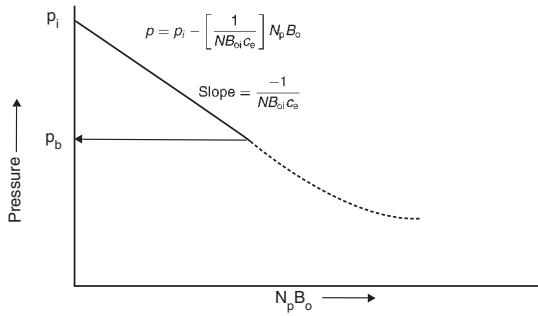
with:

$$\Delta p = p_i - p$$

where:

p_i = initial reservoir pressure
p = current reservoir pressure

Hawkins (1955) introduced the oil compressibility c_o into the MBE to further simplify the equation. The oil

Figure 5.6 *Pressure voidage relationship.*

compressed is defined as:

$$c_o = \frac{1}{B_{oi}} \frac{\partial B_o}{\partial p} \approx \frac{1}{B_{oi}} \frac{B_o - B_{oi}}{\Delta p}$$

Rearranging:

$$B_o - B_{oi} = c_o B_{oi} \Delta p$$

Combining the above expression with Equation 5.1.26 gives:

$$N = \frac{N_p B_o}{c_o B_{oi} \Delta p + B_{oi} \left[\dfrac{S_{wi} c_w + c_f}{1 - S_{wi}} \right] \Delta p} \qquad [5.1.27]$$

The *denominator* of the above equation can be regrouped as:

$$N = \frac{N_p B_o}{B_{oi} \left[c_o + \dfrac{S_{wi} c_w}{1 - S_{wi}} + \dfrac{c_f}{1 - S_{wi}} \right] \Delta p} \qquad [5.1.28]$$

Since there are only two fluids in the reservoir, i.e., oil and water, then:

$$S_{oi} = 1 - S_{wi}$$

Rearranging Equation 5.1.28 to include initial oil saturation gives:

$$N = \frac{N_p B_o}{B_{oi} \left[\dfrac{S_{oi} c_o + S_{wi} c_w + c_f}{1 - S_{wi}} \right] \Delta p}$$

The term in the square brackets is called the effective compressibility and defined by Hawkins (1955) as:

$$c_e = \frac{S_{oi} c_o + S_{wi} c_w + c_f}{1 - S_{wi}} \qquad [5.1.29]$$

Therefore, the MBE above the bubble point pressure becomes:

$$N = \frac{N_p B_o}{B_{oi} c_e \Delta p} \qquad [5.1.30]$$

Equation 5.1.30 can be expressed as the equation of a straight line by:

$$p = p_i - \left[\frac{1}{N B_{oi} c_e} \right] N_p B_o \qquad [5.1.31]$$

Figure 5.6 indicates that the reservoir pressure will decrease linearly with cumulative reservoir voidage $N_p B_o$.

Rearranging Equation 5.1.31 and solving for the cumulative oil production N_p gives:

$$N_p = N c_e \left(\frac{B_o}{B_{oi}} \right) \Delta p \qquad [5.1.32]$$

The calculation of future reservoir production, therefore, does not require a trial-and-error procedure, but can be obtained directly from the above expression.

Example 5.3 The following data is available on a volumetric undersaturated oil reservoir.

$p_i = 4000$ psi, $c_o = 15 \times 10^{-6}$ psi^{-1},

$p_b = 3000$ psi, $c_w = 3 \times 10^{-6}$ psi^{-1}

$N = 85$ MMSTB $S_{wi} = 30\%$,

$c_f = 5 \times 10^{-6}$ psi^{-1}, $B_{oi} = 1.40$ bbl/STB

Estimate cumulative oil production when the reservoir pressure drops to 3500 psi. The oil formation volume factor at 3500 psi is 1.414 bbl/STB.

Solution

Step 1. Determine the effective compressibility from Equation 5.1.29:

$$c_e = \frac{S_{oi} c_o + S_{wi} c_w + c_f}{1 - S_{wi}}$$

$$= \frac{(0.7)(15 \times 10^{-6}) + (0.3)(3 \times 10^{-6}) + 5 \times 10^{-6}}{1 - 0.3}$$

$$= 23.43 \times 10^{-6} \text{ psi}^{-1}$$

Step 2. Estimate N_p from Equation 5.1.32:

$$N_p = N c_e \left(\frac{B_o}{B_{oi}} \right) \Delta p$$

$$= (85 \times 10^6)(23.43 \times 10^{-6}) \left(\frac{1.411}{1.400} \right)(4000 - 3500)$$

$$= 985.18 \text{ MSTB}$$

5.1.4 Saturated oil reservoirs

If the reservoir originally exists at its bubble point pressure, the reservoir is referred to as a saturated oil reservoir. This is considered as the second type of solution gas drive reservoir. As the reservoir pressure declines below the bubble point, the gas begins to evolve from solution. The general MBE may be simplified by assuming that the expansion of the gas is much greater than the expansion of rock and initial water and, therefore, can be neglected. For a volumetric and saturated oil reservoir with no fluid injection, the MBE can be expressed by:

$$N = \frac{N_p B_o + (G_p - N_p R_s) B_g}{(B_o - B_{oi}) + (R_{si} - R_s) B_g} \qquad [5.1.33]$$

This MBE contains two unknowns. These are:

(1) cumulative oil production N_p;
(2) cumulative gas production G_p.

The following reservoir and *PVT* data must be available in order to predict the primary recovery performance of a depletion drive reservoir in terms of N_p and G_p.

Initial oil-in-place N: Generally the volumetric estimate of oil-in-place is used in calculating the performance. However, where there is sufficient solution gas drive history, this estimate may be checked by calculating a material balance estimate.

Hydrocarbon PVT data: Since differential gas liberation is assumed to best represent the conditions in the reservoir, differential laboratory *PVT* data should be used in reservoir material balance. The flash *PVT* data is then used to convert from reservoir conditions to stock-tank conditions.

If laboratory data is not available, reasonable estimates may sometimes be obtained from published correlations. If differential data is not available, the flash data may be used instead; however, this may result in large errors for high-solubility crude oils.

Initial fluid saturations: Initial fluid saturations obtained from a laboratory analysis of core data are preferred; however, if these are not available, estimates in some cases may be obtained from a well log analysis or may be obtained from other reservoirs in the same or similar formations.

Relative permeability data: Generally, laboratory determined k_g/k_o and k_{ro} data is averaged to obtain a single representative set for the reservoir. If laboratory data is not available, estimates in some cases may be obtained from other reservoirs in the same or similar formations.

Where there is sufficient solution gas drive history for the reservoir, calculate k_{rg}/k_{ro} values versus saturation from:

$$S_o = (1 - S_{wi}) \left(1 - \frac{N_p}{N}\right) \frac{B_o}{B_{oi}}$$

$$\frac{k_{rg}}{k_{ro}} = (GOR - R_s) \left(\frac{\mu_g B_g}{\mu_o B_o}\right)$$

The above results should be compared with the averaged laboratory relative permeability data. This may indicate a *needed adjustment* in the early data and possibly an adjustment in the overall data.

All the techniques that are used to predict the future performance of a reservoir are based on combining the appropriate MBE with the instantaneous GOR using the proper saturation equation. The calculations are repeated at a series of assumed reservoir pressure drops. These calculations are usually based on one stock-tank barrel of oil-in-place at the bubble point pressure, i.e., $N = 1$. This avoids dealing with large numbers in the calculation procedure and permits calculations to be made on the basis of the fractional recovery of initial oil-in-place.

As mentioned above, there are several widely used techniques that were specifically developed to predict the performance of solution gas drive reservoirs, including:

- the Tracy method;
- the Muskat technique;
- the Tarner method.

These methodologies are presented below.

Tracy method

Tracy (1955) suggested that the general MBE can be rearranged and expressed in terms of three functions of *PVT* variables. Tracy's arrangement is given in Chapter 4 by Equation 4.5.2 and is repeated here for convenience:

$$N = N_p \Phi_o + G_p \Phi_g + (W_p B_w - W_e) \Phi_w \qquad [5.1.34]$$

where Φ_o, Φ_g, and Φ_w are considered *PVT*-related properties that are functions of pressure and defined by:

$$\Phi_o = \frac{B_o - R_s B_g}{Den}$$

$$\Phi_g = \frac{B_g}{Den}$$

$$\Phi_w = \frac{1}{Den}$$

with:

$$Den = (B_o - B_{oi}) + (R_{si} - R_s) B_g + mB_{oi} \left[\frac{B_g}{B_{gi}} - 1\right] \qquad [5.1.35]$$

For a solution gas drive reservoir, Equations 5.1.34 and 5.1.35 are reduced to the following expressions, respectively:

$$N = N_p \Phi_o + G_p \Phi_g \qquad [5.1.36]$$

and:

$$Den = (B_o - B_{oi}) + (R_{si} - R_s) B_g \qquad [5.1.37]$$

Tracy's calculations are performed in a series of pressure drops that proceed from known reservoir conditions at the previous reservoir pressure p^* to the new, assumed, lower pressure p. The calculated results at the new reservoir pressure become "known" at the next assumed lower pressure.

In progressing from the conditions at any pressure p^* to the lower reservoir pressure p, consider that the incremental oil and gas production as ΔN_p and ΔG_p, or:

$$N_p = N_p^* + \Delta N_p \qquad [5.1.38]$$

$$G_p = G_p^* + \Delta G_p \qquad [5.1.39]$$

where:

$N_p^*, G_p^* =$ "known" cumulative oil and gas production at previous pressure level p^*

$N_p, G_p =$ "unknown" cumulative oil and gas at new pressure level p

Replacing N_p and G_p in Equation 5.1.36 with those of 5.1.38 and 5.1.39 gives

$$N = (N_p^* + \Delta N_p) \Phi_o + (G_p^* + \Delta G_p) \Phi_g \qquad [5.1.40]$$

Defining the average instantaneous GOR between the two pressures p^* and p by:

$$(GOR)_{avg} = \frac{GOR^* + GOR}{2} \qquad [5.1.41]$$

the incremental cumulative gas production ΔG_p can be approximated by Equation 5.1.6 as:

$$\Delta G_p = (GOR)_{avg} \Delta N_p \qquad [5.1.42]$$

Replacing ΔG_p in Equation 5.1.40 with that of 5.1.41 gives:

$$N = [N_p^* + \Delta N_p] \Phi_o + [G_p^* + \Delta N_p (GOR)_{avg}] \Phi_g \qquad [5.1.43]$$

If Equation 5.1.43 is expressed for $N = 1$, the cumulative oil production N_p and cumulative gas production G_p become fractions of initial oil-in place. Rearranging Equation 5.1.43 gives:

$$\Delta N_p = \frac{1 - (N_p^* \Phi_o + G_p^* \Phi_g)}{\Phi_o + (GOR)_{avg} \Phi_g} \qquad [5.1.44]$$

Equation 5.1.44 shows that there are essentially two unknowns. These are:

(1) the incremental cumulative oil production ΔN_p;
(2) the average gas–oil ratio $(GOR)_{avg}$.

The methodology involved in solving Equation 5.1.44 is basically an iterative technique with the objective of converging to the future GOR. In the calculations as described below, three GORs are included at any assumed depletion reservoir pressure. These are:

(1) the *current* (known) gas–oil ratio GOR^* at current (known) reservoir pressure p^*;
(2) the *estimated* gas–oil ratio $(GOR)_{est}$ at a selected new reservoir pressure p;
(3) the *calculated* gas–oil ratio $(GOR)_{cal}$ at the same selected new reservoir pressure p.

The specific steps of solving Equation 5.1.44 are given below:

Step 1. Select a *new* average reservoir pressure p below the previous reservoir pressure p^*.

Step 2. Calculate the values of the *PVT* functions Φ_o and Φ_g at the selected new reservoir pressure p.

Step 3. *Estimate* the GOR designated as $(GOR)_{est}$ at the selected new reservoir pressure p.

Step 4. Calculate the average instantaneous GOR:

$$(GOR)_{avg} = \frac{GOR^* + (GOR)_{est}}{2}$$

where GOR^* is a "known" GOR at previous pressure level p^*.

Step 5. Calculate the incremental cumulative oil production ΔN_p from Equation 5.1.44, as:

$$\Delta N_p = \frac{1 - \left(N_p^* \Phi_o + G_p^* \Phi_g\right)}{\Phi_o + (\text{GOR})_{\text{avg}} \Phi_g}$$

Step 6. Calculate cumulative oil production N_p:

$$N_p = N_p^* + \Delta N_p$$

Step 7. Calculate the oil and gas saturations at selected average reservoir pressure by using Equations 5.1.15 and 5.1.16, as:

$$S_o = \left(1 - S_{\text{wi}}\right)\left(1 - \frac{N_p}{N}\right)\frac{B_o}{B_{\text{oi}}}$$

Since the calculations are based on $N = 1$, then:

$$S_o = \left(1 - S_{\text{wi}}\right)\left(1 - N_p\right)\frac{B_o}{B_{\text{oi}}}$$

with gas saturation of:

$$S_g = 1 - S_o - S_{\text{wi}}$$

Step 8. Obtain the ratio $k_{\text{rg}}/k_{\text{ro}}$ at S_L, i.e., at $(S_o + S_{\text{wi}})$, from the available laboratory or field relative permeability data.

Step 9. Using the relative permeability ratio $k_{\text{rg}}/k_{\text{ro}}$, *calculate* the instantaneous GOR from Equation 5.1.1 and designate it as $(\text{GOR})_{\text{cal}}$:

$$(\text{GOR})_{\text{cal}} = R_s + \frac{k_{\text{rg}}}{k_{\text{ro}}}\left(\frac{\mu_o B_o}{\mu_g B_g}\right)$$

Step 10. Compare the estimated $(\text{GOR})_{\text{est}}$ in step 3 with the calculated $(\text{GOR})_{\text{cal}}$ in step 9. If the values are within the acceptable tolerance of:

$$0.999 \le \frac{(\text{GOR})_{\text{cal}}}{(\text{GOR})_{\text{est}}} \le 1.001$$

then proceed to the next step. If they are not within the tolerance, set the estimated $(\text{GOR})_{\text{est}}$ equal to the calculated $(\text{GOR})_{\text{cal}}$ and repeat the calculations from step 4. Steps 4 through 10 are repeated until convergence is achieved.

Step 11. Calculate the cumulative gas production

$$G_p = G_p^* + \Delta N_p \, (\text{GOR})_{\text{avg}}$$

Step 12. Since results of the calculations are based on 1 STB of oil initially in place, a final check on the accuracy of the prediction should be made on the MBE, or:

$$0.999 \le \left(N_p \Phi_o + G_p \Phi_g\right) \le 1.001$$

Step 13. Repeat from Step 1 with a new pressure and setting:

$$p^* = p$$
$$\text{GOR}^* = \text{GOR}$$
$$G_p^* = G_p$$
$$N_p^* = N_p$$

As the calculation progresses, a plot of GOR versus pressure should be maintained and extrapolated as an aid in estimating GOR at each new pressure.
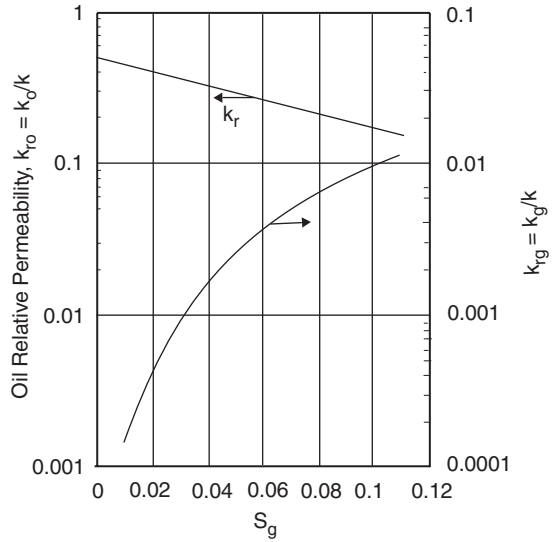
Figure 5.7   *Relative permeability data for Example 5.4 (After Economides, M., et al., Petroleum Production Systems, Prentice Hall Petroleum Engineers Series, 1994).*

Example 5.4   The following *PVT* data characterizes a solution gas drive reservoir. The relative permeability data is shown is Figure 5.7.

p (psi)	B_o (bbl/STB)	B_g (bbl/scf)	R_s (scf/STB)
4350	1.43	6.9×10	840
4150	1.420	7.1×10	820
3950	1.395	7.4×10^{-4}	770
3750	1.380	7.8×10^{-4}	730
3550	1.360	8.1×10^{-4}	680
3350	1.345	8.5×10^{-4}	640

The following additional data is available:

$N = 15$ MMSTB,	$p^* = 4350$
$p_i = 4350$ psia,	$\text{GOR}^* = 840$ scf/STB,
$p_b = 4350$ psia,	$G_p^* = 0$,
$S_{\text{wi}} = 30\%$,	$N_p^* = 0$
$N = 15$ MMSTB,	

Predict the cumulative oil and gas production to 3350 psi.

Solution   A sample of Tracy's calculation procedure is performed *at 4150* psi.

Step 1. Calculate Tracy's *PVT* functions at 4150 psia. First calculate the term "Den" from Equation 5.1.37:

$$\text{Den} = (B_o - B_{\text{oi}}) + (R_{\text{si}} - R_s)B_g$$

$$= (1.42 - 1.43) + (840 - 820)(7.1 \times 10^4)$$

$$= 0.0042$$

Then calculate Φ_o and Φ_g at 4150 psi:

$$\Phi_o = (B_o - R_s B_g)/\text{Den}$$
$$= [1.42 - (820)(7.1 \times 10^{-4})]/0.0042 = 199$$
$$\Phi_g = B_g/\text{Den}$$
$$= 7.1 \times 10^{-4}/0.0042 = 0.17$$

Similarly, these *PVT* variables are calculated for all other pressures, to give:

p	Φ_o	Φ_g
4350	–	–
4150	199	0.17
3950	49	0.044
3750	22.6	0.022
3550	13.6	0.014
3350	9.42	0.010

$\bar{p}$	ΔN_p	N_p	$(\text{GOR})_{\text{avg}}$	ΔG_p	G_p (scf/STB)	$N_p = 15 \times 10^6 N$ (STB)	$G_p = 15 \times 10^6 N$ (scf)
4350	–	–	–	–	–	–	
4150	0.00292	0.00292	845	2.48	2.48	0.0438×10^6	–
3950	0.00841	0.0110	880	7.23	9.71	0.165×10^6	37.2×10^6
3750	0.0120	0.0230	1000	12	21.71	0.180×10^6	145.65×10^6
3550	0.0126	0.0356	1280	16.1	37.81	0.534×10^6	325.65×10^6
3350	0.011	0.0460	1650	18.2	56.01	0.699×10^6	567.15×10^6

Step 2. Estimate (assume) a value for the GOR at 4150 psi:

$$(\text{GOR})_{\text{est}} = 850 \text{ scf/STB}.$$

Step 3. Calculate the average GOR:

$$(\text{GOR})_{\text{avg}} = \frac{\text{GOR}^* + (\text{GOR})_{\text{est}}}{2}$$
$$= \frac{840 + 850}{2} = 845 \text{ scf/STB}$$

Step 4. Calculate the incremental cumulative oil production ΔN_p:

$$\Delta N_p = \frac{1 - (N_p^* \Phi_o + G_p^* \Phi_g)}{\Phi_o + (\text{GOR})_{\text{avg}} \Phi_g}$$
$$= \frac{1 - 0}{199 + (845)(0.17)} = 0.00292 \text{ STB}$$

Step 5. Calculate the cumulative oil production N_p at 4150 psi:

$$N_p = N_p^* + \Delta N_p$$
$$= 0 + 0.00292 = 0.00292$$

Step 6. Calculate oil and gas saturations:

$$S_o = (1 - S_{\text{wi}})\left(1 - \frac{N_p}{N}\right)\frac{B_o}{B_{\text{oi}}}$$
$$= (1 - 0.3)(1 - 0.00292)\left(\frac{1.42}{1.43}\right) = 0.693$$

$$S_g = 1 - S_{\text{wi}} - S_o = 1 - 0.3 - 0.693 = 0.007$$

Step 7. Determine the relative permeability ratio $k_{\text{rg}}/k_{\text{ro}}$ from Figure 5.7, to give:

$$k_{\text{rg}}/k_{\text{ro}} = 8 \times 10^{-5}$$

Step 8. Using $\mu_o = 1.7$ cp and $\mu_g = 0.023$ cp, calculate the instantaneous GOR:

$$(\text{GOR})_{\text{cal}} = R_s + \frac{k_{\text{rg}}}{k_{\text{ro}}}\left(\frac{\mu_o B_o}{\mu_g B_g}\right)$$

$$= 820 + (1.7 \times 10^4)\frac{(1.7)(1.42)}{(0.023)(7.1 \times 10^{-4})}$$

$$= 845 \text{ scf/STB}$$

which agrees with the assumed value of 850.

Step 9. Calculate cumulative gas production:

$$G_p = 0 + (0.00292)(850) = 2.48$$

Complete results of the method are shown below:

Muskat method
Muskat (1945) expressed the MBE for a depletion drive reservoir in the following differential form:

$$\frac{dS_o}{dp} = \frac{\dfrac{S_o B_g}{B_o}\dfrac{dR_s}{dp} + \dfrac{S_o}{B_o}\dfrac{k_{\text{rg}}}{k_{\text{ro}}}\dfrac{\mu_o}{\mu_g}\dfrac{dB_o}{dp} - \dfrac{(1 - S_o - S_{\text{wi}})}{B_g}\dfrac{dB_g}{dp}}{1 + \dfrac{\mu_o}{\mu_g}\dfrac{k_{\text{rg}}}{k_{\text{ro}}}}$$

[5.1.45]

with:

$$\Delta S_o = S_o^* - S_o$$

$$\Delta p = p^* - p$$

where:

S_o^*, p^* = oil saturation and average reservoir pressure at the beginning of the pressure step (known values)

S_o, p = oil saturation and average reservoir pressure at the end of the time step

R_s = gas solubility at pressure p, scf/STB

B_g = gas formation volume factor, bbl/scf

S_{wi} = initial water saturation

Craft et al. (1991) suggested that the calculations can be greatly facilitated by computing and preparing in advance in graphical form the following pressure-dependent groups:

$$X(p) = \frac{B_g}{B_o}\frac{dR_s}{dp}$$ [5.1.46]

$$Y(p) = \frac{1}{B_o}\frac{\mu_o}{\mu_g}\frac{dB_o}{dp}$$ [5.1.47]

$$Z(p) = \frac{1}{B_g}\frac{dB_g}{dp}$$ [5.1.48]

Introducing the above pressure-dependent terms into Equation 5.1.45 gives:

$$\left(\frac{\Delta S_o}{\Delta p}\right) = \frac{S_o X(p) + S_o \frac{k_{rg}}{k_{ro}} Y(p) - (1 - S_o - S_{wi}) Z(p)}{1 + \frac{\mu_o}{\mu_g} \frac{k_{rg}}{k_{ro}}}$$

[5.1.49]

Given:

- initial oil-in-place N;
- current (known) pressure p^*;
- current cumulative oil production N_p^*;
- current cumulative gas production G_p^*;
- current GOR*;
- current oil saturation S_o^*;
- initial water saturation S_{wi}.

Equation 5.1.49 can be solved to predict cumulative production and fluid saturation at a given pressure drop Δp, i.e., $(p^* - p)$, by employing the following steps:

Step 1. Prepare a plot of k_{rg}/k_{ro} versus gas saturation.

Step 2. Plot R_s, B_o, and B_g versus pressure and numerically determine the slope of the *PVT* properties (i.e., dB_o/dp, dR_s/dp, and $d(B_g)/dp$) at several pressures. Tabulate the generated values as a function of pressure.

Step 3. Calculate the pressure-dependent terms $X(p)$, $Y(p)$, and $Z(p)$ at each of the selected pressures in Step 2. That is:

$$X(p) = \frac{B_g}{B_o} \frac{dR_s}{dp}$$

$$Y(p) = \frac{1}{B_o} \frac{\mu_o}{\mu_g} \frac{dB_o}{dp}$$

$$Z(p) = \frac{1}{B_g} \frac{dB_g}{dp}$$

Step 4. Plot the pressure-dependent terms $X(p)$, $Y(p)$, and $Z(p)$ as a function of pressure, as illustrated in Figure 5.8.

Step 5. Assume that the reservoir pressure has declined from initial (known) average reservoir pressure of p^* to a *selected* reservoir pressure p. Graphically determine the values of $X(p)$, $Y(p)$, and $Z(p)$ that correspond to the pressure p.

Step 6. Solve Equation 5.1.49 for $(\Delta S_o/\Delta p)$ by using the current oil saturation S_o^* at the beginning of the pressure drop interval p^*:

$$\left(\frac{\Delta S_o}{\Delta p}\right) = \frac{S_o^* X(p^*) + S_o^* \frac{k_{rg}}{k_{ro}} Y(p^*) - (1 - S_o^* - S_{wi}) Z(p^*)}{1 + \frac{\mu_o}{\mu_g} \frac{k_{rg}}{k_{ro}}}$$
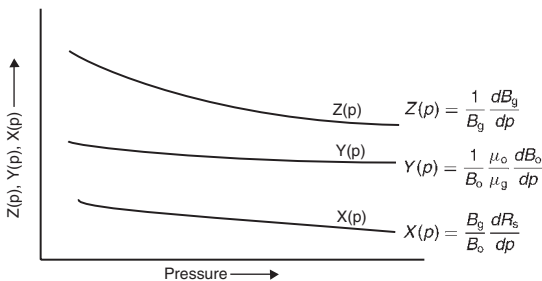

Figure 5.8 *Pressure-dependent terms vs. p.*

Step 7. Determine the oil saturation S_o at the assumed (selected) average reservoir pressure p, from:

$$S_o = S_o^* - (p^* - p)\left(\frac{\Delta S_o}{\Delta p}\right)$$

[5.1.50]

Step 8. Using the *calculated oil saturation* S_o from step 7, the updated value of the relative permeability ratio k_{rg}/k_{ro} at S_o, and the *PVT* terms at the assumed pressure p, recalculate $(\Delta S_o/\Delta p)$ by applying Equation 5.1.49:

$$\left(\frac{\Delta S_o}{\Delta p}\right) = \frac{S_o X(p) + S_o \frac{k_{rg}}{k_{ro}} Y(p) - (1 - S_o - S_{wi}) Z(p)}{1 + \frac{\mu_o}{\mu_g} \frac{k_{rg}}{k_{ro}}}$$

Step 9. Calculate the average value for $(\Delta S_o/\Delta p)$ from the two values obtained in steps 6 and 8, or:

$$\left(\frac{\Delta S_o}{\Delta p}\right)_{avg} = \frac{1}{2}\left[\left(\frac{\Delta S_o}{\Delta p}\right)_{step\ 6} + \left(\frac{\Delta S_o}{\Delta p}\right)_{step\ 8}\right]$$

Step 10. Using $(\Delta S_o/\Delta p)_{avg}$, solve for the oil saturation S_o from:

$$S_o = S_o^* - (p^* - p)\left(\frac{\Delta S_o}{\Delta p}\right)_{avg}$$

[5.1.51]

Step 11. Calculate gas saturation S_g and the GOR from:

$$S_g = 1 - S_{wi} - S_o$$

$$GOR = R_s + \frac{k_{rg}}{k_{ro}}\left(\frac{\mu_o B_o}{\mu_g B_g}\right)$$

Step 12. Using the saturation equation, i.e., Equation 5.1.15, solve for the cumulative oil production:

$$N_p = N\left[1 - \left(\frac{B_{oi}}{B_o}\right)\left(\frac{S_o}{1 - S_{wi}}\right)\right]$$

[5.1.52]

with an incremental cumulative oil production of:

$$\Delta N_p = N_p - N_p^*$$

Step 13. Calculate the incremental cumulative gas production by using Equations 5.1.40 and 5.1.41:

$$(GOR)_{avg} = \frac{GOR^* + GOR}{2}$$

$$\Delta G_p = (GOR)_{avg} \Delta N_p$$

with a total cumulative gas production of:

$$G_p = \sum \Delta G_p$$

Step 14. Repeat steps 5 through 13 for all pressure drops of interest and setting:

$$p^* = p$$

$$N_o^* = N_p$$

$$G_p^* = G_p$$

$$GOR^* = GOR$$

$$S_o^* = S_o$$

Example 5.5[a] A volumetric depletion drive reservoir exists at its bubble point pressure of 2500 psi. Detailed fluid

[a] Craft, B.C., Hawkins, M., and Terry, R. *Applied Petroleum Reservoir Engineering*, Prentice Hall, 1991, 2nd edition.

property data is listed by Craft and his co-authors and given here for only two pressures:

Fluid property	$p^* = 2500$ psi	$p = 2300$ psi
B_o, bbl/STB	1.498	1.463
R_s, scf/STB	721	669
B_g, bbl/scf	0.001048	0.001155
μ_o, cp	0.488	0.539
μ_g, cp	0.0170	0.0166
$X(p)$	0.00018	0.00021
$Y(p)$	0.00328	0.00380
$Z(p)$	0.00045	0.00050

The following additional information is available:

$$N = 56 \text{ MMSTB}, \quad S_{wi} = 20\%,$$

$$S_{oi} = 80\%$$

S_g	k_{rg}/k_{ro}
0.10	0.010
0.20	0.065
0.30	0.200
0.50	2.000
0.55	3.000
0.57	5.000

Calculate the cumulative oil production for a pressure drop of 200 psi, i.e., at 2300 psi.

Solution

Step 1. Using the oil saturation at the beginning of the pressure interval, i.e., $S_o^* = 0.8$, calculate k_{rg}/k_{ro}, to give:

$$k_{rg}/k_{ro} = 0.0 \text{ (no free gas initially in place)}$$

Step 2. Evaluate $(\Delta S_o/\Delta p)$ by applying Equation 5.1.49:

$$\left(\frac{\Delta S_o}{\Delta p}\right) = \frac{S_o^* X(p^*) + S_o^* \frac{k_{rg}}{k_{ro}} Y(p^*) - (1 - S_o^* - S_{wi}) Z(p^*)}{1 + \frac{\mu_o}{\mu_g} \frac{k_{rg}}{k_{ro}}}$$

$$= \frac{(0.8)(0.00018) + 0 - (1 - 0.8 - 0.2)(0.00045)}{1 + 0} = 0.000146$$

Step 3. Estimate the oil saturation at $p = 2300$ psi from Equation 5.1.51:

$$S_o = S_o^* - (p^* - p)\left(\frac{\Delta S_o}{\Delta p}\right)_{avg}$$

$$= 0.8 - 200(0.000146) = 0.7709$$

Step 4. Recalculate $(\Delta S_o/\Delta p)$ by using $S_o = 0.7709$, relative permeability ratio k_{rg}/k_{ro} at S_o, and the *pressure-dependent PVT terms at 2300 psi:*

$$\left(\frac{\Delta S_o}{\Delta p}\right) = \frac{S_o X(p) + S_o \frac{k_{rg}}{k_{ro}} Y(p) - (1 - S_o - S_{wi}) Z(p)}{1 + \frac{\mu_o}{\mu_g} \frac{k_{rg}}{k_{ro}}}$$

$$= 0.7709(0.00021) + 0.7709(0.00001)0.0038$$

$$- (1 - 0.2 - 0.7709)0.0005 \left/ 1 + \left(\frac{0.539}{0.0166}\right)(0.00001) \right.$$

$$= 0.000173$$

Step 5. Calculate the average $(\Delta S_o/\Delta p)$:

$$\left(\frac{\Delta S_o}{\Delta p}\right)_{avg} = \frac{0.000146 + 0.000173}{2} = 0.000159$$

Step 6. Calculate the oil saturation at 2300 psi by applying Equation 5.1.51:

$$S_o = S_o^* - (p^* - p)\left(\frac{\Delta S_o}{\Delta p}\right)_{avg}$$

$$= 0.8 - (2500 - 2300)(0.000159) = 0.7682$$

Step 7. Calculate the gas saturation:

$$S_g = 1 - 0.2 - 0.7682 = 0.0318$$

Step 8. Calculate cumulative oil production at 2300 psi by using Equation 5.1.52:

$$N_p = N\left[1 - \left(\frac{B_{oi}}{B_o}\right)\left(\frac{S_o}{1 - S_{wi}}\right)\right]$$

$$= 56 \times 10^6 \left[1 - \left(\frac{1.498}{1.463}\right)\left(\frac{0.7682}{1 - 0.2}\right)\right]$$

$$= 939\,500 \text{ STB}$$

Step 9. Calculate k_{rg}/k_{ro} at 2300 psi, to give $k_{rg}/k_{ro} = 0.00001$.

Step 10. Calculate the instantaneous GOR at 2300 psi:

$$\text{GOR} = R_s + \frac{k_{rg}}{k_{ro}}\left(\frac{\mu_o B_o}{\mu_g B_g}\right)$$

$$= 669 + 0.00001\frac{(0.539)(1.463)}{(0.0166)(0.001155)}$$

$$= 670 \text{ scf/STB}$$

Step 11. Calculate the incremental cumulative gas production:

$$(\text{GOR})_{avg} = \frac{\text{GOR}^* + \text{GOR}}{2} = \frac{669 + 670}{2}$$

$$= 669.5 \text{ scf/STB}$$

$$\Delta G_p = (GOR)_{avg} \Delta N_p$$

$$= 669.5(939500 - 0) = 629 \text{ MMscf}$$

It should be stressed that this method is based on the assumption of uniform oil saturation in the whole reservoir and that the solution will therefore break down when there is appreciable gas segregation in the formation. It is therefore applicable only when permeabilities are relatively low.

Tarner method

Tarner (1944) suggested an iterative technique for predicting cumulative oil production N_p and cumulative gas production G_p as a function of reservoir pressure. The method is based on solving the MBE and the instantaneous GOR equation simultaneously for a given reservoir pressure drop from a known pressure p^* to an assumed (new) pressure p. It is accordingly assumed that the cumulative oil and gas production has increased from known values of N_p^* and G_p^* at reservoir pressure p^* to future values of N_p and G_p at the assumed pressure p. To simplify the description of the proposed iterative procedure, the stepwise calculation is illustrated for a volumetric saturated oil reservoir; however, *the method can be used to predict the volumetric behavior of reservoirs under different driving mechanisms.*

Step 1. Select (assume) a future reservoir pressure p below the initial (current) reservoir pressure p^* and obtain the necessary *PVT* data. Assume that the cumulative oil production has increased from N_p^* to N_p. Note that

N_p^* and G_p^* are set equal to 0 at the initial reservoir pressure.

Step 2. Estimate or guess the cumulative oil production N_p at the selected (assumed) reservoir pressure p of step 1.

Step 3. Calculate the cumulative gas production G_p by rearranging the MBE, i.e., Equation 5.1.33, to give:

$$G_p = N \left[(R_{si} - R_s) - \frac{B_{oi} - B_o}{B_g} \right] - N_p \left[\frac{B_o}{B_g} - R_s \right] \qquad [5.1.53]$$

Equivalently, the above relationship can be expressed in terms of the two-phase (total) formation volume factor B_t as:

$$G_p = \frac{N(B_t - B_{ti}) - N_p(B_t - R_{si}B_g)}{B_g} \qquad [5.1.54]$$

where:

B_{oi} = initial oil formation volume factor, bbl/STB
R_{si} = initial gas solubility, scf/STB
B_o = oil formation volume factor at the assumed reservoir pressure p, bbl/STB
B_g = gas formation volume factor at the assumed reservoir pressure p, bbl/scf
B_o = oil formation volume factor at the assumed reservoir pressure p, bbl/STB
B_t = two-phase formation volume factor at the assumed reservoir pressure p, bbl/STB
N = initial oil-in-place, STB

Step 4. Calculate the oil and gas saturations at the assumed cumulative oil production N_p and the selected reservoir pressure p by applying Equations 5.1.15 and 5.1.16 respectively, or:

$$S_o = (1 - S_{wi}) \left[1 - \frac{N_p}{N} \right] \left(\frac{B_o}{B_{oi}} \right)$$

$$S_g = 1 - S_o - S_{wi}$$

and:

$$S_L = S_o + S_{wi}$$

where:

S_L = total liquid saturation
B_{oi} = initial oil formation volume factor at p_i, bbl/STB
B_o = oil formation volume factor at p, bbl/STB
S_g = gas saturation at the assumed reservoir pressure p
S_o = oil saturation at assumed reservoir pressure p

Step 5. Using the available relative permeability data, determine the relative permeability ratio k_{rg}/k_{ro} that corresponds to the calculated total liquid saturation S_L of step 4 and compute the instantaneous GOR at p from Equation 5.1.1:

$$GOR = R_s + \left(\frac{k_{rg}}{k_{ro}} \right) \left[\frac{\mu_o B_o}{\mu_g B_g} \right] \qquad [5.1.55]$$

It should be noted that all the *PVT* data in the expression *must be evaluated at the assumed reservoir pressure p*.

Step 6. Calculate again the cumulative gas production G_p at p by applying Equation 5.1.7:

$$G_p = G_p^* + \left[\frac{GOR^* + GOR}{2} \right] [N_p - N_p^*] \qquad [5.1.56]$$

in which GOR^* represents the instantaneous GOR at p^*. Note that if p^* represents the initial reservoir pressure, then set $GOR^* = R_{si}$.

Step 7. The calculations as performed in step 3 and step 6 give two estimates for cumulative gas produced G_p at the assumed (future) pressure p:

(1) G_p as calculated from the MBE;
(2) G_p as calculated from the GOR equation.

These two values of G_p are calculated from two independent methods and, therefore, if the cumulative gas production G_p as calculated from step 3 agrees with the value of step 6, the assumed value of N_p is correct and a new pressure may be selected and steps 1 through 6 are repeated. Otherwise, assume another value of N_p and repeat steps 2 through 6.

Step 8. In order to simplify this iterative process, three values of N_p can be assumed, which yield three different solutions of cumulative gas production for each of the equations (i.e., MBE and GOR equation). When the computed values of G_p are plotted versus the assumed values of N_p, the resulting two curves (one representing results of step 3 and the one representing step 5) will intersect. This intersection indicates that the cumulative oil and gas production that will satisfy both equations.

It should be pointed out that it may be more convenient to assume values of N_p as a fraction of the initial oil-in-place N. For instance, N_p could be assumed as $0.01N$, rather than as 10000 STB. In this method, a true value of N is not required. Results of the calculations would be, therefore, in terms of STB of oil produced per STB of oil initially in place and scf of gas produced per STB of oil initially in place.

To illustrate the application of the Tarner method, Cole (1969) presented the following example.

Example 5.6 A saturated oil reservoir has a bubble point pressure of 2100 psi at 175°F. The initial reservoir pressure is 2400 psi. The following data summarizes the rock and fluid properties of the field:

Original oil-in-place = 10 MMSTB

Connate water saturation = 15%

Porosity = 12%

$c_w = 3.2 \times 10^{-6}$ psi^{-1}

$c_f = 3.1 \times 10^{-6}$ psi^{-1}

Basic *PVT* data is as follows:

p (psi)	B_o (bbl/STB)	B_t (bbl/STB)	R_s (scf/STB)	B_g (bbl/scf)	μ_o/μ_g
2400	1.464	1.464	1340	–	–
2100	1.480	1.480	1340	0.001283	34.1
1800	1.468	1.559	1280	0.001518	38.3
1500	1.440	1.792	1150	0.001853	42.4

Relative permeability ratio:

S_L (%)	k_{rg}/k_{ro}
96	0.018
91	0.063
75	0.850
65	3.350
55	10.200

Predict the cumulative oil and gas production at 2100, 1800, and 1500 psi.

Solution   The required calculations will be performed under the following two different driving mechanisms:

(1) When the reservoir pressure declines from the initial reservoir pressure of 2500 to the bubble point pressure of 2100 psi, the reservoir is considered undersaturated and, therefore, the MBE can be used directly in cumulative production without restoring the iterative technique.

(2) For reservoir pressures below the bubble point pressure, the reservoir is treated as a saturated oil reservoir and the Tarner method may be applied.

Oil recovery prediction from initial pressure to the bubble point pressure:

Step 1.   The MBE for an undersaturated reservoir is given by Equation 4.4.10:

$$F = N(E_o + E_{f,w})$$

where:

$$F = N_p B_o + W_p B_w$$

$$E_o = B_o - B_{oi}$$

$$E_{f,w} = B_{oi}\left[\frac{c_w S_w + c_f}{1 - S_{wi}}\right]\Delta p$$

$$\Delta p = p_i - \bar{p}_r$$

Since there is no water production, Equation 4.4.10 can be solved for cumulative oil production, to give:

$$N_p = \frac{N[E_o + E_{f,w}]}{B_o} \qquad [5.1.57]$$

Step 2.   Calculate the two expansion factors E_o and $E_{f,w}$ for the pressure declines from the initial reservoir pressure of 2400 psi to the bubble point pressure of 2100 psi:

$$E_o = B_o - B_{oi}$$

$$= 1.480 - 1.464 = 0.016$$

$$E_{f,w} = B_{oi}\left[\frac{c_w S_w + c_f}{1 - S_{wi}}\right]\Delta p$$

$$= 1.464\left[\frac{(3.2 \times 10^{-6})(0.15) + (3.1 \times 10^{-6})}{1 - 0.15}\right]$$

$$\times (2400 - 2100) = 0.0018$$

Step 3.   Calculate the cumulative oil and gas production when the reservoir pressure declines from 2400 to 2100 psi by applying Equation 5.1.57, to give:

$$N_p = \frac{N[E_o + E_{f,w}]}{B_o}$$

$$= \frac{10 \times 10^6[0.016 + 0.0018]}{1.480} = 120\,270 \text{ STB}$$

At or above the bubble point pressure, the producing GOR is equal to the gas solubility at the bubble point and, therefore, the cumulative gas production is given by:

$$G_p = N_p R_{si}$$

$$= (120\,270)(1340) = 161 \text{ MMscf}$$

Step 4.   Determine the remaining oil-in-place at 2100 psi:

Remaining oil in place $= 10\,000\,000 - 120\,270$

$$= 9.880 \text{ MMSTB}$$

The remaining oil-in-place is considered as the initial oil-in-place during the reservoir performance below the saturation pressure. That is:

$$N = 9.880 \text{ MMSTB}$$

$$N_p = N_p^* = 0.0 \text{ STB}$$

$$G_p = G_p^* = 0.0 \text{ scf}$$

$$R_{si} = 1340 \text{ scf/STB}$$

$$B_{oi} = 1.489 \text{ bbl/STB}$$

$$B_{ti} = 1.489 \text{ bbl/STB}$$

$$B_{gi} = 0.001283 \text{ bbl/scf}$$

Oil recovery prediction below the bubble point pressure:
Oil recovery prediction at 1800 psi with the following *PVT* properties:

$$B_o = 1.468 \text{ bbl/STB}$$

$$B_t = 1.559 \text{ bbl/STB}$$

$$B_g = 0.001518 \text{ bbl/scf}$$

$$R_s = 1280 \text{ scf/STB}$$

Step 1.   Assume that 1% of the bubble point oil will be produced when the reservoir pressure drops 1800 psi. That is:

$$N_p = 0.01N$$

Calculate the corresponding cumulative gas G_p by apply Equation 5.1.54:

$$G_p = \frac{N(B_t - B_{ti}) - N_p(B_t - R_{si}B_g)}{B_g}$$

$$= \frac{N(1.559 - 1.480) - (0.01N)[1.559 - (1340)(0.001518)]}{0.001518}$$

$$= 55.17N$$

Step 2.   Calculate the oil saturation, to give:

$$S_o = (1 - S_{wi})\left(1 - \frac{N_p}{N}\right)\frac{B_o}{B_{oi}}$$

$$= (1 - 0.15)\left(1 - \frac{0.01N}{N}\right)\frac{1.468}{1.480} = 0.835$$

Step 3.   Determine the relative permeability ratio k_{rg}/k_{ro} from the tabulated data at total liquid saturation of S_L to give:

$$S_L = S_o + S_{wi} = 0.835 + 0.15 = 0.985$$

$$k_{rg}/k_{ro} = 0.0100$$

Step 4.   Calculate the instantaneous GOR at 1800 psi by applying Equation 5.1.55 to give:

$$\text{GOR} = R_s + \left(\frac{k_{rg}}{k_{ro}}\right)\left[\frac{\mu_o B_o}{\mu_g B_g}\right]$$

$$= 1280 + 0.0100(38.3)\left(\frac{1.468}{0.001518}\right)$$

$$= 1650 \text{ scf/STB}$$

Step 5.   Solve again for the cumulative gas production by using the average GOR and applying Equation 5.1.56 to yield:

$$G_p = G_p^* + \left[\frac{\text{GOR}^* + \text{GOR}}{2}\right][N_p - N_p^*]$$

$$= 0 + \frac{1340 + 1650}{2}(0.01N - 0) = 14.95N$$

Step 6. Since the cumulative gas production, as calculated by the two independent methods (step 1 and step 5), do not agree, the calculations must be repeated by assuming a different value for N_p and plotting results of the calculation. Repeated calculations converge at:

$$N_p = 0.0393N \quad \text{STB/STB of bubble point oil and}$$

$$G_p = 64.34N \quad \text{scf/STB of bubble point oil}$$

or:

$$N_p = 0.0393(9.88 \times 10^6) = 388\,284 \text{ STB}$$

$$G_p = 64.34(9.88 \times 10^6) = 635.679 \text{ MMscf}$$

It should be pointed out that the cumulative production *above the bubble point pressure must be included when reporting the total cumulative oil and gas production*. The cumulative oil and gas production as the pressure declines from the initial pressure to the bubble point pressure is:

$$N_p = 120\,270 \text{ STB}$$

$$G_p = 161 \text{ MMscf}$$

Therefore, the actual cumulative recovery at 1800 psi is:

$$N_p = 120\,270 + 388\,284 = 508\,554 \text{ STB}$$

$$G_p = 161 + 635.679 = 799.679 \text{ MMscf}$$

The final results as summarized below show the cumulative gas and oil production as the pressure declines from the bubble point pressure:

Pressure	N_p	Actual N_p (STB)	G_p	Actual G_p (MMscf)
1800	0.0393N	508 554	64.34N	799.679
1500	0.0889N	998 602	136.6N	1510.608

It is apparent from the three predictive oil recovery methods; i.e., Tracy's, Muskat's, and Tarner's, that the relative permeability ratio k_{rg}/k_{ro} is the most important single factor governing the oil recovery. In cases where no detailed data are available concerning the physical characteristics of the reservoir rock in terms of k_{rg}/k_{ro} relationship, Wahl et al. (1958) presented an empirical expression for predicting the relative permeability ratio in sandstones:

$$\frac{k_{rg}}{k_{ro}} = \zeta(0.0435 + 0.4556\zeta)$$

with:

$$\zeta = \frac{1 - S_{gc} - S_{wi} - S_o}{S_o - 0.25}$$

where:

S_{gc} = critical gas saturation
S_{wi} = initial water saturation
S_o = oil saturation

Torcaso and Wyllie (1958) presented a similar correlation for sandstones in the following form:

$$\frac{k_{rg}}{k_{ro}} = \frac{(1 - S^*)^2[1 - (S^*)^2]}{(S^*)^4}$$

with:

$$S^* = \frac{S_o}{1 - S_{wi}}$$

5.2 Phase 2. Oil Well Performance

All the reservoir performance prediction techniques show the relationship of cumulative oil production N_p, cumulative gas production G_p, and instantaneous GOR as a function of the declining average reservoir pressure but do not relate the production to time. However, reservoir performance can be related to time by the use of relationships that are designed to predict the flow rate performance of the reservoirs individual wells. Such flow rate relationships are traditionally expressed in terms of:

- the well productivity index;
- the well inflow performance relationship (IPR).

These relationships are presented below for vertical and horizontal wells.

5.2.1 Vertical oil well performance
Productivity index and IPR
A commonly used measure of the ability of the well to produce is the productivity index. Defined by the symbol J, the productivity index is the ratio of the total liquid flow rate to the pressure drawdown. For a water-free oil production, the productivity index is given by:

$$J = \frac{Q_o}{\bar{p}_r - p_{wf}} = \frac{Q_o}{\Delta p} \qquad [5.2.1]$$

where:

Q_o = oil flow rate, STB/day
J = productivity index, STB/day/psi
$\bar{p}_r$ = volumetric average drainage area pressure (static pressure)
p_{wf} = bottom-hole flowing pressure
Δp = drawdown, psi

The productivity index is generally measured during a production test on the well. The well is shut in until the static reservoir pressure is reached. The well is then allowed to produce at a constant flow rate of Q and a stabilized bottom-hole flow pressure of p_{wf}. Since a stabilized pressure at the surface does not necessarily indicate a stabilized p_{wf}, the bottom-hole flowing pressure should be recorded continuously from the time the well is to flow. The productivity index is then calculated from Equation 5.1.1.

It is important to note that the productivity index is a valid measure of the well productivity potential only if the well is flowing at pseudosteady-state conditions. Therefore, in order to accurately measure the productivity index of a well, it is essential that the well is allowed to flow at a constant flow rate for a sufficient amount of time to reach the pseudosteady state as illustrated in Figure 5.9. The figure indicates that during the transient flow period, the calculated values of the productivity index will vary depending upon the time at which the measurements of p_{wf} are made.
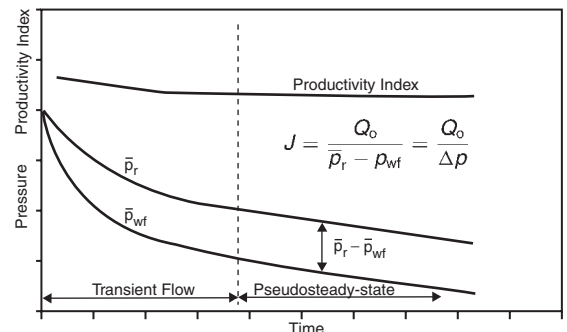

Figure 5.9 *Productivity index during flow regimes.*

The productivity index can be numerically calculated by recognizing that J must be defined in terms of semisteady-state flow conditions. Recalling Equation 1.2.137:

$$Q_o = \frac{0.00708k_o h \left(\bar{p}_r - p_{wf} \right)}{\mu_o B_o \left[\ln \left(r_e/r_w \right) - 0.75 + s \right]} \qquad [5.2.2]$$

The above equation is combined with Equation 5.2.1 to give:

$$J = \frac{0.00708k_o h}{\mu_o B_o \left[\ln \left(r_e/r_w \right) - 0.75 + s \right]} \qquad [5.2.3]$$

where:

J = productivity index, STB/day/psi
k_o = effective permeability of the oil, md
s = skin factor
h = thickness, ft

The oil relative permeability concept can be conveniently introduced into Equation 5.2.3, to give:

$$J = \frac{0.00708hk}{\left[\ln \left(r_e/r_w \right) - 0.75 + s \right]} \left(\frac{k_{ro}}{\mu_o B_o} \right) \qquad [5.2.4]$$

Since most of the well's life is spent in a flow regime that is approximating the pseudosteady state, the productivity index is a valuable methodology for predicting the future performance of wells. Further, by monitoring the productivity index during the life of a well, it is possible to determine if the well has become damaged due to completion, workover, production, injection operations, or mechanical problems. If a measured J has an unexpected decline, one of the indicated problems should be investigated. A comparison of productivity indexes of different wells in the same reservoir should also indicate that some of the wells might have experienced unusual difficulties or damage during completion. Since the productivity indexes may vary from well to well because of the variation in thickness of the reservoir, it is helpful to normalize the indexes by dividing each by the thickness of the well. This is defined as the specific productivity index J_s, or:

$$J_s = \frac{J}{h} = \frac{Q_o}{h \left(\bar{p}_r - p_{wf} \right)} \qquad [5.2.5]$$

Assuming that the well's productivity index is constant, Equation 5.2.1 can be rewritten as:

$$Q_o = J \left(\bar{p}_r - p_{wf} \right) = J \Delta p \qquad [5.2.6]$$

where:

Δp = drawdown, psi
J = productivity index

Equation 5.2.6 indicates that the relationship between Q_o and Δp is a straight line passing through the origin with a slope of J as shown in Figure 5.10.
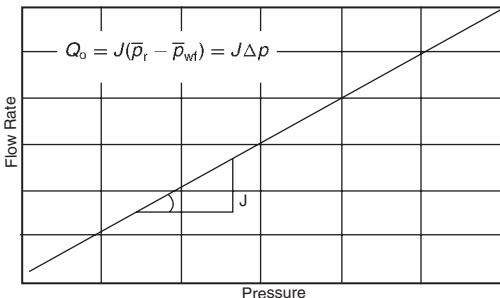

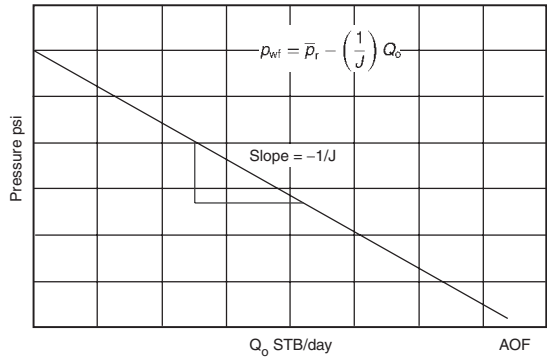**Figure 5.10** Q_o vs. Δp relationship.

Figure 5.11   IPR.

Alternatively, Equation 5.2.1 can be written as:

$$p_{wf} = \bar{p}_r - \left(\frac{1}{J} \right) Q_o \qquad [5.2.7]$$

This expression shows that the plot of p_{wf} vs. Q_o is a straight line with a slope of $-1/J$ as shown schematically in Figure 5.11. This graphical representation of the relationship that exists between the oil flow rate and bottom-hole flowing pressure is called the "inflow performance relationship" and referred to as IPR.

Several important features of the straight-line IPR can be seen in Figure 5.11:

- When p_{wf} equals the average reservoir pressure, the flow rate is zero due to the absence of any pressure drawdown.
- Maximum rate of flow occurs when p_{wf} is zero. This maximum rate is called "absolute open flow" and referred to as AOF. Although in practice this may not be a condition at which the well can produce, it is a useful definition that has widespread applications in the petroleum industry (e.g., comparing flow potential of different wells in the field). The AOF is then calculated by:

$$\text{AOF} = J\bar{p}_r$$

- The slope of the straight line equals the reciprocal of the productivity index.

Example 5.7   A productivity test was conducted on a well. The test results indicate that the well is capable of producing at a stabilized flow rate of 110 STB/day and a bottom-hole flowing pressure of 900 psi. After shutting the well for 24 hours, the bottom-hole pressure reached a static value of 1300 psi.

Calculate:

(a) the productivity index;
(b) the AOF;
(c) the oil flow rate at a bottom-hole flowing pressure of 600 psi;
(d) the wellbore flowing pressure required to produce 250 STB/day.

Solution

(a) Calculate J from Equation 5.2.1:

$$J = \frac{Q_o}{\bar{p}_r - p_{wf}} = \frac{Q_o}{\Delta p}$$

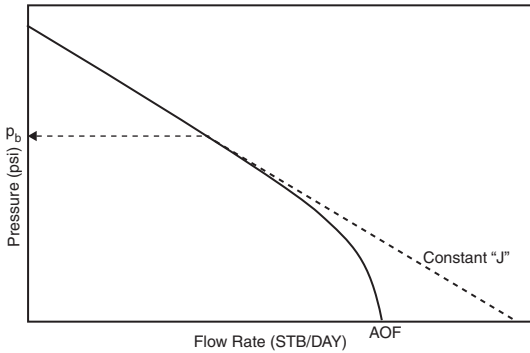$$= \frac{110}{1300 - 900} = 0.275 \text{ STB/psi}$$
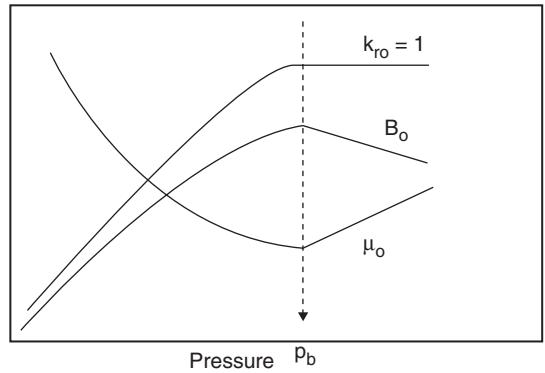
Figure 5.12   *IPR below p_b.*

Figure 5.13   *Effect of pressure on B_o, μ_o and k_{ro}.*

(b) Determine the AOF from:

$$\text{AOF} = J(\bar{p}_r - 0)$$

$$= 0.275(1300 - 0) = 375.5 \text{ STB/day}$$

(c) Solve for the oil flow rate by applying Equation 5.2.1:

$$Q_o = J(\bar{p}_r - p_{wf})$$

$$= 0.275(1300 - 600) = 192.5 \text{ STB/day}$$

(d) Solve for p_{wf} by using Equation 5.2.7:

$$p_{wf} = \bar{p}_r - \left(\frac{1}{J}\right) Q_o$$

$$= 1300 - \left(\frac{1}{0.275}\right) 250 = 390.9 \text{ psi}$$

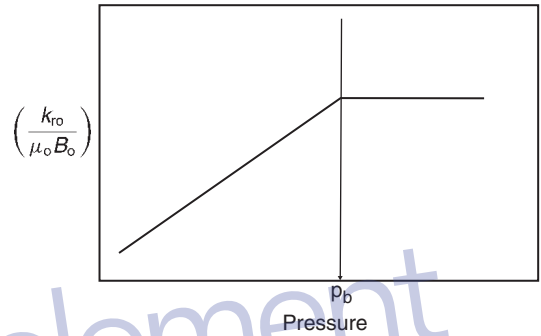The previous discussion, as illustrated by the example, suggested that the inflow into a well is directly proportional to the pressure drawdown and the constant of proportionality is the productivity index. Muskat and Evinger (1942) and Vogel (1968) observed that when the pressure drops below the bubble point pressure, the IPR deviates from that of the simple straight-line relationship as shown in Figure 5.12. Recalling Equation 5.2.4:

$$J = \frac{0.00708hk}{\ln\left(r_e/r_w\right) - 0.75 + s} \left(\frac{k_{ro}}{\mu_o B_o}\right)$$

Treating the term in the brackets as a constant c, the above equation can be written in the following form:

$$J = c \left(\frac{k_{ro}}{\mu_o B_o}\right) \tag{5.2.8}$$

with the coefficient c as defined by:

$$c = \frac{0.00708kh}{\ln\left(r_e/r_w\right) - 0.75 + s}$$

Equation 5.2.8 reveals that the variables affecting the productivity index are essentially those that are pressure dependent, namely:

- oil viscosity μ_o;
- oil formation volume factor B_o;
- relative permeability to oil k_{ro}.

Figure 5.13 schematically illustrates the behavior of these variables as a function of pressure. Figure 5.14 shows the overall effect of changing the pressure on the term $k_{ro}/\mu_o B_o$. Above the bubble point pressure p_b, the relative oil permeability k_{ro} equals unity ($k_{ro} = 1$) and the term ($k_{ro}/\mu_o B_o$) is almost constant. As the pressure declines below p_b, the gas is released from solution which can cause a large decrease

Figure 5.14 $k_{ro}/\mu_o B_o$ *as a function of pressure.*
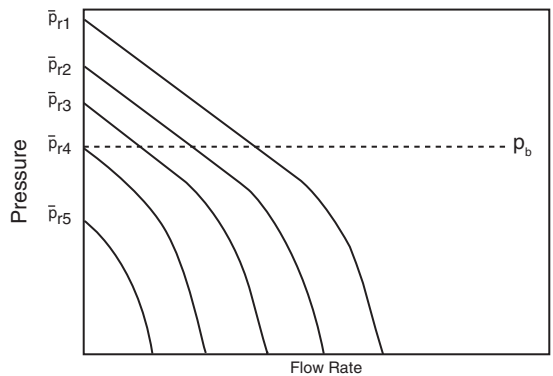
Figure 5.15   *Effect of reservoir pressure on IPR.*

in both k_{ro} and $k_{ro}/\mu_o B_o$. Figure 5.15 shows qualitatively the effect of reservoir depletion on the IPR.

There are several empirical methods that are designed to predict the non-linear behavior of the IPR for solution gas drive reservoirs. Most of these methods require at least one stabilized flow test in which Q_o and p_{wf} are measured. All the methods include the following two computational steps:

(1) Using the stabilized flow test data, construct the IPR curve at the current average reservoir pressure $\bar{p}_r$.
(2) Predict future IPRs as a function of average reservoir pressures.

The following empirical methods are designed to generate the current and future inflow performance relationships:

- the Vogel method;
- the Wiggins method;
- the Standing method;
- the Fetkovich method;
- the Klins and Clark method.

Vogel method

Vogel (1968) used a computer model to generate IPRs for several hypothetical saturated oil reservoirs that are producing under a wide range of conditions. Vogel normalized the calculated IPRs and expressed the relationships in a dimensionless form. He normalized the IPRs by introducing the following dimensionless parameters:

$$\text{Dimensionless pressure} = \frac{p_{wf}}{\bar{p}_r}$$

$$\text{Dimensionless flow rate} = \frac{Q_o}{(Q_o)_{max}}$$

where $(Q_o)_{max}$ is the flow rate at zero wellbore pressure, i.e., the AOF.

Vogel plotted the dimensionless IPR curves for all the reservoir cases and arrived at the following relationship between the above dimensionless parameters:

$$\frac{Q_o}{(Q_o)_{max}} = 1 - 0.2 \left(\frac{p_{wf}}{\bar{p}_r}\right) - 0.8 \left(\frac{p_{wf}}{\bar{p}_r}\right)^2 \qquad [5.2.9]$$

where:

$$Q_o = \text{oil rate at } p_{wf}$$
$$(Q_o)_{max} = \text{maximum oil flow rate at zero wellbore pressure, i.e., the AOF}$$
$$\bar{p}_r = \text{current average reservoir pressure, psig}$$
$$p_{wf} = \text{wellbore pressure, psig}$$

Note that p_{wf} and $\bar{p}_r$ must be expressed in psig.

The Vogel method can be extended to account for water production by replacing the dimensionless rate with $Q_L/(Q_L)_{max}$ where $Q_L = Q_o + Q_w$. This has proved to be valid for wells producing at water cuts as high as 97%. The method requires the following data:

- current average reservoir pressure $\bar{p}_r$;
- bubble point pressure p_b;
- stabilized flow test data that includes Q_o at p_{wf}.

Vogel's methodology can be used to predict the IPR curve for the following two types of reservoirs:

(1) saturated oil reservoirs: $\bar{p}_r \leq p_b$;
(2) undersaturated oil reservoirs: $\bar{p}_r > p_b$.

The vertical well IPR in saturated oil reservoirs

When the reservoir pressure equals the bubble point pressure, the oil reservoir is referred to as a saturated oil reservoir. The computational procedure of applying the Vogel method in a saturated oil reservoir to generate the IPR curve for a well with a stabilized flow data point, i.e., a recorded Q_o value at p_{wf}, is summarized below:

Step 1. Using the stabilized flow data, i.e., Q_o and p_{wf}, calculate $(Q_o)_{max}$ from Equation 5.2.9, or:

$$(Q_o)_{max} = \frac{Q_o}{1 - 0.2 \left(p_{wf}/\bar{p}_r\right) - 0.8 \left(p_{wf}/\bar{p}_r\right)^2}$$

Step 2. Construct the IPR curve by assuming various values for p_{wf} and calculating the corresponding Q_o by

applying Equation 5.2.9:

$$\frac{Q_o}{(Q_o)_{max}} = 1 - 0.2 \left(\frac{p_{wf}}{\bar{p}_r}\right) - 0.8 \left(\frac{p_{wf}}{\bar{p}_r}\right)^2$$

or:

$$Q_o = (Q_o)_{max} \left[1 - 0.2 \left(\frac{p_{wf}}{\bar{p}_r}\right) - 0.8 \left(\frac{p_{wf}}{\bar{p}_r}\right)^2\right]$$

Example 5.8   A well is producing from a saturated reservoir with an average reservoir pressure of 2500 psig. Stabilized production test data indicates that the stabilized rate and wellbore pressure are 350 STB/day and 2000 psig, respectively. Calculate:

(a) Calculate the oil flow rate at $p_{wf} = 1850$ psig.
(b) Calculate the oil flow rate assuming constant J.
(c) Construct the IPR by using the Vogel method and the constant productivity index approach.

Solution

(a)

Step 1. Calculate $(Q_o)_{max}$:

$$(Q_o)_{max} = \frac{Q_o}{1 - 0.2 \left(p_{wf}/\bar{p}_r\right) - 0.8 \left(p_{wf}/\bar{p}_r\right)^2}$$

$$= \frac{350}{1 - 0.2 \left(\frac{2000}{2500}\right) - 0.8 \left(\frac{2000}{2500}\right)^2}$$

$$= 1067.1 \text{ STB/day}$$

Step 2. Calculate Q_o at $p_{wf} = 1850$ psig by using Vogel's equation:

$$Q_o = (Q_o)_{max} \left[1 - 0.2 \left(\frac{p_{wf}}{\bar{p}_r}\right) - 0.8 \left(\frac{p_{wf}}{\bar{p}_r}\right)^2\right]$$

$$= 1067.1 \left[1 - 0.2 \left(\frac{1850}{2500}\right) - 0.8 \left(\frac{1850}{2500}\right)^2\right]$$

$$= 441.7 \text{ STB/day}$$

(b)

Step 1. Apply Equation 5.2.2 to determine J:

$$J = \frac{Q_o}{\bar{p}_r - p_{wf}}$$

$$= \frac{350}{2500 - 2000} = 0.7 \text{ STB/day/psi}$$

Step 2. Calculate Q_o:

$$Q_o = J(\bar{p}_r - p_{wf}) = 0.7(2500 - 1850)$$

$$= 455 \text{ STB/day}$$

(c) Assume several values for p_{wf} and calculate the corresponding Q_o:

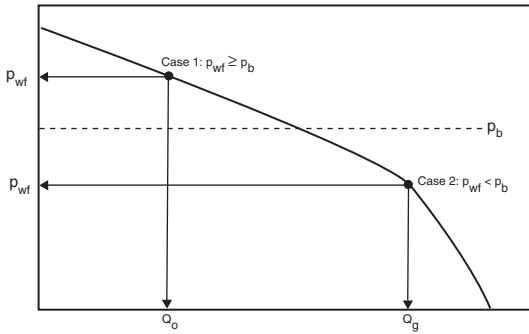| p_{wf}	*Vogel*	$Q_o = J(\bar{p}_r - p_{wf})$
2500	0	0
2200	218.2	210
1500	631.7	700
1000	845.1	1050
500	990.3	1400
0	1067.1	1750

Figure 5.16 *Stabilized flow test data.*

The vertical well IPR in undersaturated oil reservoirs
Beggs (1991) pointed out that in applying the Vogel method
for undersaturated reservoirs, there are two possible out-
comes of the recorded stabilized flow test data that must be
considered, as shown schematically in Figure 5.16:

(1) The recorded stabilized bottom-hole flowing pressure is
greater than or equal to the bubble point pressure, i.e.,
$p_{wf} \geq p_b$.
(2) The recorded stabilized bottom-hole flowing pressure is
less than the bubble point pressure $p_{wf} < p_b$.

Case 1 $p_{wf} \geq p_b$ Beggs outlined the following procedure
for determining the IPR when the stabilized bottom-hole
pressure is greater than or equal to the bubble point pressure
(Figure 5.16):

Step 1. Using the stabilized test data point (Q_o and p_{wf})
calculate the productivity index J:

$$J = \frac{Q_o}{\bar{p}_r - p_{wf}}$$

Step 2. Calculate the oil flow rate at the bubble point pres-
sure:

$$Q_{ob} = J\left(\bar{p}_r - p_b\right) \qquad [5.2.10]$$

where Q_{ob} is the oil flow rate at p_b.
Step 3. Generate the IPR values below the bubble point pres-
sure by assuming different values of $p_{wf} < p_b$ and
calculating the correspond oil flow rates by applying
the following relationship:

$$Q_o = Q_{ob} + \frac{Jp_b}{1.8}\left[1 - 0.2\left(\frac{p_{wf}}{p_b}\right) - 0.8\left(\frac{p_{wf}}{p_b}\right)^2\right]$$

$$[5.2.11]$$

The maximum oil flow rate ($Q_{o\,max}$ or AOF) occurs
when the bottom-hole flowing pressure is zero, i.e.,
$p_{wf} = 0$, which can be determined from the above
expression as:

$$Q_{o\ max} = Q_{ob} + \frac{Jp_b}{1.8}$$

It should be pointed out that when $p_{wf} \geq p_b$, the IPR
is linear and is described by:

$$Q_o = J\left(\bar{p}_r - p_{wf}\right)$$

Example 5.9 An oil well is producing from an undersat-
urated reservoir that is characterized by a bubble point
pressure of 2130 psig. The current average reservoir pres-
sure is 3000 psig. Available flow test data shows that the
well produced 250 STB/day at a stabilized p_{wf} of 2500 psig.
Construct the IPR data.

Solution The problem indicates that the flow test data
was recorded above the bubble point pressure, $p_{wf} \geq p_b$,
and therefore the "Case 1" procedure for undersaturated
reservoirs as outlined previously must be used:

Step 1. Calculate J using the flow test data:

$$J = \frac{Q_o}{\bar{p}_r - p_{wf}}$$

$$= \frac{250}{3000 - 2500} = 0.5 \text{ STB/day/psi}$$

Step 2. Calculate the oil flow rate at the bubble point pres-
sure by applying Equation 5.2.10:

$$Q_{ob} = J\left(\bar{p}_r - p_b\right)$$

$$= 0.5(3000 - 2130) = 435 \text{ STB/day}$$

Step 3. Generate the IPR data by applying the constant J
approach for all pressures above p_b and Equation
5.2.11 for all pressures below p_b:

$$Q_o = Q_{ob} + \frac{Jp_b}{1.8}\left[1 - 0.2\left(\frac{p_{wf}}{p_b}\right) - 0.8\left(\frac{p_{wf}}{p_b}\right)^2\right]$$

$$= 435 + \frac{(0.5)(2130)}{1.8}$$

$$\times \left[1 - 0.2\left(\frac{p_{wf}}{2130}\right) - 0.8\left(\frac{p_{wf}}{2130}\right)^2\right]$$

$\bar{p}_{wf}$	Q_o
$p_i = 3000$	0
2800	100
2600	200
$p_b = 2130$	435
1500	709
1000	867
500	973
0	1027

Case 2 $p_{wf} < p_b$ When the recorded p_{wf} from the stabilized
flow test is below the bubble point pressure, as shown in
Figure 5.16, the following procedure for generating the IPR
data is proposed:

Step 1. Using the stabilized well flow test data and com-
bining Equation 5.2.10 with 5.2.11, solve for the
productivity index J to give:

$$J = \frac{Q_o}{\left(\bar{p}_r - p_b\right) + \dfrac{p_b}{1.8}\left[1 - 0.2\left(\dfrac{p_{wf}}{p_b}\right) - 0.8\left(\dfrac{p_{wf}}{p_b}\right)^2\right]}$$

$$[5.2.12]$$

Step 2. Calculate Q_{ob} by using Equation 5.2.10, or:

$$Q_{ob} = J\left(\bar{p}_r - p_b\right)$$

Step 3. Generate the IPR for $p_{wf} \geq p_b$ by assuming several
values for p_{wf} above the bubble point pressure and
calculating the corresponding Q_o from:

$$Q_o = J\bar{p}_r - p_{wf}$$

Step 4. Use Equation 5.2.11 to calculate Q_o at various values
of p_{wf} below p_b, or:

$$Q_o = Q_{ob} + \frac{Jp_b}{1.8}\left[1 - 0.2\left(\frac{p_{wf}}{p_b}\right) - 0.8\left(\frac{p_{wf}}{p_b}\right)^2\right]$$

Example 5.10 The well described in Example 5.8 was retested and the following results obtained:

$$p_{wf} = 1700 \text{ psig}, \quad Q_o = 630.7 \text{ STB/day}$$

Generate the IPR data using the new test data.

Solution Notice that the stabilized p_{wf} is less than p_b.

Step 1. Solve for J by applying Equation 5.2.12:

$$J = \frac{Q_o}{(\bar{p}_r - p_b) + \dfrac{p_b}{1.8}\left[1 - 0.2\left(\dfrac{p_{wf}}{p_b}\right) - 0.8\left(\dfrac{p_{wf}}{p_b}\right)^2\right]}$$

$$= \frac{630.7}{(3000 - 2130) + \dfrac{2130}{1.8}\left[1 - \left(\dfrac{1700}{2130}\right) - \left(\dfrac{1700}{2130}\right)^2\right]}$$

$$= 0.5 \text{ STB/day/psi}$$

Step 2. Determine Q_{ob}:

$$Q_{ob} = J(\bar{p}_r - p_b)$$

$$= 0.5(3000 - 2130) = 435 \text{ STB/day}$$

Step 3. Generate the IPR data by applying Equation 5.2.6 when $p_{wf} > p_b$ and Equation 5.2.11 when $p_{wf} < p_b$:

$$Q_o = J(\bar{p}_r - p_{wf}) = J\Delta p$$

$$= Q_{ob} + \frac{Jp_b}{1.8}\left[1 - 0.2\left(\frac{p_{wf}}{p_b}\right) - 0.8\left(\frac{p_{wf}}{p_b}\right)^2\right]$$

p_{wf}	Equation	Q_o
3000	5.2.6	0
2800	5.2.6	100
2600	5.2.6	200
2130	5.2.6	435
1500	5.2.11	709
1000	5.2.11	867
500	5.2.11	973
0	5.2.11	1027

Quite often it is necessary to predict the well's inflow performance for future times as the reservoir pressure declines. Future well performance calculations require the development of a relationship that can be used to predict future maximum oil flow rates.

There are several methods that are designed to address the problem of how the IPR might shift as the reservoir pressure declines. Some of these prediction methods require the application of the MBE to generate future oil saturation data as a function of reservoir pressure. In the absence of such data, there are two simple approximation methods that can be used in conjunction with the Vogel method to predict future IPRs.

First approximation method This method provides a rough approximation of the future maximum oil flow rate $(Q_{o\,max})_f$ at the specified *future* average reservoir pressure $(\bar{p}_r)_f$. This future maximum flow rate $(Q_{o\,max})_f$ can be used in Vogel's equation to predict the future inflow performance

relationships at $(\bar{p}_r)_f$. The following steps summarize the method:

Step 1. Calculate $(Q_{o\,max})_f$ at $(\bar{p}_r)_f$ from:

$$(Q_{o\,max})_f = (Q_{o\,max})_p\left[\frac{(\bar{p}_r)_f}{(\bar{p}_r)_p}\right]\left[0.2 + 0.8\frac{(\bar{p}_r)_f}{(\bar{p}_r)_p}\right]$$

$$[5.2.13]$$

where the subscripts f and p represent future and present conditions, respectively.

Step 2. Using the new calculated value of $(Q_{o\,max})_f$ and $(\bar{p}_r)_f$, generate the IPR by using Equation 5.2.9.

Second approximation method A simple approximation for estimating future $(Q_{o\,max})_f$ at $(\bar{p}_r)_f$ was proposed by Fetkovich (1973). The relationship has the following mathematical form:

$$(Q_{o\,max})_f = (Q_{o\,max})_p\left[\frac{(\bar{p}_r)_f}{(\bar{p}_r)_p}\right]^{3.0}$$

where the subscripts f and p represent future and present conditions, respectively. The above equation is intended only to provide a rough estimation of future $(Q_{o\,max})$.

Example 5.11 Using the data given in Example 5.8, predict the IPR when the average reservoir pressure declines form 2500 psig to 2200 psig.

Solution Example 5.8 shows the following information:
- present average reservoir pressure $(\bar{p}_r)_p = 2500$ psig;
- present maximum oil rate $(Q_{o\,max})_p = 1067.1$ STB/day.

Step 1. Solve for $(Q_{o\,max})_f$ by applying Equation 5.2.13:

$$(Q_{o\,max})_f = (Q_{o\,max})_p\left[\frac{(\bar{p}_r)_f}{(\bar{p}_r)_p}\right]\left[0.2 + 0.8\frac{(\bar{p}_r)_f}{(\bar{p}_r)_p}\right]$$

$$= (1067.1)\left(\frac{2200}{2500}\right)\left[0.2 + 0.8\frac{2200}{2500}\right]$$

$$= 849 \text{ STB/day}$$

Step 2. Generate the IPR data by applying Equation 5.2.9:

$$Q_o = (Q_o)_{max}\left[1 - 0.2\left(\frac{p_{wf}}{\bar{p}_r}\right) - 0.8\left(\frac{p_{wf}}{\bar{p}_r}\right)^2\right]$$

$$= 849[1 - 0.2(p_{wf}/2200) - 0.8(p_{wf}/2200)^2]$$

p_{wf}	Q_o
2200	0
1800	255
1500	418
500	776
0	849

It should be pointed out that the main disadvantage of Vogel's methodology lies with its sensitivity to the match point, i.e., the stabilized flow test data point, used to generate the IPR curve for the well.

For a production well completed in a multilayered system, it is possible to allocate individual layer production by

applying the following relationships:

$$(Q_o)_i = Q_{oT} \frac{[1 - (\overline{S}_i f_{wT})]\dfrac{(k_o)_i(h)_i}{(\mu_o)_{Li}}}{\sum_{i=1}^{n \, \text{Layers}} [1 - (\overline{S}_i f_{wT})]\dfrac{(k_o)_i(h)_i}{(\mu_o)_i}}$$

$$(Q_w)_i = Q_{wT} \frac{[(\overline{S}_i f_{wT})]\dfrac{(k_w)_i(h)_i}{(\mu_w)_i}}{\sum_{i=1}^{n \, \text{Layers}} [(\overline{S}_i f_{wT})]\dfrac{(k_w)_i(h)_i}{(\mu_w)_i}}$$

with:

$$\overline{S}_i = \frac{(S_w)_i}{\sum_{i=1}^{n \, \text{Layers}} (S_w)_i}$$

where:

$(Q_o)_i$ = allocated oil rate for layer i
$(Q_w)_i$ = allocated water rate for layer i
f_{wT} = total well water cut
$(k_o)_i$ = effective oil permeability for layer i
$(k_w)_i$ = effective water permeability for layer i
n Layers = number of layers

Wiggins method

Wiggins (1993) used four sets of relative permeability and fluid property data as the basic input for a computer model to develop equations to predict inflow performance. The generated relationships are limited by the assumption that the reservoir initially exists at its bubble point pressure. Wiggins proposed generalized correlations that are suitable for predicting the IPR during three-phase flow. His proposed expressions are similar to that of Vogel and are expressed as:

$$Q_o = (Q_o)_{\text{max}} \left[1 - 0.52 \left(\frac{p_{wf}}{\overline{p}_r} \right) - 0.48 \left(\frac{p_{wf}}{\overline{p}_r} \right)^2 \right] \quad [5.2.14]$$

$$Q_w = (Q_w)_{\text{max}} \left[1 - 0.72 \left(\frac{p_{wf}}{\overline{p}_r} \right) - 0.28 \left(\frac{p_{wf}}{\overline{p}_r} \right)^2 \right] \quad [5.2.15]$$

where:

Q_w = water flow rate, STB/day
$(Q_w)_{\text{max}}$ = maximum water production rate at $p_{wf} = 0$, STB/day

As in the Vogel method, data from a stabilized flow test on the well must be available in order to determine $(Q_o)_{\text{max}}$ and $(Q_w)_{\text{max}}$.

Wiggins extended the application of the above relationships to predict future performance by providing expressions for estimating future maximum flow rates. He expressed future maximum rates as a function of:

- current (present) average pressure $(\overline{p}_r)_p$;
- future average pressure $(\overline{p}_r)_f$;
- current maximum oil flow rate $(Q_{o\,\text{max}})_p$;
- current maximum water flow rate $(Q_{w\,\text{max}})_p$.

Wiggins proposed the following relationships:

$$(Q_{o\,\text{max}})_f = (Q_{o\,\text{max}})_p \left[0.15 \frac{(\overline{p}_r)_f}{(\overline{p}_r)_p} + 0.84 \left(\frac{(\overline{p}_r)_f}{(\overline{p}_r)_p} \right)^2 \right] \quad [5.2.16]$$

$$(Q_{w\,\text{max}})_f = (Q_{w\,\text{max}})_p \left[0.59 \frac{(\overline{p}_r)_f}{(\overline{p}_r)_p} + 0.36 \left(\frac{(\overline{p}_r)_f}{(\overline{p}_r)_p} \right)^2 \right] \quad [5.2.17]$$

Example 5.12 The information given in Examples 5.8 and 5.11 is repeated here for convenience.

- current average pressure = 2500 psig;
- stabilized oil flow rate = 350 STB/day;
- stabilized wellbore pressure = 2000 psig.

Generate the current IPR data and predict future IPR when the reservoir pressure declines from 2500 to 2000 psig by using the Wiggins method.

Solution

Step 1. Using the stabilized flow test data, calculate the current maximum oil flow rate by applying Equation 5.2.14:

$$Q_o = (Q_o)_{\text{max}} \left[1 - 0.52 \left(\frac{p_{wf}}{\overline{p}_r} \right) - 0.48 \left(\frac{p_{wf}}{\overline{p}_r} \right)^2 \right]$$

Solve for the present $(Q_o)_{\text{max}}$, to give:

$$(Q_{o\,\text{max}})_p = \frac{350}{1 - 0.52 \left(\dfrac{2000}{2500} \right) - 0.48 \left(\dfrac{2000}{2500} \right)^2}$$

$$= 1264 \text{ STB/day}$$

Step 2. Generate the current IPR data by using the Wiggins method and compare the results with those of Vogel. Results of the two methods are shown graphically in Figure 5.17.

p_{wf}	Wiggins	Vogel
2500	0	0
2200	216	218
1500	651	632
1000	904	845
500	1108	990
0	1264	1067

Step 3. Calculate future maximum oil flow rate by using Equation 5.2.16:

$$(Q_{o\,\text{max}})_f = (Q_{o\,\text{max}})_p \left[0.15 \frac{(\overline{p}_r)_f}{(\overline{p}_r)_p} + 0.84 \left(\frac{(\overline{p}_r)_f}{(\overline{p}_r)_p} \right)^2 \right]$$

$$= 1264 \left[0.15 \left(\frac{2200}{2500} \right) + 0.84 \left(\frac{2200}{2500} \right)^2 \right]$$
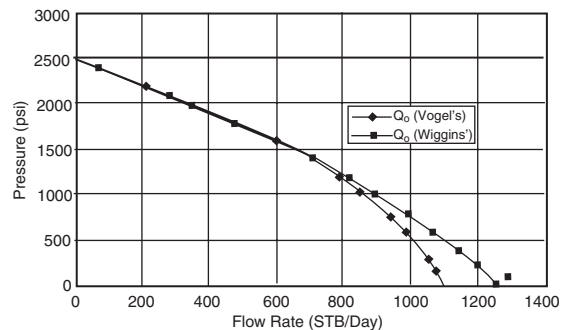
$$= 989 \text{ STB/day}$$

Figure 5.17 IPR curves.

Step 4. Generate future IPR data by using Equation 5.2.14:

$$Q_o = (Q_o)_{max} \left[1 - 0.52 \left(\frac{p_{wf}}{\bar{p}_r} \right) - 0.48 \left(\frac{p_{wf}}{\bar{p}_r} \right)^2 \right]$$

$$= 989[1 - 0.52(p_{wf}/2200) - 0.48(p_{wf}/2200)^2]$$

p_{wf}	Q_o
2200	0
1800	250
1500	418
500	848
0	989

Standing method

Standing (1970) essentially extended the application of the Vogel method to predict the future IPR of a well as a function of reservoir pressure. He noted that Vogel's equation (Equation 5.2.9) can be rearranged as:

$$\frac{Q_o}{(Q_o)_{max}} = \left(1 - \frac{p_{wf}}{\bar{p}_r} \right) \left[1 + 0.8 \left(\frac{p_{wf}}{\bar{p}_r} \right) \right] \qquad [5.2.18]$$

Standing introduced the productivity index J as defined by Equation 5.1.1 into Equation 5.2.18, to yield:

$$J = \frac{(Q_o)_{max}}{\bar{p}_r} \left[1 + 0.8 \left(\frac{p_{wf}}{\bar{p}_r} \right) \right] \qquad [5.2.19]$$

Standing then defined a "zero drawdown" productivity index as:

$$J_P^* = 1.8 \left[\frac{(Q_o)_{max}}{\bar{p}_r} \right] \qquad [5.2.20]$$

where J_P^* is the current zero-drawdown productivity index. J_P^* is related to the productivity index J by:

$$\frac{J}{J_P^*} = \frac{1}{1.8} \left[1 + 0.8 \left(\frac{p_{wf}}{\bar{p}_r} \right) \right] \qquad [5.2.21]$$

Equation 5.2.21 permits the calculation of J_P^* from a measured value of J. That is:

$$J_P^* = \frac{1.8J}{1 + 0.8 \left(\frac{p_{wf}}{\bar{p}_r} \right)}$$

To arrive at the final expression for predicting the desired IPR expression, Standing combines Equation 5.2.20 with 5.2.18 to eliminate $(Q_o)_{max}$, to give:

$$Q_o = \left[\frac{J_f^* (\bar{p}_r)_f}{1.8} \right] \left\{ 1 - 0.2 \frac{p_{wf}}{(\bar{p}_r)_f} - 0.8 \left[\frac{p_{wf}}{(\bar{p}_r)_f} \right]^2 \right\} \qquad [5.2.22]$$

where the subscript f refers to the future condition.

Standing suggested that J_f^* can be estimated from the present value of J_P^* by the following expression.

$$J_f^* = J_P^* \left(\frac{k_{ro}}{\mu_o B_o} \right)_f \bigg/ \left(\frac{k_{ro}}{\mu_o B_o} \right)_p \qquad [5.2.23]$$

where the subscript p refers to the present condition.

If the relative permeability data is not available, J_f^* can be roughly estimated from:

$$J_f^* = J_P^* \left[\frac{(\bar{p}_r)_f}{(\bar{p}_r)_p} \right]^2 \qquad [5.2.24]$$

Standing's methodology for predicting a future IPR is summarized in the following steps:

Step 1. Using the current time condition and the available flow test data, calculate $(Q_o)_{max}$ from Equation 5.2.18:

$$(Q_o)_{max} = \frac{Q_o}{\left(1 - \frac{p_{wf}}{\bar{p}_r} \right) \left[1 + 0.8 \left(\frac{p_{wf}}{\bar{p}_r} \right) \right]}$$

Step 2. Calculate J^* at the present condition, i.e., J_P^*, by using Equation 5.2.20. Note that other combinations of Equations 5.2.18 through 5.2.21 can be used to estimate J_P^*:

$$J_P^* = 1.8 \left[\frac{(Q_o)_{max}}{\bar{p}_r} \right]$$

or from:

$$J_P^* = \frac{1.8J}{1 + 0.8 (p_{wf}/\bar{p}_r)}$$

Step 3. Using fluid property, saturation, and relative permeability data, calculate both $(k_{ro}/\mu_o B_o)_p$ and $(k_{ro}/\mu_o B_o)_f$.

Step 4. Calculate J_f^* by using Equation 5.2.23. Use Equation 5.2.24 if the oil relative permeability data is not available:

$$J_f^* = J_P^* \left(\frac{k_{ro}}{\mu_o B_o} \right)_f \bigg/ \left(\frac{k_{ro}}{\mu_o B_o} \right)_p$$

or:

$$J_f^* = J_P^* \left[\frac{(\bar{p}_r)_f}{(\bar{p}_r)_p} \right]^2$$

Step 5. Generate the future IPR by applying Equation 5.2.22:

$$Q_o = \left[\frac{J_f^* (\bar{p}_r)_f}{1.8} \right] \left\{ 1 - 0.2 \frac{p_{wf}}{(\bar{p}_r)_f} - 0.8 \left[\frac{p_{wf}}{(\bar{p}_r)_f} \right]^2 \right\}$$

Example 5.13 A well is producing from a saturated oil reservoir that exists at its saturation pressure of 4000 psig. The well is flowing at a stabilized rate of 600 STB/day and a p_{wf} of 3200 psig. Material balance calculations provide the following current and future predictions for oil saturation and *PVT* properties.

	Present	*Future*
$\bar{p}_r$	4000	3000
μ_o (cp)	2.40	2.20
B_o (bbl/STB)	1.20	1.15
k_{ro}	1.00	0.66

Generate the future IPR for the well at 3000 psig by using the Standing method.

Solution

Step 1. Calculate the current $(Q_o)_{max}$ from Equation 5.2.18:

$$(Q_o)_{max} = \frac{Q_o}{(1 - p_{wf}/\bar{p}_r) \left[1 + 0.8 (p_{wf}/\bar{p}_r) \right]}$$

$$= \frac{600}{\left(1 - \frac{3200}{4000} \right) \left[1 + 0.8 \left(\frac{3200}{4000} \right) \right]}$$

$$= 1829 \text{ STB/day}$$

Step 2. Calculate J_P^* by using Equation 5.2.21:

$$J_P^* = 1.8\left[\frac{(Q_o)_{max}}{\bar{p}_r}\right]$$

$$= 1.8\left[\frac{1829}{4000}\right] = 0.823$$

Step 3. Calculate the following pressure function:

$$\left(\frac{k_{ro}}{\mu_o B_o}\right)_p = \frac{1}{(2.4)(1.20)} = 0.3472$$

$$\left(\frac{k_{ro}}{\mu_o B_o}\right)_f = \frac{0.66}{(2.2)(1.15)} = 0.2609$$

Step 4. Calculate J_f^* by applying Equation 5.2.23:

$$J_f^* = J_P^*\left(\frac{k_{ro}}{\mu_o B_o}\right)_f \bigg/ \left(\frac{k_{ro}}{\mu_o B_o}\right)_p$$

$$= 0.823\left(\frac{0.2609}{0.3472}\right) = 0.618$$

Step 5. Generate the IPR by using Equation 5.2.22:

$$Q_o = \left[\frac{J_f^*\,(\bar{p}_r)_f}{1.8}\right]\left\{1 - 0.2\frac{p_{wf}}{(\bar{p}_r)_f} - 0.8\left[\frac{p_{wf}}{(\bar{p}_r)_f}\right]^2\right\}$$

$$= \left[\frac{(0.618)(3000)}{1.8}\right]\left\{1 - 0.2\frac{p_{wf}}{3000} - 0.8\left[\frac{p_{wf}}{3000}\right]^2\right\}$$

p_{wf}	Q_o (STB/day)
3000	0
2000	527
1500	721
1000	870
500	973
0	1030

It should be noted that one of the main disadvantages of Standing's methodology is that it requires reliable permeability information; in addition, it also requires material balance calculations to predict oil saturations at future average reservoir pressures.

Fetkovich method

Muskat and Evinger (1942) attempted to account for the observed non-linear flow behavior (i.e., IPR) of wells by calculating a theoretical productivity index from the pseudosteady-state flow equation. They expressed Darcy's equation as:

$$Q_o = \frac{0.00708kh}{\left[\ln\left(r_e/r_w\right) - 0.75 + s\right]}\int_{p_{wf}}^{\bar{p}_r} f(p)\,dp \qquad [5.2.25]$$

where the pressure function $f(p)$ is defined by:

$$f(p) = \frac{k_{ro}}{\mu_o B_o} \qquad [5.2.26]$$

where:

k_{ro} = oil relative permeability
k = absolute permeability, md
B_o = oil formation volume factor
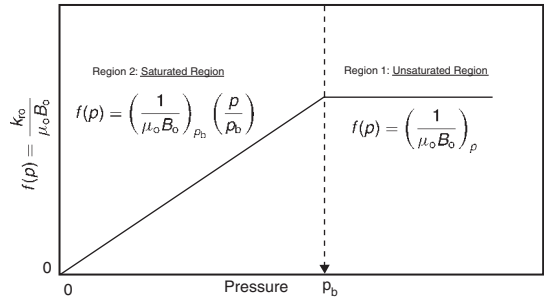μ_o = oil viscosity, cp

Figure 5.18 *Pressure function concept.*

Fetkovich (1973) suggested that the pressure function $f(p)$ can basically fall into one of the following two regions:

Region 1: *Undersaturated region:* The pressure function $f(p)$ falls into this region if $p > p_b$. Since oil relative permeability in this region equals unity (i.e., $k_{ro} = 1$), then:

$$f(p) = \left(\frac{1}{\mu_o B_o}\right)_p \qquad [5.2.27]$$

Fetkovich observed that the variation in $f(p)$ is only slight and the pressure function is considered constant as shown in Figure 5.18.

Region 2: *Saturated region:* In the saturated region where $p < p_b$, Fetkovich showed that $k_{ro}/\mu_o B_o$ changes linearly with pressure and that the straight line passes through the origin. This linear plot is shown schematically in Figure 5.18 and can be expressed mathematically as:

$$f(p) = 0 + (\text{slope})p$$

or:

$$f(p) = 0 + \left(\frac{1/(\mu_o B_o)}{p_b}\right)_{p_b} p$$

Simplifying:

$$f(p) = \left(\frac{1}{\mu_o B_o}\right)_{p_b}\left(\frac{p}{p_b}\right) \qquad [5.2.28]$$

where μ_o and B_o are evaluated at the bubble point pressure. In the application of the straight-line pressure function, there are *three cases* that must be considered:

(1) $\bar{p}_r$ and $p_{wf} > p_b$;
(2) $\bar{p}_r$ and $p_{wf} < p_b$;
(3) $\bar{p}_r > p_b$ and $p_{wf} < p_b$.

These three cases are presented below.

Case 1: $\bar{p}_r$ and p_{wf} are both greater than p_b This is the case of a well producing from an undersaturated oil reservoir where both p_{wf} and $\bar{p}_r$ are greater than the bubble point pressure. The pressure function $f(p)$ in this case is described by Equation 5.2.27. Substituting Equation 5.2.27 into Equation 5.2.25 gives:

$$Q_o = \frac{0.00708kh}{\ln\left(r_e/r_w\right) - 0.75 + s}\int_{p_{wf}}^{\bar{p}_r}\left(\frac{1}{\mu_o B_o}\right)dp$$

Since $\left(\frac{1}{\mu_o B_o}\right)$ is constant, then:

$$Q_o = \frac{0.00708kh}{\mu_o B_o\left[\ln\left(r_e/r_w\right) - 0.75 + s\right]}\left(\bar{p}_r - p_{wf}\right) \qquad [5.2.29]$$

and from the definition of the productivity index:

$$Q_o = J\left(\bar{p}_r - p_{wf}\right) \qquad [5.2.30]$$

The productivity index is defined in terms of the reservoir parameters as:

$$J = \frac{0.00708kh}{\mu_o B_o \left[\ln\left(r_e/r_w\right) - 0.75 + s\right]} \qquad [5.2.31]$$

where B_o and μ_o are evaluated at $(\bar{p}_r + p_{wf})/2$.

Example 5.14 A well is producing from an undersaturated oil reservoir that exists at an average reservoir pressure of 3000 psi. The bubble point pressure is recorded as 1500 psi at 150°F. The following additional data is available:

 stabilized flow rate = 280 STB/day,

 stabilized wellbore pressure = 2200 psi

 $h = 20$ ft, $r_w = 0.3$ ft,

 $r_e = 660$ ft, $s = -0.5$

 $k = 65$ md, μ_o at 2600 psi = 2.4 cp,

 B_o at 2600 psi = 1.4 bbl/STB

Calculate the productivity index by using both the reservoir properties (i.e., Equation 5.2.31) and flow test data (i.e., Equation 5.2.1):

Solution From Equation 5.2.30:

$$J = \frac{0.00708kh}{\mu_o B_o \left[\ln\left(r_e/r_w\right) - 0.75 + s\right]}$$

$$= \frac{0.00708(65)(20)}{(2.4)(1.4)\left[\ln\left(\frac{660}{0.3}\right) - 0.75 - 0.5\right]}$$

$$= 0.42 \text{ STB/day/psi}$$

From production data:

$$J = \frac{Q_o}{\bar{p}_r - p_{wf}} = \frac{Q_o}{\Delta p}$$

$$= \frac{280}{3000 - 2200} = 0.35 \text{ STB/day/psi}$$

Results show a reasonable match between the two approaches. However, it should be noted that several uncertainties exist in the values of the parameters used in Equation 5.2.31 to determine the productivity index. For example, changes in the skin factor k or drainage area would change the calculated value of J.

Case 2: $\bar{p}_r$ *and* $p_{wf} < p_b$ When the reservoir pressure $\bar{p}_r$ and bottom-hole flowing pressure p_{wf} are both below the bubble point pressure p_b, the pressure function $f(p)$ is represented by the straight-line relationship of Equation 5.2.28. Combining Equation 5.2.28 with 5.2.25 gives:

$$Q_o = \left[\frac{0.00708kh}{\ln\left(r_e/r_w\right) - 0.75 + s}\right]\int_{p_{wf}}^{\bar{p}_r}\frac{1}{(\mu_o B_o)_{p_b}}\left(\frac{p}{p_b}\right)dp$$

Since the term $\left[(1/\mu_o B_o)_{p_b}(1/p_b)\right]$ is constant, then:

$$Q_o = \left[\frac{0.00708kh}{\ln\left(r_e/r_w\right) - 0.75 + s}\right]\frac{1}{(\mu_o B_o)_{p_b}}\left(\frac{1}{p_b}\right)\int_{p_{wf}}^{\bar{p}_r}p\,dp$$

Integrating:

$$Q_o = \frac{0.00708kh}{(\mu_o B_o)_{p_b}\left[\ln\left(r_e/r_w\right) - 0.75 + s\right]}\left(\frac{1}{2p_b}\right)\left(\bar{p}_r^2 - p_{wf}^2\right) \qquad [5.2.32]$$

Introducing the productivity index, as defined by Equation 5.2.31, into the above equation gives:

$$Q_o = J\left(\frac{1}{2p_b}\right)\left(\bar{p}_r^2 - p_{wf}^2\right) \qquad [5.2.33]$$

The term $(J/2p_b)$ is commonly referred to as the performance coefficient C, or:

$$Q_o = C\left(\bar{p}_r^2 - p_{wf}^2\right) \qquad [5.2.34]$$

To account for the possibility of non-Darcy flow (turbulent flow) in oil wells, Fetkovich introduced the exponent n in Equation 5.2.34 to yield:

$$Q_o = C(\bar{p}_r^2 - p_{wf}^2)^n \qquad [5.2.35]$$

The value of n ranges from 1.0 for complete laminar flow to 0.5 for highly turbulent flow.

There are two unknowns in Equation 5.2.35, the performance coefficient C and the exponent n. At least two tests are required to evaluate these two parameters, assuming $\bar{p}_r$ is known.

By taking the log of both sides of Equation 5.2.35 and solving for $\log(\bar{p}_r^2 - p_{wf}^2)$, the expression can be written as:

$$\log\left(\bar{p}_r^2 - p_{wf}^2\right) = \frac{1}{n}\log Q_o - \frac{1}{n}\log C$$

A plot of $\bar{p}_r^2 - p_{wf}^2$ vs. q_o on a log–log scale will result in a straight line having a slope of $1/n$ and an intercept of C at $\bar{p}_r^2 - p_{wf}^2 = 1$. The value of C can also be calculated using any point on the linear plot once n has been determined, to give:

$$C = \frac{Q_o}{\left(\bar{p}_r^2 - p_{wf}^2\right)^n}$$

Once the values of C and n are determined from test data, Equation 5.2.35 can be used to generate a complete IPR.

To construct the future IPR when the average reservoir pressure declines to $(\bar{p}_r)_f$, Fetkovich assumed that the performance coefficient C is a linear function of the average reservoir pressure and, therefore, the value of C can be adjusted as:

$$(C)_f = (C)_p\frac{(\bar{p}_r)_f}{(\bar{p}_r)_p} \qquad [5.2.36]$$

where the subscripts f and p represent the future and present conditions.

Fetkovich assumed that the value of the exponent n would not change as the reservoir pressure declines. Beggs (1991) presented an excellent and comprehensive discussion of the different methodologies used in constructing the IPR curves for oil and gas wells.

The following example was used by Beggs (1991) to illustrate the Fetkovich method for generating the current and future IPR.

Example 5.15 A four-point stabilized flow test was conducted on a well producing from a saturated reservoir that exists at an average pressure of 3600 psi.

Q_o (STB/day)	p_{wf} (psi)
263	3170
383	2890
497	2440
640	2150

(a) Construct a complete IPR by using the Fetkovich method.
(b) Construct the IPR when the reservoir pressure declines to 2000 psi.
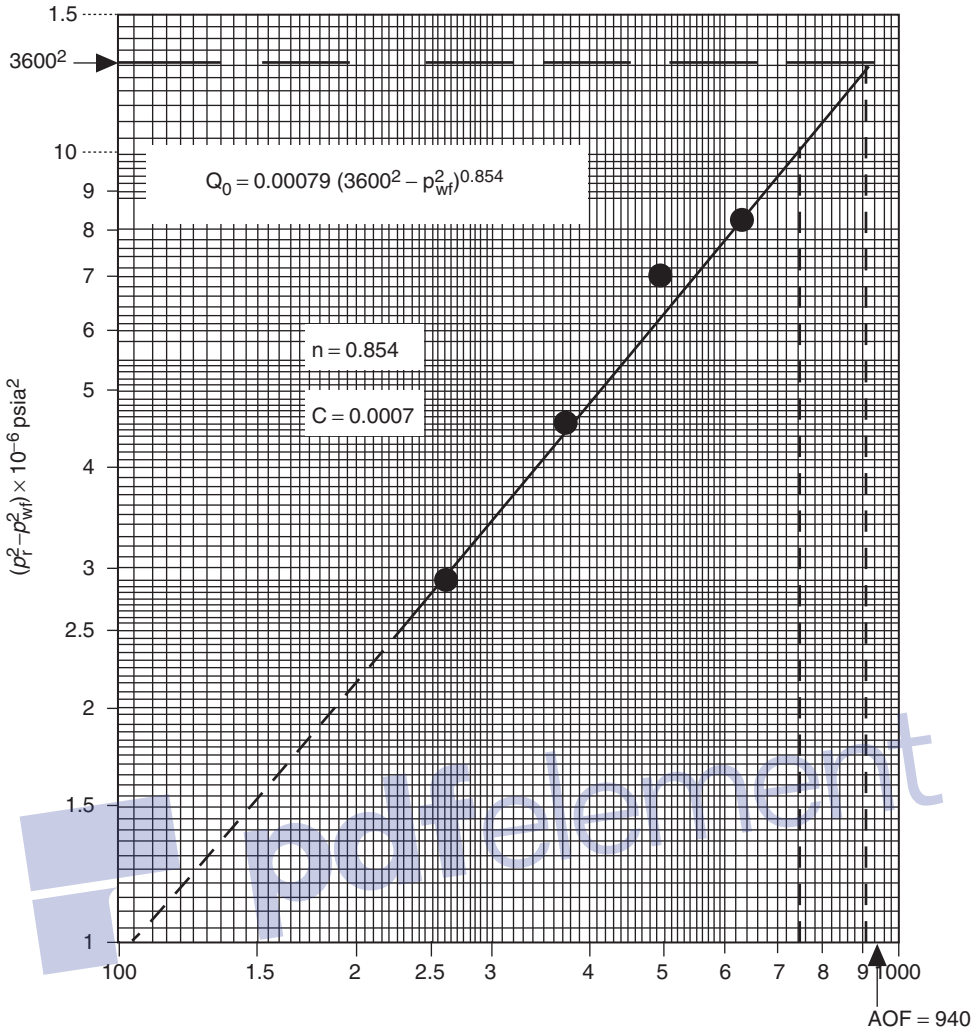
Figure 5.19 *Flow–after-flow data for Example 5.15 (After Beggs, D., Production Optimization Using Nodal Analysis, permission to publish by the OGCI, copyright OGCI, 1991).*

Solution

(a)

Step 1. Construct the following table:

Q_o (STB/day)	p_{wf} (psi)	$(\bar{p}_r^2 - p_{wf}^2) \times 10^{-6}$, (psi^2)
263	3170	2.911
383	2897	4.567
497	2440	7.006
640	2150	8.338

Step 2. Plot $(\bar{p}_r^2 - p_{wf}^2)$ vs. Q_o on log–log paper as shown in Figure 5.19 and determine the exponent n, or:

$$n = \frac{\log(750) - \log(105)}{\log(10^7) - \log(10^6)} = 0.854$$

Step 3. Solve for the performance coefficient C by selecting any point on the straight line, e.g., $(745, 10 \times 10^6)$,

and solving for C from Equation 5.2.35:

$$Q_o = C(\bar{p}_r^2 - p_{wf}^2)^n$$

$$745 = C(10 \times 10^6)^{0.854}$$

$$C = 0.00079$$

Step 4. Generate the IPR by assuming various values for p_{wf} and calculating the corresponding flow rate from Equation 5.2.35:

$$Q_o = 0.00079(3600^2 - p_{wf}^2)^{0.854}$$

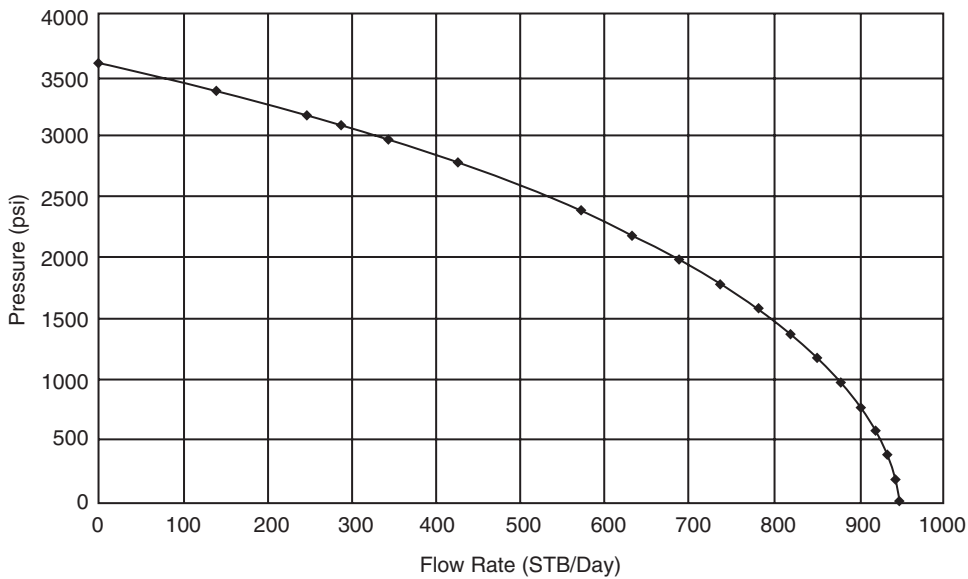| p_{wf}	Q_o (STB/day)
3600	0
3000	340
2500	503
2000	684
1500	796
1000	875
500	922
0	937

Figure 5.20 IPR using Fetkovich method.

The IPR curve is shown in Figure 5.20. Notice that the AOF, i.e., $(Q_o)_{max}$, is 937 STB/day.

(b)

Step 1. Calculate future C by applying Equation 5.2.36:

$$(C)_f = (C)_p \frac{(\bar{p}_r)_f}{(\bar{p}_r)_p}$$

$$= 0.00079 \left(\frac{2000}{3600}\right) = 0.000439$$

Step 2. Construct the new IPR curve at 2000 psi by using the new calculated C and applying the inflow equation:

$$Q_o = 0.000439(2000^2 - p_{wf}^2)^{0.854}$$

p_{wf}	Q_o (STB/day)
2000	0
1500	94
1000	150
500	181
0	191

Both the present time and future IPRs are plotted in Figure 5.21.

Klins and Clark (1993) developed empirical correlations that correlate the changes in Fetkovich's performance coefficient C and the flow exponent n with the decline in the reservoir pressure. The authors observed that the exponent n changes considerably with reservoir pressure. Klins and Clark concluded that the "future" values of $(n)_f$ and C at pressure $(\bar{p}_r)_f$ are related to the values of n and C at the bubble point pressure. Denoting C_b and n_b as the values of the performance coefficient and the flow exponent at the bubble point pressure p_b, Klins and Clark introduced the following dimensionless parameters:

- dimensionless performance coefficient = C/C_b;
- dimensionless flow exponent = n/n_b;
- dimensionless average reservoir pressure = $\bar{p}_r/p_b$.

The authors correlated C/C_b and n/n_b to the dimensionless pressure by the following two expressions:

$$\left(\frac{n}{n_b}\right) = 1 + 0.0577\left(1 - \frac{\bar{p}_r}{p_b}\right) - 0.2459\left(1 - \frac{\bar{p}_r}{p_b}\right)^2$$
$$+ 0.503\left(1 - \frac{\bar{p}_r}{p_b}\right)^3 \qquad [5.2.37]$$

and:

$$\left(\frac{C}{C_b}\right) = 1 - 3.5718\left(1 - \frac{\bar{p}_r}{p_b}\right) + 4.7981\left(1 - \frac{\bar{p}_r}{p_b}\right)^2$$
$$- 2.3066\left(1 - \frac{\bar{p}_r}{p_b}\right)^3 \qquad [5.2.38]$$

where:

C_b = performance coefficient at the *bubble point pressure*
n_b = flow exponent at the *bubble point pressure*

The procedure or applying the above relationships in adjusting the coefficients C and n with changing average reservoir pressure is detailed below:

Step 1. Using the available flow test data in conjunction with Fetkovich's equation, i.e., Equation 5.2.35, calculate the present (current) values of n and C at the present average pressure $\bar{p}_r$.

Step 2. Using the current values of $\bar{p}_r$, calculate the dimensionless values of n/n_b and C/C_b by applying Equations 5.2.37 and 5.2.38, respectively.

Step 3. Solve for the constants n_b and C_b from:

$$n_b = \frac{n}{n/n_b} \qquad [5.2.39]$$

and:

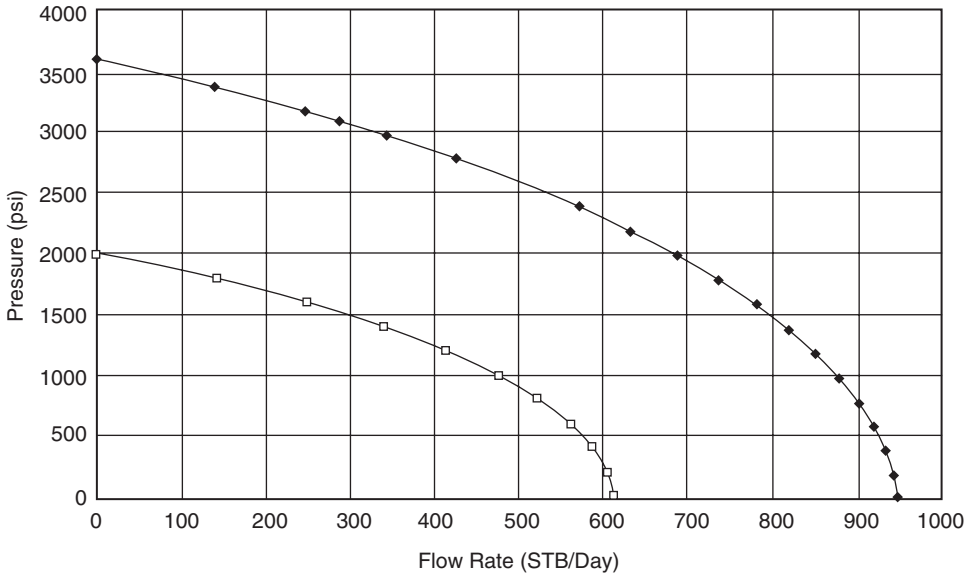$$C_b = \frac{C}{(C/C_b)} \qquad [5.2.40]$$

Figure 5.21 *Future IPR at 2000 psi.*

It should be pointed out that if the present reservoir pressure equals the bubble point pressure, the values of n and C as calculated in step 1 are essentially n_b and C_b.

Step 4. Assume future average reservoir pressure $(\bar{p}_r)_f$ and solve for the corresponding future dimensionless parameters n_f/n_b and C_f/C_b by applying Equations 5.2.37 and 5.2.38, respectively.

Step 5. Solve for future values of n_f and C_f from:

$$n_f = n_b(n/n_b)$$
$$C_f = C_b(C_f/C_b)$$

Step 6. Use n_f and C_f in Fetkovich's equation to generate the well's future IPR at the desired (future) average reservoir pressure $(\bar{p}_r)_f$. It should be noted that the maximum oil flow rate $(Q_o)_{max}$ at $(\bar{p}_r)_f$ is given by:

$$(Q_o)_{max} = C_f[(\bar{p}_r)^2]^{n_f} \qquad [5.2.41]$$

Example 5.16 Using the data given in Example 5.15, generate the future IPR data when the reservoir pressure drops to 3200 psi.

Solution

Step 1. Since the reservoir exists at its bubble point pressure, $p_b = 3600$ psi, then:

$$n_b = 0.854 \quad \text{and} \quad C_b = 0.00079$$

Step 2. Calculate the future dimensionless parameters at 3200 psi by applying Equations 5.2.37 and 5.2.38:

$$\left(\frac{n}{n_b}\right) = 1 + 0.0577\left(1 - \frac{3200}{3600}\right) - 0.2459$$
$$\times \left(1 - \frac{3200}{3600}\right)^2 + 0.5030\left(1 - \frac{3200}{3600}\right)^3$$
$$= 1.0041$$

$$\left(\frac{C}{C_b}\right) = 1 - 3.5718\left(1 - \frac{3200}{3600}\right) + 4.7981$$
$$\left(1 - \frac{3200}{3600}\right)^2 - 2.3066\left(1 - \frac{3200}{3600}\right)^3$$
$$= 0.6592$$

Step 3. Solve for n_f and C_f:

$$n_f = n_b(1.0041) = (0.854)(1.0041) = 0.8575$$

$$C_f = C_b(0.6592) = (0.00079)(0.6592) = 0.00052$$

Therefore, the flow rate is then expressed as:

$$Q_o = C(\bar{p}_r^2 - p_{wf}^2)^n = 0.00052(3200^2 - p_{wf}^2)^{0.8575}$$

The maximum oil flow rate, i.e., AOF, occurs at $p_{wf} = 0$, or

$$(Q_o)_{max} = 0.00052(3200^2 - 0^2)^{0.8575} = 534 \text{ STB/day}$$

Step 4. Construct the following table by assuming several values for p_{wf}:

$$Q_o = 0.00052\left[3200^2 - (p_{wf})^2\right]^{0.8575} = 534 \text{ STB/day}$$

p_{wf}	Q_o
3200	0
2000	349
1500	431
5000	523
0	534

Figure 5.22 compares current and future IPRs as calculated in Examples 5.10 and 5.11.

Case: $\bar{p}_r > p_b$ and $p_{wf} < p_b$ Figure 5.23 shows a schematic illustration of case 3 in which it is assumed that $p_{wf} < p_b$ and $\bar{p}_r > p_b$. The integral in Equation 5.2.25 can be expanded and written as:

$$Q_o = \frac{0.00708kh}{\ln(r_e/r_w) - 0.75 + s}\left[\int_{p_{wf}}^{p_b} f(p)\,dp + \int_{p_b}^{\bar{p}_r} f(p)\,dp\right]$$
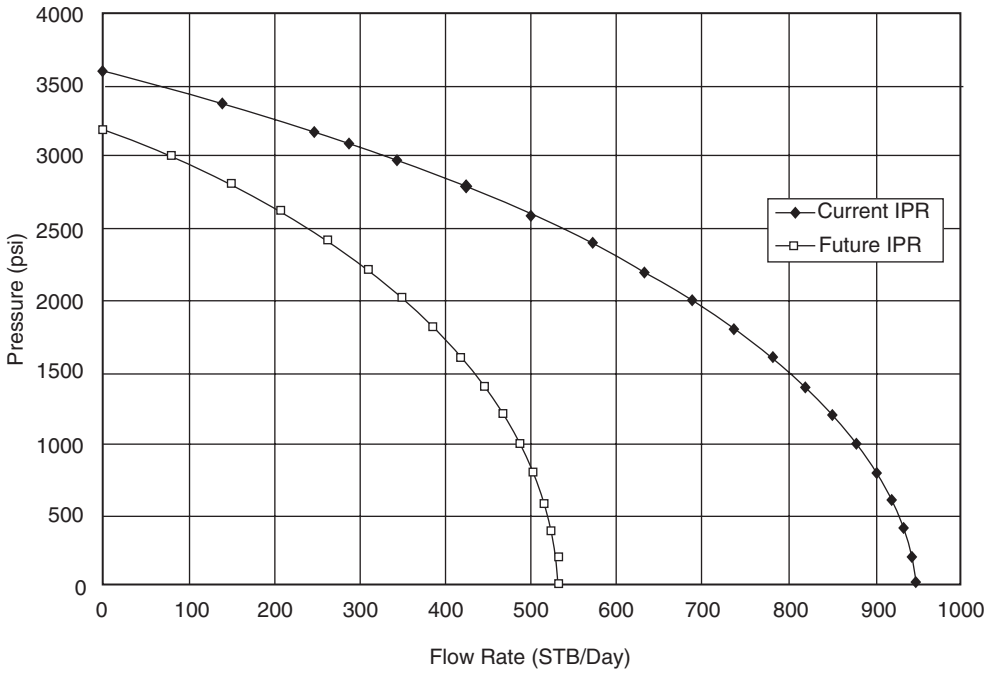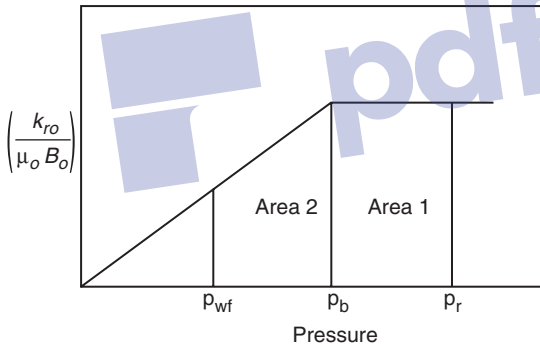
Figure 5.22 *IPR.*

Figure 5.23 *($k_{ro}/\mu_o B_o$) vs. pressure for case 3.*

Substituting Equations 5.2.27 and 5.2.28 into the above expression gives:

$$Q_o = \frac{0.00708kh}{\ln(r_e/r_w) - 0.75 + s}$$
$$\times \left[\int_{p_{wf}}^{p_b} \left(\frac{1}{\mu_o \beta_o}\right)\left(\frac{p}{p_b}\right) dp + \int_{p_b}^{\bar{p}_r} \left(\frac{1}{\mu_o \beta_o}\right) dp \right]$$

where μ_o and B_o are evaluated at the bubble point pressure p_b. Rearranging the above expression gives:

$$Q_o = \frac{0.00708kh}{\mu_o B_o [\ln(r_e/r_w) - 0.75 + s]} \left[\frac{1}{p_b}\int_{p_{wf}}^{p_b} p\,dp + \int_{p_b}^{\bar{p}_r} dp \right]$$

Integrating and introducing the productivity index J into the above relationship gives:

$$Q_o = J \left[\frac{1}{2p_b}\left(p_b^2 - p_{wf}^2\right) + (\bar{p}_r - p_b) \right]$$

or:

$$Q_o = J(\bar{p}_r - p_b) + \frac{J}{2p_b}\left(p_b^2 - p_{wf}^2\right) \qquad [5.2.42]$$

Example 5.17 The following reservoir and flow test data is available on an oil well:

pressure data: $\bar{p}_r = 4000$ psi, $p_b = 3200$ psi

flow test data: $p_{wf} = 3600$ psi, $Q_o = 280$ STB/day

Generate the IPR data of the well.

Solution

Step 1. Since $p_{wf} < p_b$, calculate the productivity index from Equation 5.2.1:

$$J = \frac{Q_o}{\bar{p}_r - p_{wf}} = \frac{Q_o}{\Delta p}$$
$$= \frac{280}{4000 - 3600} = 0.7 \text{ STB/day/psi}$$

Step 2. Generate the IPR data by applying Equation 5.2.30 when the assumed $p_{wf} > p_b$ and using Equation 5.2.42 when $p_{wf} < p_b$. That is:

$$Q_o = J(\bar{p}_r - p_{wf})$$
$$= 0.7(4000 - p_{wf})$$

and:

$$Q_o = J(\bar{p}_r - p_b) + \frac{J}{2p_b}\left(p_b^2 - p_{wf}^2\right)$$
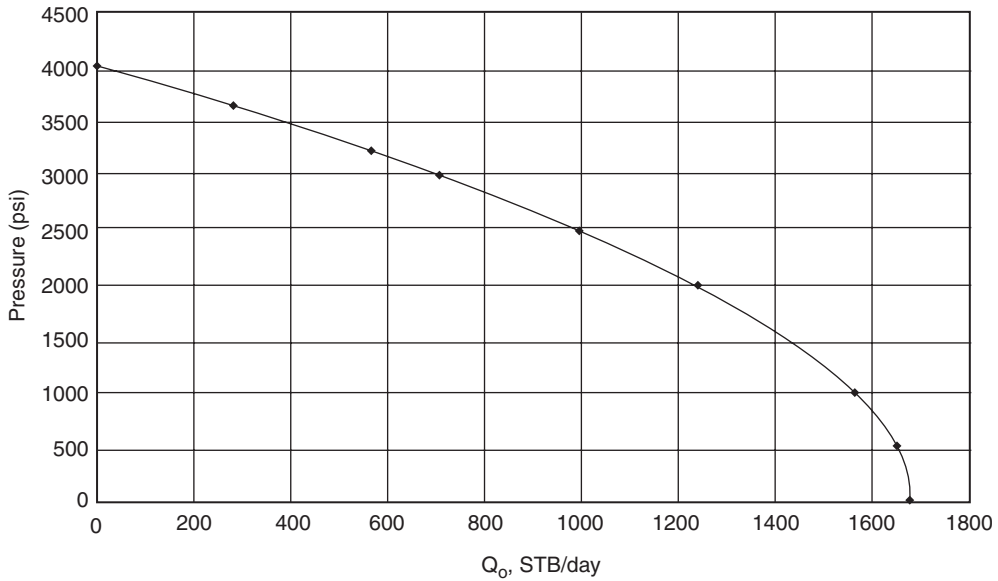$$= 0.7(4000 - 3200) + \frac{0.7}{2(3200)}[(3200)^2 - p_{wf}^2]$$

Figure 5.24   *IPR using the Fetkovich method.*

p_{wf}	*Equation*	Q_o
4000	5.2.30	0
3800	5.2.30	140
3600	5.2.30	280
3200	5.2.30	560
3000	5.2.42	696
2600	5.2.42	941
2200	5.2.42	1151
2000	5.2.42	1243
1000	5.2.42	1571
500	5.2.42	1653
0	5.2.42	1680

Results of the calculations are shown graphically in Figure 5.24.

It should be pointed out the Fetkovich method has the advantage over Standing's methodology in that it does not require the tedious material balance calculations to predict oil saturations at future average reservoir pressures.

Klins and Clark method
Klins and Clark (1993) proposed an inflow expression similar in form to that of Vogel's and can be used to estimate future IPR data. To improve the predictive capability of Vogel's equation, the authors introduced a new exponent d to Vogel's expression. The authors proposed the following relationships:

$$\frac{Q_o}{(Q_o)_{\max}} = 1 - 0.295\left(\frac{p_{wf}}{\bar{p}_r}\right) - 0.705\left(\frac{p_{wf}}{\bar{p}_r}\right)^d \qquad [5.2.43]$$

where:

$$d = \left[0.28 + 0.72\left(\frac{\bar{p}_r}{p_b}\right)\right](1.24 + 0.001p_b) \qquad [5.2.44]$$

The computational steps of the Klins and Clark method are summarized below:

Step 1. Knowing the bubble point pressure and the current reservoir pressure, calculate the exponent d from Equation 5.2.44.

Step 2. From the available stabilized flow data, i.e., Q_o at p_{wf}, solve Equation 5.2.43 for $(Q_o)_{\max}$. That is:

$$(Q_o)_{\max} = \frac{Q_o}{1 - 0.295\left(\frac{p_{wf}}{\bar{p}_r}\right) - 0.705\left(\frac{p_{wf}}{\bar{p}_r}\right)^d}$$

Step 3. Construct the current IPR by assuming several values of p_{wf} in Equation 5.2.43 and solving for Q_o.

5.2.2 Horizontal oil well performance
Since 1980, horizontal wells began capturing an ever-increasing share of hydrocarbon production. Horizontal wells offer the following advantages over vertical wells:

- The large volume of the reservoir can be drained by each horizontal well.
- Higher productions from thin pay zones.
- Horizontal wells minimize water and gas zoning problems.
- In high-permeability reservoirs, where near-wellbore gas velocities are high in vertical wells, horizontal wells can be used to reduce near-wellbore velocities and turbulence.
- In secondary and enhanced oil recovery applications, long horizontal injection wells provide higher injectivity rates.
- The length of the horizontal well can provide contact with multiple fractures and greatly improve productivity.

The actual production mechanism and reservoir flow regimes around the horizontal well are considered more complicated than those for the vertical well, especially if the horizontal section of the well is of a considerable length. Some combination of both linear and radial flow actually exists, and the well may behave in a manner similar to that of a well that has been extensively fractured. Sherrad et al. (1987) reported that the shape of measured IPRs for horizontal wells is similar to those predicted by the Vogel or Fetkovich methods. The authors pointed out that the productivity gain from drilling horizontal wells 1500 feet long is two to four times that of a vertical well.

A horizontal well can be looked upon as a number of vertical wells drilling next to each other and completed in a limited
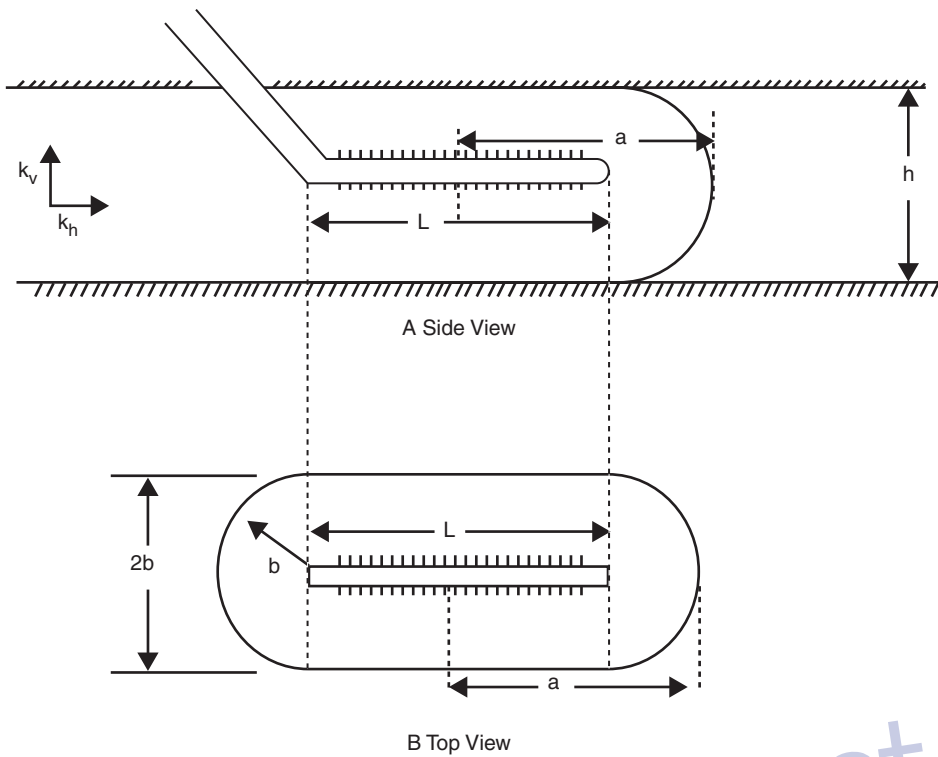
Figure 5.25   *Horizontal well drainage area.*

pay zone thickness. Figure 5.25 shows the drainage area of a horizontal well of length L in a reservoir with a pay zone thickness of h. Each end of the horizontal well would drain a half-circular area of radius b, with a rectangular drainage shape of the horizontal well.

Assuming that each end of the horizontal well is represented by a vertical well that drains an area of a semicircle with a radius of b, Joshi (1991) proposed the following two methods for calculating the drainage area of a horizontal well.

Method I

Joshi proposed that the drainage area is represented by two semicircles of radius b (equivalent to a radius of a vertical well r_{ev}) at each end and a rectangle, of dimensions $2b - L$, in the center. The drainage area of the horizontal well is then given by:

$$A = \frac{L(2b) + \pi b^2}{43\,560} \tag{5.2.45}$$

where:

A = drainage area, acres
L = Length of the horizontal well, ft
b = half minor axis of an ellipse, ft

Method II

Joshi assumed that the horizontal well drainage area is an ellipse and given by:

$$A = \frac{\pi ab}{43\,560} \tag{5.2.46}$$

with:

$$a = \frac{L}{2} + b \tag{5.2.47}$$

where a is the half major axis of an ellipse.

Joshi noted that the two methods give different values for the drainage area A and suggested assigning the average value for the drainage of the horizontal well. Most of the production rate equations require the value of the drainage radius of the horizontal well, which is given by:

$$r_{eh} = \sqrt{\frac{43\,560\,A}{\pi}}$$

where:

r_{eh} = drainage radius of the horizontal well, ft
A = drainage area of the horizontal well, acres

Example 5.18   A 480 acre lease is to be developed by using 12 vertical wells. Assuming that each vertical well would effectively drain 40 acres, calculate the possible number of either 1000 or 2000 ft long horizontal wells that will drain the Lease effectively.

Solution

Step 1.   Calculate the drainage radius of the vertical well:

$$r_{ev} = b = \sqrt{\frac{(40)(43\,560)}{\pi}} = 745 \text{ ft}$$

Step 2.   Calculate the drainage area of the 1000 and 2000 ft long horizontal well using Joshi's two methods.

Method I:
For the 1000 ft horizontal well and using Equation 5.2.45:

$$A = \frac{L\,(2b) + \pi b^2}{43\,560}$$

$$= \frac{(1000)\,(2 \times 745) + \pi\,(745)^2}{43\,560} = 74 \text{ acres}$$

For the 2000 ft horizontal well:

$$A = \frac{L\,(2b) + \pi b^2}{43\,560}$$

$$= \frac{(2000)\,(2 \times 745) + \pi\,(745)^2}{43\,560} = 108 \text{ acres}$$

Method II:
For the 1000 ft horizontal well and using Equation 5.2.46:

$$a = \frac{L}{2} + b$$

$$= \frac{1000}{2} + 745 = 1245 \text{ ft}$$

$$A = \frac{\pi a b}{43\,560}$$

$$= \frac{\pi\,(1245)\,(745)}{43\,560} = 67 \text{ acres}$$

For the 2000 ft horizontal well:

$$a = \frac{2000}{2} + 745 = 1745 \text{ ft}$$

$$A = \frac{\pi\,(1745)\,(745)}{43\,560} = 94 \text{ acres}$$

Step 3. *Averaging* the values from the two methods, the drainage area of the 1000 ft long is well:

$$A = \frac{74 + 67}{2} = 71 \text{ acres}$$

and the drainage area of 2000 ft long well is:

$$A = \frac{108 + 94}{2} = 101 \text{ acres}$$

Step 4. Calculate the number of horizontal wells 1000 ft long:

Total number of 1000 ft horizontal wells

$$= \frac{\text{total area}}{\text{drainage area per well}}$$

$$= \frac{480}{71} = 7 \text{ wells}$$

Step 5. Calculate the number of horizontal wells 2000 ft long:

Total number of 2000 ft horizontal wells

$$= \frac{\text{total area}}{\text{drainage area per well}}$$

$$= \frac{480}{101} = 5 \text{ wells}$$

From a practical standpoint, inflow performance calculations for horizontal wells are presented here under the following two flowing conditions:

(1) steady-state single-phase flow;
(2) pseudosteady-state two-phase flow.

The reference textbook by Joshi (1991) provides an excellent treatment of horizontal well technology and it contains detailed documentation of recent methodologies of generating IPRs.

5.2.3 Horizontal well productivity under steady-state flow

The steady-state analytical solutions are the simplest form of horizontal well solutions. The steady-state solution requires that the pressure at any point in the reservoir does not change with time. The flow rate equation in a steady-state condition is represented by:

$$Q_{\text{oh}} = J_{\text{h}}(p_{\text{r}} - p_{\text{wf}}) = J_{\text{h}}\,\Delta p \qquad [5.2.48]$$

where:

Q_{oh} = horizontal well flow rate, STB/day
Δp = pressure drop from the drainage boundary to wellbore, psi
J_{h} = productivity index of the horizontal well, STB/day/psi

The productivity index of the horizontal well J_{h} can always be obtained by dividing the flow rate Q_{oh} by the pressure drop Δp, or:

$$J_{\text{h}} = \frac{Q_{\text{oh}}}{\Delta p}$$

There are several methods that are designed to predict the productivity index from the fluid and reservoir properties. Some of these methods include:

- the Borisov method;
- the Giger, Reiss, and Jourdan method;
- the Joshi method;
- the Benard and Dupuy method.

Borisov method
Borisov (1984) proposed the following expression for predicting the productivity index of a horizontal well in an isotropic reservoir, i.e., $k_{\text{v}} = k_{\text{h}}$:

$$J_{\text{h}} = \frac{0.00708 h k_{\text{h}}}{\mu_o B_o \left[\ln\left(\frac{4 r_{\text{eh}}}{L} \right) + \left(\frac{h}{L} \right) \ln\left(\frac{h}{2\pi r_{\text{w}}} \right) \right]} \qquad [5.2.49]$$

where:

h = thickness, ft
k_{h} = horizontal permeability, md
k_{v} = vertical permeability, md
L = length of the horizontal well, ft
r_{eh} = drainage radius of the horizontal well, ft
r_{w} = wellbore radius, ft
J_{h} = productivity index, STB/day/psi

Giger, Reiss, and Jourdan method
For an isotropic reservoir where the vertical permeability k_{v} equals the horizontal permeability k_{h}, Giger, et al. (1984) proposed the following expression for determining J_{h}:

$$J_{\text{h}} = \frac{0.00708 L k_{\text{h}}}{\mu_o B_o \left[\left(\frac{L}{h} \right) \ln(X) + \ln\left(\frac{h}{2 r_{\text{w}}} \right) \right]} \qquad [5.2.50]$$

where:

$$X = \frac{1 + \sqrt{1 + [L/2 r_{\text{eh}}]^2}}{L/(2 r_{\text{eh}})} \qquad [5.2.51]$$

To account for the reservoir anisotropy, the authors proposed the following relationships:

$$J_{\text{h}} = \frac{0.00708 k_{\text{h}}}{\mu_o B_o \left[\left(\frac{1}{h} \right) \ln(X) + \left(\frac{\beta^2}{L} \right) \ln\left(\frac{h}{2 r_{\text{w}}} \right) \right]} \qquad [5.2.52]$$

with the parameter β as defined by:

$$\beta = \sqrt{\frac{k_h}{k_v}} \qquad [5.2.53]$$

where:

k_v = vertical permeability, md
L = length of the horizontal section, ft

Joshi method

Joshi (1991) presented the following expression for estimating the productivity index of a horizontal well in isotropic reservoirs:

$$J_h = \frac{0.00708hk_h}{\mu_o B_o\left[\ln(R) + \left(\dfrac{h}{L}\right)\ln\left(\dfrac{h}{2r_w}\right)\right]} \qquad [5.2.54]$$

with:

$$R = \frac{a + \sqrt{a^2 - (L/2)^2}}{(L/2)} \qquad [5.2.55]$$

and a is half the major axis of the drainage ellipse and given by:

$$a = (L/2)\left[0.5 + \sqrt{0.25 + (2r_{eh}/L)^4}\right]^{0.5} \qquad [5.2.56]$$

Joshi accounted for the influence of the reservoir anisotropy by introducing the vertical permeability k_v into Equation 5.2.54, to give:

$$J_h = \frac{0.00708hk_h}{\mu_o B_o\left[\ln(R) + \left(\dfrac{B^2 h}{L}\right)\ln\left(\dfrac{h}{2r_w}\right)\right]} \qquad [5.2.57]$$

where the parameters B and R are defined by Equations 5.2.53 and 5.2.55, respectively.

Renard and Dupuy method

For an isotropic reservoir, Renard and Dupuy (1990) proposed the following expression:

$$J_h = \frac{0.00708hk_h}{\mu_o B_o\left[\cosh^{-1}\left(\dfrac{2a}{L}\right) + \left(\dfrac{h}{L}\right)\ln\left(\dfrac{h}{2\pi r_w}\right)\right]} \qquad [5.2.58]$$

where a is half the major axis of the drainage ellipse and given by Equation 5.2.56.

For anisotropic reservoirs, the authors proposed the following relationship:

$$J_h = \frac{0.00708hk_h}{\mu_o B_o\left[\cosh^{-1}\left(\dfrac{2a}{L}\right) + \left(\dfrac{\beta h}{L}\right)\ln\left(\dfrac{h}{2\pi r_w'}\right)\right]} \qquad [5.2.59]$$

where:

$$r_w^\backslash = \frac{(1+\beta)\,r_w}{2\beta} \qquad [5.2.60]$$

with the parameter β as defined by Equation 5.2.53.

Example 5.19 A horizontal well 2000 feet long drains an estimated drainage area of 120 acres. The reservoir is characterized by an isotropic formation with the following properties:

$k_v = k_h = 100$ md, $h = 60$ ft,
$B_o = 1.2$ bbl/STB, $\mu_o = 0.9$ cp,
$p_e = 3000$ psi, $p_{wf} = 2500$ psi,
$r_w = 0.30$ ft

Assuming a steady-state flow, calculate the flow rate by using:

(a) the Borisov method;
(b) the Giger, Reiss, and Jourdan method;
(c) the Joshi's method;
(d) the Renard and Dupuy method.

Solution

(a) Borisov method:

Step 1. Calculate the drainage radius of the horizontal well:

$$r_{eh} = \sqrt{\frac{43\,560A}{\pi}} = \sqrt{\frac{(43\,560)\,(120)}{\pi}} = 1290 \text{ ft}$$

Step 2. Calculate J_h by using Equation 5.2.49:

$$J_h = \frac{0.00708hk_h}{\mu_o B_o\left[\ln\left(\dfrac{4r_{eh}}{L}\right) + \left(\dfrac{h}{L}\right)\ln\left(\dfrac{h}{2\pi r_w}\right)\right]}$$

$$= \frac{(0.00708)\,(60)\,(100)}{(0.9)\,(1.2)\left[\ln\left(\dfrac{(4)\,(1290)}{2000}\right) + \left(\dfrac{60}{2000}\right)\ln\left(\dfrac{60}{2\pi\,(0.3)}\right)\right]}$$

$$= 37.4 \text{ STB/day/psi}$$

Step 3. Calculate the flow rate by applying Equation 5.2.48:

$$Q_{oh} = J_h \Delta p$$

$$= (37.4)\,(3000 - 2500) = 18\,700 \text{ STB/day}$$

(b) Giger, Reiss, and Jourdan method:

Step 1. Calculate the parameter X from Equation 5.2.51:

$$X = \frac{1 + \sqrt{1 + \left(\dfrac{L}{2r_{eh}}\right)^2}}{L/(2r_{eh})}$$

$$= \frac{1 + \sqrt{1 + \left(\dfrac{2000}{(2)\,(1290)}\right)^2}}{2000/[(2)\,(1290)]} = 2.105$$

Step 2. Solve for J_h by applying Equation 5.2.50:

$$J_h = \frac{0.00708Lk_h}{\mu_o B_o\left[\left(\dfrac{L}{h}\right)\ln(X) + \ln\left(\dfrac{h}{2r_w}\right)\right]}$$

$$= \frac{(0.00708)\,(2000)\,(100)}{(0.9)\,(1.2)\left[\left(\dfrac{2000}{60}\right)\ln(2.105) + \ln\left(\dfrac{60}{2\,(0.3)}\right)\right]}$$

$$= 44.57 \text{ STB/day}$$

Step 3. Calculate the flow rate:

$$Q_{oh} = 44.57(3000 - 2500) = 22\,286 \text{ STB/day}$$

(c) Joshi method:

Step 1. Calculate the half major axis of the ellipse by using Equation 5.2.56:

$$a = (L/2)\left[0.5 + \sqrt{0.25 + (2r_{eh}/L)^4}\right]^{0.5}$$

$$= \left(\frac{2000}{2}\right)\left[0.5 + \sqrt{0.25 + [2(1290)/2000]^2}\right]^{0.5}$$

$$= 1372 \text{ ft}$$

Step 2. Calculate the parameter R from Equation 5.2.55:

$$R = \frac{a + \sqrt{a^2 - (L/2)^2}}{(L/2)}$$

$$= \frac{1372 + \sqrt{(1372)^2 - (2000/2)^2}}{(2000/2)} = 2.311$$

Step 3. Solve for J_h by applying Equation 5.2.54:

$$J_h = \frac{0.00708 hk_h}{\mu_o B_o \left[\ln (R) + \left(\frac{h}{L} \right) \ln \left(\frac{h}{2r_w} \right) \right]}$$

$$= \frac{0.00708 \, (60) \, (100)}{(0.9) \, (1.2) \left[\ln (2.311) + \left(\frac{60}{2000} \right) \ln \left(\frac{60}{(2) \, (0.3)} \right) \right]}$$

$$= 40.3 \, \text{STB/day/psi}$$

Step 4. Calculate the flow rate:

$$Q_{oh} = J_h \Delta p$$

$$= (40.3) \, (3000 - 2500) = 20\,154 \, \text{STB/day}$$

(d)   Renard and Dupuy method:

Step 1. Calculate a from Equation 5.2.56:

$$a = (L/2) \left[0.5 + \sqrt{0.25 + (2r_{eh}/L)^4} \right]^{0.5}$$

$$= \left(\frac{2000}{2} \right) \left[0.5 + \sqrt{0.25 + \left[2(1290)/2000 \right]^2} \right]^{0.5}$$

$$= 1372 \, \text{ft}$$

Step 2. Apply Equation 5.2.58 to determine J_h:

$$J_h = \frac{0.00708 hk_h}{\mu_o B_o \left[\cosh^{-1} \left(\frac{2a}{L} \right) + \left(\frac{h}{L} \right) \ln \left(\frac{h}{2\pi r_w} \right) \right]}$$

$$= \frac{0.00708 \, (60) \, (100)}{(0.9) \, (1.2) \left[\cosh^{-1} \left(\frac{(2) \, (1372)}{2000} \right) + \left(\frac{60}{2000} \right) Ln \left(\frac{60}{2\pi \, (0.3)} \right) \right]}$$

$$= 41.77 \, \text{STB/day/psi}$$

Step 3. Calculate the flow rate:

$$Q_{oh} = 41.77 (3000 - 2500) = 20\,885 \, \text{STB/day}$$

Example 5.20   Using the data in Example 5.19 and assuming an isotropic reservoir with $k_h = 100$ md and $k_v = 10$ md, calculate the flow rate by using:

(a) the Giger, Reiss, and Jourdan method;
(b) the Joshi method;
(c) the Renard and Dupuy method.

Solution

(a) Giger, Reiss, and Jourdan method:

Step 1. Solve for the permeability ratio β by applying Equation 5.2.53:

$$\beta = \sqrt{\frac{k_h}{k_v}}$$

$$= \sqrt{\frac{100}{10}} = 3.162$$

Step 2. Calculate the parameter X as shown in Example 5.19, to give:

$$X = \frac{1 + \sqrt{1 + \left(\frac{L}{2r_{eh}} \right)^2}}{L/(2r_{eh})} = 2.105$$

Step 3. Determine J_h by using Equation 5.2.52:

$$J_h = \frac{0.00708 k_h}{\mu_o B_o \left[\left(\frac{1}{h} \right) \ln (X) + \left(\frac{\beta^2}{L} \right) \ln \left(\frac{h}{2r_w} \right) \right]}$$

$$= \frac{0.00708 \, (100)}{(0.9) \, (1.2) \left[\left(\frac{1}{60} \right) \ln (2.105) + \left(\frac{3.162^2}{2000} \right) \ln \left(\frac{60}{(2) \, (0.3)} \right) \right]}$$

$$= 18.50 \, \text{STB/day/psi}$$

Step 4. Calculate Q_{oh}:

$$Q_{oh} = (18.50) \, (3000 - 2500) = 9\,252 \, \text{STB/day}$$

(b) Joshi method:

Step 1. Calculate the permeability ratio β:

$$\beta = \sqrt{\frac{k_h}{k_v}} = 3.162$$

Step 2. Calculate the parameters a and R as given in Example 5.19:

$$a = 1372 \, \text{ft}, \quad R = 2.311$$

Step 3. Calculate J_h by using Equation 5.2.54:

$$J_h = \frac{0.00708 hk_h}{\mu_o B_o \left[\ln (R) + \left(\frac{h}{L} \right) \ln \left(\frac{h}{2r_w} \right) \right]}$$

$$= \frac{0.00708 \, (60) \, (100)}{(0.9) \, (1.2) \left[\ln (2.311) + \left(\frac{(3.162)^2 \, (60)}{2000} \right) \ln \left(\frac{60}{2 \, (0.3)} \right) \right]}$$

$$= 17.73 \, \text{STB/day/psi}$$

Step 4. Calculate the flow rate:

$$Q_{oh} = (17.73) \, (3000 - 2500) = 8\,863 \, \text{STB/day}$$

(c) Renard and Dupuy method:

Step 1. Calculate $r_w^\backslash$ from Equation 5.2.60:

$$r_w^\backslash = \frac{(1 + \beta) \, r_w}{2\beta}$$

$$r_w^\backslash = \frac{(1 + 3.162) \, (0.3)}{(2) \, (3.162)} = 0.1974$$

Step 2. Apply Equation 5.2.59:

$$J_h = 0.00708 \, (60) \, (100) \Big/$$

$$(0.9) \, (1.2) \left\{ \cosh^{-1} \left[\frac{(2) \, (1372)}{2000} \right] + \left[\frac{(3.162)^2 \, (60)}{2000} \right] \ln \left(\frac{60}{(2)\pi \, (0.1974)} \right) \right\}$$

$$= 19.65 \, \text{STB/day/psi}$$

Step 3. Calculate the flow rate :

$$Q_{oh} = 19.65 (3000 - 2500) = 9\,825 \, \text{STB/day}$$

5.2.4 Horizontal well productivity under semisteady-state flow

The complex flow regime existing around a horizontal well-bore probably precludes using a method as simple as that of Vogel to construct the IPR of a horizontal well in solution gas drive reservoirs. However, if at least two stabilized flow tests are available, the parameters J and n in Fetkovich's equation (i.e., Equation 5.2.35) could be determined and used to construct the IPR of the horizontal well. In this case, the values of J and n would account not only for the effects of turbulence and gas saturation around the wellbore, but also for the effects of the non-radial flow regime existing in the reservoir.

Bendakhlia and Aziz (1989) used a reservoir model to generate IPRs for a number of wells and found that a combination of Vogel's and Fetkovich's equations would fit the generated data if expressed as:

$$\frac{Q_{oh}}{(Q_{oh})_{max}} = \left[1 - V\left(\frac{p_{wf}}{\bar{p}_r}\right) - (1-V)\left(\frac{p_{wf}}{\bar{p}_r}\right)^2 \right]^n \quad [5.2.61]$$

where:

$(Q_{oh})_{max}$ = horizontal well maximum flow rate, STB/day
n = exponent in Fetkovich's equation
V = variable parameter

In order to apply the equation, at least three stabilized flow tests are required to evaluate the three unknowns $(Q_{oh})_{max}$, V, and n at any given average reservoir pressure $\bar{p}_r$. However, Bendakhlia and Aziz indicated that the parameters V and n are functions of the reservoir pressure or recovery factor and, thus, the use of Equation 5.2.61 is not convenient in a predictive mode.

Cheng (1990) presented a form of Vogel's equation for horizontal wells that is based on the results from a numerical simulator. The proposed expression has the following form:

$$\frac{Q_{oh}}{(Q_{oh})_{max}} = 0.9885 + 0.2055\left(\frac{p_{wf}}{\bar{p}_r}\right) - 1.1818\left(\frac{p_w}{\bar{p}_r}\right)^2 \quad [5.2.62]$$

Petnanto and Economides (1998) developed a generalized IPR equation for a horizontal and multilateral well in a solution gas drive reservoir. The proposed expression has the following form:

$$\frac{Q_{oh}}{(Q_{oh})_{max}} = 1 - 0.25\left(\frac{p_{wf}}{\bar{p}_r}\right) - 0.75\left(\frac{p_{wf}}{\bar{p}_r}\right)^n \quad [5.2.63]$$

where:

$$n = \left[-0.27 + 1.46\left(\frac{\bar{p}_r}{p_b}\right) - 0.96\left(\frac{\bar{p}_r}{p_b}\right)^2 \right]$$
$$\times (4 + 1.66 \times 10^{-3} p_b) \quad [5.2.64]$$

with:

$$(Q_{oh})_{max} = \frac{J\bar{p}_r}{0.25 + 0.75n}$$

Example 5.21 A horizontal well 1000 foot long is drilled in a solution gas drive reservoir. The well is producing at a stabilized flow rate of 760 STB/day and wellbore pressure of 1242 psi. The current average reservoir pressure is 2145 psi. Generate the IPR data of this horizontal well by using the Cheng method.

Solution

Step 1. Use the given stabilized flow data to calculate the maximum flow rate of the horizontal well:

$$\frac{Q_{oh}}{(Q_{oh})_{max}} = 1.0 + 0.2055\left(\frac{p_{wf}}{\bar{p}_r}\right) - 1.1818\left(\frac{p_w}{\bar{p}_r}\right)^2$$

$$\frac{760}{(Q_{oh})_{max}} = 1 + 0.2055\left(\frac{1242}{2145}\right) - 1.1818\left(\frac{1242}{2145}\right)$$

$(Q_{oh})_{max} = 1052$ STB/day

Step 2. Generate the IPR data by applying Equation 5.2.63:

$$Q_{oh} = (Q_{oh})_{max}\left[1.0 + 0.2055\left(\frac{p_{wf}}{\bar{p}_r}\right) \right.$$
$$\left. -1.1818\left(\frac{p_w}{\bar{p}_r}\right)^2 \right]$$

p_{wf}	$(Q_{oh})_{max}$
2145	0
1919	250
1580	536
1016	875
500	1034
0	1052

5.3 Phase 3. Relating Reservoir Performance to Time

All reservoir performance techniques show the relationship of cumulative oil production and the instantaneous GOR as a function of average reservoir pressure. However, these techniques do not relate the cumulative oil production N_p and cumulative gas production G_p with time. Figure 5.26 shows a schematic illustration of the predicted cumulative oil production with declining average reservoir pressure.

The time required for production can be calculated by applying the concept of the IPR in conjunction with the MBE predictions. For example, Vogel (1968) expressed the well's IPR by Equation 5.2.9 as:

$$Q_o = (Q_o)_{max}\left[1 - 0.2\left(\frac{p_{wf}}{\bar{p}_r}\right) - 0.8\left(\frac{p_{wf}}{\bar{p}_r}\right)^2 \right]$$

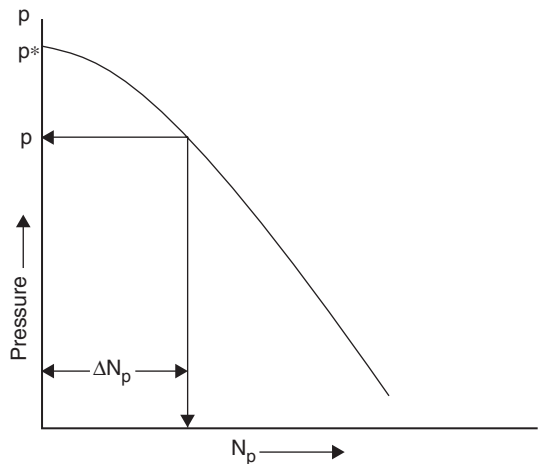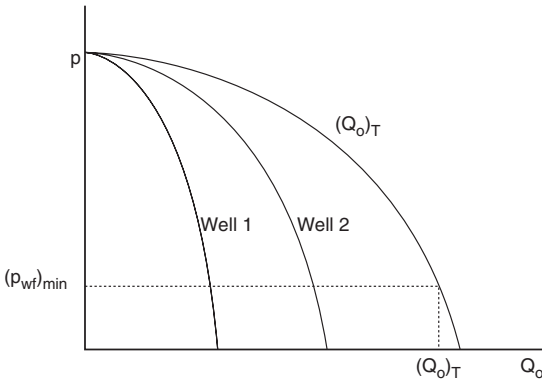**Figure 5.26** Cumulative production as a function of average reservoir pressure.

Figure 5.27 *Overall field IPR at future average pressure.*

The following methodology can be employed to correlate the predicted cumulative field production with time t:

Step 1. Plot the *predicted* cumulative oil production N_p as a function of average reservoir pressure p as shown in Figure 5.26.

Step 2. Assume that the current reservoir pressure is p^* with a current cumulative oil production of $(N_p)^*$ and total field flow rate of $(Q_o)_T^*$.

Step 3. Select a future average reservoir pressure p and determine the future cumulative oil production N_p from Figure 5.26.

Step 4. Using the selected future average reservoir pressure p, construct the IPR curve for *each well in the field* (as shown schematically in Figure 5.27 for two hypothetical wells). Establish the total field IPR by taking the summation of the flow rates of all wells at any time.

Step 5. Using the minimum bottom-hole flowing pressure $(p_{wf})_{min}$, determine the total field flow rate $(Q_o)_T$.

$$(Q_o)_T = \sum_{i=1}^{\#\ wells} (Q_o)_i$$

Step 6. Calculate the average field production rate $\left(\overline{Q}_o\right)_T$:

$$\left(\overline{Q}_o\right)_T = \frac{(Q_o)_T + (Q_o)_T^*}{2}$$

Step 7. Calculate the time Δt required for the incremental oil production ΔN_p during the first pressure drop interval, i.e., from p^* to p, by:

$$\Delta t = \frac{N_p - N_p^*}{\left(\overline{Q}_o\right)_T} = \frac{\Delta N_p}{\left(\overline{Q}_o\right)_T}$$

Step 8. Repeat the above steps and calculate the total time t to reach an average reservoir pressure p, by:

$$t = \Sigma \Delta t$$

Problems

1. An oil well is producing under steady-state flow conditions at 300 STB/day. The bottom-hole flowing pressure is recorded at 2500 psi. Given:

$$h = 23 \text{ ft}, \quad k = 50 \text{ md}, \quad \mu_o = 2.3 \text{ cp},$$
$$B_o = 1.4 \text{ bbl/STB}, \quad r_e = 660 \text{ ft}, \quad s = 0.5$$

Calculate:

(a) the reservoir pressure;
(b) the AOF;
(c) the productivity index.

2. A well is producing from a saturated oil reservoir with an average reservoir pressure of 3000 psig. Stabilized flow test data indicates that the well is capable of producing 400 STB/day at a bottom-hole flowing pressure of 2580 psig.
   Calculate the remaining oil-in-place at 3000 psi.

   (a) Oil flow rate at $p_{wf} = 1950$ psig.
   (b) Construct the IPR curve at the current average pressure.
   (c) Construct the IPR curve by assuming a constant J.
   (d) Plot the IPR curve when the reservoir pressure is 2700 psig.

3. An oil well is producing from an undersaturated reservoir that is characterized by a bubble point pressure of 2230 psig. The current average reservoir pressure is 3500 psig. Available flow test data shows that the well produced 350 STB/day at a stabilized p_{wf} of 2800 psig. Construct the IPR data, by using:

   (a) Vogel's correlation;
   (b) Wiggins method.
   (c) Generate the IPR curve when the reservoir pressure declines to 2230 and 2000 psi.

4. A well is producing from a saturated oil reservoir that exists at its saturation pressure of 4500 psig. The well is flowing at a stabilized rate of 800 STB/day and a p_{wf} of 3700 psig. Material balance calculations provide the following current and future predictions for oil saturation and *PVT* properties:

	Present	*Future*
$\overline{p}_r$	4500	3300
μ_o, cp	1.45	1.25
B_o, bbl/STB	1.23	1.18
k_{ro}	1.00	0.86

   Generate the future IPR for the well at 3300 psig by using the Standing method.

5. A four-point stabilized flow test was conducted on a well producing from a saturated reservoir that exists at an average pressure of 4320 psi.

Q_o, (STB/day)	p_{wf}, (psi)
342	3804
498	3468
646	2928
832	2580

   (a) Construct a complete IPR by using the Fetkovich method.
   (b) Construct the IPR when the reservoir pressure declines to 2500 psi.

6. The following reservoir and flow test data is available on an oil well:

   pressure data: $\quad \overline{p}_r = 3280$ psi $\quad\quad p_b = 2624$ psi

   flow test data: $\quad p_{wf} = 2952$ psi $\quad\quad Q_o = $ STB/day

   Generate the IPR data of the well.

7. A horizontal well 2500 feet long drains an estimated drainage area of 120 acres. The reservoir is characterized by an isotropic formation with the following properties:

$$k_v = k_h = 60 \text{ md}, \quad h = 70 \text{ ft},$$
$$B_o = 1.4 \text{ bbl/STB}, \quad \mu_o = 1.9 \text{ cp}$$
$$p_e = 3900 \text{ psi}, \quad p_{wf} = 3250 \text{ psi}$$
$$r_w = 0.30 \text{ ft}$$

Assuming a steady-state flow, calculate the flow rate by using:

(a) the Borisov method;
(b) the Giger, Reiss, and Jourdan method;
(c) the Joshi method;
(d) the Renard and Dupuy method.

8. A horizontal well 2000 feet long is drilled in a solution gas drive reservoir. The well is producing at a stabilized flow rate of 900 STB/day and wellbore pressure of 1000 psi. The current average reservoir pressure is 2000 psi. Generate the IPR data of this horizontal well by using the Cheng method.

9. The following *PVT* data is for the Aneth Field in Utah:

Pressure (psia)	B_o (bbl/STB)	R_{so} (scf/STB)	B_g (bbl/SCF)	μ_o/μ_g
2200	1.383	727	–	–
1850	1.388	727	0.00130	35
1600	1.358	654	0.00150	39
1300	1.321	563	0.00182	47
1000	1.280	469	0.00250	56
700	1.241	374	0.00375	68
400	1.199	277	0.00691	85
100	1.139	143	0.02495	130
40	1.100	78	0.05430	420

The initial reservoir temperature was 133°F, the initial pressure was 220 psia, and the bubble-point pressure was 1850 psia. There was no active water drive. From 1850 psia to 1300 psia a total of 720 MMSTB of oil were produced and 590.6 MMscf of gas.

(a) How many reservoir barrels of oil were in place at 1850 psia?
(b) The average porosity was 10%, and connate water saturation was 28%. The field covered 50 000 acres. What is the average formation thickness in feet?

10. An oil reservoir initially contains 4 MMSTB of oil at its bubble point pressure of 3150 psia with 600 scf/STB of gas in solution. When the average reservoir pressure has dropped to 2900 psia, the gas in solution is 550 scf/STB. B_{oi} was 1.34 bbl/STB and B_o at a pressure of 2900 psia is 1.32 bbl/STB.
Other data:

$R_p = 600$ scf/STB at 2900 psia, $S_{wi} = 0.25$,
$B_g = 0.0011$ bbl/SCF at 2900 psia
volumetric reservoir no original gas cap

(a) How many STB of oil will be produced when the pressure has decreased to 2900 psia?
(b) Calculate the free gas saturation that exists at 2900 psia.

11. The following data is obtained from laboratory core tests, production data, and logging information:

well spacing = 320 acres
net pay thickness = 50 ft with the gas/oil contact 10 ft from the top
porosity = 0.17
initial water saturation = 0.26
initial gas saturation = 0.15
bubble-point pressure = 3600 psia
initial reservoir pressure = 3000 psia
reservoir temperature = 120°F
$B_{oi} = 1.26$ bbl/STB
$B_o = 1.37$ bbl/STB at the bubble point pressure
$B_o = 1.19$ bbl/STB at 2000 psia
$N_p = 2.00$ MM/STB at 2000 psia
$G_p = 2.4$ MMMSCF at 2000 psia
gas compressibility factor, $Z = 1.0 - 0.0001p$
solution, GOR $R_{so} = 0.2p$

Calculate the amount of water that has influxed and the drive indexes at 2000 psia.

12. The following production data is available on a depletion drive reservoir:

p (psi)	GOR (scf/STB)	N_p (MMSTB)
3276	1098.8	0
2912	1098.8	1.1316
2688	1098.8	1.8532
2352	1098.8	2.8249
2016	1587.52	5.9368
1680	2938.88	9.86378
1344	5108.6	12.5632

Calculate cumulative gas produced G_p and cumulative GOR at each pressure.

13. A volumetric solution gas drive reservoir has an initial water saturation of 25%. The initial oil formation volume factor is reported at 1.35 bbl/STB. When 8% of the initial oil was produced, the value of B_o decreased to 1.28. Calculate the oil saturation and gas saturation.

14. The following data is available on a volumetric undersaturated oil reservoir.

$$p_i = 4400 \text{ psi}, \quad p_b = 3400 \text{ psi},$$
$$N = 120 \text{ MMSTB}, \quad c_f = 4 \times 10^{-6} \text{ psi}^{-1},$$
$$c_o = 12 \times 10^{-6} \text{ psi}^{-1}, \quad c_w = 2 \times 10^{-6} \text{ psi}^{-1},$$
$$S_{wi} = 25\%, \quad B_{oi} = 1.35 \text{ bbl/STB}$$

Estimate cumulative oil production when the reservoir pressure drops to 4000 psi. The oil formation volume factor at 4000 psi is 1.38 bbl/STB.

This page intentionally left blank

6

# Introduction to Oil Field Economics

Contents

The objective of this chapter is to explain the fundamentals of investment decision making with an emphasis on the methods most commonly used in the petroleum industry. To successfully evaluate investment alternatives associated with oil and gas properties, knowledge of investment decision making and petroleum engineering evaluation methods is necessary. Many of the petroleum engineering evaluation methods used to predict future hydrocarbon producing rates and recoverable reserves were presented in earlier chapters of this book. Combining those methods with the investment decision-making and evaluation methods presented in this chapter will provide the basis for determining the relative economic merits of most oil and gas investment opportunities.

6.1 Fundamentals of Economic Equivalence and Evaluation Methods

Money has a time value. The time value of money depends on many things and can be different for different individuals or companies. The concept of the time value of money can be demonstrated by considering whether someone would rather receive a particular sum of money today or receive it a year from now. Most people would prefer to receive it today. However, if the amount of money to be received a year from now is increased to an amount that would cause the person to change their preference, the time value of money for the person could be established. Some of the issues affecting the time value of money include the alternative investment opportunities for the sum of money to be received today, the perceived risk associated with receiving the money in the future, and the inflation rate during the associated time period.

The time value of money is established in the marketplace by the supply and demand for money. The supply establishes the lending market price (lending rate) and the demand establishes the borrowing market price (borrowing rate). The difference is the margin for the lender or go-between. These rates, or "interest rates" as they are commonly called, are usually expressed as a percentage of the original amount of money per unit of time. Knowing the interest rate, you can calculate the value of a specific amount of money at a different point in time. The different values are said to be "equivalent" as long as the holder of the money is indifferent to receiving payment now or in the future at the agreed interest rate. This is the concept of economic equivalence. It is this concept that provides the basis for comparing different investment alternatives and is necessary when comparing investment alternatives with different cost and payment schedules (see Figure 6.1).

With respect to all economic evaluation methods, time is relative and the time direction is very important. When determining the future worth of a present-day amount of money, the time direction is forward and the time value of money is said to be compounding. This is because the interest earned during the first period is added to the original principal to form the principal for the second period. The compounded interest concept is generally used to determine economically equivalent future values. Conversely, when determining the present worth of a future amount of money, the time direction is backward and the time value of money is said to be discounting. This is because a specific amount of money paid in the future is not worth as much as the same amount paid today. Hence, the future sum of money must be discounted to make it equivalent to a present-day sum of money. The discounting interest concept is generally used to determine equivalent present values and is considered the most important since most investors account for the time value of money using present value calculations.
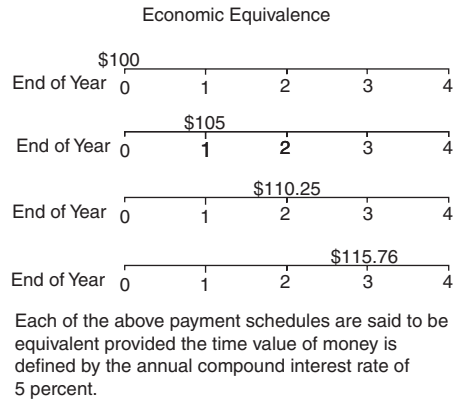
Figure 6.1 *Economic equivalent payment schedules.*

Cash flow is a term used in this text to describe the net inflow and outflow of money during a specified period of time such as a month, a quarter, or a year. For example, a particular investment alternative may generate revenue (inflows) and incur costs (outflows) for operating expenses, taxes, and additional capital investments during a single calendar year. The cash flow for the investment would be defined as the revenue received minus the costs incurred during the year. Cash flow can be negative or positive:

$$\text{Cash flow} = \text{revenues} - \text{costs} \qquad [6.1.1]$$

The term "discounted cash flow" describes a method used to evaluate the positive and negative cash flow of an investment alternative using present worth calculations. It is a method that requires an analytical approach of systematically and quantitatively evaluating all of the economic considerations that affect the economic potential of the investment. It is also the method most commonly used in the petroleum industry to evaluate different investment alternatives.

Cash flow time lines are used to graphically depict the associated timing of cash flow for a project. When applied properly, they can help simplify the complicated nature of a cash flow evaluation to properly account for the time value of money. Shown in Figure 6.2 is the basic cash flow time line used in this text to derive economic equivalence formulas and solve associated problems.

The basic cash flow time line notation used in this text is:

P = present lump sum of money
F = future lump sum of money
A = amount of each payment in a uniform series of equal payments
n = number of interest compounding periods
i = periodic interest rate (interest rate per interest compounding period)

The periodic interest rate (i) is a term used to describe the interest rate for each interest compounding period (n). It is usually expressed as a percentage of the principal. Principal is a term used to describe the sum of money on which interest is calculated during a specified period of time. For example,

Figure 6.2 *Basic cash flow time line.*

$100 deposited into a bank account paying interest at 5% annually would earn $5 after one year. The principal in this example is the $100. Simple interest is a concept rarely used. However, since it provides the basis for understanding compound interest formulas, their derivations, and equivalence applications, it makes for a good starting point. Consider a present lump sum of money P invested at a simple interest rate i for n periods; then the interest will be $P \times i \times n$. The future lump sum (F) at the end of n periods will be the present lump sum (P) plus the interest ($P \times i \times n$). The future lump sum can be calculated using the following formula:

$$F = P(1 + in) \qquad [6.1.2]$$

6.1.1 Equivalent value formulas

The formulas presented in this subsection are based on the concept of economic equivalence. They are intended to mathematically equate present-day money (P), future money (F), and a uniform series of periodic and equal payments of money (A). Six two-variable relationships or factors are derived that describe three basic types of time-value-of-money calculations. These factors are tabulated in the Appendix and can be used to simplify the calculation of economic equivalent values using the following basic formula:

$$\begin{matrix} \text{Quantity} \\ \text{calculated} \end{matrix} = \begin{matrix} \text{quantity} \\ \text{given} \end{matrix} \times \begin{matrix} \text{appropriate time-} \\ \text{value-of-money factor} \end{matrix} \quad [6.1.3]$$

Notation is used in this text to describe and simplify the reference of these factors. The first letter of the factor notation designates the value or quantity being calculated. The second letter designates the quantity given and is followed by two subscripted terms. The first subscripted term defines the periodic interest rate (i) expressed as a percentage and followed with a comma. The second subscripted term in the notation defines the number of interest compounding periods (n).

Future worth

As stated above, the compounding interest concept is defined by adding the interest earned during the period to the original amount of principal to form the principal for the next period. Combining this concept with the simple interest future lump-sum formula 6.1.2, the future worth formula can be derived. First, let us denote F with a subscript to define it as the future lump sum or future worth at the end of the number of interest compounding periods indicated by the subscript. If we consider a present-day lump sum of money (P) invested at a periodic interest rate (i), then the future lump sum at the end of the first period can be calculated by the following formula:

$$F_1 = P(1 + i) \qquad [6.1.4]$$

If we substitute F_1 for the principal at the beginning of the second period, then it follows that the future lump sum at the end of the second period can be calculated by the following formula:

$$F_2 = F_1(1 + i) \qquad [6.1.5]$$

If we substitute F_2 for the principal at the beginning of the third period, then it follows that the future lump sum at the end of the third period can be calculated by the following formula.

$$F_3 = F_2(1 + i) \qquad [6.1.6]$$

This process of substitution can be continued for n periods. To complete the derivation, if we substitute Equation 6.1.5 for F_2, Equation 6.1.6 becomes:

$$F_3 = F_1(1 + i)(1 + i) \qquad [6.1.7]$$

If we substitute Equation 6.1.4 for F_1, Equation 6.1.7 becomes:

$$F_3 = P(1 + i)(1 + i)(1 + i) \qquad [6.1.8]$$

Equation 6.1.8 can be simplified to:

$$F_3 = P(1 + i)^3 \qquad [6.1.9]$$

Since the future worth subscript is the same as the number of compounding periods, the subscript for future worth can be dropped. This leaves us with a general equation for determining the equivalent future worth of a present-day sum of money compounding at a periodic interest rate (i) for n periods as:

$$F = P(1 + i)^n \qquad [6.1.10]$$

From the general Equation 6.1.10, the term $(1 + i)^n$ is called the single-payment compound-amount factor and is designated in this text by $F/P_{i,n}$.

Example 6.1 Single-payment compound amount If $500 is deposited into a savings account paying 5% interest compounded annually, how much money will be in the account after five years?

Solution   To calculate F given P (Figure 6.3), look up the $F/P_{i,n}$ factor obtained from the Appendix for 5% interest and five interest compounding periods and substitute the appropriate values into Equation 6.1.3 as follows:

$$F = P \left[\frac{F}{P_{i,n}} \right]$$

$$= \$500(1.27628) = \$638.14$$

Alternatively, the future worth can be mathematically calculated using Equation 6.1.10 as follows:

$$F = P(1 + i)^n = \$500(1 + 0.05)^5 = \$638.14$$

Present worth

As stated above, the discounting interest concept is generally used to determine the equivalent present worth of a future lump sum of money and is considered the most important since most investors account for the time value of money using present worth or present value calculations. Recall that the primary difference between determining the value of a future lump sum and the value of a present lump sum is the time direction. It follows then that the present worth formula is simply another form of the future worth formula 6.1.10. Solving for P we get:

$$P = \frac{F}{(1 + i)^n} \qquad [6.1.11]$$

If a future amount of money (F) is to be received n periods from now, the present value (P) of that money can be determined for a given interest rate (i) by Equation 6.1.11. From this equation, the term $(1 + i)^{-n}$ is commonly referred to as the single-payment discount factor or single-payment present worth factor and is designated in this text by $P/F_{i,n}$.

Example 6.2 Single-payment discount factor If $500 is to be received five years from now, how much is it worth if the time value of money is defined by 5% interest compounded annually?
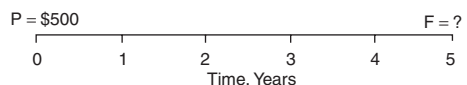
P = $500   F = ?

0   1   2   3   4   5
Time, Years

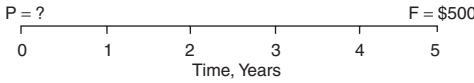**Figure 6.3**

Figure 6.4

Figure 6.6

Solution   To calculate P given F (Figure 6.4), look up the $P/F_{i,n}$ factor obtained from the Appendix for 5% interest and five interest compounding periods and substitute the appropriate values into Equation 6.1.3 as follows:

$$P = F\left[\frac{P}{F_{i,n}}\right]$$

$$= \$500(0.78353) = \$391.77$$

Alternatively, the future worth can be mathematically calculated using Equation 6.1.11 as follows with the small difference due to rounding in the look-up table:

$$P = \frac{F}{(1+i)^n}$$

$$= \frac{\$500}{(1+0.05)^5} = \$391.76$$

Future worth of a uniform series
The formula presented in this subsection is called the uniform series compound-amount formula. It is an equivalent value formula used to determine the future value (F) of a uniform series of equal payments (A) made at the end of each period of a series of interest compounding periods (n) at a given periodic interest rate (i) as shown in Figure 6.5. This formula could be used to determine the future value of an investment vehicle such as a savings plan or a retirement fund where periodic and equal deposits are made over a specified period of time accumulating at a specified interest rate. Because the payments draw interest for a different number of compounding periods, the formula must be derived by determining the future worth of each payment with the future worth formula 6.1.10 and adding the individual results. It is worth noting that the final payment in the uniform series of equal payments occurs at the same time the future worth is determined so the final payment does not earn interest.

Substituting A for P in Equation 6.1.10 and calculating the future worth for each payment in Figure 6.5, the formula for determining the future worth of the series is as follows:

$$F = A(1) + A(1+i) + A(1+i)^2 + \cdots + A(1+i)^{n-1} \tag{6.1.12}$$

To continue the derivation, if we multiply both sides of the equation by $(1+i)$, then Equation 6.1.12 becomes:

$$F(1+i) = A(1+i) + A(1+i)^2 + A(1+i)^3 + \cdots + A(1+i)^n \tag{6.1.13}$$

If we then subtract Equation 6.1.12 from 6.1.13, we get:
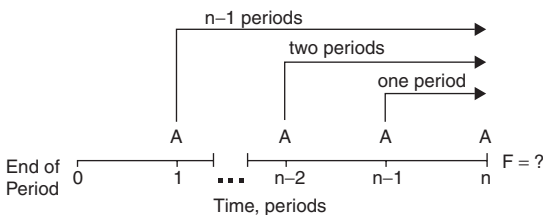
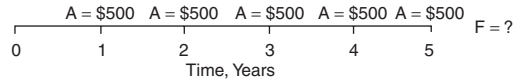$$F(1+i) - F = A(1+i)^n - A \tag{6.1.14}$$

With further simplification we get:

$$F\left[(1+i) - 1\right] = A\left[(1+i)^n - 1\right] \tag{6.1.15}$$

The final form of the equation is:

$$F = \frac{A\left[(1+i)^n - 1\right]}{i} \tag{6.1.16}$$

Equation 6.1.16 is the uniform series compound-amount formula and is used to determine the future value of a uniform series of equal payments. From the equation, the term $A\left[(1+i)^n - 1\right]/i$ is called the uniform series compound-amount factor and is designated in this text by $F/A_{i,n}$.

Example 6.3 Uniform series compound-amount factor If \$500 is deposited into a savings account at the end of every year for five years, how much will the account be worth if interest compounds annually at 5%?

Solution   To calculate F given A (Figure 6.6), look up the $F/A_{i,n}$ factor obtained from the Appendix for 5% interest and five interest compounding periods and substitute the appropriate values into Equation 6.1.3 as follows:

$$F = A\left[\frac{F}{A_{i,n}}\right]$$

$$= \$500(5.52563) = \$2762.82$$

Alternatively, the future worth can be mathematically calculated using Equation 6.1.16 as follows:

$$F = \frac{A\left[(1+i)^n - 1\right]}{i}$$

$$= \frac{\$500\left[(1+0.05)^5 - 1\right]}{0.05} = \$2762.82$$

Present worth of a uniform series
This formula is called the uniform series present worth formula. It is an equivalent value formula used to determine the present value (P) of a uniform series of equal payments (A) made at the end of each period of a series of interest compounding periods (n) at a given periodic interest rate (i) as shown in Figure 6.7. This formula could be used to determine the present value of an annuity, the right to receive
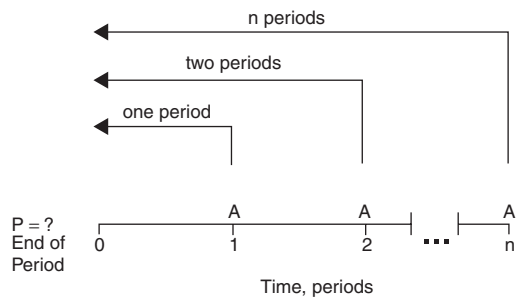

Figure 6.5 *Cash flow diagram used to derive the uniform series compound-amount formula.*

Figure 6.7 *Cash flow diagram depicting the present worth of a uniform series of equal payments.*
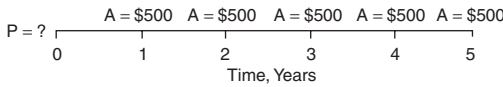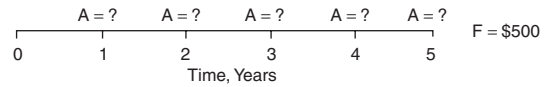
Figure 6.8

Figure 6.9

periodic payments of a fixed amount over a specified period of time.

The uniform series present worth formula can be derived by substituting F in Equation 6.1.16 with Equation 6.1.10 as follows:

$$P(1+i)^n = \frac{A\left[(1+i)^n - 1\right]}{i} \qquad [6.1.17]$$

Solving for P, Equation 6.1.17 becomes:

$$P = \frac{A\left[(1+i)^n - 1\right]}{i(1+i)^n} \qquad [6.1.18]$$

From Equation 6.1.18, the term $\left[(1+i)^n - 1\right]/i(1+i)^n$ is commonly referred to as the uniform series present worth factor and is designated in this text by $P/A_{i,n}$.

Example 6.4 Uniform series present worth factor Calculate the present value of depositing $500 into a savings account at the end of every year for five years if interest compounds annually at 5%.

Solution To calculate P given A (Figure 6.8), look up the $P/A_{i,n}$ factor obtained from the Appendix for 5% interest and five interest compounding periods and substitute the appropriate values into Equation 6.1.3 as follows:

$$P = A\left[\frac{P}{A_{i,n}}\right]$$

$$= \$500(4.32948) = \$2164.74$$

Alternatively, the future worth can be mathematically calculated using Equation 6.1.18 as follows:

$$P = \frac{A\left[(1+i)^n - 1\right]}{i(1+i)^n}$$

$$= \frac{\$500\left[(1+0.05)^5 - 1\right]}{0.05(1+0.05)^5} = \$2164.74$$

Uniform series for a future worth
This formula is called the sinking fund formula and is simply the inverse of the uniform series compound-amount formula 6.1.16. It is used to determine the periodic and equal payments (A) necessary to accumulate a specified future lump sum of money (F) after a specified number of compounding interest periods (n) at a given periodic interest rate (i). This formula could be used to determine the magnitude of the periodic deposits necessary to allow a savings plan or retirement fund to reach a future lump sum of money:

$$A = F\left[\frac{i}{(1+i)^n - 1}\right] \qquad [6.1.19]$$

From Equation 6.1.19, the term $i/(1+i)^n - 1$ is commonly referred to as the sinking fund factor and is designated in this text by $A/F_{i,n}$.

Example 6.5 Sinking fund factor How much money must be deposited into a savings account at the end of every year for five years if interest compounds annually at 5% and the goal is to have $500 in the account after the final payment?

Solution To calculate A given F (Figure 6.9), look up the $A/F_{i,n}$ factor obtained from the Appendix for 5% interest and five interest compounding periods and substitute the appropriate values into Equation 6.1.3 as follows:

$$A = F\left[\frac{A}{F_{i,n}}\right]$$

$$= \$500(0.18097) = \$90.49$$

Alternatively, the future worth can be mathematically calculated using Equation 6.1.19 as follows:

$$A = F\left[\frac{i}{(1+i)^n - 1}\right]$$

$$= 500\left[\frac{0.05}{(1+0.05)^5 - 1}\right] = \$90.49$$

Uniform series for a present worth
This formula is called the capital recovery formula and is simply the inverse of the uniform series present worth formula 6.1.18. It is used to equate a series of periodic and equal payments (A) made at the end of each period of a specified series of compounding interest periods (n) to a given present lump sum of money (P) at a given periodic interest rate (i). This formula could be used to determine the periodic payments required to pay back a loan:

$$A = \frac{P\left[i(1+i)^n\right]}{\left[(1+i)^n - 1\right]} \qquad [6.1.20]$$

From Equation 6.1.20, the term $\left[i(1+i)^n\right]/\left[(1+i)^n - 1\right]$ is commonly referred to as the capital recovery factor and it is designated in this text by $A/P_{i,n}$.

Example 6.6 Capital recovery factor How much should the end of every year payments be to repay a $500 loan in five years if the interest charged is 5% compounded annually?

Solution To calculate A given P (Figure 6.10), look up the $A/P_{i,n}$ factor obtained from the Appendix for 5% interest and five interest compounding periods and substitute the appropriate values into Equation 6.1.3 as follows:

$$A = P\left[\frac{A}{P_{i,n}}\right]$$
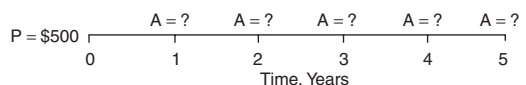
$$= \$500(0.23097) = \$115.49$$

Figure 6.10

Alternatively, the future worth can be mathematically calculated using Equation 6.1.20 as follows:

$$A = \frac{P\left[i\left(1+i\right)^{n}\right]}{\left[(1+i)^{n}-1\right]}$$

$$= \frac{\$500\left[0.05\left(1+0.05\right)^{5}\right]}{\left[(1+0.05)^{5}-1\right]} = \$115.49$$

Beginning-, end-, and midpoint-of-period timing (discounting)
All of the compound interest formulas presented in this text so far have used end-of-period timing. Beginning- or midpoint-of-period timing can be valid choices depending on the situation. The following example illustrates the impact these timing assumptions have on value determination.

Example 6.7 Beginning-, end-, and midpoint-of-period discounting Calculate the present value of receiving $500 at the beginning of the year, five years from now, assuming an annual compounded interest rate of 5%. Using the same terms, calculate the present value of receiving the same amount of money at the midpoint of the fifth year. Finally, calculate the present value of receiving two payments of $250, one at the beginning of the fifth year and the other at the end assuming the same compounded interest rate. Compare your answers to the present value calculated in Example 6.2.

Solution   See Figure 6.11:

Step 1. Recognizing that the beginning of the fifth year is the same as the end of the fourth year, substitute the given values into Equation 6.1.11 as follows:

$$P = \frac{F}{(1+i)^{n}} = \frac{\$500}{(1+0.05)^{4}} = \$411.35$$

Step 2. Recognizing that the midpoint of the fifth year is 4.5 time periods from the present, substitute the given values into Equation 6.1.11 as follows:

$$P = \frac{F}{(1+i)^{n}} = \frac{\$500}{(1+0.05)^{4.5}} = \$401.44$$

Step 3. Add the present values determined for the two $250 payments by substituting the given values into Equation 6.1.11 as follows:

$$P = \frac{\$250}{(1+0.05)^{4}} + \frac{\$250}{(1+0.05)^{5}}$$

$$= \$205.68 + \$195.88 = \$401.56$$

In Example 6.2, the present value of receiving $500 at the end of the fifth year assuming 5% interest compounded annually was equal to $391.76.
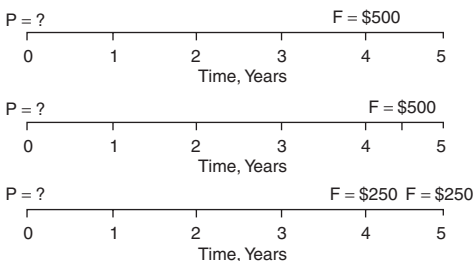
Figure 6.11

The results of this exercise demonstrate the present value differences of the different period timing assumptions. Selecting the proper timing assumption to solve a simple time-value-of-money problem is dependent on the timing of the associated cash flow. The primary thing to remember is to place the timing of costs and revenues in the calculations as close as possible to when they will actually occur. Often, oil field economic evaluations are very complicated and involve investments, revenues, and costs that occur at different times in a year and are spread over multiple years. Usually, the uncertainty associated with estimating the exact timing of the cash flow for a relatively long-life project or property makes this issue insignificant. However, most industry-accepted economic evaluation software packages offer the user the option to choose the period timing assumption. The timing assumption chosen, whether midpoint or end-of-period timing (more often called the midpoint- or end-of-period discounting) is not nearly as important as making sure that the economic evaluations that need to be compared or ranked use the same assumption. Most companies establish guidelines to standardize this assumption and if a particular evaluation justifies using a different assumption than the standard, make sure that information is provided with the results.

Nominal and effective interest rates
Financial institutions normally express their interest rates on a nominal annual basis and commonly refer to them as "annual percentage rates" or "APRs." Nominal interest is also the most commonly referenced interest rate—when someone says they are paying 5% interest, they usually mean they are paying 5% interest on an annual basis. In this text, nominal interest rate (i_n) is a term used to define the annual interest rate or APR and can be used to define the periodic interest rate (i) using the following formula where m is the number of interest compounding periods in a year:

$$i_n = i \times m \qquad [6.1.21]$$

Effective interest rate (i_e) is a term used to define the annual interest rate effectively realized as a result of compounding m times per year. The formula for calculating the effective interest rate can be derived from Equation 6.1.10. For derivation purposes, let us denote F with a subscript to denote it as a future value to be kept separate and distinct. Let us also assume that P dollars are invested at a periodic interest rate of i for m periods. Equation 6.1.10 becomes:

$$F_1 = P(1+i)^m \qquad [6.1.22]$$

If we assume that the same P dollars are invested at an effective interest rate (i_e), and we determine the future value (F_2) after one year, we get:

$$F_2 = P(1+i_e)^1 \qquad [6.1.23]$$

Since P is the same in both cases, then $F_2 = F_1$ and the remaining portions of Equation 6.1.23 can be set equal to each other as follows:

$$(1+i_e)^1 = (1+i)^m \qquad [6.1.24]$$

Solving for i_e, we get:

$$i_e = (1+i)^m - 1 \qquad [6.1.25]$$

Example 6.8 Nominal and effective interest rates—effect of compounding frequency Calculate the effective interest rate (i_e) for 5% nominal interest rate compounded quarterly, monthly, and daily.

Solution   Using Equation 6.1.25, substitute the given information as follows:
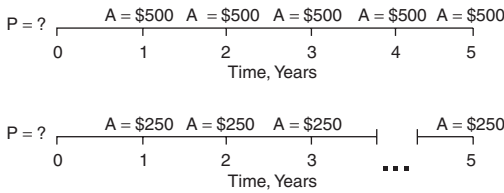
$$i_e = (1+i)^m - 1$$

Figure 6.12

Table 6.1

Option	A	n	P @ i=5% ($)	P @ i=10% ($)	P @ i=15% ($)
A	500	5	2164.74	1895.40	1676.08
B	250	15	2594.92	1901.52	1461.84

i_e compounded quarterly $= (1+0.05/4)^4 - 1 = 0.050945$ or 5.0945%

i_e compounded monthly $= (1+0.05/12)^{12} - 1 = 0.051162$ or 5.1162%

i_e compounded daily $= (1+0.05/365)^{365} - 1 = 0.051267$ or 5.1267%

As demonstrated in Example 6.8, increasing the number of compounding periods per year increases the effective interest rate. However, in the above example, had we calculated the effective interest rate for increasing numbers of compounding periods per year, we would have found diminishing returns with respect to increasing effective interest rates. As it turns out, compounding more often than monthly has negligible effect on the results of most oil field economic evaluations.

Time value of money—effect on investment decision analysis

It is important to remember that economic equivalence assumes that the agreed periodic interest rate defines the time value of money and that the holder of the money is indifferent to receiving payment now or in the future at the agreed interest rate. It was also stated that the time value of money depends on many things and can be different for different individuals or companies. Realistically defining the time value of money is very important and can affect the results of investment decision analysis especially when considering projects with long lives. The following example illustrates the impact different periodic interest rates can have on investment decision analysis.

Example 6.9 Time value of money–effect on investment decision analysis Suppose you had the choice between receiving one of two different uniform series of equal payments: $500 annually for 5 years (option A) or $250 annually for fifteen years (option B). Which would you choose if you defined the time value of money by the annual compounded interest rate of 5%? Would your preference change if you defined the time value of money by a different annual compounded interest rate, say 10% or 15%?

Solution Look up the six different $P/A_{i,n}$ factors obtained from the Appendix that correspond to the two uniform-series-of-equal-payment options (Figure 6.12) and the three different periodic interest rates:

$P/A_{5,5} = 4.32948,$ $P/A_{10,5} = 3.79079,$
$P/A_{15,5} = 3.35216,$ $P/A_{5,15} = 10.37966,$
$P/A_{10,15} = 7.60608,$ $P/A_{15,15} = 5.84737$

Substitute the appropriate values into Equation 6.1.3 and calculate the six present values. Table 6.1 contains the correct results.

Based on these results, if you define the time value of money using 5%, option B may be the better choice since the present value is almost 20% higher than the present value for option A. However, if 10% more accurately defines your

time value of money, the present values of the two options are within 1% of each other, so other issues may need to be considered before choosing. If 15% is the rate that defines the time value of money, then option A may be your preference since its present value is almost 15% higher than option B.

Although Example 6.9 is simplistic, it illustrates another reason why seemingly similar individuals or companies can determine different economic values for the same project. Not only can different cost, revenue, and timing assumptions be used by different evaluators, but choosing a different interest rate to define the time value of money can have a material impact on the results as well. Because the periodic interest rate used in investment decision analysis can represent the cost of borrowed money, the rate of return on invested capital, or the minimum rate of return, most companies establish guidelines to standardize this assumption.

Rate of return analysis

Up to this point in the text, the periodic interest rate (i) has been a given quantity used to calculate equivalent values. There are times when the costs and revenues are believed to be known but the periodic interest rate is not. In this type of problem, the periodic interest rate is more commonly referred to as the rate of return. We can solve this type of problem by developing an equation that sets the known quantities equal to each other and solving for the rate of return through a trial-and-error process. For illustrative purposes, let us take Example 6.6 and change it to read as follows.

Example 6.10 Rate of return What annual compounded interest rate is being paid on a $500 loan if the lender requires it to be repaid with five equal end-of-year payments of $115.49?

Solution To calculate i given A and P (Figure 6.13), substitute the known quantities into Equation 6.1.3 and solve for the $A/P_{i,n}$ factor as follows:

$$A = P \left[\frac{A}{P_{i,n}} \right] \$115.49 = \$500(A/P_{i,5})$$

$$A/P_{i,5} = \$115.49/\$500 = 0.23098$$

At this point, we search the Appendix for an $A/P_{i,5}$ factor that equals 0.23098. As would be expected, we find 0.23097 on the 5% interest table indicating that the lender was satisfied with a 5% rate of return on their money. The difference between the $A/P_{i,5}$ factor of 0.23097 and 0.23098 is due to rounding.

Often, the $A/P_{i,n}$ factor calculated will fall between values in the Appendix. In that case, interpolation is required to solve for the rate of return.
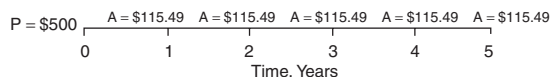

Figure 6.13

6.1.2 Oil field evaluation methods

There are four economic evaluation methods commonly used to calculate equivalent values of different investment alternatives: present worth, future worth, annual worth, and rate of return. Although when applied correctly, all of these methods will lead to the same economic conclusion, emphasis is placed in this text on the two most common economic evaluation methods used in the petroleum industry—present worth and rate of return. The other methods, annual worth and future worth, are rarely used in typical oil field evaluations so are not included in this text.

Present worth method

The present worth method is more commonly referred to as the net present value (NPV) method or the discounted cash flow method. It is a method used to evaluate the positive and negative cash flow of an investment alternative using present worth calculations that requires an analytical approach of systematically and quantitatively evaluating all of the economic considerations that affect the economic potential of the investment. The NPV of an investment alternative is determined by calculating the present worth of all the future net cash flows and summing them. It is based on the economic equivalence concepts presented earlier in this text and is highly dependent on the interest rate (commonly referred to as the discount rate) chosen to determine the time value of money. NPV calculations are commonly done on a "before-tax" and "after-tax" basis. The NPV method of investment decision analysis is illustrated in the following example.

Example 6.11   Net present value (NPV) Suppose you have the opportunity to drill an oil well for $1 500 000. The well is expected to generate revenues and incur costs as shown in Table 6.2 over a 16 year period. What is the before-tax NPV discounted at 10% (BTAX NPV10) for your investment opportunity in the proposed well?

Solution   Look up the $P/F_{10,n}$ factors obtained from the Appendix for periods 1 through 15. Substitute the BTAX cash flow value (F) shown in Table 6.2 for each time period and the appropriate $P/F_{10,n}$ factor from the Appendix into

Table 6.2

Year	Net revenue ($ × 1000)	Direct operating costs ($ × 1000)	Capital costs ($ × 1000)	BTAX net cash flow ($ × 1000)
0			1500.0	−1500.0
1	1107.8	179.7	0.0	928.2
2	886.3	146.1	0.0	740.1
3	709.0	119.3	0.0	589.7
4	567.2	97.8	0.0	469.4
5	453.8	80.7	0.0	373.1
6	363.0	66.9	0.0	296.1
7	290.4	56.0	0.0	234.5
8	232.3	47.2	0.0	185.2
9	185.9	40.1	0.0	145.7
10	148.7	34.5	0.0	114.2
11	123.7	30.0	0.0	93.7
12	102.8	26.4	0.0	76.4
13	85.3	23.5	0.0	61.7
14	70.6	21.2	0.0	49.4
15	58.5	19.4	0.0	39.1
16	0.0	0.0	0.0	0.0
	5385.3	988.9	1500.0	2896.4

Table 6.3

Year	BTAX net cash flow ($ × 1000)	$P/F_{10,n}$ factor	NPV discounted @ 10% ($ × 1000)
0	−1500.0	1.00000	−1500.0
1	928.2	0.90909	843.8
2	740.1	0.82645	611.7
3	589.7	0.75131	443.1
4	469.4	0.68301	320.6
5	373.1	0.62092	231.7
6	296.1	0.56447	167.1
7	234.5	0.51316	120.3
8	185.2	0.46651	86.4
9	145.7	0.42410	61.8
10	114.2	0.38554	44.0
11	93.7	0.35049	32.8
12	76.4	0.31863	24.3
13	61.7	0.28966	17.9
14	49.4	0.26333	13.0
15	39.1	0.23939	9.4
16	0.0		
	2896.0		1527.8

Equation 6.1.3 and solve. Repeat for each time period and sum the results. The correct results are shown in Table 6.3.

Rate of return method

The rate of return method is more often referred to as the discounted cash flow rate of return (DCFROR) method. It is a method widely used as a measure of profitability because it does not require that the discount rate or time value of money be established before making the calculation. The discounted cash flow rate of return (ROR) is calculated by discounting the estimated cash flows of an investment alternative until the sum of the cash flows equals zero. As with NPV calculations, the discounted cash flow ROR is routinely calculated on a "before-tax" and "after-tax" basis. The DCFROR method of investment decision analysis is illustrated in the following example.

Example 6.12   Discounted cash flow rate of return (DCFROR) Calculate the before-tax discounted rate of return (BTAX DCFROR) for the oil well investment opportunity in Example 6.11.

Solution   Through a trial-and-error process, the discount rate that causes the sum of the future net cash flows to equal zero is shown in Table 6.4 to be approximately 41.5%.

6.2 Reserves Definitions and Classifications

Before any quantities of hydrocarbon resources can be classified as reserves, they must meet two basic criteria. First, they must be physically producible. Second, they must be economically producible. Once hydrocarbon resources meet these two criteria, they are further classified based on the needs or the requirements placed on the owner of the reserves. For example, a privately held independent oil and gas company may need to define its reserves to meet the requirements of the owner(s) or the financial institution(s) with which it does business. However, an oil and gas company that has issued stock that is publicly traded on a stock exchange will be required to define its reserves based on the definitions established by the regulating agency of the exchange.

Table 6.4

Year	BTAX net cash flow ($ × 1000)	NPV discounted @ 10% ($ × 1000)	NPV discounted 41.5% ($ × 1000)
0	−1500.0	−1500.0	−1500.0
1	928.2	843.8	655.9
2	740.1	611.7	369.6
3	589.7	443.1	208.1
4	469.4	320.6	117.1
5	373.1	231.7	65.8
6	296.1	167.1	36.9
7	234.5	120.3	20.6
8	185.2	86.4	11.5
9	145.7	61.8	6.4
10	114.2	44.0	3.5
11	93.7	32.8	2.1
12	76.4	24.3	1.2
13	61.7	17.9	0.7
14	49.4	13.0	0.4
15	39.1	9.4	0.2
16	0.0		0
	2896.4	1527.8	0.0

Many of the terms used by the various organizations concerned with reserves classifications and definitions are the same. However, the definitions associated with the terms may not be the same. It is important that the reserve evaluator understand which reserves definitions are to be used in an evaluation and to apply the definitions rigorously.

With respect to this text, we will review the definitions published by three agencies concerned with the classification and definition of reserves. Two of the agencies, the World Petroleum Congress and the Society of Petroleum Engineers, use the same definitions. The third agency is the Securities and Exchange Commission (SEC), the regulating agency that, among other things, defines such terms for publicly traded companies in the United States. There are other widely used definitions that justify review but were not included in this text due to space considerations.

6.2.1 World petroleum congress/society of petroleum engineers

The World Petroleum Congress and the Society of Petroleum Engineers, working independently, published a set of similar reserves definitions in the late 1980s. Working together, the two organizations developed and approved a single set of definitions by March 1997 that could be used worldwide to remove some of the subjectivity that normally accompanies reserves estimation and provide a measure of reserves comparability as well. The following definitions are taken from the Society of Petroleum Engineers.

Proved reserves (WPC/SPE)

Proved reserves are those quantities of petroleum which, by analysis of geological and engineering data, can be estimated with reasonable certainty to be commercially recoverable, from a given date forward, from known reservoirs and under current economic conditions, operating methods, and government regulations. Proved reserves can be categorized as developed or undeveloped.

If deterministic methods are used, the term reasonable certainty is intended to express a high degree of confidence that the quantities will be recovered. If probabilistic methods are used, there should be at least a 90% probability that the quantities actually recovered will equal or exceed the estimate.

Establishment of current economic conditions should include relevant historical petroleum prices and associated costs and may involve an averaging period that is consistent with the purpose of the reserves estimate, appropriate contract obligations, corporate procedures, and government regulations involved in reporting these reserves.

In general, reserves are considered proved if the commercial producibility of the reservoir is supported by actual production or formation tests. In this context, the term proved refers to the actual quantities of petroleum reserves and not just the productivity of the well or reservoir. In certain cases, proved reserves may be assigned on the basis of well logs and/or core analysis that indicate the subject reservoir is hydrocarbon bearing and is analogous to reservoirs in the same area that are producing or have demonstrated the ability to produce on formation tests. The area of the reservoir considered as proved includes

- the area delineated by drilling and defined by fluid contacts, if any, and
- the undrilled portions of the reservoir that can reasonably be judged as commercially productive on the basis of available geological and engineering data.

In the absence of data on fluid contacts, the lowest known occurrence of hydrocarbons controls the proved limit unless otherwise indicated by definitive geological, engineering, or performance data.

Reserves may be classified as proved if facilities to process and transport those reserves to market are operational at the time of the estimate or there is a reasonable expectation that such facilities will be installed. Reserves in undeveloped locations may be classified as proved undeveloped provided:

- the locations are direct offsets to wells that have indicated commercial production in the objective formation,
- it is reasonably certain that such locations are within the known proved productive limits of the objective formation,
- the locations conform to existing well spacing regulations where applicable, and
- it is reasonably certain the locations will be developed. Reserves from other locations are categorized as proved undeveloped only where interpretations of geological and engineering data from wells indicate with reasonable certainty that the objective formation is laterally continuous and contains commercially recoverable petroleum at locations beyond direct offsets.

Reserves which are to be produced through the application of established improved recovery methods are included in the proved classification when:

- successful testing by a pilot project or favorable response of an installed program in the same or an analogous reservoir with similar rock and fluid properties provides support for the analysis on which the project was based, and
- it is reasonably certain that the project will proceed. Reserves to be recovered by improved recovery methods that have yet to be established through commercially successful applications are included in the proved classification only:
  - after a favorable production response from the subject reservoir from either (a) a representative pilot or (b) an installed program where the response provides support for the analysis on which the project is based; and
  - it is reasonably certain the project will proceed.

Unproved reserves (WPC/SPE)

Unproved reserves are based on geological and/or engineering data similar to that used in estimates of proved reserves—but technical, contractual, economic, or regulatory uncertainties preclude such reserves being classified as proved. Unproved reserves may be further classified as probable reserves and possible reserves.

Unproved reserves may be estimated assuming future economic conditions different from those prevailing at the time of the estimate. The effect of possible future improvements in economic conditions and technological developments can be expressed by allocating appropriate quantities of reserves to the probable and possible classifications.

Probable reserves (WPC/SPE)

Probable reserves are those unproved reserves which analysis of geological and engineering data suggests are more likely than not to be recoverable, In this context, when probabilistic methods are used, there should be at least a 50% probability that the quantities actually recovered will equal or exceed the sum of estimated proved plus probable reserves.

In general, probable reserves may include:

- reserves anticipated to be proved by normal step-out drilling where subsurface control is inadequate to classify these reserves as proved,
- reserves in formations that appear to be productive based on well log characteristics but lack core data or definitive tests and which are not analogous to producing or proved reservoirs in the area,
- incremental reserves attributable to infill drilling that could have been classified as proved if closer statutory spacing had been approved at the time of the estimate,
- reserves attributable to improved recovery methods that have been established by repeated commercially successful applications when (a) a project or pilot is planned but not in operation and (b) rock, fluid, and reservoir characteristics appear favorable for commercial application,
- reserves in an area of the formation that appears to be separated from the proved area by faulting and the geologic interpretation indicates the subject area is structurally higher than the proved area,
- reserves attributable to a future workover, treatment, retreatment, change of equipment, or other mechanical procedures, where such procedure has not been proved successful in wells which exhibit similar behavior in analogous reservoirs, and
- incremental reserves in proved reservoirs where an alternative interpretation of performance or volumetric data indicates more reserves than can be classified as proved.

Possible reserves (WPC/SPE)

Possible reserves are those unproved reserves which analysis of geological and engineering data suggests are less likely to be recoverable than probable reserves. In this context, when probabilistic methods are used, there should be at least a 10% probability that the quantities actually recovered will equal or exceed the sum of estimated proved plus probable plus possible reserves.

In general, possible reserves may include:

- reserves which, based on geological interpretations, could possibly exist beyond areas classified as probable,
- reserves in formations that appear to be petroleum bearing based on log and core analysis but may not be productive at commercial rates,
- incremental reserves attributed to infill drilling that are subject to technical uncertainty,
- reserves attributed to improved recovery methods when (a) a project or pilot is planned but not in operation and (b) rock, fluid, and reservoir characteristics are such

that a reasonable doubt exists that the project will be commercial, and
- reserves in an area of the formation that appears to be separated from the proved area by faulting and geological interpretation indicates the subject area is structurally lower than the proved area.

Reserve status categories (WPC/SPE)

Reserve status categories define the development and producing status of wells and reservoirs.

Developed reserves Developed reserves are expected to be recovered from existing wells including reserves behind pipe. Improved recovery reserves are considered developed only after the necessary equipment has been installed, or when the costs to do so are relatively minor. Developed reserves may be subcategorized as producing or non-producing.

Producing reserves subcategorized as producing are expected to be recovered from completion intervals which are open and producing at the time of the estimate. Improved recovery reserves are considered producing only after the improved recovery project is in operation.

Non-producing reserves subcategorized as non-producing include shut-in and behind-pipe reserves. Shut-in reserves are expected to be recovered from:

- completion intervals which are open at the time of the estimate but which have not started producing,
- wells which were shut in for market conditions or pipeline connections, or
- wells not capable of production for mechanical reasons. Behind-pipe reserves are expected to be recovered from zones in existing wells, which will require additional completion work or future recompletion prior to the start of production.

Undeveloped reserves Undeveloped reserves are expected to be recovered:

- from new wells on undrilled acreage,
- from deepening existing wells to a different reservoir, or
- where a relatively large expenditure is required to (a) recomplete an existing well or (b) install production or transportation facilities for primary or improved recovery projects.

6.2.2 Securities and exchange commission (SEC)

The regulations that govern the securities industry in the United States are based on a simple concept—all investors should have access to certain basic facts about an investment prior to buying it. To achieve this, the SEC has developed definitions and regulations that require public companies to disclose meaningful financial and other information to the public. With respect to publicly traded oil and gas companies, reserves are considered meaningful information and reporting of those reserves is required using SEC definitions. Because the SEC requires that only proved reserves be reported, the only definitions provided by the SEC are those for proved reserves. All other reserves are classified as unproved. The definitions listed below are taken from SEC Regulation 210.4-10, Financial Accounting and Reporting for Oil and Gas Producing Activities Pursuant to the Federal Securities Laws and the Energy Policy and Conservation Act of 1975.

Proved reserves (SEC)

Proved oil and gas reserves are the estimated quantities of crude oil, natural gas, and natural-gas liquids which geological and engineering data demonstrates with reasonable certainty to be recoverable in future years from known reservoirs under existing economic and operating conditions,

i.e., prices and costs as of the date the estimate is made. Prices include consideration of changes in existing prices provided only by contractual arrangements, but not on escalations based upon future conditions.

(1) Reservoirs are considered proved if economic producibility is supported by either actual production or conclusive formation test. The area of a reservoir considered proved includes:

- that portion delineated by drilling and defined by gas–oil and/or oil–water contacts, if any, and
- the immediately adjoining portions not yet drilled but which can be reasonably judged as economically productive on the basis of available geological and engineering data. In the absence of information on fluid contacts, the lowest known structural occurrence of hydrocarbons controls the lower proved limit of the reservoir.

(2) Reserves which can be produced economically through application of improved recovery techniques (such as fluid injection) are included in the proved classification when successful testing by a pilot project, or the operation of an installed program in the reservoir, provides support for the engineering analysis on which the project or program was based.

(3) Estimates of proved reserves do not include the following:

- oil that may become available from known reservoirs but is classified separately as indicated additional reserves;
- crude oil, natural gas, and natural-gas liquids, the recovery of which is subject to reasonable doubt because of uncertainty as to geology, reservoir characteristics, or economic factors;
- crude oil, natural gas, and natural-gas liquids that may occur in undrilled prospects; and
- crude oil, natural gas, and natural-gas liquids that may be recovered from oil shales, coal, gilsonite and other such sources.

Proved developed reserves (SEC)

Proved developed oil and gas reserves are reserves that can be expected to be recovered through existing wells with existing equipment and operating methods. Additional oil and gas expected to be obtained through the application of fluid injection or other improved recovery techniques for supplementing the natural forces and mechanisms of primary recovery should be included as proved developed reserves only after testing by a pilot project or after the operation of an installed program has confirmed through production response that increased recovery will be achieved.

Proved undeveloped reserves (SEC)

Proved undeveloped oil and gas reserves are reserves that are expected to be recovered from new wells on undrilled acreage, or from existing wells where a relatively major expenditure is required for recompletion. Reserves on undrilled acreage shall be limited to those drilling units offsetting productive units that are reasonably certain of production when drilled. Proved reserves for other undrilled units can be claimed only where it can be demonstrated with certainty that there is continuity of production from the existing productive formation. Under no circumstances should estimates for proved undeveloped reserves be attributable to any acreage for which an application of fluid injection or other improved recovery technique is contemplated, unless such techniques have been proved effective by actual tests in the area and in the same reservoir.

6.3 Accounting Principles

The accounting practices that apply to oil and gas industry activities are established by the governing tax authorities having jurisdiction. In the United States, for example, Congress passes laws that set the federal tax rates and establishes the accounting practices used to determine the taxable and non-taxable portions of the revenue from an oil and gas property. Similarly, State and local law makers set the tax rates for the oil and gas industry in their jurisdictions. The Internal Revenue Service (IRS) and the State and local tax authorities oversee the implementation of those laws. The accounting practices established in the laws and followed by the IRS are generally based on what are known as the generally accepted accounting principles (GAAP) published in the U.S. by the Financial Accounting Standards Board (FASB). Different GAAP standards are used internationally and can be very different. Under the current laws and GAAP, the respective tax authorities in the United States recognize that a portion of the revenue from a property represents the return or recovery of the invested capital, a portion of the revenue represents the return of expenses associated with operating or maintaining the investment, and a portion of the revenue represents income. This distinction is important because the United States, for example, endeavors to tax only the income portion of the revenue. The determination of which portion of the annual revenue from a property is considered income and which portion is considered the recovery of invested capital or expenses can be very complicated and varies from one tax authority to the next. It is not our intention to investigate all of the specific details of any one particular taxing authority. However, it is important to investigate some of the fundamental terminology and associated definitions commonly used throughout the industry to understand how they apply to oil field economic evaluations and investment decision analysis.

There are two classes or types of costs associated with generally accepted oil field accounting practices—capitalized costs and expensed costs. Capitalized costs are expenditures for items that can generate revenue in future periods. Examples are purchases of land, equipment, the drilling of a well, or installation of facilities to produce a well. These types of assets have the capacity to generate revenue in future periods beyond the period in which they were purchased, built, or placed into service. Capitalized items are considered assets of the individual or firm that owns them.

Expensed costs are expenditures for items that expire or are believed to expire during the accounting period they are incurred in an attempt to generate revenue during the period. Examples of expensed costs include the costs for labor, power, consumable items required for continued operations, etc. These items are expensed because they do not provide any benefit for any period other than the period in which the cost was incurred.

The primary thing to remember about expensed costs and capitalized costs is that expenses are charged against revenue during the period in which the expense was incurred whereas only a portion of capitalized costs is charged against the revenue of the period they are incurred. The recovery of the remaining, uncharged portion of the capitalized cost is charged or expensed against the revenue of future periods based on the rules established by the governing tax authority. The following subsection describes the terms and definitions associated with the accounting methods of recovering capitalized costs.

6.3.1 Depreciation, depletion, and amortization (DD&A)

Depreciation is a term used to describe a common accounting method for recovering the investment costs of the

"fixed assets," or more commonly called the "tangible assets" associated with oil and gas industry activity. Fixed or tangible assets are just as they sound: they are assets that are tangible—one can usually see or touch tangible assets. Tangible assets include such things as oil field tubulars and line pipe, wellheads, pumping equipment, tanks and tank battery equipment, buildings, cars, etc. The costs associated with tangible assets are considered investment capital and are allowed to be recovered against the current and future revenue from a property. The rate of recovery is generally established by the taxing authority based on the perceived "useful life" of the asset. However, some jurisdictions will use the rate of recovery as an incentive-allowing accelerated recoveries in certain circumstances. It is important to remember a couple of things. First, the taxing authority establishes the different recovery rates or depreciation schedules for the different types of tangible equipment based on its useful life and the useful life may not be the same as the actual property life. Second, the taxing authorities may change the depreciation rates from time to time causing depreciation schedules for the same type of tangible asset to be different. The reasons for establishing different depreciation schedules vary but are usually based on when the tax law was changed and when the asset was purchased or placed in service. From an evaluator's view point, it is imperative to understand the applicable depreciation schedules.

The concept of depreciation can be applied to a mineral resource such as oil and gas reserves and the accounting term used to define it is called depletion. Depletion is an accounting method of recovering the costs associated with the value of a natural resource. Examples are costs associated with a lease bonus or the acquisition costs of an oil or gas property in excess of the value of the depreciable equipment (tangible equipment). The recovery of the value of the natural resource is usually associated with the perceived life of the natural resource.

When this concept is applied to the recovery of an intangible item, the accounting term is called amortization. Examples of intangible items are items associated with the installation or construction of tangible assets, such as the costs for a drilling rig, labor costs for contractors or consultants to drill or complete a well, cementing services, logging and coring services, testing services, equipment rentals, etc. As with depreciation and depletion schedules, the taxing authority defines amortization schedules for intangible items.

Collectively, the terms depreciation, depletion, and amortization are referred to as DD&A. For the purposes of this text, the term amortization will be used to include and refer to all three. As stated before, it is imperative that the evaluator understand the DD&A (amortization) schedules associated with a property because the DD&A expenses are usually deducted from revenues for determining federal, State, or provincial tax purposes or used to determine the costs recovered in an international contract such as a production sharing contract (PSC).

6.3.2 Amortization schedules

As stated earlier, the capitalized costs associated with oil and gas industry activity are recovered (amortized or expensed) against current and future income. The amount recovered during an accounting period is dependent on the recovery schedule or more commonly called the depreciation or amortization schedule. Four amortization schedules for recovering capitalized costs are presented in this text. Two of the schedules are classified as accelerated recovery methods. The fourth schedule is dependent on the accounting method chosen by the company that owns the assets.

Straight-line (SL) method

Considered the simplest amortization schedule, the straight-line amortization method expenses the capital costs evenly across an asset's useful life. For example, an asset having no residual value at the end of its four year useful life would allow the owner to expense 1/4 (25%) of the asset value against income each year for four years. International contracts often times use straight-line cost recovery schedules and define them using a percentage or a rate per year such as 25%. In this case, 25% of the costs would be recovered each year for four years.

Example 6.13   Straight-line amortization Calculate the amortization schedule for a $500 asset assuming the straight-line (SL) amortization method and a five year useful life.

Solution $500 divided by five years equals $100 per year for five years.

Double declining balance (DDB) method

This is a form of accelerated cost recovery that amortizes capital costs at twice the rate of the straight-line method. Using the DDB method, twice the straight-line rate is applied each year to the remaining unamortized value of the asset. For example, an asset requiring a four year DDB would amortize 50% of the asset value in the first year. The remaining balance for the second year is 50% and the allowed amortization would be 50% of 50% or simply 25% of the asset value. The remaining balance for the third year would be 25% of the asset value so the amortized amount for the third year would be 50% of 25% or 12.5% of the asset value. The remaining balance for the fourth year would be 12.5% of the asset value so the amortized amount for the fourth year would be 50% of 12.5% or 6.25% of the asset value.

Example 6.14   Double declining balance amortization Calculate the amortization schedule for a $500 asset assuming the double declining balance (DDB) amortization method and a five year useful life.

Solution   The straight-line (SL) amortization rate assuming a five year useful life is 1/5 or 20%. Therefore, the DDB amortization rate is 40% ($2 \times 20\%$). The amount to be expensed the first year is 40% of $500 or $200. The remaining balance for the second year is $300 ($500 − $200) so the amount to be expensed during the second year is 40% of $300 or $120. The remaining balance for the third year is $180 ($500 − $200 − $120) so the amount to be expensed the third year is 40% of $180 or $72. The remaining balance for the fourth year is $108 ($500 − $200 − $120 − $72) so the amount to be expensed the fourth year is 40% of $108 or $43.20. The remaining balance for the fifth year is $64.80 ($500 − $200 − $120 − $72 − $43.20) so the amount to be expensed the fifth and final year is 40% of $64.80 or $25.92. Note that $38.88 of the original asset value is not recovered.

Sum-of-the-year's digits (SYD)

Another accelerated cost recovery method, SYD is based on an inverted scale of the summation of digits for the years of depreciable life. For example, assuming an asset is amortized over four years, the digits for each of the four years 1, 2, 3, and 4 are added to produce 10. Since SYD is based on the inverted scale, the first year's rate is 4/10 (40%) of the asset value, the second year is 3/10 (30%), the third year is 2/10 (20%), and the fourth year is 1/10 (10%).

Example 6.15   Sum-of-the-year's digits (SYD) amortization Calculate the amortization schedule for a $500 asset assuming the SYD amortization method and a five year useful life.

Solution The sum of the year's digits is 15 $(1 + 2 + 3 + 4 + 5)$. Therefore, the amortization rate for the first year is 5/15 (33.33%) of the $500 asset value or simply $166.67. The amortization rate for the remaining years 2, 3, 4, and 5 are 4/15 (26.67%), 3/15 (20%), 2/15 (13.33%), and 1/15 (6.67%), respectively. The corresponding amortization schedule for years 2, 3, 4, and 5 are $133.33, $100, $66.67, and $33.33, respectively.

Unit-of-production method

This method of amortizing capital costs associated with oil and gas industry activity is dependent on the accounting method chosen by the company owning the assets. More will be discussed later in this section concerning different accounting methods. A general formula illustrating the concept of unit-of-production amortization follows:

$$\begin{bmatrix} \text{Amortization} \\ \text{for period} \end{bmatrix} = \begin{bmatrix} \text{unamortized costs at} \\ \text{end of period} \end{bmatrix}$$

$$\times \frac{\text{production for period}}{\text{reserves at the beginning of period}} \quad [6.3.1]$$

Unamortized costs at the end of period are equal to the total capitalized costs at the end of the current period less accumulated amortization taken in prior periods. The reserves at the beginning of period should be determined by adding the estimated remaining recoverable reserves at the end of the current period to the production for the current period so that reserve revisions determined during the current period can be included.

When reserves of both oil and gas are used to determine amortization, they should be calculated on the basis of total energy equivalent units of oil or gas. Although it may be more precise to determine the actual energy equivalent content of the oil and gas, it is acceptable to use a general approximation of one barrel of oil as equivalent to 6000 cubic feet (6 MCF) of gas.

Example 6.16 Unit-of-production amortization

Assuming total capitalized costs at the end of the period are equal to $1 500 000, accumulated amortization taken in prior periods is equal to $500 000, estimated remaining recoverable reserves at the end of the period are equal to 440 000 BOE, and production during the period is equal to 60 000 BOE, calculate the amortization for the period using the unit-of-production method.

Solution

$$\text{Amortization for period} = (\$1\,500\,000 - \$500\,000)$$

$$\times 60\,000/(440\,000 + 60\,000)$$

$$= \$120\,000$$

6.3.3 Successful efforts and full cost accounting

Companies that chose the successful efforts accounting method can report considerably different earnings, return on equity, and book value for the same activity and success than if they chose full cost accounting. The primary differences between the two methods are associated with the size and use of cost centers, the capitalization of exploration costs, and the determination of unit-of-production amortization. These differences stem from different philosophical opinions concerning what capital contributes to growth. Full cost accounting borrows concepts from Research and Development accounting that argues that all capital costs, regardless of success, contribute to the growth of the company. It is generally preferred by smaller upstream oil and

gas companies including some large independents. Successful efforts accounting contends that only the capital invested in successful projects contribute to growth. Successful efforts is the preferred accounting method of the SEC and used by all large integrated oil and gas companies.

Cost centers

Successful efforts accounting allows proved properties in a common geological structure to be combined or aggregated for the purpose of forming cost centers and computing amortization. Because the definition of a geological structure can be subjective, there can be subjectivity associated with defining the cost centers. Most successful efforts companies define their cost centers through cost aggregation by well, by property, by reservoir, or by field.

Full cost accounting requires that cost centers be established on a country-by-country basis except in the rare case where a company makes a significant acquisition of properties with lives substantially shorter than the composite productive life of the cost center. As a result, all exploration, development, and acquisition costs associated with oil and gas activities within a country are aggregated together for amortization purposes.

Exploration costs

Successful efforts accounting allows exploration costs leading to the discovery of commercial quantities of oil and gas to be capitalized. All other exploration costs are to be expensed or written off since those expenditures are said to provide no further benefit. For example, using successful efforts accounting, all exploration dry hole costs are expensed in the period they are incurred.

Full cost accounting, on the other hand, allows all exploration costs to be capitalized regardless of success because they are said to contribute ultimately to the production of reserves. As a result, it is not necessary to establish a direct relationship between costs incurred and specific reserves discovered using the full cost accounting method.

Unit-of-production amortization

As noted earlier in this text, the determination of unit-of-production amortization is dependent on the accounting method a company chooses. The general equation for unit-of-production amortization Equation 6.3.1 is the same for both methods. The differences between the two methods are associated with the capital and corresponding reserves definitions. The following equations and corresponding definitions summarize the primary differences in successful efforts and full cost accounting with respect to unit-of-production amortization calculations:

$$\text{Amortization expense} = \frac{\text{UC} \times \text{PP}}{\text{PP} + \text{R}} \quad [6.3.2]$$

where:

UC = the unamortized costs at the end of the period, defined below

PP = the period production (usually defined as hydrocarbons sold)

R = the reserves at the beginning of the period, defined below

For *successful efforts* accounting, the unamortized costs (UC) are determined using the following formula:

$$\text{UC} = \text{ICC} - \text{AA} + (\text{DR\&A}) - \text{SV} - \text{EC} \quad [6.3.3]$$

where:

ICC = the incurred capitalized costs of wells and development facilities or of mineral property interests

AA = the accumulated amortization of prior periods

DR&A = the estimated undiscounted future dismantlement, restoration, and abandonment costs (P&A costs)

SV = the estimated undiscounted future salvage value of well and lease equipment

EC = the excluded capitalized development costs allowed under certain circumstances

For *full cost* accounting, the unamortized costs (UC) are determined using the following formula:

$$UC = ICC - AA + (DR\&A) - SV - EUC + FDC \qquad [6.3.4]$$

where:

ICC = the incurred capitalized costs of exploration, development, and acquisition activities

AA = the accumulated amortization of prior periods

DR&A = the estimated undiscounted future dismantlement, restoration, and abandonment costs (P&A costs)

SV = the estimated undiscounted future salvage value of well and lease equipment

EUC = the excluded capitalized unproved property costs associated with the acquisition of unproved properties and certain allowable capitalized development costs

FDC = the undiscounted estimated future development costs associated with proved undeveloped reserves

For successful efforts accounting, reserves (R) = proved reserves at the end of the period using proved developed (PD) reserves for well and equipment amortization, and total proved reserves for property acquisition amortization.

For full cost accounting, reserves (R) = total proved reserves at the end of the period.

Appendix

Table 6A.1 *Periodic Interest Rate* $(i) = 0.5\%$

n	$F/P_{i,n}$	$P/F_{i,n}$	$F/A_{i,n}$	$P/A_{i,n}$	$A/F_{i,n}$	$A/P_{i,n}$
1	1.00500	0.99502	1.00000	0.99502	1.00000	1.00500
2	1.01003	0.99007	2.00500	1.98510	0.49875	0.50375
3	1.01508	0.98515	3.01502	2.97025	0.33167	0.33667
4	1.02015	0.98025	4.03010	3.95050	0.24813	0.25313
5	1.02525	0.97537	5.05025	4.92587	0.19801	0.20301
6	1.03038	0.97052	6.07550	5.89638	0.16460	0.16960
7	1.03553	0.96569	7.10588	6.86207	0.14073	0.14573
8	1.04071	0.96089	8.14141	7.82296	0.12283	0.12783
9	1.04591	0.95610	9.18212	8.77906	0.10891	0.11391
10	1.05114	0.95135	10.22803	9.73041	0.09777	0.10277
11	1.05640	0.94661	11.27917	10.67703	0.08866	0.09366
12	1.06168	0.94191	12.33556	11.61893	0.08107	0.08607
13	1.06699	0.93722	13.39724	12.55615	0.07464	0.07964
14	1.07232	0.93256	14.46423	13.48871	0.06914	0.07414
15	1.07768	0.92792	15.53655	14.41662	0.06436	0.06936
16	1.08307	0.92330	16.61423	15.33993	0.06019	0.06519
17	1.08849	0.91871	17.69730	16.25863	0.05651	0.06151
18	1.09393	0.91414	18.78579	17.17277	0.05323	0.05823
19	1.09940	0.90959	19.87972	18.08236	0.05030	0.05530
20	1.10490	0.90506	20.97912	18.98742	0.04767	0.05267
21	1.11042	0.90056	22.08401	19.88798	0.04528	0.05028
22	1.11597	0.89608	23.19443	20.78406	0.04311	0.04811
23	1.12155	0.89162	24.31040	21.67568	0.04113	0.04613
24	1.12716	0.88719	25.43196	22.56287	0.03932	0.04432
25	1.13280	0.88277	26.55912	23.44564	0.03765	0.04265
26	1.13846	0.87838	27.69191	24.32402	0.03611	0.04111
27	1.14415	0.87401	28.83037	25.19803	0.03469	0.03969
28	1.14987	0.86966	29.97452	26.06769	0.03336	0.03836
29	1.15562	0.86533	31.12439	26.93302	0.03213	0.03713
30	1.16140	0.86103	32.28002	27.79405	0.03098	0.03598
35	1.19073	0.83982	38.14538	32.03537	0.02622	0.03122
40	1.22079	0.81914	44.15885	36.17223	0.02265	0.02765
45	1.25162	0.79896	50.32416	40.20720	0.01987	0.02487
50	1.28323	0.77929	56.64516	44.14279	0.01765	0.02265
55	1.31563	0.76009	63.12577	47.98145	0.01584	0.02084

(continued)

Table 6A.1 Periodic Interest Rate (*i*) = 0.5% (continued)

n	$F/P_{i,n}$	$P/F_{i,n}$	$F/A_{i,n}$	$P/A_{i,n}$	$A/F_{i,n}$	$A/P_{i,n}$
60	1.34885	0.74137	69.77003	51.72556	0.01433	0.01933
65	1.38291	0.72311	76.58206	55.37746	0.01306	0.01806
70	1.41783	0.70530	83.56611	58.93942	0.01197	0.01697
75	1.45363	0.68793	90.72650	62.41365	0.01102	0.01602
80	1.49034	0.67099	98.06771	65.80231	0.01020	0.01520
85	1.52797	0.65446	105.59430	69.10750	0.00947	0.01447
90	1.56655	0.63834	113.31094	72.33130	0.00883	0.01383
95	1.60611	0.62262	121.22243	75.47569	0.00825	0.01325
100	1.64667	0.60729	129.33370	78.54264	0.00773	0.01273

Table 6A.2 Periodic Interest Rate (*i*) = 1%

n	$F/P_{i,n}$	$P/F_{i,n}$	$F/A_{i,n}$	$P/A_{i,n}$	$A/F_{i,n}$	$A/P_{i,n}$
1	1.01000	0.99010	1.00000	0.99010	1.00000	1.01000
2	1.02010	0.98030	2.01000	1.97040	0.49751	0.50751
3	1.03030	0.97059	3.03010	2.94099	0.33002	0.34002
4	1.04060	0.96098	4.06040	3.90197	0.24628	0.25628
5	1.05101	0.95147	5.10101	4.85343	0.19604	0.20604
6	1.06152	0.94205	6.15202	5.79548	0.16255	0.17255
7	1.07214	0.93272	7.21354	6.72819	0.13863	0.14863
8	1.08286	0.92348	8.28567	7.65168	0.12069	0.13069
9	1.09369	0.91434	9.36853	8.56602	0.10674	0.11674
10	1.10462	0.90529	10.46221	9.47130	0.09558	0.10558
11	1.11567	0.89632	11.56683	10.36763	0.08645	0.09645
12	1.12683	0.88745	12.68250	11.25508	0.07885	0.08885
13	1.13809	0.87866	13.80933	12.13374	0.07241	0.08241
14	1.14947	0.86996	14.94742	13.00370	0.06690	0.07690
15	1.16097	0.86135	16.09690	13.86505	0.06212	0.07212
16	1.17258	0.85282	17.25786	14.71787	0.05794	0.06794
17	1.18430	0.84438	18.43044	15.56225	0.05426	0.06426
18	1.19615	0.83602	19.61475	16.39827	0.05098	0.06098
19	1.20811	0.82774	20.81090	17.22601	0.04805	0.05805
20	1.22019	0.81954	22.01900	18.04555	0.04542	0.05542
21	1.23239	0.81143	23.23919	18.85698	0.04303	0.05303
22	1.24472	0.80340	24.47159	19.66038	0.04086	0.05086
23	1.25716	0.79544	25.71630	20.45582	0.03889	0.04889
24	1.26973	0.78757	26.97346	21.24339	0.03707	0.04707
25	1.28243	0.77977	28.24320	22.02316	0.03541	0.04541
26	1.29526	0.77205	29.52563	22.79520	0.03387	0.04387
27	1.30821	0.76440	30.82089	23.55961	0.03245	0.04245
28	1.32129	0.75684	32.12910	24.31644	0.03112	0.04112
29	1.33450	0.74934	33.45039	25.06579	0.02990	0.03990
30	1.34785	0.74192	34.78489	25.80771	0.02875	0.03875
35	1.41660	0.70591	41.66028	29.40858	0.02400	0.03400
40	1.48886	0.67165	48.88637	32.83469	0.02046	0.03046
45	1.56481	0.63905	56.48107	36.09451	0.01771	0.02771
50	1.64463	0.60804	64.46318	39.19612	0.01551	0.02551
55	1.72852	0.57853	72.85246	42.14719	0.01373	0.02373
60	1.81670	0.55045	81.66967	44.95504	0.01224	0.02224
65	1.90937	0.52373	90.93665	47.62661	0.01100	0.02100
70	2.00676	0.49831	100.67634	50.16851	0.00993	0.01993
75	2.10913	0.47413	110.91285	52.58705	0.00902	0.01902
80	2.21672	0.45112	121.67152	54.88821	0.00822	0.01822
85	2.32979	0.42922	132.97900	57.07768	0.00752	0.01752
90	2.44863	0.40839	144.86327	59.16088	0.00690	0.01690
95	2.57354	0.38857	157.35376	61.14298	0.00636	0.01636
100	2.70481	0.36971	170.48138	63.02888	0.00587	0.01587

Table 6A.3 *Periodic Interest Rate* $(i) = 2\%$

n	$F/P_{i,n}$	$P/F_{i,n}$	$F/A_{i,n}$	$P/A_{i,n}$	$A/F_{i,n}$	$A/P_{i,n}$
1	1.02000	0.98039	1.00000	0.98039	1.00000	1.02000
2	1.04040	0.96117	2.02000	1.94156	0.49505	0.51505
3	1.06121	0.94232	3.06040	2.88388	0.32675	0.34675
4	1.08243	0.92385	4.12161	3.80773	0.24262	0.26262
5	1.10408	0.90573	5.20404	4.71346	0.19216	0.21216
6	1.12616	0.88797	6.30812	5.60143	0.15853	0.17853
7	1.14869	0.87056	7.43428	6.47199	0.13451	0.15451
8	1.17166	0.85349	8.58297	7.32548	0.11651	0.13651
9	1.19509	0.83676	9.75463	8.16224	0.10252	0.12252
10	1.21899	0.82035	10.94972	8.98259	0.09133	0.11133
11	1.24337	0.80426	12.16872	9.78685	0.08218	0.10218
12	1.26824	0.78849	13.41209	10.57534	0.07456	0.09456
13	1.29361	0.77303	14.68033	11.34837	0.06812	0.08812
14	1.31948	0.75788	15.97394	12.10625	0.06260	0.08260
15	1.34587	0.74301	17.29342	12.84926	0.05783	0.07783
16	1.37279	0.72845	18.63929	13.57771	0.05365	0.07365
17	1.40024	0.71416	20.01207	14.29187	0.04997	0.06997
18	1.42825	0.70016	21.41231	14.99203	0.04670	0.06670
19	1.45681	0.68643	22.84056	15.67846	0.04378	0.06378
20	1.48595	0.67297	24.29737	16.35143	0.04116	0.06116
21	1.51567	0.65978	25.78332	17.01121	0.03878	0.05878
22	1.54598	0.64684	27.29898	17.65805	0.03663	0.05663
23	1.57690	0.63416	28.84496	18.29220	0.03467	0.05467
24	1.60844	0.62172	30.42186	18.91393	0.03287	0.05287
25	1.64061	0.60953	32.03030	19.52346	0.03122	0.05122
26	1.67342	0.59758	33.67091	20.12104	0.02970	0.04970
27	1.70689	0.58586	35.34432	20.70690	0.02829	0.04829
28	1.74102	0.57437	37.05121	21.28127	0.02699	0.04699
29	1.77584	0.56311	38.79223	21.84438	0.02578	0.04578
30	1.81136	0.55207	40.56808	22.39646	0.02465	0.04465
35	1.99989	0.50003	49.99448	24.99862	0.02000	0.04000
40	2.20804	0.45289	60.40198	27.35548	0.01656	0.03656
45	2.43785	0.41020	71.89271	29.49016	0.01391	0.03391
50	2.69159	0.37153	84.57940	31.42361	0.01182	0.03182
55	2.97173	0.33650	98.58653	33.17479	0.01014	0.03014
60	3.28103	0.30478	114.05154	34.76089	0.00877	0.02877
65	3.62252	0.27605	131.12616	36.19747	0.00763	0.02763
70	3.99956	0.25003	149.97791	37.49862	0.00667	0.02667
75	4.41584	0.22646	170.79177	38.67711	0.00586	0.02586
80	4.87544	0.20511	193.77196	39.74451	0.00516	0.02516
85	5.38288	0.18577	219.14394	40.71129	0.00456	0.02456
90	5.94313	0.16826	247.15666	41.58693	0.00405	0.02405
95	6.56170	0.15240	278.08496	42.38002	0.00360	0.02360
100	7.24465	0.13803	312.23231	43.09835	0.00320	0.02320

Table 6A.4 *Periodic Interest Rate* $(i) = 3\%$

n	$F/P_{i,n}$	$P/F_{i,n}$	$F/A_{i,n}$	$P/A_{i,n}$	$A/F_{i,n}$	$A/P_{i,n}$
1	1.03000	0.97087	1.00000	0.97087	1.00000	1.03000
2	1.06090	0.94260	2.03000	1.91347	0.49261	0.52261
3	1.09273	0.91514	3.09090	2.82861	0.32353	0.35353
4	1.12551	0.88849	4.18363	3.71710	0.23903	0.26903
5	1.15927	0.86261	5.30914	4.57971	0.18835	0.21835
6	1.19405	0.83748	6.46841	5.41719	0.15460	0.18460
7	1.22987	0.81309	7.66246	6.23028	0.13051	0.16051
8	1.26677	0.78941	8.89234	7.01969	0.11246	0.14246
9	1.30477	0.76642	10.15911	7.78611	0.09843	0.12843
10	1.34392	0.74409	11.46388	8.53020	0.08723	0.11723

(continued)

Table 6A.4   *Periodic Interest Rate* (*i*) = 3% (continued)

n	$F/P_{i,n}$	$P/F_{i,n}$	$F/A_{i,n}$	$P/A_{i,n}$	$A/F_{i,n}$	$A/P_{i,n}$
11	1.38423	0.72242	12.80780	9.25262	0.07808	0.10808
12	1.42576	0.70138	14.19203	9.95400	0.07046	0.10046
13	1.46853	0.68095	15.61779	10.63496	0.06403	0.09403
14	1.51259	0.66112	17.08632	11.29607	0.05853	0.08853
15	1.55797	0.64186	18.59891	11.93794	0.05377	0.08377
16	1.60471	0.62317	20.15688	12.56110	0.04961	0.07961
17	1.65285	0.60502	21.76159	13.16612	0.04595	0.07595
18	1.70243	0.58739	23.41444	13.75351	0.04271	0.07271
19	1.75351	0.57029	25.11687	14.32380	0.03981	0.06981
20	1.80611	0.55368	26.87037	14.87747	0.03722	0.06722
21	1.86029	0.53755	28.67649	15.41502	0.03487	0.06487
22	1.91610	0.52189	30.53678	15.93692	0.03275	0.06275
23	1.97359	0.50669	32.45288	16.44361	0.03081	0.06081
24	2.03279	0.49193	34.42647	16.93554	0.02905	0.05905
25	2.09378	0.47761	36.45926	17.41315	0.02743	0.05743
26	2.15659	0.46369	38.55304	17.87684	0.02594	0.05594
27	2.22129	0.45019	40.70963	18.32703	0.02456	0.05456
28	2.28793	0.43708	42.93092	18.76411	0.02329	0.05329
29	2.35657	0.42435	45.21885	19.18845	0.02211	0.05211
30	2.42726	0.41199	47.57542	19.60044	0.02102	0.05102
35	2.81386	0.35538	60.46208	21.48722	0.01654	0.04654
40	3.26204	0.30656	75.40126	23.11477	0.01326	0.04326
45	3.78160	0.26444	92.71986	24.51871	0.01079	0.04079
50	4.38391	0.22811	112.79687	25.72976	0.00887	0.03887
55	5.08215	0.19677	136.07162	26.77443	0.00735	0.03735
60	5.89160	0.16973	163.05344	27.67556	0.00613	0.03613
65	6.82998	0.14641	194.33276	28.45289	0.00515	0.03515
70	7.91782	0.12630	230.59406	29.12342	0.00434	0.03434
75	9.17893	0.10895	272.63086	29.70183	0.00367	0.03367
80	10.64089	0.09398	321.36302	30.20076	0.00311	0.03311
85	12.33571	0.08107	377.85695	30.63115	0.00265	0.03265
90	14.30047	0.06993	443.34890	31.00241	0.00226	0.03226
95	16.57816	0.06032	519.27203	31.32266	0.00193	0.03193
100	19.21863	0.05203	607.28773	31.59891	0.00165	0.03165

Table 6A.5   *Periodic Interest Rate* (*i*) = 4%

n	$F/P_{i,n}$	$P/F_{i,n}$	$F/A_{i,n}$	$P/A_{i,n}$	$A/F_{i,n}$	$A/P_{i,n}$
1	1.04000	0.96154	1.00000	0.96154	1.00000	1.04000
2	1.08160	0.92456	2.04000	1.88609	0.49020	0.53020
3	1.12486	0.88900	3.12160	2.77509	0.32035	0.36035
4	1.16986	0.85480	4.24646	3.62990	0.23549	0.27549
5	1.21665	0.82193	5.41632	4.45182	0.18463	0.22463
6	1.26532	0.79031	6.63298	5.24214	0.15076	0.19076
7	1.31593	0.75992	7.89829	6.00205	0.12661	0.16661
8	1.36857	0.73069	9.21423	6.73274	0.10853	0.14853
9	1.42331	0.70259	10.58280	7.43533	0.09449	0.13449
10	1.48024	0.67556	12.00611	8.11090	0.08329	0.12329
11	1.53945	0.64958	13.48635	8.76048	0.07415	0.11415
12	1.60103	0.62460	15.02581	9.38507	0.06655	0.10655
13	1.66507	0.60057	16.62684	9.98565	0.06014	0.10014
14	1.73168	0.57748	18.29191	10.56312	0.05467	0.09467
15	1.80094	0.55526	20.02359	11.11839	0.04994	0.08994
16	1.87298	0.53391	21.82453	11.65230	0.04582	0.08582
17	1.94790	0.51337	23.69751	12.16567	0.04220	0.08220
18	2.02582	0.49363	25.64541	12.65930	0.03899	0.07899
19	2.10685	0.47464	27.67123	13.13394	0.03614	0.07614
20	2.19112	0.45639	29.77808	13.59033	0.03358	0.07358

(continued)

Table 6A.5 *Periodic Interest Rate* (*i*) = 4% *(continued)*

n	$F/P_{i,n}$	$P/F_{i,n}$	$F/A_{i,n}$	$P/A_{i,n}$	$A/F_{i,n}$	$A/P_{i,n}$
21	2.27877	0.43883	31.96920	14.02916	0.03128	0.07128
22	2.36992	0.42196	34.24797	14.45112	0.02920	0.06920
23	2.46472	0.40573	36.61789	14.85684	0.02731	0.06731
24	2.56330	0.39012	39.08260	15.24696	0.02559	0.06559
25	2.66584	0.37512	41.64591	15.62208	0.02401	0.06401
26	2.77247	0.36069	44.31174	15.98277	0.02257	0.06257
27	2.88337	0.34682	47.08421	16.32959	0.02124	0.06124
28	2.99870	0.33348	49.96758	16.66306	0.02001	0.06001
29	3.11865	0.32065	52.96629	16.98371	0.01888	0.05888
30	3.24340	0.30832	56.08494	17.29203	0.01783	0.05783
35	3.94609	0.25342	73.65222	18.66461	0.01358	0.05358
40	4.80102	0.20829	95.02552	19.79277	0.01052	0.05052
45	5.84118	0.17120	121.02939	20.72004	0.00826	0.04826
50	7.10668	0.14071	152.66708	21.48218	0.00655	0.04655
55	8.64637	0.11566	191.15917	22.10861	0.00523	0.04523
60	10.51963	0.09506	237.99069	22.62349	0.00420	0.04420
65	12.79874	0.07813	294.96838	23.04668	0.00339	0.04339
70	15.57162	0.06422	364.29046	23.39451	0.00275	0.04275
75	18.94525	0.05278	448.63137	23.68041	0.00223	0.04223
80	23.04980	0.04338	551.24498	23.91539	0.00181	0.04181
85	28.04360	0.03566	676.09012	24.10853	0.00148	0.04148
90	34.11933	0.02931	827.98333	24.26728	0.00121	0.04121
95	41.51139	0.02409	1012.78465	24.39776	0.00099	0.04099
100	50.50495	0.01980	1237.62370	24.50500	0.00081	0.04081

Table 6A.6 *Periodic Interest Rate* (*i*) = 5%

n	$F/P_{i,n}$	$P/F_{i,n}$	$F/A_{i,n}$	$P/A_{i,n}$	$A/F_{i,n}$	$A/P_{i,n}$
1	1.05000	0.95238	1.00000	0.95238	1.00000	1.05000
2	1.10250	0.90703	2.05000	1.85941	0.48780	0.53780
3	1.15763	0.86384	3.15250	2.72325	0.31721	0.36721
4	1.21551	0.82270	4.31013	3.54595	0.23201	0.28201
5	1.27628	0.78353	5.52563	4.32948	0.18097	0.23097
6	1.34010	0.74622	6.80191	5.07569	0.14702	0.19702
7	1.40710	0.71068	8.14201	5.78637	0.12282	0.17282
8	1.47746	0.67684	9.54911	6.46321	0.10472	0.15472
9	1.55133	0.64461	11.02656	7.10782	0.09069	0.14069
10	1.62889	0.61391	12.57789	7.72173	0.07950	0.12950
11	1.71034	0.58468	14.20679	8.30641	0.07039	0.12039
12	1.79586	0.55684	15.91713	8.86325	0.06283	0.11283
13	1.88565	0.53032	17.71298	9.39357	0.05646	0.10646
14	1.97993	0.50507	19.59863	9.89864	0.05102	0.10102
15	2.07893	0.48102	21.57856	10.37966	0.04634	0.09634
16	2.18287	0.45811	23.65749	10.83777	0.04227	0.09227
17	2.29202	0.43630	25.84037	11.27407	0.03870	0.08870
18	2.40662	0.41552	28.13238	11.68959	0.03555	0.08555
19	2.52695	0.39573	30.53900	12.08532	0.03275	0.08275
20	2.65330	0.37689	33.06595	12.46221	0.03024	0.08024
21	2.78596	0.35894	35.71925	12.82115	0.02800	0.07800
22	2.92526	0.34185	38.50521	13.16300	0.02597	0.07597
23	3.07152	0.32557	41.43048	13.48857	0.02414	0.07414
24	3.22510	0.31007	44.50200	13.79864	0.02247	0.07247
25	3.38635	0.29530	47.72710	14.09394	0.02095	0.07095
26	3.55567	0.28124	51.11345	14.37519	0.01956	0.06956
27	3.73346	0.26785	54.66913	14.64303	0.01829	0.06829
28	3.92013	0.25509	58.40258	14.89813	0.01712	0.06712
29	4.11614	0.24295	62.32271	15.14107	0.01605	0.06605
30	4.32194	0.23138	66.43885	15.37245	0.01505	0.06505
35	5.51602	0.18129	90.32031	16.37419	0.01107	0.06107
40	7.03999	0.14205	120.79977	17.15909	0.00828	0.05828

(continued)

Table 6A.6   *Periodic Interest Rate* $(i) = 5\%$ *(continued)*

n	$F/P_{i,n}$	$P/F_{i,n}$	$F/A_{i,n}$	$P/A_{i,n}$	$A/F_{i,n}$	$A/P_{i,n}$
45	8.98501	0.11130	159.70016	17.77407	0.00626	0.05626
50	11.46740	0.08720	209.34800	18.25593	0.00478	0.05478
55	14.63563	0.06833	272.71262	18.63347	0.00367	0.05367
60	18.67919	0.05354	353.58372	18.92929	0.00283	0.05283
65	23.83990	0.04195	456.79801	19.16107	0.00219	0.05219
70	30.42643	0.03287	588.52851	19.34268	0.00170	0.05170
75	38.83269	0.02575	756.65372	19.48497	0.00132	0.05132
80	49.56144	0.02018	971.22882	19.59646	0.00103	0.05103
85	63.25435	0.01581	1245.08707	19.68382	0.00080	0.05080
90	80.73037	0.01239	1594.60730	19.75226	0.00063	0.05063
95	103.03468	0.00971	2040.69353	19.80589	0.00049	0.05049
100	131.50126	0.00760	2610.02516	19.84791	0.00038	0.05038

Table 6A.7   *Periodic Interest Rate* $(i) = 6\%$

n	$F/P_{i,n}$	$P/F_{i,n}$	$F/A_{i,n}$	$P/A_{i,n}$	$A/F_{i,n}$	$A/P_{i,n}$
1	1.06000	0.94340	1.00000	0.94340	1.00000	1.06000
2	1.12360	0.89000	2.06000	1.83339	0.48544	0.54544
3	1.19102	0.83962	3.18360	2.67301	0.31411	0.37411
4	1.26248	0.79209	4.37462	3.46511	0.22859	0.28859
5	1.33823	0.74726	5.63709	4.21236	0.17740	0.23740
6	1.41852	0.70496	6.97532	4.91732	0.14336	0.20336
7	1.50363	0.66506	8.39384	5.58238	0.11914	0.17914
8	1.59385	0.62741	9.89747	6.20979	0.10104	0.16104
9	1.68948	0.59190	11.49132	6.80169	0.08702	0.14702
10	1.79085	0.55839	13.18079	7.36009	0.07587	0.13587
11	1.89830	0.52679	14.97164	7.88687	0.06679	0.12679
12	2.01220	0.49697	16.86994	8.38384	0.05928	0.11928
13	2.13293	0.46884	18.88214	8.85268	0.05296	0.11296
14	2.26090	0.44230	21.01507	9.29498	0.04758	0.10758
15	2.39656	0.41727	23.27597	9.71225	0.04296	0.10296
16	2.54035	0.39365	25.67253	10.10590	0.03895	0.09895
17	2.69277	0.37136	28.21288	10.47726	0.03544	0.09544
18	2.85434	0.35034	30.90565	10.82760	0.03236	0.09236
19	3.02560	0.33051	33.75999	11.15812	0.02962	0.08962
20	3.20714	0.31180	36.78559	11.46992	0.02718	0.08718
21	3.39956	0.29416	39.99273	11.76408	0.02500	0.08500
22	3.60354	0.27751	43.39229	12.04158	0.02305	0.08305
23	3.81975	0.26180	46.99583	12.30338	0.02128	0.08128
24	4.04893	0.24698	50.81558	12.55036	0.01968	0.07968
25	4.29187	0.23300	54.86451	12.78336	0.01823	0.07823
26	4.54938	0.21981	59.15638	13.00317	0.01690	0.07690
27	4.82235	0.20737	63.70577	13.21053	0.01570	0.07570
28	5.11169	0.19563	68.52811	13.40616	0.01459	0.07459
29	5.41839	0.18456	73.63980	13.59072	0.01358	0.07358
30	5.74349	0.17411	79.05819	13.76483	0.01265	0.07265
35	7.68609	0.13011	111.43478	14.49825	0.00897	0.06897
40	10.28572	0.09722	154.76197	15.04630	0.00646	0.06646
45	13.76461	0.07265	212.74351	15.45583	0.00470	0.06470
50	18.42015	0.05429	290.33590	15.76186	0.00344	0.06344
55	24.65032	0.04057	394.17203	15.99054	0.00254	0.06254
60	32.98769	0.03031	533.12818	16.16143	0.00188	0.06188
65	44.14497	0.02265	719.08286	16.28912	0.00139	0.06139
70	59.07593	0.01693	967.93217	16.38454	0.00103	0.06103
75	79.05692	0.01265	1300.94868	16.45585	0.00077	0.06077
80	105.79599	0.00945	1746.59989	16.50913	0.00057	0.06057
85	141.57890	0.00706	2342.98174	16.54895	0.00043	0.06043
90	189.46451	0.00528	3141.07519	16.57870	0.00032	0.06032
95	253.54625	0.00394	4209.10425	16.60093	0.00024	0.06024
100	339.30208	0.00295	5638.36806	16.61755	0.00018	0.06018

Table 6A.8 *Periodic Interest Rate* $(i) = 7\%$

n	$F/P_{i,n}$	$P/F_{i,n}$	$F/A_{i,n}$	$P/A_{i,n}$	$A/F_{i,n}$	$A/P_{i,n}$
1	1.07000	0.93458	1.00000	0.93458	1.00000	1.07000
2	1.14490	0.87344	2.07000	1.80802	0.48309	0.55309
3	1.22504	0.81630	3.21490	2.62432	0.31105	0.38105
4	1.31080	0.76290	4.43994	3.38721	0.22523	0.29523
5	1.40255	0.71299	5.75074	4.10020	0.17389	0.24389
6	1.50073	0.66634	7.15329	4.76654	0.13980	0.20980
7	1.60578	0.62275	8.65402	5.38929	0.11555	0.18555
8	1.71819	0.58201	10.25980	5.97130	0.09747	0.16747
9	1.83846	0.54393	11.97799	6.51523	0.08349	0.15349
10	1.96715	0.50835	13.81645	7.02358	0.07238	0.14238
11	2.10485	0.47509	15.78360	7.49867	0.06336	0.13336
12	2.25219	0.44401	17.88845	7.94269	0.05590	0.12590
13	2.40985	0.41496	20.14064	8.35765	0.04965	0.11965
14	2.57853	0.38782	22.55049	8.74547	0.04434	0.11434
15	2.75903	0.36245	25.12902	9.10791	0.03979	0.10979
16	2.95216	0.33873	27.88805	9.44665	0.03586	0.10586
17	3.15882	0.31657	30.84022	9.76322	0.03243	0.10243
18	3.37993	0.29586	33.99903	10.05909	0.02941	0.09941
19	3.61653	0.27651	37.37896	10.33560	0.02675	0.09675
20	3.86968	0.25842	40.99549	10.59401	0.02439	0.09439
21	4.14056	0.24151	44.86518	10.83553	0.02229	0.09229
22	4.43040	0.22571	49.00574	11.06124	0.02041	0.09041
23	4.74053	0.21095	53.43614	11.27219	0.01871	0.08871
24	5.07237	0.19715	58.17667	11.46933	0.01719	0.08719
25	5.42743	0.18425	63.24904	11.65358	0.01581	0.08581
26	5.80735	0.17220	68.67647	11.82578	0.01456	0.08456
27	6.21387	0.16093	74.48382	11.98671	0.01343	0.08343
28	6.64884	0.15040	80.69769	12.13711	0.01239	0.08239
29	7.11426	0.14056	87.34653	12.27767	0.01145	0.08145
30	7.61226	0.13137	94.46063	12.40904	0.01059	0.08059
35	10.67658	0.09366	138.23688	12.94767	0.00723	0.07723
40	14.97446	0.06678	199.63511	13.33171	0.00501	0.07501
45	21.00245	0.04761	285.74931	13.60552	0.00350	0.07350
50	29.45703	0.03395	406.52893	13.80075	0.00246	0.07246
55	41.31500	0.02420	575.92859	13.93994	0.00174	0.07174
60	57.94643	0.01726	813.52038	14.03918	0.00123	0.07123
65	81.27286	0.01230	1146.75516	14.10994	0.00087	0.07087
70	113.98939	0.00877	1614.13417	14.16039	0.00062	0.07062
75	159.87602	0.00625	2269.65742	14.19636	0.00044	0.07044
80	224.23439	0.00446	3189.06268	14.22201	0.00031	0.07031
85	314.50033	0.00318	4478.57612	14.24029	0.00022	0.07022
90	441.10298	0.00227	6287.18543	14.25333	0.00016	0.07016
95	618.66975	0.00162	8823.85354	14.26262	0.00011	0.07011
100	867.71633	0.00115	12 381.66179	14.26925	0.00008	0.07008

Table 6A.9 *Periodic Interest Rate* $(i) = 8\%$

n	$F/P_{i,n}$	$P/F_{i,n}$	$F/A_{i,n}$	$P/A_{i,n}$	$A/F_{i,n}$	$A/P_{i,n}$
1	1.08000	0.92593	1.00000	0.92593	1.00000	1.08000
2	1.16640	0.85734	2.08000	1.78326	0.48077	0.56077
3	1.25971	0.79383	3.24640	2.57710	0.30803	0.38803
4	1.36049	0.73503	4.50611	3.31213	0.22192	0.30192
5	1.46933	0.68058	5.86660	3.99271	0.17046	0.25046
6	1.58687	0.63017	7.33593	4.62288	0.13632	0.21632
7	1.71382	0.58349	8.92280	5.20637	0.11207	0.19207
8	1.85093	0.54027	10.63663	5.74664	0.09401	0.17401
9	1.99900	0.50025	12.48756	6.24689	0.08008	0.16008
10	2.15892	0.46319	14.48656	6.71008	0.06903	0.14903

(continued)

Table 6A.9   *Periodic Interest Rate* $(i) = 8\%$ *(continued)*

n	$F/P_{i,n}$	$P/F_{i,n}$	$F/A_{i,n}$	$P/A_{i,n}$	$A/F_{i,n}$	$A/P_{i,n}$
11	2.33164	0.42888	16.64549	7.13896	0.06008	0.14008
12	2.51817	0.39711	18.97713	7.53608	0.05270	0.13270
13	2.71962	0.36770	21.49530	7.90378	0.04652	0.12652
14	2.93719	0.34046	24.21492	8.24424	0.04130	0.12130
15	3.17217	0.31524	27.15211	8.55948	0.03683	0.11683
16	3.42594	0.29189	30.32428	8.85137	0.03298	0.11298
17	3.70002	0.27027	33.75023	9.12164	0.02963	0.10963
18	3.99602	0.25025	37.45024	9.37189	0.02670	0.10670
19	4.31570	0.23171	41.44626	9.60360	0.02413	0.10413
20	4.66096	0.21455	45.76196	9.81815	0.02185	0.10185
21	5.03383	0.19866	50.42292	10.01680	0.01983	0.09983
22	5.43654	0.18394	55.45676	10.20074	0.01803	0.09803
23	5.87146	0.17032	60.89330	10.37106	0.01642	0.09642
24	6.34118	0.15770	66.76476	10.52876	0.01498	0.09498
25	6.84848	0.14602	73.10594	10.67478	0.01368	0.09368
26	7.39635	0.13520	79.95442	10.80998	0.01251	0.09251
27	7.98806	0.12519	87.35077	10.93516	0.01145	0.09145
28	8.62711	0.11591	95.33883	11.05108	0.01049	0.09049
29	9.31727	0.10733	103.96594	11.15841	0.00962	0.08962
30	10.06266	0.09938	113.28321	11.25778	0.00883	0.08883
35	14.78534	0.06763	172.31680	11.65457	0.00580	0.08580
40	21.72452	0.04603	259.05652	11.92461	0.00386	0.08386
45	31.92045	0.03133	386.50562	12.10840	0.00259	0.08259
50	46.90161	0.02132	573.77016	12.23348	0.00174	0.08174
55	68.91386	0.01451	848.92320	12.31861	0.00118	0.08118
60	101.25706	0.00988	1253.21330	12.37655	0.00080	0.08080
65	148.77985	0.00672	1847.24808	12.41598	0.00054	0.08054
70	218.60641	0.00457	2720.08007	12.44282	0.00037	0.08037
75	321.20453	0.00311	4002.55662	12.46108	0.00025	0.08025
80	471.95483	0.00212	5886.93543	12.47351	0.00017	0.08017
85	693.45649	0.00144	8655.70611	12.48197	0.00012	0.08012
90	1018.91509	0.00098	12723.93862	12.48773	0.00008	0.08008
95	1497.12055	0.00067	18701.50686	12.49165	0.00005	0.08005
100	2199.76126	0.00045	27484.51570	12.49432	0.00004	0.08004

Table 6A.10   *Periodic Interest Rate* $(i) = 9\%$

n	$F/P_{i,n}$	$P/F_{i,n}$	$F/A_{i,n}$	$P/A_{i,n}$	$A/F_{i,n}$	$A/P_{i,n}$
1	1.09000	0.91743	1.00000	0.91743	1.00000	1.09000
2	1.18810	0.84168	2.09000	1.75911	0.47847	0.56847
3	1.29503	0.77218	3.27810	2.53129	0.30505	0.39505
4	1.41158	0.70843	4.57313	3.23972	0.21867	0.30867
5	1.53862	0.64993	5.98471	3.88965	0.16709	0.25709
6	1.67710	0.59627	7.52333	4.48592	0.13292	0.22292
7	1.82804	0.54703	9.20043	5.03295	0.10869	0.19869
8	1.99256	0.50187	11.02847	5.53482	0.09067	0.18067
9	2.17189	0.46043	13.02104	5.99525	0.07680	0.16680
10	2.36736	0.42241	15.19293	6.41766	0.06582	0.15582
11	2.58043	0.38753	17.56029	6.80519	0.05695	0.14695
12	2.81266	0.35553	20.14072	7.16073	0.04965	0.13965
13	3.06580	0.32618	22.95338	7.48690	0.04357	0.13357
14	3.34173	0.29925	26.01919	7.78615	0.03843	0.12843
15	3.64248	0.27454	29.36092	8.06069	0.03406	0.12406
16	3.97031	0.25187	33.00340	8.31256	0.03030	0.12030
17	4.32763	0.23107	36.97370	8.54363	0.02705	0.11705
18	4.71712	0.21199	41.30134	8.75563	0.02421	0.11421
19	5.14166	0.19449	46.01846	8.95011	0.02173	0.11173
20	5.60441	0.17843	51.16012	9.12855	0.01955	0.10955

(continued)

Table 6A.10 *Periodic Interest Rate* (i) $= 9\%$ *(continued)*

n	$F/P_{i,n}$	$P/F_{i,n}$	$F/A_{i,n}$	$P/A_{i,n}$	$A/F_{i,n}$	$A/P_{i,n}$
21	6.10881	0.16370	56.76453	9.29224	0.01762	0.10762
22	6.65860	0.15018	62.87334	9.44243	0.01590	0.10590
23	7.25787	0.13778	69.53194	9.58021	0.01438	0.10438
24	7.91108	0.12640	76.78981	9.70661	0.01302	0.10302
25	8.62308	0.11597	84.70090	9.82258	0.01181	0.10181
26	9.39916	0.10639	93.32398	9.92897	0.01072	0.10072
27	10.24508	0.09761	102.72313	10.02658	0.00973	0.09973
28	11.16714	0.08955	112.96822	10.11613	0.00885	0.09885
29	12.17218	0.08215	124.13536	10.19828	0.00806	0.09806
30	13.26768	0.07537	136.30754	10.27365	0.00734	0.09734
35	20.41397	0.04899	215.71075	10.56682	0.00464	0.09464
40	31.40942	0.03184	337.88245	10.75736	0.00296	0.09296
45	48.32729	0.02069	525.85873	10.88120	0.00190	0.09190
50	74.35752	0.01345	815.08356	10.96168	0.00123	0.09123
55	114.40826	0.00874	1260.09180	11.01399	0.00079	0.09079
60	176.03129	0.00568	1944.79213	11.04799	0.00051	0.09051
65	270.84596	0.00369	2998.28847	11.07009	0.00033	0.09033
70	416.73009	0.00240	4619.22318	11.08445	0.00022	0.09022
75	641.19089	0.00156	7113.23215	11.09378	0.00014	0.09014
80	986.55167	0.00101	10 950.57409	11.09985	0.00009	0.09009
85	1517.93203	0.00066	16 854.80033	11.10379	0.00006	0.09006
90	2335.52658	0.00043	25 939.18425	11.10635	0.00004	0.09004
95	3593.49715	0.00028	39 916.63496	11.10802	0.00003	0.09003
100	5529.04079	0.00018	61 422.67546	11.10910	0.00002	0.09002

Table 6A.11 *Periodic Interest Rate* (i) $= 10\%$

n	$F/P_{i,n}$	$P/F_{i,n}$	$F/A_{i,n}$	$P/A_{i,n}$	$A/F_{i,n}$	$A/P_{i,n}$
1	1.10000	0.90909	1.00000	0.90909	1.00000	1.10000
2	1.21000	0.82645	2.10000	1.73554	0.47619	0.57619
3	1.33100	0.75131	3.31000	2.48685	0.30211	0.40211
4	1.46410	0.68301	4.64100	3.16987	0.21547	0.31547
5	1.61051	0.62092	6.10510	3.79079	0.16380	0.26380
6	1.77156	0.56447	7.71561	4.35526	0.12961	0.22961
7	1.94872	0.51316	9.48717	4.86842	0.10541	0.20541
8	2.14359	0.46651	11.43589	5.33493	0.08744	0.18744
9	2.35795	0.42410	13.57948	5.75902	0.07364	0.17364
10	2.59374	0.38554	15.93742	6.14457	0.06275	0.16275
11	2.85312	0.35049	18.53117	6.49506	0.05396	0.15396
12	3.13843	0.31863	21.38428	6.81369	0.04676	0.14676
13	3.45227	0.28966	24.52271	7.10336	0.04078	0.14078
14	3.79750	0.26333	27.97498	7.36669	0.03575	0.13575
15	4.17725	0.23939	31.77248	7.60608	0.03147	0.13147
16	4.59497	0.21763	35.94973	7.82371	0.02782	0.12782
17	5.05447	0.19784	40.54470	8.02155	0.02466	0.12466
18	5.55992	0.17986	45.59917	8.20141	0.02193	0.12193
19	6.11591	0.16351	51.15909	8.36492	0.01955	0.11955
20	6.72750	0.14864	57.27500	8.51356	0.01746	0.11746
21	7.40025	0.13513	64.00250	8.64869	0.01562	0.11562
22	8.14027	0.12285	71.40275	8.77154	0.01401	0.11401
23	8.95430	0.11168	79.54302	8.88322	0.01257	0.11257
24	9.84973	0.10153	88.49733	8.98474	0.01130	0.11130
25	10.83471	0.09230	98.34706	9.07704	0.01017	0.11017
26	11.91818	0.08391	109.18177	9.16095	0.00916	0.10916
27	13.10999	0.07628	121.09994	9.23722	0.00826	0.10826
28	14.42099	0.06934	134.20994	9.30657	0.00745	0.10745
29	15.86309	0.06304	148.63093	9.36961	0.00673	0.10673
30	17.44940	0.05731	164.49402	9.42691	0.00608	0.10608

(continued)

Table 6A.11   *Periodic Interest Rate (i) = 10% (continued)*

n	$F/P_{i,n}$	$P/F_{i,n}$	$F/A_{i,n}$	$P/A_{i,n}$	$A/F_{i,n}$	$A/P_{i,n}$
35	28.10244	0.03558	271.02437	9.64416	0.00369	0.10369
40	45.25926	0.02209	442.59256	9.77905	0.00226	0.10226
45	72.89048	0.01372	718.90484	9.86281	0.00139	0.10139
50	117.39085	0.00852	1163.90853	9.91481	0.00086	0.10086
55	189.05914	0.00529	1880.59142	9.94711	0.00053	0.10053
60	304.48164	0.00328	3034.81640	9.96716	0.00033	0.10033
65	490.37073	0.00204	4893.70725	9.97961	0.00020	0.10020
70	789.74696	0.00127	7887.46957	9.98734	0.00013	0.10013
75	1271.89537	0.00079	12 708.95371	9.99214	0.00008	0.10008
80	2048.40021	0.00049	20 474.00215	9.99512	0.00005	0.10005
85	3298.96903	0.00030	32 979.69030	9.99697	0.00003	0.10003
90	5313.02261	0.00019	53 120.22612	9.99812	0.00002	0.10002
95	8556.67605	0.00012	85 556.76047	9.99883	0.00001	0.10001

Table 6A.12   *Periodic Interest Rate (i) = 11%*

n	$F/P_{i,n}$	$P/F_{i,n}$	$F/A_{i,n}$	$P/A_{i,n}$	$A/F_{i,n}$	$A/P_{i,n}$
1	1.11000	0.90090	1.00000	0.90090	1.00000	1.11000
2	1.23210	0.81162	2.11000	1.71252	0.47393	0.58393
3	1.36763	0.73119	3.34210	2.44371	0.29921	0.40921
4	1.51807	0.65873	4.70973	3.10245	0.21233	0.32233
5	1.68506	0.59345	6.22780	3.69590	0.16057	0.27057
6	1.87041	0.53464	7.91286	4.23054	0.12638	0.23638
7	2.07616	0.48166	9.78327	4.71220	0.10222	0.21222
8	2.30454	0.43393	11.85943	5.14612	0.08432	0.19432
9	2.55804	0.39092	14.16397	5.53705	0.07060	0.18060
10	2.83942	0.35218	16.72201	5.88923	0.05980	0.16980
11	3.15176	0.31728	19.56143	6.20652	0.05112	0.16112
12	3.49845	0.28584	22.71319	6.49236	0.04403	0.15403
13	3.88328	0.25751	26.21164	6.74987	0.03815	0.14815
14	4.31044	0.23199	30.09492	6.98187	0.03323	0.14323
15	4.78459	0.20900	34.40536	7.19087	0.02907	0.13907
16	5.31089	0.18829	39.18995	7.37916	0.02552	0.13552
17	5.89509	0.16963	44.50084	7.54879	0.02247	0.13247
18	6.54355	0.15282	50.39594	7.70162	0.01984	0.12984
19	7.26334	0.13768	56.93949	7.83929	0.01756	0.12756
20	8.06231	0.12403	64.20283	7.96333	0.01558	0.12558
21	8.94917	0.11174	72.26514	8.07507	0.01384	0.12384
22	9.93357	0.10067	81.21431	8.17574	0.01231	0.12231
23	11.02627	0.09069	91.14788	8.26643	0.01097	0.12097
24	12.23916	0.08170	102.17415	8.34814	0.00979	0.11979
25	13.58546	0.07361	114.41331	8.42174	0.00874	0.11874
26	15.07986	0.06631	127.99877	8.48806	0.00781	0.11781
27	16.73865	0.05974	143.07864	8.54780	0.00699	0.11699
28	18.57990	0.05382	159.81729	8.60162	0.00626	0.11626
29	20.62369	0.04849	178.39719	8.65011	0.00561	0.11561
30	22.89230	0.04368	199.02088	8.69379	0.00502	0.11502
35	38.57485	0.02592	341.58955	8.85524	0.00293	0.11293
40	65.00087	0.01538	581.82607	8.95105	0.00172	0.11172
45	109.53024	0.00913	986.63856	9.00791	0.00101	0.11101
50	184.56483	0.00542	1668.77115	9.04165	0.00060	0.11060
55	311.00247	0.00322	2818.20424	9.06168	0.00035	0.11035
60	524.05724	0.00191	4755.06584	9.07356	0.00021	0.11021
65	883.06693	0.00113	8018.79027	9.08061	0.00012	0.11012
70	1488.01913	0.00067	13 518.35574	9.08480	0.00007	0.11007
75	2507.39877	0.00040	22 785.44339	9.08728	0.00004	0.11004
80	4225.11275	0.00024	38 401.02500	9.08876	0.00003	0.11003
85	7119.56070	0.00014	64 714.18815	9.08963	0.00002	0.11002
90	11 996.87381	0.00008	109 053.39829	9.09015	0.00001	0.11001

Table 6A.13 *Periodic Interest Rate* (i) = 12%

n	$F/P_{i,n}$	$P/F_{i,n}$	$F/A_{i,n}$	$P/A_{i,n}$	$A/F_{i,n}$	$A/P_{i,n}$
1	1.12000	0.89286	1.00000	0.89286	1.00000	1.12000
2	1.25440	0.79719	2.12000	1.69005	0.47170	0.59170
3	1.40493	0.71178	3.37440	2.40183	0.29635	0.41635
4	1.57352	0.63552	4.77933	3.03735	0.20923	0.32923
5	1.76234	0.56743	6.35285	3.60478	0.15741	0.27741
6	1.97382	0.50663	8.11519	4.11141	0.12323	0.24323
7	2.21068	0.45235	10.08901	4.56376	0.09912	0.21912
8	2.47596	0.40388	12.29969	4.96764	0.08130	0.20130
9	2.77308	0.36061	14.77566	5.32825	0.06768	0.18768
10	3.10585	0.32197	17.54874	5.65022	0.05698	0.17698
11	3.47855	0.28748	20.65458	5.93770	0.04842	0.16842
12	3.89598	0.25668	24.13313	6.19437	0.04144	0.16144
13	4.36349	0.22917	28.02911	6.42355	0.03568	0.15568
14	4.88711	0.20462	32.39260	6.62817	0.03087	0.15087
15	5.47357	0.18270	37.27971	6.81086	0.02682	0.14682
16	6.13039	0.16312	42.75328	6.97399	0.02339	0.14339
17	6.86604	0.14564	48.88367	7.11963	0.02046	0.14046
18	7.68997	0.13004	55.74971	7.24967	0.01794	0.13794
19	8.61276	0.11611	63.43968	7.36578	0.01576	0.13576
20	9.64629	0.10367	72.05244	7.46944	0.01388	0.13388
21	10.80385	0.09256	81.69874	7.56200	0.01224	0.13224
22	12.10031	0.08264	92.50258	7.64465	0.01081	0.13081
23	13.55235	0.07379	104.60289	7.71843	0.00956	0.12956
24	15.17863	0.06588	118.15524	7.78432	0.00846	0.12846
25	17.00006	0.05882	133.33387	7.84314	0.00750	0.12750
26	19.04007	0.05252	150.33393	7.89566	0.00665	0.12665
27	21.32488	0.04689	169.37401	7.94255	0.00590	0.12590
28	23.88387	0.04187	190.69889	7.98442	0.00524	0.12524
29	26.74993	0.03738	214.58275	8.02181	0.00466	0.12466
30	29.95992	0.03338	241.33268	8.05518	0.00414	0.12414
35	52.79962	0.01894	431.66350	8.17550	0.00232	0.12232
40	93.05097	0.01075	767.09142	8.24378	0.00130	0.12130
45	163.98760	0.00610	1358.23003	8.28252	0.00074	0.12074
50	289.00219	0.00346	2400.01825	8.30450	0.00042	0.12042
55	509.32061	0.00196	4236.00505	8.31697	0.00024	0.12024
60	897.59693	0.00111	7471.64111	8.32405	0.00013	0.12013
65	1581.87249	0.00063	13 173.93742	8.32807	0.00008	0.12008
70	2787.79983	0.00036	23 223.33190	8.33034	0.00004	0.12004
75	4913.05584	0.00020	40 933.79867	8.33164	0.00002	0.12002
80	8658.48310	0.00012	72 145.69250	8.33237	0.00001	0.12001

Table 6A.14 *Periodic Interest Rate* (i) = 13%

n	$F/P_{i,n}$	$P/F_{i,n}$	$F/A_{i,n}$	$P/A_{i,n}$	$A/F_{i,n}$	$A/P_{i,n}$
1	1.13000	0.88496	1.00000	0.88496	1.00000	1.13000
2	1.27690	0.78315	2.13000	1.66810	0.46948	0.59948
3	1.44290	0.69305	3.40690	2.36115	0.29352	0.42352
4	1.63047	0.61332	4.84980	2.97447	0.20619	0.33619
5	1.84244	0.54276	6.48027	3.51723	0.15431	0.28431
6	2.08195	0.48032	8.32271	3.99755	0.12015	0.25015
7	2.35261	0.42506	10.40466	4.42261	0.09611	0.22611
8	2.65844	0.37616	12.75726	4.79877	0.07839	0.20839
9	3.00404	0.33288	15.41571	5.13166	0.06487	0.19487
10	3.39457	0.29459	18.41975	5.42624	0.05429	0.18429
11	3.83586	0.26070	21.81432	5.68694	0.04584	0.17584
12	4.33452	0.23071	25.65018	5.91765	0.03899	0.16899
13	4.89801	0.20416	29.98470	6.12181	0.03335	0.16335
14	5.53475	0.18068	34.88271	6.30249	0.02867	0.15867
15	6.25427	0.15989	40.41746	6.46238	0.02474	0.15474

(continued)

Table 6A.14 *Periodic Interest Rate (i) = 13% (continued)*

n	$F/P_{i,n}$	$P/F_{i,n}$	$F/A_{i,n}$	$P/A_{i,n}$	$A/F_{i,n}$	$A/P_{i,n}$
16	7.06733	0.14150	46.67173	6.60388	0.02143	0.15143
17	7.98608	0.12522	53.73906	6.72909	0.01861	0.14861
18	9.02427	0.11081	61.72514	6.83991	0.01620	0.14620
19	10.19742	0.09806	70.74941	6.93797	0.01413	0.14413
20	11.52309	0.08678	80.94683	7.02475	0.01235	0.14235
21	13.02109	0.07680	92.46992	7.10155	0.01081	0.14081
22	14.71383	0.06796	105.49101	7.16951	0.00948	0.13948
23	16.62663	0.06014	120.20484	7.22966	0.00832	0.13832
24	18.78809	0.05323	136.83147	7.28288	0.00731	0.13731
25	21.23054	0.04710	155.61956	7.32998	0.00643	0.13643
26	23.99051	0.04168	176.85010	7.37167	0.00565	0.13565
27	27.10928	0.03689	200.84061	7.40856	0.00498	0.13498
28	30.63349	0.03264	227.94989	7.44120	0.00439	0.13439
29	34.61584	0.02889	258.58338	7.47009	0.00387	0.13387
30	39.11590	0.02557	293.19922	7.49565	0.00341	0.13341
35	72.06851	0.01388	546.68082	7.58557	0.00183	0.13183
40	132.78155	0.00753	1013.70424	7.63438	0.00099	0.13099
45	244.64140	0.00409	1874.16463	7.66086	0.00053	0.13053
50	450.73593	0.00222	3459.50712	7.67524	0.00029	0.13029
55	830.45173	0.00120	6380.39789	7.68304	0.00016	0.13016
60	1530.05347	0.00065	11 761.94979	7.68728	0.00009	0.13009
65	2819.02434	0.00035	21 677.11035	7.68958	0.00005	0.13005
70	5193.86962	0.00019	39 945.15096	7.69083	0.00003	0.13003
75	9569.36811	0.00010	73 602.83163	7.69150	0.00001	0.13001

Table 6A.15 *Periodic Interest Rate (i) = 14%*

n	$F/P_{i,n}$	$P/F_{i,n}$	$F/A_{i,n}$	$P/A_{i,n}$	$A/F_{i,n}$	$A/P_{i,n}$
1	1.14000	0.87719	1.00000	0.87719	1.00000	1.14000
2	1.29960	0.76947	2.14000	1.64666	0.46729	0.60729
3	1.48154	0.67497	3.43960	2.32163	0.29073	0.43073
4	1.68896	0.59208	4.92114	2.91371	0.20320	0.34320
5	1.92541	0.51937	6.61010	3.43308	0.15128	0.29128
6	2.19497	0.45559	8.53552	3.88867	0.11716	0.25716
7	2.50227	0.39964	10.73049	4.28830	0.09319	0.23319
8	2.85259	0.35056	13.23276	4.63886	0.07557	0.21557
9	3.25195	0.30751	16.08535	4.94637	0.06217	0.20217
10	3.70722	0.26974	19.33730	5.21612	0.05171	0.19171
11	4.22623	0.23662	23.04452	5.45273	0.04339	0.18339
12	4.81790	0.20756	27.27075	5.66029	0.03667	0.17667
13	5.49241	0.18207	32.08865	5.84236	0.03116	0.17116
14	6.26135	0.15971	37.58107	6.00207	0.02661	0.16661
15	7.13794	0.14010	43.84241	6.14217	0.02281	0.16281
16	8.13725	0.12289	50.98035	6.26506	0.01962	0.15962
17	9.27646	0.10780	59.11760	6.37286	0.01692	0.15692
18	10.57517	0.09456	68.39407	6.46742	0.01462	0.15462
19	12.05569	0.08295	78.96923	6.55037	0.01266	0.15266
20	13.74349	0.07276	91.02493	6.62313	0.01099	0.15099
21	15.66758	0.06383	104.76842	6.68696	0.00954	0.14954
22	17.86104	0.05599	120.43600	6.74294	0.00830	0.14830
23	20.36158	0.04911	138.29704	6.79206	0.00723	0.14723
24	23.21221	0.04308	158.65862	6.83514	0.00630	0.14630
25	26.46192	0.03779	181.87083	6.87293	0.00550	0.14550
26	30.16658	0.03315	208.33274	6.90608	0.00480	0.14480
27	34.38991	0.02908	238.49933	6.93515	0.00419	0.14419
28	39.20449	0.02551	272.88923	6.96066	0.00366	0.14366
29	44.69312	0.02237	312.09373	6.98304	0.00320	0.14320
30	50.95016	0.01963	356.78685	7.00266	0.00280	0.14280

(continued)

Table 6A.15 *Periodic Interest Rate* (i) = 14% *(continued)*

n	$F/P_{i,n}$	$P/F_{i,n}$	$F/A_{i,n}$	$P/A_{i,n}$	$A/F_{i,n}$	$A/P_{i,n}$
35	98.10018	0.01019	693.57270	7.07005	0.00144	0.14144
40	188.88351	0.00529	1342.02510	7.10504	0.00075	0.14075
45	363.67907	0.00275	2590.56480	7.12322	0.00039	0.14039
50	700.23299	0.00143	4994.52135	7.13266	0.00020	0.14020
55	1348.23881	0.00074	9623.13434	7.13756	0.00010	0.14010
60	2595.91866	0.00039	18 535.13328	7.14011	0.00005	0.14005
65	4998.21964	0.00020	35 694.42601	7.14143	0.00003	0.14003
70	9623.64498	0.00010	68 733.17846	7.14211	0.00001	0.14001

Table 6A.16 *Periodic Interest Rate* (i) = 15%

n	$F/P_{i,n}$	$P/F_{i,n}$	$F/A_{i,n}$	$P/A_{i,n}$	$A/F_{i,n}$	$A/P_{i,n}$
1	1.15000	0.86957	1.00000	0.86957	1.00000	1.15000
2	1.32250	0.75614	2.15000	1.62571	0.46512	0.61512
3	1.52088	0.65752	3.47250	2.28323	0.28798	0.43798
4	1.74901	0.57175	4.99338	2.85498	0.20027	0.35027
5	2.01136	0.49718	6.74238	3.35216	0.14832	0.29832
6	2.31306	0.43233	8.75374	3.78448	0.11424	0.26424
7	2.66002	0.37594	11.06680	4.16042	0.09036	0.24036
8	3.05902	0.32690	13.72682	4.48732	0.07285	0.22285
9	3.51788	0.28426	16.78584	4.77158	0.05957	0.20957
10	4.04556	0.24718	20.30372	5.01877	0.04925	0.19925
11	4.65239	0.21494	24.34928	5.23371	0.04107	0.19107
12	5.35025	0.18691	29.00167	5.42062	0.03448	0.18448
13	6.15279	0.16253	34.35192	5.58315	0.02911	0.17911
14	7.07571	0.14133	40.50471	5.72448	0.02469	0.17469
15	8.13706	0.12289	47.58041	5.84737	0.02102	0.17102
16	9.35762	0.10686	55.71747	5.95423	0.01795	0.16795
17	10.76126	0.09293	65.07509	6.04716	0.01537	0.16537
18	12.37545	0.08081	75.83636	6.12797	0.01319	0.16319
19	14.23177	0.07027	88.21181	6.19823	0.01134	0.16134
20	16.36654	0.06110	102.44358	6.25933	0.00976	0.15976
21	18.82152	0.05313	118.81012	6.31246	0.00842	0.15842
22	21.64475	0.04620	137.63164	6.35866	0.00727	0.15727
23	24.89146	0.04017	159.27638	6.39884	0.00628	0.15628
24	28.62518	0.03493	184.16784	6.43377	0.00543	0.15543
25	32.91895	0.03038	212.79302	6.46415	0.00470	0.15470
26	37.85680	0.02642	245.71197	6.49056	0.00407	0.15407
27	43.53531	0.02297	283.56877	6.51353	0.00353	0.15353
28	50.06561	0.01997	327.10408	6.53351	0.00306	0.15306
29	57.57545	0.01737	377.16969	6.55088	0.00265	0.15265
30	66.21177	0.01510	434.74515	6.56598	0.00230	0.15230
35	133.17552	0.00751	881.17016	6.61661	0.00113	0.15113
40	267.86355	0.00373	1779.09031	6.64178	0.00056	0.15056
45	538.76927	0.00186	3585.12846	6.65429	0.00028	0.15028
50	1083.65744	0.00092	7217.71628	6.66051	0.00014	0.15014
55	2179.62218	0.00046	14 524.14789	6.66361	0.00007	0.15007
60	4383.99875	0.00023	29 219.99164	6.66515	0.00003	0.15003
65	8817.78739	0.00011	58 778.58258	6.66591	0.00002	0.15002
70	17 735.72004	0.00006	118 231.46693	6.66629	0.00001	0.15001

Table 6A.17 *Periodic Interest Rate* (i) = 20%

n	$F/P_{i,n}$	$P/F_{i,n}$	$F/A_{i,n}$	$P/A_{i,n}$	$A/F_{i,n}$	$A/P_{i,n}$
1	1.20000	0.83333	1.00000	0.83333	1.00000	1.20000
2	1.44000	0.69444	2.20000	1.52778	0.45455	0.65455
3	1.72800	0.57870	3.64000	2.10648	0.27473	0.47473
4	2.07360	0.48225	5.36800	2.58873	0.18629	0.38629
5	2.48832	0.40188	7.44160	2.99061	0.13438	0.33438

(continued)

Table 6A.17   *Periodic Interest Rate* $(i) = 20\%$ *(continued)*

n	$F/P_{i,n}$	$P/F_{i,n}$	$F/A_{i,n}$	$P/A_{i,n}$	$A/F_{i,n}$	$A/P_{i,n}$
6	2.98598	0.33490	9.92992	3.32551	0.10071	0.30071
7	3.58318	0.27908	12.91590	3.60459	0.07742	0.27742
8	4.29982	0.23257	16.49908	3.83716	0.06061	0.26061
9	5.15978	0.19381	20.79890	4.03097	0.04808	0.24808
10	6.19174	0.16151	25.95868	4.19247	0.03852	0.23852
11	7.43008	0.13459	32.15042	4.32706	0.03110	0.23110
12	8.91610	0.11216	39.58050	4.43922	0.02526	0.22526
13	10.69932	0.09346	48.49660	4.53268	0.02062	0.22062
14	12.83918	0.07789	59.19592	4.61057	0.01689	0.21689
15	15.40702	0.06491	72.03511	4.67547	0.01388	0.21388
16	18.48843	0.05409	87.44213	4.72956	0.01144	0.21144
17	22.18611	0.04507	105.93056	4.77463	0.00944	0.20944
18	26.62333	0.03756	128.11667	4.81219	0.00781	0.20781
19	31.94800	0.03130	154.74000	4.84350	0.00646	0.20646
20	38.33760	0.02608	186.68800	4.86958	0.00536	0.20536
21	46.00512	0.02174	225.02560	4.89132	0.00444	0.20444
22	55.20614	0.01811	271.03072	4.90943	0.00369	0.20369
23	66.24737	0.01509	326.23686	4.92453	0.00307	0.20307
24	79.49685	0.01258	392.48424	4.93710	0.00255	0.20255
25	95.39622	0.01048	471.98108	4.94759	0.00212	0.20212
26	114.47546	0.00874	567.37730	4.95632	0.00176	0.20176
27	137.37055	0.00728	681.85276	4.96360	0.00147	0.20147
28	164.84466	0.00607	819.22331	4.96967	0.00122	0.20122
29	197.81359	0.00506	984.06797	4.97472	0.00102	0.20102
30	237.37631	0.00421	1181.88157	4.97894	0.00085	0.20085
35	590.66823	0.00169	2948.34115	4.99154	0.00034	0.20034
40	1469.77157	0.00068	7343.85784	4.99660	0.00014	0.20014
45	3657.26199	0.00027	18 281.30994	4.99863	0.00005	0.20005
50	9100.43815	0.00011	45 497.19075	4.99945	0.00002	0.20002
55	22 644.80226	0.00004	113 219.01129	4.99978	0.00001	0.20001

Table 6A.18   *Periodic Interest Rate* $(i) = 25\%$

n	$F/P_{i,n}$	$P/F_{i,n}$	$F/A_{i,n}$	$P/A_{i,n}$	$A/F_{i,n}$	$A/P_{i,n}$
1	1.25000	0.80000	1.00000	0.80000	1.00000	1.25000
2	1.56250	0.64000	2.25000	1.44000	0.44444	0.69444
3	1.95313	0.51200	3.81250	1.95200	0.26230	0.51230
4	2.44141	0.40960	5.76563	2.36160	0.17344	0.42344
5	3.05176	0.32768	8.20703	2.68928	0.12185	0.37185
6	3.81470	0.26214	11.25879	2.95142	0.08882	0.33882
7	4.76837	0.20972	15.07349	3.16114	0.06634	0.31634
8	5.96046	0.16777	19.84186	3.32891	0.05040	0.30040
9	7.45058	0.13422	25.80232	3.46313	0.03876	0.28876
10	9.31323	0.10737	33.25290	3.57050	0.03007	0.28007
11	11.64153	0.08590	42.56613	3.65640	0.02349	0.27349
12	14.55192	0.06872	54.20766	3.72512	0.01845	0.26845
13	18.18989	0.05498	68.75958	3.78010	0.01454	0.26454
14	22.73737	0.04398	86.94947	3.82408	0.01150	0.26150
15	28.42171	0.03518	109.68684	3.85926	0.00912	0.25912
16	35.52714	0.02815	138.10855	3.88741	0.00724	0.25724
17	44.40892	0.02252	173.63568	3.90993	0.00576	0.25576
18	55.51115	0.01801	218.04460	3.92794	0.00459	0.25459
19	69.38894	0.01441	273.55576	3.94235	0.00366	0.25366
20	86.73617	0.01153	342.94470	3.95388	0.00292	0.25292
21	108.42022	0.00922	429.68087	3.96311	0.00233	0.25233
22	135.52527	0.00738	538.10109	3.97049	0.00186	0.25186
23	169.40659	0.00590	673.62636	3.97639	0.00148	0.25148
24	211.75824	0.00472	843.03295	3.98111	0.00119	0.25119
25	264.69780	0.00378	1054.79118	3.98489	0.00095	0.25095

(continued)

Table 6A.18   *Periodic Interest Rate* $(i) = 25\%$ *(continued)*

n	$F/P_{i,n}$	$P/F_{i,n}$	$F/A_{i,n}$	$P/A_{i,n}$	$A/F_{i,n}$	$A/P_{i,n}$
26	330.87225	0.00302	1319.48898	3.98791	0.00076	0.25076
27	413.59031	0.00242	1650.36123	3.99033	0.00061	0.25061
28	516.98788	0.00193	2063.95153	3.99226	0.00048	0.25048
29	646.23485	0.00155	2580.93941	3.99381	0.00039	0.25039
30	807.79357	0.00124	3227.17427	3.99505	0.00031	0.25031
35	2465.19033	0.00041	9856.76132	3.99838	0.00010	0.25010
40	7523.16385	0.00013	30 088.65538	3.99947	0.00003	0.25003
45	22 958.87404	0.00004	91 831.49616	3.99983	0.00001	0.25001

Table 6A.19   *Periodic Interest Rate* $(i) = 30\%$

n	$F/P_{i,n}$	$P/F_{i,n}$	$F/A_{i,n}$	$P/A_{i,n}$	$A/F_{i,n}$	$A/P_{i,n}$
1	1.30000	0.76923	1.00000	0.76923	1.00000	1.30000
2	1.69000	0.59172	2.30000	1.36095	0.43478	0.73478
3	2.19700	0.45517	3.99000	1.81611	0.25063	0.55063
4	2.85610	0.35013	6.18700	2.16624	0.16163	0.46163
5	3.71293	0.26933	9.04310	2.43557	0.11058	0.41058
6	4.82681	0.20718	12.75603	2.64275	0.07839	0.37839
7	6.27485	0.15937	17.58284	2.80211	0.05687	0.35687
8	8.15731	0.12259	23.85769	2.92470	0.04192	0.34192
9	10.60450	0.09430	32.01500	3.01900	0.03124	0.33124
10	13.78585	0.07254	42.61950	3.09154	0.02346	0.32346
11	17.92160	0.05580	56.40535	3.14734	0.01773	0.31773
12	23.29809	0.04292	74.32695	3.19026	0.01345	0.31345
13	30.28751	0.03302	97.62504	3.22328	0.01024	0.31024
14	39.37376	0.02540	127.91255	3.24867	0.00782	0.30782
15	51.18589	0.01954	167.28631	3.26821	0.00598	0.30598
16	66.54166	0.01503	218.47220	3.28324	0.00458	0.30458
17	86.50416	0.01156	285.01386	3.29480	0.00351	0.30351
18	112.45541	0.00889	371.51802	3.30369	0.00269	0.30269
19	146.19203	0.00684	483.97343	3.31053	0.00207	0.30207
20	190.04964	0.00526	630.16546	3.31579	0.00159	0.30159
21	247.06453	0.00405	820.21510	3.31984	0.00122	0.30122
22	321.18389	0.00311	1067.27963	3.32296	0.00094	0.30094
23	417.53905	0.00239	1388.46351	3.32535	0.00072	0.30072
24	542.80077	0.00184	1806.00257	3.32719	0.00055	0.30055
25	705.64100	0.00142	2348.80334	3.32861	0.00043	0.30043
26	917.33330	0.00109	3054.44434	3.32970	0.00033	0.30033
27	1192.53329	0.00084	3971.77764	3.33054	0.00025	0.30025
28	1550.29328	0.00065	5164.31093	3.33118	0.00019	0.30019
29	2015.38126	0.00050	6714.60421	3.33168	0.00015	0.30015
30	2619.99564	0.00038	8729.98548	3.33206	0.00011	0.30011
35	9727.86043	0.00010	32 422.86808	3.33299	0.00003	0.30003
40	36 118.86481	0.00003	120 392.88269	3.33324	0.00001	0.30001

Table 6A.20   *Periodic Interest Rate* $(i) = 40\%$

n	$F/P_{i,n}$	$P/F_{i,n}$	$F/A_{i,n}$	$P/A_{i,n}$	$A/F_{i,n}$	$A/P_{i,n}$
1	1.40000	0.71429	1.00000	0.71429	1.00000	1.40000
2	1.96000	0.51020	2.40000	1.22449	0.41667	0.81667
3	2.74400	0.36443	4.36000	1.58892	0.22936	0.62936
4	3.84160	0.26031	7.10400	1.84923	0.14077	0.54077
5	5.37824	0.18593	10.94560	2.03516	0.09136	0.49136
6	7.52954	0.13281	16.32384	2.16797	0.06126	0.46126
7	10.54135	0.09486	23.85338	2.26284	0.04192	0.44192
8	14.75789	0.06776	34.39473	2.33060	0.02907	0.42907
9	20.66105	0.04840	49.15262	2.37900	0.02034	0.42034
10	28.92547	0.03457	69.81366	2.41357	0.01432	0.41432

(continued)

Table 6A.20 *Periodic Interest Rate (i) = 40% (continued)*

n	$F/P_{i,n}$	$P/F_{i,n}$	$F/A_{i,n}$	$P/A_{i,n}$	$A/F_{i,n}$	$A/P_{i,n}$
11	40.49565	0.02469	98.73913	2.43826	0.01013	0.41013
12	56.69391	0.01764	139.23478	2.45590	0.00718	0.40718
13	79.37148	0.01260	195.92869	2.46850	0.00510	0.40510
14	111.12007	0.00900	275.30017	2.47750	0.00363	0.40363
15	155.56810	0.00643	386.42024	2.48393	0.00259	0.40259
16	217.79533	0.00459	541.98833	2.48852	0.00185	0.40185
17	304.91347	0.00328	759.78367	2.49180	0.00132	0.40132
18	426.87885	0.00234	1064.69714	2.49414	0.00094	0.40094
19	597.63040	0.00167	1491.57599	2.49582	0.00067	0.40067
20	836.68255	0.00120	2089.20639	2.49701	0.00048	0.40048
21	1171.35558	0.00085	2925.88894	2.49787	0.00034	0.40034
22	1639.89781	0.00061	4097.24452	2.49848	0.00024	0.40024
23	2295.85693	0.00044	5737.14232	2.49891	0.00017	0.40017
24	3214.19970	0.00031	8032.99925	2.49922	0.00012	0.40012
25	4499.87958	0.00022	11 247.19895	2.49944	0.00009	0.40009
26	6299.83141	0.00016	15 747.07853	2.49960	0.00006	0.40006
27	8819.76398	0.00011	22 046.90994	2.49972	0.00005	0.40005
28	12 347.66957	0.00008	30 866.67392	2.49980	0.00003	0.40003
29	17 286.73740	0.00006	43 214.34349	2.49986	0.00002	0.40002

Table 6A.21 *Periodic Interest Rate (i) = 50%*

n	$F/P_{i,n}$	$P/F_{i,n}$	$F/A_{i,n}$	$P/A_{i,n}$	$A/F_{i,n}$	$A/P_{i,n}$
1	1.50000	0.66667	1.00000	0.66667	1.00000	1.50000
2	2.25000	0.44444	2.50000	1.11111	0.40000	0.90000
3	3.37500	0.29630	4.75000	1.40741	0.21053	0.71053
4	5.06250	0.19753	8.12500	1.60494	0.12308	0.62308
5	7.59375	0.13169	13.18750	1.73663	0.07583	0.57583
6	11.39063	0.08779	20.78125	1.82442	0.04812	0.54812
7	17.08594	0.05853	32.17188	1.88294	0.03108	0.53108
8	25.62891	0.03902	49.25781	1.92196	0.02030	0.52030
9	38.44336	0.02601	74.88672	1.94798	0.01335	0.51335
10	57.66504	0.01734	113.33008	1.96532	0.00882	0.50882
11	86.49756	0.01156	170.99512	1.97688	0.00585	0.50585
12	129.74634	0.00771	257.49268	1.98459	0.00388	0.50388
13	194.61951	0.00514	387.23901	1.98972	0.00258	0.50258
14	291.92926	0.00343	581.85852	1.99315	0.00172	0.50172
15	437.89389	0.00228	873.78778	1.99543	0.00114	0.50114
16	656.84084	0.00152	1311.68167	1.99696	0.00076	0.50076
17	985.26125	0.00101	1968.52251	1.99797	0.00051	0.50051
18	1477.89188	0.00068	2953.78376	1.99865	0.00034	0.50034
19	2216.83782	0.00045	4431.67564	1.99910	0.00023	0.50023
20	3325.25673	0.00030	6648.51346	1.99940	0.00015	0.50015
21	4987.88510	0.00020	9973.77019	1.99960	0.00010	0.50010
22	7481.82764	0.00013	14 961.65529	1.99973	0.00007	0.50007
23	11 222.74146	0.00009	22 443.48293	1.99982	0.00004	0.50004
24	16 834.11220	0.00006	33 666.22439	1.99988	0.00003	0.50003
25	25 251.16829	0.00004	50 500.33659	1.99992	0.00002	0.50002

Table 6A.22 *Periodic Interest Rate (i) = 70%*

n	$F/P_{i,n}$	$P/F_{i,n}$	$F/A_{i,n}$	$P/A_{i,n}$	$A/F_{i,n}$	$A/P_{i,n}$
1	1.70000	0.58824	1.00000	0.58824	1.00000	1.70000
2	2.89000	0.34602	2.70000	0.93426	0.37037	1.07037
3	4.91300	0.20354	5.59000	1.13780	0.17889	0.87889
4	8.35210	0.11973	10.50300	1.25753	0.09521	0.79521
5	14.19857	0.07043	18.85510	1.32796	0.05304	0.75304

(continued)

Table 6A.22   *Periodic Interest Rate (i) = 70% (continued)*

n	$F/P_{i,n}$	$P/F_{i,n}$	$F/A_{i,n}$	$P/A_{i,n}$	$A/F_{i,n}$	$A/P_{i,n}$
6	24.13757	0.04143	33.05367	1.36939	0.03025	0.73025
7	41.03387	0.02437	57.19124	1.39376	0.01749	0.71749
8	69.75757	0.01434	98.22511	1.40809	0.01018	0.71018
9	118.58788	0.00843	167.98268	1.41652	0.00595	0.70595
10	201.59939	0.00496	286.57056	1.42149	0.00349	0.70349
11	342.71896	0.00292	488.16995	1.42440	0.00205	0.70205
12	582.62224	0.00172	830.88891	1.42612	0.00120	0.70120
13	990.45780	0.00101	1413.51115	1.42713	0.00071	0.70071
14	1683.77827	0.00059	2403.96895	1.42772	0.00042	0.70042
15	2862.42305	0.00035	4087.74722	1.42807	0.00024	0.70024
16	4866.11919	0.00021	6950.17027	1.42828	0.00014	0.70014
17	8272.40262	0.00012	11 816.28946	1.42840	0.00008	0.70008
18	14 063.08445	0.00007	20 088.69207	1.42847	0.00005	0.70005
19	23 907.24357	0.00004	34 151.77653	1.42851	0.00003	0.70003
20	40 642.31407	0.00002	58 059.02009	1.42854	0.00002	0.70002

Table 6A.23   *Periodic Interest Rate (i) = 90%*

n	$F/P_{i,n}$	$P/F_{i,n}$	$F/A_{i,n}$	$P/A_{i,n}$	$A/F_{i,n}$	$A/P_{i,n}$
1	1.90000	0.52632	1.00000	0.52632	1.00000	1.90000
2	3.61000	0.27701	2.90000	0.80332	0.34483	1.24483
3	6.85900	0.14579	6.51000	0.94912	0.15361	1.05361
4	13.03210	0.07673	13.36900	1.02585	0.07480	0.97480
5	24.76099	0.04039	26.40110	1.06624	0.03788	0.93788
6	47.04588	0.02126	51.16209	1.08749	0.01955	0.91955
7	89.38717	0.01119	98.20797	1.09868	0.01018	0.91018
8	169.83563	0.00589	187.59514	1.10457	0.00533	0.90533
9	322.68770	0.00310	357.43078	1.10767	0.00280	0.90280
10	613.10663	0.00163	680.11847	1.10930	0.00147	0.90147
11	1164.90259	0.00086	1293.22510	1.11016	0.00077	0.90077
12	2213.31492	0.00045	2458.12769	1.11061	0.00041	0.90041
13	4205.29835	0.00024	4671.44261	1.11085	0.00021	0.90021
14	7990.06686	0.00013	8876.74095	1.11097	0.00011	0.90011
15	15 181.12703	0.00007	16 866.80781	1.11104	0.00006	0.90006

Table 6A.24   *Periodic Interest Rate (i) = 110%*

n	$F/P_{i,n}$	$P/F_{i,n}$	$F/A_{i,n}$	$P/A_{i,n}$	$A/F_{i,n}$	$A/P_{i,n}$
1	2.10000	0.47619	1.00000	0.47619	1.00000	2.10000
2	4.41000	0.22676	3.10000	0.70295	0.32258	1.42258
3	9.26100	0.10798	7.51000	0.81093	0.13316	1.23316
4	19.44810	0.05142	16.77100	0.86235	0.05963	1.15963
5	40.84101	0.02449	36.21910	0.88683	0.02761	1.12761
6	85.76612	0.01166	77.06011	0.89849	0.01298	1.11298
7	180.10885	0.00555	162.82623	0.90404	0.00614	1.10614
8	378.22859	0.00264	342.93509	0.90669	0.00292	1.10292
9	794.28005	0.00126	721.16368	0.90795	0.00139	1.10139
10	1667.98810	0.00060	1515.44373	0.90855	0.00066	1.10066
11	3502.77501	0.00029	3183.43182	0.90883	0.00031	1.10031
12	7355.82751	0.00014	6686.20683	0.90897	0.00015	1.10015
13	15 447.23777	0.00006	14 042.03434	0.90903	0.00007	1.10007
14	32 439.19933	0.00003	29 489.27211	0.90906	0.00003	1.10003
15	68 122.31858	0.00001	61 928.47144	0.90908	0.00002	1.10002

Table 6A.25 *Periodic Interest Rate* $(i) = 130\%$

n	$F/P_{i,n}$	$P/F_{i,n}$	$F/A_{i,n}$	$P/A_{i,n}$	$A/F_{i,n}$	$A/P_{i,n}$
1	2.30000	0.43478	1.00000	0.43478	1.00000	2.30000
2	5.29000	0.18904	3.30000	0.62382	0.30303	1.60303
3	12.16700	0.08219	8.59000	0.70601	0.11641	1.41641
4	27.98410	0.03573	20.75700	0.74174	0.04818	1.34818
5	64.36343	0.01554	48.74110	0.75728	0.02052	1.32052
6	148.03589	0.00676	113.10453	0.76403	0.00884	1.30884
7	340.48254	0.00294	261.14042	0.76697	0.00383	1.30383
8	783.10985	0.00128	601.62296	0.76825	0.00166	1.30166
9	1801.15266	0.00056	1384.73282	0.76880	0.00072	1.30072
10	4142.65112	0.00024	3185.88548	0.76905	0.00031	1.30031
11	9528.09758	0.00010	7328.53660	0.76915	0.00014	1.30014
12	21 914.62443	0.00005	16 856.63418	0.76920	0.00006	1.30006
13	50 403.63619	0.00002	38 771.25861	0.76922	0.00003	1.30003
14	115 928.36325	0.00001	89 174.89480	0.76922	0.00001	1.30001
15	266 635.23546	0.00000	205 103.25805	0.76923	0.00000	1.30000

Table 6A.26 *Periodic Interest Rate* $(i) = 150\%$

n	$F/P_{i,n}$	$P/F_{i,n}$	$F/A_{i,n}$	$P/A_{i,n}$	$A/F_{i,n}$	$A/P_{i,n}$
1	2.50000	0.40000	1.00000	0.40000	1.00000	2.50000
2	6.25000	0.16000	3.50000	0.56000	0.28571	1.78571
3	15.62500	0.06400	9.75000	0.62400	0.10256	1.60256
4	39.06250	0.02560	25.37500	0.64960	0.03941	1.53941
5	97.65625	0.01024	64.43750	0.65984	0.01552	1.51552
6	244.14063	0.00410	162.09375	0.66394	0.00617	1.50617
7	610.35156	0.00164	406.23438	0.66557	0.00246	1.50246
8	1525.87891	0.00066	1016.58594	0.66623	0.00098	1.50098
9	3814.69727	0.00026	2542.46484	0.66649	0.00039	1.50039
10	9536.74316	0.00010	6357.16211	0.66660	0.00016	1.50016
11	23 841.85791	0.00004	15 893.90527	0.66664	0.00006	1.50006
12	59 604.64478	0.00002	39 735.76318	0.66666	0.00003	1.50003
13	149 011.61194	0.00001	99 340.40796	0.66666	0.00001	1.50001

Table 6A.27 *Periodic Interest Rate* $(i) = 200\%$

n	$F/P_{i,n}$	$P/F_{i,n}$	$F/A_{i,n}$	$P/A_{i,n}$	$A/F_{i,n}$	$A/P_{i,n}$
1	3.00000	0.33333	1.00000	0.33333	1.00000	3.00000
2	9.00000	0.11111	4.00000	0.44444	0.25000	2.25000
3	27.00000	0.03704	13.00000	0.48148	0.07692	2.07692
4	81.00000	0.01235	40.00000	0.49383	0.02500	2.02500
5	243.00000	0.00412	121.00000	0.49794	0.00826	2.00826
6	729.00000	0.00137	364.00000	0.49931	0.00275	2.00275
7	2187.00000	0.00046	1093.00000	0.49977	0.00091	2.00091
8	6561.00000	0.00015	3280.00000	0.49992	0.00030	2.00030
9	19 683.00000	0.00005	9841.00000	0.49997	0.00010	2.00010
10	59 049.00000	0.00002	29 524.00000	0.49999	0.00003	2.00003
11	177 147.00000	0.00001	88 573.00000	0.50000	0.00001	2.00001
12	531 441.00000	0.00000	265 720.00000	0.50000	0.00000	2.00000

Problems

1. Suppose $1000 is deposited into a savings account paying 6% APR. Assuming the interest is compounded monthly, how much money will be in the account after six years if $200 is withdrawn at the end of the second year?

2. Suppose 10 shares of common stock are purchased for $50 per share and the share price increases 5% compounded annually for two years, decreases 2% compounded annually for one half year, and increases 11% compounded annually for two and only half years, calculate the following assuming no commissions apply to the purchase or sale of the stock.
   a. The value of the shares after two years;
   b. The value of the shares after two and one half years;
   c. The value of the shares after five years;
   d. The nominal interest rate for the five year investment.

3. How much money must be deposited into a savings plan every month for ten years if interest compounds annually at 7% and the goal is to have $50 000 after the final payment?

4. Suppose $100 is invested every month into a company]savings plan and the company dollar-for-dollar contribution for this amount vests immediately. If the savings plan pays 4% compounded annually for two years and 6% compounded annually for three years, what is the value of the plan after 5 years?

5. Suppose a home buyer purchases a home for $150 000 and makes a 10% down payment. If a financial institution advertises a 15 year loan for 6% APR, what will the monthly payments be to pay off the principal and interest? Assume monthly compounding.

6. Suppose an investor believes money is worth 11% compounded annually and has the option to invest in one of two investment opportunities. The first investment (Option A) is to pay $5000 to receive a uniform series of equal annual payments of $1318.99 for five years. The second investment (Option B) is to pay the same amount of money to receive a uniform series of equal annual payments of $1318.99 for three years and a single lump sum of $3370.12 after five years. How much more is the better of the two investment opportunities worth?

7. What APR is being paid on a $20 000 loan if the lender requires it to be repaid with 60 monthly payments of $386.66 assuming monthly compounding?

8. Suppose an investor estimates a working interest in a gas well will generate the following annual cash flows. If the time value of money is 10% compounded annually, what is the working interest worth?

Year	Cash Flow
1	$4685
2	$3820
3	$3085
4	$2740
5	$1955
6	−$9000

9. Suppose an investor purchased the gas well working interest in problem 8 for $5000. What is the DCFROR?

10. Suppose a $20 000 asset has a five year useful life, calculate the amortization schedules assuming the straight-line amortization method, the double declining balance amortization method, and the sum-of-the-year's digits amortization method.

11. Assuming total capitalized costs at the end of the period are equal to $2 000 000, accumulated amortization taken in prior periods is equal to $800 000, estimated remaining recoverable reserves at the end of the prior period are 480 000 BOE, production during the period is equal to 70 000 BOE, and reserves were revised down 28 800 BOE during the current period, calculate the amortization for the period using the unit-of-production method. What would the amortization for the period have been had the reserve write-down not occurred?

References

AGARWAL, R.G. (1980). A new method to account for producing time effects when drawdown type curves are used to analyze pressure buildup and other test data. SPE Paper 9289, Presented at SPE–AIME 55th Annual Technical Conference, Dallas, Texas, Sept. 21–24

AGARWAL, R.G., AL-HUSSAINY, R., and RAMEY, H.J., JR. (1970). An investigation of wellbore storage and skin effect in unsteady liquid flow: I. Analytical treatment. *SPE J.*, Sept., 279–290

AGARWAL, R.G., CARTER, R.D., and POLLOCK, C.B. (1979). Evaluation and performance prediction of low-permeability gas wells stimulated by massive hydraulic fracturing. *J. Pet. Technol.*, Mar., 362–372; also in SPE Reprint Series No. 9

AL-GHAMDI, A. and ISSAKA, M. (2001). SPE Paper 71589, Presented at the SPE Annual Conference, New Orleans, LA, 30 Sept.–3 Oct.

AL-HUSSAINY, R., RAMEY, H.J., JR., and CRAWFORD, P.B. (1966). The flow of real gases through porous media. *Trans.* AIME, **237**, 624

ALLARD, D.R. and CHEN, S.M. (1988). Calculation of water influx for bottomwater drive reservoirs. *SPE Reservoir Eng.*, May, 369–379

ANASH, J., BLASINGAME, T.A., and KNOWLES, R.S. (2000). A semi-analytic (p/Z) rate-time relation for the analysis and prediction of gas well performance. *SPE Reservoir Eng.*, **3**, Dec.

ANCELL, K., LAMBERTS, S., and JOHNSON, F. (1980). Analysis of the coalbed degasification process. SPE/DPE Paper 8971, Presented at 1980 Unconventional Gas Recovery Symposium, Pittsburgh, PA, May 18–12, 1980

ARPS, J. (1945). Analysis of decline curve. *Trans. AIME*, **160**, 228–231

BEGGS, D. (1991). *Production Optimization Using Nodal Analysis* (Tulsa, OK: OGCI)

BEGLAND, T. and WHITEHEAD, W. (1989). Depletion performance of volumetric high-pressured gas reservoirs. *SPE Reservoir Eng*, Aug., 279–282

BENDAKHLIA, H. and AZIZ, K. (1989). IPR for solution-gas drive horizontal wells. Paper SPE 19823, Presented at the 64th SPE Annual Meeting, San Antonio, TX, Oct. 8–11

BORISOV, JU.P. (1984). *Oil Production Using Horizontal and Multiple Deviation Wells*, trans. J. Strauss and S.D. Joshi (ed.) (Bartlesville, OK: Phillips Petroleum Co., the R&D Library Translation)

BOSSIE-CODREANU, D. (1989). A simple buildup analysis method to determine well drainage area and drawdown pressure for a stabilized well. *SPE Form. Eval.*, Sept., pp. 418–420

BOURDET, D. (1985). SPE Paper 13628, Presented at the SPE Regional Meeting, Bakersfield, CA, Mar. 27–29

BOURDET, D. and GRINGARTEN, A.C. (1980). Determination of fissure volume and block size in fractured reservoirs by type-curve analysis. SPE Paper 9293, Presented at the 1980 Annual Technical Conference and Exhibition, Dallas, Sept. 21–24

BOURDET, D., WHITTLE, T.M., DOUGLAS, A.A., and PIRARD, Y.M. (1983). A new set of type curves simplifies well test analysis. *World Oil*, May, 95–106

BOURDET, D., ALAGOA, A., AYOUB, J.A., and PIRARD, Y.M. (1984). New type curves aid analysis of fissured zone well tests. *World Oil*, Apr., 111–124

BOURGOYNE, A. (1990). Shale water as a pressure support mechanism. *J. Pet. Sci.*, **3**, 305

CARSON, D. and KATZ, D. (1942). Natural gas hydrates. *Trans. AIME*, **146**, 150–159

CARTER, R. (1985). Type curves for finite radial and linear gas-floe systems. *SPE J.*, Oct., 719–728

CARTER, R. and TRACY, G. (1960). An improved method for calculations of water influx. *Trans. AIME*, **152**

CHATAS, A.T. (1953). A practical treatment of nonsteady-state flow problems in reservoir systems. *Pet. Eng.*, Aug, B-44–56

CHAUDHRY, A. (2003). *Gas Well Testing Handbook* (Houston, TX: Gulf Publishing)

CHENG, AM. (1990). IPR for solution gas-drive horizontal wells. Paper SPE 20720, Presented at the 65th SPE Annual Meeting, New Orleans, Sept. 23–26

CINCO, H. LEY and SAMANIEGO, F. (1981). Transient pressure analysis for finite conductivity fracture case versus damage fracture case. SPE Paper 10179

CLARK, N. (1969). *Elements of Petroleum Reservoirs* (Dallas, TX: Society of Petroleum Engineers)

COATS, K. (1962). A mathematical model for water movement about bottom-water-drive reservoirs. *SPE J.*, Mar., 44–52

COLE, F.W. (1969). *Reservoir Engineering Manual* (Houston, TX: Gulf Publishing)

CRAFT, B. and HAWKINS, M. (1959). *Applied Petroleum Reservoir Engineering* (Englewood Cliffs, NJ: Prentice Hall)

CRAFT, B.C. and HAWKINS, M. (Revised by TERRY, R.E.) (1991). *Applied Petroleum Reservoir Engineering*, 2nd ed. (Englewood Cliffs, NJ: Prentice Hall)

CULHAM, W.E. (1974). Pressure buildup equations for spherical flow regime problems. *SPE J.*, Dec. 545–555

CULLENDER, M. and SMITH, R. (1956). Practical solution of gas flow equations for wells and pipelines. *Trans. AIME*, **207**, 281–287

DAKE, L. (1978). *Fundamentals of Reservoir Engineering* (Amsterdam: Elsevier)

DAKE, L.P. (1994). *The Practice of Reservoir Engineering* (Amsterdam: Elsevier)

DIETZ, D.N. (1965). Determination of average reservoir pressure from buildup surveys. *J. Pet. Technol.*, Aug., 955–959

DONOHUE, D. and ERKEKIN, T. (1982). *Gas Well Testing, Theory and Practice* (Boston: International Human Resources Development Corporation)

DUGGAN, J.O. (1972). The Anderson 'L' – an abnormally pressured gas reservoir in South Texas. *J. Pet. Technol.*, **24**, No. 2, 132–138

EARLOUGHER, ROBERT C., JR. (1977). *Advances in Well Test Analysis*, Monograph Vol. 5 (Dallas, TX: Society of Petroleum Engineers of AIME)

ECONOMIDES, C. (1988). Use of the pressure derivative for diagnosing pressure-transient behavior., *J. Pet. Technol.*, Oct.

ECONOMIDES, M., HILL, A., and ECONOMIDES, C. (1994). *Petroleum Production Systems* (Englewood Cliffs, NJ: Prentice Hall)

EDWARDSON, M. et al. (1962). Calculation of formation temperature disturbances caused by mud circulation. *J. Pet. Technol.*, Apr., 416–425

ERCB (1975). *Theory and Practice of the Testing of Gas Wells*, 3 ed. (Calgary: Energy Resources Conservation Board)

FANCHI, J. (1985). Analytical representation of the van Everdingen-Hurst influence functions. *SPE J.*, June, 405–425

FETKOVICH, E.J., FETKOVICH, M.J., and FETKOVICH, M.D. (1996). Useful concepts for decline curve forecasting, reserve estimation, and analysis. *SPE Reservoir Eng.*, Feb.

FETKOVICH, M., REESE, D., and WHITSON, C. (1998). Application of a general material balance for high-pressure gas reservoirs. *SPE J.*, Mar., 923–931

FETKOVICH, M.J. (1971). A simplified approach to water influx calculations – finite aquifer systems. *J. Pet. Technol.*, July, 814–828

FETKOVICH, M.J. (1973). The isochronal testing of oil wells. Paper SPE 4529, Presented at the SPE Annual Meeting, Las Vegas, Nevada, Sept. 30–Oct. 3

FETKOVICH, M.J. (1980). Decline curve analysis using type curves. SPE 4629, *SPE J.*, June

FETKOVICH, M.J., VIENOT, M.E., BRADLEY, M.D., and KIESOW, U.G. (1987). Decline curve analysis using type curves - case histories. SPE 13169, *SPE Form. Eval.*, Dec.

GENTRY, R.W. (1972). Decline curve analysis. *J. Pet. Technol.*, Jan., 38

GIGER, F.M., REISS, L.H., and JOURDAN, A.P. (1984). The reservoir engineering aspect of horizontal drilling. Paper SPE 13024, Presented at the 59th SPE Annual Technical Conference and Exhibition, Houston, TX, Sept. 16–19

GODBOLE, S., KAMATH, V., and ECONOMIDES, C. (1988). Natural gas hydrates in the Alaskan Arctic. *SPE Form. Eval.*, Mar.

GOLAN, M. and WHITSON, C. (1986). *Well Performance*, 2nd ed. (Englewood Cliffs, NJ: Prentice Hall)

GRAY, K. (1965). Approximating well-to-fault distance. *J. Pet. Technol.*, July, 761–767

GRINGARTEN, A. (1984). Interpretations of tests in fissured and multilayered reservoirs with double-porosity behavior. *J. Pet. Technol.*, Apr., 549–554

GRINGARTEN, A. (1987). Type curve analysis. *J. Pet. Technol.*, Jan., 11–13

GRINGARTEN, A.C., RAMEY, H.J., JR., and RAGHAVAN, R. (1974). Unsteady-state pressure distributions created by a well with a single infinite-conductivity vertical fracture. *SPE J.*, Aug., 347–360

GRINGARTEN, A.C., RAMEY, H.J., JR., and RAGHAVAN, R. (1975). Applied pressure analysis for fractured wells. *J. Pet. Technol.*, July, 887–892

GRINGARTEN, A.C., BOURDET, D.P., LANDEL, P.A., and KNIAZEFF, V.J. (1979). Comparison between different skin and wellbore storage type-curves for early time transient analysis. SPE Paper 8205, Presented at SPE–AIME 54th Annual Technical Conference, Las Vegas, Nevada, Sept. 23–25

GUNAWAN GAN, RONALD and BLASINGAME, T.A. (2001). A semi-analytic (p/Z) technique for the analysis of reservoir performance from abnormally pressured gas reservoirs. SPE Paper 71514, Presented at SPE Annual Technical Conference & Exhibition, New Orleans, LA, Sept.

HAGOORT, JACQUES and HOOGSTRA, ROB (1999). Numerical solution of the material balance equations of compartmented gas reservoirs. *SPE Reservoir Eng.*, **2**, Aug.

HAMMERLINDL, D.J. (1971). Predicting gas reserves in abnormally pressure reservoirs. Paper SPE 3479 presented at the 46th Annual Fall Meeting of SPE–AIME. New Orleans, LA, Oct.

HARVILLE, D. and HAWKINS, M. (1969). Rock compressibility in geopressured gas reservoirs. *J. Pet. Technol.*, Dec., 1528–1532

HAVLENA, D. and ODEH, A.S. (1963). The material balance as an equation of a straight line: Part 1. *Trans. AIME*, **228**, I-896

HAVLENA, D. and ODEH, A.S. (1964). The material balance as an equation of a straight line: Part 2. *Trans. AIME*, **231**, I-815

HAWKINS, M. (1955). *Material Balances in Expansion Type Reservoirs Above Bubble-Point*. SPE Transactions Reprint Series No. 3, pp. 36–40

HAWKINS, M. (1956). A note on the skin factor. *Trans. AIME*, **207**, 356–357

HOLDER, G. and ANGER, C. (1982). A thermodynamic evaluation of thermal recovery of gas from hydrates in the earth. *J. Pet. Technol.*, May, 1127–1132

HOLDER, G. et al. (1987). Effect of gas composition and geothermal properties on the thickness of gas hydrate Zones. *J. Pet. Technol.*, Sept., 1142–1147

HOLDITCH, S. et al. (1988). Enhanced recovery of coalbed methane through hydraulic fracturing. SPE Paper 18250, Presented at the SPE Annual Meeting, Houston, TX, Oct. 2–5

HORN, R. (1995). *Modern Test Analysis* (Palo Alto, CA: Petroway)

HORNER, D.R. (1951). Pressure build-up in wells. Proceedings of the Third World Petroleum Congress, The Hague, Sec II, 503–523. Also *Pressure Analysis Methods*, Reprint Series, No. 9 (Dallas, TX: Society of Petroleum Engineers of AIME), pp. 25–43

HUGHES, B. and LOGAN, T. (1990). How to design a coalbed methane well. *Pet. Eng. Int.*, May, 16–23

HURST, W. (1943). Water influx into a reservoir. *Trans. AIME*, **151**

IKOKU, C. (1984). *Natural Gas Reservoir Engineering* (New York: John Wiley & Sons)

JONES, S.C. (1987). Using the inertial coefficient, b, to characterize heterogeneity in reservoir rock. SPE Paper 16949, Presented at the SPE Conference, Dallas, TX, Sept. 27–30

JOSHI, S. (1991). *Horizontal Well Technology* (Tulsa, OK: Penn Well)

KAMAL, M. (1983). Interference and pulse testing - a review. *J. Pet. Technol.*, Dec., 2257–2270

KAMAL, M. and BIGHAM, W.E. (1975). Pulse testing response for unequal pulse and shut-in periods. *SPE J.*, Oct., 399–410

KAMAL, M., FREYDER, D., and MURRAY, M. (1995). Use of transient testing in reservoir management. *J. Pet. Technol.*, Nov.

KATZ, D. (1971). Depths to which frozen gas fields may be expected. *J. Pet. Technol.*, Apr.

KAZEMI, H. (1969). Pressure transient analysis of naturally fractured reservoirs with uniform fracture distribution., *SPE J.*, Dec., 451–462

KAZEMI, H. (1974). Determining average reservoir pressure. *SPE. J.*, Feb., 55–62

KAZEMI, H. and SETH, M. (1969). Effect of anisotropy on pressure transient analysis. *J. Pet. Technol.*, May, 639–647

KING, G. (1992). Material balance tec for coal seam and Devonian shale gas reservoirs with limited water influx. *SPE Reservoir Eng.*, Feb., 67–75

KING, G., ERTEKIN, T., and SCHWERER, F. (1986). Numerical simulation of the transient behavior of coal seam wells. *SPE Form. Eval.*, Apr., 165–183

KLINS, M. and CLARK, L. (1993). An improved method to predict future IPR curves. *SPE Reservoir Eng.*, Nov., 243–248

LANGMUIR, I. (1918). The constitution and fundamental properties of solids and liquids. *J. Am. Chem. Soc.*, **38**, 1918

LEE, J. (1982). *Well Testing* (Dallas, TX: Society of Petroleum Engineers of AIME)

LEE, J. and WATTENBARGER, R. (1996). *Gas Reservoir Engineering*, SPE Textbook Series, Vol. 5 (Dallas, TX: Society of Petroleum Engineers)

LEFKOVITS, H., HAZEBROEK, P., ALLEN, E., and MATTHEWS, C. (1961). A study of the behavior of bounded reservoirs. *SPE. J.*, Mar., 43–58

LEVINE, J. (1991). The impact of oil formed during coalification on generating natural gas in coalbed reservoirs. The 1991 Coalbed Methane Symposium, The University of Alabama–Tuscaloosa, May 13–16

MAKOGON, Y. (1981). *Hydrates of Natural Gas* (Tulsa, OK: Penn Well)

MATTAR, L. and ANDERSON, D. (2003). A systematic and comprehensive methodology for advanced analysis of production data. SPE Paper 84472, Presented at the SPE Conference, Denver, CO, Oct. 5–8

MATTHEWS, C.S. and RUSSELL, D.G. (1967). *Pressure Buildup and Flow Tests in Wells*, Monograph Vol. 1 (Dallas, TX: Society of Petroleum Engineers of AIME)

MATTHEWS, C.S., BRONS, F., and HAZEBROEK, P. (1954). A method for determination of average pressure in a bounded reservoir. *Trans. AIME*, **201**, 182–191; also in SPE Reprint Series, No. 9

MAVOR, M. and NELSON, C. (1997). Coalbed reservoirs gas-in-place analysis. Gas Research Institute Report GRI 97/0263, Chicago

MAVOR, M., CLOSE, J., and MCBANE, R. (1990). Formation evaluation of coalbed methane wells. *Pet. Soc. CIM*, CIM/SPE Paper 90–101

MCLENNAN, J. and SCHAFER, P. (1995). A guide to coal bed gas content determination. Gas Research Institute Report GRI 94/0396, Chicago

MCLEOD, N. and COULTER, A. (1969). The simulation treatment of pressure record. *J. Pet. Technol.*, Aug, 951–960

MERRILL, L.S., KAZEMI, H., and COGARTY, W.B. (1974). Pressure falloff analysis in reservoirs with fluid banks. *J. Pet. Technol.*, July, 809–818

MEUNIER, D., WITTMANN, M.J., and STEWART, G. (1985). Interpretation of pressure buildup test using in-situ measurement of afterflow. *J. Pet. Technol.*, Jan., 143–152

MULLER, S. (1947). *Permafrost* (Ann Arbor, MI: J.W. Edwards)

MUSKAT, M. (1945). The production histories of oil producing gas-drive reservoirs. *J. Appl. Phys.*, **16**, 167

MUSKAT, M. and EVINGER, H.H. (1942). Calculations of theoretical productivity factor. *Trans. AIME*, **146**, 126–139

NAJURIETA, H.L. (1980). A theory for pressure transient analysis in naturally fractured reservoirs. *J. Pet. Technol.*, July, 1241–1250

NEAVEL, R. et al. (1986). Interrelationship between coal compositional parameters. *Fuel*, **65**, 312–320 1999

NELSON, C. (1989). *Chemistry of coal weathering* (New York: Elsevier Science)

NELSON, R. (1999). Effects of coalbed reservoir property analysis methods on gas-in-place estimates. SPE Paper 57443, Presented at SPE Regional Meeting, Charleston, WV, 21–22 Oct.

OSTERGAARD, K. et al. (2000). Effects of reservoir fluid production on gas hydrate phase boundaries. SPE Paper 50689, Presented at the SPE European Petroleum Conference, The Hague, The Netherlands, Oct. 20–22

PALACIO, C. and BLASINGAME, T. (1993). Decline-curve analysis using type-curves analysis of gas well production data. SPE Paper 25909, Presented at the 1993 SPE Rocky Mountain Regional Meeting, Denver, CO, Apr. 26–28

PAPADOPULOS, I. (1965). Unsteady flow to a well in an infinite aquifer. *Int. Assoc. Sci. Hydrol.*, **I**, 21–31

PAYNE, DAVID A. (1996). Material balance calculations in tight gas reservoirs: the pitfalls of p/Z plots and a more accurate technique. *SPE Reservoir Eng.*, Nov.

PERRINE, R. (1956). Analysis of pressure buildup curves. *Drill. Prod. Prac. API*, 482–509

PETNANTO, A. and ECONOMIDES, M. (1998). Inflow performance relationships for horizontal wells. SPE Paper 50659, Presented at the SPE European Conference held in The Hague, The Netherlands, Oct. 20–22

PINSON, A. (1972). Convenience in analysing two-rate flow tests. *J. Pet. Techol.*, Sept., 1139–1143

PLETCHER, J. (2000). Improvements to reservoir material balance methods. SPE 62882, SPE Annual Technical Conference, Dallas, TX, 1–4 Oct.

POSTON, S. (1987). The simultaneous determination of formation compressibility and gas in place. Presented at the 1987 Production Operation Symposium, Oklahoma City, OK

POSTON, S. and BERG, R. (1997). *Overpressured Gas Reservoirs* (Richardson, TX: Society of Petroleum Engineers)

PRATIKNO, H., RUSHING, J., and BLASINGAME, T.A. (2003). Decline curve analysis using type curves - fractured wells. SPE 84287, SPE Annual Technical Conference, Denver, CO, 5–8 Oct.

PRATT, T., MAVOR, M., and DEBRUYN, R. (1999). Coal gas resources and production potential in the Powder River Basin. Paper SPE 55599, Presented at the 1999 Rocky Mountain Meeting; Gillette, WY, May 15–18

RAMEY, H. (1975). Interference analysis for anisotropic formations. *J. Pet. Technol.*, Oct., 1290–1298

RAMEY, H. and COBB, W. (1971). A general buildup theory for a well located in a closed drainage area. *J. Pet. Technol.*, Dec.

RAWLINS, E.L. and SCHELLHARDT, M.A. (1936). *Back-pressure Data on Natural Gas Wells and Their Application to Production Practices* (US Bureau of Mines Monograph 7)

REMNER, D. et al. (1986). A parametric stuffy of the effects of coal seam properties on gas drainage. *SPE Reservoir Eng.*, Nov., 633

RENARD, G.I. and DUPUY, J.M. (1990). Influence of formation damage on the flow efficiency of horizontal wells. Paper SPE 19414, Presented at the Formation Damage Control Symposium, Lafayette, LA, Feb. 22–23

ROACH, R.H. (1981). Analyzing geopressured reservoirs - a material balance technique. SPE Paper 9968, Society of Petroleum Engineers of AIME, Dallas, TX, Dec.

RUSSELL, D. and TRUITT, N. (1964). Transient pressure behaviour in vertically fractured reservoirs. *J. Pet. Technol.*, Oct., 1159–1170

SABET, M. (1991). *Well Test Analysis* (Dallas, TX: Gulf Publishing)

SAIDIKOWSKI, R. (1979). SPE Paper 8204, Presented at the SPE Annual Conference, Las Vegas, NV, Sept. 23–25

SCHILTHUIS, R. (1936). Active oil and reservoir energy. *Trans. AIME*, **118**, 37

SEIDLE, J. (1999). A modified p/Z method for coal wells. SPE Paper 55605, Presented at the 1999 Rocky Mountain Meeting, Gillette, WY, May 15–18

SEIDLE, J. and ARRL, A. (1990). Use of the conventional reservoir model for coalbed methane simulation. CIM/SPE Paper No. 90–118

SHERRAD, D., BRICE, B., and MacDONALD, D. (1987). Application of horizontal wells in Prudhoe Bay. *J. Pet. Technol.*, May, 1417–1421

SLIDER, H.C. (1976). *Practical Petroleum Reservoir Engineering Methods*. (Tulsa, OK: Petroleum Publishing)

SLOAN, D. (1984). Phase equilibria of natural gas hydrates. Paper Presented at the 1984 Gas Producers Association Annual Meeting, New Orleans, LA, Mar. 19–21

SLOAN, E. (2000). *Hydrate Engineering* (Richardson, TX: Society of Petroleum Engineers)

SMITH, J. and COBB, W. (1979). Pressure buildup tests in bounded reservoirs. *J. Pet. Technol.*, Aug.

SOMERTON, D. et al. (1975). Effects of stress on permeability of coal. *Int. J. Rock Mech., Min. Sci. Geomech. Abstr.*, **12**, 129–145

STANDING, M.B. (1970). Inflow performance relationships for damaged wells producing by solution-gas drive. *J. Pet. Technol.*, Nov., 1399–1400

STEFFENSEN, R. (1987). Solution-gas-drive reservoirs. *Petroleum Engineering Handbook*, Chapter 37 (Dallas, TX: Society of Petroleum Engineers)

STEGEMEIER, G. and MATTHEWS, C. (1958). A study of anomalous pressure buildup behavior. *Trans. AIME*, **213**, 44–50

STROBEL, C., GULATI, M., and RAMEY, H. (1976). Reservoir limit tests in a naturally fractured reservoir. *J. Pet. Technol.*, Sept., 1097–1106

TARNER, J. (1944). How different size gas caps and pressure maintenance affect ultimate recovery. *Oil Wkly*, June 12, 32–36

TERWILLIGER, P. et al. (1951). An experimental and theoretical investigation of gravity drainage performance. *Trans. AIME*, **192**, 285–296

TIAB, D. and KUMAR, A. (1981). Application of the p_D function to interference tests. *J. Pet. Technol.*, Aug., 1465–1470

TRACY, G. (1955). Simplified form of the MBE. *Trans. AIME*, **204**, 243–246

UNSWORTH, J., FOWLER, C., and JUNES, L. (1989). Moisture in coal. *Fuel*, **68**, 18–26

VAN EVERDINGEN, A.F. and HURST, W. (1949). The application of the Laplace transformation to flow problems in reservoirs. *Trans. AIME*, **186**, 305–324

VOGEL, J.V. (1968). Inflow performance relationships for solution-gas drive wells. *J. Pet. Technol.*, Jan. 86–92

WALSH, J. (1981). Effect of pore pressure on fracture permeability. *Int. J. Rock Mech., Min. Sci. Geomech. Abstr.*, **18**, 429–435

WARREN, J.E. and ROOT, P.J. (1963). The behavior of naturally fractured reservoirs. *SPE J.*, Sept., pp. 245–255

WATTENBARGER, ROBERT A. and RAMEY, H.J., JR. (1968). Gas well testing with turbulence damage and wellbore storage. *J. Pet. Technol.*, 877–887

WEST, S. and COCHRANE, P. (1994). Reserve determination using type curve matching and extended material balance methods in The Medicine Hat Shallow Gas Field. SPE Paper 28609, Presented at the 69th Annual Technical Conference, New Orleans, LA, Sept. 25–28

WHITSON, C. and BRULE, M. (2000). *Phase Behavior* (Richardson, TX: Society of Petroleum Engineers)

WICK, D. et al. (1986). Effective production strategies for coalbed methane in the Warrior Basin. SPE Paper 15234, Presented at the SPE Regional Meeting, Louisville, KY, May 18–21

WIGGINS, M.L. (1993). Generalized inflow performance relationships for three-phase flow. Paper SPE 25458, Presented at the SPE Production Operations Symposium, Oklahoma City, OK, Mar. 21–23

YEH, N. and AGARWAL, R. (1989). Pressure transient analysis of injection wells. SPE Paper 19775, Presented at the SPE Annual Conference, San Antonio, TX, Oct. 8–11

ZUBER, M. et al. (1987). The use of simulation to determine coalbed methane reservoir properties. Paper SPE 16420, Presented at the 1987 Reservoir Symposium, Denver, CO, May 18–19

This page intentionally left blank

Index